

**Integrated Analytical Systems**  
*Series Editor: Radislav A. Potyrailo*

Ghenadii Korotcenkov

# Handbook of Gas Sensor Materials

Properties, Advantages and  
Shortcomings for Applications

*Volume 1: Conventional Approaches*

 Springer

# Integrated Analytical Systems

This comprehensive and interdisciplinary series offers the most recent advances in all key aspects of development and applications of modern instrumentation for chemical and biological analysis on the microscale.

These key aspects will include (1) innovations in sample introduction through micro- and nano-fluidic designs, (2) new types and methods of fabrication of physical transducers and ion detectors, (3) materials for sensors that became available due to the breakthroughs in combinatorial materials science and nanotechnology, and (4) innovative data processing and mining methodologies that provide dramatically reduced rates of false alarms.

Clearly, a true multidisciplinary effort is required to meet objectives for a system with previously unavailable capabilities. This cross-discipline fertilization is driven by the expanding need for chemical and biological detection and monitoring and leads to the creation of instruments with new capabilities for new demanding applications. Indeed, instruments with more sensitivity are required today to analyze ultra-trace levels of environmental pollutants, pathogens in water, and low vapor pressure energetic materials in air. Sensor devices with faster response times are desired to monitor transient in-vivo events and bedside patients. More selective instruments are wanted to analyze specific proteins in vitro and analyze ambient urban or battlefield air. For these and many other applications, new features of modern microanalytical instrumentation are urgently needed. This book series is a primary source of both fundamental and practical information on both the current state of the art and future directions for microanalytical instrumentation technologies. This book series is addressed to the rapidly growing number of active practitioners and developers and those who are interested in starting research in this direction, directors of industrial and government research centers, laboratory supervisors and managers, students and lecturers.

For further volumes:

<http://www.springer.com/series/7427>



Ghenadii Korotcenkov

# Handbook of Gas Sensor Materials

Properties, Advantages and Shortcomings  
for Applications Volume 1: Conventional Approaches

Ghenadii Korotcenkov  
Materials Science and Engineering  
Gwangju Institute of Science and Technology  
Gwangju, Korea, Republic of (South Korea)

ISSN 2196-4475                      ISSN 2195-4483 (electronic)  
ISBN 978-1-4614-7164-6            ISBN 978-1-4614-7165-3 (eBook)  
DOI 10.1007/978-1-4614-7165-3  
Springer New York Heidelberg Dordrecht London

Library of Congress Control Number: 2013936792

© Springer Science+Business Media, LLC 2013

This work is subject to copyright. All rights are reserved by the Publisher, whether the whole or part of the material is concerned, specifically the rights of translation, reprinting, reuse of illustrations, recitation, broadcasting, reproduction on microfilms or in any other physical way, and transmission or information storage and retrieval, electronic adaptation, computer software, or by similar or dissimilar methodology now known or hereafter developed. Exempted from this legal reservation are brief excerpts in connection with reviews or scholarly analysis or material supplied specifically for the purpose of being entered and executed on a computer system, for exclusive use by the purchaser of the work. Duplication of this publication or parts thereof is permitted only under the provisions of the Copyright Law of the Publisher's location, in its current version, and permission for use must always be obtained from Springer. Permissions for use may be obtained through RightsLink at the Copyright Clearance Center. Violations are liable to prosecution under the respective Copyright Law.

The use of general descriptive names, registered names, trademarks, service marks, etc. in this publication does not imply, even in the absence of a specific statement, that such names are exempt from the relevant protective laws and regulations and therefore free for general use.

While the advice and information in this book are believed to be true and accurate at the date of publication, neither the authors nor the editors nor the publisher can accept any legal responsibility for any errors or omissions that may be made. The publisher makes no warranty, express or implied, with respect to the material contained herein.

Printed on acid-free paper

Springer is part of Springer Science+Business Media ([www.springer.com](http://www.springer.com))

# Preface

Sensing materials play a key role in the successful implementation of gas sensors, which year by year find wider application in various areas from environmental control to everyday monitoring of such activities as public safety, engine performance, medical therapeutics, and many more. Gas sensors can also be found in various industries such as the chemical and petrochemical industries, food and drinks processing, semiconductor manufacturing, agriculture, and fabrication industries, not to mention the motor, ship, and aircraft industries, power generation, etc., where control and analysis of process gases are necessary. At present industrial processes increasingly involve the use and manufacture of highly dangerous substances, particularly toxic and combustible gases. Inevitably, occasional escapes of gas occur, creating a potential hazard to the industrial plant, its employees, and people living nearby. Gas sensors allow detection of toxic and combustible gases in the atmosphere and, therefore, the use of these devices can prevent disastrous consequences for people.

However, the multidimensional nature of the interactions between function and composition, preparation method, and end-use conditions of sensing materials often make their rational design for real-world applications very challenging. Moreover, the world of sensing materials is very broad, and practically all well-known materials can be used in chemical sensors. Therefore, the selection of optimal sensing material for gas sensors is a complicated and multivariate task. However, one should note that the number of published books describing the analysis of materials through their application in the field of gas sensors is very limited.

Moreover, most of them are devoted to analysis of one specific sensing material, for example, polymers or metal oxides. Therefore, it is very difficult to conduct a comparative analysis of various materials and to choose sensing material optimal for concrete applications.

Taking this situation into account, I decided to fill this gap. My main goal was to create a really useful and encyclopedic handbook of gas sensor materials. The *Handbook of Gas Sensor Materials: Properties, Advantages, and Shortcomings for Application* is the first book containing a comprehensive examination of materials suitable for gas sensor design. For convenience of practical use, the present *Handbook* is divided into two parts: Vol. 1: *Conventional Approaches* and Vol. 2: *New Trends in Materials and Technologies*. In these books one can find detailed analysis of conventional gas sensing materials such as metal oxides, polymers, metal films, and semiconductors. New trends in gas sensing materials include analysis of, among other materials, 1D metal oxide nanostructures, carbon nanotubes, fullerenes, graphene, semiconductor quantum dots, and metal nanoparticles. The properties and applications of nanocomposites, photonic crystals, calixarenes-based compounds, ion conductors, ion liquids, metal-organic frameworks, porous semiconductors, ordered mesoporous materials, and zeolites are also discussed in the books. Close attention is given in these books to examining problems connected with stability and functionalizing of gas sensing materials. It is known that high stability is the main requirement for materials aimed for use as a gas sensor. The book chapters

introduce analysis of general approaches to selection of sensing materials for gas sensor design. Auxiliary materials used in gas sensors such as substrates, catalysts, membranes, heaters, and electrodes are also discussed. Thus, in these two volumes, the reader can find comparative analyses of all materials acceptable for gas sensor design and can estimate their real advantages and shortcomings. This means that one can consider the present books as a selection guide of materials for gas sensor manufacture. In addition, the books contain a large number of tables with information necessary for gas sensor design. The tables alone make these books very helpful and comfortable for the user. Hence, my belief that these books comprise an encyclopedic handbook of gas sensor materials, which answers many questions arising during selection of optimal sensor materials and promotes an understanding of the fundamentals of sensor functioning and development of the technological route of their fabrication for applications in various types of gas sensors.

These books will be of real interest to all materials scientists, especially to researchers working or planning to begin working in the field of gas sensing materials study and gas sensor design. The books will also be interesting for practicing engineers and project managers in industries and national laboratories who are interested in the development and fabrication of gas sensors for the sensor market. With many references to the vast resource of recently published literature on the subject, these books are a significant source of valuable information, which will provide scientists and engineers with new insights for understanding and improving existing devices and for designing new materials to making better gas sensors.

I believe that these books will also be useful to university students, postdocs, and professors. The structure of the books offers the basis for courses in the field of materials sciences, chemical sensors, sensor technologies, chemical engineering, semiconductor devices, electronics, and environmental control. Graduate students could also find the books useful while conducting research and trying to understand the basics of gas sensor design and functioning. I hope very much that in these books all will find specific information that will be of interest and use in his/her area of scientific and professional interests.

Gwangju, South Korea

Ghenadii Korotcenkov

# Series Preface

*In my career I've found that "thinking outside the box" works better  
if I know what's "inside the box."*

Dave Grusin, composer and jazz musician

*Different people think in different time frames: scientists think in decades,  
engineers think in years, and investors think in quarters.*

Stan Williams, Director of Quantum Science Research,  
Hewlett Packard Laboratories

*Everything can be made smaller, never mind physics;  
Everything can be made more efficient, never mind thermodynamics;  
Everything will be more expensive, never mind common sense.*

Tomas Hirschfeld, pioneer of industrial spectroscopy

## Integrated Analytical Systems

The field of analytical instrumentation systems is one of the most rapidly progressing areas of science and technology. This rapid development is facilitated by (1) the advances in numerous areas of research that collectively provide the impact on the design features and performance capabilities of new analytical instrumentation systems and by (2) the technological and market demands to solve practical measurement problems.

The book series *Integrated Analytical Systems* reflects the most recent advances in all key aspects of development and applications of modern instrumentation for chemical and biological analysis. These key development aspects include: (1) innovations in sample introduction through micro- and nano-fluidic designs, (2) new types and methods of fabrication of physical transducers and ion detectors, (3) materials for sensors that became available due to the breakthroughs in biology, combinatorial materials science and nanotechnology, (4) innovative data processing and mining methodologies that provide dramatically reduced rates of false alarms, and (5) new scenarios of applications of the developed systems.

A multidisciplinary effort is required to design and build instruments with previously unavailable capabilities for demanding new applications. Instruments with more sensitivity are required today to analyze ultra-trace levels of environmental pollutants, pathogens in water, and low vapor pressure energetic materials in air. Sensor systems with faster response times are desired to monitor transient in-vivo events and bedside patients. More selective instruments are sought to analyze specific proteins



*in vitro* and analyze ambient urban or battlefield air. Distributed sensors for multiparameter measurements (often including not only chemical and biological but also physical measurements) are needed for surveillance over large terrestrial areas or for personal health monitoring as wearable sensor networks. For these and many other applications, new analytical instrumentation is urgently needed. This book series is intended to be a primary source on both fundamental and practical information of where analytical instrumentation technologies are now and where they are headed in the future.

Niskayuna, NY, USA

Radislav A. Potyrailo  
GE Global Research

# Acknowledgments

I would like to say great thanks to Gwangju Institute of Science and Technology, Gwangju, Korea, which invited me and gave possibility to prepare this book for publication. This work was supported by Korean BK 21 Program and by Basic Science Research Program through the National Research Foundation of Korea (NRF) funded by the Ministry of Education, Science and Technology (2012R1A1A2041564). I also wish to thank to all my colleagues such as Dr. V. Brinzari (Moldova), Professors B.K. Cho (Korea), J. Schwank (USA), A. Cornet (Spain), J.R. Morante (Spain), V. Matolin (Chezh Rep.), and V. Tolstoy (Russia) for their friendly cooperation for a long time and important contribution to this work by advice, by valuable information on the new phenomena, and participation in experiments and discussions. Last but not least, I would like to thank to my wife Irina Korotcenkova for her patience and kind understanding during preparation of the manuscript. Research into gas sensors for many years and the writing of this book would not have been possible without her warm support.

Gwangju, South Korea

G. Korotcenkov



# Contents

<b>1 Introduction</b> .....	1
1.1 Gas Sensors and Their Role in Industry, Agriculture, and Environment Control.....	1
1.2 Gas Sensors Classification .....	13
1.3 Requirements of Gas Sensors.....	26
1.4 Comparative Analysis of Gas Sensors .....	28
1.5 Materials Acceptable for Gas Sensor Applications.....	35
References .....	40
 <b>Part I Conventional Gas Sensing Materials</b>	
<b>2 Metal Oxides</b> .....	49
2.1 General View .....	49
2.2 Which Metal Oxides Are Better for Solid-State Electrochemical Gas Sensors?.....	51
2.3 Metal Oxides with Ionic Conductivity: Solid Electrolytes .....	53
2.3.1 Criteria for Metal Oxide Application in Solid Electrolyte-Based Gas Sensors .....	53
2.3.2 High-Temperature Oxygen Sensors .....	54
2.3.3 Solid Electrolyte-Based Hydrogen Sensors .....	62
2.3.4 Other Gases .....	68
2.3.5 Limitations of Solid Electrolytes Application in Gas Sensors.....	68
2.4 Semiconducting Metal Oxides .....	71
2.4.1 Metal Oxides for Chemiresistors.....	71
2.4.2 Metal-Oxide p–n Homojunction and Heterostructures .....	85
2.4.3 High-Temperature Oxygen Sensors Based on Semiconducting Metal Oxides .....	89
2.5 Metal Oxides for Room-Temperature Gas Sensors.....	92
2.6 Other Applications of Metal Oxides .....	98
2.6.1 Pyroelectric-Based Gas Sensors.....	98
2.6.2 Thermoelectric-Based Gas Sensors.....	99
2.6.3 Chemoschromic Materials for Hydrogen Sensors .....	101
References .....	104
<b>3 Polymers</b> .....	117
3.1 General View .....	117
3.2 Polymer-Based Gas Sensors.....	122
3.3 Mechanisms of Conductivity Change in Polymer-Based Gas Sensors .....	129

3.4	Ion-Conducting Polymers and Their Use in Electrochemical Sensors .....	131
3.5	Limitations of Polymer Using in Gas Sensors .....	136
3.6	Choosing a Polymer for Gas Sensor Applications .....	139
	References .....	146
<b>4</b>	<b>Thin Metal Films</b> .....	<b>153</b>
4.1	Thin Metal Films in Gas Sensors .....	153
4.2	Disadvantages of Sensors and Approaches to Sensors' Parameters Improvement .....	161
	References .....	163
<b>5</b>	<b>Semiconductors in Gas Sensors</b> .....	<b>167</b>
5.1	Silicon-Based Gas Sensors .....	167
5.2	III–V-Based Gas Sensors .....	170
5.3	Wide-Bandgap Semiconductors .....	172
5.4	Porous Semiconductors (Porous Silicon) .....	175
5.5	Other Semiconductor Materials .....	180
5.5.1	Thermoelectric Materials .....	180
5.5.2	II–VI Semiconductor Compounds .....	182
5.5.3	Semiconductor Glasses .....	186
5.5.4	Tellurium .....	188
	References .....	190
<b>6</b>	<b>Solid Electrolytes for Detecting Specific Gases</b> .....	<b>197</b>
6.1	General View on Electrochemical Gas Sensors .....	197
6.2	Ideal Solid Electrolytes .....	200
6.3	H <sub>2</sub> Sensors .....	201
6.4	CO <sub>2</sub> Sensors .....	206
6.5	NO <sub>x</sub> Sensors .....	210
6.6	SO <sub>x</sub> Sensors .....	211
6.7	Cross-Sensitivity of Solid Electrolyte-Based Gas Sensors and Limitations .....	212
6.8	Oxygen and Other Sensors Based on Fluoride Ion Conductors .....	214
	References .....	217

## Part II Auxiliary Materials

<b>7</b>	<b>Materials for Sensor Platforms and Packaging</b> .....	<b>223</b>
7.1	Conventional Platforms .....	223
7.2	Micromachining Hotplates .....	225
7.3	Flexible Platforms .....	228
7.4	Cantilever-Based Platforms .....	234
7.4.1	Silicon-Based Microcantilevers .....	235
7.4.2	Polymer-Based Microcantilevers .....	238
7.5	Paper-Based Gas Sensors .....	240
7.6	Material Requirements for Packaging of Gas Sensors .....	243
	References .....	244
<b>8</b>	<b>Materials for Thick Film Technology</b> .....	<b>249</b>
	References .....	254
<b>9</b>	<b>Electrodes and Heaters in MOX-Based Gas Sensors</b> .....	<b>255</b>
9.1	Materials for Electrodes in Conductometric Gas Sensors .....	255
9.1.1	Electrode Influence on Gas Sensor Response .....	255
9.1.2	Electrode Materials Preferable for Gas Sensor Applications .....	257

9.2	Electrodes for Solid Electrolyte-Based Gas Sensors.....	260
9.2.1	The Role of Electrode Configuration in Solid Electrolyte-Based Gas Sensors .....	260
9.2.2	Sensing Electrodes in Solid Electrolyte-Based Gas Sensors.....	261
9.3	Materials for Heater Fabrication .....	266
	References .....	267
<b>10</b>	<b>Surface Modifiers for Metal Oxides in Conductometric Gas Sensors .....</b>	<b>273</b>
10.1	General Consideration .....	273
10.2	Sensitization Mechanisms .....	276
10.3	Bimetallic Catalysts.....	279
10.4	Approaches to Noble Metal Cluster Forming .....	281
	References .....	284
<b>11</b>	<b>Catalysts Used in Calorimetric (Combustion-Type) Gas Sensors .....</b>	<b>287</b>
	References .....	291
<b>12</b>	<b>Filters in Gas Sensors.....</b>	<b>293</b>
12.1	Passive Filters .....	293
12.2	Catalytically Active Filters.....	298
12.3	Sorbents for Gas Preconcentrators .....	300
	References .....	301
 <b>Part III Materials for Specific Gas Sensors</b>		
<b>13</b>	<b>Materials for Piezoelectric-Based Gas Sensors .....</b>	<b>307</b>
13.1	Piezoelectric Materials .....	309
13.2	Saw Devices .....	311
13.2.1	Materials for Interdigital Transducers .....	312
13.3	High-Temperature Devices.....	314
13.4	Miniaturization of Piezoelectric Sensors.....	317
13.5	Sensing Layers .....	318
13.5.1	General Requirements .....	318
13.5.2	Features of Sensing Materials Used in Acoustic Wave Gas Sensors .....	319
	References .....	325
<b>14</b>	<b>Materials for Optical, Fiber Optic, and Integrated Optical Sensors.....</b>	<b>329</b>
14.1	General View on Optical Gas Sensing .....	329
14.2	Fibers for Optical Gas Sensors.....	333
14.3	Planar Waveguide and Integrated Optical Sensors .....	336
14.4	Light Sources for Optical Gas Sensors.....	338
14.5	Detectors for Optical Gas Sensors.....	342
14.6	Other Elements of Optical Gas Sensors .....	348
	References .....	350
<b>15</b>	<b>Materials for Electrochemical Gas Sensors with Liquid and Polymer Electrolytes.....</b>	<b>353</b>
15.1	Membranes .....	354
15.2	Electrolytes .....	355
15.3	Electrodes .....	356
15.4	Gas Diffusion Electrodes.....	359
	References .....	363

<b>16</b>	<b>Materials for Capacitance-Based Gas Sensors</b> .....	365
16.1	General Discussions .....	365
16.2	Polymer-Based Capacitance Gas Sensors .....	367
16.3	Other Materials.....	369
	References .....	374
<b>17</b>	<b>Sensing Layers in Work-Function-Type Gas Sensors</b> .....	377
17.1	Work-Function-Type Gas Sensors.....	377
17.2	Materials Tested by KP .....	379
17.2.1	Metallic Layers.....	379
17.2.2	Inorganic Layers .....	380
17.2.3	Organic Layers .....	384
	References .....	386
<b>18</b>	<b>Humidity-Sensitive Materials</b> .....	389
18.1	Humidity Sensors .....	389
18.2	Materials Acceptable for Application in Humidity Sensors .....	392
18.2.1	Polymers.....	393
18.2.2	Metal Oxide Ceramics.....	396
18.2.3	Porous Semiconductors (Silicon and Other) .....	400
18.2.4	Other Materials and Approaches .....	403
	References .....	404
<b>19</b>	<b>Materials for Field Ionization Gas Sensors</b> .....	409
	References .....	414
<b>20</b>	<b>Gas Sensors Based on Thin-Film Transistors</b> .....	415
20.1	Thin-Film Transistors.....	415
20.2	Gas-Sensing Characteristics of Organic Thin-Film Transistors.....	417
20.3	Metal Oxide-Based Thin-Film Transistors .....	423
20.4	Other Materials in Thin-Film Transistor-Based Gas Sensors .....	425
	References .....	429
	<b>Author Biography</b> .....	433
	<b>Index</b> .....	435

# Contents of Volume II

## Part I Nanostructured Gas Sensing Materials

### 1 Carbon-Based Nanostructures

- 1.1 Carbon Black
  - 1.2 Fullerenes
  - 1.3 Carbon Nanotubes
  - 1.4 Graphene
  - 1.5 Nanodiamond Particles
- References

### 2 Nanofibers

- 2.1 Approaches to Nanofiber Preparation
  - 2.2 Nanofiber-Based Gas Sensors
- References

### 3 Metal Oxide-Based Nanostructures

- 3.1 Metal Oxide One-Dimensional Nanomaterials
    - 3.1.1 1D Structures in Gas Sensors
    - 3.1.2 The Role of 1D Structures in the Understanding of Gas-Sensing Effects
    - 3.1.3 What Kind of 1D Structures Is Better for Gas Sensor Design?
  - 3.2 Mesoporous, Macroporous, and Hierarchical Metal Oxide Structures
- References

### 4 Metal-Based Nanostructures

- 4.1 Metal Nanoparticles
    - 4.1.1 Properties
    - 4.1.2 Synthesis
    - 4.1.3 Gas Sensor Applications
  - 4.2 Metal Nanowires
- References

### 5 Semiconductor Nanostructures

- 5.1 Quantum Dots
  - 5.1.1 General Consideration
  - 5.1.2 Gas Sensor Applications of Quantum Dots



- 5.2 Semiconductor Nanowires
  - 5.2.1 Synthesis of Semiconductor Nanowires
  - 5.2.2 Gas-Sensing Properties of Si Nanowires
- References

## **Part II Other Trends in Design of Gas Sensor Materials**

### **6 Photonic Crystals**

- 6.1 Photonic Crystals in Gas Sensors
- 6.2 Problems in the Sensing Application of PhCs
  - 6.2.1 Problems on the Fabrication of Photonic Crystal
  - 6.2.2 Problems with Coupling Losses
  - 6.2.3 Problems with Signal Detection

References

### **7 Ionic Liquids in Gas Sensors**

References

### **8 Silicate-Based Mesoporous Materials**

- 8.1 Mesoporous Silicas
  - 8.1.1 Gas Sensor Applications of Mesoporous Silicas
- 8.2 Aluminosilicates (Zeolites)
  - 8.2.1 Zeolite-Based Gas Sensors

References

### **9 Cavitands**

- 9.1 Cavitands: Characterization
- 9.2 Cavitands as a Material for Gas Sensors

References

### **10 Metallo-Complexes**

- 10.1 Gas Sensor Applications of Metallo-Complexes
- 10.2 Approaches to Improvement of Gas Sensor Parameters and Limitations

References

### **11 Metal–Organic Frameworks**

- 11.1 General Consideration
- 11.2 MOFs Synthesis
- 11.3 Gas Sensor Applications

References

## **Part III Nanocomposites**

### **12 Nanocomposites in Gas Sensors: Promising Approach to Gas Sensor Optimization**

References

### **13 Polymer-Based Composites**

- 13.1 Conductometric Gas Sensors Based on Polymer Composites
- 13.2 Problems Related to Application of Polymer-Based Composites in Gas Sensors

References

**14 Metal Oxide-Based Nanocomposites for Conductometric Gas Sensors**

- 14.1 Metal–Metal Oxide Composites
  - 14.2 Metal Oxide–Metal Oxide Composites
- References

**15 Composites for Optical Sensors**

- 15.1 Dye-Based Composites
    - 15.1.1 Sol–Gel Composites
    - 15.1.2 Polymer-Based Composites
  - 15.2 Metal Oxide-Based Nanocomposites
- References

**16 Nanocomposites in Electrochemical Sensors**

- 16.1 Solid Electrolyte-Based Electrochemical Sensors
  - 16.2 Electrochemical Sensors with Liquid Electrolyte
    - 16.2.1 Polymer-Modified Electrodes
    - 16.2.2 Carbon–Ceramic Electrodes
- References

**17 Disadvantages of Nanocomposites for Application in Gas Sensors**

References

**Part IV Stability of Gas Sensing Materials and Related Processes****18 The Role of Temporal and Thermal Stability in Sensing Material Selection**

References

**19 Factors Controlling Stability of Polymers Acceptable for Gas Sensor Application**

- 19.1 Polymer Degradation
    - 19.1.1 Thermal Degradation
    - 19.1.2 Oxidative Degradation
    - 19.1.3 Hydrolytic Degradation
    - 19.1.4 Conducting Polymers Dedoping
  - 19.2 Approaches to Polymer Stabilization
- References

**20 Instability of Metal Oxide Parameters and Approaches to Their Stabilization**

- 20.1 Role of Structural Transformation of Metal Oxides in Instability of Gas-Sensing Characteristics
- 20.2 Role of Phase Transformations in Gas Sensor Instability
- 20.3 Approaches to the Improvement of Metal Oxide Structure Stability
  - 20.3.1 Only Chemically and Thermally Stable Materials Should Be Used in the Sensor Design
  - 20.3.2 Diffusion Coefficients of Both Oxygen and Any Ions in the Sensing Material Should Be Minimized
  - 20.3.3 Gas-Sensing Materials with an Extremely Small Grain Size Should Not Be Used
  - 20.3.4 Size and Shape of the Grains That Formed a Gas-Sensing Matrix Should Be Controlled
  - 20.3.5 Elemental Composition of Gas-Sensing Material Should Be Optimized
  - 20.3.6 Use Preliminary (Accelerated) Aging Prior to Sensor Tests

- 20.3.7 Use Technological Operations Contributing to the Improvement of the Temporal Stability of the Designed Structures
- 20.3.8 Use Novel Techniques for Metal Oxide Synthesis and Deposition Able to Produce Stable Materials
- 20.3.9 Materials and Processing Should Facilitate a Reduction of the Effects of Humidity
- 20.3.10 Increase Material Porosity and Pore Size
- 20.3.11 Use New Approaches to Design Sensors

References

## **21 InstaStability of Metal and Semiconductor 1D Nanowires and Nanotubability of 1D Nanostructures**

- 21.1 Stability of Metal and Semiconductor 1D Nanowires and Nanotubes
- 21.2 Stability of Carbon-Based Nanotubes and Nanofibers

References

## **22 Temporal Stability of Porous Silicon**

- 22.1 Porous Silicon Aging
- 22.2 Temporal Stabilization of Porous Silicon Through Oxidation

References

## **Part V Structure and Surface Modification of Gas Sensing Materials**

### **23 Bulk Doping of Metal Oxides**

- 23.1 General Approach
- 23.2 Bulk Doping Influence on Response and Stability of Gas-Sensing Characteristics

References

### **24 Bulk and Structure Modification of Polymers**

- 24.1 Modifiers of Polymer Structure
  - 24.1.1 Solvents (Porogens)
  - 24.1.2 Cross-Linkers
  - 24.1.3 Initiators
  - 24.1.4 Plasticizers
- 24.2 Approaches to Polymer Functionalizing
  - 24.2.1 Polymer Doping
  - 24.2.2 Polymer Grafting
  - 24.2.3 Role of Polymer Functionalization in the Gas-Sensing Effect

References

### **25 Surface Functionalizing of Carbon-Based Gas-Sensing Materials**

- 25.1 Surface Functionalizing of Carbon Nanotubes and Other Carbon-Based Nanomaterials
- 25.2 The Role of Defects in Graphene Functionalizing

References

### **26 Structure and Surface Modification of Porous Silicon**

- 26.1 Structure and Morphology Control of Porous Silicon
  - 26.1.1 Surface Modification of Porous Semiconductors to Improve Gas-Sensing Characteristics

References

**Part VI Technology and Sensing Material Selection**

**27 Technological Limitations in Sensing Material Applications**

References

**28 Technologies Suitable for Gas Sensor Fabrication**

28.1 Ceramic Technology

28.2 Planar Sensors

28.3 Thick-Film Technology

28.3.1 General Description

28.3.2 Powder Technology

28.3.3 Advantages and Disadvantages of Thick-Film Technology

28.4 Thin-Film Technology

28.5 Polymer Technology

28.5.1 Methods of Polymer Synthesis

28.5.2 Fabrication of Polymer Films

28.6 Deposition on Fibers

28.6.1 Specifics of Film Deposition on Fibers

28.6.2 Coating Design and Tooling

References

**29 Outlook: Sensing Material Selection Guide**

References

**About the Author**

**Index**

# Chapter 1

## Introduction

### 1.1 Gas Sensors and Their Role in Industry, Agriculture, and Environment Control

The air we live in contains numerous kinds of chemical species, natural and artificial, some of which are vital to life while many others are harmful to a greater or lesser extent (Yamazoe 2005). Figure 1.1 illustrates the concentration levels of the typical gas components concerned. At the present time, industrial processes increasingly involve the use and manufacture of highly dangerous substances, particularly toxic and combustible gases. Inevitably, occasional escapes of gas occur, which create a potential hazard to the industrial plant, its employees, and people living nearby. Worldwide incidents involving asphyxiation, explosions, and loss of life are a constant reminder of this problem. Therefore, gas sensors, helping the prevention of the above-mentioned problems, play an important role in various modern technological processes, where control and analysis of gases are necessary (Taylor and Schultz 1996; Cleaver 2001; Fine et al. 2010; Korotcenkov 2011; Honeywell Analytics 2012). Gas sensors are becoming widely used in the following: chemical and petrochemical industries; environmental, scientific, and engineering research organizations; medical institutions, including hospitals; food and drinks processing; microelectronics, including semiconductor manufacturing and telecommunications; agriculture; fabrication industries, including the motor, ship, and aircraft industries; and power generation, etc. (see Table 1.1).

Some examples of the use of gas sensors are shown in Fig. 1.2. This figure illustrates how a domestic house might be equipped with gas sensors in Japan. One can see that various kinds of sensors to monitor CO<sub>2</sub>, air quality, odor, and humidity can be installed in the house. Gas sensors may be used to detect toxic gases in continuous monitoring and alarm systems such as the detection of harmful gases both outdoor and indoor, including in the workplace. As is well known, even at very low concentrations, toxic gases are very dangerous to human health (see Table 1.2). Traditionally, fire alarms have used a smoke detector or a heat detector. In the event of fire, however, various combustible gases are also produced and these gases, particularly hydrogen, diffuse more rapidly than does smoke or heat. In many cases sensing these gases is useful for earlier detection of fire (Kohl et al. 2001). Gas sensors are able to detect a gas leak and can interface with a control system so that a process can be shut down automatically. A gas detector can also sound an alarm to operators in the area where the leak is occurring, giving them the opportunity to leave the area. Thus, the use of gas sensors can prevent accidents due to gas leakages, thereby saving lives and equipment. Gas detectors can be used to detect combustible and flammable gases. This type of device can be situated in a variety of locations such as on oil rigs, gas containers, and trunk gas pipelines; they may therefore also be used in firefighting.

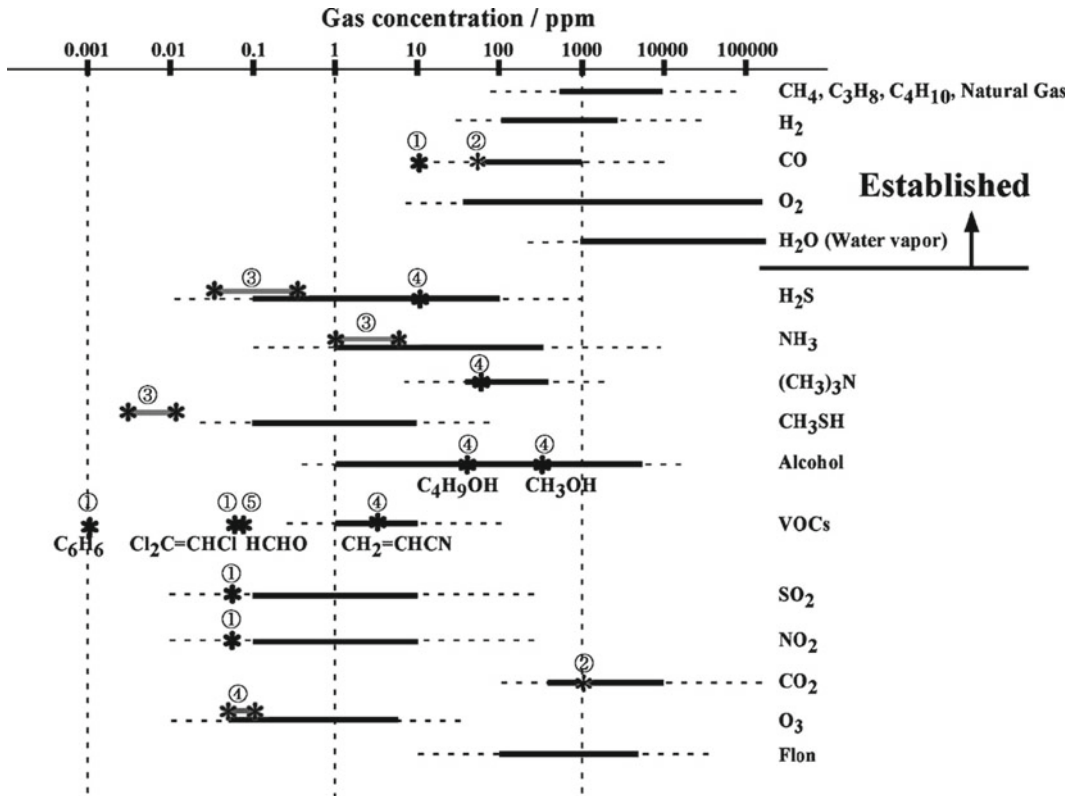


**Fig. 1.1** Concentration levels of typical gas components concerned. *Star marks* indicate the standards of the gases legislated in Japan by (1) Environmental Standard, (2) Ordinance on Health Standards in the Office, (3) Offensive Odor Control Law, (4) Working Environment Measurement Law, and (5) Ordinance by Ministry of Health, Labour and Welfare (Reprinted with permission from Yamazoe (2005). Copyright 2005 Elsevier)

Asphyxiant gases such as CO<sub>2</sub> and O<sub>2</sub> can also be detected by gas sensors. Carbon dioxide has many uses: carbonating drinks, pneumatic applications, fire extinguishers, photosynthesis. It is an essential ingredient for many processes—lasers and refrigerants are just two examples where carbon dioxide has found a use. Carbon dioxide can have substantial negative health effects in humans (Table 1.3) including drowsiness and, at high enough concentrations, suffocation. The maximum time-weighted exposure recommended by the United States Occupational Safety and Health Administration is 5,000 ppm over 8 h (CFR 1994). We all need to breathe the oxygen (O<sub>2</sub>) in air to live. Normal ambient air contains an oxygen concentration of 20.9 vol. %. When the oxygen level dips below 19.5 vol. %, the air is considered oxygen deficient. Oxygen concentrations below 16 vol. % are considered unsafe for humans. As such, it is highly desirable to be able to measure carbon dioxide and oxygen concentrations in order to control indoor air quality.

Environmental monitoring, i.e., the control of air pollution caused by industry and exhaust gases from automobiles, has also become a critical issue (Fine et al. 2010). The main gas pollutants and their features are summarized in Table 1.4. Gas sensors can control the contents of the above-mentioned hazardous gases in atmosphere, and therefore the wide application of gas sensors is one factor which can improve the quality of our lives. The principal gases that cause air pollution from automobiles are nitrogen oxides, NO<sub>x</sub> (NO and NO<sub>2</sub>), and carbon monoxide (CO). In addition, NO<sub>x</sub> gases and sulfur oxides (SO<sub>x</sub>) emitted from coal-fired plants cause acid rain and global warming and produce ozone (O<sub>3</sub>) that leads to serious metropolitan smog from photochemical reactions; these must be detected and reduced. In addition, a great amount of oil organic compounds are currently being produced by

**Table 1.1** Some examples of gas sensor applications

Field of application	Function	Examples of detected gases
Environment	Monitoring toxic gases present in the atmosphere, due to industrial emissions (weather stations, pollution monitoring)	CO, CH <sub>4</sub> , humidity, CO <sub>2</sub> , O <sub>3</sub> , NO <sub>x</sub> , VOCs, SO <sub>x</sub> , HCs, NH <sub>3</sub> , H <sub>2</sub> S
Safety at work	Control of indoor air quality; monitoring toxic gases in a working environment, for instance in a factory where dangerous chemicals are used	Toxic gases, combustible gases, O <sub>2</sub>
Domestic safety/ household application	Detection of poisonous gases or smoke in households, due to accidents such as fires and explosions; intelligent refrigerator or oven; fire alarm; natural gas heating; leak detection; air quality control; air purifiers; cooking control	CO, CH <sub>4</sub> , humidity, CO <sub>2</sub> , VOCs
Safety in car	Car ventilation control; gasoline vapor detection; alcohol breath tests	CO, CH <sub>4</sub> , LPG, VOCs
Public security	Control of indoor air quality, detection of substances dangerous for the safety of the general public	Toxic gases, combustible gases, flammable gases, explosives, O <sub>2</sub>
Medical/clinical	Diagnostics (breath analysis, disease detection); point-of-care patient monitoring; drug monitoring; artificial organs and prostheses; new drug discovery	O <sub>2</sub> , NH <sub>3</sub> , NO <sub>x</sub> , CO <sub>2</sub> , H <sub>2</sub> S, H <sub>2</sub> , Cl <sub>2</sub> , anesthesia gases
Agriculture	Plant/animal diagnostics; soil and water testing; meat/poultry inspection; waste/sewage monitoring	NH <sub>3</sub> , amines, humidity, CO <sub>2</sub> ,
Food quality control	Detection of particular molecules, which are formed when food starts to rot and it is no longer good for consumption	Humidity, CO <sub>2</sub> , etc.
Utilities/automotive/ power plants	Control of the concentration of the gases in the engine and gas boiler, to guarantee the highest possible efficiency of the combustion process. The same concept can also be applied to power plants, as the energy is generated by combustion	O <sub>2</sub> , CO, HCs, NO <sub>x</sub> , SO <sub>x</sub> , CO <sub>2</sub> , H <sub>2</sub> , HCs
Industry: Petrochemical Steel Water treatment Semiconductor	Process monitoring and control; quality control; workplace monitoring; waste stream monitoring; leakage alarms	HCs, conventional pollutants O <sub>2</sub> , H <sub>2</sub> , CO, conventional pollutants Cl <sub>2</sub> , CO <sub>2</sub> , O <sub>2</sub> , O <sub>3</sub> , H <sub>2</sub> S, CH <sub>4</sub> H <sub>2</sub> , CH <sub>4</sub> , HCl, AsH <sub>3</sub> , BCl <sub>3</sub> , PH <sub>3</sub> , CO, HF, O <sub>3</sub> , H <sub>2</sub> Cl <sub>2</sub> Si, TEOS, C <sub>4</sub> F <sub>6</sub> , C <sub>5</sub> F <sub>8</sub> , GeH <sub>4</sub> , NH <sub>3</sub> , NO <sub>2</sub> , O <sub>2</sub>
Oil and gas		HCs, H <sub>2</sub> S, CO

(continued)

**Table 1.1** (continued)

Field of application	Function	Examples of detected gases
Defense/military	Detection of chemical, biological, and toxin warfare agents; treaty verification	Agents, explosives, propellants
Aerospace	Monitoring of oxygen and toxic and flammable gases in the environment atmosphere	H <sub>2</sub> , O <sub>2</sub> , CO <sub>2</sub> , humidity
Traffic/tunnels/car parks	City traffic control and management; air quality monitoring in tunnels or underground parking garages	CO, O <sub>3</sub> , NO <sub>x</sub> , SO <sub>2</sub> , CH <sub>4</sub> , LPG

Source: Data from Taylor (1996), Stetter et al. (2003), Capone et al. (2003), etc.  
 HCs hydrocarbons, VOCs volatile organic compounds

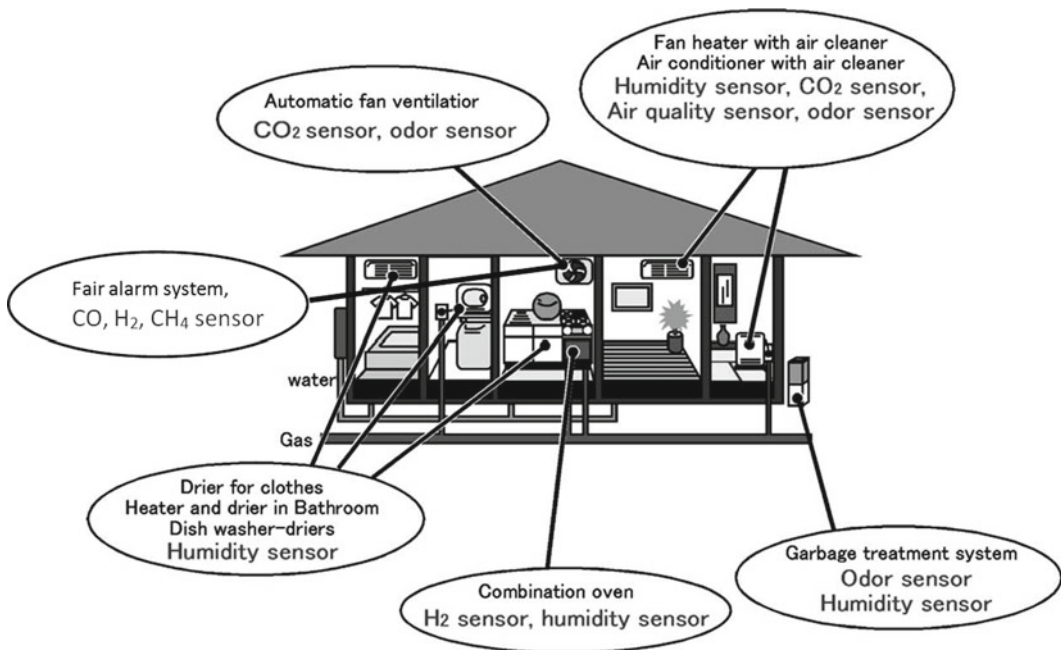


**Fig. 1.2** Various kinds of gas sensors equipped at various sites in a house [Idea from Nakahara (2004)]

applied construction materials and households; formaldehyde is the most dangerous among indoor pollutants as it can harm all kinds of organisms (see Table 1.5).

Typical examples of concentrations of regulated exposure are presented in Table 1.6 for three groups of toxic volatiles such as volatile organic compounds (VOCs), toxic industrial chemicals (TICs), and chemical warfare agents (CWAs). These examples demonstrate the need for gas-sensing capabilities with broad measurement dynamic ranges to cover two to four orders of magnitude in gas concentrations.

Gas sensors can be used for monitoring and control of combustion-related emissions (Docquier and Candel 2002). It is known that this task is a top priority in many industries. Sensors of CO, NO<sub>x</sub>, O<sub>2</sub>, CO<sub>2</sub>, hydrocarbons (HCs), and volatile organic compounds (VOCs) make it possible to provide a better control of combustion, leading to reduction of toxic emissions, efficient use of fuels, and subsequent energy savings. For example, according to a U.S. DOE report (DOE 2002),



**Table 1.2** Long- and short-term exposure limits of some typical toxic gases

Gas	Long-term exposure limit, 8 h (ppm)	Short-term exposure limit, 10 min (ppm)
H <sub>2</sub> S	10	15
CO	50	300
NO <sub>x</sub>	3	5
SO <sub>2</sub>	2	5
PH <sub>3</sub>	–	0.3
CH <sub>3</sub> OH	200	250
Cl <sub>2</sub>	0.5	1
NH <sub>3</sub>	25	35
HCl	–	5

Source: Data from <http://www.inspectapedia.com>

**Table 1.3** Detailing the effects of concentration and exposure time of CO<sub>2</sub> on human health

CO <sub>2</sub> concentration and exposure time	Effect on health (symptoms)
0.035 %	Approximate atmospheric concentration, no noticeable effect
3.3–5.4 % for 15 min	Increased depth of breathing
7.5 % for 15 min	Feeling of an inability to breathe, increased pulse rate, headache, dizziness, sweating, restlessness, disorientation, and visual distortion
3 % for over 15 h	Decreased night vision, color sensitivity
10 %, 1.5 min	Eye flickering, increased muscle activity, twitching
10+ %	Difficulty in breathing, impaired hearing, nausea, vomiting, as strangling sensation, sweating, after 15 min a loss of consciousness
30 %	Unconsciousness, convulsions. Several deaths attributed to CO <sub>2</sub> , at concentrations of more than 20 %

Source: Taken from occupational health and safety website in Canada. “Trends in atmospheric carbon dioxide (<http://www.esrl.noaa.gov/gmd/ccgg/trends/>)”

emissions-monitoring sensors are predicted to save 0.25 quadrillion British thermal units (BTU)/year of energy across all energy-consuming industries.

Gas sensors can be applied to the characterization of the aroma of food as part of a quality control process. We need to say that electronic noses satisfying this function are one of the most perspective devices among gas sensors. As is known, the sense of smell has long played a fundamental role in human development and biosocial interactions. An electronic nose system typically consists of a multi-sensor array, an information-processing unit such as an artificial neural network (ANN), software with digital pattern-recognition algorithms, and reference-library databases (Kowaiski and Bender 1972; Gardner 1991; Freund and Lewis 1995; Gardner and Bartlett 1999; Wilson and Baietto 2009; Korotcenkov and Stetter 2011). As sensor technology advances in the next decade, such gas sensor arrays will become routine on chemical and food processing lines, and more sophisticated sensors will be incorporated into automated process monitoring and control systems. In addition to the food industry, e-noses can be applied in areas such as automobile, packaging, cosmetic, drug, analytical chemistry, and biomedical industries where e-noses can be utilized for quality control of raw and manufactured products, process design, freshness and maturity (ripeness) monitoring, shelf-life investigations, authenticity assessments of premium products, classification of scents and perfumes, microbial pathogen detection, and environmental assessment studies (Table 1.7).

**Table 1.4** Pollutant gases

Features	Sources	Effects
Carbon dioxide (CO <sub>2</sub> )—colorless, odorless, and nontoxic gas	CO <sub>2</sub> is gas associated with ocean acidification, emitted from sources such as combustion, cement production, and respiration of animals, including people. The main source in urban areas is the motor vehicle and industry, especially power generation	The most abundant greenhouse gas in the atmosphere. It traps heat. It is heavier than air and, like hydrogen sulfide, will tend to accumulate just above the animal pen floor, surface of manure in a manure tank, or silage surface in a silo. The main danger with carbon dioxide is that it can create an oxygen deficiency and can result in asphyxiation or suffocation
Carbon monoxide (CO)—colorless, odorless, flammable and non-irritating, but very poisonous gas	It is a product by incomplete combustion of fuel such as natural gas, coal, or wood. Vehicular exhaust is a major source of carbon monoxide. Found in high concentrations in tunnels, mechanics' garages, and near heavy traffic	It inhibits the blood's ability to carry oxygen. Small amounts cause dizziness, headaches, fatigue, and slowed reaction times. It weakens the contractions of the heart in a healthy person and reduces their ability to do exercise. Fetuses, infants, and pregnant women are more susceptible to the effects. Large amounts are fatal
Chlorofluorocarbons—synthetic gas also called CFCs. Molecules contain chlorine, fluorine, and carbon	Used in air conditioners, refrigerators, dry cleaning solvents, some aerosol cans, and some foam plastics	Act as greenhouse gases in the troposphere with each molecule trapping 10,000 times more heat than a molecule of carbon dioxide. Break down ozone in the stratosphere, i.e., depletes the ozone layer (one chlorine atom can destroy up to 100,000 ozone molecules over an 80–120 year period)
Formaldehyde (HCHO)—an organic compound. Colorless gas with a pungent odor	The largest single use is as a resin to bond laminated wood products and to bind wood chips (particle board) used in furniture, flooring. Also used in the manufacture of carpet, wallpapers, and fiberglass insulation. Used to make creaseproof, flame-resistant, and shrinkproof fabrics (used on most cottons and linens). Cigarette smoke. Kerosene heaters. Used as a preservative in cosmetics, toiletries, food containers, and medicines	HCHO is the most dangerous among the indoor pollutants as it could harm all kinds of organisms. Can be inhaled, ingested, or absorbed through the skin, with different concentrations affecting individuals. Acute exposure: is an irritant to the eyes, sinus, and skin. It can cause a runny nose, sore throat, and sinus congestion (symptoms of a cold). It can cause difficulty in breathing, chest pain, wheezing, and asthma. Chronic and repeated exposure: causes nausea, vomiting, diarrhea, headaches, dizziness, lethargy, irritability, disturbed sleep, and skin irritation. May also cause menstrual and reproductive disorders. Repeated small level exposure may cause an allergic response. Is carcinogenic (cancer causing)

(continued)

**Table 1.4** (continued)

Features	Sources	Effects
Nitrogen dioxide (NO <sub>2</sub> )—a component of photochemical smog. This reddish-brown toxic gas has a characteristic sharp, biting odor. Soluble in water droplets to produce acid rain	Produced when a high-temperature heat source, such as an open flame, comes into contact with atmospheric nitrogen. Also a by-product from the burning of fossil fuels in places such as factories, power plants, and motor vehicles. In the home the major sources of nitrogen dioxide are gas cookers, gas or kerosene heaters, open fireplaces, and cigarette smoke	Irritates the eyes, nose, and throat when exposed to high levels. Can cause respiratory problems, especially in asthmatics. Reduces respiratory defense mechanisms and increases infection rates. Long-term exposure may cause structural damage to the lungs. Produces a smelly, dark haze. Contributes to brown haze
Ozone (O <sub>3</sub> )—a colorless gas. A slight odor in large concentrations	Ozone itself is not released during oil and gas development. But some of the main compounds that combine to form ozone (e.g., volatile organic compounds and nitrogen oxides) are released from oil and gas operations. Usually ozone is formed as a result of oxides of nitrogen reacting with organic compounds in the presence of sunlight. This results in a mixture of ozone and other pollutants which sometimes appears as a white haze. Also produced by high voltage electrical equipment such as photocopiers	Is a greenhouse gas because it traps heat in the troposphere. Irritates the mucous membranes of the nose, throat, and airways. Shortness of breath, wheezing, chest pain, coughing, and irritated eyes. People most at risk on high ozone days are those who (1) suffer from bronchitis and asthma, (2) exercise vigorously outside, (3) work physically outdoors, (4) play in parks for long periods, and (5) travel long distances on a bike. Vegetation and materials such as rubber, paints, and cloth are also damaged with long-term exposure
Natural gas—methane (CH <sub>4</sub> ) is the most important component of natural gas. Methane is odorless and not a toxic gas	Natural gas is released during venting operations or when there are leaks in equipment used during oil and gas development. Methane is also generated by anaerobic digestion of organic material. It is lighter than air and, therefore, tends to rise from the manure storage	CH <sub>4</sub> is an extremely efficient greenhouse gas which enhances global warming. CH <sub>4</sub> and other VOCs can combine with nitrogen oxides to form ground-level ozone, which can cause respiratory ailments such as asthma and decreased lung function. Methane is not toxic; however, it is extremely flammable and may form explosive mixtures with air
Reactive organic compounds (ROCs)—a group of VOCs and hydrocarbon pollutants (benzene, toluene, etc.). Most are invisible. Often have a very noticeable smell, for example, the smell of a pine tree. A component of photochemical smog	From fuel which has not actually burned during combustion in cars. Also released from oil refining, petrol stations, degreasing operations, dry cleaners, factories, power plants, glues, and solvents. Naturally released from trees such as pines, eucalypts, and citrus	Some may be toxic. Some may cause cancer. Some may damage plants. Produces photochemical smog if it reacts with nitrogen dioxide in strong sunlight

(continued)

**Table 1.4** (continued)

Features	Sources	Effects
Sulfur dioxide (SO <sub>2</sub> )—a colorless reactive gas. Distinctive choking odor. Soluble in water to produce acid rain	SO <sub>2</sub> is produced by volcanoes and in various industrial processes. Since coal and petroleum often contain sulfur compounds, their combustion generates SO <sub>2</sub> . Major sources are power plants and industrial boilers	Is a greenhouse gas because it traps heat in the atmosphere. Irritates the eyes, nose, and throat. May impair lung function by reducing a person's ability to clear foreign particles, such as dust or bacteria. Aggravates respiratory diseases such as bronchitis. High levels can affect healthy individuals during exercise who will experience symptoms such as wheezing, shortness of breath, and coughing. Kills plants. Corrodes metal
Hydrogen sulfide (H <sub>2</sub> S)—hydrogen sulfide is a toxic gas which has a characteristic rotten egg odor at low concentrations	Hydrogen sulfide occurs naturally in some oil and gas formations. When oil or gas is extracted from these formations, H <sub>2</sub> S may be released when gas is vented, when there is incomplete combustion of flared gas, or via fugitive emissions from equipment. It is also produced from the anaerobic decomposition of organic materials such as manure	Hydrogen sulfide, H <sub>2</sub> S, is the most dangerous manure gas. Hydrogen sulfide is considered a broad-spectrum poison, meaning that it can poison several different systems in the body, although the nervous system is most affected. The toxicity of H <sub>2</sub> S is comparable with that of hydrogen cyanide. It forms a complex bond with iron in the mitochondrial cytochrome enzymes, thus preventing cellular respiration. It is lethal if inhaled at high concentrations
Ammonia (NH <sub>3</sub> )—it is normally encountered as a gas with a characteristic pungent odor	NH <sub>3</sub> is emitted from agricultural processes. It is produced by the decomposition of animal manures. NH <sub>3</sub> contributes significantly to the nutritional needs of terrestrial organisms by serving as a precursor to foodstuffs and fertilizers. NH <sub>3</sub> , either directly or indirectly, is also a building block for the synthesis of many pharmaceuticals	Although in wide use, NH <sub>3</sub> is both caustic and hazardous. Ammonia gas is a severe respiratory tract irritant. Brief exposure to concentrations above 1,500 ppm can cause pulmonary edema, a potentially fatal accumulation of fluid in the lungs. The symptoms of pulmonary edema (tightness in the chest and difficulty breathing) may not develop for 1–24 h after an exposure

Sources: [http://www.environment.nsw.gov.au/resources/airwatch/airpoll\\_8.pdf](http://www.environment.nsw.gov.au/resources/airwatch/airpoll_8.pdf); [http://www.earthworksaction.org/issues/detail/air\\_contaminants](http://www.earthworksaction.org/issues/detail/air_contaminants); [http://en.wikipedia.org/wiki/Air\\_pollution](http://en.wikipedia.org/wiki/Air_pollution)

**Table 1.5** Physical symptoms of formaldehyde influence on the human's health

Concentration	Physical symptoms
40 ppb (8 h average) 100 ppb (1 h average)	Health Canada recommends these exposure limits as residential indoor air quality guidelines (Health Canada 2006)
1–10 ppm	Eye irritation; lacrimation at 4 ppm
10–20 ppm	Coughing, heart palpitations, tight feeling in chest
50–100 ppm and above	Pulmonary edema, pneumonitis, death
Contact with skin (formalin or HCHO-containing resins)	Dermatitis

**Table 1.6** Examples of regulated concentration levels (in ppm by volume) from three representative classes of toxic gases: VOCs, TICs, and CWAs

Class	Chemical or agent	IDLH (ppm)	LOC (ppm)	TLV-TWA (ppm)	TLV-STEL (ppm)	PEL (ppm)	GPL (ppm)	AEGL-3 (ppm)	AEGL-2 (ppm)	AEGL-1 (ppm)	
VOCs	Acetone	2,500	250	750	1,000	1,000		1,700	950	200	
	Benzene	500	50	0.5	2.5	1		990	200	9	
	Chloroform	500	50	10	2	50		1,600	29		
	Methanol	6,000	600	200	250	250		1,600	520	270	
	Methylene chloride	2,300	230	25	125			2,100	60		
	Phenol	250	25	5	10	5		23	6.3	1.9	
	Ammonia	300	30	25	25	50		390	110	30	
	Carbon monoxide	1,200	120	25	400	50		130	27		
	Chlorine	10	1	0.5	1	1		7.1	0.71	0.5	
	Formaldehyde	20	2	0.3	0.75	0.75		35	15	0.9	
TICs	Nitrogen dioxide	20	2	3	5	5		11	6.7	0.5	
	Phosphine	50	5	0.3	0.3	0.3		0.45	0.25		
	Sulfur dioxide	100	10	2	5	5		9.6	0.75	0.2	
	Chemical mustard	$4 \times 10^{-4}$	$4 \times 10^{-5}$	$6 \times 10^{-5}$	$4.6 \times 10^{-4}$			$3.1 \times 10^{-6}$	$4.2 \times 10^{-2}$	$2 \times 10^{-3}$	$1.2 \times 10^{-3}$
	Lewisite	$3 \times 10^{-4}$	$3 \times 10^{-5}$	$3.5 \times 10^{-4}$				$3.5 \times 10^{-4}$	$1.3 \times 10^{-2}$	$2.1 \times 10^{-3}$	
	Sarin	$3 \times 10^{-2}$	$3 \times 10^{-3}$	$9 \times 10^{-6}$	$3 \times 10^{-5}$			$3 \times 10^{-7}$	$8.7 \times 10^{-3}$	$2.2 \times 10^{-3}$	$2 \times 10^{-4}$
	Soman	$8 \times 10^{-3}$	$8 \times 10^{-4}$	$4 \times 10^{-6}$	$7.0 \times 10^{-6}$			$1.3 \times 10^{-7}$	$6.6 \times 10^{-3}$	$9 \times 10^{-3}$	$7 \times 10^{-5}$
	Tabun	$3 \times 10^{-2}$	$3 \times 10^{-3}$	$9 \times 10^{-6}$	$3 \times 10^{-5}$			$3 \times 10^{-7}$	$1.5 \times 10^{-2}$	$2 \times 10^{-3}$	$2 \times 10^{-4}$
	VX	$2 \times 10^{-3}$	$2 \times 10^{-4}$	$7 \times 10^{-7}$	$7 \times 10^{-6}$			$4 \times 10^{-7}$	$3.6 \times 10^{-4}$	$1 \times 10^{-4}$	$7 \times 10^{-7}$
	CWAs										

*IDLH* immediately dangerous to life or health, *LOC* level of concern,  $0.1 \times$  *IDLH*—established by NIOSH, U.S. National Institute for Occupational Safety and Health; *TLV-TWA* threshold limit value (time-weighted average), *TLV-STEL* threshold limit value (short-term exposure limit)—established by ACGIH, American Conference of Governmental Industrial Hygienists; *PEL* permissible exposure limit—established by OSHA, Occupational Safety and Health Administration; *GPL* general population limit—established by USACHPPM, U.S. Army Center for Health Promotion and Preventative Medicine; and *AEGL-1,2,3* acute exposure guideline levels—established by EPA, U.S. Environmental Protection Agency *Source*: Reprinted with permission from Potyrailo et al. (2011). Copyright 2011 American Chemical Society

**Table 1.7** Examples of some industry-based applications for electronic noses

Industry sector	Application area	Specific use types and examples
Agriculture	Rop protection; harvest timing and storage; meat, seafood, and fish products; plant production; pre- and post-harvest diseases	Homeland security; safe food supply; crop ripeness; preservation treatments; freshness; contamination; spoilage cultivar selection; variety characteristics plant disease diagnoses; pest identification; detect non-indigenous pests of food crops
Airline transportation	Public safety and welfare; passenger and personnel security	Explosive and flammable materials detection
Cosmetics	Personal application products; fragrance additives	Perfume and cologne development; product enhancement; consumer appeal
Environmental	Air and water quality monitoring; indoor air quality control; pollution abatement regulations	Pollution detection; effluents, toxic spills, malodor emissions; toxic/hazardous gases control of point-source pollution releases
Food and beverage	Consumer fraud prevention; quality control assessments; ripeness; food contamination taste; smell characteristics	Ingredient confirmation; standards; brand recognition; product consistency; marketable condition; spoilage, shelf life; off flavors; product variety assessments
Manufacturing	Processing controls; product uniformity; safety; security; work conditions	Product characteristics and consistency; aroma and flavor characteristics; fire alarms; toxic gas leak detection
Medical and clinical	Pathogen identification; pathogen or disease detection; physiological conditions	Patient treatment selection; prognoses disease diagnoses; metabolic disorders nutritional status, organ failures
Military	Personnel and population security; civilian and military safety	Biological and chemical weapons; explosive materials detection
Pharmaceutical	Contamination; product purity; variations in product mixtures	Quality control of drug purity; formulation consistency and uniformity
Regulatory	Consumer protection; environmental protection	Product safety; hazardous characteristics; air, water, and soil contamination tests
Scientific research	Botany; ecological studies; engineering; material properties; microbiology; pathology	Chemotaxonomy; ecosystem functions machine design; chemical processes; microbe and metabolite identifications

Source: Reprinted from Wilson and Baietto (2009). Published by MDPI

In agriculture, gas sensors can be used for: animal and plant disease diagnostics; detection of contaminants and pathogens in milk, meat, and other foods; and determination of product quality such as the ripeness and flavors of fruits and vegetables in the field (Taylor 1996; Wilson and Baietto 2009). Pharmaceuticals is another important field for gas sensor applications. Drug discovery is critical in the development and commercialization of new pharmaceuticals, providing the basis for new drugs and new therapies.

Medicine is another important field for gas sensor applications. Emerging requirements for sensors in the medical and healthcare sector are being driven by movement toward the continuous monitoring of patients. Breath analysis is one of the possible applications of gas sensors in medicine (see Table 1.8). Under these conditions, feedback on the state of the patient and the results of therapy can

**Table 1.8** Principal clinical conditions for which in vivo chemical sensors are considered to be helpful

Clinical condition	Analyte and breath markers	Physiological range of gases in human breath
Diabetes mellitus	Vapor of acetone	CH <sub>4</sub> : 4–20 ppm
Vital function monitoring in intensive care/anesthetics/prolonged surgery	NO <sub>x</sub> , O <sub>2</sub> , halothane, CO <sub>2</sub> , etc.	C <sub>2</sub> H <sub>6</sub> , C <sub>2</sub> H <sub>12</sub> : 1–11 ppb C <sub>6</sub> H <sub>8</sub> : 12–1,000 ppb C <sub>2</sub> H <sub>5</sub> OH: 13–1,000 ppb CH <sub>3</sub> OH: 160–2,000 ppb
Inflammation and oxidative stress	NO, CO	CO <sub>2</sub> : 2,500–3,000 ppm
Asthma, cystic fibrosis	NO, CO, H <sub>2</sub> O <sub>2</sub>	CO: 0.4–2.0 ppm
Pulmonary allograft dysfunction, lung cancer	NO	CO ( <i>smoker</i> ): 1–20 ppm NH <sub>3</sub> : 130–2,400 ppb
Chronic bronchitis/chest medicine	O <sub>2</sub> , CO <sub>2</sub> , pH	NO ( <i>lower respiratory tract</i> ): 1–9 ppb
Bronchial epithelial infection	NO <sub>2</sub>	NO ( <i>upper respiratory tract</i> ): 200–1,000 ppb
Respiratory monitoring	CO <sub>2</sub> /O <sub>2</sub> ratio, NO	NO ( <i>nasal level</i> ): 1,000–30,000 ppb

Source: Data from Moskalenko et al. (1996), Smith et al. (1999), Marczin et al. (2005), and Cao and Duan (2006)

be obtained without the delays associated with conventional intermittent measurement and the use of central laboratories for chemical and biochemical analysis (Moskalenko et al. 1996; Kharitonov and Barnes 2000; Cao and Duan 2006).

Experiment has shown that e-noses designed on the basis of gas sensor arrays can also be successfully applied in medicine (Wilson and Baietto 2011). Diagnosing human diseases based on the sense of smell, in addition to physical examinations, remains one of the most reliable methods used in bedside medicine for many years. The odors emitted by patients were once considered among the first major clues leading to an early diagnosis. The practice of evaluating effluvia (odor of patients), along with other extracorporeal information, was regarded with such importance that Fitzgerald and Tierney (1982) summarized a range of different types of extracorporeal observations (clues) and supplemental diagnostic techniques that provided useful physical evidence for clinical diagnostic evaluations. A list of some of these descriptive aromas that have been reported as positive indicators of specific diseases, physiological or metabolic disorders, and genetic anomalies is presented in Table 1.9. It is clear that, to emphasize the value of preserving olfactory methods in the medical profession, they provided a number of different examples of aroma bioindicators for various types of disease. The long history of human odors being used for disease diagnosis by medical doctors attests to the usefulness and effectiveness of olfactory information in providing valuable clues for assessing patient conditions and to the ingenuity and skill of medical practitioners in achieving accurate diagnoses without the aid of modern analytical equipment and chemical-detection devices now available for this purpose.

Government agencies have many singular needs for gas sensors across a wide range of applications as well. For example, gas sensors have been essential in satisfying a profusion of government-mandated regulatory requirements, including such applications as measuring chemical effluent from factories and exhaust gases from automobiles (see Table 1.10). Water quality is also one of the objectives for control using gas sensors.

A great demand for gas sensors stems from the National Aeronautics and Space Administration's Earth Orbiting Satellite program, which attempts to monitor changes in the chemical composition of the Earth's atmosphere. Reductions in the size of military forces and the resulting closures of military bases have led to a demand for gas sensors capable of monitoring the cleanup and disposal of numerous toxic organic compounds, chemical warfare agents, and obsolete munitions. Gas sensors will also be required for online control in the manufacture of low-volume specialty components or ultra-high-performance military aircraft. Without sensor-based control for these specialized needs, the unit costs of production will very likely be prohibitive.

At present, common gases measured by gas sensors include ammonia (NH<sub>3</sub>), arsine (AsH<sub>3</sub>), bromine (Br<sub>2</sub>), carbon dioxide (CO<sub>2</sub>), carbon monoxide (CO), chlorine (Cl<sub>2</sub>), chlorine dioxide (ClO<sub>2</sub>), diborane

**Table 1.9** Some early uses of descriptive aromas in diagnosing specific diseases and metabolic disorders associated with odors released from affected human tissues

Disease/disorder	Body source	Descriptive aroma
Acromegaly	Body	Strong, offensive
Anaerobic infection	Skin, sweat	Rotten apples
Azotemia (prerenal)	Urine	Concentrated urine odor
Bacterial proteolysis	Skin	Over-ripe Camembert
Bacterial vaginosis	Vaginal discharge	Amine-like
Bladder infection	Urine	Ammonia
Bromhidrosis	Skin, nose	Unpleasant
Darier's disease	Buttocks	Rank, unpleasant odor
Diabetic ketoacidosis	Breath	Rotting apples, acetone
Congestive heart failure	Heart (portcaval shunts)	Dimethyl sulfide
Cystic fibrosis	Infant stool	Foul
Diabetes mellitus	Breath	Acetone-like
Diphtheria	Sweat	Sweet
Empyema (anaerobic)	Breath	Foul, putrid
Esophageal diverticulum	Breath	Feculent, foul
Fetor hepaticus	Breath	Newly mown clover, sweet
Gout	Skin	Gouty odor
Hydradenitis suppurativa	Apocrine sweat glands	Bad body odor
Hyperhidrosis	Body	Unpleasant body odor
Hyperaminoaciduria (oasthouse syndrome)	Infant skin	Dried malt or hops
Hypermethioninemia	Infant breath	Sweet, fruity, fishy, boiled cabbage, rancid butter
Intestinal obstruction	Breath	Feculent, foul
Intranasal foreign body	Breath	Foul, feculent
Isovaleric acidemia	Skin, sweat, breath	Sweaty feet, cheesy
Ketoacidosis (starvation)	Breath	Sweet, fruity, acetone-like
Liver failure	Breath	Musty fish, raw liver, feculent, mercaptans, dimethyl sulfide
Lung abscess	Sputum, breath	Foul, putrid, full
Maple syrup urine disease	Sweat, urine, ear wax	Maple syrup, burnt sugar
Phenylketonuria	Infant skin	Musty, horsey, mousy, sweet urine
Pneumonia (necrotizing)	Breath	Putrid
Pseudomonas infection	Skin, sweat	Grape
Renal failure (chronic)	Breath	Stale urine
Rotavirus gastroenteritis	Stool	Full
Rubella	Sweat	Freshly plucked feathers
Schizophrenia	Sweat	Mildly acetic
Scrofula	Body	Stale beer
Scurvy	Sweat	Putrid
Shigellosis	Stool	Rancid
Smallpox	Skin	Pox stench
Squamous-cell carcinoma	Skin	Offensive odor
Sweaty feet syndrome	Urine, sweat, breath	Foul acetic
Trench mouth	Breath	Halitosis
Trimethylaminuria	Skin, urine	Fishy
Tuberculosis lymphadenitis	Skin	Stale beer
Tubular necrosis (acute)	Urine	Stale water
Typhoid	Skin	Freshly baked brown bread
Uremia	Breath	Fishy, ammonia, urine-like
Vagabond's disease	Skin	Unpleasant
Varicose ulcers (malignant)	Leg	Foul, unpleasant
Yellow fever	Skin	Butcher's shop

Source: Data from Wilson and Baietto (2011). Published by MDPI



**Table 1.10** Gaseous air pollutants

---

Oxides of sulfur and other sulfur compounds (SO <sub>2</sub> , etc.)
Oxides of nitrogen and other nitrogen compounds (NO, NO <sub>2</sub> , peroxyacetyl nitrate, NH <sub>3</sub> , etc.)
Oxides of carbon (CO, CO <sub>2</sub> )
Oxidizing agents (O <sub>3</sub> , Cl <sub>2</sub> , etc.)
Organic compounds and partial oxidation compounds (rubber and plastics, organic solvents, chlorinated hydrocarbons and fluorocarbons, volatile organic compounds, CH <sub>4</sub> , etc.)
Organometallic compounds
Halogens and their compounds (As, AsH <sub>3</sub> , etc.)
Phosphorus and its compounds (P, P <sub>2</sub> O <sub>5</sub> , etc.)

---

(B<sub>2</sub>H<sub>6</sub>), fluorine (F<sub>2</sub>), germanium tetrahydride (GeH<sub>4</sub>), halocarbons or refrigerants, **hydrocarbons** (CH<sub>4</sub>, C<sub>2</sub>H<sub>6</sub>, C<sub>3</sub>H<sub>8</sub>, etc.), hydrogen (H<sub>2</sub>), hydrogen chloride (HCl), hydrogen cyanide (HCN), hydrogen fluoride (HF), hydrogen selenide (H<sub>2</sub>Se), hydrogen sulfide (H<sub>2</sub>S), mercury vapor (Hg), nitrogen dioxide (NO<sub>2</sub>), nitric oxide (NO), nitrogen oxides (NO<sub>x</sub>), organic solvents (acetone (C<sub>2</sub>H<sub>2</sub>), **tetrachloroethylene** (C<sub>2</sub>Cl<sub>4</sub>), ethanol (C<sub>2</sub>H<sub>5</sub>OH), etc.), oxygen (O<sub>2</sub>), ozone (O<sub>3</sub>), phosphine (PH<sub>3</sub>), silane (SiH<sub>4</sub>), sulfur dioxide (SO<sub>2</sub>), and **water vapor** (H<sub>2</sub>O).

## 1.2 Gas Sensors Classification

At present there are a wide variety of devices based on different materials and operating on diverse principles which can be applied for gas detection. The appearance of several types of gas sensors designed by Figaro is shown in Fig. 1.3.

For gas sensor classification, various approaches can be used. For example, taking into account transduction mechanisms, we can distinguish six general categories of sensors: (1) optical sensors, (2) electrochemical sensors, (3) electrical sensors, (4) mass-sensitive sensors, (5) calorimetric sensors, and (6) magnetic sensors (see Table 1.11).

*Electrochemical sensors such as* amperometric, potentiometric, and conductometric ones are based on the detection of electroactive species involved in chemical recognition processes and make use of charge transfer from a solid or liquid sample to an electrode or vice versa (Korotcenkov et al. 2009; Stetter et al. 2011). As a rule in electrochemical sensors, three active gas diffusion electrodes are immersed in a common electrolyte, frequently a concentrated aqueous acid or salt solution, for efficient conduction of ions between the working and counter electrodes (see Fig. 1.4). Depending on the specific cell, the target gas is either oxidized or reduced at the surface of the working electrode. This reaction alters the potential of the working electrode relative to the reference electrode. The primary function of the associated electronic driver circuit connected to the cell is to minimize this potential difference by passing current between the working and counter electrodes, the measured current being proportional to the target gas concentration. Electrochemical effects in sensors may be stimulated electrically or they may result from a spontaneous interaction at the zero-current condition. Gas enters the cell through an external diffusion barrier that is porous to gas but impermeable to liquid. Many designs incorporate a capillary diffusion barrier to limit the amount of gas contacting the working electrode and thereby maintaining “amperometric” cell operation. Typical configurations of electrochemical sensors are shown in Fig. 1.5. As it is seen, for electrochemical sensors, design of liquid electrolytes (Fig. 1.5a), polymers (Fig. 1.5b), and solid electrolytes (Fig. 1.5c, d) can be used.

*Electrical sensors*, operating due to a surface interaction with target gas, cover a large group of gas sensors: polymer, metal, metal oxide, or semiconductor conductometric sensors; capacitance sensors; and work–function-type and Schottky barrier-, MOS-, and FET-based sensors (Korotcenkov 2011).

**Table 1.11** The classification of gas sensors suggested in 1991 by Analytical Chemistry Division of IUPAC

Class of gas sensors	Operating principle
Electrochemical	Changes in current, voltage, capacitance/impedance: <ul style="list-style-type: none"> <li>• Voltammetry (including amperometry)</li> <li>• Potentiometry</li> <li>• Chemically sensitized field-effect transistor</li> <li>• Potentiometry with solid electrolytes for gas sensing</li> </ul>
Electrical	Metal oxide conductivity Organic conductivity Electrolytic conductivity Heterojunction conductivity (Schottky diode, FET, MOS) Work function Electric permittivity (capacitance)
Mass sensitive	Changes in the weight, amplitude, phase or frequency, size, shape, or position: <ul style="list-style-type: none"> <li>• Quartz crystal microbalance</li> <li>• Surface acoustic wave propagation</li> <li>• Cantilever</li> </ul>
Magnetic	Changes of paramagnetic gas properties
Optical devices	Changes in light intensity, color, or emission spectra: <ul style="list-style-type: none"> <li>• Absorbance</li> <li>• Reflectance</li> <li>• Luminescence</li> <li>• Refractive index</li> <li>• Optothermal effect</li> <li>• Light scattering (Raman scattering, plasmon resonance)</li> </ul>
Thermometric (calorimetric)	Heat effects of a specific chemical reaction. Changes in temperature, heat flow, heat content: <ul style="list-style-type: none"> <li>• Thermoelectric</li> <li>• Pyroelectric</li> <li>• Catalytic bead (pellistors)</li> <li>• Thermal conductivity</li> </ul>

Source: Reprinted from Hulanicki et al. (1991). Published by International Union of Pure and Applied Chemistry



**Fig. 1.3** Gas sensors designed by Figaro <http://www.figarosensor.com/>

**Fig. 1.4** Schematic diagram of electrochemical sensor operation

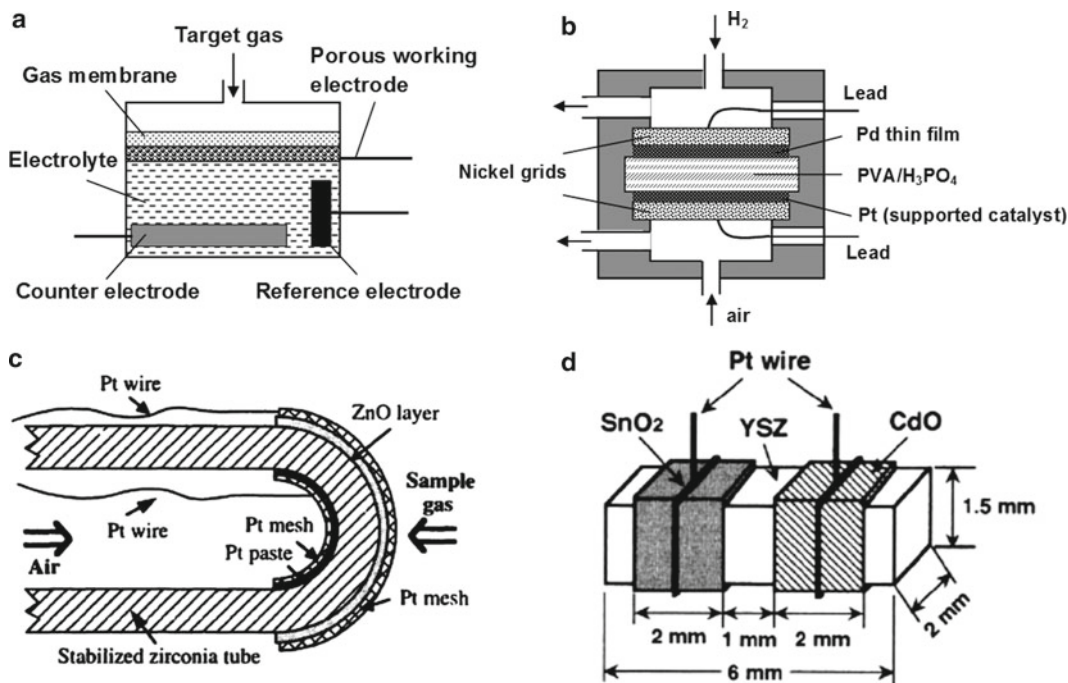
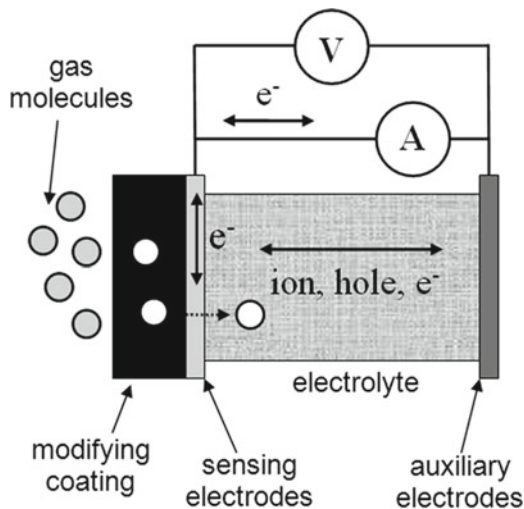


**Fig. 1.5** Schematic diagrams of electrochemical gas sensors: (a) amperometric sensor with liquid electrolyte and three-electrode configurations; (b) potentiometric polymer-based sensor for hydrogen detection; (c) mixed-potential-type  $H_2$  sensor using YSZ-based solid electrolyte and ZnO-Pt electrode; (d) chip-type YSZ-based sensor attached with CdO and  $SnO_2$  electrodes (Reprinted with permission from (a, b) Korotcenkov et al. (2009). Copyright 2009 American Chemical Society; (c) Lu et al. (1996). Copyright 1996 Elsevier; and (d) Miura et al. (1998a, b). Copyright 1998 Elsevier)

*Conductometric (resistive) sensors* have a simple structure, and their operating principle is based on the fact that their electrical conductivity (or electrical conductance) can be modulated by the presence or absence of some chemical species that comes in contact with the device (Wohltjen et al. 1985). The basis of the operation of conductometric sensors is the change in resistance under the effect of reactions (adsorption, chemical reactions, diffusion, catalysis, swelling) taking place on the surface or in the bulk of the sensing layer. The chemical species interact with the sensitive layer and thus modu-

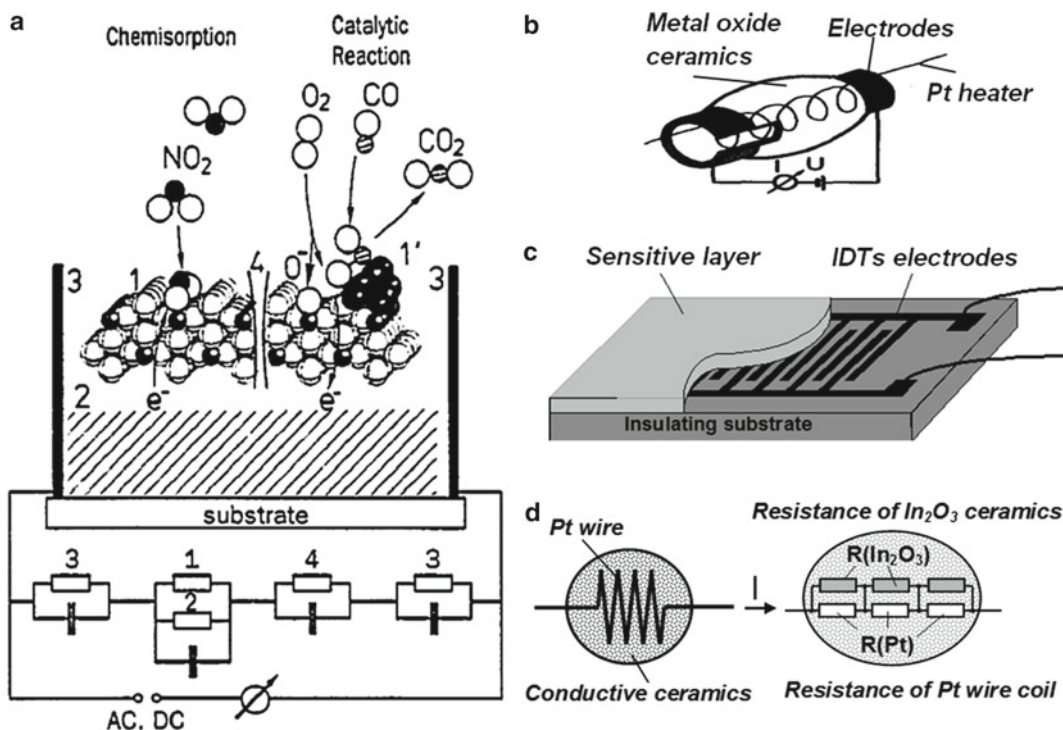


**Fig. 1.6** (a) Schematic representation of the basic steps in the detection of gas molecules using conductometric metal oxide gas sensors. Surface and bulk reactions lead to changes of the overall DC or AC conductance, which may include frequency-dependent contributions from (1) an undoped or doped surface, (2) bulk, (3) three-phase boundary or contacts, and (4) grain boundaries. Equivalent circuits with different resistance/capacitance (RC) units describe the frequency behavior formally. Each unit corresponds to a characteristic charge carrier transport (Reprinted with permission from Gopel and Schierbaum (1995). Copyright 1995 Elsevier); (b) Figaro-type gas sensor basically used dielectric ceramic support tube containing a heater spiral; (c) planar thin-film gas sensor; (d) one-electrode gas sensor

late its electrical conductivity. This can be measured as a change in the current, which is correlated to the concentration of the chemical species. Schematic representation of the basic steps in the detection of gas molecules using conductometric metal oxide gas sensors is shown in Fig. 1.6a.

In general, semiconductor materials are used as sensors of reducing gases such as  $H_2$ , CO, hydrocarbons, and vapors of organic solvents. Most of these sensors are believed to operate by adsorption of oxygen on the surface, leading to a high resistance (for n-type semiconductors such as ZnO,  $SnO_2$ ,  $TiO_2$ ,  $In_2O_3$ , and  $WO_3$ ), and the resistance is lowered when a reducing agent reacts with this surface. In the case of an n-type semiconductor, such as  $SnO_2$ , the chemistry occurring on the surface involves two main reactions. In the first reaction, atmospheric oxygen chemisorbs on the surface, consuming electrons:



where  $S_{\text{ads}}$  denotes an adsorption site and  $k_i$  and  $k_e$  are the rate constants for oxygen ionization, i.e., electron extrinsic surface state trapping and emission, respectively. This means that ionosorption of oxygen results in a decrease in conductivity of n-type semiconductor. Equation (1.1) is in fact an oversimplified picture of the surface reaction, since oxygen chemisorption can be accompanied by generation of  $O_2^-$  or  $O^{2-}$  species. In addition, of course, we need to take into account that this process

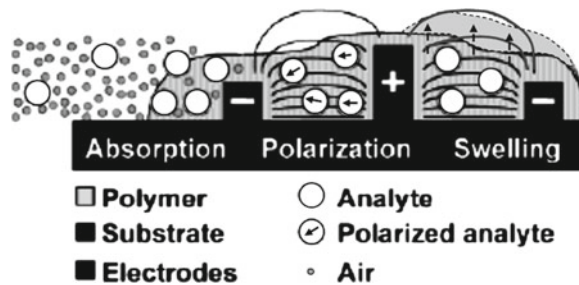


**Fig. 1.7** Schematic of sensing principle showing analyte absorption and the two relevant effects changing the sensor capacitance: change of the dielectric constant and swelling. The interdigitated electrodes (+, -) on the substrate (black) are coated with a polymer layer (gray). Big and small globes represent analyte and air molecules, respectively. Analyte molecules are polarized in the electric field (solid lines). Analyte-induced polymer swelling is indicated with the dashed lines (right side) (Reprinted with permissions from Kummer et al. (2004). Copyrights 2004 American Chemical Society)

involves also structural defects in metal oxides and water presented in surrounding air. The reducing gas ( $R$ ) presented in the ambient produces a counter reaction:



where  $k_r$  is the rate coefficient of the reaction between the reducing gas  $R$  and the preadsorbed oxygen ions  $O_{\text{ads}}^-$ . Thus, the reducing gas removes the chemisorbed oxygen, frees up an electronic carrier, and increases the conductivity of the semiconducting gas sensor. These two irreversible reactions act in opposite directions and, for a given concentration of the reducing gas, would reach a steady state. Even though in most of these sensors the primary mechanism of operation is through the changes introduced in conductivity by chemical reactions occurring on the surface, the change in conductance depends to a great extent on the physical nature of the gas-sensing element and its morphology (grain size, porosity, thickness, etc.). For polymer- or metal film-based conductometric gas sensors, the mechanism of sensitivity differs of course. One can find in the respective chapters the description of these mechanisms.

Figure 1.6 shows typical structures of conductometric sensors. Conductometric gas sensors consist of two elements, a sensitive conducting layer usually deposited on insulated substrate and contact electrodes. These electrodes are often interdigitated and embedded in the sensitive layer (Fig. 1.6c). To make the measurement, a DC voltage is applied to the device and the current flowing through the electrodes is monitored as the response. In the case of metal oxide conductometric gas sensors, the devices also include a heater for obtaining the temperature, typically 200–500 °C, required for efficient operation. Since detection occurs at high temperature, the environmental humidity and temperature are not strong interfering factors for metal oxide gas sensors as occurs with room-temperature sensors such as polymer-based devices. However, the power consumption caused by the high operating temperatures is a challenge, especially for handheld and portable systems. To address this issue, work has been undertaken within the last decade to develop systems with lower power consumption. Several types of micro-machined hotplates have been adopted to reduce the power consumption down to a range of a few hundred to tens of milliwatts, for a typical operating temperature of 400 °C (Semancik 2001; Chan et al. 2002; Wollenstein et al. 2003).

The main operating principle of capacitance sensors is that changes can be made to the relative permittivity of the dielectric ( $\epsilon$ ), the area of the electrode ( $A$ ), or the distance between the two electrodes ( $d$ ), and therefore, by measuring the change in the capacitance, the presence of the measurand can be detected (Ishihara and Matsubara 1998). With reference to polymer coating, the mechanisms

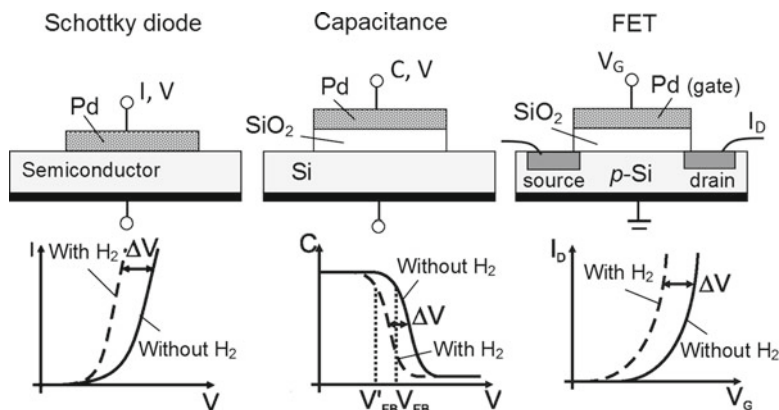


**Fig. 1.8** “Classical” schematic drawing illustrating the hydrogen-sensitive Schottky diode-based, capacitance-based, and field-effect transistor-based devices, in which hydrogen atoms adsorbed at the metal–semiconductor or metal oxide interface cause a shift of the electrical characteristics along the voltage axis in devices having catalytic metal (Pd) gates

which can be accompanied by the change of these parameters are shown in Fig. 1.7. Upon analyte absorption, the physical properties of the polymer layer change as a result of the incorporation of the analyte molecules into the polymer matrix. Changes in two physical properties influence the sensor capacitance: (1) volume (swelling) and (2) dielectric constant.

A theory for the operation of non-resistive type semiconductor gas sensor such as Schottky and MOS diode-, FET-, and MOSFET-based devices was developed by Lundström and co-workers (Lundström 1991; Ekedahl et al. 1998; Lundstrom et al. 2007). The basic theory regarding a gas FET, Schottky, or MOS diode with a Pd electrode (or similar catalytic metal, such as Pt) sensitivity to hydrogen is by modulation in the flat band potential or the Schottky barrier height. If we consider a gas FET with a thick Pd-gate film, hydrogen gas molecules are absorbed at the surface of the palladium by disassociating into atomic hydrogen. These atoms diffuse through the metal and absorb on the inner surface of the gate insulator junction, where they become polarized. The resulting dipole layer is in equilibrium with the outer layer of chemisorbed hydrogen and hence in phase with the gas. The dipole layer produces an abrupt rise in the surface potential at the metal oxide and metal–semiconductor interfaces. The gas FET response is measured as a shift in either gate-source voltage ( $V_{GS}$ ) or drain-source current ( $I_{DS}$ ) (see Fig. 1.8), and it has been shown that this response is related to a shift in the threshold voltage. The response of Schottky diode-based sensors can also be due either to *adsorption* of the species of interest at the metal surface affecting interfacial polarization by formation of a dipole layer or to *absorption* of gases or vapors of interest by the semiconductor and their interaction with the semiconductor, which changes its work function and hence the contact potential or built-in voltage of the diode (Trinchi et al. 2004; Potje-Kamloth 2008).

*Mass-sensitive gas sensors* such as microcantilever, quartz crystal microbalance (QCM), and surface acoustic wave (SAW)-based sensors rely on disturbances and changes to the mass of the sensor surface during interaction with chemicals (Fang et al. 2011). Mass-sensitive devices transform the mass change at a specially modified surface into a change in some property of the support material. The mass change is caused by accumulation of the analyte during interaction with the sensing layer (e.g., polymer) deposited on the mechanical resonator. The mass changes can be monitored either by deflecting a micromechanical structure due to stress changes or mass loading or by assessing the frequency characteristics of a resonating structure or a traveling acoustic wave upon mass loading. The sensitivity and the selectivity of *mass-sensitive gas sensors* selective for the detection of particular analyte molecules are dependent on applying an appropriate coating on the active surface. Examples of *mass-sensitive gas sensors* are shown in Fig. 1.9.

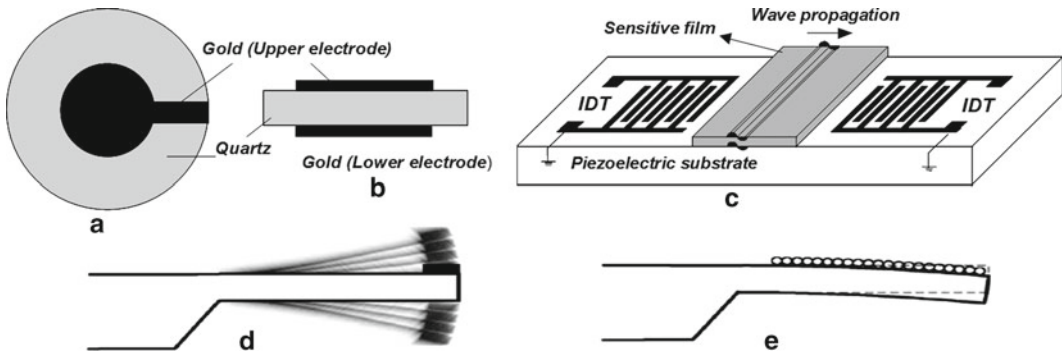
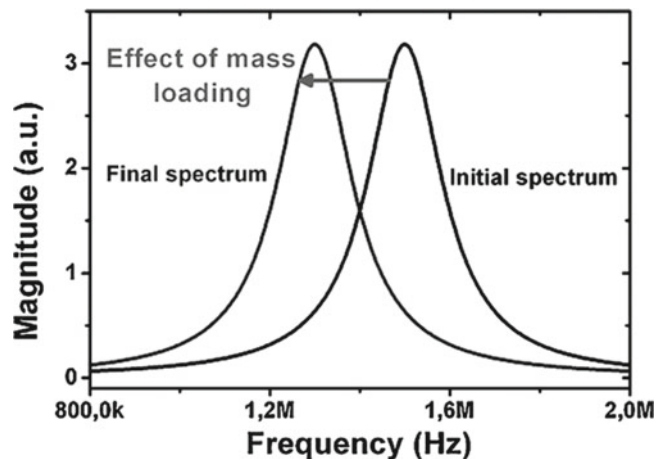


**Fig. 1.9** Schematic diagrams of mass-sensitive gas sensors: (a, b) quartz crystal microbalance (QCM) device; (c) surface acoustic wave (SAW) device; (d, e) microcantilever – (d) dynamic mode: adsorption of analyte molecules in a sensor layer leads to shift in resonance frequency, and (e) static mode: the cantilever bends owing to adsorption of analyte molecules and change of surface stress at the cantilever surface (Reprinted with permission from Battison et al. (2001). Copyright 2001 Elsevier)

**Fig. 1.10** Principle of operation of mass sensors by frequency-shift measurement (Reprinted with permission from Fanget et al. (2011). Copyright 2001 Elsevier)



The conventional quartz crystal microbalance (QCM) setup contains a piezoelectric quartz crystal wafer with deposited metal electrodes (see Fig. 1.9a, b), a quartz wafer holder (a metal base), an oscillator, a digital counter for the frequency measurements, and a computer (Voinova and Jonson 2011). Basically, the sensors are electromechanical oscillators, and the detection consists of measuring the frequency shift with respect to the mass loading as shown in Fig. 1.10. Knowing the chemical affinity of the layer with the gas molecules, the frequency shift can then be related to the gas concentration. The theoretical foundation for precise measurements of mass using quartz resonators is due to Sauerbrey (1959), who derived a linear relation between the change in the resonance frequency of a quartz oscillator and a (small) amount of extra mass attached to its surface. This result is the basis of QCM microgravimetry measurements in vacuum and air. In particular, early chemical applications of the quartz crystal microbalance include the detection of volatile compounds in various gases. One of the first papers to suggest chemical detection of analytes by means of a quartz crystal resonator was the short but important publication of King (1964). QCMs usually operate at a frequency lower than a few hundred MHz due to the limitation on how a quartz crystal can be thinned down. The relatively low operating frequency of QCMs is the main reason for its mass sensitivity limitation (Fanget et al. 2011). This problem has been solved by developing film bulk acoustic resonator (FBAR) sensors

**Table 1.12** Relative magnetic susceptibility ( $\chi_m$ ) of common gases

Gas	$\chi_m$	Gas	$\chi_m$	Gas	$\chi_m$
O <sub>2</sub>	100	H <sub>2</sub>	0.24	CH <sub>4</sub>	-0.20
NO	43	N <sub>2</sub>	0.00	CO <sub>2</sub>	-0.27
NO <sub>2</sub>	28	CO	0.01	HCl	-0.30

using silicon micro-technology (Zhang et al. 2010). The structure of an FBAR consists of a very thin piezoelectric film sandwiched by two metallic electrodes, and due to the low thickness of piezoelectric film, the acoustic wave formed can reach in this case higher frequency near GHz. Moreover, compared to QCMs, FBARs are much more compact (lower thickness and volume).

SAW devices also utilize piezoelectric crystal resonators to generate acoustic waves (Afzal and Dickert 2011; Fanget et al. 2011). It is the mode of propagation of the acoustic wave that distinguishes different types of acoustic wave resonators. A surface acoustic wave is a mechanical wave in which acoustic energy is confined to the surface of an isotropic single crystal. It can be electrically excited on a piezoelectric plate by means of interdigital transducers (IDTs) (White and Voltmer 1965), two opposing, comb-shaped, intermeshing metallic electrodes which are lithographically patterned on a polished piezoelectric substrate, normally a quartz crystal (see Fig. 1.9c). Application of voltage between differently polarized transducer fingers of a transmitter IDT generates a periodic electric field that produces a wavelike mechanical deformation of the substrate surface. Just like tiny earthquakes, an acoustic surface wave then exits the transmitter IDT on both sides and travels parallel to the surface toward the receiver IDT over a delay line, where it is retransformed into an electric signal. The SAW oscillator unit is sensitive toward any specific analyte only if it is coated with a suitable material that can interact with and distinguish between diverse molecules. It is necessary to note that the operation of the SAW and QCM sensors requires temperature and humidity control because the QC resonant frequency is affected by variation in temperature and humidity and thus affects how the frequency shifts during gas molecule collection.

Microcantilever-based devices are another type of *mass-sensitive gas sensor* (Vashist and Korotcenkov 2011). A microcantilever is the miniaturized counterpart of a diving board that moves up and down at regular intervals. This movement changes when a specific mass of analyte is adsorbed on its surface, similar to the movement of a diving board when someone steps on it. Typically, the microcantilever is made up of silicon, silicon derivatives such as silicon nitride, or polymers. When molecules adsorb on the microcantilever, they cause changes in its vibrational frequency (dynamic mode) or changes in the surface stress that leads to nanomechanical bending of the microcantilever (static mode) (see Fig. 1.9d, e). As is known, adsorption onto the sensing element composed of two chemically different surfaces produces a differential stress between the two surfaces and induces bending (Goeders et al. 2008). The analyte that induces the mechanical response may be physi- or chemisorbed onto the cantilever in either a reversible or an irreversible process. The changes in the resonant frequency and the bending of the microcantilever can be monitored by several detection techniques, such as optical, piezoresistive, capacitive, and interferometric.

*Magnetic gas sensors* are based on the change of paramagnetic properties of the gas being analyzed. These are represented by certain types of oxygen monitors (Merilainen 1990; Lee et al. 2002). It was found that oxygen has a relatively high magnetic susceptibility as compared to other gases such as nitrogen, helium, and argon, and displays a paramagnetic behavior (see Table 1.12). Usually paramagnetic oxygen sensors consist of a cylindrical container with a glass dumbbell placed inside. The dumbbell is filled with an inert gas and is suspended on a tight platinum wire. This wire has a nonuniform magnetic field. Since the dumbbell is suspended from the wire, it is allowed to move freely. When oxygen passes into the container, it is attracted to the higher magnetic field because of its high magnetic susceptibility. This causes the dumbbell to rotate. A precision optical system measures the



degree of the rotation using a light source, a photo diode, and an amplifier circuit. Then an opposing circuit is used to restore the dumbbell into its proper position. The current required to put it back into its regular position is proportional to the amount of partial pressure oxygen. This is then displayed electronically as the percentage of oxygen. In our series we will not analyze materials for this type of sensors, because these sensors' parameters depend mainly on the construction of the sensors rather than the properties of the sensing materials. One can find in the site <http://electronicsbus.com/paramagnetic-oxygen-sensor-oxygen-measurement-analyzer/> more detailed information about these sensors, including advantages and disadvantages.

*Optical gas sensors* transform changes in optical phenomena that result from an interaction of the analyte with the receptor part. More generally, optical gas sensors detect changes in visible light or other electromagnetic waves during interactions with chemicals (Korotcenkov et al. 2011). Diagrams illustrating operation principles of optical are shown in Fig. 1.11a–d. The use of optical fibers in various configurations has enabled applications of optical sensors (see Figs. 1.11e, f and 1.12). The instrumentation associated with optical chemical sensors is similar to that associated with conventional spectrophotometric techniques. Usually, optical sensor devices consist of (1) a light source, (2) a wavelength selector, (3) a recognition element for identification and interaction with the target, (4) a transducer element converting the recognition into a detectable signal, and, finally, (5) a detector unit detecting

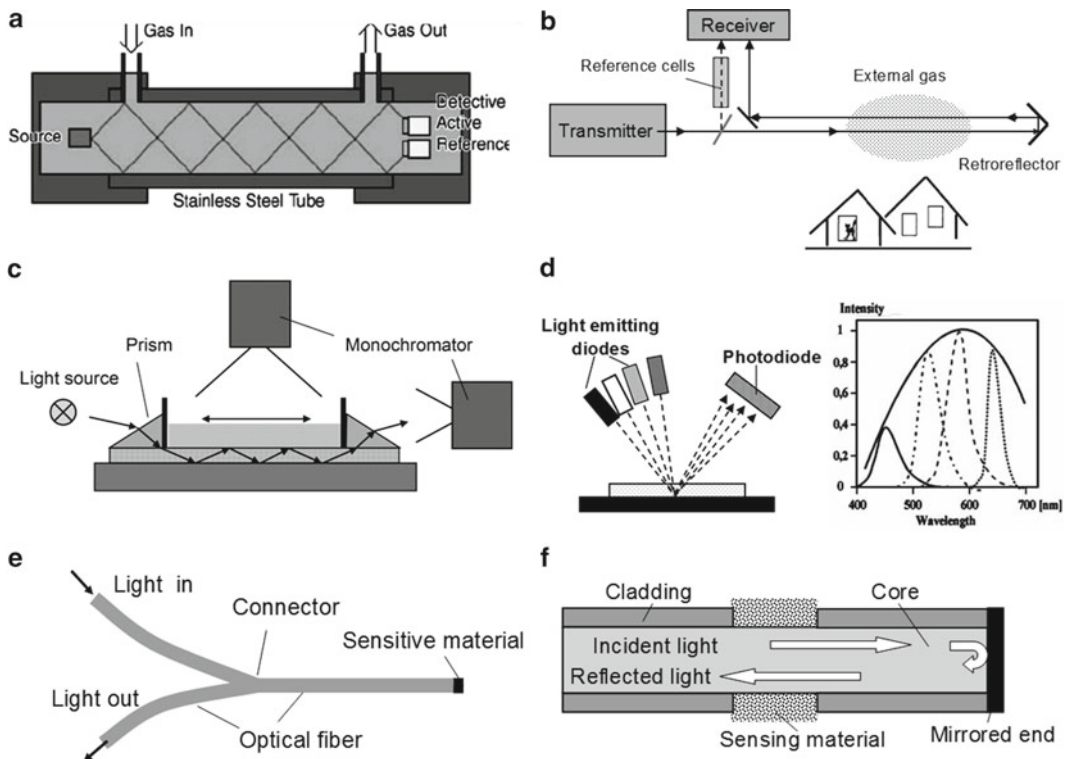


**Fig. 1.11** Schematic diagrams of optical gas sensors: (a) configuration for source/detector layout in sensor cell used in portable methane gas analyzer (Reprinted with permission from Massie et al. (2006). Copyright 2006 Elsevier); (b) experimental setup for remote atmosphere monitoring using retroreflector; (c) experimental setup used for measurements of Raman and Brillouin scattering, absorbance, and luminescence in waveguide configuration – the laser light is injected into the guide by prism coupling; (d) spectral separation using diodes emitted light at different wavelengths [Idea from Gauglitz (2005)]; (e) fiber-optic optode for gas sensing; (f) configuration of fiber-optic gas sensor with twice incident light passing through the sensing zone due to the mirrored end

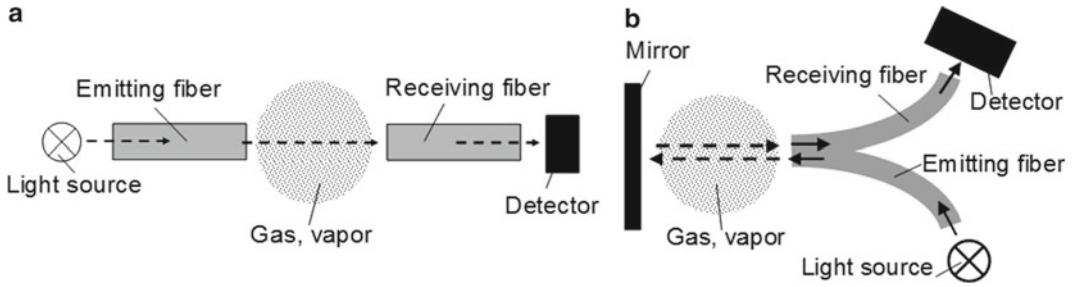


**Fig. 1.12** Variants of extrinsic optical fiber sensors (Reprinted with permission from Chan et al. (1984). Copyright 1984 IEEE)

**Table 1.13** Gases commonly detected by optical absorption

Spectral range	Gas species
IR and NIR (0.025–1.6 eV or 780–50,000 nm)	CO, CO <sub>2</sub> , CH <sub>4</sub> , C <sub>3</sub> H <sub>8</sub> , N <sub>2</sub> O, NO, NO <sub>2</sub> , SF <sub>6</sub> , NH <sub>3</sub> , H <sub>2</sub> O, HCl, H <sub>2</sub> S, SO <sub>2</sub>
UV (2.3–6.2 eV or 200–380 nm)	O <sub>3</sub> , H <sub>2</sub> S, SO <sub>2</sub> , NO, NO <sub>2</sub> , NH <sub>3</sub> , C <sub>6</sub> H <sub>6</sub> , Cl <sub>2</sub> , C <sub>2</sub> H <sub>4</sub>

and converting the change of optical properties of the sensor—maybe after amplification—into a read-out (Wolfbeis 1991, 1992; Narayanaswamy and Wolfbeis 2004). The optical radiation supplied by the light source is modulated and launched into optical fibers, and the detected light from the sensor is passed through a wavelength selector, e.g., a monochromator, and directed to the photodetector.

The mode of operation of the optical gas sensor is a consequence of the physical and chemical properties of the target molecule determining the type of interaction with the sensitive chemistry (Wolfbeis 1991). Thus, various sensing principles for optical determination are conceivable. In particular, for optically sensing chemical species, one can utilize the following basic operation principles (Baldini et al. 2006): (1) an intrinsic optical property of the analyte is utilized for its detection and (2) indicator (or label) sensing is used when the analyte has no intrinsic optical property. The first principle is used mainly in infrared and ultraviolet spectrometers. The most widely used techniques employed in optical gas sensors are optical absorption, fluorescence, and chemiluminescence (Wolfbeis 1991; Lakowicz 1999; Valeur and Brochon 2001). For example, the concentration of the target can be investigated by directly utilizing characteristic absorbance properties of the target molecule as intrinsic sensor in the infrared region of the electromagnetic spectrum. In this case, optical gas sensors detect the intensity of photon radiation that arrives at a sensor. No indicator mediation is needed. Some of the gases commonly detected by absorption at UV and IR wavelengths are shown in Table 1.13. For example, carbon dioxide and ammonia can be detected via IR absorption spectroscopy at operational wavelengths of 4.2–4.3  $\mu\text{m}$  (CO<sub>2</sub>), 1.55 or 4.6  $\mu\text{m}$  (CO), and 2.25–2.3  $\mu\text{m}$  (NH<sub>3</sub>), respectively. However, instrumentation for this method is bulky and difficult to miniaturize. Sensors based on other optical parameter spectroscopies, such as refractive index, light scattering, and reflectivity, have also been well developed (Korotcenkov et al. 2011; Mayer and Hafner 2011).

Another operation principle utilizes indicator dyes (extrinsic sensor) to transduce the concentration of the target gas into an optical measurable signal, when the particular gas has no useful intrinsic optical property. Thus the indicator or molecular recognition element is the main sensing element in a gas sensor based on the second principle, because just the indicator is exposed to the measurand system and its interaction with the analyte can provide selective sensing. This interaction causes a change in the measured optical property, the extent of this change being determined by the concentration of the analyte. Because of their simple visual readout, detection systems based on indicator dyes can be very inexpensive and are thus widely deployed. The most frequently used methods include indicator-mediated luminescence and absorption spectroscopy (Wolfbeis 1991; Lakowicz 1999; Valeur and Brochon 2001; Baldini et al. 2006). These are based on the determination of the change of

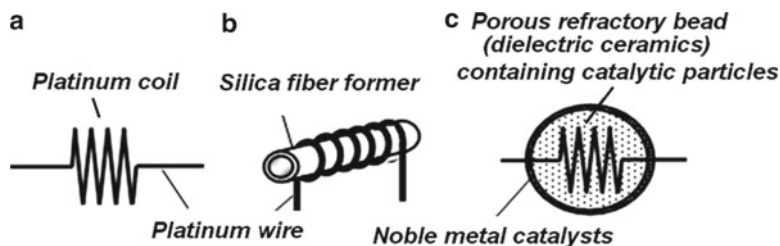


**Fig. 1.13** Schematic views of various pellistors (Reprinted with permission from Korotcenkov (2007b). Copyright 2007 Elsevier)

luminescence, mostly intensity or decay time (Lakowicz 1999), and the change of absorption properties of the indicator dye when subjected to the target molecule. In the case of oxygen sensors, decay time is the preferred parameter since it is intrinsically referenced (Lippitsch et al. 1988). For acidic or basic gases, like carbon dioxide or ammonia, the most general characterization method is the determination of the change of absorbance of a pH-sensitive dye on exposure to the target.

*Thermometric (calorimetric) sensor* devices convert the temperature changes which are generated by chemical reactions into electrical signals such as the change of the resistance, current, and voltage. The catalytic sensors widely known as “catalytic bead” or “pellistors” are the best known and used type of such gas sensors (Symons 1992; Miller 2001; Korotcenkov 2007b). Schematic views of various pellistors are shown in Fig. 1.13. In operation, the pellet and consequently the catalyst layer are heated by passing a current through the underlying coil, usually Pt. In the presence of a flammable gas or vapor, the hot catalyst allows oxidation to occur in a chemical reaction similar to combustion. Just as in combustion, the catalytic reaction releases heat, which causes the temperature of the catalyst together with that of its underlying pellet and coil to rise. This rise in temperature results in a change in the electrical resistance of the coil, and it is this change in electrical resistance which constitutes the signal from the sensor. The resistance change is then directly related to the gas concentration in the surrounding atmosphere and can be displayed on a meter or some similar indicating device. State-of-the-art catalytic sensors are stable, reliable, accurate, and rugged and have a long operating life. The output is linear because the platinum wire has a good linear coefficient of thermal resistance.

Thermoelectric-, pyroelectric-, and thermoconductivity-based devices are other representatives of thermometric gas sensors (Korotcenkov 2011). In particular the *thermal conductivity* technique for detecting gas is suitable for the measurement of high (vol. %) concentrations of binary gas mixes. The heated sensing element is exposed to the sample and the reference element is enclosed in a sealed compartment (see Fig. 1.14). If the thermal conductivity of the sample gas is higher than that of the reference, then the temperature of the sensing element decreases. The higher their thermal conductivity, the lower the concentration which can be measured (Table 1.14). Power loss of a single filament thermistor by heat conduction via the ambient gas can be expressed as

$$P = k_{TC} \lambda \Delta T, \quad (1.3)$$

where  $P$  is the power dissipation of the heater by thermal conduction of the gas,  $\lambda$  is the thermal conductivity of the given gas–gas mixture,  $k_{TC}$  is a constant characteristic for a given geometry, and  $\Delta T$  is temperature difference between heater and ambient gas.

If the thermal conductivity of the sample gas is less than that of the reference, then the temperature of the sample element increases. These temperature changes are proportional to the concentration of gas present at the sample element. *Thermal conductivity* method is mainly used for detecting gases with a thermal conductivity much greater than air, e.g., methane and hydrogen. Gases with thermal conductivities close to air cannot be detected. These include ammonia, carbon monoxide, nitric oxide, oxygen, and nitrogen. Gases with thermal conductivities less than air (see Table 1.14) are more

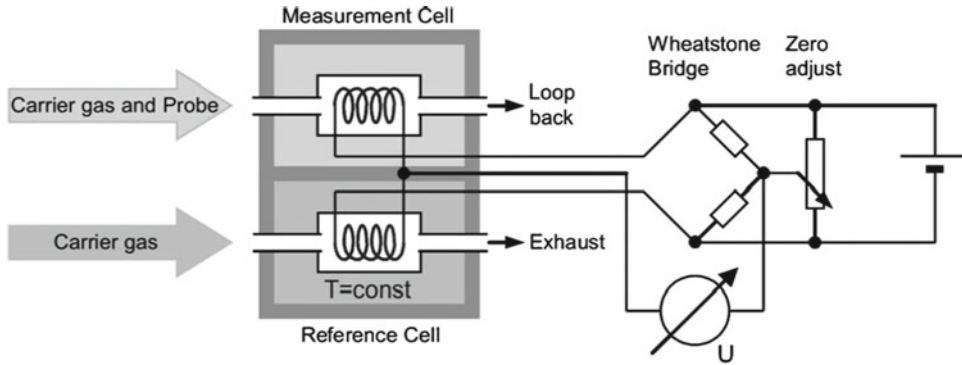


**Fig. 1.14** Measurement and reference cell of a thermal conductivity sensor connected in a Wheatstone bridge circuit (Reprinted with permission from Hubert et al. (2011). Copyright 2011 Elsevier)

**Table 1.14** Thermal conductivities relative to air at 100 °C

Gas	Thermal conductivity		
	>1	<1	~1
Helium	5.6		
Hydrogen	6.9		
Methane	1.4		
Neon	1.8		
Argon		0.7	
Butane		0.7	
Carbon dioxide		0.7	
Ethane		0.75	
Freon/halon		0.4	
Hexane		0.5	
Pentane		0.7	
Propane		0.8	
Water vapor		0.8	
Xenon		0.2	
Ammonia			1.12
Oxygen			1.01
Nitric oxide			1.003
Nitrogen			0.97

difficult to detect as water vapor can cause interference, e.g., carbon dioxide and butane. Mixtures of two gases in the absence of air can also be measured using this technique.

Two other important calorimetric devices such as pyroelectric and thermoelectric sensors detect the temperature changes which are generated by chemical reactions of gases, the heat of adsorption, and the oxidation reaction of, for instance, hydrocarbons, carbon monoxide, and hydrogen. In these devices the resulting temperature gradient caused by a catalyzed oxidation reaction is converted into an electrical signal by a pyroelectric or thermoelectric effect (Shin et al. 2011). As is well known, the thermoelectric effect, or more specifically the Seebeck effect, arises when there is a temperature difference between two points of a conductor or semiconductor material which results in a voltage difference between these points. Alkali-doped NiO and SiGe are commonly used sensing materials due to their superior thermoelectric properties. Other variants are sensors based on thin films of Si (Hubert et al. 2011). Simplified diagrams illustrating thermoelectric and pyroelectric gas sensors are shown in Fig. 1.15. As with pellistors and conductometric gas sensors, recent research efforts have focused on miniaturization to reduce power consumption. A micro-heater is used to allow the operat-

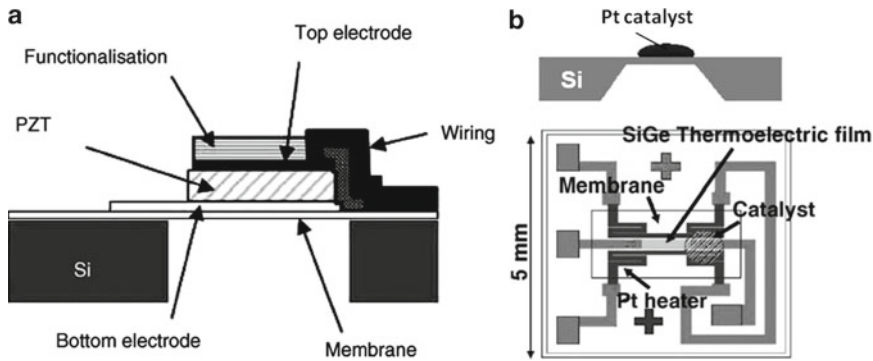


**Fig. 1.15** Schematic diagrams of (a) pyroelectric and (b) micro-thermoelectric gas sensors fabricated on Si substrates with micromachined membrane [(a) Reprinted with permission from Schreiter et al. (2006) and (b) from Shin et al. (2006). Copyright 2006 Elsevier]

**Table 1.15** The classification of gas sensors according to the detection principle

Detection principle	Examples
Sensors based on reactivity of gas	Electrochemical sensors Semiconductor sensor Combustible gas sensor/microcalorimetric gas sensor/pellistor Colorimetric paper tape Chemiluminescence Schottky barrier/heterocontact sensor/FET-based sensors
Sensor based on physical properties of gas	Nondispersive infrared UV absorption Photo acoustic sensor Thermal conductive sensor Gas ionization
Sensors based on gas sorption	Polymer sensors (swelling) Fiber-optic sensors Mass sensitive (quartz crystal microbalance (QMB); surface (SAW) and bulk acoustic wave (BAW), microcantilevers)

ing temperature to be changed rapidly to facilitate gas sensing with low power consumption, high sensitivity, and fast response times.

Of course, gas sensors may exhibit characteristics that fall into more than one of these six broad categories. For example, some mass sensors may rely on electrical excitation or optical settings. Even so, our five categories of sensors are sufficiently distinct for the purposes of this review.

We need to point out that our classification represents but one of the possible alternatives. Detection principles can also be used for gas sensor classification. According to detection principles, commonly used gas sensors can be classified into the following three groups: (1) sensors based on reactivity of gas, (2) sensors based on physical properties of gas, and (3) sensors based on gas sorption (see Table 1.15).

Of course, gas sensors can be graded according to the approach used for gas sensor design. According to this approach, gas detectors come in two main types: portable devices and fixed gas detectors. The first is used to monitor the atmosphere around personnel and is worn on clothing or on a belt/harness. The second, fixed, type may be used for detection of one or more gas types. Fixed type detectors are generally mounted near the process area of a plant or control room. Generally they are installed on fixed-type mild steel structures, and a cable connects the detectors to a SCADA system for continuous monitoring where a tripping interlock can be activated for an emergency situation.

According to technology used for gas sensor fabrication, they can be classified as ceramic, thin-film, and thick-film gas sensors. Micromachined gas sensors, which were designed during the last few decades, can also be referred to by this principle of classification.

Gas sensors can also be arranged according to their working temperature. This approach to classification gives two great groups: “hot sensors” and “cold sensors.” The group of the so-called hot sensors mainly includes the different kinds of metal oxide gas sensors. This group includes conductometric metal oxide gas sensors, pellistors, Schottky type, and MOS field-effect transistors that operate at elevated temperatures. Usually hot sensors’ selectivity and sensitivity are dependent on operating temperature and choice of metal oxide. “Cold sensors” operate at ambient temperature. This group of sensors includes the piezoelectric crystal sensors (bulk acoustic wave sensors, surface acoustic wave sensors), optical sensors, and the conducting organic polymer sensors.

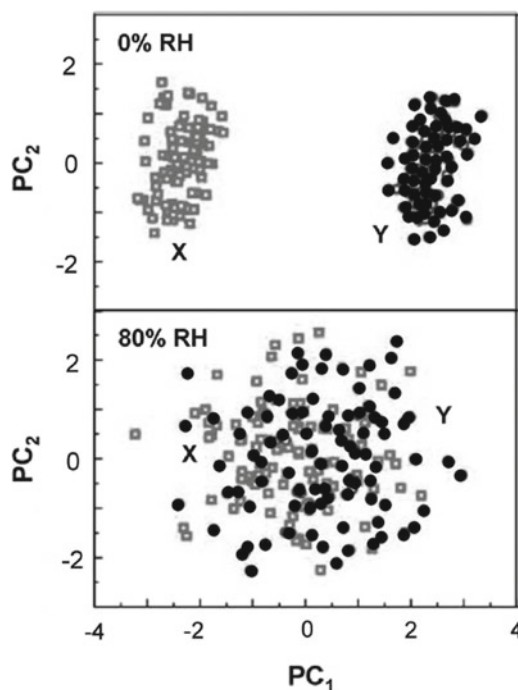
One can find in reviews and books already published more detailed description of gas sensors, including construction and principles of operation (Korotcenkov 2010, 2011).

### 1.3 Requirements of Gas Sensors

The main purpose of any gas sensors is to provide reliable real-time information about the chemical composition of the surrounding environment. Therefore, ideally, a device designed for gas sensing should operate continuously and reversibly, without disturbing the sample. An ideal gas sensor should be low cost and foolproof, working with perfect and instantaneous selectivity with reference to a particular target gas, which is present in the surrounding environment. The device should produce a measurable signal output at any required gas concentration (Ho et al. 2001). Simple fabrication, fast response, attainment of minimal measuring uncertainty, relative temperature and humidity insensitivity, high resistance to contamination and poisoning, and low noise are also useful requirements of the gas sensor designed for the gas sensor market. Chou (2000) believes that the ideal sensor should be portable and enclosed in a small, explosion-proof housing, making it suitable for use in hazardous locations and harsh environments. For portable applications, the ideal gas sensor should be small and have low energy consumption. In addition, minimal special training should be required for personnel who are to manage the sensor’s operation and maintenance. Gas sensors should provide repetitive measurements of analytes for a long time in multiple or remote locations, supporting environmental monitoring. The ideal sensor should function continuously and reliably without requiring recalibration for more than 30 days at least. Such a gas sensor should be able to function in an industrial environment for at least 2 years or longer, and should be replaceable or renewable at reasonable cost. The gas sensor should also be easy to place into a multipoint system, and either a controller or a controlled distribution system must be able to manage its functioning simply. The needed degree of quantitative reliability, such as precision and accuracy, should be provided as well.

However, we have to note that no such ideal gas sensor can be found in the sensor market today, in spite of great advances achieved over the past decades (Korotcenkov 2011). One will never find a gas sensor that satisfies all these requirements; there will always be some disadvantages. Therefore, while designing gas sensors, first of all elaborators try to meet the requirements corresponding to their planned application. For example, according to Potyrailo and Mirsky (2008), high reliability, adequate long-term stability, a low false-positive rate, and good sensitivity form the priority list for industrial sensor users, whereas often the size and the cost of sensors are the least important factors. In contrast, medical users focus on the cost of disposable sensors. Resistance to gamma radiation during sterilization, drift-free performance, and cost are the most critical specific requirements for sensors in disposable bioprocess components. The importance of continuous monitoring also differs from application to application. For instance, glucose sensing should be performed two to four times a day using home

**Fig. 1.16** Response of an array of ten chemiresistors coated with diverse surface-functionalized single-wall carbon nanotubes sensing films upon exposure to two types of vapor mixtures (X, *gray squares*, and Y, *black circles*) at 0 and 80 % RH (Reprinted with permission from Peng et al. (2008). Copyright 2008 American Chemical Society)



blood glucose biosensors, whereas blood-gas sensors for use in intensive care should be capable of continuous monitoring with subsecond time resolution.

Environmental monitoring along highways requires the control of specific amounts of toxic components (Yamazoe and Miura 1994). This control should be available for a long time and everywhere under conditions of constantly changing humidity and temperature. However, as a rule, gas sensors intended for these uses are not required to have extremely high sensitivity. Therefore, gas sensors different in sensitivity, selectivity, or other characteristics may be applied to environmental monitoring. Stability, reliability, low cost, opportunity for wide-ranging manufacturing, and good matching with measuring chains are the main requirements of gas sensors to be used for environmental monitoring. Sensors designed for environmental monitoring also should have low sensitivity to water vapor (Potyrailo et al. 2011). Water vapor is the most abundant and high concentration interferent in ambient air, with the concentration of saturated water vapor pressure ( $P_0$ ) at  $\sim 30,000$  ppm at room temperature (100 % relative humidity, RH). Thus, if a sensor under development is thought to detect 1 ppm of a toxic vapor at 50 % RH air (water vapor at  $0.5 P/P_0$ ), this new sensor must operate at a 15,000-fold overload from water vapor interference. Experience has shown that even the e-nose cannot resolve this problem and sensor arrays often cannot detect minute analyte concentrations in the presence of elevated levels of interference, e.g., water vapor in air (Peng et al. 2008). Figure 1.16 illustrates typical reduction in the ability of sensor arrays to detect low concentrations of analyte vapors in the presence of relatively high levels of water vapor interference. Thus, the sensitivity of almost all sensors to water vapor represents the largest challenge for their practical applications even when combined in arrays to form “electronic noses.” Importantly, cross-sensitivity to water vapor is not an issue in natural noses because humans and other mammals do not have receptors for water vapor (Rock et al. 2008).

Wireless sensing is a field of application with different requirements (Potyrailo et al. 2011). Wireless sensors are devices in which sensing electronic transducers are spatially and galvanically separated from their associated readout/display components, i.e., sensors have limited or no onboard

electrical power for sensor operation, and such systems therefore require devices with extremely low power consumable, because the communication distance depends first of all on the power stored on-board the sensor or delivered to the sensor and the power needed for the sensor to operate at a predetermined signal-to-noise ratio. The main benefits of wireless sensors, as compared to traditional tethered sensors, include the nonobtrusive nature of their installations, higher nodal densities, and lower installation costs without the need for extensive wiring (Messer et al. 2006).

In contrast to environmental monitoring, sensor units for chemical weapons treaty verification will likely be custom units produced in very small numbers (e.g., 100 units or less) (Singh 2007). However, the demands for selectivity and sensitivity are very high. For example, very often limits of detection of the order of 1 ppb are required together with high selectivity in order to avoid incorrect sensor response. This task is particularly difficult because Schedule II compounds (chemicals with limited dual use) are complex organic molecules without distinctive characteristics that might allow easy and rapid identification (Ho et al. 2001). In addition, these compounds can be masked by or mistaken for other organic compounds that may be present in higher concentrations. So gas sensors for chemical weapons detection may be unique devices with high cost.

Other scenarios might include stationary stations for monitoring, with permanently installed units of highly sensitive devices. In this case, high-cost gas sensors needing expensive recalibration may be acceptable. Thus, in real-world applications, the qualities of an ideal gas sensor are often weighted differently according to the application (Potyrailo and Mirsky 2008).

## 1.4 Comparative Analysis of Gas Sensors

One of the most frequently asked questions regarding sensors is “Which gas sensor is best?” Of course, there is no simple answer to this question (Chou 2000). In terms of the working characteristics of gas sensors, every type of sensor has specific advantages, for specific areas of application, and one type may compete with another type of gas sensor. For example, conductometric metal oxide-based gas sensors have low selectivity, noticeable drift of operating characteristics, and high sensitivity to air humidity (Korotcenkov 2007a). Metal oxide sensors can become “dormant” after several days of inactivity due to surface effects. However, in comparison with other sensors, these sensors have excellent sensitivity, very short response time, low cost, low noise, small size, low power consumption for adequate battery life, and very good suitability for portable instruments. Those advantages compensate for their disadvantages and open up many possibilities for application, such as sensors in alarm systems, portable instruments, electronic nose, and other specific applications, where general-purpose instruments would not be practical. Overlaid on such requirements is the prioritization imposed by the need to monitor different types of hazards in the face of finite economic resources. So, despite many limitations, conductometric gas sensors continue to hold their own in the gas sensor market and appear to have a promising future. Without doubt, in the near future we shall see more of these sensors applied to combustion and environmental monitoring, quality and process control, and safety devices.

Optical sensors, in particular integral optic (IO) gas sensors, have other features (Lambeck 1992). The strong points of IO chemical sensors arise from optical sensing and the use of waveguides and integrated structures. By sensing optically, electromagnetic interference and the danger of explosion are (almost) excluded. As well as this, optical methods often offer high sensitivity and high selectivity. By using waveguides the light path can be controlled simply, without the need for bulky components like mirrors or beam splitters. Propagation of light through waveguides also offers excellent possibilities of influencing its optical characteristics both for sensing and processing purposes. The use of integrated optic systems instead of fiber-optic ones adds another set of strong points. There is a large flexibility in the choice of construction materials and dimensions. The systems are small and rigid, and by using silicon wafers as substrates, integration of optical and electrical functions can be achieved, offering the prospect of monolithic smart multisensor systems. It also has economic advantages,



**Table 1.16** Comparison of operating parameters of gas sensors acceptable for portable applications

Parameter	Sensor technology		Work function CHEMFET	Surface plasmon resonance
	MOX chemoresistor	Polymer chemoresistor		
Sensitivity	Moderate	Moderate	High	High
Selectivity	Moderate	Poor	Moderate	High
Robustness	Moderate	Moderate	High	Moderate
Power	High	Low	Moderate	Moderate
Size	Small	Small	Medium	Moderate
Overhead	Low	Low	Moderate	High

Source: Data from Wilson et al. (2001)

which are common for most microtechnological devices: a batch-wise mass production, in which all basic functions required for the sensing system can be realized simultaneously. However, the rather complicated smart multisensory systems are still in an initial state, and a lot of research will have to be done before they will be ready for production. Moreover, the technology of IO sensors is complicated and expensive. This means that the IO chemical sensor, in general, will not be very cheap. Of course, they will be more expensive than, for example, capacitance, FET, and MOX conductometric gas sensors. Therefore their use may be restricted to applications where the above-mentioned sensors cannot meet the specifications.

The same conclusions can be drawn regarding electrochemical sensors (Korotcenkov et al. 2011, etc). Electrochemical sensors are suitable only for low-concentration, parts-per-million ranges. In addition, their life expectancy is only 2–5 years. Moreover, depending on the application, life expectancy may be much shorter. However, the electrochemical gas sensors have very low power consumption, respond quickly to gas, and are not affected by humidity. These sensors can also be exposed to gas periodically, which maximizes sensor life. Therefore, one can conclude that electrochemical sensors are a good choice for portable instruments and alarm/dosimeter systems, including lightweight, personal monitor/alarm devices, rather than for continuous monitors.

Other advantages of electrochemical sensors are conditioned by their mechanism of sensitivity. Generally, the magnitude of the current in electrochemical sensors is controlled by how much of the target gas is oxidized at the working electrode. Therefore, sensors are usually designed so that the gas supply is limited by diffusion and thus the output from the sensor is linearly proportional to the gas concentration. A linear output allows for more precise measurement of low concentrations and much simpler calibration (only baseline and one point are needed). In many other sensor technologies, output must be linearized before it can be used. Diffusion control via changing the diffusion barrier also allows the sensor manufacturer to tailor the sensor to a particular target gas concentration range. In addition, since the diffusion barrier is primarily mechanical, calibration of electrochemical sensors tends to be more stable over time, and so electrochemical sensor-based instruments require much less maintenance than some other detection technologies. In principle, the sensitivity can be calculated based on the diffusion properties of the gas path into the sensor (Warburton et al. 1998).

Thus, one can conclude that electrochemical gas sensors offer many advantages for various applications. However, it is also true that electrochemical sensors are not suitable for every gas. Since the detection mechanism involves the oxidation or reduction of the gas, electrochemical sensors are usually suitable only for gases which are electrochemically active. Inert gases can be detected electrochemically only indirectly if the gas interacts with another species in the sensor that then produces a response (Pletcher et al. 1991). Sensors for carbon dioxide are an example of this approach.

Information presented in Table 1.16 allows one to evaluate advantages of one or another gas sensor for portable applications. High sensitivity, selectivity, and robustness are desirable characteristics of any chemical sensor technology in order to meet the specifications of the sensing application. Supplemental to these basic requirements, however, portable instruments also require sensor technolo-

gies that consume low power, are compact in size, and incur low electronics overheads (Wilson et al. 2001). Control and measurement electronics overheads can play a major role in increasing the size and power consumption of the overall system beyond what is practical; in many sensing systems, electronics overheads can consume 40 % or more of the total space and often contribute at least this much to the overall power consumption as well. Comparisons of CHEMFET, chemiresistor, and surface plasmon resonance (SPR) gas sensors indicate that, in general, no single sensor technology is ideal by itself for portable instrument design. The chemiresistor is for reasons of its simplicity perhaps the most attractive chemical sensor type for portable applications. However, it also presents significant obstacles in terms of noise, drift, aging, and sensitivity to environmental parameters. The CHEMFET does not exhibit many of the fluctuations and instabilities of the chemiresistor, but it also requires more complex signal processing. The SPR gas sensor holds great promise for miniaturizable optical sensors, since it does not require the use of a laser in a portable system (SPR probes can operate using an LED as the light source). Comparison of other gas sensors acceptable for portable devices can be found in the review by Brown (2006).

Naturally, in other areas with different technical requirements for the measuring system, preference will be given to other gas sensors with other sets of advantages, which depend not only on the sensor type but also on its version. This facet can be well illustrated using the example of electrochemical sensors, which can be realized either as conductometric, potentiometric, or amperometric (voltammetric) sensors (Brett and Brett 1998; Brett 2001).

In conductometric electrochemical gas sensors the concentration of charge is obtained through measurement of solution resistance and is therefore not species selective. Conductometric detectors can, however, be useful in situations where it is necessary to ascertain, for example, whether the total ion concentration is below a certain permissible maximum level or for use as an online detector. In potentiometric sensors, the equilibrium potential of an indicator electrode is measured against a selected reference electrode using a high-impedance voltmeter, i.e., effectively at zero current. Thus, the current path between the two electrodes can be highly resistive. At an inert redox indicator electrode such as platinum, the potential measured is a mixed potential, a function of all species present in solution and their concentrations (Brett and Brett 1998). A study has shown that potentiometric electrochemical sensors are very attractive for field operation due to their high selectivity, simplicity, and low cost. Therefore, in the past, potentiometric devices have been more widely used than amperometric electrochemical sensors. However, potentiometric sensors are less sensitive and are often slower than their amperometric counterparts. Moreover, more information can usually be gained by using amperometric sensors. An applied potential in voltammetric sensors can lead to high selectivity and specificity and thence probing of speciation. Each chemical species as well as each element or oxidation state has an associated potential for oxidation and reduction. Therefore, several species that react at different applied potentials can be determined almost simultaneously in the same experiment without the need for prior separation. As a result, in recent years we have seen an increasing amount of research on amperometric probes, which should gradually shift this balance in the direction of wider application of amperometric electrochemical sensors.

Of course, the selection of an optimal construction (type) for a chemical sensor is also dependent on the sensing material used (Haug et al. 1993). So, as we have stated, there are no ideal sensors, no one sensor type demonstrates optimum performance overall, and, therefore, none can meet all the requirements for workable devices. It was found that every analyzed type of sensor has its own specific technical limitations in achieving the required parameters. This means that which technology is most suited to a given application depends on the operating requirements for that application. A listing of some of the major advantages and disadvantages associated with each sensor type is given in Table 1.17. Table 1.18 shows the similar comparison of various sensors suitable for hydrogen detection. Thus, the unique combinations of advantages and disadvantages related to individual sensor types largely determines the range of capabilities and potential applications that each sensor type provides for the analysis of various gas analytes in specific operating situations (Wilson and Baietto 2009). For example, although their measuring ranges

**Table 1.17** Summary of advantages and disadvantages of sensor types

Sensor type	Advantages	Disadvantages
Calorimetric or catalytic bead (CB)	Fast response and recovery time, high specificity for oxidized compounds	High-temperature operation, only sensitive to oxygen-containing compounds
Catalytic field-effect sensors (MOSFET)	Small sensor size, inexpensive operating costs	Requires environmental control, baseline drift, low sensitivity to ammonia and carbon dioxide
Conducting polymer sensors	Ambient temperature operation, sensitive to many VOCs, short response time, diverse sensor coatings, inexpensive, resistance to sensor poisoning	Sensitive to humidity and temperature, sensors can be overloaded by certain analytes, sensor life is limited
Electrochemical sensors (EC)	Ambient temperature operation, low power consumption, very sensitive to diverse VOCs	Bulky size, limited sensitivity to simple or low molecular weight gases
Metal oxide semiconducting (MOS)	Very high sensitivity, limited sensing range, rapid response and recovery times for low mol. wt. compounds (not high)	High-temperature operation, high power consumption, sulfur and weak acid poisoning, limited sensor coatings, sensitive to humidity, poor precision
Optical sensors	Very high sensitivity, capable of identifications of individual compounds in mixtures, multiparameter detection capabilities	Complex sensor-array systems, more expensive to operate, low portability due to delicate optics and electrical components
Quartz crystal microbalance (QMB)	Good precision, diverse range of sensor coatings, high sensitivity	Complex circuitry, poor signal-to-noise ratio, sensitive to humidity and temperature
Surface acoustic wave (SAW)	High sensitivity, good response time, diverse sensor coatings, small, inexpensive, sensitive to virtually all gases	Complex circuitry, temperature sensitive, specificity to analyte groups affected by polymeric-film sensor coating

*Source:* Reprinted from Wilson and Baietto (2009). Published by MDPI

overlap, electrochemical and semiconducting metal oxide sensors are preferred for measurement of low hydrogen concentrations as they have acceptable selectivity, whereas robust catalytic and thermal conductivity sensors of low selectivity can be favored at higher hydrogen gas concentrations. Some other important considerations for sensor selection include operational expenses, maintenance costs, training costs, and ease of use by the operator (Korotcenkov and Cho 2011). In terms of cost, it should be noted that, in addition to the cost of the sensor elements themselves, the application of these sensors also requires more or less cost-intensive electric components. Electrochemical sensors, for example, may demand costly electric equipment for amperometric or potentiometric measurement.

Regarding capacitance sensors that are not presented in Table 1.17, one can say that the main advantage of capacitive readout is the capability for high enough sensitivity combined with the simplicity of the relevant electronics that enables miniaturization of sensor arrays, low power consumption, and integration of the readout setup in the sensor (Britton et al. 2000; Lim et al. 2007). Capacitance-type devices are passive elements and therefore do not require any additional power other than what is required by their electronic readout. They are ideal in applications where the devices are operated from a battery source, i.e., portable devices, or where power is harvested from the environment, e.g., using a vibrational power generator or solar cells. This is often the case when long-term, autonomous, and unattended operation is required, as in the monitoring of stored goods. In addition, sensors of this type have low cost because capacitance-type chemical sensors are relatively simple devices, usually requiring only a few steps for their fabrication. Moreover, use of

**Table 1.18** Comparative characteristics of hydrogen sensor types

Sensor type	Operating principle/device	Physical change/measurand	Advantages	Disadvantages
Catalytic	Pellistor	Temperature; resistance	Robust; stable; long lifetime; wide operating temperature range	Not hydrogen selective; high power consumption; requires at least 5–10 % O <sub>2</sub> to operate; susceptible to poisoning by P, S, Si compounds
Thermal conduction	Thermoelectric	Thermoelectric voltage	Room-temperature operation; low power consumption	Long response time; sensitive to temperature fluctuations; requires at least 5–10 % O <sub>2</sub> to operate
	Calorimetric	Temperature; resistance; voltage	Very wide measuring range; robust; does not require O <sub>2</sub> to operate; long-term stability; resistant to poisoning; simple construction; low cost; fast measured response time	Higher lower detection limit; cross-sensitive to He; reaction with heating wire can occur
Electrochemical	Amperometric Potentiometric	Electrical current Electromotive force; voltage	Sensitive down to 100 ppm; low power consumption; resistant to poisoning; heating of sensor element not required; operation at high ambient temperature possible	Narrow temperature range using some electrolytes; restricted lifetime; regular calibration needed; cross-sensitivity to CO; aging; cost
Resistive	Semiconducting metal oxide  Metallic resistor	Resistance	High sensitivity; fast response; acceptable lifetime; wide operating temperature range; low cost; modest power consumption  Very wide detection range; rapid response; selective; long-term stability; can operate in the absence of O <sub>2</sub>	Poor selectivity; interference from humidity and temperature; high operation temperature; contamination; susceptible to aging and memory effects; requires O <sub>2</sub> to operate  Dependence on temperature; affected by total gas pressure; poisoned by SO <sub>2</sub> , H <sub>2</sub> S; susceptible to aging effects; cost

Work function	Schottky diode MOS field-effect transistor MIS capacitor	Current; voltage; capacitance	Micromachinable; low cost; small size; mass production possible Fast response; accurate measurement; low influence from ambient parameters; high sensitivity and selectivity; small size; mass production possible High sensitivity and selectivity; fast response; low power consumption; Low costs; small size; mass production possible	Susceptible to drift Baseline and hydrogen induced drift; hysteresis; saturates at modest concentrations Drift; hysteresis
Mechanical	Cantilever	Length; bending; curvature	Micromachinable; small size; no source of ignition in explosive atmospheres; does not require O <sub>2</sub> to operate	Slow response time; susceptible to poisoning; susceptible to hydrogen induced aging effects
Optical	Optrode	Transmission; reflectance; wave length; polarization; phase shift	No source of ignition in explosive atmospheres; unaffected by electromagnetic interference; wide area monitoring; can operate in the absence of O <sub>2</sub>	Interference from ambient light; drift due to aging effects; poisoning by SO <sub>2</sub> , H <sub>2</sub> S
Acoustic	Quartz crystal microbalance (QCM) Surface acoustic wave (SAW) Ultrasonic	Frequency; time; wave velocity	Very high sensitivity; room temperature to 100 °C operation; can operate in the absence of O <sub>2</sub> High sensitivity; room-temperature operation; can operate in the absence of O <sub>2</sub> Very wide detection range; in-line measurement; rapid response, usually a fraction of second; low power consumption; long-term stability; can operate in the absence of O <sub>2</sub>	Interference from humidity and temperature; drift Unstable at higher temperature; interference from humidity and temperature Knowledge of acoustic properties of materials through which the sound travels is necessary; substantial amount of electronics needed for high accuracy

Source: Reprinted with permission from Hubert et al. (2011). Copyright 2011 Elsevier

**Table 1.19** Sensors recommended for various applications

Analyte class	Recommended sensors
Toxic gases	Electrochemical; solid-state (MOS)
Combustible gases	Catalytic; solid-state (MOS); IR; thermal conductivity
Volatile organic compounds	Gas chromatography; mass spectrometry; photoionization; flame ionization; ion mobility spectrometry
Total hydrocarbons (THCs)	Flame ionization
Other gases	Thermal conductivity; calorimetry
Single gas	
O <sub>3</sub>	UV photometer; solid-state (MOS)
SO <sub>2</sub>	UV photometer; IR; flame ionization
NO <sub>x</sub>	Chemoluminescence; solid-state (MOS)
CO <sub>2</sub>	IR; ion-selective electrode; solid-state electrolyte
O <sub>2</sub>	Electrochemical; paramagnetic; zirconia-based
H <sub>2</sub>	Schottky; FET; catalytic; solid-state (MOS)
HCl	IR; mass spectrometry
CO	IR; electrochemical; solid-state (MOS)
H <sub>2</sub> S	Solid-state (MOS)
NH <sub>3</sub>	Solid-state (MOS)
CH <sub>4</sub>	IR; electrochemical; solid-state (MOS)
Multiple gases	UV/IR spectrometry; mass spectrometry Gas chromatography; electronic nose

polymers as chemically sensitive materials allows for easy and low-cost adaptation of the same basic structure to many different applications (Chatzandroulis et al. 2011). Disadvantages, associated mainly with microcantilevers, are the possibility of sticking when the capacitor plates are brought too close together and the influence of the analytes in the capacitive signal (Chatzandroulis et al. 2002). In general, a bimorph cantilever is more sensitive than a similar bimorph membrane because the latter is clamped peripherally instead of having one clamped edge as in the case of a cantilever. Nevertheless, the use of membranes enables capacitive readout in conductive media, such as electrolytes, because the gap between the capacitor plates is under the membrane and thus is isolated from the sensor environment (Chatzandroulis et al. 2011). The use of polymers as sensitive films, which are not stable in hazard environment, can also be considered as a disadvantage of capacitance sensors. We also need to take into account that the sensitivity of capacitance sensors is significantly lower in comparison with conductometric gas sensors and usually these sensors can detect limited number of gases.

More detailed information about the use of various sensors for detection of certain gases is given in Table 1.19. Data presented in this table were extracted from the work of Ho et al. (2001) and many others. One should note that recommendations given in this table do not take into account all existing opportunities for detection of gases and they do not consider the specificity of gas detection in extremely small concentrations.

Thus, choosing the right chemical sensor is an important part of the activities related to design of an efficient instrument for monitoring a specific analyte. Proper selection is based on a number of inputs: the physical properties of the target analyte, ambient conditions, required sensitivity, maintenance cycle, and method of operation, among others. For example, for H<sub>2</sub> sensing one can conclude that catalytic sensors can be used to detect the presence of higher concentrations of hydrogen; however, catalytic sensors only detect the presence of combustible gas; they are not gas specific. In areas where other flammable gases are not present, this technology may be appropriate. Electrochemical gas sensors can also be used to detect hydrogen and offer some selectivity compared to catalytic sensors. Disadvantages of electrochemical sensors are their required recalibration and periodic maintenance. Solid-state sensors can be used to detect hydrogen at low concentrations; however, they may

**Table 1.20** Sensors acceptable for CO<sub>2</sub> detection

Parameter	Method			
	Severinghaus electrode	Conductivity sensor	Solid electrolyte sensor	NDIR sensor
Application	Direct	Direct	Direct	Direct gas flow
Sensor function	Nernst logarithmic	Linear	Nernst logarithmic	Beer–Lambert linear
Concentration range	ppm–vol. %	0–5 vol. %	ppm–vol. %	0.1 ppm–vol. %
Response time	30 s	1–2 s	<1 s	Few seconds
Cross-sensitivity	Water, SO <sub>2</sub> , NO <sub>x</sub> , H <sub>2</sub> S	SO <sub>2</sub> , NO <sub>x</sub> , H <sub>2</sub> S	Combustibles, SO <sub>2</sub> , NO <sub>x</sub> , H <sub>2</sub> S	Selective, dust aerosol
Measuring temperature	<50 °C	20 °C	350–750 °C	<50 °C
Calibration	Yes	Yes	No	Yes
Energy consumption	No	Yes	Yes	Yes
Maintenance	High	High	No	Low

Conductivity sensors analyzed in the present table are based on the influence of dissociation reaction of CO<sub>2</sub> in a liquid electrolyte on its conductivity

Source: Reprinted with permission from Zosel et al. (2011). Copyright 2011 IOP

be subject to interference from various gases such as vapors of alcohol and other reducing gases. Some manufacturers offer activated carbon filters to mitigate alcohol interference. Several companies offer an acoustic sensing technique for H<sub>2</sub> sensing. A special approach to surface acoustic wave (SAW) sensor design offers a specific detection method that is not subject to interference.

Comparison of sensors acceptable for CO<sub>2</sub> measurements is listed in Table 1.20. Analysis carried out by Zosel et al. (2011) has shown that CO<sub>2</sub> solid electrolyte sensors can be applied successfully in all cases of long-term measurements in air, in breath analysis, and in process measuring, especially at higher temperature. As compared to sensors with aqueous electrolytes, the main advantages consist of a short response time and maintenance-free operation without calibration. Water vapor and traces of combustibles should not disturb the signal. This kind of sensor can be easily miniaturized. On the other hand, the sensor has to be heated electrically up to 550–700 °C. For this reason a small electric heating power is necessary. As compared to IR sensors, Severinghaus (electrochemical sensor with liquid electrolyte) and solid electrolyte-based sensors are simpler in setup and in most cases cheaper. The main advantage of the Severinghaus sensor consists in energy-free operation. However, for its application a basic knowledge of electrochemistry is necessary. Methods using CO<sub>2</sub> analysis by NDIR are frequently excessive in maintenance.

Regarding sensors designed for detection of other gases, such as NH<sub>3</sub>, O<sub>2</sub>, CH<sub>4</sub>, and O<sub>3</sub>, reviews offering comparative analyses are listed in Table 1.21. Reviews that discuss various chemical sensors suitable for specific applications are presented in Table 1.22.

## 1.5 Materials Acceptable for Gas Sensor Applications

Results of numerous items of research have shown that, in theory, any material can be used in the design of a gas sensor, regardless of its physical, chemical, structural, or electrical properties (Korotcenkov 2010, 2011). Prototypes of gas sensors based on covalent semiconductors, semiconducting metal oxides, solid electrolytes, polymers, ionic membranes, organic semiconductors, and ionic salts have already been tested (Sadaoka 1992; Gopel 1996; Haugen and Kvaal 1998; Monkman 2000; Talazac et al. 2001; Eranna et al. 2004; Adhikari and Majumdar 2004). As shown in Table 1.23, these materials may be used

**Table 1.21** Reviews related to comparative analysis of sensors aimed for detection of specific gases

Analyte	Type of sensor	Reference
O <sub>2</sub> (high temperatures)	Solid electrolyte	Maskell (1987)
	Solid electrolyte	Yamazoe and Miura (1996)
	Solid electrolyte	Suzuki et al. (1999)
	Solid electrolyte	Riegel et al. (2002)
	Solid electrolyte	Docquier and Candel (2002)
	Solid electrolyte, semiconductor oxides	Ramamoorthy et al. (2003)
	Zirconia based	Lee (2003)
O <sub>2</sub> (RT measurements)	Semiconductor oxides	Aroutiounian (2007)
	Biosensors, optical, electrochemical	Azevedo et al. (2005)
	Optochemical	Ando (2006)
O <sub>2</sub> in blood	Optical (phosphorescence)	Ast et al. (2012)
	Biosensors	Ward (2008)
O <sub>3</sub>	Optical, electrochemical	Parrish and Fehsenfel (2000)
	All types of sensors	White (2000)
	Optochemical	Ando (2006)
H <sub>2</sub>	All type of sensors	Korotcenkov and Cho (2012)
	Optochemical	Ando (2006)
	Semiconductor oxides	Aroutiounian (2007)
	Electrochemical, solid electrolyte	Korotcenkov et al. (2009)
	All types of sensors	Boon-Brett et al. (2009)
	All types of sensors	Hubert et al. (2011)
	Fiber-optic Pd-based sensors	Silva et al. (2012)
VOCs (hydrocarbons)	RT solid-state sensors	Arya et al. (2012)
	Luminescence based	Keefe et al. (2000)
	All types of sensors	Pejicic et al. (2007)
	Mass spectrometry, optical	Krol et al. (2010)
CH <sub>4</sub>	Semiconductor oxides	Basu and Basu (2009)
	Optical (diode lasers)	Shemshad et al. (2012)
CO	Chromatography, optical	Parrish and Fehsenfel (2000)
	Semiconductor oxides	Aroutiounian (2007)
CO <sub>2</sub>	Solid electrolyte, semiconductor oxides	Yamazoe and Miura (1994)
	Solid electrolyte	Yamazoe and Miura (1996)
	Solid electrolyte	Holzinger et al. (1997)
	Optochemical	Ando (2006)
	Solid electrolyte	Fergus (2008)
	Electrochemical, semiconductor oxides, polymers	Neethirajan et al. (2009)
NH <sub>3</sub>	All types of sensors	Zosel et al. (2011)
	All types of sensors	Sazhin et al. (2003)
	All types of sensors	Timmer et al. (2005)
SO <sub>2</sub>	Solid electrolyte, semiconductor oxides	Yamazoe and Miura (1994)
	Solid electrolyte, semiconductor oxides	Yamazoe and Miura (1996)
	Solid electrolyte	Fergus (2008)
H <sub>2</sub> S	Optical	Choi and Hawkin (2003)
	Solid-state sensors	Pandey et al. (2012)
NO	Solid electrolyte, semiconductor oxides	Ménil et al. (2000)
NO <sub>2</sub> (NO <sub>x</sub> )	Solid electrolyte, semiconductor oxides	Yamazoe and Miura (1994)
	Solid electrolyte, semiconductor oxides	Yamazoe and Miura (1996)
	Semiconductor oxides, carbon	Afzal et al. (2012)
	Optical	Parrish and Fehsenfel (2000)
	Solid electrolyte	Fergus (2007)

(continued)



**Table 1.21** (continued)

Analyte	Type of sensor	Reference
Formaldehyde	Polymer and solid-state sensors	Flueckiger et al. (2009)
Humidity	Ceramic type	Traversa (1995)
	Solid-state sensors	Greenblatt and Shuk (1996)
	All types of sensors	Rittersma (2002)
	Solid-state sensors	Fontes (2005)
	Solid-state sensors	Chen and Lu (2005)
	Optochemical	Ando (2006)
	Fiber optic	Yeo et al. (2008)

**Table 1.22** Reviews related to comparative analysis of sensors aimed for several specific applications

Application	Type of sensor	Reference
Environment monitoring	Electrochemical	Fleet and Gunasingham (1992)
	Solid electrolyte	Yamazoe and Miura (1994)
	All types of sensors	Parrish and Fehsenfel (2000)
	All types of sensors	Ho et al. (2005)
	All types of sensors	Pejcic et al. (2007)
Gas chromatography	All types of sensors	Drake et al. (2007)
	All types of sensors	Muñoz et al. (2010)
Clinic and medical applications	Fluorescence based	Leiner (1991)
	All types of sensors	Cutmore and James (2007)
	All types of biosensors	Justino et al. (2010)
Combustion control	All types of sensors	Docquier and Candel (2002)
Explosives detection	All types of sensors	Singh (2007)
Food and drink industry	All types of sensors	Pedersen (1991)
	All types of biosensors	Mello and Kubota (2002)
	All types of biosensors	Patel (2002)
Fire alarm systems	All types of sensors	Kohl et al. (2001)
	Conventional sensors	NFPA (2003)
Agriculture	Various types of sensors	Adamchuk et al. (2004)
Car industry, emission control	Solid electrolyte	Igarashi (1986)
	Solid electrolyte	Riegel et al. (2002)
	Mass spectrometry, spectroscopy, etc.	Maricq (2007)
Field application (portable devices)	All types of sensors	Wilson et al. (2001)
	All types of sensors	Brown (2006)
Wireless sensors	All types of sensors	Potyrailo et al. (2011)
Electronic nose	All types of sensors	Arshak et al. (2004), Wilson and Baietto (2009), Korotcenkov and Stetter (2011)

successfully in designing all types of gas sensors, including humidity sensors. It has been established that various materials can show excellent adaptability for application in gas sensors.

For example, standard semiconductors such as InAsSbP, InAsSb, GaInAsSb, PbSSe, and some others are the best materials for generators and photoreceivers for optical and fiber-optic gas sensors (Yakovlev et al. 1991; Werle et al. 2002). Wide-band-gap semiconductors (SiC, GaN) are good candidates for high-temperature Schottky, FET-based, and MOS capacitance-based gas sensors. Ionic films such as hydrated potassium halides and noble metals can provide excellent work-function sensor signals for ozone detection at room temperature (Doll et al. 1996; Eisele et al. 2001). Pd films show high sensitivity to hydrogen. Zeolites are excellent materials for designing various filters and membranes. By using

**Table 1.23** Typical materials used in gas sensor research and development

Material	Examples	Analyte (function in sensors)
Metals	Pt, Pd, Ni, Ag, Au, Sb, Rh	Gases (H <sub>2</sub> , etc.) (electrodes, sensing materials, catalysts, membranes)
Semiconductors	Si, GaAs, InP, SiC, GaN, etc.	Gases (O <sub>2</sub> , CO <sub>2</sub> , H <sub>2</sub> S, CH <sub>4</sub> , NO <sub>2</sub> , O <sub>3</sub> , etc.); H <sub>2</sub> O, etc. (sensing materials)
Metal oxides	Electronic conductors (SnO <sub>2</sub> , TiO <sub>2</sub> , In <sub>2</sub> O <sub>3</sub> , etc.); mixed conductors (Ga <sub>2</sub> O <sub>3</sub> , WO <sub>3</sub> , SrTiO <sub>3</sub> , perovskites); ionic conductors (ZrO <sub>2</sub> , CeO <sub>2</sub> , etc.); metal oxides with metallic-type conductivity (RuO <sub>2</sub> , Co <sub>3</sub> O <sub>4</sub> , PbOx, etc.)	Gases (CO, H <sub>2</sub> , CH <sub>4</sub> , NO <sub>x</sub> , O <sub>2</sub> , Cl <sub>2</sub> , etc. vapor, alcohol; dissolved oxygen O <sub>2</sub> , Cl <sub>2</sub> in solutions; dissolved oxygen in molten metals, etc. (electrodes, sensing materials, membranes)
Ionic compounds	Ionic conductors [LaF <sub>3</sub> , CaF <sub>2</sub> , Na <sub>2</sub> CO <sub>3</sub> , AgCl, Zr(HPO <sub>4</sub> ) <sub>2</sub> , SrCl <sub>2</sub> , Na <sub>2</sub> SO <sub>4</sub> , AgBr, Ag <sub>2</sub> S, CuBr, Nasicon, Nafion]	Gases (CO <sub>2</sub> , SO <sub>2</sub> , CO, etc.), ions, etc. (sensing materials, electrodes, membranes)
Molecular crystals	Phthalocyanines [PbPc, LuPc <sub>2</sub> , LiPc, FePc, CuPc, NiPc, (PcAlF) <i>n</i> , (PcGaF), etc.]	Gases, vapors, ions (sensing materials, membranes)
Langmuir-Blodgett films	Phthalocyanines, polydiacetylenes, Cd.-arachidate, etc.	Gases (NO <sub>2</sub> , NH <sub>3</sub> , Cl <sub>2</sub> , etc.), vapors, etc. (sensing materials, membranes)
Membranes	Ion-exchange membranes; neutral-carrier membranes; charged carrier membrane	Cations, anions in solutions; gas filtration (membranes)
Cage compounds	Zeolites, calixarenes, cyclodextrines, crown ethers, cyclophanes, etc.	Gases, vapors (membranes, supporting media)
Carbon	Carbon nanotubes, black carbon, diamond, fullerenes, graphene	Gases, vapors (sensing materials, electrodes, membranes)
Polymers, organic semiconductors	Polyethers, polyurethanes, polysiloxanes, polypyrroles, polythiophenes, polyolefins, polyphenyl acetylene, phthalocyanine, polyamides, polyimides, polyfluorocarbons, polytetrafluoroethylene, Nafion, etc.	Gases (CO, CO <sub>2</sub> , CH <sub>4</sub> , NO <sub>x</sub> , etc.), H <sub>2</sub> O, chlorinated, hydrocarbons, etc. (sensing materials, membranes)

Source: Data from Korotcenkov (2010, 2011)

metal films and metal nanoparticles, effective gas sensors can be designed based on surface plasmon resonance. Porous semiconductors can be incorporated in biosensors and optical gas sensors (Korotcenkov and Cho 2010). Solid electrolytes guarantee good parameters of electrochemical gas sensors which can operate at high temperatures in tough conditions (Fergus 2008). The use of polymeric materials in either surface acoustic wave-based gas sensors or in electrochemical systems can improve their analyte sensitivity and selectivity.

This means that in this book we have to consider a wide variety of gas-sensing layers for forming a real concept of materials suitable for application in gas sensors. It is important to note that in spite of the great number of materials analyzed in this book regarding their use in gas sensors elaboration, the reader should be aware of the fact that just a small, limited, amount of materials described in the book might be applied in real devices, aimed at the sensors market. For example, at present a majority of devices available on the sensors market are being elaborated on the base of sensing materials such as metal oxides and polymers only, which can be referred to as traditional or conventional sensing materials.

Experience shows that materials aimed at the sensor market should meet a large number of tough requirements. For example, Wolfbeis (2005), while analyzing materials suitable for optical gas sensors

use, reached the conclusion that, for the incorporation of a sensor material in a real device, its quality should be estimated by the number of yes answers to the following questions:

- Does the sensor, on the basis of tested material, give an optical signal of high signal-to-noise ratio?
- Does the response of the sensing material change much with the analyte?
- Is the sensor material stable over time on storage?
- Do the components used for making the sensor material leach or deteriorate on exposure to the (often complex or aggressive) analyte?
- Is the indicator photostable for at least 24 h in operation?
- Does the sensor material adequately adhere to the support?
- Can the analytical signal be referenced to another signal (such as another wavelength, a modulation phase, an excitation pulse, or the plane of polarization)?
- Can the optical response of the material be described (or at least modeled) by a fairly uncomplicated mathematical equation?
- Are the materials used affordable and do they come (or can they be made) in constant quality?
- Can the sensor, using tested materials, be made at acceptable cost?
- Has it been demonstrated that the materials used are nontoxic?

According to Wolfbeis (2005), some of the above criteria are so-called killer criteria.

No doubt parameters of sensing materials can be optimized with regard to their use in gas sensors. The problem of optimization exists while either designing or manufacturing any electronic device. The problem of optimization is present in both the design and the manufacture of all electronic devices. However, in the case of gas sensors (GS), this problem has some specific peculiarities due to the absence of strict quantitative theory which would describe their operation. Some semiquantitative approaches can be found in the literature (Clifford 1983; Morrison 1987; Zemel 1988; Geistlinger 1993, 1994; Moseley et al. 1991; Brinzari et al. 2000; Barsan and Weimar 2001; Yamazoe et al. 2012). However, since the number of physical and chemical parameters that characterize sensor properties is large, and some of these parameters are difficult to control, the problem of optimization is largely empirical and remains a form of art.

At present, therefore, the field of gas sensors is characterized by a search for optimal sensing materials and design of adequate theoretical models that may promote optimization of gas sensors. The term *optimization* here means achieving either the necessary or the best available values of sensitivity, selectivity, and response time of gas sensors at given operating conditions. For example, according to at least one earlier view of the problem of gas sensor design (Moseley et al. 1991), almost any metal oxide can serve as the basis for a solid-state gas sensor. For this purpose one need only prepare this metal oxide as a sufficiently fine dispersed porous substance with properties controlled by the surface state. However, as requirements for gas sensors became more complex and precise, and understanding of the nature of the gas-sensing effects was became more fundamental, our conception of material compatibility for gas sensor elaboration began to change. We began to understand that for the implementation of such requirements as (1) strong response to the target agent, (2) low cross-sensitivity, (3) wide measuring range, (4) long operating/field lives, (5) fast and reversible interaction with analytes, (6) low sensitivity of the signal to a change in air humidity, (7) absence of long-term drift, (8) short time to operational status, (9) effective low-cost technology, (10) high reproducibility, (11) uniform and strong binding to the surface of the substrate, and (12) easy connection to control units, materials for gas sensors have to possess specific combination of physical and chemical properties, and not every material can fulfill these requirements.

A systematic consideration of the required properties of materials for gas sensor applications indicates that the key properties which determine a specific choice include (1) adsorption ability, (2) electronic, electrophysical, and chemical properties, (3) catalytic activity, (4) permittivity, (5) thermodynamic stability, (6) crystallographic structure, (7) interface quality, (8) compatibility with current or expected

materials to be used in processing, and (9) reliability. Many different materials appear to be favorable in terms of some of these properties, but very few materials are promising with respect to all of these requirements.

Many applications require gas sensors with high selectivity, and, therefore, it would seem that the selection of sensing material should take this requirement into account. Over the years, different approaches to develop materials with molecular selectivity have been explored including the use of molecularly imprinted polymers, zeolites, porphyrins, cavitands, metal-organic frameworks (MOFs), and other supramolecular compounds. However, it was established that the requirement for sensor selectivity often conflicts with the requirement for sensor reversibility (Potyrailo et al. 2011). Unfortunately, highly selective recognition could be associated with high binding energies and, thus, lack of full sensor reversibility. Quite the contrary, full reversibility of sensor response is achieved via weak interactions between the analyte and the sensing film.

## References

- Adamchuk VI, Hummel IW, Morgan MT, Upadhyaya SK (2004) On-the-go soil sensors for precision agriculture. *Comput Electron Agric* 44(1):71–91
- Adhikari B, Majumdar S (2004) Polymers in sensor applications. *Prog Polym Sci* 29:699–766
- Afzal A, Dickert FL (2011) Surface acoustic wave sensors for chemical applications. In: Korotcenkov G (ed) *Chemical sensors: comprehensive sensor technologies*, vol 3, Solid state devices. Momentum Press, New York, pp 447–484
- Afzal A, Cioffi N, Sabbatini L, Torsi L (2012) NO<sub>2</sub> sensors based on semiconducting metal oxide nanostructures: progress and perspectives. *Sens Actuators B* 171–172:25–42
- Ando M (2006) Recent advances in optochemical sensors for the detection of H<sub>2</sub>, O<sub>2</sub>, O<sub>3</sub>, CO, CO<sub>2</sub> and H<sub>2</sub>O in air. *Trends Anal Chem* 25(10):937–948
- Aroutiounian V (2007) Metal oxide hydrogen, oxygen, and carbon monoxide sensors for hydrogen setups and cells. *Int J Hydrogen Energy* 32(9):1145–1158
- Arshak K, Moore E, Lyons GM, Harris J, Clifford S (2004) A review of gas sensors employed in electronic nose applications. *Sensor Rev* 24(2):181–198
- Arya SK, Krishnan S, Silva H, Jeana S, Bhansali S (2012) Advances in materials for room temperature hydrogen sensors. *Analyst* 137:2743–2756
- Ast C, Schmälzlin E, Löhmansröben H-G, van Dongen JT (2012) Optical oxygen micro- and nanosensors for plant applications. *Sensors* 12:7015–7032
- Azevedo AM, Prazeres DMF, Cabral JMS, Fonseca LP (2005) Ethanol biosensors based on alcohol oxidase. *Biosens Bioelectron* 21(2):235–247
- Baldini F, Chester AN, Homola J, Martellucci S (eds) (2006) *Optical chemical sensors*. Springer, Dordrecht
- Barsan N, Weimar U (2001) Conduction model of metal oxide gas sensors. *J Electroceram* 7:143–167
- Basu S, Basu PK (2009) Nanocrystalline metal oxides for methane sensors: role of noble metals. *J Sensors* 2009, 861968
- Battison FM, Ramseyer J-P, Lang HP, Baller MK, Gerber C, Gimzewski JK, Meyer E, Guntherodt H-J (2001) A chemical sensor based on a microfabricated cantilever array with simultaneous resonance-frequency and bending readout. *Sens Actuators B* 77:122–131
- Boon-Brett L, Bousek J, Moretto P (2009) Reliability of commercial available hydrogen sensors for detection of hydrogen at critical concentrations: part II – selected sensor test results. *Int J Hydrogen Energy* 34:562–571
- Brett CMA (2001) *Electrochemical sensors for environmental monitoring. Strategy and examples*. *Pure Appl Chem* 73(12):1969–1977
- Brett CMA, Brett AMO (1998) *Electroanalysis*. Oxford University Press, Oxford
- Brinzari V, Korotchenkov G, Dmitriev S (2000) Theoretical study of semiconductor thin film gas sensitivity: attempt to consistent approach. *J Electron Technol* 33:225–235
- Britton CL Jr, Jones RL, Oden PI, Hu Z, Warmack RJ, Smith SF, Bryan WL, Rochelle JM (2000) Multiple-input micro-cantilever sensors. *Ultramicroscopy* 82:17–21
- Brown VR (2006) Sensor selection for hand-held portable gas detection. In: Mars-Proietti L (ed) *The grey house safety and security directory*. Grey House Publishing, Millerton, NY, pp 291–293, <http://www.enmet.com>
- Cao W, Duan Y (2006) Breath analysis: potential for clinical diagnosis and exposure assessment. *Clin Chem* 52(5):800–811

- Capone S, Forleo A, Francioso L, Rella R, Siciliano P, Spadavecchia J, Presicce DS, Taurino AM (2003) Solid state gas sensors: state of the art and future activities. *J Optoelectron Adv Mater* 5(5):1335–1348
- CFR (1994) Code of Federal Regulations: the Superintendent of Documents. U.S. Government Printing Office, Washington, DC
- Chan K, Ito H, Inaba H (1984) An optical fiber-based gas sensor for remote absorption measurements of low-level methane gas in the near-infrared region. *J Lightwave Technol* 2:234–237
- Chan PCH, Yan G, Sheng L, Sharma RK, Tang Z, Sin JKO, Hising L-M, Wang Y (2002) An integrated gas sensor technology using surface micromachining. *Sens Actuators B* 82:277–283
- Chatzandroulis S, Tserepi A, Goustouridis D, Normand P, Tsoukalas D (2002) Fabrication of single crystal Si cantilevers using a dry release process and application in a capacitive-type humidity sensor. *Microelectron Eng* 61–62: 955–961
- Chatzandroulis S, Tsouti V, Raptis I, Goustouridis D (2011) Capacitance-type chemical sensors. In: Korotcenkov G (ed) *Chemical sensors: comprehensive sensor technologies*, vol 4, Solid state sensors. Momentum Press, New York, pp 229–260
- Chen Z, Lu C (2005) Humidity sensors: a review of materials and mechanisms. *Sensor Lett* 3:274–295
- Choi MMF, Hawkin P (2003) Development of an optical hydrogen sulphide sensor. *Sens Actuators B* 90:211–215
- Chou J (2000) Hazardous gas monitors: a practical guide to selection, operation and application. McGraw-Hill, New York
- Cleaver KD (2001) The analysis of process gases: a review. *Accred Qual Assur* 6(1):8–15
- Clifford PK (1983) Microcomputational selectivity enhancement of semiconductor gas sensors. In: *Proceeding of international meeting on chemical sensors*, Fukuoka, 19–22 Sept 1983, pp 153–158
- Cutmore TRH, James DA (2007) Sensors and sensor systems for psychophysiological monitoring: a review of current trends. *J Psychophysiol* 21(1):51–71
- Docquier N, Candel S (2002) Combustion control and sensor: a review. *Prog Energy Combust Sci* 28:107–150
- DOE (2002) Glass industry: technology road map. DOE Report, Apr 2002
- Doll T, Lechner J, Eisele I, Schierbaum KD, Gopel W (1996) Ozone detection in the ppb range with work function sensors operating at room temperature. *Sens Actuators B* 34:506–510
- Drake C, Deshpande S, Bera D, Seal S (2007) Metallic nanostructured materials based sensors. *Intern Mater Rev* 52(5):289–317
- Eisele I, Doll T, Burgmair M (2001) Low power gas detection with FET sensors. *Sens Actuators B* 78:19–25
- Ekedahl L-G, Eriksson M, Lundström I (1998) Hydrogen sensing mechanisms of metal-insulator interfaces. *Acc Chem Res* 31:249–256
- Eranna G, Joshi BC, Runthala DP, Gupta RP (2004) Oxide materials for development of integrated gas sensors: a comprehensive review. *Crit Rev Solid State Mater Sci* 29:111–188
- Fanget S, Hentz S, Puget P, Arcamone J, Matheron M, Colinet E, Andreucci P, Duraffourg L, Ed M, Roukes ML (2011) Gas sensors based on gravimetric detection—a review. *Sens Actuators B* 160:804–821
- Fergus JW (2007) Materials for high temperature electrochemical NOx gas sensors. *Sens Actuators B* 121:652–663
- Fergus JW (2008) A review of electrolyte and electrode materials for high temperature electrochemical CO<sub>2</sub> and SO<sub>2</sub> gas sensors. *Sens Actuators B* 134:1034–1041
- Fine GF, Cavanagh LM, Afonja A, Binions R (2010) Metal oxide semiconductor gas sensors in environmental monitoring. *Sensors* 10:5469–5502
- Fitzgerald FT, Tierney LM Jr (1982) The bedside Sherlock Holmes. *West J Med* 137:169–175
- Fleet B, Gunasingham H (1992) Electrochemical sensors for monitoring environmental pollutants. *Talanta* 39:1449–1457
- Flueckiger J, Ko FK, Cheung KC (2009) Microfabricated formaldehyde gas sensors. *Sensors* 9:9196–9215
- Fontes J (2005) Humidity sensors. In: Wilson JS (ed) *Sensor technology handbook*. Elsevier, Oxford, pp 271–284
- Freund MS, Lewis NS (1995) A chemically diverse conducting polymer-based electronic nose. *Proc Natl Acad Sci USA* 92:2652–2656
- Gardner JW (1991) Detection of vapours and odours from a multisensor array using pattern recognition: principal component and cluster analysis. *Sens Actuators* 4:109–115
- Gardner JW, Bartlett PN (1999) *Electronic noses. Principles and applications*. Oxford University Press, Oxford
- Gauglitz G (2005) Direct optical sensors: principles and selected applications. *Anal Bioanal Chem* 381:141–155
- Geistlinger H (1993) Electron theory of thin film gas sensors. *Sens Actuators B* 17:47–60
- Geistlinger H (1994) Accumulation layer model for Ga<sub>2</sub>O<sub>3</sub> thin-film gas sensors based on the Volkenstein theory of catalysis. *Sens Actuators B* 18–19:125–131
- Goeders KM, Colton JS, Bottomley LA (2008) Microcantilevers: sensing chemical interactions via mechanical motion. *Chem Rev* 108:522–542
- Gopel W (1996) Ultimate limits in the miniaturization of chemical sensors. *Sens Actuators A* 56:83–102
- Gopel W, Schierbaum KD (1995) SnO<sub>2</sub> sensors: current status and future prospects. *Sens Actuators B* 26–27:1–12
- Greenblatt M, Shuk P (1996) Solid-state humidity sensors. *Solid State Ionics* 86–88:995–1000
- Haug M, Schierbaum KD, Gauglitz G, Göpel W (1993) Chemical sensors based upon polysiloxanes: comparison between optical, quartz microbalance, calorimetric, and capacitance sensors. *Sens Actuators B* 11:383–391

- Haugen JE, Kvaal K (1998) Electronic nose and artificial neural network. *Meat Sci* 49:S273–S286  
Health Canada 2006 (<http://www.hc-sc.gc.ca/ewh-semt/air/in/res-in/index-eng.php>)
- Ho CK, Itamura MT, Kelley M, Hughes RC (2001) Review of chemical sensors for in-situ monitoring of volatile contaminants. Sandia Report SAND2001-0643, Unlimited release, Sandia National Laboratories, Albuquerque, NM. <http://www.sandia.gov/sensor>
- Ho CK, Robinson A, Miller DR, Davis MJ (2005) Overview of sensors and needs for environmental monitoring. *Sensors* 5:4–37
- Holzinger M, Maier J, Sitte W (1997) Potentiometric detection of complex gases: application to CO<sub>2</sub>. *Solid State Ionics* 94:217–225
- Honeywell Analytics (2012) Gas handbook. [http://www.honeywellanalytics.com/Technical %20Library/EMEA/1 %20Types %20of %20Documents/Gas %20Book/Gas %20Book %20English.pdf](http://www.honeywellanalytics.com/Technical%20Library/EMEA/1%20Types%20of%20Documents/Gas%20Book/Gas%20Book%20English.pdf)
- Hubert T, Boon-Brett L, Black G, Banach U (2011) Hydrogen sensors – a review. *Sens Actuators B* 157:329–352
- Hulanicki A, Geab S, Ingman F (1991) Chemical sensors definitions and classification. *Pure Appl Chem* 63(9):1247–1250
- Igarashi I (1986) New technology of sensors for automotive applications. *Sens Actuators* 10:181–193
- Ishihara T, Matsubara S (1998) Capacitive type gas sensors. *J Electrocer* 2:215–228
- Justino CIL, Rocha-Santos TA, Duarte AC, Rocha-Santos TA (2010) Review of analytical figures of merit of sensors and biosensors in clinical applications. *Trends Anal Chem* 29(10):1172–1183
- Keefe MK, Benkstein KD, Hup JT (2000) Luminescent sensor molecules based on coordinated metals: a review of recent developments. *Coord Chem Rev* 205(1):201–228
- Kharitonov SA, Barnes PJ (2000) Clinical aspects of exhaled nitric oxide. *Eur Respir J* 16:781–792
- King WH Jr (1964) Piezoelectric sorption detector. *Anal Chem* 36:1735–1739
- Kohl D, Kelleter J, Petig H (2001) Detection of fires by gas sensors. In: Balthes H, Gopel W, Hesse J (eds) *Sensors update*, vol 9(1). Wiley-VCH, Weinheim, pp 161–223
- Korotcenkov G (2007a) Metal oxides for solid state gas sensors. What determines our choice? *Mater Sci Eng B* 139:1–23
- Korotcenkov G (2007b) Practical aspects in design of one-electrode semiconductor gas sensors: status report. *Sens Actuators B* 121:664–678
- Korotcenkov G (ed) (2010) *Chemical sensors: fundamentals of sensor materials*, vols 1–3. Momentum Press, New York
- Korotcenkov G (ed) (2011) *Chemical sensors: comprehensive sensor technologies*, vol 6, *Sensors application*. Momentum Press, New York
- Korotcenkov G, Cho BK (2010) Porous semiconductors: advanced material for gas sensor applications. *Crit Rev Solid State Mater Sci* 35(1):1–37
- Korotcenkov G, Cho BK (2011) Chemical sensor selection and application guide. In: Korotcenkov G (ed) *Chemical sensors: comprehensive sensor technologies*, vol 6, *Sensors application*. Momentum Press, New York, pp 281–348
- Korotcenkov G, Cho BK (2012) Ozone measuring: what can limit the application of SnO<sub>2</sub>-based gas sensors? *Sens Actuators B* 161:28–44
- Korotcenkov G, Han S-D, Stetter JR (2009) Review of electrochemical hydrogen sensors. *Chem Rev* 109(3): 1402–1433
- Korotcenkov G, Cho BK, Narayanaswamy R, Sevilla F III (2011) Optical and fiber optic chemical sensors. In: Korotcenkov G (ed) *Chemical sensors: comprehensive sensor technologies*, vol 5, *Electrochemical and optical sensors*. Momentum Press, New York, pp 311–476
- Korotcenkov G, Stetter JR (2011) Chemical gas mixture analysis and the electronic nose: current status, future trends. In: Korotcenkov G (ed) *Chemical sensors: comprehensive sensor technologies*, vol 6, *Chemical sensors applications*. Momentum, New York, pp 1–56
- Kowalski BR, Bender CF (1972) Pattern recognition: a powerful approach to interpreting chemical data. *J Am Chem Soc* 94:5632–5639
- Krol S, Zabiegata B, Namiesnik J (2010) Monitoring VOCs in atmospheric air. I. On-line gas analyzers. *Trends Anal Chem* 29(9):1092–1100
- Kummer AM, Hierlemann A, Balthes H (2004) Tuning sensitivity and selectivity of complementary metal oxide semiconductor-based capacitive chemical microsensors. *Anal Chem* 76:2470–2477
- Lakowicz JR (1999) *Principles of fluorescence spectroscopy*, 2nd edn. Kluwer Academic/Plenum, New York
- Lambeck PV (1992) Integrated opto-chemical sensors. *Sens Actuators B* 8:103–116
- Lee J-H (2003) Review on zirconia air-fuel ratio sensors for automotive applications. *J Mater Sci* 38:4247–4257
- Lee J-H, Tsai C-L, Fann C-S, Wang S-H (2002) Design of an acousto-magnetic oxygen sensor. *J Med Biol Eng* 22(4):193–198
- Leiner MJP (1991) Luminescence chemical sensors for biomedical applications: scope and limitations. *Anal Chim Acta* 255:209–222
- Lim SH, Jaworski J, Satyanarayana S, Wang F, Raorane D, Lee S-W, Majumdar A (2007) Nanomechanical chemical sensor platform. In: *Proceedings of the 2nd IEEE international conference on nano/micro engineered and molecular systems*, Bangkok, 16–19 Jan, pp 886–889
- Lippitsch ME, Pusterhofer J, Leiner MJP, Wolfbeis OS (1988) Fiber-optic oxygen sensor with the fluorescence decay time as the information carrier. *Anal Chim Acta* 205:1–6

- Lu G, Miura N, Yamazoe N (1996) High-temperature hydrogen sensor based on stabilized zirconia and a metal oxide electrode. *Sens Actuators B* 35–36:130–135
- Lundström I (1991) Field effect chemical sensors. In: Gopel W, Hesse J, Zemel JN (eds) *Sensors: a comprehensive survey*, vol 1. VCH, Weinheim, pp 467–529
- Lundstrom I, Sundgren H, Winquist F, Eriksson M, Krantz-Rulcker C, Lloyd-Spetz A (2007) Twenty-five years of field effect gas sensor research in Linköping. *Sens Actuators B* 121:247–262
- Marczin N, Kharitonov SA, Yacoub MH, Barnes PJ (eds) (2005) *Disease markers in exhaled breath*. Taylor and Francis, Oxford
- Maricq MM (2007) Chemical characterization of particulate emissions from diesel engines: a review. *J Aerosol Sci* 38(11):1079–1118
- Maskell WC (1987) Inorganic solid state chemically sensitive devices: electrochemical oxygen gas sensors. *J Phys E: Sci Instrum* 20:1156–1168
- Massie C, Stewart G, McGregor G, Gilchrist JR (2006) Design of a portable optical sensor for methane gas detection. *Sens Actuators B* 113:830–836
- Mayer KM, Hafner JH (2011) Localized surface plasmon resonance sensors. *Chem Rev* 111:3828–3857
- Mello LD, Kubota LT (2002) Review of the use of biosensors as analytical tools in the food and drink industries. *Food Chem* 77(2):237–256
- Ménil F, Coillard V, Lucat C (2000) Critical review of nitrogen monoxide sensors for exhaust gases of lean burn engines. *Sens Actuators B* 67:1–23
- Meriläinen PT (1990) A differential paramagnetic sensor for breath-by-breath oximetry. *J Clin Monit* 6(1):65–73
- Messer H, Zinevich A, Alpert P (2006) Environmental monitoring by wireless communication networks. *Science* 312:713
- Miller JB (2001) Catalytic sensors for monitoring explosive atmospheres. *IEEE Sensors J* 1(1):88–93
- Miura N, Ono M, Shimanoe K, Yamazoe N (1998a) A compact solid-state amperometric sensor for detection of NO<sub>2</sub> in ppb range. *Sens Actuators B* 49:101–109
- Miura N, Raisen T, Lu G, Yamazoe N (1998b) Highly selective CO sensor using stabilized zirconia and a couple of oxide electrodes. *Sens Actuators B* 47:84–91
- Monkman G (2000) Monomolecular Langmuir-Blodgett films—tomorrow’s sensors? *Sensor Rev* 20:127–131
- Morrison SR (1987) Mechanism of semiconductor gas sensor operation. *Sens Actuators* 11:283–287
- Moseley PT, Norris JOW, Williams DE (eds) (1991) *Techniques and mechanisms in gas sensing*. Adam Hilger, Bristol
- Moskalenko KL, Nadezhdinskii AI, Adamovskaya IA (1996) Human breath trace gas content study by tuneable diode laser spectroscopy. *Infrared Phys Technol* 37:181–192
- Muñoz R, Sivret EC, Parcsi G, Lebrero R, Wang X, Suffet IH, Stuetz RM (2010) Monitoring techniques for odour abatement assessment. *Water Res* 44(18):5129–5149
- Nakahara T (2004) Development of gas sensors and cultivation of new markets for air quality. In: *Proceedings of the 38th chemical sensor symposium*, Tokyo, 24–26 Mar, pp 73–75
- Narayanaswamy R, Wolfbeis OS (eds) (2004) *Optical sensors—industrial, environmental and diagnostic applications*, vol 1, Chemical sensors and biosensors. Springer, Berlin
- Neethirajan S, Jayas DS, Sadistap S (2009) Carbon dioxide (CO<sub>2</sub>) sensors for the agri-food industry—a review. *Food Bioprocess Technol* 2:115–121
- NFPA (2003) *Operation of fire protection systems*. National Fire Protection Association, Quincy, MA
- Pandey SK, Kim K-H, Tang K-T (2012) A review of sensor-based methods for monitoring hydrogen sulfide. *Trends Anal Chem* 32:87–99
- Parrish DD, Fehsenfel FC (2000) Methods for gas-phase measurements of ozone, ozone precursors and aerosol precursors. *Atmos Environ* 34(12–14):1921–1957
- Patel PD (2002) Biosensors for measurement of analytes implicated in food safety: a review. *Trends Anal Chem* 21(2):96–115
- Pedersen LD (1991) Assessment of sensors used in the food industry. *Food Control* 2(2):87–98
- Pejčić D, Eadington P, Ross A (2007) Environmental monitoring of hydrocarbons: a chemical sensor perspective. *Environ Sci Technol* 41(18):6333–6342
- Peng G, Trock E, Haick H (2008) Detecting simulated patterns of lung cancer biomarkers by random network of single-walled carbon nanotubes coated with nonpolymeric organic materials. *Nano Lett* 8:3631–3636
- Pletcher D, Evans J, Warburton PR, Gibbs TK (1991) Acidic gas sensors and method of using the same. US Patent 5,071,526
- Potje-Kamloth K (2008) Semiconductor junction gas sensors. *Chem Rev* 108:367–399
- Potyraiilo RA, Mirsky VM (2008) Combinatorial and high-throughput development of sensing materials: the first 10 years. *Chem Rev B* 108:770–813
- Potyraiilo RA, Surman C, Nagraj N, Burns A (2011) Materials and transducers toward selective wireless gas sensing. *Chem Rev* 111:7315–7354
- Ramamoorthy R, Dutta PK, Akbar SA (2003) Oxygen sensors: materials, methods, designs and applications. *J Mater Sci* 38:4271–4282

- Riegel J, Neumann H, Wiedenmann N-M (2002) Exhaust gas sensors for automotive emission control. *Solid State Ionics* 152–153:783–800
- Rittersma ZM (2002) Recent achievements in miniaturised humidity sensors—a review of transduction techniques. *Sens Actuators A* 96:196–210
- Rock F, Barsan N, Weimar U (2008) Electronic nose: current status and future trends. *Chem Rev* 108:705–725
- Sadaoka Y (1992) Organic semiconductor gas sensors. In: Sberveglieri G (ed) *Gas sensors*. Kluwer Academic, Dordrecht, pp 187–218
- Sauerbrey G (1959) Verwendung von Schwingquarzen zur Wagung dünner Schichten und zur Mikrowagung. *Z Physik* 155:206–212
- Sazhin SG, Soborover EI, Tokarev SV (2003) Sensor methods of ammonia inspection. *Russ J Nondestruct Test* 39(10):791–806
- Schreiter M, Gabl R, Lerchner J, Hohlfeld C, Delan A, Wolf G, Bluhner A, Katzschner B, Mertig M, Pompe W (2006) Functionalized pyroelectric sensors for gas detection. *Sens Actuators B* 119:255–261
- Semancik S (2001) Microhotplate platform for chemical sensors research. *Sens Actuators B* 77:579–591
- Shemshad J, Aminossadati SM, Kizil MS (2012) A review of developments in near infrared methane detection based on tunable diode laser. *Sens Actuators B* 171–172:77–92
- Shin W, Tajima K, Choi Y, Nishibori M, Izu N, Matsubara I, Murayama N (2006) Micro-thermoelectric devices with ceramic combustors. *Sens Actuators A* 130–131:411–418
- Shin W, Nishibori M, Matsubara I (2011) Gas sensors using pyroelectric and thermoelectric effects. In: Korotcenkov G (ed) *Chemical sensors: comprehensive sensor technologies*, vol 4, Solid-state devices. Momentum Press, New York, pp 261–319
- Silva SF, Coelho L, Frazão O, Santos JL, Malcata FX (2012) A review of palladium-based fiber-optic sensors for molecular hydrogen detection. *IEEE Sensors J* 12(1):93–102
- Singh S (2007) Sensors—an effective approach for the detection of explosives. *J Hazard Mater* 144:15–28
- Smith D, Spanel P, Davies S (1999) Trace gases in breath of healthy volunteers when fasting and after a protein-calorie meal: a preliminary study. *J Appl Physiol* 87:1584–1588
- Stetter JR, Penrose WR, Yao S (2003) Sensors, chemical sensors, electrochemical sensors, and ECS. *J Electrochem Soc* 150(2):S11–S16
- Stetter JR, Korotcenkov G, Zeng X, Tang Y, Liu Y (2011) Electrochemical gas sensors: fundamentals, fabrication and parameters. In: Korotcenkov G (ed) *Chemical sensors: comprehensive sensor technologies*, vol 3, Electrochemical and optical sensors. Momentum Press, New York, pp 1–123
- Suzuki S, Noda Y, Sawaki N (1999) Market overview: oxygen sensors. In: Baltes H, Gopel W, Hesse J (eds) *Sensors update*, vol 6(1). Wiley-VCH, Weinheim, pp 381–396
- Symons EA (1992) Catalytic gas sensors. In: Sberveglieri G (ed) *Gas sensors*. Kluwer, Dordrecht, pp 169–185
- Talazac L, Brunet J, Battut V, Blanc JP, Pauly A, Germain JP, Pellier S, Soulier C (2001) Air quality evaluation by monolithic InP-based resistive sensors. *Sens Actuators B* 76:258–264
- Taylor RF (1996) Chemical and biological sensors: markets and commercialization. In: Taylor RF, Schultz JS (eds) *Handbook of chemical sensors and biosensors*. IOP Publishing, Bristol
- Taylor RF, Schultz JS (eds) (1996) *Handbook of chemical sensors and biosensors*. IOP Publishing, Bristol
- Timmer B, Olthuis W, van den Berg A (2005) Ammonia sensors and their applications—a review. *Sens Actuators B* 107:666–677
- Traversa E (1995) Ceramic sensors for humidity detection: the state-of-the-art and future developments. *Sens Actuators B* 23:135–156
- Trinchi A, Woldarski W, Li YX (2004) Hydrogen sensitive  $\text{Ga}_2\text{O}_3$  Schottky diode sensor based on SiC. *Sens Actuators B* 100:94–98
- Valeur B, Brochon JC (eds) (2001) *New trends in fluorescence spectroscopy: applications to chemical and life sciences*. Springer, Berlin
- Vashist SK, Korotcenkov G (2011) Microcantilever-based chemical sensors. In: Korotcenkov G (ed) *Chemical sensors: comprehensive sensor technologies*, vol 3, Solid state devices. Momentum Press, New York, pp 321–376
- Voinova M, Jonson M (2011) The quartz crystal microbalance. In: Korotcenkov G (ed) *Chemical sensors: comprehensive sensor technologies*, vol 3, Solid state devices. Momentum Press, New York, pp 377–483
- Warburton PR, Pagano MP, Hoover R, Logman M, Crytzer K, Warburton YJ (1998) Amperometric gas sensor response times. *Anal Chem* 70(5):998–1006
- Ward JPT (2008) Oxygen sensors in context. *Biochim Biophys Acta Bioenerg* 1777(1):1–14
- Werle P, Slemr F, Maurer K, Kormann R, Mucke R, Janker B (2002) Near- and mid-infrared laser-optical sensors for gas analysis. *Opt Lasers Eng* 37:101–1114
- White LT (2000) *Hazardous gas monitoring: a guide for semiconductor and other hazardous occupancies*. Noyes/William Andrew, Norwich, NY
- White RM, Voltmer FW (1965) Direct piezoelectric coupling to surface elastic waves. *Appl Phys Lett* 7:314–315
- Wilson AD, Baietto M (2009) Applications and advances in electronic-nose technologies. *Sensors* 9:5099–5148



- Wilson AD, Baietto M (2011) Advances in electronic-nose technologies developed for biomedical applications. *Sensors* 11:1105–1176
- Wilson DM, Hoyt S, Janata J, Booksh K, Obando L (2001) Chemical sensors for portable, handheld field instruments. *IEEE Sensors J* 1:256–274
- Wohltjen H, Barger WR, Snow AW, Jarvis NL (1985) A vapor-sensitive chemiresistor fabricated with planar microelectrodes and a Langmuir-Blodgett organic semiconductor film. *IEEE Trans Electron Dev* ED-32:1170–1174
- Wolfbeis OS (1991) Fiber optic chemical sensors and biosensors, vol 1. CRC, Boca Raton, FL
- Wolfbeis OS (1992) Fiber optic chemical sensors and biosensors, vol 2. CRC, Boca Raton, FL
- Wolfbeis OS (2005) Materials for fluorescence-based optical chemical sensors. *J Mater Chem* 15:2657–2669
- Wollenstein J, Plaza JA, Canè C, Min Y, Bottner H, Tuller HL (2003) A novel single chip thin film metal oxide array. *Sens Actuators B* 93:350–355
- Yakovlev YP, Baranov AN, Imenkov AN, Mikhailova MP (1991) Optoelectronic LED-photodiode pairs for moisture and gas sensors in spectral range 1.8–4.8  $\mu\text{m}$ . In: Wolfbeis S (ed) *Chemical and medical sensors*. Proc SPIE 1510:170–177
- Yamazoe N (2005) Toward innovations of gas sensor technology. *Sens Actuators B* 108:2–14
- Yamazoe N, Miura N (1994) Environmental gas sensing. *Sens Actuators B* 20:95–102
- Yamazoe N, Miura N (1996) Prospect and problems of solid electrolyte-based oxygenic gas sensors. *Solid State Ionics* 86–88:987–993
- Yamazoe N, Suematsu K, Shimano K (2012) Extension of receptor function theory to include two types of adsorbed oxygen for oxide semiconductor gas sensors. *Sens Actuators B* 163:128–135
- Yeo TL, Sun T, Grattan KTV (2008) Fibre-optic sensor technologies for humidity and moisture measurement. *Sens Actuators A* 144:280–295
- Zemel J (1988) Theoretical description of gas film interaction on SnO<sub>x</sub>. *Thin Solid Films* 163:89–195
- Zhang H, Pang W, Kim ES, Yu H (2010) Micromachined silicon and polymer probes integrated with film-bulkacoustic-resonator mass sensors. *J Micromech Microeng* 20:125008
- Zosel J, Oelßner W, Decker M, Gerlach G, Guth U (2011) The measurement of dissolved and gaseous carbon dioxide concentration. *Meas Sci Technol* 22:072001

**Part I**  
**Conventional Gas Sensing Materials**

## Chapter 2

# Metal Oxides

### 2.1 General View

Metal oxides form the class of materials which has seen the widest application in gas sensors (Park and Akbar 2003; Korotcenkov 2007a, b). As can be seen in Table 2.1 and Fig. 2.1, they can be used in every type of gas sensor. For example, in conductometric sensors, semiconducting metal oxides are typically used as gas-sensing materials that change their electrical resistance upon exposure to oxidizing or reducing gases.

Specific properties of the metal oxides, such as the wide variety of materials with different electro-physical, optical, and chemical characteristics, their high thermal and temporal stability, and their ability to function in harsh environments, make metal oxides very suitable materials for use in chemical sensors (Korotcenkov 2010, 2011a). Furthermore, their role in chemical sensors is not limited to being used just as sensing materials. They are also being used successfully as substrates, electrodes, promoters, and structure modifiers and as membranes and fibers (Table 2.2). Among other advantages of metal oxides are the simplicity of device structure, low fabrication cost, robustness in practical applications, and adaptability to a wide variety of reducing or oxidizing gases. Furthermore, many of the metal oxides can be prepared in thin-film form using deposition techniques that are compatible with standard microelectronic technology. This last factor is very important for large-scale production, because the microelectronic approach promotes low cost for mass production, offers the possibility of manufacturing a sensor array on a chip, and guarantees good, reproducible sampling. Gas sensors in the form of thin or thick films seem to be more promising detectors over the pellet form, because they are potentially smaller in size, rugged, and consume only small amounts of electrical power. A handy sensor system is an added advantage for a field application and also for urban and remote areas, to avoid the bulky systems that are presently used. On the other hand, low selectivity is the main shortcoming of sensors based on metal oxides. Metal oxide-based gas sensors appear to respond to a wide spectrum of reducing gases, thereby making it difficult to assign the signal to a particular gas of interest in a mixture of several reducing gases. There are several methods to overcome this difficulty. One method is the use of thermal cycling of the sensor element (Sears et al. 1989). As different reducing gases react at different rates as a function of sensor temperature, varying the temperature in a cyclic manner could lead to unique signatures of the gas of interest. In some cases, thermal cycling has been reported to cause a great increase in the selectivity of gas detection. The incorporation of passive and catalytically active filters in the sensors also promotes the increase of sensor selectivity. These filters can create situation where only the gas(es) of interest can reach the sensor, while the gases that are of no interest cannot. This approach will be discussed in Chap. 12 (Vol. 1). The other more common approach to selectivity is through the use of additional surface

**Table 2.1** Metal oxides preferred for applications in various types of chemical sensors

Sensor type and (sensor elements)	Detected gas	Metal oxides preferred for application
Chemiresistor (semiconductor)	Reducing gases (CO, H <sub>2</sub> , CH <sub>4</sub> )	SnO <sub>2</sub> ; CTO; Ga <sub>2</sub> O <sub>3</sub> ; In <sub>2</sub> O <sub>3</sub>
	Oxidizing gases (O <sub>3</sub> , NO <sub>x</sub> , Cl <sub>2</sub> )	In <sub>2</sub> O <sub>3</sub> ; WO <sub>3</sub> ; ZnO; TiO <sub>2</sub>
	H <sub>2</sub> S; SO <sub>2</sub>	SnO <sub>2</sub> /CuO; SnO <sub>2</sub> /Ag <sub>2</sub> O
	NH <sub>3</sub>	WO <sub>3</sub> ; MoO <sub>3</sub> ; In <sub>2</sub> O <sub>3</sub>
	CO <sub>2</sub>	SnO <sub>2</sub> /La <sub>2</sub> O <sub>3</sub> ; Al <sub>2</sub> O <sub>3</sub> /V <sub>2</sub> O <sub>5</sub> ; BaTiO <sub>3</sub> /CuO; BaSnO <sub>3</sub>
	Alcohol	La <sub>2</sub> O <sub>3</sub> /In <sub>2</sub> O <sub>3</sub> ; La <sub>2</sub> O <sub>3</sub> /SnO <sub>2</sub> ; In <sub>2</sub> O <sub>3</sub> /Fe <sub>2</sub> O <sub>3</sub>
	Oxygen	Ga <sub>2</sub> O <sub>3</sub> ; SrTiO <sub>3</sub> ; SrTiFeO <sub>3</sub> ; TiO <sub>2</sub> ; Nb <sub>2</sub> O <sub>5</sub> ; ZnO
	Humidity	In <sub>2</sub> O <sub>3</sub> /SiO <sub>2</sub> ; TiO <sub>2</sub> /MgCr <sub>2</sub> O <sub>4</sub> ; SrTiO <sub>3</sub> ; LaFeO <sub>3</sub>
Electrochemical (solid electrolyte)	Oxygen	ZrO <sub>2</sub> :Y; Bi <sub>2</sub> O <sub>3</sub> /MoO <sub>3</sub> ; SrCeO <sub>3</sub> ; SrTiO <sub>3</sub> ; SrTiFeO <sub>3</sub>
	H <sub>2</sub>	Sb <sub>2</sub> O <sub>5</sub> ; BaCeO <sub>3</sub> ; BaCeO <sub>3</sub> :Gd; ZrO <sub>2</sub> :Y; SrCeO <sub>3</sub> ; SrCeO <sub>3</sub> :Yb, In; SrZrO <sub>3</sub> ; BaZrO <sub>3</sub> ; CaZrO <sub>3</sub>
Surface acoustic wave Quartz crystal balance	Humidity; NO <sub>2</sub> ; H <sub>2</sub> ; ethanol; O <sub>3</sub>	ZnO; In <sub>2</sub> O <sub>3</sub> ; LiNbO <sub>3</sub> ; SiO <sub>2</sub> ; WO <sub>3</sub> ; GaPO <sub>4</sub> ;
	Hg vapor; NH <sub>3</sub> ; NO <sub>x</sub> ; SO <sub>x</sub> ; H <sub>2</sub> S	La <sub>3</sub> Ga <sub>3</sub> SiO <sub>14</sub>
Work function (RT)	CH <sub>4</sub> ; CO; Cl <sub>2</sub>	NiO; Fe <sub>2</sub> O <sub>3</sub> ; Co <sub>3</sub> O <sub>4</sub>
Capacitance	H <sub>2</sub> ; NH <sub>3</sub> ; C <sub>2</sub> H <sub>5</sub> OH	(Pd, Pt, Ir)/SiO <sub>2</sub>
	Humidity	Al <sub>2</sub> O <sub>3</sub>
	CO <sub>2</sub>	CuO/BaTiO <sub>3</sub> ; CeO <sub>2</sub> /BaCO <sub>2</sub> /CuO; Co <sub>3</sub> O <sub>4</sub> /BaTiO <sub>3</sub> ; NiO/BaTiO <sub>3</sub>
Pelistor	NO <sub>x</sub>	CoO/In <sub>2</sub> O <sub>3</sub> ; NiO/ZnO
	Combustible gases and vapors	Al <sub>2</sub> O <sub>3</sub> ; SiO <sub>2</sub>
Pyroelectric	H <sub>2</sub> ; CH <sub>4</sub>	ZnO; LiTaO <sub>3</sub> ; LiTiO <sub>3</sub>
Heterostructural	CO	ZnO/Zn <sub>2</sub> SnO <sub>4</sub> ; SnO <sub>2</sub> /TiO <sub>2</sub> ; SnO <sub>2</sub> /Zn <sub>2</sub> SnO <sub>4</sub>
	H <sub>2</sub> S	ZnO/CuO; SnO <sub>2</sub> /CuO/SnO <sub>2</sub>
Schottky diode	H <sub>2</sub>	ZnO; TiO <sub>2</sub>
Optochemical (fiber optic)	H <sub>2</sub> ; CO; alcohol	WO <sub>3</sub> ; Mn <sub>2</sub> O <sub>3</sub> ; Co <sub>3</sub> O <sub>4</sub> ; NiO; CuO
Surface plasmon resonance	NO <sub>2</sub> ; H <sub>2</sub> S; NH <sub>3</sub>	Ta <sub>2</sub> O <sub>5</sub> ; SiO <sub>x</sub> N <sub>y</sub> ; TiO <sub>2</sub>
Cataluminescence	Organic vapors	MgO; TiO <sub>2</sub> ; Y <sub>2</sub> O <sub>3</sub> ; LaCoO <sub>3</sub> ; Sr
	Ethanol	ZnO
Electronic nose	Gases; vapors	SnO <sub>2</sub> ; In <sub>2</sub> O <sub>3</sub> ; WO <sub>3</sub> ; ZnO

Source: Data from Korotcenkov (2007)

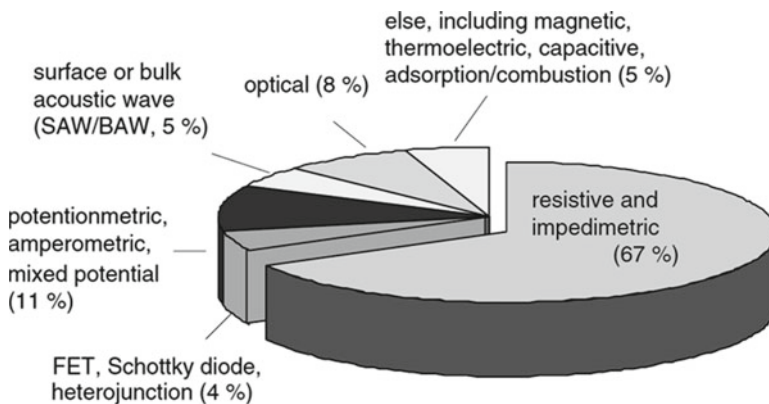


**Fig. 2.1** Literature review: various types of metal oxide-based gas sensors discussed in 2007 (based on a total of 340 papers available via ISI Web of Science) (Reprinted with permission from Sahner and Tuller (2010). Copyright 2010 Springer)

**Table 2.2** Functions of metal oxides in chemical sensors

Function	Type of sensor	Examples
Sensing layer	Conductometric, SAW, QCM, optical, calorimetric	SnO <sub>2</sub> , In <sub>2</sub> O <sub>3</sub> , WO <sub>3</sub> , TiO <sub>2</sub> , ZrO <sub>2</sub> , SrCeO <sub>3</sub> ; SrTiO <sub>3</sub> ; SrTiFeO <sub>3</sub> ; etc.
Substrate	Conductometric SAW, QCM Thermoelectric	Al <sub>2</sub> O <sub>3</sub> , SiO <sub>2</sub> , BeO; LiNbO <sub>3</sub> ; ZrO <sub>2</sub> :Y ZnO; La <sub>3</sub> Ga <sub>2</sub> SiO <sub>14</sub> Al <sub>2</sub> O <sub>3</sub> ; MgO
Electrode	Electrochemical	In <sub>2</sub> O <sub>3</sub> , ZnO, NiO/Ni; PdO/Pd; Al <sub>2</sub> O <sub>3</sub> /Pt; MgAl <sub>2</sub> O <sub>3</sub> /Pt; Au/Ga <sub>2</sub> O <sub>3</sub>
Membrane, filter	Electrochemical, gas sensors	Al <sub>2</sub> O <sub>3</sub> , SiO <sub>2</sub> , zeolites
Fiber	Fiber optic	SiO <sub>2</sub> , GeO <sub>2</sub> -Sb <sub>2</sub> O <sub>3</sub>
Promoter	Conductometric, SAW, QCM, optical, calorimetric	PdO; RhO; Ag <sub>2</sub> O; CuO; Fe <sub>2</sub> O <sub>3</sub> ; P <sub>2</sub> O <sub>5</sub> ; Co <sub>3</sub> O <sub>4</sub> ; NiO; MnO
Structure modifier (stabilizer)	Conductometric, calorimetric	Al <sub>2</sub> O <sub>3</sub> ; SiO <sub>2</sub> ; CaO; MgO; BaO; Y <sub>2</sub> O <sub>3</sub> ; La <sub>2</sub> O <sub>3</sub> ; Ta <sub>2</sub> O <sub>5</sub> ; CeO <sub>2</sub>

*QCM* quartz crystal microbalance, *SAW* surface acoustic wave

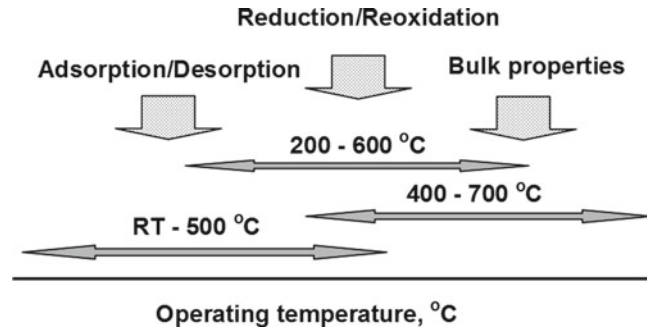
catalysts and promoters. This approach will be discussed in details in Chap. 10 (Vol. 1) and Chap. 23 (Vol. 2). Addition of a noble metal (such as Pt, Pd, Au, and Ag), an alloy of noble metals (such as Pd/Au and Pd/Rh), or transition metals (such as Cu, Fe, and Ni) has long been known to enhance the sensitivity and selectivity of the sensor elements. However, we need to recognize that all the above-mentioned approaches do not resolve the problem of low selectivity completely.

## 2.2 Which Metal Oxides Are Better for Solid-State Electrochemical Gas Sensors?

The choice of a suitable material for a gas sensor should be based on good sensor response, low sensitivity to air humidity, high selectivity, low hysteresis, high stability of parameters over time, a wide range of operating temperatures, good thermal cycling, and durability in the face of exposure to the various chemicals likely to be present in the environment (Kulwicki 1991; Eranna et al. 2004; Korotcenkov 2005, 2007a, b; Sadek et al. 2006). This means that, in addition to high gas-sensing properties, metal oxides designed for gas sensor applications must fulfill criteria such as: (1) high chemical stability, without solid-state transformation or thermal decomposition; metal oxides must also be inert with respect to the gases and materials in contact; (2) good mechanical stability, with high stiffness, no creep at the operating temperature and good heat shock strength; and (3) good compatibility of expansion coefficient with expansion coefficients of the other constituents of the sensor – this criterion is especially important when the working temperature is high. Unfortunately, we do not have the answer to the question—which metal oxide is better for the above-mentioned application?

For example, as is known, the gas sensitivity of heated MOX conductometric gas sensors is caused either by chemisorption processes and catalytic reactions of the molecules to be detected or by bulk point defect equilibrium with the surrounding atmosphere (Schierbaum 1995; Brynzari et al. 2000). While the first mechanism is realized in chemiresistors that operate in the temperature range 20–500 °C, the second is used in solid electrolyte-based gas sensors that operate at high temperatures, usually in the range from 300 to 1,000 °C (see Fig. 2.2). In ion conductors, current flow occurs by the movement of ions through the crystal lattice. This movement is a result of thermally activated hopping of the ions, moving from crystal lattice site to crystal lattice site, with a superimposed drift in the direction of the electric field. The ionic conductivity is consequently strongly temperature dependent, but at

**Fig. 2.2** Processes controlling response of high-temperature and low-temperature MOX-based gas sensors



high temperatures can approach values close to  $1 \text{ S cm}^{-1}$ , comparable to the levels of ionic conductivity found in liquid electrolytes.

In solid electrolytes the time necessary to reach equilibrium between the concentration of bulk point defects and the surrounding gas is controlled by the diffusion coefficient of oxygen. Therefore, faster diffusion decreases both the required operating temperature and the response time of solid electrolyte-based gas sensors. In chemiresistors, due to low operating temperatures and surface nature of processes taking place during interaction with target gas, the change in ambient gas concentration does not lead to equilibrium between MOX bulk properties (stoichiometry) and the surrounding gas. The gas chemisorption at the oxide surface results in capture of free electrons at the localized states induced by adsorption species. The diffusion of oxygen in/out of the bulk of oxide crystallites is only a source of long-term drift of sensor parameters (Jamnik et al. 2002). This means that the above-mentioned types of gas sensors require different material platforms, which force the diffusion of oxygen vacancies or foreign impurity point defects to go very slowly (chemiresistors) or very quickly (solid electrolytes). It was established that lattice vacancies promote oxygen bulk diffusion (Murch and Nowick 1984). Therefore, oxides with intrinsic defects are not favorable for the development of chemisorptions-type sensors when diffusion processes should be avoided. On the other hand, materials with specific structural properties are necessary to develop sensors operated under high temperatures through diffusion processes (Tuller 2003). Perovskites, such as  $\text{SrTiO}_3$  and  $\text{SrTi}_{(1-x)}\text{Fe}_x\text{O}_3$ , which have been intensively investigated in recent years as promising materials for high-temperature sensors, have such internal imperfections of the crystal structure (Kreuer 2003).

One can find the analysis of advantages and disadvantages of indicated types of gas sensors in review papers (Korotcenkov 2007a). Gas sensors operated at low temperatures are more compatible with other microelectronic devices, which often have limitations on temperature. By employing such sensors, it is easier to maintain better selectivity and to create sensor arrays for “electronic nose” instruments (Gardner and Bartlett 1992, 1999).  $\text{SnO}_2$ - and  $\text{In}_2\text{O}_3$ -based sensors operating in the temperature range 150–450 °C are typical examples of low-temperature sensors. High-temperature sensors, however, are more suitable for carrying out in situ monitoring of many high-temperature technological processes such as those observed in engines (Fleischer and Meixner 1997, 1998). For example, Blase et al. (1997) found that the response time of such sensors could be  $\sim 1 \text{ ms}$ . Another advantage of high-temperature operation is that the sensing behavior of such sensors is well explained and well predicted from known thermodynamic principles (Brynn and Tseung 1979). In addition, it has been shown that the conductivity of some oxide materials, such as  $\text{Ga}_2\text{O}_3$ , at high operating temperatures does not depend on grain boundaries, and also that the oxide surface is well self-cleaned, which allows the development of stable and reproducible sensors (Fleischer and Meixner 1997). The analysis of operation mechanisms of solid electrolyte-based sensors has been covered elsewhere (Park et al. 2009).

## 2.3 Metal Oxides with Ionic Conductivity: Solid Electrolytes

Metal oxide solid-state electrolytes or fast solid-state ionic conductors are an important class of materials that have received great attention because of their potential applications in various fields such as gas separations heterogeneous catalysis, solid oxide fuel cells, solid-state batteries, and gas sensors (Marnellos and Stoukides 1998; Zisekas et al. 2008; Amar et al. 2011; Garagounis et al. 2011). Basically, the solid electrolytes are characterized according to the conduction ions. Among these ions, proton ( $H^+$ ), oxygen ( $O^{2-}$ ), lithium ( $Li^+$ ), copper ( $Cu^+$ ), sodium ( $Na^+$ ), silver ( $Ag^+$ ), and fluorine ( $F^-$ ) are very common (Stoukides 1988) (Table 2.3). However, as seen in Table 2.3, metal oxides are mainly oxygen and proton conductors.

It is also necessary to take into account that the process of solid electrolyte doping differs from the doping process peculiar to semiconductors. Studies of doping solid electrolytes resulted in some general rules with regard to the effect on the transport and phase stability properties (Weppner 2000). These are:

1. p- and n-type conducting dopants increase the partial hole and electron conductivity, respectively, in the case where there is about the same activity of the anionic component, e.g., oxygen. This rule is quite independent of the crystal structure and chemical environment.
2. The ionic conductivity commonly decreases by the addition of dopants because of entropy effects and local lattice distortions. The magnitude of solid solubility of the dopant seems not to be related directly to the lattice distortion, however.
3. The diffusion coefficients of the electronic charge carriers and mobile ions are related to each other. Both decrease with increasing amounts of dopants.
4. The electrochemical redox potentials are obviously not changed by the dopant as compared to the undoped electrolyte.
5. The dopants control the phase formation based on the valence of the dopant. Aliovalent dopants generate vacancies which may be necessary for specific structures.

### 2.3.1 Criteria for Metal Oxide Application in Solid Electrolyte-Based Gas Sensors

Numerous experimental studies have shown that for electrochemical sensors to be acceptable for gas sensor market, solid electrolytes should satisfy the following requirements (Thangadurai and Weppner 2006; Amar et al. 2011).

**Table 2.3** Typical examples of ion-conducting electrolytes

Predominant conducting ion	Compounds
Fluorine ( $F^-$ )	$CaF_2$ ; $MgF_2$ ; $PbF_2$ ; $NaF$ ; $SrF_2$
Silver ( $Ag^+$ )	$\alpha$ - and $\beta$ - $AgI$ ; $AgCl$ ; $AgBr$ ; $Ag_3SI$
Oxygen ( $O^{2-}$ )	$Zr_{1-x}M_x^{2+}O_{2-x}$ ; $Zr_{1-x}M_x^{3+}O_{2-(x/2)}$ ; $Th_{1-x}M_x^{2+}O_{2-x}$ ; $Th_{1-x}M_x^{3+}O_{2-(x/2)}$ ; $La_{0.9}Sr_{0.1}Ga_{0.8}Mg_{0.2}O_{2.85}$
Sodium ( $Na^+$ )	$\beta$ - $Na_2O \cdot 11Al_2O_3$ ; NASICON
Lithium ( $Li^+$ )	LIPON; $Li_{1+x}Al_xTi_{2-x}(PO_4)_3$ ; $La_{0.51}Li_{0.34}TiO_{2.94}$
Proton ( $H^+$ )	$SrCe_{1-x}Yb_xO_3$ ; $BaCe_{1-x}Gd_xO_3$ ; $SrZr_{1-x}In_xO_3$ ; $CaZr_{1-x}In_xO_3$ ; $BaZr_{1-x}Yb_xO_3$
Bromine ( $Br^-$ )	$CsPbBr_3$
Chlorine ( $Cl^-$ )	$CsPbCl_3$

LIPON lithium phosphorus oxynitride, NASICON sodium super-ionic conductor

Source: Data from Park et al. (2003), Iwahara (2009), etc.

To be used successfully in a chemical sensor, conduction in the ionic conductor should preferably:

- Be highly specific to one ion only; i.e., the transference number of this ion should be equal to unity. If the electrolyte in a potentiometric sensor is not specifically conductive, a mixed potential may arise and the EMF may not respond uniquely to the target component.
- The electrolyte materials at the operating temperatures (400–1,000 °C) should exhibit high ionic conductivity in the range of  $>10^{-2}$  S cm<sup>-1</sup> in order to minimize the ohmic losses.
- The electronic contribution to conductivity must also be negligible, as otherwise ions will be transferred across the electrolyte and the EMF will be reduced. It is furthermore important for reproducibility that both electrolyte/electrode interfaces reach equilibrium.
- Mechanical strength and chemical (electrochemical) stability without structural phase transition and decomposition in both oxidizing/reducing environments are properties, which are required for solid electrolytes as well. In particular, solid electrolytes should be stable in an atmosphere containing moisture and CO<sub>2</sub>.
- The solid electrolyte must be highly dense in order to be gas tight. Pore-free material should have good adhesion to both anode and cathode. Electrolyte–electrode interfaces must have negligible charge transfer resistances.
- The electrolyte material should possess high stability against chemical reactions with anode, cathode, and sealing materials over an extended period of operation time.
- The thermal expansion coefficients of the electrolyte must be matched to that of both electrodes used in the sensor structure to give stable interfaces and prevent material failure of the electrolyte due to the thermal expansion mismatch with other cell components.
- The cost of raw materials and fabrication should be as low as possible. The nontoxicity of raw materials is also advisable.

We need to say that the requirement of a “pure” ion for conducting is the most difficult for fulfillment, because, in this case, the level of any electronic contribution to the total electrical conductivity must be negligible. However, this is not at all easy to achieve. Even very low concentrations of electronic carriers will give rise to a significant electronic component because of the very high mobility of electrons and holes in comparison with the ionic mobilities. Therefore, most ion conductors are, in fact, mixed conductors, and only very few are capable of being classed as pure ionic conductors.

### 2.3.2 High-Temperature Oxygen Sensors

The oxygen sensor is the main field of solid electrolyte-based sensors application. Monitoring oxygen under ambient conditions and especially as dissolved oxygen is necessary in medical, food processing, waste management industries, etc. However, the predominant use of oxygen sensors is in the control of air–fuel mixtures in the combustion engine of the automobiles and is an integral part of the “on-board diagnostic” (OBD) facility of the exhaust emission control system. The oxygen sensor, sometimes called exhaust gas oxygen (EGO) or lambda sensor, is usually a potentiometric-type sensor.

Solid-state potentiometric oxygen sensors typically use an oxygen ion-conducting material as electrolyte. Many metal oxides have been investigated from this viewpoint (Tuller 2000; Stefanik and Tuller 2001; Toan et al. 2003; Litzelman et al. 2005; Rothschild et al. 2005; Rothschild and Tuller 2006; Moos et al. 2011). Table 2.4 provides a partial list. The fluorite oxides are the classical oxygen ion-conducting oxide materials (Skinner and Kilner 2003). The crystal structure consists of a simple cubic oxygen lattice with alternate body centers occupied by eight coordinated cations. The general formula of a fluorite oxide is AO<sub>2</sub>, where A is a large tetravalent cation. The materials that readily form in the fluorite crystal structure are uranium dioxide (UO<sub>2</sub>), thorium dioxide (ThO<sub>2</sub>), and ceria



**Table 2.4** Electrical conductivity values of solid oxide electrolytes at 600 °C

Oxygen ion-conducting solid electrolytes	Conductivity (S cm <sup>-1</sup> )
Bi <sub>2</sub> O <sub>3</sub>	3 × 10 <sup>-3</sup>
Gd <sub>2</sub> O <sub>3</sub> doped CeO <sub>2</sub>	4 × 10 <sup>-3</sup>
Bi <sub>2</sub> Cu <sub>0.1</sub> V <sub>0.9</sub> O <sub>5.35</sub>	1 × 10 <sup>-1</sup>
YSZ (8 mol.% Y <sub>2</sub> O <sub>3</sub> )	5 × 10 <sup>-2</sup>

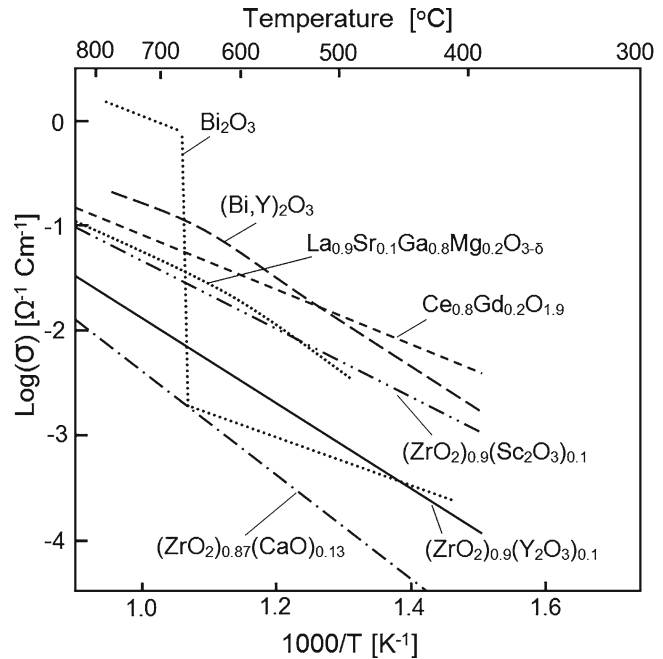
Source: Data from Ramamoorth et al. (2003)

(CeO<sub>2</sub>). The Zr<sup>4+</sup> cation is too small to sustain the fluorite structure and only forms either at high temperatures or when the zirconium ion is partially substituted with another (usually larger) cation. Borrowing terminology from semiconductor technology, this substitution is known as doping. Doping is usually performed by substituting lower valence cations into the lattice, with the added effect of introducing oxygen vacancies to maintain overall charge neutrality. These oxygen vacancies supply the equivalent sites allowing the oxygen ions to migrate, as mentioned above, and are the prerequisite for high ionic conductivity. A further peculiar feature of the fluorite structure is that it is able to sustain a high degree of substitution and consequent non-stoichiometry, making these very highly disordered materials. These MOXs satisfy a number of the above-mentioned criteria including high oxygen ion conductivity, low electronic conductivity, high density, mechanical strength, thermal shock resistance, and chemical compatibility with electrodes and/or substrates.

Experiments have shown that, in principle, all the oxides indicated above can work as high-temperature oxygen sensors (Logothetis 1980). The operation of an oxide in this temperature range is limited only by parameters such as insufficient conductivity, slow oxygen diffusion, and bad stability of the material. For example, fluorite-related solid oxygen ion conductors, such as  $\delta$ -bismuth sesquioxide (Bi<sub>2</sub>O<sub>3</sub>) and cerium oxide (CeO<sub>2</sub>), have the advantage of higher ionic conductivity at lower temperatures (Kharton et al. 2001). The ionic conductivity of some of the most promising oxide ion conductors as a function of the temperature is shown in Fig. 2.3. In particular, the ionic conductivity of ceria-based metal oxides is approximately an order of magnitude greater than that of stabilized zirconia for comparable doping conditions. This is a result of the larger ionic radius of Ce<sup>4+</sup> (0.87 Å in sixfold coordination) than Zr<sup>4+</sup> (0.72 Å), which produces a more open structure through which O<sup>2-</sup> ions can easily migrate. However, the indicated metal oxides are characterized by lower chemical and structural stability and enhanced electronic conduction. An additional challenge related to use of CeO<sub>2</sub> lays with the chemical expansion of ceria under reducing conditions and the internal stress that results (Haile 2003). The same effects take place in Bi<sub>2</sub>O<sub>3</sub>. Kharton et al. (2001) have shown that limitations of Bi<sub>2</sub>O<sub>3</sub> application are connected with high reactivity, volatilization of bismuth oxide, easy reducibility at low oxygen pressure, low mechanical strength, and high thermal expansion. Phase transitions in the course of heating–cooling cycles lead to sharp volume changes of sintered Bi<sub>2</sub>O<sub>3</sub> ceramics. In addition, the stabilized  $\delta$ -Bi<sub>2</sub>O<sub>3</sub>-type phases decompose at temperatures below 870 K. Thorium oxide has traditionally been an attractive alternative to zirconia. It was established that thorium oxide exhibits higher oxygen sensitivity of conductance. However, research has shown that ThO<sub>2</sub> has a conductance that is inconveniently low (Jones et al. 1985). Moreover, modern legislation has now essentially banned further use of this material. Oxygen ion conduction may also be found to prevail in some pyrochlore, spinel, apatite, lanthanum silicates with the apatite structure, and perovskite structures. Excellent reviews are available on these types of solid electrolytes (Adachi and Imanaka 1995; West 1999; Kumar and Iwahara 2000; Haile 2003; Skinner and Kilner 2003; Kharton et al. 2004; Stolen et al. 2006; Traqueia et al. 2006; Ishihara 2009).

For example, one of the examples of oxygen ion conductors is the family of sesquioxides with the C-type cubic structure, namely, Y<sub>2</sub>O<sub>3</sub> (Marques and Wirtz 1991; Marques et al. 2006; Traqueia et al. 2006). These oxides form solid solutions with either divalent cations or tetravalent cations, compensated by formation of oxygen vacancies or oxygen interstitials, respectively. The versatility of this

**Fig. 2.3** The ionic conductivity of some of the most promising oxide ion conductors as a function of the temperature. [Data from Haile (2003)]



structure derives from the existence of large interstitial positions, similar in size to those occupied by the oxygen ions in normal positions. These interstitial positions form a continuous network throughout the lattice, suggesting an easy pathway for interstitial motion. However, the ionic conductivity observed for divalent-doped yttria is very much larger than the corresponding value observed for tetravalent-doped  $\text{Y}_2\text{O}_3$ . Besides a poor ionic conductivity, the activation energy for ionic motion in yttria-based solid solutions with a tetravalent dopant is also larger than for most competitive oxygen ion conductors. The same is true for other isostructural materials.

A family of materials with the apatite structure are also ionic conductors (Nakayama and Sakamoto 1998; Tao and Irvine 2001; Kharton et al. 2004). The ideal stoichiometry of these apatites is  $(\text{M}_1, \text{M}_2)_{10}(\text{XO}_4)_6\text{Z}_2$ , with all sites fully occupied (Nakayama and Sakamoto 1998). If we compare the formula of  $\text{La}_{10}(\text{SiO}_4)_6\text{O}_3$ , a reference for this new group of materials, with the ideal apatite composition, we realize that the metal site has excess positive charge, balanced in this case by one excess oxygen ion. With all normal lattice positions fully occupied, this oxygen must occupy an interstitial position, as confirmed by neutron powder diffraction. Not all normal oxygen sites are occupied, suggesting the formation of oxygen vacancies together with interstitial defects for some compositions. Furthermore, La deficiency apparently has an important role in the formation of interstitial oxygen defects, enhancing this process with respect to the metal stoichiometric materials. These results are coherent with the relatively high ionic conductivities found in materials with excess oxygen (more than 26 per formula) or with La deficiency. Besides their interesting performance in the low–intermediate temperature range, their cost is relatively low. However, as for other ionic conductors with dominant interstitial mechanism, the ionic conductivity of apatites is lower than in ionic conductors with highly symmetrical and highly disordered lattices with vacancy-migration mechanisms, such as fluorite-type  $\delta\text{-Bi}_2\text{O}_3$  and LSGM (Kharton et al. 2004).

The LAMOX family of oxide ion conductors, based initially on the  $\text{La}_2\text{Mo}_2\text{O}_9$  parent compound, are competitive with existing electrolytes at temperatures above 600 °C at which point there is an  $\alpha$ – $\beta$  phase transition (Lacorre et al. 2000). Associated with this transition is a dramatic improvement in the

**Table 2.5** Examples of stoichiometric and nonstoichiometric perovskite oxides

The perovskite structure $ABO_3$	
<i>Characterization</i>	
A–B combinations:	I–V in, e.g., $\text{KNbO}_3$ II–IV in, e.g., $\text{BaTiO}_3$ III–III in, e.g., $\text{LaMnO}_3$
Can also have vacancies on:	A site in, e.g., $\text{Na}_x\text{WO}_3$ B site in, e.g., $(\text{Ba}_{1-x}\text{La}_x)\text{Ti}_{1-x/4}\text{O}_3$ O site in, e.g., $\text{CaMnO}_{3-x}$
Basic crystal structure:	Octahedral B, 12-coordinate A, cubic unit cell ideally
Properties:	Properties depend on chemical constituents, local coordination environments, and defect structure
Isovalent doping:	e.g., $\text{Al}_2\text{O}_3:\text{Cr}^{3+}$ in $(\text{Al}_{2-x}\text{Cr}_x)\text{O}_3$ Ruby color depends critically on $x$ : local structure of $\text{Cr}^{3+}$ within $\text{Al}_2\text{O}_3$ crystal lattice
Aliovalent doping:	Introduce ions of different charge; need charge compensation to preserve electroneutrality Doping can generate vacancies, interstitials, and mixed valence

*Source:* Data from West (2006)

ionic conductivity by approximately two orders of magnitude, such that a value of  $0.03 \text{ S cm}^{-1}$  was achieved at  $\sim 720^\circ\text{C}$ . Unfortunately, the Mo content of this material leaves it susceptible to reduction and phase transitions (Collado et al. 2002), and therefore, significant development of this material is needed before it is commercially useful, either as an electrolyte in fuel cells or indeed as an oxygen separator.

Typical perovskite oxides having the  $ABO_3$  structure are cerates, titanates, and zirconates (Ishihara 2009). The perovskite structure contains two-size cations, which makes it amenable to a variety of dopant additions (Kreuer 2003; Thangadurai and Weppner 2006; West 2006). This doping flexibility allows control of the transport and catalytic properties to optimize sensor performance for particular applications (Moos et al. 2011). Table 2.5 presents examples and general characterization of stoichiometric and nonstoichiometric perovskite oxides. Given the large difference in size of the A and B ions, most cations in the periodic table are able to enter one or other site in the perovskite structure, giving enormous possibilities for property modification, leading to the labeling of perovskite as an “inorganic chameleon” (West 2006). Within the large family of materials that have the same basic perovskite structure, it is possible to encounter almost any physical property imaginable, as shown for a selection of materials and properties in Table 2.6.

Highly conductive perovskites derived from  $\text{LaGaO}_3$  (LSGM), usually doped with Sr in the A site and Mg in the B site, contain large concentrations of oxygen vacancies, the mobile defect involved in oxygen transport (Tao et al. 2000). The close packing of ions in this structure leaves no room for formation of oxygen interstitial defects. In the case of perovskites, the most obvious pathway for oxygen ion hopping is through a triangle formed by two large A-cations and one small B-cation (Kharton et al. 2004; Traqueia et al. 2006). Perovskite-type  $ABO_3$  phases derived from lanthanum gallate,  $\text{LaGaO}_3$ , possess a higher ionic conductivity than that of stabilized zirconia and are thus promising materials for gas sensors operating in the intermediate temperature range, 770–1,100 K. However, the concentration of transition-metal dopants should be limited to below 3–7% as further additions lead to increasing electronic and decreasing ionic conductivities. Disadvantages of  $\text{LaGaO}_3$ -based materials include possible reduction and volatilization of gallium oxide, formation of stable secondary phases in the course of processing, the relatively high cost of gallium, and significant reactivity with perovskite electrodes under oxidizing conditions as well as with metal anodes in reducing conditions (Kharton et al. 2004).

**Table 2.6** A selection of materials with the perovskite structure illustrating the enormous range of properties found in different materials with the same basic crystal structure

Perovskite: an inorganic chameleon	
Oxide	Physical property
CaTiO <sub>3</sub>	Dielectric
BaTiO <sub>3</sub>	Ferroelectric
Pb(Mg <sub>1/3</sub> Nb <sub>2/3</sub> )O <sub>3</sub>	Relax or ferroelectric
Pb(Zr <sub>1-x</sub> Ti <sub>x</sub> )O <sub>3</sub>	Piezoelectric
(Ba <sub>1-x</sub> La <sub>x</sub> )TiO <sub>3</sub>	Semiconductor
(Y <sub>1/3</sub> Ba <sub>2/3</sub> )CuO <sub>3-x</sub>	Superconductor; O <sup>-</sup> ion conductor
Na <sub>x</sub> WO <sub>3</sub>	Mixed conductor (Na <sup>+</sup> , e <sup>-</sup> ); electrochromic
SrCeO <sub>3</sub> :H	Proton conductor
LaMnO <sub>3-x</sub>	Mixed conductor (O <sup>-</sup> , e <sup>-</sup> )
Li <sub>0.5-3x</sub> La <sub>0.5+x</sub> TiO <sub>3</sub>	Li <sup>+</sup> ion conductor
A MnO <sub>3-δ</sub>	Giant magnetoresistor

Source: Data from West (2006)

The conductivity of ion-conducting perovskite oxides is strongly dependent on the operating temperature. Experiments have shown that perovskites become sufficiently conductive only at temperatures exceeding 400 or 600 °C. In this temperature range, up to more than 1,000 °C, they have high ionic conductivity and good gas-sensing properties. It was established that thick films of perovskite compounds have rather high response to partial pressures of oxygen and some reducing gases (Miura et al. 1989). The perovskites are advantageous for practical applications in oxygen sensors because of (1) great chemical stability at high and low oxygen partial pressures, from 1 bar to 10<sup>-13</sup> bar, (2) adequate oxygen sensitivity of the electrical resistance, and (3) excellent reversibility of the electrical properties under oxygen absorption/desorption. The melting and decomposition temperature of perovskites is high enough to keep stable both the microstructure and the morphology that are necessary for long-term sensor operation. Usually, embedding a fourth chemical element into perovskite oxides is done to control the conductivity. For example, doping of SrCeO<sub>3</sub> with 5% of Yb<sup>3+</sup> allows one to obtain a maximum of ionic conductivity (Scherban and Nowick 1989).

However, it is necessary to recognize that at present the lion's share of the oxygen sensor market is held by ZrO<sub>2</sub>-based sensors (Tuller 2000; Park et al. 2009; Lopez-Gandara et al. 2009). Zirconium oxide (ZrO<sub>2</sub>) sensors, otherwise known as high-temperature electrochemical sensors, consist of a cell made of yttria-stabilized zirconia ceramic. Yttria-stabilized zirconia (YSZ) is the best-known solid electrolyte with the fluorite structure (Traqueia et al. 2006). The ionic motion in fluorite-based systems is the well-established vacancy-based mechanism, where one vacancy shifts position with a neighboring oxygen ion in a normal lattice position (Fig. 2.4). So, in this system, oxygen vacancies move to neighboring oxygen ion positions. The easiest jump is along the edge of the cube formed by eight oxygen ions/vacancies. Optimization of oxygen transport can be addressed based on simple considerations on dopant size, charge, and concentration. In particular, in stabilized cubic zirconia (e.g., Zr<sub>1-x</sub>Y<sub>x</sub>O<sub>2-x/2</sub>), the disorder is induced by the addition of aliovalent elements (see Fig. 2.5). For comparison, the high-temperature phase of bismuth oxide contains intrinsic oxygen vacancies. The structure of δ-Bi<sub>2</sub>O<sub>3</sub> is similar to the fluorine structure with one quarter of the anion sites vacant and is formed at temperatures above 730 °C.

Nevertheless high concentration of oxygen vacancies in doped ZrO<sub>2</sub>, temperatures of the order of 900–1,000 °C are required to reach levels of ionic conductivity of ~0.1 S cm<sup>-1</sup> needed for achievement of required gas sensor parameters (Tuller 2000). To avoid lattice distortion and strong defect association, host and dopant cations should have similar sizes and minimum charge difference. High concentrations of defects increase defect interaction and decrease the ionic conductivity (Subbarao and Maiti 1984).

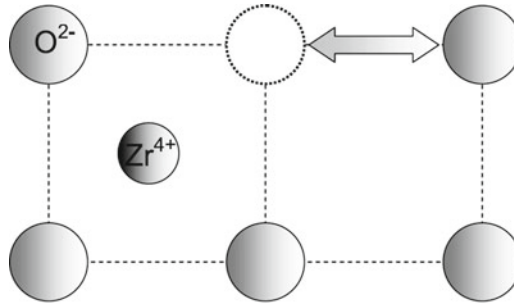
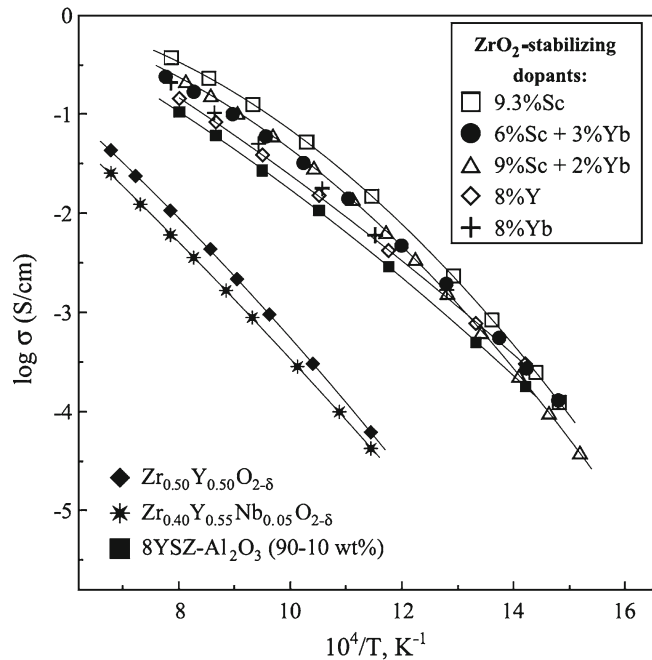


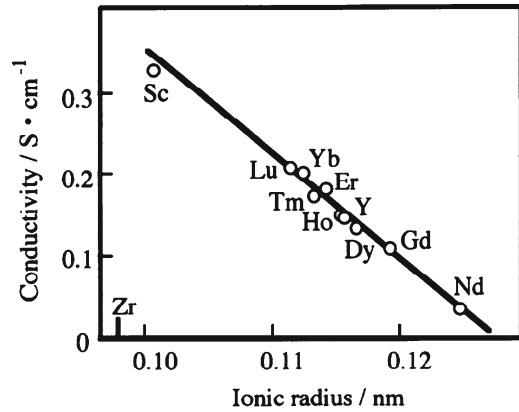
**Fig. 2.4** Schematic view of the vacancy motion mechanism in the fluorite-type structure. Ionic positions are shown as *filled circles*, while the oxygen vacancy is shown as an *empty circle* within a *dashed line*. The metal cation is located below the plane containing the anions, in the center of a cube formed by eight oxygen ions/vacancies. [Idea from Traqueia et al. (2006)]

**Fig. 2.5** Total conductivity of  $\text{ZrO}_2$ -based solid electrolytes in air. (Reprinted with permission from Kharton et al. (2004). Copyright 2004 Elsevier)



We need to note that the necessity of zirconia (zirconium oxide) stabilization follows from the phase instability of pure  $\text{ZrO}_2$  (Imanaka and Adachi 1997). It was established that pure zirconia exists in a monoclinic form at room temperature. It transforms to a tetragonal phase at elevated temperatures, around 1,100 °C. On further heating, tetragonal  $\text{ZrO}$  undergoes another phase transition to a cubic form at temperature equaled 2,370 °C. At the first transition, the cell volume of the oxide shrinks by almost about 4%. Therefore, by cooling the sample after heating at high temperature for sintering, cracks appear in the oxide bulk, which degrades the sample. Such a behavior is a crucial limitation in practical applications. In order to maintain the high-temperature cubic phase, one appropriate way is to substitute the Zr site in  $\text{ZrO}_2$  with another cation and thereby keep the cubic phase in a wider temperature range. Here, the candidate ions are trivalent rare earths and divalent alkali earths, for example, CaO (Etsell and Flengas 1970). The substitution of the Zr site with a lower valent ion

**Fig. 2.6** Electrical conductivity change upon mixing of various rare-earth ions in ZrO at 1,273 K. (Reprinted with permission from Imanaka and Adachi (1997). Copyright 1997 Elsevier)

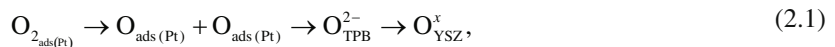


introduces oxide vacancies in the bulk and contributes very much to both holding the cubic phase even at room temperature and to enhancing the oxide ion conductivity. Because the vacancies cause the crystal to shrink, it is necessary to dope a larger cation compared with Zr ion in the Zr site. The structures of cubic zirconia and C-type rare-earth oxide are closely similar, and this resemblance accounts for the high solubility of rare-earth oxides in cubic ZrO<sub>2</sub>.

Other rare-earth oxides, such as Gd<sub>2</sub>O<sub>3</sub> and Lu<sub>2</sub>O<sub>3</sub>, can also be used for ZrO<sub>2</sub> stabilization. These oxides have the same crystal structures as Y<sub>2</sub>O<sub>3</sub> and cations, which are comparable in size to Y or smaller than Y<sup>3+</sup> (Etsell and Flengas 1970). The rare-earth oxides such as Ce<sub>2</sub>O<sub>3</sub>, Pr<sub>2</sub>O<sub>3</sub>, and Tb<sub>2</sub>O<sub>3</sub> are not valency stable and have been purposely omitted from consideration even though a stable cubic solid solution can be formed between these oxides and ZrO<sub>2</sub>. These cations are easily oxidized to the tetravalent state, which renders them unsuitable as solid-state electrolyte constituents, because electronic conduction appears in addition to ionic conduction. In the series of rare-earth oxides, Sc<sub>2</sub>O<sub>3</sub> is an interesting dopant because of the similar radii between Zr and Sc<sup>3+</sup> ions. The ionic conductivity of the solid solution is the highest among the ZrO<sub>2</sub>-R<sub>2</sub>O<sub>3</sub> solid solutions, as shown in Fig. 2.6. However, the lower stability of the solid solution restricts practical application (Imanaka and Adachi 1997).

Typical construction and its output characteristics of ZrO<sub>2</sub>-based sensors are shown in Fig. 2.7. The cell in oxygen sensors is usually shaped like a test tube where the inner and outer surfaces are each coated with ultrathin layers of porous platinum which act as the cathode and anode electrodes. The output of this potentiometric sensor is due to the combined effect of chemical and electrical processes. At high temperatures >650 °C, zirconium dioxide exhibits two mechanisms (Park et al. 2009): (1) ZrO<sub>2</sub> partly dissociates to produce oxygen ions, which can be transported through the material when a voltage is applied and (2) ZrO<sub>2</sub> behaves like a solid electrolyte for oxygen.

When the sensor is exposed to a test gas environment, the oxygen molecules get adsorbed onto the porous electrode, commonly made of platinum, and dissociate into atomic oxygen. Then the oxygen atoms diffuse into the boundary of the electrode (Pt), electrolyte (YSZ), and the gas called the “triple phase boundary” (TPB), where electron transfer takes place from the electrode to the atomic oxygen forming O<sup>2-</sup> ions (reduction). The overall electrode reactions are as follows (Robertson and Michaels 1990; Mitterdorfer and Gauckler 1999):



All the reaction steps in Eq.(2.1) can be represented in a simpler form as



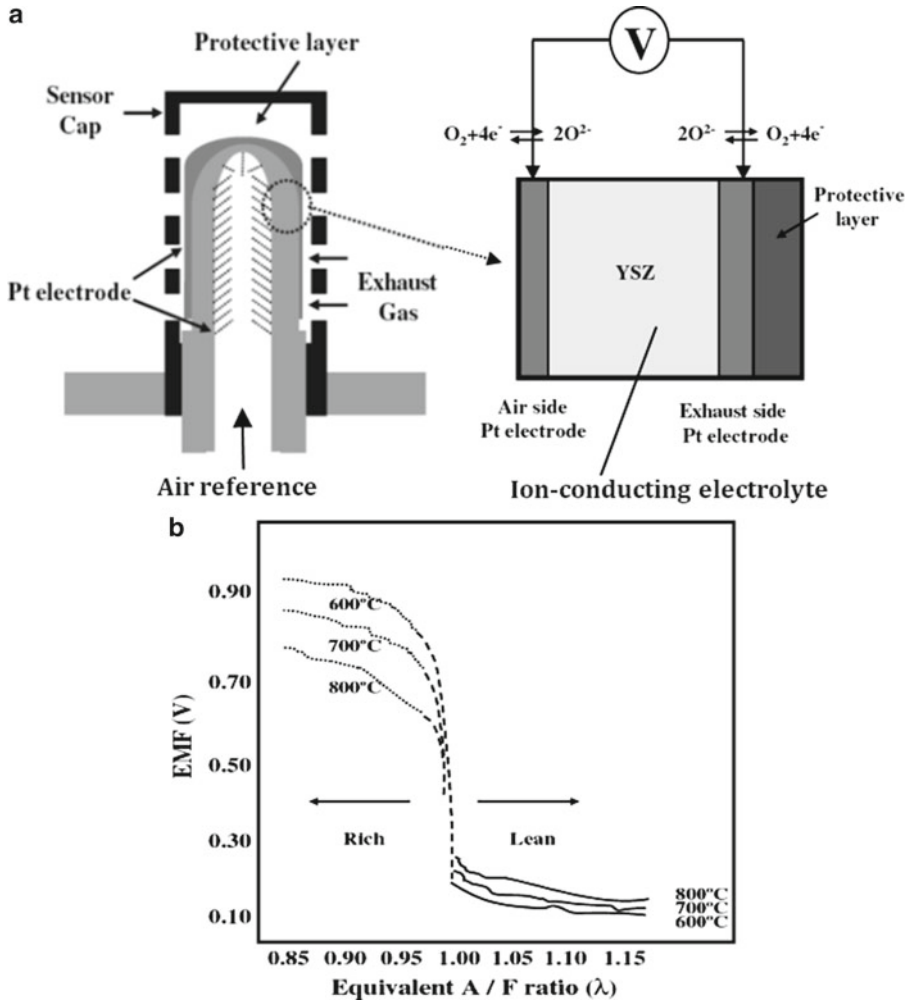


**Fig. 2.7** Cross-sectional view of EGO sensor with its output characteristics: (a) the sensor geometry; (b) *emf* response (Reprinted with permission from Park et al. (2003, 2009). Copyright 2003 and 2009 Springer)

Thus, when a sample gas is introduced on one side, oxygen ions migrate within the crystal lattice to form a concentration gradient from the higher  $O_2$  partial pressure side to the lower pressure side. The gradient is determined by the ratio of the  $O_2$  partial pressures between a sample gas on one side of the lattice and a reference gas (typically ambient air) on the other side of the lattice. This concentration gradient of oxygen ions within the  $ZrO_2$  lattice produces a voltage potential between the two platinum electrodes, which can be expressed in terms of the difference between the chemical potentials of oxygen at two electrodes according to the Nernst equation

$$U = \frac{RT}{4F} \cdot \ln \left( \frac{pO_{2, \text{measure}}}{pO_{2, \text{reference}}} \right) \quad (2.3)$$

where  $R$  is the gas constant,  $F$  is the Faraday constant,  $T$  is temperature in K, and  $pO_2$  is oxygen partial pressure.

In order to facilitate processes involved in Eq. (2.1), the electrode needs to be a good catalyst for oxygen reduction and oxidation. The electrode microstructure needs to be porous to manifest enough triple phase boundaries, and the electrolyte needs to be a good oxygen ion conductor at the operating temperature of the device (Ramamoorth et al. 2003). The sensitivity of the equilibrium potentiometric sensors is given by  $RT/4F$  and depends only on temperature, provided the electrolyte is a pure ionic conductor. On the other hand, the response time is influenced by rate constants involved in Eq. (2.1). The slowest process will be the rate-determining step for the response time of the sensor.

Since the 1980s, oxygen sensors have also been designed in planar type. Although the planar structure requires lower size, lower power consumption for the heating element, and lower fabrication costs and enables better stability in the measurements, the physical principles governing the behavior of the sensors are essentially the same in both thimble and planar types (Tuller 2000; Park et al. 2009). Some planar sensors work with no air reference in one of their electrodes (Lopez-Gandara et al. 2009).

It was established that zirconium oxide oxygen analyzers have fast speeds of response. Also, due to the high operating temperature requirement, they make an ideal choice for oxygen measurements in combustion applications because the sensor can be inserted into the stack or exhaust directly for in situ measurements. For example,  $ZrO_2$ -based sensors are suitable for gasoline engines that work optimally at the stoichiometric air-to-fuel ratio (Rothschild and Tuller 2006). Because combustion applications measure percent  $O_2$  levels, the error caused by catalytic reaction of the residual hydrocarbons in the post-combustion gas is not significant. The major disadvantages of the zirconium oxide sensors are the relatively short life span and high replacement cost. Sensors typically require replacement every 12–24 months of continuous use due to the gradual diffusion of the platinum of the electrodes into the  $ZrO_2$  crystal lattice, eventually shorting the two electrodes together (Delta Corporation *n.d.*). In addition, given their relatively low sensitivity to variations in the oxygen partial pressure ( $pO_2$ ), these sensors are not well suited to trace  $O_2$  analysis.

### 2.3.3 Solid Electrolyte-Based Hydrogen Sensors

The majority of solid electrolyte  $H_2$  sensors are based on proton conductors (Miura et al. 1989, Alberti and Casciola 2001). Metal oxides that can potentially meet the requirements for application in solid electrolyte  $H_2$  sensors are listed in Table 2.7. These proton conductors typically do not have high porosity but rather can reach 96–99% of the theoretical density (Jacobs et al. 1993). Similar to oxygen sensors, solid-state electrochemical cells for hydrogen sensing are typically constructed by combining a membrane of solid electrolyte (proton conductor) with a pair of electrodes (electronic conductors). Most of the  $H_2$  sensors that use solid electrolytes are operated potentiometrically. The voltage produced is from the concentration dependence of the chemical potential, which at equilibrium is represented by the Nernst equation (Eq. 2.3).

Experiments have shown that metal oxide-based solid electrolyte  $H_2$  sensors can operate in wide range of temperatures from RT to 1,000 °C (Alberti et al. 2001, Fergus 2007c). In particular, layered perovskite oxides such as  $ACa_2Nb_3O_{10}$ , where A is an alkali metal, are promising candidates for designing low-temperature  $H_2$  sensors (Nowick et al. 1999; Thangadurai and Weppner 2001a, b). It was found that  $KCa_2Nb_3O_{10}$ -based sensors are able to work in the temperature range of RT–65 °C. In these niobates, the A atom is sandwiched between  $Ca_2Nb_3O_{10}$  perovskite slabs composed of corner-sharing  $NbO_6$  octahedral and Ca ions. The electrical conductivity has been explained to be due to the migration of alkali metal ions in interlayer conduction paths (Toda et al. 1996). However, when the compound is exposed to hydrogen, a large increase in the ionic conductivity is observed. This is attributed to the added mobility of protons. For example, 2D-layered  $KCa_2Nb_3O_{10}$  exhibits an electrical conductivity of  $3.2 \times 10^{-4} \text{ S cm}^{-1}$  with activation energy of 0.25 eV at 45 °C in an  $H_2$  atmosphere (Thangadurai and Weppner 2001a, b). Proton conductivity in  $H_2$  is commonly understood by assuming point defects according to the specific defect equations for  $KCa_2Nb_3O_{10}$  under hydrogen atmosphere as follows:

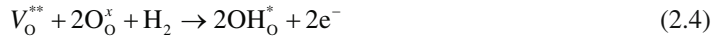


**Table 2.7** Metal oxide solid electrolytes used in electrochemical H<sub>2</sub> gas sensors

Metal oxide solid electrolytes	Temp. of stability (°C)	Type of gas sensor
YSZ	>1,000	P
$\alpha$ -Al <sub>2</sub> O <sub>3</sub> :Mg	>1,500	
Ce <sub>0.8</sub> Gd <sub>0.2</sub> O <sub>1.9</sub>	>1,000	P
<i>Perovskites:</i>		
SrCeO <sub>3</sub> (SrCeO <sub>3</sub> :Yb)	>1,000	C, P
CaZrO <sub>3</sub> (CaZrO <sub>3</sub> :In)	>1,000	P
BaCeO <sub>3</sub>	>1,000	P
BaCe <sub>0.8</sub> Gd <sub>0.2</sub> O <sub>3</sub>	>1,000	P
BaZr <sub>0.4</sub> Ce <sub>0.4</sub> In <sub>0.2</sub> O <sub>3</sub>	>1,000	
Ba <sub>3</sub> Ca <sub>1.18</sub> Nb <sub>1.82</sub> O <sub>9.6</sub>	>1,000	P
KCa <sub>2</sub> Nb <sub>3</sub> O <sub>10</sub>	>1,000	P

*P* potentiometric, *A* amperometric, *C* conductometric

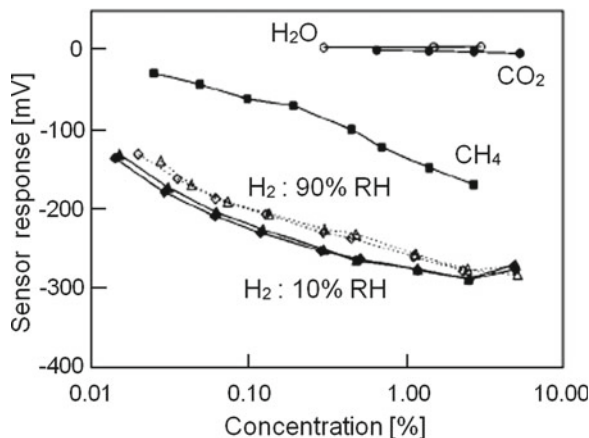
Source: Data from Korotcenkov et al. (2009c)



where  $V_O^{**}$ ,  $O_O^x$ ,  $e^-$ ,  $h^*$ ,  $H^*$ ,  $OH_O^*$ ,  $H_K^*$ , and  $H_i^*$  represent oxygen vacancy, lattice oxygen, excess electrons, holes, protons, protons attached to lattice oxygen, protons at a vacant  $K$  site in the lattice, and interstitial protons, respectively. The proton conductivity mechanism in acceptor-doped 3D perovskite oxides due to the migration of hydroxyl ions or protons has been described in detail (Bonanos 2001). The  $KCa_2Nb_3O_{10}$ -layered perovskite contains neither oxygen vacancies nor structural protons nor water, but yet behaves as an electrolyte. Amperometric-type H<sub>2</sub> sensors using  $KCa_2Nb_3O_{10}$  have been described (Sakhthivel and Weppner 2007). The sensitivity of this type of sensor is highly influenced by the electrode particle size and the operating temperature. The optimum particle size of 300–500 nm and a Pt loading of 1.85 mg cm<sup>-2</sup> were found to have high catalytic activity and be useful for H<sub>2</sub> detection. The best operating temperature for the sensor appeared to be about 45 °C with respect to long-term stability, and at this temperature, the sensor exhibited reproducible results in 1–8 % H<sub>2</sub>.

However, we have to note that most metal oxide-based solid electrolyte H<sub>2</sub> sensors were designed for operation at high temperatures. Specific advantages of high-temperature solid-state potentiometric hydrogen sensors include accuracy and sensitivity, rugged construction, and the wide concentration range that can be measured. The use of ceramic solid electrolytes in electrochemical gas sensors at elevated temperatures allows for the detection of H<sub>2</sub> under harsh conditions where typical aqueous electrolytes, liquids, or polymeric materials cannot be used. For example, because of the exceptional

**Fig. 2.8** Response at 500 °C of an aged ITO/YSZ/Pt sensor with an ~13 μm ITO electrode; H<sub>2</sub> in 10% (closed symbols) and ~90% (open symbols) RH. The two curves at each humidity level represent before (diamonds) and after (triangles) 18 h at 90% relative humidity. Responses to CH<sub>4</sub>, CO<sub>2</sub>, and H<sub>2</sub>O are also shown (Reprinted with permission from Martin and Glass (2005). Copyright 2005 The Electrochemical Society)



thermal and chemical stability of the materials, a hydrogen sensor for molten metals has been developed and widely used in process control in the metal melting industry (Yajima et al. 1995; Nishimura et al. 1996; Fukatsu et al. 1998). In order to produce high-quality castings it is necessary to reduce the hydrogen concentration in the molten metals during the casting process to an acceptable level, and a hydrogen sensor provides important process control data (Yajima et al. 1995). The high operating temperature frequently reduces the RH influence that is bothersome in many sensing applications. This advantage can be clearly seen if one considers the performance of potentiometric sensors using the ITO/YSZ/Pt system (Martin and Glass 2005). In Fig. 2.8, the response to H<sub>2</sub> at 500 °C for a sensor with a 13-μm ITO electrode is shown after aging in air for over 100 h at 500 °C. These measurements were carried out in the atmosphere with 10% (closed symbols) and 90% (open symbols) relative humidity. Each pair of curves represents measurements taken before and after 18 h at 90% relative humidity. These data indicate that the sensor is fairly insensitive to relative humidity in the 10–90% range, with a change in response of <10% (decreasing with increasing humidity) and no visible hysteresis on cycling the humidity. In addition, the sensor response is stable and reproducible in this humidity range over the duration of the test.

Typical solid electrolytes for high-temperature H<sub>2</sub> sensors include YSZ and perovskite oxides, such as SrCeO<sub>3</sub>, SrCeO<sub>3</sub>/Yb, SrCeO<sub>3</sub>/In, BaCeO<sub>3</sub>, BaCeO<sub>3</sub>/Gd, SrZrO<sub>3</sub>, BaZrO<sub>3</sub>, and CaZrO<sub>3</sub>, that become sufficiently conductive only when the temperature exceeds 400 °C (Tejuca and Fierro 1993; Hashimoto et al. 2001; Sundmacher et al. 2005; Fergus 2007a, b, c, 2008; Park et al. 2009; Amar et al. 2011). The ceramics of these perovskite-type oxide solid solutions exhibit p-type electronic (hole) conduction under oxidizing atmosphere free of hydrogen or water vapor at high temperatures. H<sup>+</sup> ion conductivities for several perovskites are shown in Fig. 2.9. Over a wide range of temperatures they have a high ionic conductivity with low activation energy at elevated temperatures (>700 °C) (Yajima et al. 1991; Nowick et al. 1999; Wakamura 2005). Ion conductivities of selected metal oxides in comparison with polymers are shown in Fig. 2.10. As a rule, the embedding of the fourth element is used to control conductivity; for example, in the case of SrCeO<sub>3</sub>/Yb, doping with 5% of Yb<sup>3+</sup> achieved the maximum of ionic conductivity. Y<sup>+3</sup>, In<sup>+3</sup>, Gd<sup>+3</sup>, or Nd<sup>+3</sup> can also be used for doping. As a rule, the concentration of a certain rare-earth element in perovskite-type oxide should be less than its upper limit of its solid solution formation range (usually less than 0.2) and represents the oxygen deficiency per unit formula.

Proton conductivity of metal oxides can be obtained if protonic defects exist. In perovskite-type oxides with proton conductivity, proton defects can have concentrations of a few mole percent or more. There are two mechanisms for proton conduction (Sundmacher et al. 2005). The first is proton hopping, also called the Grotthuss mechanism, in which the proton jumps between adjacent oxygen ions.

**Fig. 2.9** Total mass of constituent atoms in a unit cell vs the H<sup>+</sup> ion conductivity at 600 °C for several perovskite-type proton conductors. A least-squares *line* is drawn through the data. (Reprinted with permission from Wakamura (2005), Copyright 2005 Elsevier)

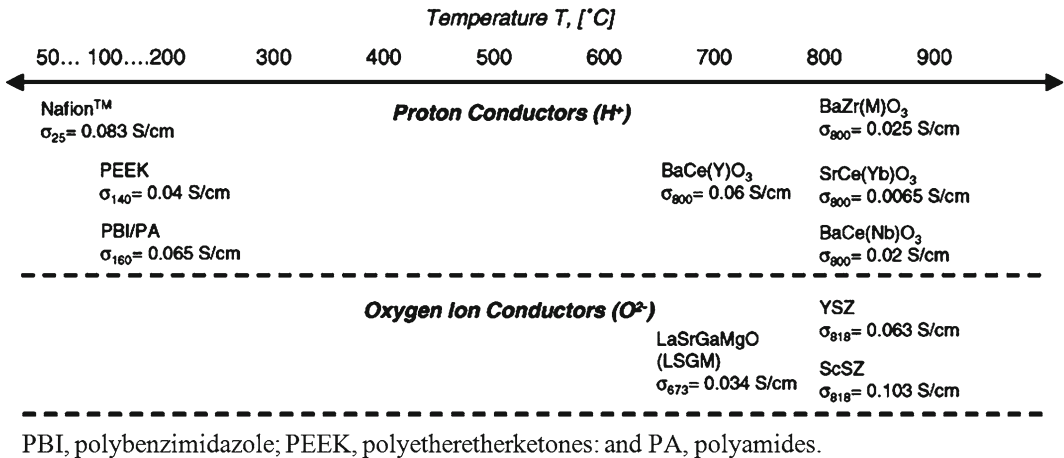
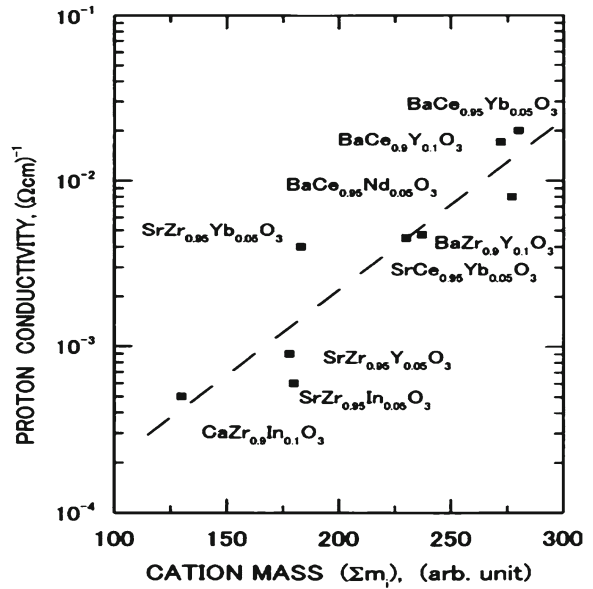
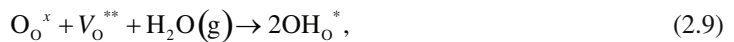


**Fig. 2.10** Ion conductivities of selected metal oxides in comparison with polymers (Reprinted with permission from Sundmacher et al. (2005). Copyright 2005 Elsevier)

The second mechanism is hydroxyl ion migration, also called the “vehicle” mechanism. Protonic defects can be formed by reaction between water molecules and oxygen vacancies according to the equation



where two effectively positive hydroxyl groups on regular oxygen positions are formed. Another important mechanism forming protonic defects is the reaction of hydrogen with electron holes according to

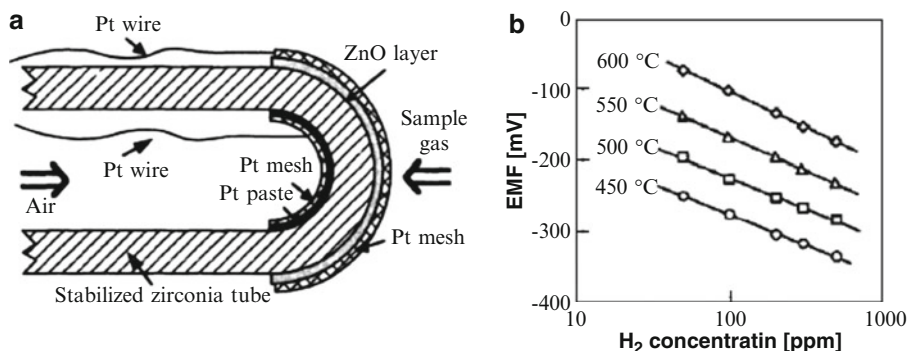


**Fig. 2.11** Mixed-potential-type  $H_2$  sensor using a YSZ and ZnO/Pt electrode. (a) Device structure with the ZnO layer deposited around the YSZ tube. (b) EMF as a function of concentration of  $H_2$  in air (Reprinted with permission from Lu et al. (1996a). Copyright 1996 Elsevier)

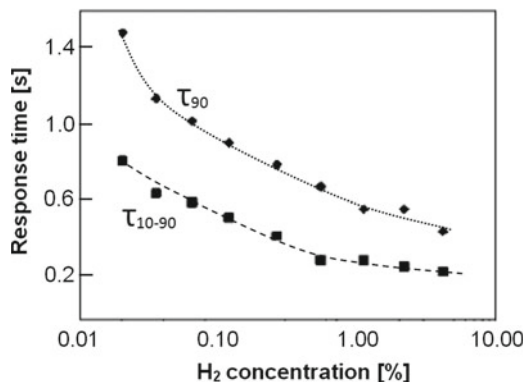


for which the presence of excess holes is obviously necessary.

An example of a high-temperature solid-state mixed-potential gas sensor designed for hydrogen detection and aimed at commercialization is given in Fig. 2.11a. The  $H_2$  sensors were fabricated by using a half-open, yttrium-stabilized zirconia tube (YSZ, 8 mol%  $Y_2O_3$  doped, NKT) (Lu et al. 1996a, b). The tube was 30 mm in length and 5 and 8 mm in inner and outer diameter, respectively. This design is essentially the same structure as that used for potentiometric YSZ oxygen sensors except that the sensing electrode on the outer surface is provided with a porous ZnO layer. The Pt mesh is designed to work as an electron collector. Pt black and Pt mesh were pressed on the inner surface of the YSZ tube at the closed end to form a reference electrode. This RE was always exposed to static atmospheric air. An oxide powder paste containing  $\alpha$ -terpineol and ethyl cellulose was applied belt like (width, 10 mm; total area, 2.5 cm<sup>2</sup>) on the outside of the tube, followed by calcination at 650 °C for 2 h, to form the sensing oxide layer. The oxide layer thus formed was porous and about 30  $\mu$ m thick. This device generated a fairly large EMF response to  $H_2$  in air at temperatures in the range 450–600 °C, as shown in Fig. 2.11b.

As seen in Fig. 2.8, the typical sensor is not responsive to  $H_2O$  and  $CO_2$  over the ranges tested. However, it is still not possible to achieve complete selectivity with high-temperature  $H_2$  sensor measurements. Various gases other than  $H_2$  can also be detected (Fig. 2.8) whenever they produce or consume protons through any electrode reaction. Typical examples are CO and  $NH_3$  (Miura et al. 2000) and especially various combustible hydrogen-containing gases including hydrocarbons ( $CH_4$ ,  $C_2H_6$ ,  $C_3H_8$ ,  $C_4H_{10}$ , etc.) (Martin and Glass 2005). Research has shown that the easiest way of resolving this problem is the creation of additional passive filters, preventing penetration of unwanted reacting molecules, and yet allowing the fast diffusing and very penetrating hydrogen to access the sensing surface. This would also suggest the use of time-dependent thermal, chemical, or electrical properties to sort out the various specific molecular interactions, as can be utilized in sensor arrays. For example, a Pd film has been used as a barrier to prevent chemical attack of the solid electrolyte by aggressive gases but allow hydrogen permeation for sensing (Jacobs et al. 1993). A solid Teflon membrane was used on low-temperature sensors (Chao et al. 2005), and certain ceramics and glasses only a few hundred nanometers thick (e.g.,  $SiO_2$  or  $Si_3N_4$ ) can also make an effective barrier for gases while allowing hydrogen to pass. While Pd is a most suitable material for a barrier, Pd can change crystal form in  $H_2$  (this effect is reduced by alloys with Ni or Ag) and can also change permeation rate with deposits on its surface. It remains a challenge to engineer a barrier that does not grossly slow the response time

**Fig. 2.12** Sensor response times as a function of  $H_2$  concentration measured from the baseline to 90% of the full response  $t_{(90)}$  and from 10 to 90% of the full response  $t_{(10-90)}$ ,  $T_{oper} = 500\text{ }^\circ\text{C}$  (Reprinted with permission from Martin and Glass (2005). Copyright 2005 The Electrochemical Society)



(theoretical calculations show that a 10 s slower response is expected if a Pd protection cap with a thickness of 0.25 mm is used) while greatly increasing the lifetime and retaining the sensitivity and stability of the measurement.

As a rule, high-temperature sensors have a fast rate of response (see Fig. 2.12). Response times of 2 s (Okamura et al. 2007) or even less than 1 s (at 500 °C) have been observed (Martin and Glass 2005). Such a response may be acceptable for hydrogen leak sensor applications (Glass et al. 2000).

In addition to the perovskite-type electrolytes, nonperovskite oxides including pyrochlores and fluorites exhibit protonic conduction at elevated temperatures under hydrogen-containing atmospheres (Shimura et al. 1996, 2001). Pyrochlore-type oxides have the general formula  $A_2B_2O_7$  with two types of cations ( $A^{3+}$  and  $B^{4+}$ ). Pyrochlores can be regarded as (A, B) $O_2$  fluorite structures depending on the cation radius ratio: when  $r^{3+}/r^{4+} > 1.22$ , it is considered as a pyrochlore ( $La_2Zr_2O_7$ ) while it is a fluorite structure otherwise ( $La_2Ce_2O_7$ ). Furthermore, at high temperature—generally as high as 1,377–2,227 °C—most pyrochlores disorder into fluorite structures (Kharton et al. 2004; Wang et al. 2005). Generally, these materials have attracted great attention as fast ionic conductors because of the presence of many non-occupied sites (Shimura et al. 1996; Wuensch et al. 2000).

Liang et al. (Liang and Nowick 1993; Liang et al. 1994) have shown that nonstoichiometric complex or mixed perovskite-type oxides of the formulas  $A_2B(1)_{1+x}B(2)_{1-x}O_{6-\delta}$  and  $A_3B(1)_{1+x}B(2)_{2-x}O_{9-\delta}$  can also be proton conductors upon exposure to  $H_2O$  vapor. Among them, the  $A_3B(1)_{1+x}B(2)_{2-x}O_{9-\delta}$  (A=Sr, Ba) compounds are particularly interesting because of their excellent protonic conductivity (Du and Nowick 1996). In addition, unlike Ce-based perovskites, these compounds have a wide band gap (Lecomte et al. 1984) and are superior insulators without producing detectable electronic conduction under either oxidizing or reducing gas mixtures up to 1,000 °C (Du and Nowick 1996).

The fluorite-type oxides are considered as the traditional oxygen ion-conducting electrolytes. The fluorite oxide has the general formula  $AO_2$  in which A is a large tetravalent cation. Examples of materials that easily adopt the fluorite structure are ceria ( $CeO_2$ ), uranium dioxide, and thorium dioxide (Skinner and Kilner 2003). It is worth bearing in mind that the protonic conductivity of these materials has been overlooked for a long time; however, Nigara et al. (1998) was the first to suggest the possibility of protonic conductivity. Since then, several subsequent pieces of research have been conducted to confirm this possibility (Sakai et al. 1999). According to Liu et al. (2006), the protonic conductivity of doped- $CeO_2$  electrolytes would lead to a lowering of the cell efficiency and fuel permeation which is not desirable for SOFC. However, it is a valuable property for hydrogen sensors. In particular, results presented by Mukundan et al. (1999) have shown that Pt/ $Ce_{0.8}Gd_{0.2}O_{1.9}$ /Au mixed-potential sensors can be used to detect  $H_2$  in a gas mixture of  $H_2$ -air. The sensor response was maximum for  $H_2$  and negligible for methane; other gases followed the trend methane < propane < CO, propylene <

hydrogen. Another novel protonic conductor is  $\text{BaZr}_{0.4}\text{C}_{0.4}\text{In}_{0.2}\text{O}_3$  (BZCI), a material that has practical durability in the presence of steam and has relatively high conductivity (Taniguchi et al. 2005). This material was able to produce a very stable  $\text{H}_2$  sensor at 800 and 1,000 °C in a wet but pure hydrogen atmosphere. The crystal structure and the composition of all samples did not change during a test with hydrogen. The actual EMFs almost coincided with the theoretical values below 800 °C but were lower than the theoretical values at 1,000 °C. Protonic conduction in BZCI was confirmed below 800 °C and seems to decrease at higher temperature.

### 2.3.4 Other Gases

We need to note that, besides oxygen and hydrogen, other gases can also be detected by sensors based on solid electrolytes. However, for these purposes sensors of Type II and Type III need to be used (Garzon et al. 2000). These mixed-potential sensors will be discussed in detail in Chap. 6 (Vol. 1). Usually these sensors are designed on zirconia-based electrolyte and metal-oxide electrodes acting as selective catalysts for target gas. Using the above-mentioned approach, sensors for detection of CO (Miura et al. 1998), hydrocarbons (Hibino et al. 1998, 1999; Zosel et al. 2004),  $\text{NO}_2$  (Miura and Yamazoe 1998, Elumalai and Miura 2005), and  $\text{NH}_3$  (Wang et al. 2006a; Satsuma et al. 2011) were developed. For example, Wang et al. (2006a) examined various metals and metal oxides as sensing electrodes for ammonia sensors and demonstrated that  $\text{V}_2\text{O}_5$ ,  $\text{BiVO}_4$ ,  $\text{MoO}_3$ , and  $\text{WO}_3$  are all effective for the sensing of  $\text{NH}_3$ . In particular,  $\text{BiVO}_4$  showed the best output voltage in the presence of  $\text{NH}_3$ , which was far higher than those for CO,  $\text{C}_3\text{H}_6$ , and NO. Schönauer et al. (2009) developed a novel selective ammonia sensor based on the mixed-potential effect using a porous  $\text{V}_2\text{O}_5$ - $\text{WO}_3$ - $\text{TiO}_2$ -based SCR catalyst as a sensing material. The proposed sensor showed good cross-sensitivity to  $\text{NH}_3$ , and they demonstrated that the sensor can detect very small  $\text{NH}_3$  slips at the downstream of a real SCR catalyst. Elumalai et al. (2008) fabricated a planar mixed-potential-type sensor using a YSZ electrolyte and NiO/Au sensing electrode. Satsuma et al. (2011) fabricated YSZ-based sensors and shown that the selective sensing of ammonia can be achieved by modification of the sensing electrode using  $\text{MoO}_3$ ,  $\text{Bi}_2\text{O}_3$ , and  $\text{V}_2\text{O}_5$ , while the use of  $\text{WO}_3$ ,  $\text{Nb}_2\text{O}_5$ , and MgO was not effective. Operating characteristics of Pt/YSZ/ $\text{Bi}_2\text{O}_3$ -Au sensors are shown in Fig. 2.13. It is seen that sensors have low cross-sensitivity to many gases and vapors, including  $\text{O}_2$  and  $\text{H}_2\text{O}$ . Satsuma et al. (2011) reported that the sensing selectivity to ammonia was in the order of  $\text{MoO}_3 > \text{Bi}_2\text{O}_3 > \text{V}_2\text{O}_5$ , which was in agreement with the corresponding acidity of the metal oxides. It was clarified that the acidity of metal oxides is the determining factor for the selective sensing of  $\text{NH}_3$ . Table 2.8 and Chap. 9 (Vol. 1) present details of electrode materials which can be used for the detection of other gases.

### 2.3.5 Limitations of Solid Electrolytes Application in Gas Sensors

Of course, it is difficult to meet all requirements addressed to metal oxide solid electrolytes aimed for gas sensor applications. First of all, these limitations are connected with insufficient temporal, thermal, and chemical stability of these materials. Therefore, although numerous metal oxides with high ionic conductivity are available, at present the lion's share of solid electrolyte-based gas sensor market, including oxygen and hydrogen sensors, is held by  $\text{ZrO}_2$ -based sensors. For example, a comparative study of perovskite oxides used in high-temperature gas sensors has shown that the conductivities of cerates are generally higher than those of zirconates. However, low chemical stability and mechanical

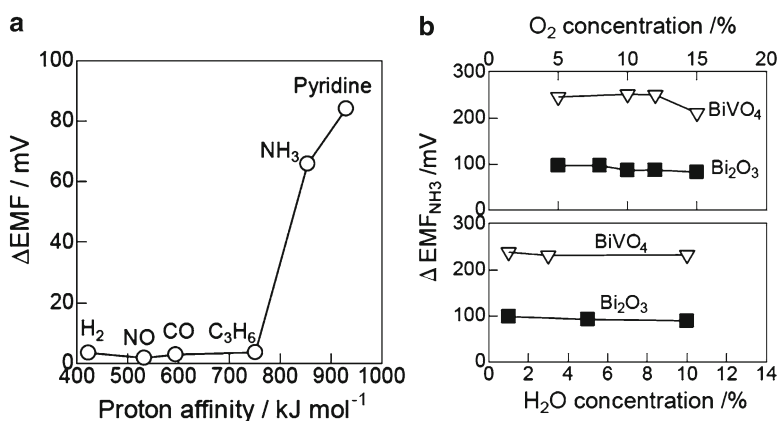


**Fig. 2.13** (a) The  $\Delta\text{EMF}$  of the YSZ/ $\text{Bi}_2\text{O}_3$ -based sensors in the presence of 500 ppm of various gases as a function of the proton affinity. (b) Influence of  $\text{O}_2$  and water vapor on the response of the  $\text{Bi}_2\text{O}_3$  and  $\text{BiVO}_4$  electrodes to 500 ppm  $\text{NH}_3$  at 600 °C (Reprinted from Satsuma et al. (2011). Published by MDPI as open access article, <http://www.mdpi.com/journal/sensors>)

**Table 2.8** Metal oxides used as sensing electrodes in zirconia-based gas sensors

Gas	Oxide SE materials
<i>Mixed-potential</i>	
$\text{NO}_x$	$\text{WO}_3$ ; $\text{NiCr}_2\text{O}_4$ ; $\text{ZnCr}_2\text{O}_4$ ; $\text{ZnFe}_2\text{O}_4$ ; $\text{ZnO}$ ; $\text{Cr}_2\text{O}_3$ ; $\text{NiO}$ ; $\text{LaFeO}_3$ ; $\text{La}_{0.8}\text{Sr}_{0.2}\text{CrO}_3$ ; $\text{CuO}$ ; $\text{La}_{0.6}\text{Ca}_{0.4}\text{Mn}_{1-x}\text{Me}_{x-3-5}\text{O}_{3-5}$ ; $\text{La}_{0.85}\text{Sr}_{0.15}\text{CrO}_3/\text{Pt}$ ; tin-doped indium (ITO); $\text{NiO}$ (+ YSZ); $\text{La}_{0.6}\text{Sr}_{0.4}\text{Fe}_{0.8}\text{Co}_{0.2}\text{O}_3$ ; $\text{CuO} + \text{CuCr}_2\text{O}_4$
CO	$\text{LaCoO}_3$ ; $\text{Nb}_2\text{O}_5$ ; $\text{Y}_{0.16}\text{Tb}_{0.30}\text{Zr}_{0.54}\text{O}_2$ ; $\text{WO}_3 + \text{LaFeO}_3$
$\text{C}_x\text{H}_y$	$\text{CdO}$ ; $\text{SrCe}_{0.95}\text{Yb}_{0.05}\text{O}_{3-\alpha}$ ; $\text{Au} + \text{Nb}_2\text{O}_5$ ; $\text{La}_{0.8}\text{Sr}_{0.2}\text{CrO}_3$ ; $\text{Pr}_6\text{O}_{11}$ ; $\text{Au} + \text{NiO}$ ; $\text{In}_2\text{O}_3$ $\text{In}_2\text{O}_3 + \text{MnO}_2$ ; $\text{La}_{1-x}\text{Sr}_x\text{Cr}_{1-y}\text{Ga}_y\text{O}_{3-5}$
$\text{NH}_3$	$\text{MoO}_3$ ; $\text{Bi}_2\text{O}_3$ ; $\text{V}_2\text{O}_5$ ; $\text{NiO}$ ; $\text{BiVO}_4$
<i>Impedancemetric</i>	
$\text{NO}_x$	$\text{ZnCr}_2\text{O}_4$
NO	$\text{NiCr}_2\text{O}_4$ ; $\text{NiO}$ ; $\text{Pt-WO}_3/\text{TiO}_2$
CO	$\text{Au-Ga}_2\text{O}_3$
$\text{C}_x\text{H}_y$	$\text{ZnO}$ ; $\text{Pt} + \text{ZnO}$
$\text{H}_2\text{O}$	$\text{In}_2\text{O}_3$
<i>Amperometric</i>	
$\text{NO}_x$	$\text{CdCr}_2\text{O}_4$ ; Zeolite + Pt
$\text{C}_x\text{H}_y$	$\text{ZnO} + \text{Pt}$

Source: Data from Zhuiykov and Miura (2007), Satsuma et al. (2011), etc.

strength limit their use in practical applications (Iwahara et al. 2004). It was established that many of the cerates discussed above ( $\text{SrCeO}_3$ ,  $\text{BaCeO}_3$ ,  $\text{BaCe}_{0.8}\text{Gd}_{0.2}\text{O}_3$ , i.e., BCG) react readily with carbon dioxide to form carbonates of the alkaline earth elements and therefore are not good candidates for applications in sensors exposed to  $\text{CO}_2$ , including ambient atmosphere sensors (Tanner and Virkar 1996; Sakthivel and Weppner 2007, 2008). For example, the  $\text{SrCeO}_3/\text{Yb}$  reacts with 10%  $\text{CO}_2$  at temperatures below 800 °C, and this reaction can even take place at 500 °C (Wang and Virkar 2005). In addition, cerates such as  $\text{BaCeO}_3$  are thermodynamically unstable when a critical  $\text{H}_2\text{O}$  vapor pressure is exceeded (Tanner and Virkar 1996). It was established that  $\text{BaCeO}_3$  in an  $\text{H}_2\text{O}$  vapor-containing

**Table 2.9** Potential oxide ion electrolytes and their problems when employed in gas sensors

Oxide ion electrolyte (Structure type)	Critical materials issues
Y <sub>2</sub> O <sub>3</sub> -doped ZrO <sub>2</sub> (Fluorite)	Poor ionic conductor, incompatible with perovskite-type cathode materials (e.g., Sr-doped LaMO <sub>3</sub> (M = Mn, Co) at elevated temperatures and long period of operation time
Sc <sub>2</sub> O <sub>3</sub> -doped ZrO <sub>2</sub> (Fluorite)	Expensive, long-term performance is not known
Rare-earth-doped CeO <sub>2</sub> (Fluorite)	Not stable in the low-oxygen partial pressure, poor mechanical stability, large grain boundary resistance at lower temperature
Sr + Mg-doped LaGaO <sub>3</sub> (Perovskite)	Not stable at low-oxygen partial pressures, forms carbonates in CO and CO <sub>2</sub> atmospheres, Ga evaporates in H <sub>2</sub> atmosphere, incompatible with Ni anode at elevated temperatures
Ba <sub>2</sub> In <sub>2</sub> O <sub>5</sub> (Brownmillerite)	Not stable at low-oxygen partial pressures, poor ionic conductor at low temperature, shows first-order phase transition accompanied by structural change, degradation in CO <sub>2</sub> atmosphere with the formation of BaCO <sub>3</sub>
Doped Bi <sub>4</sub> V <sub>2</sub> O <sub>11</sub> (Aurivillius)	Stable over a limited range of oxygen partial pressures
BaBi <sub>4</sub> Ti <sub>3</sub> InO <sub>14.5</sub> (Aurivillius)	Moderate ionic conductor, electrochemical stability at low- and high-oxygen partial pressures is not known, may form carbonates in CO <sub>2</sub> atmosphere
Gd <sub>2</sub> Ti <sub>2</sub> O <sub>7</sub> (Pyrochlore)	Poor ionic conductor and not stable at low-oxygen partial pressures at elevated temperatures
Doped BaCeO <sub>3</sub> (Perovskite)	Chemically not stable in CO <sub>2</sub> -containing atmospheres, exhibits hole (p-type) and electronic (n-type) conduction at high- and low-oxygen partial pressures, respectively, at elevated temperatures
Sr <sub>3</sub> Ti <sub>1.9</sub> Al <sub>0.1</sub> O <sub>7-x</sub> (Ruddlesden–Popper)	Poor ionic conductor, p-type electronic conduction at high-oxygen partial pressures

Source: Data from Thangadurai and Weppner (2006)

environment (~430 Torr H<sub>2</sub>O) decomposed into CeO<sub>2</sub> and Ba(OH)<sub>2</sub> in relatively short periods of time at temperatures less than 900 °C. Furthermore, it has been demonstrated that strontium cerate is not stable in a simulated coal gasification atmosphere containing 0.0033 vol.% H<sub>2</sub>S at 800 °C, since SrS and CeO<sub>2</sub> are formed (Luyten et al. 1991).

Zirconates such as CaZrO<sub>3</sub> and BaZrO<sub>3</sub> are less reactive with CO<sub>2</sub> than cerates and are more stable in H<sub>2</sub>O- and CO<sub>2</sub>-containing atmospheres (Yajima et al. 1990; Iwahara et al. 1993). Therefore, the zirconates with Ca, Ba, and Sr in the A site are the most widely used proton conductors. For example, In-doped CaZrO<sub>3</sub> has been successfully developed as a commercial hydrogen probe and is being used for the detection of dissolved hydrogen in molten aluminum in more than 150 foundries and laboratories (Iwahara et al. 2004). Y-doped BaZrO<sub>3</sub>-based electrolytes are also promising for gas sensor applications. These electrolytes combine high thermodynamic stability with high-bulk proton conductivity, which exceeds the conductivity of the best oxide ion conductors for temperatures below about 700 °C. The perovskite-structured oxides indicated above, having high melting and/or decomposition temperatures, can provide microstructural and morphological stability to improve the reliability and long-term performance of sensors. However, we need to note that even the above-mentioned perovskites cannot replace YSZ electrolytes. Critical material issues of several other solid electrolytes, which can be used in gas sensors, are listed in Table 2.9.



## 2.4 Semiconducting Metal Oxides

### 2.4.1 Metal Oxides for Chemiresistors

Conductometric sensors (chemiresistors) have a simple structure, and their operating principle is based on the fact that their electrical conductivity (or electrical conductance) can be modulated by the presence or absence of some chemical species that comes in contact with the device (Wohltjen and Snow 1998; Kohl 1989). Figure 2.14 shows a typical structure of a conductometric sensor. It consists of three elements, a sensitive conducting layer, heater, and contact electrodes. These electrodes are often interdigitated and embedded in the sensitive layer. To make the measurement, a DC voltage is applied to the device, and the current flowing through the electrodes is monitored as the response. The main advantages of these sensors are easy fabrication, simple operation, and low production cost, which means that well-engineered metal-oxide conductometric sensors can be mass produced at reasonable cost. Moreover, these sensors are compact and durable. As a result, they are amenable to being placed in situ in monitoring wells.

The basis of the operation of conductometric sensors is the change in resistance under the effect of reactions (adsorption, chemical reactions, diffusion, catalysis) taking place on the surface of the sensing layer. The chemical species interact with the sensitive layer and thus modulate its electrical conductivity (Chap. 1). This can be measured as a change in the current, which is correlated to the concentration of the chemical species. The main processes controlling gas-sensing effect are shown in Fig. 2.15. As is seen, a number of processes and factors influence the gas-sensitive properties of the MOX gas sensors. The porosity, grain size, active surface area, area of intergrain contacts, thickness, and conductivity of the MOXs also influence the operating characteristics of the gas sensors (see Fig. 2.16). For example, numerous investigations have shown that decreasing crystallite size leads to an increase of gas sensitivity (Yamazoe et al. 1983; Korotcenkov 2008; Korotcenkov et al. 2009a). For example, a dramatic increase in sensitivity for metal oxides with grain size smaller than a Debye length has been demonstrated many times for various materials, such as  $\text{SnO}_2$  (Suzuki and Yamazaki 1990; Xu et al. 1991; Yamazoe and Miura 1992; Brinzari et al. 2001; Korotcenkov 2005, 2008; Korotcenkov et al. 2009a),  $\text{WO}_3$  (Kanda and Maekawa 2005; Gillet et al. 2005), and  $\text{In}_2\text{O}_3$  (Gurlo et al. 1997; Korotcenkov et al. 2004a, b, 2007a, b, 2009a). In particular, Shimizu and Egashira (1999) established that the sensitivity of sensors based on tin oxide nanoparticles increased dramatically when the particle size was reduced to 6 nm. Below this critical grain size, sensor sensitivity decreased rapidly. As the calculated Debye length of  $\text{SnO}_2$  is  $L_D = 3$  nm at 250 °C (Ogawa et al. 1982), the greatest sensitivity was actually reached when the particle diameter was 2 nm. For  $\text{In}_2\text{O}_3$  this effect is

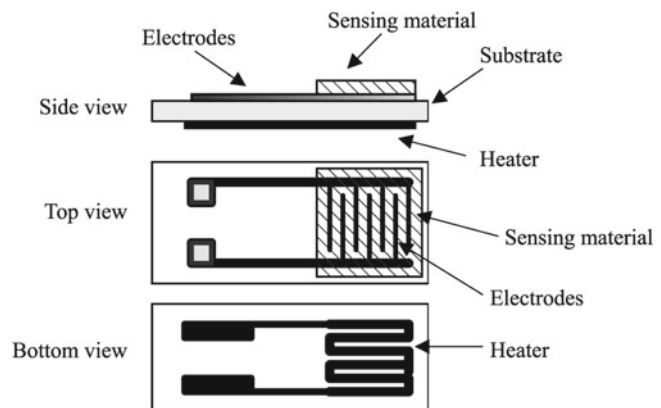


**Fig. 2.14** Schematic diagram of typical conductometric metal oxide-based gas sensors

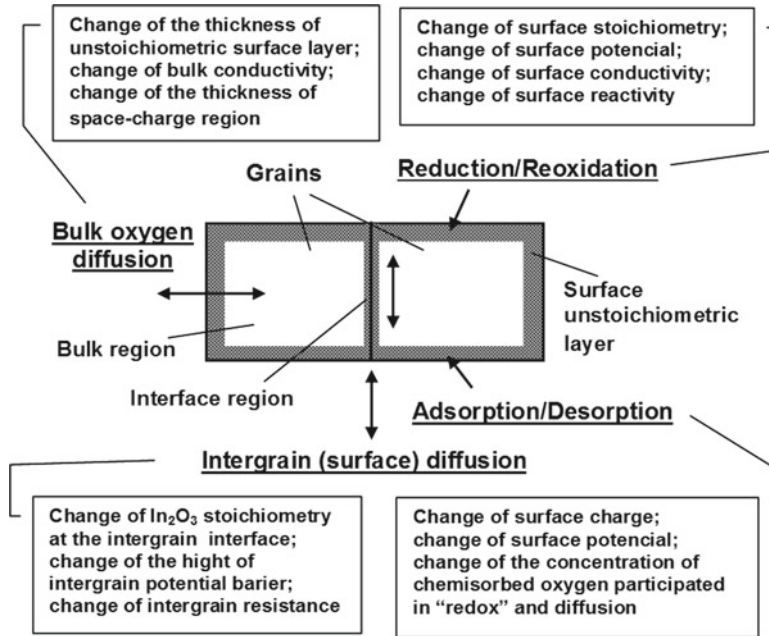


**Fig. 2.15** Processes affecting gas sensitivity of MOXs

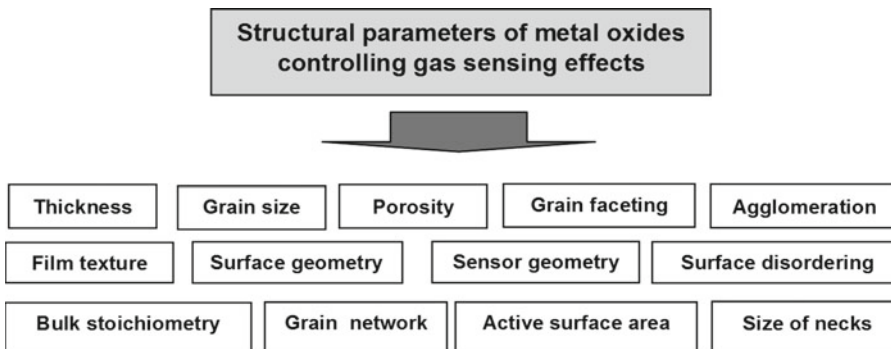


**Fig. 2.16** Structural parameters of MOXs that influence their gas-sensing properties (Reprinted with permission from Korotcenkov (2008). Copyright 2008 Elsevier)

illustrated in Fig. 2.17a. For  $\text{In}_2\text{O}_3$ , it was also found that sensors fabricated using thin films with minimal crystallite size had minimal response time (see Fig. 2.17b) in addition to maximum sensor response. For example, a decrease in grain size from 60–80 nm to 10–15 nm decreased  $t_{\text{res}}$  during ozone detection in dry air by a factor of 50–100 times. In a humidified atmosphere, however, the correlation was significantly weakened (Korotcenkov et al. 2004a, c). Therefore, at present polycrystalline materials with nano-dimensional grains are most often considered as a basis for prospective gas sensors. However, there are considerable challenges in achieving and retaining these small dimensions for practical gas sensors (Korotcenkov and Han 2009; Sysoev et al. 2009).

Dependences illustrating the influence of other structural and morphological parameters of metal oxides on the response of metal oxide gas sensors are shown in Fig. 2.18. These dependences show that as the porosity and active surface area of the gas-sensing material increases, the sensor response

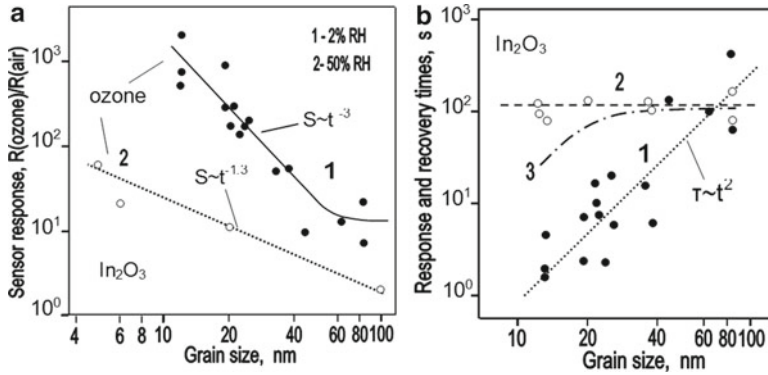


**Fig. 2.17** (a) Influence grain size on sensor response to (1) ozone ( $\sim 1$  ppm) and (2)  $\text{NO}_2$  ( $\sim 1$  ppm) of undoped  $\text{In}_2\text{O}_3$ -based devices. (1) Thin-film technology. Films deposited by spray pyrolysis at  $T_{\text{pyr}} = 475$  °C ( $T_{\text{oper}} = 270$  °C; RH = 1–2%). (2) Thick-film technology.  $\text{In}_2\text{O}_3$  powders were synthesized by the sol–gel method ( $d$  200 nm;  $T_{\text{oper}} = 150$  °C; RH = 50%). [Experimental data from Korotcenkov et al. (2004a) and Gurlo et al. (1997)]. (b) Influence of grain size on (1, 2) the response and (3) recovery times of the undoped  $\text{In}_2\text{O}_3$ -based sensors during ozone detection:  $T_{\text{pyr}} = 475$  °C (0.2 M),  $T_{\text{oper}} = 270$  °C, 1 and 2, RH = 1–2%; 3, RH = 45–50% (Adapted with permission from Korotcenkov (2004a). Copyright 2004 Elsevier)

increases as well (see Fig. 2.18b). This is consistent with the conclusion of Matko et al. (2002) that the porosity and specific surface area are basic factors that influence the solid/gas interactions and ultimately the material performance in gas detection. This is an important conclusion, because experiment has shown that the simplest method to achieve maximum sensitivity independently on gas-sensing material is to increase the film's porosity (Sberveglieri 1992; Park and Mackenzie 1996; Basu et al. 2001; Ahmad et al. 2003; Hyodo et al. 2003; Lee and Kang 2005; Jin et al. 2005; Tesfamichael et al. 2007). In the case of compact layers, interaction with gases takes place only at the geometric surface. In porous material the volume of the layer is accessible to the gases and therefore the active surface is much greater than the geometric area and the sensor response is higher (Barsan et al. 1999). Higher porosity results in a smaller number of contacts with the necks that are not overlapped under interaction with the surrounding gas. Increased porosity also decreased the probability of forming so-called capsulated zones in the volume of the gas-sensing layer. Capsulated zones are isolated from contact with the atmosphere, and therefore their resistance does not depend on the surrounding gas (McAleer et al. 1987). As has been established, all these parameters have a direct correlation with grain size (see Fig. 2.17). As a rule, an increase in specific surface area of a gas-sensing material is accompanied by a shift in the sensitivity maximum into the range of lower operating temperatures (see Fig. 2.18d). One can assume that this effect is caused by the thermally activated nature of gas diffusion inside the gas-sensing matrix (Ruiz et al. 2005). Several studies (Park and Mackenzie 1996; De Souza Brito et al. 1995; Korotcenkov et al. 2004a) have shown that gas sensors with higher porosity have faster responses.

Park and Mackenzie (1996) established that the refractive index correlates with film porosity. If the porosity is higher, the refractive index is smaller. It is known that only nonporous metal oxides have refractive indices equal to the tabular data estimated for these materials. Pores in metal oxides can be considered as a component with a refractive index equal to 1.0. Therefore, films with smaller refractive indexes along with invariability of the main parameters must have higher degrees of porosity and better gas permeabilities. Figure 2.18c shows that  $\text{In}_2\text{O}_3$  films with low refractive indexes really have minimal  $t_{\text{res}}$  and  $t_{\text{re}}$ . Korotcenkov et al. (2004b) concluded that, for the detection of reducing gases in  $\text{In}_2\text{O}_3$  films, the porosity or the gas permeability is a more important factor than grain size. We also need to note that, with an increase in porosity, the influence of film thickness on both the magnitude of sensor response and the response time is appreciably weakened. In particular, Korotcenkov and

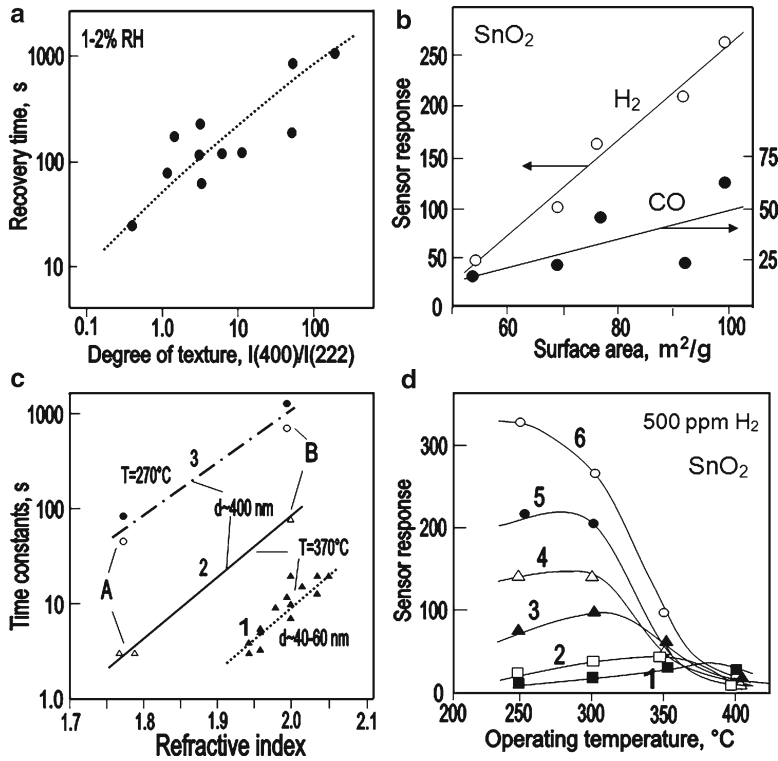


**Fig. 2.18** (a) Influence of  $In_2O_3$  film texture on recovery time during ozone detection. Films with thicknesses of 40–300 nm were deposited by spray pyrolysis from 1.0 M  $InCl_3$ –water solution ( $T_{oper} = 270^\circ C$ ). (b) Relationship between surface areas of  $SnO_2$  sensors and their sensitivity to 500 ppm of  $H_2$  and CO at  $300^\circ C$ . Sensors were fabricated by pressing and annealing at  $450^\circ C$  calcined  $SnO_2$  powders into 14-mm-diameter and 1-mm-thick pellets with two Pt electrodes.  $SnO_2$  for these experiments were prepared by a surfactant-templating method. [Data extracted from Li et al. (1999)]. (c) Time constants of sensor response to CO vs  $In_2O_3$  film refraction index: (1, 2)  $T_{oper} = 370^\circ C$ ; (3)  $T_{oper} = 270^\circ C$ ; (1)  $d$  40–60 nm; (2, 3)  $d$  400 nm; (A)  $In_2O_3$  films were deposited from 0.2 M  $InCl_3$ –water solution; (B) from 1.0 M  $InCl_3$ –water solution. (d) Influence of surface area of  $SnO_2$ -based thick-film sensors on response to 500 ppm of  $H_2$ : 1, 3  $m^2/g$ ; 2, 54  $m^2/g$ ; 3, 69  $m^2/g$ ; 4, 77  $m^2/g$ ; 5, 92  $m^2/g$ ; 6, 99  $m^2/g$ . [Data extracted from Li et al. (1999)]. (a, c) Reprinted with permission from Korotcenkov et al. (2004a). Copyright 2004 Elsevier. (b, d) Reprinted with permission from Korotcenkov (2008). Copyright 2008 Elsevier

coworkers (Korotcenkov 2005; Korotcenkov et al. 2005a, b, 2007c), studying the influence of the modes of deposition on the structural and gas-sensing properties of  $SnO_2$  and  $In_2O_3$  films deposited by spray pyrolysis, found that for dense films an increase of film thickness in the range 30–200 nm was accompanied by a decrease in sensitivity to ozone by almost two orders of magnitude; for porous films, the same change of thickness did not affect gas sensitivity.

The most accepted mechanism, explaining the sensitivity of n-type metal oxide-based sensors, involves consideration of the role of the chemisorbed oxygen (Kohl 1989; Barsan et al. 1999; Gurlo 2006). Oxygen chemisorption means the formation of  $O_2^-$ ,  $O^-$ ,  $O^{2-}$  species on the surface. Among these,  $O^-$  proved to be more reactive than  $O_2^-$ , while  $O^{2-}$  is not stable. So the dominant species is the  $O^-$  species. According to Barsan et al. (1999) and Batzill (2006),  $O^-$  species start to be dominant oxide surfaces, in particular  $SnO_2$ , at  $T > 150$ – $220^\circ C$  (see Fig. 2.19). However, it is necessary to note that some controversy on this subject still persists (Gurlo 2006). The oxygen chemisorption results in a modification of the space charge region toward depletion. The amount of charged adsorbates determines both the height of the surface potential  $eV_s$  and the width  $d_s$  of the depletion layer (see Fig. 2.20).

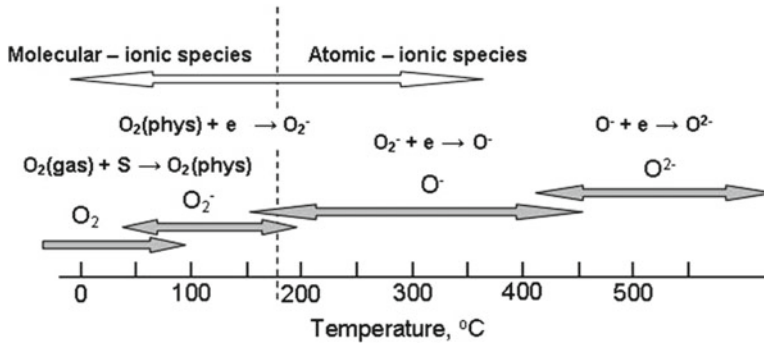


**Fig. 2.19** Literature survey of oxygen species detected at different temperatures on SnO<sub>2</sub> surfaces with infrared analysis (IR), temperature-programmed desorption (TPD), and electron paramagnetic resonance (EPR) [Data from Barsan and Weimar (2001)]

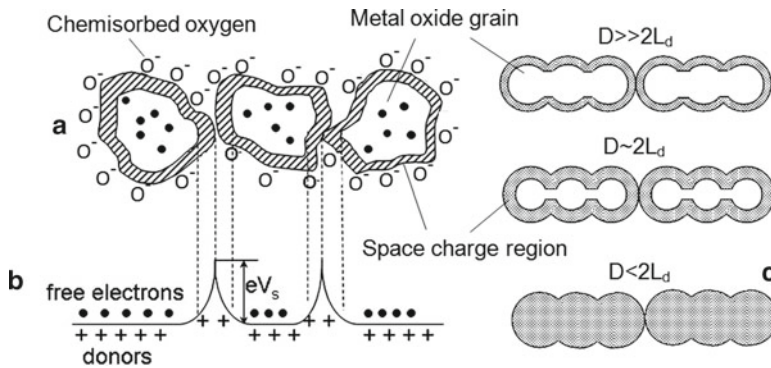


**Fig. 2.20** Double Schottky barrier in polycrystalline oxide layers: (a) physical model; (b) energy zone diagram; (c) grain size influence on mechanism of polycrystalline MOX layer conductance. The *filled* and *empty* areas indicate high and low resistances, respectively [Idea from Yamazoe (1991) and Yamazoe and Miura (1992)]

The resistance corresponding to this state is considered the base resistance. The appearance of a reducing gas leads to partial consumption of the adsorbed oxygen, resulting in a decrease in resistance, while the appearance of oxygen increases the surface oxygen coverage and hence the resistance. The above mechanisms suggest the existence of a grain boundary (connected to the modification of the space charge region (Barsan and Weimar 2001)). The relationship between the change in resistance and the concentration of a combustible gas can be expressed by a power-law equation (Barsan et al. 1999):

$$G = \frac{1}{R} = kC^n, \tag{2.11}$$

where  $C$  is the concentration of analyte and  $k$  and  $n$  are individual constants, which depend on the mechanism of sensitivity and must be determined empirically by calibration.

A key observation on MOX gas sensors is that those chemical surface interactions that lead to a combustible gas response are thermally activated. This fact is apparent in Fig. 2.21, which shows typical responses of a metal oxide-based gas sensor as a function of its operation temperature and adsorption/

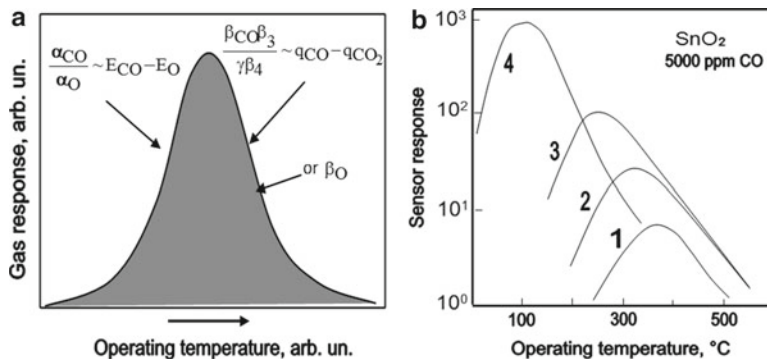


**Fig. 2.21** (a) Typical shape of operating temperature influence on response of metal oxide gas sensors and adsorption/desorption parameters controlling this dependence. (b) Simulation of the influence of adsorption/desorption parameters on temperature dependence of SnO<sub>2</sub> gas response to CO. Here  $E_{CO}$  is the activation energy of CO adsorption, and  $q_{CO}$  is the activation energy of CO desorption.  $E_{CO}$ : 1, 0.9 eV; 2, 0.85 eV; 3, 0.8 eV; 4, 0.7 eV; 5, 0.6 eV.  $q_{CO}$ : 1, 2, 3, 4, 1.6 eV; 5, 1.4 eV. Reprinted with permission from Korotcenkov (2007). Copyright 2007 Elsevier)

desorption parameters. As far as reducing analyte molecules are concerned, the shape of these sensitivity curves can be understood on the basis of two opposite trends: (1) a thermally activated surface combustion of the adsorbed analyte molecules which limits the response on the low-temperature side, and (2) a thermally activated and concentration-dependent desorption rate which limits the response at the high-temperature side (Brynzari et al. 1999, 2000; Ahlers et al. 2005; Helwig et al. 2009). Simulations carried out by Brynzari et al. (2000) have shown that the decrease of activation energy of CO and O<sub>2</sub> adsorption processes may really change the sensor sensitivity and shift the temperature of the maximum sensor response considerably. In addition, this process may be accompanied by a considerable decrease of response and recovery times.

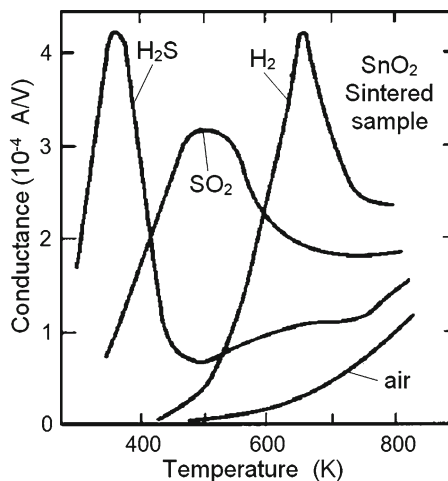
According to Brynzari et al. (2000), the influence of some adsorption/desorption parameters on the surface potential ( $\Delta U_s$ ) and SnO<sub>2</sub> conductivity ( $\Delta G$ ) during CO detection can be presented as the following pattern:

$$\frac{\alpha_R}{\alpha_O} -, \beta_4 -, \beta_{RO} -, N^* \downarrow, N_{ss} \downarrow, \beta_3 \downarrow, \beta_R \downarrow \Rightarrow \Delta U_s -, \Delta G -, \quad (2.12)$$

where  $\alpha_R$  and  $\alpha_O$  are the coefficients of R and O<sub>2</sub> adsorption,  $\beta_R$  and  $\beta_{RO}$  are the coefficients of R and RO desorption,  $\beta_3$  and  $\beta_4$  are the coefficients of charging and neutralization of RO, and  $N^*$  and  $N_{ss}$  are the total number of adsorption sites and sites originating from native (biographic) surface charge;  $\uparrow$  indicates an increase and  $\downarrow$  indicates a decrease. The scheme at Eq. (2.12) shows the directions of adsorption/desorption parameter changes, which are necessary to improve sensor response, i.e., increase both the change of surface potential and film resistance during interaction with target gas.

The above testifies to the fact that the response of metal oxide gas sensor should have a maximum at a certain temperature. For example, the maximum sensitivity to reducing gases such as H<sub>2</sub> for pristine SnO<sub>2</sub>-based sensors is observed at a  $T_{max}$  of about 400 °C (Fig. 2.22). At low temperatures the concentration of chemisorbed oxygen (O<sup>-</sup>) on the surface of SnO<sub>2</sub>, which may interact with reducing gases, is low. As we mentioned above, chemisorbed oxygen appears on the surface of SnO<sub>2</sub> only at temperatures higher than 180–200 °C. Therefore, accounting for low activation of surface catalysis processes, exposure of the oxides to the target gases results in only negligible sensor response. With an increase in operating temperature, the conductance response of the sensor is increased as well, due

**Fig. 2.22** Influence of gas nature on the temperature dependencies of conductivity response of SnO<sub>2</sub>-based sensors to H<sub>2</sub>S (40 ppm in air), SO<sub>2</sub> (1,000 ppm in air), and H<sub>2</sub> (500 ppm in air) [Data from Pijolat (1986)]



to enhancement of both the concentration of chemisorbed oxygen and the rate of interaction of the adsorbed gases with oxygen. However, the desorption rate of adsorbed gases, including oxygen, is also increased at higher operating temperatures. As a result, further increase of the temperature “cleans” the oxide surface, and the number of adsorbed species which participate in surface reactions is decreased. At a certain operating temperature, the latter processes begin dominating the sensor response, and therefore, the sensor response to gases is decreased. So the operating temperature of the sensor is optimized empirically to be set close to  $T_{\max}$ . However, the actual operating temperature may exceed the value of  $T_{\max}$  if a faster response time is required. It is worth noting that  $T_{\max}$  may vary for the same sensor when it is exposed to different target gases. As is well known, every gas has specific reactivity and adsorption/desorption parameters (Kohl 1989). An example of gas nature influence on temperature dependencies of SnO<sub>2</sub> conductivity response to H<sub>2</sub>S, SO<sub>2</sub>, and H<sub>2</sub> is shown in Fig. 2.22. This fact is frequently utilized to improve selectivity of metal oxide-based gas sensors.

#### 2.4.1.1 Binary Metal Oxides

Early work on chemisorptions-type sensors (chemiresistors) focused mostly on studying SnO<sub>2</sub> and ZnO (Seiyama et al. 1962; Taguchi 1971; Chiba 1992). Sensors based on these oxides have high sensitivity and rather low operating temperatures, 250–400 °C. These oxides have negligible concentration of electron states in the gap and high reactivity to many gaseous species. The crystal structures of these metal oxides are shown in Fig. 2.23. Zinc oxide is crystallized in a wurtzite crystal lattice. Tin dioxide is crystallized in the tetragonal structure of rutile. More recently, other oxide materials, such as WO<sub>3</sub>, TiO<sub>2</sub>, and In<sub>2</sub>O<sub>3</sub>, have been used successfully to design conductometric gas sensors as well (see Table 2.10). The study of other MOXs is a subject of interest to advance various parameters of conductometric sensors. For example, WO<sub>3</sub>-based gas sensors have excellent selective response to NH<sub>4</sub>, H<sub>2</sub>S, and NO<sub>2</sub>. Moreover, the larger range of sensing materials is required to tailor sensitivity and cross-sensitivity profiles to particular applications and to develop multisensor arrays (Meier et al. 2007a, b). A more detailed comparison of metal oxides tested for gas sensor application is given in Table 2.11.

As summarized in Fig. 2.24 and Tables 2.9 and 2.10, MOX gas sensors exhibit broad-range sensitivity to a wide variety of analyte molecules.

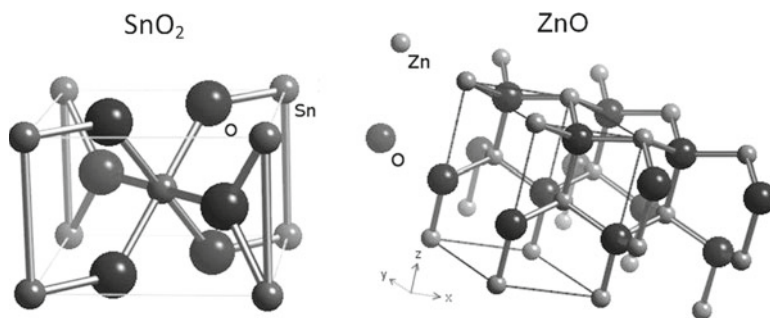


**Fig. 2.23** Crystal structures of basic MOXs employed in the design of chemisorption-type conductometric gas sensors. (Reprinted from <http://www.webelements.com>)

**Table 2.10** Characterization of gas sensors based on MOXs

Material	Operating temperature (°C)	Implementation	Additives	Target gases
SnO <sub>2</sub>	100–500	Ceramic Thick film Thin film	Pd, Pt, Au, Sb, Ag, Rh, CuO, Al <sub>2</sub> O <sub>3</sub> , In <sub>2</sub> O <sub>3</sub> , TiO <sub>2</sub> , Fe <sub>2</sub> O <sub>3</sub> , CaO, Nb <sub>2</sub> O <sub>5</sub> , Bi <sub>2</sub> O <sub>3</sub> , Mn, CeO, La, MoO <sub>3</sub> , SiO <sub>2</sub>	CO, C <sub>2</sub> H <sub>5</sub> OH, H <sub>2</sub> , CCl <sub>4</sub> , O <sub>3</sub> , CHCl <sub>3</sub> , CH <sub>4</sub> , C <sub>2</sub> H <sub>10</sub> , CH <sub>3</sub> CN, NH <sub>3</sub> , SO <sub>2</sub> , H <sub>2</sub> S, NO, PH <sub>3</sub> , NO <sub>2</sub> , HF, O <sub>2</sub> , H <sub>2</sub> O, CH <sub>2</sub> SH, C <sub>2</sub> H <sub>5</sub> OH
In <sub>2</sub> O <sub>3</sub>	50–500	Ceramic Thick film Thin film	Pd, Pt, Li <sub>2</sub> O, Er <sub>2</sub> O <sub>3</sub> , GdO <sub>3</sub> , WO <sub>3</sub> , CaO, Al <sub>2</sub> O <sub>3</sub> , SnO <sub>2</sub> , SiO <sub>2</sub>	CO, O <sub>2</sub> , O <sub>3</sub> , CH <sub>4</sub> , H <sub>2</sub> , H <sub>2</sub> S, HCOH, NO <sub>2</sub> , NO, H <sub>2</sub> O, NH <sub>3</sub> , C <sub>2</sub> H <sub>5</sub> OH
WO <sub>3</sub>	200–500	Ceramic Thin film	Sb, Pt, Au	O <sub>2</sub> , O <sub>3</sub> , H <sub>2</sub> S, HCOH, NO <sub>2</sub>
ZnO	200–600	Ceramic Thick film Thin film	Ni, Li <sub>2</sub> O, Er <sub>2</sub> O <sub>3</sub> , WO <sub>3</sub> , CaO, Al <sub>2</sub> O <sub>3</sub> , In <sub>2</sub> O <sub>3</sub> , SnO <sub>2</sub>	O <sub>2</sub> , O <sub>3</sub> , CO, H <sub>2</sub> , CH <sub>4</sub> , NH <sub>3</sub> , NO <sub>2</sub> , C <sub>2</sub> H <sub>5</sub> OH
Ga <sub>2</sub> O <sub>3</sub>	400–800	Thin film		O <sub>2</sub> , H <sub>2</sub> , CO, CH <sub>4</sub>
Fe <sub>2</sub> O <sub>3</sub>	200–500	Ceramic Thick film Thin film	Pd, SnO <sub>2</sub> , Mg, TiO <sub>2</sub> , MgO, SO <sub>4</sub>	CH <sub>4</sub> , C <sub>4</sub> H <sub>10</sub> , H <sub>2</sub> , CO, NH <sub>3</sub> , F <sub>2</sub> , C <sub>2</sub> H <sub>5</sub> OH
TiO <sub>2</sub>	40–600	Ceramic Thick film Thin-film gel	Pt, Ru, Au, Rh, Cr, Li, Na, In, Y, Sr, Tb, SnO <sub>2</sub> , Sb <sub>2</sub> O <sub>5</sub> , Ta <sub>2</sub> O <sub>5</sub> , Nb <sub>2</sub> O <sub>5</sub> , Ga <sub>2</sub> O <sub>3</sub> , CeO <sub>2</sub> ,	O <sub>2</sub> , H <sub>2</sub> , H <sub>2</sub> O, C <sub>3</sub> H <sub>3</sub> N, CO, NO <sub>x</sub> , C <sub>2</sub> H <sub>5</sub> OH, NH <sub>3</sub>
V <sub>2</sub> O <sub>5</sub>	300–400	Thin film		H <sub>2</sub> , C <sub>2</sub> H <sub>5</sub> OH
MoO <sub>3</sub>	100–500	Thin film	Pt, ZrO <sub>2</sub> ,	H <sub>2</sub> , CO

#### 2.4.1.2 Complex and Mixed Metal Oxides

Except for binary oxides, chemisorption-type conductometric sensors employ complex oxides such as CdIn<sub>2</sub>O<sub>4</sub>, NiTa<sub>2</sub>O<sub>6</sub>, CoTa<sub>2</sub>O<sub>6</sub>, CuTa<sub>2</sub>O<sub>6</sub>, BaSnO<sub>3</sub>, LnFeO<sub>3</sub>, CdFe<sub>2</sub>O<sub>4</sub>, Bi<sub>2</sub>Sn<sub>2</sub>O<sub>7</sub>, YBa<sub>2</sub>Cu<sub>3</sub>O<sub>7–8</sub>, Bi<sub>x</sub>Mo<sub>y</sub>O<sub>2</sub>, Sn<sub>1–x</sub>Fe<sub>x</sub>O<sub>y</sub>, and NiFe<sub>2</sub>O<sub>4</sub>. More complicated metal oxides, such as LiSmFe<sub>2</sub>O<sub>4</sub>, Ni<sub>0.99</sub>Co<sub>0.01</sub>M<sub>0.01</sub>Fe<sub>1.99</sub>O<sub>4</sub>, BaSn<sub>0.95</sub>Zr<sub>0.05</sub>O<sub>3</sub>, Na<sub>0.1</sub>Nb<sub>0.1</sub>W<sub>0.8</sub>O<sub>3</sub>, CS<sub>4</sub>SiW<sub>12</sub>O<sub>40</sub>, or CoMn<sub>0.65</sub>Fe<sub>1.35</sub>O<sub>4</sub>, can be used as well (Lample et al. 1996;



**Table 2.11** Operating parameters of solid-state gas sensors based on metal oxides and particulars of their fabrication

Metal oxide	Optimal gases for detection	Operating temperature (°C)	Stability	Compatibility with standard fabrication techniques	Complexity of fabrication	Sensitivity to air humidity	Stability in reducing atmosphere	Readiness of synthesis and deposition
SnO <sub>2</sub>	Reducing gases (CO, H <sub>2</sub> , CH <sub>4</sub> , etc.)	200–400	Excellent	Imperfect	Acceptable	High	Good	High
WO <sub>3</sub>	O <sub>3</sub> , NO <sub>x</sub> , H <sub>2</sub> S, SO <sub>2</sub>	300–500	Excellent	Low	Moderate	Reduced	Good	Medium
Ga <sub>2</sub> O <sub>3</sub>	O <sub>2</sub> , CO	600–900	High	Good	Acceptable	Low	Moderate	Medium
In <sub>2</sub> O <sub>3</sub>	O <sub>3</sub> , NO <sub>x</sub>	200–400	Moderate	Good	Acceptable	Reduced	Moderate	High
MoO <sub>3</sub>	NH <sub>3</sub> , NO <sub>2</sub>	200–450	Moderate	Moderate	Moderate		Good	
TiO <sub>2</sub>	O <sub>2</sub> , CO, SO <sub>2</sub>	350–800	Enhanced	Moderate	Moderate	Low	Excellent	Medium
ZnO	CH <sub>4</sub> , C <sub>4</sub> H <sub>10</sub> , O <sub>3</sub> , NO <sub>x</sub>	250–350	Satisfactory	Good	Acceptable		Excellent	High
CTO	H <sub>2</sub> S, NH <sub>3</sub> , CO, VOCs	300–450	High	Imperfect	Moderate	Low	Moderate	Medium
Fe <sub>2</sub> O <sub>3</sub>	Alcohols, CH <sub>4</sub> , NO <sub>2</sub>	250–450	Low	Moderate	Acceptable	High	Low	Medium

Source: Reprinted with permission from Korotcenkov (2007a). Copyright 2007 Elsevier

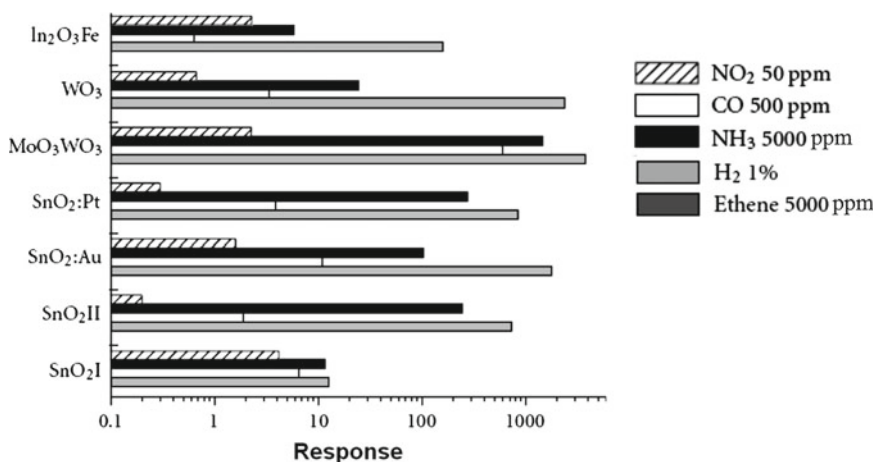


**Fig. 2.24** Gas sensitivity profiles of different MOX materials. Reprinted from Helwig et al. (2009). Published by Hindawi Publishing Corporation as open access article

Ifitimie et al. 2006; Sandu et al. 2006; Gadkari et al. 2011). Such complex oxide-based sensors exhibit both n-type and p-type responses to gases under different operating temperatures (see, e.g., Wu et al. 1990; Mosley et al. 1991; Lampe et al. 1992, 1995a, b, 1996; Solis and Lantto 1995; Dawson et al. 1995; Siemons et al. 2007).

Mixed metal oxides such as SnO<sub>2</sub>-In<sub>2</sub>O<sub>3</sub> (ITO), SnO<sub>2</sub>-ZnO, SnO<sub>2</sub>-WO<sub>3</sub>, or In<sub>2</sub>O<sub>3</sub>-ZnO based on stable conductive metal oxides SnO<sub>2</sub>, In<sub>2</sub>O<sub>3</sub>, WO<sub>3</sub>, and ZnO with high gas sensitivity form other group of metal oxides which has been of great of interest during the last decade. Many groups recently focused on investigating the above-mentioned mixed metal oxides with different metal-to-metal ratios in order to fine-tune gas response and selectivity issues (Zampiceni et al. 2003; Ferro et al. 2005; Rummyantseva et al. 2006; Choi et al. 2009; Shouli et al. 2010). In such mixed metal oxides, the content of second oxide phase can exceed 10%. In particular, Table 2.12 presents noteworthy NO<sub>x</sub> sensor data revealed recently using mixed metal oxides as sensing materials.

Experiments have shown that multicomponent and mixed metal oxides may sometimes be more promising materials for a specific application than SnO<sub>2</sub> and other binary oxides (Gas'kov and Rummyantseva 2001, 2009). For example, the majority of semiconducting metal oxide sensors operate by the measurement of resistance changes. However, there are several examples of mixed metal oxide compositions (e.g., CuO-BaTiO<sub>3</sub>, ZnO-WO<sub>3</sub>) that exhibit changes in permittivity, providing the ability to perform capacitance measurements using semiconducting metal oxides (Ishihara et al. 1991a, b, 1992, 1996; Herran et al. 2008). Gadkari et al. (2011) believe that nickel ferrite (NiFe<sub>2</sub>O<sub>4</sub>) can be promising for the detection of chlorine and acetone, and zinc ferrite (ZnFe<sub>2</sub>O<sub>4</sub>) for the detection of ethanol, whereas magnesium ferrite (MgFe<sub>2</sub>O<sub>4</sub>) and cadmium ferrite (CdFe<sub>2</sub>O<sub>4</sub>) could be used for the design of LPG and ethanol sensors. Bangale et al. (2011) established that zinc ferrite (ZnFe<sub>2</sub>O<sub>4</sub>) can be used for the detection of chlorine as well. Gawas et al. (2011) have shown that manganese and nickel doped zinc ferrite (Mn<sub>0.3</sub>Ni<sub>0.3</sub>Zn<sub>0.4</sub>Fe<sub>2</sub>O<sub>4</sub>) is very promising for room-temperature NH<sub>3</sub> sensors. Gawas et al. (2011) believe that a remarkable decrease in the resistance of the Mn<sub>0.3</sub>Ni<sub>0.3</sub>Zn<sub>0.4</sub>Fe<sub>2</sub>O<sub>4</sub>-based sensor at room temperature is due to the surface reaction of ammonia with physisorbed H<sub>2</sub>O or by proton conductivity via NH<sub>4</sub><sup>+</sup> cations. Ammonium hydroxide NH<sub>4</sub>OH produced during the surface reaction is volatile in nature. The high volatility of NH<sub>4</sub>OH explains the quick response and fast recovery of the sensor. A careful selection of mixed metal oxide SnO<sub>2</sub>-TiO<sub>2</sub> compositions was recently demonstrated to reduce significantly (but not eliminate) humidity effects (Tricoli et al. 2009). Ivanovskaya et al. (2003) and Rummyantseva et al. (2006) believe that Fe<sub>2</sub>O<sub>3</sub>-based mixed metal oxides are promising for ethanol gas sensors.

**Table 2.12** NO<sub>x</sub> conductometric gas sensors employing mixed metal oxides as active layers

Metal oxides	Optimal mixing ratio	Morphology	Method	Optimal T <sub>oper</sub> (°C)	Detection range (ppm)	Response/ppm		Time <sup>b</sup> (s)
						S <sup>a</sup>	ppm	
SnO <sub>2</sub>		Hollow spheres	Wet chemical	160	5–100	2.5 × 10 <sup>3</sup>	50	10
WO <sub>3</sub>		Nanoparticles	Thermal evaporation	50	1	4.7 × 10 <sup>3</sup>	1	~200
In <sub>2</sub> O <sub>3</sub>		Powders	Spray pyrolysis	100	10	381	10	>1,013
ZnO		Nanoparticles	Commercial	200	0.2–5	49	0.4	–
In <sub>2</sub> O <sub>3</sub> -SnO <sub>2</sub>	SnO <sub>2</sub> (15%)	Thin film	RF magnetron sputtering	327	5–200	27	50	–
In <sub>2</sub> O <sub>3</sub> -SnO <sub>2</sub>	SnO <sub>2</sub> (17%)	Nanofibers	Electrospinning	160	1–50	2.4	1	–
SnO <sub>2</sub> -WO <sub>3</sub>	WO <sub>3</sub> (5%; 7%)	Thin film	RF diode sputtering	100	10	5.4 × 10 <sup>4</sup>	10	67
SnO <sub>2</sub> -WO <sub>3</sub>	WO <sub>3</sub> (5%; 7%)	Thin film	Sol-gel	300	0.1–3	36	1	<60
SnO <sub>2</sub> -WO <sub>3</sub>	WO <sub>3</sub> (20%)	Thick film	Sol-precipitation	200	0.01–40	186	200	–
SnO <sub>2</sub> -ZnO	ZnO coating	Nanofibers	Electrospinning-ALD	200	1–5	1.1	1	>100
SnO <sub>2</sub> -ZnO	ZnO (40%)	Powders	Microemulsion	250	100–1,000	34	500	–
SnO <sub>2</sub> -Fe <sub>2</sub> O <sub>3</sub>	Fe <sub>2</sub> O <sub>3</sub> (1.5 %)	Thick film	Sol-gel	150	0.06–10,000	200	1	–
ZnO-SnO <sub>2</sub>	Zn: Sn (1:1)	Thick film	Wet chemical	RT	0.5	1,066	0.5	–
ZnO-SnO <sub>2</sub>	Zn: Sn (4:6)	Thick film	Reverse microemulsion	200	200–1,000	13.5	500	–
ZnO-SnO <sub>2</sub>	SnO <sub>2</sub> coating	Nanofibers	Electrospinning-PLD	200	0.1–4	105	4	>100
ZnO-CdO	CdO (14–28 %)	Thin films	Spray pyrolysis	230	0.2–6	14	3	–

T<sub>oper</sub>—the temperature at which the best sensor performance, usually in terms of the highest response toward NO<sub>x</sub>, is observed

<sup>a</sup>Herein, gas response is always reported as S = (R<sub>g</sub>-R<sub>0</sub>)/R<sub>0</sub>

<sup>b</sup>The time required to reach 90 % of the total response toward specific concentration of NO<sub>x</sub>

Source: Data extracted from Ferro et al. (2005), Rumyantseva et al. (2006), Liangyuan et al. (2008), Afzal et al. (2012), etc.

**Fig. 2.25** Responses of the sensor based on the composite materials with the various molar ratio of ZnO to SnO<sub>2</sub> to 500 ppb NO<sub>2</sub> at room temperature with and without UV light irradiation.

Structural parameters of tested films are presented in Table 2.13 (Reprinted with permission from Lu et al. (2012). Copyright 2012 Elsevier)

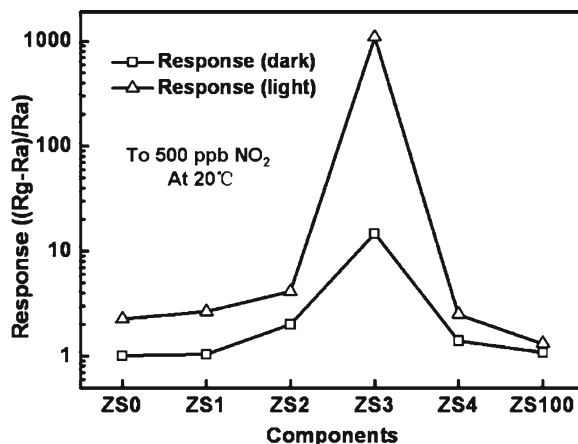
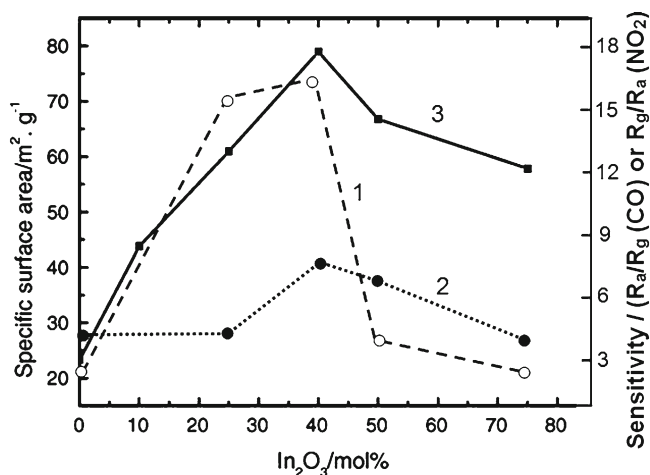


**Fig. 2.26** Influence

In<sub>2</sub>O<sub>3</sub>-SnO<sub>2</sub> mixed metal oxide composition on (1, 2) sensor response and (3) specific surface area of gas-sensing matrix calcined at 600 °C: (1) response to 1,000 ppm of CO at  $T_{oper} = 250$  °C and (2) response to 450 ppm of NO<sub>2</sub> at  $T_{oper} = 150$  °C (Adapted with permission from Aifan et al. (2006). Copyright 2006 Elsevier)



However, we need to recognize that the use of the above-mentioned mixed metal oxides and multicomponent metal oxides do not, as a rule, give any considerable improvement in gas-sensing characteristics in comparison with binary metal oxides. For example, as seen in Table 2.12, binary metal oxides with optimal morphology and mixed metal oxides have practically the same sensor response. Of course, at certain concentrations of the second component in mixed metal oxides we can observe a great increase of sensor response (see Figs. 2.25 and 2.26). However, this increase is reached mainly due to improvement of structural parameters such as grain size, porosity, and surface area (see Table 2.13 and Fig. 2.25), but is not due to a specific composition of gas-sensing matrix. Moreover, in many cases mixed metal oxides have low gas sensitivity though complex composition. The complex nature of these materials also limits their use for integrated gas sensors. The large number of elements in these metal oxides makes it hard to deposit thin films with good and repeatable stoichiometric ratios (Eranna et al. 2004).

Experiment has shown that complex metal oxides can be successfully applied only for design of gas sensors intended for the detection of specific gases such as H<sub>2</sub>S (Tamaki et al. 1998; Jianping et al. 2000) or CO<sub>2</sub>. In particular, Chapelle et al. (2010) have shown that CuO-Cu<sub>x</sub>Fe<sub>3-x</sub>O<sub>4</sub> films can be used for design conductometric sensors for CO<sub>2</sub> detection. It was found that as a rule film conductance changes in CO<sub>2</sub>-sensitive materials upon interaction with CO<sub>2</sub> are achieved via the rapid and reversible formation of carbonates. We have to note that conventional binary metal oxides due to high

**Table 2.13** Average particle size and BET surface area of ZnO/SnO<sub>2</sub> composite materials

Label	Composition	Average crystal size (nm)		BET surface area (m <sup>2</sup> /g)
		ZnO	SnO <sub>2</sub>	
ZS0	ZnO	40	–	4
ZS1	Zn/Sn=10:1	35	6	27
ZS2	Zn/Sn=2:1	32	10	34
ZS3	Zn/Sn=1:1	17	11	50
ZS4	Zn/Sn=1:5	–	14	32
ZS100	SnO <sub>2</sub>			

Source: Reprinted with permission from Lu et al. (2012). Copyright 2012 Elsevier

**Table 2.14** Comparison of responses of metal oxide-based conductometric sensors to 2,000 ppm CO<sub>2</sub> in synthetic air

Material	Operating temperature (°C)	Sensor response ( $R_g/R_0$ )	References
SnO <sub>2</sub>	100	1.1	Tamaki et al. (1990)
SnO <sub>2</sub>	400	1.02	Mizuno et al. (1993)
SnO <sub>2</sub> -La <sub>2</sub> O <sub>3</sub>	400	1.4	Kim et al. (2000)
SnO <sub>2</sub> -La <sub>2</sub> O <sub>3</sub>	400	1.6	Mizuno et al. (1993)
SnO <sub>2</sub> -LaOCl	350–425	1.4–1.6	Marsal et al. (2003a, b)
BaTiO <sub>3</sub> -CuO	300	1.08	Herrán et al. (2009)
BaTiO <sub>3</sub> -CuO-La <sub>2</sub> O <sub>3</sub>	550	2.5	Lee and Meyer (2000)
BaSnO <sub>3</sub>	500	3.1	Cavanagh et al. (2012)

chemical stability have very low sensitivity to CO<sub>2</sub>. Other studies have reported promising metal-oxide candidates such as La-doped SnO<sub>2</sub> and BaTiO<sub>3</sub>, which display reliable CO<sub>2</sub> sensing properties (Mizuno et al. 1993; Kim et al. 2000; Lee and Meyer 2000; Marsal et al. 2003a, b). However, the CO<sub>2</sub> sensitivity was found to be significantly reduced in the presence of humidity. BaTiO<sub>3</sub>-CuO and CuO-BaSnO<sub>3</sub> composites are also sensitive to CO<sub>2</sub> (Ishihara et al. 1991a, b, 1992, 1996; Herrán et al. 2009). The sensing mechanism appears due to gas interaction on a p–n heterojunction. However, the sensitivity of these devices to concentrations of interest for indoor air quality (300–2,000 ppm) is too low. Nd<sub>2</sub>O<sub>2</sub>CO<sub>3</sub> has also been reported as a strong candidate for a CO<sub>2</sub> sensor (Djerdj et al. 2009). In this case it was noted that the response of the material was enhanced in the presence of humidity, but the exposure to water vapor leads to a pronounced decrease in resistance (opposite of the CO<sub>2</sub> effect). Cavanagh et al. (2012) studied BaSnO<sub>3</sub> and found that BaSnO<sub>3</sub> prepared as porous screen-printed thick films and running at elevated temperature exhibits a significant resistance change upon exposure to CO<sub>2</sub> concentrations in the indoor air quality application range. The achieved CO<sub>2</sub> sensitivity of 3.1 at 2,000 ppm is larger than the current highest reported literature values for other metal oxide systems (see Table 2.14). Some authors believe that alarm systems based on such sensors can be developed. However, it is necessary to recognize that the sensitivity to CO<sub>2</sub> is not great. Moreover, there is also strong interference with other gases and humidity. Temporal drift and problems with stability are present as well.

### 2.4.1.3 Metal Oxide Comparison and Selection

We need to note that all the metal oxides indicated before which are used in chemiresistors are post-transition-metal oxides, such as ZnO and SnO<sub>2</sub>, which have cations with the filled  $d^{10}$  configuration, and transition-metal oxides with  $d^0$  and  $d^{10}$  electronic configurations. As we know, the  $d^0$  configuration is found in binary transition-metal oxides such as TiO<sub>2</sub> and WO<sub>3</sub> and also in perovskites such as

**Table 2.15** Advantages and disadvantages of MOXs for conductometric gas sensor applications

Material	Advantages	Disadvantages
SnO <sub>2</sub>	High sensitivity Good stability in reducing atmosphere	Low selectivity Dependence on air humidity
WO <sub>3</sub>	Good sensitivity to oxidizing gases Good thermal stability	Low selectivity Low sensitivity to reducing gases Dependence on air humidity Slow recovery
Ga <sub>2</sub> O <sub>3</sub>	High stability Ability to operate at high temperatures	Low selectivity Average sensitivity
In <sub>2</sub> O <sub>3</sub>	High sensitivity to oxidizing gases Fast response and recovery Low sensitivity to air humidity	Low selectivity Low stability at low-oxygen partial pressure
CTO (CrTiO)	High stability Low sensitivity to air humidity	Low selectivity Moderate sensitivity

Source: Reprinted with permission from Korotcenkov (2007b). Copyright 2007 Elsevier

ScTiO<sub>3</sub> and LiNbO<sub>3</sub>. These compounds share many features with non-transition-metal oxides. They have a filled valence band of predominantly O2p character and a gap between the valence band and an empty conduction band. Typical band gaps are 3–4 eV. Unlike transition-metal oxides with  $0 < n < 10$ , stoichiometric, post-transition-metal oxides ZnO, SnO<sub>2</sub>, and  $d^0$  transition-metal oxides may be reduced but not oxidized. The post-transition oxides ZnO, In<sub>2</sub>O<sub>3</sub>, SnO<sub>2</sub>, as well as the majority of transition-metal oxides, are active in “redox” reactions since the electron configuration of the solid may be altered. However, the reaction with oxidizing species such as O<sub>2</sub> is expected only with samples that have been bulk reduced or where the surfaces have been made oxygen deficient (Calatayud et al. 2003). The reduction of post-transition oxides as a rule leads to the formation of free carriers, which greatly increase the metal-oxide conductivity, a fact that is crucial for sensor applications.

Advantages and disadvantages of the most studied MOXs are listed in Table 2.15. Analysis of information listed in Tables 2.11 and 2.15 testifies that no single metal oxide can satisfy all possible requirements for efficient elaboration of gas sensors. For example, it is known that the response of gas sensors that operate in a temperature range lower than 450 °C can be controlled by either chemisorption or redox processes (Morrison 1982, 1987; Williams and Pratt 1998; Golovanov et al. 2005; Korotcenkov et al. 2007a, b). Sensors based on SnO<sub>2</sub> are sensors of the first type, whereas those based on In<sub>2</sub>O<sub>3</sub> are of the second type. SnO<sub>2</sub>-based sensors have been studied more extensively and are more widely used (Eranna et al. 2004), but this does not mean that the chemisorption mechanism necessarily has advantages compared to the redox mechanism for design of a particular sensor. It has been established that SnO<sub>2</sub>-based sensors have better sensitivity to reducing gases and better stability during operation in reducing atmospheres. However, In<sub>2</sub>O<sub>3</sub>-based sensors have better conductivity response to oxidizing gases and are less affected by changes in air humidity (Korotcenkov et al. 2004c; Korotcenkov 2005; Korotcenkov and Stetter 2008). Which is better, high response to reducing gases or to oxidizing gases? Only the designer can answer this question, depending on the requirements for a particular sensor.

The same can be said for other pairs of metal oxides, for example SnO<sub>2</sub>–CTO or SnO<sub>2</sub>–WO<sub>3</sub>. Titanium-substituted chromium oxide, Cr<sub>2-x</sub>Ti<sub>x</sub>O<sub>3+z</sub> (CTO), with  $0.01 < x < 0.45$ , has high chemical stability at its operating temperature, an easily measurable range of resistance, and good conductivity response (Williams 1999). In contrast to SnO<sub>2</sub>-based sensors, the effect of water vapor on the parameters of CTO-based sensors, such as the baseline and sensitivity, is much less than that on the parameters of SnO<sub>2</sub>-based devices operating at the same temperatures. This has been the key to the successful commercial development of CTO-based sensors for detection of carbon monoxide and volatile organic compounds in the air. On the other hand, CTO sensors, unlike SnO<sub>2</sub> sensors, are not sensitive to

methane, though they are sensitive to the higher hydrocarbons and to carbon monoxide,  $\text{H}_2\text{S}$ ,  $\text{NH}_3$ , and a wide range of solvents.

Considering the pair  $\text{SnO}_2\text{-WO}_3$ ,  $\text{SnO}_2$  shows both strong and fast gas response to ozone at sufficiently low temperature ( $\sim 200\text{--}300\text{ }^\circ\text{C}$ ), though there are problems of baseline stability at such low temperatures. The effect decreases with increasing temperature, to virtually zero at  $400\text{ }^\circ\text{C}$ .  $\text{WO}_3$  shows a particularly large resistivity increase at high temperatures ( $400\text{--}500\text{ }^\circ\text{C}$ ) in response to the presence of ozone. However, the response to ozone is relatively slow, as is the recovery when the gas is removed. In addition, the signal depends on the flow rate of the gas to the surface and on the partial pressures of water vapor and oxygen (Williams 1999). At the same time, however, experiments carried out by Solis et al. (2001) showed that  $\text{WO}_3$ -based sensors have unique and excellent sensitivity to low concentrations of  $\text{H}_2\text{S}$  in air at room temperature.

Hoefler et al. (2001) believe that  $\text{Ga}_2\text{O}_3$ -based sensors also have certain advantages in comparison with  $\text{SnO}_2$ -based sensors.  $\text{Ga}_2\text{O}_3$  sensors are high-temperature devices ( $T_{\text{oper}} = 600\text{--}900\text{ }^\circ\text{C}$ ) and therefore show faster response and recovery and lower cross-sensitivity to humidity than  $\text{SnO}_2$ -based sensors.  $\text{Ga}_2\text{O}_3$  sensors also show stable long-term sensing properties and good reproducibility even in sulfur-containing atmospheres. This last property makes these sensors suitable for use in domestic burner controls. No cleaning cycles are necessary, and smut or other organic residues are burned off. Additionally, no pre-aging is necessary (compared to  $\text{SnO}_2$ ). On the other hand, the sensitivity of  $\text{Ga}_2\text{O}_3$  sensors to a number of gases is lower compared to  $\text{SnO}_2$ -based sensors, and the power consumption of  $\text{Ga}_2\text{O}_3$ -based sensors is comparably high due to their high operating temperatures.

Grimes and coworkers (Mor et al. 2004; Varghese et al. 2004) found that  $\text{TiO}_2$  nanotubes were excellent room-temperature hydrogen sensors not only with a high sensitivity but also with an ability to self-clean photoactively after environmental contamination (Mor et al. 2004). The hydrogen-sensing capabilities of the sensors were largely recovered by ultraviolet (UV) light exposure after being completely extinguished by a rather extreme means of sensor contamination: immersion of the sensor in motor oil.  $\text{SnO}_2$  does not possess such properties.

All these factors mean that the choice of a metal oxide for gas sensor design is determined by the type of gas sensor to be designed (see Tables 2.15 and 2.16), the apparatus or device in which the sensor will be used, the structure chosen for the sensor's fabrication, and conditions of exploitation (Wilson et al. 2001; Varghese et al. 2003; Eranna et al. 2004; Korotcenkov 2005; Tamaki et al. 2005; Kanda and Maekawa 2005; Sadek et al. 2006; Chung and Oh 2006). However, any competition between potential materials can be ignored if the device is to become part of an "electronic nose." Different behavior during interaction with the same gas is one of the most important requirements for sensors designed for this application (Gardner and Bartlett 1992, 1999; Haugen and Kvaal 1998; Tomchenko et al. 2003).

One can find in review papers and books more detailed comparative analysis of different metal oxides aimed for gas sensors (Korotcenkov 2007a, b, 2011a, b; Fine et al. 2010; Wetchakun et al. 2011; Arafat et al. 2012; etc.).

### 2.4.2 Metal-Oxide p-n Homojunction and Heterostructures

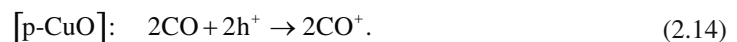
Normally, metal oxides such as  $\text{SnO}_2$ ,  $\text{TiO}_2$ ,  $\text{WO}_3$ ,  $\text{ZnO}$ , and  $\text{In}_2\text{O}_3$  usually used for gas sensor design are n-type semiconductors (see Fig. 2.27). However, there are few metal oxides such as  $\text{CrO}$ ,  $\text{CuO}$ , and  $\text{NiO}$  that also exhibit p-type conductivity (Krillov and Kisilev 1981; Stamataki et al. 2008). Recently p-type conductivity was reported in  $\text{ZnO}$  (Basu and Hazra 2005; Hazra and Basu 2006). Thus, the fabrication of semiconducting metal oxide p-n homojunctions could also be achieved with  $\text{ZnO}$ . It was shown that p-n  $\text{ZnO}$  homojunction is sensitive to  $\text{H}_2$  as there is a substantial shift in the forward bias  $I\text{-}V$  characteristics on exposure to the reducing gases (Basu and Hazra 2005; Hazra and Basu 2006).

**Table 2.16** Examples of metal oxide-based sensors with maximum sensitivity to specific gases

Gas tested	Metal oxide	$T_{\text{oper}}$ (°C)	Sensitivity	Gas concentration	Reference
Ethanol	SnO <sub>2</sub> :Zn (thick film)	250	$3.9 \times 10^3$	300 ppm	Hemmati et al. (2011)
	ZnO:Sn (thick film)	300	$1.2 \times 10^3$	300 ppm	Hemmati et al. (2011)
	SnO <sub>2</sub> :Pd (nanofiber)	330	$1 \times 10^3$	100 ppm	Choi et al. (2010)
	In <sub>2</sub> O <sub>3</sub> :Fe <sub>2</sub> O <sub>3</sub> (thick film)	300	220	100 ppm	Ivanovskaya et al. (2003)
	SnO <sub>2</sub> :La <sub>2</sub> O <sub>3</sub> (thick film)	200	213	100 ppm	Shi et al. (2009)
LPG	SnO <sub>2</sub> :Ru (thin film)	250	$2.5 \times 10^3$	1,000 ppm	Mulla et al. (2004)
H <sub>2</sub> S	SnO <sub>2</sub> :CuO (nanoribbon)	50	$1.8 \times 10^4$	3 ppm	Kong and Li (2005)
	SnO <sub>2</sub> :Pt (nanofiber)	300	$5.1 \times 10^3$	20 ppm	Dong et al. (2011)
H <sub>2</sub>	In <sub>2</sub> O <sub>3</sub> :Pt (nanofiber)	200	$1.5 \times 10^3$	600 ppm	Zheng et al. (2009)
	TiO <sub>2</sub> (nanotube array)	RT	$10^9$	1,000 ppm (H <sub>2</sub> +N <sub>2</sub> )	Paulose et al. (2006)
	SnO <sub>2</sub> /SBA-15	250	$1.4 \times 10^3$	1,000 ppm	Yang et al. (2008)
	SnO <sub>2</sub> /SiO <sub>2</sub> (thick film)	250	$3.2 \times 10^3$	3,000 ppm	Wada and Egashira (2000)
	SnO <sub>2</sub> (mesoporous)	300	100	500 ppm	Li and Kawi (1998)
CO	SnO <sub>2</sub> (thick film)	120	$10^3$	1,000 ppm	Aroutiounian (2007)
	In <sub>2</sub> O <sub>3</sub> :Au (nanowire)	RT	104	5 ppm	Singh et al. (2011)
	In <sub>2</sub> O <sub>3</sub> (nanofibers)	300	500	100 ppm	Lim et al. (2010)
	SnO <sub>2</sub> :In:Pt (thick film)	140	20	50 ppm	Zhang et al. (2009)
	TiO <sub>2</sub> (nanofiber)	300	21	100 ppm	Biao et al. (2010)
O <sub>3</sub>	WO <sub>3</sub> (thin film)	120	$(0.6-7) \times 10^3$	90 ppb	Berger et al. (2004)
	SnO <sub>2</sub> (thin film)	150	$\sim 10^5$	1 ppm	Korotcenkov et al. (2009b)
	In <sub>2</sub> O <sub>3</sub> (thick film)	300-350	$(1-6) \times 10^3$	76 ppb 100 ppb	Sahm et al. (2006); Epifani et al. (2008)
	WO <sub>3</sub> (thin film)	300	$1.5 \times 10^3$	500 ppb	Vallejos et al. (2008)
	In <sub>2</sub> O <sub>3</sub> (thin film)	200-300	$10^3-10^4$	1 ppm	Korotcenkov et al. (2004a)
NH <sub>3</sub>	ZnO:Fe <sub>2</sub> O <sub>3</sub> (thick film)	350	$3.6 \times 10^3$	300 ppm	Patil (2009)
CH <sub>4</sub>	ZnO:Sb (thick film)	360	25	1,000 ppm	Dayan et al. (1998)
	SnO <sub>2</sub> :Pd (nanofibers)	385	8.5	500 ppm	Choi et al. (2010)
SO <sub>2</sub>	WO <sub>3</sub> :Pt (thin film)	200	6	1 ppm	Stankova et al. (2004)
	SnO <sub>2</sub> and SnO <sub>2</sub> :V <sub>2</sub> O <sub>5</sub> (thick film)	350	35-70	100 ppm	Das et al. (2008)
	WO <sub>3</sub> (thin film)	350	3	20 ppm	Ghimbeu et al. (2009)

Thick films and thin films mean that sensors were fabricated using thick-film or thin-film technologies; Sensitivity:  $S = R_a/R_g$

The use of heterostructures in gas detection was introduced by Nakamura et al. (1986, 1990) who employed bulk p-CuO and n-ZnO disks mechanically pressed into contact. Experimental results from this device showed CO sensitivities that were two to three times higher at  $T_{\text{oper}} = 260$  °C than that for propane or H<sub>2</sub>. Subsequent studies for individual ZnO and CuO disks yielded negligible sensitivities for CO, and, thus, an interaction between the ZnO and CuO was proposed as follows (Nakamura et al. 1990):





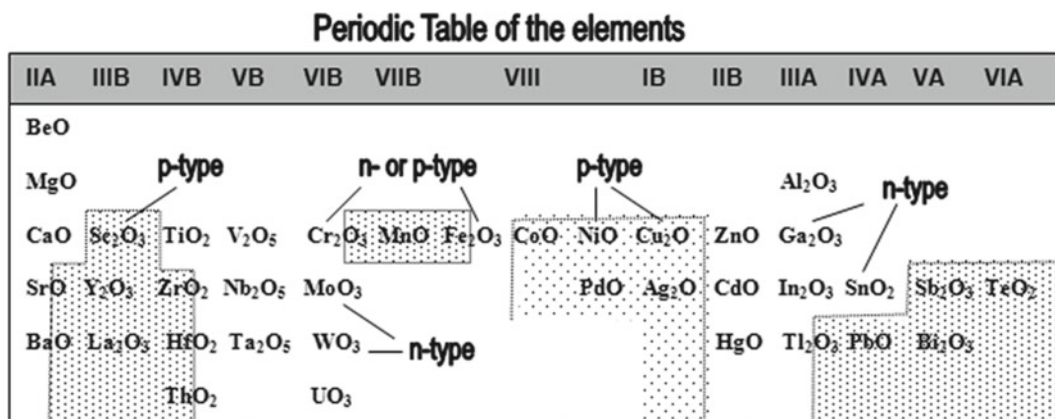


**Fig. 2.27** Dependence of the metal oxide's type of conductivity on the position of metals in the Periodic Table. *Hatched*, metal oxides with a predominance of p-type conductivity. *Unhatched*, metal oxides with a predominance n-type conductivity [Data extracted from Krilov and Kisilev (1981)]

The reaction in Eq. (2.15) serves to free up both electrons and holes, thus allowing for the sensitive detection of CO through a decrease in interfacial resistance. It was found that high sensitivity and selectivity to CO was conditioned by the presence of Na (>1 mol%) in CuO. It was concluded that the excess electropositive Na stabilized molecular chemisorption and promoted the dissociation of such molecules as CO and O<sub>2</sub>, thus leading to the observed CO sensitivity (Jung and Yanagida 1996). The doping of CuO/ZnO heterostructures in the improvement of H<sub>2</sub> sensitivity has also been studied. Research by Aygun and Cann (2005) demonstrated improved hydrogen sensitivity when CuO was doped with monovalent and divalent metals. This effect was attributed to a possible increase in hole density and the potential for second phase hydrogen adsorption sites.

Vasiliev et al. (1998, 1999) showed that CuO/SnO<sub>2</sub> heterostructures have a high sensitivity to H<sub>2</sub>S. In addition Vasiliev et al. (1998) found that heterostructure-based sensors had shorter response times to 25–300 ppm H<sub>2</sub>S in N<sub>2</sub> at 100–250 °C compared to those of SnO<sub>2</sub>(CuO) films. Operating characteristics of SnO<sub>2</sub>/CuO heterostructures sensitive to H<sub>2</sub>S are presented in Fig. 2.28. It is suggested that the improvement of dynamic sensor properties of SnO<sub>2</sub>/CuO heterostructures is caused by the localization of electrical barrier between CuO and SnO<sub>2</sub> layers.

Experiment has shown that the possibility to control the capacitance during gas detection is applicable to heterostructure-based sensors as well. Vasiliev et al. (1999) observed this effect for SnO<sub>2</sub>/SiO<sub>2</sub>/Si heterostructures (see Fig. 2.28d), while Kwon and Cann (2005) reported on the capacitance behavior of Ni-doped CuO/ZnO heterostructures during H<sub>2</sub> detection. Kwon and Cann (2005) have found that heterostructure capacitance displayed a strong frequency dependence in ambient hydrogen at low (~100 Hz) frequencies.

Other heterostructures were also studied. In particular, ZnO/CuO is relatively a widely explored structure for sensing CO (Baek and Tuller 1993; Ushio et al. 1994) and H<sub>2</sub> (Dandeneau et al. 2009). Hu et al. (2003) showed that ZnO/CuO also has good response toward H<sub>2</sub>S and alcohol. The NO<sub>2</sub> and CO<sub>2</sub> sensing properties of a heterojunction gas sensor formed between n-type ZnO and a p-type composite based on a mixture of BaTiO<sub>3</sub>/CuO/La<sub>2</sub>O<sub>3</sub> were evaluated by Ling et al. (2001). Heterostructures such as SnO<sub>2</sub>/a-MoO<sub>3</sub> and TiO<sub>2</sub>/Ti<sub>1-x</sub>Sn<sub>x</sub>O<sub>2</sub> as sensors to ethanol were studied by Xing et al. (2011) and Wu (2011), respectively.

It should be noted that, similarly to conventional metal oxide gas sensors, high porosity of material used for heterostructure forming is one of the main requirements for achievement of high sensitivity.

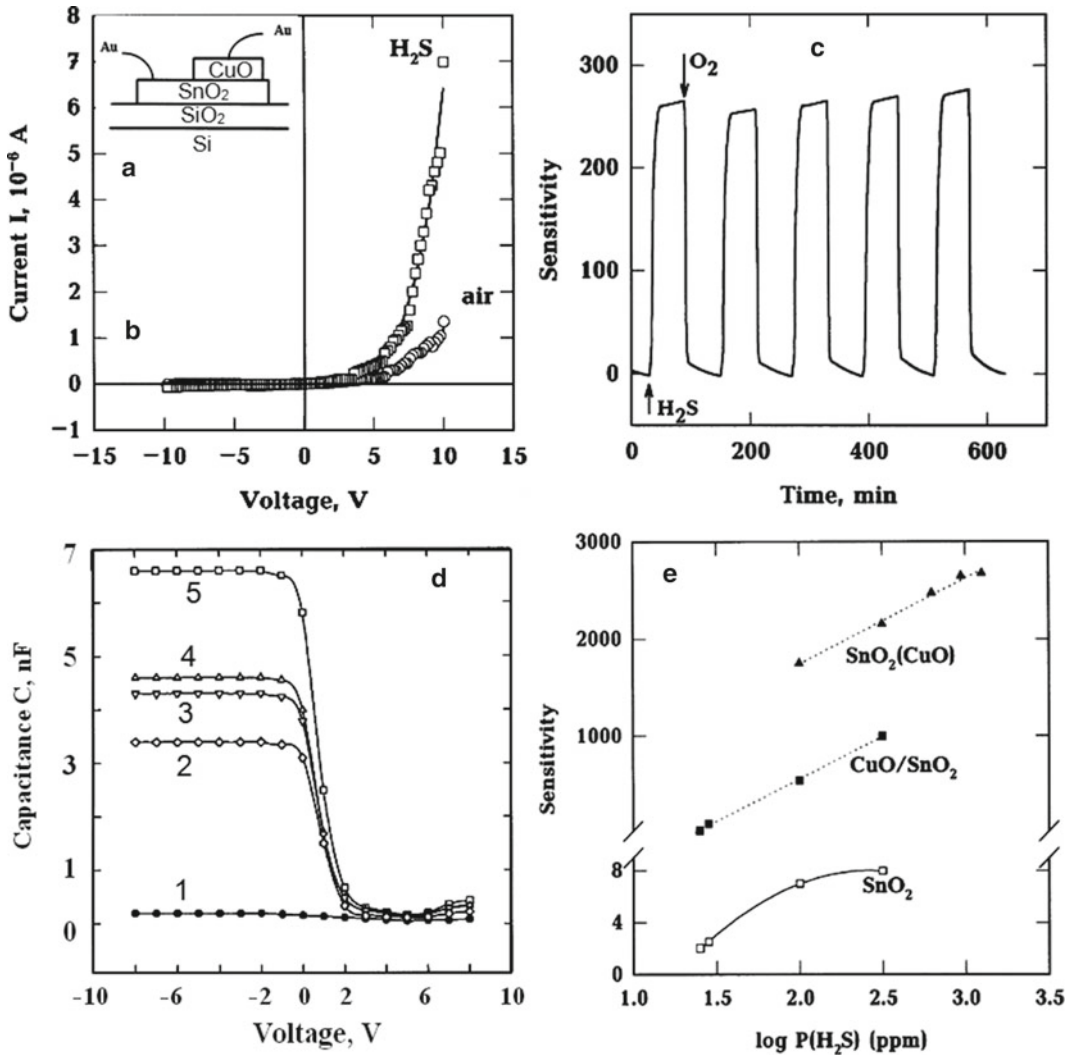


**Fig. 2.28** Operating characteristics of heterostructure-based gas sensors. (a) CuO:SnO<sub>2</sub> heterostructures configuration. (b)  $I-V$  characteristics in air and 100 ppm H<sub>2</sub>S in N<sub>2</sub> at 200 °C. (c) Typical electrical response of CuO:SnO<sub>2</sub> heterostructure to a periodic change of gas phase composition at 160 °C. (d) Typical capacitance-voltage characteristics of an n-SnO<sub>2</sub>/SiO<sub>2</sub>/p-Si heterostructure in air (curve 1) after a 10-min exposure to mixtures of air and 1% C<sub>2</sub>H<sub>5</sub>OH (2), 1% H<sub>2</sub>O (3), and 1% NH<sub>3</sub> (4) and after a 24-h to a mixture of air and 1% H<sub>2</sub>O (5).  $T_{oper}=20$  °C. (e) Sensitivity of CuO:SnO<sub>2</sub> heterostructure, SnO<sub>2</sub>, and SnO<sub>2</sub>(CuO) nanocomposite film vs H<sub>2</sub>S content in H<sub>2</sub>S+N<sub>2</sub> gas mixture (Reprinted with permission from Vasiliev et al. (1998). Copyright 1998 Elsevier, and Vasiliev et al. (1999). Copyright 1999 American Institute of Physics)

In particular, Tongpool et al. (2000) studied CuO/ZnO heterostructure-based hydrogen sensors and found that the response to H<sub>2</sub> was significantly larger in the more porous structures.

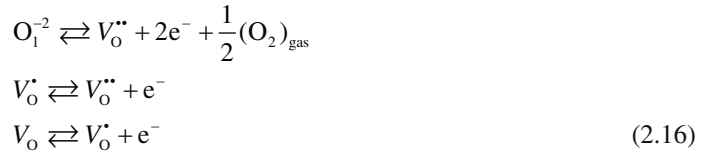
Of course, the possibility to design gas sensors using p-n junctions and heterostructures gives additional resources for fabrication devices with new performances. However, we need to acknowledge that such sensors cannot find widespread applications. First, the technology of these sensors is more complicated, and second, the application of p-n junction and heterostructures does not give the improvement of gas-sensing characteristics in comparison with conventional devices. For example, Vasiliev et al. (1998) found that SnO<sub>2</sub>/CuO heterostructures had smaller response to H<sub>2</sub>S as compared to sensitivity of the SnO<sub>2</sub>(CuO) films (see Fig. 2.28e). In addition, CuO-based heterostructures have increased

both the drift and sensitivity to air humidity (Katti et al. 2003). As a result, CuO/ZnO and La<sub>2</sub>CuO<sub>4</sub>/ZnO heterostructures were studied as in humidity sensors (Traversa 1995). According to Traversa (1995), the mechanism of these sensors is based on the electrolysis of water at the heterocontact interface.

### 2.4.3 High-Temperature Oxygen Sensors Based on Semiconducting Metal Oxides

Experiment has shown that semiconducting metal oxides can operate at high temperature as well. For example, it was established that resistive oxygen sensors based on semiconducting metal oxides such as TiO<sub>2</sub>, CeO<sub>2</sub>, Nb<sub>2</sub>O<sub>5</sub>, SnO<sub>2</sub>, CoO, Ga<sub>2</sub>O<sub>3</sub>, or WO<sub>3</sub> provide an alternative solution for high-temperature oxygen sensors (instead of solid electrolytes) with wide dynamic range and simplified design (Logothetis 1980). Table 2.17 lists properties of several common semiconducting metal oxides which are the most suitable for application in high-temperature oxygen sensors.

The change in conductance of semiconducting metal oxides at high temperature upon exposure to the test gas is due to the change in concentration of oxygen species in the bulk and is a reflection of the defect structure (Moseley and Crocker 1996). So, in this temperature region, sensors do not work as chemiresistors as discussed in previous sections. The predominant defects in oxide semiconductors are oxygen vacancies and their associated free charge carriers. According to the oxygen-vacancy model proposed by Kröger and Vink (1956), the reactions between the oxygen vacancies, the ambient oxygen gas, and the conduction electrons are



where  $\text{e}^-$ ,  $\text{V}_\text{O}^{\bullet\bullet}$ ,  $\text{V}_\text{O}^{\bullet}$ ,  $\text{V}_\text{O}$ ,  $1/2(\text{O}_2)_{\text{gas}}$ , and  $\text{O}_1^{-2}$  represent, respectively, a conduction electron, a doubly ionized oxygen vacancy, a singly ionized oxygen vacancy, an un-ionized oxygen vacancy, an atom of oxygen in the ambient gas, and an oxygen ion at an anion lattice position. Subjecting an oxide film, such as TiO<sub>2</sub> or SnO<sub>2</sub>, to decreasing oxygen partial pressure,  $P_{\text{O}_2}$ , at kinetically favorable temperatures will lead to increasing levels of oxygen deficiency and consequently increasing levels of n-type conductivity. Applying defect chemical concepts (Hill and Tuller 1991), it is straightforward to show that  $\ln$  conductivity has the following linear dependence on  $\ln P_{\text{O}_2}$  (Moseley 1992; Moseley and Crocker 1996):

$$\ln \sigma = K(T) + \frac{1}{N} \ln P_{\text{O}_2} \quad (2.17)$$

or

$$\sigma = A \exp\left(-\frac{E_A}{kT}\right) P_{\text{O}_2}^{1/N}, \quad (2.18)$$

where  $\sigma$  is the electronic conductivity,  $A$  is a constant,  $E_A$  the activation energy for conduction,  $P_{\text{O}_2}$  is oxygen partial pressure, and  $N$  is a parameter determined by both the type of the carrier (n or p) and the bulk defects in the semiconductor involved in the equilibrium between oxygen and the sensor (e.g., oxygen vacancy) (Kofstad 1972). The positive and negative signs of  $N$  correspond to p-type and n-type conduction, correspondingly. The value of  $|1/N|$  is the sensitivity of the sensor; the higher the  $|1/N|$  value the higher the sensitivity, and vice versa. A high diffusion coefficient in metal oxides produces a decrease in both operation temperatures and response time. Table 2.17 lists the  $N$  values for a

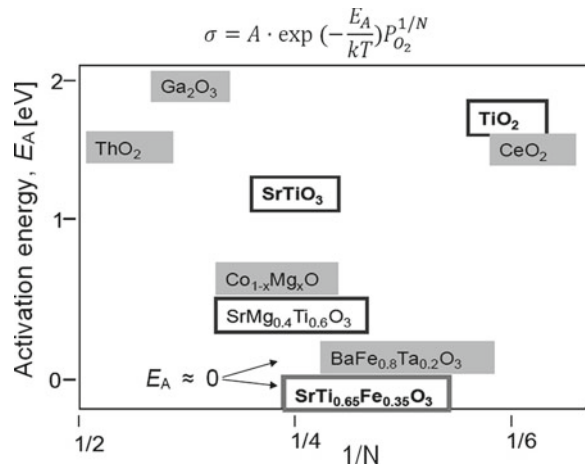
**Table 2.17** Carrier, defect type, and sensitivity parameters of semiconducting metal oxides for oxygen sensing in the temperature range 600–800 °C

Semiconductor metal oxides	Carrier type	Defect type	Oxygen sensitivity ( $N$ in Eq. (2.18))
CeO <sub>2</sub>	n	$V_o^{\bullet\bullet}$	-5 to -7
Nb <sub>2</sub> O <sub>5</sub>	n	$V_o^{\bullet\bullet}$	-4 to -8
Ga <sub>2</sub> O <sub>3</sub>	n	$V_o^{\bullet\bullet}$	-2 to -4
TiO <sub>2</sub>	n	$V_o^{\bullet\bullet}$ , $Ti_{int}$	-4 to -6
SrTiO <sub>3</sub> <sup>a</sup>	n, p	$V_o^{\bullet\bullet}$ , $V''_{Sr}$	-4 to -6 and 4

<sup>a</sup>Strontium titanate adopts different conduction mechanisms in different  $P_{O_2}$  ranges

Source: Data from Moseley (1992) and Ramamoorth et al. (2003)

**Fig. 2.29** Parameters controlling conductivity of several metal oxides. [Idea of Meneskloou (2011)]

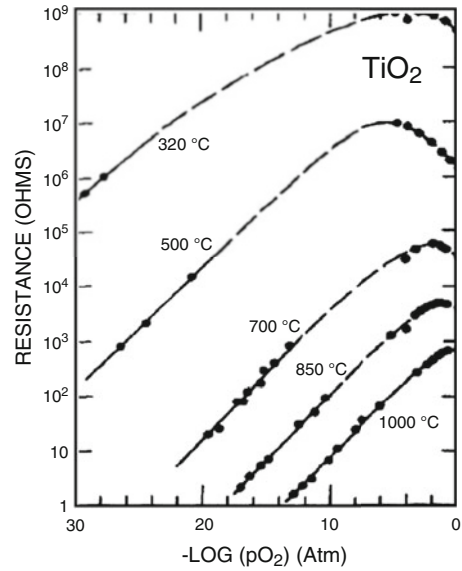


series of semiconducting oxygen sensor materials.  $E_A$  is also an important parameter, because the lower the value of  $E_A$ , the lower the sensitivity of the response will be to temperature fluctuation.  $E_A$  for several metal oxides is presented in Fig. 2.29.

However, these sensors also have considerable disadvantage. Unfortunately, the conductivity also depends, in most cases, on temperature, rendering these sensors very sensitive to temperature fluctuations (see Fig. 2.30) (Logothetis 1980; Knauth and Tuller 1999). For example, for TiO<sub>2</sub> and Ga<sub>2</sub>O<sub>3</sub>, the activation energies are equal to ~1.5 eV and ~1.9 eV, respectively. This means that, for precise measurements of oxygen partial pressure with these materials, there will be a need for close control of temperature. Thus, to limit erroneous signals, minimization of cross-sensitivity to temperature is desired. Experiments have shown that all the above-mentioned problems can be resolved through application of perovskites (BaTiO<sub>3</sub>, SrTiO<sub>3</sub>, BaFe<sub>0.8</sub>Ta<sub>0.2</sub>O<sub>3</sub>, LaFeO<sub>3</sub>, SrTiFeO<sub>3</sub>, BaSnO<sub>3</sub>, etc.) (Rothschild et al. 2005; Rothschild and Tuller 2006; Moos et al. 2011).

The considerable attention paid to other perovskites such as BaTiO<sub>3</sub> as oxygen sensors is a result of the fact that the conductivity of these materials can be independent of operating temperatures. It has been suggested that the Fermi level lies in the semiconductor gap far above the valence band, and the concentration and mobility of free charge carriers (holes) depend on the operating temperature under different signs. This effect compensates the temperature-induced variations of the conductivity and results in zero temperature coefficient of resistance (Rothschild et al. 2005). It was

**Fig. 2.30** Temperature influence on  $R(pO_2)$ -characteristics of a  $TiO_2$  ceramics (Reprinted with permission from Logothetis (1980). Copyright 1980 Elsevier)



established that for achievement of the indicated effect, two points should be made (Moseley 1992). First, this balance of thermal effects must not alter the effect of changes in oxygen partial pressure at a fixed temperature. Second, such a balance is only possible for oxides in the p-type regime, where the thermal activation of charge carriers and the stoichiometry effect are opposed. Perovskites make it possible to realize such a situation. For example,  $BaTiO_3$  is an n-type at low oxygen partial pressure, but above certain minimum conductance values the material is p-type. In this range of oxygen partial pressures, the isothermal data lines really are very much closer together than in the n-type range. In other words, the temperature dependence of conduction is considerably less in the p-type than in the n-type range. As was explained earlier, the reasons for this characteristic are quite interesting. In general, as the temperature is raised at a fixed oxygen partial pressure, the oxides of transition metals lose oxygen, and if they are in the p-type range of oxygen partial pressure, conductivity will tend to decrease. This effect is in contrast to the thermal promotion of charge carriers, and it makes it possible to dope the oxide to such an extent that the two effects cancel each other out and the temperature changes have hardly any effect on the conductivity. However, for  $BaTiO_3$ , the thermal activation and stoichiometric effects are not quite in balance so the activation energy is small but not zero. It was found that perovskites  $SrTi_{(1-x)}Fe_xO_3$  ( $x=0.3-0.4$ ) have much better characteristics, and the conductivity of these materials does not depend on operating temperatures higher than 700 °C at oxygen partial pressures exceeding 1 Pa (Litzelman et al. 2005; Rothschild et al. 2005; Rothschild and Tuller 2006; Menesklou 2011). This effect is illustrated in Fig. 2.31. The negligible cross-sensitivity to temperature fluctuations makes these MOX structures promising candidates for the development of oxygen sensors for lean-burn engines (Litzelman et al. 2005; Rothschild et al. 2005). Moseley and Williams (1989) have shown that  $BaFe_{1-y}Ta_yO_3$  ( $y=0.2-0.3$ ) also possesses a temperature independency of conductivity (Menesklou 2011). Some years later, Blase et al. (1997) found that  $La_2CuO_{4+\delta}$  (lanthanum cuprate) thick-film sensors also behave temperature independently. Moreover, the long-term stability under cyclic temperature loading was found to be excellent. In Fig. 2.32 the resistance of a  $La_2CuO_{4+\delta}$  ceramic pellet is plotted vs  $pO_2$  for 600 °C, 700 °C, and 800 °C. However, it was established that this material type shows instability toward reducing atmospheres and limited high-temperature stability.

**Fig. 2.31** Conductivity as a function of oxygen partial pressure and temperature for  $\text{Sr}(\text{Ti}_{1-x}\text{Fe}_x)\text{O}_3$  polycrystals with  $x=0.01$  and  $x=0.35$ . Reprinted from Menesklou et al. (1999)

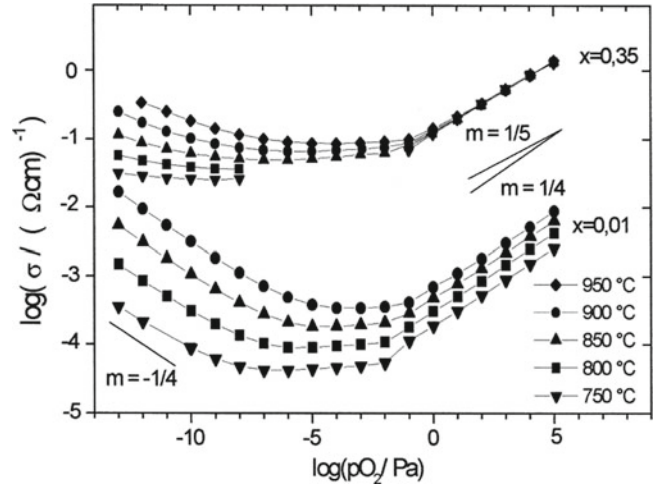
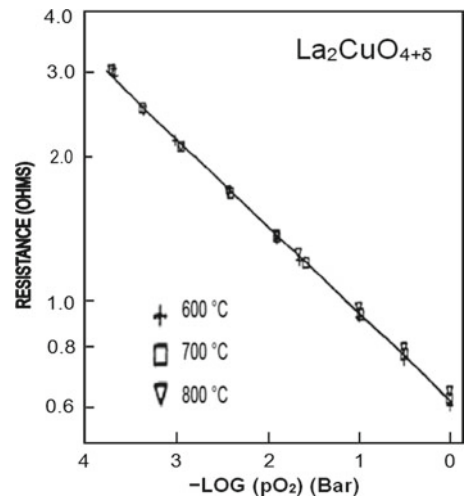


**Fig. 2.32** Temperature influence on  $R(p\text{O}_2)$ -characteristics of  $\text{La}_2\text{CuO}_{4+\delta}$  ceramics. Reprinted with permission from Blase et al. (1997). Copyright 1997 Elsevier



## 2.5 Metal Oxides for Room-Temperature Gas Sensors

As shown earlier, only post-transition-metal oxides, which have cations with the filled  $d^{10}$  ( $\text{ZnO}$ ,  $\text{SnO}_2$ ,  $\text{Ga}_2\text{O}_3$ ) configuration, and transition-metal oxides with  $d^0$  ( $\text{TiO}_2$ ) electronic configurations have found wide application in conductometric gas sensors (Fleischer and Meixner 1997; Barsan et al. 1999; Korotcenkov 2005, 2007a, b; Jing et al. 2006). However, limited use of pure transition-metal oxides ( $1 < n < 10$ ) for conductometric gas sensor fabrication does not mean that transition-metal oxides are not of interest of gas sensor designers. Numerous experiments, conducted by various authors, testify that, as a rule, oxides with electron configuration  $d^3$  ( $\text{Cr}_2\text{O}_3$ ,  $\text{MnO}_2$ ) and  $d^{6-8}$  ( $\text{Co}_3\text{O}_4$ ,  $\text{NiO}$ ) are the most catalytically active ones (Krilov and Kisilev 1981). In addition,  $dn$  oxides with  $n \geq 1$  are potentially susceptible to oxidation, as well as reduction. The most obvious consequence is that many transition elements have several stable oxides with different compositions. It is also much easier than with non-transition-metal oxides to make defects, having different electron configurations. Such big differences in pre-transition- and transition-metal oxides' behavior mean that transition-metal oxides are more sensitive to the change of the surroundings. Such unique properties of transition-metal oxides make them very attractive for various sensor applications, including functionalizing of more stable and wide band gap oxides and

forming of more complicated nanocomposite materials (Kanazawa et al. 2001). We have to admit that a choice of metal oxide as additive for properties' modification of other metal oxides is often connected with the catalytic properties of those oxides (Yamazoe et al. 1983; Oelerich et al. 2001; Pijolat et al. 2006). For example, the catalytic activity to a selected gas is the most important parameter for application in membranes, used for sensor response selectivity improvement (Yamazoe et al. 1983).

Room-temperature (RT) gas sensors are another possible field of application for catalytic active metal oxides. Doll and Eisele (1998) have found that RT work-function sensors based on catalytically active oxides such as CeO, Fe<sub>2</sub>O<sub>3</sub>, and NiO have shown good operation parameters. Transition-metal oxides such as Co<sub>3</sub>O<sub>4</sub>, NiO, Mn<sub>3</sub>O<sub>4</sub>, CuO, and WO<sub>3</sub> are also preferred for use in optochemical sensors based on optical absorption change during interaction with detected gas (Ando et al. 1997, 2001). For optical waveguide gas sensors, the change of optical refraction index is more important than the change of electroconductivity. Therefore the reversible absorbance change in the visible–near IR range and the relatively fast response make these oxides potential candidates for optical detection of CO, H<sub>2</sub>, alcohol (WO<sub>3</sub>), and air humidity (Dakin and Culshaw 1988; Ando et al. 1996, 1997, 1999; Yadav et al. 2007). In particular, it was found that Mn<sub>2</sub>O<sub>3</sub>, Co<sub>3</sub>O<sub>4</sub>, and NiO with p-type semiconducting properties under the influence of CO demonstrate reversible changes in the visible–near IR absorption band at 250–350 °C (Kobayashi et al. 1990). The absorbance change was assumed to be caused by a change in positive hole density during catalytic CO oxidation. Metal oxides such as WO<sub>3</sub>, MoO<sub>3</sub>, and V<sub>2</sub>O<sub>5</sub> showed reversible sensitivity to H<sub>2</sub> (see also Sect. 2.6.3 and Chap. 15 (Vol. 2)) and cobalt oxide (Co<sub>3</sub>O<sub>4</sub>) films, prepared by pyrolysis of an organometallic precursor, showed a humidity-sensitive absorbance change in the visible wavelength region around 350–400 nm (Ando et al. 1996). The reversible absorbance changes and the relatively fast response time (within a few minutes) make the Co<sub>3</sub>O<sub>4</sub> film a potential candidate for optical humidity detection. Co<sub>3</sub>O<sub>4</sub>-based optochemical sensors can also operate at room temperature (Ando et al. 1997). Nanosized NiO films prepared by plasma oxidation of nickel–carbon composite films (Ando et al. 1999) and TiO<sub>2</sub> films fabricated by sol–gel and thermal evaporation methods (Yadav et al. 2007) also showed humidity sensitive absorbance changes at room temperature. However, a comparative study carried out by Yadav et al. (2007) established that humidity sensors with a TiO<sub>2</sub> film prepared by the thermal evaporation method are more sensitive in the range 5–80% than the sensor based on the sol–gel method, while sensors based on sol–gel films are sensitive in the higher range of humidity, i.e., from 80% to 95%. Of course, these sensors do not possess so high a sensitivity as standard semiconductor gas sensors. However, this type of sensor has some peculiarities, which can be used in real applications. The advantages of optochemical sensors over conventional electricity-based gas sensors are higher resistivity to electromagnetic noise, compatibility with optical fibers, and the potential of multi-gas detection using differences in the intensity, wavelength, phase, and polarization of the output light signals (Ando et al. 2001).

In plasmon resonance gas sensors, which also usually operate at room temperatures, we have another situation. In these devices, in order to shift the operating point of the surface plasmon resonance toward an aqueous environment, a thin high-refractive index dielectric overlayer can be employed. The use of overlayers with higher refractive indexes allow for thinner overlayers and potentially better sensor sensitivity. Analysis of results obtained indicates that tantalum pentoxide, which has high refractive index (see Table 2.18) and good environmental stability, may be used for this purpose (Dostálek et al. 2001; Boozer 2003).

Adsorption sensors designed for operation at room temperature, for example, such sensors as SAW and cantilever ones, where the change in weight of sensing element is a determinant factor (Houser et al. 2001) have other requirements as sensing materials. It is known that the role of the sensing material in such devices is selectively and reversibly to adsorb an analyte of interest from sampled air. Therefore, maximum and reversible sorption of specific analytes or classes of analytes, with rapid sorption kinetics and minimal sorption of interferences, are key goals in the development of a successful chemiselective coating for SAW and work-function sensors (Thompson and Stone 1997). For example, measurements of various metal oxide capabilities for adsorption of both isopropanol and methanol (Badlani and Wachs 2001; Kulkarni and Wachs 2002) have shown that the average active surface site

**Table 2.18** Refractive indices and dielectric constants of some sensing materials

Refractive indices		Dielectric constants	
Material	$n$	Material	$\epsilon$
<i>Metal oxides</i>		<i>Metal oxides</i>	
Al <sub>2</sub> O <sub>3</sub> , SiO <sub>2</sub>	1.4–1.7	MgO, CaO, BaO, SiO <sub>2</sub>	3–5
MgO, CaO, SrO	1.7–2.0	Cr <sub>2</sub> O <sub>3</sub> , NiO, CuO, ZnO, Al <sub>2</sub> O <sub>3</sub>	5–10
BaO, ZrO <sub>2</sub> , HfO <sub>2</sub> , Nb <sub>2</sub> O <sub>5</sub> , ZnO, SnO <sub>2</sub> , Sb <sub>2</sub> O <sub>3</sub>	~2–2.1	Y <sub>2</sub> O <sub>3</sub> , ZrO <sub>2</sub> , V <sub>2</sub> O <sub>5</sub> , WO <sub>3</sub> , SnO <sub>2</sub>	10–20
Cr <sub>2</sub> O <sub>3</sub> , Fe <sub>2</sub> O <sub>3</sub> , NiO, Bi <sub>2</sub> O <sub>3</sub> , TiO <sub>2</sub> , Ta <sub>2</sub> O <sub>5</sub> , CuO	2.1–2.5 >2.5	La <sub>2</sub> O <sub>3</sub> , HfO <sub>2</sub> , CeO <sub>2</sub> , Nb <sub>2</sub> O <sub>5</sub> , Ta <sub>2</sub> O <sub>5</sub>	20–50
		TiO <sub>2</sub>	>50
<i>Semiconductors</i>		<i>Semiconductors</i>	
Si, InP, GaAs	3.4–3.6	Si, InP, GaAs	11.8–12.9
SiC, GaN	2.3–2.6	SiC, GaN	8.9–10.6
Diamond	2.4	Diamond	5.5
<i>Polymers</i>		<i>Polymers</i>	
Polypyrrole	1.8	Polypyrrole	8

density ( $N_s$ ) for isopropanol and methanol adsorption on the majority of metal oxide surfaces was found to be 0.2–4  $\mu\text{mol m}^{-2}$ . Some of the active metal oxides (MgO, La<sub>2</sub>O<sub>3</sub>, Cr<sub>2</sub>O<sub>3</sub>, Sb<sub>2</sub>O<sub>3</sub>) possess a higher active site density, which gives those oxides a sufficient advantage for the design of adsorption sensors sensitive to isopropanol and ethanol. Cr<sub>2</sub>O<sub>3</sub>, WO<sub>3</sub>, and BaO show a somewhat lower active surface site density. SiO<sub>2</sub> is extremely unreactive and has a low  $N_s$  in spite of having a high surface area. However, we have to note that this conclusion is not a universal one. Every technical task requires an individual solution, considering both the nature of tested gas and operating conditions. For example, in the case of CO<sub>2</sub> adsorption, an absolutely different situation applies (Horiuchi et al. 1998).

Dielectric constant is another important parameter for gas-sensing materials. Dielectric constants for several materials are presented in Table 2.17. Its value plays an important role during selection of materials for capacitance-type gas sensors operated at room temperature (Ishihara and Matsubara 1998). Capacitive-type sensors have good prospects given that the capacitor structure is so simple, enabling miniaturization and achieving high reliability and low cost. In addition, application of capacitance is easily performed by oscillator circuits, and thus capacitive-type sensors enable sensitive detection. In addition, oscillator circuits consist of only a standard resistor and sensor capacitor. Therefore the signal treatment circuit is also very simple and low cost. The humidity sensor is the best known capacitive-type sensor. Since water has an abnormally large dielectric constant, the adsorption of water in porous metal oxide changes the relative permittivity of a gas-sensing matrix. In relation to other types of humidity sensors, the capacitive type has the advantage of high sensitivity over a wide humidity range. Porous Al<sub>2</sub>O<sub>3</sub> is the best known metal oxides used in such sensors (Ishihara and Matsubara 1998).

As was shown before, conventional gas-sensing metal oxides, such as SnO<sub>2</sub>, In<sub>2</sub>O<sub>3</sub>, WO<sub>3</sub>, ZnO, as a rule are used in conductometric gas sensors operated at high temperatures. However, during experiments carried out recently (last decade) it was established that conductometric gas sensors based on these metal oxides can operate at room temperatures as well. Examples of these sensors are presented in Table 2.19.

It is seen that metal oxides with the smallest grain size, doped or modified by noble metals, have the greatest sensitivity. In addition, the sensitivity measured in an inert atmosphere is greater than when measured in air. It is necessary to note that several metal oxide sensors listed in Table 2.19 have much better parameters than room-temperature sensors based on other gas-sensing materials. Room-temperature conductivity responses of Pd/WO<sub>3</sub>-based sensors are shown in Fig. 2.33. Zhao et al. (2012) reported that Pd/WO<sub>3</sub>-based sensors fabricated from nanosized WO<sub>3</sub> clusters with diameters in the range 3–5 nm have large sensor signals (~1,200 at 3,000 ppm of H<sub>2</sub> in air), low detection limits (~0.042 ppm), and responses to H<sub>2</sub> over a broad range from 4 to 20,000 ppm. This means that, in



**Table 2.19** Room-temperature conductometric gas sensors designed on the base of conventional metal oxides

MeOx geometry	Material (grain size, nm)	S % R/R	Gas tested	$t_r$ (s)	Reference
Nanoclusters	WO <sub>3</sub> (3–5)	725	H <sub>2</sub> (40,000 ppm in Ar)	1,500	Zhao et al. (2012)
Nanowire	WO <sub>3</sub> (<5)	13	H <sub>2</sub> (20,000 ppm in air)	5,220	Zhao and Zhu (2009)
Nanorods	WO <sub>3</sub> (4)	0.06	NH <sub>3</sub> (2 ppm in air)	n/a	Kim et al. (2005)
		0.1	NH <sub>3</sub> (10 ppm in air)	>1,000	
		0.14	NO <sub>2</sub> (3 ppm in air)		
Mesoporous	WO <sub>3</sub>	2–15	NO <sub>2</sub> (0.2 ppm in air)	>1,500	Manzanares et al. (2009)
Nanobelt	SnO <sub>2</sub> (80)	0.65	H <sub>2</sub> (20,000 in N <sub>2</sub> )	220	Fields et al. (2006)
Nanowire	ZnO (100)	0.52	H <sub>2</sub> (100 ppm in air)	64	Lupan et al. (2010)
Nanorods	ZnO (60–80)	1.7	H <sub>2</sub> S (50 ppb)	>1,500	Wang et al. (2006b)
Nanotetrapods	ZnO (50–150)	80	H <sub>2</sub> S (5 ppm in air)	~250	Gupta et al. (2010)
		120	NO (10 ppm in air)	~150	Lin et al. (2011)
Nanotubes	TiO <sub>2</sub>	0.37	HCHO (50 ppm in air)	~150	
		0.02	NH <sub>3</sub> (50 ppm in air)	6,000	
		0.13	Ethanol (1,000 ppm)	~100	
Whiskers	In <sub>2</sub> O <sub>3</sub>	0.035	H <sub>2</sub> S (200 ppb in air)	~300	Kaur et al. (2008)
<i>Composites and metal oxides modified</i>					
Nanoclusters	Pd/WO <sub>3</sub> (3–5)	1.2 × 10 <sup>3</sup>	H <sub>2</sub> (3,000 ppm in air)	15	Zhao et al. (2012)
Nanoclusters	Pd (10%)–WO <sub>3</sub> (20)	2.5 × 10 <sup>4</sup>	H <sub>2</sub> (1,300 ppm in air)	1300	Fardindoost et al. (2010)
Nanoclusters	Pt/WO <sub>3</sub> (35–65)	0.89	H <sub>2</sub> (100%)	3000	Shanak et al. (2004)
Nanorods	Pt/SnO <sub>2</sub> :In (1–3)	2.0 × 10 <sup>5</sup>	H <sub>2</sub> (900 ppm in N <sub>2</sub> )	500	Shukla et al. (2008)
Nanorods	Pt/SnO <sub>2</sub> :In (6–7)	1.1 × 10 <sup>3</sup>	H <sub>2</sub> (40,000 ppm in N <sub>2</sub> )	10000	Shukla et al. (2004)
Nanowires	Ru/SnO <sub>2</sub>	22	NO <sub>2</sub> (100 ppm in air)	>100	Ramgir et al. (2005)
Nanoclusters	Graphene/SnO <sub>2</sub> (<5)	0.15	NH <sub>3</sub> (50 ppm in N <sub>2</sub> )	~200	Lin et al. (2012)
		0.08	NH <sub>3</sub> (50 ppm in air)	<60	
Crystallites	MWCNTs/SnO <sub>2</sub>	100	NO <sub>2</sub> (100 ppb in air)	~100	Espinosa et al. (2007)
Crystallites	CNT/SnO <sub>2</sub> (~10)	2–12	NH <sub>3</sub> (100 ppm in air)	<300	Hieu et al. (2008)
Nanorods	Pt/ZnO (50–150)	0.10	H <sub>2</sub> (500 ppm in N <sub>2</sub> )	500	Tien et al. (2005)
Nanorods	CuO/ZnO	13.7	NH <sub>3</sub> (100 ppm in air)		Bahu et al. (2012)

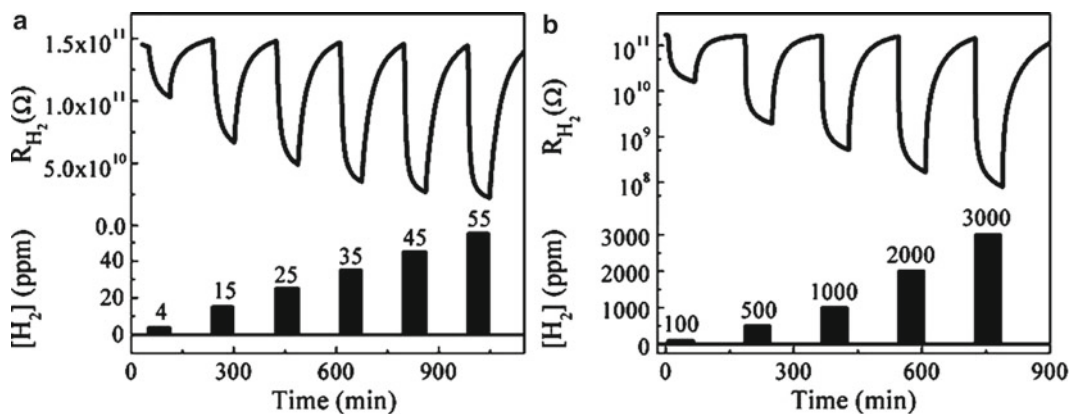


**Fig. 2.33** Response of Pd/WO<sub>3</sub>-based sensors to H<sub>2</sub> measured at 20 °C. Pd ( $d \sim 5$  nm) coated tungsten oxide films ( $d \sim 140$  nm) were prepared by using supersonic cluster beam deposition (SCBD) (Reprinted with permission from Zhao et al. (2012). Copyright 2012 IOP)

principle, room-temperature gas sensors based on conventional metal oxides can compete for the place in the market of room-temperature sensors.

However, at the same time, we have to recognize that, similar to other room-temperature solid-state gas sensors (Dickey et al. 2002; Burgmair et al. 2003; Oprea et al. 2009), the response and recovery times of these sensors are long enough and operating characteristics are very sensitive to air humidity. For information, the parameters presented in Table 2.19 were measured in a dry atmosphere. In addition, the size of grains in the most sensitive metal oxide films is too small for long-term stable operation. The number of gases which can be detected at room temperature is also limited.

Unfortunately, till now the mechanism of room temperature sensitivity has remained debatable, especially for decorated metal oxides and composite-based sensors. Generally the room temperature sensitivity of sensors based on undoped metal oxides is explained in the frame of simple adsorption/desorption mechanism. However, we have to note that the situation is more complicated. It is known that at temperatures below 80–100 °C, a thin layer of adsorbed humidity is likely to exist and to cover the surface of all studied metal oxides. Under these conditions a direct gas-sensing interaction with the semiconductor surface, which is characteristic for heating metal oxides at  $T_{oper} > 100$ –150 °C, cannot occur. Helwig et al. (2009) believe that low-temperature response in a humid atmosphere is controlled by the pH of a thin layer of adsorbed water. This layer with the semiconductor material act as a pH sensor: possible pH changes in the surface electrolyte due to interaction with analyte can be communicated to the electronic system in the underlying semiconductor, and a conductometric gas response can be obtained. Therefore, this form of gas sensitivity is limited to gases which are able to undergo electrolytic dissociation in water, and it is therefore called “dissociative gas response mechanism.” Gases that cannot undergo electrolytic dissociation remain largely undetected. This mechanism looks realistic. Moreover, it seems that this mechanism can be applied for sensors presented in Table 2.19 as well, because the layer of adsorbed water is present on the surface of tested metal oxides, even when measuring in a dry atmosphere. Bahu et al. (2012) also believe that the ammonia response of ZnO/CuO sensors at room temperature is expected to be monitored by adsorption of moisture on the activated ZnO film. Results reported by Pavelko et al. (2009) are also important. Pavelko et al. (2009) found that small SnO<sub>2</sub> particles ( $t < 3$  nm) having a high density of surface defects are characterized by the intensive formation of Sn–OH groups and the accumulation of molecular water. As was indicated before, maximum sensitivity at room temperature results from metal oxides with the smallest grain sizes. For composite-based sensors, the influence of p–n and heterojunctions is also possible (Espinosa et al. 2007; Hieu et al. 2008).

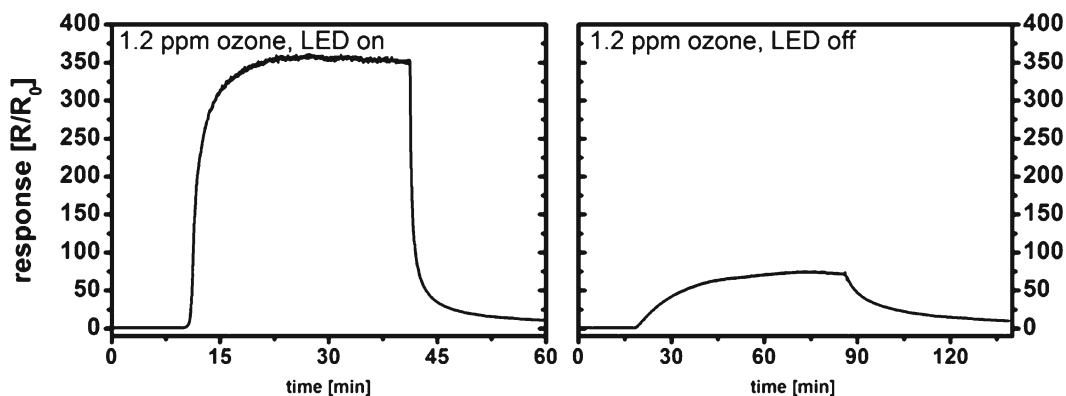
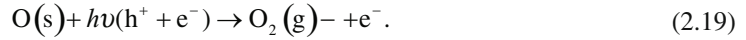


**Fig. 2.34** Response of  $\text{In}_2\text{O}_3$ -based sensor at room temperature to 2.4 ppm ozone in dry atmosphere with (left) and without (right) illumination by a blue LED. The LED has its maximum of emission at 459.6 nm with a FWHM of 40.5 nm (Reprinted with permission from Wagner et al. (2011). Copyright 2011 Elsevier)

Experimental results, including data presented in Table 2.19, show that  $\text{WO}_3$ - and  $\text{ZnO}$ -based sensors are the most promising for room-temperature application.  $\text{SnO}_2$ -based sensors as a rule have low sensitivity at room temperature (Manzanares et al. 2009). However, it was established that its gas-sensing properties can be improved by using the observed effects of UV light exposure (Comini et al. 2000, 2001; Yang et al. 2003; Mishra et al. 2004; Fu 2007; Helwig et al. 2007). For instance, Gui et al. (2008) found that pure and  $\text{TiO}_2$ -doped  $\text{ZnO}$  sensors under UV light illumination may operate at room temperature. The response and recovery times of these sensors under exposure to ethanol vapors were found to be less than 8 s. Gases which were tested under such conditions were  $\text{O}_2$ ,  $\text{NO}_2$ ,  $\text{NH}_3$ ,  $\text{H}_2\text{S}$ , formaldehyde, and a number of short-chain alcohols, and in all cases an increase of sensitivity was observed. Peng et al. (2008) demonstrated that the gas response of  $\text{ZnO}$  nanorods to 110 ppm formaldehyde with UV light irradiation was about 120 times higher than that without UV light irradiation. The same increase of RT response under UV radiation was observed by Lu et al. (2012) for  $\text{ZnO}/\text{SnO}_2$  sensors during detection of  $\text{NO}_2$  and by Sun et al. (2012) for  $\text{TiO}_2/\text{SnO}_2$  sensors during detection of ethanol. Besides  $\text{ZnO}$  (Gui et al. 2008; Peng et al. 2008; Lu et al. 2012) and  $\text{TiO}_2$  (Yang et al. 2003), the same effects of lowering the operating temperature and increasing sensitivity under application of UV light were observed for  $\text{SnO}_2$ ,  $\text{In}_2\text{O}_3$  (Xirouchaki et al. 1996; Comini et al. 2000; Comini et al. 2001; Kiriakidis et al. 2001; Anothainart et al. 2003; Zhang et al. 2003), and some other metal oxide-based sensors (Herrán et al. 2010). In addition to an increase of sensor response, Comini et al. (2001) have shown that exposure of UV radiation also results in a decrease in the response and recovery time of a tin oxide gas sensor at low temperature with no poisoning effect when  $\text{NO}_2$  comes into contact. The same effect was observed for other metal oxides as well. Hong et al. (2009) established that UV radiation also promotes regeneration of Pd, Pt- $\text{TiO}_2$ -based sensors after catalytic poisoning by  $\text{H}_2\text{S}$ . For  $\text{In}_2\text{O}_3$ -based ozone sensors, the influence of UV radiation on sensor response is shown in Fig. 2.34. We need to note that UV radiation increases sensor sensitivity at elevated temperatures as well. For example, under UV irradiation ( $\lambda = 368$  nm and a power of  $3.25$  mW  $\text{cm}^{-2}$ ), the sensitivity of  $\text{TiO}_2$ -based sensors to 300 ppm CO at  $T_{\text{oper}} = 225$  °C can be increased by a factor of 30 (Yang et al. 2003). It follows from this short survey that parameters of  $\text{ZnO}$ -,  $\text{TiO}_2$ -, and  $\text{In}_2\text{O}_3$ -based sensors are the most sensitive to UV irradiation.

It is generally suggested that the absorbed photons modulate the receptor function of the MOX via (1) excitation of the solid (in other words, enhancement of the concentration of charge carriers in the solid), (2) producing highly reactive surface radical species, (3) shifting both the surface density of adsorption sites of various kinds and the surface coverage by the gas adspecies, and (4) filling the defects by charge carriers (Xirouchaki et al. 1996; Kiriakidis et al. 2001; Mishra et al. 2004; Prades et

al. 2008; Comini et al. 2009; Brinzari et al. 2010). For example, UV photoactivation can promote desorption of oxygen and increase of target gas particle population on metal oxide surfaces (Prades et al. 2009). It was established that adsorbed oxygen participates in recombination with photogenerated holes with a subsequent desorption of oxygen species from the surface. A simple explanation of the observed effect can be given by the following equation:



According to Comini et al. (2009a), these photoexcitation processes may modulate the charge transport across the grain boundaries by (1) increasing the concentration of free charge carriers throughout the material (as Eq. (2.19) indicates, an annihilation of photogenerated holes by the electrons of the ionosorbed oxygen is accompanied by molecular oxygen desorption and a conductivity increase due to the electrons remaining in the conduction band, (2) decreasing the barrier height at the grain contacts by changing the charge of interface states, or (3) increasing the probability of charge carrier tunneling through the inter-grain barriers by decreasing the depletion layer widths in the adjacent grains. However, the consistent mechanisms responsible for the photo-assisted gas-sensing properties of the MOXs still need to be thoroughly developed (Comini et al. 2009).

## 2.6 Other Applications of Metal Oxides

### 2.6.1 Pyroelectric-Based Gas Sensors

The development of electric dipoles in certain crystalline materials as a result of temperature changes is often called the **pyroelectric effect**. This phenomenon is present in crystallized dielectrics which lack a center of symmetry and have one or more polar axes of symmetry. These conditions are fulfilled for 10 of the 32 crystal classes. Spontaneous polarization is temperature dependent; thus, any change in temperature causes a change of the dipole moments, measurable as a change of electric charges at both ends of the polar axis. Thus, the functional principle of a pyroelectric sensor is given by the conversion of a change of temperature into an electrical signal such as voltage or current. It was established that this effect can be successfully applied for designing gas sensors intended for the detection of CO<sub>2</sub>, H<sub>2</sub>, VOCs, CH<sub>4</sub>, and heptane (D'Amico and Zemel 1985; Schreiter et al. 2006; Qiu et al. 2008). Pyroelectric detectors are capacitors, having metallic electrodes applied to opposite surfaces of a temperature sensitive ferroelectric crystal or film. Pyroelectric detectors are especially suited for optical IR-based gas detection due to their robustness and low sensitivity to environmental temperature influences. Pyroelectric detectors are primarily used in the mid-infrared range, but they also function in the NIR, visible, UV, and far-infrared ranges. A selective IR window in the detector allows the precise spectral selection of a gas. The great advantage of these devices is that they can be operated at room temperature without cooling. At present, one can find single, dual, and quad channel gas sensors packaged in industry standard TO packages, intended for various gas detection applications in the gas sensor market (<http://www.optoelectronics.perkinelmer.com>). These sensors can be used for fire, flame, and explosion detection as well. The **pyroelectric effect** is also interesting for calorimetric sensor applications where signal is controlled by the interaction between the gases and catalyst of Pt (Polla et al. 1985).

It is important to note that all ferroelectric crystals possess piezoelectric and pyroelectric properties. It was also found that all pyroelectric materials are piezoelectric, but the opposite is not true. For example, quartz is piezoelectric but not pyroelectric. At the same time zinc oxide with its wurtzite

**Table 2.20** Materials for pyroelectric-based gas sensors

Material	Pyroelectric coefficient (nC cm <sup>-2</sup> ) K
ZnO thin film	0.95–1.05
PZT thin film	50–70
PbTiO <sub>3</sub> thin film	95–125
LiTiO <sub>3</sub> single crystal	19
Polyvinylidene fluoride (PVDF)	3

Source: Data from Ye et al. (1991), Hsieh et al. (1991)

**Table 2.21** Typical parameters of pyroelectric and thermoelectric gas sensors

Sensor type	Transducer type	Detected gas	Threshold sensitivity (ppm)	Response time (s)
Pyroelectric	LiTaO <sub>3</sub> -Pd	H <sub>2</sub>	100	30
Pyroelectric	PVDF-Pd	H <sub>2</sub>	750	>100
Pyroelectric	PZT-Pt cluster	H <sub>2</sub>	5,000	
Pyroelectric	PZT-PDMS	Heptane	10	
Pyroelectric	PZT film, gold black	CH <sub>4</sub>	10,000	
Thermoelectric	Si	Ethanol	3	
Thermoelectric	SnO <sub>2</sub>	H <sub>2</sub>	1,000	10
Thermoelectric	SiGe	H <sub>2</sub>		5
Thermoelectric	SiGe	CO	50	5

Source: Data from Shin et al. (2011)

crystal structure and many perovskite oxides such as PZT, LiTaO<sub>3</sub>, and PbTiO<sub>3</sub> fulfill these requirements and also have ionic bonding, which induces high ferroelectric performance, i.e., feature an intrinsic dipole moment. Moreover, it was established that these materials show pyroelectricity even in thin-film form. Studies have shown that the temperature change in the sample is larger for a smaller specific heat under constant heating and the voltage generated by a given induced charge is larger for a smaller dielectric constant. Other factors important for application in gas sensors include materials stability, reproducibility, and ease of fabrication. It was also found that while this pyroelectric function of thermal sensitivity is very important, the materials intended for sensor applications should have very weak dependence of their pyroelectricity on temperature over the working range of the device. In order to assure this, the materials should have sufficiently high Curie temperature. It was found that triglycine sulfate (TGS) has a high figure of merit, but it is a fragile and water-soluble crystal. In addition, the Curie temperature of TGS is very low (~49 °C). Therefore, this material is not used in gas sensor design. Tantalates have much better stability. Curie temperatures for these materials were found to lie in the range from 230 °C (PbZrO<sub>3</sub>) to 665 °C (LiTaO<sub>3</sub>). The strongest pyroelectric effect for a thin film was measured with the sol-gel-processed tetragonal PbTiO<sub>3</sub> ( $T_C = 494$  °C). However, lithium tantalate is readily grown as a single crystal, is insensitive to moisture, and is stable in vacuum to the temperatures required to enable outgassing (Moulson and Herbert 1990). Data on several pyroelectric materials are listed in Table 2.20. Typical parameters of pyroelectric-based gas sensors are listed in Table 2.21.

### 2.6.2 Thermoelectric-Based Gas Sensors

Thermoelectric gas sensors are other field of possible application of metal oxides. The thermoelectric effect is the direct conversion of temperature differences to electric voltage. A thermoelectric device

creates a voltage when there is a different temperature on each side. A basic gas sensor setup comprises a heater to bring the whole device to operation temperature, insulating layers, and a heater providing a modulated temperature gradient  $\Delta T$  over the gas-sensitive film. Alumina and magnesium oxide can be used as the substrate material in these sensors (Rettig and Moos 2007a). A temperature gradient is usually created due to catalytic reaction of combustion on one of the sides of sensing material. For example, the first thermoelectric gas sensor consisted of electrodes of Au and Pt coated on a tin dioxide pellet, and the Pt electrode worked as a catalyst (McAleer et al. 1985). The Seebeck voltage was then measured across electrodes on both sides of the pellet. The measured thermovoltage of the material,  $V_s$ , is a function of the Seebeck coefficient of the film material ( $S$ ) and of the applied temperature difference  $\Delta T$ , which is controlled by the rate of catalytic reaction with participation of targeted gas. In principle,  $S$  describes the position of the Fermi level in the band scheme, and hence it is correlated with the concentration of the electronic charge carriers in semiconducting materials. For example, in n-type semiconducting oxides,  $S$  is related with the electron density  $n$  by Eq. (2.20) (Moos et al. 1995):

$$S = -\frac{k}{e} \left( \ln \frac{N_C}{n} + A_e \right), \quad (2.20)$$

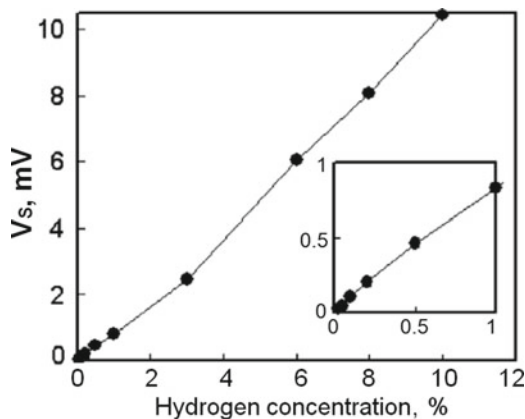
where  $k$  is the Boltzmann constant,  $e$  the electron charge,  $N_C$  the effective density of states in the conduction band, and  $A_e$  is a scattering mechanism-dependent transport coefficient for electrons.

According to Moos et al. (2009), thermoelectric gas sensors in comparison with conventional chemiresistors have the following advantage: in a direct thermoelectric sensor, the signal does not depend on the film geometry and morphology (Rettig and Moos 2007a, 2009). As is well known, this problem is crucial for chemiresistors. For that reason, the sensor signal in chemiresistors is also affected by cracks in the film, by abrasion of the film, or by sintering of the film during operation. All these issues strongly affect reproducibility of manufacturing and long-term stability. As seen in Eq. (2.19), unlike the conductivity,  $S$  is independent of the geometry of the gas-sensitive material.

It was established that, in principle, materials suitable for thermoelectric gas sensor design are almost all semiconducting oxides if their oxygen diffusion coefficient is high enough for a fast sensor response and if a  $pO_2$ -variation affects significantly the mobile electronic charge concentrations (Moos et al. 2009). However, at present only doped  $SrTi_{1-x}Fe_xO_{3-\delta}$  (Rettig and Moos 2007a, 2008),  $SnO_2$  (Ionescu 1998; Rettig and Moos 2007b), YSZ (Ahlgren and Poulsen 1995; Röder-Roith et al. 2009), and NiO (Shin et al. 2001) were tested. Based on these materials, oxygen sensors were designed showing almost linear slope in the  $S(pO_2)$ -plot of  $186 \mu V K^{-1}$  per decade  $pO_2$  (Rettig and Moos 2008), as well as sensors of reducing gases like hydrocarbons (Ionescu 1998; Rettig and Moos 2007b), and hydrogen sensors (Shin et al. 2001). Hydrogen sensors were fabricated on an alumina substrate, with a Pt catalyst deposited on one side of an alkali-doped NiO thick film. Reaction of  $H_2$  with the catalyst warmed the one side of the device, producing a thermoelectric voltage (Shin et al. 2001, 2005). The measured voltage signal,  $V_s$ , for the thermoelectric hydrogen sensor (THS), Pt/NiO/alumina exposed in various  $H_2$  concentrations in air with the gas flow of  $100 \text{ ml min}^{-1}$ , is shown in Fig. 2.35.

It was shown that the development of thermoelectric-based gas sensors is not limited to oxygen, hydrogen, and inflammable gas species such as hydrocarbons. Carbon monoxide can also be detected (see Table 2.20). It was found that, when the catalyst layer was replaced by Au nanoparticle from Pt, only carbon monoxide was selectively oxidized and gave off a highly selective signal (Nishibori et al. 2006). It was also established that the signal in thermoelectric sensors was almost independent of the technology of sensing material preparation (Rettig and Moos 2007b). The last point is a huge advantage for direct thermoelectric gas sensors. However, we need to recognize that the sensitivity of thermoelectric-based gas sensors is considerably lower than the sensitivity of conventional sensors such as chemiresistors. For example, Shin et al. (2003, 2005) reported that sensors were possible to detect

**Fig. 2.35** Voltage signal,  $V_s$ , of the THS for wide-range hydrogen concentration in air. The operating temperature of the THS was 80 °C (Reprinted with permission from Shin et al. (2003). Copyright 2003 Elsevier)



hydrogen for the concentration from 0.025% to 10% in air. However, Shin et al. (2003, 2005) believe that this limitation is not important for commercial instruments designed to measure high hydrogen concentration. In addition, as has been pointed out (Siroky 1993), the use of metal oxides such as tin oxide or indium oxide in thermoelectric sensors encounters a problem; the Seebeck coefficient of the oxide also changes if it is exposed to the combustible gas. However, we should note that Moos and coworkers used exactly this effect for designing their thermoelectric-based gas sensors (Rettig and Moos 2007a, b, 2008).

It was found that metal oxides in thermoelectric gas sensors may be applied as catalysts instead of Pt for specific gases such as hydrocarbons ( $\text{SnO}_2$ ) (Rettig and Moos 2007a) and CO ( $\text{TiO}_2$ :Au) (Nishibori et al. 2006).

### 2.6.3 Chemochromic Materials for Hydrogen Sensors

The application of chemochromic materials for hydrogen detection is a new direction in the design of optical gas sensor. Chemochromic materials are derived from electrochromic materials described in the seminal work of Deb and coworkers during the mid-1960s and early 1970s at American Cyanamid Company (Deb and Witzke 1975). These materials are transition-metal oxides, which undergo dramatic changes in absorption in the visible spectrum with the insertion of electrons and intercalating ions, typically lithium or hydrogen. The basis of the effect is a reduction–oxidation reaction. For example, according to the electrochromic model, based on electrochemical “insertion” of hydrogen into the amorphous  $\text{WO}_3$  (Granqvist 1995), hydrogen is thought to be inserted as an ion–electron pair with the proton residing in a  $\text{WO}_3$  lattice interstice adjacent to a  $\text{W}^{+5}$  ion. This is the “double-charge injection model.” The characteristic optical absorption is thought to result from either electron exchange between adjacent  $\text{W}^{+5}$  and  $\text{W}^{+6}$  ions or self-trapped, nearly free electrons called polarons. However, Zhang et al. (1996) believe that electron exchange between the  $\text{W}^{+4}$  and  $\text{W}^{+5}$  ions during hydrogen insertion is more important than  $\text{W}^{+5}$ – $\text{W}^{+6}$  exchange. The charges are inserted or removed reversibly by the application of small electric fields, hence the name electrochromic.

Much of this early work was oriented toward making display materials, but recently interest has focused on using these oxide materials in the windows of buildings to control the transmission of light. In 1984, Japanese scientists Kentaro Ito and K. Kubo suggested that these metal oxide materials might also be useful for detecting hydrogen gas if a suitable catalyst to dissociate the hydrogen molecule covered them (Ito et al. 1987). As a rule, platinum group metals perform this function and diffuse hydrogen readily. However, experiments have shown that palladium and its alloys work best.

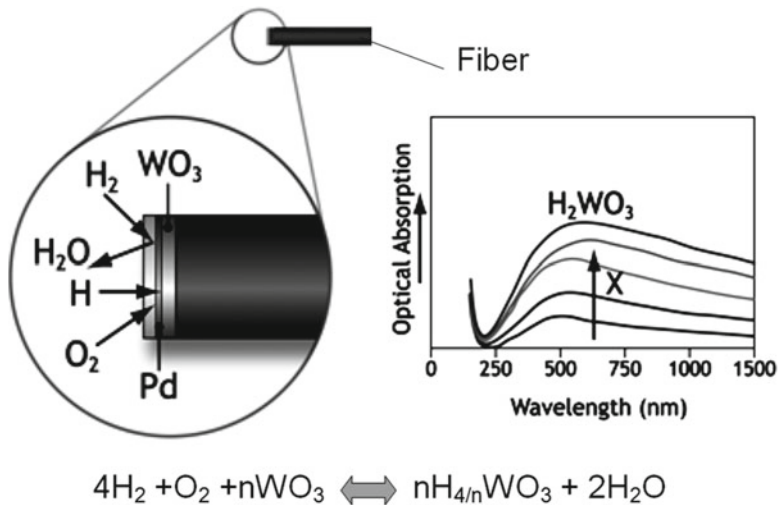


**Fig. 2.36** Schematic of fiber-optic hydrogen sensor [Idea from Benson et al. (1998), Pitts (2002), Smith et al. (2004)]

**Table 2.22** Hydrogen sensors designed on the basis of chemochromic materials

Chemochromic material	Sensor type	Reference
$\text{WO}_3$ ; $\text{V}_2\text{O}_5$ ; $\text{WO}_3:\text{Ni}$ (Pd)	Fiber-optic sensors	Pitts (2002)
$\text{Ag}-\text{WO}_3$ (Pd)	Fiber-optic sensors/surface plasmon resonance	Benson et al. (1998)
$\text{V}_2\text{O}_5$ (Pd)	Optical	Liu et al. (2003)
$\text{WO}_3$ (Pd)	Fiber-optic sensors	Smith et al. (2001, 2004)
$\text{WO}_3$ (Pd)	Optical	Ando et al. (2001)
Polyoxo compounds of W and Mo:	Smart paint sensors	Mohajeri et al. (2009)
$\text{H}_4[\text{SiW}_{12}\text{O}_{40}]$ -Pt; $\text{H}_3[\text{P}(\text{W}_3\text{O}_{10})_4]$ -Pt; $\text{H}_3[\text{P}(\text{Mo}_3\text{O}_{10})_4]$ -Pt		

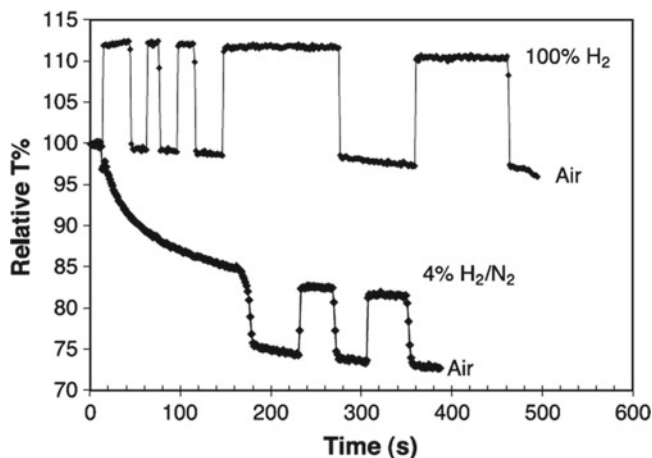
$\text{H}_4[\text{SiW}_{12}\text{O}_{40}]$ —silico-tungstic acid (STA);  $\text{H}_3[\text{P}(\text{W}_3\text{O}_{10})_4]$ —phospho-tungstic acid (PTA);  $\text{H}_3[\text{P}(\text{Mo}_3\text{O}_{10})_4]$ —phospho-molybdic acid (PMA)

When hydrogen is present in the air, some of it dissociates on the catalyst surface and then diffuses through the catalyst layer and into the chemochromic layer to produce a change in color. In this case a change in the reflected or transmitted light intensity indicates the presence of hydrogen. A conceptual schematic of such a fiber-optic sensor is presented in Fig. 2.36. It should be noted that without catalysts the color change would occur very slowly (hours to days) or may not occur at all (Ando et al. 2001). For reversibility to proceed, it is believed that the sensor composition must also allow oxidizing species, such as oxygen, to permeate to the pigment to regenerate the original color (Bechinger et al. 1993).

Typical chemochromic materials acceptable for hydrogen sensor design are listed in Table 2.22. As is seen at present for hydrogen sensor design, metal oxides such as tungsten oxide ( $\text{WO}_3$ ) and vanadium oxide ( $\text{V}_2\text{O}_5$ ) are mainly used. The sensitivity of these materials is 200–1,000 ppm of hydrogen in air, depending on the material selected, and the response time (0–90% of signal) is less than 1 s. When  $\text{V}_2\text{O}_5$  is used, the thin-film system is extraordinarily stable to cycling in higher concentrations



**Fig. 2.37** Optical response at 545 nm of a Pd/V<sub>2</sub>O<sub>5</sub> device upon exposure to 4% H<sub>2</sub>/N<sub>2</sub>, air, and 100% H<sub>2</sub>. The mesoporous vanadium oxide layer was prepared by electrodeposition (Reprinted with permission from Liu et al. (2003). Copyright 2003 Elsevier)



of hydrogen, even up to 100% (Pitts 2002). Liu et al. (2003) have shown that, after an initial irreversible coloration (see Fig. 2.37), vanadium oxide is found to be an optically passive proton host that is critical for the long-term stability of the sensor. However, experiment has shown that such parameter devices show only in lab conditions. When the sensor materials are stored or used under less than ideal conditions, such as in the presence of pollutants in the air, the sensitivity and speed of the devices change with time.

Smith et al. (2004) believe that the main mode of degradation in thin-film chemochromic hydrogen sensors is the poisoning of the palladium (Pd) catalyst layer by airborne contaminants. This problem is hard to resolve because the fouling of the Pd surface inhibits the dissociation of hydrogen on the catalyst surface, severely degrading the device. However, it was found that a photocatalytic TiO<sub>2</sub> coating, which was developed by Smith et al. (2004) for protection of the Pd catalyst, can prolong the working life of the Pd from days or weeks up to 3 years. It was also found that sensors have shown a significant increase in response time at relative humidities greater than 50% and they have a pronounced peak in sensitivity at room temperature. Below the freezing point, the accumulation of ice slows response time. Heating is one of the possible decisions, but the incorporation of a heater would complicate the sensors and increase consumable power.

Benson et al. (1998) also observed a strong influence of air humidity on the parameters of WO<sub>3</sub>-based sensors. Water adsorbed onto the nanoporous structure of the WO<sub>3</sub> increases its refractive index. Conversely, exposure of the sensor to dry air causes rapid loss of adsorbed water from the film and a shift in the SPR that mimics exposure to hydrogen. The use of a protective layer decreases this effect. However, the sensor SPR was still susceptible to severe drift under conditions of changing humidity.

Mohajeri et al. (2009) have shown that polyoxo compounds of W and Mo such as STA and PTA also have very fast kinetics (seconds) for both coloration and bleaching reactions, whereas PMA rapidly acquires color (seconds to minutes) but bleaches very slowly (days). Thus, depending on the particular application, the sensor provides an opportunity to fine-tune the kinetics of bleaching by changing the composition of the H<sub>2</sub> sensor formulation. Control experiments indicated that reversible H<sub>2</sub> sensors are not sensitive (i.e., do not change color) due to exposure to other reducing gases such as CO, CH<sub>4</sub>, and other hydrocarbons. The encapsulation of the reversible chemochromic pigment in the PDMS matrix somewhat slows down the kinetics of both coloration and bleaching processes due to the diffusion limitation of H<sub>2</sub> and O<sub>2</sub> transport through the matrix material.

It was found that, for sensor design, both thin-film (Benson et al. 1998) and thick-film (Whitten et al. 2006; Mohajeri et al. 2009) technologies can be used. In the latter case, various light-colored metal oxides in the form of fine powders (0.01–100  $\mu\text{m}$ ) can be used as a support for the POC of W and Mo, e.g.,  $\text{TiO}_2$ ,  $\text{Al}_2\text{O}_3$ ,  $\text{SiO}_2$ ,  $\text{ZrO}_2$ , and molecular sieves. Noble metal dopants are usually added to the formulation at the level of 0.001–5.0 wt% (of total).

## References

- Adachi G, Imanaka N (1995) Chemical sensors. In: Gschneidner KA Jr, Eyring L (eds) Handbook on the physics and chemistry of rare earths, vol 21. Elsevier Science, Amsterdam, pp 179–262
- Afzal A, Cioffi N, Sabbatini L, Torsi L (2012)  $\text{NO}_x$  sensors based on semiconducting metal oxide nanostructures: progress and perspectives. *Sens Actuators B* 171–172:25–42
- Ahlers S, Muller G, Doll T (2005) A rate equation approach to the gas sensitivity of thin film metal oxide materials. *Sens Actuators B* 107:587–599
- Ahlgren EO, Poulsen FW (1995) Thermoelectric power of stabilized zirconia. *Solid State Ionics* 82:193–201
- Ahmad A, Walsh J, Wheat TA (2003) Effect of processing on the properties of tin oxide-based thick-film gas sensors. *Sens Actuators B* 93:538–545
- Aifan C, Xiaodong H, Zhangfa T, Shouli B, Ruixian L, Chiun LC (2006) Preparation, characterization and gas-sensing properties of  $\text{SnO}_2$ – $\text{In}_2\text{O}_3$  nanocomposite oxides. *Sens Actuators B* 115:316–321
- Alberti G, Casciola M (2001) Solid state protonic conductors, present main applications and future prospects. *Solid State Ion* 145:3–16
- Alberti G, Carbone A, Palombari R (2001) Solid state potentiometric sensor at medium temperatures (150–300  $^\circ\text{C}$ ) for detecting oxidizable gaseous species in air. *Sens Actuators B* 75:125–128
- Ando M, Kobayashi T, Haruta M (1996) Humidity-sensitive optical absorption of  $\text{Co}_3\text{O}_4$  film. *Sens Actuators B* 32:157–160
- Ando M, Kobayashi T, Iijima S, Haruta M (1997) Optical recognition of CO and  $\text{H}_2$  by use of gas-sensitive Au– $\text{Co}_3\text{O}_4$  composite films. *J Mater Chem* 7(9):1779–1783
- Ando M, Sato Y, Tamura S, Kobayashi T (1999) Optical humidity sensitivity of plasma-oxidized nickel oxide films. *Solid State Ionics* 121:307–311
- Ando M, Chabicovsky R, Haruta M (2001) Optical hydrogen sensitivity of noble metal–tungsten oxide composite films prepared by sputtering deposition. *Sens Actuators B* 76:13–17
- Anothainart K, Burgmair A, Karthigeyan A, Zimmer M, Eisele I (2003) Light enhanced  $\text{NO}_2$  gas sensing with tin oxide at room temperature: conductance and work function measurements. *Sens Actuators B* 93:580–584
- Amar IA, Lan R, Petit CTG, Tao S (2011) Solid-state electrochemical synthesis of ammonia: a review. *J Solid State Electrochem* 15:1845–1860
- Arafat MM, Dinan B, Akbar SA, Haseeb ASMA (2012) Gas sensors based on one dimensional nanostructured metal-oxides: a review. *Sensors* 12:7207–7258
- Aroutiounian V (2007) Metal oxide hydrogen, oxygen, and carbon monoxide sensors for hydrogen setups and cells. *Int J Hydrogen Energy* 32:1145–1158
- Aygun S, Cann D (2005) Hydrogen sensitivity of doped CuO/ZnO heterocontact. *Sens Actuators B* 106:837–842
- Badlani M, Wachs IE (2001) Methanol: a “smart” chemical probe molecule. *Catal Lett* 75(3–4):137–149
- Baek K-K, Tuller HL (1993) Electronic characterization of ZnO/CuO heterojunctions. *Sens Actuators B* 13:238–240
- Bahu M, Kumar K, Bahu T (2012) CuO–ZnO semiconductor gas sensors for ammonia at room temperatures. *J Electron Devices* 14:1137–1141
- Bangale SV, Patil DR, Bamane SR (2011) Nanostructured spinel  $\text{ZnFe}_2\text{O}_4$  for the detection of chlorine gas. *Sens Transducers J* 134(11):107–119
- Barsan N, Weimar U (2001) Conduction model of metal oxide gas sensors. *J Electroceram* 7(3):143–167
- Barsan N, Schweizer-Berberich M, Gopel W (1999) Fundamental and practical aspects in the design of nanoscaled  $\text{SnO}_2$  gas sensors. A status report. *Fresen J Anal Chem* 365:287–304
- Basu S, Hazra SK (2005) ZnO *p-n* homojunctions for hydrogen gas sensors at elevated temperature. *Asian J Phys* 14:65–69
- Basu S, Saha M, Chatterjee S, Mistry KK, Bandyopadhyay S, Sengupta K (2001) Porous ceramic sensor for measurement of gas moisture in the ppm range. *Mater Lett* 49:29–33
- Batzill M (2006) Surface science studies of gas sensing materials:  $\text{SnO}_2$ . *Sensors* 6:1345–1376
- Bechinger C, Oefinger G, Herminghaus S, Leidered P (1993) On the fundamental role of oxygen for the photochromic effect in  $\text{WO}_3$ . *J Appl Phys* 74:4527–4533

- Benson DK, Tracy CE, Lee S-H, Hishmeh GA, Haberman DP, Ciszek PA (1998) Low-cost, fiber-optic hydrogen gas detector using guided-wave, surface-plasmon resonance in chemochromic thin films. NREL/CP-590-25611, pp 1–18
- Berger O, Hoffmann T, Fischer W-J, Melev V (2004) Tungsten-oxide thin films as novel materials with high sensitivity and selectivity to NO<sub>2</sub>, O<sub>3</sub>, and H<sub>2</sub>S. Part II: application as gas sensors. *J Mater Sci Mater Electron* 15:483–493
- Biao W, Dong ZY, Ming HL, Sheng CJ, Li GF, Yun L, Jun WL (2010) Improved and excellent CO sensing properties of Cu-doped TiO<sub>2</sub> nanofibers. *Chin Sci Bull* 55:228–232
- Blase R, Härdtl KH, Schönauer U (1997) Oxygen sensor based on non-doped cuprate. US Patent 5,792,666
- Bonanos N (2001) Oxide-based protonic conductors: point defects and transport properties. *Solid State Ionics* 145:265–274
- Boozer C (2003) Surface functionalization for self-referencing surface plasmon resonance (SPR) biosensors by multi-step self-assembly. *Sens Actuators B* 90:22–30
- Brinzari V, Korotcenkov G, Golovanov V (2001) Factors influencing the gas sensing characteristics of tin dioxide films deposited by spray pyrolysis: understanding and possibilities for control. *Thin Solid Films* 391(1/2):167–175
- Brinzari V, Ivanov M, Cho BK, Kamei M, Korotcenkov G (2010) Photoconductivity in In<sub>2</sub>O<sub>3</sub> nanoscale thin films: interrelation with chemisorbed-type conductometric response towards oxygen. *Sens Actuators B* 148:427–438
- Brynn DH, Tseung CC (1979) The reduction of sulphur dioxide by carbon monoxide on La<sub>0.5</sub>Sr<sub>0.5</sub>CoO<sub>3</sub> catalyst. *J Chem Technol Biotechnol* 29:713–718
- Brynzari V, Korotchenkov G, Dmitriev S (1999) Simulation of thin film gas sensor kinetics. *Sens Actuators B* 61:143–153
- Brynzari V, Korotchenkov G, Dmitriev S (2000) Theoretical study of semiconductor thin film gas sensitivity: attempt to consistent approach. *J Electron Technol* 33:225–235
- Burgmair M, Zimmer M, Eisele I (2003) Humidity and temperature compensation in work function gas sensor FETs. *Sens Actuators B* 93:271–275
- Calatayud M, Markovits A, Menetrey M, Mguig B, Minot C (2003) Adsorption on perfect and reduced surfaces of metal oxides. *Catal Today* 85:125–143
- Cavanagh LM, Smith P, Binions R (2012) BaSnO<sub>3</sub> thick film as a carbon dioxide sensor. *J Electrochem Soc* 159(3):J67–J71
- Chao Y, Buttner WJ, Yao S, Stetter JR (2005) Amperometric sensor for selective and stable hydrogen measurement. *Sens Actuators B* 106:784–790
- Chapelle A, Oudrhiri-Hassani F, Presmanes L, Barnabé A, Tailhades P (2010) CO<sub>2</sub> sensing properties of semiconducting copper oxide and spinel ferrite nanocomposite thin film. *Appl Surf Sci* 256(14):4715–4719
- Chiba A (1992) Development of the TGS gas sensor. In: Yamauchi S (ed) *Chemical sensor technology*, vol 4. Elsevier, Amsterdam, pp 1–18
- Choi SW, Park JY, Kim SS (2009) Synthesis of SnO<sub>2</sub>-ZnO core-shell nanofibers via a novel two-step process and their gas sensing properties. *Nanotechnology* 20:465603
- Choi J-K, Hwang I-S, Kim S-J, Park J-S, Park S-S, Jeong U, Kang YC, Lee J-H (2010) Design of selective gas sensors using electrospun Pd-doped SnO<sub>2</sub> hollow nanofibers. *Sens Actuators B* 150:191–199
- Chung W-Y, Oh S-J (2006) Remote monitoring system with wireless sensors module for room environment. *Sens Actuators B* 113:64–70
- Collado JA, Aranda MAG, Cabeza A, Olivera-Pastor P, Bruque S (2002) Synthesis, structures, and thermal expansion of the La<sub>1-x</sub>W<sub>2x</sub>Mo<sub>x</sub>O<sub>9</sub> series. *J Solid State Chem* 167:80–85
- Comini E, Cristalli A, Faglia G, Sberveglieri G (2000) Light enhanced gas sensing properties of indium oxide and tin dioxide sensors. *Sens Actuators B* 65:260–263
- Comini E, Faglia G, Sberveglieri G (2001) UV light activation of tin oxide thin films for NO<sub>2</sub> sensing at low temperatures. *Sens Actuators B* 78:73–77
- Comini E, Faglia G, Sberveglieri G (2009) Electrical-based gas sensing. In: Comini E, Faglia G, Sberveglieri G (eds) *Solid state gas sensing*. Springer, New York, pp 47–107
- D'Amico A, Zemel JN (1985) Pyroelectric enthalpimetric detection. *J Appl Phys* 57:2640–2643
- Dakin J, Culshaw B (eds) (1988) *Optical fiber sensors: principles and components*, vol 1. Artech House, Boston, MA
- Dandaneau CS, Jeon Y-H, Shelton CT, Plant TK, Cann DP, Gibbons BJ (2009) Thin film chemical sensors based on p-CuO/n-ZnO heterocontacts. *Thin Solid Films* 517:4448–4454
- Das S, Chakraborty S, Parkash O, Kumarb D, Bandyopadhyay S, Samudrala SK, Sena A, Maiti HS (2008) Vanadium doped tin dioxide as a novel sulfur dioxide sensor. *Talanta* 75:385–389
- Dawson DH, Henshaw GS, Williams DE (1995) Description and characterization of hydrogen sulfide gas sensor based on Cr<sub>2-y</sub>TiO<sub>3+x</sub>. *Sens Actuators B* 26–27:76–80
- Dayan NJ, Sainkar SR, Karekar RN, Aiyer RC (1998) Formulation and characterization of ZnO:Sb thick-film gas sensors. *Thin Solid Films* 325:254–258
- De Souza Brito GE, Santilli CV, Pulcenelli SH (1995) Evolution of the fractal structural during sintering of SnO<sub>2</sub> compacted sol-gel powders. *Colloids Surf A* 97:217–225
- Deb SK, Witzke H (1975) The solid state electrochromic phenomenon and its applications to display devices. *Proc IEEE Int Electron Devices Mtng* 21:393–397

- Delta Corporation (n.d.) Application note No. 107, Risks in using zirconium oxide analyzers for trace oxygen measurements. <http://www.delta-f.com/AppNotes/apnote7.htm>
- Dickey EC, Varghese OK, Ong KG, Gong D, Paulose M, Grimes CA (2002) Room temperature ammonia and humidity sensing using highly ordered nanoporous alumina films. *Sensors* 2:91–110
- Djerdj I, Haensch A, Koziej D, Pokhrel S, Barsan N, Weimar U, Niederberger M (2009) Neodymium dioxide carbonate as a sensing layer for chemoresistive CO<sub>2</sub> sensing. *Chem Mater* 21:5375–5381
- Doll T, Eisele I (1998) Gas detection with work function sensors. In: Proceedings of SPIE conference on chemical microsensors and applications, vol 3539, Nov 1998, Boston, MA, pp 96–105
- Dong K-Y, Choi J-K, Hwang I-S, Lee J-W, Kang BH, Ham D-J, Lee J-H, Ju B-K (2011) Enhanced H<sub>2</sub>S sensing characteristics of Pt doped SnO<sub>2</sub> nanofibers sensors with micro heater. *Sens Actuators B* 157:154–161
- Dostálek J, Tyroky J, Homola J, Brynda E, Skalský M, Někviňová P, Spirková J, Skvor J, Schröfel J (2001) Surface plasmon resonance biosensor based on integrated optical waveguide. *Sens Actuators B* 76:8–12
- Du Y, Nowick AS (1996) Galvanic cell measurements on a fast proton conducting complex perovskite electrolyte. *Solid State Ionics* 91(1–2):85–91
- Elumalai P, Miura N (2005) Performances of planar NO<sub>x</sub> sensor using stabilized zirconia and NiO sensing electrode at high temperature. *Solid State Ion* 31–34:2517–2522
- Elumalai P, Plashnitsa VV, Fujio Y, Miura A (2008) Stabilized zirconia-based sensor attached with NiO/Au sensing electrode aiming for highly selective detection of ammonia in automobile exhausts. *Electrochem Solid State Lett* 11:J79–J81
- Epifani M, Comini E, Arbiol J, Diaz R, Sergent N, Pagnier T, Siciliano P, Faglia G, Morante JR (2008) Chemical synthesis of In<sub>2</sub>O<sub>3</sub> nanocrystals and their application in highly performing ozone-sensing devices. *Sens Actuators B* 130:483–487
- Eranna G, Joshi BC, Runthala DP, Gupta RP (2004) Oxide materials for development of integrated gas sensors – a comprehensive review. *Crit Rev Solid State Mater Sci* 29:111–188
- Espinosa EH, Ionescu R, Chambon B, Bedis G, Sotter E, Bittencourt C, Felten A, Pireaux J-J, Correig X, Llobet E (2007) Hybrid metal oxide and multiwall carbon nanotube films for low temperature gas sensing. *Sens Actuators B* 127:137–142
- Etsell TH, Flengas SN (1970) Electrical properties of solid oxide electrolytes. *Chem Rev* 70:339–376
- Fardindoost S, Zad AI, Rahimi F, Ghasempour R (2010) Pd doped WO<sub>3</sub> films prepared by sol–gel process for hydrogen sensing. *Int J Hydrogen Energy* 35:854–860
- Fergus JW (2007a) Perovskite oxides for semiconductor-based gas sensors. *Sens Actuators B* 123:1169–1179
- Fergus JW (2007b) Solid electrolyte based sensors for the measurement of CO and hydrocarbon gases. *Sens Actuators B* 122:683–693
- Fergus JW (2007c) Materials for high temperature electrochemical NO<sub>x</sub> gas sensors. *Sens Actuators B* 121:652–663
- Fergus JW (2008) A review of electrolyte and electrode materials for high temperature electrochemical CO<sub>2</sub> and SO<sub>2</sub> gas sensors. *Sens Actuators B* 134:1034–1041
- Ferro R, Rodriguez JA, Jimenez I, Ciera A, Cerda J, Morante JR (2005) Gas-sensing properties of sprayed films of (CdO)<sub>x</sub>(ZnO)<sub>1-x</sub> mixed oxide. *IEEE Sens J* 5:48–52
- Fields LL, Zheng JP, Cheng Y, Xiong P (2006) Room-temperature low-power hydrogen sensor based on a single tin dioxide nanobelt. *Appl Phys Lett* 88:263102
- Fine GF, Cavanagh LM, Afonja A, Binions R (2010) Metal oxide semiconductor gas sensors in environmental monitoring. *Sensors* 10:5469–5502
- Fleischer M, Meixner H (1997) Fast gas sensors based on metal oxides which are stable at high temperatures. *Sens Actuators B* 43:1–10
- Fleischer M, Meixner H (1998) Selectivity in high-temperature operated semiconductor gas-sensors. *Sens Actuators B* 52:179–187
- Fu T (2007) Sensing properties and mechanism of gas sensor for H<sub>2</sub>S and NO<sub>2</sub> based on [Cu<sub>5</sub>(bipyO<sub>2</sub>)<sub>6</sub>Cl<sub>8</sub>]Cl<sub>2</sub>. *Sens Actuators B* 123:1113–1119
- Fukatsu N, Kurita N, Koide K, Ohashi T (1998) Hydrogen sensor for molten metals usable up to 1500 K. *Solid State Ionics* 113–115:219–227
- Gadkari AB, Shinde TJ, Vasambekar PN (2011) Ferrite gas sensors. *IEEE Sens J* 11(4):849–861
- Garagounis I, Kyriakou V, Anagnostou C, Bourganis V, Papachristou I, Stoukides M (2011) Solid electrolytes: applications in heterogeneous catalysis and chemical cogeneration. *Ind Eng Chem Res* 50:431–472
- Gardner JM, Bartlett PN (eds) (1992) *Sensors and sensory systems for an electronic nose*. Kluwer Academic, Dordrecht
- Gardner JM, Bartlett PN (1999) *Electronic noses: principles and applications*. Oxford University Press, Oxford
- Garzon FH, Mukundan R, Brosha EL (2000) Solid-state mixed potential gas sensors: theory, experiments and challenges. *Solid State Ionics* 136–137:633–638
- Gas'kov AM, Rummyantseva MN (2001) Nature of gas sensitivity in nanocrystalline metal oxides. *Russ J Appl Chem* 74(3):440–444
- Gas'kov A, Rummyantseva M (2009) Metal oxide nanocomposites: synthesis and characterization in relation with gas sensing phenomena. In: Baraton MI (ed) *Sensors for environment, health and security*. Springer Science + Business Media B.V., Dordrecht, pp 3–29

- Gawas UB, Verenkar VMS, Patil DR (2011) Nanostructured ferrite based electronic nose sensitive to ammonia at room temperature. *Sens Transducers J* 134(11):45–55
- Ghimbeu CM, Lumbreiras M, Schoonman J, Siadat M (2009) Electro sprayed metal oxide semiconductor films for sensitive and selective detection of hydrogen sulfide. *Sensors* 9:9122–9132
- Gillet M, Aguir K, Bendahan M, Mennini P (2005) Grain size effect in sputtered tungsten trioxide thin films on the sensitivity to ozone. *Thin Solid Films* 484:358–363
- Glass RS, Milliken J, Howden K, Sullivan R (eds) (2000) Sensor needs and requirements for proton-exchange membrane fuel cell systems and direct-injection engines. Lawrence Livermore National Laboratory, UCRL-ID-137767, Livermore, CA, p 11
- Golovanov V, Maki-Jaskari MA, Rantala TT, Korotcenkov G, Brinzari V, Cornet A, Morante J (2005) Experimental and theoretical studies of the indium oxide-based gas sensors deposited by spray pyrolysis. *Sens Actuators B* 106:563–571
- Granqvist CG (1995) *Handbook of inorganic electrochromic materials*. Elsevier, New York
- Gui Y, Li S, Xu J, Li C (2008) Study on TiO<sub>2</sub>-doped ZnO thick film gas sensors enhanced by UV light at room temperature. *Microelectron J* 39:1120–1125
- Gupta SK, Joshi A, Kaur M (2010) Development of gas sensors using ZnO nanostructures. *J Chem Sci* 122(1):57–62
- Gurlo A (2006) Interplay between O<sub>2</sub> and SnO<sub>2</sub>: oxygen ionosorption and spectroscopic evidence for adsorbed oxygen. *ChemPhysChem* 7:2041–2052
- Gurlo A, Ivanovskaya M, Barsan N, Schweizer-Berberich M, Weimar U, Gopel W, Dieguez A (1997) Grain size control in nanocrystalline In<sub>2</sub>O<sub>3</sub> semiconductor sensors. *Sens Actuators B* 44:327–333
- Haile SM (2003) Fuel cell materials and components. *Acta Mater* 51:5981–6000
- Hashimoto A, Hibino T, Mori K, Sano M (2001) High-temperature hydrocarbon sensors based on a stabilized zirconia electrolyte and proton conductor-containing platinum electrode. *Sens Actuators B* 81:55–63
- Haugen JE, Kvaal K (1998) Electronic nose and artificial neural network. *Meat Sci* 49:S273–S286
- Hazra SK, Basu S (2006) Hydrogen sensitivity of ZnO p-n homojunctions. *Sens Actuators B* 117:177–182
- Helwig A, Muller G, Eickhoff M, Sberveglieri G (2007) Dissociative gas sensing at metal oxide surfaces. *IEEE Sens J* 7:1675–1679
- Helwig A, Muller G, Sberveglieri G, Eickhoff M (2009) On the low-temperature response of semiconductor gas sensors. *J Sens* 2009:620720
- Hemmati S, Firooz AA, Khodadadi AA, Mortazavi Y (2011) Nanostructured SnO<sub>2</sub>-ZnO sensors: highly sensitive and selective to ethanol. *Sens Actuators B* 160:1298–1303
- Herran J, Mandayo GG, Castano E (2008) Solid state gas sensor for fast carbon dioxide detection. *Sens Actuators B* 129:705–709
- Herrán J, Ga MG, Castaño E (2009) Semiconducting BaTiO<sub>3</sub>-CuO mixed oxide thin films for CO<sub>2</sub> detection. *Thin Solid Films* 517:6192–6197
- Herrán J, Fernández-González O, Castro-Hurtado I, Romero T, Ga Mandayo G, Castano E (2010) Photoactivated solid-state gas sensor for carbon dioxide detection at room temperature. *Sens Actuators B* 149:368–372
- Hibino T, Kuwahara Y, Wang S, Kakimoto S, Sano M (1998) Nonideal electromotive force of zirconia sensors for unsaturated hydrocarbon gases. *Electrochem Soc Lett* 1(4):197–199
- Hibino T, Kakimoto S, Sano M (1999) Non-Nernstian behavior at modified Au electrodes for hydrocarbon gas sensing. *J Electrochem Soc* 146:3361–3366
- Hieu NV, Thuy LTB, Chien ND (2008) Highly sensitive thin film NH<sub>3</sub> gas sensor operating at room temperature based on SnO<sub>2</sub>/MWCNTs composite. *Sens Actuators B* 129:888–895
- Hill DC, Tuller HL (1991) *Ceramic sensors: theory and practice*. In: Buchanan RC (ed) *Ceramic materials for electronics*, 2nd edn. Marcel Dekker, New York, pp 249–347
- Hofer U, Frank J, Fleischer M (2001) High temperature Ga<sub>2</sub>O<sub>3</sub>-gas sensors and SnO<sub>2</sub>-gas sensors: a comparison. *Sens Actuators B* 78:6–11
- Hong DU, Han C-H, Park SH, Kim I-J, Gwak J, Han S-D, Kim HJ (2009) Recovery properties of hydrogen gas sensor with Pd/titanate and Pt/titanate nanotubes photo-catalyst by UV radiation from catalytic poisoning of H<sub>2</sub>S. *Curr Appl Phys* 9:172–178
- Horiuchi T, Hidaka H, Fukui T, Kubo Y, Horio M, Suzuki K, Mori T (1998) Effect of added basic metal oxides on CO<sub>2</sub> adsorption on alumina at elevated temperatures. *Appl Catal A Gen* 167:195–202
- Houser EJ, Mlsna TE, Nguyen VK, Chung R, Mowery EL, McGill RA (2001) Rational materials design of sorbent coatings for explosives: applications with chemical sensors. *Talanta* 54:469–485
- Hsieh HY, Spetz A, Zemel JN (1991) Wide range pyroelectric anemometers for gas flow measurements. In: *Digest of technical papers of TRANSDUCERS '91*. International conference on solid-state sensors and actuators, 24–27 June 1991, San Francisco, CA, pp 38–40
- Hu Y, Zhou X, Han Q, Cao Q, Huang Y (2003) Sensing properties of CuO-ZnO heterojunction gas sensors. *Mater Sci Eng B* 99(1–3):41–43

- Hyodo T, Abe S, Shimuzu Y, Egashira M (2003) Gas sensing properties of ordered mesoporous SnO<sub>2</sub> and effects of coatings thereof. *Sens Actuators B* 93:590–600
- Iftimie N, Rezlescu E, Popa PD, Rezlescu N (2006) Gas sensitivity of nanocrystalline nickel ferrite. *J Optoelectron Adv Mater* 8(3):1016–1018
- Imanaka N, Adachi G (1997) Rare earth contribution in solid state electrolytes, especially in the chemical sensor field. *J Alloys Compd* 250:492–500
- Ionescu R (1998) Combined Seebeck and resistive SnO<sub>2</sub> gas sensors, a new selective device. *Sens Actuators B* 48:392–394
- Ishihara T (ed) (2009) *Perovskite oxide for solid oxide fuel cells*. Springer, Dordrecht
- Ishihara T, Matsubara S (1998) Capacitive type gas sensors. *J Electroceram* 2(4):215–228
- Ishihara T, Kometani K, Mizuhara Y, Takita Y (1991a) Mixed oxide capacitor of CuO-BaSnO<sub>3</sub> as a sensor for CO<sub>2</sub> detection over a wide range of concentration. *Chem Lett* 20(10):1711–1714
- Ishihara T, Kometani K, Hashida M, Takita Y (1991b) Application of mixed oxide capacitor to the selective carbon dioxide sensor. I. Measurement of carbon dioxide sensing characteristics. *J Electrochem Soc* 138:173–176
- Ishihara T, Kometani K, Mizuhara Y, Takita Y (1992) Application of a mixed oxide capacitor to the selective carbon dioxide sensor. II. CO<sub>2</sub> sensing characteristics of a CuO-based oxide capacitor. *J Electrochem Soc* 139:2881–2885
- Ishihara T, Sato S, Takita Y (1996) Sensitive detection of nitrogen oxides based upon capacitance changes in binary oxide mixture. *Sens Actuators B* 30:43–45
- Ito K, Kubo T, Yamauchi Y (1987) Gas sensor. US Patent 4,661,320
- Ivanovskaya M, Kotsikau D, Faglia G, Nelli P (2003) Influence of chemical composition and structural factors of Fe<sub>2</sub>O<sub>3</sub>/In<sub>2</sub>O<sub>3</sub> sensors on their selectivity and sensitivity to ethanol. *Sens Actuators B* 96:498–503
- Iwahara H, Yajima T, Hibino T, Ozaki K (1993) Protonic conduction in calcium, strontium and barium zirconates. *Solid State Ionics* 61:65–69
- Iwahara H, Asakura Y, Katahira K, Tanaka M (2004) Prospect of hydrogen technology using proton-conducting ceramics. *Solid State Ionics* 168:299–310
- Jacobs A, Vangrunderbeek J, Beckers H, De Schumr F, Luyten J, Van Landschoot R, Schoonman J (1993) Hydrogen measuring probe for coal gasification processes. *Fuel Process Technol* 36:251–258
- Jamnik J, Kamp B, Merkle R, Maier J (2002) Space charge influenced oxygen incorporation in oxides: in how far does it contribute to the drift of Taguchi sensors? *Solid State Ionics* 150:157–166
- Jianping L, Yue W, Xiaoguang G, Qing M, Li W, Jinghong H (2000) H<sub>2</sub>S sensing properties of the SnO<sub>2</sub>-based thin films. *Sens Actuators B* 65:111–113
- Jin CJ, Yamazaki T, Shirai Y, Yoshizawa T, Kikuta T, Nakatani N, Takeda H (2005) Dependence of NO<sub>2</sub> gas sensitivity of WO<sub>3</sub> sputtered films on film density. *Thin Solid Films* 474:255–260
- Jing Z, Wang Y, Wu S (2006) Preparation and gas sensing properties of pure and doped γ-Fe<sub>2</sub>O<sub>3</sub> by an anhydrous solvent method. *Sens Actuators B* 113:177–181
- Jones TA, Firth JG, Mann B (1985) The effect of oxygen on the electrical conductivity of some metal oxides in inert and reducing atmospheres at high temperature. *Sens Actuators* 8:281–306
- Jung SJ, Yanagida H (1996) The characterization of a CuO/ZnO heterocontact-type gas sensor having selectivity for CO gas. *Sens Actuators B* 37:55–60
- Kanazawa E, Sakai G, Shimanoe K, Kanmura Y, Teraoka Y, Miura N, Yamazoe N (2001) Metal oxide semiconductor N<sub>2</sub>O sensor for medical use. *Sens Actuators B* 77:72–77
- Kanda K, Maekawa T (2005) Development of a WO<sub>3</sub> thick-film-based sensors for the detection of VOC. *Sens Actuators B* 108:97–101
- Katti VR, Debnath AK, Muthea KP, Kaur M, Dua AK, Gadkari SC, Gupta SK, Sahni VC (2003) Mechanism of drifts in H<sub>2</sub>S sensing properties of SnO<sub>2</sub>:CuO composite thin film sensors prepared by thermal evaporation. *Sens Actuators B* 96:245–252
- Kaur M, Jain N, Sharma K, Bhattacharya S, Mainak Roy M, Tyagi AK, Gupta SK, Yakhmia JV (2008) Room-temperature H<sub>2</sub>S gas sensing at ppb level by single crystal In<sub>2</sub>O<sub>3</sub> whiskers. *Sens Actuators B* 133:456–461
- Kharton V, Naumovich EN, Yaremchenko AA, Marques FMB (2001) Research on the electrochemistry of oxygen ion conductors in the former Soviet Union. IV. Bismuth oxide-based ceramics. *J Solid State Electrochem* 5:160–187
- Kharton V, Marques F, Atkinson A (2004) Transport properties of solid oxide electrolyte ceramics: a brief review. *Solid State Ionics* 174:135–149
- Kim DH, Yoon JY, Park HC, Kim KH (2000) CO<sub>2</sub>-sensing characteristics of SnO<sub>2</sub> thick film by coating lanthanum oxide. *Sens Actuators B* 62:61–66
- Kim YS, Ha S-C, Kim K, Yang H, Choi S-Y, Kim YT (2005) Room-temperature semiconductor gas sensor based on nonstoichiometric tungsten oxide nanorod film. *Appl Phys Lett* 86:213105
- Kiriakidis G, Bender M, Katsarakis N, Gagaoudakis E, Hourdakis E, Doulofakis E, Cimalla V (2001) Ozone sensing properties of polycrystalline indium oxide films at room temperature. *Physica Status Solidi A Appl Res* 185(1):27–32

- Knauth P, Tuller HL (1999) Electrical and defect thermodynamic properties of nanocrystalline titanium dioxide. *J Appl Phys* 85:897–902
- Kobayashi T, Haruta M, Sano H, Delmon B (1990) Optical detection of CO in air through catalytic chromism of metal-oxide thin films. In: Proceedings of the third international meeting on chemical sensors, Cleveland, pp 318–321
- Kofstad P (1972) Nonstoichiometry, diffusion and electrical conductivity in binary metal oxides. Wiley, New York
- Kohl D (1989) Surface processes in the detection of reducing gases with SnO<sub>2</sub>-based devices. *Sens Actuators* 18:71–113
- Kong X, Li Y (2005) High sensitivity of CuO modified SnO<sub>2</sub> nanoribbons to H<sub>2</sub>S at room temperature. *Sens Actuators B* 105:449–453
- Korotcenkov G (2005) Gas response control through structural and chemical modification of metal oxides: state of the art and approaches. *Sens Actuators B* 107:209–232
- Korotcenkov G (2007a) Metal oxides for solid state gas sensors. What determines our choice? *Mater Sci Eng B* 139:1–23
- Korotcenkov G (2007b) Practical aspects in design of one-electrode semiconductor gas sensors: status report. *Sens Actuators B* 121:664–678
- Korotcenkov G (2008) The role of morphology and crystallographic structure of metal oxides in response of conductometric-type gas sensors. *Mater Sci Eng R* 61:1–39
- Korotcenkov G (ed) (2010) Chemical sensors: fundamentals of sensing materials, vols 1, 2. Momentum, New York
- Korotcenkov G (ed) (2011a) Chemical sensors: fundamentals of sensing materials, vol 3. Momentum, New York
- Korotcenkov G (ed) (2011b) Chemical sensors: comprehensive sensor technologies, vols 4–6. Momentum, New York
- Korotcenkov G, Han SD (2009) (Cu, Fe, Co and Ni)-doped SnO<sub>2</sub> films deposited by spray pyrolysis: doping influence on thermal stability of SnO<sub>2</sub> film structure. *Mater Chem Phys* 113:756–763
- Korotcenkov G, Stetter JR (2008) Comparative study of SnO<sub>2</sub>- and In<sub>2</sub>O<sub>3</sub>-based ozone sensors. *ECS Trans* 6(20):29–41
- Korotcenkov G, Brinzari V, Cerneavski A, Ivanov M, Golovanov V, Cornet A, Morante J, Cabot A, Arbiol J (2004a) The influence of film structure on In<sub>2</sub>O<sub>3</sub> gas response. *Thin Solid Films* 460:308–316
- Korotcenkov G, Brinzari V, Cerneavski A, Ivanov M, Cornet A, Morante J, Cabot A, Arbiol J (2004b) In<sub>2</sub>O<sub>3</sub> films deposited by spray pyrolysis: gas response to reducing (CO, H<sub>2</sub>) gases. *Sens Actuators B* 98:236–243
- Korotcenkov G, Cerneavski A, Brinzari V, Vasiliev A, Cornet A, Morante J, Cabot A, Arbiol J (2004c) In<sub>2</sub>O<sub>3</sub> films deposited by spray pyrolysis as a material for ozone gas sensors. *Sens Actuators B* 99:304–310
- Korotcenkov G, Golovanov V, Cornet A, Brinzari V, Morante J, Ivanov M (2005a) Distinguishing feature of metal oxide films' structural engineering for gas sensor application. *J Phys Conf Ser (IOP)* 15:256–261
- Korotcenkov G, Brinzari V, Ivanov M, Cerneavski A, Rodriguez J, Cirera A, Cornet A, Morante J (2005b) Structural stability of In<sub>2</sub>O<sub>3</sub> films deposited by spray pyrolysis during thermal annealing. *Thin Solid Films* 479:38–51
- Korotcenkov G, Blinov I, Stetter JR (2007a) Kinetics of indium oxide-based thin film gas sensor response: the role of "redox" and adsorption/desorption processes in gas sensing effects. *Thin Solid Films* 515:3987–3996
- Korotcenkov G, Brinzari V, Stetter JR, Blinov I, Blaja V (2007b) The nature of processes controlling the kinetics of indium oxide-based thin film gas sensor response. *Sens Actuators B* 128:51–63
- Korotcenkov G, Blinov I, Ivanov M, Stetter JR (2007c) Ozone sensors on the base of SnO<sub>2</sub> films deposited by spray pyrolysis. *Sens Actuators B* 120:679–686
- Korotcenkov G, Han SD, Cho BK, Brinzari V (2009a) Grain size effects in sensor response of nanostructured SnO<sub>2</sub>- and In<sub>2</sub>O<sub>3</sub>-based conductometric gas sensor. *Crit Rev Solid State Mater Sci* 34:1–17
- Korotcenkov G, Cho BK, Gulina L, Tolstoy V (2009b) Ozone sensors based on SnO<sub>2</sub> films modified by SnO<sub>2</sub>-Au nanocomposites synthesized by the SILD method. *Sens Actuators B* 138:512–517
- Korotcenkov G, Han SD, Stetter JR (2009c) Review of electrochemical hydrogen sensors. *Chem Rev* 109:1402–1433
- Kreuer KD (2003) Proton-conducting oxides. *Annu Rev Mater Res* 33:333–359
- Krilov OV, Kisilev VF (1981) Adsorption and catalysis on the transition metals and their oxides. Chemistry, Moscow
- Kröger FA, Vink HJ (1956) Relations between concentrations of imperfections in crystalline solids. In: Seitz F, Turnbull D (eds) *Solid state physics*, vol 3. Academic, New York, pp 307–435
- Kulkarni D, Wachs IE (2002) Isopropanol oxidation by pure metal oxide catalysts: number of active surface sites and turnover frequencies. *Appl Catal A* 237:121–137
- Kulwicki BM (1991) Humidity sensors. *J Am Ceram Soc* 74:697–708
- Kumar RV, Iwahara H (2000) Solid electrolytes. In: Gschneidner KA Jr, Eyring L (eds) *Handbook on the physics and chemistry of rare earths*, vol 28. Elsevier Science, Amsterdam, pp 131–185
- Kwon S, Cann DP (2005) Capacitive response of doped CuO/ZnO heterocontacts to hydrogen. *Sens Lett* 3(3):258–262
- Lacorre P, Goutenoire F, Bohnke O, Retoux R, Laligantet Y (2000) Designing fast oxide-ion conductors based on La<sub>2</sub>Mo<sub>2</sub>O<sub>6</sub>. *Nature* 404:856–858
- Lampe U, Gerblinger J, Meixner H (1992) Comparison of structural response of exhaust-gas sensors based on thin films of selected metal oxides. *Sens Actuators B* 7:787–791
- Lampe U, Gerblinger J, Meixner H (1995a) Carbon-monoxide sensors based on thin films of BaSnO<sub>3</sub>. *Sens Actuators B* 24–25:657–660

- Lampe U, Gerblinger J, Meixner H (1995b) Nitrogen oxide sensors based on thin films of  $\text{BaSnO}_3$ . *Sens Actuators B* 26–27:97–98
- Lample U, Fleischer M, Reitmeier N, Meixner H, McMonagle JB, Marsh A (1996) New metal oxide sensors: materials and properties. In: *Sensors update*, Chap 1, vol 2. Wiley, New York, pp 1–36
- Lecomte J, Loup JP, Bossier G, Hervieu M, Raveau B (1984) Defect structure and electrical conductivity of niobates with related perovskite-type structures. *Solid State Ionics* 12:113–118
- Lee GG, Kang S-JK (2005) Formation of large pores and their effect on electrical properties of  $\text{SnO}_2$  gas sensors. *Sens Actuators B* 107:392–396
- Lee M-S, Meyer J-U (2000) A new process for fabricating  $\text{CO}_2$ -sensing layers based on  $\text{BaTiO}_3$  and additives. *Sens Actuators B* 68:293–299
- Li JG, Kawi S (1998) Synthesis, characterization and sensing application of novel semiconductor oxides. *Talanta* 45:759–766
- Li GJ, Zhang XH, Kawi S (1999) Relationships between sensitivity, catalytic activity and surface areas of  $\text{SnO}_2$  gas sensors. *Sens Actuators B* 60:64–70
- Liang KC, Nowick AS (1993) High-temperature protonic conduction in mixed perovskite ceramics. *Solid State Ionics* 61:77–81
- Liang KC, Du Y, Nowick AS (1994) Fast high-temperature proton transport in nonstoichiometric mixed perovskites. *Solid State Ionics* 69:117–120
- Liangyuan C, Shouli B, Guojun Z, Dianqing L, Aifan C, Liu CC (2008) Synthesis of  $\text{ZnO-SnO}_2$  nanocomposites by microemulsion and sensing properties for  $\text{NO}_2$ . *Sens Actuators B* 134:360–366
- Lim SK, Hwang S-H, Chang D, Kim S (2010) Preparation of mesoporous  $\text{In}_2\text{O}_3$  nanofibers by electrospinning and their application as a CO gas sensor. *Sens Actuators B* 149:28–33
- Lin S, Li D, Wu J, Li X, Akbar SA (2011) A selective room temperature formaldehyde gas sensor using  $\text{TiO}_2$  nanotube arrays. *Sens Actuators B* 156:505–509
- Lin Q, Li Y, Yang M (2012) Tin oxide/graphene composite fabricated via a hydrothermal method for gas sensors working at room temperature. *Sens Actuators B* 173:139–147
- Ling Z, Leach C, Freer R (2001) Heterojunction gas sensors for environmental  $\text{NO}_2$  and  $\text{CO}_2$  monitoring. *J Eur Ceram Soc* 21(10–11):1977–1980
- Litzelman SJ, Rothschild A, Tuller HL (2005) The electrical properties and stability of  $\text{SrTi}_{0.65}\text{Fe}_{0.35}\text{O}_{3-\delta}$  thin films for automotive oxygen sensor applications. *Sens Actuators B* 108:231–237
- Liu P, Lee S-H, Tracy CE, Turner JA, Pitts JR, Deb SK (2003) Electrochromic and chemochromic performance of mesoporous thin-film vanadium oxide. *Solid State Ionics* 165:223–228
- Liu RQ, Xie YH, Wang JD, Li ZJ, Wang BH (2006) Synthesis of ammonia at atmospheric pressure with  $\text{Ce}_{0.8}\text{M}_{0.2}\text{O}_2$ -delta (M=La, Y, Gd, Sm) and their proton conduction at intermediate temperature. *Solid State Ionics* 177:73–76
- Logothetis EM (1980) Resistive-type exhaust gas sensors. *Ceram Eng Sci Proc* 2:281–301
- Lopez-Gandara C, Ramos FM, Cirera A (2009) YSZ-based oxygen sensors and the use of nanomaterials: a review from classical models to current trends. *J Sens* 2009:258489
- Lu G, Miura N, Yamazoe N (1996a) High temperature hydrogen sensor based on stabilized zirconia and a metal oxide electrode. *Sens Actuators B* 35:130–135
- Lu G, Miura N, Yamazoe N (1996b) Mixed potential hydrogen sensor combining oxide ion conductor with oxide electrode. *J Electrochem Soc* 143:L154–L155
- Lu G, Xu J, Sun J, Yu Y, Zhang Y, Liu F (2012) UV-enhanced room temperature  $\text{NO}_2$  sensor using  $\text{ZnO}$  nanorods modified with  $\text{SnO}_2$  nanoparticles. *Sens Actuators B* 162:82–88
- Lupan O, Ursaki VV, Chai G, Chow L, Emelchenko GA, Tiginyanu IM, Gruzintsev AN, Redkin AN (2010) Selective hydrogen gas nanosensor using individual  $\text{ZnO}$  nanowire with fast response at room temperature. *Sens Actuators B* 144:56–66
- Luyten J, De Schutter F, Schram J, Schoonman J (1991) Chemical and electrical properties of Yb-doped strontium cerates in coal combustion atmospheres. *Solid State Ionics* 46:117–120
- Manzanares M, Prades JD, Cirera A, Andreu T, Hernández-Ramírez F, Jiménez-Rodríguez R, Romano-Rodríguez A, Morante JR (2009) Room temperature conductometric gas sensors based on metal oxide nanowires and nanocrystals. In: *Proceedings of the Spanish conference on electron devices*, 11–13 Feb 2009, Santiago de Compostela, Spain, pp 320–322
- Marnellos G, Stoukides M (1998) Ammonia synthesis at atmospheric pressure. *Science* 282:98–100
- Marques FMB, Wirtz GP (1991) Electrical properties of ceria-doped yttria. *J Am Ceram Soc* 74:598–605
- Marques FMB, Kharton VV, Naumovich EN, Shaula AL, Kovalevsky AV, Yaremchenko AA (2006) Oxygen ion conductors for fuel cells and membranes: selected developments. *Solid State Ionics* 177:1697–1703
- Marsal A, Cornet A, Morante JR (2003a) Study of the CO and humidity interference in La doped tin oxide  $\text{CO}_2$  gas sensor. *Sens Actuators B* 94:324–329
- Marsal A, Dezanneau G, Cornet A, Morante JR (2003b) Study of the CO and humidity interference in La doped tin oxide  $\text{CO}_2$  gas sensor. *Sens Actuators B* 95:266–270



- Martin LP, Glass RS (2005) Hydrogen sensor based on YSZ electrolyte and tin doped indium oxide electrode. *J Electrochem Soc* 152:H43–H47
- Matko I, Gaidi M, Chenevier B, Charai A, Saikaly W, Labeau M (2002) Pt doping of SnO<sub>2</sub> thin films. *J Electrochem Soc* 149:H153–H158
- McAlear JF, Moseley PT, Bourke P, Norris JO, Stephan R (1985) Tin dioxide gas sensors: use of the Seebeck effect. *Sens Actuators* 8:251–256
- McAlear JF, Moseley PT, Norris JO, Williams DE (1987) Tin dioxide gas sensors: I. Aspects of the surface chemistry revealed by electrical conductance variations. *J Chem Soc Faraday Trans I* 83:1323
- Meier DC, Semancik S, Button B, Strelcov E, Kolmakov A (2007a) Coupling nanowire chemiresistors with MEMS microhotplate gas sensing platforms. *Appl Phys Lett* 91:063118
- Meier DC, Evju JK, Boger Z, Raman B, Benkstein KD, Martinez CJ, Montgomery CB, Semancik S (2007b) The potential for and challenges of detecting chemical hazards with temperature-programmed microsensors. *Sens Actuators B* 121:282–294
- Menesklou W (2011) Systematische Produktentwicklung in der Sensorik. [http://www.iwe.kit.edu/plainhtml/lehre/spids/SPIDS\\_1.2\\_Sensor\\_Prinzipien\\_WS2011\\_12.pdf](http://www.iwe.kit.edu/plainhtml/lehre/spids/SPIDS_1.2_Sensor_Prinzipien_WS2011_12.pdf)
- Menesklou W, Schreiner H-J, Hardtl KH, Tiffée EI (1999) High temperature oxygen sensors based on doped SrTiO<sub>3</sub>. *Sens Actuators B* 59:184–189
- Mishra S, Ghanshyam C, Ram N, Bajpai RP, Bedi RK (2004) Detection mechanism of metal oxide gas sensor under UV radiation. *Sens Actuators B* 97:387–390
- Mitterdorfer A, Gauckler LJ (1999) Identification of the reaction mechanism of the Pt, O<sub>2</sub>(g)/yttria-stabilized zirconia system: Part I: General framework, modelling, and structural investigation. *Solid State Ionics* 117:187–202
- Miura N, Yamazoe N (1998) High-temperature potentiometric/amperometric NO<sub>x</sub> sensors combining stabilized zirconia with mixed-metal oxide electrode. *Sens Actuators B* 52:169–178
- Miura N, Harada T, Yamazoe N (1989) Sensing characteristics and working mechanism of four-probe type solid-state hydrogen sensor using proton conductor. *J Electrochem Soc* 136:1215–1219
- Miura N, Raisen T, Lu G, Yamazoe N (1998) Highly selective CO sensor using stabilized zirconia and a couple of oxide electrodes. *Sens Actuators B* 47:84–91
- Miura N, Lu G, Yamazoe N (2000) Progress in mixed-potential type devices based on solid electrolyte for sensing redox gases. *Solid State Ionics* 136–137:533–542
- Mizuno N, Yoshioka T, Kato K, Iwamoto M (1993) CO<sub>2</sub>-sensing characteristics of SnO<sub>2</sub> element modified by La<sub>2</sub>O<sub>3</sub>. *Sens Actuators B* 13:473–476
- Mohajeri N, Muradov N, Bokerman G, T-Raissi A, Captain J, Peterson B, Whitten M (2009) Gas permeable chemochromic compositions for hydrogen sensing. NASA/CR – 2009–215441, pp 20–148
- Moos R, Gnudi A, Härdtl KH (1995) Thermopower of Sr<sub>1-x</sub>La<sub>x</sub>TiO<sub>3</sub> ceramics. *J Appl Phys* 78:5042–5047
- Moos R, Sahnner K, Fleischer M, Guth U, Barsan N, Weimar U (2009) Solid state gas sensor research in Germany – a status report. *Sensors* 9:4323–4365
- Moos R, Izu N, Rettig F, Reiß S, Shin W, Matsubara I (2011) Resistive oxygen gas sensors for harsh environments. *Sensors* 11:3439–3465
- Mor GK, Carvalho MA, Varghese OK, Pishko MV, Grimes CA (2004) A room-temperature TiO<sub>2</sub>-nanotube hydrogen sensor able to self-clean photoactively from environmental contamination. *J Mater Res* 19:628
- Morrison SR (1982) Chemisorption on nonmetallic surfaces. In: Anderson JR, Boudart M (eds) *Catalysis science and technology*. Springer, Berlin
- Morrison SR (1987) Mechanism of semiconductor gas sensor operation. *Sens Actuators* 11:283–287
- Moseley PT (1992) Materials selection for semiconductor gas sensors. *Sens Actuators B* 6:149–156
- Moseley PT, Crocker AJ (1996) *Sensor materials*. IOP Publishing, Bristol
- Moseley P, Williams DE (1989) Gas sensors based on oxides of early transition metals. *Polyhedron* 8:1615–1618
- Mosley PT, Norris J, Williams DE (eds) (1991) *Techniques and mechanisms in gas sensing*. Adam Hilger, New York
- Moulson AJ, Herbert JM (1990) *Electroceramics materials, properties, applications*. Chapman and Hall, London
- Mukundan R, Brosha E, Brown D, Garzon F (1999) Ceria-electrolyte-based mixed potential sensors for the detection of hydrocarbons and carbon monoxide. *Electrochem Soc Lett* 2(8):412–414
- Mulla IS, Ramgir NS, Hwang YK, Chang J-S (2004) Semiconductor tin oxide gas sensors: from bulk to thin films. *J Ind Eng Chem* 10(7):1242–1256
- Murch GE, Nowick AS (eds) (1984) *Diffusion in crystalline solids*. Academic, New York
- Nakamura Y, Ando A, Tsurutani T, Okada O, Miyayama M, Koumoto K, Yanagida H (1986) Gas sensitivity of CuO/ZnO hetero-contact. *Chem Lett* 1986:413–416
- Nakamura Y, Yoshioka H, Miyayama M, Yanagida H (1990) Selective CO gas sensing mechanism with CuO/ZnO heterocontact. *J Electrochem Soc* 137:940–943
- Nakayama S, Sakamoto M (1998) Electrical properties of new type high oxide ionic conductor RE<sub>10</sub>Si<sub>6</sub>O<sub>27</sub> (RE = La, Pr, Nd, Sm, Gd, Dy.). *J Eur Ceram Soc* 18:1413–1418

- Nigara Y, Mizusaki J, Kawamura K, Kawada T, Ishigame M (1998) Hydrogen permeability in  $(\text{CeO}_2)_{0.9}(\text{CaO})_{0.1}$  at high temperatures. *Solid State Ionics* 113:347–354
- Nishibori M, Tajima K, Shin W, Izu N, Itoh T, Matsubara I (2006) CO oxidation catalyst of Au-TiO<sub>2</sub> on the thermoelectric gas sensor. *J Ceram Soc Jpn* 115:34–41
- Nishimura R, Toba K, Yamakawa K (1996) The development of a ceramic sensor for the prediction of hydrogen attack. *Corros Sci* 38:611–621
- Nowick AS, Du Y, Liang KC (1999) Some factors that determine proton conductivity in nonstoichiometric complex perovskites. *Solid State Ionics* 125:303–311
- Oelerich W, Klassen T, Bormann R (2001) Metal oxides as catalysts for improved hydrogen sorption in nanocrystalline Mg-based materials. *J Alloys Compd* 315:237–242
- Ogawa H, Nishikawa M, Abe A (1982) Hall measurement studies and an electrical conduction model of tin oxide ultrafine particle films. *J Appl Phys* 53:4448–4455
- Okamura K, Ishiji T, Iwaki M, Suzuki Y, Takahashi K (2007) Electrochemical gas sensor using a novel gas permeable electrode modified by ion implantation. *Surf Coat Technol* 201:8116–8119
- Oprea A, Courbat J, Bârsan N, Briand D, de Rooij NF, Weimar U (2009) Temperature, humidity and gas sensors integrated on plastic foil for low power applications. *Sens Actuators B* 140:227–232
- Park CO, Akbar SA (2003) Ceramics for chemical sensing. *J Mater Sci* 38:4611–4637
- Park SS, Mackenzie JD (1996) Thickness and microstructure effect on alcohol sensing of tin oxide thin films. *Thin Solid Films* 274:154–159
- Park CO, Akbar SA, Weppner W (2003) Ceramic electrolytes and electrochemical sensors. *J Mater Sci* 38:4639–4660
- Park CO, Fergus JW, Miura N, Park J, Choi A (2009) Solid-state electrochemical gas sensors. *Ionics* 15:261–284
- Patil LA (2009) Fe<sub>2</sub>O<sub>3</sub> - ZnO based gas sensors. *Sens Transducers J* 104(5):68–75
- Paulose M, Varghese OK, Mor GK, Grimes CA, Ong KG (2006) Unprecedented ultra-high hydrogen gas sensitivity in undoped titania nanotubes. *Nanotechnology* 17:398–402
- Pavelko RG, Vasiliev AA, Llobet E, Vilanova X, Barrabés N, Medina F, Sevastyanov VG (2009) Comparative study of nanocrystalline SnO<sub>2</sub> materials for gas sensor application: thermal stability and catalytic activity. *Sens Actuators B* 137:637–643
- Peng L, Xie TF, Yang M, Xu D, Pang S, Wang DJ (2008) Light induced enhancing gas sensitivity of copper-doped zinc oxide at room temperature. *Sens Actuators B* 131:660–664
- Pijolat C (1986) Etude des proprietes physico-chimiques et des proprietes electriques du dioxyde d'étain en fonction de l'atmosphère gazeuse environnante. Application a la detection selective des gaz. PhD Thesis, l'Institut National Polytechnique de Grenoble
- Pijolat C, Viricelle JP, Tournier G, Montment P (2006) Application of membranes and filtering films for gas sensors improvements. *Thin Solid Films* 490:7–16
- Pitts JR (2002) Detecting hydrogen with chemochromic thin films. *Ind Physicist (AIP) Forum* June/July:31
- Polla DL, White RM, Muller RS (1985) Integrated chemical-reaction sensor. In: Digest of technical papers of TRANSDUCERS '85. 1985 International conference on solid-state sensors and actuators, 11–14 June 1985, Philadelphia, pp 33–36
- Prades JD, Jimenes-Diaz R, Hernandez-Ramirez F, Fernandez-Romero L, Andreu T, Cirera A, Romano-Rodriguez A, Cornet A, Morante JR, Barth S, Mathur S (2008) Toward a systematic understanding of photodetectors based on individual metal oxide nanowires. *J Phys Chem C* 112:14639–14644
- Prades JD, Jimenes-Diaz R, Manzanares M, Hernandez-Ramirez F, Cirera A, Romano-Rodriguez A, Marthur S, Morante JR (2009) A model for the response towards oxidizing gases of photoactivated sensors based on individual SnO<sub>2</sub> nanowires. *Phys Chem Chem Phys* 11:1–9
- Qiu S, Gao C, Zheng X, Chen J, Yang C, Gan X, Fan H (2008) Pb(Zr<sub>0.95</sub>Ti<sub>0.05</sub>)O<sub>3</sub> powders prepared by aqueous Pechini method using one-step pyrolysis process: characterization and porous ceramics. *J Mater Sci* 43(9):3094–3100
- Ramgir NS, Mulla IS, Vijayamohan KP (2005) A room temperature nitric oxide sensor actualized from Ru-doped SnO<sub>2</sub> nanowires. *Sens Actuators B* 107:708–715
- Ramamoorthy R, Dutta PK, Akbar SA (2003) Oxygen sensors: materials, methods, designs and applications. *J Mater Sci* 38:4271–4282
- Rettig F, Moos R (2007a) Direct thermoelectric gas sensors: design aspects and first gas sensors. *Sens Actuators B* 123:413–419
- Rettig F, Moos R (2007b) Direct thermoelectric hydrocarbon gas sensors based on SnO<sub>2</sub>. *IEEE Sens J* 7:1490–1496
- Rettig F, Moos R (2008) Morphology dependence of thermopower and resistance in semiconducting oxides with space charge regions. *Solid State Ionics* 179:2299–2307
- Rettig F, Moos R (2009) Temperature modulated direct thermoelectric gas sensors: thermal modeling and results for fast hydrocarbon sensors. *Meas Sci Technol* 20:065205
- Robertson NL, Michaels JN (1990) Oxygen exchange on platinum electrodes in zirconia cells: location of electrochemical reaction sites. *J Electrochem Soc* 137:129–135

- Röder-Roith U, Rettig F, Röder T, Janek J, Moos R, Sahner K (2009) Thick-film solid electrolyte oxygen sensors using the direct ionic thermoelectric effect. *Sens Actuators B* 136:530–535
- Rothschild A, Tuller HL (2006) Gas sensors: new materials and processing approaches. *J Electroceram* 17:1005–1012
- Rothschild A, Litzelman SJ, Tuller HL, Menesklou W, Schneider T, Ivers-Tiffée E (2005) Temperature-independent resistive oxygen sensors based on  $\text{SrTi}_{1-x}\text{Fe}_x\text{O}_{3-\delta}$  solid solutions. *Sens Actuators B* 108:223–230
- Ruiz AM, Cornet A, Shimanoe K, Morante JR, Yamazoe N (2005) Effects of various metal additives on the gas sensing performances of  $\text{TiO}_2$  nanocrystals obtained from hydrothermal treatments. *Sens Actuators B* 108:34–40
- Rumyantseva M, Kovalenko V, Gaskov A, Makshina E, Yuschenko V, Ivanova I, Ponzoni A, Faglia G, Comini E (2006) Nanocomposites  $\text{SnO}_2/\text{Fe}_2\text{O}_3$ : sensor and catalytic properties. *Sens Actuators B* 118:208–214
- Sadek Z, Wlodarski W, Shin K, Kaner RB, Kalantar-zadeh K (2006) A layered surface acoustic wave gas sensor based on a polyaniline/ $\text{In}_2\text{O}_3$  nanofibre composite. *Nanotechnology* 17:4488–4492
- Sahm T, Gurlo A, Barsan N, Weimar U (2006) Properties of indium oxide semiconducting sensors deposited by different techniques. *Particulate Sci Technol* 24(4):441–452
- Sahner K, Tuller HL (2010) Novel deposition techniques for metal oxide: prospects for gas sensing. *J Electroceram* 24:177–199
- Sakai N, Yamaji K, Horita T, Yokokawa H, Hirata Y, Sameshima S, Nigara Y, Mizusaki J (1999) Determination of hydrogen solubility in oxide ceramics by using SIMS analyses. *Solid State Ionics* 125:325–331
- Sakthivel M, Weppner W (2007) Application of layered perovskite type proton conducting  $\text{KCa}_2\text{Nb}_3\text{O}_{10}$  in  $\text{H}_2$  sensors: Pt particle size and temperature dependence. *Sens Actuators B* 125:435–440
- Sakthivel M, Weppner W (2008) A portable limiting current solid-state electrochemical diffusion hole type hydrogen sensor device for biomass fuel reactors: engineering aspect. *Int J Hydrogen Energy* 33:905–911
- Sandu I, Presmanes L, Alphonse P, Tailhades P (2006) Nanostructured cobalt manganese ferrite thin films for gas sensor application. *Thin Solid Films* 495:130–133
- Satsuma A, Katagiri M, Kakimoto S, Sugaya S, Shimizu K (2011) Effects of calcination temperature and acid–base properties on mixed potential ammonia sensors modified by metal oxides. *Sensors* 11:2155–2165
- Sberveglieri G (1992) Classical and novel techniques for the preparation of  $\text{SnO}_2$  thin-film gas sensors. *Sens Actuators B* 6:239–247
- Scherban E, Nowick AS (1989) Bulk protonic conduction in Yb-doped  $\text{SrCeO}_3$ . *Solid State Ionics* 35:189–194
- Schierbaum KD (1995) Engineering of oxide surfaces and metal/oxide interfaces for chemical sensors: recent trends. *Sens Actuators B* 24–25:239–247
- Schönauer D, Wiesner K, Fleischer M, Moos R (2009) Selective mixed potential ammonia exhaust gas sensor. *Sens Actuators B* 140:585–590
- Schreiter M, Gabl R, Lerchner J, Hohlfeld C, Delan A, Wolf G, Blüher A, Katzschner B, Mertig M, Poempec W (2006) Functionalized pyroelectric sensors for gas detection. *Sens Actuators B* 119:255–261
- Sears WM, Colbow K, Consadori F (1989) General characteristics of thermally cycled tin oxide gas sensors. *Semicond Sci Technol* 4:351–359
- Seiyama T, Kato A, Fujiishi K, Nagatani M (1962) A new detector for gaseous components using semiconductive thin films. *Anal Chem* 34:1502–1503
- Shanak H, Schmitt H, Nowoczin J, Ziebert C (2004) Effect of Pt-catalyst on gasochromic  $\text{WO}_3$  films: optical, electrical and AFM investigations. *Solid State Ionics* 171:99–106
- Shi S, Liu Y, Chen Y, Zhang J, Wang Y, Wang T (2009) Ultrahigh ethanol response of  $\text{SnO}_2$  nanorods at low working temperature arising from  $\text{La}_2\text{O}_3$  loading. *Sens Actuators B* 140:426–431
- Shimizu Y, Egashira M (1999) Basic aspects and challenges of semiconductor gas sensors. *MRS Bull* 24:18–24
- Shimura T, Komori M, Iwahara H (1996) Ionic conduction in pyrochlore-type oxides containing rare earth elements at high temperature. *Solid State Ionics* 86:685–689
- Shimura T, Fujimoto S, Iwahara H (2001) Proton conduction in non-perovskite-type oxides at elevated temperatures. *Solid State Ionics* 143:117–123
- Shin W, Imai K, Izu N, Murayama N (2001) Thermoelectric thick-film hydrogen gas sensor operating at room temperature. *Jpn J Appl Phys* 2 Lett 40:L1232–L1234
- Shin W, Matsumiya M, Izu N, Murayama N (2003) Hydrogen-selective thermoelectric gas sensor. *Sens Actuators B* 93:304–308
- Shin W, Choi Y, Tajima K, Izu N, Matsubara I, Murayama N (2005) Planar catalytic combustor film for thermoelectric hydrogen sensor. *Sens Actuators B* 108:455–460
- Shin W, Nishibori M, Matsubara I (2011) Gas sensors using pyroelectric and thermoelectric effects. In: Korotcenkov G (ed) *Chemical sensors: comprehensive sensor technologies*, vol 4, Solid state devices. Momentum, New York, pp 261–285
- Shouli B, Dianqing L, Dongmei H, Ruixian L, Aifan C, Liu CC (2010) Preparation, characterization of  $\text{WO}_3$ - $\text{SnO}_2$  nanocomposites and their sensing properties for  $\text{NO}_2$ . *Sens Actuators B* 150:749–755
- Shukla S, Seal S, Ludwig L, Parish C (2004) Nanocrystalline indium oxide-doped tin oxide thin film as low temperature hydrogen sensor. *Sens Actuators B* 97:256–265

- Shukla S, Zhang P, Cho HJ, Ludwig L, Seal S (2008) Significance of electrode-spacing in hydrogen detection for tin oxide-based MEMS sensor. *Int J Hydrogen Energy* 33:470–475
- Siemons M, Leifert A, Simon U (2007) Preparation and gas sensing characteristics of nanoparticulate *p*-type semiconducting  $\text{LnFeO}_3$  and  $\text{LnCrO}_3$  materials. *Adv Funct Mater* 17:2189–2197
- Singh N, Gupta RK, Lee PS (2011) Gold-nanoparticle-functionalized  $\text{In}_2\text{O}_3$  nanowires as CO gas sensors with a significant enhancement in response. *Appl Mater Int* 3:2246–2252
- Siroky K (1993) Use of the Seebeck effect for sensing flammable gas and vapors. *Sens Actuators B* 17:13–17
- Skinner SJ, Kilner JA (2003) Oxygen ion conductors. *Mater Today* 6:30–37
- Smith RD II, Benson DK, Pitts RJ, Oison DL, Wildeman TR (2001) Diffusible weld hydrogen measurement by fiber optic sensors. *Materialpruefung/Mater Test* 43(1–2):26–29
- Smith RD II, Pitts JR, Lee S-H, Tracy E (2004) Protective coatings for Pd-based hydrogen sensors. *Prep Pap Am Chem Soc Div Fuel Chem* 49(2):968–969
- Solis JL, Lantto V (1995) A study of gas-sensing properties of sputtered  $\alpha\text{-SnWO}_4$  thin films. *Sens Actuators B* 24–25:591–595
- Solis JL, Saukko S, Kish L, Granqvist CG, Lantto V (2001) Semiconductor gas sensors based on nanostructured tungsten oxide. *Thin Solid Films* 391:255–260
- Stamatakis M, Tsamakis D, Brilis N, Fasaki I, Giannoudakis A, Kompitsas M (2008) Hydrogen gas sensors based on PLD grown NiO thin film structures. *Physica Status Solidi* 205(8):2064–2068
- Stankova M, Vilanova X, Calderer J, Llobet E, Ivanov P, Gracia I, Cane C, Correig X (2004) Detection of  $\text{SO}_2$  and  $\text{H}_2\text{S}$  in  $\text{CO}_2$  stream by means of  $\text{WO}_3$ -based micro-hotplate sensors. *Sens Actuators B* 102:219–225
- Stefanik TS, Tuller HL (2001) Ceria-based gas sensors. *J Eur Ceram Soc* 21:1967–1970
- Stolen S, Bakken E, Mohn CE (2006) Oxygen-deficient perovskites: linking structure, energetics and ion transport. *Phys Chem Chem Phys* 8:429–447
- Stoukides M (1988) Applications of solid electrolytes in heterogeneous catalysis. *Ind Eng Chem Res* 27:1745–1750
- Subbarao EC, Maiti HS (1984) Solid electrolytes with oxygen ion conduction. *Solid State Ionics* 11:317–338
- Sun J, Xu JY, Yu SP, Liu FG, Lu G (2012) UV-activated room temperature metal oxide based gas sensor attached with reflector. *Sens Actuators B* 169:291–296
- Sundmacher K, Rihko-Struckmann LK, Galvita V (2005) Solid electrolyte membrane reactors: status and trends. *Catal Today* 104:185–199
- Suzuki T, Yamazaki T (1990) Effect of annealing on the gas sensitivity of thin oxide ultra-thin films. *J Mater Sci Lett* 9:750–751
- Sysoev VV, Schneider T, Goschnick J, Kiselev I, Habicht W, Hahn H, Strelcov E, Kolmakov A (2009) Percolating  $\text{SnO}_2$  nanowire network as a stable gas sensor: direct comparison of long-term performance versus  $\text{SnO}_2$  nanoparticle films. *Sens Actuators B* 139:699–703
- Taguchi N (1971) Gas detecting device. US Patent 3,631,436
- Tamaki J, Akiyama M, Xu C, Miura N, Yamazoe N (1990) Conductivity change of  $\text{SnO}_2$  with  $\text{CO}_2$  adsorption. *Chem Lett* 1990:1243–1246
- Tamaki J, Shimanoe K, Yamada Y, Yamamoto Y, Miura N, Yamazoe N (1998) Dilute hydrogen sulfide sensing properties of  $\text{CuO-SnO}_2$  thin film prepared by low-pressure evaporation method. *Sens Actuators B* 49:121–125
- Tamaki J, Miyaji A, Makinodan J, Ogura S, Konishi S (2005) Effect of micro-gap electrode on detection of dilute  $\text{NO}_2$  using  $\text{WO}_3$  thin film microensors. *Sens Actuators B* 108:202–206
- Taniguchi N, Kuroha T, Nishimura C, Iijima K (2005) Characteristics of novel  $\text{BaZr}_{0.4}\text{Ce}_{0.4}\text{In}_{0.2}\text{O}_3$  proton conducting ceramics and their application to hydrogen sensors. *Solid State Ionics* 176:2979–2983
- Tanner CW, Virkar AV (1996) Instability of  $\text{BaCeO}_3$  in  $\text{H}_2\text{O}$ -containing atmospheres. *J Electrochem Soc* 143:1386–1389
- Tao S, Irvine JTS (2001) Preparation and characterisation of apatite-type lanthanum silicates by a sol-gel process. *Mat Res Bull* 36:1245–1258
- Tao S, Poulsen FW, Meng G, Sørensen OT (2000) High-temperature stability study of the oxygen-ion conductor  $\text{La}_{0.9}\text{Sr}_{0.1}\text{Ga}_{0.8}\text{Mg}_{0.2}\text{O}_{3-x}$ . *J Mater Chem* 10:1829–1833
- Tejuca LJ, Fierro JLG (eds) (1993) Properties and applications of perovskite-type oxides. Marcel Dekker, New York
- Tesfamichael T, Motta N, Bostrom T, Bell JM (2007) Development of porous metal oxide thin films by coevaporation. *Appl Surf Sci* 253:4853–4859
- Thangadurai V, Weppner W (2001a)  $\text{AA}_2\text{M}_3\text{O}_{10}$  ( $\text{A} = \text{K, Rb, Cs}$ ;  $\text{A} = \text{Ca}$ ;  $\text{M} = \text{Nb}$ ) layered perovskites: low-temperature proton conductors in hydrogen atmospheres. *J Mater Chem* 11:636–639
- Thangadurai V, Weppner W (2001b) Electrical properties of  $\text{A}'\text{Ca}_2\text{Nb}_3\text{O}_{10}$  ( $\text{A}' = \text{K, Rb, Cs}$ ) layered perovskite ceramics. *Ionics* 7:22–31
- Thangadurai V, Weppner W (2006) Recent progress in solid oxide and lithium ion conducting electrolytes research. *Ionics* 12:81–92
- Thompson M, Stone DC (1997) Surface-launched acoustic wave sensors: chemical sensing and thin-film characterization. Wiley, New York
- Tien LC, Sadik PW, Norton DP, Voss LF, Pearton SJ, Wang HT, Kang BS, Ren F, Jun J, Lin J (2005) Hydrogen sensing at room temperature with Pt-coated ZnO thin films and nanorods. *Appl Phys Lett* 87:222106

- Toan NN, Saukko S, Lantto V (2003) Gas sensing with semiconducting perovskite oxide  $\text{LaFeO}_3$ . *Phys B Condens Matter* 327:279–282
- Toda K, Kameo Y, Kurita S, Sato M (1996) Crystal structure determination and ionic conductivity of layered perovskite compounds  $\text{NaLnTiO}_4$  ( $\text{Ln} = \text{Rare Earth}$ ). *J Alloys Compd* 234:19–25
- Tomchenko AA, Harmer GP, Marquis BT, Allen JW (2003) Semiconducting metal oxide sensor array for the selective detection of combustion gases. *Sens Actuators B* 93:126–134
- Tongpool R, Leach C, Freer R (2000) Temperature and microstructural dependence of the sensitivity of heterocontacts between zinc oxide and copper oxide in reducing environments. *J Mater Sci Lett* 19:119–121
- Traqueia LSM, Marques FMB, Khartov VV (2006) Oxygen ion conduction in oxide materials: selected examples and basic mechanisms. *Bol Soc Esp Ceram* 45(3):115–121
- Traversa E (1995) Ceramic sensors for humidity detection: the state-of-the-art and future developments. *Sens Actuators B* 23:135–156
- Tricoli A, Righettoni M, Pratsinis SE (2009) Minimal cross-sensitivity to humidity during ethanol detection by  $\text{SnO}_2$ – $\text{TiO}_2$  solid solutions. *Nanotechnology* 20:315502
- Tuller HL (2000) Ionic conduction in nanocrystalline materials. *Solid State Ionics* 131:143–157
- Tuller HL (2003) Defect engineering: design tools for solid state electrochemical devices. *Electrochim Acta* 48:2879–2887
- Ushio Y, Miyayama M, Yanagida H (1994) Effects of interface states on gas-sensing properties of a  $\text{CuO}/\text{ZnO}$  thin-film heterojunction. *Sens Actuators B* 17:221–226
- Vallejos S, Khatko V, Calderer J, Gracia I, Cane C, Llobet E, Correig X (2008) Micromachined  $\text{WO}_3$ -based sensors selective to oxidizing gases. *Sens Actuators B* 132:209–215
- Varghese OK, Gong D, Paulose M, Grimes CA, Dickey EC (2003) Crystallization and high-temperature structural stability of titanium oxide nanotube arrays. *J Mater Res* 18(1):156–165
- Varghese OK, Mor GK, Grimes CA, Paulose M, Mukherjee N (2004) A titania nanotube-array room-temperature sensor for selective detection of hydrogen at low concentrations. *J Nanosci Nanotechnol* 4:733–737
- Vasil'ev RB, Rumyantseva MN, Ryabova LI, Akimov BA, Gas'kov AM, Labeau M, Langlet M (1999) Electric-field-controlled memory effect in heterostructures for gas sensors. *Tech Phys Lett* 25(6):471–474
- Vasiliev RB, Rumyantseva MN, Yakovlev NV, Gaskov AM (1998)  $\text{CuO}:\text{SnO}_2$  thin film heterostructures as chemical sensors to  $\text{H}_2\text{S}$ . *Sens Actuators B* 50:186–193
- Vasiliev RB, Rumyantseva MN, Podguzova SE, Ryzhikov AS, Ryabova LI, Gaskov AM (1999) Effect of interdiffusion on electrical and gas sensor properties of  $\text{CuO}:\text{SnO}_2$  heterostructure. *Mater Sci Eng B* 57:241–246
- Wada K, Egashira M (2000) Hydrogen sensing properties of  $\text{SnO}_2$  subjected to surface chemical modification with ethoxysilanes. *Sens Actuators B* 62:211–219
- Wagner T, Hennemann J, Kohl C-D, Tiemann N (2011) Photocatalytic ozone sensor based on mesoporous indium oxide: influence of the relative humidity on the sensing performance. *Thin Solid Films* 520:918–921
- Wakamura K (2005) Empirical relationships for ion conduction based on vibration amplitude in perovskite-type proton and superionic conductors. *J Phys Chem Solids* 66:133–142
- Wang W, Virkar AV (2005) Ionic and electron–hole conduction in  $\text{BaZr}_{0.93}\text{Y}_{0.07}\text{O}_{3-d}$  by 4-probe DC measurements. *J Power Sources* 142(1–2):1–9
- Wang JD, Xie YH, Zhang ZF, Liu RQ, Li ZJ (2005) Protonic conduction in  $\text{Ca}^{2+}$ -doped  $\text{La}_2\text{M}_2\text{O}_7$  ( $\text{M} = \text{Ce}, \text{Zr}$ ) with its application to ammonia synthesis electrochemically. *Mater Res Bull* 40:1294–1302
- Wang DY, Symons WT, Farhat RJ, Valdes CA, Briggs EM, Polikarpus KK, Kupe J (2006a) Ammonia gas sensors. US Patent 7,074,319 B2
- Wang CH, Chu XF, Wu MW (2006b) Detection of  $\text{H}_2\text{S}$  down to ppb levels at room temperature using sensors based on  $\text{ZnO}$  nanorods. *Sens Actuators B* 113:320–323
- Weppner W (2000) Concepts and materials aspects of developing solid state ionic devices. In: Chowdari BVR, Wang W (eds) Proceedings of the 7th Asian conference on solid state ionics: materials and devices. World Scientific, River Edge, NJ, pp 3–12
- West AR (1999) Basic solid state chemistry, 2nd edn. Wiley, Chichester
- West AR (2006) Inorganic functional materials: optimization of properties by structural and compositional control. *Chem Rec* 6:206–216
- Wetchakun K, Samerjai T, Tamaekong N, Liewhiran C, Siriwong C, Kruefu V, Wisitsoraat A, Tuantranont A, Phanichphant S (2011) Semiconducting metal oxides as sensors for environmentally hazardous gases. *Sens Actuators B* 160:580–591
- Whitten MC, Janine EC, Peterson BV, Trigwell S, Berger CM, Mohajeri N, Bokerman G, Muradov N, T-Raissi A, McPherson J (2006) Chemoschromic hydrogen detection. *Proc SPIE* 6222:62220C
- Williams D (1999) Semiconducting oxides as gas-sensitive resistors. *Sens Actuators B* 57:1–16
- Williams DE, Pratt KFE (1998) Classification of reactive sites on the surface of polycrystalline tin dioxide. *J Chem Soc Faraday Trans* 94:3493–3500
- Wilson DM, Hoyt S, Janata J, Booksh K, Obando L (2001) Chemical sensors for portable, handheld field instruments. *IEEE Sens J* 1:256–274
- Wohltjen H, Snow AW (1998) Colloidal metal-insulator-metal ensemble chemiresistor sensor. *Anal Chem* 70:2856–2859

- Wu JM (2011)  $\text{TiO}_2/\text{Ti}_{1-x}\text{Sn}_x\text{O}_2$  heterojunction nanowires: characterization, formation, and gas sensing performance. *J Mater Chem* 21:14048–14055
- Wu L, Wu C-C, Wu M-M (1990) Humidity sensitivity of  $\text{Sr}(\text{Sn}, \text{Ti})\text{O}_3$  ceramics. *J Electron Mater* 19:197–200
- Wuensch BJ, Eberman KW, Heremans C, Ku EM, Onnerud P, Yeo EME, Haile SM, Stalick JK, Jorgensen JD (2000) Connection between oxygen-ion conductivity of pyrochlore fuel-cell materials and structural change with composition and temperature. *Solid State Ionics* 129:111–133
- Xing L-L, Yuan S, Chen Z-H, Chen Y-J, Xue X-Y (2011) Enhanced gas sensing performance of  $\text{SnO}_2/a\text{-MoO}_3$  heterostructure nanobelts. *Nanotechnology* 22:225502
- Xirouchaki C, Kiriakidis G, Pedersen TF, Fritzsche H (1996) Photoreduction and oxidation of as-deposited microcrystalline indium oxide. *J Appl Phys* 79:9349–9352
- Xu C, Tamaki J, Miura N, Yamazoe N (1991) Grain size effects on gas sensitivity of porous  $\text{SnO}_2$ -based elements. *Sens Actuators B* 3:147–155
- Yadav BC, Pandey NK, Srivastava A, Sharma P (2007) Optical humidity sensors based on titania films fabricated by sol-gel and thermal evaporation methods. *Meas Sci Technol* 18:260–264
- Yajima T, Iwahara H, Uchida H, Koide K (1990) Relation between proton conduction and concentration of oxide ion vacancy in  $\text{SrCeO}_3$  based sintered oxides. *Solid State Ionics* 40–41:914–917
- Yajima T, Iwahara H, Koide K, Yamamoto K (1991)  $\text{CaZrO}_3$ -type hydrogen and steam sensors: trial fabrication and their characteristics. *Sens Actuators B* 5:145–147
- Yajima T, Koide K, Takai H, Fukatu N, Iwahara H (1995) Application of hydrogen sensor using proton conductive ceramics as a solid electrolyte to aluminum casting industries. *Solid State Ionics* 79:333–337
- Yamazoe N (1991) New approaches for improving semiconductor gas sensors. *Sens Actuators B* 5:7–19
- Yamazoe N, Miura N (1992) Some basic aspects of semiconductor gas sensors. In: Yamauchi S (ed) *Chemical sensors technology*, vol 4. Kodansha/Elsevier, Tokyo/Amsterdam, pp 20–41
- Yamazoe N, Kurokawa Y, Seiyama T (1983) Effects of additives on semiconductor gas sensors. *Sens Actuators* 4:283–289
- Yang T-Y, Lin H-M, Wie B-Y, Wu C-Y, Lin C-K (2003) UV enhancement of the gas sensing properties of nano- $\text{TiO}_2$ . *Rev Adv Mater Sci* 4:48–54
- Yang J, Hidajat K, Kawi S (2008) Synthesis of nano- $\text{SnO}_2/\text{SBA-15}$  composite as a highly sensitive semiconductor oxide gas sensor. *Mater Lett* 62:1441–1443
- Ye C, Tamagawa T, Polla DL (1991) Experimental studies on primary and secondary pyroelectric effects in  $\text{Pb}(\text{Zr}, \text{Ti}_{1-x})\text{O}_3$ ,  $\text{PbTiO}_3$ , and  $\text{ZnO}$  thin films. *J Appl Phys* 70(10):5538–5543
- Zampiceni E, Comini E, Faglia G, Sberveglieri G, Kaciulis S, Pandolfi L, Viticoli S (2003) Composition influence on the properties of sputtered Sn–W–O films. *Sens Actuators B* 89:225–231
- Zhang J-G, Benson DK, Tracy CE, Deb SK, Czanderna AW, Bechinger C (1996) Electrochromic mechanism in  $a\text{-WO}_3$  films. *J Electrochem Soc* 24:251–259
- Zhang D, Li C, Han S, Liu X, Tang T, Jin W, Zhou C (2003) Ultraviolet photodetection properties of indium oxide nanowires. *Appl Phys A* 77:163–166
- Zhang T, Liu L, Qi Q, Li S, Lu G (2009) Development of microstructure In/Pd-doped  $\text{SnO}_2$  sensor for low-level CO detection. *Sens Actuators B* 139:287–291
- Zhao YM, Zhu YQ (2009) Room temperature ammonia sensing properties of  $\text{W}_{18}\text{O}_{49}$  nanowires. *Sens Actuators B* 137:27–31
- Zhao M, Huang JX, Ong CW (2012) Room-temperature resistive  $\text{H}_2$  sensing response of  $\text{Pd}/\text{WO}_3$  nanocluster-based highly porous film. *Nanotechnology* 23:315503
- Zheng W, Lu X, Wang W, Li Z, Zhang H, Wang Z, Xu X, Li S, Wang C (2009) Assembly of Pt nanoparticles on electrospun  $\text{In}_2\text{O}_3$  nanofibers for  $\text{H}_2\text{S}$  detection. *J Colloid Interface Sci* 338:366–370
- Zhuykov S, Miura N (2007) Development of zirconia-based potentiometric  $\text{NO}_x$  sensors for automotive and energy industries in the early 21st century: what are the prospects for sensors? *Sens Actuators B* 121:639–651
- Zisekas S, Karagiannakis G, Kokkofitis C, Stoukides M (2008)  $\text{NH}_3$  decomposition in a proton conducting solid electrolyte cell. *J Appl Electrochem* 38:1143–1149
- Zosel J, Ahlborn K, Müller R, Westphal D, Vashook V, Gutha U (2004) Selectivity of HC-sensitive electrode materials for mixed potential gas sensors. *Solid State Ionics* 169:115–119

# Chapter 3

## Polymers

### 3.1 General View

Polymers constitute another class of materials which are also very promising for various applications including gas sensors (Skotheim et al. 1998; Dai et al. 2002; Dimitrakopoulos and Malenfant 2002; Potyrailo 2006; Thomas et al. 2006; Skotheim and Reynolds 2007; Rahman et al. 2008; Ahmad 2009). Except for a few, polymers are organic macromolecules made of carbon and hydrogen atoms as the major percentage, with some heteroatoms such as nitrogen, oxygen, sulfur, phosphorus, and halogens as minor constituents. A polymer molecule is formed by the repetitive union of a large number of reactive small molecules in a regular sequence. Examples of such molecules are shown in Fig. 3.1. Some polymers that are used in the design of gas sensors are presented in Table 3.1. Of course, this list of polymers is not complete; the number of polymers which have been tested is much more extensive.

Studies have shown that conducting polymers (CPs) are the main class of these organic materials with most promise for gas sensor applications (Janata and Huber 1985; Janata and Josowicz 2003). In particular, common classes of organic conducting polymers acceptable for conductometric gas sensor application include poly(acetylene)s, poly(pyrrole)s, poly(thiophene)s, poly(terthiophene)s, poly(aniline)s, poly(fluorine)s, poly(3-alkylthiophene)s, polytetrathiafulvalenes, polynaphthalenes, poly(*p*-phenylene sulfide)s, and poly(*para*-phenylene vinylene)s (Nalwa 1997). Conducting polymers are also known for their ability to be compatible with biological molecules in neutral aqueous solutions (Chaubey and Malhotra 2002). In conjugated polymers, the chemical bonding leads to one unpaired electron (the  $\pi$ -electron) per carbon atom. For example, in polyacetylene  $(-\text{CH})_n$ , the classic example of CP, each carbon is  $\sigma$ -bonded to only two neighboring carbons and one hydrogen atom with one  $\pi$ -electron on each carbon. Moreover,  $\pi$ -bonding, in which the carbon orbitals are in the  $sp^2p_z$  configuration and in which the orbitals of successive carbon atoms along the backbone overlap, leads to electron delocalization along the backbone of the polymer (Epstein and Mele 2001; Heeger 2001). This electronic delocalization provides the “highway” for charge mobility along the backbone of the polymer chain. As a result, the electronic structure in conducting polymers is determined by the chain symmetry, i.e., the number and kind of atoms within the repeat unit. The driving force for the delocalization of these states is associated with the resonance-stabilized structure of the polymer. The bond alternation combined with the consequent restriction on the extent of delocalization leads to the formation of an energy gap. For example, in real polyacetylene the structure is dimerized as a result of the Peierls instability, with two carbon atoms in the repeat unit  $(-\text{CH}=\text{CH})_n$ . Thus, the  $\pi$ -band is divided into  $\pi$ - and  $\pi^*$ -bands. Since each band can hold two electrons per atom (spin up and spin down), the  $\pi$ -band is filled and the  $\pi^*$ -band is empty. The energy difference between the highest occupied

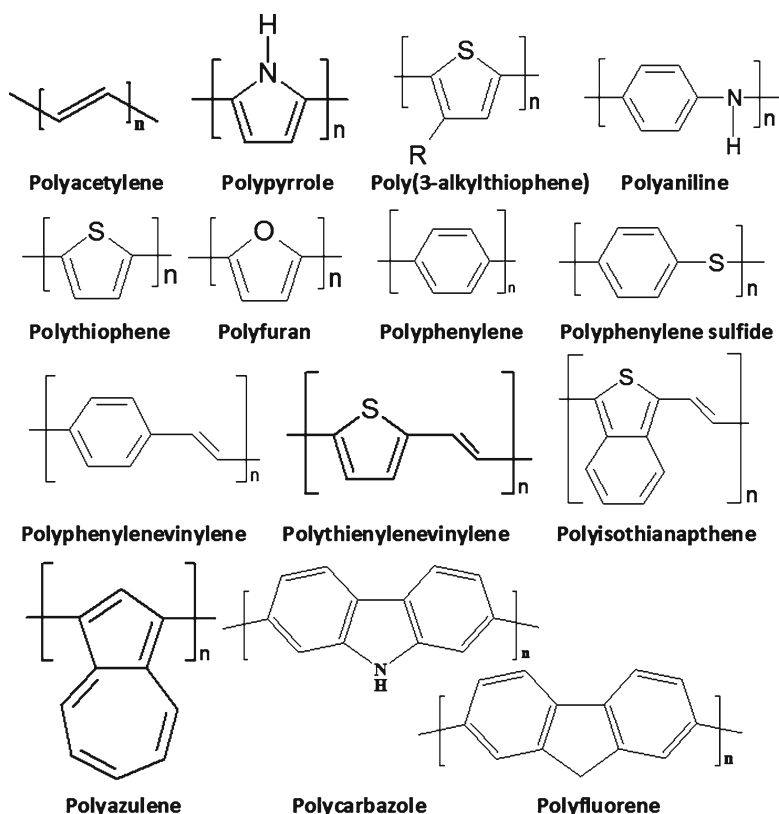


**Fig. 3.1** Repeating unit structures of some common conducting polymers

state in the  $\pi$ -band and the lowest unoccupied state in the  $\pi^*$ -band is the  $\pi$ - $\pi^*$  energy gap,  $E_g$ . Consequently, since there are no partially filled bands, conjugated polymers are typically semiconductors. Because  $E_g$  depends upon the molecular structure of the repeat unit, synthetic chemists are provided with the opportunity and the challenge to control the energy gap by design at the molecular level (Heeger 2002).

Most CPs, such as polyaniline (PAni), polypyrrole (PPy) (Nalwa 1997), and poly(phenylene sulfide-phenyleneamine) (PPSA) (Leuninger et al. 1998), are p-type semiconductors, unstable in the undoped state. In contrast, polythiophene (PT) films are stable when undoped or very lightly doped. The primary dopants (anions), introduced during the chemical or electrochemical polymerization, maintain charge neutrality and generally increase the electrical conductivity. For these purposes, HCl, FeCl<sub>3</sub>, HBF<sub>4</sub>, BF<sub>3</sub>, AsF<sub>5</sub>, NaCl, I<sub>2</sub>, Br<sub>2</sub>, H<sub>3</sub>PO<sub>4</sub>, HClO<sub>4</sub>, R-SO<sub>3</sub>H, CH<sub>3</sub>SO<sub>3</sub>H, CF<sub>3</sub>COOH, etc., can be used (Han and Eisenbaumer 1989; Chandrasekhar 1999). Approaches which can be used for doping, and applications where doped polymers can be used, are shown in Fig. 3.2. For additional information related to polymer doping, one can find it in a review (Heeger 2002) and in Chapter 24 (Vol. 2).

Doping generates charge carriers in the polymer chain through chemical modification of the polymer structure and involves charge exchange between the polymer and the dopant species. In particular, the neutral chain can be partially oxidized or reduced, i.e., “doped,” by inducing an excess or deficiency of  $\pi$ -electrons into the polymer lattice. This process for PPy is shown in Fig. 3.3 (Al-Mashat et al. 2008). Just the redox reaction of PPy is responsible for large changes in its electrical resistance (Skotheim et al. 1998). This effect can be reversed by “dedoping” through the removal or chemical compensation of charge carriers. Since every repeat unit is a potential redox site, conjugated polymers can be doped n-type (reduced) or p-type (oxidized) to a relatively high density of charge carriers (Persaud 2005).



**Table 3.1** Preferred polymers for gas sensor applications

Sensor type	Analyte	Preferred polymers
Chemiresistors (conductometric)	CO, NH <sub>3</sub> , HCl	PAni
	H <sub>2</sub> , CO	Cu-PPy; Pd-PPy
	NO <sub>x</sub> , NH <sub>3</sub>	P3HTH; PPy; PAni; PAni-PMA
	H <sub>2</sub> S	PPy; PTh
	VOCs (acetone, toluol, etc.)	PPy; poly(5-carboxyindole); PTh; PAni; P3MT
	Alcohol	PPy; PAni
Electrochemical	Humidity	Polyfuran; PTh; PAni
	H <sub>2</sub> O <sub>2</sub>	Polyester
	Oxygen	Nafion; 1,5-diaminonaphthalene; PDMS; polyacrylamide
	H <sub>2</sub>	Nafion; PBI; S-PEEK; PVA/H <sub>3</sub> PO <sub>4</sub>
Surface acoustic wave	NO <sub>2</sub>	Pt/Nafion; PDMS
	CO <sub>2</sub>	Polyacrylamide; polyethylene glycol
	CO, NO <sub>2</sub>	PAni
Quartz crystal microbalance	CH <sub>3</sub> CN, CH <sub>2</sub> Cl <sub>2</sub>	PIB; PECH; PDMS
	Ethane	Phthalocyanine
Cantilever	Tetrachloride, benzene, and chlorobenzene	Polybutyl methacrylate
	SO <sub>2</sub>	DMEDA; DMPDA; DPEDA
Capacitance	VOCs	PHEMA; PMMA
Optochemical	VOCs, humidity	PEUT; PDMS; PECH; PHEMA; EPN
	NH <sub>3</sub>	PAni-PMMA
UV-visible	VOCs	PPy; PAni-PMMA; PTFE; PVA
	Nitroaromatic compounds	BkF
Surface plasmon resonance	Ozone	PAni; <i>m</i> -chloro-PAni
Raman spectroscopy	H <sub>2</sub> S, NO <sub>2</sub>	PAni
	H <sub>2</sub> O <sub>2</sub>	PAni + horseradish peroxidase
Chemiluminescence (fluorescence)	Trinitrotoluene	3-Aminopropyltriethoxysilane (APTES)
	Oxygen	Phenyl-trimethoxysilane and tetramethoxysilane; poly(1-trimethylsilyl-1-propyne); PS; Teflon AF; PS-co-fluoroacrylate
Fiber optic	Alcohol	Phenanthroline-containing polymers
	Explosives	Dibenzochrysenes-based PPEs; poly(iptycenebutadiynylene)s
Work function	NH <sub>3</sub> , VOCs	PDPAHB; PDPIHB; PAni
Field-effect transistor	Volatile organic compounds	PPy
	Cl, O, S, ClO <sub>4</sub> <sup>-</sup> ions	PPSA
Gas-permeable membranes (filters)	Volatile organic compounds	Alkyl- and alkoxy-substituted regioregular PTh; PPy
	O <sub>2</sub> , CO <sub>2</sub> , etc.	Teflon; ePTFE; Nafion; PVC; polysiloxane

*BkF* benzo(k)fluoranthene, *DMEDA* *N,N*-dimethylethylenediamine, *DMPDA* *N,N*-dimethyl propane diamine, *DPEDA* *N,N*-dimethyl-*p*-phenylene diamine, *EPN* epoxidized novolac, *PAni* polyaniline, *PBI* polybenzimidazole, *PDMS* polydimethylsiloxane, *PDPAHB* poly(4,4'-diphenylamine *p*-heptyloxy)benzylidene, *PDPIHB* poly(4,4'-diphenylimine *p*-heptyloxy)benzylidene, *PECH* polyepichlorohydrin, *PEUT* poly(ether urethane), *P3HTH* poly(3-hexylthiophene), *P3MT* poly(3-methylthiophene), *P3OTH* poly(3-octylthiophene), *PHEMA* poly(hydroxyethyl methacrylate), *PIB* polyisobutylene, *PMMA* poly(methyl methacrylate), *PNMA* poly(*N*-methylaniline), *PPSA* poly(phenylenesulfideohylenylamine), *PPy* polypyrrole, *PPV* poly(*p*-phenylenevinylene), *ePTFE* polytetrafluoroethylene, *PS* polystyrene, *PTh* polythiophene, *PVA* poly(vinyl alcohol), *PVC* poly(vinyl chloride), *PU* polyurethane, *S-PEEK* sulfonated poly(ether ether ketone), *VOCs* volatile organic compounds

Nafion—sulfonated tetrafluoroethylene (PTFE) copolymer; polyester—polyethylene terephthalate (PET); polyfuran—heterocyclic polymers based on the five-membered heteroaromatic ring compounds; Teflon—polytetrafluoroethylene (PTFE)

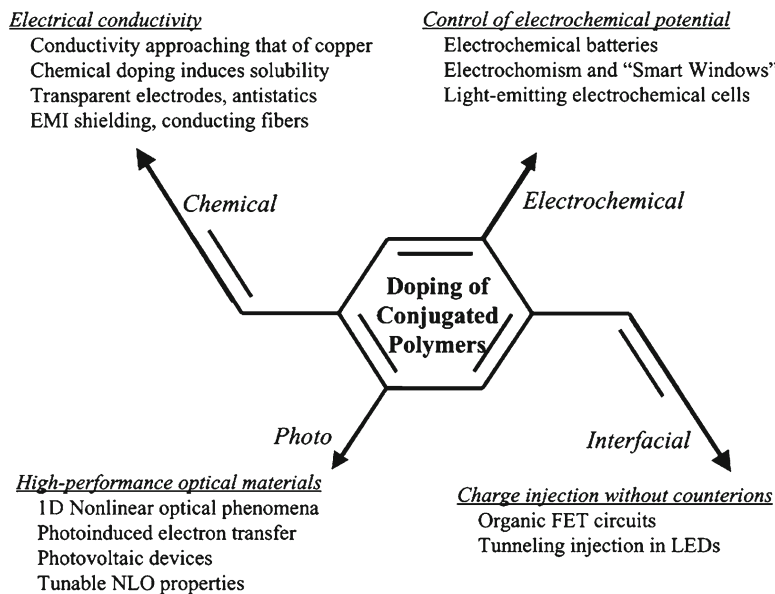


**Fig. 3.2** Doping mechanisms and related applications (Reprinted with permission from Heeger (2002). Copyright 2002 Elsevier)

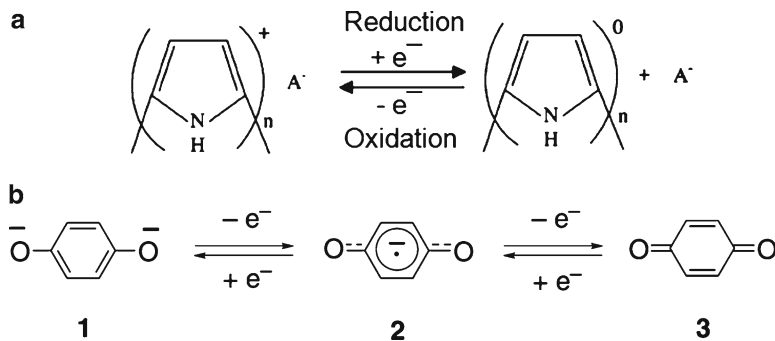


**Fig. 3.3** Diagrams illustrating the redox reactions of PPy (a) and p-benzoquinone (b) Data from Al-Mashat et al. (2008) and Hirao (2002)

Possible ranges of conductivity change for several polymers in comparison with other materials are shown in Fig. 3.4. It is seen that conductivity of polymers can reach a level approaching that of a metal. Disorder caused by doping, however, limits the carrier mobility and, in the metallic state, limits the electrical conductivity. The level of primary doping depends on the type of the dopant and on its distribution in the polymer. It was established that the nature of the anion also strongly influences the morphology of the polymer (Pron and Rannou 2002). In addition, anions can serve as specific binding sites for interaction of the conducting polymer with the analyte gas (Cabala et al. 1997).

Experiments have shown that polymers are inexpensive to manufacture and can be prepared as films, which is very important for device application. Conductive polymers may be synthesized by any one of the following techniques (Kumar and Sharma 1998): (1) chemical polymerization, (2) electrochemical polymerization, (3) photochemical polymerization, (4) metathesis polymerization, (5) concentrated emulsion polymerization, (6) inclusion polymerization, (7) solid-state polymerization, (8) plasma polymerization, (9) pyrolysis, and (10) soluble precursor polymer preparation. Several methods of

**Fig. 3.4** Comparison of conductivity ranges for several conducting polymer systems compared with conventional materials

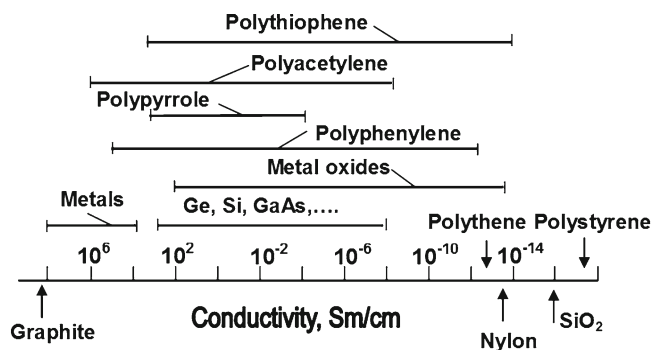


**Table 3.2** List of synthesis techniques of conductive polymers

Method used	Polymer
Chemical polymerization	Polyacetylene; polythiophene; polyaniline; polypyrrole; PVC; poly( <i>p</i> -phenylene); poly(aniline- <i>co-o</i> -anisidine)
Electrochemical polymerization	Polythiophene; polyaniline; polypyrrole; poly( <i>p</i> -phenylene-terephthalamide); polypyrrole-polyimide composites; poly( $\alpha$ -naphthylamine); 3-octylthiophene-3-methylthiophene; poly(1,4-phenylene)
Inclusion polymerization	Polyisoprene; polybutadiene; poly(2, 3-dimethyl-butadiene)
Concentrated emulsion polymerization	Polystyrene

Source: Data from Kumar and Sharma (1998)

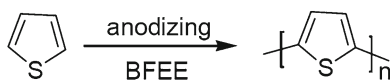


**Fig. 3.5** Electrosynthesis of polythiophene in BFEE (BFEE boron trifluoride diethyl ether). From Bai and Shi (2007). Published by MDPI (<http://www.mdpi.org>) (open access)

polymerization used for preparing selected polymers are listed in Table 3.2. However, among all the above categories, chemical and electrochemical polymerizations are the most useful methods for preparing large amounts of conducting polymers designed for gas sensor application (Bai and Shi 2007). Chemical oxidation involves mixing monomer and oxidant in solution. For example, for PANi synthesis, a proton acid is necessary to ensure the production of a linear structured polymer product. The most widely used oxidants are ammonium persulfate, ferrum chloride, hydrogen peroxide, potassium dichromate, cerium sulfate, and so on. For chemical synthesis, both aqueous and organic media can be used. The electrochemical process of synthesizing a typical conducting polymer, polythiophene, is shown in Fig. 3.5. For electrochemical synthesis, several methods can be used: galvanostatic, potentiostatic, cyclic voltammetry, and other potentiodynamic methods. For all these techniques, a three-electrode system is the best choice to realize syntheses. This system comprises a working electrode, a counter electrode, and a reference electrode. Working electrodes made of various materials, such as platinum, stainless steel, gold, and indium tin oxide (ITO) glass, have been successfully applied in depositing conducting polymers. In many cases the polymers deposited on the electrode surface can be peeled off into self-stand states.

However, we need to note that other chemical routes, rather than oxidation polymerization, can also be applied for conducting polymer synthesis. For example, polymers such as poly(phenylene vinylene), poly(phenylene ethynylene), and their derivatives are usually synthesized using the Wittig reaction (Wittig and Schöllkopf 1954), Heck reaction (Heck and Nolley 1972), and Gilch

polymerization (Gilch and Wheelwright 1966). Polythiophene and its derivatives can also be synthesized via coupling reactions (McCullough 1998). That is because their backbones consist not only of aromatic rings but also of C–C double or triple bonds.

Regarding polymer films, one can say that there are a number of different techniques for depositing polymer layers. Many of these techniques are suitable for laboratory scale fabrication only, while others are adaptations of methods used in the silicon-integrated circuit industry to fabricate reproducible membranes in large numbers. For preparing polymer films one can use methods such as solution casting, spin coating, screen printing, dip coating, electropolymerization, evaporation, inkjet printing, and layer-by-layer (LBL) self-assembly techniques (Bai and Shi 2007). One can find in Chap. 28 (Vol. 2) a short description of the methods suitable for polymer film deposition.

In addition, polymers are relatively open materials that allow ingress of gases into their interior. Moreover, conducting polymers can be deposited over defined areas of electrodes. In addition, unlike metal and metal oxide semiconductor materials, there is no need for special clean room, high-temperature, or special high-cost process techniques to fabricate sensor devices using polymers. This means that polymers can be readily incorporated into microfabricated structures and therefore CPs are inherently compatible with solid-state integrated gas sensors.

## 3.2 Polymer-Based Gas Sensors

Earlier inert polymers were used only to provide mechanical strength to membranes. However, experiment has shown that conducting polymers can improve the sensitivity of gas sensors due to their electrical conductivity or charge transport properties. In general, as seen in Table 3.1, polymers, due to their great design flexibility, could be used in all types of gas sensors and a variety of gases can be detected using polymer-based gas sensors (Milella and Penza 1998; Leclerc 1999; Michalska and Lewenstam 2000; Osada and De Rossi 2000; McQuade et al. 2000; Angelopoulos 2001; Gerard et al. 2002; Janata and Josowicz 2003; Persaud 2005; Gonzalez-Rodriguez and Schenning 2011). Several examples of polymer-based gas sensors with their short characterization are presented in Table 3.3.

The conductometric-type gas sensor (chemiresistor) is one sort of gas sensor which can be designed on the basis of polymers. Typical operating characteristics of polymer-based chemiresistors are shown in Fig. 3.6. Experiments have shown that polymer-based chemiresistors can detect various gases and vapors, including  $\text{NO}_2$ ,  $\text{SO}_2$ ,  $\text{NH}_3$ , VOCs, and  $\text{H}_2$ . The mechanism of sensitivity of polymer-based conductometric gas sensors will be discussed latter in Sect. 3.3 of present Chapter. Here, we only say that gases interacting with CP can be divided in two main classes: gases which chemically react with CP and gases which physically adsorb on CP (Table 3.4). Chemical reactions lead to changes in the doping level of CP and therefore alter their physical properties like resistance. For example, electron acceptors like  $\text{NO}_2$ ,  $\text{I}_2$ ,  $\text{O}_3$ , and  $\text{O}_2$  are able to oxidize partially reduced CPs and therefore increase their doping level. To oxidize CP, the gas should have a higher electron affinity than the CP. Electron-donating gases like  $\text{H}_2\text{S}$ ,  $\text{NH}_3$ , and  $\text{N}_2\text{H}_4$  reduce and therefore dedope CP, which leads to an increase in resistance (Lange et al. 2008). Mechanisms of conductivity change due to weak physical interactions were not studied in detail till now (Lange et al. 2008). An adsorption of ethanol and hexanol on dipentoxo-substituted polyterthiophene was supposed to change the potential barrier at the boundaries between CP grains (Torsi et al. 2004). Resistance increases due to adsorption of chloroform, acetone, ethanol, acetonitrile, toluene, and hexane on PANi, PPy, PTh, and polythiophene derivatives were explained by CP swelling leading to a greater distance between the PANi chains (Reemts et al. 2004; Li et al. 2007) or by modification of dielectric constant of CP (Vercelli et al. 2002).

The flexibility of polymers' properties is attained at the expense of doping and the introduction of functional additives (see Chaps. 13 and 24 [Vol. 2]). Polymers can have either electronic or ionic conductivity when conductivity is controlled by migration of ionic species. This means that polymers

**Table 3.3** Polymers used in various gas sensors

Gas	Device/principles	Polymer	Sensor characteristics
NH <sub>3</sub>	Optical	PAni–PMMA	Sensitivity of PAni–PMMA coatings is 10–4,000 ppm, reversible response
	Conductometric	Polypyrrole	Response time, 20 s; recovery time, 60 s
	Conductometric	PPy–PVA composite	Resistance increases with NH <sub>3</sub> concentration but becomes irreversible beyond 10% NH <sub>3</sub>
	Conductometric	PAni–isopolymolybdic acid nanocomposite	Resistance increases with NH <sub>3</sub> concentration and is reversible up to 100 ppm NH <sub>3</sub>
	Conductometric	Acrylic acid-doped polyaniline	Highly sensitive to even 1 ppm of NH <sub>3</sub> at room temperature and shows stable responses up to 120 days
NO <sub>2</sub>	Conductometric	PAni–isopolymolybdic acid nanocomposite	Resistance increases with NO <sub>2</sub> concentration
	Amperometric	Nafion	Electrode shows sensitivity of 0.16 mA/ppm at room temperature, response time of 45 s and recovery time of 54 s, a long-term stability >27 days
	Amperometric	SPE (10% PVC, 3% tetra butyl ammonium hexafluoro-phosphate, 87% 2-nitrophenyl octyl ether)	Sensitivity is 277 nA/ppm, recovery time is 19 s
NO	Amperometric	Polydimethylsiloxane (PDMS)	Shows sensitivity to 20 nM gas, high performance characteristics in terms of response time and selectivity
O <sub>2</sub>	Amperometric	PDMS	Analyte can be measured up to 1.2 mM
	Optical	Tris(4,70-diphenyl-1,100-phenanthroline)Ru(II) perchlorate-aluminescent dye dissolved in polystyrene layer	–
	Conductometric	Nafion	Sensitivity 38.4 mA/ppm, lowest limit 3.8 ppm, stability excellent (30 h)
SO <sub>2</sub>	QCM-type	Amino-functional poly(styrene-cochloromethyl styrene) derivatives	DPEDA functional copolymer with 5 wt% of siloxane oligomer shows 11 min response time and good reversibility even near RT (50 °C)
HCl	Optochemical	5,10,15,20-Tetra (40-alkoxyphenyl) porphyrin [TP(OR)PH <sub>2</sub> ] embedded in poly(hexyl acrylate), poly(hexylmethacrylate), poly(butyl methacrylate)	Reversibly sensitive to sub-ppm levels of HCl
	Optochemical	Ethylcellulose, poly(hexylmethacrylate)	Sensitivity smaller but faster recovery time compared to that of tetra-hydroxy-substituted tetraphenylporphin
H <sub>2</sub> S	Electrochemical	Nafion	High sensitivity (45 ppb v/v), good reproducibility, short response time (0.5 s)

Source: Reprinted with permission from Adhikari and Majumdar (2004). Copyright 2004 Elsevier

**Fig. 3.6** Dynamic responses of PPy/PVA-based sensor and pure PPy sensor upon exposure to methanol gas at room temperature. Polymers were spin-coated onto an interdigitated Pt/Pd alloy electrode. (Reprinted with permission from Jiang et al. (2005). Copyright 2005 Elsevier)

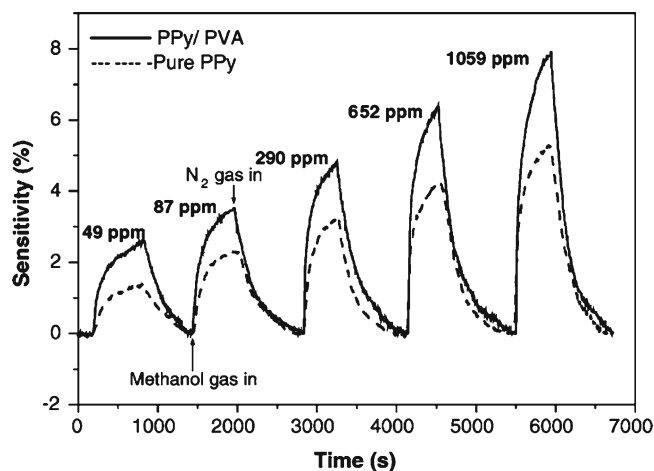


**Table 3.4** Mechanisms of interaction of different gases and vapors with conducting polymers

Interaction of gases with conducting polymers			
	Chemical interaction		
Physical interaction	Oxidation	Reduction	Protonation/deprotonation
CHCl <sub>3</sub> , CH <sub>2</sub> Cl <sub>2</sub> , alcohols, acetonitrile, toluene, acetone, alkanes, cyclohexane, benzene	NO <sub>2</sub> , SO <sub>2</sub> , O <sub>3</sub> , I <sub>2</sub> , O <sub>2</sub>	H <sub>2</sub> , N <sub>2</sub> H <sub>4</sub> , NH <sub>3</sub> , H <sub>2</sub> S	HCl, NH <sub>3</sub>

Source: Reprinted with permission from Lange et al. (2008). Copyright 2008 Elsevier

besides solid-state gas sensors, such as chemiresistors, can be used as the electrolyte in the development of electrochemical sensors. There are two types of polymeric electrolyte, based on their conduction mechanisms (Tierney 1996). The first group is the polyelectrolyte in which the polymer itself contains an anionic or cationic group, usually on a side chain. The counterions for these groups are typically small, inorganic ions that are mobile within the polymer matrix. Nafion, a perfluorinated sulfonated ionomer, is an example of this type of electrolyte. The second type of polymer electrolyte does not itself possess charged moieties along its chain. Rather, the polymer acts as the solvent for electrolyte ions which are able to move through the polymer matrix much as in a liquid electrolyte. Thus, the polymer serves as a solid ionic conductor. An example of this type of polymer is polyethylene oxide in which lithium and other small cations have high mobility. Hydrogels are actually a third type of polymer electrolyte (Tierney 1996). However, in hydrogels the solvent for the ions is water; the water-soluble polymer serves only to increase the viscosity of the solution. Hydrogel electrolytes are formed when the dissolved polymer is cross-linked into a rigid three-dimensional matrix which can contain up to 98 vol.% water. To this extent, the hydrogel can be considered as a “solid” and, thus, a more easily processed form of liquid water. An example of a polymer that can form hydrogels is poly(vinylalcohol) (PVA). PVA can be cross-linked by a variety of agents and can form gels containing as little as 2–3 wt% PVA. Hydrogels have found application as replacements for liquid electrolytes. Because of their viscosity, they resist leakage from sensor housings, and many sensing components can be incorporated into them, such as ionic salts and electrochemical mediators.

Gas-permeable membranes and diffusion barriers are fields of polymer applications as well (Harsanyi 1995; Tierney 1996). A typical gas-permeable membrane is hydrophobic and has a high rate of gas transport relative to other species. The membrane may be solid or microporous. Gas-permeable membranes serve a number of functions. They provide the sensor with a selective membrane covering and, thus, reducing contamination of the sensor by incompatible materials in the environment. They allow passage of gases only, preventing excess electrolyte loss in electrochemical sensors.

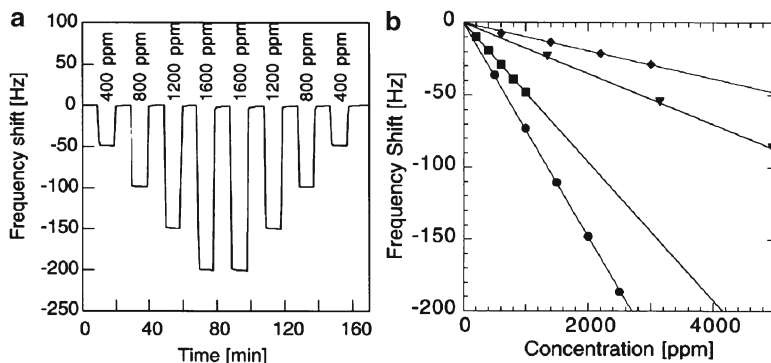


**Fig. 3.7** (a) Frequency shifts of a PEUT-coated cantilever ( $f_0 = 353$  kHz) upon alternate exposure to different concentrations of toluene and air. (b) Frequency shifts of a resonant cantilever as a function of analyte concentration for various organic volatiles: from left to right, toluene, *n*-octane, ethyl acetate, and ethanol (PEUT layer thickness  $3.7 \mu\text{m}$ ) (Reprinted with permission from Hierlemann et al. (2000). Copyright 2000 Elsevier)

Although the gas-permeable membrane cannot totally eliminate electrolyte loss through evaporation, the rate of diffusion of water vapor through the hydrophobic membrane is often many orders of magnitude slower than the gas transport rate. The membrane can also act as a diffusion barrier to lower the flux of gas reaching the electrode of an amperometric sensor, and thus bring the sensor into diffusion-limited operation. The addition of a diffusion barrier can reduce the flux of analyte to the sensor and so bring the effective analyte concentration down into a linear portion of the sensor's response curve. In this way, a diffusion barrier can increase the sensor's usable measurement range. Diffusion barriers are typically used where the chemical reaction responsible for sensing is slow relative to the diffusion rate of the analyte to the active portion of the sensor. Polymer membranes can also be used as permselective electrode coatings to prevent electroactive interferences from reaching the electrode and generating spurious background currents (Tierney 1996). Polymers with anionic or cationic charges exclude ions of similar charge by electrostatic repulsion. More commonly, permselective membranes create a differential in the transport rate of different species. The permeability differences may be based on physical size, solubility differences, or specific interactions between the polymer and the diffusing species. A commonly used permselective membrane is Nafion which demonstrates an extremely high affinity for organic cations, reasonable affinity for inorganic cations, and almost completely excludes both organic and inorganic anions. Thus, coating a sensor with a thin, pinhole-free layer of Nafion with its anionic sulfonate side groups forms an efficient barrier to anionic interferences. In an analogous manner, polycationic polymers, such as polymers with amine side groups, prevent cations from reaching the electrode.

Polymers can sorb molecules from their surroundings. A great variety of polymers, such as polysiloxanes and polyetherurethanes, could be mentioned here. This means that polymers can be used in SAW-, QCM-, and cantilever-based gas sensors (Grate and Abraham 1991; Grate et al. 1995; Maute et al. 1999; Baller et al. 2000; Jesenius et al. 2000). The natural resonant frequency of SAW-, QCM-, and cantilever-based gas sensors is disturbed by a change in mass from the adsorption of molecules onto the coating. For example, the sensitivities to VOCs of a CMOS resonance gas sensor based on a  $150 \mu\text{m}$  long silicon cantilever beam were studied by Hierlemann et al. (2000). It was established that polymer-based microcantilever gas sensors can detect VOCs with high reliability. Figure 3.7a shows the measured frequency shift of a cantilever coated with  $3.7 \mu\text{m}$  of poly(etherurethane) (PEUT) upon exposure to different concentrations of toluene. The concentrations were ramped up and down to test for reproducibility. The linear response of a PEUT-coated cantilever to varying concentrations of different analytes is shown in Fig. 3.7b. Different slopes for the respective analytes are observed due to their different molecular weights and saturation vapor pressures in air. So, the developed sensor system is capable of quantitative analysis of complex gas mixtures in combination with principal-component regression.

**Table 3.5** Permeability and permselectivity data for polymers of interest for membrane separation

Polymer	Permeability (Barrers)					Permselectivity ( $\alpha$ )		
	O <sub>2</sub>	N <sub>2</sub>	He	CO <sub>2</sub>	CH <sub>4</sub>	O <sub>2</sub> /N <sub>2</sub>	He/N <sub>2</sub>	CO <sub>2</sub> /CH <sub>4</sub>
PTMSP	9,710	6,890	6,750	37,000	18,400	1.41	0.98	2.01
Poly(4-methyl-1-pentyne)	2,700	1,330	2,630	10,700	2,900	2.03	3.69	1.98
Silicone rubber	781	351	590	4,550	1,430	2.22	1.68	3.18
<sup>a</sup> TMPA-6FDA polyimide	122	35.6	440		28.2	3.43		15.6
Poly(4-methyl-1-pentene)	27.0	6.79	5.4	84.6	14.9	4.03	14.2	5.68
<sup>b</sup> PPO	14.6	3.5	82.3	65.5	4.1	4.17	23.5	16.0
Tetrabromobisphenol A polycarbonate	1.36	0.18	17.6	4.23	0.126	7.47	96.7	33.6
Polysulfone	1.2	0.20	11.0	4.9	0.21	6.0	52.4	23.3

<sup>a</sup>TMDA52,3,5,6-tetramethyl phenylene diamine; 6FDA55,5''-(1,1,1-trifluoromethyl)ethylidene)bis-1,3 isobenzofurandione

<sup>b</sup>PPO5poly(2,6-dimethyl-1,4-phenylene oxide); temperature 25 °C for PTMSP and poly(4-methyl-1-pentyne); other polymers at 35 °C

Source: Reprinted with permission from Robeson (1999). Copyright 1999 Elsevier

Various filters and preconcentrators designed for gas sensor applications can also be fabricated using polymer materials (see Chap. 12 [Vol. 1]). Experiment has shown that polymers can be applied to the separation of different gaseous and liquid-state constituents as well (Robeson 1999). In this case, a membrane works as a selective semipermeable barrier that allows different gases, vapors, or liquids to move through it at different rates. A wide range of mechanisms are available for this control: for example, size variability of the molecules, affinity for the membrane material, and permeation driving forces—typically concentration or pressure difference. The rate is usually determined by the ability of the component to dissolve in and diffuse through the membrane material. Thus, the membrane restricts the motion of molecules passing across it so that some molecules move more slowly than others or are excluded, i.e., each gas component in a feed mixture has a characteristic permeation rate through the membrane. Examples of the polymers proposed for gas separation are tabulated in Table 3.5 with their respective permeability ( $P$ ) and permselectivity ( $\alpha$ ) values. For common (inert) gases, the permeability coefficient,  $P$ , is the product of the diffusion coefficient,  $D$ , and the solubility constant,  $S$ , with the common units noted:

$$P = DS, (\text{cm} / (\text{cm}^2 \cdot \text{s} \cdot \text{cmHg})), \quad (3.1)$$

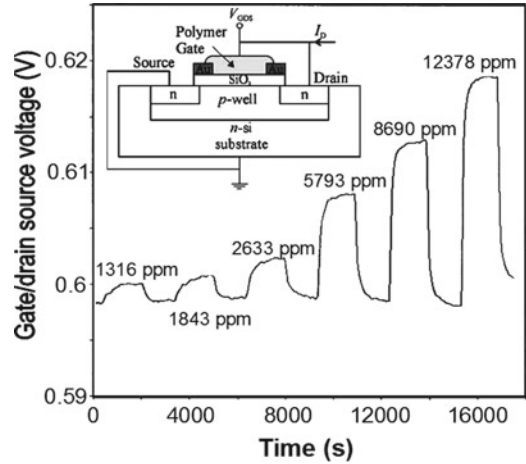
$$1 \text{ Barrer} = 10^{-10} (\text{cm}^3 \text{ O}_2) \text{cm} / (\text{cm}^2 \cdot \text{s} \cdot \text{cmHg}) \quad (3.2)$$

Here, ( $\text{cm}^3 \text{ O}_2$ ) represents a molar quantity of oxygen rather than a true volume. The separation factor,  $\alpha$ , is defined as the ratio of  $P_i/P_j$ , where  $i, j =$  gases being separated.

Polymer field-effect transistors (polyFET) also are promising devices for gas sensor applications. Work carried out using electrochemically deposited polypyrrole (Josowicz and Janata 1986), poly(ethylene-co-vinyl acetate), poly(styrene-co-butadiene), poly(9-vinylcarbazole) (Covington et al. 2001, 2004), or dipentoxo-substituted polyterthiophene (Torsi et al. 2003, 2004) as a field-effect transistor gate material have demonstrated devices sensitive to a series of alcohol vapors (ethanol, isopropanol, etc.) and VOCs (see Fig. 3.8). These devices consist of a polymer gate on a Si substrate. In insulated gate field-effect transistors (IGFETs), the gate contact is on the surface of the device and is the sensing part exposed to the analyte. The buried inorganic semiconductor, where the field-effect transport takes place, is normally not exposed to the analyte. The transduction principle is based on the linear relationship between the transistor threshold voltage and the gate-metal/semiconductor work-function offset. Chemical selectivity can be induced using conducting polymers as the gate contact material. Upon exposure, the work function of the polymer/gate-dielectric system changes (Janata and Josowicz 1997) and can be measured by passing a small current through the conducting polymer. Such a combination of technologies could lead to a



**Fig. 3.8** *n*-Channel polyFET sensor circuit and typical response of poly(styrene-*co*-butadiene)-FET gas sensor to toluene at 37 °C. Polymer films were deposited at room temperature by spraying. Films had thickness varied from 1.9 to 3.6 μm (Adapted with permission from Covington et al. (2001). Copyright 2001 Elsevier)



new generation of low-cost, low-power gas sensors for handheld monitors (Persaud 2005). Thin-film transistor-based gas sensors will be discussed in details in Chap. 20 (Vol. 1).

Experiment has shown that the design of work-function-based sensors, including Schottky diodes, and capacitance-type gas sensors based on polymers is possible as well (Kummer and Hierlemann 2006). It was found that in some ways semiconducting polymers are more robust than their inorganic counterparts. In particular, whereas pinning of the Fermi energy by surface states is a major problem in conventional semiconductors, the Fermi energy can be controlled and shifted all the way across the energy gap in conjugated polymers. The absence of Fermi level pinning and the ability to shift the chemical potential all the way across the energy gap are fundamentally important for work-function-based gas sensors. Work-function gas sensors will be discussed in Chap. 17 (Vol. 1). Analysis of capacitance-based gas sensors can be found in Chap. 16 (Vol. 1). An exhaustive review of Schottky diodes and their sensing applications has recently been published (Nguyen and Potje-Kamloth 1999; Potje-Kamloth 2001). The relation between current density and voltage in Schottky diode is described by Richardson's equation:

$$J = J_0 \exp\left(\frac{eV}{nkT}\right), \text{ where } J_0 = A^* T^2 \exp\left(\frac{\phi_B}{kT}\right), \quad (3.3)$$

where  $A^*$  is the effective Richardson's constant,  $\phi_B$  is the effective barrier height,  $k$  is the Boltzmann's constant,  $n$  is the ideality factor,  $e$  is the electronic charge, and  $T$  is the absolute temperature. The effective barrier height  $\phi_B$  at the metal-polymer interface can be modulated by analyte. Thus, after exposure to an analyte, several electric parameters of the diode such as current density, voltage shift, capacitance, and rectification ratio will change. Sensors of this type are relatively simple to fabricate, but the choice of functional metals is critical. Because most CPs are p-type semiconductors having rather large values of work function, the choice of suitable metals to form Schottky contacts is limited. Nevertheless, metals of low work function such as Al, Ca, In, or Na have been used. This poses an obvious problem with the stability of such junctions in the ambient air (Janata and Josowicz 2003).

The change of optical properties of many conducting polymers during switching between the insulating and conducting forms is another feature of polymers important for gas sensor design (Jin et al. 2001; Elizalde-Torres et al. 2004). For example, nonconducting poly(3-octylthiophene) is deep red in color but becomes light blue on doping; poly(*N*-methylpyrrole) is transparent in the neutral state and brown when oxidized. Poly(ethylenedioxythiophene) also changes color from blue to colorless on oxidation (Persaud 2005). This means that the exposure of polymers to certain gases or vapors, which results in a change in the electronic structure of the polymer, can be accompanied by changes in their optical spectra as well. It was established that many polymers, such as polyaniline, polythiophene,

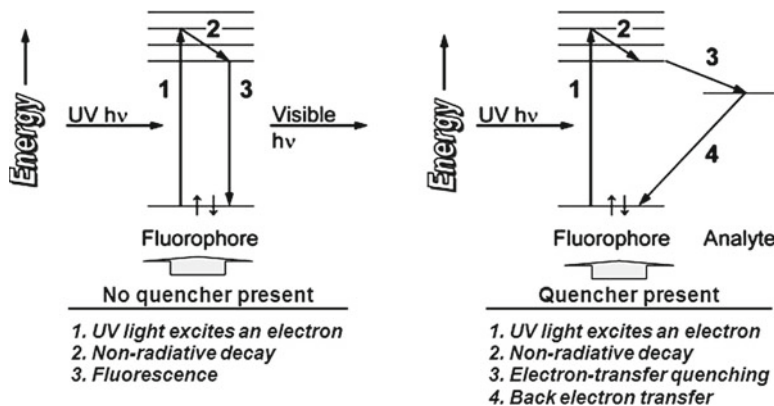


**Fig. 3.9** Electron-transfer fluorescence quenching in conjugated polymers (Reprinted with permission from Toal and Trogler (2006). Copyright 2006 Royal Society of Chemistry)

polypyrrole, and polyphenylene, whose common feature is a conjugated  $\pi$ -electron system extending over the whole polymer backbone, have high optical sensitivities to a broad range of gases and organic vapors, and in most cases responses are rapid. For example, polyaniline can be switched very quickly between insulating and conducting forms when exposed to an acidic or alkaline environment. Electronic transitions from the valence band to the polaron or bipolaron bands occur in the near-infrared to near-ultraviolet regions. The emeraldine base form of polyaniline exhibits two absorption peaks at  $\sim 328$  nm and 620–650 nm, which have been identified as the  $\pi$ - $\pi^*$  and exciton transitions in the benzenoid and quinoid ring, respectively (Nalwa 1996). It was established that poly(4,4'-diphenylamine *p*-heptyloxy)benzylidene (PDPAHB) and poly(4,4'-diphenylimine *p*-heptyloxy)benzylidene (PDPIHB) also have optical changes that occur when they are exposed to different relative humidities (RH) or  $\text{NH}_3$  concentrations (Kondratowicz et al. 2001). This means that optical sensors can also be designed based on polymers. Experiments confirmed this statement (Nalwa 1996; Skotheim et al. 1998; Lange et al. 2008). During the last few decades, gas sensors for HCl,  $\text{NH}_3$ , and  $\text{O}_3$ , based on UV-vis spectroscopy, and sensors for detection of HCl,  $\text{H}_2\text{S}$ ,  $\text{NO}_2$ , and  $\text{H}_2\text{O}_2$ , based on surface plasmon resonance (SPR) effect, were designed (Agbor et al. 1997; Christie et al. 2003; Ando et al. 2005).

Modification of the optical properties of CP due to analyte binding can also be detected by fluorescence measurements. It was established that derivatives of pyrene, dansyl, anthracene, polyacetylenes, poly(*p*-phenylenevinyls), porphyrins, polysilanes, etc., have fluorescence properties dependent on the surrounding gas (Toal and Trogler 2006; Zhang et al. 2007). These conducting polymers have high fluorescent efficiency, and, when they react with electron acceptor, the electron-transfer process mentioned above will lead to a quenching of fluorescence, as depicted in Fig. 3.9. For example, nitroaromatic explosives act as electron acceptors for photoexcited electrons of the CP and quench fluorescence (Toal and Trogler 2006). The detection limit of the sensors designed on the base of these polymers can be very low (several ppb for TNT [Toal and Trogler 2006]).

It was found that in several polymers, such as stretched and poled poly(vinylidene fluoride) (PVDF) and its copolymer, poly(vinylidene fluoride-trifluoroethylene) (P(VDF-TrFE)), a strong polarization effect is observed under influence on mechanical stress and temperature. This means that piezoelectric and pyroelectric gas sensors can also be designed based on polymers (see Chap. 13 [Vol. 1]).

It is mentioned above that, in gas sensors, polymers can be used as the sensing layer or as the transducer itself. Polymers can form selective layers in which the interaction between the analyte and the sensing matrix generates a primary change in a physical parameter in the transduction mechanism. Polymers can also form different membranes, providing selectivity of chemical reactions in electrochemical gas sensors.

It is important that all indicated devices can function at room temperatures. This means that polymer-based sensors have low power consumption (of the order of microwatts) because no heater element is required for their operation. Properties of polymers that influence the operating parameters of sensors can be physicochemical, chemical, optical (photo- and electroluminescence, optoelectronic), redox, hydrophobic/hydrophilic, piezoelectric/pyroelectric, and electrical (conductivity, resistivity). Moreover, the polymer itself can be modified to bind biomolecules to a biosensor (Mulchandani and Wang 1996). It is mentioned above that polymers have considerable potential for fabrication of multisensing arrays required for e-nose fabrication (Janata and Huber 1985).

We need to say that insulating polymers, in which all four valence electrons of carbon are used up in covalent bonds, can also be applied in gas sensor design. Moreover, experiment has shown that, for several types of gas sensors such as capacitive sensors (see Chap. 16 [Vol. 1]) and resistive sensors based on composite materials (Chap. 13 [Vol. 2]), the application of insulating polymers is actually preferable.

### 3.3 Mechanisms of Conductivity Change in Polymer-Based Gas Sensors

Research has shown that the sensor response of CP films upon the effect of any analyte can be related to the following processes (Posudievsky et al. 2011): (1) absorption of the analyte vapor by the polymer and ion-dipole interaction between polycation-radical fragments of polymer and anion dopants and the molecules of analyte and (2) change of the electron state of the polymer due to specific interaction (e.g., formation of hydrogen bonds, charge transfer complexes, redox interaction) between the molecules of analyte and polymer chain. It should be noted that absorption/desorption of an analyte in the form of gas or vapors can be considered as a basic principle of polymer-based gas sensors operation. This property of polymers is especially important because, in addition to the change in film conductivity, a change in polymer volume takes place. The process of absorption is determined mainly by the polymer film morphology (porosity) and polarity of interacted molecules and leads to the weakening of Coulomb interaction between the charged fragments of the polymer and anion dopants, resulting in an increase of mobility of the charge carriers in CPs and thus an increase of its conductivity.

As described above, the physical properties of conducting polymers strongly depend on their doping levels. Fortunately, the doping levels of conducting polymers can be easily changed by chemical reactions with many analytes at room temperature, and this provides a simple technique to detect the analytes. In particular, most of the conducting polymers are doped/undoped by redox reactions; therefore, their doping level can be altered by transferring electrons from or to the analytes. Electron transfer can cause changes in resistance and work function of the sensing material (Bai and Shi 2007). Specific interaction is mainly determined by the chemical nature of the analyte and the electron state of the polymer; it could lead to either increase or decrease of the polymer conductivity. In particular, as the CP interacts with gaseous species, it can act either as an electron donor or an electron acceptor. If a p-type CP donates electrons to the gas, its hole conductivity increases. Conversely, when the same CP acts as an electron acceptor, its conductivity decreases. Besides the change in the number of carriers, there can be a change in their bulk mobility. It is usually due to conformational changes of the polymer backbone (Zheng et al. 1997).

The above-mentioned process occurred when PPy, PTh, and in some case PANi films were exposed in  $\text{NH}_3$ ,  $\text{NO}_2$ ,  $\text{I}_2$ ,  $\text{H}_2\text{S}$ , and other redox-active gases (Van and Potje-Kamloth 2001; Bai and Shi 2007). Electron acceptors, such as  $\text{NO}_2$  and  $\text{I}_2$ , can remove electrons from the aromatic rings of conducting polymers. When this occurs at a p-type conducting polymer, the doping level as well as the electric conductance of the conducting polymer is enhanced. The opposite process will occur when detecting an electron-donating gas. However, this mechanism is not clearly understood and further studies are still needed to make the mechanism clear. For example, some toxic gas, such as CO, was rather inert to redox at room temperature. However, response of PANi toward CO was also observed (Misra et al. 2004; Dixit et al. 2005).

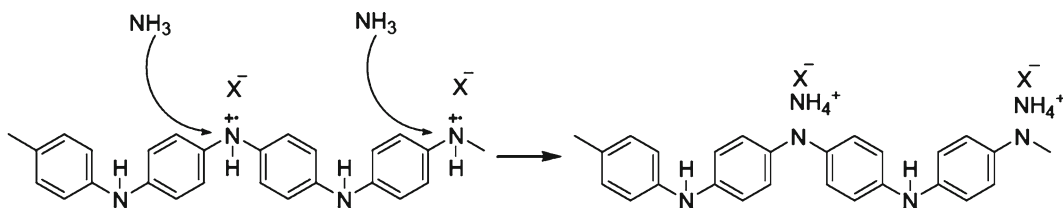


**Fig. 3.10** Possible mechanism of PAni interaction with  $\text{NH}_3$  (Reprinted from Bai and Shi (2007). Published in 2007 by MDPI)

PAni is a special conducting polymer since its doped state can be controlled by acid–base reactions. This effect is widely used to detect acidic and basic gases, in particular ammonia gas, because when exposed in ammonia gas, PAni undergoes dedoping by deprotonation (Jin et al. 2001; Hu et al. 2002; Bai and Shi 2007). The mechanism of this interaction is shown in Fig. 3.10.

It was supposed that during interaction with  $\text{NH}_3$ , the protons on  $-\text{NH}-$  groups can transfer to  $\text{NH}_3$  molecules to form ammonium ions while PAni itself turns into its base form. This process is reversible, and, in fact, when ammonia atmosphere is removed, the ammonium ion can be decomposed to ammonia gas and proton. After reaction with acidic gases, such as  $\text{HCl}$ ,  $\text{H}_2\text{S}$ , and  $\text{CO}_2$  (in presence of water), PAni will be doped (Agbor et al. 1995; Virji et al. 2004). Experiments have shown that when the polyaniline was exposed to  $\text{HCl}$ , a rapid drop in resistance was observed within a short period of time (Huang et al. 2003; Virji et al. 2004). It was found that this doping of polyaniline is achieved by protonation of the imine nitrogens by  $\text{HCl}$ . The charge created along the backbone by this protonation was counterbalanced by the resulting negatively charged chloride counterions. The change in conductivity was brought about by the formation of polarons (radical cations) that traveled along the polymer backbone. According to Huang et al. (2003) and Virji et al. (2004), the mechanism for base dedoping of polyaniline is different from that for acid doping and may account for the slower response times and smaller resistance changes, characteristic for  $\text{NH}_3$  sensors. In addition to the emeraldine salt and base forms, polyaniline can exist in several different oxidation states, including the fully reduced leucoemeraldine form, the half-oxidized emeraldine form, and the fully oxidized pernigraniline form. Water is also able to transfer protons to PAni (Jain et al. 2003). Virji et al. (2006) reported that  $\text{H}_2$  can be adsorbed onto the positive-charged nitrogen atoms of PAni and then dissociate into hydrogen atoms. The following formation of new  $\text{N}-\text{H}$  bonds between the hydrogen atoms and nitrogens can reduce the resistance of PAni. Proton transfer is also present in PPy. Krivan et al. (2000) observed a decrease in resistance of PPy film when it was exposed to the vapor of weak acid such as  $\text{H}_2\text{S}$  and  $\text{CH}_3\text{COOH}$ , indicating a proton transfer from acidic gas to PPy and an increase of doping level of the polymer. Geng et al. (2006) gave the same interpretation. Furthermore,  $\text{NH}_3$  was reported to be able to remove protons from PPy (Gustafsson et al. 1989). If the formed ammonium was bound close to the counter anion, the proton transfer process is reversible. However, in fact, a nucleophilic attack on the carbon atom of PPy backbones usually occurs, which may cause an irreversible change in PPy (Kemp et al. 2006).

Swelling and polymer chain conformational changes can also be responsible for the sensing by polymer-based gas sensors (Huang et al. 2003; Virji et al. 2004). In particular, the sensing mechanism for chloroform molecules sensing is that chloroform molecules are relatively small and can diffuse efficiently into the polymeric matrix, which expands the structure and decreases the conductivity of the film. We need to note that like other polymers, conducting polymers can swell in many organic solvents, and this has been detected by AFM. Swelling is controlled by the vapor molecular volume, the affinity of the vapor to the sensing polymer, and the physical state of the polymer (Segal et al. 2002). This mechanism makes it possible to detect gases such as benzene, toluene, and some other volatile organic compounds (VOCs) which are not reactive at room temperature and under mild conditions.

Therefore, it is difficult to detect them by their chemical reactions with conducting polymers (Bai and Shi 2007). However, they may have weak physical interactions with the sensing polymers, involving absorbing or swelling the polymer matrixes, etc. These interactions do not change the oxidation levels of conducting polymers, but can also influence the properties of the sensing materials and make these gases detectable. As will be shown later in Chap. 13 (Vol. 2), the role of the swelling effect is especially important in sensor response of polymer-based composites (Segal et al. 2002). Small alcohol molecules have a different response mechanism to polyaniline from those of halogenated solvents. They interact with the nitrogen atoms of polyaniline, leading to an expansion of the compact polymer chains into a linear form, thus decreasing the resistance of the film. It was established that not only polymer chains but also the counterions or the side chains may be involved in the acid–base reaction.

Hydrogen bonding and dipole–dipole interactions are also reported to play important roles in sensing processes (Bai and Shi 2007). For example, the infrared spectra of a PPy film after exposure to acetone indicated the formation of hydrogen bonds (H-bonds) between C=O groups of acetone molecules and N–H groups of pyrrole units (Ruangchuay et al. 2004). Tan and Blackwood (2000) investigated the interaction between methanol and PANi salt and base and found that the H-bonds in the two types of PANis were different. In PANi base, one methanol molecule forms two H-bonds as a bridge between PANi chains. Twisting caused by these H-bonds localizes the polarons and decreases the conductance of PANi.

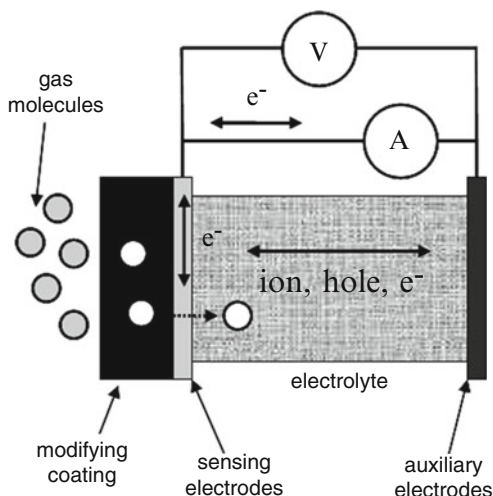
Another possible interaction between analytes and conducting polymer films is dissolving of the counterions of conducting polymers in analytes. Counterions are usually bound along the polymer chains and their mobility is rather low. The analyte diffused into the film can act as a solvent for small counterions, resulting in an ionic conduction (Miller et al. 2000; Tan and Blackwood 2000). Besides, solvent, for example water, can result in a delocalization of counterion, which in some cases allows easier intrachain electron transfer and reduces the resistance of the film (Ogura et al. 1997).

### 3.4 Ion-Conducting Polymers and Their Use in Electrochemical Sensors

A large group of organic polymers, having as a constituent ionic monomer or inorganic salt, exhibits ionic conductivity which can be modulated by the environment. The copolymer of poly(tetrafluoroethylene) with poly(sulfonylfluoride vinyl ether), known under the commercial name Nafion, poly(hydroxyethyl methacrylate) (PHEMA), alkali salt-polyether complexes such as poly(propylene oxide), polystyrene sulfonate, and poly(vinyl pyridine) (PVPy), and many other polymers can be mentioned as examples. As discussed earlier, polymers can be incorporated in electrochemical sensors as well. As we know, ionic conductivity is a necessary condition for the design of electrochemical sensors, such as amperometric, potentiometric, and conductometric (see Fig. 3.11). Solid polymer electrolytes became important during the mid-1970s because of the inefficiencies and maintenance requirements of liquid electrolytes. Originally, a solid polymer electrolyte (SPE) was described as a solid plastic sheet of perfluorinated sulfuric acid polymer that, when saturated with water, became an excellent ionic conductor.

Bobacka (2006) underlined the following reasons to explain the utility of using conducting polymers in electrochemical sensors: (1) conducting polymers can form an ohmic contact to materials with high work function, such as carbon, gold, and platinum; (2) conducting polymers can be conveniently electrodeposited on the electronic conductor by electrochemical polymerization of a large variety of monomers; (3) several conducting polymers are soluble and can therefore be deposited from solution; and (4) conducting polymers are often materials with mixed electronic and ionic conductivity, which means that they can transduce an ionic signal into an electronic one in the solid state. These multifunctional properties are advantageous for ion-to-electron transduction solid-state devices. Configurations and parameters of polymer-based amperometric-type electrochemical gas sensors are presented in Table 3.6.

**Fig. 3.11** Schematic diagram of electrochemical sensor operation



Studies have shown that ionic polymers in contact with a conductive medium such as a metal allow electrochemical reactions at this interface. Table 3.7 lists possible electrochemical reactions for gas analysis.

Of course, the reactions shown in Table 3.7 reflect only a general view of the processes taking place in electrochemical sensors. In practice, these processes are more complicated. We need to take into account that the above-mentioned reactions are the idealized versions, and the actual electrode reaction at the electrode surface is dependent on the nature of the electrode material, the electrolyte solution, the thermodynamic potential, the interface of the electrode/electrolyte, and, of course, the analyte. In addition, the electrode reaction, i.e., electron-transfer reaction at the WE, which is part of a mechanism of response, has several steps, including gas diffusion to the electrode–electrolyte interface, dissolution of the analyte gas, adsorption of the analyte onto the surface, electroreaction at the triple phase boundary, and desorption of products from the electrode surface (Vaihinger et al. 1991; Chang et al. 1993; Stetter and Li 2008). For example, the reaction of  $H_2$  detection consists of two stages. In general, the electrode processes in a  $H_2$  sensor with a Nafion (DuPont) electrolyte electrode include the anode reaction



and the cathode reduction



Under short-circuit condition, the reaction at Eq.(3.4) occurs at the sensing or working electrode, WE, whereas the reaction at Eq.(3.5) occurs at the counter, or CE, electrode. Simultaneously, the protons move toward the counter electrode through the proton-conducting electrolyte Nafion. This process results in a flow of an equivalent number of electrons in an external electrical current. The anodic oxidation reaction of hydrogen is often limited by the diffusion process to the sensing electrode by the sensor design. The number of protons produced is proportional to the hydrogen concentration. Since the number of  $H_2$  molecules reaching the WE is limited by the diffusion of  $H_2$  from the bulk air sample to the WE surface, the external current is proportional to the hydrogen concentration in the gas phase (Nikolova et al. 2000).

As seen in Table 3.6, at present Nafion is the most used polymer for the design of electrochemical gas sensors. Experiment has shown that Nafion has good proton conductivity, high gas permeability, outstanding chemical stability, and good mechanical strength, i.e., possesses parameters important for gas sensor fabrication, especially  $H_2$  sensors. However, it is necessary to take into account that, in general,

**Table 3.6** Amperometric sensors for electroactive gases

Analyte	Type	Arrangement	Detection limit (ppm)	Upper limit of dynamic range (ppm)	
H <sub>2</sub>	SPE <sup>a</sup>	Pt/Nafion/0.1 M H <sub>2</sub> SO <sub>4</sub>	n/a	5,000	
	GDE <sup>a</sup>	Teflon-bonded WC/5 M H <sub>2</sub> SO <sub>4</sub>	n/a	40,000	
CH <sub>4</sub>	SPE	Pt/Nafion/10 M H <sub>2</sub> SO <sub>4</sub>	1,300	80%	
	GDE	Teflon-bonded Pt/2 M NaClO <sub>4</sub> in $\gamma$ -butyrolactone	60,000	100%	
C <sub>2</sub> H <sub>4</sub>	SPE	Au/Nafion/0.5 M H <sub>2</sub> SO <sub>4</sub>	0.001	500	
C <sub>2</sub> H <sub>2</sub>	SPE	Au/Nafion/0.5 M H <sub>2</sub> SO <sub>4</sub>	0.02 <sup>b</sup>	10	
CH <sub>2</sub> CH <sub>2</sub> O	SPE	Pt/Nafion/10 M H <sub>2</sub> SO <sub>4</sub>	0.015	100	
CH <sub>2</sub> O	SPE	Au/Nafion/0.5 M H <sub>2</sub> SO <sub>4</sub>	0.013	1	
C <sub>2</sub> H <sub>5</sub> OH	SPE	Au/Nafion/1 M NaOH	0.002	0.5	
	SPE	Au/Nafion/1 M NaOH	1	476	
CO	SPE	Pt/Nafion/1 M H <sub>2</sub> SO <sub>4</sub>	1.7	33,000	
CO <sub>2</sub>	GDE	Gore-Tex/Pt/0.5 M H <sub>2</sub> SO <sub>4</sub>	<5% <sup>b</sup>	50%	
	GDE	Teflon/Pt/DMSO	40,000	100%	
	Clark	Nonporous Teflon/Au/DMSO	n/a	15	
O <sub>2</sub>	SPE	Pt/Nafion/1 M H <sub>2</sub> SO <sub>4</sub>	n/a	5%	
	GDE	Silicon-sieve/Pt/Nafion/H <sup>+</sup>	n/a	80%	
	Clark	Nonporous Teflon/Au/DMSO	n/a	90%	
O <sub>3</sub>	SPE <sup>c</sup>	Au/Nafion/H <sub>2</sub> SO <sub>4</sub>	0.2	350	
	SPE	Au/Nafion/1 M HClO <sub>4</sub>	0.22	44,800	
	SPE	Au/Nafion/0.5 M H <sub>2</sub> SO <sub>4</sub>	0.0006	n/a	
N <sub>2</sub> O	Clark	Nonporous Teflon/Au/DMSO	n/a	90%	
NO	SPE	Au, Pt/Nafion/10 M H <sub>2</sub> SO <sub>4</sub>	0.0010	1	
	SPE <sup>c</sup>	Au/ <i>a</i> -ZrPO <sub>4</sub> /TiH <sub>x</sub>	0.2	20	
	GDE	Silicon-sieve/Au/Nafion/H <sup>+</sup>	5	100	
	SPE <sup>d</sup>	Au/NASICON-NaNO <sub>2</sub>	n/a	1	
NO <sub>2</sub>	SPE	Au, Pt/Nafion/10 M H <sub>2</sub> SO <sub>4</sub>	0.004; 0.017	1	
	SPE <sup>d</sup>	Au/NASICON-NaNO <sub>2</sub>	0.01	1	
	SPE	C, Au/ <i>a</i> -ZrPO <sub>4</sub> /TiH <sub>x</sub>	0.01; 0.1	20	
	SPE	Au/PVC/TBAHFPe	0.075	5	
	SPE	C/PVC/TBAHFPe	0.08	2.2	
	SPE	Au/Nafion/0.5 M H <sub>2</sub> SO <sub>4</sub>	n/a	100	
	SPE	Au/Nafion/1 M HClO <sub>4</sub>	0.2	7	
	SO <sub>2</sub>	SPE	Au/Nafion, ADP/1 M NaOH	0.0005	0.1
		SPE	Au/Nafion/0.5 M H <sub>2</sub> SO <sub>4</sub>	0.0025	0.1
		SPE	Pt/Nafion/1 M HClO <sub>4</sub>	0.18	4,500
GDE		Teflon/Au/5 M H <sub>2</sub> SO <sub>4</sub> in DMSO	0.5	200	
SPE		Teflon/Au, Au/Nafion/4 M H <sub>2</sub> SO <sub>4</sub>	n/a	50	
H <sub>2</sub> S	SPE	Teflon-bonded Au/0.33 M H <sub>3</sub> PO <sub>4</sub>	n/a	500	
		Ag/Nafion/0.01 M HClO <sub>4</sub> +0.99 M NaClO <sub>4</sub>	0.045	450	

SPE solid polymer electrolyte, GDE gas diffusion electrode

<sup>a</sup>Galvanic mode

<sup>b</sup>(Absorptive) preconcentration step followed by anodic oxidation or cathodic reduction

<sup>c</sup>With porous Teflon membrane as additional diffusion barrier

<sup>d</sup>Operating temperature > 150 °C

Source: Reprinted with permission from Knake et al. (2005). Copyright 2005 Elsevier

**Table 3.7** Example of electrode reactions for aqueous electrolyte amperometric gas sensors

Target gas	Electrode reaction
H <sub>2</sub>	H <sub>2</sub> + 2OH <sup>-</sup> = 2H <sub>2</sub> O + 2e <sup>-</sup>
CO	CO + H <sub>2</sub> O = CO <sub>2</sub> + 2H <sup>+</sup> + 2e <sup>-</sup>
O <sub>2</sub>	O <sub>2</sub> + 4H <sup>+</sup> + 4e <sup>-</sup> = 2H <sub>2</sub> O
NO <sub>2</sub>	NO <sub>2</sub> + 2H <sup>+</sup> + 2e <sup>-</sup> = NO + H <sub>2</sub> O
NO	NO + 2H <sub>2</sub> O = NO <sub>3</sub> <sup>2-</sup> + 4H <sup>+</sup> + 3e <sup>-</sup>
H <sub>2</sub> S	H <sub>2</sub> S + 4H <sub>2</sub> O = SO <sub>4</sub> <sup>2-</sup> + 10H <sup>+</sup> + 8e <sup>-</sup>
SO <sub>2</sub>	SO <sub>2</sub> + 2H <sub>2</sub> O = SO <sub>4</sub> <sup>2-</sup> + 4H <sup>+</sup> + 2e <sup>-</sup>
CO <sub>2</sub>	CO <sub>2</sub> + H <sub>2</sub> O + 2e <sup>-</sup> = HCOO <sup>-</sup> + OH <sup>-</sup>
MMH	(CH <sub>3</sub> ) <sub>2</sub> N <sub>2</sub> H <sub>3</sub> + 4OH <sup>-</sup> = CH <sub>3</sub> OH + N <sub>2</sub> + 3H <sub>2</sub> O + 4e <sup>-</sup>
CH <sub>3</sub> CH <sub>2</sub> OH	CH <sub>3</sub> CH <sub>2</sub> OH + H <sub>2</sub> O = CH <sub>3</sub> COOH + 4H <sup>+</sup> + 4e <sup>-</sup>
CH <sub>3</sub> CHO	CH <sub>3</sub> CHO + H <sub>2</sub> O = CH <sub>3</sub> COOH + 2H <sup>+</sup> + 2e <sup>-</sup>

Source: Data from Chang et al. (1993), Hodgson et al. (1999a, b), Stetter and Li (2008)

perfluorinated polymer membranes show high ionic conductivities at high water vapor pressure (Anantaraman and Gardner 1996). Nafion electrolyte gas sensors, because Nafion conductivity is a function of RH, typically produce a gas response that depends on the RH (Samec et al. 1995; Opekar 1992; Yasuda et al. 1992). The RH response is not desired for an ambient air sensor wherein the RH can change over wide limits and typically is either eliminated or compensated.

Polymer electrolytes such as PBI (sulfonated polybenzimidazole), S-PEEK (sulfonated polyether ether ketone) (Bouchet et al. 2000; Alberti and Casciola 2001; Sundmacher et al. 2005), and PVA/H<sub>3</sub>PO<sub>4</sub> can also be used in gas sensors (Ramesh et al. 2003, 2004). Some of these solid polymer electrolytes have excellent mechanical and thermal properties and good protonic conductivity even in dry atmospheres (Ramesh et al. 2003; Bouchet and Siebert 1999). The remarkable properties of these polymers lie in the combination of the high hydrophobicity of the perfluorinated polymer backbone and the high hydrophilicity of the sulfonic acid branch. The hydrophilic branches act as a plasticizer, and the backbone retains strong mechanical properties (Colomban 1999). New polymers, based on hybrid inorganic/organic phosphosilicate polymers prepared from orthophosphoric acid, dichlorodimethylsilane, and tetraethoxysilane, have also been synthesized (Mika et al. 2007). Membranes fabricated based on these polymers are amorphous, translucent, and flexible. The proton conductivity increases with rising temperature following Arrhenius behavior and an activation energy of 20 kJ/mol. Under dry conditions at 120 °C, the conductivity was 1.6 S/m. It was established that potentiometric gas sensors with a TiH<sub>x</sub> reference electrode and a Pt sensing electrode exhibited a fast, stable, and reproducible response to dry H<sub>2</sub> and O<sub>2</sub> gases at temperatures above 100 °C.

Typical operating characteristics of amperometric electrochemical H<sub>2</sub> sensors designed based on Nafion and PVA-H<sub>3</sub>PO<sub>4</sub> polymers are shown in Fig. 3.12. It is seen that the response of many polymer H<sub>2</sub> sensors is sensitive enough to detect below 10 ppm and perhaps even 1 ppm with the appropriate electronics and controlled exposures (Ramesh et al. 2003; Sakthivel and Weppner 2006a). Results presented in Fig. 3.12a were obtained using a PVA/H<sub>3</sub>PO<sub>4</sub> electrolyte that was prepared by casting the structure onto a Teflon sheet (Ramesh et al. 2003, 2004). The electrolyte film was fixed to a supporting ring and coated with palladium as an anode on the sensing side and platinum as a cathode on the counter electrode side. The electrolyte thickness was about 2 mm. The housing assembly for the sensor was made from polycarbonate. The schematic diagram of this sensor is shown in Fig. 3.12a. The palladium anode was deposited by vacuum vapor deposition. The thickness of the anode film in the sensor was of the order of 1,000 Å. The cathode on the counter electrode side of the sensor was platinum supported on carbon prepared by screen printing. Before coating, 20–25% of a Teflon emulsion was added to the mixture. The electrode was sintered at 100 °C under vacuum. Two gold-coated nickel grids were used as current collectors on both sides.



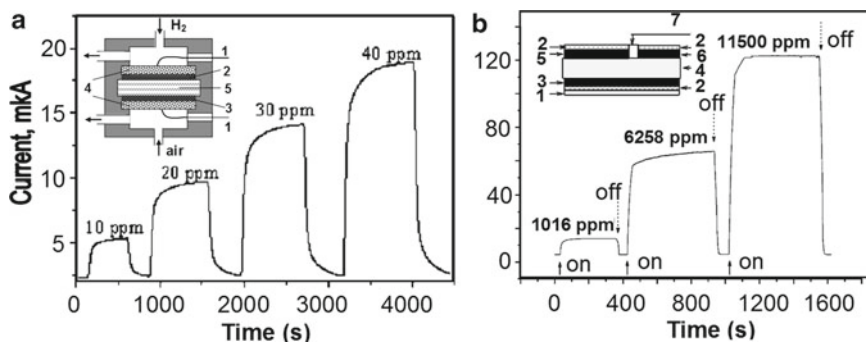


**Fig. 3.12** Responses and schematic diagrams of polymer-based  $H_2$  amperometric sensors. (a) The Pd/PVA- $H_3PO_4$ /Pt-based sensor for various concentrations of  $H_2$  in air: (1) lead; (2) Pd thin film; (3) Pt (supported catalyst); (4) nickel grids; (5) PVA- $H_3PO_4$ . (Reprinted with permission from Ramesh et al. (2003). Copyright 2003 Springer). (b) Nafion-based sensor: (1) PTFE membrane; (2) Pt/Ru mesh (embedded into the catalyst layer); (3) working electrode (Pt/C catalyst thin layer); (4) Nafion-117 membrane; (5) counter electrode; (6) reference electrode; (7) insulator. (Reprinted with permission from Lu et al. (2005). Copyright 2005 Elsevier)

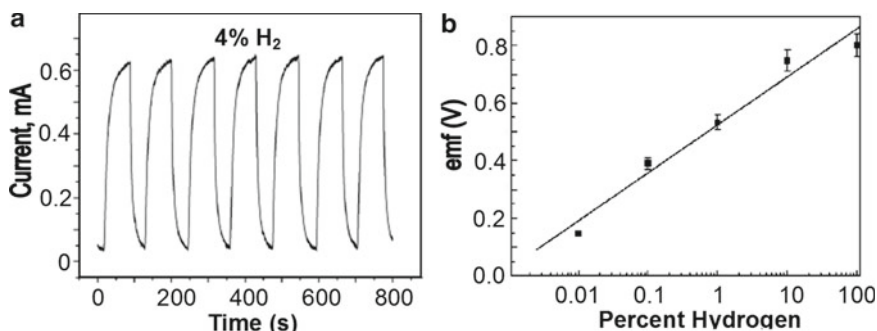


**Fig. 3.13** (a) Cyclic behavior of 4%  $H_2$  exposure to the sensor Pt Nafion WE with an area of  $2\text{ cm}^2$  in a 1 min time interval. (Reprinted with permission from Sakthivel and Weppner (2006b). Copyright 2006 Elsevier.) (b) Equilibrium EMF of a Pd/Nafion-based sensor vs the logarithm of the hydrogen partial pressure for hydrogen/air gas mixtures (Reprinted with permission from Maffei and Kuriakose (2004). Copyright 2004 Elsevier)

Nafion-based sensors also have good operating characteristics. As seen in Fig. 3.12b, for a step change of the hydrogen concentration, the  $t_{90}$  response time (time required to reach 90% of the steady-state current) of the sensor is about 20–50 s, suitable for most monitoring applications (Lu et al. 2005). Sensors show good reproducibility of sensor response (Sakthivel and Weppner 2006a, b). For example, Fig. 3.13 shows cyclic exposure of the Pt Nafion sensor element to 4% hydrogen and no hydrogen. These results can be used to calculate the measurement precision during cyclic exposures. Short-term drift and long-term drift under laboratory conditions (downward drift in the output current) were also reported to be about 2% of signal per day.

The potentiometric response of a polymer sensor is shown in Fig. 3.12b, and, as is typical for potentiometric sensors,  $H_2$  can be detected over many orders of magnitude in concentration. The EMF dependence on the logarithm of the hydrogen partial pressure is very close to linear but is non-Nernstian. A nonlinear least-squares fit (NLLSF) of the data yielded a slope of 166 mV, well above the value predicted by the Nernst equation. If the data for 0.01% hydrogen is discarded, the value of the resultant

slope is 145 mV and still significantly greater than the expected theoretical value. The reasons for the non-Nernstian behavior of this sensor to hydrogen/air mixtures are not clear. The fast, linear, reproducible, and large stable output of the sensor makes it very useful for detection of hydrogen leaks in air. The sensor performance thus suggests that it can be incorporated into a fuel cell or into other hydrogen process applications to detect explosive levels of hydrogen gas.

More detailed information about polymers used in electrochemical gas sensors can be found in various reports in the literature (Josowicz 1995; Shi and Anson 1996; Colombari 1999; Wroblewski et al. 2004; Lukow and Kounaves 2005; Michalska 2006).

The polymers or hydrogels can prevent the evaporation of electrolyte during sensor fabrication, especially for microsensor devices where very small amounts of electrolyte are used. Using polymer electrolytes provides opportunities for the design of planar sensors and the applications of standard microelectronic fabrication technologies (Shi and Anson 1996). Polymers allow decreases essentially of both the size and weight of electrochemical sensors. In addition, polymer electrolytes allow a larger range of operating temperatures for the electrochemical sensor. As research has shown, polymer-based  $H_2$  sensors successfully operate in the temperature range RT–100 °C (Sakthivel and Weppner 2006b; Ramesh et al. 2008), and, compared to liquid electrolytes, solid polymer electrolytes can be used as separators in electrochemical cells, do not dissolve impurities from the gas easily, and permit the construction of miniaturized devices that are leakproof to help avoid premature sensor failure.

### 3.5 Limitations of Polymer Using in Gas Sensors

Strong water vapor influence (see Figs. 3.14 and 3.15c) is one of the main disadvantages of polymer-based gas sensors, because water vapor is the most common interferant for gas sensors operating at room temperature (Buchler and Ryan 1997; James et al. 2005; Pejic et al. 2007). For example, Kaplan and Brahm (1998) showed that an e-nose based on polymer gas sensors lost sensitivity in the presence of water vapor. Therefore, when humidity levels are not compensated for or controlled, it is possible that the humidity is responsible for some successful discriminations. For example, the

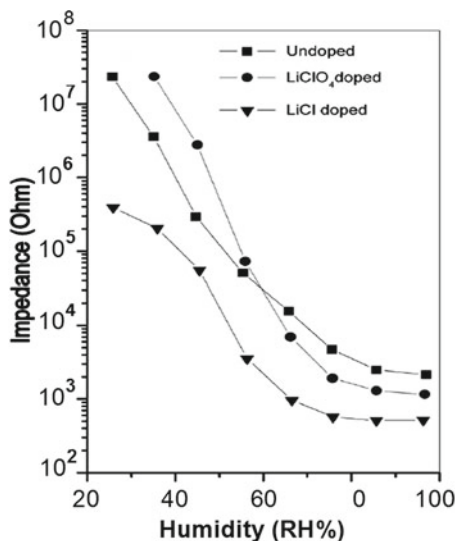


**Fig. 3.14** The impedance response to humidity of undoped and doped anionic poly(phenylenevinylene) derivative. (Reprinted with permission from Liu et al. (2008). Copyright 2008 Elsevier)

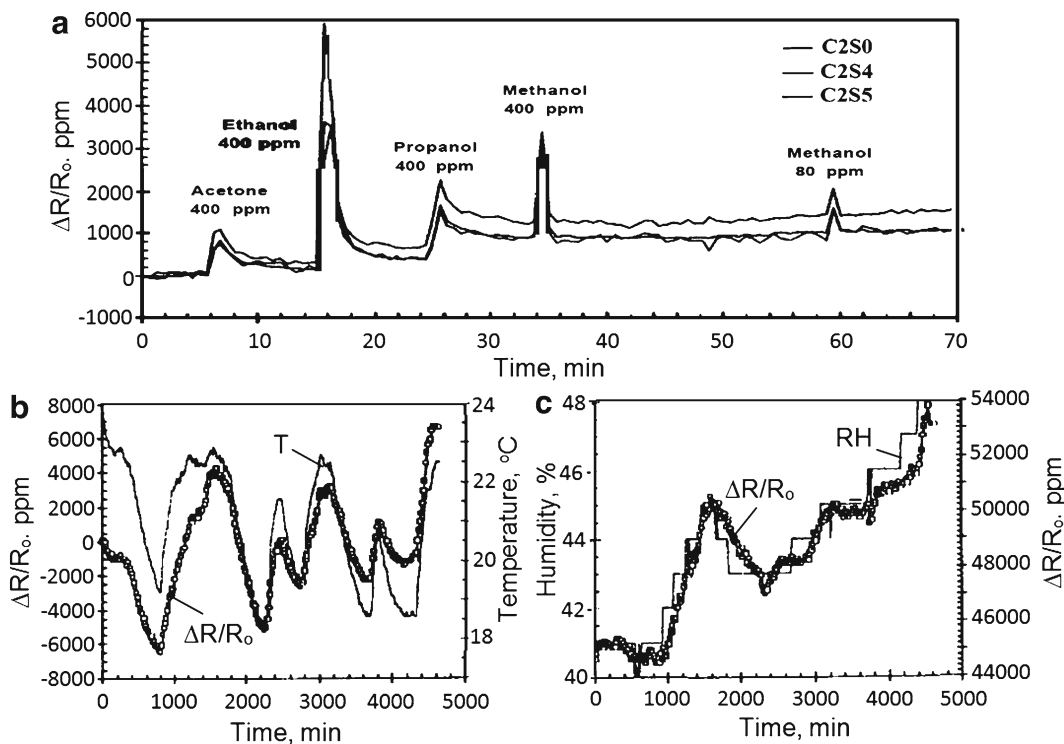


**Fig. 3.15** (a) Conductivity responses for three donut-shaped thin-film sensors based on carbon-doped poly 4-vinyl phenol; (b, c) conductivity responses of carbon-doped polyvinyl acetate to (b) temperature and (c) air humidity. The polymer films swell in response to the presence of a particular gas which increases the distance between the carbon dopants and changes the resistance of the film. These results were obtained from 3-day experiments in an air ambient where the gas sensors were kept in stagnant air (Data from Buchler and Ryan (1997))

electrical properties of Nafion (primarily its conductivity) are strongly dependent on the amount of water contained in the polymer. The maximum water content, corresponding to 22 water molecules per single sulfo group of the polymer, is attained by boiling Nafion in water, and this number decreases to 14 for the polymer which is in contact with a gaseous phase saturated in water vapor; the water content fluctuating in its dependence on the humidity of the surrounding medium (Opekar and Stulik 1999). Therefore, the response of a Nafion-containing sensor in a gaseous phase depends on the gas relative humidity. Changes in the water content also cause the Nafion membrane to swell physically (Sondheimer et al. 1986). This swelling alters the size and shape of the membrane and thereby changes the rate of proton diffusion; that is, proton diffusion is the charge-carrier mechanism within the polymer. Therefore, a changeable very dry or very wet atmosphere provides a difficult working environment for Nafion-based gas sensors. Even Nafion in contact with a water phase to maintain the water content constant is sometimes insufficient to remove the signal dependence on RH, since local chemical and physical effects at the sample–electrode interface can dominate the response (Opekar and Stulik 1999) and the rate of water exchange in the Nafion itself can change (Opekar and Svozil 1995). Of course, this complicates the detection of volatile odors in the presence of high levels of water vapor. Wang et al. (1999) have shown that making the substrate surface hydrophobic before the deposition of the CP may alleviate this problem. However, this improvement is negligible.

The required operating temperatures can add complexity to a gas sensor system. For example, sensors using Nafion 117 often do not reach a steady state at temperatures in excess of about 50 °C (Mika et al. 2007).

This instability is caused by the rapid and continuous drying of the membrane in gas streams that affect the membrane's conductivity. The strong influence of the surrounding temperature on polymer conductivity (see Fig. 3.15b) is also a factor, which decreases detection limit of polymer-based chemiresistive sensors (Buchler and Ryan 1997).

During sensor design, it is also necessary to take into account the fact that the conductivity of otherwise identical CP samples varies from preparation to preparation. Much of this variability is due to the method of preparation and the thickness of the film (Stussi et al. 1997), which has a considerable influence on the surface morphology. For example, Li et al. (2002) have shown that thin (<300 nm) films of PANi grown electrochemically are compact and smooth, but thicker films have filamental or dendritic surface structure.

Difficulty in the interpretation of the chemical response of polymer-based sensors is also a big problem for such sensors (Huang et al. 2003; Virji et al. 2004). For example, localized energy states can affect the value of the work function but do not affect the conductivity of the CP (Polk et al. 2002). In addition, there are too many different factors influencing sensor response. These factors depend on both the type of polymer and the type of dopant. For example, Posudievsky et al. (2011) studying sensor responses of thin conducting polymer films to organic solvent vapors have shown that the main factors determining the magnitude of response of PANi films doped with "conventional" acids to the effect of organic solvents were the films' morphology and acceptor ability of the analyte molecules, while the magnitude of response of PANi films doped with heteropoly acids (HPA) was apparently also determined by additional donor-acceptor interaction of the analyte molecules with the dopant. For PPy-based VOCs sensors, the situation was different. The response of PPy depended not only on the morphology of films but also on the type of charge carriers in the polymer, both determined by the nature of anion dopant, and also on polarity and nucleophilicity/electrophilicity of the analyte molecules. In case of P3MT films, the magnitude and sign of sensor response were determined by the ratio of the quantities of cation-radical and dication states in the polymer, which depends on the nature of anion dopant and polarity of analyte. At the same time, response of P3MT to chloroform was always positive independently of the nature of the used anion dopant, and its magnitude was an order greater than that of the response to other analytes. That makes P3MT-based arrays specifically sensitive to this analyte among all studied organic solvents (Posudievsky et al. 2011).

It was also established that some polymers undergo degradation or an irreversible swelling process when exposed to certain environments (Pejcic et al. 2007). As a result, the temporal drift of sensor baseline is present in most polymer-based conductometric gas sensors (see Fig. 3.15a). Irreversible changes in polymers under influence of UV radiation and oxidizers such as ozone and NO<sub>2</sub> also limit appreciably the application of polymers for designing sensors aimed at environment control. Problems related to polymer degradation will be discussed later in Chap. 19 (Vol. 2). We need to note that long-time instability is a big drawback of the sensors based on conducting polymers (Bai and Shi 2007). The performances of this kind of sensors decreased dramatically as they were stored in air for a relatively long time (Kondratowicz et al. 2001). This phenomenon can be explained as dedoping of conducting polymers. Many conducting polymers, such as PPy and PTh, are easily dedoped when they are exposed to air. For example, Jiang et al. (2005) reported that the sensitivity of PPy/PVA composite sensor was only maintained for 2 weeks, while the sensitivity of pure PPy sensor was maintained over 1 month. Of course, this time is too short. In the case of an ozone-containing atmosphere, this time is considerably shorter. For example, the lifetime in an ozone-containing atmosphere for several polymer-based materials used for ozone gas sensor design is summarized in Table 3.8. Experiment has shown that the reaction of ozone with the polymer is irreversible and the average useful lifetime is found to range from 20 to 3,000 ppb hours only.

Another problem is the irreversibility of these sensors (Bai and Shi 2007). The responses of sensors gradually decrease in the sensing cycles, or the signal cannot return to the original value after exposure to analytes. In particular, Hao et al. (2005) reported these results. It was believed that the irreversibility of PPy in ammonia is caused by nucleophilic attack on the carbon backbone (Kemp et al. 2006). The mechanism of irreversibility is still not clear.

**Table 3.8** A summary of the lifetimes of the coating studied during work operating of QCM-based sensors

Coating compound	Lifetime (ppb hours)
Polybutadiene	97.2 <sup>a</sup>
Beeswax	14.8
Indigo carmine	45.6
Sodium nitrite	>3,264
KI	794.8
Gallic acid	2,778.89 <sup>b</sup> ; 82.7 <sup>c</sup>

Beeswax is a mixture of organic compounds such as unsaturated and saturated fatty acids, alcohols, and esters, and polybutadiene contains unsaturated alkenes

<sup>a</sup>Lifetime calculated for coating prepared by cast solution

<sup>b</sup>Lifetime for dip coated

<sup>c</sup>Lifetime for spin coated

Source: Data from Muller et al. (2011)

In addition, due to the low temperature of operation, polymer-based sensors as a rule have long response and recovery times (tens of seconds to tens of minutes), often accompanied by hysteresis. This means that these sensors cannot be applied to in situ monitoring of fast processes. Usually, slow kinetics of sensor response is caused by slow penetration of gases into the CP. It was found that the porosity of polymers depends mainly on technology route used and the type of dopant. For example, Desilvestro and Scheifele (1993) reported that the porosity of electrochemically synthesized PANi films increased within the following row of the parent acid solutions:  $\text{H}_2\text{SO}_4 \gg \text{HCl} > \text{HNO}_3 \gg \text{HClO}_4$ .

One can consider as a disadvantage the low selectivity of polymer-based gas sensors. However, not only the sensors based on conducting polymers but also the other sensors, including sensors designed on the base of metal oxides and many other sensing materials, face this problem.

### 3.6 Choosing a Polymer for Gas Sensor Applications

As we have shown before in Table 3.6, there is a large variety of polymers which can be used for gas sensors design. This means that, similar to metal oxides, we do not have one polymer which is most suitable for all chemical sensor applications. This is because, for every type of sensor, we need polymers with specific combinations of properties. A polymer that is to be used as a hydrogel should be hydrophilic (Tierney 1996). On the other hand, gas-permeable membranes are often made of hydrophobic polymers to prevent passage of water through the membrane. A polymer electrolyte for a sensor operating with nonaqueous electrochemistry may be less hydrophilic. The hydrophilic or hydrophobic properties of a polymer are easily determined by looking at its solubility in various solvents. Polymers for chemiresistor sensors must be conductive while, for optical and capacitance sensor applications, this property of polymers is not important. Polymers in optical sensors can have insulating properties. Reversible change of optical properties such as refraction, transmittance, and fluorescence during interaction with target gas is more important for polymers aimed at applications in optical sensors. A hygroscopic polymer in humidity sensors should be simultaneously highly sensitive and resistive to water molecules.

QCM-, SAW-, and cantilever-based gas sensors are adsorption-type sensors in which the change in weight of the sensing element is the determining factor (Houser et al. 2001). Therefore, polymers applied in such devices should have the ability to sorb selectively and reversibly an analyte of interest from sampled air and to concentrate it so that lower concentrations can be detected. How specific adsorption properties of polymers can be, one can estimate on the base of results presented in Table 3.9. We need to note that for other analytes, polymers optimal for application will be different.

**Table 3.9** Adsorption of strychnine (a pesticide) at 45 °C by various films immobilized on a QCM surface

Immobilized film	Strychnine, $\Delta m$ (ng)
Uncoated	2
2C <sub>18</sub> N <sup>+</sup> 2C <sub>1</sub> /poly(styrene sulfonate) (PSS)	533
Dimyristoylphosphatidyl ethanolamine (DMPE)	560
Poly(vinyl alcohol)	4
Poly(methyl glutamate)	5
Poly(styrene)	7
Bovine plasma albumin cross-linked with glutaraldehyde	5
Keratin	7

Source: Data from Forster (1998)

Polymer electrolyte in electrochemical sensors finds its place in a sandwich manner between the electrodes and is in close interaction with both electrodes, so it needs to be compatible with the electrodes. The interfaces between the electrolyte and both the electrodes dictate the device performance. Therefore, the electrolyte should be stable toward both the cathode and anode surfaces (Ahmad 2009). In addition, according to Ahmad (2009), polymer electrolytes (1) should be good ionic conductors and electronic insulators, so that ion transport can be facilitated and self-discharge can be minimized; (2) should have wide electrochemical windows, so that electrolyte degradation would not occur within the range of the working potentials of the electrodes; (3) should be inert to other cell components such as cell separators, electrode substrates, and cell packaging materials; (4) should be robust against electrical, mechanical, or thermal abuses; and (5) should be environmentally friendly. It is necessary to note that some of indicated requirements can be applied to polymers designed for other types of gas sensors.

Chatzandroulis et al. (2011) believe that physical properties of polymers also are important for achievement of better gas-sensing characteristics. For example, it was established that an amorphous state of polymers is optimal for adsorption-type gas sensors, and the sensing performance is higher when the amorphous polymer is at the elastomeric state, i.e., the glass transition temperature ( $T_g$ ) is lower than the temperature of operation (Kitsara et al. 2007). In the elastomeric phase, the thermal motion of the polymer chains allows rapid vapor diffusion and leads to higher absorption compared to the glassy state. When an absorption/desorption cycle is complete, the polymer returns to the initial state. However, it is necessary to take into account that, when the polymer is in the elastomeric state, the shape and thickness of the polymer film can vary continuously (e.g., if the sensor is placed in a vertical position, the polymer film will start to flow), and the sensing performance will be affected significantly and become unstable. Polymers in the glassy state present important drawbacks such as limited diffusion, absorption, and permeability. The slower vapor diffusion results in longer response times. During desorption, the diffusion rate becomes slower as the vapor concentration in the film decreases and the polymer stiffens, whereas some vapors may still remain in the film. This remaining vapor could cause partial sensor reversibility loss and hysteresis. Despite those drawbacks, glassy polymers cannot be excluded for use in chemical sensors. Ultrathin films (a few nanometers thick) might provide enhanced absorption; however, the application of such film thicknesses in particular geometries, such as interdigitated electrodes, is not possible (Manoli et al. 2006). Partially crystalline polymers have additional disadvantages to those of glasses. The processing is more difficult and the crystalline domains do not contribute to vapor absorption. Therefore, the final volume contributing to the absorption is smaller. For these reasons, this class of materials should be avoided (Chatzandroulis et al. 2011).

The features of analyte interaction with polymers also influence sensor parameters. We have to take into account that weak interactions between the analyte and the polymer produce sensors with good

performance in terms of reversibility and hysteresis associated with low selectivity and sensitivity values. On the other hand, strong interactions lead to the opposite behavior—limited reversibility and hysteresis values along with higher sensitivity and selectivity performance.

Chatzandroulis et al. (2011) believe that the optimum approach appears to be the selection of polymeric films which interact with the vapors through solubility interactions. Dipole–dipole and hydrogen bonding interactions are examples of orientation-dependent solubility interactions. In ideal situations, the interactions are limited to nonoriented interactions such as induced-dipole–induced-dipole interactions, also known as dispersion interactions. In order to achieve the optimum performance in gas sensors, materials which maximize specific-oriented interactions with the absorbed analyte molecules, thus achieving selectivity and sensitivity, should be identified. In particular, for the achievement of high sensitivity to vapors, which have hydrogen-bond base adsorption, it was suggested to incorporate the same hydrogen-bond basic functional groups into the sensor-coating material. However, Grate and Abraham (1993) found that the incorporation of hydrogen-bond acidic groups gives stronger and more selective interactions and makes a better sensor-coating material.

It is known that the polymer chemical structure determines its solubility properties, and hence the sensor sensitivity and selectivity. Therefore, the greatest sensitivity to the target analyte can be achieved by including structural elements in the coating material which maximize the solubility properties that interact with the analyte vapor (Kummer et al. 2004). There is assumption (Chatzandroulis et al. 2011) that the selectivity of a coating material will be greatest if it can be designed to interact with vapors by only a single type of solubility interactions. However, in the real world, it is not possible to make a polymer that will interact only through a single solubility property. For example, it is quite difficult to have a polymer that presents significantly different absorption characteristics on the various members of the same family of analytes, i.e., with the same functional group. The strategy for selectivity must be to select a particular solubility property, incorporate it into a coating material at maximum strength, and minimize all other solubility properties. However, this task is very hard to resolve (Kummer et al. 2006; Kurzawski et al. 2006).

So we see that requirements for polymers aimed at application in various gas sensors are really different. However, it was established that even for one type of sensor, depending on the task, we need polymers with different properties. For example, much research with different polymers, including phthalocyanine, polymer–ceramic composite, epoxy resin, and cellulose, have shown that using polymer-coated QCMs, hydrogen bond-forming acidic volatiles are best detected by hydrogen bond-forming basic polymers (Slater and Paynter 1994; Grate et al. 1997) while alkanes could be distinguished by the use of strong hydrogen bond-forming acidic polymers that could interact with the weak hydrogen-bond basicity of the alkenes (Adhikari and Majumdar 2004). The same situation takes place during designing specific sensors which can operate using different operation principles. Polymers, used in humidity sensors and listed in Table 3.10, illustrate this situation. The electrical conductivity of the PANi-PAV composite film is plotted vs atmospheric humidity and time in Fig. 3.16.

Based on the above-mentioned discussions and information presented in Table 3.10, we can only say that polyaniline (PANi) and polypyrrole (PPy) are most often used in various designs. Polyaniline and polypyrrole are formed through the oxidation of aniline and pyrrole, respectively. The oxidation is usually carried out either by electropolymerization on a conductive substrate (electrode) with the application of an external potential or by chemical polymerization in solution through the use of a chemical oxidant (Wallace et al. 1997). It was established that PPy- and PANi-based sensors have considerable response to various organic vapors (Bartlett and Ling-Chung 1989) and inorganic gases such as  $O_2$ ,  $NH_3$ ,  $NO_x$  (Blanc et al. 1990; Li et al. 2000),  $H_2$  (Virji et al. 2006; Al-Mashat et al. 2008),  $CO$  (Liu et al. 1997), and  $CO_2$  (Waghuley et al. 2008).

According to Macagnano et al. (2011), an intrinsically conducting polymer polyaniline (PANi) has the following advantages. In fact, its synthesis is easy to perform (the most common is based on oxidative polymerization in aqueous acidic media using a variety of oxidizing agents such as  $(NH_4)_2S_2O_8$ ,  $KIO_3$ , and  $K_2Cr_2O_7$ ), it is capable of existing in intrinsically distinct redox states (pernigraniline, emeraldine,

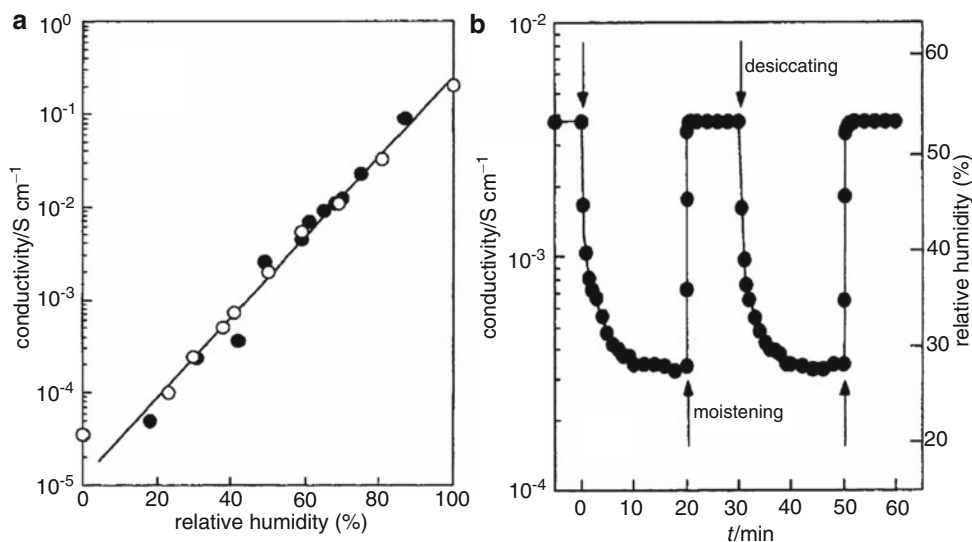


**Fig. 3.16** (a) Relationship between the conductivity of PANi-PVA composite and relative humidity in the (*open circle*) desiccating and (*filled circle*) moistening processes. (b) Conductivity and relative humidity as a function of time. Desiccating and moistening processes were begun at the point indicated by the *arrow*. The composite film was prepared with 0.28 vol% PANi and 99.72 vol% PVA (Reprinted with permission from Ogura et al. (1997). Copyright 1997 Royal Society of Chemistry)

**Table 3.10** Different polymers used in humidity sensors

Principles	Polymer	Sensor properties
Electrical property measurement	2-Acrylamido-2-methyl propane sulfonate modified with tetraethyl orthosilicate	Less hysteresis, 2%, good linearity, 30–90% working range humidity, long-term stability of at least 31 days
	Iron oxide-polypyrrole nanocomposite	Sensitivity increases with increasing concentration of polypyrrole
	Nano-BaTiO <sub>3</sub> -quaternary acrylic resin (RMX) composite	Maximum humidity hysteresis is 3% RH, 7–98% working humidity range, $\tau_{res} \sim 15$ s and $\tau_{rec} \sim 120$ s in 33–98% RH, about 1 year long-term stability
	PAni-PAV (0.28–99.72%)	Good linear dependence in all RH range. Hysteresis is absent
QCM	Poly( <i>o</i> -phenylenediamine) (PoPD)-PVA (0.2–99.8%)	Good linear dependence in all RH range, small hysteresis
	Quaternized and cross-linked poly(chloromethyl styrene)	Hysteresis decreases with increase in quaternization
SAW	PVA (polyvinyl alcohol)	60% RH measured as a frequency change of about 211.5 MHz at room temperature
Optical	Crystal violet and methylene blue incorporated in PVA/H <sub>3</sub> PO <sub>4</sub> SPE	Shows linearity of response

Source: Data from Ogura et al. (1997); Adhikari and Majumdar (2004)



and leucoemeraldine) (MacDiarmid 2002), it is rather stable to environmental changes (e.g., the base form of the emeraldine oxidation state (PAniEb) can tolerate up to 300 °C, depending on dopants) (Skotheim and Reynolds 2007), and, finally, it is soluble in a variety of organic solvents (e.g., dimethylsulfoxide, dimethylformamide, 1-methyl 2-pyrrolidinone, tetrahydrofuran, and chloroform for PAniEb). Furthermore, PAni is an excellent example of conjugated polymers that can be tailored for specific applications through the doping process; it can result in electrically conductive material as well when the emeraldine oxidation state is doped with an acid which protonates the iminic nitrogen on the polymer backbone. Incidentally, dopants (e.g., common protonic acids such as hydrochloric acid) can be added to polymer until all iminic nitrogens (half of the total) are doped, thus tuning the polymer conductivity from the undoped insulating base form ( $\sigma$   $10^{-10}$  S/cm) to the fully doped, conductive acidic form ( $\sigma$  1 S/cm). Therefore, the acidic doping (and conversely the undoping) can end up being a pivotal event in the sensing mechanism of PAni. For instance, a dedoping effect through deprotonation is thought to happen when ammonia gas is adsorbed onto PAni molecules: the protons present on  $\text{NH}$  groups, in fact, happen to move onto  $\text{NH}_3$  molecules to form  $\text{NH}_4^+$ , while PAni itself turns into its base form (less conductive). In contrast, acidic gases ( $\text{HCl}$ ,  $\text{H}_2\text{S}$ , and  $\text{CO}_2$  with water) can cause doping through protonation. All these processes are reversible (Bai and Shi 2007). Each of these changes, following the polymer exposure to analytes, can be detected as current variation commonly measured by suitable resistors.

However, the above-mentioned does not mean that PAni- and PPy-based devices have better parameters and other types of polymers do not have prospects for application. For example, experiments have shown that heteroaromatic polymers can act as sensors for both gases and solutions. Simple polythiophenes show conductivity changes upon exposure to oxidizing gases, such as nitrogen dioxide, and to reducing gases such as ammonia (Walton 1990). Thin-film polyaniline-based gas sensors have shown satisfactory selectivity to  $\text{CO}$ ,  $\text{NH}_3$ , and  $\text{HCl}$ , while conductive polymers such as polyfuran and polythiophene have been seriously considered as humidity gas sensors. The conductivity of perchlorate-doped polyfuran varies from  $10^{-8}$  to  $10^{-2}$  Sm/cm when it is exposed to humidity varying from 10% to 80% (Kumar and Sharma 1998). Penza and Cassano (2000) reported that poly(vinyl alcohol) (PVA) film provided high RH sensitivity, as well as high water resistance. Therefore, PVA is more preferable than PAni for operation in an aqueous environment. In addition, it is necessary to note that PAni, similar to other polymers, is inclined to aging and degradation. For example, Šeděnková et al. (2008a, b) studied the stability of the PAni films prepared under different conditions and leading to different morphologies (nanotubular and granular) at elevated temperature. They established that a dramatic change in the resistivity dependence on time was observed when temperature of aging exceeded 85 °C. They also found that the degradation at 80 °C over 3 months is accompanied by deprotonation, oxidation, and thermal transition due to the chemical cross-linking reactions among PAni molecules. In addition, Šeděnková et al. (2008a, b) have shown that the molecular structure corresponding to nanotubular morphology, which contains the cross-linked phenazine- and oxazine-like groups, is more stable than the molecular structure with granular morphology. Brožová et al. (2008) reported that the media, strongly alkaline or acidic, also influences the stability of polyaniline.

The same can be said about Nafion, which is most usable for electrochemical gas sensors (Opekar and Stulik 1999). Nafion is a hydrated copolymer of poly(tetrafluoroethylene) with poly(sulfonylfluoride vinyl ether) manufactured by DuPont, USA. This is a cation exchanger containing hydrophilic sulfo groups firmly bound to the hydrocarbon backbone, whose charge is compensated for by counterions (mostly  $\text{H}^+$ ). The counterions are released by dissociation of the water present within the polymer structure and cause ionic (proton) conductivity of the polymer. The water required is bound in the hydration mantles of the ions present and thus the polymer is a solid which contains no macroscopic liquid phase (Opekar and Stulik 1999). Experiments have shown that Nafion exhibits extraordinary properties important for electrochemical gas sensor design (Opekar and Stulik 1999). However, the geometric dimensions of Nafion and its electroconductivity are strongly dependent on the amount of

water contained in the polymer, which fluctuates depending on the humidity of the surrounding medium (Zawodzinski et al. 1993). Therefore, the response of a Nafion-containing sensor in a gaseous phase depends on the gas relative humidity (Opekar 1992). Some sensor designs thus employ Nafion in contact with a water phase to maintain the water content constant. However, this is only a partial solution to the problem because only the bulk water concentration is constant, while the local water contents at the boundary of the test gas, the indicator electrode, and the Nafion membrane, which is decisive for the sensor response, still fluctuate, leading to changes not only in the conductivity but also in polymer dimensions and thus also in the length of the gas/electrode/polymer boundary. It is difficult to correct for the sensor response variations with varying humidity because the rates of water intake and release by Nafion are different (Opekar and Svozil 1995). Attempts at replacing hydrophilic Nafion by a hydrophobic solid electrolyte polymer (Langmaier et al. 1997) led only to a decrease in the dependence but not to its complete elimination.

The use of polymers able to operate at high temperature might be at least one way to resolve the RH response of polymer gas sensors. For example, a polymer,  $\text{H}_3\text{PO}_4$ -doped polybenzimidazole (PBI), which is promising for gas sensor application, has sufficiently high proton conductivity even in dry air (Bouchet and Siebert 1999; Rosini and Siebert 2005). Experiments carried out by Bouchet et al. (2001) have confirmed operation of  $\text{H}_3\text{PO}_4$ -PBI-based sensors in RH of only 10–30%, and this is about the same as the performance of the PVA/ $\text{H}_3\text{PO}_4$  polymer electrolyte (Ramesh et al. 2003). However, at higher temperatures, any degradation mechanism will be enhanced. Mika et al. (2007) found that hybrid polymers appeared to be stable up to 400 °C, but the membrane slowly degrades, as was revealed by thermal analysis. As a result, the new hybrid inorganic/polymer electrolyte sensors exhibited drift, which results in a need for frequent calibration (Mika et al. 2007).

In addition, it was established that through the functionalizing of polymers, it is possible to change their properties significantly and to obtain the same sensing parameters even using different polymers. The process of polymer functionalizing will be discussed later in Chap. 24 (Vol. 2). An extreme example of this process is Nafion. Its backbone is Teflon, a very hydrophobic polymer that is insoluble in all common solvents. However, upon grafting polyether side chains which terminate in sulfonate groups onto the main chain, the polymer becomes much more hydrophilic and is then soluble in polar organic solvents. This means that polymers due to flexibility of their properties give a strong possibility of polymer-based gas sensors. Sometimes, however, the multitude of choices of polymers makes selection of the proper polymer difficult. Janata and Josowicz (2003) noted that the abundant literature dealing with various applications of polymers can be divided into two groups: polymers in electronic, optoelectronic, and electromechanical devices on the one hand and polymers in gas sensors based on optical and mechanical mechanism (Osada and De Rossi 2000) on the other. Acceptable operation of the first group relies on their chemical stability in the ambient environment, whereas the sensor applications take advantage of the physical changes that take place in the polymers when they are exposed to different chemicals. This property has its origin in the molecular and macroscopic structure of polymers. Thus, *tunability* is an important bonus of polymers that aids in the preparation of a variety of sensing layers, but it can be troublesome where performance independent of ambient factors is desired. Thus, we believe that only sufficient knowledge of the physical and chemical properties of the analyte, the potential interferences, and the environment in which sensor will operate, combined with insight into the desired function of the polymer, can make the selection of a polymer for sensor fabrication a much less daunting task. We constantly need to take into account that, for every polymer, we can find specific properties which would be useful for design of one type of sensor but unsuitable for design of another. For example, Nafion, which is commonly used as a permselective membrane, has extremely high affinity for organic cations, reasonable affinity for inorganic cations, and almost completely excludes both organic and inorganic anions.

Thus, it is apparent that polymers display promising analytical results. It was shown that the changes in polymer properties can be correlated quantitatively to the concentration of the analyte and can be readily reversed when the analyte is removed (Persaud 2005). For example, Bissell et al. (2002) demonstrated that, for analyte functional classes (alcohols, esters, alkanes, and hydrocarbon-only aromatics),

**Table 3.11** Examples of polymers used for sensor array design

Electrochemical polymerization; array of chemiresistive sensors <sup>a</sup>	Carbon-polymer composites; silicon-based micromachined array of chemiresistive gas sensors <sup>b</sup>	Polymer films; array of QCM-based sensors <sup>c</sup>
1. Polypyrrole(PPy)-butane sulfonic acid	1. Poly(styrene- <i>co</i> -allyl alcohol)	1. <i>t</i> -Bu-Calix-[6]arene
2. PPy-PSA	2. Poly(4-methylstyrene)	2. <i>t</i> -Bu-Calix-[8]arene
3. PPy-hexanesulfonic acid	3. Poly(caprolactone)	3. Pentacene
4. PPy-heptane sulfonic acid	4. Polystyrene-black-polyisoprene-black-polystyrene	4. Tetracene
5. PPy-octane sulfonic acid	5. Cellulose acetate	5. Phthalocyanine
6. PPy-decanesulfonic acid	6. Poly(styrene- <i>co</i> -methyl methacrylate)	6. Dibenzotetraazaannulene
7. PPy- <i>p</i> -toluenesulfonic acid sodium salt	7. Poly(styrene- <i>co</i> -butadiene)	7. Tetramethyl-dibenzotetraazaannulene
8. PPy- <i>p</i> -toluenesulfonic acid monohydrate	8. Poly(vinyl stearate)	
9. PPy-tetraethylammonium toluenesulfonate	9. Hydroxypropyl cellulose	
10. Ployaniline-NaHSO <sub>4</sub>	10. Poly(butadiene)	
11. Poly(3-methylthiophene-tetraethylammonium tetrafluoroborate)	11. Poly(vinyl butyral)- <i>co</i> -vinyl alcohol- <i>co</i> -vinyl acetate	
	12. Ethyl cellulose	
	13. Poly(vinyl acetate)	
	14. Poly(4-vinyl pyridine)	

<sup>a</sup>Breer et al. (1996)

<sup>b</sup>Kim et al. (2005), Ha et al. (2005)

<sup>c</sup>Snopok and Kruglenko (2005)

the electrical resistance changes of various polypyrrole- and polythiophene-based conducting polymer sensors conform to a linear relationship with vapor concentration, producing a fixed amplitude of sensor response at an analyte-saturated vapor pressure. As a result, a lot of polymers were developed as odor-sensing devices, and many materials have been synthesized and characterized for odor transduction. However, we need to note that, till now, there are problems which create difficulties to achieve the desired selectivity, sensitivity, and stability in real samples of polymer-based gas sensors.

Research has shown that at present the problem of selectivity can be resolved only by e-noses, which are an array of nonselective gas sensors. Fundamental to the artificial nose is the idea that each sensor in the array has a different sensitivity (Gardner 2004). Selectivity is maximized when each gas sensor responds more selectively to a certain chemical parameter or chemical quality of chemical compounds such that the array is able to image in “chemical” space. As we wrote before, polymers have great variability of gas-sensing parameters and they can impart a wide variety of response characteristics to sensors. Therefore, the fabrication of differentially sensitive polymer-based elements for sensor array of e-nose is not a big problem. As a result, one of the early commercial e-nose systems was designed based on polymer-based sensors (Hatfield et al. 1994; Hodgins 1995; Gardner 2004). Examples of polymers used for the design of sensor arrays are given in Table 3.11.

Arrays of conductive polymer sensors are typically prepared electrochemically (Slater et al. 1993; Hodgins 1995; Gardner and Bartlett 1995; Partridge et al. 1996). The electrochemical deposition of CPs is reasonably controllable because films can be electrodeposited onto metalized areas and the film thickness can be varied by monitoring the total charge passed during the deposition process. The polymerization is usually carried out in a three-electrode configuration in which the working electrode is the sensor substrate. The electrodes are typically interdigitated electrodes or are a pair of metal leads separated by approximately 10–50 μm. Microfabrication of large arrays of CPs with microscale dimensions is possible using interdigitated microelectrodes (Imisides et al. 1996) created by photolithography.

Regarding polymer structure preferable for application in solid-state gas sensors, we can say that to achieve better response characteristics we should use thin films or make them porous. Many results demonstrated that conductometric gas sensors with thinner or more porous active films have higher

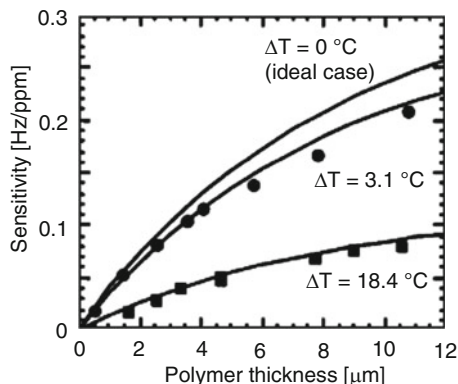


**Fig. 3.17** Measured and modeled (*solid lines*) *n*-octane sensitivity vs polymer thickness for different cantilever temperatures.  $\Delta T$  refers to ambient temperature (gas phase and sensor chip). The 150- $\mu\text{m}$ -long resonant cantilever was fabricated using CMOS technology (Reprinted with permission from Lange et al. (2002). Copyright 2002 American Chemical Society)

sensitivities (Stussi et al. 1997). Increasing the volume ratio of micropores in the film can also enhance the response (Matsuguchi et al. 2003). However, this trend is not obvious in porous films. For example, Huang et al. (2004) found, as the porosity of the film is high enough, the response of the film is insensitive to its thickness. On the other hand, as a thin film fabricated by LB technique was used as the sensing layers, the sensitivity of the sensor increased with the number of LB layer (Xie et al. 2002; Prasad et al. 2005). Maybe this effect takes place because the LB layers have too small a thickness. Due to diffusion, the sorption of analytes is not the key step in the ultrathin LB film, and the sensitivity of the device is determined by the amount of polymer. In particular, Lange et al. (2002) found that for cantilevers coated with polymer films, the sensitivity increases linearly with increasing layer thickness in the range of thin polymer layers (2–4  $\mu\text{m}$ ) and then shows saturation-like behavior at larger thickness (>4  $\mu\text{m}$ ), as is seen in Fig. 3.17. However, whatever the morphology of active layer, the response time is always decreased as the thickness of layer decreases (Xie et al. 2002; Prasad et al. 2005).

## References

- Adhikari B, Majumdar S (2004) Polymers in sensor applications. *Prog Polym Sci* 29:699–766
- Agbor NE, Petty MC, Monkman AP (1995) Polyaniline thin-films for gas-sensing. *Sens Actuators B* 28:173–179
- Agbor NE, Cresswell JP, Petty MC, Monkman AP (1997) An optical gas sensor based on polyaniline Langmuir-Blodgett films. *Sens Actuators B* 41:137–141
- Ahmad S (2009) Polymer electrolytes: characteristics and peculiarities. *Ionics* 15:309–321
- Alberti G, Casciola M (2001) Solid state protonic conductors, present main applications and future prospects. *Solid State Ionics* 145:3–16
- Al-Mashat L, Tran HD, Wlodarski W, Kaner RB, Kalantar-Zadeh K (2008) Conductometric hydrogen gas sensor based on polypyrrole nanofibers. *IEEE Sensors J* 8(4):365–370
- Anantaraman AV, Gardner CL (1996) Studies on ion-exchange membranes. I. Effect of humidity on the conductivity of Nafion. *J Electroanal Chem* 414:115–120
- Ando M, Swart C, Pringsheim E, Mirsky VM, Wolfbeis OS (2005) Optical ozone-sensing properties of poly(2-chloroaniline), poly(*N*-methylaniline) and polyaniline films. *Sens Actuators B* 108:528–534
- Angelopoulos M (2001) Conducting polymers in microelectronics. *IBM J Res Dev* 45:57–75
- Bai H, Shi G (2007) Gas sensors based on conducting polymers. *Sensors* 7:267–307
- Baller MK, Lang HP, Fritz J, Gerber C, Gimzewski JK, Drechsler U, Rothuizen H, Despont M, Vettiger PF, Battiston FM, Ramseyer JP, Fornaro P, Meyer E, Güntherodt HJ (2000) A cantilever array-based artificial nose. *Ultramicroscopy* 82:1–9

- Bartlett PN, Ling-Chung SK (1989) Conducting polymer gas sensors. Part III: results for four different polymers and five different vapors. *Sens Actuators* 20:287–292
- Bissell RA, Persaud KC, Travers P (2002) The influence of non-specific molecular partitioning of analytes on the electrical responses of conducting organic polymer gas sensors. *Phys Chem Chem Phys* 4(14):3482–3490
- Blanc JP, Derouiche N, El HA, Germain JP, Maleysson C, Robert H (1990) Study of the action of gases on a polypyrrole film. *Sens Actuators B* 1:130–133
- Bobacka J (2006) Conducting polymer-based solid-state ion-selective electrodes. *Electroanalysis* 18:7–18
- Bouchet R, Siebert E (1999) Proton conduction in acid doped polybenzimidazole. *Solid State Ionics* 118:287–299
- Bouchet R, Siebert E, Vitter G (2000) Polybenzimidazole-based hydrogen sensors. I. Mechanism of response with an E-TEK gas diffusion electrode. *J Electrochem Soc* 147:3125–3130
- Bouchet R, Rosini S, Vitter G, Siebert E (2001) Solid-state hydrogen sensor based on acid-doped polybenzimidazole. *Sens Actuators B* 76:610–616
- Breer H, Wanner I, Strotmann J (1996) Molecular genetics of mammalian olfaction. *Behav Genet* 26:209–219
- Brožová L, Holler P, Ková ová J, Stejskal J, Trchová M (2008) The stability of polyaniline in strongly alkaline and acidic aqueous media. *Polym Degrad Stab* 93:592–600
- Buchler MG, Ryan MA (1997) Temperature and humidity dependence of a polymer-based gas sensor. *Proc SPIE* 3082:40–48. <http://enose.jpl.nasa.gov/publications/sensors/97-0482.pdf>
- Cabala R, Meister V, Potje-Kamloth K (1997) Effect of composite doping on sensing properties of polypyrrole. *J Chem Soc Faraday Trans* 93:131–137
- Chandrasekhar P (ed) (1999) *Conducting polymers. Fundamentals and applications*. Kluwer, Boston, MA
- Chang SC, Stetter JR, Cha CS (1993) Amperometric gas sensors. *Talanta* 40:461–477
- Chatzandroulis S, Tsouti V, Raptis I, Goustouridis D (2011) Capacitance-type chemical sensors. In: Korotcenkov G (ed) *Chemical sensors: comprehensive sensor technologies, vol 4, Solid state devices*. Momentum Press, New York, NY, pp 229–259
- Chaubey A, Malhotra BD (2002) Mediated biosensors. *Biosens Bioelectron* 17:441–456
- Christie S, Scorsone E, Persaud K, Kvasnik F (2003) Remote detection of gaseous ammonia using the near infrared transmission properties of polyaniline. *Sens Actuators B* 90:163–169
- Colomban P (1999) Latest developments in proton conductors. *Ann Chim Sci Mater* 24:1–18
- Covington JA, Gardner JW, Briand D, de Rooij NF (2001) A polymer gate FET sensor array for detecting organic vapours. *Sens Actuators B* 77:155–162
- Covington JA, Gardner JW, Bartlett PN, Toh CS (2004) Conductive polymer gate FET devices for vapour sensing. *IEEE Proc Circ Dev Syst* 151(4):326–334
- Dai L, Soundarajan P, Kim T (2002) Sensors and sensor arrays based on conjugated polymers and carbon nanotubes. *Pure Appl Chem* 74(9):1753–1772
- Desilvestro J, Scheifele W (1993) Morphology of electrochemically prepared polyaniline. Influence of polymerization parameters. *J Mater Chem* 3(3):263–272
- Dimitrakopoulos CD, Malenfant PRL (2002) Organic thin film transistors for large area electronics. *Adv Mater* 14:99–117
- Dixit V, Misra SCK, Sharma BS (2005) Carbon monoxide sensitivity of vacuum deposited polyaniline semiconducting thin films. *Sens Actuators B* 104:90–93
- Elizalde-Torres J, Hu HL, Garcia-Valenzuela A (2004) NO<sub>2</sub>-induced optical absorbance changes in semiconducting polyaniline thin films. *Sens Actuators B* 98:218–226
- Epstein AJ, Mele EJ (eds) (2001) *Symposium proceedings on synthetic metals, 4–5 May 2000*. *Synth Met* 125:138
- Forster RJ (1998) Miniaturized chemical sensors. In: Diamond D (ed) *Principles of chemical and biological sensors*. Wiley, New York, NY, p 243
- Gardner JW (2004) Review of conventional electronic noses and their possible application to the detection of explosives. In: Gardner JW, Yinou L (eds) *Electronic noses and sensors for the detection of explosives*. Kluwer, Dordrecht, pp 1–28
- Gardner JW, Bartlett PN (1995) Application of conducting polymer technology in microsystems. *Sens Actuators A* 51:57–66
- Geng L, Wang SR, Zhao YQ, Li P, Zhang SM, Huang WP, Wu SH (2006) Study of the primary sensitivity of polypyrrole/r-Fe<sub>2</sub>O<sub>3</sub> to toxic gases. *Mater Chem Phys* 99:15–19
- Gerard M, Chaubey A, Malhotra BD (2002) Application of conducting polymers to biosensors. *Biosens Bioelectron* 17:345–359
- Gilch HG, Wheelwright WL (1966) Polymerization of  $\alpha$ -halogenated p-xylenes with base. *J Polym Sci A* 4:1337–1349
- Gonzalez-Rodriguez D, Schenning APHJ (2011) Hydrogen-bonded supramolecular  $\pi$ -functional materials. *Chem Mater* 23:310–325
- Grate JW, Abraham MH (1991) Solubility interactions and the selection of sorbent coating materials for chemical sensors and arrays. *Sens Actuators B* 3:85–111

- Grate JW, Abraham MH (1993) Solubility interactions and the design of chemically selective sorbent coatings for chemical sensors and arrays. *Sens Actuators B* 3:85–111
- Grate JW, Patrash SJ, Abraham MH (1995) Method for estimating polymer-coated acoustic wave vapor sensor responses. *Anal Chem* 67:2162–2169
- Grate JW, Abraham MH, McGill RA (1997) Sorbent polymer materials for chemical sensors and arrays. In: Kress-Rogers E (ed) *Handbook of biosensors and electronic noses: medicine, food and the environment*. CRC, Boca Raton, FL, pp 593–612
- Gustafsson G, Lundrom I, Liedberg B, Wu CR, Inganas O, Wennerstrom O (1989) The interaction between ammonia and polypyrrole. *Synth Met* 31:163
- Ha S, Kim YS, Yang Y, Kim YJ, Cho S, Yang H, Kim YT (2005) Integrated and microheater embedded gas sensor array based on the polymer composites dispensed in micromachined wells. *Sens Actuators B* 105:549–555
- Han CC, Elsenbaumer RL (1989) Protonic acids: general applicable dopants for conducting polymers. *Synth Met* 30:123–131
- Hao QL, Wang X, Lu LD, Yang XJ, Mirsky VM (2005) Electropolymerized multilayer conducting polymers with response to gaseous hydrogen chloride. *Macromol Rapid Commun* 26:1099–1103
- Harsanyi G (1995) Polymeric sensing films: new horizons in sensorics? *Sens Actuators A* 46–47:85–88
- Hatfield JV, Neaves P, Hicks PJ, Persaud K, Travers P (1994) Towards an integrated electronic nose using conducting polymer sensors. *Sens Actuators B* 18:221–228
- Heck RF, Nolley JP Jr (1972) Palladium-catalyzed vinylic hydrogen substitution reactions with aryl, benzyl, and styryl halides. *J Org Chem* 37(14):2320–2322
- Heeger AJ (2001) Semiconducting and metallic polymers: the fourth generation of polymeric materials (Nobel lecture). *Angew Chem Int Ed* 40:2591–2611
- Heeger AJ (2002) Semiconducting and metallic polymers: the fourth generation of polymeric materials. *Synth Met* 125:23–42
- Hierlemann A, Lange D, Hagleitner C, Kerness N, Koll A, Brand O, Baltes H (2000) Application-specific sensor systems based on CMOS chemical microsensors. *Sens Actuators B* 70:2–11
- Hirao T (2002) Conjugated systems composed of transition metals and redox-active  $\pi$ -conjugated ligands. *Coord Chem Rev* 226:81–91
- Hodgins DM (1995) The development of an electronic ‘nose’ for industrial and environmental applications. *Sens Actuators B* 27:255–258
- Hodgson AWE, Jacquinet P, Jordan LR, Hauser PC (1999a) Amperometric gas sensors of high sensitivity. *Electroanalysis* 11:782–787
- Hodgson AWE, Jacquinet P, Hauser PC (1999b) Electrochemical sensor for the detection of SO<sub>2</sub> in the low-ppb range. *Anal Chem* 71:2831–2837
- Houser EJ, Mlsna TE, Nguyen VK, Chung R, Mowery EL, McGill RA (2001) Rational materials design of sorbent coatings for explosives: applications with chemical sensors. *Talanta* 54:469–485
- Hu H, Trejo M, Nicho ME, Saniger JM, Garcia-Valenzuela A (2002) Adsorption kinetics of optochemical NH<sub>3</sub> gas sensing with semiconductor polyaniline films. *Sens Actuators B* 82:14–23
- Huang JX, Virji S, Weiller BH, Kaner RB (2003) Polyaniline nanofibers: facile synthesis and chemical sensors. *J Am Chem Soc* 125:314–315
- Huang J, Virji S, Weiller BH, Kaner RB (2004) Nanostructured polyaniline sensors. *Chem Eur J* 10:1315–1319
- Imisides MD, John R, Wallace GG (1996) Microsensors based on conducting polymers. *Chemtech* 26:19–25
- Jain S, Chakane S, Samui AB, Krishnamurthy VN, Bhoraskar SV (2003) Humidity sensing with weak acid-doped polyaniline and its composites. *Sens Actuators B* 96:124–129
- James D, Scott SM, Ali Z, O’Hare WT (2005) Chemical sensors for electronic nose systems. *Microchim Acta* 149:1–17
- Janata J, Huber RJ (eds) (1985) *Solid state chemical sensors*. Academic, New York, NY
- Janata J, Josowicz MA (1997) A fresh look at some old principles: the Kelvin probe and the Nernst equation. *Anal Chem* 69:293–296
- Janata J, Josowicz M (2003) Conducting polymers in electronic chemical sensors. *Nat Mater* 2:19–24
- Jesenius H, Thaysen J, Rasmussen AA, Veje LH, Hansen O, Boisen A (2000) A microcantilever-based alcohol vapor sensor-application and response model. *Appl Phys Lett* 76:2615–2617
- Jiang L, Jun H-K, Hoh Y-S, Lim J-O, Lee D-D, Huh J-S (2005) Sensing characteristics of polypyrrole–poly(vinyl alcohol) methanol sensors prepared by in situ vapor state polymerization. *Sens Actuators B* 105:132–137
- Jin Z, Su YX, Duan YX (2001) Development of a polyaniline-based optical ammonia sensor. *Sens Actuators B* 72:75–79
- Josowicz M (1995) Applications of conducting polymers in potentiometric sensors. *Analyst* 120:1019–1024
- Josowicz M, Janata J (1986) Suspended gate field effect transistors modified with polypyrrole as alcohol sensor. *Anal Chem* 58(3):514–517
- Kaplan G, Brahm R (1998) The how and why of electronic noses. *IEEE Spectrum* September:22–31

- Kemp NT, Kaiser AB, Trodahl HJ, Chapman B, Buckley RG, Partridge AC, Foot PJS (2006) Effect of ammonia on the temperature-dependent conductivity and thermopower of polypyrrole. *J Polym Sci B* 44:1331–1338
- Kim YS, Ha S-C, Yang Y, Kim YY, Cho SM, Yang H, Kim YT (2005) Portable electronic nose system based on the carbon black–polymer composite sensor array. *Sens Actuators B* 108:285–291
- Kitsara M, Goustouridis D, Chatzandroulis S, Chatzichristidi M, Raptis I, Ganetsos T, Igreja R, Dias CJ (2007) Single chip interdigitated electrode capacitive chemical sensor arrays. *Sens Actuators B* 127:186–192
- Knake R, Jacquinet P, Hodgson AWE, Hauser PC (2005) Amperometric sensing in the gas-phase. *Anal Chim Acta* 549:1–9
- Kondratowicz B, Narayanaswamy R, Persaud KC (2001) An investigation into the use of electrochromic polymers in optical fibre gas sensors. *Sens Actuators B* 74:138–144
- Krivan E, Visy C, Dobay R, Harsanyi G, Berkesi O (2000) Irregular response of the polypyrrole films to H<sub>2</sub>S. *Electroanalysis* 12:1195–1200
- Kumar D, Sharma RC (1998) Advances in conductive polymers. *Eur Polym J* 34(8):1053–1060
- Kummer AM, Hierlemann A (2006) Configurable electrodes for capacitive-type sensors and chemical sensors. *IEEE Sensors J* 6(1):3–10
- Kummer AM, Hierlemann A, Baltes H (2004) Tuning sensitivity and selectivity of complementary metal oxide semiconductor based capacitive chemical microsensors. *Anal Chem* 76:2470–2477
- Kummer AM, Burg TP, Hierlemann A (2006) Transient signal analysis using complementary metal oxide semiconductor capacitive chemical microsensors. *Anal Chem* 78:279–290
- Kurzawski P, Hagleitner C, Hierlemann A (2006) Detection and discrimination capabilities of a multitransducer single-chip gas sensor system. *Anal Chem* 78:6910–6920
- Lange D, Hagleitner C, Hierlemann A, Brand O, Baltes H (2002) Complementary metal oxide semiconductor cantilever arrays on a single chip: mass-sensitive detection of volatile organic compounds. *Anal Chem* 74:3084–3095
- Lange U, Roznyatovskaya NV, Mirsky VM (2008) Conducting polymers in chemical sensors and arrays. *Anal Chim Acta* 614:1–26
- Langmaier J, Opekar F, Samec Z (1997) Amperometric solid-state NO<sub>2</sub> sensor based on plasticized PVC matrix containing a hydrophobic electrolyte. *Sens Actuators B* 41:1–6
- Leclerc M (1999) Optical and electrochemical transducers based on functionalized conjugated polymers. *Adv Mater* 11:1491–1498
- Leuninger J, Wang C, Soczka-Guth T, Enkelmann V, Pakula T, Müllen K (1998) Poly(phenylene sulfide-phenyleneamine) (PPSA): the first hybrid structure of poly(phenylene sulfide) and polyaniline. *Macromolecules* 31:1720–1727
- Li D, Jiang Y, Wu Z, Chen X, Li Y (2000) Self-assembly of polyaniline ultrathin films based on doping-induced deposition effect and applications for chemical sensors. *Sens Actuators B* 66:125–127
- Li G, Josowicz M, Janata J (2002) Electrochemical assembly of conducting polymer films on an insulating surface. *Electrochem Solid State* 5:5–8
- Li B, Santhanam S, Schultz L, Jeffries-EL M, Iovu MC, Sauve G, Cooper J, Zhang R, Revelli JC, Kusne AG (2007) Inkjet printed chemical sensor array based on polythiophene conductive polymers. *Sens Actuators B* 123:651–660
- Liu DM, Aguilar-Hernandez J, Potje-Kamloth K, Liess HD (1997) A new carbon monoxide sensor using a polypyrrole film grown on an interdigital-capacitor substrate. *Sens Actuators B* 41:203–206
- Liu K, Li Y, Honga L, Yang M (2008) Humidity sensitive properties of an anionic conjugated polyelectrolyte. *Sens Actuators B* 129:24–29
- Lu X, Wu S, Wang L, Su Z (2005) Solid-state amperometric hydrogen sensor based on polymer electrolyte membrane fuel cell. *Sens Actuators B* 107:812–817
- Lukow SR, Kounaves SP (2005) Analysis of simulated Martian regolith using an array of ion selective electrodes. *Electroanalysis* 17:1441–1449
- Macagnano A, Zampetti E, Pantalei S, De Cesare F, Bearzotti A, Persaud KC (2011) Nanofibrous PANI-based conductive polymers for trace gas analysis. *Thin Solid Films* 520:978–985
- MacDiarmid AG (2002) Synthetic metals: a novel role for organic polymers. *Synth Met* 125:11–22
- Maffei N, Kuriakose AK (2004) A solid-state potentiometric sensor for hydrogen detection in air. *Sens Actuators B* 98:73–76
- Manoli K, Goustouridis D, Chatzandroulis S, Raptis I, Valamontes ES, Sanopoulou M (2006) Vapor sorption in thin supported polymer films studied by white light interferometry. *Polymer* 47:6117–6122
- Matsuguchi M, Okamoto A, Sakai Y (2003) Effect of humidity on NH<sub>3</sub> gas sensitivity of polyaniline blend films. *Sens Actuators B* 94:46–52
- Maute M, Raible S, Prins FE, Kern DP, Ulmer H, Weimar U, Göpel W (1999) Detection of volatile organic compounds (VOCs) with polymer-coated cantilevers. *Sens Actuators B* 58:505–511
- McCullough RD (1998) The chemistry of conducting polythiophenes. *Adv Mater* 10:93–116
- McQuade DT, Pullen AE, Swager TM (2000) Conjugated polymer-based chemical sensors. *Chem Rev* 100:2537–2574
- Michalska A (2006) Optimizing the analytical performance and construction of ion-selective electrodes with conducting polymer-based ion-to-electron transducers. *Anal Bioanal Chem* 384:391–406

- Michalska A, Lewenstam A (2000) Potentiometric selectivity of p-doped polymer films. *Anal Chim Acta* 406:159–169
- Mika M, Paidar M, Klapste B, Masinova M, Bouzek K, Vondrak J (2007) Hybrid inorganic–organic proton conducting membranes for fuel cells and gas sensors. *J Phys Chem Sol* 68:775–779
- Milella E, Penza M (1998) SAW gas detection using Langmuir–Blodgett polypyrrole films. *Thin Solid Films* 329:694–697
- Miller LL, Bankers JS, Schmidt AJ, Boyd DC (2000) Organic vapors, organic polymers and electrical conductivity. *J Phys Org Chem* 13:808–815
- Misra SCK, Mathur P, Srivastava BK (2004) Vacuum-deposited nanocrystalline polyaniline thin film sensors for detection of carbon monoxide. *Sens Actuators A* 114:30–35
- Mulchandani AK, Wang CL (1996) Bienzyme sensors based modified electrodes. *Electroanalysis* 8:414–419
- Muller JBA, Smith CE, Newton MI, Percival CJ (2011) Evaluation of coated QCM for the detection of atmospheric ozone. *Analyst* 136:2963–22968
- Nalwa HS (ed) (1996) Handbook of organic conductive molecules and polymers, vol 2 and 3. Wiley, New York, NY
- Nalwa HS (ed) (1997) Handbook of organic conductive molecules and polymers, vol 4. Wiley, New York, NY
- Nguyen VC, Potje-Kamloth K (1999) Electrical and chemical sensing properties of doped polypyrrole/gold Schottky barrier diodes. *Thin Solid Films* 338:142–148
- Nikolova V, Nikolov I, Andreev P, Najdenov V, Vitanov T (2000) Tungsten carbide-based electrochemical sensors for hydrogen determination in gas mixtures. *J Appl Electrochem* 30:705–710
- Ogura K, Saino T, Nakayama M, Shiigi H (1997) The humidity dependence of the electrical conductivity of a soluble polyaniline-poly(vinyl alcohol) composite film. *J Mater Chem* 7:2363–2366
- Opekar F (1992) An amperometric solid-state sensor for nitrogen dioxide based on a solid polymer electrolyte. *Electroanalysis* 4:133–138
- Opekar F, Stulik K (1999) Electrochemical sensors with solid polymer electrolytes. *Anal Chim Acta* 385:151–162
- Opekar F, Svozil D (1995) Electric resistance in a Nafion membrane exposed to air after a step change in the relative humidity. *J Electroanal Chem* 385:269–271
- Osada Y, De Rossi DE (eds) (2000) Polymer sensors and actuators. Springer, Berlin
- Partridge AC, Harris PD, Andrews MK (1996) High sensitivity conducting polymer sensors. *Analyst* 121:1349–1353
- Pejčić B, Eadington P, Ross A (2007) Environmental monitoring of hydrocarbons: a chemical sensor perspective. *Environ Sci Technol* 41(18):6333–6342
- Penza M, Cassano G (2000) Relative humidity sensing by PVA coated dual resonator SAW oscillator. *Sens Actuators B* 68:300–306
- Persaud KC (2005) Polymers for chemical sensing. *Mater Today* April:28–44
- Polk BJ, Potje-Kamloth K, Josowicz M, Janata J (2002) Role of protonic and charge transfer doping in solid-state polyaniline. *J Phys Chem* 106:11457–11462
- Posudievsky OY, Konoschuk NV, Kukla AL, Pavluchenko AS, Shirshov YM, Pokhodenko VD (2011) Comparative analysis of sensor responses of thin conducting polymer films to organic solvent vapors. *Sens Actuators B* 151:351–359
- Potje-Kamloth K (2001) Conducting polymer-based Schottky barrier and heterojunction diodes and their sensor application. In: Nalwa HS (ed) Handbook of surfaces and interfaces of materials, vol 5. Academic, San Diego, CA, pp 445–494
- Potyrailo RA (2006) Polymeric sensor materials: toward an alliance of combinatorial and rational design tools? *Angew Chem Int Ed* 45:702–723
- Prasad GK, Radhakrishnan TP, Kumar DS, Krishna MG (2005) Ammonia sensing characteristics of thin film based on polyelectrolyte templated polyaniline. *Sens Actuators B* 106:626–631
- Pron A, Rannou P (2002) Processible conjugated polymers: from organic semiconductors to organic metals and superconductors. *Prog Polym Sci* 27:135–190
- Rahman MA, Kumar P, Park D-S, Shim Y-B (2008) Electrochemical sensors based on organic conjugated polymers. *Sensors* 8:118–141
- Ramesh C, Velayutham G, Murugesan N, Ganesan V, Dhathathreyan KS, Periaswami G (2003) An improved polymer electrolyte-based amperometric hydrogen sensor. *J Solid State Electrochem* 7:511–516
- Ramesh C, Velayutham G, Murugesan N, Ganesan V, Manivannan V, Periaswami G (2004) Studies on modified anode polymer hydrogen sensor. *Ionics* 10:50–55
- Ramesh C, Murugesan N, Krishnaiah MV, Ganesan V, Periaswami GJ (2008) Improved Nafion-based amperometric sensor for hydrogen in argon. *J Solid State Electrochem* 12(9):1109–1116
- Reemts J, Parisi J, Schlettwein D (2004) Electrochemical growth of gas-sensitive polyaniline thin films across an insulating gap. *Thin Solid Films* 466:320–325
- Robeson LM (1999) Polymer membranes for gas separation. *Curr Opin Solid State Mater Sci* 4(6):549–552
- Rosini S, Siebert E (2005) Electrochemical sensors for detection of hydrogen in air: model of the non-Nernstian potentiometric response of platinum gas diffusion electrodes. *Electrochim Acta* 50:2943–2953



- Ruangchuay L, Sirivat A, Schwank J (2004) Electrical conductivity response of polypyrrole to acetone vapor: effect of dopant anions and interaction mechanisms. *Synth Met* 140:15–21
- Sakthivel M, Weppner W (2006a) Response behaviour of a hydrogen sensor based on ionic conducting polymer-metal interfaces prepared by the chemical reduction method. *Sensors* 6:284–297
- Sakthivel M, Weppner W (2006b) Development of a hydrogen sensor based on solid polymer electrolyte membranes. *Sens Actuators B* 113:998–1004
- Samec Z, Opekar F, Crijns GJEF (1995) Solid-state hydrogen sensor based on a solid-polymer electrolyte. *Electroanalysis* 7:1054–1058
- Šeděnková I, Trchová M, Stejskal J (2008a) Thermal degradation of polyaniline films prepared in solutions of strong and weak acids and in water – FTIR and Raman spectroscopic studies. *Polym Degrad Stab* 93:2147–2157
- Šeděnková I, Prokeš J, Trchová M, Stejskal J (2008b) Conformational transition in polyaniline films – spectroscopic and conductivity studies of ageing. *Polym Degrad Stab* 93:428–435
- Segal E, Tchoudakov R, Narkis M, Siegmann A (2002) Thermoplastic polyurethane-carbon black compounds: structure, electrical conductivity and sensing of liquids. *Polym Eng Sci* 42:2430–2439
- Shi M, Anson FC (1996) Effects of hydration on the resistances and electrochemical responses of “Nafion” coatings on electrodes. *J Electroanal Chem* 415:41–46
- Skotheim TA, Reynolds JR (2007) *Handbook of conducting polymers*, 3rd edn. CRC/Taylor & Francis, Boca Raton, FL
- Skotheim TA, Elsenbaumer R, Reynolds JR (eds) (1998) *Handbook of conducting polymers*, 2nd edn. Dekker, New York, NY
- Slater JM, Paynter J (1994) Prediction of gas sensor response using basic molecular parameters. *Analyst* 119:191–195
- Slater JM, Paynter J, Watt EJ (1993) Multi-layer conducting polymer gas sensor arrays for olfactory sensing. *Analyst* 118:379–384
- Snopok BA, Kruglenko IV (2005) Nonexponential relaxations in sensor arrays: forecasting strategy for electronic nose performance. *Sens Actuators B* 106:101–113
- Sondheimer SJ, Bunce NJ, Fyfe CA (1986) Structure and chemistry of Nafion-H: a fluorinated sulfonic acid polymer. *J Macromol Sci Rev Macromol Chem C* 26:353–413
- Stetter JR, Li J (2008) Amperometric gas sensors—a review. *Chem Rev* 108:352–366
- Stussi E, Stella R, De Rossi D (1997) Chemoresistive conducting polymer-based odour sensors: influence of thickness changes on their sensing properties. *Sens Actuators B* 43:180–185
- Sundmacher K, Rihko-Struckmann LK, Galvita V (2005) Solid electrolyte membrane reactors – status and trends. *Catal Today* 104:185–199
- Tan CK, Blackwood DJ (2000) Interactions between polyaniline and methanol vapour. *Sens Actuators B* 71:184–191
- Thomas SW III, Joly GD, Swager TM (2006) Chemical sensors based on amplifying fluorescent conjugated polymers. *Mater Sci Eng R* 52:49–91
- Tierney MJ (1996) Practical examples of polymer-based chemical sensors, chapter 13. In: Taylor RF, Schultz JS (eds) *Handbook of chemical and biological sensors*. IOP Publishing, Bristol
- Toal SJ, Trogler WC (2006) Polymer sensors for nitroaromatic explosives detection. *J Mater Chem* 16:2871–2883
- Torsi L, Tanese MC, Cioffi N, Gallazzi MC, Sabbatini L, Zambonin PG, Raos G, Meille SV, Giangregorio MM (2003) Side-chain role in chemically sensing conducting polymer field-effect transistors. *J Phys Chem B* 107(31):7589–7594
- Torsi L, Tanese MC, Cioffi N, Gallazzi MC, Sabbatini L, Zambonin PG (2004) Alkoxy-substituted polyterthiophene thin-film-transistors as alcohol sensors. *Sens Actuators B* 98:204–207
- Vaihinger S, Goepel W, Stetter JR (1991) Detection of halogenated and other hydrocarbons in air: response functions of catalyst/electrochemical sensor systems. *Sens Actuators B* 4:337–343
- Van CN, Potje-Kamloth K (2001) Electrical and NO<sub>x</sub> gas sensing properties of metallophthalocyanine-doped polypyrrole/silicon heterojunctions. *Thin Solid Films* 392:113–121
- Vercelli B, Zecchin S, Comisso N, Zotti G, Berlin A, Dalcanale E, Groenendaal LB (2002) Solvoconductivity of polyconjugated polymers: the roles of polymer oxidation degree and solvent electrical permittivity. *Chem Mater* 14:4768–4774
- Virji S, Huang JX, Kaner RB, Weiller BH (2004) Polyaniline nanofiber gas sensors: examination of response mechanisms. *Nano Lett* 4:491–496
- Virji S, Kaner RB, Weiller BH (2006) Hydrogen sensors based on conductivity changes in polyaniline nanofibers. *J Phys Chem B* 110:22266–22270
- Waghuley SA, Yenorkar SM, Yawale SS, Yawale SP (2008) Application of chemically synthesized conducting-polymer polypyrrole as a carbon dioxide gas sensor. *Sens Actuators B* 128:366–373
- Wallace GG, Spinks GM, Teasdale PR (1997) *Conductive electroactive polymers*. Technomic, Lancaster, PA
- Walton DJ (1990) Electrically conducting polymers. *Mater Des* 11:142–152
- Wang PC, Huang Z, MacDiarmid AG (1999) Critical dependency of the conductivity of polypyrrole and polyaniline films on the hydrophobicity/hydrophilicity of the substrate surface. *Synth Met* 101:852–853

- Wittig G, Schöllkopf U (1954) Über Triphenyl-phosphin-methylene als olefinbildende Reagenzien I. *Chem Ber* 87(9):1318–1330
- Wroblewski W, Dybko A, Malinowska E, Brzozka Z (2004) Towards advanced chemical microsensors—an overview. *Talanta* 63:33–39
- Xie D, Jiang YD, Pan W, Li D, Wu ZM, Li YR (2002) Fabrication and characterization of polyaniline-based gas sensor by ultra-thin film technology. *Sens Actuators B* 81:158–164
- Yasuda A, Doi K, Yamaga N, Fujioka T, Kusanagi S (1992) Mechanism of the sensitivity of the planar CO sensor and its dependency on humidity. *J Electrochem Soc* 139:3224–3229
- Zawodzinski TA, Springer TE, Uribe F, Gottesfeld S (1993) Characterization of polymer electrolytes for fuel cell applications. *Solid State Ionics* 60:199–211
- Zhang S, Lii F, Gao L, Ding L, Fang Y (2007) Fluorescent sensors for nitroaromatic compounds based on monolayer assembly of polycyclic aromatics. *Langmuir* 23:1584–1590
- Zheng W, Min Y, MacDiarmid AG, Angelopoulos M, Liao Y-H, Epstein AJ (1997) Effect of organic vapors on the molecular conformation of nondoped polyaniline. *Synth Met* 84:63–64

## Chapter 4

# Thin Metal Films

### 4.1 Thin Metal Films in Gas Sensors

Thin metal films have a long history in gas sensor applications, because all types of gas sensors include metal films playing the role of either electrode or sensing material. Metal films such as group VIII transition metals, nickel, palladium, and platinum nanostructured films are used for hydrogen detection in SAW devices (Jakubik and Urbanczyk 2005), work-function-based sensors (Dus et al. 2005), resistance-based sensors (Pundt 2004), optical sensors (Villatoro and Monzon-Hernandez 2005), and fiber-optic sensors (Zhao et al. 2006). Sensors with either palladium or palladium alloy films—the best for sensor applications—have the ability to detect hydrogen below its explosive limits. The high affinity of palladium nanostructured films toward hydrogen changes the electrical conductivity of metals upon adsorption of molecules together with the optical and mechanical properties of the film, including reflectance and the palladium lattice parameter, due to formation of hydrides of palladium at room temperature. Therefore, for example, optical detection of hydrogen typically involves measurement of the optical transmission or reflectivity of a tin-palladium film, either via conventional transmission (reflectivity) measurements or the more sensitive but more expensive and complicated surface plasmon resonance or interferometric measurements (Villatoro and Monzon-Hernandez 2005; Hubert et al. 2011).

The resistance change of palladium film in  $H_2$  atmosphere takes place because palladium hydride has a higher electrical resistance compared to palladium. The following may be the explanation of the observed sensitivity to hydrogen (Noh et al. 2011). When a palladium film is exposed to  $H_2$ , hydrogen molecules are adsorbed onto the palladium surface and dissociate into hydrogen atoms (Kay et al. 1986). These hydrogen atoms diffuse until they occupy the interstitial sites of the palladium lattice, causing a certain amount of lattice expansion (Smith and Otterson 1970; Sakamoto et al. 1996). In particular, in  $PdH_x$  the hydrogen atoms occupy octahedral sites in the cubic close-packed palladium lattice (see Fig. 4.1). As there are four palladium atoms and four octahedral interstitial sites per unit cell of palladium, the maximum theoretical composition corresponds to  $PdH$  ( $x=1$ ). The diffusion generally takes place through high-diffusivity paths such as grain boundaries and dislocations or via a vacancy exchange mechanism (Smith and Otterson 1970; Sakamoto et al. 1996; Pundt and Kirchheim 2006; Fukai and Sugimoto 2007), resulting in the defect density dependence of  $H_2$  intake. The absorbed hydrogen atoms interact with palladium atoms to form palladium hydrides and increase the frequency of scattering events

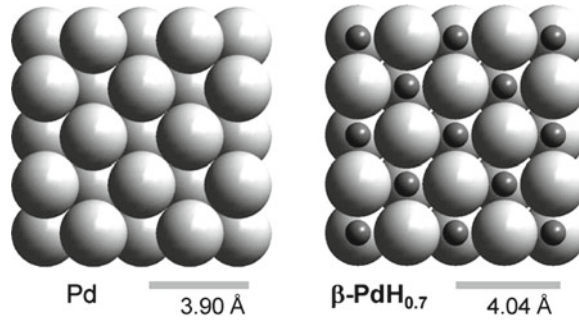


**Fig. 4.1** Palladium swelling due to hydrogen dissolution. Comparison between two extremes: {100} surfaces of fcc-Pd (left) and  $\beta$ -PdH<sub>0.7</sub> (right). The bars represent the shortest distances between two palladium atoms corresponding to the lattice parameters. Palladium atoms ( $r_{\text{at}} = 120$  pm) are shown as large circles, hydrogen atoms ( $r_{\text{at}} = 53$  pm) as small circles (Reprinted with permission from Gurlo and Clarke (2011). Copyright 2011 Wiley)

of charge carriers, which directly leads to the resistance increase of the palladium. In this context, it is expected that the magnitude of resistance increase is proportional to the atomic fraction of absorbed hydrogen atoms to palladium atoms, as expressed by the Sieverts' law below (Sieverts 1929):

$$\text{Sensitivity} \propto \frac{[\text{H}]}{[\text{Pd}]} = \frac{1}{K_s} (p\text{H}_2)^{1/2}, \quad (4.1)$$

where [H] and [Pd] are the respective concentrations of hydrogen atoms and palladium atoms in the Pd–H system,  $K_s$  is the Sieverts' constant, and  $p\text{H}_2$  is the  $\text{H}_2$  partial pressure in the environment (Sieverts 1929; Lewis 1967; Mueller et al. 1968). Sieverts' law refers to the bulk Pd–H system in the isothermal state. According to Eq.(4.1), the resistance change with respect to a reference value, termed sensitivity, is proportional to the relative hydrogen concentration in the solid state, which is correlated with the square root of the hydrogen partial pressure in the gas phase. From this equation it is inferred that the resistance change on exposure to  $\text{H}_2$  is determined by the  $\text{H}_2$  flux impinging the palladium surface, number of hydrogen accommodation sites, and the hydrogen diffusion rate in the palladium. It is important to note that, according to Kay et al. (1986), the hydrogen absorption rate of palladium is limited by the diffusion process of hydrogen atoms in the bulk rather than the chemisorption of  $\text{H}_2$  molecules on the surface of the palladium.

Typically metallic resistor sensors are fabricated by deposition of a film of metal on a substrate (e.g., silicon) between two electrical contacts. A low-cost, thick-film palladium resistive sensor measures hydrogen concentration in the range 0.5–30% at temperatures 0–200 °C (Hoffheins et al. 1999; Ravi Prakash et al. 2007; Hubert et al. 2011). Detection is selective to hydrogen, but the sensor can be poisoned by gases like CO,  $\text{SO}_2$ , and  $\text{H}_2\text{S}$ . A hydrogen sensor comprising a thin-film Pd–Ni (Hughes and Schubert 1992; Lee et al. 2010a) alloy has also been reported and claims a wide measuring range of 0.1–100%. Typical operating characteristics of palladium and Pd–Ni  $\text{H}_2$  sensors are shown in Fig. 4.2. Lee et al. (2010b) found that the addition of nickel decreased the response time as well.

According to Drake et al. (2007), the removal of adsorbed hydrogen gas molecules on the palladium layer is the most important drawback of the palladium-based hydrogen sensors. It was established that metal palladium could absorb large amounts of hydrogen gas forming Pd–H alloy. A heating arrangement is required in order to avoid the  $\text{H}_2$  association with palladium.

Schottky barrier, metal oxide semiconductor (MOS), and field-effect transistors (MOSFETs) sensors are other types of gas sensor which involve metal films. These types of sensors were pioneered by Lundstrom et al. (1975). Besides silicon, compound semiconductors such as GaAs, InP, GaN,  $\text{Ga}_2\text{O}_3$ , and SiC have been alternatively employed as substrate materials for the above-mentioned

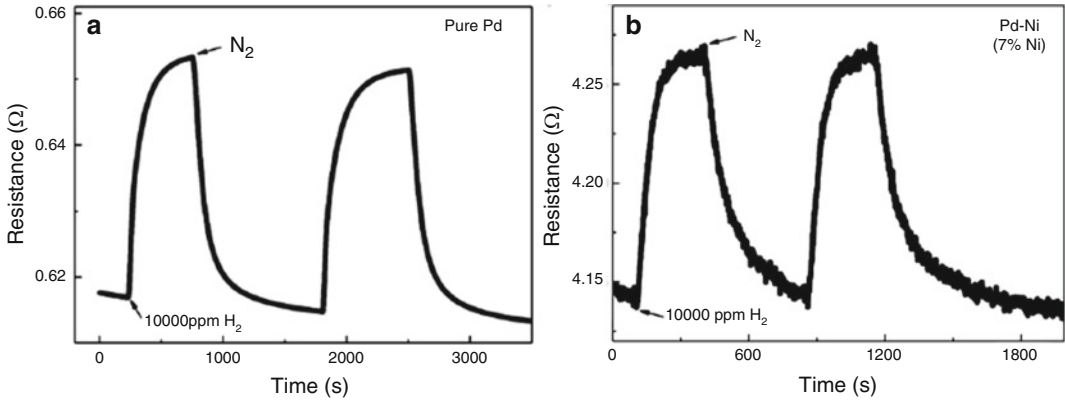
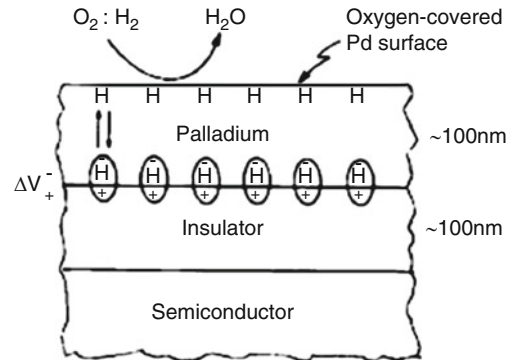


**Fig. 4.2** Plots of real-time electrical resistance responses after exposure to 1%  $H_2$  for pure palladium (a) and Pd–Ni (7% Ni) (b) alloy sensors, respectively, at room temperature. The measurement chamber had a volume of 250 mL (Reprinted with permission from Lee et al. (2010a). Copyright 2010 Elsevier)

**Fig. 4.3** Mechanism of MOSFET operation in a hydrogen atmosphere (Reprinted with permission from Lundstrom et al. (2007). Copyright 2007 Elsevier)



hydrogen sensors (Chen and Chou 2003; Trinchi et al. 2003). GaN,  $Ga_2O_3$ , and SiC have a wide bandgap, and hence operating temperatures up to 900 °C are achievable, as compared to silicon substrates, for which operating temperatures are limited to 250 °C (Trinchi et al. 2003). The basic theory regarding a gas FET or MOS capacitor with a palladium electrode (or similar catalytic metal, such as platinum), sensitivity to hydrogen is by a modulation in the flat band potential. If we consider a gas FET with a palladium-gate film ( $d \sim 100$  nm), hydrogen gas molecules are absorbed at the surface of the palladium by disassociating into atomic hydrogen. These atoms diffuse through the metal and absorb on the inner surface of the gate insulator junction, where they become polarized as shown in Fig. 4.3. This dipole layer corresponds to a measurable voltage change,  $\Delta V$ , which is added to the externally applied voltage. In the above-mentioned hydrogen sensors, the key role is played by the metallization, mostly belonging to the platinum group metals (palladium and platinum), which ensures the catalytic dissociation of molecular hydrogen into hydrogen atoms. It should be noted that the semiconducting substrate in such devices plays an auxiliary role.

Since the response of a hydrogen sensor is mainly governed by the hydrogen adsorption reaction on the palladium-semiconductor interface, the decrease in film thickness would lead to increased response and recovery rates. It was established that such a device with 10–100-nm thick palladium layer could easily detect 10 ppm of hydrogen in air in the range 27–300 °C (Lundstrom et al. 1975; Choi et al. 1986).

Palladium- and platinum-based Schottky diodes, MOS sensors, and FET sensors also respond to hydrogen-containing molecules such as hydrocarbons, provided that the molecules are also dissociated on the catalytic metal surface (Trinchi et al. 2003). It was shown that, besides hydrogen, palladium- and iridium-based sensors can be used for detection of various specific gases, for example, ammonia, carbon monoxide, and organic vapors such as ethanol (Lundstrom et al. 1993). Oxygen atoms and  $\text{NO}_x$  (Tuyen et al. 2002) are also dissociated on the catalytic metal surface. Water formation with oxygen atoms from oxygen-containing molecules consumes hydrogen and therefore decreases the sensor response. In other words, catalytic metal gates have a direct response to hydrogen and hydrocarbons as well as an indirect response to other gases, for example oxygen molecules, the effect of which is to decrease the direct response.

Optical surface plasmon resonance gas sensors also include a metal layer that plays a significant role in sensing effects, and, therefore, careful selection of the metal used is an important step in SPR-based sensor design. Detailed analyses of metals acceptable for design of SPR sensors were carried by Stewart et al. (2008) and by Kashyap and Nemova (2009). According to Kashyap and Nemova (2009), for metallic coating on a prism base or fiber core, mainly either silver or gold is used. The sharpness of the resonance curve depends on the imaginary part of the dielectric constant of the metal. Silver, having a larger value of the imaginary part of the dielectric constant, shows narrower width of the SPR curve, causing the higher signal-to-noise ratio (SNR) or detection accuracy. On the other hand, the shift of the resonance curve depends on the real part of the dielectric constant of the metal. The real part of the dielectric constant is larger for gold than for silver, and, hence, gold demonstrates a higher shift of resonance parameter in response to a change in the refractive index of the sensing layer. The chemical stability of silver is poor due to its tendency to oxidize. The oxidation of silver occurs as soon as it is exposed to air and especially to water, which makes it difficult to obtain a reproducible result, and, hence, the sensor remains unreliable for practical applications. Treatment of the silver surface with a thin and dense cover is required. In this regard, a new structure of resonant metal film based on bimetallic layers (with gold as the outer layer) on a prismatic base with an angular interrogation method has been reported (Zynio et al. 2002; Sharma and Gupta 2007). The structure displayed a large shift of resonance angle as gold film and also showed a narrower resonance curve as silver film along with protecting the silver film against oxidation. Other metals, such as copper and aluminum, can also be used for SPR sensors (Kashyap and Nemova 2009). However, copper has some of the same limitations as silver. It is chemically vulnerable to oxidation and corrosion, so its protection is required for a stable sensing application. The application of aluminum is limited by its low sensitivity (Sharma and Gupta 2007).

It was found that structural changes due to the interaction of  $\text{H}_2$  with palladium induce a change in its optical as well as its electrical properties. In particular, Fedtke et al. (2004) have found that on exposure to  $\text{H}_2$  a reversible increase in the optical transmittance of palladium in the visible region takes place [the opposite effect has also been observed in the case of extremely thin films of palladium (Wang et al. 2001)]. As was shown before, the hydration of palladium leads to crystallographic changes associated with an increment in lattice parameters. The palladium film consequently expands, and the volume density of free electrons consequently decreases, which cause reduction of both the real and imaginary parts of the palladium complex refractive index (Avila et al. 2010). Bévenot et al. (2000) proposed a simple empirical equation to describe this effect, in which the complex permittivity of the  $\text{PdH}_x$  film,  $\epsilon_{\text{PdH}_x}$ , is expressed as

$$\epsilon_{\text{PdH}_x} = h \cdot \epsilon_{\text{Pd}}, \quad (4.2)$$

where  $\epsilon_{\text{Pd}}$  is the complex permittivity of the hydrogen-free palladium film and  $h$  is a nonlinear function that decreases with concentration and takes values below unity. This means that palladium films may therefore be used directly in the optical detection of hydrogen, such as in the case of micromirror sensors (Fedtke et al. 2004). An example of such a sensor is shown in Fig. 4.4. Palladium films approximately

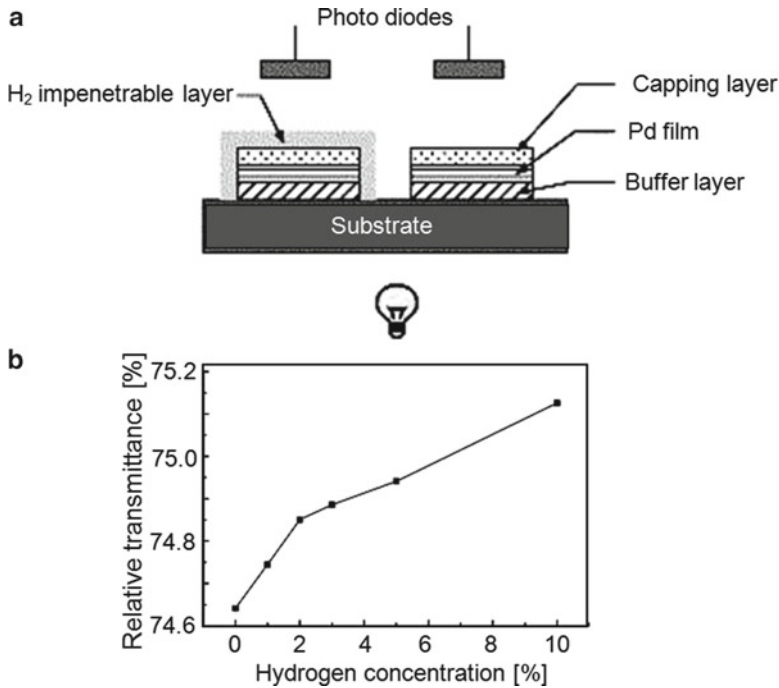


**Fig. 4.4** (a) Schematic of Pd-based optical H<sub>2</sub> sensor and (b) calibration curve of a 40-nm thick Pd-polymer nano-composite film at 370 nm (Reprinted with permission from Fedtke et al. (2004). Copyright 2004 Elsevier)

40 nm thick were deposited by DC plasma sputtering. The films had a columnar structure and showed proportionality between the relative transmittance at 545 nm and hydrogen concentration. The relative transmittance information is provided by the differential measurements between the structure exposed to hydrogen and the other isolated by the impenetrable layer. The capping layer, which can be an inert metal (such as gold or platinum) transparent and permeable to hydrogen, should prevent poisoning of the active palladium film by atmospheric contaminants. The buffer layer is used to accommodate the residual stresses and to improve the adhesion and the time stability of the sensor.

It was established that fiber-optic sensors based on palladium films can be designed as well (Silva et al. 2012). Approaches used for designing such sensors are shown in Fig. 4.5. Several examples of fiber-optic palladium-based hydrogen gas sensors are listed in Table 4.1. As may be seen, these sensors may in turn be classified according to their working principle: (1) interferometric-based, (2) intensity-based, or (3) fiber grating-based sensors. A palladium-based optical device is usually an optical fiber structure previously coated with a palladium film, ranging in thickness from a few nanometers to tens of micrometers. When the device is exposed to H<sub>2</sub>, the expansion of the palladium film induces mechanical stress in the optical fiber, so two responses may occur (Silva et al. 2012): (1) changes of the real part of the palladium complex refractive index—which produce an effective phase alteration of the guided light, according to the elasto-optic effect that can be detected using interferometric techniques, or (2) changes of the imaginary part of the palladium-complex refractive index—which cause alterations in absorption of the guided light that can be detected via monitoring the intensity of the optical signal. Analysis carried out by Silva et al. (2012) has shown that, in general, interferometric-based sensors are potentially more sensitive, while fiber Fabry–Perot devices have indeed shown short time responses, with the possibility of use as single point sensors because of their small dimensions. However, these sensors are more complex structures—and often require thermal isolation and high stability to ensure good a performance. Fiber grating-based sensors are robust

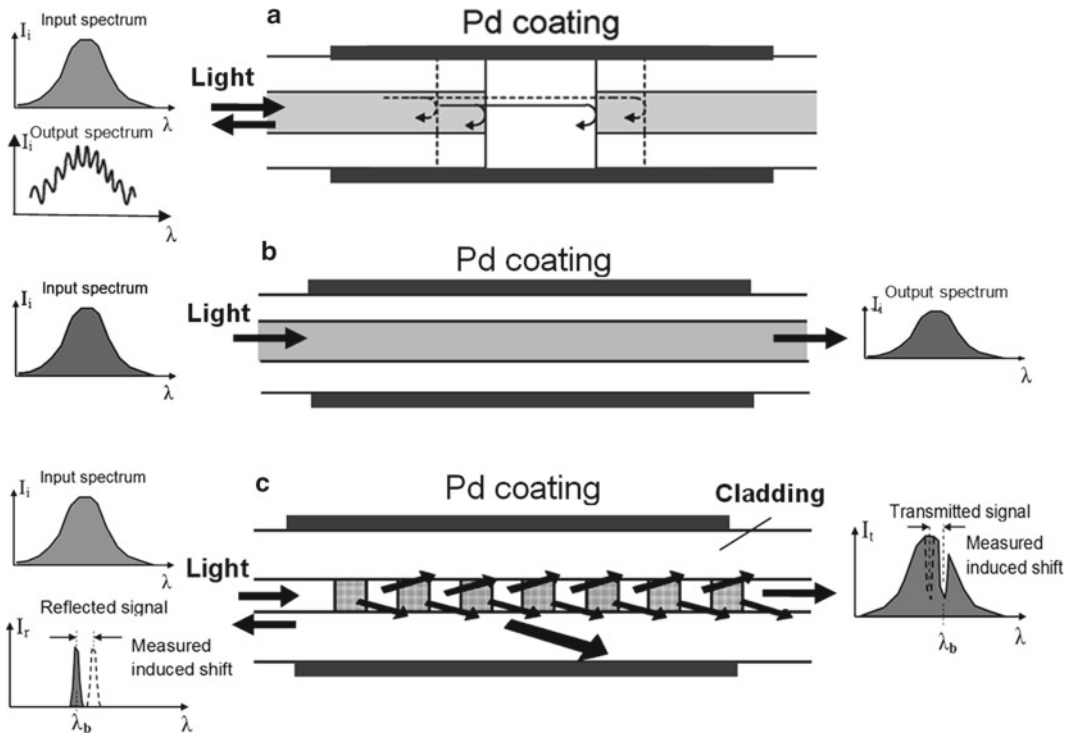


**Fig. 4.5** Generic form of optical-based  $H_2$  sensors and underlying operating principles: (a) interferometric-based, (b) intensity-based, and (c) fiber gratin-based sensors (Idea from Silva et al. (2012))

**Table 4.1** Examples of fiber-optic Pd-based hydrogen gas sensors

Sensing head	Concentration range	Response time	References
<i>Interferometric-based sensors</i>			
10-nm Ti, 10- $\mu$ m Pd, 30 mm/28 cm long SMF	0.6%/(2 ppb-2%)	<3 min/<30 s	Butler (1984), Butler and Ginley (1988)
LPG Mach-Zehnder interferometer coated with 50-nm Pd	4%	8 min	Kim et al. (2008)
2- $\mu$ m Pd, SMF and MMF Fabry-Perot cavity, 50 $\mu$ m cavity length	0.5% (33 ppm sensitivity)	<5 s	Zeakes et al. (1994)
<i>Intensity-based sensors</i>			
13-nm Pd-coated MMF tip	1-17%	<5 s	Bévenot et al. (2000)
Pt/ $WO_3$ sol-gel, 15 cm long MMF (100 $\mu$ m)	1%	5 min	Sumida et al. (2005)
SPR-MMF core coated with 12-nm Pd	0.8-100%	3-300 s	Bévenot et al. (2002)
Tapered MMF 30 and 60 $\mu$ m diameter, 10 mm length, 14-nm Pd	0.3-3.5%	30 s (2%)	Villatoro et al. (2005)
FBG (15 mm length) side-polished, 50-nm Pd	0.1-4%	30 s (4%), 2 min (<1%)	Schroeder et al. (2009)
<i>Grating-based sensors</i>			
Tapered SMF+FBG, 8 mm length, 25 $\mu$ m diameter, 8-nm Pd	0-9%	50 s (4%)	Zalvidea et al. (2004)
FBG-coated 350-nm Pd	0.5%	<10 s	Buric et al. (2007)
70-nm Pd-coated LPG	0-16%	<70 s (4%)	Wei et al. (2008)

SMF single-mode fiber, MMF multimode fiber, LPG long-period fiber grating, FBG fiber Bragg grating, SPR surface plasmon resonance



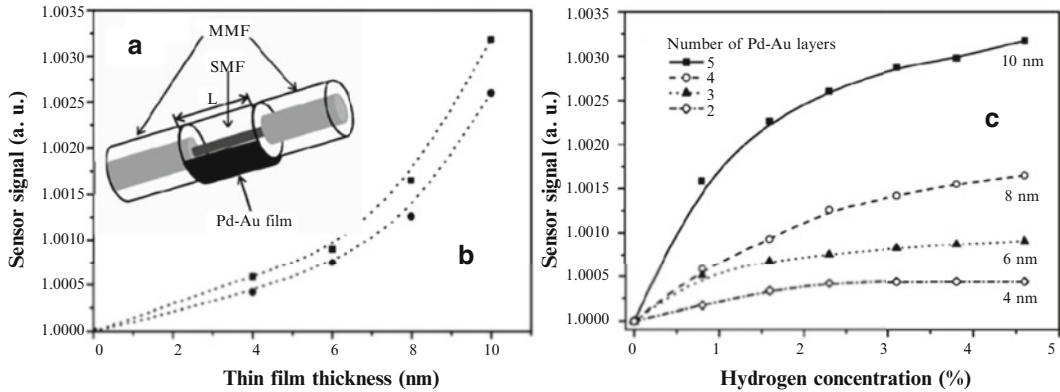


**Fig. 4.6** (a) Final structure of the optical fiber hetero-core sensor, consisting of a piece of single-mode fiber (SMF) of length ( $L$ ) longitudinally sandwiched between two multimode fibers (MMFs); (b, c) experimental sensor signals vs hydrogen concentration for samples with different thin-film thickness. In all cases, only the single-mode fiber section,  $L=8$  mm, was coated (Reprinted with permission from Monzón-Hernández et al. (2009). Copyright 2009 Elsevier)

structures, easily reproducible, and exhibit the unique advantage that they can be multiplexed. However, fiber Bragg grating (FBG) usually requires etching to enhance sensitivity, which in turn reduces mechanical strength. Conversely, long-period fiber grating (LPG) presents high stability for hydrogen detection.

Interferometric sensors were the first type of hydrogen sensors reported in the literature, yet intensity-based sensors have been the most common in terms of practical applications. In particular, evanescent wave absorption-based intensity sensors, relying on palladium-coated, etched, or tapered optical fibers, have been the most usual configurations, owing to their good performance in terms of response time (usually below 1 min). For example, Monzón-Hernández and coworkers (Luna-Moreno and Monzón-Hernández 2007; Monzón-Hernández et al. 2009) designed intensity-based fiber-optic hydrogen sensors (see Fig. 4.6). The resulting sensor consists of a multimode fiber in which a short section of single-mode fiber is coated with layered Pd/Au film (Monzón-Hernández et al. 2009) or thick-film Pd–Au alloy (Luna-Moreno and Monzón-Hernández 2007). Testing sensors in a mixture of hydrogen and nitrogen (carrier gas), Monzón-Hernández et al. (2009) established that the response time was 4.5 s for hydrogen concentration of 4%. When the hydrogen flow was turned off the multi-layer thin film desorbed the gas in 13 s. It was concluded that the operation mechanism of the sensors is based on the attenuation changes of the evanescent wave due to the diminution of real and imaginary parts of the refractive index of Pd/Au film. Palladium-capped magnesium hydride was used as an alternative sensing material in a fiber-optic hydrogen detector (Slaman et al. 2007).

Thermoelectric hydrogen sensors are also promising for thin metal film applications (Shin et al. 2003; Qiu et al. 2003; Hubert et al. 2011). Thermoelectric sensors generate an electrical signal based on the catalyzed exothermic oxidation reaction of hydrogen but use the thermoelectric effect to generate the electrical signal. The thermoelectric effect, or more specifically the Seebeck effect, arises when there is a temperature difference between two points of a conductor or semiconductor material which results in a voltage difference between these points. This hydrogen sensor is usually fabricated with a thermoelectric film coated with a catalyst, mainly platinum, on half of its surface. When exposed to  $H_2$  gas, the catalytic reaction starts, causing a change in the thermoelectric voltage across the hot and the cold region of the thermoelectric oxide film. Glass, alumina, and magnesium oxide are often used as the substrate material (Matsumiya et al. 2002; Casey et al. 2003). Platinum is used extensively as the catalyst because of its high catalytic activity at relatively low operating temperatures. Since only hydrogen can be oxidized effectively by a palladium catalyst near room temperature, thermoelectric sensors have, in principle, a low cross-sensitivity to other combustible species.

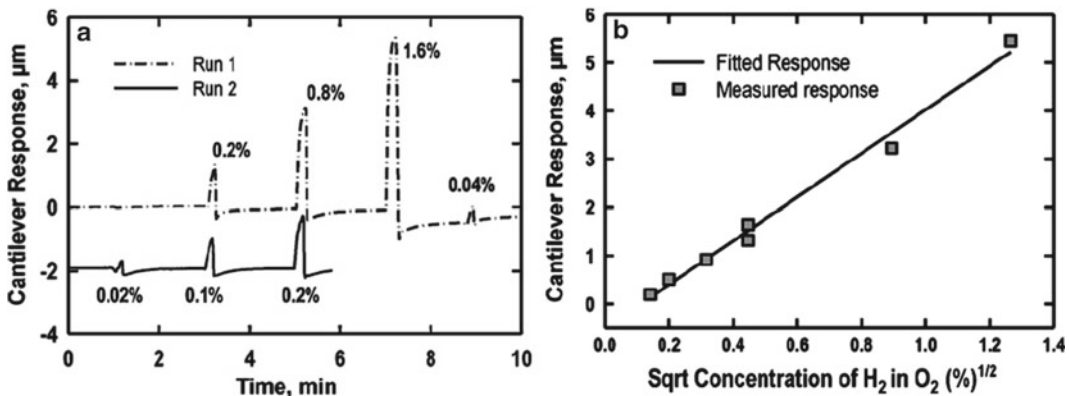


**Fig. 4.7** (a) Calibration data shown as responses to injections of H<sub>2</sub> over a large range of concentrations showing a limit of detection of approximately 100 ppm. (b) Linear calibration plot showing the expected square root dependence as described by Sievert's law and a regression constant of 0.992 (Reprinted with permission from Patton et al. (2010). Copyright 2010 Elsevier)

It was established that hydrogen, when absorbed by a metal, occupies interstitial sites in the metal lattice, causing this lattice to expand and thereby changing the physical properties of the metal. Experiment has shown that this effect, the expansion of palladium, can be used for hydrogen detection using micro-fabricated palladium-coated cantilever-based sensors (Chou et al. 2008; Patton et al. 2010). Mechanical changes, caused by volume expansion of a palladium film produced by hydrogen absorption, are monitored by parameters such as deflection, resonance frequency, and capacitance. Operating characteristics for a palladium-modified cantilever-based H<sub>2</sub> sensor are shown in Fig. 4.7. Specifically, a 3-s response time and a 10-s recovery time have been measured for these sensors. Additionally, these sensors have very low H<sub>2</sub> detection thresholds (100 ppm), wide dynamic range, and very good selectivity relative to common interferents. Kirby et al. (2009) have found that LaAl<sub>0.3</sub>Ni<sub>4.7</sub> films also have appreciable lattice expansion during interaction with hydrogen, making them suitable for the design of cantilever-based capacitance gas sensors. The device showed a stable response to 400-ppm hydrogen and can measure up to 100% hydrogen. The sensor was not poisoned by CO and was mechanically robust following repeated exposure to hydrogen. The measured response time,  $t_{90}$ , was greater than 10 s.

Lomperski et al. (2000) reported that the hydrogen influence on the velocity of sound in palladium can be the basis for gas sensor design as well. As is known, the acoustic wave velocity in a solid waveguide depends on the material density and on the amount of stress and strain to which it is subjected. When palladium absorbs hydrogen, its density and mechanical properties change, and this can therefore be detected as a difference in the velocity of sound waves traveling through it. An acoustic palladium wire sensor fabricated by Lomperski et al. (2000) had a measuring range of 0.1–100% hydrogen and an operating temperature range of 200–400 °C. This relatively high operating temperature range is set to avoid the  $\alpha \rightarrow \beta$  phase transition of the palladium wire. The measured response time of the sensor decreases with increasing temperature and ranges from 30 s at 180 °C to 8 s at 380 °C.

As has been demonstrated, the fields of quartz crystal microbalance (QCM)- and surface acoustic wave (SAW)-based gas sensors are also of interest in metal film application (Miura 1991; Jakubik et al. 2003; Jakubik and Urbanczyk 2005). When the palladium or palladium-based alloy layer absorbs hydrogen, both its mass density and electrical conductivity change, and this produces a detectable change in the frequency of the SAW and resonance frequency of QCM. Devices were able to detect hydrogen gas in a range of 1.5–4.0% concentration in air.

## 4.2 Disadvantages of Sensors and Approaches to Sensors' Parameters Improvement

Simplicity of the sensor structures, manufacturability of the sensors, good compatibility with Si microelectronic technology, and ease of microminiaturization are the main advantages of metal film-based gas sensors, while temporal and thermal instability is the main disadvantage of these devices. It was established that palladium is susceptible to cracking, blistering, and delamination on repeated exposure to hydrogen. For example, Baselt et al. (2003) observed palladium delamination after several exposures to hydrogen. Pitts et al. (2000) reported that lifetimes of these sensors did not exceed ten cycles. Fedtke et al. 2004 established that palladium films were destroyed at hydrogen concentrations higher than 4%. This effect takes place due to strong volumetric expansion during interaction with H<sub>2</sub> (see Table 4.2). It is also necessary to note that, in spite of the high selectivity to hydrogen of palladium-based sensors, these sensors are not yet sensitive enough to detect low hydrogen concentrations. Pitts et al. (2000) also found that the surface plasmon-based sensors had a slow response and that the repeatability of signals upon cyclic exposure was poor.

It was also observed (Skucha et al. 2010) that response and recovery times are strongly affected by humidity and other contaminants, such as sulfur and carbon monoxide, present in the surrounding atmosphere. These contaminants are known to degrade response and recovery times of palladium-based H<sub>2</sub> sensors operated at room temperature (Ruths et al. 1981; Pitts et al. 2000; Zhao et al. 2006). In particular, Pitts et al. (2000) have found that CO and CH<sub>4</sub> adsorb on the surface and restrict access to hydrogen dissociation sites. However, this adsorption appears to be weak and reversible when the sensor is exposed for extended periods in synthetic air. The effect observed with exposure to H<sub>2</sub>S is much more dramatic. Exposure to 10-ppm H<sub>2</sub>S for 5 min is sufficient to kill the sensor completely for the detection of hydrogen. Moreover, this effect is not reversible after exposure to synthetic air, indicating that the H<sub>2</sub>S has chemisorbed to the surface. This conclusion is consistent with much literature on the binding of sulfur-bearing compounds to noble and semi-noble metal surfaces. In order to remove most of these impurities, Skucha et al. (2010) proposed heating sensors in N<sub>2</sub> at  $T \sim 150$  °C before taking measurements. This treatment was accompanied by a strong decrease of response and recovery times. However, such an approach decreases the advantages of room temperature sensors.

Strong hysteresis, especially in the range of high hydrogen concentration, is another disadvantage of palladium-based sensors (see Fig. 4.8). The abrupt increase in resistance takes place due to phase transformation [ $\alpha \rightarrow (\alpha + \beta) \rightarrow \beta$ ] and is attributed to the plastic deformation caused mainly by dislocation formation and pile-up. The steep resistance increase in the  $\beta$  phase and the following hysteresis during desorption process can be alleviated at elevated temperatures. However, in the range of room temperatures the hysteretic resistance behavior and plastic deformation in the high H/Pd region may be potential serious issues of palladium-based sensors.

**Table 4.2** Phase and structure transformation of Pd film during interaction with H<sub>2</sub>

Property	Value
Lattice constant (nm at 298 K)	
Pd	0.3890
PdH <sub>0.015</sub> ( $\alpha_{\max}$ )	0.3894
PdH <sub>0.607</sub> ( $\beta_{\min}$ )	0.4025
Temperature and equilibrium pressure for PdH <sub>0.6</sub> formation	0.02 bar, 298 K
Volumetric expansion ( $\alpha/\beta$ phase, %)	10.4

Source: Data extracted from Flanagan and Oates (1991)

**Fig. 4.8** Sensitivity vs  $H_2$  concentration curves for palladium films with different thicknesses of 5–400 nm undergoing cyclic  $H_2$  absorption and desorption processes (Reprinted with permission from Lee et al. (2010a). Copyright 2011 Elsevier)

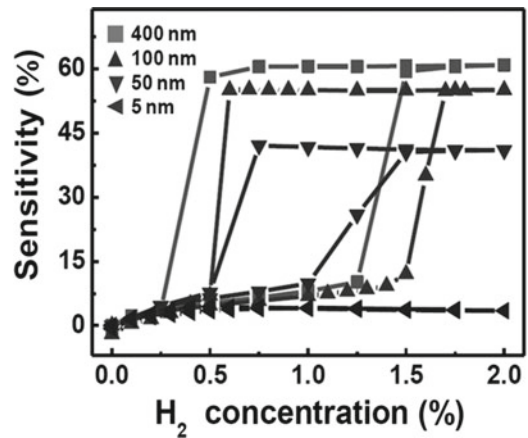
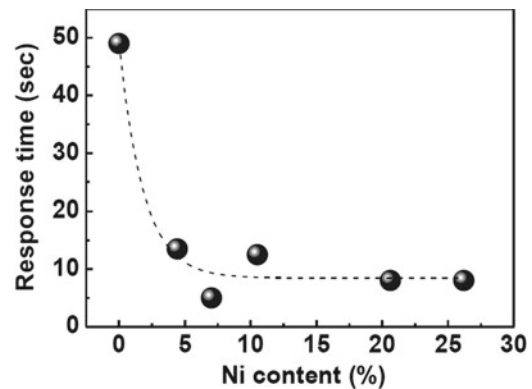


**Fig. 4.9** Response time of Pd–Ni alloy films as a function of nickel content in the presence of 1%  $H_2$  at room temperature (Reprinted with permission from Lee et al. (2010b). Copyright 2011 Elsevier)



Two principal approaches have been adopted to address this susceptibility to mechanical damage (Hubert et al. 2011). First, alloying of palladium with metals such as gold (Zhao et al. 2006; Luna-Moreno et al. 2007), silver (Cui et al. 2009), and nickel (Hughes and Schubert 1992; Chadwick et al. 1994; Hughes et al. 1995; Jung et al. 1998) suppresses the phase transition found in pure palladium due to hydrogen absorption and shifts the damaging phase transition to higher hydrogen concentrations. As a result, such an approach allows the preparation of more durable, stable, and reversible sensors. Among these, Pd–Au and Pd–Ag alloys have been more widely studied due to their advantages such as crystal structures similar to that of palladium, higher hydrogen solubility than pure palladium, and good capability to suppress structural deformations. However, these alloys have problems too. For instance, the gold in the Pd–Au alloy easily segregates on the surface owing to its high mobility (Butler et al. 1996), causing a reliability problem. For the Pd–Ag alloy, good sensor performance, particularly, high hydrogen permeability, is observed only in high silver concentration of more than 20 wt%, and the hydrogen dissociation capability of the alloy becomes worse than pure palladium in this concentration range (Gielens et al. 2004). Moreover, both alloys are expensive, adding more cost to sensors incorporating those materials. Comparing Pd–Ni alloy to these alloys, nickel can be introduced to the palladium matrix in a smaller amount to suppress structural deformations. Nickel is less likely to segregate in the alloy, is inexpensive, and helps to shorten response times (see Fig. 4.9). The attributes of the Pd–Ni alloy like good durability, fast response, and consistency of crystal structure with palladium make it an attractive material for hydrogen sensing. According to Noh et al. (2011),

the addition of a small amount of nickel to palladium effectively suppresses the structural deformations. However, we need to note that the addition of nickel strongly decreases the sensitivity as well. Okuhara et al. (1999) have found that palladium doping by tungsten also gives an optimizing effect. Composite materials can also be used for improving stability of palladium-based  $H_2$  sensors. Fedtke et al. (2004) have shown that the structure with palladium-polymer nano-composite thin films allowed the accommodation of the palladium lattice expansion during hydrogen exposure up to 10%  $H_2/N_2$ .

Second, the use of a supporting sub-layer such as titanium and chromium with high adhesion may improve the stability of the palladium sensing layer. Different materials have proved effective for this purpose including nickel (Butler 1994),  $VO_x$  (Smith et al. 2002),  $V_2O_5$  (Liu et al. 2002),  $CaF_2$  (Fedtke et al. 2004), and  $MgF_2$  (Chtanov and Gal 2001). For example, Fedtke et al. (2004) found that structures with  $CaF_2$  buffer layers and palladium cap showed a better time stability and behavior up to 6%  $H_2$ . Palladium-polymer nano-composite thin films allowed the accommodation of the palladium lattice expansion during hydrogen exposure up to 10%  $H_2/N_2$ . Liu et al. (2002) have shown that  $Pd/V_2O_5$  sensors are durable and allow detection of hydrogen concentration in excess of 4% up to 10%. At that concentration, sensors exhibit a very fast response time and can undergo more than 500 cycles without degradation of performance. A more detailed description of the above-mentioned applications of thin metal films in gas sensors can be found in a review paper of Drake et al. (2007). As was shown by Chou et al. (2008), the use of sputtering bombardment for metal deposition improves adhesion characteristics of palladium layers as well.

Optimizing the mechanical behavior of palladium films can also be achieved by optimizing the microstructure, and this may be done by reducing the grain size or thickness of the films and by using optimal substrate. In particular, Butler (1991) has shown that films with thickness larger than 50 nm are destroyed by exposure to high hydrogen concentrations. Wang et al. (1999b) and Mandelis and Garcia (1998) have used PVDF-polymer instead of glass substrates to achieve the accommodation of the lattice constant expansion by the polymer. The most practical solution, however, is to keep the sensor at an elevated temperature so that the phase transition does not occur. Unfortunately, maintenance of a high temperature leads to increased manufacturing cost and poor reliability. Moreover, the presence of an electric circuit in a hydrogen environment raises safety concerns and defeats the purpose of an optically based sensor.

As was noted before, the kinetics of palladium-based sensor response is limited by bulk diffusion. This means that response at room temperatures cannot be fast. Ding et al. (2006) proposed to resolve this problem by forming nanoporous palladium thin films using anodic aluminum oxide (AAO) templates. Ding et al. (2006) have found that porous films had lower  $H_2$  detection limit and faster and sharper response than the dense palladium films. Ding et al. (2006) believe that the film delamination problem may be alleviated in the nanoporous structures as well.

Gurlo and Clarke (2011) believe that an approach based on the use of reversible swelling of multiple cracked palladium films in which the cracks act as nanogaps (Lee et al. 2010b) and elastomeric substrates as a compliant support for palladium films to accommodate the swelling can also lead to improvement of gas-sensing parameters of palladium-based  $H_2$  sensors.

## References

- Avila JI, Matelon RJ, Trabol R, Favre M, Lederman D, Volkmann UG, Cabrera AL (2010) Optical properties of Pd thin films exposed to hydrogen studied by transmittance and reflectance spectroscopy. *J Appl Phys* 107:023504
- Baselt DR, Fruhberger B, Klaassen E, Cemalovic S, Britton CL Jr, Patel SV, MIsna TE, McCorkle D, Warmack B (2003) Design and performance of a microcantilever-based hydrogen sensor. *Sens Actuators B* 88:120–131
- Bévenot X, Trouillet A, Veillas C, Gagnaire H, Clément M (2000) Hydrogen leak detection using an optical fibre sensor for aerospace applications. *Sens Actuators B* 67:57–67
- Bévenot X, Trouillet A, Veillas C, Gagnaire H, Clément M (2002) Surface plasmon resonance hydrogen sensor using an optical fibre. *Meas Sci Tech* 13(1):118–124

- Buric M, Chen KP, Bhattarai M, Swinehart PR, Maklad M (2007) Active fibre Bragg grating hydrogen sensors for all-temperature operation. *IEEE Photonics Technol Lett* 19(5):255–257
- Butler MA (1984) Optical fiber hydrogen sensor. *Appl Phys Lett* 45(10):2736–2740
- Butler MA (1991) Fiber optic sensor for hydrogen concentrations near the explosive limit. *J Electrochem Soc* 138:L46–L47
- Butler MA (1994) Micromirror optical-fibre hydrogen sensor. *Sens Actuators B* 22:142–145
- Butler MA, Ginley DS (1988) Hydrogen sensing with palladium coated optical fibers. *J Appl Phys* 64(7):3706–3712
- Butler MA, Sanchez R, Dulleck GR (1996) Fiber optic hydrogen sensor. Sandia report SAND-96-1 133. Sandia National Labs, Albuquerque, NM
- Casey V, Cleary J, D'Arcy G, McMonagle JB (2003) Calorimetric combustible gas sensor based on a planar thermopile array: fabrication, characterisation, and gas response. *Sens Actuators B* 96:114–123
- Chadwick B, Tann J, Brungs M, Gal M (1994) A hydrogen sensor based on the optical generation of surface plasmons in a palladium alloy. *Sens Actuators B* 17:215–220
- Chen HI, Chou YI (2003) A comparative study of hydrogen sensing performances between electroless plated and thermal evaporated Pd/InP Schottky diodes. *Semicond Sci Technol* 18:104–110
- Choi SY, Takahashi K, Esashi M, Matsuo T (1986) Stabilization of MISFET hydrogen sensors. *Sens Actuators* 9:353–361
- Chou YI, Chiang HC, Wang CC (2008) Study on Pd functionalization of microcantilever for hydrogen detection promotion. *Sens Actuators B* 129:72–78
- Chtanov A, Gal M (2001) Differential optical detection of hydrogen gas in the atmosphere. *Sens Actuators B* 79:196–199
- Cui L, Chen Y, Zhang G (2009) An optical fiber hydrogen sensor with Pd/Ag film. *Optoelectron Lett* 5:220–223
- Ding D, Chen Z, Lu C (2006) Hydrogen sensing of nanoporous palladium films supported by anodic aluminum oxides. *Sens Actuators B* 120:182–186
- Drake C, Deshpande S, Bera D, Seal S (2007) Metallic nanostructured materials based sensors. *Int Mater Rev* 52(5):289–317
- Dus R, Nowakowski R, Nowicka E (2005) Chemical and structural components of work function changes in the process of palladium hydride formation within thin Pd film. *J Alloys Compd* 404–406:284–287
- Fedtko P, Wienecke M, Bunesco M-C, Pietrzak M, Deistung K, Borchardt E (2004) Hydrogen sensor based on optical and electrical switching. *Sens Actuators B* 100:151–157
- Flanagan TB, Oates WA (1991) The palladium-hydrogen system. *Annu Rev Mater Sci* 21:269–304
- Fukai Y, Sugimoto H (2007) Formation mechanism of defect metal hydrides containing superabundant vacancies. *J Phys Condens Matter* 19:4362011–43620124
- Gielens FC, Tong HD, van Rijn CJM, Vorstman MAG, Keurentjes JTF (2004) Microsystem technology for high-flux hydrogen separation membranes. *J Membr Sci* 243:203–213
- Gurlo A, Clarke DR (2011) High-sensitivity hydrogen detection: hydrogen-induced swelling of multiple cracked palladium films on compliant substrates. *Angew Chem Int Ed* 50:10130–10132
- Hoffheins B, Maxey LC, Holmes W Jr, Lauf RJ, Salter C, Walkeret D (1999) Development of low cost sensors for hydrogen safety applications. *Proceedings of the 1999 U.S. DOE Hydrogen Program Review. NREL/CP-570-26938*
- Hubert T, Boon-Brett L, Black G, Banach U (2011) Hydrogen sensors – a review. *Sens Actuators B* 157:329–352, Available online 29 April 2011
- Hughes RC, Schubert WK (1992) Thin films of Pd/Ni alloys for detection of high hydrogen concentrations. *J Appl Phys* 71:542–544
- Hughes RC, Schubert WK, Buss RJ (1995) Solid-state hydrogen sensors using palladium-nickel alloys: effect of alloy composition on sensor response. *J Electrochem Soc* 142:249–254
- Jakubik WP, Urbanczyk MW (2005) SAW hydrogen sensor with a bilayer structure based on interaction speed. *Sens Actuators B* 106:602–608
- Jakubik WP, Urbanczyk MW, Kochowski S, Bodzenta J (2003) Palladium and phthalocyanine bilayer films for hydrogen detection in a surface acoustic wave sensor system. *Sens Actuators B* 96:321–328
- Jung CC, Saaski EW, McCrae DA (1998) Fiber optic hydrogen sensor. In: Jung CC, Udd E (eds) *Proceedings of the SPIE, Fourth Pacific Northwest Fiber Optic Sensor Workshop*, vol 3489, pp 9–15
- Kashyap R, Nemova G (2009) Surface plasmon resonance-based fiber and planar waveguide sensors. *J Sensors* 2009:645162
- Kay BD, Peden CHF, Goodman DW (1986) Kinetics of hydrogen absorption by Pd(110). *Phys Rev B* 34:817–822
- Kim YH, Kim MJ, Park M, Jang J, Lee BH (2008) Hydrogen sensor based on a palladium-coated long-period fiber grating pair. *J Opt Soc Korea* 12(4):221–225
- Kirby DJ, Chang DT, Stratton FP, Zinck JJ (2009) A differential capacitive thin film hydrogen sensor. *Sens Actuators B* 141:424–430
- Lee E, Lee JM, Koo JH, Lee W, Lee T (2010a) Hysteresis behavior of electrical resistance in Pd thin films during the process of absorption and desorption of hydrogen gas. *Int J Hydrogen Energy* 35:6984–6991

- Lee E, Lee JM, Noh JS, Joe JH, Lee W (2010b) Hydrogen gas sensing performance of Pd-Ni alloy thin films. *Thin Solid Films* 519:880–884
- Lewis FA (1967) *The palladium hydrogen system*. Academic, London, UK
- Liu P, Lee S, Cheong HM, Tracy CE, Pitts JR, Smith RD (2002) Stable Pd/V<sub>2</sub>O<sub>5</sub> optical H<sub>2</sub> sensor. *J Electrochem Soc* 149:H76–H80
- Lomperski S, Anselmi M, Huhtiniemi I (2000) Ultrasonic and resistive hydrogen sensors for inert gas–water vapour atmospheres. *Meas Sci Technol* 11:1–8
- Luna-Moreno D, Monzón-Hernandez D (2007) Effect of the Pd-Au thin film thickness uniformity on the performance of an optical fiber hydrogen sensor. *Rev Appl Surf Sci* 253:8615–8619
- Luna-Moreno D, Monzón-Hernandez D, Villatoro J, Badenes G (2007) Optical fiber hydrogen sensor based on core diameter mismatch and annealed Pd–Au thin films. *Sens Actuators B* 125:66–71
- Lundstrom I, Shivaraman MS, Svensson C, Lundkvist L (1975) A hydrogen-sensitive MOS field-effect transistor. *J Appl Phys Lett* 26:55–57
- Lundstrom I, Sevansson J, Spetz A, Sundgren H, Winquist E (1993) From hydrogen sensors to olfactory images—twenty years with catalytic field-effect devices. *Sens Actuators B* 13:16–23
- Lundstrom I, Sundgren H, Winquist F, Eriksson M, Krantz-Rulcker C, Lloyd-Spez A (2007) Twenty-five years of field effect gas sensor research in Linköping. *Sens Actuators B* 121:247–262
- Mandelis A, Garcia JA (1998) Pd/PVDF thin film hydrogen sensor based on laser-amplitude-modulated optical-transmittance: dependence on H<sub>2</sub> concentration and device physics. *Sens Actuators B* 49:258–267
- Matsumiya M, Qiu F, Shin W, Izu N, Murayama N, Kanzaki S (2002) Thin-film Li-doped NiO for thermoelectric hydrogen gas sensor. *Thin Solid Films* 419:213–217
- Miura N (1991) New-type calorimetric gas sensor using temperature characteristics of piezoelectric quartz crystal fitted with noble metal catalyst film. *Sens Actuators B* 5:211–217
- Monzón-Hernández D, Luna-Moreno D, Martínez-Escobar D (2009) Fast response fiber optic hydrogen sensor based on palladium and gold nano-layers. *Sens Actuators B* 136:562–566
- Mueller WM, Blackledge JP, Libowitz GG (1968) *Metal hydrides*. Academic, New York, NY
- Noh J-S, Lee JM, Lee W (2011) Low-dimensional palladium nanostructures for fast and reliable hydrogen gas detection. *Sensors* 11:825–851
- Okuhara Y, Imai Y, Noguchi Y, Takata M (1999) Influence of phase transformation in Pd hydride on the recovery characteristics of optical hydrogen sensors. *Bull Mater Sci* 22:999–1001
- Patton JF, Hunter SR, Sepaniak MJ, Daskos PG, Smith DB (2010) Rapid response microsensor for hydrogen detection using nanostructured palladium films. *Sens Actuators B* 163:464–470
- Pitts JR, Liu P, Lee S-H, Tracy CE, Smith RD, Salter C (2000) Interfacial stability of thin film hydrogen sensors. In: *Proceedings of the 2000 DOE Hydrogen Program Review*. NREL/CP-570-28890
- Pundt A (2004) Hydrogen in nano-sized metals. *Adv Eng Mater* 6:11–21
- Pundt A, Kirchheim R (2006) Hydrogen in metals: microstructural aspects. *Annu Rev Mater Res* 36:555–608
- Qiu F, Shin W, Matsumiya M, Izu N, Murayama N (2003) Hydrogen sensing properties of multi-layer device Pt/SiGe sputtered on oxidized silicon substrate. *Mater Chem Phys* 82:575–582
- Ravi Prakash J, McDaniel AH, Horn M, Pilione L, Sunal P, Messier R, McGrath RT, Schweighardt FK (2007) Hydrogen sensors: role of palladium thin film morphology. *Sens Actuators B* 120:439–446
- Ruths PF, Ashok S, Fonash SJ, Ruths JM (1981) A study of Pd/Si MIS Schottky barrier diode hydrogen detector. *IEEE Trans Electron Devices* 28:1003–1009
- Sakamoto Y, Takai K, Takashima I, Imada M (1996) Electrical resistance measurements as a function of composition of palladium-hydrogen(deuterium) systems by a gas phase method. *J Phys Condens Matter* 8:3399–3411
- Schroeder K, Ecke W, Willsch R (2009) Optical fibre Bragg grating hydrogen sensor based on evanescent-field interaction with palladium thin-film transducer. *Opt Lasers Eng* 47(10):1018–1022
- Sharma AK, Gupta BD (2007) On the performance of different bimetallic combinations in surface plasmon resonance based fiber optic sensors. *J Appl Phys* 101(9):093111
- Shin W, Matsumiya M, Izu N, Murayama N (2003) Hydrogen-selective thermoelectric gas sensor. *Sens Actuators B* 93:304–308
- Sieverts A (1929) Absorption of gases by metals. *Z Metallkund* 21:37–46
- Silva SF, Coelho L, Frazão O, Santos JL, Malcata FX (2012) A review of palladium-based fiber-optic sensors for molecular hydrogen detection. *IEEE Sensors J* 12(1):93–102
- Skucha K, Fan Z, Jeon K, Javey A, Boser B (2010) Palladium/silicon nanowire Schottky barrier-based hydrogen sensors. *Sens Actuators B* 145:232–238
- Slaman M, Dam B, Pasturel M, Borsa DM, Schreuders H, Rector JH, Griessen R (2007) Fiber optic hydrogen detectors containing Mg-based metal hydrides. *Sens Actuators B* 123:538–545
- Smith RJ, Otterson DA (1970) Electrical resistivity of PdH<sub>x</sub> system for H/Pd atom ratios to 0.97. *J Phys Chem Solids* 31:187–189

- Smith RD II, Liu P, Lee SH, Tracy CE, Pitts JR (2002) Low-cost fiber optic hydrogen sensors. *Fuel Chem Div Preprints* 47:825–827
- Stewart ME, Anderton CR, Thompson LB, Maria J, Gray SK, Rogers JA, Nuzzo RG (2008) Nanostructured plasmonic sensors. *Chem Rev* 108:494–521
- Sumida S, Okazaki S, Asakura S, Nakagawa H, Murayama H, Hasegawa T (2005) Distributed hydrogen determination with fibre-optic sensor. *Sens Actuators B* 108:508–514
- Trinchi A, Galatsis K, Wlodarski W, Li YX (2003) A Pt/Ga<sub>2</sub>O<sub>3</sub>-ZnO/SiC Schottky diode-based hydrocarbon gas sensor. *IEEE Sensors J* 3:548–553
- Tuyen LTT, Vinh DX, Khoi PH, Gerlach G (2002) Highly sensitive NO<sub>x</sub> gas sensor based on a Au/n-Si Schottky diode. *Sens Actuators B* 84:226–230
- Villatoro J, Monzon-Hernandez D (2005) Fast detection of hydrogen with nano fiber tapers coated with ultra thin palladium layers. *Opt Express* 13:5091–5092
- Villatoro J, Luna-Moreno D, Monzón-Hernández D (2005) Optical fibre hydrogen sensor for concentrations below the lower explosive limit. *Sens Actuators B* 110:23–27
- Wang C, Mandelis A, Garcia JA (1999) Pd/PVDF thin film hydrogen sensor system based on photopyroelectric purely-thermal-wave interference. *Sens Actuators B* 60:228–237
- Wang C, Mandelis A, Au-leong KP (2001) Physical mechanism of reflectance inversion in hydrogen gas sensor with Pd/PVDF structures. *Sens Actuators B* 73:100–105
- Wei X, Wei T, Xiao H, Lin YS (2008) Nano-structured Pd-long period fibre gratings integrated optical sensor for hydrogen detection. *Sens Actuators B* 134:687–693
- Zalvidea D, Díez A, Cruz JL, Andrés MV (2004) Wavelength multiplexed hydrogen sensor based on palladium-coated fibre-taper and Bragg grating. *Electron Lett* 40(5):301–302
- Zeakes JS, Murphy KA, Elshabini-Raid A, Claus RU (1994) Modified extrinsic Fabry-Perot interferometric hydrogen gas sensor. In: *Proceedings of IEEE conference, LEOS'94*, vol 2, pp 235–236
- Zhao Z, Carpenter MA, Xia H, Welch D (2006) All-optical hydrogen sensor based on a high alloy content palladium thin film. *Sens Actuators B* 113:532–538
- Zynio SA, Samoylov AV, Surovtseva ER, Mirsky VM, Shirshov YM (2002) Bimetallic layers increase sensitivity of affinity sensors based on surface plasmon resonance. *Sensors* 2(2):62–70



## Chapter 5

# Semiconductors in Gas Sensors

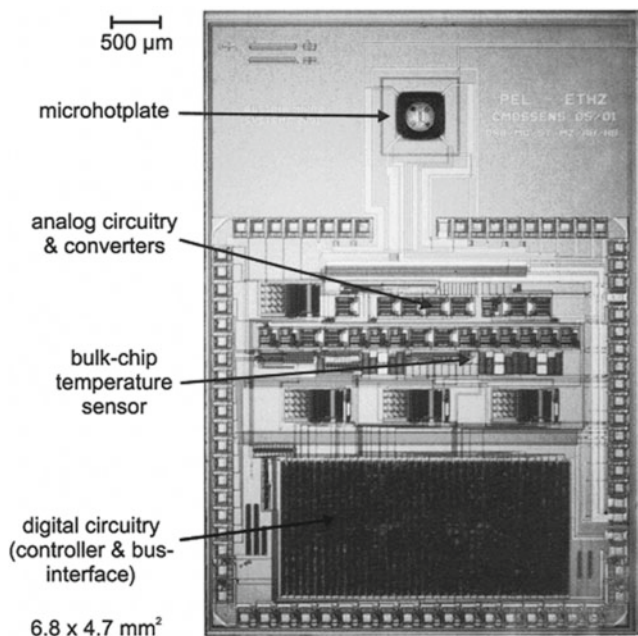
### 5.1 Silicon-Based Gas Sensors

Silicon is the best material for microelectronics, especially for integrated circuit manufacture. First, silicon is abundant and cheap to process. Silicon is highly abundant in the Earth's crust. A silicon crystal has an extremely stable structure mechanically and it can be grown to very large diameter boules and can be processed with very high yields. It is also a decent thermal conductor, thus enabling very dense packing of transistors, all very desirable for design and manufacturing of very large ICs. Good mechanical characteristics also make silicon a suitable material for the rapidly developing field of cantilever-based devices. Thin film and photolithographic fabrication procedures make it possible to realize a great variety of extremely small, high-precision mechanical structures using the same processes that have been developed for electronic circuits. High-volume batch-fabrication techniques can be utilized in the manufacture of complex miniaturized mechanical components, which may not be possible with other methods. The second major advantage of silicon is the existence of silicon dioxide—one of the best insulators and capsulation coatings. Silicon dioxide can easily be incorporated into silicon circuits, and such layers are adherent to the underlying silicon. In addition, silicon has a nearly perfect lattice, and its impurity density is very low, allowing one to build very small structures. Taking into account the qualities mentioned above, one can conclude that, in the case of silicon, using both the sensing and the electronic functions can be realized at the same platform by applying a common set of processing steps, which can all be carried out on wafer-scale, i.e., in a batch process, which allows the large economic benefits of mass production.

However, at the same time silicon is a chemically active material and, due to oxidation and interaction with surrounding atmosphere, especially at higher temperatures, has unstable surface properties. The operation temperature of silicon-based devices is also limited due to the small band gap of silicon. This means that silicon-based devices have strong limitations for operation at high temperatures and in corrosive atmospheres. Unfortunately, conventional gas sensors mainly operate in such conditions. As a result, silicon-based sensors are absent from the gas sensor market.

Meanwhile, research carried out during the last decade has shown that, in spite of the above-mentioned properties of silicon, there are great prospects for the use of silicon in gas sensors. First of all these prospects are connected with development of microelectromechanical systems (MEMS) and micromachining technology, which allows one to design silicon-based cantilever and membrane (hotplates) structures acceptable for fabrication various types of gas sensors (Gotz et al. 1997; Cane et al. 2000; Afridi et al. 2001, 2002; Semancik et al. 2001; Lee et al. 2003; Mitzner et al. 2003; Bhattacharyya et al. 2008). The aim of these developments is to yield families of miniaturized devices that offer economic and operational improvements over conventional gas sensor types. Of course, Si is

**Fig. 5.1** Micrograph of the single-chip gas sensor microsystem layout for flip-chip packaging. The components include: flip-chip frame; micro-hotplate; temperature sensor, controller, and digital interface (Reprinted with permission from Graf et al. (2004). Copyright 2004 American Chemical Society)



not a sensing material in these devices. However, the application of silicon and resources of Si-based technologies makes it possible to increase the sensitivity of mass sensitive RT gas sensors and strongly decrease the power consumption by pellistors, conductometric and thermoelectric-type sensors. Sensor arrays for e-nose, smart sensors, and integration of gas sensors and data processing on the one platform can also be realized using a silicon-based approach. It is known that the integration of electronics with gas sensors in a single chip improves the sensor signal in terms of both robustness and signal-to-noise ratio. On-chip integration also improves microsystem functionality and interconnection and facilitates more efficient packaging. At high volumes of production, monolithic solutions present economic advantages, and they are especially attractive for portable and high-sensitivity systems (Hagleitner et al. 2002; Zaghoul and Voiculescu 2011). Examples of gas sensor systems incorporated on a silicon substrate are shown in Fig. 5.1. In this section we will not discuss features of the above-mentioned devices, because silicon-based hotplates and cantilevers will be discussed in Chap. 7 (Vol. 1). We will say only that coated micromachined silicon-based resonators, such as beams and cantilevers, and resonator arrays can be extremely sensitive due to the low masses of the resonators—as little as 10 ng in some cases—and varying degrees of selectivity to volatile organic compounds (VOCs) can be achieved through the use of appropriate coatings, generally polymers. A reader interested in the detailed study of MEMS technology can refer to excellent reviews already published (Comini et al. 2009).

Research has shown that silicon-based catalytic-gate MOS (metal oxide semiconductor) field-effect transistors and diode-type gas sensors can also be designed. These devices were first described by the Lundström group (Lundström et al. 1975a, b, 1990, 2007). In the meantime, all these devices have been developed to a considerable degree of sophistication. The functioning of both kinds of devices is based on the interaction of the analyte gas species with SiO<sub>2</sub> surfaces, i.e., with the surface of those oxide layers that naturally form on Si surfaces and capsulate the silicon surface. A severe constraint of catalytic-gate MOS gas sensors is that, in the normal operating temperature range of silicon devices, such sensors are almost completely selective to H<sub>2</sub>. They therefore do not provide a sufficiently generic micro-gas-sensor. However, Si-based sensors even with SiO<sub>2</sub> capsulation rapidly lose their electronic performance at temperatures approaching 200 °C. This has so far limited the widespread adoption of SiMOS sensors to gas-sensing applications. For fabrication of MOSFET, MOS capacitors and MOS diode gas sensors, polysilicon may be used as well (Juang et al. 2011). A gas sensor designed on the basis of low temperature polysilicon (LTPS) is shown in Fig. 5.2.

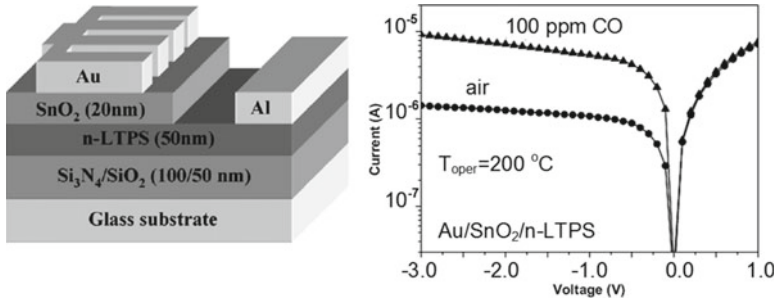
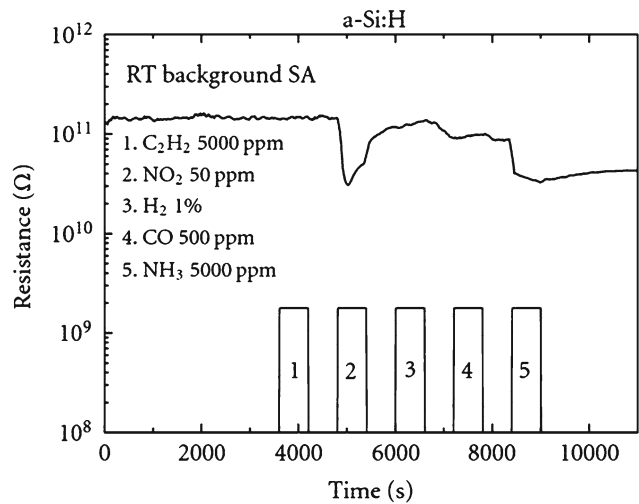


**Fig. 5.2** The schematic cross section and  $I$ - $V$  characteristics of the developed Au/SnO<sub>2</sub>/n-LTPS MIS Schottky diode under 200 °C with and without CO gas ambient (Adapted with permission from Juang et al. (2011). Copyright 2011 Elsevier)

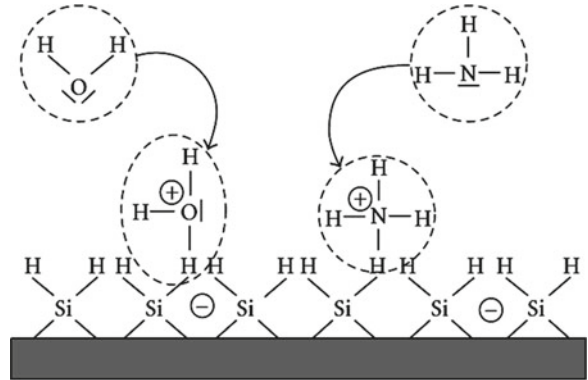
**Fig. 5.3** Resistivity response at room temperature of an undoped  $a$ -Si:H film towards a representative range of analyte gases (Reprinted from Helwig et al. (2009). Published by Hindawi Publishing Corporation)



It was found that amorphous silicon can also be used in gas sensors of resistive (Helwig et al. 2007, 2009) and heterostructure-type devices (Tucci et al. 2004). For these purposes hydrogenated amorphous silicon ( $a$ -Si:H) is normally used. This material has found widespread commercial application in photovoltaic solar energy conversion and in large-area thin-film electronic devices (Kanicki 1992). In the course of these developments, the basic material properties of  $a$ -Si:H have been intensively investigated (Luft and Tsuo 1993). It should be noted that  $a$ -Si:H is a stable material and the H-termination remains up to annealing temperatures on the order of 800 °C in vacuum (Cui et al. 1999).

It has been established that ambient humidity gives rise to adsorbed layers of water on  $a$ -Si:H surfaces (Tanielian et al. 1978). Furthermore, it has been shown that NH<sub>3</sub> and NO<sub>2</sub> exposure of undoped  $a$ -Si:H films at room temperature can increase the conductance by several orders of magnitude (Tanielian et al. 1978). However, very long recovery time constants were observed after the  $a$ -Si:H films had been exposed to NO<sub>2</sub> and particularly NH<sub>3</sub>. At higher operating temperatures,  $a$ -Si:H-based devices keep their sensitivity toward NO<sub>2</sub> and NH<sub>3</sub>. With regard to water-free MOX surfaces, the surprising result is that the high-temperature  $a$ -Si:H gas sensitivity is far more selective than that of MOX materials. Helwig et al. (2009) demonstrated that  $a$ -Si:H films do respond predominantly to nitrogen-bearing gases. Gases which simply exhibit combustibility and which can easily be detected with heated MOX gas sensors such as H<sub>2</sub> and ethene lead to a response that is 2 orders of magnitude smaller than the NO<sub>2</sub> and NH<sub>3</sub> responses (see Fig. 5.3).

**Fig. 5.4** Proposed interaction of  $\text{H}_2\text{O}$  and  $\text{NH}_3$  molecules on a water-free  $a\text{-Si:H}$  surface (Reprinted from Helwig et al. (2009). Published by Hindawi Publishing Corporation)



Helwig et al. (2009) believe that a low-temperature ( $T_{\text{oper}} < 140\text{ }^{\circ}\text{C}$ ) response-mechanism is mediated by a thin layer of adsorbed water with the semiconductor materials themselves acting as pH sensors. In this adsorbate-limited state, the gas sensitivity is limited to molecular species that can easily dissolve in  $\text{H}_2\text{O}$  and subsequently undergo electrolytic dissociation. At higher temperatures, where a closed layer of adsorbed water can no longer exist, the gas response is limited by direct molecule–semiconductor interactions. In this latter mode of operation, MOX gas sensors respond to adsorbed gases according to their different oxidizing or reducing properties. Helwig et al. (2007) have shown that hydrogenated amorphous silicon ( $a\text{-Si:H}$ ) films exhibit H-terminated surfaces that can easily interact with molecules which exhibit lone-pair orbitals like  $\text{H}_2\text{O}$  and  $\text{NH}_3$  or electron-deficient three-center orbitals like  $\text{NO}_2$ . The proposed surface interactions of  $\text{H}_2\text{O}$  and  $\text{NH}_3$  are illustrated in Fig. 5.4.

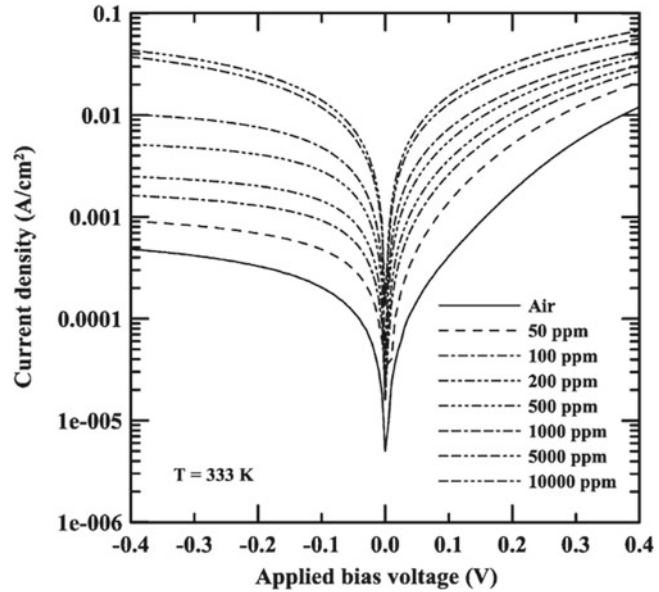
Another major research theme related to silicon is the development of MEMS-based analytical instruments for gas sensing, such as miniaturized silicon photoacoustic and thermal conductivity gas sensors, MEMS Fourier transform and other spectrometers, and integrated nondispersive IR absorption (NDIR) sensors. Unfortunately, there are several problems to be overcome here. According to Bogue (2007), part of the difficulty lies with the fact that miniaturization is not always particularly beneficial: miniaturized NDIR optical sensors suffer from low sensitivity due to the necessarily short optical path lengths; silicon photoacoustic sensors cannot offer the low limits of detection that characterize their conventional counterparts, and as yet, MEMS spectrometers only offer low resolution.

## 5.2 III–V-Based Gas Sensors

Of course, in the literature one can find gas sensors designed on the base of other conventional semiconductors such as InP, GaAs, and GaP (Yousuf et al. 1982; Lechuga et al. 1992; Kang and Gürbüz 1994; Liu et al. 2001a, b, 2002; Chen et al. 2003; Chen and Chou 2004; Lin et al. 2004; Lin and Hsu 2011; Chou et al. 2005; Kimura et al. 2006). Usually these sensors are hydrogen sensors of Schottky, MIS, or FET types. Typical operating characteristics of Pd-n-InP-based hydrogen sensors are shown in Fig. 5.5. The mechanism of sensitivity of such sensors was discussed earlier in Chap. 1 (Vol. 1). However, we need to note that sensors fabricated on the base of indicated III–V compounds do not have the required stability and therefore these devices are not promising for the sensor market. These sensors can be of interest only for incorporation in ICs fabricated on the basis of III–V compounds.

InP, AlGaAs, GaAs, and InGaAs compounds can also be found in integrated optical gas sensors, where these compounds can be used as waveguides. It should be noted that this field of application is more promising for III–V compounds. The technology of integrated optical sensors (IOSs) is a branch

**Fig. 5.5** Effect of hydrogen concentration on  $I$ – $V$  characteristics of the studied Pd–InP Schottky diode at 333 K (flow rate  $\frac{1}{4}$  500 mL/min; ambient pressure) (Reprinted with permission from Chen et al. (2003). Copyright 2003 Elsevier)



of microoptics and integrated optics (IO) (Palais 2002; Hunsperger 2002; Pollock and Lipson 2003), which emerged from the successful techniques of microelectronics together with micromechanics and other microtechnologies. Integrated optics combines thin-film and microfabrication techniques to make optical waveguides and devices in planar form and offers the advantages of compactness, power efficiency, and multifunctionality with single-chip capabilities. An integrated optical sensing system is a complex sensing system, which, besides exhibiting a gas-sensing function, also encompasses functions to connect the optical to the electrical domain (light sources and optoelectrical detectors) and electronics (for processing the electrical signals obtained from the detectors and sometimes also for controlling the state of some optical functions) (Syms and Cozens 1993). Integrated optics in solid-state semiconductor materials such as GaAs or InP allows simple integration of optical and electronic functions. Absorption is relatively high in these compounds but acceptable for short path lengths in integrated optical sensors. Semiconductor waveguides are often made as ridges, because of the ease with which a mesa structure may be made by etching. There are two basic semiconductor waveguide types: *heterostructure guides*, which operate by the refractive index differences obtained between different materials, and *homostructure guides*, which use the index reduction following from an increase in the majority carrier density (Syms and Cozens 1993). At present the most common semiconductor waveguides are fabricated on the basis of GaAs/Ga<sub>1-x</sub>Al<sub>x</sub>As and InP/Ga<sub>1-x</sub>In<sub>x</sub>As<sub>1-y</sub>P<sub>y</sub> systems. The variation of the alloy content between the layers in the heterostructure provides the refractive index difference necessary for a waveguide. The index change obtained by doping may be found for n-type GaAs as  $\Delta n = -0.01$ , when  $N = 5 \times 10^{18} \text{ cm}^{-3}$  and  $\lambda_0 = 1 \mu\text{m}$ . This implies that the index changes possible in homostructures are much lower than in heterostructures, giving reduced confinement in any guide structure. A further problem arising in homostructures is that the increased carrier concentration in the substrate causes a rise in absorption, which can result in unacceptable propagation loss. Heterostructures therefore offer several advantages. Examples of semiconductor waveguides are shown in Fig. 5.6.

The light sources (solid state lasers and light diodes) and photoreceivers are another field for III–V compounds application in gas sensors (Monroy et al. 2003). Features of these devices will be discussed in Chap. 14 (Vol. 1).

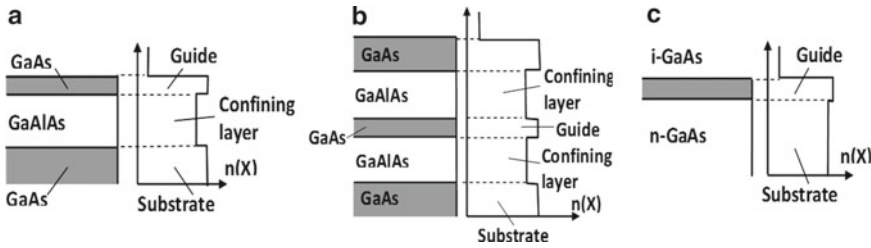


**Fig. 5.6** (a) GaAs/GaAlAs planar waveguide. (b) Double heterostructure GaAs/GaAlAs planar waveguide. (c) Planar waveguide in GaAs formed by changes in free carrier concentration (Idea from Syms and Cozens (1993))

### 5.3 Wide-Bandgap Semiconductors

As indicated before, silicon- and III–V-based sensors are not suited for operation in harsh environments, for instance in high temperature or corrosive ambient conditions. In these conditions Si-based and III–V-based gas sensors have low temporal stability. Therefore, in recent years there has been intense effort toward the design of new semiconductor materials, other than silicon and conventional III–V compounds, for use in power electronics and other applications, including gas sensor design (Lundström 2001; Grant et al. 2005; Lundström et al. 2007; Pearton et al. 2010). Among these materials, emphasis has been given to relatively large bandgap (wide-bandgap semiconductors, WBSs) semiconductors such as diamond, silicon carbide (SiC), gallium nitride (GaN), and AlGaInN materials systems, which are materials with unique properties (Lundström 2001, Lundström et al. 2007; Schalwig et al. 2002; Kang et al. 2004; Nebel et al. 2007; Qureshi et al. 2009; Pearton et al. 2010). Several selected parameters of wide-bandgap semiconductors in comparison with Si and GaAs are presented in Table 5.1. Of the wide-bandgap materials, SiC is by far the most developed (Wright and Horsfall 2007). In fact, SiC exists in a large number of polytypes—different crystal structures built from the same Si–C subunit organized into a variety of stacking sequences. There are over a hundred of these polytypes known, but the preponderance of research and development has concentrated on only three: 3C, 6H, and 4H. Of these, the 4H polytype is the most common for electronic devices due to its overall superior material properties, the suitability for which drives the investment in this area. The bandgap of 4H SiC is 3.23 eV at room temperature (compared with 1.12 eV for silicon). The 3C–SiC polytype is more common for MEMs-based sensors due to the fact that it may be grown by CVD or PECVD methods on standard Si wafers (thus reducing overall wafer cost compared with pure SiC technology). For comparison, the size of diamond layers usually does not exceed 4 mm × 4 mm (Nebel et al. 2007). In addition, all forms of SiC have high radiation tolerance, a high thermal conductivity (better than copper), high hardness and Young’s modulus (typically ~400 GPa compared with ~130 GPa for silicon), and a high critical electric field (in excess of 2 MV/cm) (Wright and Horsfall 2007).

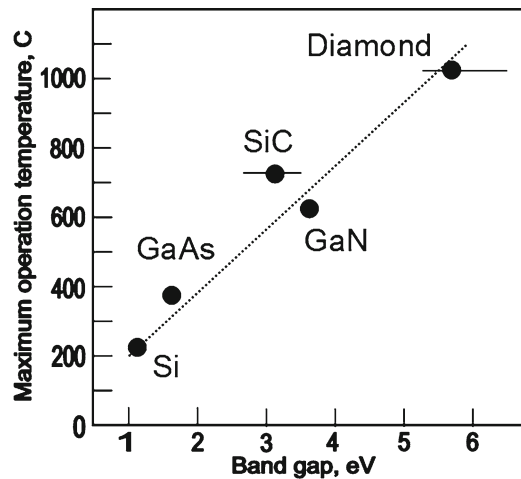
Due to the wide band gap mentioned above, these materials are very thermally stable, and electronic devices can be operated at high temperatures (see Fig. 5.7). This means that WBS-based devices have a wider operating temperature range. Much better chemical, thermal, and mechanical stability in comparison with silicon make these new semiconductor materials more acceptable for the development of biosensor systems and specific gas sensors aimed for operation in harsh environments. For example, GaN is not etched by any acid or base at temperatures below a few hundred degrees. Immunity to corrosion makes wide-bandgap semiconductors very suitable for operation in chemically harsh environments. Besides, the wide band gap of diamond, GaN, and SiC minimizes the generation of charge carriers due to undesirable background optical or thermal excitation. This is very important for gas sensor operation at high temperature. Regarding GaN we can also say that a unique advantage

**Table 5.1** Selected properties of semiconductors

Property	Si	GaAs	SiC	GaN	C (diamond)
Energy gap (eV)	1.12	1.42	2.3–3.2	3.39	5.45
Density (g/cm <sup>3</sup> )	2.3	5.3	3.1	6.1	3.5
Electron mobility (cm <sup>2</sup> /V s)	1,450	8,500	500–900	400–2,000	1,000–4,000
Semi-insulating	No	Yes	Yes	Yes	No
Dielectric constant	13.1	12.9	9.7	8.9–9.5	5.7
Refractive index	3.4	3.7	2.55	2.4–2.6	2.4
Melting point (K)	1,687	1,511	3,003	>2,700	3,820
Thermal conductivity (W/m K)	149	46–55	330–460	130–220	3,300
Thermal expansion (μm/m K)	2.6	5.7	2.2–4.2	3–5.5	0.8–1.2
Young's modulus (GPa)	130–185	85.5	350–450	280–300	1,050
Poisson ratio	0.28	0.31	0.14–0.22	0.183	0.1

For pure materials at room temperature

**Fig. 5.7** Influence of band gap on the maximum operating temperature of semiconductor devices (Data were extracted from Bogue (2002a, b))



of a GaN gas sensor is that it can be integrated with GaN-based optical devices or high-power, high-temperature electronic devices on the same chip. Another advantage of nitride-based semiconductor devices according to Irokawa (2011) is utilization of AlGaIn/GaN heterostructure. In an AlGaIn/GaN heterostructure, the polarization-induced two-dimensional electron gas (2DEG) concentration at the AlGaIn/GaN interface is extremely sensitive to surface states. Any potential changes on the surface by adsorption of gas or liquid polar molecules would affect the surface potential and modulate the 2DEG density. Irokawa (2011) believes that GaN has advantages in technology as well. First, GaN-based sensors, similarly to SiC, can be fabricated on silicon substrate that contributes to lower production costs. Second, the other promising wide-bandgap semiconductor, SiC, has several technical drawbacks for SiC device fabrication; the processing, particularly of SiC FETs (field-effect transistors), is inherently complicated, requiring high-temperature implantation, and very high-temperature postimplantation annealing steps, leading to higher cost.

The use of WBS-based devices as gas sensors for hydrogen and hydrocarbons has been extensively investigated by several groups (Arbab et al. 1993; Kim et al. 2001; Schalwig et al. 2002; Kang et al. 2004). The development of WBS-based Schottky diodes for gas detection began in the early 1990s. Experiments have shown that GaN-, SiC-, and diamond-based Schottky-diode, FET-type, and MOS capacitance-type sensors are optimal approaches used for WBS-based gas sensors design (Lloyd Spetz et al. 2001; Pearton et al. 2010). One of the possible variants of WBS-based gas sensors is shown in Fig. 5.8.

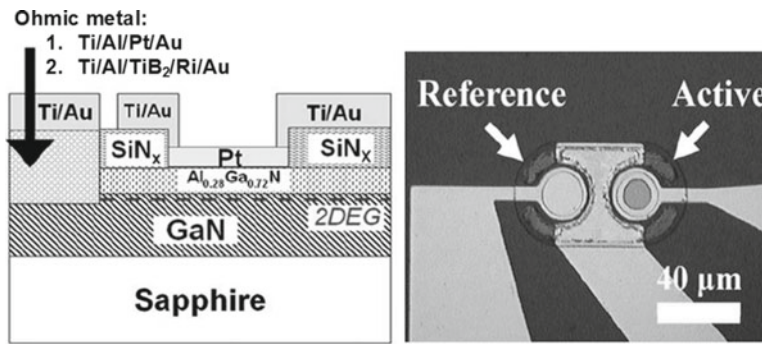
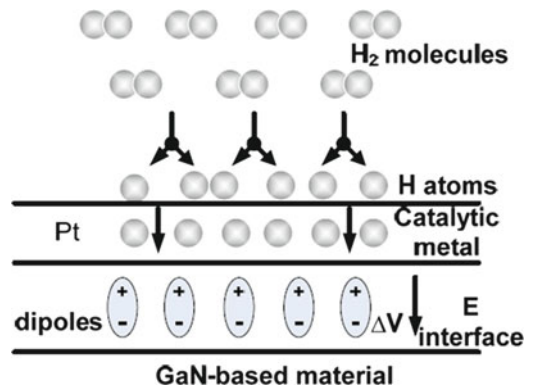


**Fig. 5.8** Cross-sectional schematic of completed Schottky diode on AlGaIn/GaN HEMT layer structure (*top*) and plan-view photograph of device (*bottom*) (Reprinted with permission from Pearton et al. (2010). Copyright 2010 Elsevier)

**Fig. 5.9** Schematic of sensing mechanism (Reprinted with permission from Kim and Ren (2003). Copyright 2003 American Institute of Physics)

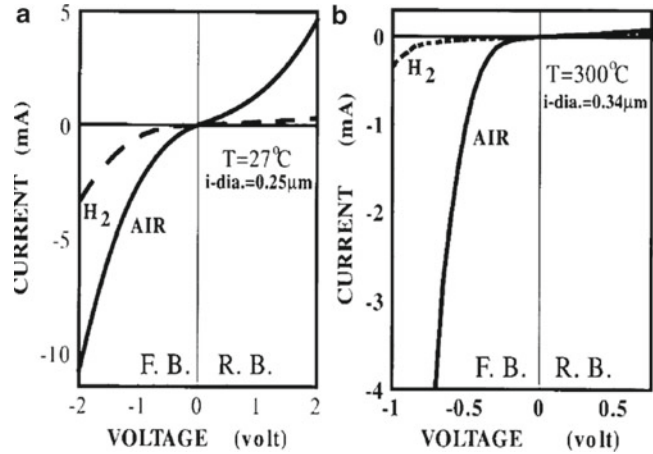


The detection mechanism of gas-sensitive Schottky-diode, field-effect, or MOS capacitance gas sensors is based on the dissociative adsorption of gas species on surfaces or interfaces and diffusion of hydrogen atoms through a catalytic metal (see Fig. 5.9). The adsorbed molecules form a dipole layer leading to a work function change in the sensing material. Decomposition of adsorbed gases occurs at temperatures above 150 °C and occurs in the sub-millisecond time scale (Nakagomi et al. 1997). This high response speed makes WBS sensors suitable for the detection of gas species in rapidly varying environments, such as close to the manifold region in car exhausts, unlike conventional ceramic-based sensors, which have a response time in the region of 10 s under these conditions (Xiong and Kale 2005).

The major advantage of using diode type structures in gas sensors is that any electrochemical change at the interface of catalytic metal–semiconductor causes an exponential change in the device current (see Fig. 5.10). In other words, the diode structure enhances the detection signal and simplifies the need for detection-signal processing/enhancing. The presence of a metal oxide layer between the WBS and the catalytic metal has also been reported and seems to increase the sensitivity and stability of hydrogen and hydrocarbon sensors. According to results of research carried out by Lundström's group, WBSs-based gas sensors, in particular SiC-based GAS-FETs, due to the large band gap of semiconductors, can operate in a range of temperatures up to 800 °C. The presence of dielectric layers, separating the metal from the WBSs, provides yet another increase of operating temperatures. For example, MOS SiC-based devices can operate at temperatures higher than 900 °C (Lloyd Spetz et al. 1997). Therefore a potential application of WBSs-based gas sensors is flue gas sensing in combustion engines (Baranzahi et al. 1997; Wingbrant et al. 2005). However, it is necessary to know that



**Fig. 5.10**  $I$ - $V$  characteristics of diamond-based  $H_2$  sensor in air and  $H_2$  environment ( $Ar/H_2 = 5:1$ ) at (a) 27 °C and (b) 300 °C (Reprinted with permission from Gurbuz et al. (2004). Copyright 2004 Elsevier)



the nature of the dielectric used in MOS-based gas sensors plays an important role in the gas-sensing effect and the change of dielectric can be accompanied by a dramatic change in operating characteristics. For example, Irokawa (2011) studying Pt-GaN, Pt-SiO<sub>2</sub>-GaN, and Pt-Si<sub>x</sub>N<sub>y</sub>-GaP structures established that the MOS Pt-GaN diode with a 10-nm SiO<sub>2</sub> dielectric showed a marked improvement in hydrogen detection sensitivity, which is twice as high as that of the conventional Pt-GaN Schottky diode. In sharp contrast, an MOS Pt-GaN diode with a 10-nm Si<sub>x</sub>N<sub>y</sub> dielectric did not show any hydrogen response.

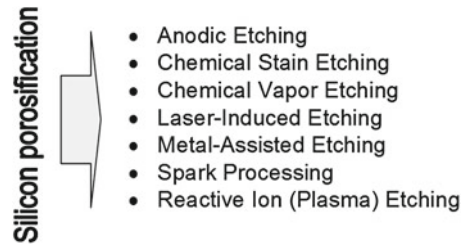
Among the disadvantages of WBS-based gas sensors one can select strong dependence of sensor parameters on the temperature. In addition, wide-bandgap materials still suffer from many technological difficulties that preventing near-term commercial application. For example, making synthetic diamond thin films that are sufficiently conducting to be electrochemically active at room temperature has always been difficult. p-Type doping (conduction occurs through holes) turned out to be relatively easy but n-type doping (conduction occurs through electrons) has remained an elusive goal until recently (Qureshi et al. 2009). The limited number of gases which can be detected is other disadvantage of the above-mentioned sensors. At present, most results are related to H<sub>2</sub> and hydrocarbon detection.

## 5.4 Porous Semiconductors (Porous Silicon)

In terms of sensor applications, porous semiconductors, in particular porous silicon layers (PSi), are very attractive because of their unique combination of crystalline structure, a huge internal surface area of up to 200–800 m<sup>2</sup>/cm<sup>3</sup>, which enables enhancement of adsorbate effects, and very high activity in surface chemical reactions. Several investigations have shown that electrical and optical characteristics of porous silicon may change considerably upon adsorption of molecules onto their surfaces and/or by filling the pores (Feng and Tsu 1994; Mares et al. 1995; Canham 1997; Cullis et al. 1997). This means that surface adsorption and capillary condensation effects in PSi layers can be used for development of effective sensor systems (Parkhutik 1999; Anderson et al. 1990). One can find in a review paper (Korotcenkov and Cho 2010b) the detailed description of approaches used for silicon porosification..

As shown in Fig. 5.11, there are many different methods that could be used for Si porosification. It was established that, besides conventional electrochemical etching, chemical stain etching, chemical vapor etching, spark processing, laser-induced etching, and reactive ion etching could be used.

**Fig. 5.11** Methods used for silicon porosification (Data extracted from Korotcenkov and Cho (2010b))



For example, stain etching, in which the silicon sample is simply immersed in an HF-based solution, is the easiest way of producing PSi. It has been reported that the physical structure of those layers was similar to that fabricated by the anodization method. The resulting pores are in the range of 1 nm to micrometers. Stain etching is an electroless process, and therefore has several advantages in comparison with electrochemical etching. It yields, however, layers of low photoluminescence efficiency, deficient homogeneity, and poor reproducibility (Cullis et al. 1997). HF spray and vapor etching methods are also electroless processes. Vapor etching was also investigated to address the difficulty of isolating metal contacts of devices from the electrolyte solution in anodic etching (Kalem and Yavuzcetin 2000). Spark erosion was also tested for preparing porous Si (Hummel and Chang 1992). Noble metal-assisted etching of Si to form PSi is also a simple process that does not require the attachment of any electrodes and can be performed on objects of arbitrary shape and size (Cullis et al. 1997; Kolasinski 2005).

However, it should be noted that, despite the wide variety of methods that can be used for silicon porosification, electrochemical (anodic) etching is the most successful and the technique used for producing pores in semiconductors. All the above-mentioned methods allow forming of porous silicon with its unique parameters, but none of them have reached a stage of maturity, similar to anodization. Besides, many methods have essential limitations on reproducibility, attainment of required porosity, and thickness of formed layer. For example, reactive ion etching (RIE) has limitations in preparing nanoporous Si. RIE also becomes quite complicated in the case of deep structures (tens to hundreds of micrometers) because of the aspect ratio dependence on etching rate and various pattern density effects (Cardinaud et al. 2000). Therefore, the attention of developers is attracted mainly to anodic oxidation, which is the most controllable process, and provides reproducible parameters (Korotcenkov and Cho 2010a). We must note that the standard method of electrochemical etching has appreciably more resources for fabrication of high quality PSi layers in comparison with the above-mentioned methods, such as stain etching, metal-assisted stain etching, laser-induced etching, and spark processing. Electrochemical etching is simple, inexpensive, and gives designers a sufficiently free hand for fabrication PSi layers with required structures (see Fig. 5.12).

Sberveglieri and coworkers (Di Francia et al. 1998) noted the following advantages of porous Si over other porous materials such as ceramics or nano- and polycrystalline films of metal oxides used for sensor design: (1) PSi is basically a crystalline material and thus, in principle, is perfectly compatible with common microelectronic processes devices; (2) PSi can be fabricated using very simple and inexpensive equipment; and (3) PSi can be produced in a large variety of morphologies (see Fig. 5.12), all exhibiting large values of surface-to-volume ratio (Korotcenkov and Cho 2010a). Other advantages of PSi include the possibility of creating three-dimensional structures and designing multisensors, based on the use of various registration techniques for gas detection, e.g., optical, electrical, luminescent, etc. Lower power consumption of PSi-based devices in comparison with metal oxide gas sensors, because PSi-based sensors can work at room temperature, is another important advantage of gas sensors based on porous semiconductors.

In addition, because PSi sensors are based on silicon wafers, they can be manufactured using established integrated circuit production techniques, and can be operated at room temperature using

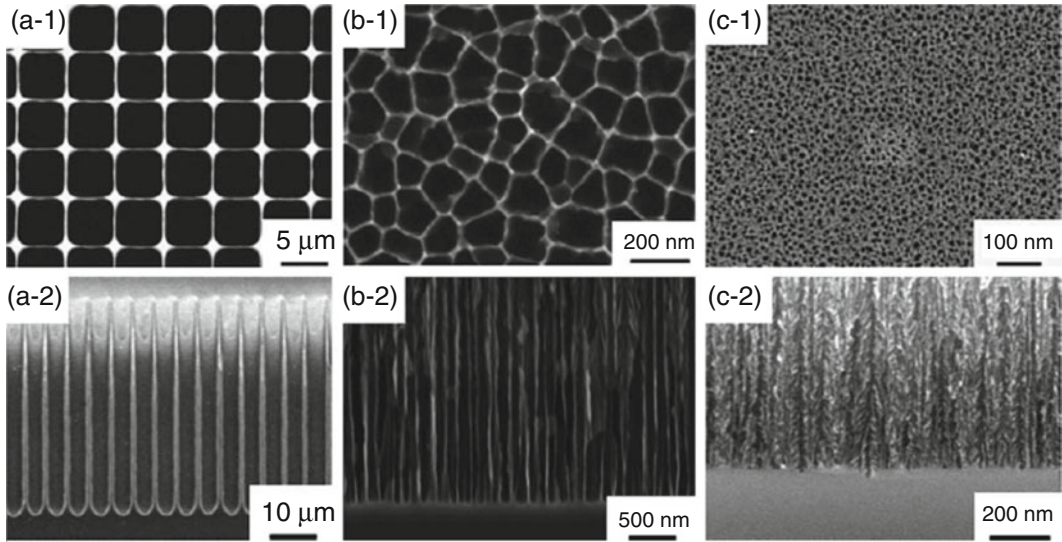


**Fig. 5.12** Top views (a-1, b-1, c-1) and cross-sectional views (a-2, b-2, c-2) of porous silicon with different pore diameters: (a) ordered macro pores, (b) medium-sized pores, and (c) meso pores. Actual average diameters of the pores, which are determined from the SEM images, are 20 nm (meso pore), 120 nm (medium-sized pore), and 5  $\mu\text{m}$  (macro pore), respectively (Reprinted with permission from Fukami et al. (2008). Copyright 2008 Elsevier)

relatively low voltages. They are particularly well suited for producing compact and low-cost sensor systems on a chip, where both the sensing element and the read-out electronics can be effectively integrated on the same wafer. Some authors contend that sensors based on PSi are so simple that they may ultimately be mass-produced for a few cents apiece, and this perspective is a powerful inducement for further development. Moreover, these new sensors could be integrated into electronic equipment and used for building sensing arrays for environmental monitoring, laboratory testing, process control, chemical warfare, biochemistry, and medicine.

Thus, porous semiconductors really have very strong potential for practical applications in gas sensor design. As was shown by Korotcenkov and Cho (2010a), many parameters of porous semiconductors such as the photoluminescence intensity, the capacity of the porous layer, the conductance, the reflection coefficient, infrared (IR) absorption, work function, the resonance frequency of a Fabry–Pérot resonator made of the PSi, and so on are sensitive to the surrounding gas. For example, a repetitive change of the photoluminescence band of porous silicon from green to red and vice versa may be observed when removing the sample from an electrolyte and replacing it. Exposing porous silicon to chemical reagents strongly alters its photoluminescence intensity and conductance features. This means that the measurement of all parameters of porous semiconductors may be the basis for gas sensor design. Types of gas sensors which can be designed on the basis of porous Si are shown in Fig. 5.13. Typical parameters of PSi-based conductometric and photoluminescence quenching RT gas sensors are shown in Table 5.2.

However, analysis carried out by Korotcenkov and Cho (2010a) has shown that porous materials are promising first of all for fabrication of micromachining gas sensor platform, while applications as sensing materials will depend on improvements in the stability and reproducibility of their gas-sensing characteristics. To realize the potential advantages of either porous silicon or other porous semiconductors as practically important materials, further work is necessary. This will provide a better understanding of important physical and chemical factors determining their growth and properties. For example, till now the problem of irreversible surface deviation that leads to the instability of optical and electrical properties of porous materials during sensor aging under ambient gases remains

**Fig. 5.13** Types of gas sensors designed on the base of porous silicon

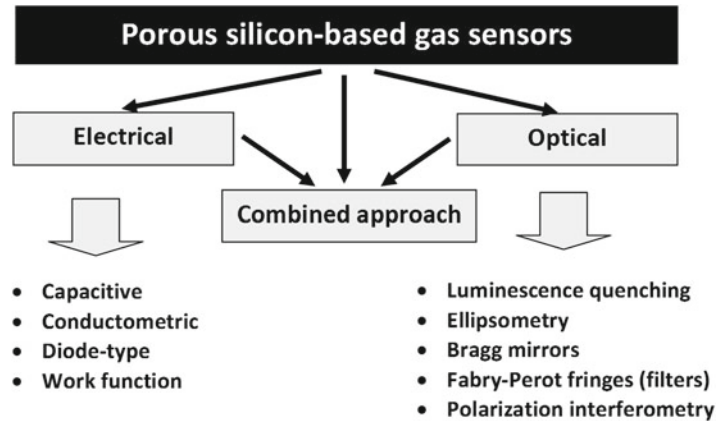


**Table 5.2** Parameters of conductometric and photoluminescence quenching RT gas sensors based on porous silicon

Conductometric sensors		Photoluminescence quenching effect	
Detected gas	Parameters	Target gas	Parameters
Ethanol (4,000 ppm)	$S_m \sim 19$	SO <sub>2</sub> (Ar) (3 ppm)	$S_m \sim 0.6$ ; $P_1 \sim 400$ ppb
H <sub>2</sub> (1%)	$S_m \sim 2$	NO (vacuum) (130 ppm)	$S_m \sim 0.7$ ; $P_1 \sim 2$ ppm
NO <sub>2</sub> (50–2,000 ppb)	$S_m \sim 10\text{--}110$	NO <sub>2</sub> (vacuum)	$S_m \sim 0.9$ ; $P_1 \sim 70$ ppb
NO <sub>x</sub>	$P_g < 1$ ppm		$\tau_{res} \sim$ few seconds, $\tau_{rec} \sim 5$ min
CO	$P_g < 5$ ppm	Vapor alcohols (50 $\mu$ g/mL)	$S_m \sim 0.5\text{--}0.75$
NH <sub>3</sub>	$P_g < 500$ ppb	Methanol, hexanol (150 ppm) (N <sub>2</sub> )	$S_m \sim 0.55\text{--}0.6$
SO <sub>2</sub>	$P_g \sim 1$ ppm		$\tau_{res} < 10$ s
Humidity (35–70% RH)	$S_m \sim 2\text{--}100$	EtOH, pentanol (10 mg/L)	$S_m \sim 0.1$
Ethanol (4%)	$S_m \sim 32$	Methanol	
Methanol (4%)	$S_m \sim 40$	Butanol (10 mg/L)	$S_m \sim 0.15$
Acetone (4%)	$S_m \sim 40$	Pentanol (10 mg/L)	$S_m \sim 0.3$
Butanol (1,000 ppm)	$S_m \sim 3$	Hexanol (10 mg/L)	$S_m \sim 0.5$
Isopropanol (1,000 ppm)	$S_m \sim 1.3$	Protein (in air)	$P_1 < 1$ $\mu$ g/mL
Acetic acid (1,000 ppm)	$S_m \sim 3$	Oxygen (10–100%)	$S_m \sim 0.7$
O <sub>2</sub> (1–100 Torr)	$S_m \sim 1.32$		

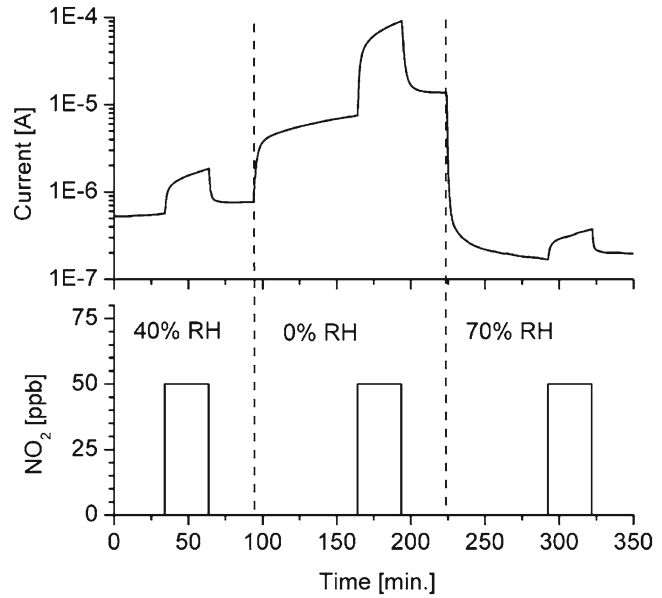
$S_m$ —maximum sensitivity  $|R(\text{air})/R(\text{gas})|$  or  $I(\text{gas})/I(\text{air})$ ;  $P_g$ ,  $P_1$ —threshold of sensitivity

Source: Data from Korotcenkov and Cho (2010a)

unsolved. Several attempts have been made to stabilize a PSi surface against oxidation through the substitution or surface-layer protection of highly reactive Si–H bonds, and it has been shown that this problem can be partially resolved. Approaches used for stabilization of PSi properties will be discussed later in Chap. 22 (Vol. 2) and Chap. 26 (Vol. 2).

The low selectivity of PS-based sensors is another important disadvantage of such kinds of sensors. Due to the sensing mechanism, this kind of device is not able to identify the components of a complex mixture. However, it is necessary to note that this disadvantage is peculiar to all adsorption type sensors, including metal oxide-based gas sensors (Korotcenkov 2005, 2007a, b). In order to enhance the sensor selectivity through specific interactions, some researchers have proposed chemically or physically modifying the PS surface. Likewise, binding of the compounds with structurally recognizing properties was found to enhance the selectivity of PSi sensor response. However, a suitable “all-purpose” surface modification procedure for improving both the stability of a PSi surface and its selectivity and sensitivity toward structurally different analytes has not been found. Therefore, detailed study of the aging mechanisms of freshly formed material is urgently needed. No doubt, some improvement

**Fig. 5.14** Dynamic response of a sensor based on Au-PSi-Si structures in the presence of different relative humidity levels and NO<sub>2</sub> concentrations. The graph above represents the sensor response and the graph below represents NO<sub>2</sub> concentration as a function of time. The dashed vertical lines divide regions with different relative humidity values (Reprinted with permission from Pancheri et al. (2003). Copyright 2003 Elsevier)



of the parameters of gas sensors based on porous semiconductors can be expected in using porous SiC and GaN. However, there are not yet enough experimental results from studies of gas sensors based on those materials to draw any integrating conclusions. Moreover, unfortunately, any appreciable success in this direction has not been achieved.

The strong dependence of sensor parameters on air humidity is another important disadvantage of PSi-based devices. For example, Pancheri et al. (2003) established for PSi-based NO<sub>2</sub> sensors that a switch from 40% RH to dry air, without introducing NO<sub>2</sub>, leads to a conductance increase of around 1 order of magnitude, which is about half of the change obtained by adding 50 ppb of NO<sub>2</sub> without changing the RH (kept at 40%). In particular, Fig. 5.14 shows sensor response and recovery by applying 50 ppb of NO<sub>2</sub> at different RH levels.

One can see that an increase in RH leads to a decrease in conductivity and, therefore, in sensor current. This effect was observed for all kinds of analyzed sensors. For example, it was established by Massera et al. (2004) that the increase of air humidity in the range of 0–60% RH decreases the sensitivity of PSi-based conductometric NO<sub>2</sub> sensors more than four times. The observed behavior could be qualitatively explained by the donor-like character of water molecules adsorbed at PSi surface defects. The relative change of conductivity,  $\Delta G/G$ , in the presence of NO<sub>2</sub> (50 ppb) decreases with increasing relative humidity, passing from 11.7 for 0% RH, to 2.2 for 40% RH, to 1.2 for 70% RH. For comparison, the change of relative humidity in the range 0–60% was accompanied by a change of PSi resistance of more than 20 times (Baratto et al. 2001). Such behavior is undesirable, because the conductometric measurement alone cannot distinguish between variations. The decrease in sensitivity could be due to a partial compensation effect between the acceptor-like NO<sub>2</sub> molecules and donor-like water molecules.

The fabrication of stable contacts with low resistance is a great problem for PSi as well (Lewis et al. 2005). It was established that the physical methods of metal deposition do not minimize contact resistance due to a small contact area, whereas during chemical methods of metal deposition a strong degradation of gas-sensing characteristics could occur. Some technical approaches for resolving these problems were proposed (Gole et al. 2000; Tucci et al. 2004; Lewis et al. 2005). In particular, in research carried out by Lewis et al. (2005), the optimization of technology of contact forming allowed considerable improvement of the operating characteristics of PSi-based sensors, including their

stability. Using a designed metallization process, Gole and his collaborators dramatically reduced the resistance of the electrodes, allowing their PSi-based sensors to operate at between 1 and 10 mV. This is a very good result, because sensors based on earlier porous silicon usually required an operating voltage of as much as 3–5 V due to high resistance in the electrodes connected to the porous silicon.

Relatively slow response and recovery due to operation at low temperatures are also disadvantages. The other important disadvantage of the devices based on PSi is strong nonreproducibility of the properties of porous silicon. The diversity of the morphology of porous silicon is too high, and the dependence of its parameters on the layer structure is too strong (Foll et al. 2002).

One can understand how relevant the problem of the irreproducibility of parameters of porous films is from the fact that the samples prepared by different research groups are hardly comparable even if the preparation conditions are apparently the same (Parkhutik 1999). In many published papers there is no information relating to a detailed structural characterization of the studied porous semiconductors. With such an approach it is hard to expect sufficient progress in the understanding of the nature of phenomena that provide the gas sensitivity of porous semiconductors.

Therefore, the elaboration of new technologies promoting the essential reproducibility of the porous films morphology, and, as a result, the parameters of sensors based on them, is the task of the greatest importance. From our point of view, the unification of the porous semiconductor parameters, which need to be controlled for correct description of the studied objects, is extremely necessary. At present several approaches are being employed for the characterization of porous materials, which might use such parameters as average pore and silicon branch widths, porosity, pore and branch orientation, and layer thickness. Unfortunately, because of the complexity of the porous material structure, the indicated parameters are unable to characterize correctly the porous layers used in experiments individually. For example, the pore diameter does not contain any information about the pore morphology.

The term *pore morphology* is used for such properties as shape (smooth, branched, faceted, etc.), orientation, interconnection of pores, etc. The morphology is the least quantifiable aspect of porous silicon. We understand that it is difficult to characterize systematically the morphology of porous silicon, which has extremely rich details with respect to variations in pore size, shape, and spatial distribution. For example, microporous and mesoporous silicon typically exhibit a sponge-like structure with densely and randomly branched pores. The tendency to branching increases with decrease of pore diameter.

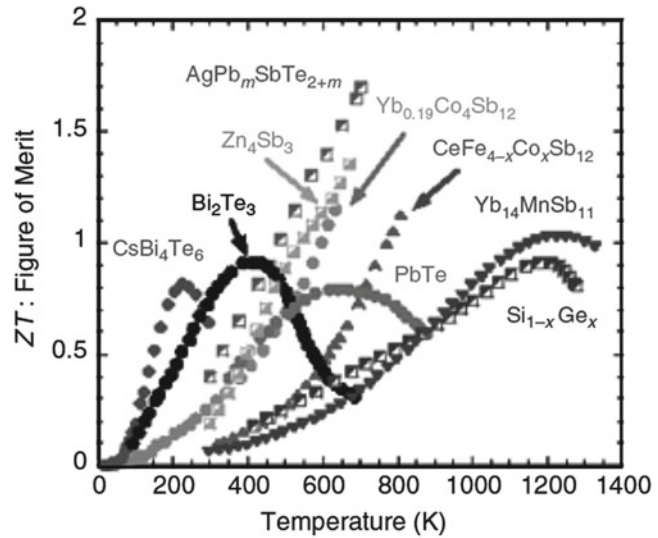
In contrast, macroporous silicon can have discrete pores with smooth walls, with either short branches or dendritic branches. Undoubtedly all those peculiarities of porous films morphology have an effect on the gas-sensing characteristics of sensors and therefore they should be taken into account when designing and testing gas sensors. The better the structural characterization, the deeper will be our understanding of the nature of processes controlling gas-sensing characteristics of PSi-based devices. The improvement of characterization can be attained only at the expense of enlarging the number of methods used for this purpose. At present the techniques used to assess these properties include various microscopy techniques (pore diameter, microstructure, and layer thickness), gravimetric analysis (Brumhead et al. 1993) (porosity and layer thickness), and gas adsorption isotherms (Herino et al. 1987) (pore diameter).

## 5.5 Other Semiconductor Materials

### 5.5.1 *Thermoelectric Materials*

We showed above that wide-bandgap semiconductors are promising for the development of high temperature gas sensors such as FET, Schottky, and MOS-based devices aimed at operation in corrosive environments. However, there are fields of gas sensing where semiconductors with much smaller band gap and lower chemical stability can be applied. Thermoelectric gas sensors are applicable in this

**Fig. 5.15** Figure of merit ( $ZT$ ) as a function of temperature for several high-efficiency bulk thermoelectric materials (Reprinted with permission from Tritt et al. (2008). Copyright 2008 MRS)



field, because thermoelectric gas sensors can operate at low temperatures and the surface of the active area in these devices is covered by the insulating layer of  $\text{SiO}_2$ , i.e., does not come into contact with the corrosive environment.

Early in the twentieth century it was recognized that good thermoelectric materials should possess large Seebeck coefficients, high electrical conductivity, and low thermal conductivity (Ioffe 1957). High electrical conductivity is necessary to minimize Joule heating, while low thermal conductivity helps to retain heat at the junctions and maintain a large temperature gradient. These three properties were later embodied in the so-called figure of merit called  $Z$ . Since  $Z$  varies with temperature, a useful dimensionless figure of merit can be defined as  $ZT$  (where  $T$  is absolute temperature). The figure of merit of a thermoelectric material is defined as

$$Z = \frac{\alpha^2 \sigma}{\kappa}, \quad (5.1)$$

where  $\alpha$  is the Seebeck coefficient of the material,  $\sigma$  is the electrical conductivity of the material, and  $\kappa$  is the total thermal conductivity of the material.

Research carried out during the last century has shown that semiconductor materials can have  $Z$  values significantly higher than those of metals or metal alloys. It was established that materials based on bismuth telluride,  $\text{BiTe}$ , lead telluride,  $\text{PbTe}$ , and silicon–germanium alloys,  $\text{SiGe}$ , emerged as the best thermoelectric materials for operating temperatures of about 450, 900, and 1,400 K, respectively. Current thermoelectric materials, as shown in Fig. 5.15, have  $ZT=1$  (where  $T$  is absolute temperature), and new materials with  $ZT$  values of 2–3 are sought to provide the desired conversion efficiencies. The current materials exhibit conversion efficiencies of 7–8% depending on the specific materials and the temperature differences involved (Tritt et al. 2008). In addition to familiar materials, Si films also became attractive. Because of its large Seebeck coefficient, polycrystalline Si film is also an attractive material for thermocouple devices (Malcovati 1996). For example, for 2- $\mu\text{m}$  thick n-type Si films with a sheet resistance of 2,600  $\Omega/\square$  the Seebeck coefficient is equaled  $\sim 500 \mu\text{V/K}$  (Malcovati 1996) at 300 K.

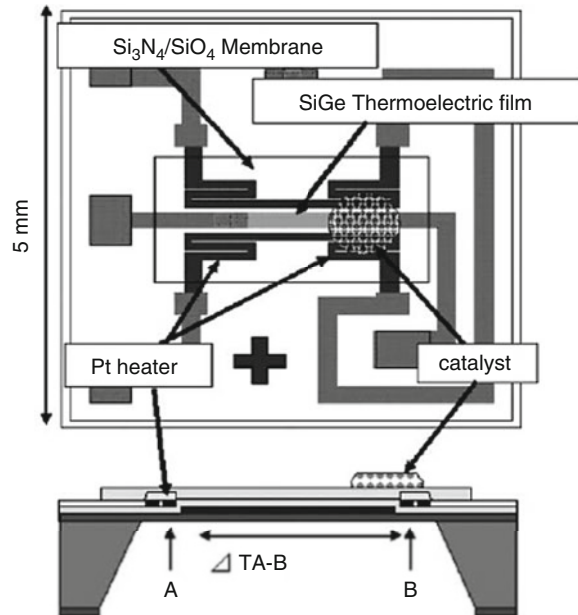
It should be noted, however, that in spite of the great number of thermoelectric materials, only  $\text{SiGe}$  and  $\text{Si}$  are applied in gas sensors (see Table 5.3). The typical configuration of thermoelectric gas sensors is shown in Fig. 5.16. The power factors of  $\text{Si}$  and  $\text{SiGe}$  are almost the same. Films of these materials can be deposited using the same technological methods. For example, they can be deposited

**Table 5.3** Thin-film materials used in thermoelectric-based gas sensors

Material	Seebeck coefficient ( $\mu\text{V/K}$ )	Detected gas	Threshold sensitivity
p-Si	103–307	Ethanol	3 ppm
n-Si	–57 to –500		
p-SiGe	59–115	$\text{H}_2$ , CO	50 ppm
n-SiGe	–77 to –290		

Source: Data from Malcovati (1996), Strasser et al. (2004), Tajima et al. (2005, 2007), Cavicchi et al. (2004), Nishibori et al. (2006a, b), and Shin et al. (2005)

**Fig. 5.16** Device structure of the  $\mu\text{THS}$  on Si substrate ( $5\text{ mm} \times 5\text{ mm} \times 0.35\text{ mm}$ ) using micro-hotplates. A sintered target of 1 at.% boron-doped  $\text{Si}_{0.8}\text{Ge}_{0.2}$  (p-type) with the purity of 99.997% was used for the RF magnetron sputtering deposition of SiGe thin film (Reprinted with permission from Shin et al. (2006). Copyright 2006 Elsevier)



by chemical vapor deposition (CVD) or sputtering, processes which are compatible with the complementary metal oxide semiconductor (CMOS) technology used for designing gas sensors in MEMS implementation. However, the thermal conductivity of SiGe is lower than that of Si, an important advantage of SiGe. It was established that the application of SiGe films instead of metal oxides greatly improved the reliability and sensitivity of the sensors, providing, e.g., for hydrogen detection limits in the low-ppm range (Shin et al. 2005, 2006).

### 5.5.2 II–VI Semiconductor Compounds

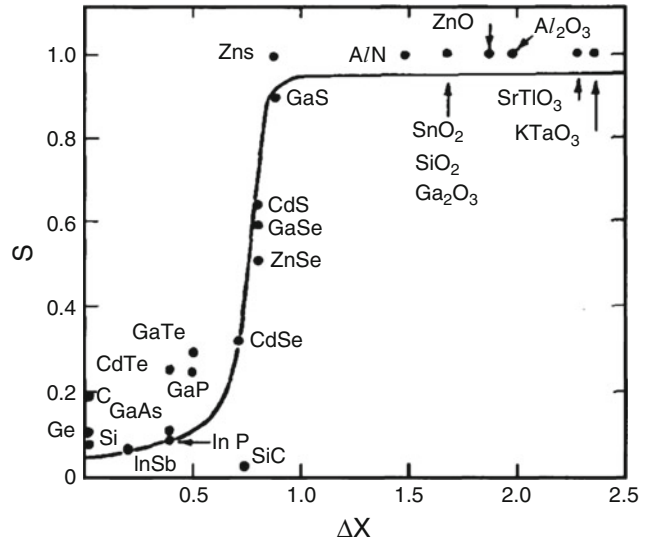
II–VI semiconductor compounds, such as ZnS, ZnSe, CdS, CdSe, etc., are stable materials with high photosensitivity and good luminescence characteristics. Therefore, these materials are highly useful in the making of thin-film solar cells, various devices of optoelectronics, photoresistors, LEDs, and phosphores. Nanoparticles of these materials are also used as quantum dots (Chun et al. 2011). Some parameters of II–VI compounds important for applications are listed in Table 5.4. However, II–VI semiconductor compounds can be used for gas sensor design as well. Research has shown that II–VI semiconductor compounds do not have the surface Fermi level pinning (see Fig. 5.17). It has been generally recognized that semiconductors can be classified into two broad groups based on the properties of the semiconductor–metal interface. “Ionic” materials display little or no Fermi-level



**Table 5.4** Parameters of chalcogenides used in gas sensors

Semiconductor	$E_g$ (eV)	$T_{\text{melting}}$ (°C)	$T_{\text{sublimation}}$ (°C)	$T_{\text{oxidation}}$ (°C)
ZnS	3.54–3.91	1,827–1,850	1,178	<500
ZnSe	2.7–2.721	1,525	800–900	<300
ZnTe	2.25–2.27	1,238–1,290	~600	
CdS	2.42–2.46	1,475–1,750	980	<450–500
CdSe	1.74–1.751	1,268	600–700	
CdTe	1.49–1.51	1,092	~500	

**Fig. 5.17** Influence of electronegativity on the value of  $S$  in  $\Phi_{\text{Bn}} = S\Delta X$  (Adapted with permission from Kurtin et al. (1969). Copyright 1969 American Physical Society)



stabilization at the interface; “covalent” materials display virtually complete stabilization. Figure 5.17 illustrates this statement. The slope  $d\Phi_{\text{Bn}}/dX_{\text{M}}$ , which is inversely correlated to the extent of Fermi-level stabilization, was found to be 1 (no Fermi-level stabilization) for “ionic” materials and 0.1 (nearly complete Fermi level stabilization) for “covalent” materials. As we can see, for II–VI compounds the slope  $S$  varies from 0.3 for CdTe and CdSe to 1.0 for ZnS. This means that the surface Fermi-level position, i.e., the band bending in these semiconductors, can be changed over a wide range, contributing to the achievement of high sensor response due to interaction with the gas surrounding. Gas sensors based on II–VI semiconductor compounds are presented in Table 5.5. For comparison, for semiconductors such as Si, GaAs, and InP, the surface Fermi level is firmly pinned within their band gap due to high surface state density. For information, for all metal oxides  $S$  is equal to 1.0.

As can be seen, II–VI semiconductor compounds can be used as sensing materials in all types of gas sensors, including chemiresistors, SAW, heterojunction based, and optical. They can be applied to surface functionalizing and composites forming as well. The application of II–VI semiconductor compounds in quantum dots-based gas sensors will be discussed in Chap. 5 (Vol. 2). Operating characteristics of several II–VI-based gas sensors are shown in Figs. 5.18 and 5.19.

It is important that the sensitivity of II–VI-based gas sensors of the conductometric type for various semiconductors changes according to the value of  $S$  from Fig. 5.17. For example, in the couple CdS–CdSe, CdS-based sensors had much better sensitivity to vapors of water, ethanol, ammonia, acetone, and iodine (Nesheva et al. 2006). We also need to note that all regularities established for metal oxides work in II–VI-based gas sensors as well (Lantto and Golovanov 1995). This means that for better sensitivity, II–VI semiconductor compounds should be porous with small both the grain size

**Table 5.5** Gas sensors designed on the base of II–VI compounds

Semiconductor	Preparing	Sensor type	Gas tested	Reference
CdS	Films, 30–200 nm (evaporation); Powders	Photoconductivity, RT	H <sub>2</sub> O, CO, H <sub>2</sub> , NH <sub>3</sub> , I, ethanol, acetone	Nesheva et al. (2006), Miremadi et al. (1997)
	Films (spray pyrolysis)	Chemiresistors, 200–280 °C	O <sub>2</sub>	Afify and Battisha (2000)
	Film (spray pyrolysis)	SAW, 160 °C	SO <sub>2</sub>	Lee et al. (1998)
CdSe	Films, 50 nm (evaporation)	Photoconductivity, RT	H <sub>2</sub> O, NH <sub>3</sub> , I, ethanol, acetone	Nesheva et al. (2006)
	Films (evaporation)	Chemiresistors	CO <sub>2</sub>	Patel et al. (1994)
ZnS	Powders (wet chemical)	Cataluminescence, 330 °C	CCl <sub>4</sub>	Luo et al. (2009)
	Nanobelts	Chemiresistors, 300 °C	H <sub>2</sub>	Chen et al. (2008)
	Nanobelts	Chemiresistors, RT+UV	O <sub>2</sub>	Liu et al. (2007)
ZnS/cyclohexylamine	Nanowires (solvothermal)	Chemiresistors	Ethanol	Xu et al. (2011)
n-CdSe/p-polyaniline n-CdTe/p-polyaniline	Film (electrodeposition)	Heterojunction, RT	LPG	Joshi et al. (2007, 2008)
CdS, PbS, ZnS/ (PEO:NH <sub>4</sub> ClO <sub>4</sub> )	Powders	Solid electrolyte (conductometric, RT)	NH <sub>3</sub>	Saroch et al. (2008)
ZnS/TiO <sub>2</sub> nanotubes	Powders	Chemiresistors, 160 °C	H <sub>2</sub>	Li et al. (2010)
ZnS/ZnO	Powders (hydrothermal)	Chemiresistors, 210 °C	Ethanol	Yu et al. (2010)

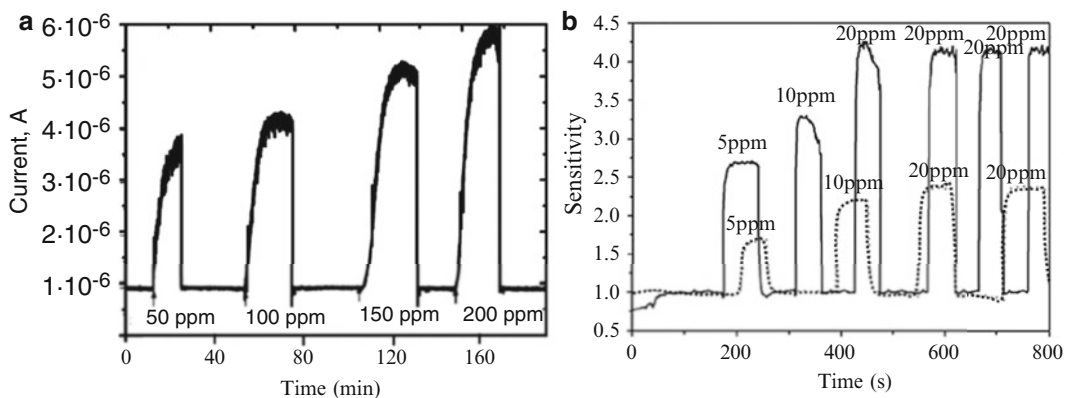


**Fig. 5.18** (a) The response of ZnS nanostructures to H<sub>2</sub> at a working temperature of 300 °C toward H<sub>2</sub> and N<sub>2</sub> pulses. Reprinted with permission from Chen et al. (2008). Copyright 2008 IOP. (b) Response curves of ZnO dumbbells (*dotted*) and ZnO/ZnS hollow nanocages (*full curve*) to ethanol with increasing concentrations at 210 °C (Reprinted with permission from Yu et al. (2010). Copyright 2010 Springer)

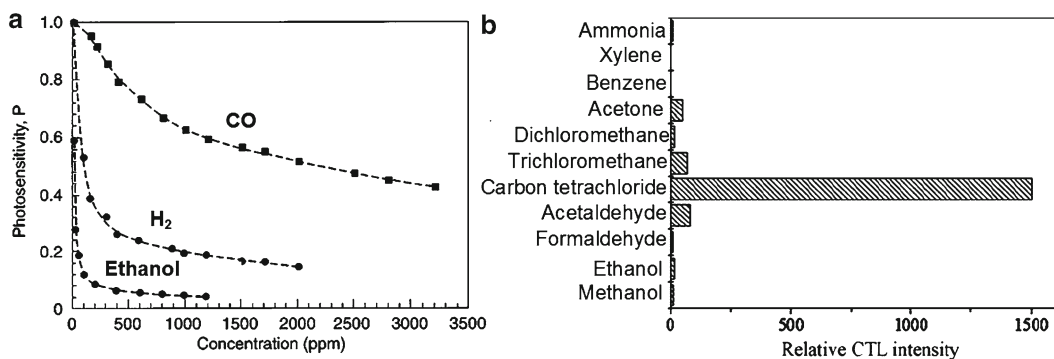


**Fig. 5.19** (a) Variation of normalized photosensitivity of CdS films with concentration for hydrogen, carbon monoxide, and ethanol at 200 °C and 200 Hz. (Reprinted with permission from Mirejadi et al. (1997). Copyright 1997 AIP. (b) Selectivity of the carbon tetrachloride ZnS-based gas sensor. Conditions: wavelength, 460 nm;  $T_{\text{oper}} = 335$  °C; gas concentration, 4.5  $\mu\text{g}/\text{mL}$ ; and air flow rate, 210 mL/min (Reprinted with permission from Luo et al. (2009). Copyright 2009 Elsevier)

and diameter of nanowires or nanofibers (Xu et al. 2011). The thinner films have also shown higher sensitivity and shorter response time (Afify and Battisha 2000). The increase of operating temperature decreases response and recovery times (Afify and Battisha 2000). Surface modification by noble metals improves the selectivity and the sensitivity of II–VI semiconductor compounds as well (Mirejadi et al. 1997).

However, in spite of results presented before, one can assert that gas sensors based on II–VI semiconductor compounds do not have perspectives in the gas sensor market. From all types of II–VI-based gas sensors, maybe only cataluminescence sensors designed by Luo et al. (2009) for detection of  $\text{CCl}_4$  vapors due to high selectivity are of interest (see Fig. 5.19b). Regarding other sensors one can say that they cannot replace metal oxide gas sensors, because they are sensitive to the same gases and vapors, have low selectivity, and the application of these materials does not give an improvement of operating characteristics in comparison with metal oxide-based sensors. As a rule, parameters of II–VI-based gas sensors are considerably worse. Moreover, parameters of II–VI semiconductor compounds depend strongly on lighting and temperature. In addition, in spite of high melting temperatures, sublimation and especially irreversible oxidation take place at considerably lower temperatures (see Table 5.4) (Dimitrov and Boyanov 2000; Dimitrov et al. 2002). As a result, operating temperatures of II–VI-based gas sensors do not exceed 300–350 °C for the most stable compounds ZnS and CdS. This means that II–VI semiconductor compounds cannot resolve the problems of selectivity and temporal instability of gas sensors. Too high resistance of the ZnS and CdS also creates difficulties in gas sensor design (Fang et al. 2011).

Liu et al. (2007) believe that the above-mentioned problems could be resolved using UV radiation. The response of ZnS nanobelts to different oxygen pressures with or without UV illumination was measured at room temperature. It was found that response time was about 2.5 s. When the light was turned off, the current recovered to the original dark level within 0.2 s. According to Liu et al. (2007) the illumination enhances the modulation of conductance by adsorbed oxygen. The fast response and rapid recovery arose from the generation and recombination of the electron–hole pairs in ZnS. The slow increase in response time was attributed to the oxygen desorption process on the ZnS nanobelt surface, taking place due to hole capture. It was found that the conductance of the ZnS nanobelt is roughly proportional to the logarithm of the oxygen pressure, which indicates that these nanobelts can be promising oxygen sensors for RT operation. However, it is necessary to note that the same effect of UV activation was observed in metal oxide-based sensors.

**Table 5.6** Chalcogenide glasses used in gas sensors operated at room temperature

Glass	Sensor type	Detected gas (threshold of sensitivity)	Reference
As <sub>2</sub> Se <sub>3</sub>	Optic sensor (acousto-optic element)	CO <sub>2</sub> ( $\lambda$ -4.3 and 4.7 $\mu$ m) (~1%)	Saito and Miyagi (1991)
(As <sub>2</sub> S <sub>3</sub> ) <sub>x</sub> -(As <sub>2</sub> Se <sub>3</sub> ) <sub>y</sub>	Chemiresistor	CO; H <sub>2</sub> (<10 ppm)	Dmitriev and Dementiev (2005)
As-S-Te	Chemiresistor	NO <sub>2</sub> (<100 ppb); CO (<200 ppm); SO <sub>2</sub> (<10 ppm)	Marian et al. (2001a)
As-Tl-S-Se	Chemiresistor	CO; CH <sub>4</sub> ; H <sub>2</sub> ; NO <sub>2</sub>	Dmitriev et al. (2004)
As <sub>4</sub> S <sub>3</sub>	Chemiresistor	Propylamine vapor (~40 ppm)	Marian et al. (2000)
Ge-As-Te	FET-based	NO <sub>2</sub> (<100 ppb); CO (<200 ppm); NH <sub>3</sub> , SO <sub>2</sub> (<5 ppm)	Marian et al. (2001b)
(GeS <sub>x</sub> ) <sub>(100-y)</sub> (AgI) <sub>y</sub>	Cantilevers	Acetone (~1–3%)	Monchev et al. (2007)
(As <sub>2</sub> S <sub>3</sub> ) <sub>(100-x)</sub> (AgI) <sub>x</sub>	Cantilevers	Acetone (~5%); isopropanol, ethanol (~10%)	Koleva et al. (2009)
Ge-As-S	Quartz crystal microbalance	NH <sub>3</sub> (<100 ppm)	Georgieva et al. (2009)

### 5.5.3 Semiconductor Glasses

#### 5.5.3.1 Chalcogenide Glasses

Semiconductor chalcogenide glasses have many current and potential applications in optics, optoelectronics, chemistry, and electrochemistry, including gas sensing due to their flexible structure, high chemical stability, enormous variation in properties such as electroconductivity, photoconductivity, thermal diffusivity, optical band gap, absorption of amorphous chalcogenides, and an almost unlimited ability for doping and alloying (Borisova 1981; Popescu 2000; Marian et al. 2000; Reithmaier et al. 2010). For example, Monchev et al. (2007) have developed cantilever-based gas sensors for acetone and ammonia detection where the change of the resonance frequency is caused by the Ge-S-AgI chemisorption of these gases. Kozicki and Mitkova (2006) have described the change of the resonance frequency and the Q-factor caused by an electrically forced Ag-ion transport. The mobile silver can move to the surface where it will form stable or unstable compounds with NH<sub>3</sub>, SO<sub>2</sub> (Barber et al. 1974), halogen-hydrogen compounds, etc. Marian et al. (2000) reported about As-S-Te-based chemiresistors making it possible to detect NO<sub>2</sub>, CO, and SO<sub>2</sub>. The response and the recovery times were rapid, with good reproducibility and high sensibility. All the above-mentioned sensors operated at room temperatures. We need to note that the possibility for preparation of chalcogenide-based gas sensors, which work at room temperatures in contrast to the oxide sensors, is an advantage of these devices. Moreover, chalcogenide films can be deposited on both hard and flexible substrates (Dmitriev et al. 2004; Dmitriev and Dementiev 2005). Chalcogenide glasses used for gas sensor design are listed in Table 5.6.

However, we need to recognize that optical gas sensing is the most promising area for chalcogenide glasses application. In many cases polymer-based room temperature gas sensors show better operation characteristics. The wide practical application in optical and fiber optic gas sensors of chalcogenides such as arsenic sulfide (As<sub>2</sub>S<sub>3</sub>) and arsenic selenide (As<sub>2</sub>Se<sub>3</sub>), especially of vitreous Ge-containing condensates, is closely connected with their transparency in the visible and near IR spectral regions and with the possibility to create optical media with defined values of refractive index, dispersion, and extinction coefficient (Dixon 1967; Ohmachi and Uchida 1972; Lyubin et al. 2004a). The relatively low energy of the chemical bonds in Ge-based chalcogenide glasses offers the

**Table 5.7** Glass-based solid electrolyte gas sensors

Glass	Sensor type	$T_{\text{oper}}$ (°C)	Detected gas	Reference
$\text{V}_2\text{O}_5\text{-Sb}_2\text{O}_3\text{-TeO}_2$	Solid electrolyte (conductometric)	30–200	$\text{O}_2$ (10–100%)	Mori and Sakata (1996)
$\text{P}_2\text{O}_5\text{-SiO}_2$ (5:95)	Solid electrolyte (potentiometric)	–30 to +30	$\text{H}_2$ (0.1–4.0 vol.%)	Nogami et al. (2006), Matsumura et al. (2007)
	Solid electrolyte (potentiometric)	25	Methanol (0.01–2.0%)	Nogami et al. (2009)
$\text{V}_2\text{O}_5\text{-SrO-Sb}_2\text{O}_3$ (73:18:9)	Solid electrolyte (conductometric)	60–170	$\text{O}_2$ (10–100%)	Sakata et al. (1994)
$\text{V}_2\text{O}_5\text{-SnO-TeO}_2$ (50:20:30)	Solid electrolyte (conductometric)	30–200	$\text{O}_2$ (10–100%)	Mori and Sakata (1997)
$\text{CuTi}_2(\text{PO}_4)_3$	Solid electrolyte (potentiometric)	100	$\text{O}_2$ (20–100%)	Yamamoto et al. (1998)

opportunity for photostructural transformations and a number of other light-induced effects, all of which are typically accompanied by considerable changes in the optical constants of the chalcogenides. At present, chalcogenide glasses have been utilized to fabricate mid-IR fibers (Zhang et al. 2004), planar waveguides (Curry et al. 2005), gratings (Vlcek et al. 2009), all-optical switches (Bhargava and Suthar 2009), and fiber amplifiers (Moon and Schaafsma 2000). Due to specific optical properties, the waveguides based on chalcogenides allow the detection of the vibrations of various molecules such as  $\text{CO}_2$ , NOX, SOX,  $\text{H}_2\text{O}$ , etc., present in the IR spectral range (Hess 1989; Meyer and Sigrist 1990). As is well known, germanium chalcogenides have transmission windows up to 12 mm. Chalcogenide glasses are also advantageous in terms of availability of large size element, simple fabrication process, and low cost of production.

We must also note that several properties of chalcogenides which were indicated as advantages can be considered as disadvantages as well. Sensors based on chalcogenides can operate only at low temperatures. It was established that very often dissociation and fractional evaporation of individual components of the glasses can be observed during the preparation and operation process at low temperatures. In addition, chalcogenides are sensitive to light (Kolobov and Tanaka 2001). In particular, the illumination by band gap light changes the internal and/or surface structure of the chalcogenide materials and leads to red or blue shifts of the optical absorption edge (de Neufville et al. 1974). This shift causes changes of the optical constants and variations of physical–chemical properties (microhardness, density, solubility). Moreover, it was found that illumination of chalcogenide/metal film structures with light with photon energies comparable to that of the band gap of the material leads to rapid penetration of the metal into the semiconductor (Kostyshin et al. 1966). This process was named photodiffusion or “photodoping” (Wagner et al. 2001; Lyubin et al. 2004b; Kovalskiy et al. 2009). High diffusion coefficient of various metals even in the dark can also influence the parameters of gas sensors (Kozicki and Mitkova 2006). In addition, we do not observe improvement of sensor response in comparison with conventional gas sensing materials.

### 5.5.3.2 Other Glasses

Glasses are a big class of materials and many of them can be used for gas sensor design. Examples of these sensors are listed in Table 5.7. Several glasses are also presented in Table 5.6.

As one can see, solid electrolyte-based gas sensor is the main application of these materials. In particular, Matsumura et al. (2007) reported on solid-state potentiometric thin-film hydrogen gas sensors fabricated using sol–gel-derived high proton-conducting  $\text{P}_2\text{O}_5\text{-SiO}_2$  glass films. High ion conductivity at low temperatures is the main advantage of these glasses in comparison with metal oxides.

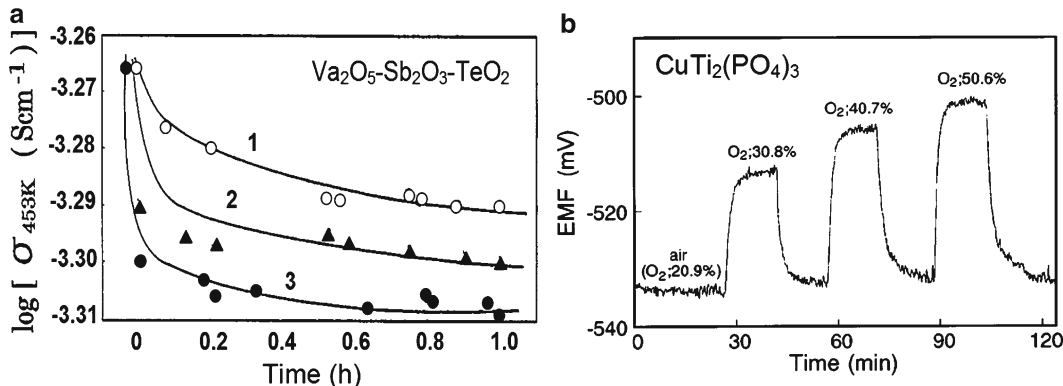


**Fig. 5.20** (a) Variations in conductivity of 62.3 $\text{Va}_2\text{O}_5$ -4.3 $\text{Sb}_2\text{O}_3$ -33.3 $\text{TeO}_2$  glass (mol%) as a function of oxygen partial pressure,  $P_{O_2}$ , at 453 K: (1)  $P_{O_2} = 0.15 \text{ atm}$ ; (2)  $P_{O_2} = 0.20 \text{ atm}$ ; (3)  $P_{O_2} = 0.35 \text{ atm}$ . Adapted with permission from Mori and Sakata (1996). Copyright 1996 Elsevier. (b) EMF response upon changing oxygen partial pressure to the reference ( $P_{O_2} = 20.9\%$ ), measured at 100 °C, for the  $\text{CuTi}_2(\text{PO}_4)_3$ -precipitated glass ceramic obtained by heating at 800 °C (Reprinted with permission from Yamamoto et al. (1998). Copyright 1998 American Institute of Physics)

As a result, the sensor designed exhibited high speed, responding within 10 s and 120 s at 30 °C and -30 °C, respectively, for 1 vol.% hydrogen gas. A linear relationship between the electromotive force (EMF) and the logarithmic hydrogen concentration of 0.1–1 vol.% was obtained in the temperature ranging from -30 to 30 °C. However, oxygen sensors designed by Mori and Sakata (1996) based on  $\text{V}_2\text{O}_5$ - $\text{Sb}_2\text{O}_3$ - $\text{TeO}_2$  glasses had considerably slower responses even at 200 °C. The same result was observed for other glasses (Mori and Sakata 1997). This means that sensors designed based on the indicated glasses are not acceptable for in situ measurements. In this regard,  $\text{CuTi}_2(\text{PO}_4)_3$ -based potentiometric oxygen sensors have much better characteristics (Yamamoto et al. 1998). Operating characteristics of  $\text{CuTi}_2(\text{PO}_4)_3$ -based oxygen sensors are shown in Fig. 5.20. The glass ceramics investigated by Yamamoto et al. (1998) exhibited good stability under a high oxygen concentration at high temperature, which is advantageous for practical applications.

### 5.5.4 Tellurium

Polycrystalline tellurium thin films were the subject of many investigations in the past due to their interesting electrical (Dinno and Schwartz 1974; Chakrabarti and Pal 1980) and optical (Swan et al. 1991) properties. One of the advantages of tellurium films over compound semiconductors in sensor and other device applications is the exemption from stoichiometry problems. This advantage allows the use of a large variety of methods for their preparation including thermal evaporation, sputtering, chemical precipitation, and hot wall epitaxy. Tellurium films show p-type conduction due to lattice defects acting as acceptors; the band gap is about 0.34 eV and the carrier concentration at room temperature is in the range of  $(1-5) \times 10^{18} \text{ cm}^{-3}$ . The Hall mobility at room temperature is typically in the range 20–50  $\text{cm}^2/\text{V s}$ . The grain sizes of tellurium film depend on the fabrication conditions, being usually less than 100 nm (Tsiulyanu 2010).

It was established that the electrical conductivity of tellurium films may be influenced by localized surface states at the crystalline boundaries due to impurities and gas atoms adsorbed during and after the growth process. This phenomenon related to oxygen influence on the electrical properties of tellurium was first observed by Tabatadze and Myasnikov (1973). However, the real interest in tellurium thin-films-based gas sensors was initiated only in the early 2000s by Tsiulyanu and coworkers

**Table 5.8** Comparison of Te-based thin-film gas sensors operated at room temperature

Target gas	Technology of preparation	Dynamic range	Reference
NO <sub>2</sub>	Thermal vacuum evaporation	0.01–1.0 ppm	Tsiulyanu et al. (2005)
	Thermal vacuum evaporation	0.2–1.0 ppm	Bhandarkar et al. (2006)
	RF sputtering	1.0–100 ppm	Siciliano et al. (2008)
	1-D structures ( $T_{\text{cond}} = 300\text{--}350\text{ }^{\circ}\text{C}$ )	10–200 ppm	Siciliano et al. (2009)
NH <sub>3</sub>	Thermal vacuum evaporation	10–150 ppm	Sen et al. (2004)
H <sub>2</sub> S	Thermal vacuum evaporation	0.1–1.0 ppm	Sen et al. (2006), Bhandarkar et al. (2006)
CO	Thermal vacuum evaporation	50–400 ppm	Tsiulyanu et al. (2002)
	Te:Ti thermal vacuum evaporation	0.1 vol.%	Duk and Lee (2005)
C <sub>3</sub> H <sub>7</sub> NH <sub>2</sub>	Thermal vacuum evaporation	1.0–10 ppm	Tsiulyanu et al. (2002)
Cl <sub>2</sub>	1-D structures (synthesis under atmospheric conditions, $T = 30\text{--}50\text{ }^{\circ}\text{C}$ )	0.1–2.0 ppm	Sen et al. (2009)

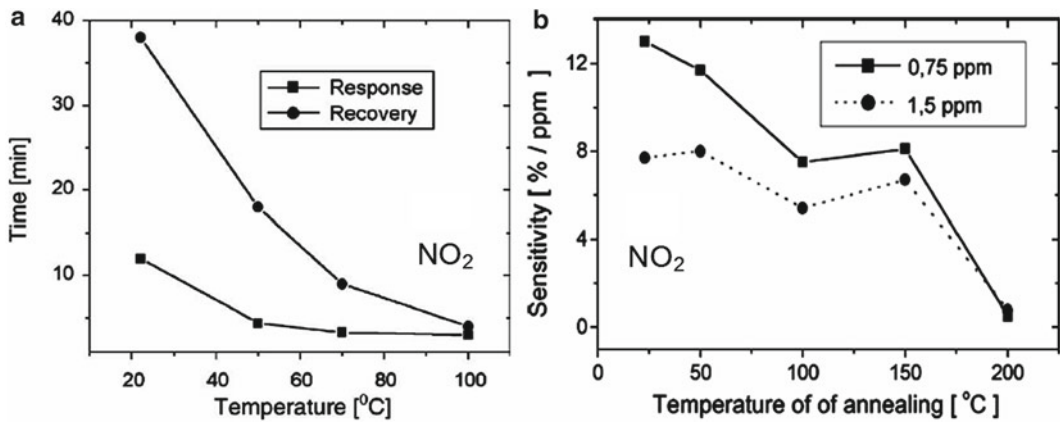


**Fig. 5.21** (a) The response and the recovery times of tellurium-based gas sensors during NO<sub>2</sub> detection ( $d \sim 110$  nm). (b) Influence of annealing on sensor response to NO<sub>2</sub> (Reprinted with permission from Tsiulyanu et al. (2005). Copyright 2005 Elsevier)

(Tsiulyanu et al. 2001, 2002; Marian et al. 2001b) who showed that tellurium thin films exhibit a high sensitivity to nitrogen dioxide even at room temperature. This advantage allows a miniaturization of gas-sensitive devices and a reduction of the power consumption. Then similar research was started in other groups. Results of that research are shown in Table 5.8.

As a result of that research, it was found that tellurium-based gas sensors show comparatively short response times and a good sensitivity in the ppm and sub-ppm concentration ranges. Recovery process is much slower. During H<sub>2</sub>S and NO<sub>2</sub> detection, the recovery time at room temperatures exceeds 7–10 min (Tsiulyanu et al. 2005; Bhandarkar et al. 2006) (see Fig. 5.21). The flexible structure and high compatibility with alloying allow variation of the properties of these materials over wide ranges and make it possible to design sensors sensitive to different gases (see Table 5.8). Bhandarkar et al. (2006) established that for tellurium films deposited at temperatures similar to those used for metal oxides in chemiresistors, gas sensitivity improves with reduction in the grain size. This has been attributed to increase in effective surface area for gas–film interaction. Investigation of the gas sensing mechanism of tellurium thin films is still in progress, but in principle it can be explained by direct or indirect interaction of adsorbed species with lone-pair electrons, which form the upper part of the valence band, and/or reversible chemical reactions on the grain surfaces (Tsiulyanu et al. 2004)

However, we have to note that tellurium-based gas sensors hardly have any real applications. Such sensors have a very restricted temperature range of operation. Experiments have shown that the sensitivity of the films to  $\text{NO}_2$  was reduced strongly at temperatures around  $80\text{ }^\circ\text{C}$  (Tsiulyanu et al. 2004). Sen et al. (2004) observed a strong decrease of sensitivity to  $\text{NH}_3$  even at temperatures higher than  $30\text{ }^\circ\text{C}$ . Postdeposition annealing of tellurium films at temperatures above  $100\text{ }^\circ\text{C}$  also noticeably influences their electrical conductivity and sensitivity to target gases (Tsiulyanu et al. 2004). Moreover, at temperatures higher than  $150\text{ }^\circ\text{C}$  the conductivity sharply and irreversibly increases simultaneously with the decrease of the gas sensitivity (see Fig. 5.21). Tsiulyanu et al. (2005) found that thermal treatment of the films at temperatures greater than  $100\text{ }^\circ\text{C}$  leads to recrystallization of the films.

## References

- Afify HH, Battisha IK (2000) Oxygen interaction with CdS based gas sensors by varying different preparation parameters. *Indian J Pure Appl Phys* 38(2):119–126
- Afridi MY, Suehle JS, Zaghoul ME, Tiffany JE, Cavicchi RE (2001) Implementation of CMOS compatible conductance-based micro-gas-sensor system. In: Proceedings ECCTD'01, European conference on circuit theory and design, Espoo, Finland, 28–31 Aug, pp 381–384
- Afridi MY, Suehle JS, Zaghoul ME, Berning DW, Hefner AR, Cavicchi RE, Semacik S, Montgomery CB, Taylor CJ (2002) A monolithic CMOS microhotplate-based gas sensor system. *IEEE Sens J* 2(6):644–655
- Anderson RC, Muller RS, Tobias CW (1990) Investigation of porous silicon for vapour sensing. *Sens Actuators A Phys* 21–23:835–839
- Arbab A, Lloyd Spetz A, Lundström I (1993) Gas sensors for high temperature operation based on metal oxide silicon carbide (MOSiC) devices. *Sens Actuators B Chem* 15:19–23
- Baranzahi A, Lloyd Spetz A, Glavmo M, Carlsson C, Nytomt J, Salomonsson P, Jobson E, Haggendal B, Martensson P, Lundström I (1997) Response of metal-oxide-silicon carbide sensors to simulated and real exhaust gases. *Sens Actuators B Chem* 43:52–59
- Baratto C, Faglia G, Sberveglieri G, Boarino L, Rossi AM, Amato G (2001) Front-side micromachined porous silicon nitrogen dioxide gas sensor. *Thin Solid Films* 391:261–264
- Barber M, Sharpe P, Vickerman JC (1974) An investigation of the  $\text{SO}_2/\text{Ag}$  surface reaction using secondary ion mass spectrometry. *Chem Phys Lett* 27:436–438
- Bhandarkar V, Sen S, Muthe KP, Kaur M, Kumar MS, Deshpande SK, Gupta SK, Yakmi JV, Sahni VC (2006) Effect of deposition conditions on the microstructure and gas-sensing characteristics of Te thin films. *Mater Sci Eng B* 131:156–161
- Bhargava A, Suthar B (2009) Optical switching in Kerr non-linear chalcogenide photonic crystal. *J Ovonic Res* 5:187–193
- Bhattacharyya P, Basu PK, Mondal B, Saha H (2008) A low power MEMS gas sensor based on nanocrystalline ZnO thin films for sensing methane. *Microelectron Reliab* 48(11–12):1772–1779
- Bogue RW (2002a) The role of materials in advanced sensor technology. *Sensor Rev* 22(4):289–299
- Bogue R (2002b) Advanced automotive sensors. *Sensor Rev* 22(2):113–118
- Bogue R (2007) MEMS sensors: past, present and future. *Sensor Rev* 27(1):7–13
- Borisova ZU (1981) Glassy semiconductors. Plenum, New York, NY
- Brumhead D, Canham LT, Seekings DM, Tufton PJ (1993) Gravimetric analysis of pore nucleation and propagation in anodized silicon. *Electrochim Acta* 38:191–197
- Cane C, Gracia I, Gotz A, Fonseca L, Tamay EL, Horrillo MC (2000) Detection of gases with arrays of micromachined tin oxide gas sensors. *Sens Actuators B Chem* 65:244–246
- Canham L (ed) (1997) Properties of porous silicon. INSPEC, London
- Cardinaud C, Peignon MC, Tessier PY (2000) Plasma etching: principles, mechanisms, application to micro- and nano-technologies. *Appl Surf Sci* 164:72–83
- Cavicchi RE, Poirier GE, Tea NH, Afridi M, Berning D, Hefner A, Suehle J, Gaitan M, Semancik S, Montgomery C (2004) Micro-differential scanning calorimeter for combustible gas sensing. *Sens Actuators B Chem* 97:22–30
- Chakrabarti B, Pal AK (1980) Electrical and galvanomagnetic properties of Te films. *Jpn J Appl Phys* 19:591–596
- Chen HI, Chou YI (2004) Evaluation of the perfection of the Pd–InP Schottky interface from the energy viewpoint of hydrogen adsorbates. *Semicond Sci Technol* 19:39–44
- Chen HI, Chou YI, Hsiung CK (2003) Comprehensive study of adsorption kinetics for hydrogen sensing with an electroless-plated Pd–InP Schottky diode. *Sens Actuators B Chem* 92:6–16



- Chen Z-G, Zou J, Liu G, Lu HF, Feng LF, Lu G-Q, Cheng HM (2008) Silicon-induced oriented ZnS nanobelts for hydrogen sensitivity. *Nanotechnology* 19:055710
- Chou YI, Chen CM, Liu WC, Chen HI (2005) Schottky hydrogen sensor fabricated by electrophoretic deposition with Pd nanoparticles. *IEEE Electron Device Lett* 26:62–64
- Chun J, Yang W, Kim JS (2011) Thermal stability of CdSe/ZnS quantum dot-based optical fiber temperature sensor. *Mol Crystallogr Liq Crystallogr* 538(1):333–340
- Comini E, Faglia G, Sberveglieri G (eds) (2009) *Solid state gas sensing*. Springer, Berlin
- Cui JB, Ristein J, Ley L (1999) Dehydrogenation and the surface phase transition on diamond (111): kinetics and electronic structure. *Phys Rev B* 59(8):5847–5856
- Cullis AG, Canham LT, Calcott PDG (1997) The structural and luminescence properties of porous silicon. *J Appl Phys* 82:909–965
- Curry RJ, Mairaj AK, Huang CC, Eason RW, Grivas C, Hewak DW, Badding JV (2005) Chalcogenide glass thin films and planar waveguides. *J Am Ceram Soc* 88(9):2451–2455
- De Neufville JP, Moss SC, Ovshinsky SR (1974) Photostructural transformation in amorphous As<sub>2</sub>Se<sub>3</sub> and As<sub>2</sub>S<sub>3</sub> films. *J Non Cryst Solids* 13:191–223
- Di Francia G, De Filippo F, La Ferrara V, Quercia L, Lancellotti L, Barotto C, Comini E, Faglia G, Sberveglieri G (1998) Porous silicon layers for the detection at RT of low concentrations of vapours from organic compounds, In: White NM (ed.) *Proceedings of European Conference Eurosensors XII*, 1:544. IOP: Southampton, UK
- Dimitrov RI, Boyanov BS (2000) Oxidation of metal sulphides and determination of characteristic temperatures by DTA and TG. *J Therm Anal Calorim* 61:181–189
- Dimitrov RI, Moldovanska N, Bonev IK (2002) Cadmium sulphide oxidation. *Thermochim Acta* 385:41–49
- Dinno MA, Schwartz M (1974) Structural dependence of electrical conductivity of thin tellurium films. *J Appl Phys* 45:3328–3331
- Dixon RW (1967) Photoelastic properties of selected materials and their relevance for applications to acoustic light modulators and scanners. *J Appl Phys* 38:5149–5153
- Dmitriev SV, Dementiev IV (2005) Vitreous chalcogenide semiconductors for gas sensing application. *MRS Proc* 828:235–240
- Dmitriev S, Duca G, Dementiev I, Craciun A (2004) Flexible substrate based gas sensors for air pollution monitoring. *MRS Proc* 814:169–174
- Duk S-K, Lee D-D (2005) Micro sensor operated at room temperature. *Mater Res Soc Symp Proc* 828:A7.1.1
- Fang X, Zhai T, Gautam UK, Li L, Wua L, Bando Y, Golberg D (2011) ZnS nanostructures: from synthesis to applications. *Prog Mater Sci* 56:175–287
- Feng ZC, Tsu R (eds) (1994) *Porous silicon*. World Science, Singapore
- Foll H, Christophersen M, Carstensen J, Hasse G (2002) Formation and application of porous silicon. *Mater Sci Eng R Rep* 39:93–141
- Fukami K, Harraz FA, Yamauchi T, Sakka T, Ogata YH (2008) Fine-tuning in size and surface morphology of rod-shaped polypyrrole using porous silicon as template. *Electrochem Commun* 10:56–60
- Georgieva V, Yordanov Tz, Pamukchieva V, Arsova D, Gadjanova V, Vergov L (2009) Gas sensing properties of Ge-As-S thin films. In: Angelopoulos A, Fildis T (eds) *Proceedings of 7th international conference of the Balkan physical union*, American Institute of Physics, pp 1079–1084
- Gole JL, Seals LT, Lillehei PT (2000) Patterned metallization of porous silicon from electroless solution for direct electrical contact. *J Electrochem Soc* 147:3785–3789
- Gotz A, Gracia I, Cane C, Lora-Tamayo E, Horrilo MC, Getino J (1997) A micromachined solid state integrated gas sensor for the detection of aromatic hydrocarbons. *Sens Actuators B Chem* 44:483–487
- Graf M, Barrettino D, Taschini S, Hagleitner C, Hierlemann A, Baltes H (2004) Metal oxide-based monolithic complementary metal oxide semiconductor gas sensor microsystem. *Anal Chem* 76:4437–4445
- Grant J, Cunningham W, Blue A, O'Shea V, Vaitkus J, Gaubas E, Rahman M (2005) Wide bandgap semiconductor detectors for harsh radiation environments. *Nucl Instrum Methods Phys Res A* 546:213–217
- Gurbuz Y, Kang WP, Davidson JL, Kerns DV (2004) Diamond microelectronic gas sensor for detection of benzene and toluene. *Sens Actuators B Chem* 99:207–215
- Hagleitner C, Lange D, Hierlemann A, Brand O, Baltes H (2002) CMOS single-chip gas detection system comprising capacitive, calorimetric and mass-sensitive microsensors. *IEEE J Solid State Circuits* 37(12):1867–1878
- Helwig A, Muller G, Sberveglieri G, Faglia G (2007) Gas sensing properties of hydrogenated amorphous silicon films. *IEEE Sens J* 7(11):1506–1512
- Helwig A, Muller G, Sberveglieri G, Eickhoff M (2009) On the low-temperature response of semiconductor gas sensors. *J Sensors* 2009:620720
- Herino R, Bomchil G, Barla K, Bertrand C (1987) Porosity and pore size distribution of porous silicon layers. *J Electrochem Soc* 134:1994–2000
- Hess P (ed) (1989) *Photoacoustic, photothermal and photochemical processes in gases*, vol 46, *Topics in current physics*. Springer, Berlin

- Hummel RE, Chang S-S (1992) Novel technique for preparing porous silicon. *Appl Phys Lett* 61:1965–1967
- Hunsperger RG (2002) *Integrated optics: theory and practice*, 5th edn. Springer, Berlin
- Ioffe AF (1957) *Semiconductor thermoelements and thermoelectric cooling*. Infosearch, London
- Irokawa Y (2011) Hydrogen sensors using nitride-based semiconductor diodes: the role of metal/semiconductor interfaces. *Sensors* 11:674–695
- Joshi SS, Lokhande CD, Han S-H (2007) A room temperature liquefied petroleum gas sensor based on all-electrodeposited *n*-CdSe/*p*-polyaniline junction. *Sens Actuators B Chem* 123:240–245
- Joshi SS, Gujar TP, Shinde VR, Lokhande CD (2008) Fabrication of *n*-CdTe/*p*-polyaniline heterojunction-based room temperature LPG sensor. *Sens Actuators B Chem* 132:349–355
- Juang F-R, Fang Y-K, Chiang Y-T, Chou T-H, Lin C-I, Lin C-W (2011) The low temperature polysilicon (LTPS) thin film MOS Schottky diode on glass substrate for low cost and high performance CO sensing applications. *Sens Actuators B Chem* 156:338–342
- Kalem S, Yavuzcetin O (2000) Possibility of fabricating light emitting porous silicon from gas phase etchants. *Opt Express* 6:7–11
- Kang WP, Gürbüz Y (1994) Comparison and analysis of Pd- and Pt-GaAs Schottky diodes for hydrogen detection. *J Appl Phys* 75:8175–8181
- Kang WP, Davidson JL, Wong YM, Soh KL, Gurbuz Y (2004) Carbon-derived micro- and nanostructures for chemical sensing. *IEEE Trans* 2004:376–394
- Kanicki J (1992) *Amorphous and microcrystalline semiconductor devices*. Artech House, Boston, MA
- Kim J, Ren F (2003) Reversible barrier height changes in hydrogen-sensitive Pd/GaN. *Appl Phys Lett* 82:739–741
- Kim CK, Lee JH, Choi SM, Noh IH, Kim HR, Cho NI, Hong C, Jang GE (2001) Pd- and Pt-SiC Schottky diodes for detection of H<sub>2</sub> and CH<sub>4</sub> at high temperature. *Sens Actuators B Chem* 77(1–2):455–462
- Kimura T, Hasegawa H, Sato T, Hashizume T (2006) Sensing mechanism of InP hydrogen sensors using Pt Schottky diodes formed by electrochemical process. *Jpn J Appl Phys* 45:3414–3422
- Kolasinski KW (2005) Silicon nanostructures from electroless electrochemical etching. *Curr Opin Solid State Mater Sci* 9(1–2):73–83
- Koleva K, Popov CL, Petkova T, Petkov P, Mihailescu IN, Reithmaier JP (2009) Complex (As<sub>2</sub>S<sub>3</sub>)<sub>(100-x)</sub>(AgI)<sub>x</sub> chalcogenide glasses for gas sensors. *Sens Actuators B Chem* 143:395–399
- Kolobov AV, Tanaka K (2001) Handbook of advanced electronic and photonic materials and devices. In: Nalwa HS (ed) *Chalcogenide glasses and sol-gel materials*, vol 5. Academic, New York, NY
- Korotcenkov G (2005) Gas response control through structural and chemical modification of metal oxides: state of the art and approaches. *Sens Actuators B Chem* 107:209–232
- Korotcenkov G (2007a) Metal oxides for solid state gas sensors. What determines our choice? *Mater Sci Eng B* 139:1–23
- Korotcenkov G (2007b) Practical aspects in design of one-electrode semiconductor gas sensors: status report. *Sens Actuators B Chem* 121:664–678
- Korotcenkov G, Cho BK (2010a) Porous semiconductors: advanced material for gas sensor applications. *Crit Rev Solid State Mater Sci* 35(1):1–37
- Korotcenkov G, Cho BK (2010b) Silicon porosification: state of the art. *Crit Rev Solid State Mater Sci* 35(3):153–260
- Kostyshin MT, Mikhailovskaya EV, Romanenko PF (1966) About effect of photographic sensitivity of thin semiconductor films being of metallic substrates. *Sov Phys Solid State* 8:451–452
- Kovalskiy A, Jain H, Mitkova M (2009) Evolution of chemical structure during silver photodiffusion into chalcogenide glass thin films. *J Non Cryst Solids* 355:1924–1929
- Kozicki MN, Mitkova M (2006) Mass transport in chalcogenode electrolyte films – materials and applications. *J Non Cryst Solids* 352:567–577
- Kurtin S, McGill TC, Mead CA (1969) Fundamental transition in the electronic nature of solids. *Phys Rev Lett* 22:1433–1436
- Lantto V, Golovanov V (1995) A comparison of conductance behaviour between SnO<sub>2</sub> and CdS gas-sensitive films. *Sens Actuators B Chem* 24–25:614–618
- Lechuga LM, Calle A, Golmayo D, Briones F (1992) Different catalytic metals (Pt, Pd and Ir) for GaAs Schottky barrier sensors. *Sens Actuators B Chem* 7:614–618
- Lee YJ, Kim HB, Roh YR, Cho HM, Baik S (1998) Development of a SAW gas sensor for monitoring SO<sub>2</sub> gas. *Sens Actuators A Phys* 64:173–178
- Lee SM, Dyer DC, Gardner JW (2003) Design and optimisation of a high-temperature silicon micro-hotplate for nanoporous palladium pellistors. *Microelectron J* 43:115–126
- Lewis SE, De Boer JR, Gole JL, Hesketh PJ (2005) Sensitive, selective, and analytical improvements to a porous silicon gas sensor. *Sens Actuators B Chem* 110:54–65
- Li H, Zhang Y, Huang W (2010) Novel selective sensors based on TiO<sub>2</sub> nanotubes supported MS(TiO<sub>2</sub>@MS, M=Cd, Zn) for their gas sensing properties. *Nano Biomed Eng* 2:143–148

- Lin K-W, Hsu C-S (2011) Analysis of hydrogen gas sensing characteristics based on a grey polynomial differential model (GPDM) algorithm. *IEEE Sens J* 11(9):1894–1898
- Lin KW, Chen HI, Chuang HM, Chen CY, Lu CT, Cheng CC, Liu WC (2004) Characteristics of Pd/InGaP Schottky diodes hydrogen sensors. *IEEE Sens J* 4(1):72–79
- Liu WC, Pan HJ, Chen HI, Lin KW, Chen SY, Yu KH (2001a) Hydrogen-sensitive characteristics of a novel Pd/InP MOS Schottky diode hydrogen sensor. *IEEE Trans Electron Devices* 48:1938–1944
- Liu WC, Pan HJ, Chen HI, Lin KW, Wang CK (2001b) Comparative hydrogen-sensing study of Pd/GaAs and Pd/InP metal-oxide-semiconductor Schottky diodes. *Jpn J Appl Phys* 40:6254–6259
- Liu WC, Lin KW, Chen HI, Wang CK, Cheng CC, Cheng SY, Lu CT (2002) A new Pt/oxide/In<sub>0.49</sub>Ga<sub>0.51</sub>P MOS Schottky diode hydrogen sensor. *IEEE Electron Dev Lett* 23(11):640–642
- Liu YG, Feng P, Xue XY, Shi SL, Fu XQ, Wang C, Wang YG, Wang TH (2007) Room-temperature oxygen sensitivity of ZnS nanobelts. *Appl Phys Lett* 90:042109
- Lloyd-Spets A, Unéus L, Svenningstorp H, Tobias P, Ekedahl L-G, Larsson O, Goras A, Savage S, Harris C, Martensson P, Wigren R, Salomonsson P, Haggendahl B, Ljung P, Mattsson M, Lundström I (2001) SiC based field effect gas sensors for industrial applications. *Physica Status Solidi A* 185:15–25
- Lloyd Spetz A, Baranzahi A, Tobias P, Lundström I (1997) High temperature sensors based on metal–insulator–silicon carbide devices. *Phys Status Solidi (a)* 162:493–511
- Luft W, Tsuo YS (1993) Hydrogenated amorphous silicon alloy deposition processes. Dekker, New York, NY
- Lundström I (2001) SiC based field effect gas sensors for industrial applications. *Phys Status Solidi (a)* 185(1):15–25
- Lundström I, Shirvamavan MS, Svensson C (1975a) A hydrogen-sensitive MOS field-effect transistor. *Appl Phys Lett* 26:55–57
- Lundström I, Shirvamavan MS, Svensson C (1975b) A hydrogen sensitive Pd-gate MOS transistor. *J Appl Phys* 46:3876–3881
- Lundström I, Lloyd Spetz A, Winquist F, Ackelid U, Sundgren H (1990) Catalytic metals and field effect devices – a useful combination. *Sens Actuators B Chem* 1:15–20
- Lundström I, Sundgren H, Winquist F, Eriksson M, Krantz-Rulcker C, Lloyd Spetz A (2007) Twenty-five years of field effect gas sensor research in Linköping. *Sens Actuators B Chem* 121:247–262
- Luo L, Chen H, Zhang L, Xu K, Lv Y (2009) A cataluminescence gas sensor for carbon tetrachloride based on nanosized ZnS. *Anal Chim Acta* 635:183–187
- Lyubin VM, Klebanov M, Sfez B, Ashkinadze B (2004a) Photoluminescence and photodarkening effect in erbium-doped chalcogenide glassy films. *Mater Lett* 58:1706–1708
- Lyubin V, Klebanov M, Froumin N (2004b) Photoinduced phenomena in chalcogenide glassy film/Al structures. *Physica B Condens Matter* 348:121–127
- Malcovati P (1996) CMOS thermoelectric sensor interfaces. Ph.D. thesis, Physical Electronics Laboratory, Swiss Federal Institute of Technology (ETH)
- Mares JJ, Kristofik J, Hulcius E (1995) Influence of humidity on transport in porous silicon. *Thin Solid Films* 255:272–275
- Marian S, Potje-Kamloth K, Tsiulyanu D, Liess H-D (2000) Dimorphite based gas sensitive thin films. *Thin Solid Films* 349:108–112
- Marian S, Tsiulyanu D, Marian T, Liess H-D (2001a) Chalcogenide-based chemical sensors for atmospheric pollution control. *Pure Appl Chem* 73(12):2001–2004
- Marian S, Tsiulyanu D, Liess H-D (2001b) Ge-As-Te-based gas sensor selective to low NO<sub>2</sub> concentrations. *Sens Actuators B Chem* 78:191–194
- Massera E, Nasti I, Quercia L, Rea I, Di Francia G (2004) Improvement of stability and recovery time in porous-silicon-based NO<sub>2</sub> sensor. *Sens Actuators B Chem* 102:195–197
- Matsumura M, Daiko Y, Nogami M (2007) Hydrogen-sensor prepared using proton-conducting glass films. *Diffus Defect Data B* 124–126(1):627–630
- Meyer PL, Sigrist MW (1990) Atmospheric pollution monitoring using CO<sub>2</sub>-laser photoacoustic spectroscopy and other techniques. *Rev Sci Instrum* 61:1779–1807
- Miremadi BK, Colbow K, Harima Y (1997) A CdS photoconductivity gas sensor as an analytical tool for detection and analysis of hazardous gases in the environment. *Rev Sci Instrum* 68(10):3898–3902
- Mitzner KD, Sternhagen J, Galipeau DW (2003) Development of a micromachined hazardous gas sensor array. *Sens Actuators B Chem* 93:92–99
- Monchev B, Filenko D, Nikolov N, Popov C, Ivanov T, Petkov P, Rangelow IW (2007) Investigation of the sorption properties of thin Ge–S–AgI films deposited on cantilever-based gas sensor. *Appl Phys A* 87:31–36
- Monroy E, Omnes F, Calle F (2003) Wide-bandgap semiconductor ultraviolet photodetectors. *Semicond Sci Technol* 18:R33–R51
- Moon JA, Schaafsma DT (2000) Chalcogenide fibers: an overview of selected applications. *Fiber Integr Opt* 19:201–210

- Mori H, Sakata H (1996) Oxygen gas-sensing properties of  $V_2O_5$ - $Sb_2O_3$ - $TeO_2$  glass. *Mater Chem Phys* 45:211–215
- Mori H, Sakata H (1997) Oxygen gas-sensing behaviour of  $V_2O_5$ - $SnO$ - $TeO_2$  glass. *J Mater Sci* 32:5243–5247
- Nakagomi S, Tobias P, Baranzahi A, Lundström I, Martensson P, Lloyd Spetz A (1997) Influence of carbon monoxide, water and oxygen on high temperature catalytic metal–oxide–silicon carbide structures. *Sens Actuators B Chem* 45:183–191
- Nebel CE, Rezek B, Shin D, Uetsuka H, Yang N (2007) Diamond for bio-sensor applications. *J Phys D Appl Phys* 40:6443–6466
- Nesheva D, Aneva Z, Reynolds S, Main C, Fitzgerald AG (2006) Preparation of micro- and nanocrystalline CdSe and CdS thin films suitable for sensor applications. *J Optoelectron Adv Mater* 8(6):2120–2125
- Nishibori M, Shin W, Houlet L, Tajima K, Izu N, Itoh T, Murayama N, Matsubara I (2006a) New structural design of micro-thermoelectric sensor for wide range hydrogen detection. *J Ceram Soc Jpn* 114:853–856
- Nishibori M, Tajima K, Shin W, Izu N, Itoh T, Matsubara I (2006b) CO oxidation catalyst of Au-TiO<sub>2</sub> on the thermoelectric gas sensor. *J Ceram Soc Jpn* 115:34–41
- Nogami M, Matsumura M, Daiko Y (2006) Hydrogen sensor prepared using fast proton-conducting glass films. *Sens Actuators B Chem* 120:266–269
- Nogami M, Maeda T, Uma T (2009) A methanol gas sensor based on inorganic glass thin films. *Sens Actuators B Chem* 137:603–607
- Ohmachi Y, Uchida N (1972) Vitreous  $As_2Se_3$ : investigation of acousto-optical properties and application to infrared modulator. *J Appl Phys* 43:1709–1712
- Palais JC (2002) Micro-optics-based components for networking. In: Bass M, Van Stryland EW (eds) *Fiber optic handbook: fiber, devices, and systems for optical communications*. McGraw-Hill, New York, NY, Ch. 10
- Pancheri L, Oton CJ, Gaburro Z, Soncini G, Pavesi L (2003) Very sensitive porous silicon NO<sub>2</sub> sensor. *Sens Actuators B Chem* 89:237–239
- Parkhutik V (1999) Porous silicon—mechanisms of growth and applications. *Solid State Electron* 43:1121–1141
- Patel NG, Panchal CJ, Makhija KK (1994) Use of cadmium selenide thin films as a carbon dioxide gas sensor. *Cryst Res Technol* 29(7):1013–1020
- Pearnton SJ, Ren F, Wang Y-L, Chu BH, Chen KH, Chang CY, Lim W, Lin J, Norton DP (2010) Recent advances in wide bandgap semiconductor biological and gas sensors. *Prog Mater Sci* 55:1–59
- Pollock CP, Lipson M (2003) *Integrated photonics*. Kluwer, Boston, MA
- Popescu MA (2000) *Non-crystalline chalcogenides*. Kluwer, Dordrecht
- Qureshi A, Kang WP, Davidson JL, Gurbuz YR (2009) Review on carbon-derived, solid-state, micro and nano sensors for electrochemical sensing applications. *Diam Relat Mater* 18:1401–1420
- Reithmaier JP, Paunovic P, Kulisch W, Popov C, Petkov P (eds) (2010) *Nanotechnological basis for advanced sensors*. In: *Proceedings of the NATO advanced study institute on nanotechnological basis for advanced sensors*, Sozopol, Bulgaria, 30 May–11 June. Springer, Dordrecht, The Netherlands
- Saito M, Miyagi M (1991) COP gas sensor using acousto-optic Bragg diffraction in  $As_2Se_3$  glass. *Rev Sci Instrum* 62(9):2105–2108
- Sakata H, Amano M, Kawashima Y, Okamoto T (1994) Oxygen gas-sensing properties of semiconductive  $V_2O_5$ - $SrO$ - $Sb_2O_3$  glass at high temperature. *J Ceram Soc Jpn* 102:317–320
- Saroeh M, Srivastava S, Fink D, Chandra A (2008) Room temperature ammonia gas sensing using mixed conductor based TEMPOS structures. *Sensors* 8:6355–6370
- Schalwig J, Muller G, Eickhoff M, Ambacher O, Stutzmann M (2002) Group III-nitride-based gas sensors for combustion monitoring. *Mater Sci Eng B* 93:207–214
- Semancik S, Cavicchi RE, Wheeler MC, Tiffany JE, Poirier GE, Walton RM, Suehle JS, Panchapakesan B, DeVoe DL (2001) Microhotplate platforms for chemical sensor research. *Sens Actuators B Chem* 77:579–591
- Sen S, Muthe KP, Joshi N, Gadkari SC, Gupta SK, Roy JM, Deshpande SK, Yakmi JV (2004) Room temperature operating ammonia sensor based on tellurium thin films. *Sens Actuators B Chem* 98:154–159
- Sen S, Bhandarkar V, Muthe KP, Roy M, Deshpande SK, Aiyer RC, Gupta SK, Yakmi JV, Sahni VC (2006) Highly sensitive hydrogen sulphide sensors operable at room temperature. *Sens Actuators B Chem* 115:270–275
- Sen S, Sharma M, Kumar V, Muthe KP, Satyam PV, Bhatta UM, Roy M, Gaur NK, Gupta SK, Yakhmi JV (2009) Chlorine gas sensors using one-dimensional tellurium nanostructures. *Talanta* 77:1567–1572
- Shin W, Choi Y, Tajima K, Izu N, Matsubara I, Murayama N (2005) Planar catalytic combustor film for thermoelectric hydrogen sensor. *Sens Actuators B Chem* 108:455–460
- Shin W, Nishibori M, Tajima K, Houlet LF, Choi Y, Izu N, Murayama N, Matsubara I (2006) Integration of ceramic catalyst on micro-thermoelectric gas sensor. *Sens Actuators B Chem* 118:283–286
- Siciliano T, Di Giulio M, Tepore M, Filippo E, Micocci G, Tepore A (2008) Tellurium sputtered thin films as NO<sub>2</sub> gas sensors. *Sens Actuators B Chem* 135:250–254
- Siciliano T, Filippo E, Genga A, Micocci G, Siciliano M, Tepore A (2009) Single-crystalline Te microtubes: synthesis and NO<sub>2</sub> gas sensor application. *Sens Actuators B Chem* 142:185–190

- Strasser M, Aigner R, Lauterbach C, Sturm T, Franosch M, Wachutka G (2004) Miniaturized thermoelectric generators based on poly-Si and poly-SiGe surface micromachining. *Sens Actuators A Phys* 97–98:362–370
- Swan R, Ray AK, Hogarth CA (1991) Optical absorption in thin tellurium films. *Phys Status Solidi (a)* 127:555–560
- Syms RRA, Cozens JR (1993) *Optical guided waves and devices*. Academic, London
- Tabatadze DG, Myasnikov IA (1973) Influence of oxygen adsorption on the electroconductivity of thin films of elementary semiconductors. *Russ J Phys Chem A* 47:1633–1635
- Tajima K, Choi Y, Shin W, Izu N, Matsubara I, Murayama N (2005) Preparation of phosphorus-doped  $\text{Si}_{0.8}\text{Ge}_{0.2}$  thermoelectric thin film using RF-induction coil. *J Ceram Soc Jpn* 113:558–561
- Tajima K, Shin W, Houlet FL, Itoh T, Izu N, Matsubara I (2007) Boron-doped  $\text{Si}_{0.8}\text{Ge}_{0.2}$  thin film deposited by helicon sputtering for micro-thermoelectric hydrogen sensor. *J Electrochem Soc* 154:J53–J58
- Tanielian M, Fritzsche H, Tsai CC, Symbalisky E (1978) Effect of adsorbed gases on the conductance of amorphous films of semiconducting silicon-hydrogen alloys. *Appl Phys Lett* 33(4):353–356
- Tritt TM, Böttner H, Chen L (2008) Thermoelectrics: direct solar thermal energy conversion. *MRS Bull* 33:336–338
- Tsiulyanu D (2010) Tellurium thin films in sensor technology. In: Reithmaier JP, Paunovic P, Kulisch W, Popov C, Petkov P (eds) *Nanotechnological basis for advanced sensors, proceedings of the NATO advanced study institute on nanotechnological basis for advanced sensors, Sozopol, Bulgaria, 30 May–11 June 2010*. Springer, Dordrecht, The Netherlands, pp 363–380
- Tsiulyanu DI, Marian SI, Miron VS, Liess H-D (2001) High sensitive tellurium based  $\text{NO}_2$  gas sensor. *Sens Actuators B Chem* 73:35–39
- Tsiulyanu D, Marian S, Liess H-D (2002) Sensing properties of tellurium based thin films to propylamine and carbon oxide. *Sens Actuators B Chem* 85:232–238
- Tsiulyanu D, Marian S, Liess H-D, Eisele I (2004) Effect of annealing and temperature on the  $\text{NO}_2$  sensing properties of tellurium based films. *Sens Actuators B Chem* 100:380–386
- Tsiulyanu D, Marian S, Liess H-D, Eisele I (2005) Characterization of tellurium-based films for  $\text{NO}_2$  detection. *Thin Solid Films* 485:252–256
- Tucci M, La Ferrara V, Della Noce M, Massera E, Quercia L (2004) Bias enhanced sensitivity in amorphous/porous silicon heterojunction gas sensors. *J Non Cryst Solids* 338–340:776–779
- Vlcek M, Schroeter S, Brueckner S, Fehling S (2009) Direct fabrication of surface relief gratings in chalcogenide glasses by excimer laser interference lithography. *J Mater Sci Mater Electron* 20:S290–293
- Wagner T, Kasap SO, Vlcek M, Frumar M, Nesladek P, Vlcek M (2001) The preparation of the  $\text{Ag}_x(\text{As}_{0.33}\text{S}_{0.67})_{100-x}$  amorphous films by optically-induced solid state reaction and the films properties. *Appl Surf Sci* 175–176:117–122
- Wingbrant H, Svenningstorp H, Salomonsson P, Kubinski D, Visser JH, Lofdahl M, Lloyd Spetz A (2005) Using a MISiC-FET sensor for detecting  $\text{NH}_3$  in SCR systems. *IEEE Sens J* 5(5):1099–1105
- Wright NG, Horsfall AB (2007) SiC sensors: a review. *J Phys D Appl Phys* 40:6345–6354
- Xiong W, Kale G (2005) Novel high-selectivity  $\text{NO}_2$  sensor incorporating mixed-oxide electrode. *Sens Actuators B Chem* 114:101–108
- Xu L, Song H, Zhang T, Fan H, Fan L, Wang Y, Dong B, Bai X (2011) A novel ethanol gas sensor-ZnS/cyclohexylamine hybrid nanowires. *J Nanosci Nanotechnol* 11(3):2121–2125
- Yamamoto K, Kasuga T, Nogami M (1998) An oxygen sensor based on copper(I)-conducting  $\text{CuTi}_2(\text{PO}_4)_3$  glass ceramics. *Appl Phys Lett* 73(22):3297–3299
- Yousuf M, Kuliyeve B, Lalevic B, Poteat TL (1982) Pd–InP Schottky diode hydrogen sensors. *Solid State Electron* 25:753–758
- Yu X-L, Ji H-M, Wang H-L, Sun J, Du X-W (2010) Synthesis and sensing properties of ZnO/ZnS nanocages. *Nanoscale Res Lett* 5:644–648
- Zaghloul ME, Voiculescu I (2011) Integrated chemical sensors. In: Korotcenkov G (ed) *Chemical sensors: comprehensive sensor technologies*, vol 4, Solid state devices. Momentum Press, New York, NY, pp 485–514
- Zhang XH, Ma H, Lu J (2004) Evaluation of glass fibers from the Ga–Ge–Sb–Se system for infrared applications. *Opt Mater* 25:85–89

## Chapter 6

# Solid Electrolytes for Detecting Specific Gases

### 6.1 General View on Electrochemical Gas Sensors

As we have shown before in Chap. 2 (Vol. 1), metal oxides have the best combination of properties necessary for designing gas sensors aimed at the detection of a great number of gases and vapors. However, it was found that in several cases related to detection of specific gases, such as CO<sub>2</sub>, H<sub>2</sub>, SO<sub>2</sub>, and NO<sub>x</sub> at low operating temperatures, other materials, in particular solid electrolytes based on various salts, can be preferable (Kumar and Fray 1988; Kleperis et al. 1992; Miura and Yamazoe 1992a; Ukshe and Leonova 1992; Zosel et al. 2006). Some designers believe that there are advantages in working at low temperature because materials are more stable and corrosion reactions are much slower. Of course, in low-temperature ranges one can use standard electrochemical sensors based on liquid electrolytes. However, due to better chemical and physical durability, solid electrolyte ion conductors provide both improved operating characteristics of electrochemical sensors, especially at elevated temperatures and wider applications of electrochemical gas sensors.

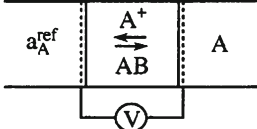
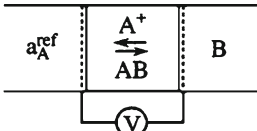
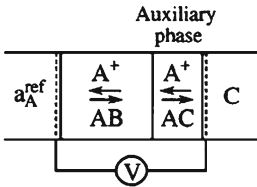
Most gas sensors that use solid electrolytes are operated potentiometrically. Configurations for potentiometric gas sensors have been reported (Yamazoe and Miura 1998; Miura et al. 2000). The simplest scheme for such sensors is represented in Table 6.1 as Type I. In this diagram illustrating the potentiometric sensor mechanism, A is the analyte with variable activity/concentration,  $a_{\text{ref}}$  is the constant activity of analyte A on the reference side of the solid electrolyte membrane, AB is a solid electrolyte membrane (A<sup>+</sup> ion conductor), and the electrodes facilitate the reaction A<sup>+</sup> + e<sup>-</sup> = A; when the activity of A is different on each side of the membrane, a potential, V, is observed. The voltage produced is from the concentration dependence of the chemical potential, which at equilibrium is represented by the Nernst equation:

$$E = \frac{RT}{nF} \ln \frac{P_x}{P_{\text{ref}}}, \quad (6.1)$$

with  $R$  the gas constant,  $F$  the Faraday constant,  $T$  the temperature (K),  $P_x$  the partial gas pressure in the sample gas mixture,  $P_{\text{ref}}$  the reference partial pressure, and  $n$  the number of electrons involved in the basic electrochemical reaction of the sensor ( $n = 2$  for hydrogen and  $n = 4$  for oxygen). As is seen from Eq. (6.1), the sensing electrode potential is a function of the logarithm of the gas concentration in air.

Similar to liquid systems, solid-state electrochemical cells for gas sensing are typically constructed by combining a membrane of solid electrolyte (ion conductor) with a pair of electrodes (electronic conductors). As typical of all electrochemical systems, the interface of solid electrolyte and electrode

**Table 6.1** Classification of solid electrolyte gas sensors and examples of their realization

Type	Cell structure	Solid electrolyte	Auxiliary phase	Target gas
Type I		HUO <sub>2</sub> PO <sub>4</sub> •4H <sub>2</sub> O		H <sub>2</sub>
Type II		Li <sub>2</sub> SO <sub>4</sub> -Ag <sub>2</sub> SO <sub>4</sub> Na <sub>2</sub> SO <sub>4</sub> Ba(NO <sub>3</sub> ) <sub>2</sub> -AgCl K <sub>2</sub> CO <sub>3</sub> SrCl <sub>2</sub> -KCl SrCl <sub>2</sub> -KCl-AgCl		SO <sub>x</sub> SO <sub>x</sub> NO <sub>2</sub> CO <sub>2</sub> Cl <sub>2</sub> Cl <sub>2</sub>
Type III		β-Alumina β-Alumina β-Alumina NASICON NASICON NASICON NASICON NASICON NASICON Li <sup>+</sup> conductor LaF <sub>3</sub> LaF <sub>3</sub>	Na <sub>2</sub> SO <sub>4</sub> AgCl NaNO <sub>3</sub> Na <sub>2</sub> CO <sub>3</sub> Li <sub>2</sub> CO <sub>3</sub> Ba(NO <sub>3</sub> ) <sub>2</sub> NaNO <sub>3</sub> NaNO <sub>3</sub> NaNO <sub>2</sub> Li <sub>2</sub> CO <sub>3</sub> LaOF Li <sub>2</sub> CO <sub>3</sub>	SO <sub>x</sub> Cl <sub>2</sub> NO <sub>2</sub> CO <sub>2</sub> CO <sub>2</sub> NO <sub>x</sub> NO <sub>2</sub> NO CO <sub>2</sub> O <sub>2</sub> CO <sub>2</sub>

Source: Data from Yamazoe and Miura (1998)

plays a most important role in determining the gas sensor's analytical characteristics. Solid electrolyte electrochemical sensors function much like their liquid and polymer electrolyte counterparts except that the mobility of ions in crystalline or polycrystalline solids is typically much lower than that in liquids. This often requires solid electrolyte sensors to operate at higher temperatures in order to have high concentrations of mobile ions in the bulk solid phase (Alberti and Casciola 2001). The solid-state ions, similar to ions in liquid electrolytes, participate in the electrode reactions involving gaseous components and electrons, and the electrodes act as a catalyst for the electrode reactions, very similar to their liquid electrolyte sensor counterparts. Detailed analysis of these electrochemical sensors can be found in review papers prepared by Park et al. (2009).

We note that due to different conditions of exploitation, there is not yet a universal electrochemical sensor for all applications. The water presented in gas can often interfere because water can affect the activity of the proton through well-known reactions such as H<sub>2</sub>O (H<sup>+</sup> + OH<sup>-</sup>) and these reactions can be accelerated at high temperature. The presence or absence of oxygen also often affects certain solid electrolytes, because oxides can be formed in oxygen-containing atmospheres. Finally, poisoning by strongly adsorbed species such as CO or CO<sub>2</sub> can affect the electrode or electrolyte performance and thereby affect observed sensor operating characteristics. This means solid electrolyte sensors must be characterized for each application to ensure the required analytical performance, and the choice of materials for electrodes, filters, and solid electrolytes is extremely important to the development of the desired analytical characteristics.

As shown in Table 6.1, at present three types of potentiometric gas sensors can be designed based on solid electrolytes (Yamazoe and Miura 1998). The well-known oxygen YSZ-based probe with an oxygen ion conductor is a sensor of Type I. This means that a gas sensor of Type I is constructed from a solid electrolyte for which the mobile ion is the same as that electrochemically derived from the gas phase. In this case, the interface potential can be obtained from the local equilibrium reaction, occurring at the electrode/electrolyte/gas three-phase boundary involving the mobile O<sup>2-</sup> ions in the electrolyte, electrons

**Fig. 6.1** Schematic representation of an example of Type II arrangement, designed for SO<sub>2</sub> detection. Sensor has the configuration (-)O<sub>2</sub>, Pt, Ag | Ag<sub>2</sub>SO<sub>4</sub> | Pt, SO<sub>2</sub>, O<sub>2</sub>(+)

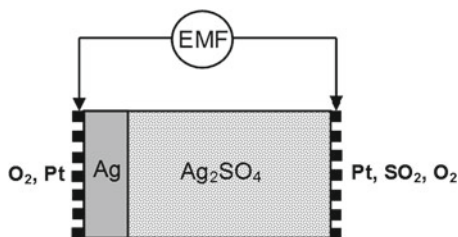
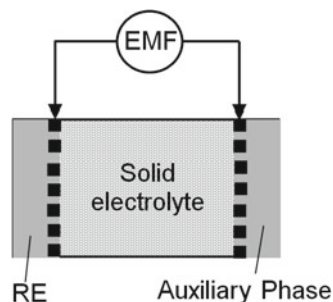


**Fig. 6.2** Schematic representation of Type III sensors



at the electrode, and the O<sub>2</sub> gas component in the ambient. However, Type I sensors are restricted to the detection of the species which correspond to the mobile ion species in the electrolyte. Though this restriction requires the use of an appropriate electrolyte, it makes the sensor inherently selective.

Sensors of Type II have another configuration (see Table 6.1). This type of sensor can be designed if an electrolyte exhibits a known equilibrium relationship between the chemical species to be detected and the component involving the mobile species in the electrolyte. In this case, the chemical potential of the conjugate (immobile) component in the electrolyte can be measured using an interpretation similar to a Type I sensor (Park et al. 2003). The Type II electrochemical sensor enables one to measure the activities of immobile conjugate components in electrolytes such as Na<sub>2</sub>CO<sub>3</sub>, Na<sub>2</sub>SO<sub>4</sub>, and AgNO<sub>3</sub>. In particular, the galvanic cell of Type II shown in Fig. 6.1 can measure SO<sub>3</sub> gas concentration, which is the immobile conjugate species in the silver-ion-conducting Ag<sub>2</sub>SO<sub>4</sub> electrolyte (Worrell and Liu 1984). The acid–base equilibrium reaction at Eq. (6.2) takes place in Ag<sub>2</sub>SO<sub>4</sub> where Ag<sub>2</sub>O and SO<sub>3</sub> are the basic and acidic components of the electrolyte, respectively:



At the platinum working electrode, the equilibrium reaction at Eq. (6.3) occurs:

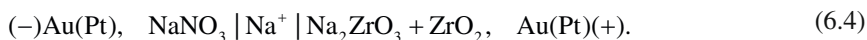


However, Type II sensors are still restricted by the limited number of suitable solid ionic conductors where a known equilibrium reaction exists with the species to be detected.

When the electrolyte does not have a suitable immobile component, its activity cannot be detected using a Type II sensor. To overcome this limitation, a Type III sensor involves an electrode with an electronically conducting auxiliary phase and the same mobile ion as the electrolyte. The schematic structure of Type III sensors is shown in Table 6.1 and in Fig. 6.2. The electronic conductivity allows the chemical activity of the neutral component corresponding to the mobile ion to be uniform throughout the auxiliary phase. In the best case, the auxiliary phase should possess a high diffusivity or be porous. For the surface-modified Type III electrochemical sensor, the activities of Cl<sub>2</sub>, NO<sub>2</sub>, S<sub>2</sub>, and CO<sub>2</sub> gases can be measured, using a Ag<sup>+</sup>-conducting or a Na<sup>+</sup>-conducting electrolyte with a corresponding



gas-sensitive auxiliary layer of AgCl, AgNO<sub>3</sub> and NaNO<sub>3</sub>, Ag<sub>2</sub>S, and Na<sub>2</sub>CO<sub>3</sub>, respectively (Park et al. 2003). The same approach can be applied for NO<sub>2</sub> measuring with a cell (Eq. 6.4) involving a Type III electrode, adopting NASICON or  $\beta/\beta''$ -alumina as a Na<sup>+</sup> ion-conducting electrolyte, NaNO<sub>3</sub> as an auxiliary phase, and the mixture of Na<sub>2</sub>ZrO<sub>3</sub> and ZrO<sub>2</sub> for a reference electrode (Miura et al. 1993):



We note that the above-mentioned sensors usually operate in mixed-potential mode. That takes place because more than one electrochemical reaction usually occurs at an electrode. In particular, in such reactions, gaseous oxygen and CO<sub>2</sub> present in the atmosphere can participate simultaneously with the target gas. In this case, the resulting electrode potential becomes a mixed potential which is generated from competition of the various reactions occurring at the electrode.

## 6.2 Ideal Solid Electrolytes

In general, ideal solid electrolytes, which can be incorporated in gas sensors, should satisfy the following demands (West 1984; Weppner 1987; Rao and Gopalakrishnan 1997; Boivin and Mairesse 1998; Kumar and Yashonath 2006):

1. A large number of the ions of one species should be mobile. This requires a large number of empty sites, either vacancies or accessible interstitial sites. As is well known, empty sites are needed for ions to move through the lattice.
2. The empty and occupied sites should have similar potential energies with a low activation energy barrier for jumping between neighboring sites. High activation energy decreases carrier mobility and can lead to carrier localization.
3. The structure should have a solid framework, preferably 3D, permeated by open channels. The migrating ion lattice should be “molten,” so that a solid framework of other ions is needed in order to prevent the entire material from melting.
4. The framework ions, usually anions, should be highly polarizable. Such ions can deform to stabilize transition-state geometries of the migration ion through covalent interactions.

At present, it has been established that there are quite a large number of solid-state materials that can potentially meet the requirements for application in solid electrolyte gas sensors (see Table 6.1). We should note that, among fast ionic conductors (FICs), one can find crystalline inorganic, amorphous, glass, organic, and/or composite materials. Since ionic conduction represents the movement of ions between near-equivalent atomic sites in a solid, the structure of crystalline FICs must be optimum in providing continuous open channels for the ready motion of ions in the complementary disordered sublattice between such sites. It has been established that such properties can be realized in the immobile frameworks or sublattices characterized by their highly ordered nature. For example, it was found that one-, two-, and three-dimensional tunnels exist in  $\beta$ -Al<sub>2</sub>O<sub>3</sub>. For amorphous and glass-based fast ion conductors we have another situation, which clearly negates the requirement of long-range periodicity. This group is characterized by a high degree of intrinsic disorder on a particular ionic sublattice. This follows from the fact that the carrier ions, e.g., silver in  $\alpha$ -AgI, populate only a fraction of the equivalent sites in the structure. This results in a random distribution of the ions over an excess number of equipotential sites, thereby in principle allowing all the ions in the sublattice to be mobile. Early papers used terms such as “liquid like” and “molten” to describe ion motion in such solids (Tuller and Moon 1988). It was also established that glasses, which are characterized by short-range order, may be modified or manipulated by composition variation within the glass-forming region of the system. For example, the addition of network modifiers (e.g., Li<sub>2</sub>O and Na<sub>2</sub>S) and/or dopant salts (e.g., LiCl and NaBr) to the glass network (e.g., B<sub>2</sub>O<sub>3</sub> and P<sub>2</sub>O<sub>5</sub>) can increase the conductivity. The glass network structure and therefore the glass’s physical and chemical properties can also be substantially

modified by the addition of the so-called network modifiers. In silica glass, for example, the alkali ions are incorporated into the network interstices, while the excess oxygen is accommodated by the network by rupturing “bridging” oxygen bonds between adjacent Si–O tetrahedra and replacing them with “non-bridging oxygen” bonds. So, it is clear that in spite of the great difference in properties, in all groups of solid electrolytes the structure plays a predominant role both in the generation of carriers and in their motion.

However, as was shown by Weppner (2000), any material used for gas sensor design taken by itself has no meaning. As in semiconductor electronics, only combinations of materials play a practical role in electrochemical gas sensors, which as a rule include both ion and electron conductors. At that, material combinations have to be considered individually to evaluate stability and performance of the galvanic cell. For example, according to Dell (1975), four distinct cases may be identified depending on the nature of electrode material used:

1. The electrode is a good electronic conductor but a poor ionic conductor; the reaction product will be deposited at the interface and may impede further reaction leading to rapid polarization. The device will operate well provided that the product is itself an ionic conductor.
2. The electrode is a good ionic conductor but a poor electronic conductor; the reaction product will form at the interface with the current collector and may impede further reaction. The device will operate well provided that the product is itself an electronic conductor.
3. The electrode is a poor ionic and electronic conductor; this incorporates the worst features of both the previous cases. Such an electrode may be used only in devices where a very low current is required.
4. The electrode shows good ionic and electronic conduction; this is the most favorable case. The reaction occurs through the bulk of the electrode. So the reaction product will spread rapidly through the electrode preventing any polarization.

From these considerations it is clear that, to achieve given sensor parameters, the selection of the couples in electrode–electrolyte–electrode systems should be subject to careful analysis. Moreover, activities should be analyzed for both the electroactive components and all other components of the electrolyte and the electrodes. For example, for any application of solid electrolytes, it is also essential to take into account the activity range of the immobile components since these may react with electrodes and form reaction products which may have an effect on the cell voltage and the current that may be drawn (Weppner 2000). The development of electrochemical sensors based on the transport of ions must also take into account the kinetics of both the ionic and electronic spaces. Electrons occur as minority charge carriers, but they play a fundamental role in the electrode processes. We also need to recognize that many of the requirements for materials intended for ionic devices are contradictory. For example, for many applications it is essential to use materials with high decomposition voltages on the one hand and with high ionic conductivities on the other. However, strong chemical bonds and easy displacement of the ions with low activation enthalpies are conflicting requirements (Akridge and Balkanski 1990). In addition, long-term chemical stabilities of the materials and their contacts are required together with low electrochemical polarization losses. So, the above short discussion shows that the selection of an electrolyte for achievement of optimal operating characteristics can be based only on the detailed consideration of all processes which can take place in electrochemical sensors (Weppner 1987, 2003).

### 6.3 H<sub>2</sub> Sensors

The majority of electrochemical H<sub>2</sub> sensors are based on proton conductors (Miura et al. 1989a, b; Miura and Yamazoe 1992b). A list of solid electrolytes that have been tested as materials for H<sub>2</sub> sensors is presented in Table 6.2. Electroconductivities of solid electrolytes which can be used in the

**Table 6.2** Solid electrolytes used in electrochemical solid electrolyte H<sub>2</sub> gas sensors

Low-temperature sensors		
Solid electrolytes sensor	Temp. of stability (°C)	Type of gas
HUO <sub>2</sub> PO <sub>4</sub> ·4H <sub>2</sub> O	<100	P; C
Sb <sub>2</sub> O <sub>5</sub> ·4H <sub>2</sub> O	<100	P; A
Sb <sub>2</sub> O <sub>5</sub> ·H <sub>2</sub> O–H <sub>3</sub> PO <sub>4</sub>	<100	P
Zr(HPO <sub>4</sub> ) <sub>2</sub> ·nH <sub>2</sub> O	<350	P; A
H <sub>4</sub> SiW <sub>12</sub> O <sub>40</sub> ·nH <sub>2</sub> O	100	P
MexH <sub>3-x</sub> PW <sub>12</sub> O <sub>40</sub> ·nH <sub>2</sub> O	100	P
(NH <sub>4</sub> ) <sub>2</sub> HPW <sub>12</sub> O <sub>40</sub> ·nH <sub>2</sub> O	100	P
Hydronium NASICON	100	P
5P <sub>2</sub> O <sub>5</sub> ·95SiO <sub>2</sub> glass		P
Na <sub>3</sub> PO <sub>4</sub>	>600	P
K <sub>3</sub> PO <sub>4</sub>	>600	P
In <sup>3+</sup> -doped SnP <sub>2</sub> O <sub>7</sub>		

Source: Data from Korotcenkov et al. (2009)

P potentiometric, A amperometric, C conductometric, NASICON Na<sub>3</sub>Zr<sub>2</sub>Si<sub>2</sub>PO<sub>12</sub>

design of H<sub>2</sub> sensors are presented in Table 6.3. Experiments have shown that each solid material has its own range of temperatures over which it possesses the required proton conductivity and is stable. Figure 6.3 illustrates this for some solids vs liquids and polymers. This means that each material has an optimum temperature or temperature range for operation. Many of these materials compare favorably with Nafion and should be suitable for H<sub>2</sub>-sensing applications.

The compounds HUO<sub>2</sub>PO<sub>4</sub>·4H<sub>2</sub>O (Velasco et al. 1982; Yamazoe and Miura 1998) and Sb<sub>2</sub>O<sub>5</sub>·4H<sub>2</sub>O (Miura et al. 1983, 1990) were two of the earliest low-temperature solid electrolytes tested in protonic conductor H<sub>2</sub> sensors. Compounds such as H<sub>4</sub>SiW<sub>12</sub>O<sub>40</sub>·28H<sub>2</sub>O, H<sub>3</sub>PW<sub>12</sub>O<sub>40</sub>·29H<sub>2</sub>O, HSbP<sub>2</sub>O<sub>8</sub>·10H<sub>2</sub>O, and H<sub>3</sub>Mo<sub>12</sub>PO<sub>40</sub>·29H<sub>2</sub>O can also be included in the category of low-temperature solid electrolytes with sufficient proton conductivity (Alberti and Casciola 2001). Proton conductivities of the order of 10<sup>-2</sup> S/cm are routinely achieved at room temperature for pure compounds. These heteropoly compounds are electrocatalytically active in reactions involving hydrogen (Treglazov et al. 2005) and can be used in the design of H<sub>2</sub> sensors. Reports have shown solid-state sensors for hydrogen concentrations from 10<sup>-2</sup> to 5 vol.% in inert gases and air without the need for maintaining constant temperature (Treglazov et al. 2005). Operation over the ambient temperature range from -60 to +60 °C has been reported (Treglazov et al. 2005). The performance of this solid electrolyte cell is shown in Fig. 6.4. Although the sensor response and recovery rate decreased with decrease in temperature, the concentration dependence remained virtually unchanged over all operating temperatures, an important advantage in ambient sensors. However, under conditions of low humidity, the above-mentioned hydrates lose their water of crystallization, leading to a decrease in the proton conductivity. Furthermore, pelletization of the compounds can also force the water of crystallization out of the compound, affecting the ionic conductivity (Phair and Badwal 2006). A P<sub>2</sub>O<sub>5</sub>-SiO<sub>2</sub> glass also has high conductivity, e.g., ~10<sup>-2</sup> S/cm at room temperature (Nogami et al. 2006), and very good chemical and thermal stability as well as a potentially low fabrication cost (Daiko et al. 2003). Nogami et al. (2006) reported a thin-film potentiometric H<sub>2</sub> sensor with this same glass that does not require the use of reference gas.

As might be anticipated, hydrogen sensors are extremely sensitive to water vapor (Miura et al. 1990). This RH effect is generally applicable and is found in solid electrolyte room temperature protonic conductors such as uranylphosphate (Velasco et al. 1982), zirconium phosphate (Alberti and Palombari 1989; Alberti et al. 2001), P<sub>2</sub>O<sub>5</sub>-SiO<sub>2</sub> glass (Miura et al. 1990), and antimonite acid (Miura et al. 1990). In this regard, they operate like the polymer sensors described above and are generally

**Table 6.3** Conductivity of potential proton-conducting materials for hydrogen gas sensors

Material	$T_{opt}$ (°C)	Proton conductivity (S cm <sup>-1</sup> )
<i>Hydrated sulfonated polymers</i>		
Nafion	<100	$5 \times 10^{-2}$ at 25 °C, $4 \times 10^{-2}$ at 160 °C
S-PBI	<100	$1 \times 10^{-2}$ at 25 °C
S-PEEK	<100	$3 \times 10^{-2}$ at 25 °C, $4 \times 10^{-2}$ at 160 °C
<i>Heteropoly acid hydrates</i>		
H <sub>4</sub> SiW <sub>12</sub> O <sub>40</sub> ·28H <sub>2</sub> O	<100	$2 \times 10^{-2}$ at 25 °C
H <sub>3</sub> PW <sub>12</sub> O <sub>40</sub> ·29H <sub>2</sub> O	<100	$8 \times 10^{-2}$ at 25 °C
H <sub>3</sub> PMo <sub>12</sub> O <sub>40</sub> ·29H <sub>2</sub> O	<100	$1.7 \times 10^{-1}$ at 25 °C
<i>Layered hydrates</i>		
HUO <sub>2</sub> PO <sub>4</sub> ·4H <sub>2</sub> O	<100	$5 \times 10^{-3}$ at 25 °C
$\alpha$ -Zr(HPO <sub>4</sub> ) <sub>2</sub> ·nH <sub>2</sub> O	<100	$1 \times 10^{-4}$ at 25 °C
$\gamma$ -Zr(PO <sub>4</sub> )(H <sub>2</sub> PO <sub>4</sub> )·2H <sub>2</sub> O	<100	$3 \times 10^{-4}$ at 25 °C
$\gamma$ -Zr sulfo phosphonates	<180	$1 \times 10^{-2}$ at 25, 100 °C
<i>Oxide hydrates</i>		
Sb <sub>2</sub> O <sub>5</sub> ·4H <sub>2</sub> O	<300	$3 \times 10^{-4}$ at 25 °C
V <sub>2</sub> O <sub>5</sub> ·nH <sub>2</sub> O, ZrO <sub>2</sub> ·nH <sub>2</sub> O,	<150	$1 \times 10^{-2}$ at 100 °C
SnO <sub>2</sub> ·nH <sub>2</sub> O	<300	$4 \times 10^{-4}$ at 25 °C
Ce(HPO <sub>4</sub> ) <sub>2</sub> ·nH <sub>2</sub> O	<150	$1 \times 10^{-3}$ at 100 °C
<i>Polyphosphate composite</i>		
NH <sub>4</sub> PO <sub>3</sub> /(NH <sub>4</sub> ) <sub>2</sub> SiP <sub>4</sub> O <sub>13</sub>	200–300	$8.7 \times 10^{-3}$ (dry), $3.3 \times 10^{-1}$ (wet) at 300 °C
NH <sub>4</sub> PO <sub>3</sub> /TiP <sub>2</sub> O <sub>7</sub>	150–250	$2.4 \times 10^{-2}$ at 250 °C
Layered polyvalent (Zr or Ta) hydrogen phosphate	25 (Ta>Zr)	$2 \times 10^{-4}$ at 25 °C
Sr-doped La <sub>3</sub> P <sub>3</sub> O <sub>9</sub>	700	$7 \times 10^{-7}$ – $3 \times 10^{-4}$ at 300–700 °C
Sr-doped LaPO <sub>4</sub>	500–925	$6 \times 10^{-6}$ – $3 \times 10^{-4}$ (wet) at 500–925 °C
<i>Perovskites</i>		
BaCe <sub>0.9</sub> Y <sub>0.1</sub> O <sub>3</sub> · $\alpha$ (BCY)	500–900	$1.8 \times 10^{-2}$ – $7 \times 10^{-2}$ at 600–1,000 °C
BaZr <sub>0.9</sub> Y <sub>0.1</sub> O <sub>3</sub> · $\alpha$ (BZY)	500–900	$1.6 \times 10^{-3}$ – $6 \times 10^{-3}$ at 600–1,000 °C
Ba <sub>3</sub> Ca <sub>1.18</sub> Nb <sub>1.82</sub> O <sub>8.73</sub> (BCN18)	500–900	$5.5 \times 10^{-4}$ at 600 °C
<i>Oxo acid salts</i>		
K <sub>3</sub> H(SO <sub>4</sub> ) <sub>2</sub>	100–200	$9.5 \times 10^{-6}$ – $2.2 \times 10^{-2}$ at 80–250 °C
CsHSO <sub>4</sub>		$2 \times 10^{-7}$ – $3 \times 10^{-2}$ at 110–190 °C
H <sub>3</sub> OClO <sub>4</sub>		$3.5 \times 10^{-4}$ at 25 °C
<i>Oxo acid composites</i>		
MeNO <sub>4</sub> –SiO <sub>2</sub> (Me = Rb, Cs)	100–200	$1 \times 10^{-6}$ – $1 \times 10^{-2}$ at 60–280 °C
Cs <sub>3</sub> (HSO <sub>4</sub> ) <sub>2</sub> (H <sub>2</sub> PO <sub>4</sub> )		$1 \times 10^{-6}$ – $1 \times 10^{-2}$ at 40–180 °C
<i>Pyrochlore</i>		
(La <sub>1.95</sub> Ca <sub>0.05</sub> )Zr <sub>2</sub> O <sub>7</sub> · $\delta$	500–900	$6.8 \times 10^{-2}$ at 600 °C
La <sub>2</sub> Ce <sub>2</sub> O <sub>7</sub> ·Eu <sub>2</sub> Zr <sub>2</sub> O <sub>7</sub>		$7 \times 10^{-7}$ – $1 \times 10^{-2}$ at 300–800 °C

Source: Reprinted with permission from Phair and Badwal (2006). Copyright 2006 Springer

applied only in a gas with defined or constant RH (as a rule at the highest RH) because the conductivity of these solid electrolytes strongly depends on the relative humidity of the ambient air. Quantitative investigation of the RH effects on the conductivity of HSbP<sub>2</sub>O<sub>8</sub>·H<sub>2</sub>O has measured a more than four orders of magnitude change in conductance with RH varying from 0 to 100% (Deniard-Courant et al. 1988). For the P<sub>2</sub>O<sub>5</sub>–SiO<sub>2</sub> glass, it is possible to work only in a humid atmosphere with an RH of 50% or more at room temperature (Daiko et al. 2003).

Potentiometric hydrogen sensors designed using a NASICON solid electrolyte similarly exhibited a strong RH effect, and this makes it difficult to work in a dry atmosphere (Chehab et al. 1991).

**Fig. 6.3** Conductivity as a function of temperature for some proton conductors (Reprinted with permission from Alberti and Casciola (2001). Copyright 2001 Elsevier)

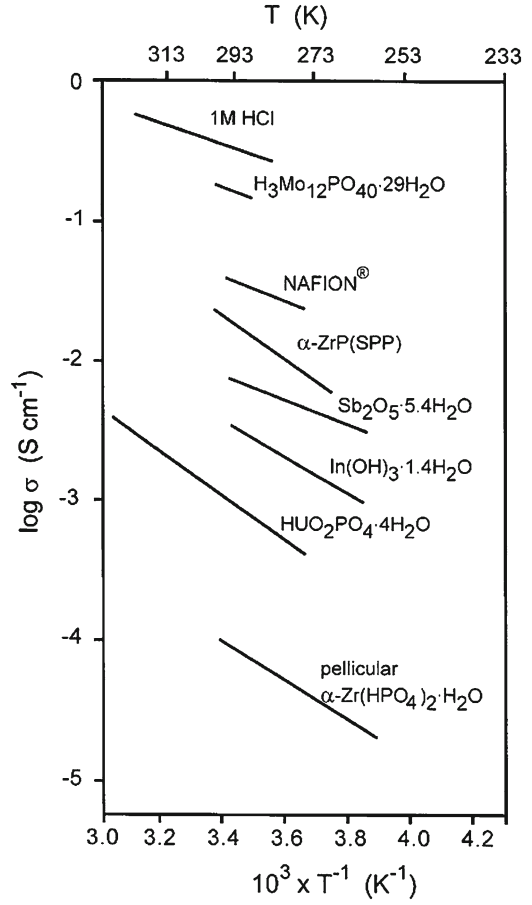


**Fig. 6.4** H<sub>2</sub> concentration vs the absolute EMF in air at different temperatures (Reprinted with permission from Treglazov et al. (2005). Copyright 2005 Elsevier)

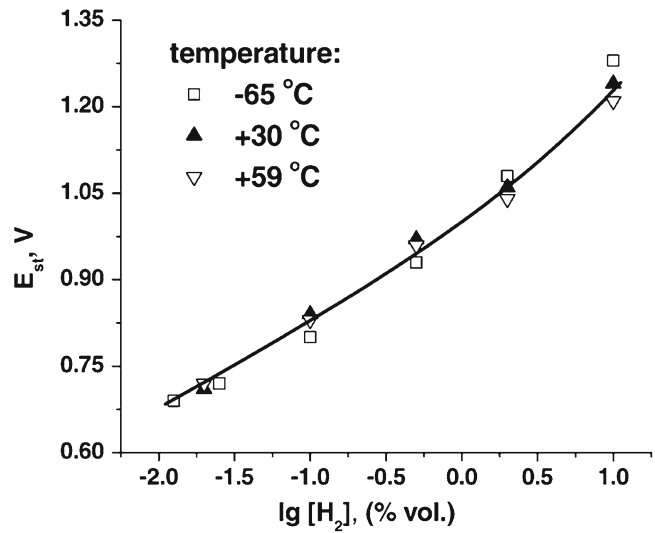


**Fig. 6.5** Pt/NASICON/  
Pt-based sensor EMF vs cell  
relative humidity (Reprinted  
with permission from Chehab  
et al. (1991). Copyright 1991  
Elsevier)

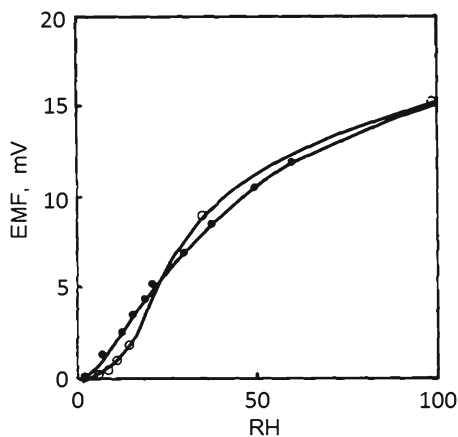
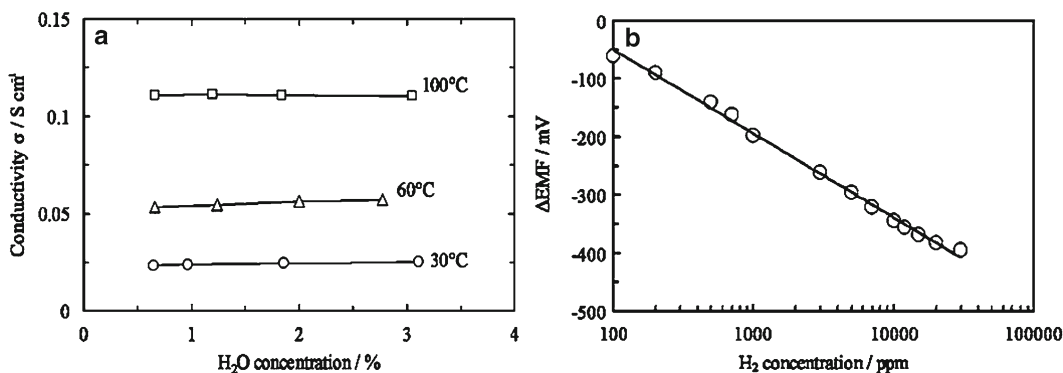


Figure 6.5 illustrates the large orders of magnitude changes that can occur in the sensor signal with RH changes. This electrolyte (a bonded hydronium NASICON) was produced by the two-stage process of powder ion exchange followed by a bonding and pressing operation. Engelhard platinum paste A-4338 with a modified curing procedure was used as the electrode material for both the anode and cathode. Measurements of EMF were made at constant hydrogen concentration with a Hewlett-Packard digital voltmeter with input impedance  $>10^{12} \Omega$  for accurate potential determination.

We need to say the same about heteropoly compounds, such as the ammonium salts of phosphotungstic acid. These compounds are very stable to environmental oscillations of RH and temperature. However, at low RH the conductivity of the salt and hence the sensor signal are reported to change significantly. Moreover, such salts are able to be reduced if they are in very high hydrogen concentration for extended periods of time, and this is confirmed by the appearance of electronic conductivity in the material. Treglazov et al. (2005) believe that the problems with low-temperature heteropoly compound solid electrolytes can be resolved through the development of composite structures. For example, a four-layer cell containing two solid electrolytes has been constructed (Treglazov et al. 2005). In this structure, platinum directly contacts the ammonium salt of phosphotungstic acid, and the rate of the hydrogen exchange reaction is rapid at this electrode. Lead dioxide is in contact with silicotungstic acid such that it is not rapidly reduced chemically on exposure to hydrogen. The entire cell only produces a signal when hydrogen is present, due to the asymmetry of the electrode/electrolyte.

Other investigators (Ponomareva et al. 1997) have suggested that composites based on hydrated antimony pentoxide and phosphoric acid are less sensitive to humidity in comparison with other known protonic electrolytes (Velasco et al. 1982; Alberti and Palombari 1989; Miura et al. 1990). Experiments related to differential thermal analysis (DTA) demonstrate that these composite materials retain water better than the initial pure  $\text{Sb}_2\text{O}_5 \cdot x\text{H}_2\text{O}$  material. The conductivity of the electrolyte  $\text{Sb}_2\text{O}_5 \cdot \text{H}_2\text{O} \cdot \text{H}_3\text{PO}_4$  does not depend greatly on the relative humidity in the midrange of RH (20–80% RH). Hence, an H<sub>2</sub>-sensitive element with this electrolyte should operate without RH drift under conditions where the humidity varies throughout the midrange of RH, and experiments confirm this prediction (20–95% RH produces a 15-mV EMF change at constant H<sub>2</sub> concentration). Sensors, based on hydrated antimony pentoxide and phosphoric acid, were also found not to degrade with long-term storage (4 years) under ambient conditions (Ponomareva et al. 1997). This successful sensor consisted of an Ag or Ag/(Ag + Ag<sub>2</sub>SO<sub>4</sub>) RE, the solid composite electrolyte, and a platinum or palladium H<sub>2</sub>-sensitive electrode. The sensor detection limit was in the low-ppm range (10 ppm), and the EMF of the sensor varied logarithmically with H<sub>2</sub> concentration for hydrogen partial pressures in the range 100–2,000 ppm. The slope of the EMF vs  $\log(\text{pH}_2)$  plot was 170 and 200 mV for platinum and palladium, respectively, which exceeds the Nernst value, presumably due to the formation of a mixed



**Fig. 6.6** Dependencies of (a) conductivity of  $\text{Sn}_{0.9}\text{In}_{0.1}\text{P}_2\text{O}_7$  in air on water vapor concentration at 30, 60, and 100 °C and (b) EMF response of  $\text{Sn}_{0.9}\text{In}_{0.1}\text{P}_2\text{O}_7$ -based sensor on  $\text{H}_2$  concentration in air at 30 °C (Reprinted with permission from Tomita et al. (2007). Copyright 2007 The Electrochemical Society)

potential in air. Moreover, the sensor's characteristics did not appear to depend on the temperature within the range 286–303 K. It has been suggested that many problems of low-temperature solid electrolyte  $\text{H}_2$  sensors could be resolved by using pellicular zirconium phosphates (Alberti and Casciola 2001; Alberti et al. 2001). These compounds are sufficiently good proton conductors, have thermal stability up to 350 °C, and can be directly deposited over the reference electrode as a very thin skin. The limitations of this electrolyte include the relatively low chemical and mechanical stability (Colomban 1999).

However, Tomita et al. (2007) noted that these proton conductors need to be penetrated with large quantities of water in order to achieve sufficient proton conductivities. Thus, it is necessary to operate sensors using these proton conductors under highly humidified conditions, requiring complicated water management in the sensor system. To overcome this challenge, Tomita et al. (2007) proposed to use anhydrous proton conductors, such as  $\text{Sn}_{0.9}\text{In}_{0.1}\text{P}_2\text{O}_7$ , that show high proton conductivities  $\geq 10^{-1}$  S/cm between 150 and 350 °C under dehumidified conditions (Fig. 6.6a). This means that  $\text{Sn}_{0.9}\text{In}_{0.1}\text{P}_2\text{O}_7$ -based  $\text{H}_2$  sensors can operate under dry conditions (Nagao et al. 2006). Experiments carried out by Tomita et al. (2007) have shown that the EMF of sensors prepared from this material and an active Pt/C working electrode varied linearly with the logarithm of the  $\text{H}_2$  concentration in the range from 100 ppm to 3% (see Fig. 6.6b) and the EMF was really minimally affected by the water vapor concentration. It was established that the proton conductivity of  $\text{Sn}_{0.9}\text{In}_{0.1}\text{P}_2\text{O}_7$  was maintained at an almost constant value of 0.023 S/cm in the water vapor concentration range of 0.6–3.1% at 30 °C (see Fig. 6.6a).

## 6.4 CO<sub>2</sub> Sensors

CO<sub>2</sub> sensors are usually sensors of Type III (see Table 6.4), which were designed as combination of  $\beta$ -alumina (Liu and Weppner 1992; Holzinger et al. 1996) or NASICON (Maruyama et al. 1987; Porta and Kumar 2000) with  $\text{Na}_2\text{CO}_3$  as auxiliary phase. These materials are generally accepted as good solid-state ionic conductors. Other solid electrolytes, of course, can also be used in the design of CO<sub>2</sub> sensors (Holzinger et al. 1996).

Electrochemical sensors of Type II based on  $\text{Na}_2\text{CO}_3$  ( $\text{Na}_2\text{CO}_3 + \text{BaCO}_3$ ) or  $\text{LiCO}_3$  are also reported (Holzinger et al. 1996; Singh et al. 1999). However, it was established that in sensors of such type, the

**Table 6.4** Materials used in solid-state electrochemical CO<sub>2</sub> gas sensors

	Electrolyte material	Sensing electrode	Reference electrode
K conductor	K <sub>2</sub> CO <sub>3</sub>	Pt, CO <sub>2</sub> , O <sub>2</sub> Au, CO <sub>2</sub> , O <sub>2</sub>	Pt, CO <sub>2</sub> , O <sub>2</sub> Au, CO <sub>2</sub> , O <sub>2</sub> , CaCO <sub>3</sub> +CaO
Na conductor	Na-β-alumina; NASICON	Pt, Na <sub>2</sub> CO <sub>3</sub> , CO <sub>2</sub> , O <sub>2</sub> Pt, Na <sub>2</sub> CO <sub>3</sub> /BaCO <sub>3</sub> , CO <sub>2</sub> , O <sub>2</sub> Pt, Li <sub>2</sub> CO <sub>3</sub> /MCO <sub>3</sub> , CO <sub>2</sub> , O <sub>2</sub> Au, Na <sub>2</sub> CO <sub>3</sub> , CO <sub>2</sub> , O <sub>2</sub> Pt, Na <sub>2</sub> CO <sub>3</sub> /BaCO <sub>3</sub> , CO <sub>2</sub> , O <sub>2</sub>	Au, Na <sub>2</sub> ZrO <sub>3</sub> +ZrO <sub>2</sub> , CO <sub>2</sub> , O <sub>2</sub> Pt, O <sub>2</sub> (air reference) NaCoO <sub>2</sub> , Na <sub>x</sub> NiO <sub>2</sub> Au, Na <sub>2</sub> Ti <sub>6</sub> O <sub>13</sub> +TiO <sub>2</sub> Na <sub>2</sub> Ti <sub>3</sub> O <sub>7</sub> +Na <sub>2</sub> Ti <sub>6</sub> O <sub>13</sub> , CO <sub>2</sub> , O <sub>2</sub> Pt, O <sub>2</sub> (air reference)
Li conductor	LiTi <sub>5</sub> (PO <sub>4</sub> ) <sub>3</sub> +0.2Li <sub>3</sub> PO <sub>4</sub> Li <sub>2</sub> CO <sub>3</sub> +Li <sub>3</sub> PO <sub>4</sub> +Al <sub>2</sub> O <sub>3</sub> Li <sub>2</sub> CO <sub>3</sub> +MgO Li <sub>2.88</sub> PO <sub>3.73</sub> N <sub>0.14</sub>	Au, Li <sub>2</sub> CO <sub>3</sub> , CO <sub>2</sub> , O <sub>2</sub> Au, CO <sub>2</sub> , O <sub>2</sub>	Au, Li <sub>2</sub> CO <sub>3</sub> , CO <sub>2</sub> , O <sub>2</sub> , CaCO <sub>3</sub> +CaO Au, CO <sub>2</sub> , O <sub>2</sub> (air reference) Pt, LiCoO <sub>2</sub> -Co <sub>3</sub> O <sub>4</sub> , CO <sub>2</sub> , O <sub>2</sub> Au, LiMn <sub>2</sub> O <sub>4</sub> (sealed) Au, LiCoO <sub>2</sub> -Co <sub>3</sub> O <sub>4</sub> , CO <sub>2</sub> , O <sub>2</sub>
Hybrid sensor (alkali conductor +anion conductor)	NASICON and YSZ; MSZ or LaF <sub>3</sub> ; (Al <sub>0.2</sub> Zr <sub>0.8</sub> ) <sub>20/19</sub> Nb(PO <sub>4</sub> ) <sub>3</sub> and YSZ LiTi <sub>5</sub> (PO <sub>4</sub> ) <sub>3</sub> +0.2Li <sub>3</sub> PO <sub>4</sub> and Bi <sub>2</sub> O <sub>3</sub> -Y <sub>2</sub> O <sub>3</sub> , CeO <sub>2</sub> - Gd <sub>2</sub> O <sub>3</sub> , ZrO <sub>2</sub> -Ln <sub>2</sub> O <sub>3</sub> ; Li <sub>2</sub> CO <sub>3</sub> +Li <sub>3</sub> PO <sub>4</sub> +Al <sub>2</sub> O <sub>3</sub> and L <sub>0.9</sub> Sr <sub>0.1</sub> Mn <sub>0.3</sub> ; Sc <sub>1/3</sub> Zr <sub>2/3</sub> (PO <sub>4</sub> ) <sub>3</sub> and YSZ; Sc <sub>2</sub> (WO <sub>4</sub> ) <sub>3</sub> or Al <sub>2</sub> (WO <sub>4</sub> ) <sub>3</sub> and YSZ	Au, Na <sub>2</sub> CO <sub>3</sub> , CO <sub>2</sub> , O <sub>2</sub> Au, Li <sub>2</sub> CO <sub>3</sub> , CO <sub>2</sub> , O <sub>2</sub> ; Au, 0.8La <sub>2</sub> O <sub>5</sub> SO <sub>4</sub> - 0.2Li <sub>2</sub> CO <sub>3</sub> , CO <sub>2</sub> , O <sub>2</sub> Au, CO <sub>2</sub> , O <sub>2</sub>	Au, CO <sub>2</sub> , O <sub>2</sub> Pt, CO <sub>2</sub> , O <sub>2</sub> Pt, CO <sub>2</sub> , O <sub>2</sub>

Source: Data extracted from Côté et al. (1984), Imanaka et al. (1990), Yao et al. (1990), Miura et al. (1995), Narita et al. (1995), Lee et al. (2001), etc.

charge compensation occurs by migration of sodium ions from the side having lower CO<sub>2</sub> and O<sub>2</sub> concentrations to the side with higher concentration (Zosel et al. 2011). If a current flows, sodium carbonate is formed on the side with higher gas concentration and it disappears on the other side. This is the reason why measurement of cell EMF should be made with an instrument having high input impedance. Therefore, carbonate cells cannot be used stably in amperometric or coulometric mode. Nevertheless, the sintered solid carbonates remain gas-tight over a long period of time. Using such cells, CO<sub>2</sub> can be measured continuously from ppm to the percentage level over more than 1 year in the cell temperature range of 450–700 °C according to Nernst's equation (Gauthier and Chamberland 1977; Guth 2008) provided that the cell is heated continuously. According to Zosel et al. (2011), there are two main problems which have to be solved for practical applications. Pressed alkali carbonates are often hygroscopic and tend to sublime so that electrolytes become porous. Besides this effect, the realization of a stable reference system is a topic of interest. To establish a gas reference, CO<sub>2</sub> and O<sub>2</sub> concentrations have to be fixed. This is not possible using air (as in the case of oxygen concentration cells) because the CO<sub>2</sub> content in the air is normally not fixed.

NASICON- and β-alumina-based CO<sub>2</sub> sensors have much better operating characteristics. NASICON is a silico-phosphate (Na<sub>1+x</sub>Zr<sub>2</sub>Si<sub>x</sub>P<sub>3-x</sub>O<sub>12</sub> [0 < x < 3]) which shows a maximum conductivity at x ≈ 2. The NASICON phases are solid solutions in the phase diagram Na<sub>4</sub>SiO<sub>4</sub>-ZrSiO<sub>4</sub>-Na<sub>3</sub>PO<sub>4</sub>-Zr<sub>3</sub>(PO<sub>4</sub>)<sub>4</sub>. These phases show high sodium ion conductivity, so these compounds were termed NASICON (NAtrium Super Ionic CONductor). β-Alumina has a composition of (Na<sub>2</sub>O)<sub>1+x</sub>·11Al<sub>2</sub>O<sub>3</sub> where the maximum conductivity occurs at x = 0.2–0.3 (Stevens and Binner 1984). According to Fig. 6.7, when β-alumina with a given activity of Na<sub>2</sub>O is exposed to the CO<sub>2</sub>-containing ambient at CO<sub>2</sub> level where Na<sub>2</sub>O and Na<sub>2</sub>CO<sub>3</sub> coexist, Na<sub>2</sub>CO<sub>3</sub> can form continuously between the two electrodes



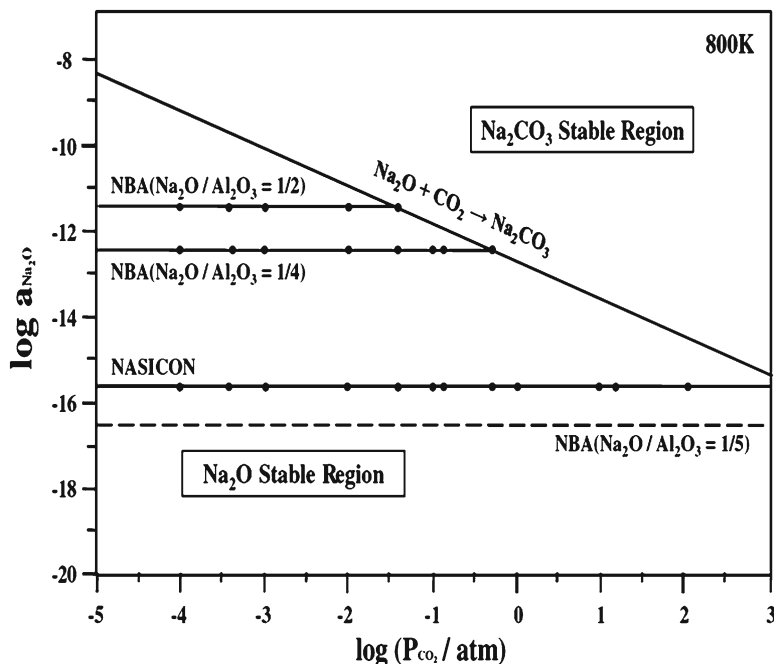


**Fig. 6.7** The stabilities of NASICON and  $\beta$ -alumina upon exposure to  $\text{CO}_2$  gas at 800 K. (Reprinted with permission from Park et al. (2009). Copyright 2009 Springer)

and lead to a symmetric cell with no cell voltage (Park et al. 2009). Because NASICON has a lower  $\text{Na}_2\text{O}$  activity than  $\beta$ -alumina, it is more stable and subsequently has a wider detection range than  $\beta$ -alumina. In addition, NASICON shows a good conductivity at temperatures as low as 600 K whereas  $\beta$ -alumina cannot be used at temperatures lower than 700 K. Unfortunately, NASICON and  $\beta$ -alumina can easily react with  $\text{H}_2\text{S}$  or  $\text{SO}_2$  in the ambient to form sodium sulfate. It is reported that greater than 50 ppb  $\text{SO}_2$  in the ambient could result in an irreversible breakdown of NASICON (Lang et al. 1996). It was established that sodium  $\beta$ -alumina and NASICON also have poor resistance to humidity. In this situation, lithium ion conductors such as lithium phosphorus oxynitride ( $\text{Li}_{2.88}\text{PO}_{3.73}\text{N}_{0.14}$ ) (Lee et al. 2001) and  $\text{LiTi}_2(\text{PO}_4)_3 + 0.2\text{Li}_3\text{PO}_4$  (Imanaka et al. 1995) look very promising for development of  $\text{CO}_2$  gas sensors due to fast ionic conduction and less reactivity with water (Szabo et al. 2003). Imanaka et al. (1991) have shown that a  $\text{CO}_2$  sensor with the lithium ionic-conducting solid electrolyte can detect  $\text{CO}_2$  accurately even in the atmosphere under the coexistence of  $\text{NO}_2$ ,  $\text{CH}_4$ , and water vapor. For selective  $\text{CO}_2$  detection with an atmosphere containing  $\text{SO}_2$ , the concentration of the  $\text{SO}_2$  should be lower than approximately 20 ppm. Kim et al. (2001) have found that lithium ion conductors such as  $\text{Li}_2\text{CO}_3$ - $\text{Li}_3\text{PO}_4$ - $\text{Al}_2\text{O}_3$  can also be used for  $\text{CO}_2$  sensor design. The EMF of the  $\text{CO}_2$  sensor showed superior long-term stability (see Fig. 6.8).

Yamazoe and Miura (1992) established that  $\text{Na}_2\text{CO}_3$  used as an auxiliary phase in  $\text{CO}_2$  sensors is also responsible for the strong sensitivity of response (EMF) and response rate to the appearance of water vapors. In an effort to overcome this problem, it has been found that the use of a binary system of  $\text{Na}_2\text{CO}_3$ - $\text{BaCO}_3$  instead of pure  $\text{Na}_2\text{CO}_3$  not only eliminates the water vapor interference (see Fig. 6.9) but also increases the response rates quite remarkably. It was established that the absence of free crystalline  $\text{Na}_2\text{CO}_3$  in the binary system is related to the elimination of the interference by water vapor. Other binary systems such as  $\text{CaCO}_3$ - $\text{Na}_2\text{CO}_3$  and  $\text{SrCO}_3$ - $\text{Na}_2\text{CO}_3$  were also effective for making the  $\text{CO}_2$  sensors resistant to the disturbance by water vapor.

**Fig. 6.8** (a) Responses of Li<sub>2</sub>CO<sub>3</sub>-Li<sub>3</sub>PO<sub>4</sub>-Al<sub>2</sub>O<sub>3</sub> electrolyte-based sensors with LiMn<sub>2</sub>O<sub>4</sub> reference electrode to CO<sub>2</sub> gas at 420 °C in dry and wet (50% RH) air. (b) Long-term stability of sensor in 1,000 ppm CO<sub>2</sub> at 420 °C (Reprinted with permission from Kim et al. (2001). Copyright 2001 Elsevier)

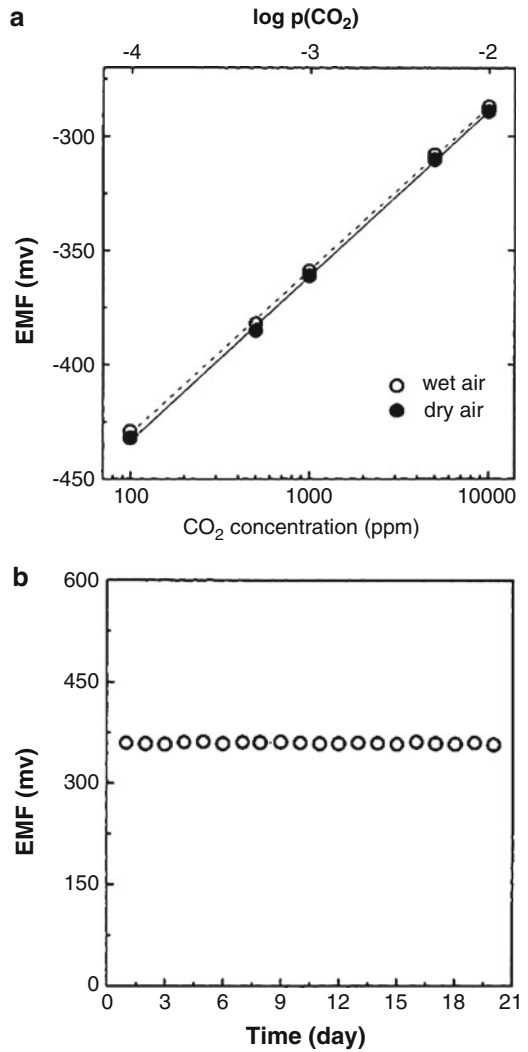


**Fig. 6.9** The amperometric signals of NASICON-Na<sub>2</sub>CO<sub>3</sub>-BaCO<sub>3</sub>-based sensors as a function of the CO<sub>2</sub> concentration in dry and wet atmospheres. The humid atmosphere was prepared by bubbling air through water at 20 °C (operation voltage=0.1 V) (Reprinted with permission from Lee et al. (2003). Copyright 2003 Elsevier)

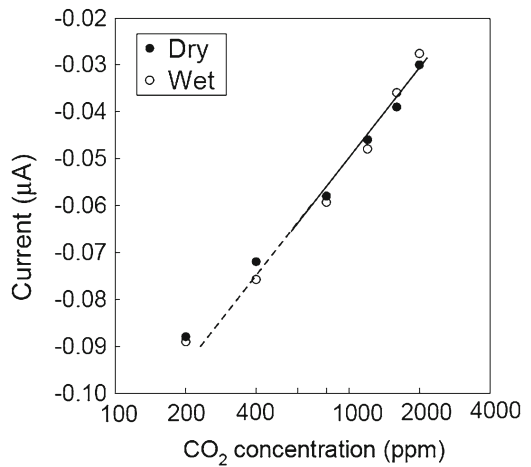
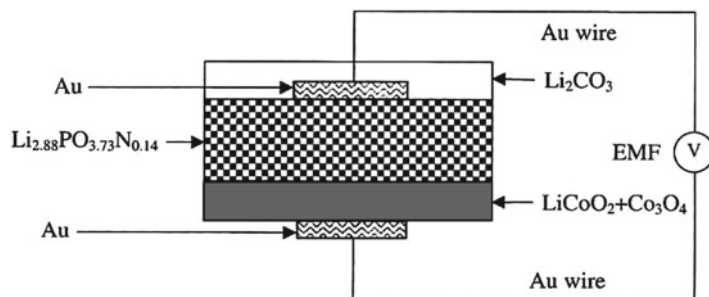


**Fig. 6.10** Configuration of CO<sub>2</sub> sensor with lithium ion conductor (Reprinted with permission from Lee et al. (2001). Copyright 2001 Elsevier)

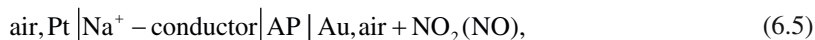


It has been found that the NASICON-based elements fitted with LiCO<sub>3</sub> or LiCO<sub>3</sub>-based binary carbonates also work as CO<sub>2</sub> sensors (Yao et al. 1991; Szabo et al. 2003). The sensors using Li<sub>2</sub>CO<sub>3</sub>–CaCO<sub>3</sub> binary system were particularly distinguished with its high resistance to deliquescence during storage at room temperature in addition to excellent CO<sub>2</sub>-sensing performances. The Li-based binary system was found to stand in a very humid ambient at room temperature for more than 800 h without showing any significant changes in physical appearance (Yamazoe and Miura 1992). Thus, one can expect that lithium ion conductor-based CO<sub>2</sub> gas sensors will have faster response and minimal interference from humidity. One of the possible configurations of Li-based CO<sub>2</sub> gas sensors is shown in Fig. 6.10.

We note that solid electrolytes can be used in other types of CO<sub>2</sub> sensors as well. For example, Matsubara et al. (2000) reported about CeO–BaCO<sub>3</sub>/CuO-based capacitor-type CO<sub>2</sub> sensors. They have shown that these sensors exhibit a high sensitivity to CO<sub>2</sub> plus selectivity within a concentration range of 100–100,000 ppm.

## 6.5 NO<sub>x</sub> Sensors

The typical structure of a NO<sub>2</sub> sensor can be represented as



where AP is an auxiliary phase and where either NASICON (Na<sub>3</sub>Zr<sub>2</sub>Si<sub>2</sub>PO<sub>12</sub>) or NBA (Na-β/β''Al<sub>2</sub>O<sub>3</sub>) has been widely adopted as a Na ion conductor. As an auxiliary phase, NaNO<sub>2</sub> (Yao et al. 1993) or NaNO<sub>3</sub> (Hotzel and Weppner 1987) alone or as a binary mixture with Ba(NO<sub>3</sub>)<sub>2</sub> (Miura et al. 1993) or Li<sub>2</sub>NO<sub>3</sub> (Miura et al. 1994) have been used. At that it is necessary to note that sensors using nitrates are not suited intrinsically for detecting NO, which is major component of NO<sub>x</sub> in combustion exhausts, while elements fitted with NaNO<sub>2</sub> could respond excellently to NO and NO<sub>2</sub> (Yamazoe and Miura 1992). Moreover, the elements with NaNO<sub>2</sub> were even superior to the element fitted with NaNO<sub>3</sub> with respect to the rates of response to NO<sub>2</sub> and the sensitivity to NO<sub>2</sub> in the lower concentration range.

The detection limit of these devices is determined by the concentration where the low extension of the sensor output intersects with the background EMF value measured in air. Miura et al. (1994) showed that mixing NaNO<sub>2</sub> with Li<sub>2</sub>CO<sub>3</sub> in molar ratio of 9:1 substantially decreased background EMF, which subsequently lowered the detection limit down to 5 ppb NO<sub>2</sub> (see Fig. 6.11). However, the major drawback of this type of sensors is the inherent low melting point of the auxiliary phase for the application of emission control, which usually requires the operation at more than 500 °C, sometimes up to 1,000 °C if they are installed close to the engine. For example, the melting points of NaNO<sub>2</sub>, NaNO<sub>3</sub>, and Ba(NO<sub>3</sub>)<sub>2</sub> are 271 °C, 309 °C, and 592 °C, respectively (Miura et al. 1993; Park et al. 2009). As a result, application of these sensors is limited to environmental monitoring,

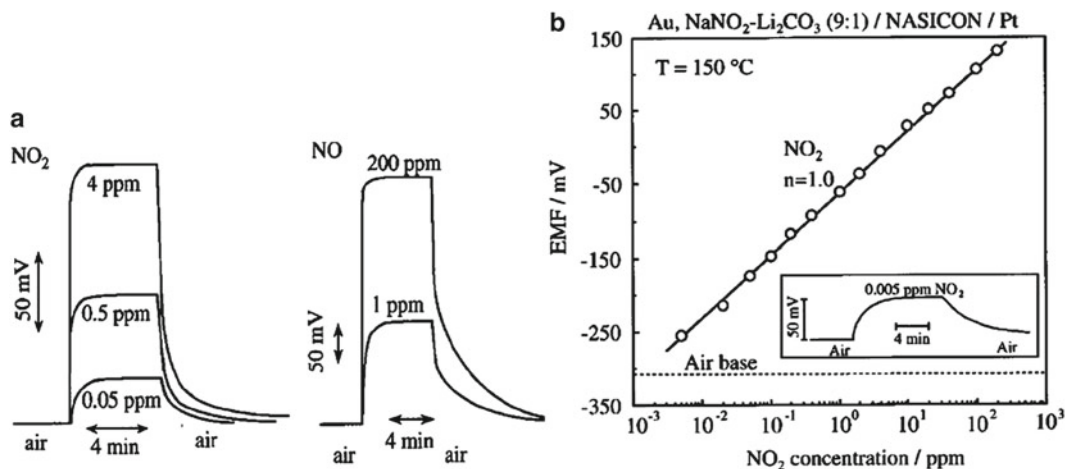
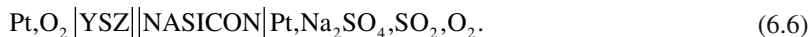


**Fig. 6.11** Dependence of EMF of (a) [Au,NaNO<sub>2</sub>/NASICOM/Pt] and (b) [Au,NaNO<sub>2</sub>-Li<sub>2</sub>CO<sub>3</sub>/NASICOM/Pt] cells on the concentration of NO<sub>2</sub> and NO ( $T_{\text{oper}} = 150\text{ }^{\circ}\text{C}$ ) (Reprinted with permission from Yamazoe and Miura (1998). Copyright 1998 Kluwer Academic)

for which detection limit becomes important. Miura et al. (1993) tried to improve operating characteristics of the above-mentioned sensors using a solid electrolyte disc (Na- $\beta/\beta''$ -alumina) which was ion-exchanged with Ba<sup>2+</sup> by dipping it in a molten salt of Ba(NO<sub>3</sub>)<sub>2</sub>-BaCl<sub>2</sub> (62:38 in molar ratio) overnight before use. Unfortunately, the introduction of Ba(NO<sub>3</sub>)<sub>2</sub> was found to induce a serious adverse affect; the devices showed high cross-sensitivity to CO<sub>2</sub>, making them unable to work as NO<sub>2</sub> sensors in combustion exhausts.

## 6.6 SO<sub>x</sub> Sensors

Research in this area mainly focuses on electrochemical sensors of Type II based on K<sub>2</sub>SO<sub>4</sub> (Gauthier and Chamberland 1977), Na<sub>2</sub>SO<sub>4</sub> (Jacob and Rao 1979), Li<sub>2</sub>SO<sub>4</sub>, Ag<sub>2</sub>SO<sub>4</sub> (Liu and Worrell 1986), and Na<sub>2</sub>SO<sub>4</sub>-Li<sub>2</sub>SO<sub>4</sub>-Y<sub>2</sub>(SO<sub>4</sub>)<sub>3</sub>-SiO<sub>2</sub> (Imanaka et al. 1987) and electrochemical sensor of Type III based on a Na<sup>+</sup> conductor, such as NASICON and beta-alumina (Maruyama et al. 1985; Rao et al. 1992), with Na<sub>2</sub>SO<sub>4</sub> as an auxiliary phase. It was established that the indicated electrolytes provide fairly good SO<sub>2</sub>-sensing properties when adopted in prototype devices. However, the feasibility of practical sensors using them is yet to be determined. It was found that both types of devices have their own stability problems. For example, the EMF output from K<sub>2</sub>SO<sub>4</sub>- or Na<sub>2</sub>SO<sub>4</sub>-based sensors often drifts with time because of electronic conductivity in the electrolytes, lack of intimate contact between electrode and electrolyte, and possible chemical reactions occurring at electrode to form polysulfates (Park et al. 2009). On the other hand, in the case of Na<sup>+</sup> conductor-based sensors, sodium sulfate is so stable that it can easily be formed on Na<sup>+</sup>-conducting electrolytes (NASICON and a beta-alumina) at the reference electrode as well as in the atmosphere containing SO<sub>2</sub> as low as 5 ppb (Holzinger et al. 1996), resulting in a symmetric cell with no voltage output. A recent approach to overcome this problem is to use a bi-electrolyte structure that has an oxygen reference instead of sodium reference by placing an oxide ion conductor between the reference electrode and the sodium ion conductor and thus avoid the formation of sodium sulfate at electrolyte and reference electrode. The arrangement of the cell in this case can be represented as (Kale et al. 2003)



Yamazoe and Miura (1992) have shown that stabilized zirconia, a typical oxide ion conductor, can be utilized for an  $\text{SO}_x$  sensor as well if it is coated with metal sulfates as an auxiliary phase. It was established that with pure  $\text{Na}_2\text{SO}_4$  or  $\text{Li}_2\text{SO}_4$  as the auxiliary phase, the element responded quickly to turning on  $\text{SO}_2$  but recovery was rather sluggish on turning off  $\text{SO}_2$ . The rates of recovery increased significantly when  $\text{Li}_2\text{SO}_4$  was mixed with  $\text{CaSO}_4$ . Imanaka (2005) has shown that  $\text{La}_2\text{O}_2\text{SO}_4$  can also be used for mixing with  $\text{Li}_2\text{SO}_4$ .

Bhoga and Singh (2007) believe that multiphase  $\text{Ag}_2\text{SO}_3$ -based solid electrolytes can also be promising for use in  $\text{SO}_2$  gas sensors. The  $\text{Ag}_2\text{SO}_4$ -based solid electrolytes offer the following additional advantages when compared with  $\text{Li}_2\text{SO}_4$ : (1)  $\text{Ag}_2\text{SO}_4$  solid electrolyte is stable in the Ag–O–S system, (2)  $\text{Ag}_2\text{SO}_4$  is not hygroscopic, (3) it has no cationic interdiffusion between electrolyte and reference electrode, (4) it exhibits low activation enthalpy, (5) it has better mechanical integrity with the Ag: $\text{Ag}_2\text{SO}_4$  solid reference electrode, and (6) it has good sinterability.

## 6.7 Cross-Sensitivity of Solid Electrolyte-Based Gas Sensors and Limitations

The results obtained so far with solid electrochemical gas sensors and discussed in the present chapter have shown that solid electrolytes are promising materials for detecting a large number of gases. The sensitivity is generally high over many orders of magnitude, but limited by the decomposition of the solid separator and the small number of species being exchanged between the phases at very low partial pressures (Weppner 1992).

Experimental studies have also shown that selective detection is an important advantage of an electrochemical sensor, but sometimes their responses are affected by the presence of other gases (Park et al. 2003). As established in numerous experiments, cross-sensitivity is often observed when Type II or Type III potentiometric sensors are exposed to gas species that form thermodynamically more stable compounds or kinetically more favorable compounds in spite of lower thermodynamic stability (Weppner 1992).

For instance, the application of  $\text{AgCl}$  as a surface-modifying layer in Type III sensors of  $\text{Cl}_2$  is very advantageous from the point of view of the high stability of  $\text{AgCl}$ . However,  $\text{Ag}_2\text{SO}_4$  is clearly thermodynamically more stable than  $\text{AgCl}$ . This means that even a trace of  $\text{SO}_2$  should result in the formation of  $\text{Ag}_2\text{SO}_4$  instead of  $\text{AgCl}$  as the galvanic cell reaction and this will affect the sensor response (Weppner 1992). This is illustrated in Fig. 6.12a. At any combination of partial pressures of  $\text{Cl}_2$  and  $\text{SO}_2$  above the straight lines given for various temperatures,  $\text{Ag}_2\text{SO}_4$  is more stable, whereas  $\text{AgCl}$  is formed thermodynamically at the partial pressure combinations below the straight lines. Fortunately, however, as shown by Weppner (1992), the formation of  $\text{Ag}_2\text{SO}_4$  is kinetically unfavorable; the interaction with  $\text{SO}_2$  is negligibly small in most cases and  $\text{AgCl}$  persists in spite of its lower stability unless  $\text{SO}_2$  is sufficiently abundant in the ambient. In contrast, the formation of  $\text{Ag}_2\text{S}$  is kinetically favorable due to a large number of silver defects with high mobility which allow the fast formation of this compound. A major cross-sensitivity for the chlorine sensor occurs as shown in Fig. 6.12b for several concentrations of  $\text{H}_2\text{S}$  in the gas, because  $\text{Ag}_2\text{S}$  forms upon exposure of an  $\text{AgCl}$  surface-modifying layer to  $\text{H}_2\text{S}$  gas, in spite of the lower  $\text{Ag}_2\text{S}$  stability compared to  $\text{AgCl}$ . A decrease in the cell voltage is observed when the  $\text{H}_2\text{S}$  partial pressure approaches the  $\text{Cl}_2$  partial pressure, in fact, at an  $\text{H}_2\text{S}$  concentration of about 10% of the  $\text{Cl}_2$  pressure (Weppner 1992). In this case, the cell voltage is established by the formation of  $\text{Ag}_2\text{S}$ , and any further reaction toward the more stable  $\text{AgCl}$  no longer occurs. Thus, the influence of  $\text{H}_2\text{S}$  is critical to the interpretations because the voltage drop caused by

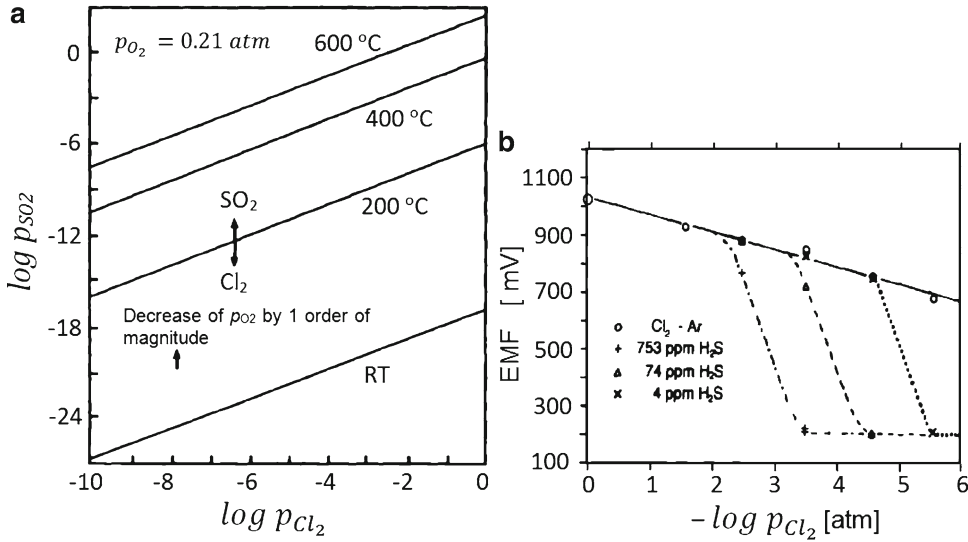
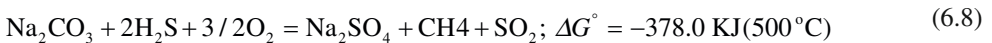
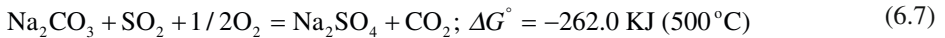


**Fig. 6.12** (a) Thermodynamic stabilities of  $\text{Ag}_2\text{SO}_4$  and  $\text{AgCl}$  at various temperatures and (b) cross-sensitivity of a  $\text{Cl}_2$  sensor to  $\text{H}_2\text{S}$  (Reprinted with permission from Weppner (1992). Copyright 1992 Elsevier)

the presence of  $\text{H}_2\text{S}$  simulates a lower chlorine concentration than really exists. Weppner (1992) has shown that  $\text{H}_2\text{O}$  also has an influence on the cell voltage. However, the influence of water vapor is not as critical as that of  $\text{H}_2\text{S}$ . The influence may be tolerated or may be taken into account quantitatively by the application of a sensor for the water vapor and calibration of the  $\text{Cl}_2$  sensor for various water vapor pressures.

We need to note that similar analyses can be carried out for other systems as well. For example, it was established that many interference effects (or cross-sensitivity) for a Type III sensor designed for  $\text{CO}_2$  detection involving a  $\text{Na}^+$  ion-conducting electrolyte can result from the chemical reactivity of sodium carbonate, which is generally used as the auxiliary phase with Au or Pt probes as sensing electrode (Liu and Weppner 1990). Iwahara et al. (1993) have found that sodium sulfate is usually formed when carbonate is exposed to an ambient containing  $\text{SO}_2$  or  $\text{H}_2\text{S}$  because of the negative standard Gibbs free energies for the reactions at Eqs. (6.7) and (6.8):



The presence of water vapor in the ambient is also reported to cause strong interference with  $\text{CO}_2$  detection; the response time increases and the EMF values become far larger than those for dry  $\text{CO}_2$ . This degradation is believed to result from the reaction of the carbonate with water, producing hydrated compounds such as  $\text{NaHCO}_3$  and  $\text{NaOH}$  (Park et al. 2003). Miura et al. (1992) identified auxiliary phases with good water resistance by mixing carbonates with low water solubility such as  $\text{BaCO}_3$ ,  $\text{CaCO}_3$ , and  $\text{SrCO}_3$  with  $\text{Na}_2\text{CO}_3$ . Especially good performances were obtained for the hypereutectic composition of  $\text{BaCO}_3$  and  $\text{Na}_2\text{CO}_3$  (molar ratio of 1.7:1.0) (see Fig. 6.13a). Though Li-electrolyte-based Type III sensors show suppressed interference from humidity, the response tends to deviate from the Nernstian behavior. Two possible reasons can cause this deviation: mixed (ionic and electronic) conduction in the electrolyte and the effect of a nonreversible electrode (Park et al. 2003). Imanaka et al. (1993) have also found that  $\text{CO}_2$  sensors with sodium carbonate are not affected by  $\text{NO}_2$

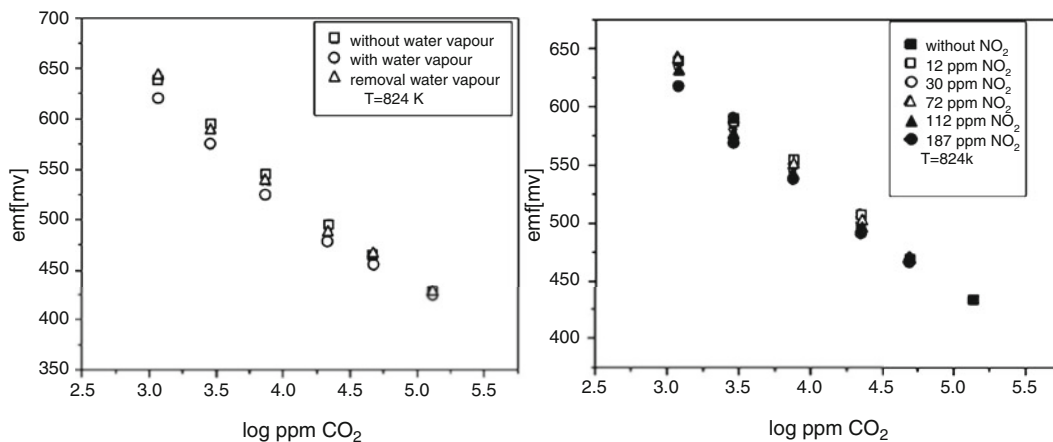


**Fig. 6.13** The EMF results for the CO<sub>2</sub> sensor with configuration [CO<sub>2</sub>,O<sub>2</sub>,Pt|BaCO<sub>3</sub>/Na<sub>2</sub>CO<sub>3</sub>|Na-β-Al<sub>2</sub>O<sub>3</sub>|Nasicon|Pt,O<sub>2</sub>,CO<sub>2</sub>] (a) in wet and dry conditions and (b) in atmosphere containing NO<sub>2</sub> in the range 0–187 ppm at 824 K (Reprinted with permission from Wang and Kumar (2004). Copyright 2004 IOP)

gas at concentrations up to 100 ppm, because nitrate salts are not very stable when the operating temperatures are relatively high. The same effect was observed for binary carbonate auxiliary electrode, such as Na<sub>2</sub>CO<sub>3</sub>–BaCO<sub>3</sub> by Wang and Kumar (2004). At a concentration less than 100 ppm, NO<sub>2</sub> does not affect the sensor signal (see Fig. 6.13b). In addition, Wang and Kumar (2004) established that humidity and oxygen have no significant influence on the performance of sensors with configuration [CO<sub>2</sub>,O<sub>2</sub>,Pt|BaCO<sub>3</sub>/Na<sub>2</sub>CO<sub>3</sub>|Na-β-Al<sub>2</sub>O<sub>3</sub>|Nasicon|Pt,O<sub>2</sub>,CO<sub>2</sub>]. However, the above-mentioned sensors, similar to Na<sub>2</sub>CO<sub>3</sub>-based electrochemical gas sensors, can resist any effects from SO<sub>2</sub> only up to a concentration of 1.7 ppm. The sensing ability is greatly limited by Na<sub>2</sub>SO<sub>4</sub> formation on the sensing auxiliary electrode and/or the surface of the electrolytes when SO<sub>2</sub> gas is present with CO<sub>2</sub>.

Regarding NO<sub>x</sub> sensors based on Na<sup>+</sup> conductor with NaNO<sub>3</sub> as an auxiliary phase, one can say that, according to Nernst theory for a sealed reference electrode, there should be a high sensitivity to oxygen pressure  $p(\text{O}_2)$ . However, in practice, sensitivity to oxygen partial pressure was found to depend on the presence or absence of NO<sub>2</sub>. In the presence of even ppm levels of NO<sub>2</sub>, sensitivity to oxygen is suppressed, particularly at low oxygen levels (see Fig. 6.14). Cross-sensitivity to oxygen is therefore unlikely to interfere seriously in exhaust gas NO<sub>x</sub> sensing, except possibly in switching between the extreme conditions of stoichiometric and lean-burn. Research carried out by Ionotec Ltd. has also shown that the NO<sub>x</sub> sensor is relatively insensitive to most other gas species likely to be encountered in an exhaust gas, in particular water vapor, CO, CO<sub>2</sub>, and unburnt hydrocarbons. As in the case of oxygen, cross-sensitivity to most interfering gas species is to some extent suppressed in the presence of NO<sub>2</sub>. It should be noted, however, that the sensor is known to respond to chlorine and fluorine with a sensitivity similar to that of NO<sub>2</sub> itself.

## 6.8 Oxygen and Other Sensors Based on Fluoride Ion Conductors

At present, various oxygen sensors using metal oxide ionic conductors or oxide semiconductors are available for a wide variety of applications. It was shown that fluoride ion conductors such as LaF<sub>3</sub>, PbF<sub>2</sub> (Yamazoe and Miura 1990), and PbSnF<sub>4</sub> (Kuwato et al. 1990, 1997; Wakagi and Kuwano 1994) can also be used for these purposes. Table 6.5 summarizes solid-state oxygen sensors based on fluoride

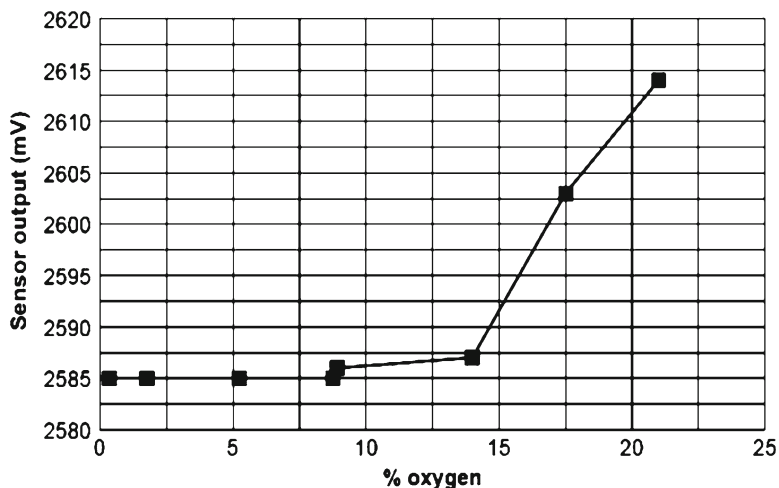


**Fig. 6.14** Cross-sensitivity to oxygen of  $\text{NO}_x$  electrochemical gas sensors fabricated by Ionotec Ltd. (68 ppm  $\text{NO}_2$ ,  $T_{\text{oper}} = 350^\circ\text{C}$ ) (Reprinted with permission from <http://www.ionotec.com/pdfs/noxsensor.pdf>)

**Table 6.5** Oxygen sensors based on fluoride ion conductors

Sensor configuration	Sensing mode	$P_{\text{O}_2}$ , range	$T_{\text{oper}}$ ( $^\circ\text{C}$ )	Response time (90%)
Bi/LaF <sub>3</sub> /Au	Amperometric	$\text{N}_2 \leftrightarrow \text{O}_2$ (linear)	RT	4 min (drift)
Ag/LaF <sub>3</sub> /Au		$\text{N}_2 \leftrightarrow \text{O}_2$	RT	1 min
Au/LaF <sub>3</sub> /La		1–100% (log.)	36	3 min
Au/PbF <sub>2</sub> /Au	Potentiometric	–	RT	2–3 min
Pt/LaF <sub>3</sub> /Sn, SnF <sub>2</sub>		2–100% (log.)	25	0.3–3 min
Bi/PbF <sub>2</sub> /LaOF/Pt		$10^{-3}$ –1 atm (log.)	20	5 min
RuO <sub>2</sub> /PbF <sub>2</sub> /RuO <sub>2</sub>		$10^{-4}$ –1 atm (log.)	160	8 min
FePc/PbSnF <sub>4</sub> (+BaO <sub>2</sub> )/Sn, SnF <sub>2</sub>		$10^{-4}$ –1 atm (log.)	150	1 min
RuO <sub>2</sub> /PbSnF <sub>4</sub> (+BaO <sub>2</sub> )/Sn, SnF <sub>2</sub>		$10^{-2}$ –1 atm (log.)	170	6 min
FePc/PbSnF <sub>4</sub> (+BaO <sub>2</sub> )/Sn, SnF <sub>2</sub>		3–100% (log.)	20	10 min

Source: Data from Yamazoe and Miura (1990)

ion conductors that have been reported to work at temperatures below ca. 200  $^\circ\text{C}$ . Experiments have shown that all of these amperometric sensors had an intrinsic difficulty in obtaining a stable output signal and/or baseline because the main electric carrier of the conductors used is not an oxide ion but a fluoride ion. However, this difficulty was overcome when potentiometric sensing was adopted.

Research also established that LaF<sub>3</sub> with high enough F<sup>-</sup> ionic conductivity is the most promising (Yamazoe and Miura 1990, 1992). Experiments have shown that LaF<sub>3</sub>-based sensors are capable of detecting gaseous oxygen as well as dissolved oxygen in water at room temperature. The sensing element shown in Fig. 6.15a had the Pt-sensing electrode on the upper side of LaF<sub>3</sub> and Sn/SnF<sub>2</sub> counter (or reference) electrode on the back side (Yamazoe et al. 1987). However, this response was slow (Fig. 6.15b). For a change of  $P_{\text{O}_2}$  from 0.21 atm to 1.0 atm, the 90% response time of a virgin sensor was about 15 min at 150  $^\circ\text{C}$  and more than 90 min at 25  $^\circ\text{C}$ . Only after treatment with water vapor under adequate conditions did the sensors show sharp response at room temperature. FTIR measurements have shown that the water vapor treatment causes the LaF<sub>3</sub> surface to be hydroxylated (Yamazoe et al. 1987). It is important that the oxygen-sensing rates were optimized when the surface was partially hydroxylated; too much hydroxylation was accompanied by an adverse effect. It was established



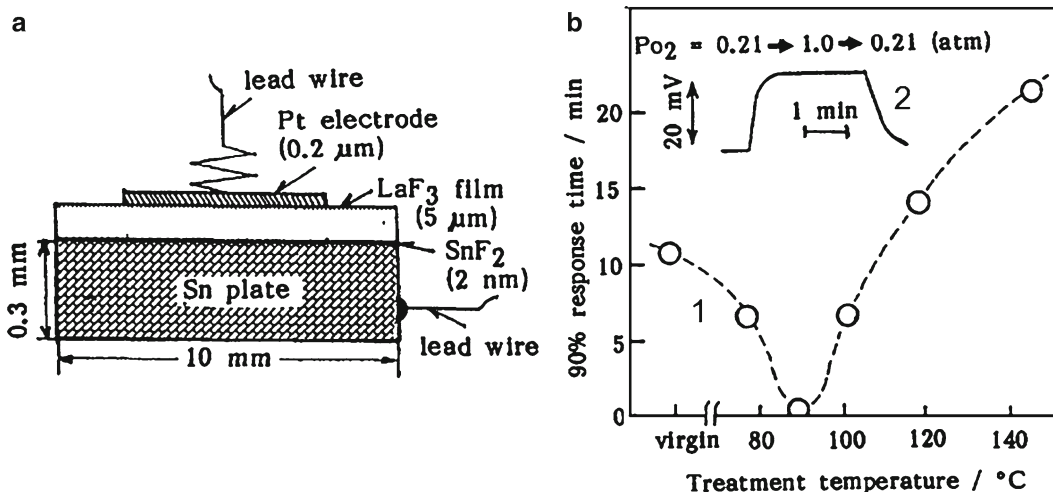


**Fig. 6.15** (a) Configuration of  $\text{LaF}_3$ -based RT oxygen sensor proposed by Yamazoe et al. (1987). (b) 1-Dependence of 90% response time at 30 °C of the sputtered  $\text{LaF}_3$  film sensor on temperature of the vapor treatment, and 2-response transient of the sensor treated at 90 °C to the change in oxygen concentration at 30 °C (Reprinted with permission from Yamazoe and Miura (1990). Copyright 1990 Elsevier)

that the implication of the partial hydroxylation is due to forming an auxiliary phase between the Pt electrode and the  $\text{F}^-$ -conducting bulk ( $\text{LaF}_3$ ) (Miura et al. 1989a). It was also found that the sensitivity to oxygen, i.e., EMF change to a change in oxygen partial pressure, can be drastically modified when the Pt electrode is replaced by perovskite-type oxide electrode. In particular, testing  $\text{LaFeO}_3$ ,  $\text{LaCrO}_3$ ,  $\text{LaCoO}_3$ ,  $\text{LaMnO}_3$ ,  $\text{La}_{0.6}\text{Ca}_{0.4}\text{CoO}_3$ , and  $\text{La}_{0.8}\text{Ca}_{0.2}\text{MnO}_3$  perovskite oxides as sensing electrodes for  $\text{LaF}_3$  oxygen sensors, Yamazoe and Miura (1990) established that the magnitudes of EMF change with a change from dry air to dry oxygen depends on the activity of perovskite oxides and decreases roughly stepwise on going from a group exhibiting low activity through a group exhibiting high activity in the electrochemical reduction of oxygen in an alkaline solution.

Moritz et al. (1999) have shown that fluoride ion conductors can be applied to the detection of fluorine in air as well. They designed an MIS gas sensor with a structure  $\text{SiC}/\text{epi-SiC}/\text{SiO}_2/\text{LaF}_3/\text{Pt}$ , which can be used at temperatures up to 400 °C for the measurement of  $\text{F}_2$ , HF, and fluorocarbons such as  $\text{CF}_3\text{CH}_2\text{F}$ ,  $\text{CF}_3\text{CCl}_3$ ,  $\text{CHClF}_2$ ,  $\text{CF}_3\text{CH}_2\text{Cl}$ , and  $\text{CCl}_3\text{F}$ . The suggested sensitivity mechanism consists of direct interaction of chemisorbed fluorocarbon molecules with platinum gate material followed by insertion of the fluorine ion into the  $\text{LaF}_3$  lattice. A selective detection of molecules containing fluorine was achieved at temperatures near to 400 °C. A similar approach was used by Bartholomaus and Moritz (2000). For detection of fluorine in air they proposed to use the  $n\text{-Si-SiO}_2/\text{Si}_3\text{N}_4/\text{LaF}_3/\text{Pt}$  sensor structure operated on the basis of the field effect in the silicon substrate.

However, we need to recognize that, at present, fluoride ion conductors are rarely used for designing electrochemical gas sensors. Stability is the main problem of these devices. For example, Dénès et al. (1998) have shown that tetragonal  $\alpha\text{-PbSnF}_4$  and orthorhombic  $o\text{-PbSnF}_4$  are stable at ambient conditions, even in air. However, all undergo significant deterioration when heated in air: the color changes from white to yellowish and tin hydrolysis and oxidation takes place. They are much more stable under inert conditions (nitrogen or argon). However,  $\text{PbSnF}_4$  undergoes several phase transitions at high temperatures:  $o$  to  $\alpha$  starting at ca. 100 °C,  $\alpha$  to  $\beta$  (reversible, but the reverse reaction is very sluggish) starting at 250 °C, and  $\beta$  to  $\gamma$  (reversible) at 390 °C.  $\beta\text{-PbSnF}_4$  can be quenched to ambient temperature and is metastable for long periods of time; however, eventually, it starts changing to stable  $\alpha\text{-PbSnF}_4$  and this change is uncontrollable and is faster above ambient temperature. In addition, for all  $\text{MSnF}_4$ , hydrolysis of the Sn–F bonds to Sn–O occurs with traces of moisture.

LaF<sub>3</sub> has better stability but, as we indicated before, properties of LaF<sub>3</sub>-based sensors strongly depend on the water vapor treatment. The water vapor treatment needs extensive optimization, since excessive water vapor may lead to the decomposition of LaF<sub>3</sub> material (Miura et al. 1989b). Further, the low stability of the superoxide and peroxide ions causes the drift in the sensor voltage. Hence, research activities have been spurred to develop technology either for stabilizing LaF<sub>3</sub> properties or preparing LaF<sub>3</sub> thin films with the desired ions without water vapor treatment. In particular, Lukaszewicz et al. (1992) used the metal phthalocyanines (MePc) as auxiliary electrodes to stabilize the desired ions. However, no great success in this direction was achieved. Even with MePc electrodes, LaF<sub>3</sub>-based sensors had high sensitivity to air humidity (Tan et al. 1996). Moreover, Sun et al. (2011), basing their arguments on the high sensitivity of LaF<sub>3</sub> to air humidity, proposed to use this material for designing humidity sensors. Yamazoe and Miura (1990) have found that LaF<sub>3</sub>-based sensors with perovskite oxides as sensing electrodes had rather short 90% response times even without the water vapor treatment of the LaF<sub>3</sub> surface. Ninety percent of the response times for various sensors varied in the range from 3 to 8 min. These results suggest that an improvement of the sensing electrode may lead to higher sensitivity and faster response times than those achieved by the platinum electrode.

## References

- Akridge JR, Balkanski M (eds) (1990) Solid state microbatteries. Plenum, New York, pp 381–393
- Alberti G, Casciola M (2001) Solid state protonic conductors, present main applications and future prospects. *Solid State Ionics* 145:3–16
- Alberti G, Palombari R (1989) All solid state hydrogen sensors based on pellicular  $\alpha$ -zirconium phosphate as a protonic conductor. *Solid State Ionics* 35:153–156
- Alberti G, Carbone A, Palombari R (2001) Solid state potentiometric sensor at medium temperatures (150–300 °C) for detecting oxidable gaseous species in air. *Sens Actuators B* 75:125–128
- Bartholomaus L, Moritz W (2000) Super-sensitivity of an all solid-state fluorine sensor: mechanistic investigations. *Solid State Ionics* 132:31–37
- Bhoga SS, Singh K (2007) Electrochemical solid state gas sensors: an overview. *Ionics* 13:417–427
- Boivin JC, Mairesse G (1998) Recent material development in fast oxide ion conductors. *Chem Mater* 10:2870–2888
- Chehab SF, Canaday JD, Kuriakose AK, Wheat TA, Ahmad A (1991) A hydrogen sensor based on bonded hydronium NASICON. *Solid State Ionics* 45:299–310
- Colomban P (1999) Latest developments in proton conductors. *Ann Chim Sci Mater* 24:1–18
- Côté R, Bale CW, Gauthier M (1984) K<sub>2</sub>CO<sub>3</sub> solid electrolyte as a CO<sub>2</sub> probe: decomposition measurements of CaCO<sub>3</sub>. *J Electrochem Soc* 131:63–67
- Daiko Y, Kasuga T, Nogami M (2003) Sol–gel preparation of fast proton-conducting P<sub>2</sub>O<sub>5</sub>-SiO<sub>2</sub> glasses. *J Sol Gel Sci Technol* 26:1041–1044
- Dell RM (1975) The application of solid state ionic devices. In: Kletzt M (ed) *Electrode processes in solid state ionics*, NATO advanced study institute series C. Kluwer, Dordrecht, pp 387–410
- Dénès G, Madamba MC, Muntasar A (1998) Reactivity and stability of superionics MSnF<sub>4</sub> at high temperature in various media. *MRS Proc* 547:371–376
- Deniard-Courant S, Piffard Y, Barboux P, Livage J (1988) Relative humidity influence on the water content and on the protonic conductivity of the phosphoantimonic acids  $HnSbnP_2O_3n_{+5} \cdot xH_2O$  ( $n=1, 3, 5$ ). *Solid State Ionics* 27:189–194
- Gauthier M, Chamberland A (1977) Solid-state detectors for the potentiometric determination of gaseous oxides. *J Electrochem Soc* 124:1579–1583
- Guth U (2008) Gas sensors. In: Bard AJ, Inzelt G, Scholz F (eds) *Electrochemical dictionary*. Springer, Berlin, pp 294–299
- Holzinger M, Maier J, Sitte W (1996) Fast CO<sub>2</sub>-selective potentiometric sensor with open reference electrode. *Solid State Ionics* 86–88:1055–1062
- Hotzel G, Weppner W (1987) Potentiometric gas sensors based on fast solid electrolytes. *Sens Actuators* 12:449–453
- Imanaka N (2005) Novel multivalent cation conducting ceramics and their application. *J Ceram Soc Jpn* 113(6):387–393
- Imanaka N, Yamaguchi Y, Adachi G, Shiokawa J (1987) Sulfur dioxide gas detection with Na<sub>2</sub>SO<sub>4</sub>-Li<sub>2</sub>SO<sub>4</sub>-Y<sub>2</sub>(SO<sub>4</sub>)<sub>3</sub>-SiO<sub>2</sub> solid electrolyte by a solid reference electrode method. *J Electrochem Soc* 134:725–728

- Imanaka N, Kawasato T, Adachi G (1990) A carbon dioxide gas sensor probe based on a lithium ionic conductor. *Chem Lett* 1990:497–500
- Imanaka N, Kawasato T, Adachi G (1991) Selective CO<sub>2</sub> detection with a lithium conductor based sensor. *Chem Lett* 1991:13–16
- Imanaka N, Murata T, Kawasato T, Adachi G (1993) CO<sub>2</sub> detection with lithium solid electrolyte sensors. *Sens Actuators B* 13–14:476–479
- Imanaka N, Hirota Y, Adachi G (1995) A tip-type carbon dioxide gas-sensor probe based on lithium and oxide ionic conductors. *Sens Actuators B* 24–25:380–382
- Iwahara H, Yamajima T, Hibino T, Ozaki K, Suzuki H (1993) Protonic conduction in calcium, strontium and barium zirconates. *Solid State Ionics* 61:65–69
- Jacob KT, Rao DB (1979) A solid-state probe for SO<sub>2</sub>/SO<sub>3</sub> based on Na<sub>2</sub>SO<sub>4</sub>-I electrolyte. *J Electrochem Soc* 126:1842–1847
- Kale GM, Wang L, Hong YR (2003) Planar SOX sensor incorporating a bi-electrolyte couple. *Solid State Ionics* 161:155–163
- Kim D-H, Yoon J-Y, Park H-C, Kim K-H (2001) Fabrication and characteristics of CO<sub>2</sub>-gas sensor using Li<sub>2</sub>CO<sub>3</sub>-Li<sub>3</sub>PO<sub>4</sub>-Al<sub>2</sub>O<sub>3</sub> electrolyte and LiMn<sub>2</sub>O<sub>4</sub> reference electrode. *Sens Actuators B* 76:594–599
- Kleperis J, Bayars G, Vairvars G, Kranevskis A, Lulis A (1992) Solid electrolytes in sensor technology. *Sov Electrochem* 28:1181–1186
- Korotcenkov G, Han S-D, Stetter JR (2009) Review of electrochemical hydrogen sensors. *Chem Rev* 109:1402–1433
- Kumar RV, Fray DJ (1988) Development of solid-state hydrogen sensors. *Sens Actuators* 15:185–191
- Kumar PP, Yashonath S (2006) Ionic conduction in the solid state. *J Chem Sci* 118(1):135–154
- Kuwano J, Eguchi T, Saito Y (1997) Ambient temperature oxygen sensors based on fluoride solid electrolyte: the roles of the constituents in the sensing electrode mixtures containing phthalocyanines. *Talanta* 44(4):705–712
- Kuwano J, Asano M, Shigehara K, Kato M (1990) Ambient temperature solid-state oxygen sensor using fast ion conductors PbSnF<sub>4</sub> and Ag<sub>6</sub>I<sub>4</sub>WO<sub>4</sub>. *Solid State Ionics* 40(41):472–475
- Lang T, Wiemhofer H-D, Gopel W (1996) Carbonate based CO<sub>2</sub> sensors with high performance. *Sens Actuators B* 34:383–387
- Lee C, Akbar SA, Park CO (2001) Potentiometric type CO<sub>2</sub> gas sensor with lithium phosphorous oxynitride electrolyte. *Sens Actuators B* 80:234–242
- Lee J-S, Lee J-H, Hong S-H (2003) NASICON-based amperometric CO<sub>2</sub> sensor using Na<sub>2</sub>CO<sub>3</sub>-BaCO<sub>3</sub> auxiliary phase. *Sens Actuators B* 96:663–668
- Liu J, Weppner W (1990) “Beta” – alumina solid electrolytes for solid state electrochemical CO<sub>2</sub> gas sensors. *Solid State Comm* 76(3):311–313
- Liu J, Weppner W (1992) A new concept for advanced solid-state ionic gas sensors. In: Balkanski M, Takahashi T, Tuller HL (eds) *Solid state ionics*. Elsevier Science, Amsterdam, pp 61–68
- Liu QG, Worrell WL (1986) Electrical conductivity of Li<sub>2</sub>SO<sub>4</sub>-Ag<sub>2</sub>SO<sub>4</sub> solid electrolytes. *Solid State Ionics* 18–19:524–528
- Lukaszewicz JP, Miura N, Yamazoe N (1992) LaF<sub>3</sub>-based oxygen sensor using Pb phthalocyanine electrode for quick response at room temperature. *Sens Actuators B* 9:55–58
- Maruyama T, Saito Y, Matsumoto Y, Yano Y (1985) Potentiometric sensor for sulfur oxides using NASICON as a solid electrolyte. *Solid State Ionics* 17:281–286
- Maruyama T, Sasaki S, Saito Y (1987) Potentiometric gas sensor for carbon dioxide using solid electrolytes. *Solid State Ionics* 23:107–112
- Matsubara S, Kaneko S, Morimoto S, Shimizu S, Ishihara T, Takita Y (2000) A practical capacitive type CO<sub>2</sub> sensors using CeO/BaCO<sub>3</sub>/CuO. *Sens Actuators B* 65:128–132
- Miura N, Yamazoe N (1992a) Development of new chemical sensors based on low-temperature proton conductors. *Solid State Ionics* 53–56:975–982
- Miura N, Yamazoe N (1992b) Solid-state gas sensors operating at room temperature. In: Colomban P (ed) *Chemistry of solid state materials 2: proton conductors*. Cambridge University Press, Cambridge, p 527
- Miura N, Kato H, Yamazoe N, Seiyama T (1983) Mixed potential type NO<sub>x</sub> sensor based on stabilized zirconia. In: *Proceedings of international meeting of chemical sensors*, Fukuoka, Japan. Kodansha/Elsevier, Tokyo/Amsterdam, p 233
- Miura N, Harada T, Yamazoe N (1989a) Sensing characteristics and working mechanism of four-probe type solid-state hydrogen sensor using proton conductor. *J Electrochem Soc* 136:1215–1219
- Miura N, Hisamoto J, Yamazoe N, Kuwata S, Salardenne J (1989b) Solid-state oxygen sensor using sputtered LaF<sub>3</sub> film. *Sens Actuators* 16:301–310
- Miura N, Harada T, Shimizu Y, Yamazoe N (1990) Cordless solid-state hydrogen sensor using proton-conductor thick film. *Sens Actuators B* 1:125–129
- Miura N, Yao S, Shimizu Y, Yamazoe N (1992) High-performance solid-electrolyte carbon dioxide sensor with a binary carbonate electrode. *Sens Actuators B* 9:165–170

- Miura N, Yao S, Shimizu Y, Yamazoe N (1993) Development of high-performance solid electrolyte sensors for NO and NO<sub>2</sub>. *Sens Actuators B* 13–14:387–390
- Miura N, Yao S, Shimizu Y, Yamazoe N (1994) New auxiliary sensing materials for solid electrolyte NO<sub>2</sub> sensors. *Solid State Ionics* 70–71:572–577
- Miura N, Yan Y, Sato M, Yao S, Nonaka S, Shimizu Y, Yamazoe N (1995) Solid state potentiometric CO<sub>2</sub> sensors using anion conductor and metal carbonate. *Sens Actuators B* 24–25:260–265
- Miura N, Lu G, Yamazoe N (2000) Progress in mixed-potential type devices based on solid electrolyte for sensing redox gases. *Solid State Ionics* 136–137:533–542
- Moritz W, Fillipov V, Vasiliev A, Bartholomaus L, Terentjev A (1999) Field-effect sensor for the selective detection of fluorocarbons. *J Fluor Chem* 93:61–67
- Nagao M, Namekata Y, Hibino T, Sano M, Tomita A (2006) Intermediate-temperature NO<sub>x</sub> sensor based on an In<sup>3+</sup>-doped SnP<sub>2</sub>O<sub>7</sub> proton conductor. *Electrochem Solid State Lett* 9:H48–H51
- Narita H, Zhang YC, Mizusaki J, Tagawa H (1995) Solid state CO<sub>2</sub> sensor using an electrolyte in the system Li<sub>2</sub>CO<sub>3</sub>-Li<sub>3</sub>PO<sub>4</sub>-Al<sub>2</sub>O<sub>3</sub>. *Solid State Ionics* 79:349–353
- Nogami M, Matsumura M, Daiko Y (2006) Hydrogen sensor prepared using fast proton-conducting glass films. *Sens Actuators B* 120:266–269
- Park CO, Akbar SA, Weppner W (2003) Ceramic electrolytes and electrochemical sensors. *J Mater Sci* 38:4639–4660
- Park CO, Fergus JW, Miura N, Park J, Choi A (2009) Solid-state electrochemical gas sensors. *Ionics* 15:261–284
- Phair JW, Badwal SPS (2006) Review of proton conductors for hydrogen separation. *Ionics* 12:103–115
- Ponomareva VG, Lavrova GV, Hairtdinov EF (1997) Hydrogen sensor based on antimonium pentoxide-phosphoric acid solid electrolyte. *Sens Actuators B* 40:95–98
- Porta MA, Kumar RV (2000) Use of NASICON/Na<sub>2</sub>CO<sub>3</sub> system for measuring CO<sub>2</sub>. *Sens Actuators B* 71:173–178
- Rao CNR, Gopalakrishnan J (1997) New directions in solid state chemistry. Cambridge University Press, Cambridge, pp 409–416
- Rao N, van den Bleek CM, Schoonman J (1992) A novel temperature-gradient Na<sup>+</sup>-β-alumina solid electrolyte based SO<sub>x</sub> gas sensor without gaseous reference electrode. *Solid State Ionics* 53–56:30–38
- Singh K, Ambekar P, Bhoga SS (1999) An investigation of Na<sub>2</sub>CO<sub>3</sub>-ABO<sub>3</sub> (A=Li/K/Ba and B=Nb/Ti) heterogeneous solid electrolyte systems for electrochemical CO<sub>2</sub> gas sensor application. *Solid State Ionics* 122:191–196
- Stevens R, Binner JGP (1984) Structure, properties and production of β-alumina. *J Mater Sci* 19:695–715
- Sun G, Wang H, Jiang Z (2011) Humidity response properties of a potentiometric sensor using LaF<sub>3</sub> thin film as the solid electrolyte. *Rev Sci Instrum* 82(8):083901
- Szabo N, Lee C, Trimboli J, Figueroa O, Ramamoorthy R, Midlam-Mohler S, Soliman A, Verweij H, Dutta P, Akbar S (2003) Ceramic-based chemical sensors, probes and field-tests in automobile engines. *J Mater Sci* 38:4239–4245
- Tan G-L, Wu X-J, Wang LR, Chen Y-Q (1996) Investigation for oxygen sensor of LaF<sub>3</sub> thin film. *Sens Actuators B* 34:417–421
- Tomita A, Namekata Y, Nagao M, Hibino T (2007) Room-temperature hydrogen sensors based on an In<sup>3+</sup>-doped SnP<sub>2</sub>O<sub>7</sub> proton conductor. *J Electrochem Soc* 154:J172–176
- Treglavov I, Leonova L, Dobrovolsky Y, Ryabov A, Vakulenko A, Vassiliev S (2005) Electrocatalytic effects in gas sensors based on low-temperature superprotonics. *Sens Actuators B* 106:164–169
- Tuller HL, Moon PK (1988) Fast ion conductors: future trends. *Mater Sci Eng B* 1:171–191
- Ukshe E, Leonova L (1992) Potentiometric hydrogen sensors with proton conducting solid electrolytes. *Sov Electrochem* 28:1166–1175
- Velasco G, Schneli JP, Croset M (1982) Thin solid-state electrochemical gas sensors. *Sens Actuators* 2:371–384
- Wakagi A, Kuwano J (1994) Amperometric PbSnF<sub>4</sub>-based oxygen sensors: rapid response at room temperature in the operating pressure range 10 kPa–7.2 MPa. *J Mater Chem* 4(6):973–975
- Wang L, Kumar RV (2004) Cross-sensitivity effects on a new carbon dioxide gas sensor based on solid bielectrolyte. *Meas Sci Technol* 15:1005–1010
- Weppner W (1987) Solid-state electrochemical gas sensors. *Sens Actuators* 12:107–119
- Weppner W (1992) Advanced principles of sensors based on solid state ionics. *Mater Sci Eng B* 15:48–55
- Weppner W (2000) Concepts and materials aspects of developing solid state ionic devices. In: Chowdari BVR, Wang W (eds) Proceedings of the 7th Asian conference on solid state ionics: materials and devices. World Scientific, River Edge, NJ, pp 3–12
- Weppner W (2003) Engineering of solid state ionic devices. *Ionics* 9:444–464
- West AR (1984) Solid state chemistry and its applications. Wiley, Chichester, Ch. 13
- Worrell WL, Liu QG (1984) A new sulphur dioxide sensor using a novel two-phase solid-sulphate electrolyte. *J Electroanal Chem* 168:355–362
- Yamazoe N, Miura N (1990) Solid-state electrochemical oxygen sensors for operation at room temperature. *Trends Anal Chem* 9(5):170–175
- Yamazoe N, Miura N (1992) New approaches in the design of gas sensors. In: Sberverglieri G (ed) Gas sensors: principles, operation, and development. Springer, Berlin, pp 1–42
- Yamazoe N, Miura N (1998) Potentiometric gas sensors for oxidic gases. *J Electroceram* 2:243–255

- Yamazoe N, Hisamoto J, Miura N, Kuwata S (1987) Potentiometric solid-state oxygen sensor using lanthanum fluoride operative at room temperature. *Sens Actuators* 12:415–423
- Yao S, Shimizu Y, Miura N, Yamazoe N (1990) Solid electrolyte CO<sub>2</sub> sensor using binary carbonate electrode. *Chem Lett* 1990:2033–2036
- Yao S, Hosohara S, Shimizu Y, Miura N, Futata H, Yamazoe N (1991) Solid electrolyte CO<sub>2</sub> sensor using NASICON and Li-based binary carbonate electrode. *Chem Lett* 1991:2069–2072
- Yao S, Shimizu Y, Miura N, Yamazoe N (1993) Development of high-performance solid-electrolyte sensors for NO and NO<sub>2</sub>. *Sens Actuators B* 13:387–390
- Zosel J, Schiffel G, Gerlach F, Ahlborn K, Sasum U, Vashook V, Guth U (2006) Electrode materials for potentiometric hydrogen sensors. *Solid State Ionics* 177:2301–2304
- Zosel J, Oelßner W, Decker M, Gerlach G, Guth U (2011) The measurement of dissolved and gaseous carbon dioxide concentration. *Meas Sci Technol* 22:072001

## **Part II**

# **Auxiliary Materials**

## Chapter 7

# Materials for Sensor Platforms and Packaging

### 7.1 Conventional Platforms

The substrate to be used in gas sensors must have good dielectric properties, excellent thermal stability, and be chemically inert. There must be no undesirable reactions between the substrate and the gas-sensitive layer during the production and operation of the sensor. In addition, good adhesion of the gas-sensitive layer deposited on these substrates must be ensured. The thermal coefficient of expansion is also an important parameter of materials used as substrates in gas sensors. This coefficient is a major factor determining the compatibility between the substrate and the added components. It has a significant effect on film adhesion. If not properly matched, during the lifetime and in the presence of thermal excursions, it can have a catastrophic effect on the integrity of the added components, including the thick film gas-sensing layer, heater, and electrodes. Experience has shown that taking into account manufacturing concerns, substrates should also provide (Prudenziati 1994: (1) the ability to withstand high temperatures – typically between 500 and 1,000 °C; (2) mechanical strength – important for easy handling and basic for several sensors; (3) surface finish – important for good line definition and printed film uniformity; (4) good planarity – there should be a minimum distortion of the substrate. Excess can result in screening problems in thick-films and photo-processing problems in thin-films; (5) the absence of visual defects – surface defects such as small pits or burrs can result in circuit defects such as open circuits and pin holes; (6) good compatibility of materials – the surface should be chemically and physically compatible with the chemicals and material used in fabrication. Generally speaking, the chemical inertness of ceramic substrates is particularly useful for sensors designed to work in very aggressive media; (7) low cost of producing large quantities; and (8) small tolerance – should be possible to achieve the suitable tolerances in overall dimensions.

Typical configurations of conventional planar gas sensors are shown in Fig. 7.1. Substrates for such planar gas sensors are most often developed from alumina ceramics, but other oxides such as MgO, ZrO<sub>2</sub>, and quartz might be used. A comparison of materials suitable for application as substrates in gas sensors is presented in Table 7.1. Ceramics based on Al<sub>2</sub>O<sub>3</sub> are generally preferred because this compound has excellent temperature stability as well as excellent dielectric and temperature conductance properties (William and Boardman 1975). Moreover, Al<sub>2</sub>O<sub>3</sub> is characterized by good chemical stability when exposed to many gas atmospheres, good adhesion to many gas-sensitive materials, and a relatively modest price. According to the industrial standard, alumina ceramics is now 96% Al<sub>2</sub>O<sub>3</sub> composition, which is used in approximately 90% of worldwide manufactured circuits. The additional 4% weight fraction of the content makes complete densification possible without grain growth and also makes it possible to optimize the electrical properties. The most common additives are magnesia and silica. Magnesia inhibits the growth of alumina grains (crystallites) by segregation at the

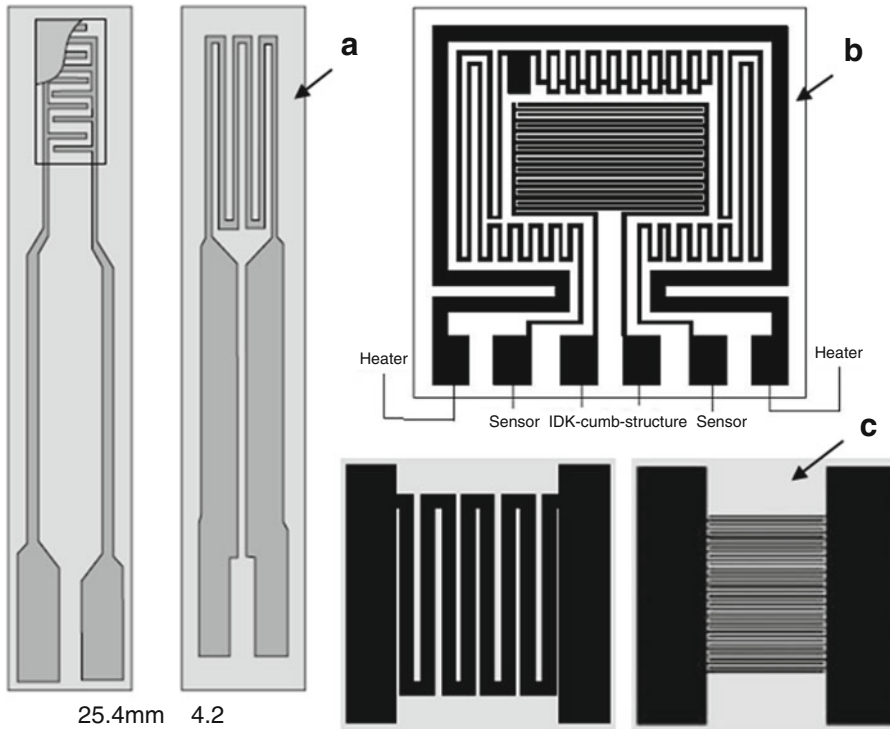


**Fig. 7.1** Commercially available configurations of planar sensors: (a, c) “double-sided” platforms fabricated using thick-film technology (Siemens AG); (b) multisensor platform with customer-specific sensor layers, heater layers, and measurement electrodes in mono- and multilayer versions [Reprinted from Heraeus Sensor Technology (<http://www.dwmai.com>)]

**Table 7.1** Parameters of materials used as gas sensor platforms

Parameter	Al <sub>2</sub> O <sub>3</sub>	MgO	ZrO <sub>2</sub> (YSZ)	SiO <sub>2</sub> (quartz)	Si
Melting point, °C	2,072	2,852	2,590	1,600	1,414
Thermal conductivity, W/m K (20 °C)	35	30	2	1.3	149
Refractive index	1.77	1.74	2.13	1.52	3.42
Density, g/cm <sup>3</sup>	3.95	3.58	6	2.65	2.3
Volume resistivity, ohm cm (20 °C)	>10 <sup>14</sup>	>10 <sup>14</sup>	>10 <sup>10</sup>	10 <sup>12</sup> –10 <sup>16</sup>	–
Dielectric constant (1 MHz)	9.8	9.8	–	3.9	11.9
Coefficient of thermal expansion, 10 <sup>-6</sup> /°C (100 °C)	8.4	8.0	5–10	0.55	2.6
Maximum use temperature, °C	1,750	1,650	1,650	1,100	300

alumina boundaries, which prevents them from moving. Silica is useful since the interaction between SiO<sub>2</sub> and Al<sub>2</sub>O<sub>3</sub> gives rise to a new inter-grain phase (mullite), which binds the whole system. The elastic moduli and mechanical strength of alumina ceramic are high, which means that it is one of the strongest refractory oxides.

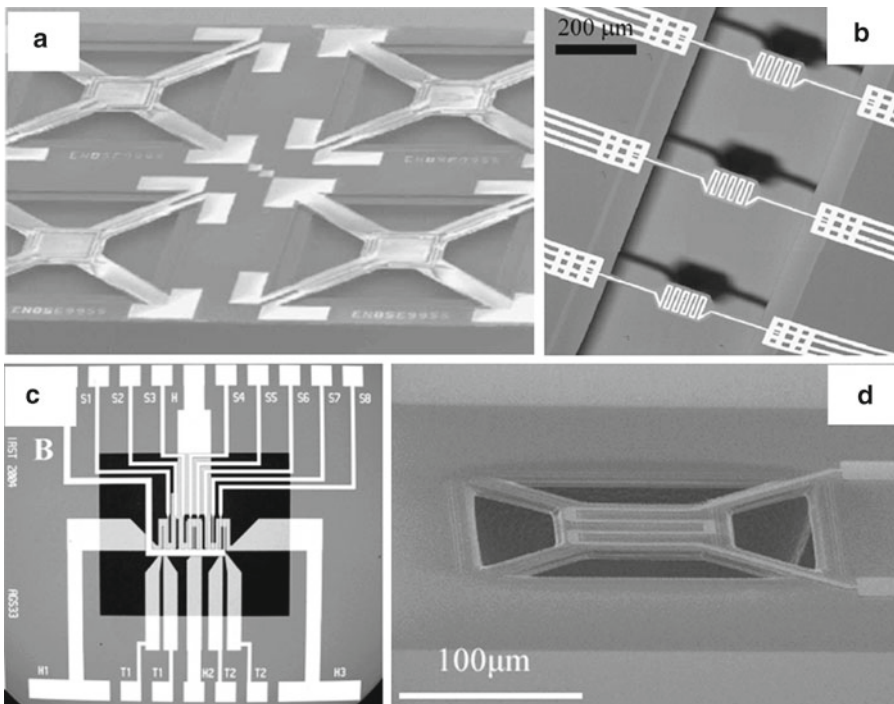
Frequently, planar gas sensors are developed using Si substrates which are largely preoxidized. Still, the thin-film technologies require substrates with very flat surfaces. Si is also used for fabrication platforms with micro-hotplates, the application of which for sensor fabrication permits a considerable reduction in the consumption power of the heaters incorporated in the platforms of sensors such as conductometric (Splinter et al. 2001; Simon et al. 2001), pellistors (Furjes et al. 2004), or thermoelectric ones (Shin et al. 2003, 2005). As well known, the minimization of power consumption is one of the main requirements for sensor technology, especially when the aim is a portable system.



## 7.2 Micromachining Hotplates

Micro-hotplates are based on suspended membranes configured after etching of cavities at the Si substrates. The heating and sensing element are thermally isolated from the substrate. As a rule, the interdigital metal electrodes are patterned over the membrane and covered by the MOX gas-sensing layer by microelectronic technologies such as sputtering, drop coating, chemical vapor deposition, physical vapor deposition, etc. (Guidi et al. 1998). The membrane therefore needs to be very robust to allow deposition of the metal oxide and heating to high temperatures. The materials chosen for the membrane of the micro-hotplate should in theory combine low thermal conductivity—in other words, small thickness—with high mechanical strength—in other words, large thickness (Horrillo et al. 1999). The first requirement is crucial because the gas-sensing properties of semiconducting MOXs are temperature dependent. The second requirement requires reliable production, particularly when the sensing layer is deposited and annealed. SEM views of several hotplates used for gas sensor design are presented in Fig. 7.2 and Table 7.2, correspondingly. It is seen that indicated platforms allow temperatures in the range of 100–800 °C to be achieved with extremely low power of 3–30 mW (Han et al. 2001; Furjes et al. (2004).

To fabricate the hotplates one can use either silicon bulk or surface micromachining (Mlcak et al. 1994; Lang 1996; Simon et al. 2001). The features of membranes developed using these two approaches are shown in Figs. 7.3 and 7.4. Surface micromachining creates free-standing membranes using

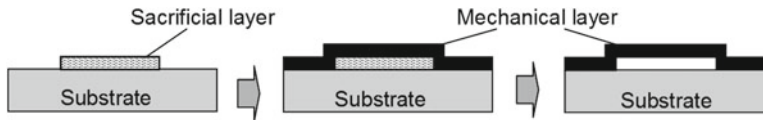
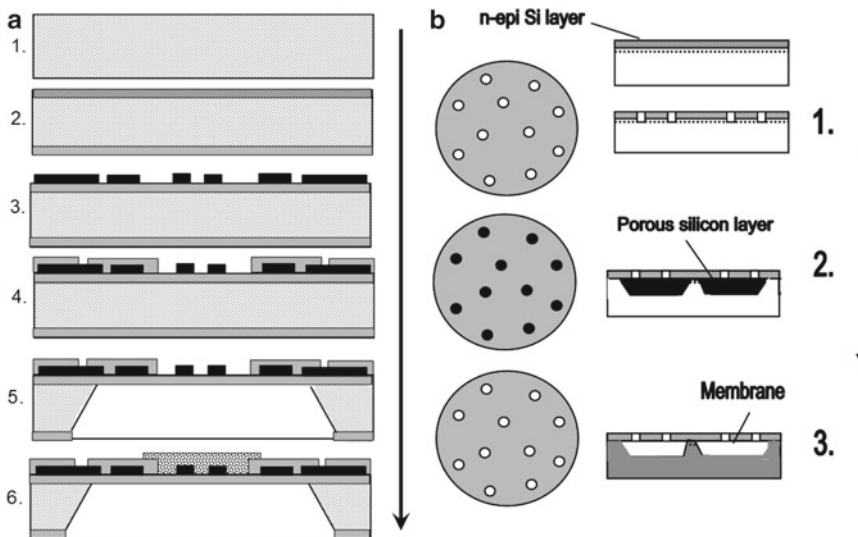


**Fig. 7.2** (a) SEM view of thermally decoupled membrane array. [Reprinted with permission from Splinter et al. (2001). Copyright 2004 Elsevier]. (b) SEM view of a free-standing sensor platform fabricated using a sacrificial layer of porous silicon [Reprinted with permission from Furjes et al. (2004). Copyright 2004 Elsevier]. (c) Optical microscope photograph of a three-section heater sensor array. [Reprinted with permission from Francioso et al. (2008). Copyright 2008 Elsevier]. (d) Suspended porous silicon micro-hotplate with a Pt heater. The thickness of the membrane is 4 μm. The depth of the cavity under the membrane is more than 60 μm [Reprinted with permission from Tsamis et al. (2003). Copyright 2003 Elsevier]

**Table 7.2** Thermal characterization of designed micro-hotplates

Reference	Parameter			
	Dimension of the sensor element ( $\mu\text{m}^2$ )	Maximum temperature ( $^{\circ}\text{C}$ )	Dissipation power ( $^{\circ}\text{C}/\text{mW}$ )	$t_{\text{T}}$ (ms) <sup>a</sup>
Furjes et al. (2004)	100×100	550	27	4.2
Adam et al. (2008)	300×300			
Tsamis et al. (2003)	100×100	600	20	
Triantafyllopoulou et al. (2006)	100×100	900	180–340	

<sup>a</sup>Time necessary to obtain maximum operating temperature

**Fig. 7.3** Diagram illustrating surface micromachining

**Fig. 7.4** (a) Fabrication of a micromachined gas sensor using bulk etching: 1, Si substrate; 2, deep oxidation of Si substrate and deposition of additional dielectric layer; 3, metallization to form heaters and metal contacts; 4, passivation; 5, back-side etching; 6, deposition of gas-sensing MOX layer [Adapted from Comini et al. (2009a)]. (b) Fabrication of a membrane using porous silicon as a sacrificial layer: 1, photolithography; 2, Si porosification; 3, porous silicon etching

sacrificial layers (see, e.g., Zeitschel et al. 1999). The sacrificial layer is deposited over the substrate surface and covered by a second layer (mechanical layer) which is intended to form a membrane. Then the sacrificial layer is removed by etching, leaving a cavity beneath the membrane layer. The drawback of this method is the limited distance between the membrane and substrate, which is typically several micrometers according to the thickness of the sacrificial layer. Although this distance is usually sufficient for other functional units, such as, for example, micromotors, gas sensors often require the thickness of the sacrificial layer to be of the order of several dozens of micrometers to reduce heat transfer to the substrate. This basic process is illustrated in Fig. 7.3. The process can be

**Table 7.3** Examples of sacrificial and mechanical layers with a suitable etchant

Sacrificial layer	Mechanical layer	Sacrificial etchant
Silicon dioxide	Polysilicon, silicon nitride, silicon carbide	HF-based
Silicon dioxide	Aluminum	Pad etch, 73% HF
Polysilicon	Silicon nitride, silicon carbide	KOH-based
Polysilicon	Silicon dioxide	TMAH-based
Resist, polymers	Aluminum, silicon carbide	Acetone, oxygen plasma

*TMAH* tetramethylammonium hydroxide. Similar to KOH etching, TMAH-based etchant is commonly used for fast removal and silicon micromachining

further expanded to produce multiple mechanical layers to yield more complex mechanical structures. There are a number of choices for both sacrificial and mechanical layers and some examples are listed in Table 7.3.

In bulk micromachining the silicon wafer is etched on the back of the silicon wafer to build the required cavities under a masking layer structured by photolithography (Lang et al. 1994a, b; Lang 1996). The typical procedure for producing bulk micromachined substrates includes: (1) covering the silicon bulk substrate, which may be hundreds of micrometers thick, with a dielectric layer; (2) deposition of a metal layer to form the heater and electrodes by patterning; (3) passivation of the heater; and (4) etching of the back to reduce the thermal mass of the heated part (see Fig. 7.4).

In the first papers silicon and silicon oxide were used as membrane material. The Si membranes show good mechanical stability, but owing to the thermal conductivity of the highly doped silicon thin film serving as an etch-stop, the thermal resistance of the micro-hotplate is reduced. In addition, the resulting silicon oxide layer is under very high compressive stress, which causes the SiO<sub>2</sub>/Si/SiO<sub>2</sub> membrane to bend until the energy of compression of SiO<sub>2</sub> balances the energy of elongation of Si. Therefore, a stress-optimized silicon oxynitride membrane has been used to replace the silicon layer and silicon oxide in later designs (Graf et al. 2007). Bulk micromachining by anisotropic silicon etching has been used intensively by NIST to study MOX gas sensors and sensor arrays (Suehle et al. 1993; Friedberger et al. 2003; Spannhake et al. 2006).

It has been shown that the bulk and surface micromachinings have good compatibility with porous silicon (PSi) technology (Lang et al. 1994a, b; Lang 1996) as shown in Fig 7.4b. This gives additional advantages to the discussed technologies (Steiner and Lang 1995; Dusco et al. 1997; Hedrich et al. 2000; Simon et al. 2001; Splinter et al. 2001). Porous silicon technology has the following specific features (Lang et al. 1994a, b; Lang 1996; Hedrich et al. 2000):

- Very thick layers can be produced which extend over the whole wafer thickness. This property is employed to develop thermal sensor membranes that need a sacrificial layer thicker than 50 μm, which cannot be obtained using such conventional layers as silicon dioxide or doped silicate glasses. Due to the large thickness, PSi offers options for creating a wide air gap between the membrane and the substrate.
- Chemical reactions occurring at internal surfaces of the PSi layer are very fast. This permits quick and easy removal of the sacrificial layer, even at room temperature, with low-concentration alkaline solutions rather than the aggressive HF employed in other cases.
- Back-side lithography is not necessary, which makes packaging the final sensor and the use of adhesives easier, gives higher yields, and provides better mechanical stability of the wafer.
- The heat conductivity of PSi is lower than that of bulk silicon by two or three orders of magnitude, depending on the preparation of the PSi layers (Tsamis et al. 2003).
- There are no geometric restrictions caused by the crystallographic orientation of the substrate. Unlike anisotropic etching, the geometry of the PSi is not limited to certain planes, and so they can be placed locally on a wafer with controlled undercutting. This is a considerable advantage in the development of special sensors, e.g., for optical applications where circular designs are required.

- The PSi layer is very selective in terms of type and doping level of the substrate. This property is used to define a finish of silicon etching.
- Any PSi layer geometry can be created via appropriate surface masking layers.
- The PSi layers can be further covered with other thin films, by such as epitaxy processes, which are widely employed in complementary metal oxide–semiconductor (CMOS) technologies.
- The use of PSi as a sacrificial layer requires it to contain pores with sizes in the range of 4–50 nm, which ensures mechanical stability of the layers (Steiner and Lang 1995; Dusco et al. 1997; Splinter et al. 2001).

Thus, surface micromachining using PSi layers allows the production of chips of small sizes at low cost. However, the PSi layers are subjected to stresses and stick to the substrates because of the narrow gap, which may limit their application (Lang 1996). In addition, PSi structures cannot be made by lateral undercutting, and the fabrication of free-standing planes requires holes to be made for the entrance of an etchant.

The removal of PSi to make a sacrificial layer is conventionally carried out with a highly dilute alkaline solution, such as KOH or NaOH, at a concentration of 0.5–5 wt% at room temperature or by employing a high-density plasma (Tsamis et al. 2003). Etching the PSi sacrificial layer made with low-concentration alkali at room temperature makes it possible to retain other chip components. This is especially important when the sacrificial layer is removed as the last step in chip production.

It has recently been suggested that for some applications the PSi need not be removed to create the air gap (Salcedo et al. 2004), as was originally demonstrated over a decade ago for flow sensors (Tabata 1986). Due to its low thermal conductivity, PSi itself may provide sufficient thermal isolation from the substrate. This approach may actually improve the mechanical strength of the device with almost identical thermal isolation.

### 7.3 Flexible Platforms

A new trend has recently arisen with the integration of sensors directly on flexible plastic foils. Their flexibility and their simplified processing, targeting the production of devices on large area using roll to roll and printed electronics processing (see Fig. 7.5), bring new opportunities and will also reduce several technical limitations that characterize the production processes of conventional microelectronics (Logothetidis 2008). In conventional Si microelectronics, patterning is most often carried out using photolithography, in which the active material is deposited initially over the entire substrate area, and selected areas of it are removed by physical or chemical processes. Despite its high resolution, the photolithographic process is very complex, expensive, uses extremely expensive equipment, requires many steps, and is time consuming, subtractive, and only suitable for patterning of small areas. Moreover, the harsh conditions required for dissolving resists, etching the underlying layers, and removing the photo-resist destroy the activity of most organic electronic materials. De Rooij and coworkers (Courbat et al. 2010a, b) believe that the printing technology applied in flexible electronics is experiencing a significant growth and the sensors field can benefit from these developments with the availability of new types of materials and fabrication processes. In particular, the above-mentioned approach to gas sensor design guarantees reduced price, new functionalities, and the possibility to integrate sensors where it was impossible to imagine them a decade ago, in smart textiles (wearable) or wireless radio frequency identification (RFID) tags for logistics applications for instance (Vergara et al. 2007). In addition, plastic substrates possess many attractive properties including biocompatibility, flexibility, light weight, shock resistance, softness, and transparency (Xu 2000).

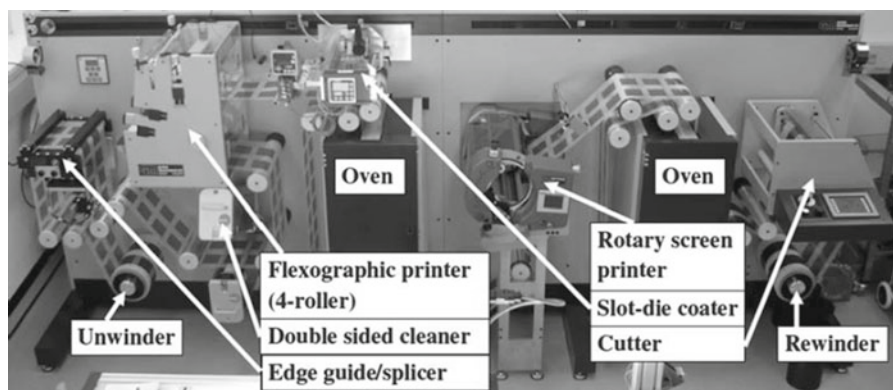


**Fig. 7.5** Inline printing machine with two ovens and three different coating and printing methods. The system has three independent web tension zones [Reprinted with permission from Krebs et al. (2010). Copyright 2010 Royal Society of Chemistry]

One of the most fundamental difficulties in flexible electronic systems is the substrate, because a material for such substrates presents a unique balance of properties (Crawford 2005). Substrates should, of course, be flexible. Specifically, this means the substrate must be able to bend and not crack or lose its other properties. Ideally, the substrate could repeatedly bend without significant long-term degradation. Along with bending, it must be robust. It cannot stretch. The substrate is required to be able to withstand reasonable processing temperatures. This means that the melting temperature of the substrate must be sufficiently high. Additionally, the coefficient of thermal expansion (CTE) must be sufficiently low. If the film expands or shrinks (or both) from too much under heating, the layers deposited on top (probably a mixture of inorganics that typically have low CTEs) are likely to crack or de-adhere, just as they would from an external stress. Substrate should be thermally stable as well. Thermal stability is important primarily for fabrication reasons because the ability to achieve very low processing temperatures is still the subject of much investigation. Stability in aggressive environments is also required. In addition, a flexible substrate must be smooth yet sufficiently adhesive, transparent, and above all economically viable. There are a number of materials that meet most of these requirements and could possibly be tuned to function as a flexible electronics substrate. However, the perfect material is yet to be discovered and, at present, compromises must be made and the choice of substrate depends on the application in question. Thus, in order to choose a substrate, there are multiple important material properties that must be considered. Plastic substrates which could be used for gas sensor design are listed in Table 7.4.

As shown in Table 7.4, most plastics which can be used as substrates for flexible gas sensors deform or melt at temperatures of only 100–300 °C, placing severe limitations on the quality of crystalline semiconductors that can be grown directly on plastic. Therefore, in many cases designers prefer to use polymer as sensing material. However, it is known that polymer-based gas sensors have limitations in many applications. For resolving the above-mentioned problem with crystalline material deposition, three categories of approaches for overcoming temperature restriction have been proposed (McAlpine et al. 2007). The first approaches are crystallization methods, in which an inferior inorganic semiconductor is vapor deposited at low temperatures onto plastic and subsequently crystallized. An example is the conversion of amorphous material into polycrystalline via laser crystallization. Second are wet-transfer or “bottom-up” methods. Single-crystalline material is prepared at high

**Table 7.4** Polymers acceptable as flexible substrates and their parameters

Material	Parameters
<i>Polytetrafluoroethylene (PTFE)</i>	<i>PTFE</i> is most well known by the <b>DuPont</b> brand name Teflon. It is highly resistant to chemicals and wear. According to DuPont, its melting point is 327 °C, but its mechanical properties degrade above 260 °C. Therefore, PTFE allows for processing steps in the 250 °C range. PTFE has excellent dielectric properties
<i>Polyimide (PI)</i>	Thermosetting <i>polyimides</i> are known for thermal stability, good chemical resistance, excellent mechanical properties, and characteristic orange/yellow color. Polyimide is available commercially from DuPont as a product called Kapton®. Polyimides compounded with graphite or glass fiber reinforcements have excellent flexible properties. Thermoset polyimides exhibit very low creep and high tensile strength. Molded polyimide parts and laminates have very good heat resistance. Polyimides maintain their properties during continuous use to temperatures from cryogenic to 232 °C and, for short excursions, as high as 482 °C. As a result polyimides are suitable for processing around 350 °C. Polyimides are also inherently resistant to flame combustion and do not usually need to be mixed with flame retardants. Typical polyimide parts are not affected by commonly used solvents and oils—including hydrocarbons, esters, ethers, alcohols, and freons. They also resist weak acids but are not recommended for use in environments that contain alkalis or inorganic acids. The above-mentioned properties make polyimide an excellent choice as a substrate from a stability and processing point of view
<i>Polyethylenes (PET) and (PEN)</i>	Two polymers in the <i>polyethylene</i> family showing significant promise are polyethylene terephthalate (PET) and polyethylene naphthalate (PEN). PET and PEN films are commercially available from DuPont under the names Melinex® and Teonex®, respectively. As compared to polyimide films, they offer transparency. Depending on its processing and thermal history, PET may exist both as an amorphous (transparent) and as a semicrystalline polymer. The semicrystalline material might appear transparent or opaque and white depending on its crystal structure and particle size. However, the glass transition temperature of these polymers is only in the range of 100–300 °C. This limits the processability of these films and requires the design of new techniques in processing. PET can be semi-rigid to rigid, depending on its thickness, and it is very lightweight. It makes a good gas and fair moisture barrier, as well as a good barrier to alcohol and solvents

temperatures; the synthesized material is then transferred onto plastic at ambient temperatures in the form of solution or paste and is then exposed to annealing admissible (acceptable) to (for) substrate used (Oprea et al. 2012). Local ink-jet printing is also a very promising method for preparing different sensing layers (Weng et al. 2010). The third category of techniques are dry-transfer methods involving the relocation of semiconductor materials or fully fabricated devices from inorganic substrates to plastic using poly(dimethylsiloxane) (PDMS) stamps or soluble glues. We should note that all the above-mentioned methods can be used for gas sensor fabrication. Examples of gas sensors based on plastic and flexible substrates are listed in Table 7.5 and are shown in Fig. 7.6.

Short analysis shows that no one polymer satisfies all the requirements. At present the most suitable for the widest number of applications appears to be PET, offering curing advantages, or PEN, offering thermal and dimensional stability. However, experiments and results presented in Table 7.5 have shown that PI offers more options in terms of processing as long as transparency isn't a requirement. For example, Briand et al. (2006) have shown that polyimide-based flexible micro-hotplates on polyimide sheets and on silicon for gas-sensing and thermal actuating applications can be realized. Moreover, platinum and aluminum microheating elements on polyimide exhibited promising

**Table 7.5** Examples of plastic substrates using in gas sensors

Substrate	Sensor type ( $T_{oper}$ )	Sensing material (deposition technology)	Target gas	References
PET	Conductometric (RT)	Polypyrrole (PPy) (self-assembling)	NH <sub>3</sub>	Su et al. (2009a)
PET	FET-based (RT)	Si-nanowires (dry transfer)	Acetone, hexane, NO <sub>2</sub>	McAlpine et al. (2007)
PET	Colorimetric (RT)	Poly(methyl methacrylate) (spin-coating)	NH <sub>3</sub>	Courbat et al. (2009c)
PET	Conductometric (RT)	MWCNTs (layer-by-layer)	NO <sub>2</sub>	Su et al. (2009b)
PET, PI	Conductometric (200 °C)	SnO <sub>2</sub> , ink jet	CO, NO <sub>2</sub>	Courbat et al. (2010a, b, c)
PEN or PI	Capacitance (RT)	Poly cellulose acetate, poly cellulose acetate butyrate, poly (methacrylate), or polyvinylpyrrolidone (spray or screen-printing)	Humidity	Oprea et al. (2008)
PI	Conductometric (200–300 °C)	SnO <sub>2</sub> :Pd or WO <sub>3</sub> (drop coating, $T_{an} = 400$ °C)	CO, CH <sub>4</sub> and NO <sub>2</sub>	Courbat et al. (2009a, b)
PI	Conductometric (RT)	C black/vinyl acetate (direct writing)	Dimethyl methyl-phosphonate	Marinov et al. (2007)
PI	Conductometric (RT–300 °C)	CNTs (reduced graphene hybrid films)	NO <sub>2</sub>	Jeong et al. (2010)
PI	Conductometric (RT–300 °C)	ZnO nanorods (chemical solution method)	Ethanol	Ahn et al. (2010)
PI	Capacitance (RT–300 °C)	Cellulose acetate butyrate Polydimethylsiloxane (drop coating)	Humidity VOCs	Courbat et al. (2009b)
PI	Conductometric (RT)	Polyaniline emeraldine (evaporating)	NH <sub>3</sub>	Pecora et al. (2008)
PI	Capacitance (RT)	Bisbenzocyclobutene (casting)	Humidity	
PI	Conductometric (300 °C)	SnO <sub>2</sub> :0.2% Pd and WO <sub>3</sub> (drop-coating)	CO, NO <sub>2</sub> , EtOH	Oprea et al. (2012)
	Capacitance (RT)	Cellulose acetate butyrate (CAB) (drop-coating) Polyether urethane (PEUT) (drop-coating)	Humidity VOCs	
PU	Conductometric (RT)	SnO <sub>2</sub>	CO	Huo et al. (2011)

characteristics for their integration in low-power gas sensors and thermal actuators. In particular, a high operating temperature (up to 400–500 °C) was obtained at a relatively low power (100–150 mW) and the thermal stability of the structure allowed the annealing of a metal oxide film to realize metal oxide gas sensors. Compared to micro-hotplates on silicon with their membranes made of dielectric layers, the fabrication of micro-hotplates with polyimide-based membranes brings the advantages of simplified processing and improved robustness and flexibility. Meanwhile, Briand et al. (2011) believe that polyimide will only be used for applications with specific requirements regarding temperature and the robustness of the substrate: most devices will be produced on PET and PEN substrates.

Kinkeldei et al. (2012) also compared different polymeric substrates such as PEN, PI, PPS, and PEI (see Table 7.6), and concluded that the selection of polymer for gas sensor platform depends on the working principle of the sensor designed. In the case of metal oxide-based gas sensors, the substrate has to be heated during operation of the sensors. This requires temperatures above the melting point of PET/PEN and PPS. This means that these materials are unacceptable for application in metal oxide chemiresistors. In the case of capacitive sensors, the substrate material should be inert against

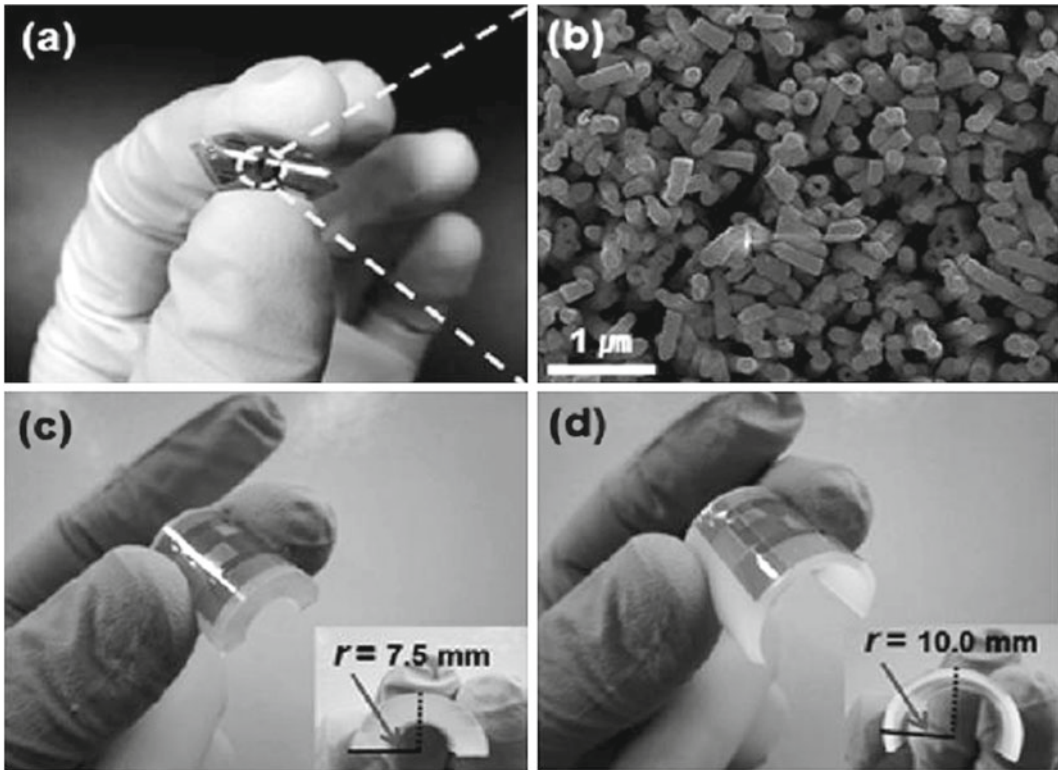


**Fig. 7.6** Flexible Pd nanotube-based gas sensor: (a) photograph of a flexible sensor based on Pd nanotube arrays; (b) SEM image of Pd nanotube arrays prepared on polyimide film; (c, d) photographs of flexible sensors attached on the cylindrical surface of silicone tubes with different radii ( $r=7.5, 10.0$  mm) [Reprinted with permission from Lim et al. (2012). Copyright 2012 American Chemical Society]

**Table 7.6** Properties of polymer materials used in flexible substrates

Parameter	Flexible polymer substrate			
	PEN	PI	PPS	PEI
$T_G$	121 °C	354 °C	92 °C	217 °C
$T_M$	269 °C	–	285 °C	–
CTE	18 ppm/°C	16 ppm/°C	30 ppm/°C	31 ppm/°C
Solvent stability	++	++	++	++
Transparency	Transparent	–	Translucent	Translucent
CHE	n.a.	8 ppm/%RH	1.5 ppm/%RH	n.a.
Water absorption	0.3%	1.8%	0.05%	0.2%

*PEN* polyethylene naphthalate, *PI* polyimide, *PPS* polyphenylene sulfide, *PEI* polyethylenimine,  $T_G$  glass transition temperature (the glass transition temperature is the temperature at which the amorphous phase of the polymer is converted between rubbery and glassy states),  $T_M$  melting point, *CTE* coefficient of thermal expansion, *CHE* coefficient of hygroscopic expansion

Source: Data from Kinkeldei et al. (2012)

environmental changes so that the signal is only dependent on the gas sensitive layer. PI has a high water adsorption that affects the sensing performance (Oprea et al. 2007), while PEN/PET, compared to PI, have a lower water absorption coefficient and are less affected from humidity changes (Oprea et al. 2008). Therefore, bare PI and PEN substrates have been used by Oprea et al. (2007, 2008) for capacitive humidity sensors. Kinkeldei et al. (2012) have found that PEI substrates also have low



water absorption coefficients. Experiments with metal oxide-resistive sensors have shown that the influence of water on the gas sensor performance was least with PEI as substrate materials. According to Kinkeldei et al. (2012), besides the stable measurement results with PEI substrates, the PEI combines several benefits of the other substrates. It is translucent and can be heated up to 200 °C without degradation (soldering is possible). Further, the evaporation of metal films on the substrate showed excellent adhesion on non-plasma-treated substrates.

For comparison, the adhesion was poor on PEN substrates and scratched metal lines were destroyed. Kinkeldei et al. (2012) believe that these properties make PEI a promising substrate material for resistive-type gas sensor applications.

More detailed information about achievements and perspectives in the field of gas sensor design on plastic foils can be found in the review prepared by Briand et al. (2011). They have shown that, in spite of limited number of publications on gas sensors on plastic/flexible foils, in the literature one can find information about various gas-sensing devices fabricated on plastic substrates. A major part of the published work consists of single flexible humidity sensors, sometimes combined with temperature sensors on the same platform (Ki 2006; Huanget al. 2006; Lee et al. 2008; Arena et al. 2009; Miyoshi et al. 2009; Su et al. 2009c; Zampetti et al. 2009). Capacitive and resistive transducers are commonly used as sensor architectures. Some groups developed organic thin-film transistors (OTFT) for sensing air humidity and volatile organic compounds (VOCs) (Subramanian et al. 2005). However, the gas sensors based on organic transistors require further development to achieve the required sensing performance and reliability needed for commercialization (Lee et al. 2005). Ammonia and hydrogen sulfide sensors have also been reported, some of which use printing technologies to deposit gas-sensitive conducting polymers and silver electrodes (Cho et al. 2008; Crowley et al. 2008; Su et al. 2009a; Weng et al. 2010). However, the gas-sensing performance has been poor. The colorimetric detection of gases on foil has also been demonstrated with the use of gas-sensitive dyes combined with an optical waveguide on plastic, with the detection of concentrations of CO<sub>2</sub> below 1% in nitrogen, and the sub-ppm detection of NH<sub>3</sub> in air (Mayr et al. 2009). Great success was achieved by EPFL-IMT SAMLAB and the University of Tuebingen (Courbat et al. 2009a, b, c, 2010a, b, c; Oprea et al. 2009, 2012; Briand et al. 2011). They demonstrated the continuous operation of metal oxide gas sensors made on polyimide hotplates for several months. A multi-parameter-sensing platform (for VOCs, temperature, humidity, reducing and oxidizing gases) on plastic foil, based on standard clean room processes, was also designed (Courbat et al. 2009c; Oprea et al. 2009, 2012; Briand et al. 2011). In particular, Oprea et al. (2012) demonstrated that by joint operation of the Pt thermo-resistive thermometer, polymer-based capacitive sensors, and metal oxide conductometric sensors (Fig. 7.6), several interfering gases can be detected and, to some extent, separated at hardware level. Thus, the capacitive structures monitored the humidity and ethanol (as representative VOC), while the metal oxide structures monitored the oxidizing and reducing gases (NO<sub>2</sub>, CO) as well as the reducing ethanol vapors. Oprea et al. (2012) reported that all the integrated devices were stable and gave reproducible signals for more than 2 months of operation, even when the MOXs ran continuously at 300 °C. A typical result of the multisensor platform is presented in Fig. 7.7. Finally, some groups have started to look at the implementation of gas-sensitive nanomaterials on plastic foil with the transfer or self-assembly of nanowires, nanotubes, and nanoparticles on flexible substrates (Parikh et al. 2006; McAlpine et al. 2007; Gu et al. 2009; Ahn et al. 2010; Jeong et al. 2010; Wang et al. 2010a, b).

It should be noted that a hybrid approach to design gas-sensing devices on plastic substrates can be used as well. In particular, a surface acoustic wave (SAW) chip, which require substrates with very different properties, can be transferred onto a plastic substrate Cobianu et al. (2007). Another interesting and new approach is the coating of passive (no power source on board) conventional RFID (radio-frequency identification) tags with chemically sensitive films to form a chemical sensor (Potyrailo and Morris 2007). The detection of several vapors of industrial, health, law enforcement, and security

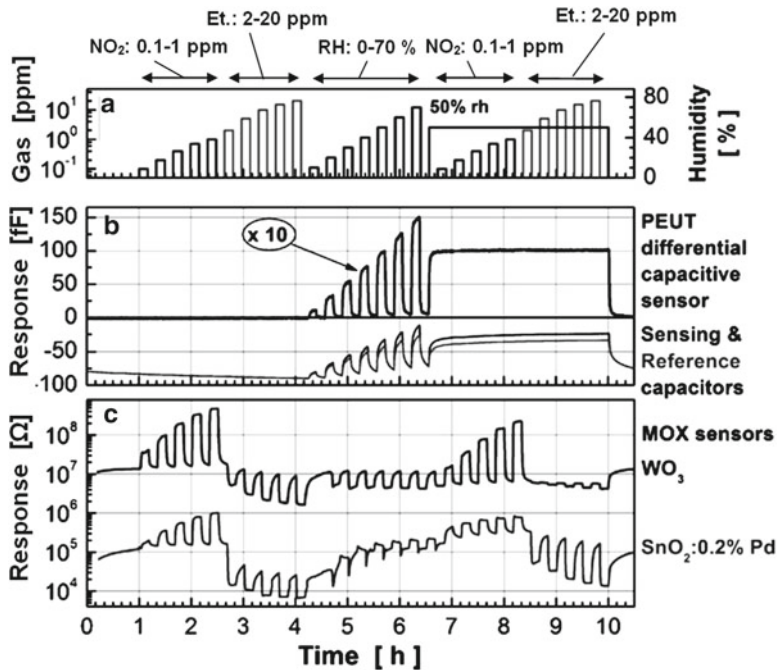


**Fig. 7.7** Gas response of the capacitive (RT) and chemoresistive (300 °C) gas sensors to nitrogen dioxide (0.1–1 ppm), ethanol (2–20 ppm), and relative humidity (0–70%). (a) Gas protocol; (b) differential PEUT capacitive sensor response (ten times magnified), PEUT-sensing capacitor signal, and reference capacitor signal. The PEUT-sensing capacitor and reference capacitor signals (in fact in the 2 pF range) have been arbitrarily shifted in order to be displayed on the same panel with the differential capacitive sensor response; (c) gas response of the SnO<sub>2</sub>:0.2% Pd and respectively WO<sub>3</sub> MOX sensors [Reprinted with permission from Oprea et al. (2012). Copyright 2012 Elsevier]

interest (ethanol, methanol, acetonitrile, and water vapors) was demonstrated with a single 13.56-MHz RFID tag coated with a solid polymer electrolyte-sensing film.

Regarding the integration of temperature sensors on plastic-flexible foil, the conventional platinum resistance temperature detector (RTD) has been realized on a flexible polyimide substrate, for operation up to 400 °C, and resistors made of TaSiN have been shown to exhibit high temperature coefficient of resistance (TCR) values (Moser and Gijs 2007; Chung et al. 2009). Some approaches utilizing thermo-sensitive polymers, based on graphite or metallic powders in a PDMS matrix, which suffered from nonlinearity and were limited to 100 °C, have also been evaluated (Chuang and Wereley 2009; Shih et al. 2010). Another approach that has been reported is the screen printing of a polymeric thermo-sensitive material on Kapton for textronic applications, e.g., measurement of the temperature of the human body (Bielska et al. 2009).

## 7.4 Cantilever-Based Platforms

Microcantilevers are very promising sensor platforms, which make possible both decreased power dissipated by the heater of conductometric and calorimetric sensors and improved sensitivity of capacitance and various mass sensitive devices. The recently developed nanocantilevers present a major technology breakthrough that have given rise to nanoelectromechanical systems used for gas detection (Guntherodt 2001; Lavrik et al. 2004; Papadimitriou and Tsamis 2005; Lang and Gerber 2008; Goeders et al. 2008; Lang et al. 2009; Battison et al. 2009). Schematic diagrams illustrating the work of cantilever-based mass-sensitive sensors are shown in Fig. 7.8.

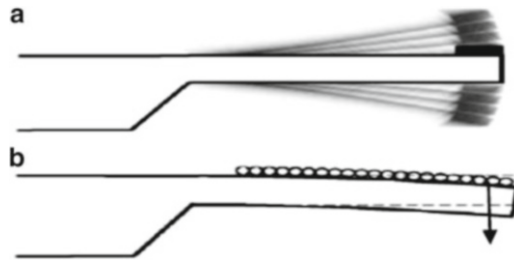


**Fig. 7.8** (a) Dynamic mode: absorption of analyte molecules in a sensor layer leads to shift in resonance frequency. (b) Static mode: the cantilever bends owing to adsorption of analyte molecules and change of surface stress at the cantilever surface [Reprinted with permission from Battiston et al. (2001). Copyright 2001 Elsevier]

**Table 7.7** Material properties of Si and several polymers. RT measurements

Material	Young's modulus (GPa)	Poisson's ratio
Si	169	0.3
Polyimide	3.3	0.35
SU-8	3.6	0.33

Source: Data from Fragakis et al. (2005) and Chung et al. (2006)

Cantilevers are normally made of silicon or related materials that have a high Young's modulus. However, it is known that cantilever sensitivity depends critically on the spring constant of material used, i.e., Young's module. It has long been established that the lower the spring constant of the cantilever, the higher the sensitivity. This means that a cantilever made of a softer material will be more sensitive for static deflection measurements in comparison with Si-based cantilevers. Young's moduli for several polymers acceptable for cantilever design are listed in Table 7.7.

The design of microcantilevers based on SU-8, a photopolymerizable epoxy-acrylate polymer, is one such attempt. SU-8 is a negative photosensitive polymer used as structuring material in micro electro mechanical systems (MEMS) and for fabrication purposes within the micro-total-analysis-system ( $\mu$ TAS) area (Carlier et al. 2004). SU-8 is highly transparent in the ultraviolet region, allowing fabrication of relatively thick (hundreds of micrometers) structures with nearly vertical side walls. After exposition and developing, its highly cross-linked structure gives it high stability to chemicals and radiation damage. Cured cross-linked SU-8 shows very low levels of outgassing. The latter is good for gas sensor design. As shown by Fragakis et al. (2005), polyimides can also be used for cantilever design. In particular, silicon/polyimide-based cantilevers were used in capacitive-type bimorph humidity sensors (Fragakis et al. 2005). The top-surface view of such cantilevers is shown in Fig. 7.9. During operation, the polyimide layer swells as it is exposed to ambient humidity; the induced compressive stress decreases in value, and the cantilever tends to return to its horizontal position, effectively increasing the device capacitance.

#### 7.4.1 Silicon-Based Microcantilevers

Silicon-based microcantilevers are made using well-established fabrication techniques, which generally include thin-layer deposition, photolithographic patterning, etching, and micromachining (surface and bulk), discussed earlier in Sect. 7.2. In particular, Si cantilever sensor arrays can be microfabricated using a dry etching silicon-on-insulator (SOI) fabrication technique developed in the Micro-/Nanomechanics Department at IBM's Zurich Research Laboratory. One example of a microcantilever fabrication process is shown in Fig. 7.10, where a scheme of the masks used and a top view of the

**Fig. 7.9** Top-surface view of the polyimide covered cantilevers. The devices are bent upward due to the polyimide precursor shrinking after curing [Reprinted with permission from Fragakis et al. (2005). Copyright 2005 IOP]

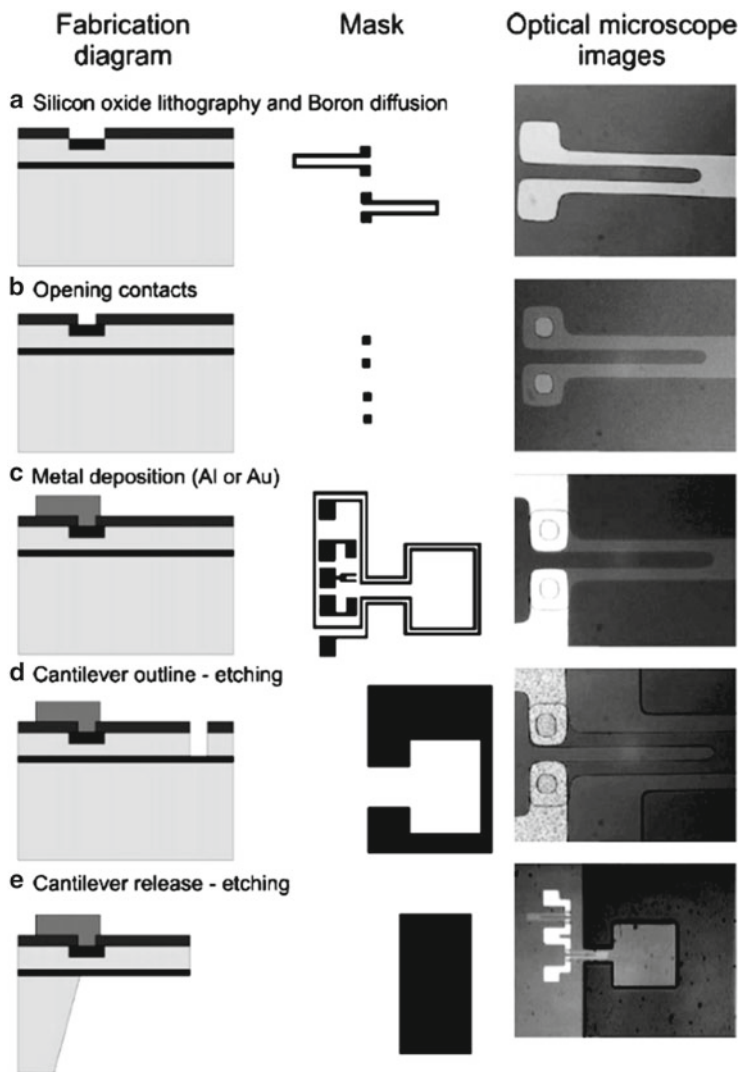
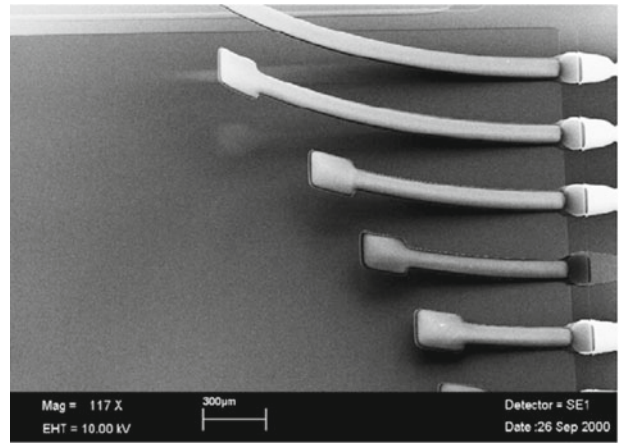


**Fig. 7.10** Scheme of the microcantilever fabrication process: (a) oxidation, aperture, and doping; (b) contacts opening; (c) aluminum or gold deposition; (d) front-face etching; (e) back-side etching [Reprinted with permission from Urbiztondo et al. (2009). Copyright 2009 Elsevier]

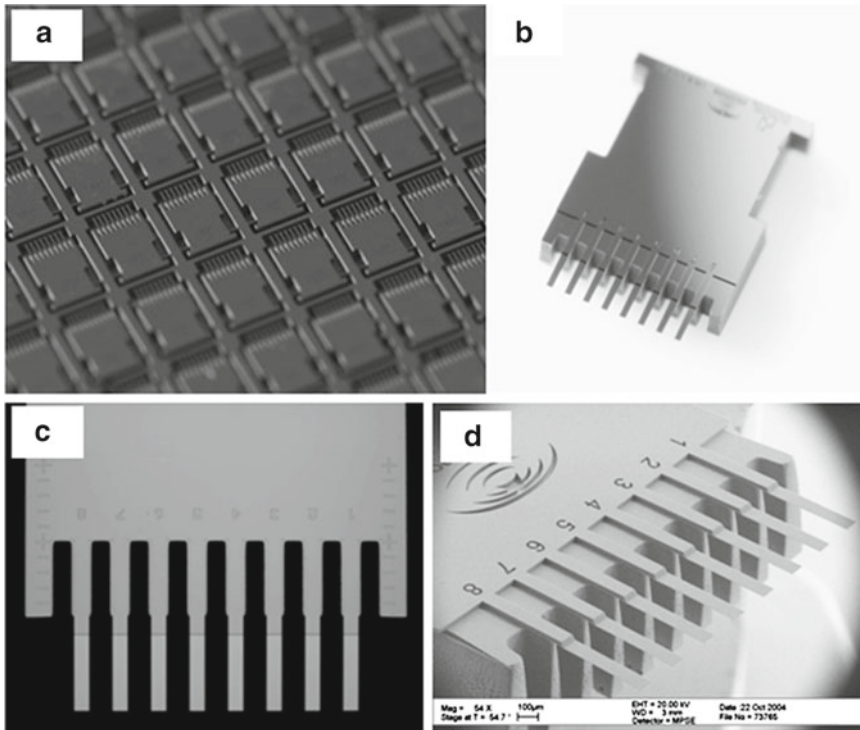


**Fig. 7.11** Views of commercially possible cantilevers: (a) cantilever array wafer; (b–d) single cantilever arrays (Uploaded from <http://www.concentris.ch> and <http://cantion.com>)

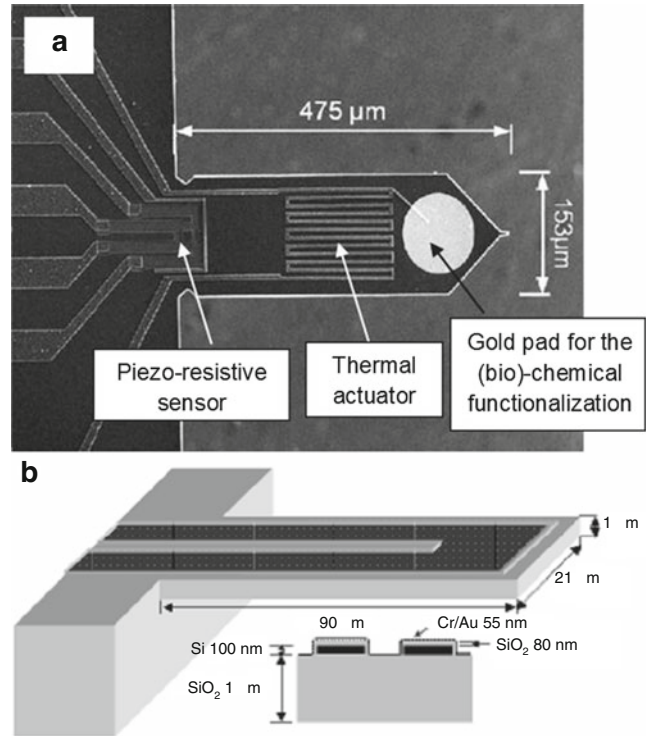
cantilever during the different stages are also provided. Briefly, a five-step photolithography procedure was used first to achieve the development of the strain gauges and electrical contacts and then to define the geometry of the microcantilever.

The above-mentioned processing technologies enable batch fabrication of cantilevers with high yield, good reproducibility, and low cost. Thus it is possible to make thousands of microcantilevers in an array format on a wafer (see Fig. 7.11). A more detailed description of microcantilever fabrication using commercial CMOS technology can be found in the literature (Hierlemann et al. 2000; Lavrik et al. 2004; Martorelli 2008; Boisen and Thundat 2009).

When the piezoresistive technique is applied to monitor cantilever deflection, the cantilever is fabricated with an integrated resistor having piezoresistive properties, and its resistance changes as a function of cantilever bending (Boisen and Thundat 2009). The extent of cantilever bending can be accurately found by a simple electrical measurement. The commonly fabricated piezoresistors are based on boron-doped silicon layers. The doped silicon layers are then capped with insulating materials. To enhance sensitivity, the piezoresistive layer of the cantilever should be placed in the region of maximum stress, preferably on the surface. One such cantilever is shown in Fig. 7.12. For a first approximation, the resulting relative change in resistance is directly proportional to the stress, and therefore to the deflection.

The silicon resistor is defined in microcrystalline or single-crystal silicon and usually encapsulated in silicon nitride. The thickness of the deposited silicon nitride on either side of the cantilever is adjusted so that the neutral axis of the cantilever lies inside the silicon nitride layer rather than in the silicon layer. This asymmetry in material composition ensures that the resistor is placed close to one of the cantilever surfaces for optimal sensitivity. In addition, the silicon nitride serves as

**Fig. 7.12** Thermally driven piezoresistive cantilevers. (a) Reprinted with permission from Woszczyna et al. (2009). Copyright 2009 Elsevier. (b) Reprinted with permission from Li and Li (2006). Copyright 2006 IOP



efficient electrical insulation for the resistor and ensures that the device can be operated in liquids. The signal-to-noise ratio of the piezoresistive cantilever is highly dependent on the doping and the crystallinity of the silicon layer. The best performance is clearly found for single-crystalline resistors, which can detect deflections below 1-nm resolution (<http://www.cantion.com>).

#### 7.4.2 Polymer-Based Microcantilevers

Microcantilevers fabricated from polymers inherently possess readily tailored mechanical and chemical properties (Goeders et al. 2008). To alter the stiffness of silicon-based cantilevers, their geometry must be changed or a rigid coating must be applied to the surface. In contrast, the stiffness of polymeric cantilevers requires only a change in material. In this way, microcantilevers with the same geometry but different properties can be produced. This reduces manufacturing costs and simplifies the apparatus required for detection. The materials used for polymer-based cantilevers span a wide range of thermosets, thermoplastics, and polymeric composites. Examples of polymer composites include silver nanoparticles and SU-8 (Jiguet et al. 2004), carbon nanotubes and poly(*m*-phenylenevinylene-*co*-2,5-dioctoxy-*p*-phenylenevinylene) (Curran et al. 1998), and many other combinations. The fabrication of such cantilevers is inexpensive and fast. Polymeric microcantilevers can be fabricated in a variety of ways; the method used is determined by the type of polymer to be used. For example, the process for fabricating SU-8-based cantilevers is quite similar to that used for silicon-based cantilevers. The fabrication process is shown in Fig. 7.13. A thin film of SU-8 is deposited onto a wafer by spin-coating. Photolithography is then used to define the regions that will comprise both the cantilever and the chip to which it is attached. The unwanted material is removed and the

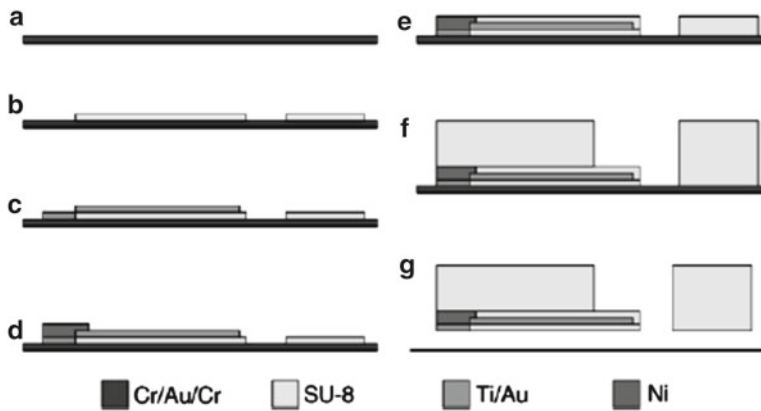
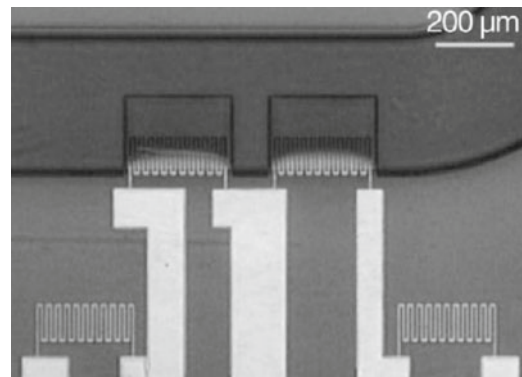


**Fig. 7.13** Polymer cantilever fabrication process. (a) Evaporation of 5/50/50 nm of Cr/Au/Cr as release layer on a Si wafer. (b) Patterning of 1.5- $\mu\text{m}$ -thick SU-8 for the cantilever. (c) Evaporation of 5/60 nm Ti/Au for the resistors and wires. (d) Electroplating approximately 5  $\mu\text{m}$  of Ni for the contact pads. (e) Patterning 3.5- $\mu\text{m}$ -thick SU-8 for encapsulation of the resistors. (f) Patterning 200- $\mu\text{m}$ -thick SU-8 for the microfluidic channel. (g) Release of the chip from the wafer by etching the Cr layer [Reprinted with permission from Johansson et al. (2005). Copyright 2005 Elsevier]

**Fig. 7.14** Image of polymer (SU-8) cantilevers with integrated gold resistors. These devices are softer than similar silicon devices and are much faster to fabricate. However, polymers with the same stability as silicon still need to be identified [Reprinted with permission from Johansson et al. (2005). Copyright 2005 Elsevier]



polymer cantilevers are released from the substrate by immersion in an appropriate solvent. SU-8 cantilevers have been made into arrays for optical lever (Calleja et al. 2005; Ransley et al. 2006) and piezoresistive (Johansson et al. 2006) detection schemes.

An example of a polymer cantilever with integrated gold resistor is shown in Fig. 7.14. The gold resistors serve as low-noise piezoresistors; the signal-to-noise ratio is comparable to the value for silicon nitride cantilevers with single-crystal resistors (Johansson et al. 2005). The relative resistance change of gold is approximately 40 times smaller than for single-crystal silicon, and new materials are therefore being investigated as possible candidates for even better piezoresistors. The challenge is to find a material that is soft while having a large change in resistance upon deflection. Moreover, the electrical noise in the system should be low (Boisen and Thundat 2009).

Injection molding, an economical mass production technique, has also been used to fabricate microcantilevers out of thermoplastic polymers (McFarland et al. 2004; McFarland and Colton 2005a, b). In this process, a molten polymer such as polypropylene is forced under pressure into a steel cavity (mold); the shape of the cavity defines the dimensions of both the base and the cantilever(s). Injection-molded microcantilevers have been shown to be of equal caliber to commercial silicon microcantilevers. McFarland et al. (2004) and McFarland and Colton (2005a, b) specified in detail the fabrication of injection-molded microcantilevers. Despite their advantages over silicon-based cantilever arrays, polymeric cantilever arrays are not commercially available.

## 7.5 Paper-Based Gas Sensors

Paper-based sensors are a new alternative technology for fabricating simple, low-cost, portable, and disposable analytical devices for many application areas including clinical diagnosis, food quality control, and environmental monitoring (Liana et al. 2012). The unique properties of paper, which allow passive liquid transport and compatibility with chemicals/biochemicals, are the main advantages of using paper as a sensing platform. Paper is a well-known material for writing, printing, drawing, and packaging. The potential utility of paper beyond these simple and traditional means stems from its versatility, high abundance, low cost, and unique physical properties (Martinez et al. 2010). It is a highly sophisticated material as it can be made thin, lightweight, and flexible, depending on its pulp processing. In addition, paper is combustible and biodegradable. It can be easily stored, transported, and disposed. The main constituent of paper is cellulose fiber, and this can be highly attractive for certain applications as it allows liquid to penetrate within its hydrophilic fiber matrix without the need for an active pump or external source (Martinez et al. 2010). The use of glass and plastic substrates requires pumping. Moreover, cellulose fibers can be functionalized, thus changing properties such as hydrophilicity, if desired, as well as permeability and reactivity (Bracher et al. 2010). The paper surface can be easily manipulated through printing, coating, and impregnation, and can be fabricated in large quantities. Depending on the main goal to be achieved in paper-based sensors, the fabrication methods and analysis techniques can be tuned to fulfill the needs of the end-user.

There are a variety of paper materials available to the user, although the choice is based mainly on the fabrication steps required in developing a device and also on the specific application area. In the development of sensors and microfluidic technologies, filter paper has seen widespread use in recent years for producing paper-based sensors due to its wicking ability (Li et al. 2010; Martinez et al. 2010). In particular, the Whatman® cellulose range is popular with the important parameters of porosity, particle retention, and flow rate differentiating the filter paper types.

At present, most of the research is focused on microfluidic delivery of solution to the detection site, whereas more advanced designs involve complex 3D geometries based on the same microfluidic principles (Li et al. 2010; Martinez et al. 2010; Liana et al. 2012). This means that designed sensors are mainly electrochemical or *colorimetric* sensors aimed at the detection of ions in solution (water, blood, etc.). These paper-based devices provide a solid platform for low-cost high-throughput biochemical analysis (Martinez et al. 2010). However, research has shown that paper-based gas sensors can be designed as well. For example, for resolving the problems connected with elaborations of portable ozone sensors, Koutrakis et al. (1993) and Geyh et al. (1997) have suggested using diffusive and pumped ozone badges, which are small, inexpensive, and acceptable for microenvironmental and personal monitoring. Sodium nitrite impregnated on a filter is oxidized to nitrate in the presence of ozone. Sodium nitrite ( $\text{NaNO}_2$ ) is a promising trapping reagent in detecting ambient ozone, because it offers sufficient sensitivity and few interference problems. Less favorable features of the method is the time-consuming analysis (because the amount of nitrate is determined by ion chromatography) and poorer time resolution. An accumulated sensor with an hourly resolution for ambient ozone monitoring has also been developed by Maruo (2007) and Maruo et al. (2009). The sensor operated by employing the reaction of ozone with indigo carmine. This reaction results in colorless reaction products in pores that can be determined by measuring the transmittance of the color change. The simple fabricated device consisted of porous substrate (paper) impregnated with the reagent. It was found that the combination of a cellulose sheet, humectant, acid, and indigo carmine is required for good response. The detection limit of the sensor with the optimal sensing layer was about 3 ppb for a 1-h exposure. Maruo et al. (2010) have shown that azo dyes can also be used for design of the above-mentioned sensors. Thus, the proposed passive sampler methods are simple, inexpensive, do not require power or a pump, and can be widely used at exposure points. A limitation of all of the above badge methods is that they only yield a single integrated ozone measurement over averaging times



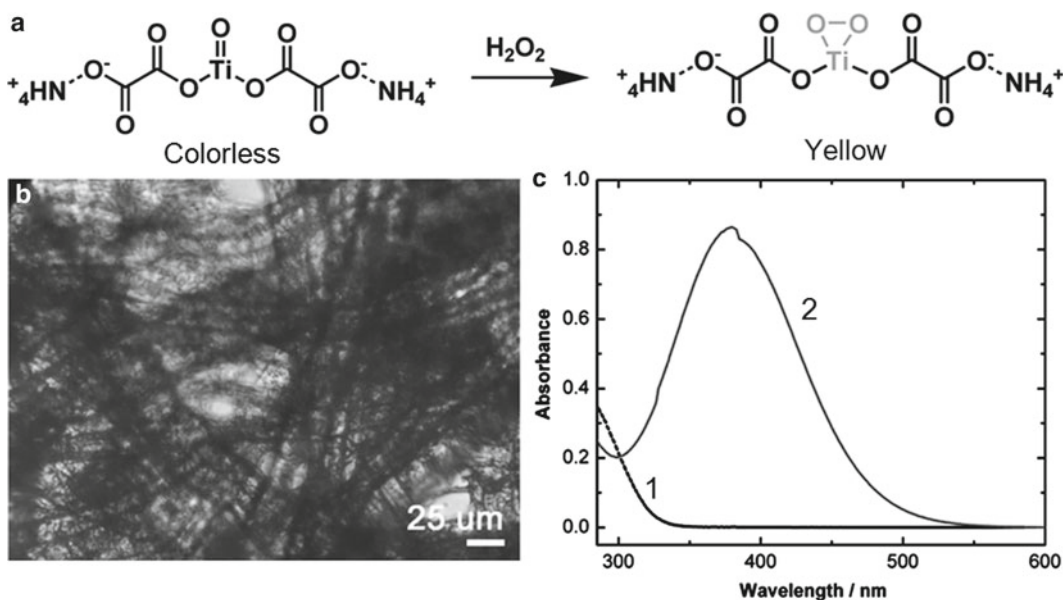


**Fig. 7.15** (a) Colorimetric sensing based on peroxide complexation with Ti(IV) oxo moiety ( $>Ti=O$ ). (b) An optical microscope photograph of the paper towel, revealing the cellulose fibril network. (c) The UV-vis absorption spectra were obtained for a water solution of titanyl oxalate ( $1.0 \times 10^{-3}$  M) before (1) and after (2) addition of 0.04 wt%  $H_2O_2$  (Adapted with permission from Xu et al. (2011). Copyright 2011 American Chemical Society)

(weekly in many cases) that are long relative to time scales over which ozone concentrations change (Black et al. 2000). While such measurements may be useful in calculating long-term average ozone exposures, they do not supply information regarding temporal changes of ozone concentration. Furthermore, the time and expense involved in extracting and analyzing the badge samples can be high. Besides, it was found that relative humidity had a strong influence on the ozone response (Maruo et al. 2009, 2010).

Research has shown that other types of gas sensors can also be fabricated on the paper substrates. In particular, Mitchell et al. (2012) reported about paper-based plasmon resonance VOCs sensors. A porous sol-gel polymer thin film doped with 20-nm gold nanoparticles was drop-coated onto 6 mm  $\times$  6 mm squares of filter paper. Sensors demonstrated limits of detection (LOD) of 160 ppm for methanol and 100 ppm for ethanol. Dossi et al. (2012) designed a paper-based electrochemical sensor for VOCs detection. A sensitive and fast-responding membrane-free amperometric gas sensor consisted of a small filter paper foil soaked with a room temperature ionic liquid (RTIL), upon which three electrodes were screen printed with carbon ink, using a suitable mask. This sensor takes advantage of the high electrical conductivity and negligible vapor pressure of RTILs as well as their easy immobilization into a porous and inexpensive supporting material such as paper.

Although filter paper is widely used, it does not always possess the desired physical characteristics, so other types of paper or paper modifications have been explored. For example, a colorimetric sensor system that can detect hydrogen peroxide vapor down to parts per billion levels was designed by Xu et al. (2011) using the cellulose microfibril network of paper towels (see Fig. 7.15). Xu et al. (2011) found that this sensor material provides a tunable interface for modification with Ti(IV) oxo complexes for binding and reacting with  $H_2O_2$ . According to Xu et al. (2011), paper-based sensory materials have the following unique features that are desirable for vapor sampling and detection: (1) continuous pore channels, allowing for efficient diffusion of gaseous molecules throughout the film matrix, making

it possible to fabricate a thick film to increase the optical density and thus enhance the sensing accuracy; (2) a three-dimensional microscopic structure that allows for maximal distribution of the Ti(IV) oxo moiety on the surface, thus enabling maximal exposure to the gaseous analytes; and (3) a colorless background in the pristine state (i.e., before exposure to hydrogen peroxide) allowing for high contrast measurement of the color formation. The Ti(IV)–peroxide bond thus formed turns the complex from colorless to bright yellow with an absorption maximum around 400 nm (Fig. 7.15c). Such a complexation-induced color change is exclusively selective for hydrogen peroxide, with no color change observed in the presence of water, oxygen, common organic reagents, or other chelating reagents. This paper-based sensor material is disposable and is for one-time use, representing a cheap, simple approach to detect peroxide vapors. The reported sensor system also proves the technical feasibility of developing enhanced colorimetric sensing using nanofibril materials that will provide plenty of room to enlarge the surface area (by shrinking the fiber size), so as to enhance the surface interaction with the gas phase.

Instead of using filter paper as the main material to create paper-based sensing devices, other types of paper, such as glossy paper, have been reported as suitable platforms in sensor technologies. Glossy paper is a flexible substrate made of cellulose fiber blended with an inorganic filler. In particular, Arena et al. (2010) used glossy paper for developing a flexible paper-based sensor for the detection of ethanol vapors in air using indium tin oxide nanoparticulate powder as a sensing material and multi-walled carbon nanotubes as electrodes. The addition of poly-diallyldimethylammonium chloride as the binder promoted the adhesion of the indium tin oxide nanoparticulate powder to the glossy paper substrate. Subsequent analysis of ethanol was carried out in air by measuring the current upon using triangular-applied voltage. Due to the nondegradability and relatively smooth surface of glossy paper, it is a good substitute for filter paper, especially when modifying nanomaterials onto a surface rather than within the fiber matrix is necessary.

The same approach was used by Steffens et al. (2009). They developed a low-cost gas sensor using graphite interdigitated electrodes coated with a thin-sensing layer of doped polyaniline. Tracing paper (weight 63 g/m<sup>2</sup>) was used as a substrate. Thin films of PANI-HCl were deposited by in situ polymerization on interdigitated graphite electrodes printed over a rectangular area of 16 mm by 14 mm. Changes in conductivity were observed in response to the presence of nitrogen gas. Later Manzoli et al. (2011) showed that these differently doped sensors incorporated in sensor arrays can be used as electronic noses. Manzoli et al. (2011) believe that the development of this low-cost apparatus will provide a more efficient monitoring of the maturation of fruits, bringing consumers better quality products.

Although paper-based sensors are very promising, they still suffer from certain limitations such as accuracy and sensitivity. However, it is anticipated that in the future, with advances in fabrication and analytical techniques, that there will be more new and innovative developments in paper-based sensors. These sensors could better meet the current objectives of a viable low-cost and portable device in addition to offering high sensitivity and selectivity and multiple analyte discrimination (Liana et al. 2012). For example, Liu et al. (2011) reported MEMS piezoresistive sensors constructed using paper as the structural material instead of silicon. They have also shown that paper can be used as a substrate for laying out simple electrical circuits and permits electrical circuits for signal processing to be readily integrated with the paper-based sensor to form monolithic paper-based chips. At the same time Liu et al. (2011) have noted that the paper-based MEMS force sensor has several limitations, of which three are (1) it has lower sensing performance (i.e., measurement range, resolution, and sensitivity) than the silicon-based force sensor, (2) because paper has a lower Young's modulus (2 GPa) than silicon (130–170 GPa), it has a low natural resonant frequency (~25 Hz), and is therefore limited to low frequency or static measurement of forces, and (3) paper-based MEMS will be more sensitive than silicon-based devices to high temperatures, atmospheric components (e.g., water vapor, ozone, prolonged exposure to dioxygen or peroxides); these sensitivities may, of course, also be advantageous in some contexts.

## 7.6 Material Requirements for Packaging of Gas Sensors

Sensor packaging is a very important issue in sensor development, because no sensor can be designed without considering the final package and its cost (Mastrangelo and Tang 1994). The nature of any sensor requires the sensing element to be exposed to the sensing environment. This requirement differs from that of common microelectronic components which are often completely encapsulated or sealed. Consequently, the material and the dimensions of the encapsulation are not as critical as those for a sensor.

We need to note that the packaging of gas sensors has two functions. First, the packaging must allow the target gas to enter the sensor and interact with the sensing element. When packaging a sensor, any area which should not be exposed must be covered properly. Second, the packaging should protect the sensor from harmful environments and destruction (Mastrangelo and Tang 1994).

Of course, the packaging of each type of sensor is different and has different requirements. However, we believe that when choosing the packaging and ways to mount the gas sensors it is necessary to take into account the following issues:

1. The packaging process needs to avoid the presence of gaseous components which may poison the sensor active layer.
2. The housing should not prevent access of the target gas to the sensor.
3. The materials utilized to package the sensor cannot emit gaseous components during sensor operation.
4. The materials utilized to package the sensors have to be inert in relation to the atmosphere in which the sensor will operate.
5. In the development of gas sensors, different layers are commonly used. Thus, the choice of a proper packaging layer, such as silicon dioxide, silicon nitride, glass-based dielectric materials, or other, for example, epoxy, should consider the adhesive properties of these layers as well as the thermal match and mismatch of these layers in order to ensure the overall integrity of the sensor (Liu 1996). Glass-based dielectric materials can be applied by thick-film techniques. Various conventional thin-film techniques can be applied for deposition of silicon dioxide and silicon nitride. For electrochemical gas sensors designed for operation in an aqueous environment, the problem of packaging is particularly important because the connection and insulation of the sensor are subjected to potential water penetration. This poses a critical challenge to the long-term operational life of the sensor, underscoring the importance of proper sensor packaging.

Analysis of presently available information shows that gas sensors are often mounted in a transistor outline (TO)-like casing which contains a filter such as charcoal. In addition, the nylon or metal cap is equipped with a mesh to allow the gas access. It should be noted that the packaging shown in Fig. 7.16

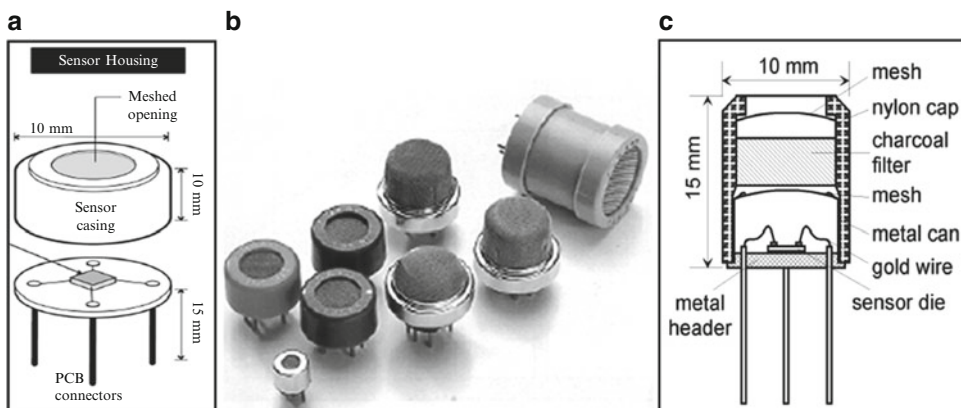


**Fig. 7.16** Photos of some sensors available on the market. (a) Ceramic-type gas sensors (<http://www.figaro.co.jp>). (b) Schematic diagram of typical gas sensor housing. (Adapted from Miller et al. 2006). (c) Packaging of micromachined gas sensors in MiCS [Reprinted with permission from Schweizer-Berberich et al. (1999). Copyright 1999 Elsevier]

represents a conventional way to mount sensors and is frequently utilized for sensors on ceramic substrates as well. The sensor is glued to the socket and the electrical contacts are bonded to the pins. This contact is usually achieved with an external lead wire connecting the sensing element to a bonding pad where connection to the external electronic or measuring instrument is made. Taking into account aggressive environments, the material used for connection should be stable in the relevant atmosphere. Therefore, depending on the operating temperature and target gas, Pt, Au, or Al wire is commonly used for these purposes. In many cases, as shown in Fig. 7.16c, the additional mesh is mounted underneath the charcoal filter to prevent contamination of the sensitive layer.

## References

- Adam M, Mohacsy T, Jonas P, Ducso C, Vazsonyi E, Barsony I (2008) CMOS integrated tactile sensor array by porous Si bulk micromachining. *Sens Actuators A* 142:192–195
- Ahn H, Park J-H, Kim S-B, Jee SH, Yoon YS, Kim DJ (2010) Vertically aligned ZnO nanorod sensor on flexible substrate for ethanol gas monitoring. *Electrochem Solid-State Lett* 13(11):J125–J128
- Arena A, Donato B, Saitta G (2009) Capacitive humidity sensors based on MWCNTs/polyelectrolyte interfaces deposited on flexible substrates. *Microelectron J* 40:887–890
- Arena A, Donato N, Saitta G, Bonavita A, Rizzo G, Neri G (2010) Flexible ethanol sensors on glossy paper substrates operating at room temperature. *Sens Actuators B* 145:488–494
- Battison FM, Ramseyer J-P, Lang HP, Baller MK, Gerber C, Gimzewski JK, Meyer E, Boisen AJ, Thundat T (2009) Design and fabrication of cantilever array biosensors. *Mater Today* 12(September):32–38
- Battison FM, Ramseyer J-P, Lang HP, Baller MK, Gerber C, Gimzewski JK, Meyer E, Guntherodt H-J (2001) A chemical sensor based on a microfabricated cantilever array with simultaneous resonance-frequency and bending readout. *Sens Actuators B* 77:122–131
- Bielska S, Sibinski M, Lukasik A (2009) Polymer temperature sensor for textronic applications. *Mater Sci Eng B* 165:50–52
- Black DR, Harley RA, Hering SV, Stolzenburg MR (2000) A new, portable, real time ozone monitor. *Environ Sci Technol* 34(14):3031–3040
- Boisen A, Thundat T (2009) Design and fabrication of cantilever array biosensors. *Mater Today* 12:32–38
- Bracher PJ, Gupta M, Whitesides GM (2010) Patterning precipitates of reactions in paper. *J Mater Chem* 20:5117–5122
- Briand D, Colin S, Gangadharaiyah A, Vela E, Dubois P, Thiery L, de Rooij NF (2006) Micro-hotplates on polyimide for sensors and actuators. *Sens Actuators A* 132:317–324
- Briand D, Oprea A, Courbat J, Bârsan N (2011) Making environmental sensors on plastic foil. *Mater Today* 14(9):416–423
- Calleja M, Nordstrom M, Alvarez M, Tamayo J, Lechuga LM, Boisen A (2005) Highly sensitive polymer-based cantilever-sensors for DNA detection. *Ultramicroscopy* 105:215–222
- Carlier J, Arscott S, Thomy V, Fourrier JC, Caron F, Camart JC, Druon C, Tabourier P (2004) Integrated microfluidics based on multi-layered SU-8 for mass spectrometry analysis. *J Micromech Microeng* 14:619–624
- Cho N-B, Lim T-H, Jeon Y-M, Gong M-S (2008) Humidity sensors fabricated with photo-curable electrolyte inks using an ink-jet printing technique and their properties. *Sens Actuators B* 130:594–598
- Chuang H-S, Wereley S (2009) Design, fabrication and characterization of a conducting PDMS for microheaters and temperature sensors. *J Micromech Microeng* 19:45010
- Chung S, Makhar S, Ackler H, Park S (2006) Material characterization of carbon-nanotube-reinforced polymer composite. *Electron Mater Lett* 2(3):175–181
- Chung CK, Chang YL, Wu JC, Jhu JJ, Chen TS (2009) Characterization and patterning of novel high-TCR Ta–Si–N thin films for sensor application. *Sens Actuators A* 156:323–327
- Cobianu C, Georgescu I, Buiculescu V (2007) Chip level packaging for wireless surface acoustic wave sensor. US patent 0114889 A1
- Comini E, Faglia G, Sberveglieri G (2009a) Electrical-based gas sensing. In: Comini E, Faglia G, Sberveglieri G (eds) *Solid state gas sensing*. Springer, New York, pp 47–107
- Courbat J, Briand D, Yue L, Raible S, de Rooij NF (2009a) Ultra-low power metal oxide gas sensor on plastic foil. In: *Proceedings of IEEE transducers 2009, Denver, CO, 21–25 June 2009a*, pp 584–587
- Courbat J, Briand D, Oprea A, Bârsan N, Weimar U, de Rooij NF (2009b) Multi sensor platform on plastic foil for environmental monitoring. *Procedia Chem* 1:597–600

- Courbat J, Briand D, Wöllenstein J, de Rooij NF (2009c) Colorimetric gas sensors based on optical waveguides made on plastic foil. *Procedia Chem* 1:576–579
- Courbat J, Canonica M, Teyssieux D, Briand D, de Rooij NF (2010a) Design and fabrication of micro-hotplates made on a polyimide foil: electrothermal simulation and characterization to achieve power consumption in the low mW range. *J Micromech Microeng* 21(1):015014
- Courbat J, Briand D, de Rooij N (2010b) Ink-jet printed colorimetric gas sensors on plastic foil. In: *Proceedings of SPIE photonic devices + applications conference 2010*, San Diego, USA, July 31–August 5
- Courbat J, Briand D, de Rooij NF (2010c) Foil level packaging of a chemical gas sensor. *J Micromech Microeng* 20:055026
- Crawford GP (ed) (2005) *Flexible flat panel displays*. Wiley, Chichester
- Crowley K, Morrin A, Hernandez A, O'Malley E, Whitten PG, Wallace GG, Smyth MR, Killard AJ (2008) Fabrication of an ammonia gas sensor using inkjet-printed polyaniline nanoparticles. *Talanta* 77(2):710–717
- Curran S, Ajayan PM, Blau W, Carroll DL, Coleman JN, Dalton A, Davey AP, McCarthy B (1998) A composite from poly(*m*-phenylenevinylene-*co*-2,5-dioctoxy-*p*-phenylenevinylene) and carbon nanotubes: a novel material for molecular optoelectronics. *Adv Mater* 10:1091–1093
- Dossi N, Toniolo R, Pizzariello A, Carrilho E, Piccin E, Battiston S, Bontempelli G (2012) An electrochemical gas sensor based on paper supported room temperature ionic liquids. *Lab Chip* 12(1):153–158
- Dusco C, Vazzonyi E, Adam M, Szabo I, Barsony I, Gardeniers JGE, Van den Berg A (1997) Porous silicon bulk micro-machining for thermally isolated membrane formation. *Sens Actuators A* 60:235–239
- Fragakis J, Chatzandroulis S, Papadimitriou D, Tsamis C (2005) Simulation of capacitive type bimorph humidity sensors. *J Phys Confer Ser* 10:305–308
- Francioso L, Forleo A, Taurino AM, Siciliano P, Lorenzelli L, Guarnieri V, Adami A, Agnusdei G (2008) Linear temperature microhotplate gas sensor array for automotive cabin air quality monitoring. *Sens Actuators B* 134:660–665
- Friedberger A, Kreis P, Rose E, Muller G, Kuhner G, Wollenstein J, Bottner H (2003) Micromechanical fabrication of robust low-power metal-oxide gas sensors. *Sens Actuators B* 93:345–349
- Furjes P, Ducso C, Adam M, Zettner J, Barsony I (2004) Thermal characterisation of micro-hotplates used in sensor structures. *Superlattice Microstruct* 35:455–464
- Geyh AS, Wolfson JM, Koutrakis P, Mulik JD, Avol EL (1997) Development and evaluation of a small active ozone sampler. *Environ Sci Technol* 31:2326–2330
- Goeders KM, Colton JS, Bottomley LA (2008) Microcantilevers: sensing chemical interactions via mechanical motion. *Chem Rev* 108:522–542
- Graf M, Barrettino D, Baltes HP, Hierlemann A (2007) *CMOS hotplate chemical microsensors*. Springer, Berlin
- Gu P-G, Lee C-T, Chou C-Y, Cheng K-H, Chuang Y-S (2009) Fabrication of flexible NO<sub>2</sub> sensors by layer-by-layer self-assembly of multi-walled carbon nanotubes and their gas sensing properties. *Sens Actuators B* 139:488–493
- Guidi V, Cardinali G, Dori L, Faglia G, Ferroni M, Martinelli G, Nelli P, Sberveglieri G (1998) Thin-film gas sensor implemented on a low-power-consumption micromachined silicon structure. *Sens Actuators B* 49:88–92
- Guntherodt H-J (2001) A chemical sensor based on a microfabricated cantilever array with simultaneous resonance frequency and bending readout. *Sens Actuators B* 77:122–131
- Han PG, Wong H, Poon MC (2001) Sensitivity and stability of porous polycrystalline silicon gas sensor. *Colloids Surf A* 179:171–175
- Hedrich F, Billat S, Lang W (2000) Structuring of membrane sensors using sacrificial porous silicon. *Sens Actuators A* 84:315–323
- Hierlemann A, Lange D, Hagleitner C, Kerness N, Koll A, Brand O, Baltes H (2000) Application-specific sensor systems based on CMOS chemical microsensors. *Sens Actuators B* 70:2–11
- Horrillo M, Sayago I, Ares L, Rodrigo J, Gutierrez J, Gotz A, Gracia I, Fonseca L, Cane C, Lora-Tamayo E (1999) Detection of low NO<sub>2</sub> concentrations with low power micromachined tin oxide gas sensors. *Sens Actuators B* 58:325–329
- Huang A, Wong VTS, Ho C-M (2006) Silicone polymer chemical vapor sensors fabricated by direct polymer patterning on substrate technique (DPPOST). *Sens Actuators B* 116:2–10
- Huo H, Ren H, Wang C, Shen M (2011) Highly sensitive gas sensors on low-cost nanostructured polymer substrates. *Intern J Smart Nano Mater* 2(1):1–8
- Jeong HY, Lee D-S, Choi HK, Lee DH, Kim J-E, Lee JL, Lee WJ, Kim SO, Choi S-Y (2010) Flexible room-temperature NO<sub>2</sub> gas sensors based on carbon nanotubes/reduced graphene hybrid films. *Appl Phys Lett* 96:213105
- Jiguet S, Bertsch A, Hofmann H, Renaud P (2004) SU8-silver photosensitive nanocomposite. *Adv Eng Mater* 6:719–724
- Johansson A, Calleja M, Rasmussen PA, Boisen A (2005) SU-8 cantilever sensor system with integrated readout. *Sens Actuators A* 123–124:111–115
- Johansson A, Blagoi G, Boisen A (2006) Polymeric cantilever-based biosensors with integrated readout. *Appl Phys Lett* 89:173505

- Ki YS (2006) Microheater-integrated single gas sensor array chip fabricated on flexible polyimide substrate. *Sens Actuators B* 114:410–417
- Kinkeldei T, Zysset C, Münzenrieder N, Tröster G (2012) Influence of flexible substrate materials on the performance of polymer composite gas sensors. In: *Proceedings of the 14th international meeting on chemical sensors, IMCS 2012, Nuremberg, Germany, May 20–23*, pp 537–540
- Koutrakis P, Wolfson J, Bunyaviroch A, Forchlich SE, Hirano K, Mulik JD (1993) Measurement of ambient ozone using a nitrite-coated filter. *Anal Chem* 65:209–214
- Krebs FC, Fyenbo J, Jørgensen M (2010) Product integration of compact roll-to-roll processed polymer solar cell modules: methods and manufacture using flexographic printing, slot-die coating and rotary screen printing. *J Mater Chem* 20(41):8994–9001
- Lang W (1996) Silicon microstructuring technology. *Mater Sci Eng R* 17:1–55
- Lang HP, Gerber C (2008) Microcantilever sensors. *Top Curr Chem* 285:1–27
- Lang W, Steiner P, Schaber U, Richter A (1994a) A thin film bolometer using porous silicon technology. *Sens Actuators A* 43:185–187
- Lang W, Steiner P, Richter A, Maruszczyk K, Weimann G, Sandmaier H (1994b) Applications of porous silicon as a sacrificial layer. *Sens Actuators A* 43:239–242
- Lang HP, Filippi A, Tonin A, Huber F, Backmann N, Zhang J, Gerber C (2009) Towards a modular, versatile and portable sensor system for measurements in gaseous environments based on microcantilevers. *Procedia Chem* 1:208–211
- Lavrik NV, Sepaniak MJ, Datskosa PG (2004) Cantilever transducers as a platform for chemical and biological sensors. *Rev Sci Instrum* 75(7):2229–2253
- Lee JB, Heeney M, Tiemey S, McCulloch I, Murphy A, Liu J, Fréchet JMJ, Subramanian V (2005) Stability in OTFT gas sensors. *MRS Symp Proc* 871:6–11
- Lee C-Y, Wu G-W, Hsieh W-J (2008) Fabrication of micro sensors on a flexible substrate. *Sens Actuators A* 147:173–176
- Li P, Li X (2006) A single-sided micromachined piezoresistive SiO<sub>2</sub> cantilever sensor for ultra-sensitive detection of gaseous chemicals. *J Micromech Microeng* 16:2539–2546
- Li X, Tian JF, Garnier G, Shen W (2010) Fabrication of paper-based microfluidic sensors by printing. *Colloid Surf B* 76:564–570
- Liana DD, Raguse B, Gooding JJJ, Chow E (2012) Recent advances in paper-based sensors. *Sensors* 12:11505–11526
- Lim MA, Kim DH, Park C-O, Lee YW, Han SW, Li Z, Williams RS, Park I (2012) A new route toward ultrasensitive, flexible chemical sensors: metal nanotubes by wet-chemical synthesis along sacrificial nanowire templates. *ACS Nano* 6(1):598–608
- Liu C-C (1996) Electrochemical sensors: microfabrication techniques. In: Taylor RF, Schultz JS (eds) *Handbook of chemical and biological sensors*. IOP, Bristol, Chapter 16
- Liu X, Mwangi M, Li X-J, O'Brien M, Whitesides G.M. M (2011) Paper-based piezoresistive MEMS sensors. *Lab Chip* 11:2189–2196
- Logothetidis S (2008) Flexible organic electronic devices: materials, process and applications. *Mater Sci Eng B* 152:96–104
- Manzoli A, Steffens C, Paschoalin RT, Correa AA, Alves WF, Leite FL, Herrmann PSP (2011) Low-cost gas sensors produced by the graphite line-patterning technique applied to monitoring banana ripeness. *Sensors* 11:6425–6434
- Marinov VR, Atanasov YA, Khan A, Vaselaar D, Halvorsen A, Schulz DL, Chrisey DB (2007) Direct-write vapor sensors on FR4 plastic substrates. *IEEE Sensor J* 7(6):937–944
- Martinez AW, Phillips ST, Whitesides GM, Carrilho E (2010) Diagnostics for the developing world: microfluidic paper-based analytical devices. *Anal Chem* 82:3–10
- Martorelli JV (2008) Monolithic CMOS-MEMS resonant beams for ultrasensitive mass detection. Ph.D. thesis, Universitat Autònoma de Barcelona, Spain
- Maruo YY (2007) Measurement of ambient ozone using newly developed porous glass sensor. *Sens Actuators B* 126:485–491
- Maruo YY, Kunioka T, Akaoka K, Nakamura J (2009) Development and evaluation of ozone detection paper. *Sens Actuators B* 135:575–580
- Maruo YY, Akaoka K, Nakamura J (2010) Development and performance evaluation of ozone detection paper using azo dye orange I: effect of pH. *Sens Actuators B* 143:487–493
- Mastrangelo C, Tang W (1994) Semiconductor sensor technologies. In: Sze S (ed) *Semiconductor sensors*. Wiley, New York, pp 17–95
- Mayr T, Abel T, Enko B, Borisov S, Konrad C, Köstler S, Lamprecht B, Sax S, List EJW, Klimant I (2009) A planar waveguide optical sensor employing simple light coupling. *Analyst* 134:1544–1547
- McAlpine MC, Ahmad H, Wang D, Heath JR (2007) Highly ordered nanowire arrays on plastic substrates for ultrasensitive flexible chemical sensors. *Nat Mater* 6:379–384
- McFarland AW, Colton JS (2005a) Role of material microstructure in plate stiffness with relevance to microcantilever sensors. *J Micromech Microeng* 15:1060–1067
- McFarland AW, Colton JS (2005b) Chemical sensing with micromolded plastic microcantilevers. *J Microelectromech Syst* 14:1375–1385

- McFarland AW, Poggi MA, Bottomley LA, Colton JS (2004) Injection moulding of high aspect ratio micron-scale thickness polymeric microcantilevers. *Nanotechnology* 15:1628–1632
- Miller TA, Bakrania SD, Perez C, Wooldridge MS (2006) Nanostructured tin dioxide materials for gas sensor applications. In: Geckeler KE, Rosenberg E (eds) *Functional nanomaterials*. American Scientific Publishers, Stevenson Ranch, CA, pp 1–24
- Mitchell JS, Oliver R, Jordan B (2012) Printable paper-based polymer sensors for detection of vapor phase alcohols. In: *Proceedings of the 14th international meeting on chemical sensors, IMCS 2012, Nuremberg, Germany, May 20–23*, pp 1109–1111
- Miyoshi Y, Miyajima K, Saito H, Kudo H, Takeuchi T, Karube I, Mitsubayashi K (2009) Flexible humidity sensor in a sandwich configuration with a hydrophilic porous membrane. *Sens Actuators B* 142:28–32
- Mlcak R, Tuller HL, Greiff P, Sohn J, Niles L (1994) Photoassisted electrochemical micromachining of silicon in HF electrolytes. *Sens Actuators A* 40:49–55
- Moser Y, Gijs MAM (2007) Miniaturized flexible temperature sensor. *J Microelectromech Syst* 16(6):1349–1354
- Oprea A, Barsan N, Weimar U, Courbat J, Briand D, de Rooij NF (2007) Integrated temperature, humidity and gas sensors on flexible substrates for low-power applications. In: *Proceedings IEEE sensors conference, Atlanta, USA, Oct 28–31*, pp 158–161
- Oprea A, Barsan N, Weimar U, Bauersfeld ML, Ebling D, W llenstein J (2008) Capacitive humidity sensors on flexible RFID labels. *Sens Actuators B* 132:404–410
- Oprea A, Courbat J, Bârsan N, Briand D, de Rooij NF, Weimar U (2009) Temperature, humidity and gas sensors integrated on plastic foil for low power applications. *Sens Actuators B* 140:227–232
- Oprea A, Courbat J, Briand D, Bârsan N, Weimar U, de Rooij NF (2012) Environmental monitoring with a multisensor platform on polyimide foil. *Sens Actuators B* 171–172:190–197
- Papadimitriou D, Tsamis C (2005) Simulation of capacitive type bimorph humidity sensors. *J Phys Conf Ser* 10:305–308
- Parikh K, Cattanaach K, Rao R, Suh D-S, Wu A, Manohar SK (2006) Flexible vapour sensors using single walled carbon nanotubes. *Sens Actuators B* 113:55–63
- Pecora A, Zampetti E, Pantalei S, Valletta A, Minotti A, Maiolo L, Simeone D, Cuscuna M, Bearzotti A, Macagnano A, Mariucci L, Fortunato G (2008) Interdigitated sensorial system on flexible substrate. In: *Proceedings of the seventh IEEE conference on sensors, IEEE SENSORS, Lecce, Italy, Oct 26–29*, 21–24
- Potyrailo RA, Morris WG (2007) Multianalyte chemical identification and quantitation using a single radio frequency identification sensor. *Anal Chem* 79:45–51
- Prudenziati M (ed) (1994) *Thick film sensors* (Middelhoek S. (series ed) *Handbook of sensors and actuators*, vol. 1. Elsevier, Amsterdam
- Ransley JHT, Watari M, Sukumaran D, McKendry RA, Seshia AA (2006) SU8 bio-chemical sensor microarrays. *Microelectron Eng* 83:1621–1625
- Salcedo WJ, Ramirez Fernandez FJ, Rubim JC (2004) Photoluminescence quenching effect on porous silicon films for gas sensors application. *Spectrochim Acta A* 60:1065–1070
- Schweizer-Berberich M, Strathmann S, Weimar U, Sharma R, Seube A, Peyre-Lavigne A, Göpel W (1999) Strategies to avoid VOC cross-sensitivity of SnO<sub>2</sub>-based CO sensors. *Sens Actuators B* 58:318–324
- Shih W-P, Tsao L-C, Lee C-W, Cheng M-Y, Chang C, Yang Y-J, Fan K-C (2010) Flexible temperature sensor array based on a graphite-polydimethylsiloxane composite. *Sensors* 10:3597–3610
- Shin W, Matsumiya M, Izu N, Murayama N (2003) Hydrogen-selective thermoelectric gas sensor. *Sens Actuators B* 93:304–308
- Shin W, Choi Y, Tajima K, Izu N, Matsubara I, Murayama N (2005) Planar catalytic combustor film for thermoelectric hydrogen sensor. *Sens Actuators B* 108:455–460
- Simon I, Bârsan N, Bauer M, Weimar U (2001) Micromachined metal oxide gas sensors: opportunities to improve sensor performance. *Sens Actuators B* 73:1–26
- Spannhake J, Schulz O, Helwig A, Krenkow A, Müller G, Doll T (2006) High-temperature MEMS heater platforms: long-term performance of metal and semiconductor heater materials. *Sensors* 6:405–419
- Splinter A, Bartels O, Benecke W (2001) Thick porous silicon formation using implanted mask technology. *Sens Actuators B* 76:354–360
- Steffens C, Manzoli A, Francheschi E, Corazza M, Corazza F, Oliveira JV, Herrmann P (2009) Low-cost sensors developed on paper by line patterning with graphite and polyaniline coating with supercritical CO<sub>2</sub>. *Synth Met* 159:2329–2332
- Steiner P, Lang W (1995) Micromachining applications of porous silicon. *Thin Solid Films* 255:52–58
- Su PG, Lee CT, Chou CY (2009a) Flexible NH<sub>3</sub> sensors fabricated by in situ self-assembly of polypyrrole. *Talanta* 80(2):763–769
- Su P-G, Lee C-T, Chou C-Y, Cheng K-H, Chuang Y-S (2009b) Fabrication of flexible NO<sub>2</sub> sensors by layer-by-layer self-assembly of multi-walled carbon nanotubes and their gas sensing properties. *Sens Actuators B* 139:488–493
- Su P-G, Tseng J-Y, Huang Y-C, Pan H-H, Li P-C (2009c) Novel fully transparent and flexible humidity sensor. *Sens Actuators B* 137:496–500

- Subramanian V, Chang P, Lee JB, Molesa SE, Volkman SK (2005) Printed organic transistors for ultra-low-cost RFID applications. *IEEE Trans Comp Packag Technol* 28(4):742–747
- Suehle JS, Cavicchi RE, Gaitan M, Semancik M (1993) Tin oxide gas sensor fabricated using CMOS micro hotplates and in-situ processing. *IEEE Electron Device Lett* 14:118–120
- Tabata O (1986) Fast-response silicon flow sensor with an on-chop fluid temperature sensing element. *IEEE Trans Electron Devices* Ed-33:361–365
- Triantafyllopoulou R, Chatzandroulis S, Tsamis C, Tserapi A (2006) Alternative micro-hotplate design for low power sensor arrays. *Microelectron Eng* 83:1189–1191
- Tsamis C, Nassiopoulou AG, Tserapi A (2003) Thermal properties of suspended porous silicon micro-hotplates for sensor applications. *Sens Actuators B* 95:78–82
- Urbiztondo MA, Pellejero I, Villarroya M, Sese J, Pina MP, Dufour I, Santamaria J (2009) Zeolite-modified cantilevers for the sensing of nitrotoluene vapors. *Sens Actuators B* 137:608–616
- Vergara A, Llobet E, Ramhrez JL, Ivanov P, Fonseca L, Zampolli S, Scorzoni A, Becker T, Marco S, Wullenstein J (2007) An RFID reader with onboard sensing capability for monitoring fruit quality. *Sens Actuators B* 127:143–149
- Wang Y, Yang Z, Hou Z, Xu D, Wei L, Kong ES-W, Zhang Y (2010a) Flexible gas sensors with assembled carbon nanotube thin films for DMMP vapor detection. *Sens Actuators B* 150:708–714
- Wang L, Luo J, Yin J, Zhang H, Wu J, Shi X, Crew E, Xu Z, Rendeng Q, Lu S, Poliks M, Sammakia B, Zhong C-J (2010b) Flexible chemiresistor sensors: thin film assemblies of nanoparticles on a polyethylene terephthalate substrate. *J Mater Chem* 20:907–915
- Weng B, Shepherd RL, Crowley K, Killard AJ, Wallace GG (2010) Printing conducting polymers. *Analyst* 135:2779–2789
- William W, Boardman J (1975) Semiconductor gas sensor and method therefore. US Patent 3901067
- Woszczyzna M, Gotszalk T, Zawierucha P, Zielony M, Ivanow T, Ivanowa K, Sarov Y, Nikolov N, Mielczarski J, Mielczarska E, Rangelow IW (2009) Thermally driven piezoresistive cantilevers for shear-force microscopy. *Microelectron Eng* 86:1212–1215
- Xu JM (2000) Plastic electronics and future trends in microelectronics. *Synth Met* 115:1–3
- Xu M, Bunes BR, Zang L (2011) Paper-based vapor detection of hydrogen peroxide: colorimetric sensing with tunable interface. *ACS Appl Mater Interfaces* 3:642–647
- Zampetti E, Pantalei S, Pecora A, Valletta A, Maiolo L, Minotti A, Macagnano A, Fortunato G, Bearzotti A (2009) Design and optimization of an ultra thin flexible capacitive humidity sensor. *Sens Actuators B* 143:302–397
- Zeitschel A, Friedberger A, Welser W, Muller G (1999) Breaking the isotropy of porous silicon formation by current focusing. *Sens Actuators A* 74:113–117



## Chapter 8

# Materials for Thick Film Technology

Thick film technology is one of the major technologies used for gas sensor fabrication (Prudenziati 1994; Ihokura and Watson 1994; Galan-Vidal et al. 1995; White and Turner 1997; Grundler 2007; Bakrania and Wooldridge 2009; Patil 2011). The ability to form a gas sensing layer with required composition and porosity makes it possible to design gas sensors with high operating characteristics. There are several approaches used in thick film technology (Agnew 1973; Holmes and Loasby 1976; Prudenziati 1994) – drop-coating, tape casting, etc. However, one of the most important thick-film deposition methods is screen printing (see Fig. 8.1), which is similar to that used for traditional silk-screen printing. The main difference lies in the screen materials and the degree of sophistication of the printing machine. Special thick-film pastes (or inks) can be formulated to paint or print an active layer onto a substrate. To formulate the paste, finely milled metal oxides or other sensing materials are combined with small amounts of special additives and an organic vehicle to form a printable paste. The paste is spread on the substrate by means of a screen made from mesh mounted on a metallic frame. The mesh is coated with an ultra-violet (UV) sensitive emulsion onto which the required pattern can be formed photographically. The finished stencil has open mesh areas through which the desired pattern can be printed and is held in position at a distance of around 0.5 mm from the substrate surface of the screen-printing machine. The ink is placed on the opposite side of the screen and a squeegee traverses the screen under pressure, thereby bringing it into contact with the substrate and also forcing the ink through the open areas of the mesh. The required circuit pattern is thus left on the substrate. Then the paste is dried to remove the organic solvents from the paste and fired (calcination) at temperatures between 500 and 1,000 °C for 1 h or more to form a solid, composite material. Further screen-printed layers may be added after firing if necessary. Standard printable thick-film materials for resistive heaters and conductor lines may also be fabricated by thick film technology on the substrate before or after the sensor layer (noble metals like platinum and gold are normally used in pastes).

The screen defines the pattern of the printed film and also regulates the amount of paste that is deposited. It is a very important part of the screen-printing equipment, and is essentially a stencil through which the paste is forced during the printing process. The most common type of screen consists of a frame, normally cast aluminum, onto which a finely woven mesh is stretched.

The mesh itself is usually based on a plain weave pattern. Some important properties of the screen mesh are the size and density of the strands (usually quoted in terms of lines per inch), the tension, the orientation, and the material. In addition, the choice of mesh material must ensure that the printed deposit is uniform. The mesh material must be precisely woven and have uniform mesh apertures. The fabric should also be flexible enough to enable good contact all over the substrate. The fabric needs to be resilient so that the mesh returns to its original position after the printing stroke. The squeegee itself is in contact with the fabric for most of the printing stroke, so the finish of the fabric must be slippery and smooth so that the resistance to the squeegee is minimal. The mesh material must also be chemically stable and very resistant to attack

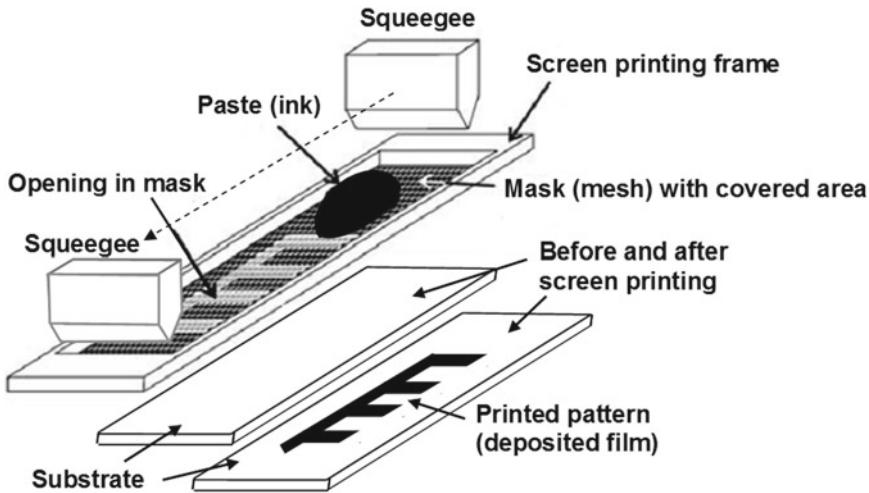


**Fig. 8.1** Manufacture of thick-film structures by screen printing [Idea from Grundler (2007)]

from the various solvents and other chemicals used in the thick-film process. Finally, the fabric must have an economic working lifetime and suitable mechanical support for the emulsion.

At present the three most common materials used for thick-film screen meshes are (1) polyester, (2) nylon, and (3) stainless steel. They all have their own advantages and disadvantages. Polyester is flexible and can be used for printing onto uneven surfaces. It is also much more resilient than nylon and stainless steel. The elastic properties of polyester are better than those of stainless steel but cannot match those of nylon. The registration and definition properties are generally good. Polyester screens have a long lifetime and give low squeegee wear. Nylon is the most elastic of the three screen fabrics, which can be an advantage in certain circumstances. Unfortunately, this also means that the open areas of the screen tend to deform during a print stroke, thereby resulting in elongated images. Another disadvantage of nylon is that its low resilience means that high viscosity inks should not be used. The mesh tends to stick to the substrate and not peel off which results in poor print quality. The main advantages of stainless-steel screens are that they produce high standards of line definition and registration and also good control of ink deposition. The mesh filaments can be drawn finer than those of nylon or polyester and can therefore provide a higher percentage of open area for a given mesh count. Stainless steel is ideal for printing onto flat surfaces but, because of its poor flexibility and resilience, it is much more difficult to use on uneven surfaces. It is generally recommended that stainless steel screens be used for printing on small areas where high definition and registration are needed.

The squeegee is essentially a flexible blade whose function is to transfer the paste through the screen and onto the substrate. During printing, the squeegee forces ink through the open areas of the mesh and, by virtue of the surface tension between the film and substrate, the required pattern is transferred to the substrate as the screen and substrate separate. The squeegee's shape, material, and pressure are all factors which dictate the life of the screen and the squeegee. Clearly, the squeegee must be resistant to the solvents and inks used in thick-film processing. Polyurethane and neoprene are common materials used for squeegee fabrication.

As a rule, the basic constituents of thick-film ink are (1) active material, (2) a low softening temperature glass frit, and (3) organic carrier. Of course the inks can contain other components such as catalytically active noble metals (Pd, Pt, Au, Ag) or metal oxides ( $\text{Al}_2\text{O}_3$ ,  $\text{SiO}_2$ , etc.), which can be added for improving porosity, catalytic activity, and stability. The glass frit acts as a binder, which holds the active particles together and bonds the film to the substrate. During the firing cycle the glass melts, typically migrates to the substrate–metal interface, and forms a mechanical key at the film-to-substrate interface. As a result the film is firmly bonded to the substrate. Glass frit also provides a

suitable matrix for the active material of the film. The organic carrier gives the paste the desired viscosity for screen printing. The characteristics required of the ink viscosity depend on the printing stage. When the ink is being forced through the screen, viscosity must be low. After printing, however, viscosity must be high because the film must retain its printed geometry and not run. For ideal (Newtonian) fluids, the viscosity is independent of the shear rate and only varies with temperature. However, for a thick-film paste the viscosity must change with the pressure applied.

The active material in inks for gas sensing layer forming is essentially a finely divided powder of metal oxides with a typical particle size in the range from a few nanometers to a few microns. However, nowadays powders with nanometric grain size are very commonly used for gas sensor fabrication, because better sensing properties of the active layer can be obtained. Conductor pastes can contain a precious metal or metal alloy like silver, platinum, gold, palladium, and their alloys. After processing, the metallic particles fuse to form continuous electrical paths through the carrier glass. Sheet resistivities of the order of  $10 \text{ m}\Omega/\text{cm}^2$  are typical. In sensor applications, conducting inks have an important function in the formation of electrode patterns, which range from simple rectangular structures to interdigitated pairs. Platinum is also used for resistance thermometry and for combined heaters and thermometers in gas sensing, where control at a variety of temperatures is an all important technique. The dielectric pastes usually have ceramic powders as the active material. Dielectric inks are mainly used as insulants, either at crossovers or when a conducting substrate has been employed.

Choosing the glass content for thick-film components is mainly dictated by the following requirements:

- The linear coefficient of thermal expansion (CTE) should be as close as possible to the CTE of the substrate. A slightly lower CTE can be tolerated, since the glass is put slightly in compression, i.e., in a condition safer than the opposite, which creates tensile strains.
- The softening point ( $T_s$ ) should fall between 400 and 600 °C. In these circumstances, the viscosity of the glass will be low enough at the peak temperatures of the common firing cycles (850–1,000 °C) for a continuous glassy matrix to form in a few minutes, and/or for there to be a liquid phase which assists the sintering of metal particles and the required reactions with the other components of the paste.
- No ions should be in motion under electric bias if mass transport and the degradation of the properties of the film are to be avoided. These conditions are prerequisites for the stability of the thick-film layers at relatively high temperatures.

It was established that pure silica does not meet these requirements (mainly because the softening point is too high and the CTE is too low). Adding  $\text{Bi}_2\text{O}_3$  decreases the  $T_s$  value and increases the CTE but makes the glass too “short” (namely the viscosity  $\eta$  changes too rapidly when the firing temperature is changed); moreover,  $\text{Bi}_2\text{O}_3$  may induce devitrification. Alkaline or alkaline earth cations, widely used in the glass industry as a means for controlling the viscosity and workability of silicate glasses, cannot be used in large quantities because of their consistent ion mobilities. Experience has shown that lead is the most suitable additive for achieving the required properties of the glass.  $\text{PbO}$  may be added to silica in large fractions without devitrification. Its cation exhibits low mobility in the glass and makes it very stable up to relatively high temperatures. Therefore, lead borosilicate glasses ( $\text{Pb}/\text{B}_2\text{O}_3/\text{SiO}_2$  with  $\text{Bi}_2\text{O}_3$  as fluxing agent) are often used as a glass frit in inks designed for gas sensor fabrication.

The crucial point here is that the specific composition of the glass (e.g., the relative amounts of  $\text{SiO}_2$ ,  $\text{Bi}_2\text{O}_3$ ,  $\text{PbO}$ ,  $\text{B}_2\text{O}_3$ ) greatly affects the dissolution kinetics of Al and Be (from alumina and beryllia substrates), the reactions with the active ingredients of the ink, and the reproducibility of the glass batches because it affects the degree of volatilization of Pb from the melted glass during the preparation of both the frit and the components. In addition it is necessary to take into account that, in excessively high firing temperature profiles, glass may “float” on the conductor surface and result in poor solderability, poor adhesion, and wire bondability. The chemical and physical properties of the substrate also play an important role in determining how the glass binder phase wets the substrate surface

**Table 8.1** Examples of inks used in thick film technology of conductometric gas sensors

Ink	Metal oxide	Reference
MeO <sub>x</sub> (68–72%) + Bi <sub>2</sub> O <sub>3</sub> (5%) + organic carrier (23–27%) (see Table 8.2)	WO <sub>3</sub> , SnO <sub>2</sub>	Ivanov (2004)
MeO <sub>x</sub> (68–74%) + (Bi <sub>2</sub> O <sub>3</sub> +Cu <sub>2</sub> O) (5%) + organic carrier (21–26 %) (see Table 8.2)	WO <sub>3</sub> , SnO <sub>2</sub>	Ivanov (2004)
ZnO (65%) + (70wt% PbO; 18wt% Al <sub>2</sub> O <sub>3</sub> ; 9wt% SiO <sub>2</sub> and 3 wt% B <sub>2</sub> O <sub>3</sub> ) 5% + organic carrier (30%) (see Table 8.2)	ZnO:Sb	Jayadev et al. (1998)
SnO <sub>2</sub> +MgO + ThO <sub>2</sub> (5%) +SiO <sub>2</sub> + organic carrier (see Table 8.2)	SnO <sub>2</sub> :Pd	Nitta and Haradome (1979)
(96 wt% SnO <sub>2</sub> + 4 wt% Al <sub>2</sub> O <sub>3</sub> ) 70% + organic carrier (30%) (see Table 8.2)	SnO <sub>2</sub>	Choi et al. (2005)

and is attached to it. Variation in surface chemistry, grain size, and smoothness of the substrate can cause wide variation in thick-film conductor performances.

For obtaining the required thick-film adhesion, oxides (fritless conductors) can also be used. Small amounts (0.1–1%) of chemically active oxides like CuO, CdO, or NiO, added to the paste, react at high temperatures with alumina substrates to form oxides like CuAlO<sub>2</sub>, which provide better adhesion. A combination of glass and oxides also is used, but the amount of glass in this case is much lower than in the fritted systems. Adhesion is believed to be related to a combination of the above-mentioned effects. Table 8.1 shows several examples of inks used for gas sensor fabrication.

“Organic vehicle” is a generic term that describes a blend of volatile solvents and polymers or resins together with a surfactant, which are needed to provide a homogeneous suspension of the particles of the functional materials and a rheology that is suitable for the printing of the film configuration. The vehicle is a temporary, sacrificial ingredient, which should be completely removed in the following steps of the process, during which the microstructure of the deposits is formed. The composition of the organic vehicle determines (or helps to determine) the shelf life of the paste, its drying rate on the screen, the change in printability with ambient temperature, the resolution of fine lines, some electrical properties of the fired films, and their cosmetic appearance. The cooperative effects and the relationships between the properties (density, wettability, surface energies, viscosity, etc.) of the organic vehicle and inorganic constituents of the paste contribute to the static and dynamic properties of the paste. Moreover, the solvents should not be so volatile that after a short time they leave a hard unprintable paste on the screen mesh but, at the same time, they should evaporate early in the drying phase of the process. Finally, the fluid properties (rheology) of the vehicle should prevent penetration through the screen when the paste is at rest, but should enable printing to be fast under the squeeze pressure and the film to settle quickly in the desired configuration on the substrate without bleeding or smearing from the defined geometry.

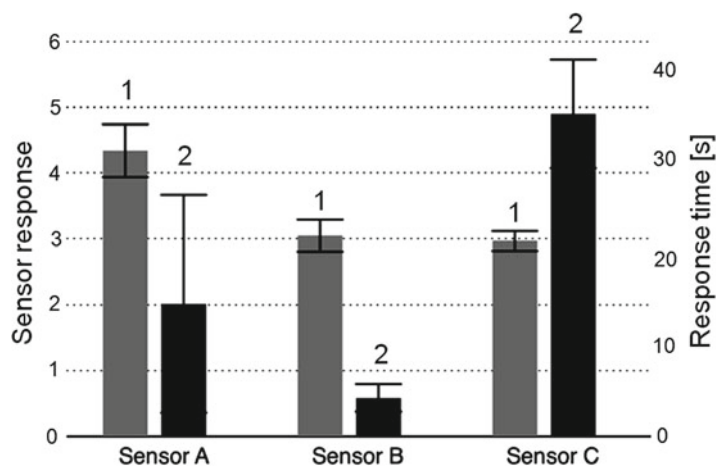
Organic vehicle formulations are usually blends of cellulose-type resins or cellulose acetate (the polymeric viscosifier) and solvents like terpineol, butylcarbitol, ethyl cellulose, cyclohexanone, or ethylene glycol. Several examples may be seen in Table 8.2. The relative fractions of these ingredients are varied according to the types and amounts of the inorganic materials of the paste. The ratio of the inorganic to organic part in the paste has usually been kept at (70–75)/(25–30). These simple vehicles perform well with many solid systems in a variety of printing conditions and environments. However, requirements of fine line resolution, fast printing rates, smooth surfaces, and the like have stimulated the development of complex vehicles.

We need to note that the composition of the ink used for gas sensor fabrication and the size of inorganic particles added in the paste has a determining influence on the operating characteristics of the gas sensors designed because the composition controls the porosity and surface chemistry of the gas sensing matrix. For example, it is necessary to take into account that the excess of the glass in the ink decreases the porosity, i.e., the gas penetrability of the gas sensing layer (Willett et al. 1998). Therefore, in many cases the ink does not contain the glass. The presence of other components such as CuO, added for improvement of film adhesion, can also be accompanied by undesirable effects,

**Table 8.2** Examples of organic vehicles (binder + solvent) used in thick film technology of conductometric gas sensors

Organic carrier	Metal oxide	Reference
Terpineol HVS100: ethyl cellulose: Texaphor 963: Rilanit spez = 89.3: 1.2: 6.0: 3.5 wt%	WO <sub>3</sub> , SnO <sub>2</sub>	Ivanov (2004)
Terpineol HVS100: ethyl cellulose: Texaphor 963: Rilanit spez: Disponil = 85.5: 1.1: 5.7: 3.4: 4.3 wt%	WO <sub>3</sub> , SnO <sub>2</sub>	Ivanov (2004)
8% Ethyl cellulose and 92% butyl carbitol acetate	ZnO:Sb	Jayadev et al. (1998)
β-Terpeneol: butyl carbitol acetate: ethyl cellulose	SnO <sub>2</sub> :Pd	Nitta and Haradome (1979)
Ethyl cellulose	In <sub>2</sub> O <sub>3</sub> -TiO <sub>2</sub>	Zhang et al. (2012)
Ethyl cellulose: butyl cellulose: butyl carbitol acetate: terpineol	ZnO:Cu	Deore et al. (2011)
Diethyl glycol monobutyl: α-terpinol	SnO <sub>2</sub> :CdS	Yadava et al. (2010)
Deionized water: α-terpinol	SnO <sub>2</sub>	Choi et al. (2005)
α-Terpineol: ethyl cellulose = 89:11 wt%	SnO <sub>2</sub>	Lee et al. (2007)
Isopropyl alcohol : hydroxylpropyl cellulose		

**Fig. 8.2** Comparison of (1) sensor response to 500 ppm CO in dry air and (2) time response for sensors fabricated using the three binder recipes. Sensor A: SnO<sub>2</sub> + hydroxypropyl cellulose + isopropyl alcohol. Sensor B: SnO<sub>2</sub> + ethyl cellulose + α-terpineol soln. Sensor C: TEOS + ethanol + H<sub>2</sub>O + 4% HCl + SnO<sub>2</sub> with 6 wt% silica [Reprinted from Bakrania and Wooldridge (2009). Published by MDPI]



because the CuO promotes the metal oxide film densification during high temperature annealing. Moreover, the additives can be incorporated in the lattice of metal oxides with proper changes in their bulk and surface properties. This means that a change of the ink composition will always be accompanied by a change of gas sensors. For example, Ivanov (2004) has studied the influence of film adhesion promoters such as Bi<sub>2</sub>O<sub>3</sub> and Cu<sub>2</sub>O on the response of SnO<sub>2</sub>- and WO<sub>3</sub>-based sensors and found that tungsten oxide sensors containing only Bi<sub>2</sub>O<sub>3</sub> were more sensitive to nitrogen dioxide than to ammonia when operated at low temperatures. At the same time, WO<sub>3</sub> sensors with Bi<sub>2</sub>O<sub>3</sub> and Cu<sub>2</sub>O were found to be very sensitive to ammonia. Their selectivity to ammonia can be improved by increasing the amount of Cu<sub>2</sub>O in the ink. The same regularity was observed for SnO<sub>2</sub> sensors as well. However, it was established that the inclusion of Cu<sub>2</sub>O in the paste increases the response to water vapor. Moreover, tin oxide sensors containing only Bi<sub>2</sub>O<sub>3</sub> were found to be sensitive and very selective to ethanol vapors. Another example is shown in Fig. 8.2 and relates to the influence of three binder recipes on the response of SnO<sub>2</sub>-based gas sensors. It is seen that composition of the paste influences both the magnitude of response and the response time.

## References

- Agnew J (1973) Thick film technology: fundamentals and applications in microelectronics. Hayden, Rochelle Park, NJ
- Bakrania SD, Wooldridge MS (2009) The effects of two thick film deposition methods on tin dioxide gas sensor performance. *Sensors* 9:6853–6868
- Choi N-J, Lee Y-S, Kwak J-H, Park J-S, Park K-B, Shin K-S, Park H-D, Kim J-C, Huh J-S, Lee D-D (2005) Chemical warfare agent sensor using MEMS structure and thick film fabrication method. *Sens Actuators B* 108:177–183
- Deore MK, Gaikwad VB, Jain GH (2011) LPG gas sensing properties of CuO loaded ZnO thick film resistors. In: Proceedings of fifth international conference on sensing technology, Palmerston North, New Zealand, IEEE, 28 Nov–1 Dec, pp 233–238
- Galan-Vidal CA, Munoz J, Dominguez C, Alegret S (1995) Chemical sensors, biosensors and thick-film technology. *Trends Anal Chem* 14(5):225–231
- Grundler P (2007) Chemical sensors: an introduction for scientists and engineers. Springer, Berlin
- Holmes PJ, Loasby RG (eds) (1976) Handbook of thick film technology. Electrochemical Publications, Ayr, Scotland
- Ihokura K, Watson J (1994) The stannic oxide gas sensor: principles and applications. CRC, Boca Raton, FL
- Ivanov PT (2004) Design, fabrication and characterization of thick-film gas sensors. PhD thesis, University Rovira i Virgili, Tarragona, Spain
- Jayadev DN, Sainkar SR, Karekar RN, Aiyer RC (1998) Formulation and characterization of ZnO:Sb thick-film gas sensors. *Thin Solid Films* 325:254–258
- Lee S, Lee G, Kim J, Kang SL (2007) A novel process for fabrication of SnO<sub>2</sub>-based thick film gas sensors. *Sens Actuators B* 123:331–335
- Nitta M, Haradome M (1979) Thick-film CO gas sensors. *IEEE Trans El Dev ED-26*(3):247–249
- Patil A (2011) ZnO thick films gas sensor: electrical, structural and gas sensing characteristics with different dopants. Lambert Academic, Saarbrücken
- Prudenziati M (ed) (1994) Thick film sensors (Middelhoek S (series ed) Handbook of sensors and actuators, vol 1). Elsevier, Amsterdam
- White NM, Turner JD (1997) Thick-film sensors: past, present and future. *Meas Sci Technol* 8(1):1–20
- Willett MJ, Burganos VN, Tsakiroglou CD, Payatakes AC (1998) Gas sensing and structural properties of various pre-treated nanopowders tin (IV) oxide samples. *Sens Actuators B* 53:76–90
- Yadava L, Verma R, Dwivedi R (2010) Sensing properties of CdS-doped tin oxide thick film gas sensor. *Sens Actuators B* 144:37–42
- Zhang ML, Song JP, Yuan ZH, Zheng C (2012) Response improvement for In<sub>2</sub>O<sub>3</sub>-TiO<sub>2</sub> thick film gas sensors. *Curr Appl Phys* 12(3):678–683

## Chapter 9

# Electrodes and Heaters in MOX-Based Gas Sensors

### 9.1 Materials for Electrodes in Conductometric Gas Sensors

#### 9.1.1 *Electrode Influence on Gas Sensor Response*

Another crucial issue, beyond the sensing layer and the sensor design, is the choice of the metal used to make the electrical contacts to the sensing layer. For example, the electrodes must provide at least two electrical contacts to the MOX to measure its conductance changes. In selecting an ideal electrode material, the following considerations need to be taken into account: (1) the contact has to provide as low a sheet resistance as possible in order to minimize voltage drops at the interconnections; (2) the contact should be stable at the advanced operation temperature, which may reach hundred degrees; and (3) the contact should be ohmic. For example, the Schottky barrier that appears at the electrode–MOX interface may be gas sensitive and may contribute to overall sensor performance (Comini et al. 2009).

It is known that commonly used electrode materials, such as Pt, Pd, and Au, are active catalysts with specific catalytic properties. As a result, in the area close to contact (spillover zones), electrode materials act as catalysts able to increase the activity of gas-sensing metal oxides (Yamazoe et al. 1983; McAleer et al. 1988; Kohl 1990; Brinzari et al. 2002). In other words, electrodes made of noble metal may promote surface reactions via a spillover effect. Spillover is a very important term in catalysis (Bowker et al. 2000). It is used as a shorthand description of the diffusion of adsorbed species from an active adsorbent to an otherwise inactive support. For instance, this could be the diffusion of atoms from active metal nanoparticles, where the dissociation is nonactivated, to a support, metal oxide in our case, where the dissociation directly from the gas phase is activated. Therefore, if the distance between contacts is comparable with the width of the spillover zone, the influence of geometric parameters of sensors on their gas sensing characteristics would become noticeable. It is also still possible that an increased catalytic reaction at the electrode might create desorption processes, leading to gas consumption and not contributing to the modulation of the oxide conductance (Gurlo et al. 2004). The consequence is that such gas consumption reduces the analyte concentration and thus makes the sensor signal lower. The interaction of electrode metal with analyte and diffusion of analyte to the electrode metal/metal oxide interface may affect the work function of contacting materials with corresponding changes in the height of the potential barrier, i.e., resistance of this interface as well. This means that the operating characteristics of the designed sensor may be controlled by electrode material, and the possibility of this effect should be taken into account. In other words, it is possible to control the sensing properties of semiconductor gas sensors simply by varying both electrode materials and distances between contacts (Jain et al. 1990; Williams 1999; Vilanova et al. 1998; Saukko and Lantto 2003). It is known that every noble metal has a specific catalytic activity. Experiments carried out in various laboratories support

**Fig. 9.1** Influence of electrode material on gas-sensing characteristics of  $\text{SnO}_2$  sensors, based on thin films deposited by electrostatic spray pyrolysis (Adapted with permission from Gourari et al. (1999). Copyright 1999 Elsevier)

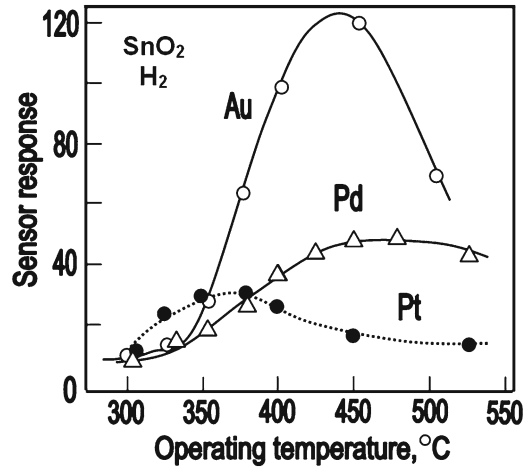
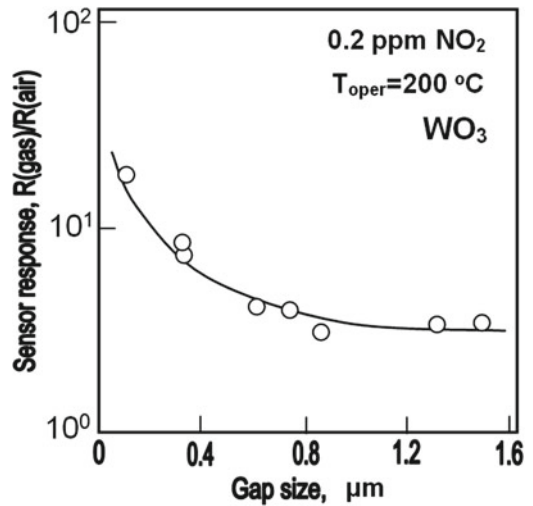


**Fig. 9.2** Sensitivities to dilute  $\text{NO}_2$  of  $\text{WO}_3$  microsensors as a function of gap size.  $\text{WO}_3$  microsensors with micro-gap electrodes were fabricated by means of MEMS techniques (photolithography and FIB) and the suspension dropping method.  $\text{WO}_3$  powders were prepared by wet process. Powders were calcined at 400 °C for 3 h (Adapted with permission from Tamaki et al. (2005). Copyright 2005 Elsevier)



this statement (Lalauze et al. 1984; Fukui and Nakane 1993; Schweizer-Berberich et al. 1997; Faglia et al. 1998; Barsan et al. 1999; Capone et al. 2001; Montmeat et al. 2002).

For example, Lalauze et al. (1984) and Gourari et al. (1999) found very large differences in the operation of sintered  $\text{SnO}_2$  sensors fabricated using different electrodes. Figure 9.1 illustrates how strong this influence could be. One can see that the change of electrode metal affects both the magnitude of the sensor response to  $\text{H}_2$  and the temperature position of the maximum sensitivity. A similar effect was observed by Pijolat (1986) for  $\text{SnO}_2$  sensors with Au and Pt contacts during detection of benzene. Sensors with Pt electrodes had maxima in lower temperature ranges.

Bertrand et al. (2006, 2007) studied  $\text{SnO}_2$  sensors with Au and Pt electrodes using DC conductance and DRIFTS measurements and demonstrated that the different nature of the electrodes changes the chemistry involved in CO sensing. Different distribution between carbonates and carboxylates, which are the reaction intermediates when CO is converted to  $\text{CO}_2$ , were identified.

That the metal–semiconductor junction may be the main gas-sensing element responsible for the observed sensor response was confirmed by Tamaki et al. (2005). In this study, the effect of gap size between Au electrodes on the sensor response to dilute  $\text{NO}_2$  was investigated (see Fig. 9.2). Gap sizes in  $\text{WO}_3$  microsensors were varied from 0.1 to 1.5 mm. It was found that the response to dilute  $\text{NO}_2$  was unchanged for gap sizes larger than 0.8 mm, whereas below 0.8 mm the sensor response



tended to increase with decreasing gap size. The sensitivity to 0.5 ppm  $\text{NO}_2$  was as high as 57 at a gap size of 0.11 mm. For an explanation of the observed effect it was assumed that the contribution of resistance at the electrode–grain interface to the total sensor resistance becomes larger when the gap size is decreased. It was concluded that the resistance change at the electrode–grain interface is much larger than that at the inter-grain boundary when the microsensor is exposed to  $\text{NO}_2$ . Thus, the sensitivity increases with decreasing gap size.

Shalan et al. (2011) observed a similar effect for nanowire  $\text{SnO}_2$ -based gas sensors with Au electrodes during  $\text{NO}_2$  detection. They established the following: (1) for low concentrations of  $\text{NO}_2$  gas the sensitivity was improved when the gap size was reduced, and the sensors with a small gap (1  $\mu\text{m}$ ) had the highest sensitivity; (2) the sensors with a large gap (30  $\mu\text{m}$ ) became highly sensitive to high concentration of  $\text{NO}_2$  – thus, it is preferable to use a sensor with a large-gap electrode for detecting high concentrations and a sensor with a small-gap electrode for detecting low concentrations; and (3) finally, the highest sensitivity of sensors was observed for the sensor with ohmic contacts or linear I–V behavior, i.e., there is a correlation between sensitivity and linearity of I–V characteristics.

Other studies also established that different electrode materials can affect sensor behavior (Ylinampa et al. 1993; Capone et al. 2001; Saukko and Lantto 2003). In particular, Ylinampa et al. (1993) compared characteristics of  $\text{SnO}_2$ -based sensors with Pt, Au, and Pt–Au contacts. It was shown that at approximately 550 °C the conductance was about the same and independent of the electrode material. However, below 150 °C the conductance of the sensors with a Pt electrode was about three orders of magnitude higher than for those with Au electrodes. Durrani (2006) used four different electrodes – Ag, Al, Au, and Pt – and found that a big difference appears between sensors: Ag and Al are less sensitive whereas Au and Pt are more sensitive. Lin et al. (1998) compared ZnO sensors with Ag and Au electrodes and found that, in contrast to Au, the conductivity of a nanocrystalline ZnO sensor with Ag electrodes cannot be recovered after turning off the  $\text{NO}_2$  gas. This result indicates that Ag electrodes are poisoned by  $\text{NO}_2$  gas. Ylinampa et al. (1993) and Schweizer-Berberich et al. (1997) also observed big difference in response to CO of sensors with Pt and Au contacts. The sensor with Pt electrodes had a much stronger response. Moreover, Schweizer-Berberich et al. (1997) observed this effect for both doped and undoped material. Saukko and Lantto (2003) also studied the impact of electrode materials on the performance of a sensor utilizing Pt or Au electrodes. They have shown that in some cases the energy barrier between electrode and the sensing semiconductor could be significant compared to the energy between the semiconductor grains. It was established that use of a Pt electrode was more sensitive to  $\text{H}_2$  whereas Au seems to give a better response to CO. In these experiments, an inter-digital electrode design with a 5-mm gap was used. The same effect was observed by Gourari et al. (1999) and Bender et al. (2001). Bender et al. (2001) have shown that a chlorine detector, made from  $\text{WO}_3$  and aluminum electrodes, had a sensor response of about 400 for 1 ppm  $\text{Cl}_2$  in air. The sensor response dropped to 1 with Pt electrodes.

Response to humidity was also affected by the electrode material. Ylinampa et al. (1993) and Capone et al. (2001) established that the influence of water on the CO response of  $\text{SnO}_2$ -based sensors is greater in the case of Au contacts and lower in the case of Pt contacts.

### 9.1.2 Electrode Materials Preferable for Gas Sensor Applications

It is clear that high stability is one of the most important requirements of materials destined for electrode fabrication. A study has shown that degradation of contacts takes place mainly due to diffusion processes occurring at either the electrode–oxide interface or the electrode interaction with the surrounding atmosphere (Meixner and Lampe 1996). Among noble metals, characterizing a maximum stability in air over a wide range of temperatures, the most intensive aging and degradation effects become apparent for Ag contacts. Silver can easily move if the electric field applied to the electrode at operating temperature is higher than 300 °C. Gold also diffuses quickly at low temperatures,

**Table 9.1** Guide for selection of materials for wiring

Parameter	Al	Ti/Pt	Polycryst. Si	TiSi <sub>2</sub>	NiFe
Heat transfer	a	a	a	a	a
Resistivity and TCR	++	++	–	+	++
Contact (if any)	++	–(TiN)	++	+	–
Stress	+	+/a	+	a/–	a
e <sup>–</sup> migration	a	a	+	+	a
Chemical compatibility	–	+	++	a	–

++, excellent; +, good; a, acceptable; –, not acceptable

Source: Reprinted with permission from Furjes et al. (2002). Copyright 2002 IOP

and it may introduce an unintentional doping of the metal oxide. Contacts based on Pt are the most stable (Park and Kim 1999; Esch et al. 2000). Pt is not oxidized at high temperatures; it has low diffusivity and is resistive to corrosive gases (Fleischer et al. 1994; Dziedzic et al. 1997). In addition, platinum has a good ohmic contact with most MOXs.

However, we need to note that even for the most stable metals there are some stability limitations. For example, at high temperatures ( $T > 1,200$  °C) platinum under oxidation can create volatile oxides (Alcock 1961) that destroy sensor metallization layers. Another potential reason for possible parameter changes in contacts is the bad adhesion of platinum. Therefore, an intermediate thin film of an “adhesion” metal such as Cr, Ti, or W, 10–100 nm thick, is deposited between the MOX and electrode layers. Good adhesion materials for Pt films over substrates used have been found to be Ta (Hoefler et al. 1994) and TiN (Michel et al. 1995). However, it was established that using a sublayer does not resolve all the problems. Of course, the use of Ti/Pt layers as the electrical contacts, which are more stable than Ti/Au or Ti/Pd/Au, might help to prevent the rather fast degradation of contacts (Sozza et al. 2004). However, Esch et al. (2000), while analyzing the behavior of Ti–Pt layers destined for the heater elements of chemical sensors, established that during exploitation the Pt surface lost its metallic luster and, at a temperature of 650 °C, hillocks appeared on the heater surface. In other words, this thermal treatment induced the diffusion and oxidation of Ti, especially for annealing times of up to 2 h at 450 °C. Longer heat treatments did not affect the chemical composition further; however, the annealing at 650 °C gave rise to hillock formation and strong adhesion problems.

In the case of micro-hotplates fabrication using micromachining technology, we have a more complicated situation because, as well as the thermodynamic stability of the materials used, we need to take into account the compatibility of these materials with silicon technology. A more detailed analysis of electrode materials acceptable for micro-hotplates fabrication was carried out by Furjes et al. (2002). Materials acceptable for realization of micro-hotplates are presented in Table 9.1.

As seen in Table 9.1, there are several alternatives for fabrication electrodes in micromachining devices; however, according to Furjes et al. (2002), materials with ideal properties cannot be found when having to consider their high thermal and low electrical conductivity, unfavorable TCR dependence vs temperature, high residual stress, chemical reactivity with Si at high temperature, and noncompatibility with silicon processing. Most of the materials are soluble in HF as used in porous Si processing (in the case of Pt the adhesive Ti layer); therefore, the wires have to be encapsulated by another SiN<sub>1.05</sub> layer. Unfortunately, the high deposition temperature of the second SiN<sub>1.05</sub> layer makes the application of Al impossible. NiFe is far from being a CMOS-compatible material at all. According to Furjes et al. (2002), the materials presented in Table 9.1 have the following advantages and shortcomings:

- *Ti/Pt*. The excellent chemical compatibility and low resistivity of Pt offer the most attractive solution for wiring. The generated heat is negligible in the Pt wires, while the heat transfer can be kept at a low level by the formation of a minimized cross section in the suspension beams. Nevertheless, the high operational temperature of the contacts between the Si heater and Pt results in continuous deterioration by the formation and lateral creeping of a silicide phase (Fig. 9.3). A conductive diffusion barrier

**Fig. 9.3** Silicide formation in high temperature contacts as degraded after annealing at 800 °C for 2 h. Microscopic view (Reprinted with permission from Furjes et al. (2002). Copyright 2002 IOP)

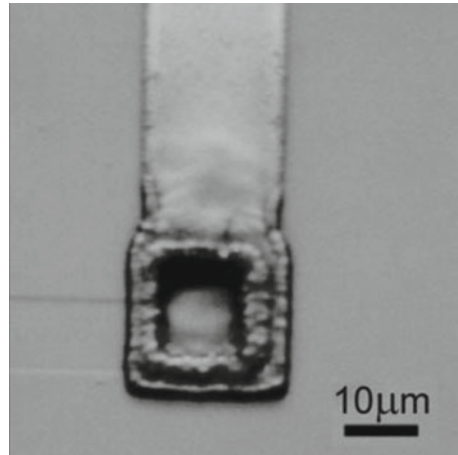
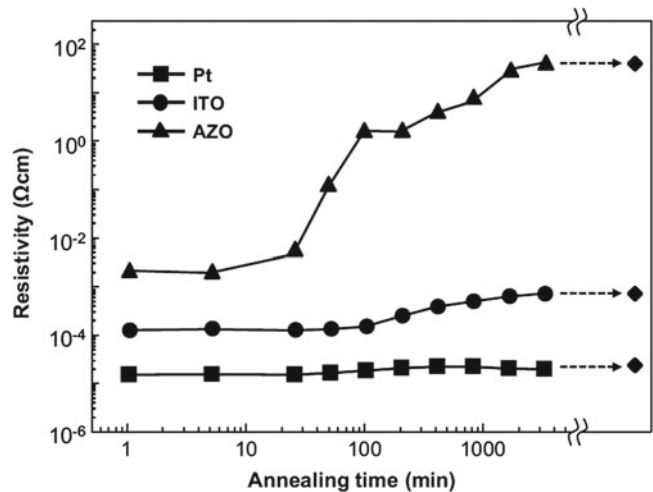


**Fig. 9.4** Resistivities of 200 nm thick Pt, ITO, and AZO films as a function of annealing time at 300 °C for 3,200 min in air. The resistivities indicated by filled square represent those after additional annealing at 500 °C for 60 min (Reprinted with permission from Shim et al. (2011). Copyright 2011 Elsevier)



between Si and Pt, such as TiN, may eliminate the problem, provided it can withstand the high temperature and cycling without losing its mechanical integrity and low contact resistance.

- *Polycrystalline silicon.* Although the contacts between polycrystalline silicon and the filament are inherently perfect, the high resistance in combination with the high positive TCR of the poly-Si limits the operation temperature of the structure. Increasing the input power (and temperature) the resistance of the polysilicon wires on the suspension beams may dominate, resulting in malfunction of the device.
- *TiSi<sub>2</sub>.* TiSi<sub>2</sub> and other refractory silicides are among the most promising materials because of their low resistivity, low contact resistance, stability at high temperature, and chemical compatibility. Due to the superior electromigration resistance of TiSi<sub>2</sub>, thin layers can be formed; therefore the high stress and the thermal loss via wiring can be reduced to an acceptable level.

Shim et al. (2011) have shown that conductive metal oxides can also be used as electrode materials in gas sensors. Analyzing the behavior of indium–tin oxide (ITO) and aluminum-doped zinc oxide (AZO) films in WO<sub>3</sub>- and SnO<sub>2</sub>-based sensors, they established that ITO can replace Pt electrodes in these devices. Upon exposure to 50 ppm CO at 300 °C, WO<sub>3</sub> or SnO<sub>2</sub> thin-film sensors with ITO interdigitated electrodes (IDEs) on glass substrates displayed higher responses than sensors with Pt IDEs, attributed to the low-resistance ohmic contacts between the electrode (ITO) and the sensing material (WO<sub>3</sub> or SnO<sub>2</sub>). It is necessary only to take into account that contacts should be stabilized at T~500 °C before using ITO (see Fig. 9.4).

Of course, in the case of gas sensors operated at room temperature we do not have such strong requirements from electrode materials, and therefore other materials, which are not as stable as Pt, can be used. In particular, gold (front and back) electrodes are used in most conventional QCMs. Other electrode materials such as aluminum, copper, silver, chromium, nickel, titanium, tungsten, zinc, as well as carbon and silicon can also be used in gas sensors (ICM, <http://www.icmfg.com/crystals.html>).

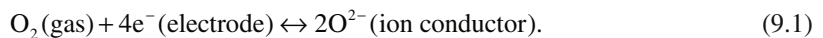
In particular, Manzoli et al. (2011) designed a low-cost polymer-based sensor array system for banana ripeness monitoring with graphite electrodes fabricated using a graphite line-patterning technique. However, even in this case the selection of electrode materials requires attention. For example, it was established that the electrical sensitivity of quartz resonators working at high frequencies (e.g., mesa-shaped QCMs) depends not only on geometry but also on the electrode material. Recently it was found that in mesa-shaped quartz resonators operated in the frequency range 1.4–3.4 GHz, the electromagnetic radiation losses in Al electrodes were significantly greater (by an order of magnitude) than their viscoelastic losses at frequencies higher than 2.3 GHz (Yong et al. 2009). In these experiments it was found that at high frequencies the vibrating aluminum electrodes worked as an emitter of electromagnetic waves.

## 9.2 Electrodes for Solid Electrolyte-Based Gas Sensors

### 9.2.1 *The Role of Electrode Configuration in Solid Electrolyte-Based Gas Sensors*

As it was shown in Chaps. 2 and 6, solid electrolyte-based gas sensors include two electrodes, which should correspond to several requirements such as: (1) electrodes should possess sufficiently high catalytic activity with respect to target gas; (2) both electrodes must be stable at the operating temperature; (3) they must have suitable porosity and pore size to improve the catalyst surface area and enhance the catalytic activity; and (4) the catalyst should possess high electronic conductivity (Amar et al. 2011).

The morphology of the electrode (porosity) is of great importance in achieving the required parameters of solid electrolyte-based gas sensors, because the main process controlling sensor response (adsorption–catalysis–electron transfer) takes place in the electrode. The triple phase boundary (TPB) is an important concept for illustrating this assertion (Jaccoud et al. 2007; Nielsen and Jacobsen 2007). TPB sites are the regions where the measured atmosphere, the metal catalyst, and the electrolyte coexist. It was established that reactions in electrochemical systems involving ion-conduction can only appear in TPB sites or nearby contact zones if the sensing electrode is metallic. For instance, the reaction at Eq. (9.1) taking place in YSZ-based oxygen sensors is assumed to occur only where O<sub>2</sub> molecules can reach a Pt/YSZ contact zone; otherwise it is not possible to exchange electrons from the metal and change the amount of oxygen ions in the electrolyte:



Experiment has shown that reactions in a nonporous pure metallic electrode are relatively difficult as the TPB sites are located exclusively in the contour of the electrode in contact with the electrolyte. Although gas molecules may adsorb over the entire surface of the electrode, most of them cannot react, providing or extracting oxygen ions from the electrolyte as the contacts gas/catalyst/electrolyte are only in the contour of the electrode. This low density of TPB sites causes a current constriction as a high fraction of the contact area between metal and YSZ is inactive (Sridhar et al. 1997; Aaberg et al. 2000). Subsequently, the response time of sensors with this structure is slow.

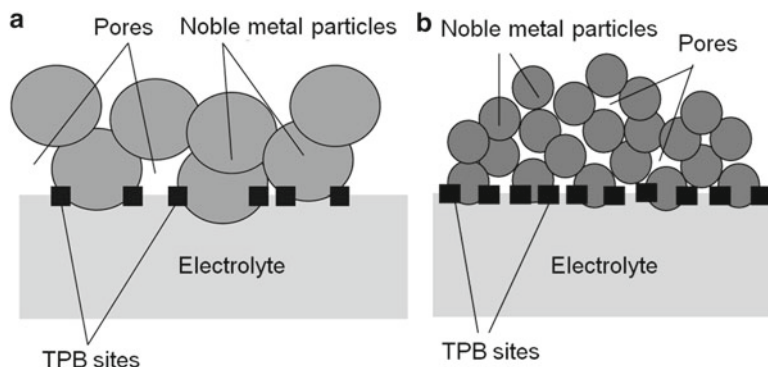


**Fig. 9.5** Scheme of the three-phase boundary sites in an interface electrode—electrolyte for electrodes with different sizes of metal particles. Porous electrodes help to increase the density of three-phase boundary sites. Idea from Lopez-Gandara et al. (2009)

Porous metal is much better in the configuration of electrodes in solid electrolyte gas sensors. Most of the commercial sensors incorporate porous metal electrodes. Gas molecules can diffuse across the pores and therefore the density of TPB sites in porous electrode increases (Yoon et al. 2003, 2004; O’Hayre et al. 2005). Figure 9.5 shows a scheme of such a porous electrode. As a result, gas sensor performance can be improved (Jaccoud et al. 2007). For example, a high number of TPB sites ensures a good response time as it lowers the double layer capacitance. An electrode made of a ceramic/metal composite is known as a cermet electrode. These electrodes provide even more TPB sites. Using a porous metal/YSZ composite as a contact to the YSZ electrolyte instead of a dense metal phase multiplies the number of interfaces between the catalyst and the electrolyte (Bultel et al. 2005). TPB length is increased and problems with current constriction are avoided. It seems obvious that particles with lower grain size and higher specific surface help to increase the number of TPB sites (Lopez-Gandara et al. 2009). As an alternative to metal/YSZ cermet electrodes, other cermet electrodes containing metal oxides mixed with a metal catalyst can also be used in order to modify the mixed potential of the sensors and/or improve gas selectivity due to the promotion of one of the competing chemical reactions in the catalysts (see next section).

### 9.2.2 Sensing Electrodes in Solid Electrolyte-Based Gas Sensors

Catalytically active and chemically stable noble metals, such as Pt and Au, were first used as sensing electrode (SE) materials in high temperature electrochemical gas sensors (Moseley and Tofield 1987; Hibino et al. 1998a; Mukundan et al. 1999). Pt electrodes, of course, found the widest application. It was established that the response of a Pt electrode was stable up to 600 °C. Bulk Au electrodes had been described for mixed potential sensors for detection of CO (Thiemann et al. 1996; Zosel et al. 2008) and hydrocarbons (Hibino et al. 1998b; Zosel et al. 2004b; Plashnitsa et al. 2008a, b, c). Plashnitsa et al. (2008c) have found that sensors using nanoparticle-based Au electrodes show high sensitivity to NO<sub>2</sub>. However, the Au electrode had stability problems at temperatures higher than 500 °C (Mukundan et al. 2000). The rapid recrystallization rate of gold electrodes at elevated temperatures has made Au electrodes unstable in high-temperature long-term operations. Therefore, in general, the noble metal Pt was more acceptable as a sensing electrode for mixed-potential type solid-electrolyte-based gas sensors (Miura et al. 2000).

Unfortunately, sensors using Pt electrodes exhibited small EMF responses to target gases at operating temperatures above  $\sim 500$  °C and gave poor gas selectivity at temperature below  $\sim 400$  °C unless covered with an additional catalyst layer. In order to get over these difficulties, a search for sensing electrode materials was carried out to include other metals and noble alloys. However, other metals often did not have the required activity; for example, a Ni-sensing electrode was considerably less sensitive to hydrogen (Ponomareva et al. 1997). Kimura and Goto (2005) established that only iridium may have similar or higher catalytic activity than Pt. They prepared Ir-YSZ nanocomposite electrodes by metalorganic chemical vapor deposition (MOCVD). The composite consisted of crystalline Ir and amorphous YSZ, with an average Ir particle size of 3 nm. Several composites were prepared with a controlled Ir composition of 3–71 vol.%. Kimura and Goto (2005) found that the electrical conductivity of the sensors with Ir-YSZ electrodes was up to 1,000 times higher than that with Pt electrodes. Later, the electrochemical performance of IrO<sub>2</sub>/YSZ nanocomposite electrodes was investigated by Torres-Huerta et al. (2007), with grain sizes between 15 and 30 nm. Although this work was in the area of fuel cells, the observed properties are applicable to gas sensors. Torres-Huerta et al. (2007) established that the polarization resistance of IrO<sub>2</sub>/YSZ electrodes was lower than that of Pt conventional electrodes and Ir-YSZ electrodes (Kimura and Goto 2005), probably due to a higher density of triple phase boundary sites. Furthermore, the activation energy for the interfacial conductivity of the composites was in agreement with the energy of dissociation of oxygen molecules. By making comparisons with the activation energy for La<sub>1-x</sub>Sr<sub>x</sub>MnO<sub>3</sub> (LSM) or Pt electrodes (Barbucci et al. 2002), the authors suggested that the IrO<sub>2</sub>-YSZ cermet might offer an efficient and competitive performance as electrode materials for YSZ electrolytes, although further analysis would be necessary.

Experiment has shown that sensors using Pt-based alloy electrodes, which included Au, Ag, Cu, Ni, or Rh, can also provide better sensor performance. For example, such sensors had higher EMF responses to H<sub>2</sub> at temperatures of about 550 °C in comparison with Pt electrodes (Vogel et al. 1993). Among the Pt-based alloys investigated as electrode materials, a Pt–Au alloy electrode applied in electrochemical sensors gives the highest response to H<sub>2</sub>. Tests of a non-Nernstian type zirconia sensor with a Pt–Au sensing electrode (Vogel et al. 1993) also established improved selectivity for CO against H<sub>2</sub>. An interesting improvement of the electrode's impedance was proposed by Wang et al. (2008), also valid for fuel cells and electrochemical gas sensors. Based on quantum ab initio calculations, it was found that both the surface energy of a Pt<sub>0.7</sub>Ni<sub>0.3</sub> cluster and the energy change of the Pt–Ni alloy cluster upon ripening on YSZ were lower than pure Pt. Also, changes in microstructure properties after annealing nanoporous Pt and Pt–Ni thin films were compared. No changes were found in Pt–Ni nanoporous thin films, but a dramatic porosity reduction was observed in pure nanoporous platinum. Therefore, a lower electrode impedance, better thermal stability, and lower temperature of operation were expected. The use of nanocomposites made of Pt mixed with carbon nanotubes has sometimes been suggested for application in oxygen sensors (Gong et al. 2005). Wang et al. (2004) reported that such nanocomposite-based electrodes can be applied in hydrocarbon electrochemical sensors as well. However, should be recognized that the use of alloy and nanocomposites did not resolve the problem of thermal and temporal instability of electrochemical gas sensors. The lack of a “perfect” material for SE in solid electrolyte sensors, in particular YSZ sensors, till now is a fundamental limitation to the use of zirconia-based sensors.

Experiments have shown that using metal oxides as sensing electrodes instead of Pt alone or in combination provided much better results (Zhuiykov and Miura 2005; Zhuiykov 2007; Fergus 2007a, b, 2008; Chevallier et al. 2008; Miura et al. 2009; Pasierb and Rekas 2009). The metal oxides which were tested as sensing electrodes in H<sub>2</sub> sensors, are listed in Table 9.2. It was established that the use of refractory conductive metal oxides for sensing electrodes offers promise in improving both the selectivity and the long-term stability of solid electrolyte gas sensors (Lu et al. 1996a, b; Miura et al. 1996; Miura and Yamazoe 1998). For example, YSZ-based sensors with metal oxide electrodes such as SnO<sub>2</sub> or CdO, configured as shown in Fig. 9.6a, can operate at rather high temperatures up to 700 °C, and certain formulations can give good sensing performances even under rather severe operating conditions

**Table 9.2** EMF response to H<sub>2</sub> and CO at 600 °C for the YSZ-electrolyte device using various oxides

Oxides	EMF (mv)	
	200 ppm H <sub>2</sub>	200 ppm CO
AuO	-136	-9
ZnO	-125	-44
CdO	-104	-126
SnO <sub>2</sub>	-95	-50
In <sub>2</sub> O <sub>3</sub>	-70	-47
Sb <sub>2</sub> O <sub>3</sub>	-15	-7
WO <sub>3</sub>	-7	0
TiO <sub>2</sub>	-7	0
MoO <sub>3</sub>	-5	-1
Fe <sub>2</sub> O <sub>3</sub>	-4	-2
Pt (only)	-3	-1
CuO	-1	0
Mn <sub>2</sub> O <sub>3</sub>	0	0
Co <sub>3</sub> O <sub>4</sub>	0	0
Cr <sub>2</sub> O <sub>3</sub>	0	0
NiO	0	0
PbO <sub>2</sub>	0	0

Source: Data extracted from Sakhivel and Weppner (2008) and Miura and Yamazoe (1998)

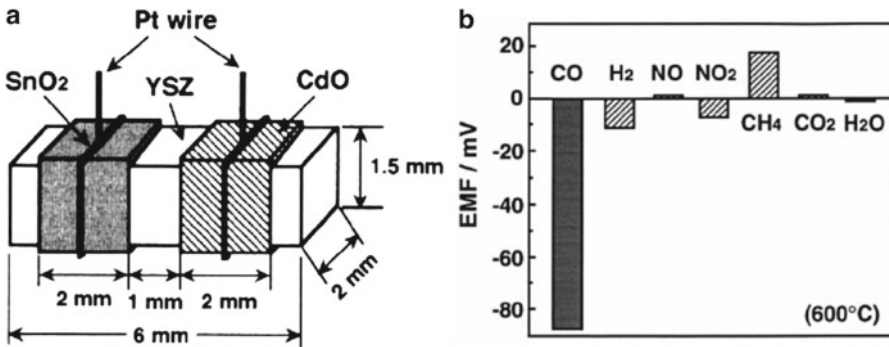


**Fig. 9.6** (a) Schematic view of YSZ-based device structure with metal oxide sensing electrodes and (b) cross-sensitivities to various gases at 600 °C for the YSZ-based device using CdO and SnO<sub>2</sub> electrodes. (Gas concentration CO, H<sub>2</sub>, NO, NO<sub>2</sub>, CH<sub>4</sub>; 200 ppm each, CO<sub>2</sub>; 10,000 ppm, H<sub>2</sub>O; 1.5 kPa) (Reprinted with permission from Miura and Yamazoe (1998). Copyrights 1998 Elsevier)

(Miura and Yamazoe 1998; Martin et al. 2004; Nakatou and Miura 2005). We also need to take into account that metal oxides are considerably cheaper than Pt. Results related to EMF response to H<sub>2</sub> and CO of YSZ-based sensors with various metal oxide sensing electrodes are presented in Table 9.2.

In Table 9.2, the EMF response is shown to be clearly dependent on the oxides used. In particular it was found that TiO<sub>2</sub>, with many transition metal oxides such as Fe<sub>2</sub>O<sub>3</sub>, Cr<sub>2</sub>O<sub>3</sub>, NiO, Mn<sub>3</sub>O<sub>4</sub>, and Co<sub>3</sub>O<sub>4</sub>, shows insignificant or no response to CO and H<sub>2</sub>. These results suggest that semiconducting oxides with modest catalytic activity tend to make the best sensing electrodes. It is seen that the maximum H<sub>2</sub> response was obtained with ZnO electrodes. Moreover, these oxide electrode sensors exhibited an excellent selectivity to H<sub>2</sub> in the presence of NO, NO<sub>2</sub>, CH<sub>4</sub>, CO<sub>2</sub>, and H<sub>2</sub>O. In the device with a Pt-sensing electrode, for comparison, the EMF response was not observed above 500 °C. The maximum response to CO with good selectivity was obtained with CdO electrodes (see Fig. 9.6b).

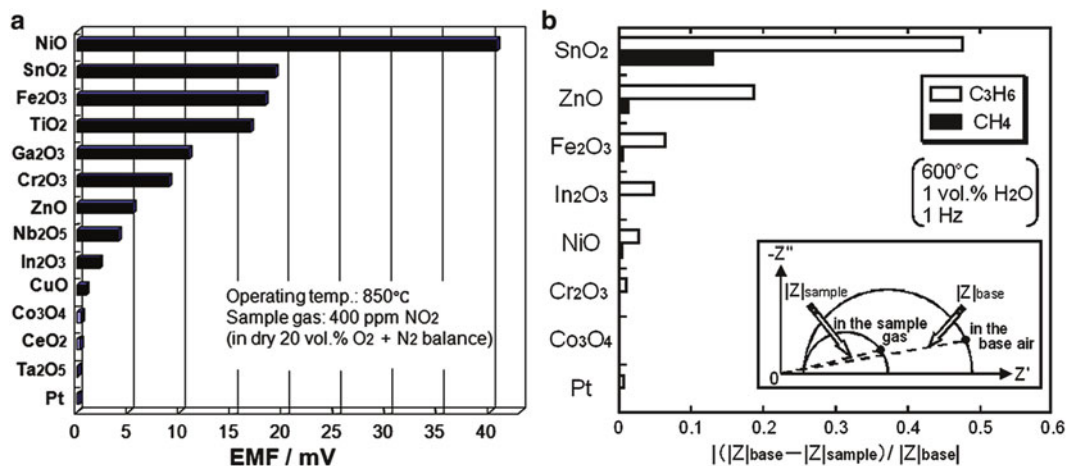


**Fig. 9.7** Histograms showing (a) typical response of various oxide SEs to 400 ppm NO<sub>2</sub> at 850 °C and (b) relative sensitivity to C<sub>3</sub>H<sub>6</sub> and CH<sub>4</sub> (400 ppm each) of impedancemetric sensors using each of various single-oxide SEs at 600 °C. *Inset* shows modeling of complex impedance plots. *Points* on *dashed lines* correspond to 1 Hz. (a) Reprinted with permission from Zhuiykov and Miura (2007). Copyright 2007 Elsevier and (b) Reprinted with permission from Nakatou and Miura (2005). Copyright 2006 Elsevier

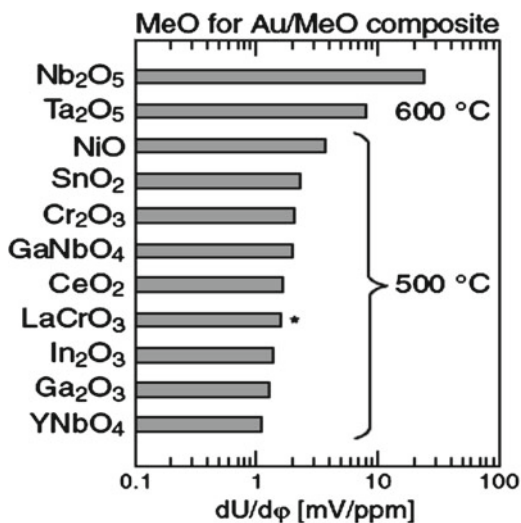
Results presented in Fig. 9.6b also illustrate that it is possible to detect CO sensitively and selectively even in the presence of H<sub>2</sub>, which is an important problem. The response to CO was visible with ZnO, In<sub>2</sub>O<sub>3</sub>, and SnO<sub>2</sub> as well, but it was much smaller than the response to H<sub>2</sub>. Using ITO with a thickness of 2–13 μm as the sensing electrode succeeded in decreasing the RH influence on the operating characteristics of sensor devices (Martin and Glass 2005). Li and Kale (2005a, b, 2006, 2007) also studied electrodes made of tin-doped indium oxide (ITO) nanoparticles. Sensors with the structure ITO nanoparticles/YSZ/Pt exposed to air mixed with several CO concentrations near 900 K got higher sensitivities for CO and lower potentiometric response times than in previous works. This net response is non-Nernstian and was attributed to the mixed potential of electrodes made of ITO nanoparticles. In comparison with CdO, ZnO, and SnO<sub>2</sub>, the perovskite LaCr<sub>0.8</sub>Ga<sub>0.2</sub>O<sub>3-δ</sub> provides an example of an electrode material with very low sensitivity to H<sub>2</sub>, and this is more typical of these composites' analytical characteristics from data reported originally with regard to the detection of hydrocarbons (HCs) (Zosel et al. 2004b, 2006).

Results related to other target gases can be found in Fig. 9.7. This figure illustrates that, among the many single metal oxides investigated, NiO provides the highest NO<sub>2</sub> sensitivity at 850 °C (Elumalai and Miura 2005; Plashnitsa et al. 2008a, b), while SnO<sub>2</sub> provides the highest response to C<sub>3</sub>H<sub>6</sub> and CH<sub>4</sub> (Zhuiykov 2007), and ZnO has a smaller response to C<sub>3</sub>H<sub>6</sub>. However, since methane is not regulated as an air pollutant, ZnO has the advantage for C<sub>3</sub>H<sub>6</sub> sensor design because it provides rather high sensitivity to propene but negligible sensitivity to methane (see Fig. 9.7b). Experiment has shown that CuO-doped NiO electrodes (Plashnitsa et al. 2007), nanostructured perovskites such as LaFeO<sub>3</sub> (Di Bartolomeo et al. 2004), and more sensitive and stable version with LaFeO<sub>3</sub>-doped Pt (Yoon et al. 2001) are also promising for NO<sub>2</sub> sensors design.

Composite electrodes have also been studied (Hibino et al. 1999; Westphal et al. 2001; Zosel et al. 2004a). Compared to electrodes made of single metal oxides, electrodes made of composites—particularly those made of gold and metal oxides (MeO)—show elevated sensitivities to a variety of hydrocarbons and H<sub>2</sub> (Fig. 9.8). It was established that the decreasing catalytic activity of the electrode materials is closely correlated with increasing sensitivity (Zosel et al. 2002, 2004a). At 600 °C, the composite materials Au–MeO with Nb<sub>2</sub>O<sub>5</sub> and Ta<sub>2</sub>O<sub>5</sub> have the highest sensitivities to H<sub>2</sub>. It has been established that the Eu-NbO<sub>4</sub>/Au composite electrode has higher sensitivity, but the signal



**Fig. 9.8** Hydrogen sensitivity of YSZ-based devices with composite electrodes (Au/20 wt% MeO) at  $p(\text{H}_2) \sim 10$  ppmv,  $p(\text{O}_2) \sim 1.5$  vol.%. The REs were prepared from commercially available Pt-paste. (Reprinted with permission from Zosel et al. (2002), Copyright 2006 Elsevier)



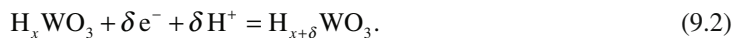
drifts even at constant  $\text{H}_2$  concentration and the rate of electrochemical oxidation was dependent on the time of exposure to hydrogen (Zosel et al. 2002). This observation is not unique and was also observed at some composite electrodes containing  $\text{TbNbO}_4$ ; this can be due, at least in part, to the elevated  $\text{H}_2$  solubility in these materials. Wu et al. (2005) proposed the use of a porous  $\text{CuO-ZnO}$  nanocomposite over a Pt conventional paste for selective CO detection. An output voltage of about 8 mV was detected for an 800 ppm CO concentration in air near 800 K for sensors with the structure  $\text{CuO-ZnO/Pt/YSZ/Pt}$ . However, the response equilibration time of the sensor was significantly slow, on the order of 30 min.

The transition to composites improves the characteristics of NiO-based sensing electrodes as well. Research has been conducted on composites such as  $\text{NiO-Rh}$  (3 wt%) (Wang et al. 2006),  $\text{NiO-WO}_3$  (10 wt%) (Miura et al. 2007),  $\text{NiO-CuO}$  (10 wt%) (Plashnitsa et al. 2006, 2007), and  $\text{NiO-(Pd, Pt, Ru, or Rh)}$  (Miura et al. 2007). It has been shown that among the noble metals such as palladium, platinum, ruthenium, and rhodium, rhodium (3 wt%) provided substantial improvement in  $\text{NO}_2$  sensitivity (Miura et al. 2007).

It was also found that this approach based on use of composites has apparently contributed to sensor stability. For example, the use of nanocomposites of  $\text{Au-MeO}_x$  seems to resolve the instability of gold electrodes (Westphal et al. 2001). It was established that electrodes made from  $\text{Au-Ga}_2\text{O}_3$ , containing 20 wt%  $\text{Ga}_2\text{O}_3$  nanoparticles, in a potentiometric YSZ sensor, kept working and remained stable up to 850 °C. These  $\text{Au-Ga}_2\text{O}_3$  nanocomposite electrodes were prepared by using thick film technology and were sintered at between 900 and 950 °C.

Considerable success in sensing  $\text{H}_2$  was demonstrated with electrodes of metal(IV) hydrides (Alberti and Casciola 2001). If a  $\text{MeH}_x$  is unable to catalyze electrode processes, any possible interference due to the diffusion of gaseous hydrogen from the sensing to the reference compartment is avoided. Therefore, even highly hydrogen-permeable membranes of protonic conductors can be used with these electrode materials as well as very thin films which can significantly lower device electrical resistance and facilitate the design of simple and miniaturized sensors. Noncatalytic metal hydrides with very low hydrogen pressure include  $\text{ZrH}_x$  and  $\text{TiH}_x$  ( $p_{\text{H}_2} \sim 10^{-10}$  and  $10^{-17}$  atm, respectively, at room temperature). In practice, however, research has shown that the  $\text{TiH}_x$  electrode, especially at higher temperature, tends to become covered by a layer of oxide, making it increasingly less reversible. Further, although sufficient for a reference electrode, its exchange current density is only of the order of  $0.3 \mu\text{A}/\text{cm}^2$  (Alberti et al. 2001). The candidate material for the sensor electrode must have two main characteristics: (1) a viable electron concentration and (2) the capability to insert reversibly

protons that come from the electrolyte (Alberti et al. 2001). Another possible candidate of questionable stability includes tungsten bronze ( $H_xWO_3$ ), which is an electron conductor and can exchange protons through the following electrochemical reaction:



### 9.3 Materials for Heater Fabrication

The majority of gas sensors, including conductometric MOX sensors, thermoelectric sensors, and pellistors, operate at high temperatures. So the heater is an important part of these devices, which influences their operating characteristics. For instance, MOX sensors have a clearly expressed sensitivity dependence on operating temperature ( $T_{oper}$ ) (Morrison 1987; Ihokura and Watson 1994; Korotcenkov 2007a, b). Therefore, in the absence of temperature control, even small changes in the resistance of a heater will be accompanied by a change in the sensors' temperature mode. Hence, at higher temperatures of exploitation, degradation of heaters could become the main reason for the observed changes in sensor parameters (Benkstein et al. 2006). This means that electrode materials used for heaters should be very stable, because they need to provide maximal stability while working at high temperatures.

Heaters for planar sensors are conventionally fabricated in the shape of meanders made of various metals or alloys. The most commonly utilized material is platinum deposited as thin or thick layers (e.g., Dziedzic et al. 1994; Mailly et al. 2001; Mo et al. 2001; Aslam et al. 2004; Dai 2007). Platinum is often chosen for the reasons discussed in the previous section. In some work related to heater manufacturing it was suggested that polysilicon be used (Vincenzi et al. 2001), NiCr or Si–Ni–Cr alloys (Korotchenkov et al. 1999), SiC (Chen and Mehregany 2007), TiN (Creemer et al. 2008), and RuO<sub>2</sub> (Dziedzic et al. 1994; Jelenkovic et al. 2003; Bai et al. 2006). The main advantage of RuO<sub>2</sub> is its weak dependence on temperature. For comparison, the resistance of platinum film approximately doubles when it reaches temperatures of 350–400 °C, although testing has shown that at  $T > 350$ –400 °C the platinum heater has more stable characteristics. In addition, platinum heaters can be used to monitor temperature in low-price gas sensors. In addition, while using polysilicon, some problems with formation of stable contacts may occur; while using RuO<sub>2</sub>, other problems may arise. For example, in an ambient hydrogen atmosphere at temperatures as low as 150–250 °C, RuO<sub>2</sub> tends to reduce to ruthenium (Jelenkovic et al. 2003).

In ceramic gas sensors, including Figaro-type, pellistors, and one-electrode conductometric gas sensors, the heater is also usually fabricated from platinum wire (Korotcenkov 2007a, b) and Cr–Ni alloy (Qi et al. 2009; Guo et al. 2012). As we wrote before, platinum has excellent chemical properties – it is corrosion resistant and can be operated at elevated temperatures for a long period of time without changing its physical properties. Platinum wire has diameters in the range 20–50 μm. Of course, it is possible to use even thinner platinum spirals. However, any further decrease of the platinum spiral's diameter sharply diminishes the reliability of gas sensors. Cr–Ni alloy also has good stability in the temperature range up to 600–700 °C.

To avoid catalytic interaction of the analyte with a heater made of noble metal, the films are frequently coated with a thin, chemically inert layer of SiO<sub>2</sub>. Such passivation very often serves as a support for further functional layers in top-down microelectronic technologies. It should be noted that the passivation of electrode materials allows a reduction in requirements relating to their thermodynamic stability. In particular, the indicated approach is used in micro-hotplate fabrication. As a result most micro-hotplate designers consider polycrystalline silicon doped with boron or phosphorus impurities to be a very appropriate material for making heaters and temperature sensors because, with capsulation covering, it is stable up to 1,000 °C (Panchapakesan et al. 2001; Hwang

et al. 2011) and it does not contaminate the IC processing equipment. Moreover, when the polysilicon layer is doped with boron at a concentration close to  $1 \times 10^{20}$  atoms/cm<sup>3</sup>, its electrical resistance becomes almost independent of temperature. Therefore, if the polysilicon is employed as a heater, it generates a uniform heat flow which is not affected by temperature variations. When the polysilicon layer is doped with boron at a concentration close to  $2 \times 10^{19}$  atoms/cm<sup>3</sup>, its electrical resistance is a linear function of temperature, which makes it possible to design a reliable thermometer. Boron is frequently selected as a dopant because the amount can be accurately controlled in order to predict the electrical resistivity of the polysilicon layer. Following implantation, the structures are annealed to let the boron diffuse and to recrystallize the silicon layer. Of course, as discussed earlier, TiSi<sub>2</sub> can be used for making heaters as well.

## References

- Aaberg RJ, Tunold R, Odegard R (2000) On the electrochemistry of metal-YSZ single contacts. *Solid State Ionics* 136–137:707–712
- Alberti G, Casciola M (2001) Solid state protonic conductors, present main applications and future prospects. *Solid State Ionics* 145:3–16
- Alberti G, Carbone A, Palombari R (2001) Solid state potentiometric sensor at medium temperatures (150–300 °C) for detecting oxidizable gaseous species in air. *Sens Actuators B* 75:125–128
- Alcock CB (1961) The gaseous oxides of the platinum metals. *Platin Met Rev* 5(4):134–139
- Amar IA, Lan R, Petit CTG, Tao S (2011) Solid-state electrochemical synthesis of ammonia: a review. *J Solid State Electrochem* 15:1845–1860
- Aslam M, Gregory C, Hatfield JV (2004) Polyimide membrane for micro-heated gas sensor array. *Sens Actuators B* 103:153–157
- Bai Z, Wang A, Xie C (2006) Laser grooving of Al<sub>2</sub>O<sub>3</sub> plate by a pulsed Nd:YAG laser: characteristics and application to the manufacture of gas sensors array heater. *Mater Sci Eng A* 435–436:418–424
- Barbucci A, Bozzo R, Cerisola G, Costamagna P (2002) Characterisation of SOFC composite cathodes using electrochemical impedance spectroscopy. Analysis of Pt/YSZ and LSM/YSZ electrodes. *Electrochim Acta* 47:2183–2188
- Barsan N, Schweizer-Belberich M, Gopel W (1999) Fundamental and practical aspects in the design of nanostructured SnO<sub>2</sub> gas sensors: a status report. *Fresenius J Anal Chem* 365:287–304
- Bender F, Kim C, Mlsna T, Vetelino JF (2001) Characterization of a WO<sub>3</sub> thin film chlorine sensor. *Sens Actuators B* 77:281–286
- Benkstein KD, Martinez CJ, Li G, Meier DC, Montgomery CB, Semancik S (2006) Integration of nanostructured materials with MEMS microhotplate platforms to enhance chemical sensor performance. *J Nanopart Res* 8:809–822
- Bertrand J, Koziej D, Barsan N, Viricelle JP, Pijolat C, Weimar U (2006) Influence of the nature of the electrode on the sensing performance of SnO<sub>2</sub> sensors; impedance spectroscopy studies. In: *Proceeding of European conference on solid state transducers, eurosensors XX*, Goteborg, Sweden, 17–20 Sept., pp 100–101
- Bertrand J, Viricelle JP, Pijolat C, Haensch A, Koziej D, Barsan N, Weimar U (2007) Metal/SnO<sub>2</sub> interface effects on CO sensing: operando studies. In: *Proceedings of the 6th IEEE sensors conference*, Atlanta, GA, 28–31 Oct, pp 492–495
- Bowker M, Bowker LJ, Bennett RA, Stone P, Ramirez-Cuesta A (2000) In consideration of precursor states, spillover and Boudart's "collection zone" and of their role in catalytic processes. *J Mol Cat A Chem* 163:221–232
- Brinzari V, Korotcenkov G, Schwank J, Boris Y (2002) Chemisorptional approach to kinetic analysis of SnO<sub>2</sub>:Pd-based thin film gas sensors (TFGS). *J Optoelect Adv Mater (Romania)* 4(1):147–150
- Bultel L, Vernoux P, Gaillard F, Roux C, Siebert E (2005) Electrochemical and catalytic properties of porous Pt-YSZ composites. *Solid State Ionics* 176:793–801
- Capone S, Siciliano P, Quaranta F, Rella R, Epifani M, Vasanelli L (2001) Moisture influence and geometry effect of Au and Pt electrodes on CO sensing response of SnO<sub>2</sub> microsensors based on sol-gel thin film. *Sens Actuators B* 77:503–511
- Chen L, Mehregany M (2007) Exploring silicon carbide for thermal infrared radiators. In: *Proceedings of the 6th IEEE sensors conference*, Atlanta, GA, USA, 28–31 Oct 2007, pp 620–623
- Chevallier L, Di Bartolomeo E, Grilli ML, Mainas M, White B, Wachsman ED, Traversa E (2008) Non-Nernstian planar sensors based on YSZ with a Nb<sub>2</sub>O<sub>5</sub> electrode. *Sens Actuators B* 129:591–597
- Comini E, Faglia G, Sberveglieri G (2009) Electrical-based gas sensing. In: Comini E, Faglia G, Sberveglieri G (eds) *Solid state gas sensing*. Springer, New York, NY, pp 47–107

- Creemer JF, Briand D, Zandbergen HW, Vlist W, Boer CR, Rooij NF, Sarro PM (2008) Microhotplates with TiN heaters. *Sens Actuators A* 148:416–421
- Dai CL (2007) A capacitive humidity sensor integrated with micro heater and ring oscillator circuit fabricated by CMOS-MEMS technique. *Sens Actuators B* 122:375–380
- Di Bartolomeo E, Kaabbuathong N, D'Epifanio A, Grilli ML, Traversa E, Aono H, Sadaoka Y (2004) Nano-structured perovskite oxide electrodes for planar electrochemical sensors using tape casted YSZ layers. *J Euro Ceram Soc* 24(6):1187–1190
- Durrani SMA (2006) The influence of electrode metals and its configuration on the response of tin oxide thin film CO sensor. *Talanta* 68(5):1732–1735
- Dziedzic A, Golonka LJ, Licznernski BW, Hielscher G (1994) Heaters for gas sensors from thick conductive or resistive films. *Sens Actuators B* 19:535–539
- Dziedzic A, Golonka LJ, Kozlowski J, Licznernski BW, Nitsch K (1997) Thick-film resistive temperature sensors. *Meas Sci Technol* 8:78–85
- Elumalai P, Miura N (2005) Performances of planar NO<sub>2</sub> sensor using stabilized zirconia and NiO sensing electrode at high temperature. *Solid State Ionics* 31–34:2517–2522
- Esch H, Huyberechts G, Mertens R, Maes G, Manca J, DeCeuninck W, De Schepper L (2000) The stability of Pt heater and temperature sensing elements for silicon integrated tin oxide gas sensors. *Sens Actuators B* 65:190–192
- Faglia G, Comini E, Sberveglieri G, Rella R, Siciliano P, Vasanelli L (1998) Square and collinear four probe array and Hall measurements on metal oxide thin film gas sensors. *Sens Actuators B* 53:69–75
- Fergus JW (2007a) Solid electrolyte based sensors for the measurement of CO and hydrocarbon gases. *Sens Actuators B* 122:683–693
- Fergus JW (2007b) Materials for high temperature electrochemical NO<sub>x</sub> gas sensors. *Sens Actuators B* 121:652–663
- Fergus JW (2008) A review of electrolyte and electrode materials for high temperature electrochemical CO<sub>2</sub> and SO<sub>2</sub> gas sensors. *Sens Actuators B* 134:1034–1041
- Fleischer M, Hollbauer L, Meixner H (1994) Effect of the sensor structure on the stability of Ga<sub>2</sub>O<sub>3</sub> sensors for reducing gases. *Sens Actuators B* 18–19:119–124
- Fukui K, Nakane M (1993) Effects of tin oxide semiconductor-electrode interface on gas sensitivity characteristics. *Sens Actuators B* 13–14:589–590
- Furjes P, Zs V, Adam M, Barsony I, Morrissey A, Cs D (2002) Materials and processing for realization of micro-hotplates operated at elevated temperature. *J Micromech Microeng* 12:425–429
- Gong K, Yan Y, Zhang M, Su L, Xiong S, Mao L (2005) Electrochemistry and electroanalytical applications of carbon nanotubes: a review. *Anal Sci* 21(12):1383–1393
- Gourari H, Lumbreras M, Van Landschoot R, Schoonman J (1999) Electrode nature effects on stannic oxide type layers prepared by electro-static spray deposition. *Sens Actuators B* 58:365–369
- Guo W, Liu T, Zhang H, Sun R, Chen Y, Zeng W, Wang Z (2012) Gas-sensing performance enhancement in ZnO nanostructures by hierarchical morphology. *Sens Actuators B* 166–167:492–499
- Gurlo A, Bârsan N, Weimar U (2004) Gas sensors based on semiconducting metal oxides. In: Fierro JLG (ed) *Metal oxides: chemistry and applications*. Dekker, New York, NY
- Hibino T, Kuwahara Y, Wang S, Kakimoto S, Sano M (1998a) Nonideal electromotive force of zirconia sensors for unsaturated hydrocarbon gases. *Electrochem Soc Lett* 1(4):197–199
- Hibino T, Wang S, Kakimoto S, Sano M (1998b) Detection of propylene under oxidizing conditions using zirconia-based potentiometric sensor. *Sens Actuators B* 50:149–155
- Hibino T, Kakimoto S, Sano M (1999) Non-Nernstian behavior at modified Au electrodes for hydrocarbon gas sensing. *J Electrochem Soc* 146:3361–3366
- Hofer U, Kuhner G, Schweizer W, Sulz G, Steiner K (1994) CO and CO<sub>2</sub> thin film SnO<sub>2</sub> gas sensors on Si substrates. *Sens Actuators B* 22:115–119
- Hwang W-J, Shin K-S, Roh J-H, Lee D-S, S.-H S-H (2011) Development of micro-heaters with optimized temperature compensation design for gas sensors. *Sensors* 11:2580–2591
- Ihokura K, Watson J (1994) *The stannic oxide gas sensor—principles and applications*. CRC, Boca Raton, FL, pp 79–85
- Jaccoud A, Foti G, Wuthrich R, Jotterand H, Comninellis C (2007) Pt/YSZ microstructure and electrochemistry. *Top Catal* 44(3):409–417
- Jain U, Hanker AM, Stoneham M, Williams DE (1990) Effect of electrode geometry on sensor response. *Sens Actuators B* 2:111–114
- Jelenkovic EV, Tong KY, Cheung WY, Wong SP (2003) Degradation of RuO<sub>2</sub> thin films in hydrogen atmosphere at temperatures between 150 and 250 °C. *J Microelectron Reliab* 43:49–55
- Kimura T, Goto T (2005) Ir-YSZ nano-composite electrodes for oxygen sensors. *Surf Coat Technol* 198:36–39
- Kohl D (1990) The role of noble metals in the chemistry of solid-state gas sensors. *Sens Actuators B* 1:158–165
- Korotcenkov G (2007a) Metal oxides for solid state gas sensors. What determines our choice? *Mater Sci Eng B* 139:1–23

- Korotcenkov G (2007b) Practical aspects in design of one-electrode semiconductor gas sensors: status report. *Sens Actuators B* 121:664–678
- Korotchenkov GS, Dmitriev SV, Brynzari VI (1999) Processes development for low cost and low power consuming SnO<sub>2</sub> thin film gas sensors (TFGS). *Sens Actuators B* 54:202–209
- Lalauze R, Bui N, Pijolat C (1984) Interpretation of the electrical properties of SnO<sub>2</sub> gas sensors after treatments with sulphur dioxide. *Sens Actuators* 6:119–125
- Li X, Kale GM (2005a) Novel nanosized ITO electrode for mixed potential gas sensors. *Electrochem Solid State Lett* 8:27–30
- Li X, Kale GM (2005b) Planar mixed-potential CO sensor utilizing novel BLIO and ITO interface. *Electrochem Solid State Lett* 9:12–15
- Li X, Kale GM (2006) Influence of thickness of ITO sensing electrode film on sensing performance of planar mixed potential CO sensor. *Sens Actuators B* 120:150–155
- Li X, Kale GM (2007) Influence of sensing electrode and electrolyte on performance of potentiometric mixed potential gas sensors. *Sens Actuators B* 123:254–261
- Lin H-M, Tzeng S-J, Hsiao P-J, Tsai W-L (1998) Electrode effects on gas sensing properties of nanocrystalline zinc oxide. *Nanostructure Mater* 10(3):465–477
- Lopez-Gandara C, Ramos FM, Cirera A (2009) YSZ-based oxygen sensors and the use of nanomaterials: a review from classical models to current trends. *J Sensors* 2009:258489
- Lu G, Miura N, Yamazoe N (1996a) High temperature hydrogen sensor based on stabilized zirconia and a metal oxide electrode. *Sens Actuators B* 35:130–135
- Lu G, Miura N, Yamazoe N (1996b) Mixed potential hydrogen sensor combining oxide ion conductor with oxide electrode. *J Electrochem Soc* 143:L154–L155
- Maily F, Giani A, Bonnot R, Temple-Boyer P, Pascal-Delannoy F, Foucaran A, Boyer A (2001) Anemometer with hot platinum thin film. *Sens Actuators A* 94:32–38
- Manzoli A, Steffens C, Paschoalin RT, Correa AA, Alves WF, Leite FL, Herrmann PSP (2011) Low-cost gas sensors produced by the graphite line-patterning technique applied to monitoring banana ripeness. *Sensors* 11:6425–6434
- Martin LP, Glass RS (2005) Hydrogen sensor based on YSZ electrolyte and tin doped indium oxide electrode. *J Electrochem Soc* 152:H43–H47
- Martin LP, Pham A-Q, Glass RS (2004) Electrochemical hydrogen sensor for safety monitoring. *Solid State Ionics* 175:527–530
- McAlear JF, Moseley PT, Norris JOW, Williams DE, Tofield BC (1988) Tin dioxide gas sensors. Part 2. The role of surface additives. *J Chem Soc, Faraday Trans 1* 84(2):441–457
- Meixner H, Lampe U (1996) Metal oxide sensors. *Sens Actuators B* 33:198–202
- Michel H-J, Michel H-J, Leiste H, Halbritter J (1995) Structural and electrical characterization of PVD-deposited SnO<sub>2</sub> films for gas-sensor application. *Sens Actuators B* 24–25:568–572
- Miura N, Yamazoe N (1998) High-temperature potentiometric/amperometric NO<sub>x</sub> sensors combining stabilized zirconia with mixed-metal oxide electrode. *Sens Actuators B* 52:169–178
- Miura N, Lu G, Yamazoe N, Kurosawa H, Hasei M (1996) Mixed potential type NO<sub>x</sub> sensor based on stabilized zirconia and oxide electrode. *J Electrochem Soc* 143:L33–L35
- Miura N, Lu G, Yamazoe N (2000) Progress in mixed-potential type devices based on solid electrolyte for sensing redox gases. *Solid State Ionics* 136–137:533–542
- Miura N, Wang J, Elumalai P, Ueda T, Terada D, Hasei M (2007) Improving NO<sub>2</sub> sensitivity by adding WO<sub>3</sub> during processing of NiO sensing electrode of mixed-potential-type zirconia-based sensor. *J Electrochem Soc* 154:J246–J250
- Miura N, Elumalai P, Plashnitsa VV, Ueda T, Wama R, Utiyama M (2009) Solid-state electrochemical gas sensing. In: Comini E, Faglia G, Sbervegliery G (eds) *Solid state gas sensing*. Springer, New York, NY, pp 181–208
- Mo YW, Okawa Y, Tajima M, Nakai T, Yoshiike N, Katukawa K (2001) Micro-machined gas sensor array based on metal film micro-heater. *Sens Actuators B* 79:175–181
- Montmeat P, Lalauze R, Viricelle J-P, Tornier G, Pijolat C (2002) Influence of SnO<sub>2</sub> thick film thickness on the detection properties. In: *Proceedings of Eurosensors XVI, European conference on solid-state transducers, Prague, Czech Republic, 15–18 Sept*, pp 1116–1119
- Morrison SR (1987) Mechanism of semiconductor gas sensor operation. *Sens Actuators* 11:283–287
- Moseley PT, Tofield BC (eds) (1987) *Solid state gas sensors*. Adam Hilger, Bristol
- Mukundan R, Brosha E, Brown D, Garzon F (1999) Ceria-electrolyte-based mixed potential sensors for the detection of hydrocarbons and carbon monoxide. *Electrochem Solid State Lett* 2(8):412–414
- Mukundan R, Brosha EL, Brown DR, Garzon FG (2000) A mixed-potential sensor based on a Ce<sub>0.8</sub>Gd<sub>0.2</sub>O<sub>1.9</sub> electrolyte and platinum and gold electrodes. *J Electrochem Soc* 147:1583–1588
- Nakatou M, Miura N (2005) Detection of combustible hydrogen-containing gases by using impedancemetric zirconia-based water-vapor sensor. *Solid State Ionics* 176:2511–2515
- Nielsen J, Jacobsen T (2007) Three-phase boundary dynamics at Pt/YSZ microelectrodes. *Solid State Ionics* 178:1001–1009

- O'Hayre R, Barnett D, Prinz FB (2005) The triple phase boundary: a mathematical model and experimental investigations for fuel cells. *J Electrochem Soc* 152:439–444
- Panchapakesan B, DeVoe DL, Widmaier MR, Cavicchi R, Semancik S (2001) Nanoparticle engineering and control of tin oxide microstructures for chemical microsensor applications. *Nanotechnology* 12:336–349
- Park JH, Kim KH (1999) Improvement of long-term stability in SnO<sub>2</sub>-based gas sensor for monitoring offensive odor. *Sens Actuators B* 56:50–58
- Pasierb P, Rekas M (2009) Solid-state potentiometric gas sensors—current status and future trends. *J Solid State Electrochem* 13:3–25
- Pijolat C (1986) Etudes des propriétés physico-chimiques et des propriétés électriques du dioxyde d'étain en fonction de l'atmosphère gazeuse environnante. Application à la detection sélective des gaz. PhD Thesis, De L'Institut National Polytechnique de Grenoble
- Plashnitsa VV, Ueda T, Miura N (2006) Improvement of NO<sub>2</sub> sensing performances by an additional second component to the nano-structured NiO sensing electrode of YSZ-based mixed-potential-type sensor. *Int J Appl Ceram Technol* 3:127–133
- Plashnitsa VV, Ueda T, Miura N (2007) Improvement of NO<sub>2</sub> a sensing performances by an additional second component to the nano-structured NiO sensing electrode of a YSZ-based mixed-potential-type sensor. *Int J Appl Ceram Technol* 3(2):27–133
- Plashnitsa VV, Ueda T, Elumalai P, Miura N (2008a) NO<sub>2</sub> sensing performances of planar sensor using stabilized zirconia and thin-NiO sensing electrode. *Sens Actuators B* 130:231–239
- Plashnitsa VV, Ueda T, Elumalai P, Miura N (2008b) Zirconia-based planar NO<sub>2</sub> sensor using ultrathin NiO or laminated NiO-Au sensing electrode. *Ionics* 14(1):15–25
- Plashnitsa VV, Elumalai P, Miura N (2008c) Sensitive and selective zirconia-based NO<sub>2</sub> sensor using gold nanoparticle coatings as sensing electrodes. *J Electrochem Soc* 155:301–306
- Ponomareva VG, Lavrova GV, Hairetdinov EF (1997) Hydrogen sensor based on antimonium pentoxide-phosphoric acid solid electrolyte. *Sens Actuators B* 40:95–98
- Qi Q, Zhang T, Liu L, Zheng X (2009) Synthesis and toluene sensing properties of SnO<sub>2</sub> nanofibers. *Sens Actuators B* 137:471–475
- Sakthivel M, Weppner W (2008) A portable limiting current solid-state electrochemical diffusion hole type hydrogen sensor device for biomass fuel reactors: engineering aspect. *Int J Hydrogen Energy* 33:905–911
- Saukko S, Lantto V (2003) Influence of electrode material on properties of SnO<sub>2</sub>-based gas sensor. *Thin Solid Films* 436:137–140
- Schweizer-Berberich M, Barsan N, Weimar U, Morante JR, Gopel W (1997) Electrode effects on gas sensing properties of nanocrystalline SnO<sub>2</sub> gas sensors. In: Proceedings of the 11th European conference on solid state transducers, Eurosensors XI, Warsaw, Poland, 21–24 Sept, pp 1377–1380
- Shaan NM, Yamazaki T, Kikuta T (2011) Effect of micro-electrode geometry on NO<sub>2</sub> gas-sensing characteristics of one-dimensional tin dioxide nanostructure microsensors. *Sens Actuators B* 156:784–790
- Shim Y-S, Moon HG, Kim DH, Jang HW, Kang C-Y, Yoon YS, Yoon S-J (2011) Transparent conducting oxide electrodes for novel metal oxide gas sensors. *Sens Actuators B* 160:357–363
- Sozza A, Dua C, Kerlain A, Brylinski C, Zanoni E (2004) Long-term reliability of Ti–Pt–Au metallization system for Schottky contact and first-level metallization on SiC MESFET. *Microelectron Reliab* 44:1109–1113
- Sridhar S, Stancovski V, Pal UB (1997) Effect of oxygen containing species on the impedance of the Pt/YSZ interface. *Solid State Ionics* 100:17–22
- Tamaki J, Miyaji A, Makinodan J, Ogura S, Konishi S (2005) Effect of micro-gap electrode on detection of dilute NO<sub>2</sub> using WO<sub>3</sub> thin film microsensors. *Sens Actuators B* 108:202–206
- Thiemann S, Hartung R, Wulff H, Klimke J, Mobius H-H, Guth U, Schonauer U (1996) Modified Au/YSZ electrodes—preparation, characterization and electrode behaviour at higher temperatures. *Solid State Ionics* 86–88:873–876
- Torres-Huerta AM, Vargas-Garcia JR, Dominguez-Crespo A (2007) Preparation and characterization of IrO<sub>2</sub>-YSZ nanocomposite electrodes by MOCVD. *Solid State Ionics* 178:1608–1616
- Vilanova X, Llobet E, Brezmes J, Calderer J, Correig X (1998) Numerical simulation of the electrode geometry and position effects on semiconductor gas sensor response. *Sens Actuators B* 48:425–431
- Vincenzi D, Butturi MA, Guidi V, Carotta MC, Martinelli G, Guarnieri V, Brida S, Margesin B, Giacomozzi F, Zen M, Pignatelli GU, Vasiliev AA, Pislakov AV (2001) Development of a low-power thick-film gas sensor deposited by screen-printing technique onto a micromachined hotplate. *Sens Actuators B* 77:95–99
- Vogel A, Baier G, Schule V (1993) Non-Nernstian potentiometric zirconia sensors: screening of potential working electrode materials. *Sens Actuators B* 15:147–150
- Wang J, Chen G, Wang M, Chatrathi MP (2004) Carbon nanotube/copper composite electrodes for capillary electrophoresis microchip detection of carbohydrates. *Analyst* 129(6):512–515
- Wang J, Elumalai P, Terada D, Hasei M, Miura N (2006) Mixed-potential-type zirconia-based NO<sub>x</sub> sensor using Rh-loaded NiO sensing electrode operating at high temperatures. *Solid State Ionics* 177:2305–2311

- Wang X, Huang H, Holme T, Tian X, Prinz FB (2008) Thermal stabilities of nanoporous metallic electrodes at elevated temperatures. *J Power Sources* 175(1):75–81
- Westphal D, Jakobs S, Guth U (2001) Gold-composite electrodes for hydrocarbon sensors based on YSZ solid electrolyte. *Ionics* 7:182–186
- Williams DE (1999) Semiconducting oxides as gas-sensitive resistors. *Sens Actuators B* 57:1–16
- Wu N, Zhao M, Zheng JG, Jiang C, Myers B, Le S, Chyu M, Mao SX (2005) Porous CuO-ZnO nanocomposite for sensing electrode of high-temperature CO solid-state electrochemical sensor. *Nanotechnology* 16(12):2878–2881
- Yamazoe N, Kurokawa Y, Seiyama T (1983) Effects of additives on semiconductor gas sensors. *Sens Actuators* 4:283–289
- Ylinampa A, Lantto V, Leppavuori S (1993) Some differences between Au and Pt electrodes in SnO<sub>2</sub> thick-film gas sensors. *Sens Actuators B* 13–14:602–604
- Yong YK, Patel M, Vig J, Ballato A (2009) Effects of electromagnetic radiation on the Q of quartz resonators. *IEEE Trans Ultrason Ferroelectr Freq Control* 56:353–360
- Yoon JW, Grilli ML, Bartolomeo ED, Polini R, Traversa E (2001) The NO<sub>2</sub> response of solid electrolyte sensors made using nano-sized LaFeO<sub>3</sub> electrodes. *Sens Actuators B* 76:483–488
- Yoon SP, Nam SW, Kim SG, Hong SA, Hyun SH (2003) Characteristics of cathodic polarization at Pt/YSZ interface without the effect of electrode microstructure. *J Power Sources* 115:27–34
- Yoon SP, Nam SW, Han J, Lim TH, Hong SA, Hyun SH (2004) Effect of electrode microstructure on gas-phase diffusion in solid oxide fuel cells. *Solid State Ionics* 166:1–11
- Zhuyikov S (2007) *Electrochemistry of zirconia gas sensors*. CRC, Boca Raton, FL
- Zhuyikov S, Miura N (2005) Solid-state electrochemical gas sensors for emission control. In: Sorrell CC, Sugihara S, Nowotny J (eds) *Materials for energy conversion devices*. Woodhead Publishing, Cambridge, pp 303–335, Ch. 12
- Zhuyikov S, Miura N (2007) Development of zirconia-based potentiometric NO<sub>x</sub> sensors for automotive and energy industries in the early 21st century: what are the prospects for sensors? *Sens Actuators B* 121:639–651
- Zosel J, Westphal D, Jakobs S, Müller R, Guth Y (2002) Au-oxide composites as HC-sensitive electrode material for mixed potential gas sensors. *Solid State Ionics* 152–153:525–529
- Zosel J, Müller R, Vashook V, Guth U (2004a) Response behavior of perovskites and Au/oxide composites as HC-electrodes in different combustibles. *Solid State Ionics* 175:531–533
- Zosel J, Ahlborn K, Müller R, Westphal D, Vashook V, Guth U (2004b) Selectivity of HC-sensitive electrode materials for mixed potential gas sensors. *Solid State Ionics* 169:115–119
- Zosel J, Schiffel G, Gerlach F, Ahlborn K, Sasum U, Vashook V, Guth U (2006) Electrode materials for potentiometric hydrogen sensors. *Solid State Ionics* 177:2301–2304
- Zosel J, Tuchtenhagen D, Ahlborn K, Guth U (2008) Mixed potential gas sensor with short response time. *Sens Actuators B* 130:326–329

# Chapter 10

## Surface Modifiers for Metal Oxides in Conductometric Gas Sensors

### 10.1 General Consideration

The gas-sensing effect is usually a surface phenomenon, i.e., changes in the concentration of conduction electrons in metal oxides and semiconductors result from surface chemical reactions, such as chemisorption, reduction/reoxidation (“redox”), and/or catalysis, which take place during interaction with surrounding gas (Gentry and Jones 1986; Kohl 1989). Both experimental and theoretical studies have demonstrated that various surface sites participate in combustion, electrical response, and interactions with water vapor and adsorbed species. Different gases interact differently with different surface sites as well. For example, as an explanation of SnO<sub>2</sub> gas response to methane, Williams and Pratt (1998) proposed that four different types of reactive surface sites may participate in gas-sensing effects on polycrystalline SnO<sub>2</sub>: the electrically neutral oxygen, which catalyzes methane; two electrically charged oxygen states, which respectively mediate methane response and dissociative water chemisorption; and a site where molecular chemisorption of water occurs. Williams and Pratt (2000) believed that the neutral site could be attributed to a coordinately unsaturated lattice oxygen. The two different electrically charged sites could be associated with oxygen adsorbed on or at two different types of surface vacancy associated with reduced (Sn<sup>2+</sup>) surface cations. All these surface sites are related directly to the surface stoichiometry of metal oxides, and thus it is clear that surface modification, i.e., surface engineering, is a powerful instrument for control of sensor response. Effects which can be achieved due to surface modification by various additives are shown in Table 10.1.

Any method of influencing the surface state can be used to modify the metal oxide or semiconductor surface, including (Wada and Egashira 1998; Kiv et al. 2001; Kim et al. 2002; Zhang et al. 2003): (1) oxygen plasma treatment; (2) UV irradiation; (3) treatment with various chemical reagents; (4) low-energy ion irradiation, and so on. As a result of such treatments, the surface stoichiometry, work function, binding energy of atoms, concentration of carbon contaminants, chemical activity of surface, and so on can all be changed. However, in spite of the availability of numerous methods by which to influence the surface state, surface modification of metal oxides and semiconductors by catalytically active atoms remains the most used method to improve gas sensor performances. The appearance of catalysts on the surface of metal oxides and semiconductors can accelerate surface reactions and increase sensitivity.

It is clear that the catalyst chosen influences the selectivity of the sensor. The ideal case is that the catalyst catalyzes the oxidation of the gas of interest but not that of any of the other gases. Unfortunately, these cases are not easy to find. Experience has shown that noble metals such as Pt, Pd, Au, Ag, Ru, and Rh and transition metals such as Fe, Cu, Ni, and Co are the most widely used surface modifiers (Yamazoe 1991; Yamazoe et al. 1983; Shimizu et al. 1998; Kolmakov et al. 2008). For their deposition



**Table 10.1** Influence of surface doping on gas-sensing characteristics of SnO<sub>2</sub> and In<sub>2</sub>O<sub>3</sub> sensors

Surface additive	Effect	Role of additive
Noble metals (Pd, Pt, Au, Rh) (thickness $d < 10$ nm)	Increases sensor response to reducing gases Decreases operating temperature Decreases response time	Catalyst
Noble metals (Pd, Pt, Au, Rh) (thickness $d > 10$ nm)	Improves selectivity	Catalytically active membrane
Al <sub>2</sub> O <sub>3</sub> , SiO <sub>2</sub>	Improves selectivity Increases response to H <sub>2</sub>	Passive membrane
Oxides of transition metals (thickness $d < 10$ nm)	Improves sensitivity and selectivity	Catalyst
Oxides of transition metals (thickness $d > 20$ nm)	Improves selectivity	Catalytically active membrane

**Table 10.2** Precursors for surface modification by selected metals and their oxides

Additive	Precursors
Au	HAuCl <sub>4</sub> · 4H <sub>2</sub> O
Ag(Ag <sub>2</sub> O)	AgNO <sub>3</sub> ; Ag(acac)
Pd(PdO)	PdCl <sub>2</sub> ; Pd(acac) <sub>2</sub> ; Pd(NH <sub>3</sub> ) <sub>4</sub> ; Pd(NO <sub>3</sub> ) <sub>2</sub>
Pt	PtCl <sub>2</sub> ; H <sub>2</sub> PtCl <sub>6</sub> · 6H <sub>2</sub> O; (CH <sub>3</sub> ) <sub>3</sub> (CH <sub>3</sub> C <sub>5</sub> H <sub>4</sub> )Pt; (NH <sub>4</sub> ) <sub>2</sub> PtCl <sub>4</sub>
Cu(CuO)	Cu(NO <sub>3</sub> ) <sub>2</sub> ; Cu(acac) <sub>2</sub>
Ni(NiO)	NiCl <sub>2</sub> ; Ni(NO <sub>3</sub> ) <sub>2</sub>
Rh(Rh <sub>2</sub> O <sub>3</sub> )	RhCl <sub>3</sub> · 3H <sub>2</sub> O
Ru(RuO)	RuCl <sub>3</sub>
Co(Co <sub>2</sub> O <sub>3</sub> )	Co(acac) <sub>2</sub>
Fe(Fe <sub>2</sub> O <sub>3</sub> )	FeCl <sub>3</sub> ; Fe(NO <sub>3</sub> ) <sub>3</sub>
Si(SiO <sub>2</sub> )	Diethoxydimethylsilane (DMES)
Al <sub>2</sub> O <sub>3</sub>	Al(acac)

one can use any method from thermal vacuum evaporation to chemical vapor deposition and electroless deposition. The choice of method will be determined by the objects being subjected to surface modification, the materials used, and the requirements for surface additives. For example, Diaz et al. (2002) established that for surface modification of powders by noble metals, the most appropriate technique is to use both impregnation and an electroless method able to provide uniform covering of the powder from every side. Precursors which can be used for these purposes are presented in Table 10.2. It is necessary to underline that, independent of the method used for surface modification (impregnation, electroless, vacuum evaporation, spraying, etc.), after deposition of noble metals it is necessary to carry out subsequent annealing in the temperature range 300–600 °C (Zhang and Colbow 1997). This annealing promotes the formation of metallic clusters, improves the homogeneity of their distribution across the layer thickness, and stabilizes the properties of the gas-sensing matrix. However, the temperature should not be too high. This is important for achieving a high sensor response. High-temperature treatment sufficient to cause agglomeration of catalyst particles resulted in the loss of any optimizing effect.

Table 10.3 summarizes the effects which can be obtained using these additives for modification of the SnO<sub>2</sub> surface. The same effects were observed for other metal oxides. For example, Penza et al. (1998) have shown that sensitivity and selectivity to reducing gases can be significantly improved by adding thin layers of noble metals such as palladium, platinum, and gold to the surface of WO<sub>3</sub> films operating at low temperatures. Maekawa et al. (1992) have shown that surface modification by Au improves

**Table 10.3** Influence of surface modification of metal oxides (SnO<sub>2</sub>) on sensitivity and selectivity of gas response

Additive	Improved sensor response and selectivity to the following gases and vapors	Reference
Pd	CO, H <sub>2</sub> , CH <sub>4</sub>	Cabot et al. (2002)
Pt	CO, H <sub>2</sub>	Cabot et al. (2002)
Au	CO	
Ru	Hydrocarbons, H <sub>2</sub>	Chaudhary et al. (1998a)
Ag	H <sub>2</sub> , H <sub>2</sub> S	Tong et al. (2000)
Fe(Fe <sub>2</sub> O <sub>3</sub> )	Alcohol	Ivanovskaya (2000)
Pt/La(La <sub>2</sub> O <sub>3</sub> )	Ethanol	Yamazoe (1991)
Pd/La(La <sub>2</sub> O <sub>3</sub> )	Ethanol	Yamazoe (1991)
Cu(CuO)	H <sub>2</sub> S	Yamazoe (1991)
Ru/Pd	H <sub>2</sub>	Chaudhary et al. (1998b)
Co	CO	Yamaura et al. (2000)
Au/La(La <sub>2</sub> O <sub>3</sub> )	CO	
Pt/SiO <sub>2</sub>	NO	Benard et al. (2005)
Co/Au	CO	Yamaura et al. (2000)
Co, Fe	O <sub>3</sub>	Takada et al. (1993)

sensitivity to NH<sub>3</sub> of WO<sub>3</sub>-based sensors as well. Other studies have shown that Au, Pd, and Pt, when deposited on transition metal oxides, have important applications in the catalytic oxidation of CO to CO<sub>2</sub> at room temperature and function as selective gas sensors for CO and H<sub>2</sub>S (Lin et al. 1994; Haruta 1997). Boccuzzi and Guglielminotti (1994) found that TiO<sub>2</sub> modified by Ru had improved sensitivity to NH<sub>3</sub>.

It was established that nanoscaled particles of noble metals (Pd, Rh, Pt, Au, Ag) and oxides of other elements (Co, Fe, Zn, B, Se, Cu, etc.) that are deposited on the surface of metal oxides can act as surface sites for adsorbates, catalysts, or promoters for surface reactions and as elements promoting improvement in the thermal stability of the film nanostructure. By definition the catalyst increases the chemical reaction without itself changing. It does not change the free energy of the reaction but lowers the activation energy (Gentry and Jones 1986). Noble metals are classical examples of catalysts. The heat of adsorption of oxygen on the noble metals is sufficiently low to allow relatively low activation energy of oxidation and consequently rapid rate of reaction. For example, Pt can be considered as the catalyst in the oxidation of hydrogen. The Pt effectively dissociates the hydrogen molecule and presents the hydrogen in the active form. Thus, the overall reaction has very low activation energy and can proceed at relatively low temperatures. If the sensor depends on such a reaction, the catalyst will lower the response time. In addition Pt, Pd, and Rh have the highest activity to oxidation of combustible gases. Ruthenium is one of the most active of the precious metals in the reactions involving nitrogen containing molecules (King and Woodruff 1982). Gold nanosize clusters are good catalysts for CO oxidation (Valden et al. 1998a, b). A promoter is a second additive, one that improves the catalyst's performance (Gentry and Jones 1986). The obvious mechanisms for promoting action are stabilizing the surface so the reaction cannot irreversibly change the surface, inducing phase changes in the catalyst so that it provides a more active phase, stabilizing the surface area, or stabilizing the favorable valence state. Promoters are particularly important with metal oxide catalysts, where they increase the number of suitable donor or acceptor species involved in the electron transfer processes. Where promoters can enhance the rate of reaction of one species relative to another, they can have a marked effect on catalyst selectivity. Surface additives can also act as inhibitors or activators of the surface reactions. They can provide adsorption sites and surface electronic states which can mediate the electronic transfer processes (Morrison 1986; Williams and Pratt 2000; Barsan et al. 1999; Williams 1999). As a result, the parameters of gas sensors such as sensor response, rate of response, and selectivity can be dramatically improved (McAleer et al. 1988; Cabot et al. 2000; Brinzari et al. 2002; Korotcenkov et al. 2003a, b, 2004) (see Fig. 10.1).

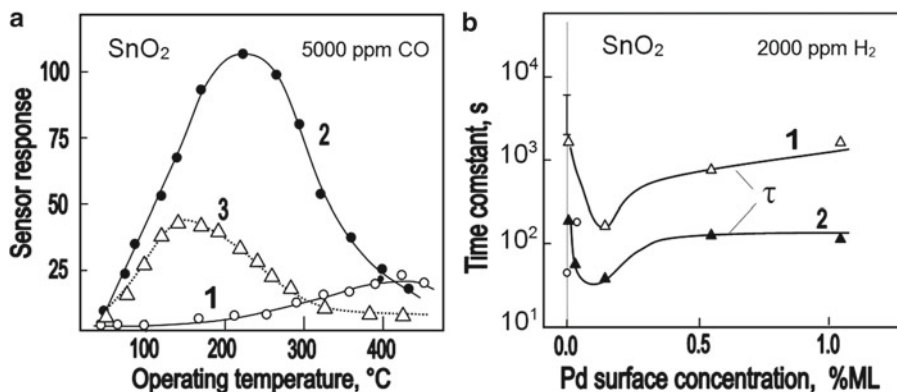
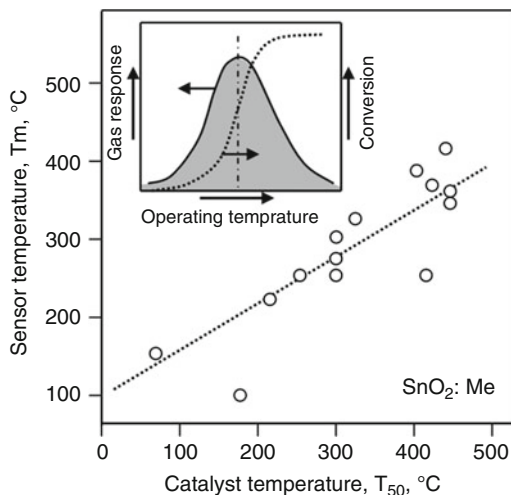


**Fig. 10.1** Influence of Pd surface additives on (a) temperature dependencies and (b) response times of SnO<sub>2</sub>:Pd thin film gas response. Pd was deposited by spray pyrolysis: 1—initial SnO<sub>2</sub>; 2—0.12% ML; 3—1.1% ML (Reprinted from Korotcenkov et al. (2003b). Copyright 2003 Elsevier)

**Fig. 10.2** Correlation between catalysis temperature of 50% conversion ( $T_{50}$ ) and temperature of SnO<sub>2</sub> gas response maximum ( $T_m$ ).



A shift of sensor response maximum in the range of low operating temperatures during surface modification by noble metals also takes place (see Fig. 10.1). For example, in experiments with SnO<sub>2</sub> films modified with Pd, this shift reached 100–200 °C (Korotcenkov et al. 2001, 2003b; Brinzari et al. 2002). It should be noted that, as a rule, a position of maximum of sensor response on temperature dependence  $S(T_{oper})$  coincides with temperature, corresponding to 50% conversion of detected gas (see Fig. 10.2) (Yamazoe et al. 1983; Cabot et al. 2002). This means that the temperature of maximum sensitivity is determined by effectiveness of catalytic reactions with detected gas participation, taking place at the surface of the gas sensing material, i.e., by the catalyst present at the surface of metal oxide.

## 10.2 Sensitization Mechanisms

At present, two types of sensitization mechanisms—“chemical” and “electronic”—are the most accepted ones (Matsushima et al. 1988; McAleer et al. 1988; Brinzari et al. 2002; Kolmakov et al. 2008). The first mechanism corresponds to “spillover” of dissociated products from the

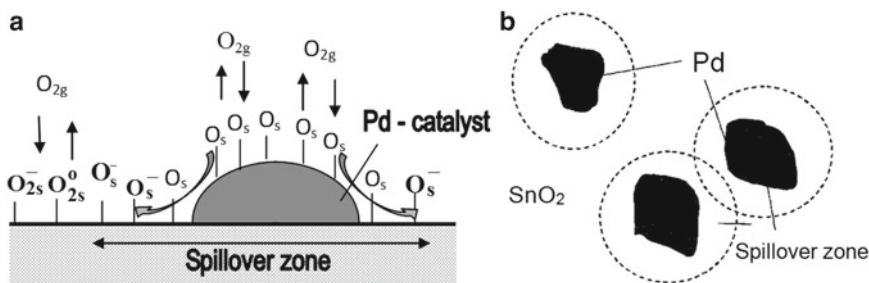


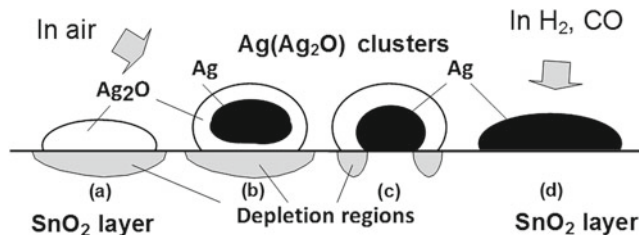
**Fig. 10.3** (a) Illustration of Pd influence on adsorbed species on the  $\text{SnO}_2$  surface; (b) spillover zones on the surface of  $\text{SnO}_2$  modified by Pd nanoclusters [(a) Reprinted with permission from Korotcenkov (2005) and Korotcenkov et al. (2003b). Copyright 2003 and 2005 Elsevier]

metal clusters out to the solid surface (see Fig. 10.3). This effect is quite popular in literature devoted to catalysis and is considered to occur mainly during early stages of gas sensor development. The gas molecules adsorbed at the metal cluster are excited and dissociate (Kohl 1990) and then migrate to the MOX surface. When a reducing gas is adsorbed, these ions may interact with adsorbed or lattice surface oxygen and modulate the semiconductor conductance. Thus, the promoter activates a test gas to facilitate its catalytic oxidation on the semiconductor surface. In other words, the promoter does not affect the resistance of the element directly, leaving the gas-sensing mechanism essentially the same as in the case without it. The promoter increases the gas sensitivity, as it increases the rate of the chemical processes, leading to a decrease in the concentration of the negatively charged adsorbed oxygen. In this case, the important factor is the electronegativity of the metal, which is a measure of electron attraction by the atoms (de Fressart et al. 1982). If the gas adsorption or dissociation manages the surface reaction kinetics and change of the MOX conductance, then the gas response of this sensor correlates with the electronegativity (Ionescu and Vancu 1994). The spillover effect explains the decrease in operating temperature in gas-sensing layers doped with catalytic metals. The chemical mechanism of sensitization is usually applied to explain the behavior of metal oxides ( $\text{SnO}_2$ ) modified with Pt (Kohl 1990; Ionescu et al. 1994). It was found that part of the Pt remains in a metallic state in air, not only providing catalytic adsorption sites for oxygen but also helping activated oxygen species to spin over onto the metal oxide surface where they get ionosorbed by trapping electrons from the metal oxide. For comparison, Pd forms a stable compound with oxygen at the temperatures used in gas sensing (Yamazoe 1991).

We note in passing that for dissociation of many gases the adsorption of molecules from the gas phase directly upon the surface of catalyst nanoparticles is not necessary. Tsu and Boudart (1961) and others (Henry et al. 1991; Bowker 1996) showed that the molecules can first adsorb onto the oxide support and diffuse to a catalyst particle. This means that the effective capture radius of a catalyst nanoparticle (Pd, Pt, etc.) can be much greater than the nanoparticle's physical radius. As with the "spillover" zones, the molecule-collection zones (Tsu and Boudart 1961) overlap when the coverage of catalyst nanoparticles exceeds some threshold value, effectively converting the entire surface of the nanostructure into a molecular delivery system for the metal catalyst nanoparticles. This so-called back-spillover effect further increases the likelihood of molecular dissociation and ionosorption on the metal oxide surface.

The "electronic" mechanism at the contact between the metal and the semiconducting oxide is due to direct electronic interaction between the metal additive and the semiconductor surface (Norris 1987). In this case there is no mass transfer between the foreign particles and the semiconductor. Instead, there is an electronic interaction between them, through the space charge created in

**Fig. 10.4** Schematic diagram of changes taken place at the interface Ag–SnO<sub>2</sub> under influence of reducing gases (Reprinted with permission from Korotcenkov et al. (2012). Copyright 2012 Elsevier)



the semiconductor by the presence of the surface clusters (see Fig. 10.4). Additives at the surface of the metal oxides act as “receptors,” while the semiconductor oxide acts as a “transducer” of the changes taking place at the surface under gas adsorption. If the metal is well dispersed over the oxide surface, the local surface change regions (SCRs) underlying each metal cluster may join together, and the surface position of the Fermi level will depend entirely on the catalyst state (Sukharev et al. 1993; Tofield 1988). The change at the catalyst surface upon interaction with a reducing gas makes a difference in the electronic exchange between the surface and the bulk of the oxide support, which results in a change in its conductance (Ioannides and Verykios 1996). This type of sensitization has been proposed for SnO<sub>2</sub> elements modified with Ag, Pd, Ni, and Cu, which form stable metal oxides when they are exposed to air (Yamazoe et al. 1983; Kolmakov et al. 2008). If a Schottky barrier appears, the gas sensitivity of the doped MOX may correlate with the work function of the metal (Vlachos et al. 1996). If so, the size of the metal clusters is of great importance. If the metal is rather thick, surface processes do not influence the bulk, and the height of the potential Schottky barrier is not changed (Madou and Morrison 1989). Therefore, the metal catalyst should be configured to be thinner to allow effective use of the potential barrier modulation due to the surface processes. Experimental evidence of the catalyst layer thickness affecting the gas sensitivity of SnO<sub>2</sub>:Ag has been reported by Zhang and Colbow (1997).

In addition to the two mechanisms considered so far, Papadopoulos and Avaritsiotis (1995) suggested that the appearance of surface conductance over an MOX doped with surface metal clusters is due to electron tunneling between the clusters (for the example of SnO<sub>2</sub>:Pd, SnO<sub>2</sub>:Pt systems exposed to CO). In this case, the gas sensitivity is caused by this surface conductance, and the bulk properties of the materials play only a minor role. Moreover, in some systems, such as SnO<sub>2</sub>:Ag, it is possible to observe mobile metal clusters which migrate under high operating temperatures over the oxide surface and change its conductivity (Sears and Love 1993; Zhang et al. 1993). Therefore, when analyzing the properties of surface-modified MOX gas sensors, experiments should be considered to compare the contributions from different mechanisms, because all the above mechanisms can actually be present at the same time.

Experiment has shown that the nature of the surface modifiers and their electronic state are the main determining factors in promoting gas sensor sensitivity and selectivity. For example, it was found that, depending on the metal deposited, the loading method, and the interacting gas, surface clusters may be in metallic or oxidized forms, which have different catalytic activities and therefore different influences on sensing characteristics (Kohl 1990). In particular, it was found that electronic interactions actually appear between Ag, Pd, and Cu in oxide form and SnO<sub>2</sub> and disappear when these oxides are converted to metals. This means that the mechanism of sensitization is dependent on the operating temperature. For example, Kohl (1990) believed that at low operating temperatures (around 100 °C) the influence of Pd on SnO<sub>2</sub> could follow the electronic mechanism, while higher temperatures facilitate the domination of chemical mechanisms. Kolmakov et al. (2008) also believe that during surface modification by Pd we need to take into

account spillover and back spillover processes, which have catalytic natures. In addition, it was shown that, for a given additive, its distribution both over the support surface and in the film also have important effects on the device response, in addition to that arising from the nature of the catalytic material itself.

### 10.3 Bimetallic Catalysts

When choosing additives it is also necessary to remember that high catalytic activity of additives is an essential, but insufficient, requirement. To achieve high sensor response, the method of surface modification should create optimal conditions for both electron and ion (spillover) exchange between the surface nanoclusters and the metal oxide support. Only in this case will catalytic reaction on the surface of the additives be accompanied by a change in film electroconductivity, which is controlled in metal oxide films during gas detection. For example, research (Tsud et al. 2001; Skala et al. 2003; Nehasil et al. 2003) has shown that, in the system of either Pd(Rh)-SnO<sub>2</sub> or Pd(Rh)-In<sub>2</sub>O<sub>3</sub>, the formation of alloys of the noble metal-Sn(In) may promote an improvement of both electron and ion exchange between the nanoclusters of the noble metal and the metal oxide support. In particular, a decrease of CO desorption energy from the SnO<sub>2</sub>:Rh surface after Rh-Sn alloy formation has been observed (Tsud et al. 2001; Skala et al. 2003; Nehasil et al. 2003). According to Tsud et al. (2001), specific properties of such alloys (Pd-Sn) were provided by the strong interaction between Pd and Sn through the hybridization of Pd *d* and Sn *s* states, leading to the formation of a Pd-Sn alloy with a noble metal-like electronic structure.

This effect is apparently normal for bimetallic catalysts. For example, Rodriguez (1996), analyzing the interaction of Co with Pd-based bimetallic catalysts, established that bimetallic surfaces have lower CO desorption temperature than Pd (see Table 10.4).

It is important to emphasize that the use of alloys of palladium for surface modification is the most promising direction of surface modification of sensitive materials. For example, Chaudhary et al. (1998b) have shown that alloys of Ru/Pd really are much more effective surface catalysts than the same metals alone for attaining the required selectivity of gas sensors. It was established that, by using alloys of Ru/Pd, it is possible to achieve a considerably greater increase of sensitivity and selectivity for hydrogen detection with sensors based on tin oxide than with sensors modified using Ru or Pd metal (1–2 wt%) separately (Chaudhary et al. 1999). The optimum seems to be at a ratio Ru/Pd » 1.28.

One may judge the effectiveness of such modification by studying the results given in Table 10.5. The tested ceramic sensors were fabricated using sol-gel technology. Ru and Pd were deposited on the surface of SnO<sub>2</sub> powders from millimolar RuCl<sub>3</sub> and PdCl<sub>2</sub> aqueous solutions using techniques described by Chaudhary et al. (1997). These techniques included dipping for 5 h, drying, and then heating at 350 °C for 2 h. The selectivity was calculated as the ratio  $S(\text{H}_2)/S(\text{gas})$ .

A considerable increase of the promotion effect was also observed using a Co/Au alloy. Studying the influence of additives on gas-sensing characteristics of In<sub>2</sub>O<sub>3</sub>-based sensors, Yamaura et al. (2000) established that a binary catalyst consisting of 0.5 wt% Co and 0.04 wt% Au gave dramatically improved sensitivity and selectivity to CO detection (see Table 10.6).

It should be noted that bimetallic catalysts that contain Group 10 metals such as Pt, Pd, or Ni are ideal catalysts for many applications: isomerization of hydrocarbons, olefin hydrogenation, CO oxidation, alcohol synthesis, etc. With an overlayer of Group 10 metals, there is very good correlation between the changes in the electronic and chemical properties induced by bimetallic bonding (Rodriguez 1996). Comparing the behavior of Pt, Pd, and Ni, it was found that among the Group 10 metals, Pd showed the strongest effects, while Ni exhibited the weakest (Ni < Pt < Pd). For these

**Table 10.4** Effects of bimetallic bonding on properties of Pd

Bimetallic catalyst	CO desorption temperature (K)	Shift in Pd( $3d_{5/2}$ ) binding energy (eV)
Pd(100)	480	0.00
Pd/Re	370	0.65
Pd/Ru	335	0.30
Pd/Mo	320	0.90
Pd/W	300	0.85
Pd/Cu	280	0.60
Pd/Zn	250	0.70
Pd/Ta	245	0.90

Source: Data from Benard et al. (2005)

**Table 10.5** Influence of surface modification with Ru/Pd (Ru/Pd 1.28) alloy on sensitivity and selectivity of H<sub>2</sub> detection by SnO<sub>2</sub>-based gas sensors

Gases and vapors, 1,000 ppm ( $T_{oper} = 250$ °C)	Pure SnO <sub>2</sub>		SnO <sub>2</sub> modified with Ru/Pd	
	Sensitivity	Selectivity (H <sub>2</sub> )	Sensitivity	Selectivity (H <sub>2</sub> )
Hydrogen	7.6	1.0	1,350	1.0
LPG	3.0	0.39	375	0.28
Ammonia	0.12	0.02	0.14	0.0001
Nitrogen dioxide	0.40	0.05	0.24	0.0002
Alcohol	6.5	0.86	20.50	0.015
Carbon monoxide	4.0	0.53	0.08	0.00006

Source: Data from Chaudhary et al. (1997)

**Table 10.6** Gas response of In<sub>2</sub>O<sub>3</sub>-based sensors modified with Co and Co/Au

Material	Sensor response ( $T_{oper} = 250$ °C; 1,000 ppm)		
	CO	H <sub>2</sub>	S(CO)/S(H <sub>2</sub> )
Undoped In <sub>2</sub> O <sub>3</sub>	7	4	1.5–2.0
In <sub>2</sub> O <sub>3</sub> :Co (0.5 wt%)	50–60	6–10	5–10
In <sub>2</sub> O <sub>3</sub> :Co/Au	160	4–6	25–40

Source: Data from Yamaura et al. (2000)

admetals, the magnitude of the electronic and chemical changes increased when the fraction of empty states in the valence band of the metal substrate rose.

However, at present the phenomena responsible for the catalytic behavior of these bimetallic systems are not fully understood. Rodriguez (1996) gave the following explanation of the properties of bimetallic catalysts. A Group 10 adatom in contact with the surface of an *s*, *p*, or early transition metal exhibits large perturbations in its electronic and chemical properties. In this type of system there is an important redistribution of charge that shifts *d* electrons from around the Group 10 metal to the interface region between the admetal and the substrate, producing an accumulation of electrons around the bimetallic bonds. This redistribution of charge affects the stability of the core levels and the valence *d* band of the Group 10 metal. The larger the movement of *d* electrons from the Group 10 metal toward the admetal–substrate interface, the stronger the bimetallic bond, and the lower the ability of the Group 10 metal to bond CO through  $\pi$  back-donation.

## 10.4 Approaches to Noble Metal Cluster Forming

Experiment has shown that the main attention during surface modification by various catalysts should be focused on the influence of dimensional effects, such as the size of surface clusters and the average distance between them. Even during early studies of semiconductor gas sensors, it was noted (Kanazawa et al. 2001) that the kind of catalyst distribution, both throughout the device and in terms of catalyst particle size, has an important influence on sensor response in addition to that arising from the nature of the catalyst material itself. For example, it was established by McAleer et al. (1988) that, to achieve optimal effect, the cluster size for many surface catalysts should not exceed 1–10 nm. For example, according to Valden et al. (1998a, b), for high catalytic activity Au clusters should have a size of ~3 nm (see Fig. 10.5a). Bulk Au is of course a noble metal. Valden et al. (1998b), however, found that Au nanocrystals supported on a titania surface show a marked size effect in their catalytic ability for CO oxidation reaction, with Au nanoparticles in the region of 3.5 nm exhibiting the maximum chemical reactivity. A metal-to-nonmetal transition was observed as the cluster size is decreased to below 3.5 nm<sup>3</sup> (consisting of ~300 atoms). This result is quite similar to that obtained with Pd particles supported on an oxide substrate (Xu et al. 1997). In another study of Au particles supported on a zinc oxide surface, smaller particles (<5 nm) exhibited a marked tendency to adsorb CO, while those with diameters above 10 nm did not significantly adsorb CO (Vinod et al. 2003). Sanchez et al. (1999) have found that small Au clusters (Au<sub>n</sub>, n < 20) exhibit size-dependent catalytic activity above a nuclearity of 8 (see Fig. 10.6). The increased activity of these metal particles is attributed to the charge transfer between the oxide support and the particle surface. It is possible that defects on the oxide surface also play a role in determining the catalytic activity of the nanocrystals.

For other metals, optimal sizes, of course, will differ (see Fig. 10.5b). According to some estimates (Brinzari et al. 2002; Korotcenkov et al. 2003b), an optimal distance between clusters approximately equals the oxygen surface diffusion length at the operating temperature (spillover zone). Research on the Pd–SnO<sub>2</sub> system showed that, as a rule, these conditions are reached at an average surface concentration of noble metals of ~1% of the monolayer (Brinzari et al. 2002; Korotcenkov et al. 2003b). Apparently, at that concentration an optimal covering of spillover zones around noble metal clusters was attained (see Fig. 10.3). Simple calculations showed that at such a degree of coverage, the average distance between clusters with sizes from 1 to 5 nm may change from 6 to 12 nm, correspondingly. According to scanning tunneling microscopy studies carried out by Bennett et al. (1999), the size of the spillover zone for oxygen around Pd nanoparticles on a TiO<sub>2</sub> (110) surface can be varied from ~10 nm to several tenths of a nanometer in diameter depending on particle size and experimental conditions. This implies that at

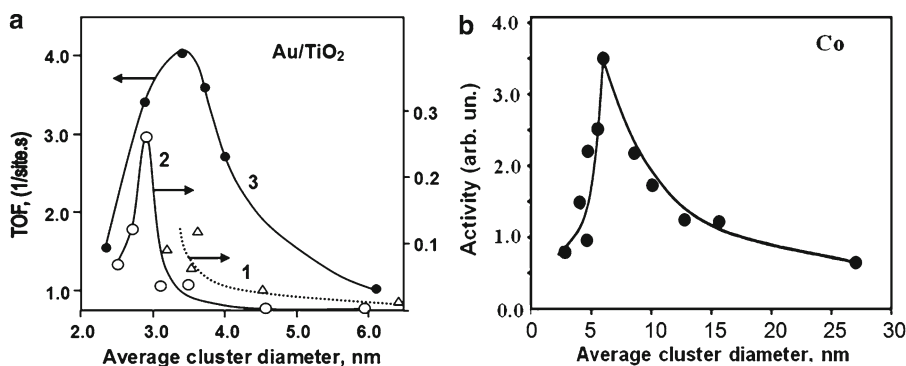
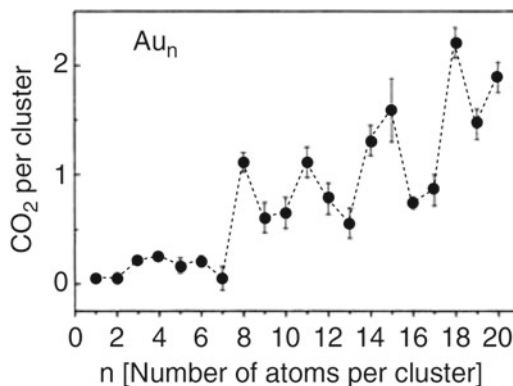


**Fig. 10.5** (a) Specific activity for CO conversion as a function of average Au cluster diameter on Au/TiO<sub>2</sub> at (1, 2) 300 K and (3) 350 K. The activity is expressed as the specific reaction rate ((product molecules) × (surface site)<sup>-1</sup> × s<sup>-1</sup>) or turnover frequency (TOF). The number of surface sites was computed using cluster morphology determined by STM.  $P_{\text{total}} = 40$  Torr, CO/O<sub>2</sub> = 1/5. [Data from (1) Valden et al. (1998a), (2) Valden et al. (1998b), and (3) Haruta (1997)]. (b) Influence of cobalt particle size on activity in the Fischer-Tropsch reaction normalized to the cobalt loading (220 °C) (Reprinted with permission from Bezemer et al. (2006). Copyright 2006 American Chemical Society)



**Fig. 10.6** Plot of the number of catalytically produced  $\text{CO}_2$  molecules against the nuclearity of Au clusters supported on a defect-rich  $\text{MgO}(100)$  surface. The  $\text{CO}_2$  molecules produced by oxidation of CO are studied by means of temperature programmed desorption mass spectrometry (Reproduced with permission from Sanchez et al. (1999). Copyright 1999 American Chemical Society)



particle coverages of  $\sim 10^{12} \text{ cm}^{-2}$  the spillover zones overlap, thereby effectively covering the entire nanostructure surface continuously, leading to the observed saturation in chemical reactivity of the functionalized nanowires beyond a certain Pd particle density. These estimations show that the amount and distribution of the metallic nanoparticles in a metal oxide matrix is an important parameter to be controlled in order to obtain the highest gas sensing sensitivity. In particular, the distribution of these small dopant particles on the surface is assumed to be more or less homogeneous. High dispersion of the bulk catalyst over the semiconductor support is also essential to obtain a good performance of gas sensors.

Attempts to evaluate the size of Pd particles on the surface of  $\text{SnO}_2$  films deposited by spray pyrolysis were made by Veltruska et al. (2001), but they were successful only for films with a coverage level over 18%. According to estimates made by Veltruska et al. (2001), the Pd grew three dimensionally; the average size of a Pd cluster was  $\sim 3.5 \text{ nm}$  for  $\sim 18\%$  Pd coverage and  $\sim 4.0 \text{ nm}$  for  $\sim 30\%$  Pd coverage. Later, Tsud et al. (2001) confirmed this estimate. The results of this research showed that with a small amount of deposited Pd, equivalent to one monolayer (ML), Pd forms an atomically dispersed layer on the  $\text{SnO}_2$  surface, and only higher quantities, several ML of Pd, led to the formation of three-dimensional Pd particles, which had mixed metallic and Pd–Sn bimetallic character. Taking into account the results presented in Fig. 10.3, one can conclude that to achieve the maximum sensitivity of  $\text{SnO}_2$ :Pd sensors, Pd should have strong dispersion, i.e., the size of the Pd clusters should be minimal. Results reported by Seal and Shukla (2002) (see Fig. 10.7) confirm this conclusion.

The initial structure of modified grains should be taken into account when evaluating the influence of surface modification on gas-sensing properties as well. Recent work has provided a direct experimental confirmation that noble metal clusters accumulate at step edges of metal oxides (El-Azab et al. 2002). Due to this behavior of noble metals, an increase of terrace area should be accompanied by an increase in the size of clusters, which can be accumulated at step edges of the terrace. This means that for the same degree of surface coverage by noble metals, the number of clusters will be smaller, while the distance between the clusters will be greater on the surface that has the larger terrace area. Illustration of this process is presented in Fig. 10.8. It follows from this that the appearance of extended, atomically flat surface planes facilitates the process of cluster formation. At the same time, the presence of atomically step-like surfaces in the case of small nanograins leads to a high probability of the conditions for atomic dispersion of palladium being provided. Results obtained during  $\text{SnO}_2$  surface modification by Pd have confirmed this conclusion. Optimal influence of Pd on gas-sensing characteristics of  $\text{SnO}_2$  films containing small grains (spherulites) was observed at considerably lower Pd concentration than for larger crystallites with clearly visible faceting.

**Fig. 10.7** The variation in the sensitivity of semiconductor  $\text{SnO}_2$  gas sensor as a function of PdO particle size, which is present on the  $\text{SnO}_2$  particle surface as a surface modifier (From Seal and Shukla (2002). Copyright 2002 The Minerals, Metals and Materials Society)

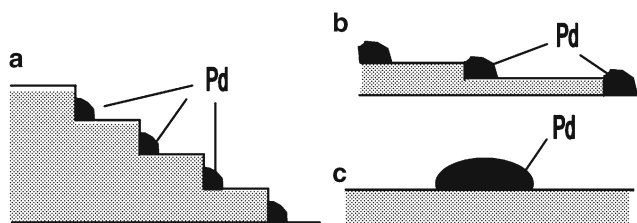
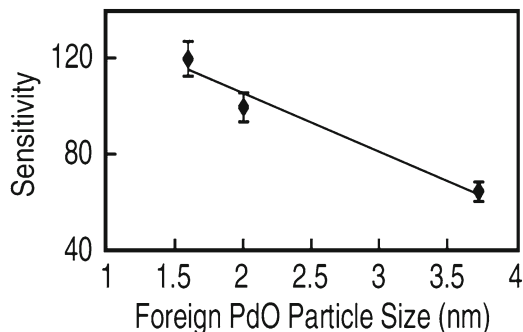


**Fig. 10.8** Influence of surface morphology on the size and distribution of Pd clusters: (a), (b), and (c) correspond to the structures with different sizes of flat surfaces (Reprinted with permission from Korotcenkov (2005). Copyright 2005 Elsevier)

Detailed analysis of the noble metal impregnation of as-obtained  $\text{SnO}_2$  sol-gel carried out by Cabot et al. (2000) confirmed many earlier conclusions. The existence of different chemical states of the noble metals localized at the grain surface, which gives rise to different sensing sites, was established. These sites responded in a different way to different gas molecules such as  $\text{CO}$  or  $\text{CH}_4$ , as well as to humidity, showing different sensitivities at the working temperatures. Moreover, it was also found that additives can introduce a strong distortion at the grain surface. All this means that the introduction of additives must be controlled with high accuracy in order to fix the type and density of sites where the gas-molecule detection takes place. According to Cabot et al. (2000), it is necessary to define not only the best noble metal to be used as catalytic additive but also its introduction technique and technical steps to be applied, such as grinding, calcinating, and firing. Earlier, Yamazoe (1991) reached the same conclusion. Analyzing the influence of different methods of Pd loading on  $\text{SnO}_2$  gas response to  $\text{H}_2$ , Yamazoe (1991) established that the fixation method gives the best results in comparison with impregnation and colloidal methods. It was found that this effect was related to the size of PdO particles formed on the surface of  $\text{SnO}_2$  grains. The finer the PdO particles, the greater the promoting effect at a fixed loading.

We also need to take into account that the presence of noble metals in metal oxide matrix might be one of the reasons for both decreased reproducibility and increased temporal instability of gas sensor parameters (Korotcenkov and Cho 2011). It is known that the reactivity of noble metal clusters depends strongly on their size (see Fig. 10.5), while the size of noble metal clusters depends strongly on the synthesis method and the shape and size of the grains (see Fig. 10.8). The size of noble metal clusters also depends on the parameters of the following thermal treatments. This means that any changes in technological parameters can be accompanied by the change of cluster size and catalyst activity, and, as a result, the effect of additives on sensor performance will be strongly dependent on the synthesis method and postdeposition heat treatments employed during sensor fabrication (Miller et al. 2006). Thus, during gas sensor design one should learn not only how to create clusters of specified size in a noble metal-metal oxide composite but also how to stabilize their size in the desired range during fabrication and exploitation.

## References

- Barsan N, Schweizer-Berberich M, Gopel W (1999) Fundamental and practical aspects in the design of nanoscaled SnO<sub>2</sub> gas sensors: a status report. *Fresenius J Anal Chem* 365:287–304
- Benard S, Retailleau L, Gaillard F, Vernoux P, Giroir-Fendler A (2005) Supported platinum catalysts for nitrogen oxide sensors. *Appl Catal B Environ* 55:11–21
- Bennett RA, Stone P, Bowker M (1999) Scanning tunnelling microscopy studies of the reactivity of the TiO<sub>2</sub>(110) surface: re-oxidation and the thermal treatment of metal nanoparticles. *Faraday Discuss* 114:267–277
- Bezemer GL, Bitter JH, Kuipers HP, Oosterbeek H, Holeyijn JE, Xu X, Kapteijn F, Van Dillen A, De Jong KP (2006) Cobalt particle size effects in the Fischer-Tropsch reaction studied with carbon nanofiber supported catalysts. *J Am Chem Soc* 128:3956–3964
- Bocuzzi F, Guglielminotti E (1994) IR study of TiO<sub>2</sub>-based gas sensor materials: effect of ruthenium on the oxidation of NH<sub>3</sub>, (CH<sub>3</sub>)<sub>3</sub>N and NO. *Sens Actuators B* 21:27–31
- Bowker M (1996) ‘Seeing’ the active site in catalysis. STM and molecular beam studies of surface reactions. In: Hightower JW, Delgass WN, Iglesia E, Bell AT (eds) *Studies in surface science and catalysis*, vol 101. Elsevier, Amsterdam, pp 287–295
- Brinzari V, Korotcenkov G, Schwank J, Boris Y (2002) Chemisorptional approach to kinetic analysis of SnO<sub>2</sub>:Pd-based thin film gas sensors (TFGS). *J Optoelect Adv Mater* 4(1):147–150
- Cabot A, Arbiol J, Morante J, Weimar U, Barsan N, Gopel W (2000) Analysis of the noble metal catalytic additives introduced by impregnation of as obtained SnO<sub>2</sub> sol–gel nanocrystals for gas sensors. *Sens Actuators B* 70:87–100
- Cabot A, Vila A, Morante JR (2002) Analysis of the catalytic activity and electrical characteristics of different modified SnO<sub>2</sub> layers for gas sensors. *Sens Actuators B* 84:2–20
- Chaudhary VA, Mulla IS, Vijayamohan K (1997) Synergetic sensitivity effects in surface modified tin oxide hydrogen sensors using ruthenium and palladium oxides. *J Mater Sci Lett* 16:1819–1821
- Chaudhary VA, Mulla IS, Sainkar SR, Belhekar AA, Vijayamohan K (1998a) Surface rutenated tin oxide as a novel hydrocarbon sensor. *Sens Actuators A* 65:197–202
- Chaudhary VA, Mulla IS, Vijayamohan K (1998b) Comparative studies of doped and surface modified tin oxide towards hydrogen sensing: synergistic effects of Pd and Ru. *Sens Actuators B* 50:45–51
- Chaudhary VA, Mulla IS, Vijayamohan K (1999) Selective hydrogen sensing properties of surface functionalized tin oxide. *Sens Actuators B* 55:154–160
- De Fressart E, Darville J, Gilles JM (1982) Influence of the work function and surface conductance of (110) SnO<sub>2</sub>. *Appl Surf Sci* 11/12:637–651
- Diaz R, Arbiol J, Sanz F, Cornet A, Morante JR (2002) Electroless addition of platinum to SnO<sub>2</sub> nanopowders. *Chem Mater* 14:3277–3283
- El-Azab A, Gan S, Liang Y (2002) Binding and diffusion of Pt nanoclusters on anatase TiO<sub>2</sub>(001)-(1 × 4) surface. *Surf Sci* 506:93–104
- Gentry SJ, Jones TA (1986) The role of catalysis in solid-state gas sensors. *Sens Actuators* 10:141–163
- Haruta M (1997) Size and support-dependency in the catalysis of gold. *Catal Today* 36:153–188
- Henry CR, Chapon C, Duriez C (1991) Precursor state in the chemisorption of CO on supported palladium clusters. *J Chem Phys* 95:700–705
- Ioannides T, Verykios XE (1996) Charge transfer in metal catalysts supported on doped TiO<sub>2</sub>: a theoretical approach based on metal–semiconductor contact theory. *J Catal* 161:560–569
- Ionescu R, Vancu A (1994) Time-dependence of the conductance of SnO<sub>2</sub>:Pt:Sb in atmospheres containing oxygen, carbon monoxide and water vapour I. Non-oscillatory behavior. *Appl Surf Sci* 74:207–212
- Ionescu R, Vancu A, Tomescu A (1994) Time-dependence of the conductance of SnO<sub>2</sub>:Pt:Sb in atmospheres containing oxygen, carbon monoxide and water vapour II. Oscillatory behavior. *Appl Surf Sci* 74:213–219
- Ivanovskaya M (2000) Ceramic and film metal oxide sensors obtained by sol–gel method: structure features and gas-sensitive properties. *J Electron Technol* 33:108–112
- Kanazawa E, Sakai G, Shimano K, Kanmura Y, Teraoka Y, Miura N, Yamazoe N (2001) Metal oxide semiconductor N<sub>2</sub>O sensor for medical use. *Sens Actuators B* 77:72–77
- Kim H, Lee J, Park C (2002) Surface characterization of O<sub>2</sub>-plasma-treated indium-tin-oxide (ITO) anodes for organic light-emitting-device applications. *J Korean Phys Soc* 41(3):395–399
- King DA, Woodruff DP (eds) (1982) *The chemical physics of solid surfaces and heterogeneous catalysis*, vol 4. Elsevier, Amsterdam, pp 143–194
- Kiv AE, Maximova TI, Soloviev VN (2001) MD simulation of the ion-stimulated processes in Si surface layers. In: Baraton MI, Uvarova IV (eds) *Functional gradient materials and surface layers prepared by fine particles technology*. Kluwer, Dordrecht, The Netherlands, pp 297–303
- Kohl D (1989) Surface processes in the detection of reducing gases with SnO<sub>2</sub>-based devices. *Sens Actuators* 18:71–113

- Kohl D (1990) The role of noble metals in the chemistry of solid-state gas sensors. *Sens Actuators B* 1:158–165
- Kolmakov A, Chen X, Moskovits M (2008) Functionalizing nanowires with catalytic nanoparticles for gas sensing application. *J Nanosci Nanotechnol* 8(1):111–121
- Korotcenkov G (2005) Gas response control through structural and chemical modification of metal oxides: state of the art and approaches. *Sens Actuators B* 107:209–232
- Korotcenkov G, Cho BK (2011) Instability of metal oxide-based conductometric gas sensors and approaches to stability improvement. *Sens Actuators B* 156:527–538
- Korotcenkov G, Brinzari V, Schwank J, Cerneavschi A (2001) Possibilities of aerosol technology for deposition of SnO<sub>2</sub>-based films with improved gas sensing characteristics. *J Mater Sci Eng C* 19:73–77
- Korotcenkov G, Macsanov V, Boris Y, Brinzari V, Tolstoy V, Schwank J, Morante J (2003a). Using of SILD technology for surface modification of SnO<sub>2</sub> films for gas sensor applications. In: Kumar A, Merg WJ, Cheng YT (eds) *Surface engineering, synthesis, characterization, and applications*. MRS Proceedings, 750, Y5.25.1–Y.5.25.6.
- Korotcenkov G, Brinzari V, Boris Y, Ivanov M, Schwank J, Morante J (2003b) Surface Pd doping influence on gas sensing characteristics of SnO<sub>2</sub> thin films deposited by spray pyrolysis. *Thin Solid Films* 436:119–126
- Korotcenkov G, Macsanov V, Brinzari V, Tolstoy V, Schwank J, Cornet A, Morante J (2004) Influence of Cu, Fe, Co, and Mn oxide nanoclusters on sensing behavior of SnO<sub>2</sub> films. *Thin Solid Films* 467:209–214
- Korotcenkov G, Cho BK, Gulina LB, Tolstoy VP (2012) Gas sensor application of Ag nanoclusters synthesized by SILD method. *Sens Actuators B* 166–167:402–410
- Lin HM, Hsu CM, Yang NY, Lee PY, Yang CC (1994) Nanocrystalline WO<sub>3</sub>-based H<sub>2</sub>S sensors. *Sens Actuators B* 22:63–68
- Madou MJ, Morrison SR (1989) *Chemical sensing with solid state devices*. Academic, San Diego, CA
- Maekawa T, Tamaki J, Miura N, Yamazoe N (1992) Gold-loaded tungsten oxide sensor for detection of ammonia in air. *Chem Lett* 2:639–642
- Matsushima S, Teraoka Y, Miura N, Yamazoe N (1988) Electronic interaction between metal additives and tin dioxide-based gas sensors. *Jpn J Appl Phys* 27:1798
- McAlear JF, Moseley PT, Norris JOW, Williams DE, Tofield BC (1988) Tin dioxide gas sensors. Part 2—The role of surface additives. *J Chem Soc Faraday Trans 1* 84(2):441–457
- Miller TA, Bakrania SD, Perez C, Wooldridge MS (2006) Nanostructured tin dioxide materials for gas sensor applications. In: Geckeler KE, Rosenberg E (eds) *Functional nanomaterials*. American Scientific Publishers, Stevenson Ranch, CA, pp 1–24
- Morrison SR (1986) Selectivity in semiconductor sensors. In: *Proceedings of the 2nd International Meeting on Chemical Sensors*. Bourdeaux, France, pp 39–48
- Nehasil V, Janecek P, Korotchenkov G, Matolin V (2003) Investigation of behavior of Rh deposited onto polycrystalline SnO<sub>2</sub> by means of TPD, AES and EELS. *Surf Sci* 532–535:415–419
- Norris JOW (1987) The role of precious metal catalysts. In: Moseley PT, Tofield BC (eds) *Solid state gas sensors*. Adam Hinger, Bristol, UK, pp 124–138
- Papadopoulos CA, Avaritsiotis JN (1995) A model for the gas sensing properties of tin oxide thin films with surface catalysts. *Sens Actuators B* 28:201–210
- Penza M, Martucci C, Cassano G (1998) NO<sub>x</sub> gas sensing characteristics of WO<sub>3</sub> thin films activated by noble metals (Pd, Pt, Au) layers. *Sens Actuators B* 50:52–59
- Rodriguez JA (1996) Electronic and chemical properties of Pt, Pd and Ni in bimetallic surfaces. *Surf Sci* 345:347–362
- Sanchez A, Abbet S, Heiz U, Schneider W-D, Hakkinen H, Narnett RN, Landman U (1999) When gold is not noble: nanoscale gold catalysts. *J Phys Chem* 103:9573–9578
- Seal S, Shukla S (2002) Nanocrystalline SnO<sub>2</sub> gas sensors in view of surface reactions and modifications. *JOM* 54(9):35–38, 60.
- Sears WM, Love DA (1993) Measurements of the electrical mobility of silver over a hot tin oxide surface. *Phys Rev B* 47:12972–12975
- Shimizu Y, Kanazawa E, Takao Y, Egashira M (1998) Modification of H<sub>2</sub>-sensitive breakdown voltages of SnO<sub>2</sub> varistors with noble metals. *Sens Actuators B* 52:38–44
- Skala T, Veltruska K, Moroseac M, Matolinova I, Korotcenkov G, Matolin V (2003) Study of Pd-in interaction during Pd deposition on pyrolytically prepared In<sub>2</sub>O<sub>3</sub>. *Appl Surf Sci* 205:196–205
- Sukharev V, Cavicchi R, Semancik S (1993) Solid state sensors based on semiconducting metal oxides with surface-dispersed metal additives: modeling of the mechanism of response formation. In: *Proceedings of the NIST workshop on gas sensors: strategies for future technologies*. Gaithersburg, MD, p 88
- Takada T, Suzuki K, Nakane M (1993) Highly sensitive ozone sensor. *Sens Actuators B* 13–14:40–407
- Tofield BC (1988) Tin dioxide gas sensors. Part 2: the role of surface additives. *J Chem Soc Faraday Trans* 84:441–457
- Tong MS, Dai GR, Wu YD, Gao DS (2000) High sensitivity and switching-like response behavior of SnO<sub>2</sub>-Ag-SnO<sub>2</sub> element to H<sub>2</sub>S at room temperature. *J Mater Sci Mater Electron* 11:661–665
- Tsu K, Boudart M (1961) Recombination of atoms at the surface of thermocouple probes. *Can J Chem* 39:1239–1246

- Tsud N, Johaneck V, Stara I, Veltruska K, Matolin V (2001) XPS, ISS and TPD study of Pd-Sn interaction on Pd-SnO<sub>2</sub> systems. *Thin Solid Films* 391:204–208
- Valden M, Lai X, Goodman DW (1998a) Onset of catalytic activity of gold clusters on titania with the appearance of nonmetallic properties. *Science* 281:1647–1650
- Valden M, Pak S, Lai X, Goodman DW (1998b) Structure sensitivity of CO oxidation over model Au/TiO<sub>2</sub> catalysts. *Catal Lett* 56:7–10
- Veltruska K, Tsud N, Brinzari V, Korotcenkov G, Matolin V (2001) CO adsorption on Pd clusters deposited on pyrolytically prepared SnO<sub>2</sub> studied by XPS. *Vacuum* 61:129–134
- Vinod CP, Kulkarni GU, Rao CNR (2003) Nanoscale catalysis by gold. In: Carley A, Davies P, Hutchings G, Spencer M (eds) *Surface chemistry and catalysis*. Kluwer Academic, New York, pp 191–206
- Vlachos DS, Papadopoulos CA, Avaritsiotis JN (1996) On the electronic interaction between additives and semiconducting oxide gas sensors. *Appl Phys Lett* 69:650–652
- Wada K, Egashira M (1998) Improvement of gas-sensing properties of SnO<sub>2</sub> by surface chemical modification with diethoxydimethylsilane. *Sens Actuators B* 53:147–154
- Williams DE, Pratt KFE (1998) Classification of reactive sites on the surface of polycrystalline tin dioxide. *J Chem Soc Faraday Trans* 94:3493–3500
- Williams DE (1999) Semiconducting oxides as gas-sensitive resistors. *Sens Actuators B* 57:1–16
- Williams DE, Pratt KFE (2000) Microstructure effects on the response of gas-sensitive resistors based on semiconducting oxides. *Sens Actuators B* 70:214–221
- Xu C, Lai X, Zajac GW, Goodman DW (1997) Scanning tunneling microscopy studies of the TiO<sub>2</sub>(110) surface: structure and the nucleation growth of Pd. *Phys Rev* 56:13464–13482
- Yamaura H, Moriya K, Miura N, Yamazoe N (2000) Mechanism of sensitivity promotion in CO sensors using indium oxide and cobalt oxide. *Sens Actuators B* 65:39–41
- Yamazoe N (1991) New approaches for improving semiconductor gas sensors. *Sens Actuators B* 5:7–19
- Yamazoe N, Kurokawa Y, Seiyama T (1983) Effects of additives on semiconductor gas sensors. *Sens Actuators* 4:283–289
- Zhang J, Colbow K (1997) Surface silver clusters as oxidation catalysts on semiconductor gas sensors. *Sens Actuators B* 40:47–52
- Zhang J, Liu D, Colbow K (1993) Growth of fractal clusters on thin solid films and scaling of the active zone. *Phys Rev B* 48:9130–9133
- Zhang D, Li C, Han S, Liu X, Tang T, Jin W, Zhou C (2003) Ultraviolet photodetection properties of indium oxide nanowires. *Appl Phys A* 77:163–166

## Chapter 11

# Catalysts Used in Calorimetric (Combustion-Type) Gas Sensors

The calorimetric gas sensor is a gas sensor that uses calorimetry as the transduction principle by measuring the heat of a reaction on the sensor surface (Firth et al. 1973). It is known that the exothermic nature of the combustion (the oxidation reaction) causes a rise in the temperature. This class of devices, in various configurations, is also known by the names pellistor, catalytic bead, catalytic gas sensor, combustible gas sensor, or thermometric gas sensor (see Fig. 11.1a, b). Taking into account that the change of temperature depends on the rate of combustion, it becomes clear that calorimetric sensors require a catalyst that efficiently promotes combustion of the target analyte. This means that the catalyst which interfaces with the gas is the key element in calorimetric gas sensors. It is the properties of the catalyst used which determine the selectivity, response, and stability of these sensors. The heterogeneous catalytic reactions of combustible gases in air have a temperature dependence on the heat generated during combustion, as shown in Fig. 11.1c. At low temperature only small heat generation can be observed. With rising temperature, the heat generation increases exponentially and saturates at higher temperatures, leaving only a small temperature dependence. The temperature region of the steep increase (transition region) is characteristic of a specific combustible gas and a certain catalyst (Riegel and Härdtl 1990). For different gases and the same catalyst, the transition region can be observed at different temperatures (Fig. 11.1c, curves Gas 1 and Gas 2). The same effect takes place for different catalysts and the same gas. It should be noted that, although calorimetric sensors are reputed to be non-selective, selective gas detection is possible by measuring the heat generation of the catalytic reaction over a broad temperature range as shown in Fig. 11.1c. Catalysts typically used in calorimetric gas sensors are listed in Table 11.1.

As can be seen in Table 11.1, noble metals Pt, Pd, and Rh are the most usable catalysts in calorimetric gas sensors designed. It was established that of all the catalysts known they have the highest activity with respect to oxidation of combustible gases (see Fig. 11.2) and provide acceptable operation temperatures. Morooka and coworkers (Morooka and Ozaki 1966; Morooka et al. 1967) showed that activity for a model reaction, propylene oxidation, correlates with the strength of the metal–oxygen (M–O) bond. Because an LEL sensor must oxidize all ambient hydrocarbon species, the highest activity catalysts hold the most promise for the application. Therefore, the choice of palladium and platinum and sometimes rhodium for application in combustion gas sensors is natural (Miller 2001). This explains why the automobile exhaust system is treated with platinum or palladium compounds and is called a catalytic converter.

Experiment has shown that Pd and Pt can be deposited on the surface of a sensor platform in the form of films (Cavicchi et al. 2004) (see Fig. 11.1b). However, such a configuration does not provide the required rate of combustion due to small active surface area. As a result, sensors have low sensitivity. Therefore, as a rule, catalysts used Pt and Pd nanoparticles dispersed on a porous metal oxide support (Debeda et al. 1995; Lee et al. 1997; Katti et al. 2002; Furjes et al. 2005) (Fig. 11.1a). It was found

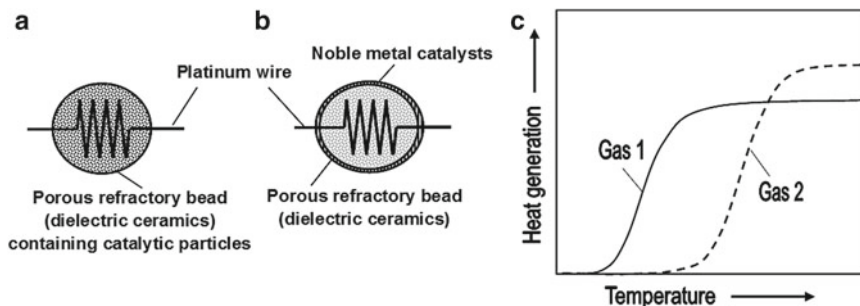
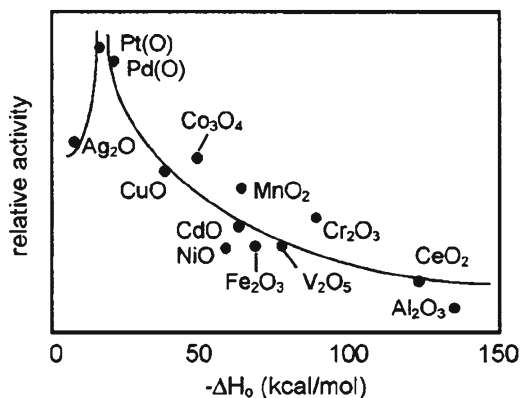


**Fig. 11.1** (a, b) Configurations of pellistor (catalytic bead) gas sensors and (c) temperature-dependent heat generation of a catalytic combustion of combustible gases in air

**Table 11.1** Catalyst typically used in calorimetric gas sensors

Gas or vapor	Catalyst
Methanol, ethanol, benzene, acetone, isopropanol	Pd; Pt; Pt-impregnated $\text{Al}_2\text{O}_3$
Methane, propane, butane, isobutene, ethane, propylene	Pt; Pd; Pd/Pt on $\text{Al}_2\text{O}_3$ ; Pd/Pt on $\text{TiO}_2$ ; Pt on $\text{Al}_2\text{O}_3$ ; Pd on $\text{Al}_2\text{O}_3$ ; Pd/Pt on $\text{Al}_2\text{O}_3$ ; Pd/Pt on $\text{Al}_2\text{O}_3$ :Ce
CO	Pd; Pd-activated zeolite; Pt/Ir; Pd/Au; Au/ $\text{TiO}_2$ ; Au/ $\text{Co}_3\text{O}_4$
$\text{H}_2$	Pt; Pd; Pd/Pt on $\text{TiO}_2$ ; Pt on $\text{Al}_2\text{O}_3$ ; Pd/Rh on $\text{Al}_2\text{O}_3$ ; Pt/Pd on F-doped $\text{SnO}_2$

**Fig. 11.2** Relative activities of various metals for oxidation of propylene (Reprinted with permission from Morooka and Ozaki (1966). Copyright 1966 Elsevier)



that the support stabilizes the catalytic metal in its most active chemical and physical state. Experiments with gas showed that such configurations of catalysts also improve the poison resistance of the sensors. Of course, for the indicated functions, the bead material must itself be stable at high temperature. Alumina and, to a lesser extent, zirconia are common choices. Both oxides are routinely doped with a variety of materials to minimize sintering at high temperatures (Zwinkels et al. 1993). Supports can also make important contributions to the catalytic chemistry of the bead, especially with respect to oxygen storage potential (Haack and Otto 1995). Catalysts for combustion sensors can be prepared by impregnation of an alumina support with aqueous solutions of palladium or platinum salts, such as platinum(IV) chloride pentahydrate. Usually the content of Pd or Pt in  $\text{Al}_2\text{O}_3$  for the best catalytic activity was found to be 15–40 wt % (Choi et al. 2005; Han et al. 2007a).  $\text{TiO}_2$  support can also be used (Han et al. 2007b). Recently, zeolites have been used as a support material with the idea of using the pore size to enhance chemical selectivity (Yasuda et al. 2009). The zeolite materials are activated with Pd by stirring with an ammonia/palladium(II) nitrate solution. In fact, sensors made from

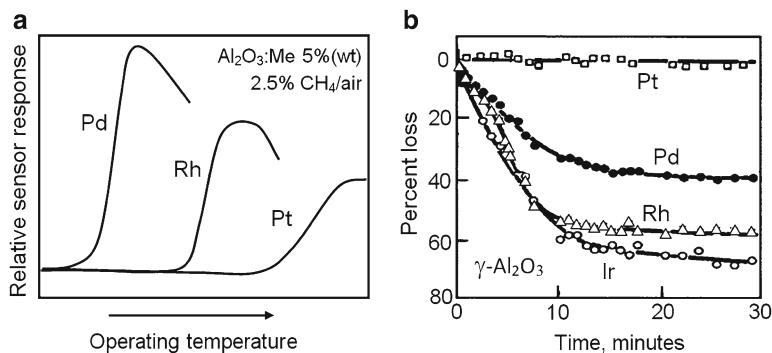


**Fig. 11.3** (a) Response of sensors with different catalytic metals to 2.5%  $\text{CH}_4/\text{air}$ : all samples 5% (wt) on  $\gamma\text{-Al}_2\text{O}_3$ . (Data from Miller 2001). (b) Responses of combustion gas sensors to 1%  $\text{CH}_4/\text{air}$  in atmosphere containing 100 ppm  $\text{H}_2\text{S}$  (all catalysts supported on  $\gamma\text{-Al}_2\text{O}_3$ ). (Data from Gentry and Walsh (1983) and Miller (2001))

zeolites with pores of average size 0.4 nm were selective to CO, while sensors of pore size 0.75 nm showed a similar response to CO, but also a response to *n*-hexane and cyclohexane.

The selection of Pd or Pt as a catalyst depends on the nature of the target gas and the temperature required for operation. For example, Pt catalyst combusts inflammable gases effectively at as low as room temperature (Casey et al. 2003). For Pd-based catalysts, the operation temperature should be higher at 200 °C. At an operating temperature of 400 °C, the Pd-coated sensor is sensitive to all combustible gases, while the Pt-coated sensor detects most combustible gases except methane. For methane combustion, Pd works more effectively than Pt (see Fig. 11.3). Figure 11.3a shows a series of light-off curves for catalytic gas sensors made from alumina-supported 5 wt % platinum (Pt), palladium (Pd), and rhodium (Rh) catalysts, exposed to 2.5 % methane (50 % of methane's LEL) in air (Miller 2001). Pd has the lowest light-off temperature in this group, Pt the highest. Alone, these results suggest that palladium would always be the catalyst of choice for an LEL sensor. However, as was established, there are other considerations, primarily those of poison tolerance, that do not allow palladium to be a universal choice. As an example of sulfur-gas poisoning, Fig. 11.3b shows the effect of hydrogen sulfide ( $\text{H}_2\text{S}$ ) exposure on catalytic beads made with a series of catalytic metals supported by gamma-alumina (Firth et al. 1973). Of this trio, only the platinum catalyst was unaffected by  $\text{H}_2\text{S}$ .

For increasing reactivity of a  $\text{TiO}_2/\text{Pd}$  catalyst at lower temperature, Han et al. (2007a) incorporated in the sensor an ultraviolet light source to create oxygen species on the  $\text{TiO}_2$  catalyst support. They observed the reduction of operating temperature from 253 to 82 °C for hydrogen gas sensing. Taking into account the various reactivities of Pd- and Pt-based catalysts to methane, Debeda et al. (1995, 1997) proposed to use an array of sensors for achievement of better chemical selectivity of calorimetric gas sensors. Debeda et al. (1995, 1997) designed a dual sensor, one sensor with a Pd coating and a second with a Pt coating. By subtracting the results (after appropriate scaling), the concentration of methane even in gas mixture can be determined. However, we need to note that in the most gas sensors aimed at application in alarm systems, catalysts containing both Pt and Pd are used. In this case sensors have a good response to all inflammable gases and vapors, including methane which is often encountered in many applications.

Studies have shown that, in addition to Pd and Pt, an Au catalyst can also be used in calorimetric sensors. Gold is not a good catalyst material, but it becomes active when its size is in the nanometer range. At that, it was established that nanosized Au combusts CO gas more selectively than other gases. Therefore, optimized Au–metal oxide system such as Au- $\text{TiO}_2$  and Au/ $\text{Co}_3\text{O}_4$  with fixed sizes of Au nanoparticles could be promising for selective CO gas sensing (Nishibori et al. 2006). However, it was established that Au-based catalysts showed strong deactivation. Nishibori et al. (2011) believe



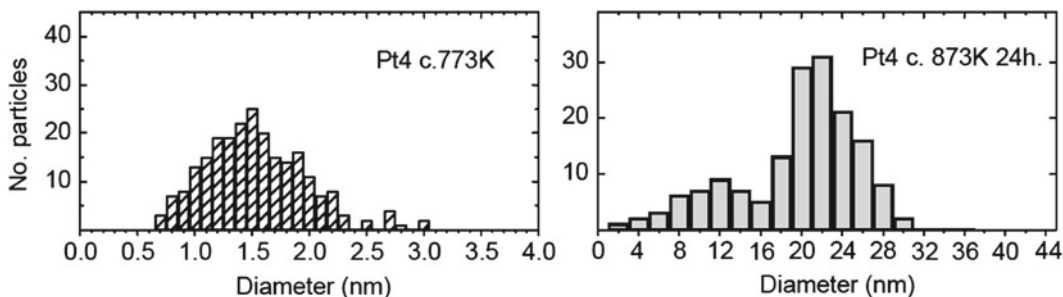


**Fig. 11.4** The change of platinum particle size distribution in Pt/Al<sub>2</sub>O<sub>3</sub> catalyst prepared by sol-gel method using H<sub>2</sub>PtCl<sub>6</sub> as metal precursor after calcination at 773 K for 2 h and 873 K for 24 h (Reprinted with permission from Romero-Pascual et al. (2002). Copyright 2002 Elsevier)

that the deactivation of the Au-based catalyst occurs due to formation of the thin layer of the carbonate on the catalyst surface.

During research it was also established that, for better long-term reliability and temperature independence, a thicker catalyst combustor film is preferred. The aging process after fabrication of the catalyst combustor is also essential for long-term stability (Nishibori et al. 2008). Nishibori et al. (2008) believe that the degradation of the Pt/alumina catalyst is mainly caused by the sintering of Pt particles. As the bonding between noble metals and alumina is weak, it seems that some weak-bond noble metal particles move on the surface of the alumina by thermally activated migration during the aging treatment and is fixed to a stable site by the anchor effect. In addition, the migration and coalescence of the particles cause the growth of the Pt grain size and the loss of the active surface area, i.e., the loss of its activity. How strong the change in particle size can be is shown in Fig. 11.4. Therefore, it seems that the aging treatment is considered effective in preventing the further migration of Pt particles and degradation of catalyst performance. The effect of aging treatment on the stability of micro-thermoelectric hydrogen sensor is shown in Fig. 11.5.

It was also established that the reduction of catalyst activity due to contaminating gases in the environment is another important factor affecting the life of calorimetric gas sensor sensors. Gentry and Walsh performed comprehensive studies of the poisoning effects in pellistors (Gentry and Walsh 1984, 1987). Halogenated gases were found to inhibit reversibly the catalytic activity of the catalysts. Sulfur-containing species also often resulted in partially irreversible changes that took longer to establish. Gentry and Walsh assumed that an SO<sub>2</sub> species is formed through a reaction with the catalyst. When the poison is removed, partial recovery takes place through the desorption of SO<sub>2</sub>. For both halogenated and sulfur-containing species, when comparing three catalysts, both the gas sensitivity and susceptibility to poisoning were found to proceed as Pd > Rh > Pt. Phosphate esters also poison the catalyst. It was established that poisoning induces the loss of sensitivity because the strongly adsorbed gases preoccupy catalyst sites and inhibit catalytic reaction (combustion) between the catalyst and the gases (Katti et al. 2002). Deng et al. (1993) also compared Pd, Rh, and Ir catalysts in a study of sulfur poisoning. They found that Ir, while less catalytically active for methane oxidation, was the least affected by SO<sub>2</sub> poisoning. It was reported that hexamethyldisiloxane (HMDS) also irreversibly poisons catalysts (Gentry and Walsh 1984, 1987; Ehrhardt et al. 1997). The effect is reduced with increased porosity of the support and increased dispersion of the catalyst. In an early study of a MEMS methane sensor, Krebs and Grisel (1993) found thick-film catalysts to be more resistant to HMDS poisoning as well. It is also possible to add protective coatings for protection from poisoning. For example, a polytetrafluoroethylene coating was used to reduce poisoning due to HMDS, H<sub>2</sub>S, and iodine for a hydrogen calorimetric gas sensor (Katti et al. 2002), while Miller (2001) reported the use of an alumina coating. Another approach was used by Wang et al. (2011). They found that better performance of combustion-type methane gas sensors regarding activity, anti-sulfur ability, and thermal

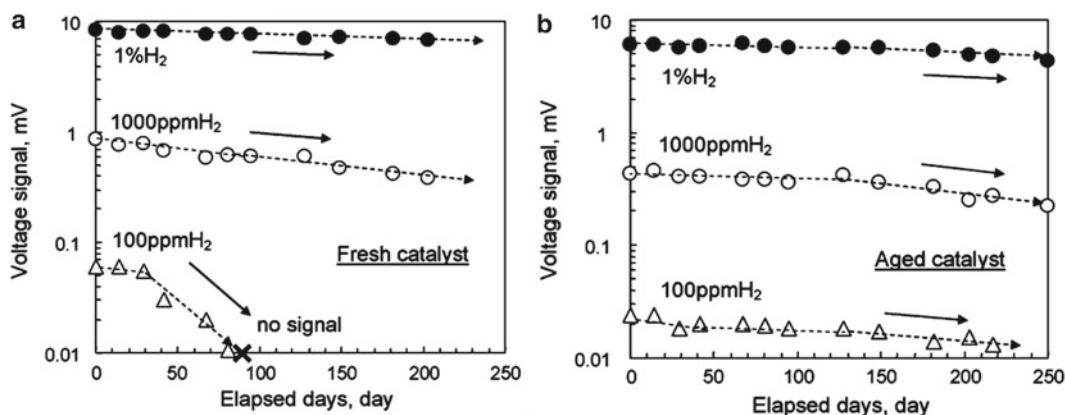


**Fig. 11.5** Aging process of the hydrogen thermoelectric sensors with thick Pt/Al<sub>2</sub>O<sub>3</sub> catalyst at operating temperature of 100 °C: (a) fresh catalyst and (b) after aging treatment at 160 °C for 14 days (Reprinted with permission from Nishibori et al. (2008). Copyright 2008 Elsevier)

stability can be achieved by the introduction of Ce in a Pt/Pd catalyst (Pt/Pd-Ce-Al<sub>2</sub>O<sub>3</sub>). The experiment indicated that catalytic elements fabricated with cerium-modified alumina have stronger oxygen storage and release ability than other conventional catalytic elements. In addition, it has been shown that, by doping cerium with pure alumina, the vacancies in alumina are easy to fill by Ce<sup>3+</sup> ions and the reversible oxidation reaction  $\text{Ce}_2\text{O}_3 + 1/2\text{O}_2 \rightarrow 2\text{CeO}_2$  occurs. The spinel structure possesses a strong ability to restrain the calcination.

## References

- Casey V, Cleary J, D'arcy G, Mcmonagle JB (2003) Calorimetric combustible gas sensor based on a planar thermopile array: fabrication, characterisation, and gas response. *Sens Actuators B* 96:114–123
- Cavicchi RE, Poirier GE, Tea NH, Afridi M, Berning D, Hefner A, Suehle J, Gaitan M, Semancik S, Montgomery C (2004) Micro-differential scanning calorimeter for combustible gas sensing. *Sens Actuators B* 97:22–30
- Choi Y, Tajima K, Sawaguchi N, Shin W, Izu N, Matsubara I, Murayama N (2005) Planar catalytic combustor application for gas sensing. *Appl Catal A* 287:19–24
- Debeda H, Rebiere D, Pistre J, Menil F (1995) Thick-film pellistor array with a neural-network posttreatment. *Sens Actuators B* 27:297–300
- Debeda H, Dulau L, Dondon P, Menil F, Lucat C, Massok P (1997) Development of a reliable methane detector. *Sens Actuators B* 44:248–256
- Deng YQ, Nevell TG, Ewen RJ, Honeybourne CL, Jones MG (1993) Sulfur poisoning, recovery and related phenomena over supported palladium, rhodium and iridium catalysts for methane oxidation. *Appl Catal A* 101:51–62
- Ehrhardt JJ, Colin L, Jamois D (1997) Poisoning of platinum surfaces by hexamethyldisiloxane (HMDS): application to catalytic methane sensors. *Sens Actuators B* 40:117–124
- Firth JG, Jones A, Jones TA (1973) The principles of the detection of flammable atmospheres by catalytic devices. *Combust Flame* 21:303–311
- Furjes P, Adam M, Ducso C, Zettner J, Barsony I (2005) Thermal effects by the sensitive coating of calorimetric gas sensors. *Sens Actuators B* 111:96–101
- Gentry SJ, Walsh PT (1984) Poison-resistant catalytic flammable-gas sensing elements. *Sens Actuators* 5:239
- Gentry SJ, Walsh PT (1983) Thioresistant flammable gas sensing elements. *Stud Surf Sci Catal* 16:203–212
- Gentry SJ, Walsh PT (1987) The theory of poisoning of catalytic flammable gas-sensing elements. In: Moseley PT, Tofield BC (eds) *Solid state gas sensors*. Adam Hilger, Bristol
- Haack LP, Otto K (1995) X-Ray photoelectron spectroscopy of Pd/ $\gamma$ -alumina and Pd foil after catalytic methane oxidation. *Catal Lett* 34:31–40

- Han CH, Hong DW, Han SD, Gwak J, Singh KC (2007a) Catalytic combustion type hydrogen gas sensor using  $\text{TiO}_2$  and UV-LED. *Sens Actuators B* 125:224–228
- Han CH, Hong DW, Kim IJ, Gwak J, Han SD, Singh KC (2007b) Synthesis of Pd or Pt/titanate nanotube and its application to catalytic type hydrogen gas sensor. *Sens Actuators B* 128:320–325
- Katti VR, Debnath AK, Gadkari SC, Gupta SK, Sahni VC (2002) Passivated thick film catalytic type  $\text{H}_2$  sensor operating at low temperature. *Sens Actuators B* 84:219–225
- Krebs P, Grisel A (1993) A low-power integrated catalytic gas sensor. *Sens Actuators B* 13:155–158
- Lee JS, Park JW, Shin SM (1997) Fabrication of a micro catalytic gas sensor using thin film process and Si anisotropic etching techniques. *Sens Actuators B* 45:265–269
- Miller JB (2001) Catalytic sensors for monitoring explosive atmospheres. *IEEE Sensors J* 1(1):88–93
- Morooka Y, Ozaki A (1966) Regularities in catalytic properties of metal oxides in propylene oxidation. *J Catal* 5:116–124
- Morooka Y, Morikawa Y, Ozaki A (1967) Regularity in the catalytic properties of metal oxides in hydrocarbon oxidation. *J Catal* 7:23–32
- Nishibori M, Tajima K, Shin W, Izu N, Itoh T, Matsubara I (2006) CO oxidation catalyst of Au- $\text{TiO}_2$  on the thermoelectric gas sensor. *J Ceram Soc Jpn* 115:34–41
- Nishibori M, Shin W, Houlet L, Tajima K, Izu N, Itoh T, Matsubara I (2008) Long-term stability of Pt/alumina catalyst combustors for micro-gas sensor application. *J Eur Ceram Soc* 28:2183–2190
- Nishibori M, Shin W, Izu N, Itoh T, Matsubara I (2011) CO combustion catalyst for micro gas sensor application. *J Mater Sci* 46:1176–1183
- Riegel J, Hardtl KH (1990) Analysis of combustible gases in air with calorimetric gas sensors based on semiconducting  $\text{BaTiO}_3$  ceramics. *Sens Actuators B* 1:54–57
- Romero-Pascual E, Larrea A, Monzon WA, Gonzalez RD (2002) Thermal stability of Pt/ $\text{Al}_2\text{O}_3$  catalysts prepared by sol-gel. *J Solid State Chem* 168:343–353
- Wang Y, Tong MM, Zhang D, Gao Z (2011) Improving the performance of catalytic combustion type methane gas sensors using nanostructure elements doped with rare earth cocatalysts. *Sensors* 11:19–31
- Yasuda KE, Visser JH, Bein T (2009) Molecular sieve catalysts on microcalorimeter chips for selective chemical sensing. *Microporous Mesoporous Mater* 119:356–359
- Zwinkels MFM, Jaras SG, Menon PG (1993) Catalytic materials for high-temperature combustion. *Catal Rev Sci Eng* 35(3):319–358

## Chapter 12

# Filters in Gas Sensors

The use of additional various physical/passive and catalytically active/chemical filters incorporated into the measuring unit or directly into the sensor construction is one of the most effective methods to improve both sensor selectivity and sensor resistivity to poisoning (Feng et al. 1994; Sauvan and Pijolat 1999; Pijolat et al. 1999, 2005; Fleischer et al. 2000; Mandayo et al. 2002; Ryzhikov et al. 2009; Prasad et al. 2010). As is well known, low selectivity and insufficient stability are the most important shortcomings of gas sensors. The filter or adsorbent incorporated in gas sensors helps to resolve this problem because it can selectively remove interferences or transform them into an inactive phase. Physical filters are based on materials with well-defined pore sizes in order to block larger molecules from diffusion toward the sensitive material. Chemical filters eliminate interfering gases via a chemical reaction (Fleischer et al. 2000) or preferentially transform the target gas into a more active species (Hubalek et al. 2004). Additional filters can also be employed to protect the sensor surface from contamination, although they not only influence metal oxide surface properties but also can provoke an electrical short circuit (Billi et al. 2002). However, Kitsukawa et al. (2000) believe that, unlike existing filters with adsorbing materials, filters with decomposing material have stronger immunity against higher concentration and prolonged exposure of the interfering gases. Note that filters can also be used for gas desiccation. The decrease in the humidity influence of the sensor parameters considerably improves the stability of its operating characteristics.

### 12.1 Passive Filters

It was established that numerous inorganic and organic materials, such as  $\text{CaCl}_2$ ,  $\text{CaO}$ ,  $\text{MgO}$ ,  $\text{ZnO}$ ,  $\text{MgSiO}_3$ , activated carbon, cellulose, collagen, wool, zeolite, and silica gel, can be used as adsorbents (Knaebel 2004). For application as adsorbents, they must have high abrasion resistance, high thermal stability, and small pore diameters, which results in more exposed surface area and hence high surface capacity for adsorption. The adsorbents must also have a distinct pore structure which enables fast transport of the gaseous vapors. In this section we will discuss only adsorbents, which are commercial products and are frequently encountered. Those included here are listed in alphabetical order rather than by importance.

**Activated Carbon** Activated carbon is a highly porous, amorphous solid consisting of microcrystallites with a graphite lattice. The base materials that comprise activated carbon include wood, coal, peat, coconut shells, saran, recycled tires, and others. The final adsorbents all look the same, i.e., black granules or pellets. Effective surface area and pore size are strongly dependent on the activation conditions. The content of inorganic components in activated carbon varies between 2 and 25 %, but the average is about 7 %. Effective surface area generally ranges from 300 to 1,500 m<sup>2</sup>/g, depending on the base material, activation method, density, etc. Some typical applications are removing volatile organic compounds or other specific contaminants in gas that impart odor or are hazardous and upgrading methane from substandard natural gas wells. It is the most widely used adsorbent since most of its chemical (e.g., surface groups) and physical properties (e.g., pore size distribution and surface area) can be tuned according to what is needed. Pretreatment for gas-phase applications requires heating to about 200 °C. At present there is a new type of product called a “carbon molecular sieve” which is analogous to the zeolite molecular sieve. While micropores in zeolites tend to have rounded apertures, the carbon-based counterparts are more slit-like, as in the space between layers of graphite. This material is used for separation of nitrogen from air. This pressure swing process exploits the difference between sizes of oxygen (0.343 nm) and nitrogen (0.368 nm) and can achieve 99.9 % nitrogen purity. One of the main drawbacks with activated carbon is that it reacts with oxygen at moderate temperatures (over 300 °C).

**Aluminas** Activated alumina is produced from hydrated alumina, Al<sub>2</sub>O<sub>3</sub>·*n*H<sub>2</sub>O, where *n*=1 or 3, by dehydration (calcining) under carefully controlled conditions to get *n*=0.5. Aluminas have defect spinel form which leads to higher concentrations of surface acid sites. Surface areas are from 200 to 400 m<sup>2</sup>/g. Aluminas uses as an adsorbent are for removal of oxygenates and mercaptans from hydrocarbon feed streams and HCl from hydrogen and others. Pretreatment, for most gas-phase applications, requires heating to about 250 °C.

**Polymers** Instead of being limited to styrene-divinylbenzene, polymer adsorbents are also made from polymethacrylate, divinylbenzene/ethylvinylbenzene, or vinylpyridine and are sometimes sulfonated or chloromethylated, much as are ion exchange resins. As a result, some are sufficiently hydrophilic to be used as desiccants, while others are quite hydrophobic. The effective surface area is usually smaller than for activated carbon, e.g., 5–800 m<sup>2</sup>/g. Pore diameters range from about 0.3 to 200 nm. The range of application is somewhat restricted due to a higher price in comparison with other adsorbents. Currently, the main application includes removing VOCs from off-gas.

**Silicas** At present, several forms of silicas are available – silica gel, porous borosilicate glass, and aerogels. The last material is relatively new. However, its unique characteristics make it an interesting prospect for the future. Silica gel is a chemically inert, nontoxic, polar, and dimensionally stable (<400 °C) amorphous form of SiO<sub>2</sub>. It is prepared by the reaction between sodium silicate and acetic acid, which is followed by a series of after-treatment processes such as aging and pickling. These after-treatment methods result in various pore size distributions. Silica gel and porous glass are both non-dusting and resistant to attrition. Effective surface areas range from 300 to 900 m<sup>2</sup>/g, depending on the density. The widest uses of silica gel and porous glass are as a desiccant. Ancillary uses as an adsorbent are for separation of hydrocarbons (adsorption of heavy (polar) hydrocarbons from natural gas) and for drying of process air (e.g., oxygen, natural gas). Pretreatment, for gas-phase application (especially as a desiccant) requires heating to about 200 °C.

**Zeolites** Zeolites are natural or synthetic crystalline aluminosilicates which have a repeating pore network and release water at high temperature. Zeolites are polar in nature. Properties of zeolites are discussed in detail in Chap.8 (Vol.2). Therefore, we will only say that zeolites exhibit micropore structure with very small size and uniform distribution, as depicted in the pore size distribution shown in Fig. 12.1. The channel diameter of zeolite cages usually ranges from 0.2 to 0.9 nm. Applications of zeolites include gas drying, CO<sub>2</sub> removal from natural gas, CO removal from reforming gas, and

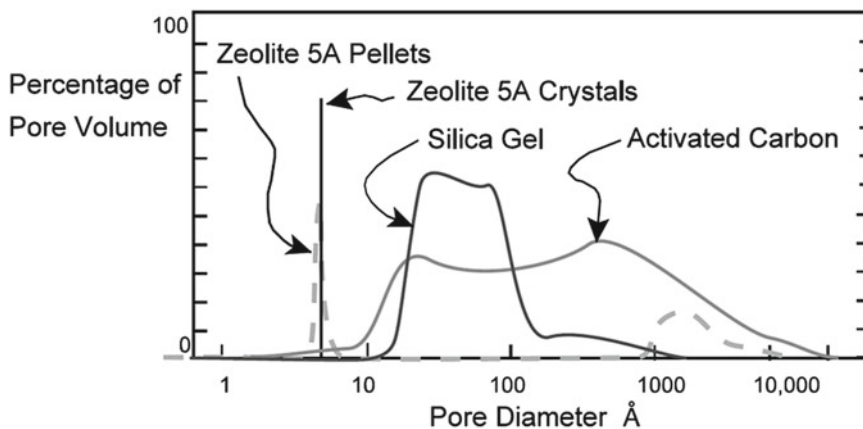


**Fig. 12.1** Pore size distribution of common classes of adsorbents. From Knaebel (2004) (<http://www.adsorption.com/publications/AdsorbentSel1B.pdf>)

separation of oxygen from air. Other possible applications are discussed in Chap. 8 (Vol. 2). Activation for gas-phase applications typically requires more stringent conditions than for silica or alumina, namely, 300 °C under full vacuum or an inert purge gas. For gas-phase applications they may require conditioning prior to use, e.g., washing in water and/or another solvent followed by drying.

We need to note that none of the adsorbents mentioned above has the same adsorption affinity for a given component. Therefore, selecting a proper adsorbent for a specific application is most important for the development of filters (Park and Yang 2005). It has long been thought that a good adsorbent should have a high adsorption capacity and good regenerability (Yang 1997). Regenerability is a measure of how well the adsorbent is regenerated by purging with an inert gas or by thermal treatment. Usually a working capacity for the adsorbent, defined as the difference between the amount adsorbed under the feed condition and that at the impurity concentration just leaving the adsorber at the end of the purge step, is employed for selecting the best adsorbent. This working capacity depends on the adsorption capacity, isotherm nonlinearity, and operating conditions such as the purge-to-feed ratio. Thus, in selecting the best adsorbent and determining the optimal bed layering, all these factors should be accounted for (Park and Yang 2005). For example, when an isotherm is of the favorable type, it is unfavorable for desorption. The more it is favorable for adsorption, the more it becomes unfavorable for desorption. Often the adsorbent that holds the higher adsorption capacity also yields a more favorable isotherm. So, an adsorbent showing a high adsorption capacity suffers from poor regenerability. Because of these two conflicting tendencies, it is not straightforward to determine which adsorbent is more suitable for gas sensor application. However, Park and Yang (2005) believe that if two adsorbents show the same working capacity at some concentration of impurity and that concentration is within the range of the gas sensor operating conditions, a layered bed of two adsorbents is better than a single adsorbent bed. If the working capacity of one of the adsorbents is always higher than the other under the operating conditions, then a single adsorbent bed with higher working capacity is better than layered beds of two adsorbents. Several examples of adsorbent applications for specific tasks are listed in Table 12.1.

Filters conventionally developed for gas sensors use three types of materials: porous layers, which physically absorb gas molecules; porous membranes, which realize separation by diffusion; and catalytic films, which decompose gases. Passive absorption filters usually employ a granular, highly porous sorption material which provides a large collection area. In some cases, filters include up to three different absorbent materials to enhance the efficiency of absorption of various undesirable gas

**Table 12.1** Examples of adsorbents for environmental separations

Application	Adsorbent
CH <sub>4</sub> storage	Super-activated carbon and activated carbon fibers
H <sub>2</sub> storage	Carbon nanotubes
N <sub>2</sub> /CH <sub>4</sub> separation	Clinoptilolite, Sr-ETS-4
CO <sub>2</sub> adsorption	MCM-41-polyethylenimine composite
CO removal from H <sub>2</sub> (to <10 ppm)	$\pi$ -Complexation sorbents such as CuCl/ $\gamma$ -Al <sub>2</sub> O <sub>3</sub> , CuY, and AgY
NO <sub>x</sub> removal	Fe–Mn–Ti oxides, Fe–Mn–Zr oxides, Cu–Mn oxides
Removal of dienes from olefins (to <1 ppm)	$\pi$ -Complexation sorbents such as Cu(I) and AgY

Source: Data extracted from Yang (2003)

components. The second type, which may also be considered as passive filters, often employ zeolites which contain pores of diameter ranging from 0.2 to 1 nm. Other passive filters use films of SiO<sub>2</sub> or Al<sub>2</sub>O<sub>3</sub> deposited directly on the surface of the sensing element. It has been found that porous layers in which various gases may have different diffusion coefficients have the possibility to improve the selectivity of gas sensors (Feng et al. 1994). For example, small pores allow the filter to store some long gas molecules. In particular, it was established that a dense SiO<sub>2</sub> layer, 10–100  $\mu$ m thick, can act as a molecular sieve to reduce the penetration of large molecules, such as C<sub>2</sub>H<sub>5</sub>OH and CH<sub>4</sub>, while H<sub>2</sub> molecules pass through easily (Katsuki and Fukui 1998; Zhan et al. 2005). Wong et al. (1996) have shown that polymer membranes also can be applied for improvement selectivity of metal oxide gas sensors. Wong et al. (1996) covered the surface of the tin dioxide thick films of Figaro series gas sensors by heat-resistant polymer membranes XU218 and PMDA-ODA (polyimide type) and found that the polymer gas separation membranes XU218 and PMDA-ODA, at medium gas concentration, can largely decrease the sensitivity to polar gas ammonia and slightly decrease the sensitivity to slightly polar gas carbon monoxide, not affecting the sensitivity to nonpolar gases, hydrogen and methane, at any concentration. Miller (2001) has found that, in addition to restricting diffusion of high-molecular-weight poisons, the overcoat layer provides a hot surface upon which they can decompose before reaching the catalytic sites. Other examples include metal-organic pastes which have been used as humidity filters (Vlachos et al. 1995) and thick Al<sub>2</sub>O<sub>3</sub> layers which have been used as alcohol filters in methane sensors (De Angelis and Riva 1995). There are also filters based on specific chemical reactivity of reference gas. For example, the filter for reducing the cross-sensitivity of a chlorine dioxide detector to hydrogen sulfide includes a high surface area substrate impregnated with a silver(I) salt or copper(II) salt which is effective in removing hydrogen sulfide from a gas stream without producing undesirable compounds which might be detected by the sensor. Examples of applications of some surface filters to one-electrode semiconductor sensors are given in Table 12.2. It is necessary to note, however, that such filters become completely filled under high gas concentrations, which would require their regeneration via, say, heating.

The best known example of filter application in gas sensors is CO sensor. Various devices developed to detect CO successfully utilize charcoal as a filter to avoid the interfering effect of hydrocarbons and alcohols (McGeekin 1996; Schweizer-Berberich et al. 2000; Kitsukawa et al. 2000). In this case, activated charcoal is placed inside the packaging casing between sensor and surrounding atmosphere (see Fig. 12.2a). A nylon cap with charcoal cloth filter was pressed over the metal can of the sensor housing. Schweizer-Berberich et al. (2000) established that charcoal filters with a diameter of 8 mm and a thickness of 10 mm were sufficient for preventing a false alarm by interfering gases, such as CH<sub>4</sub>, within the required exposure time of 2 h. Smaller filter thickness led to a breakthrough of the UL-test gases. Miller (2001) has found that external activated carbon filters can also be used to prevent poisoning by hexamethyldisiloxane (HMDS). As shown in Fig. 12.2, activated carbon filters are extremely effective for limiting silicones. However, this class of filter also prevents passage of hydrocarbons heavier than methane.

**Table 12.2** Surface filters employed in one-electrode semiconductor gas sensors to improve sensor selectivity

Gas-sensing material	Membrane	Effect
SnO <sub>2</sub>	Dense SiO <sub>2</sub>	Improves H <sub>2</sub> selectivity; decreases response to humidity
SnO <sub>2</sub>	Al <sub>2</sub> O <sub>3</sub>	Improves durability to Si-containing gas poisoning
SnO <sub>2</sub>	ZnO	Increases sensitivity to H <sub>2</sub> and C <sub>2</sub> H <sub>5</sub> OH
In <sub>2</sub> O <sub>3</sub>	Dense SiO <sub>2</sub>	Improves H <sub>2</sub> selectivity
ZnO	WO <sub>3</sub> -Al <sub>2</sub> O <sub>3</sub>	Improves C <sub>2</sub> H <sub>4</sub> O selectivity

Source: Reprinted with permission from Korotcenkov (2007b). Copyright 2007 Elsevier

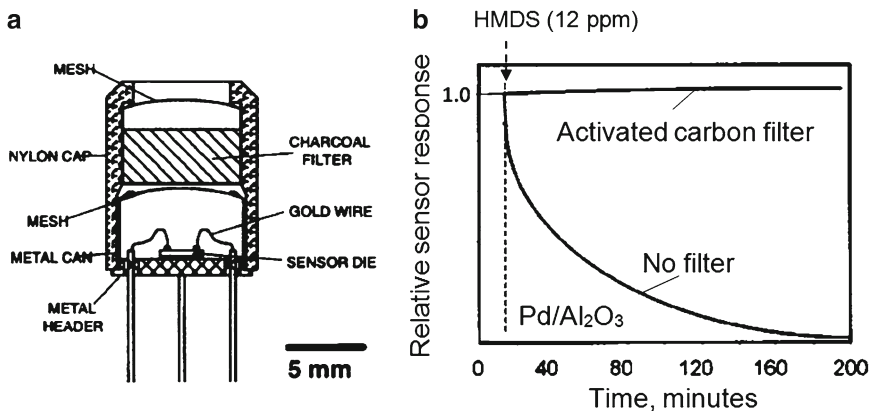


**Fig. 12.2** (a) SnO<sub>2</sub>-based MGS1100 gas sensor with filter included in the nylon cap. (Reprinted with permission from Schweizer-Berberich et al. (2000). Copyright 2000 Elsevier). (b) Pd/Al<sub>2</sub>O<sub>3</sub> catalytic detectors with and without activated carbon filter exposed to 15 ppm HMDS in 2.5 % CH<sub>4</sub>/air. [Data from Miller (2001)]

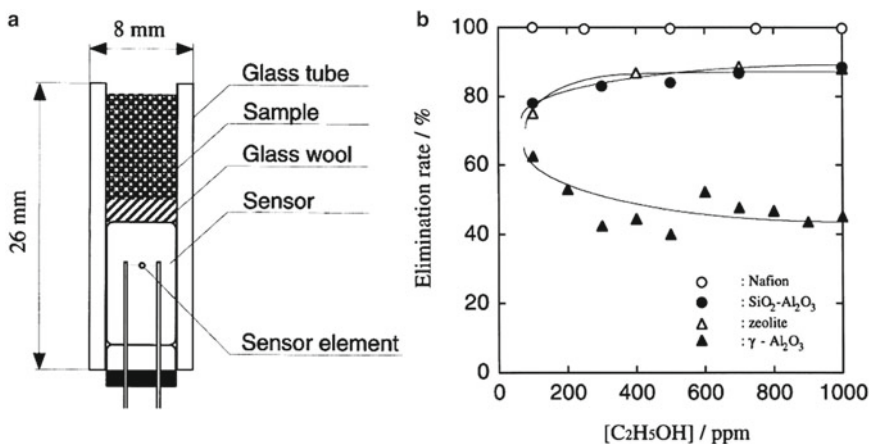


**Fig. 12.3** (a) Model sensor unit and (b) elimination effect of filtering materials (Reprinted with permission from Kitsukawa et al. (2000). Copyright 2000 Elsevier)

Another example of CO sensor with increase selectivity is shown in Fig. 12.3. Kitsukawa et al. (2000) tested different materials, such as Nafion, SiO<sub>2</sub>-Al<sub>2</sub>O<sub>3</sub>, zeolite, γ-Al<sub>2</sub>O<sub>3</sub>, BaO, and CaO, and established that the ethanol interference for CO sensor is almost removed by Nafion filter without a sensitivity change to CO gas. It was also found that this effect was remarkably improved by the treatment of the Nafion to be formed into complete acidic type before measurement. In the case of barium oxide and calcium oxide, no effect of elimination was observed.



We need to note that the filters strongly increase response and recovery times simultaneously with improving sensor selectivity. For example, studying Pd/Al<sub>2</sub>O<sub>3</sub> catalytic detectors, Miller (2001) established that the sensor without the filter had a pentane response time of 300 s, while, with activated carbon filter, no pentane response was seen even after 30 min. Miller (2001) concluded that such filter influence of sensor parameters illustrates a key trade-off in the design of modern gas sensors—it is difficult to obtain rapid response, high selectivity, and good tolerance to poisons in the same design. In addition, we need to note that the above-mentioned filters can also limit O<sub>2</sub> diffusion into the gas-sensing layer. It was established that the limited O<sub>2</sub> diffusion into the SnO<sub>2</sub> layer can cause a strong reduction of the SnO<sub>2</sub> upon exposure to H<sub>2</sub> in the inner layer covered with the dense SiO<sub>2</sub> layer. This results in decay of sensor output and irreversible degradation of the device due to deactivation of the SnO<sub>2</sub>. To resolve this issue, it was suggested to dope SnO<sub>2</sub> with Ce, which stabilizes the characteristics of the sensor material compared to the undoped version (Katsuki and Fukui 1998). In addition, it was found that sensors based on the SnO<sub>2</sub>:Ce layer with built-in SiO<sub>2</sub> surface coating layer had a negligible signal to humidity and were resistant to highly reactive gases such as hexamethylenediamine (HMDA) and SO<sub>2</sub> (Katsuki and Fukui 1998).

It is also necessary to take into account that the lifetime of filters is limited, and therefore, in the absence of control of their conditions, changes in their filtering capacities could be a reason for the observed drift in sensor characteristics. In addition, the adsorption capacity of filters often decreases with temperature (Schweizer-Berberich et al. 2000). Thus the filter sorption capacity becomes dependent on both the surrounding temperature and the heater temperature. Taking all these considerations into account, one should carefully interpret any results pertaining to improvement of the temporal stability of sensor parameters, especially at the expense of adding filtering layers to the gas-sensing layer (Zhan et al. 2004). Most of the results stated here were obtained in clean lab conditions, and therefore it is unknown how these filters—especially those with small pore sizes—would behave in a highly polluted atmosphere.

Prasad et al. (2010) have shown that an additional protective layer, formed on the surface of SnO<sub>2</sub>, can also stabilize the behavior of metal oxide in reduced atmosphere. They found that the additional microporous ceramic Si-B-C-N layer, acting as a filter, prevents the reduction of SnO<sub>2</sub> in H<sub>2</sub>/CO atmosphere. The microporous amorphous Si-B-C-N layers were obtained via the polymer pyrolysis route. The main feature of the tested Si-B-C-N polymer-derived ceramics is their increased stability against crystallization and high temperature stability. It was established that the Si-B-C-N-coated SnO<sub>2</sub> sensors showed stable sensor signals toward hydrogen and carbon monoxide (550 °C) in the absence of oxygen, whereas the unprotected SnO<sub>2</sub> sample becomes reduced over time. It is known that in hydrogen-rich atmospheres at high temperatures, SnO<sub>2</sub> is not stable being reduced to metallic tin (Wurzinger and Reinhardt 2004).

## 12.2 Catalytically Active Filters

The catalytic filters are designed with noble metals (Pt, Pd) and MOXs (Fe<sub>2</sub>O<sub>3</sub>, CuO) which can be deposited directly on the sensing material. For example, the combination of a thin gas-sensing film and a thick filtering film was considered by Meixner's group when they developed Ga<sub>2</sub>O<sub>3</sub> sensors, in order to reduce the ethanol and acetone effect (Flingelli et al. 1998). However, most catalyst filters employ noble metals. One of the first prototypes of such a noble metal-based filter was composed of a Pt-porous thick film deposited over a thick film of Pd:SnO<sub>2</sub> (Menil et al. 1994). This device was said to reduce the effects of alcohol and CO to aid in CH<sub>4</sub> detection. Dutronc et al. (1993a, b) have shown that the use of Pd filters also enhances the selectivity of sensors for CH<sub>4</sub>. A similar approach was used

by Mandayo et al. (2002), who dropped a Pt:SnO<sub>2</sub> thick film as a filter over a film, 200 nm thick, of the same material. This allowed the authors to reduce the ethanol signal of the sensor, which was targeted to CH<sub>4</sub> and CO detection.

It was established, however, that the use of metallic films in direct contact with the gas-sensing semiconductor makes the effect rather complex. For instance, thick metal may shunt the MOX layer, among other effects. Therefore, very thin films of the metal dispersed over the gas-sensitive oxide are mainly used. Examples include a Pd film, 5–15 nm thick, which improves the selectivity of SnO<sub>2</sub> film response to H<sub>2</sub> and C<sub>2</sub>H<sub>5</sub>OH against CH<sub>4</sub> and CO (Sberveglieri 1992), or a Pt film, 5 nm thick, which improves the selectivity of SnO<sub>2</sub> film response to CO against NO<sub>2</sub> and O<sub>3</sub> (Wollenstein et al. 2000). However, such thin metallic films or dispersed clusters do not have enough thickness to yield effective filtration. To improve this situation, an intermediate porous insulating layer may be introduced in gas sensor (Sberveglieri 1992). This layer separates the gas-sensing oxide layer and metal film and therefore gives possibility to use thicker metal films with better filtration ability. Recently, Frietsch et al. (2000) employed an Al<sub>2</sub>O<sub>3</sub> thin film, 30 nm thick, as such an insulating layer between an SnO<sub>2</sub> film, 300 nm thick, and the catalytic layer of CuO, 5–30 nm thick, in order to exclude its influence on the resistivity of the gas-sensing layer. Cabot et al. (2003) proposed using mesoporous silica which, due to high resistivity and high surface area, is ideally suited as a base material for this application. Figure 12.4 shows transitory resistance of the SnO<sub>2</sub> material heated at 350 °C with different gas conditions. Cabot et al. (2003) found that SiO<sub>2</sub> has no observable influence on the CO and CH<sub>4</sub> sensor response. The low density of the silica-deposited layer and the well-defined spacious mesoporous channels in the mesoporous filter layer allow efficient diffusion of the species involved in the sensing mechanism. Consequently, it does not induce any physical filtering to O<sub>2</sub>, CO, and CH<sub>4</sub>, resulting in no slowdown of the sensor response or signal recovery speed. Catalytic filters consisting of Pd- and Pt-loaded mesoporous silica (SiO<sub>2</sub>:Pd and SiO<sub>2</sub>:Pt filters), on the other hand, eliminate the response to CO without affecting the response to CH<sub>4</sub>.

MnO<sub>2</sub> thick film, deposited on the surface of metal oxides such as SnO<sub>2</sub> and WO<sub>3</sub> with the purpose of reducing the interference of O<sub>3</sub> for NO<sub>2</sub> sensors, acts as a catalytically active filter as well (Pijolat et al. 2003; Viricelle et al. 2006; Zhang et al. 2012). Fortunately, O<sub>3</sub> is unstable and can be transformed to O<sub>2</sub> by catalysts, e.g., manganese dioxide (MnO<sub>2</sub>) (Dhandapani and Oyama 1997). The results obtained have shown that the sensors with thin MnO<sub>2</sub> filters are able to reduce the O<sub>3</sub> interference while keeping a good response to NO<sub>2</sub>.

Regarding technological approaches used for filter fabrication, we can say that the additional filter or sandwich coatings at the surface of gas-sensing materials can be deposited by conventional methods such as chemical vapor deposition or sputtering (Katsuki and Fukui 1998; Zhan et al. 2005), electrophoretic deposition (Dougami and Takada 2003), and successive ionic layer deposition (SILD) (Korotcenkov et al. 2006; Tolstoy et al. 2009). The last, rather new method is realized by consistent dipping of the sample into reagent solutions. SILD chemistry is based on hydroxylation of a growing layer, proton–metal cation exchange between the hydroxylated layer and the aqueous solution, and additional oxidation by hydrogen peroxide, which results in higher oxidation states of the chemisorbed metal ions and yields poorly soluble peroxocomplexes. The thickness of film developed by this method depends on the number of deposition cycles and follows a linear law. The advantage of this method is that the film, usually of nanodomain thickness, is placed continuously and uniformly over the whole surface, with morphology determined by the nature of the synthesized material. This method is also attractive because the reaction of cation metal adsorption during the second step of the deposition cycle is self-stopped when the monolayer coverage is attained. The synthesis can be carried out at room temperature in a rather simple apparatus. Screen printing can also be used to fabricate filter membranes (see, e.g., Goldberg et al. 1994). Membranes of different compositions can be deposited just by repeating the screen print/cure cycles. The use of screen printing has rheological constraints but does not require additional processing such as etching and lift-off.

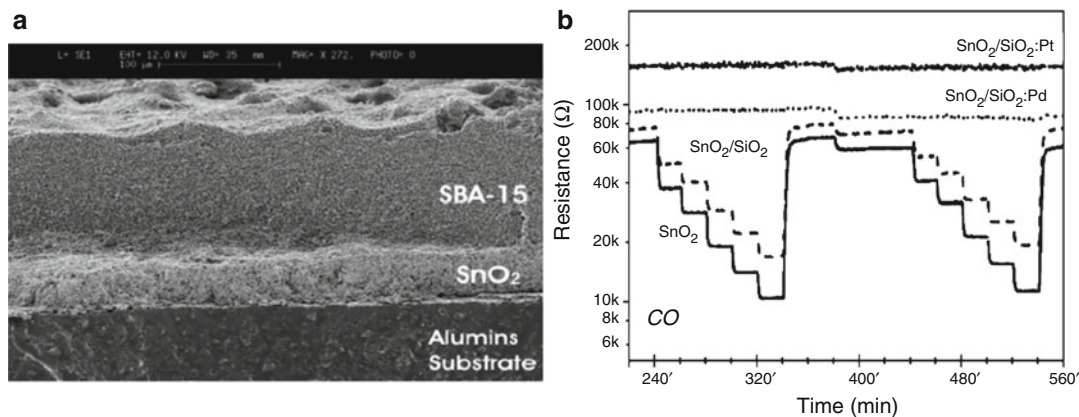


**Fig. 12.4** (a) SEM cross-sectional view of a  $\text{SnO}_2$  sensor with a filter ( $\sim 100\text{-}\mu\text{m}$ ) fabricated from SBA-15 mesoporous silica. (b) Transitory resistances of the  $\text{SnO}_2$ ,  $\text{SnO}_2\text{-SiO}_2$ ,  $\text{SnO}_2\text{-SiO}_2\text{:Pd}$ , and  $\text{SnO}_2\text{-SiO}_2\text{:Pt}$  gas sensors when exposed to different concentrations of CO, from 20 to 400 ppm. Two different relative humidity conditions are considered: 30–50 % (Reprinted with permission from Cabot et al. (2003). Copyright 2003 Elsevier)

### 12.3 Sorbents for Gas Preconcentrators

Preconcentration is a useful way to improve sensor selectivity and detection limits for certain analytes. Besides, the preconcentration is one of the methods used for gas sampling. The preconcentrator is conventionally placed at the front end of the analytical system and concentrates and purifies the analyte at the sorption material, which is developed to absorb selectively the analyte molecules over a period of time. Following heating to high temperature, the sorption material releases the analyte and supplies the gas-sensing unit with the gas at relatively high concentration to allow its efficient detection by the sensor. The preconcentrator obviously needs time to collect the analyte, which limits its application to cases when analyte detection is carried out over a rather long period of time. The most significant figure of merit for a preconcentrator is the concentration factor, which is the ratio of the analyte concentration delivered to the sensor and the analyte concentration present in the inlet airflow.

The conventional preconcentrators, so-called microtraps, comprise a stainless steel tube or glass capillary tube (Janata 1989; Bakker and Telting-Diaz 2002; Hierlemann and Baltes 2002; Pierce et al. 2003; Hu et al. 2003; Camara et al. 2010). To heat the unit and to desorb the gas, a current is passed through the stainless steel tube or a metal spiral heater coiled around the glass capillary tube. These units are characterized by large dead volumes and limited heating efficiency due to their relatively large thermal mass, which contributes to a rather long time for the analyte pulse. Microfabricated preconcentrator devices based on micro-hotplates overcome these limitations through a significant reduction of dead volume and thermal mass, which allows them to deliver the analyte gas with a short time pulse for analysis (Simon et al. 2001; Shen et al. 2004; Voiculescu et al. 2008; Camara et al. 2010).

Preconcentrators used in detection of complex organic vapors employ a granular, highly porous sorption material which provides a large collection area. Some preconcentrators are packed with up to three different absorbent materials to enhance the efficiency of collection and concentration of various organic compounds. Silica gel, polyurethane foam (PUF), and other sorbents can be used for these purposes. Sorbents usually used for atmospheric air monitoring are shown in Table 12.3.

A potential problem encountered in these techniques is reactions occurring during the sampling between the concentrated organic gases of interest and other reactive air constituents such as ozone, halogens, the hydroxyl radical, nitrogen oxides, water, or hydrogen peroxide. Reactions of this kind

**Table 12.3** Sorbents usually used for atmospheric air control

Type of sorbent	Specific area (m <sup>2</sup> /g)	Maximum temperature (°C)	VOC analytes retained	Preferred analyte-liberation technique
<b>Porous organic polymers</b>				
Tenax TA and GR	35	<350	Aromatic compounds, nonpolar VOC	Thermal desorption
Chromosorb 102 ( <i>styrene-divinylbenzene copolymer</i> )	750	20–250	Alcohols, ketones, aliphatic hydrocarbons	Thermal desorption
Chromosorb 106 ( <i>polystyrene</i> )	350	20–250	C <sub>5</sub> –C <sub>12</sub> hydrocarbons, oxygenated VOCs	Thermal desorption
Porapak N ( <i>polyvinylpyrrolidone</i> )	300	20–190	Acetylene, aliphatic hydrocarbons	Thermal desorption
Porapak Q ( <i>ethylvinylbenzene-divinylbenzene copolymer</i> )	550	20–190	Acetylene, aliphatic hydrocarbons, and oxygenated VOCs	Solvent extraction
<b>Graphitized carbon blacks (specific surface depends on the degree of graphitization)</b>				
Carbotrap	12	>400	Hydrocarbons less than C <sub>20</sub> , alkylbenzenes	Thermal desorption
Carbograph	100	>400	Ketones, alcohols, and aldehydes	
Carbopack	12	>400		
<b>Molecular sieves (formed during the pyrolysis of organic polymers, e.g., polyvinyl chloride)</b>				
Spherocarb	1,200	>400	Very volatile organic compounds, methanol, acetone	Thermal desorption
Unicarb	>1,000	>400		
Carbosieve III	800	400		
Carboxen	>1,200	400		
Molecular Sieve 13X, 5A		350–400	1,3-Butadiene	
<b>Activated carbon (formed by the low-temperature oxidation of vegetable carbon)</b>				
Activated carbon	>1,000	400	Aliphatic and aromatic hydrocarbons, e.g., C <sub>2</sub> –C <sub>4</sub>	Solvent extraction or thermal desorption

Source: Reprinted with permission from Krol et al. (2010a, b). Copyright 2010 Elsevier

may alter the quantities of the trace gases of interest and may also contribute to the formation of artifact products which may mistakenly be interpreted as atmospheric constituents (Helmig 1997). Therefore, the investigation of interference from reactions during sampling is an important part of method development and improvement strategies for atmospheric monitoring.

## References

- Bakker E, Telting-Diaz M (2002) Electrochemical sensors. *Anal Chem* 74:2781–2800
- Billi E, Viricelle J-P, Montanaro L, Pijolat C (2002) Development of a protected gas sensor for exhaust automotive applications. *IEEE Sensor J* 2(4):342–348
- Cabot A, Arbiol J, Cornet A, Morante JR, Chen F, Liu M (2003) Mesoporous catalytic filters for semiconductor gas sensors. *Thin Solid Films* 436:64–69
- Camara EHM, Breuil P, Briand D, Guillot L, Pijolat C, de Rooij NF (2010) Micro gas preconcentrator in porous silicon filled with a carbon absorbent. *Sens Actuators B* 148:610–619
- De Angelis L, Riva R (1995) Selectivity and stability of a tin dioxide sensor for methane. *Sens Actuators B* 28:25–29
- Dhandapani B, Oyama ST (1997) Gas phase ozone decomposition catalysts. *Appl Catal* 11:129–166
- Dougami N, Takada T (2003) Modification of metal oxide semiconductor gas sensor by electrophoretic deposition. *Sens Actuators B* 93:316–320

- Dutronec P, Lucat C, Menil F, Loesch M, Horillo MC, Sayago I, Gutierrez J, De Agapito JA (1993a) A potentially selective methane sensor based on the differential conductivity responses of Pd and Pt-doped tin oxide thick layers. *Sens Actuators B* 15–16:384–389
- Dutronec P, Lucat C, Menil F, Loesch M, Combes L (1993b) A new approach to selectivity in methane sensing. *Sens Actuators B* 15–16:24–31
- Feng CD, Shimizu Y, Egashira M (1994) Effect of gas diffusion process on sensing properties of SnO<sub>2</sub> thin film sensors in a SiO<sub>2</sub>/SnO<sub>2</sub> layer-built structure fabricated by sol–gel process. *J Electrochem Soc* 141:220–225
- Fleischer M, Kornely S, Weh T, Frank J, Meixner H (2000) Selective gas detection with high-temperature operated metal oxides using catalytic filters. *Sens Actuators B* 69:205–210
- Flingelli G, Fleischer M, Meixner H (1998) Selective detection of methane in domestic environments using a catalyst sensor system based on Ga<sub>2</sub>O<sub>3</sub>. *Sens Actuators B* 48:258–262
- Frietsch M, Zudock F, Goschnick J, Bruns M (2000) CuO catalytic membrane as selectivity trimmer for metal oxide gas sensors. *Sens Actuators B* 65:379–381
- Goldberg HD, Brown RB, Liu DP, Meyerhoff ME (1994) Screen printing: a technology for the batch fabrication of integrated chemical-sensor arrays. *Sens Actuators B* 21:171–183
- Helmig D (1997) Ozone removal techniques in the sampling of atmospheric volatile organic trace gases. *Atmos Environ* 31:3635–3651
- Hierlemann A, Baltes H (2002) CMOS-based chemical microsensors. *Analyst* 128:15–28
- Hu J, Zhu F, Zhang J, Gong H (2003) A room temperature indium tin oxide/quartz crystal microbalance gas sensor for nitric oxide. *Sens Actuators B* 93:175–180
- Hubalek J, Malysz K, Prasek J, Vilanova X, Ivanov P, Llobet E, Brezmes J, Correig X, Sverak Z (2004) Pt-loaded Al<sub>2</sub>O<sub>3</sub> catalytic filters for screen-printed WO<sub>3</sub> sensors highly selective to benzene. *Sens Actuators B* 101:277–283
- Janata J (1989) *Principle of chemical sensors*. Plenum, New York
- Katsuki A, Fukui K (1998) H<sub>2</sub> selective gas sensor based on SnO<sub>2</sub>. *Sens Actuators B* 52:30–37
- Kitsukawa S, Nakagawa H, Fukuda K, Asakura S, Takahashi S, Shigemori T (2000) The interference elimination for gas sensor by catalyst filters. *Sens Actuators B* 65(1):120–121
- Knaebel KS (2004) Adsorbent selection. Adsorption Research Inc. <http://www.adsorption.com/publications/AdsorbentSel1B.pdf>
- Korotcenkov G (2007) Practical aspects in design of one-electrode semiconductor gas sensors: status report. *Sens Actuators B* 121:664–678
- Korotcenkov G, Tolstoy V, Schwank J (2006) Successive ionic layer deposition (SILD) as a new sensor technology: synthesis and modification of metal oxides. *Meas Sci Technol* 17:1861–1869
- Krol S, Zabiegata B, Namiesnik J (2010a) Monitoring VOCs in atmospheric air. I. On-line gas analyzers. *Trends Anal Chem* 29(9):1092–1100
- Krol S, Zabiegata B, Namiesnik J (2010b) Monitoring VOCs in atmospheric air. II. Sample collection and preparation. *Trends Anal Chem* 29(9):1101–1112
- Mandayo GC, Castano E, Gracia FJ, Cirera A, Cornet A, Morante JR (2002) Built-in active filter for an improved response to carbon monoxide combining thin and thick-film technologies. *Sens Actuators B* 87:88–94
- McGeehin P (1996) Self-diagnostic gas sensors which differentiate carbon monoxide from interference gases for residential applications. *Sensor Rev* 16:37–39
- Menil F, Lucat C, Debich A (1994) The thick-film route to selective gas sensors. *Sens Actuators B* 25:415–420
- Miller JB (2001) Catalytic sensors for monitoring explosive atmospheres. *IEEE Sensors J* 1(1):88–93
- Park J-H, Yang RT (2005) Simple criterion for adsorbent selection for gas purification by pressure swing adsorption processes. *Ind Eng Chem Res* 44:1914–1921
- Pierce TC, Schiffma SS, Nagle HT, Gardner JW (eds) (2003) *Handbook of machine olfaction: electronic nose technology*. Wiley-VCH, Weinheim
- Pijolat C, Pupier C, Sauvan M, Tournier G, Lalauze R (1999) Gas detection for automotive pollution control. *Sens Actuators B* 59:195–202
- Pijolat C, Riviere B, Kamionka M, Viricelle JP, Breuil P (2003) Tin dioxide gas sensor as a tool for atmospheric pollution monitoring: problems and possibilities for improvements. *J Mater Sci* 38:4333–4346
- Pijolat C, Viricelle JP, Tournier G, Montmep P (2005) Application of membranes and filtering films for gas sensors improvements. *Thin Solid Films* 490:7–16
- Prasad RM, Gurlo A, Riedel R, Hübner M, Barsan N, Weimar U (2010) Microporous ceramic coated SnO<sub>2</sub> sensors for hydrogen and carbon monoxide sensing in harsh reducing conditions. *Sens Actuators B* 149:105–109
- Ryzhikov A, Labeau M, Gaskov A (2009) Selectivity improvement of semiconductor gas sensors by filters. In: Baraton M-I (ed) *Sensors for environment, health and security*, NATO science for peace and security series C: environmental security. Springer, Dordrecht, pp 141–157
- Sauvan M, Pijolat C (1999) Selectivity improvement of SnO<sub>2</sub> films by superficial metallic films. *Sens Actuators B* 58:295–301

- Sberveglieri G (1992) Classical and novel techniques for the preparation of SnO<sub>2</sub> thin-film gas sensors. *Sens Actuators B* 6:239–247
- Schweizer-Berberich M, Strathmann S, Gopel W, Sharma R, Peyre-Lavigne A (2000) Filters for tin dioxide CO gas sensors to pass the UL2034 standard. *Sens Actuators B* 66:34–36
- Shen CY, Huang CP, Huang WT (2004) Gas-detecting properties of surface acoustic wave ammonia sensors. *Sens Actuators B* 101:1–7
- Simon I, Bărsan N, Bauer M, Weimar U (2001) Micromachined metal oxide gas sensors: opportunities to improve sensor performance. *Sens Actuators B* 73:1–26
- Tolstoy V, Han SD, Korotcenkov G (2009) Successive ionic layer deposition (SILD): advanced method for deposition and modification of functional nanostructured metal oxides aimed for gas sensor applications. In: Umar A, Hahn YB (eds) *Metal oxide nanostructures and their applications*, vol 3. American scientific, Stevenson Ranch, CA, pp 1–58
- Viricelle J, Pauly A, Mazet L, Brunet J, Bouvet M, Varenne C, Pijolat C (2006) Selectivity improvement of semi-conducting gas sensors by selective filter for atmospheric pollutants detection. *Mater Sci Eng C* 26:186–195
- Vlachos DS, Scafidas PD, Avaritsiotis JN (1995) The effect of humidity on tin-oxide thick-film gas sensors in the presence of reducing and combustible gases. *Sens Actuators B* 25:491–494
- Voiculescu I, Zaghoul M, Narasimhan N (2008) Microfabricated chemical preconcentrators for gas-phase microanalytical detection systems. *Trends Anal Chem* 27:327–342
- Wollenstein J, Bottner H, Jaegle M, Becker WJ, Wagner E (2000) Material properties and the influence of metallic catalysts at the surface of highly dense SnO<sub>2</sub> films. *Sens Actuators B* 70:196–202
- Wong KKL, Tang Z, Sin JKO, Chan PCH, Cheung PW, Hiraoka H (1996) Sensing mechanism of polymer for selectivity enhancement of gas sensors. In: *Proceedings of IEEE international conference on semiconductor electronics, ICSE'96*, Penang, 26–28 Nov 1996, pp 217–220
- Wurzinger O, Reinhardt G (2004) CO-sensing properties of doped SnO<sub>2</sub> sensors in H<sub>2</sub>-rich gases. *Sens Actuators B* 103:104–110
- Yang RT (1997) *Gas separation by adsorption processes*. Imperial College Press, London
- Yang RT (2003) *Adsorbents: fundamentals and applications*. Wiley-Interscience, Hoboken, NJ
- Zhan ZL, Jiang DG, Xu JQ (2004) Enhancement of H<sub>2</sub> sensing properties of In<sub>2</sub>O<sub>3</sub>-based gas sensor by chemical modification with SiO<sub>2</sub>. *Chin Chem Lett* 15(12):1509–1512
- Zhan Z, Jiang D, Xu J (2005) Investigation of a new In<sub>2</sub>O<sub>3</sub>-based selective H<sub>2</sub> gas sensor with low power consumption. *Mater Chem Phys* 90:250–254
- Zhang C, Boudiba A, Navio C, Olivier M-G, Snyders R, Debliquy M (2012) Study of selectivity of NO<sub>2</sub> sensors composed of WO<sub>3</sub> and MnO<sub>2</sub> thin films grown by radio frequency sputtering. *Sens Actuators B* 161:914–922

**Part III**  
**Materials for Specific Gas Sensors**

## Chapter 13

# Materials for Piezoelectric-Based Gas Sensors

Piezoelectric-based or acoustic wave (AW) sensors such as surface acoustic wave (SAW), quartz crystal microbalance (QCM) or bulk acoustic wave (BAW), and cantilever-based devices create a specific class of gas sensors widely used in various applications (Ippolito et al. 2009; Korotcenkov 2011) (see Fig. 13.1). Virtually all acoustic wave-based devices use a piezoelectric material to generate the acoustic wave which propagates along the surface in SAW devices or throughout the bulk of the structure in BAW devices. Piezoelectricity involves the ability of certain crystals to couple mechanical strain to electrical polarization and will only occur in crystals that lack a center of inversion symmetry (Ballantine et al. 1996).

Acoustic wave devices come in a number of configurations, each with their own distinct acoustic and electrical characteristics [see Chap. 1 (Vol. 1)]. The first are bulk acoustic wave (BAW) devices, which involve acoustic wave propagation through the bulk of the structure. This category of devices includes the quartz crystal microbalance (QCM) and thin-film resonators (TFRs), the latter encapsulating thin-film bulk acoustic resonator (FBAR) and solidly mounted resonator (SMR) structures. Two typical structures of FBAR-based sensors are shown in Fig. 13.2. The first (Fig. 13.2a) shows the electrodes and thin piezoelectric film deposited on top of an optional insulating layer (typically silicon nitride) supported by a substrate. A portion of the substrate is removed, typically by a wet chemical etching process, thereby defining the resonator. The top electrode may be patterned in a ground–signal–ground configuration, with the bottom electrode serving as the electrical ground plane (Lakin 2005). The second TFBAR structure (Fig. 13.2b) shows the vibrating membrane suspended over an air gap. However, for gas-sensing applications, the first configuration is the most widely utilized. In most gas-sensing applications, a sensitive layer is deposited on one side of the structure. For the supporting substrate with the etched cavity, the sensitive layer is typically deposited in the region of this etched cavity as shown in Fig. 13.2a. However, for the air gap-based structure, the sensitive layer is deposited on the top side. The fundamental difference between FBAR and QCM or TSM is in the operating frequency. FBARs have a fundamental resonant frequency around 1 GHz due to the thinner piezoelectric layer. This also means higher mass sensitivity.

The second type utilizes acoustic waves confined to the surface of the piezoelectric material and are known as surface acoustic wave (SAW) devices. Both BAW and SAW sensors use longitudinal waves or shear waves (SH). Surface acoustic waves are generated by converse piezoelectric effect at the input interdigital transducer (IDT), and they are converted back into an electric signal by direct piezoelectric effect. In their basic form, they consist of a piezoelectric substrate, on top of which two metallic interdigital transducers (IDTs) are patterned to form a delay line structure, as shown in Fig. 13.3. This is the most commonly utilized structure for gas-sensing applications with the sensitive layer normally deposited in between the two IDT ports.



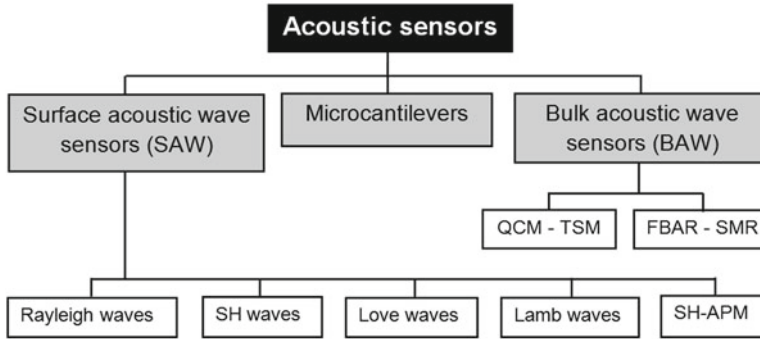


**Fig. 13.1** Different types of acoustic devices that can be used for sensing application: *FBAR* film bulk acoustic resonators, *TSM* thickness shear mode, *SMR* solidly mounted resonators. Other designations are in the text

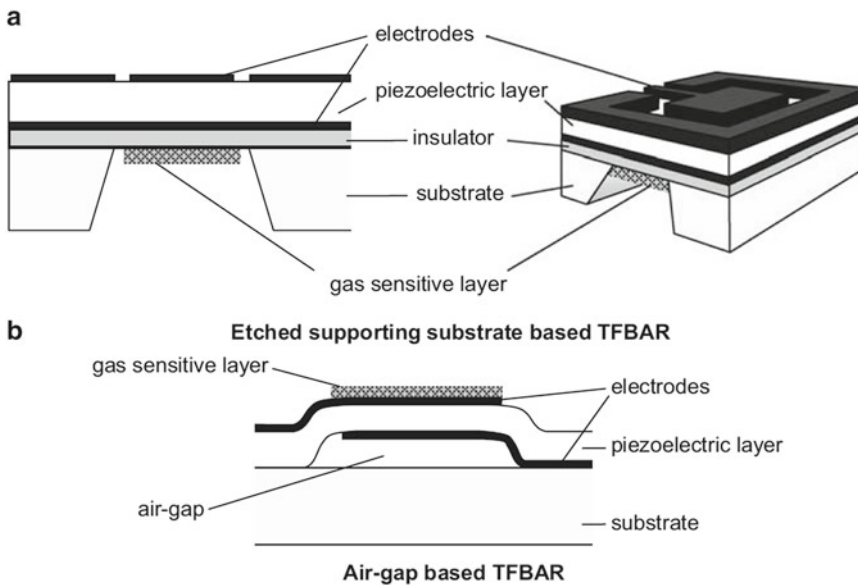


**Fig. 13.2** (a) Cross-section and diagram of a TFBAR with etched supporting substrate and (b) diagram of TFBAR having the vibrating part suspended over an air gap (Reprinted with permission from Ippolito et al. (2009). Copyright 2009 Springer, New York)

There are many different types of surface acoustic waves that are used for sensor applications (Ballantine et al. 1997; Mortet et al. 2008; Ippolito et al. 2009). Rayleigh waves have longitudinal and vertical shear components. Longitudinal waves have particle displacements parallel to the direction of wave propagation while shear waves have particle displacements normal to the direction of wave propagation. The particle displacements in shear waves are either normal to the sensing surface (vertical shear wave) or parallel to the sensing surface (horizontal shear wave). Because of the shear component that couples with the medium in contact with the device's surface, SAW devices operating with Rayleigh waves cannot operate in liquids. They are generally used to make high-frequency gas sensors. Shear-horizontal surface acoustic waves (SH-SAW) have particle displacements perpendicular to the propagation direction and parallel to the surface. Acoustic devices operating with horizontal shear waves are of particular interest since there are no acoustic losses when operated in liquids

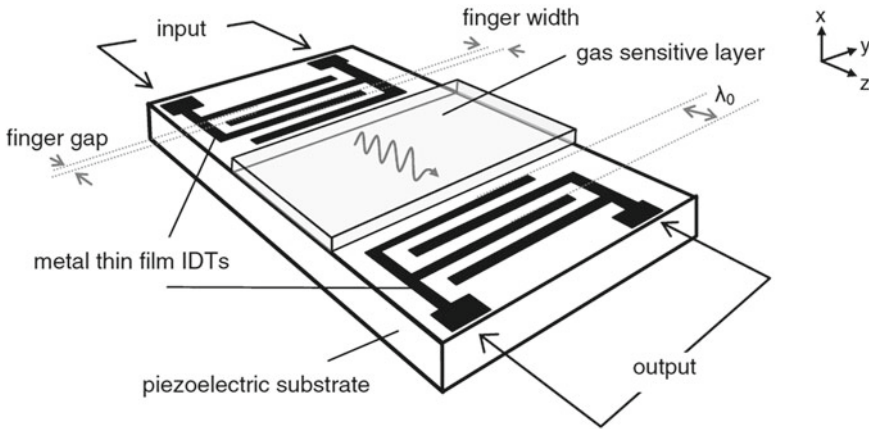


**Fig. 13.3** Two-port delay line SAW device with gas-sensitive layer (Reprinted with permission from Ippolito et al. (2009). Copyright 2009 Springer, New York)

compared to vertical shear waves. Thus, they are adequate for sensing applications in liquids. Love waves are a particular form of SH surface waves, and they can be used for sensors operating in liquids. They are formed by the constructive interference of multiple reflections at the thin coating interface layer that has an acoustic velocity lower than the substrate. Love waves are dispersive, i.e., the wave velocity is not solely determined by the material constants but also by the ratio between the thickness of the piezoelectric layer and the wavelength defined by the IDTs special period. Bulk acoustic waves generated by IDTs can be confined between the upper and lower surfaces of a plate that acts as an acoustic waveguide. As a result, both sides of the plate vibrate. Thus, IDTs can be placed on one side of the plate, and the other side can be used for sensing purposes. Shear-horizontal acoustic plate mode (SH-APM) sensors can also be operated in liquids. If the substrate thickness is smaller than the wavelength (membrane), longitudinal and flexural waves, called Lamb waves, are generated. Devices based on such waves, also called flexural plate wave sensors (FPW), are of special interest since they are more sensitive than other SAW sensors and they can be operated in liquids.

The nature of acoustic waves generated in piezoelectric materials is determined by the piezoelectric material orientation as well as the metal electrodes configuration employed to generate the electric field that induces acoustic waves by converse piezoelectric effect. As gas sensors, the resonators are coated with layers which selectively absorb or adsorb analytes of interest and thereby induce a mass change that is then detected via a shift in the resonant frequency of the device (Kurosawa et al. 1990). The detection limits and the relative ( $S_r$ ) mass sensitivities for different types of acoustic sensors are presented in Table 13.1. The comparison of various types of AW sensors is also presented in Table 13.2. Several books and reviews (Ballantine et al. 1997; Ippolito et al. 2009) provide a more detailed analysis of AW-based sensors operation.

## 13.1 Piezoelectric Materials

In these devices, piezoelectric materials play one of the main roles. Usually,  $\alpha$ -quartz ( $\text{SiO}_2$ ) and non-stoichiometric lithium niobate ( $\text{LiNbO}_3$ ) are used in such devices (Jakubik et al. 2002). Quartz is a piezoelectric material that is widespread in nature (Rosen et al. 1992). Quartz, a crystalline form of  $\text{SiO}_2$ , presents an excellent crystal quality, and this material can be very weakly sensitive to parasitic temperature effects (compared to other piezoelectric materials) according to its cut. These two

**Table 13.1** Comparison of the relative sensitivity and minimum detectable mass density of the different acoustic sensors

Sensors	Sensitivities (cm <sup>2</sup> /g)	Minimum detectable mass density (ng/cm <sup>2</sup> )
Flexural plate wave	100–1,000	~0.5
SH-SAW	65	1
FBAR	1,000–10,000	0.1–0.01
Quartz microbalance	10	10
SAW	151	1.2
Microcantilever	1,000–10,000	0.02–0.04

Source: Reprinted with permission from Mortet et al. (2008). Copyright 2008 Wiley-VCH Verlag

**Table 13.2** Typical properties of commonly utilized acoustic wave-based sensors

Parameter	QCM	TFR	SAW
Operating frequency range	5–30 MHz	500 MHz–20 GHz	40 MHz–1 GHz
Sensitivity towards mass	Yes	Yes	Yes
Sensitivity towards conductivity	No	No	Yes
Fractional frequency change to gas	~0.01 %	~0.1 %	~0.1 %
Quality factor (approx.)	Up to 10 <sup>5</sup>	Up to 10 <sup>3</sup>	Up to 10 <sup>4</sup>

Source: Data from Ippolito et al. (2009)

properties explain its widespread use as a platform for AW sensors (Wang et al. 2006; Fanget et al. 2011). Though it is far from easy to grow, quartz's widespread use has led to its availability in comparatively large sizes and large quantities from several suppliers. Artificially grown quartz crystals show high stability over long times at room temperature and good resistance to adverse chemical conditions. In addition, various crystallographic orientations that minimize the temperature coefficient (near-room temperature) of AW devices have been characterized over the years and are now widely available; these include the ST cut for AW devices and the AT and BT cuts for “thickness-shear-mode” (TSM) resonators or quartz crystal microbalance (QCM) sensors.

Among the most common and important piezo materials are zinc oxide (ZnO) (Özgür et al. 2005; Lang 2005), aluminum nitrate (AlN) films (Tadigadapa and Mateti 2009), lithium tantalate (LiTaO<sub>3</sub>) (Fechete et al. 2006), and lead zirconate titanate (PZT) (Ferrari et al. 2000; Lee et al. 2004, 2006). Lithium niobate (LiNbO<sub>3</sub>) has a relatively large electromechanical coupling coefficient ( $K^2$ ) that allows two-port acoustic wave devices to utilize IDTs comprised of nearly an order of magnitude fewer pairs of fingers than quartz. The coupling coefficient represents the ratio of the mechanical (electrical) energy converted to the input electrical (mechanical) energy for the piezoelectric material (Schwartz et al. 2004). The orientation of the coupling coefficient is important and must be distinguished clearly. The planar coupling coefficient,  $k_p$ , describes the radial coupling in a thin disc, when the electrical field is applied through the thickness, and the thickness coupling coefficient,  $k_t$ , is identical to  $k_{33}$  when the element is clamped laterally (Setter 2002). Unfortunately, LiNbO<sub>3</sub> suffers from a very large temperature coefficient—approximately 80 ppm/°C for an SAW device with propagation in the Z direction on Y-cut LiNbO<sub>3</sub>. The consequences of this are that LiNbO<sub>3</sub> is thermally quite fragile and that exceptional temperature stability is necessary when using LiNbO<sub>3</sub> to detect anything other than temperature changes (Ballantine et al. 1997).

Zinc oxide is a wide-band gap chemically stable semiconductor of interesting physical properties that can be changed in a controlled way during chemical preparation. ZnO is both piezoelectric (Özgür et al. 2005) and pyroelectric (Lang 2005). The high wettability of zinc oxide is employed in superhydrophobic coatings, and particularly in humidity sensors (Zhou et al. 2007). An advantage of the ZnO-based resonators is that it is possible to fabricate them in a solidly mounted resonator (SMR)

**Table 13.3** Comparison of piezoelectric and related properties of several important piezoelectric materials

Parameter	Quartz	BaTiO <sub>3</sub>	PbTiO <sub>3</sub> :Sm	PZT 4	PZT 5H	LF4T	PVDF
$d_{33}$ (pC/N)	2.3	190	65	289	593	410	33
$g_{33}$ (10 <sup>-3</sup> Vm/N)	57.8	12.6	42	26.1	19.7	20.2	380
$k_t$	0.09	0.38	0.50	0.51	0.50	0.45	0.30
$k_p$		0.33	0.03	0.58	0.65	0.6	
$\epsilon_{33}/\epsilon_0$	5	1,700	175	1,300	3,400	2,300	6
$Q_m$		>10 <sup>5</sup>	900	500	65	–	3–10
$T_c$ (°C)		120	355	328	193	253	

$d_{33}$ : piezoelectric charge sensor constant;  $g_{33}$ : piezoelectric voltage constant;  $k$ : electromechanical coupling factor;  $\epsilon_{33}/\epsilon_0$ : dielectric constant;  $Q_m$ : mechanical quality factor;  $T_c$ : Curie temperature

Source: Data from Kholkin et al. (2009)

configuration and to integrate them with integrated circuit (IC) systems. ZnO materials offer lower cost, easier fabrication, and highly sensitive sensor components for SAW and “electronic nose” devices in comparison with quartz crystals (Lozano et al. 2006). Aluminum nitrate crystals are piezoelectrics with high stiffness, low losses, and large electromechanical coupling constants (Tadigadapa and Mateti 2009). The main advantage of AlN as well as of ZnO for film bulk acoustic resonator (FBAR) technology is their compatibility with IC components and lower costs, which are important objectives of sensor miniaturization efforts and for commercial success. Because extremely thin piezoelectric films are readily fabricated, both ZnO and AlN have been used to make bulk resonators that operate at much higher frequencies (e.g., 100–3,000 MHz) than TSM resonators made from quartz disks, which typically resonate at 5–20 MHz (Ballantine et al. 1997).

Lead zirconate titanate is a piezoelectric ceramic material (Pb(Zr,Ti)O<sub>3</sub> (PZT), Pb(La,Zr,Ti)O<sub>3</sub>, or Pb(Zr,Ti,Zn)O<sub>3</sub>) which demonstrates an exceptional combination of pyroelectric, piezoelectric, and inverse piezoelectric effects, high-temperature stability, and large electromechanical coupling coefficients (Ferrari et al. 2000; Lee et al. 2004, 2006). The sensitivity of PZT is double that of quartz. These properties enable the development through advanced engineering of PZT-based microelectromechanical systems (MEMS), including micromachined cantilevers (Ferrari 2004; Lee et al. 2004), pyroelectric sensors (Ferrari 2004), and biosensors (Lee et al. 2004). Piezoelectric polymers, PVDF, generally known as piezo-films, allow for extremely low-cost sensors but generally do not provide acceptable stability for many applications. For these reasons, the vast majority of piezoelectric sensors use PZT ceramic elements.

The comparison of piezoelectric properties of several of the major piezoelectric ceramics discussed above is given in Table 13.3. In this table, PZT 4 is hard PZT (PZT doped with acceptor ions, such as K<sup>+</sup> or Na<sup>+</sup> at the A site, or Fe<sup>3+</sup>, Al<sup>3+</sup>, or Mn<sup>3+</sup> at the B site), PZT 5H is soft PZT (PZT doped with donor ions, such as La<sup>3+</sup> at the A site, or Nb<sup>5+</sup> or Sb<sup>5+</sup> at the B site), LF4T is (K<sub>0.44</sub>Na<sub>0.52</sub>Li<sub>0.04</sub>)(Nb<sub>0.86</sub>Ta<sub>0.10</sub>Sb<sub>0.04</sub>)O<sub>3</sub>, and PVDF is piezoelectric polymer synthesized using copolymerization of vinylidene difluoride with trifluoroethylene (TrFE).

## 13.2 Saw Devices

The fundamental parameters controlling operating characteristics of SAW-based sensors are the SAW velocity, the temperature coefficients of delay (TCD), the electromechanical coupling factor, and the propagation loss. In SAW applications, the coupling factor  $k_p^2$  relates to the maximum bandwidth obtainable and the amount of signal loss between input and output that determines the fractional

**Table 13.4** Material parameters for representative SAW materials

Material	Cut-propagation direction	$k^2$ (%)	TCD (ppm/°C)	$V_0$ (m/s)	$\epsilon_r$
<i>Single crystal</i>					
Quartz	ST-X	0.16	0	3,158	4.5
LiNbO <sub>3</sub>	128°Y-X	5.5	-74	3,960	35
LiTaO <sub>3</sub>	X112°-Y	0.75	-18	3,290	42
Li <sub>2</sub> B <sub>4</sub> O <sub>7</sub>	(110)-<001>	0.8	0	3,467	9.5
<i>Ceramic</i>					
PZT-In(Li <sub>3/5</sub> W <sub>2/5</sub> )O <sub>3</sub>		1.0	10	2,270	690
(Pb,Nd)(Ti,Mn,In)O <sub>3</sub>		2.6	<1	2,554	225
<i>Thin film</i>					
ZnO/glass		0.64	-15	3,150	8.5
ZnO/sapphire		1.0	-30	5,000	8.5

Source: Data from Uchino and Ito (2009)

bandwidth vs minimum insertion loss for a given material and a filter. Propagation loss, one of the major factors that determine the insertion loss of a device, is caused by wave scattering by crystalline defects and surface irregularities. Materials that have high electromechanical coupling factors combined with small TCD times are likely to be required. Table 13.4 shows some important material parameters which can be applied in SAW devices. The free surface velocity,  $V_0$ , of the material is a function of cut angle and propagative direction. The TCD is an indication of the frequency shift expected from a transducer due to a temperature change and is also a function of the cut angle and the propagation direction.

At present, the most popular single-crystal SAW materials are quartz, lithium niobate, and lithium tantalite (see Table 13.4). These substrates are chosen on the basis of the device's design specifications for operating temperature, fractional bandwidth, and insertion loss. ZnO thin films,  $c$  axis oriented and deposited on a fused quartz, glass, or sapphire substrate, have also been commercialized for SAW devices (Uchino and Ito 2009). The ZnO microcrystals can be oriented in the process of the structure growth with the crystallite  $c$  axis (001 direction) either perpendicular to or aligned in the substrate plane. Due to this property, textured ZnO films (Yanagitani et al. 2007) can be used in SAW, Love mode, and BAW types of devices as active elements or as wave-guiding layers. An example of the latter use is ZnO-based thin-film bulk acoustic resonators operated at gigahertz frequencies, with applications both as gas sensors (Roy and Basu 2002) and in liquid-phase applications (Weber et al. 2006). Typical parameters of SAW-based gas sensors, based on the substrates discussed earlier, are presented in Table 13.5.

### 13.2.1 Materials for Interdigital Transducers

The excitation and detection of surface acoustic waves, flexural plate waves, and other plate waves on piezoelectric substrates is most readily accomplished by use of an interdigital transducer (IDT). The comb-like structure of the IDT is typically made from a lithographically patterned thin metal film that has been deposited onto the surface of a piezoelectric substrate. The metal film used to make the IDT must be thick enough to offer low electrical resistance and thin enough so that it does not present an excessive mechanical load to the AW. Typical IDTs have thickness of ~100–200 nm.

**Table 13.5** Important attributes of experimental SAW-based gas sensors

SAW platform	Coating material	Gas, vapor	Operating frequency (MHz)	Max. sensitivity (Hz/ppm)
Langasite (LGS)	Pt/WO <sub>3</sub>	H <sub>2</sub>	167	6–8
	Pt/WO <sub>3</sub>	Ethylene	167	100–150
YZ LiNbO <sub>3</sub>	WO <sub>3</sub> ; WO <sub>3</sub> ; Au	H <sub>2</sub> S	38–60	50–366
	Lead phthalocyanine	NO <sub>2</sub>	43–110	15.4–360
ST quartz	WO <sub>3</sub>	H <sub>2</sub> S	260	400
	Iron phthalocyanine; copper phthalocyanine	NO <sub>2</sub>	79	42–72
	TiO <sub>2</sub>	O <sub>2</sub>	63	30–45
	Ru/WO <sub>3</sub>	NO	261	1.7 × 10 <sup>3</sup>
	Fluoropolyol; –OH and –CH <sub>3</sub> terminated thiols	DMMP	250	66
ZnO/ST quartz	Ag(I)/cryptand-22 complex	Heptene	315	50–60
	B-Cyclodextrins	Toluene	1,000	61
	Carbosilane polymer	DNT	250	6.7 × 10 <sup>5</sup>
	ZnO	O <sub>2</sub>	90	220

DMMP Dimethyl methylphosphonate, DNT 2,4-Dinitrotoluene

Source: Data from Afzal and Dickert (2011)

The two “metallizations” most commonly used to fabricate transducers on SAW devices are gold-on-chromium and aluminum (Ballantine et al. 1997). Au is often chosen for gas detection applications because of its inertness and resistance to corrosion. Unfortunately, the inertness of Au also prevents its adhesion to quartz and other oxides utilized for AW device substrates. Therefore an underlayer of Cr (2–10 nm thick) is utilized to promote the adhesion of Au to the substrate: the electropositive (reactive) nature of Cr allows it to form strong bonds with oxide surfaces, while alloying between the Cr and Au chemically binds the two metal layers tightly together. Care must be taken not to expose a freshly deposited Cr layer to oxygen (air) before the Au is deposited, as a chromium oxide layer will form instantaneously, preventing adhesion of the Au to the Cr. At elevated temperatures (ca. 300 °C and above), Cr and Au interdiffuse; the unfortunate result of this is that the conductivity of the Au layer decreases significantly, eventually rendering the metallization too resistive for use. This problem can be partially circumvented by substitution of Ti for Cr as an adhesion layer, although Ti is more difficult to deposit (see below).

Aluminum has the advantage that it adheres well to common oxide substrates, is easy to deposit, is only 17 % less conductive (for an equivalent thickness) than Au, and is far less dense. The lower density is significant because reflections of AWs from Au IDT fingers in delay-line applications can cause appreciable pass band ripple in the IDT frequency response. Al’s main disadvantage is the relative ease with which it corrodes; this problem is sometimes addressed, particularly for (non-sensor) commercial applications of SAW devices, by passivating the Al using a relatively impermeable layer of a material such as  $\text{Si}_3\text{N}_4$  or AlN.

Although it is not yet common for AW devices, other areas of microelectronics have demonstrated the utility of more exotic metallization, such as Pt–Ti, for demanding, high-temperature applications; this combination would also be very corrosion resistant, though the relatively high density and poor conductivity of Pt are less than optimal for SAW devices.

Deposition of metals can be accomplished using various methods. However, thermal evaporation, electron-beam-induced evaporation, and sputtering are the most used methods.

### 13.3 High-Temperature Devices

High-temperature sensors are desired for the automotive, aerospace, and energy industries. Specifically, high-temperature sensors are critical for high-performance engine development as well as engine control and health assessment, in which the sensors must be able to operate reliably under harsh environments, where the sensors often need to be close to the engine component of interest for adequate sensitivity, for fuel combustion efficiency studies, and engine prognostic and engine health management. Other applications that benefit from high-temperature sensors include power plants, for the structure health monitoring of the furnace components or reactor systems. However, it was established that materials discussed in the previous section cannot be used at elevated temperatures (see Table 13.6). For example, the phase transition at 573 °C and the strong decreasing resonator quality factor (Q-factor) of quartz permit its use up to around 450 °C. The phase transitions in general lead to instability and irreversibility of the properties with temperature. The chemical instability of nonstoichiometric lithium niobate, i.e., its tendency to decompose, limits its application temperature to about 450 °C (Fachberger et al. 2004). The decrease of electrical resistivity of  $\text{LiNbO}_3$  at high temperature (Smith and Welsh 1971), which contributes to charge drift interfering with piezoelectrically induced charges, also limits the application at high temperatures of the materials discussed above. Many factors, including the above-mentioned ones, together with increased attenuation of acoustic waves and dielectric losses, must be considered when choosing a material appropriate for a particular high-temperature application.

**Table 13.6** Operation temperature limits of piezoelectric materials

Material	Temperature limit (°C)	Reasons
Li <sub>2</sub> B <sub>4</sub> O <sub>7</sub>	230	Excessive ionic conductivity
LiNbO <sub>3</sub>	300	Decomposition
LiTaO <sub>3</sub>	300	Decomposition
α-SiO <sub>2</sub> (α-quartz)	573	Phase transformation
AlPO <sub>4</sub>	588	Phase transformation
GaPO <sub>4</sub>	970	Phase transformation
AlN	~1,000	Oxidation resistance
La <sub>3</sub> Ga <sub>3</sub> SiO <sub>14</sub>	1,470	Melting point

Source: Data from Fritze (2011)

**Table 13.7** Properties of various high-temperature piezoelectric crystals and commercially available ferroelectric materials

Material	Structure (crystal symmetry)	T <sub>c</sub> /T <sub>mel</sub> (°C)	ε <sub>r</sub>	d <sub>33</sub> (pC/N)
<i>Ferroelectric ceramics/single crystals</i>				
BaTiO <sub>3</sub>	Perovskite	115	1,700	190
PZT-5A	Perovskite	330	2,000	400
PbTiO <sub>3</sub> (modified)	Perovskite	470	200	60
PbNb <sub>2</sub> O <sub>6</sub> (modified)	Tungsten bronze	500	300	85
Bi <sub>4</sub> Ti <sub>3</sub> O <sub>12</sub>	Aurivillius	675	180	20
CaBi <sub>4</sub> Ti <sub>4</sub> O <sub>12</sub>	Aurivillius	800	150	14
La <sub>2</sub> Ti <sub>2</sub> O <sub>7</sub>	Perovskite layer	1,460	60	2.6
LiTaO <sub>3</sub> (crystal)	Trigonal, 3m	720	43	6
LiNbO <sub>3</sub> (crystal)	Trigonal, 3m	1,150	28	6
<i>Piezoelectric single crystals</i>				
α-Quartz	Trigonal, 32	570	4.5	~3
Tourmaline	Trigonal, 3m	1,100–1,200	6	~2
GaPO <sub>4</sub>	Trigonal, 32	1,650	6–7	4–5
Langasite (La <sub>3</sub> Ga <sub>3</sub> SiO <sub>14</sub> )	Trigonal, 32	~1,470	16–20	4–7
Oxyborate (ReCa <sub>4</sub> O(BO <sub>3</sub> ) <sub>3</sub> or ReCOB)	Monoclinic <i>m</i> point group			

Source: Reprinted with permission from Zhang et al. (2011). Copyright 2011 Elsevier

**Fig. 13.4** Usage temperature range of various piezoelectric single crystals, showing different sensitivities (piezoelectric coefficient) (Reprinted with permission from Zhang et al. (2011). Copyright 2011 Elsevier)

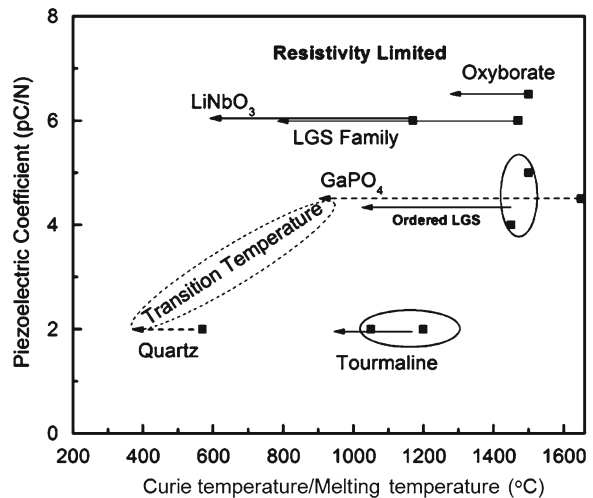
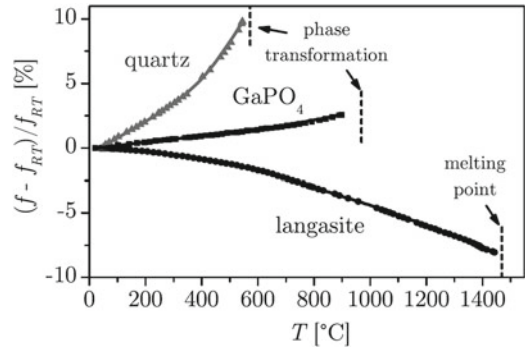




**Fig. 13.5** Temperature-dependent resonance frequency of langasite, gallium phosphate, and quartz BAW resonators normalized using the resonance frequency at room temperature  $f_{RT}$ . (Reprinted with permission from Fritze (2011). Copyright 2011 IOP)



Commonly used ferroelectric and piezoelectric materials which can be applied at high temperature are listed in Table 13.7. The materials are categorized into different groups, including ferroelectric materials with perovskite, tungsten bronze, Aurivillius and perovskite layer structures, and non-ferroelectric single crystals (Zhang et al. 2011). The sensitivities of indicated piezoelectric crystals vs their usage temperature range are shown in Fig. 13.4. Perovskite ferroelectric ceramics, such as PZT, have high piezoelectric sensitivity. Although the electrical resistivity remains sufficiently high up to Curie temperature  $T_c$ , the usage is generally limited to  $1/2T_c$ , above which aging occurs rapidly (Setter 2002). Ferroelectric ceramics with Aurivillius and/or perovskite layer structures possess Curie temperatures  $>600$  °C. However, their application is limited due to low piezoelectric properties and reduced electrical resistivity at elevated temperatures (Setter 2002; Ye 2008). The mineral tourmaline has the same limitations.

It was found that langasite ( $\text{La}_3\text{Ga}_5\text{SiO}_{14}$ , LGS) and gallium orthophosphate ( $\text{GaPO}_4$ ), which are also piezoelectric materials, have much better characteristics at high temperatures (Smythe et al. 2000; Fritze and Tuller 2001). Experiments have shown that the phase transformation of  $\text{GaPO}_4$  limits its operation to temperatures below 970 °C, whereas LGS has been shown to exhibit bulk acoustic wave vibrations up to at least 1,400 °C (Schulz et al. 2009). Both materials exhibited very good Q-factors at elevated temperatures. The most critical issues for the indicated materials are stoichiometry changes due to, e.g., low oxygen partial pressures, and high losses. According to Schulz et al. (2009), the mechanical loss in langasite is significantly impacted by the electrical conductivity due to the piezoelectric coupling. The effect of the piezoelectric coupling on the loss is negligible for gallium phosphate since it shows an extremely low electrical conductivity. Besides, gallium phosphate has minimal dependence of resonance frequency on the temperature (see Fig. 13.5). However, the poor availability of  $\text{GaPO}_4$  single crystals and an expensive, time-intensive growth process limit its large-scale applications. LGS has better manufacturability and is therefore a more promising candidate for design of high-temperature gas sensors (Tuller 2003; Richter et al. 2006; Fritze et al. 2006). In addition, it has been found that small donor doping suppresses the electrical conductivity and the losses in LGS in the entire temperature range of measurement. The main problems during LGS-based sensors operation are related to instability of oxygen vacancies and water influence. Fritze et al. (2006) established that, in the absence of hydrogen, the formation of oxygen vacancies limits the stable operation of langasite at fairly low oxygen partial pressures, e.g., at about  $10^{-24}$  and  $10^{-36}$  bar at 800 and 600 °C, respectively. The oxygen vacancy concentration remains almost constant, and a stable resonance frequency is expected in this range. However, water vapor results in a frequency shift at higher oxygen partial pressure, starting below about  $10^{-15}$  and  $10^{-20}$  at 800 and 600 °C, respectively.

Zhang et al. (2011) believe that oxyborates  $\text{ReCa}_4\text{O}(\text{BO}_3)_3$  (Re: rare earth element; abbreviated as ReCOB) are also promising piezoelectric crystals for high-temperature-sensing applications.

Large-sized and high-quality crystals can be readily grown by the Czochralski growth method. In contrast to quartz and  $\text{GaPO}_4$  crystals, no phase transformations are observed prior to their melting points, being in the order of  $\sim 1,500$  °C. Moreover, the resistivity of ReCOB was found to be  $\sim 2 \times 10^8$  ohm cm at 800 °C, two orders higher than langasite.

### 13.4 Miniaturization of Piezoelectric Sensors

There are essentially three approaches to realizing piezoelectric MEMS devices: (1) deposition of piezoelectric thin films on silicon substrates with appropriate insulating and conducting layers followed by surface or silicon bulk micromachining to realize the micromachined transducers (“additive approach”), (2) direct bulk micromachining of single crystal or polycrystalline piezoelectrics and piezoceramics which are thereafter appropriately electroded to realize micromachined transducers (“subtractive approach”), and (3) integrate micromachined structures in silicon via bonding techniques onto bulk piezoelectric substrates (“integrative approach”) (Tadigadapa and Mateti 2009). Depending upon the exact physical size of the desired mechanical sensors, each of these approaches offers specific advantages as illustrated schematically in Fig. 13.6.

As indicated before, there are many piezoelectric materials which can be used for gas sensor design. However, experiment has shown that for MEMS devices we have limitations in application of several of these materials. It was established that the deposition of the piezoelectric material in the form of thin films from 1/10th of a micron to several tens of microns in thickness with piezoelectric properties approaching those of the corresponding bulk materials is critical to the realization of a piezoelectric micromachined transducer. Unfortunately, materials such as quartz, langasite, lithium niobate, and lithium tantalate are only available as bulk single crystals, and currently no effective processes for their deposition in single-crystal thin film form exist (Tadigadapa and Mateti 2009). This means that these materials can be integrated in micromachined transducers only through direct bulk micromachining or hybrid integration methods.

At the same time, ZnO, AlN, and PZT do not have technological limitations in film deposition. Thin films of these materials can be prepared using various methods including sputtering, chemical solution methods, screen printing, and atomic layer deposition technique. It was found that properties of thin-film piezoelectric materials depend upon (1) stoichiometry, (2) film morphology, (3) film density, (4) impurities, and (5) defects. In order to obtain a large response to mechanical deformations, piezoelectric films have to be grown with a textured structure with a high degree of alignment of the

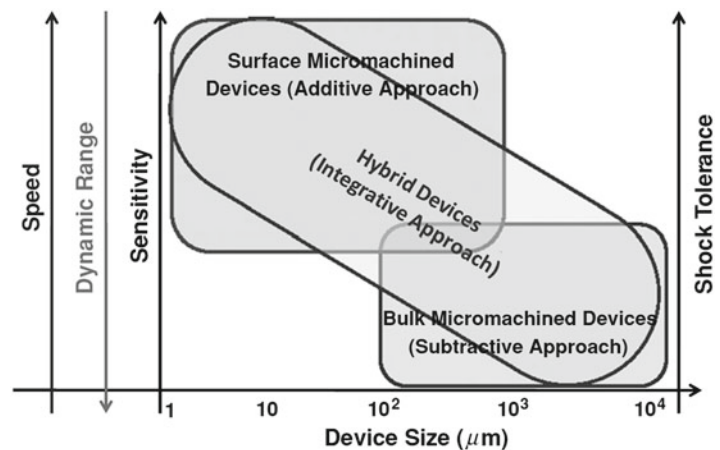


**Fig. 13.6** Three approaches towards fabricating piezoelectric MEMS devices (Reprinted with permission from Tadigadapa and Mateti (2009). Copyright 2009 IOP)

piezoelectric (poling) axis. In addition to the conditions used for the growth process, the orientation and quality of the substrate material is also found to have a strong influence on the nucleation and subsequent growth of the piezoelectric films. One can find in the review by Tadigadapa and Mateti (2009) a more detailed description of the technological approaches used for fabricating microminaturized AW sensors (wet and dry etching, bulk and surface micromachining, etc.).

## 13.5 Sensing Layers

### 13.5.1 General Requirements

The detection of gas analytes using acoustic wave (AW) sensors can be based on changes in one or more of the physical characteristics of a thin film or layer in contact with the device surface (Ballantine et al. 1997). Some of the intrinsic film properties that can be utilized for gas detection include mass/area, elastic stiffness (modulus), viscoelasticity, viscosity, electrical conductivity, and permittivity. Variations in any of these parameters alter the mechanical and/or electrical boundary conditions producing a measurable shift in the propagating acoustic wave phase velocity,  $v_0$ . Equation (13.1) illustrates the change in acoustic phase velocity,  $\Delta v$ , as a result of external perturbations, assuming that the perturbations are small and linearly combined (Ippolito et al. 2009):

$$\frac{\Delta v}{v_0} \cong \frac{1}{v_0} \left( \frac{\delta v}{\delta T} \Delta T + \frac{\delta v}{\delta \varepsilon} \Delta \varepsilon + \frac{\delta v}{\delta E} \Delta E + \frac{\delta v}{\delta \sigma} \Delta \sigma + \frac{\delta v}{\delta m} \Delta m + \frac{\delta v}{\delta \rho} \Delta \rho + \dots \right) \quad (13.1)$$

However, the temperature dependence of each parameter, in addition to the overall temperature coefficient of the device structure, must also be considered, as the sensor response for many gas-phase-sensing applications is strongly dependent on operating temperature.

An increase in mass loading alone produces a decrease in frequency without affecting attenuation. In contrast, changes in mechanical properties of the coating can produce changes in both the frequency and the attenuation of the AW (Ballantine et al. 1997). Furthermore, these changes can either increase or decrease either or both of the two AW propagation parameters, depending on the details of the relationship between film thickness, acoustic wavelength, and the complex modulus of the film at the frequency and temperature of operation. In addition, changes in extrinsic variables such as temperature and pressure can also produce a sensor response, affecting the AW either directly or via changes in the film's intrinsic properties. Of course, not all detection mechanisms are of practical significance for all types of sensors, and several mechanisms can operate simultaneously (synergistically or antagonistically) to affect a response. In addition, we need to take into account that the nature of the sensitive coating—both its inherent physicochemical properties and the physical particulars (thickness, uniformity, etc.) of a specific layer deposited on a specific device—often influences the detection process.

An attractive feature of acoustic wave-based chemical sensors is that they impose relatively few constraints on the materials that can be used as chemically selective coatings. In brief, the film must be uniform, adherent, thin, chemically and physically stable when in contact with its working medium (gas), and it must not electrically short-circuit the IDTs. Thickness, uniformity, and other characteristics are affected by the method of deposition, be it painting, dipping, solvent casting, spraying (air-brushing), spin-casting, or subliming. These methods are detailed in Chap. 28 (Vol. 2). Typically, uniformity in film thickness is not crucial but can be important in some circumstances, especially in the case when devices are designed for the sensor market. The selected material must adhere to the device surface in such a manner that it moves synchronously with the AW and must maintain this adhesion in the presence of the expected analytes and interferents. The adhesion of thin films to many

types of surfaces, including those that are chemically very dissimilar to the coating material, is a much-studied topic outside the sensor field. Adhesion promoting interlayers have often been developed for general classes of problems, such as securing a highly nonpolar polymer film to a very polar substrate. Anyone attempting to construct a reliable sensor would do well to examine the relevant literature (Lee 1991). Highly conductive coatings (i.e., all metals and most semiconductors) must, of course, be electrically insulated from IDT electrodes in order to prevent shorting; this is not a concern with the planar electrodes of QCM devices. A final constraint is that the coating be acoustically thin (Ballantine et al. 1997). A somewhat standard rule of thumb is that thicknesses less than 1 % of the acoustic wavelength are appropriate. In fact, whether or not a particular coating thickness is acoustically thin depends critically upon the acoustic properties of that material under the particular set of conditions (temperature, nature, and concentration of contacting gaseous species) being evaluated. In other words, it is the acoustic wavelength in the coating film that is relevant; this can differ appreciably from the acoustic wavelength in the device substrate, particularly in materials such as rubbery polymers, which have vastly different sound velocities than, for example, quartz. In practice, coating thicknesses from a few angstroms to several micrometers have been utilized in sensing applications.

AW devices can certainly work without coatings. However, experiment has shown that the lack of specificity and low sensitivity are two major drawbacks of gas sensors with uncoated surfaces.

### 13.5.2 Features of Sensing Materials Used in Acoustic Wave Gas Sensors

Most physical and chemical interactions between analytes and sensor coatings lead to changes of mass. Surface mass changes can result from sorptive interactions (i.e., adsorption or absorption) or chemical reactions between analyte and coating (Kurosawa et al. 1990). Thus, this sensing mechanism offers the greatest latitude in the selection of sorptive or reactive coating materials (Monreal and Marl 1987). In addition, the performance of a given coating can sometimes be predicted a priori through knowledge of chemical reactions or by reference to solubility theory and/or appropriate models (Ballantine et al. 1997). It follows from general consideration that the working relationship between mass loading and frequency shift,  $\Delta f_m$ , for AW devices can be written as

$$\Delta f_m = -K \cdot S_m \cdot \Delta m_A \quad (13.2)$$

in which  $S_m$  is a device-specific constant that depends upon factors such as the nature of the piezoelectric substrate, device dimensions, frequency of operation, and the acoustic mode that is utilized,  $K$  is a geometric factor for the fraction of the active device area being perturbed, and  $\Delta m_A$  is the change in mass/area on the device surface. It is clear that all other properties being equal, a film having a higher surface area results in a larger number of analyte molecules being adsorbed for a given ambient-phase analyte concentration, the consequences of which are enhanced sensitivity and limit of detection. For reactive and (irreversible) adsorptive coatings, higher surface area translates to higher capacity and thus greater dynamic range. It is also necessary to take into account that, as the plate thickness decreases, the operating frequency and mass sensitivity increase proportionally. The maximal operating frequency is usually limited by the mechanical stability of the substrate.

Examples of high surface area solid adsorbents suitable for sensor coatings are microporous materials such as activated charcoal, silica gel, alumina gel, porous polymers, and molecular sieves, in particular zeolites and metal-organic framework materials (MOF). One can find in other chapters, in particular Chaps. 3 and 12 (Vol. 1) and Chaps. 1, 8, 11, and 13 (Vol. 2), more detailed discussions of these materials. For most of the above-mentioned materials, high adsorption capacity arises from the presence of large numbers of micropores and/or mesopores. The total surface area of a single gram of such materials can exceed 1,000 m<sup>2</sup> (Cheremisinof and Ellerbusch 1980). Table 13.8 lists several

**Table 13.8** Adsorbent materials and typical adsorbates

Adsorbent	Adsorbates (vapors)
Activated charcoal	Most nonpolar and moderately polar organic vapors; alkanes, alkenes, chlorinated aliphatics, ketones, esters, ethers, higher alcohols
Silica and alumina gels, zeolites	Polar vapors: water, alcohols, phenols, chlorophenols, glycols, aliphatic and aromatic amines
Porous polymers (Tenax, XAD, Chromosorb, etc.)	Higher boiling-point organics: acidic and basic organics, multifunctional organics, pesticides, polynuclear aromatic hydrocarbons, etc.

Source: Data from Ballantine et al. (1997)

**Table 13.9** Sorption capacity of activated charcoal and natural rubber for vapors of several organic solvents

Vapor	Capacity at saturation, g(vapor)/g(charcoal)	Capacity at saturation, g(vapor)/g(rubber)
Acetone	0.4	0.104
Chloroform	1.1	–
Hexane	0.4	1.444
Carbon tetrachloride	0.9	9.111
Ethanol	0.5	0.008

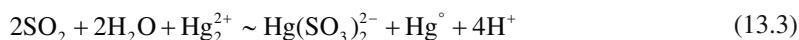
Source: Data from Comyn (1985) and Wood and Moyer (1991)

adsorbents along with some of the types of compounds that can be collected with them. The adsorption capacity for different vapors varies widely with the structure and volatility (saturation vapor pressure) of the adsorbate (see Table 13.9) as well as the process used for both preparing (synthesis) and activation of the adsorbent.

Because piezoelectric substrates are used for AW chemical sensing applications, an electric field accompanies the propagating wave as it travels through the substrate. This field can interact with mobile charge carriers in a surface layer/coating and affect both the velocity and amplitude of the wave (Ballantine et al. 1997). The design of gas sensors, which use this detection mechanism, requires judicious selection of the piezoelectric substrate (Ricco and Martin 1992). Changes in the attenuation and velocity of surface acoustic waves depend on the square of the electromechanical coupling coefficient of the substrate,  $K^2$ , which varies by orders of magnitude from one material to another. YZ-lithium niobate ( $\text{LiNbO}_3$ ), for example, has a  $K^2$  value of 0.048, which is more than 40 times higher than that of ST quartz ( $K^2=0.0011$ ). Thus,  $\text{LiNbO}_3$  is a more appropriate substrate to choose if this detection mechanism is to be employed. Appropriate temperature controls will be essential, however, since the temperature coefficient of  $\text{LiNbO}_3$  SAW devices is over 20 times that of comparable ST-quartz devices. If a coating material is used to concentrate the analyte near the sensor surface, it must be a semiconductive material with a sheet conductivity (the product of film thickness and bulk conductivity) that falls within a “window of sensitivity” determined by the substrate. Using values for  $\text{LiNbO}_3$  (Ricco et al. 1985), maximum sensitivity is obtained in the range  $10^{-7}$  to  $10^{-5} \Omega^{-1}$ , and the maximum possible frequency shift ( $\Delta f/f_0$ ) is  $K^2/2=24,000$  ppm. For quartz, the window of sensitivity is an order of magnitude lower ( $10^{-8}$  to  $10^{-6} \Omega^{-1}$ ) and the maximum shift obtainable is only 550 ppm; this is, however, more than adequate for the observation of a significant effect (i.e., sensor response) under the proper conditions (Ricco and Martin 1992). In addition to having sheet conductivity within the aforementioned window of sensitivity, the sheet conductivity of the coating material must be altered as a result of a chemical stimulus. As shown before, conductive polymers (phthalocyanines, polypyrrole, etc.), metal oxides ( $\text{ZnO}$ ,  $\text{In}_2\text{O}_3$ , etc.), and metals (Pd) have such properties.

If interaction with an analyte increases the conductivity of the coating film (in the appropriate range), the frequency decreases and the conductivity change enhances frequency shifts due to increased mass or decreased modulus. If it is desired to isolate the conductivity effects from mass and mechanical effects, a reference device can be coated with an initial layer of metal whose sheet conductivity significantly exceeds the window of sensitivity, thereby shorting the electric field (this does not affect sensitivity to mass changes). The chemically sensitive coating material is then applied over the metal film (Ricco et al. 1985). The signal from this device can be compared with that from a sensing device having no metal layer, and the resulting difference in frequency shifts depends only on conductivity changes. The substrate material can also be important in isolating the conductivity effect;  $\text{LiNbO}_3$  is again the material of choice, with a mass sensitivity less than half that of other common substrates such as quartz and ZnO-on-Si (Ricco et al. 1985).

A very wide range of materials which change properties under the influence of gas can be used for AW-based gas sensor design. Experiments carried out during the last few decades have confirmed this statement. Thin metal films (Pt, Pd) have been used for the adsorption and detection of gases such as  $\text{H}_2$  and  $\text{NH}_3$  (D'Amico et al. 1982, 1987). It is well known that  $\text{H}_2$  dissolves to a significant extent in Pd, with concomitant changes in the density, electrical conductivity, and mechanical properties of the film. The  $\text{H}_2$ /Pt interaction as well as the interaction of  $\text{NH}_3$  with both Pd and Pt undoubtedly involves chemisorption on surface sites. Metal thin films deposited by nearly all techniques are polycrystalline; chemisorption along grain boundaries can often lead to a response that is considerably larger than that predicted from the properties of metal single crystals. The amalgamation of noble metals, specifically gold (Au), by mercury (Hg) has been used to detect ambient Hg levels in the atmosphere (Scheide and Taylor 1974). The amalgamation reaction has also been used for the detection of atmospheric  $\text{SO}_2$  (Suleiman and Guilbault 1984a). Bubbling an  $\text{SO}_2$  stream through a solution of mercurous nitrate produces elemental mercury via the reaction

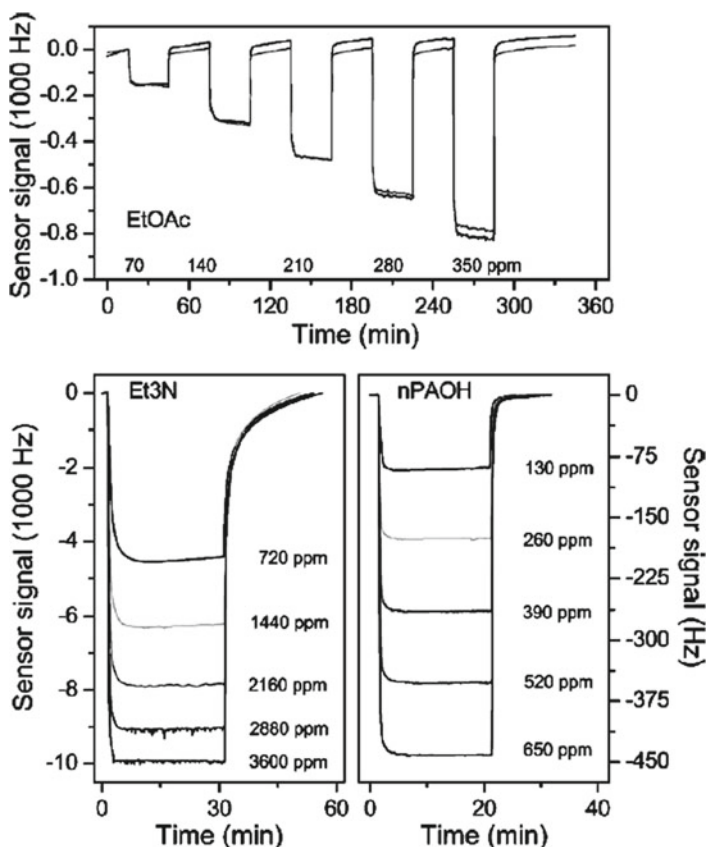


The quantity of evolved elemental Hg, which is proportional to the  $\text{SO}_2$  concentration, is measured by amalgamation onto an Au QCM device electrode surface. The collected Hg can be thermally stripped from the electrode and the QCM resonator reused for subsequent analyses.

Various metal oxide films have also been applied with some success. Tungsten trioxide ( $\text{WO}_3$ ) was applied for the detection of  $\text{H}_2\text{S}$  using SAW devices (Bryant et al. 1983). This sensor was operated at elevated temperatures ( $>100^\circ\text{C}$ ). Sol-gel derived indium-tin oxide (ITO) thin films coated onto 10-MHz QCMs have shown an approximately linear relationship with sensitivity towards NO concentrations around 1,000 ppm at room temperature (Zhang et al. 2004). Edmonds et al. (1988) reported using manganese dioxide for the detection of  $\text{NO}_2$  using a TSM device. One of the more unique adsorbent films used for vapor sensing is sputtered polycrystalline zinc oxide, ZnO. Under the appropriate conditions, the grain boundaries provide adequate surface area for the adsorption of gases and vapors (Wohltjen 1984; Martin et al. 1984). An advantage of this material is that it can simultaneously function as the piezoelectric transduction layer for the construction of thin film-based SAW and FPW devices supported on Si (or virtually any other) substrates.

It was found that activated charcoal, silica, zeolite, MOFs, and other molecular sieve-based piezoelectric gas sensors can provide good sensitivity for the detection of vapor-phase species and humidity (King 1964; Sanchez-Pedreno et al. 1986; Bein et al. 1989; Kreno et al. 2012). For example, it was established that MOFs have the ability to adsorb large quantities of water. It is reported that HKUST-1 can adsorb as much as 40 wt % water (Wang et al. 2002). Of course, this makes them attractive for humidity sensing, which has been demonstrated using a variety of sensing platforms. In particular, Ameloot et al. (2009) demonstrated water vapor detection with an MOF-coated QCM, using electrochemically synthesized Cu-BTC films grown directly on the device. They showed that changes in

**Fig. 13.7** (Top) transient signals of two QCM sensors with a vic-dioxime coating to pulses of ethyl acetate (EtOAc) vapor. (Bottom) superimposed response curves of a QCM sensor with a vic-dioxime coating to pulses of (left) triethylamine (Et3N) and (right) *n*-propanol (nPAOH) vapors (Reprinted with permission from Harbeck et al. (2011). Copyright 2011 Elsevier)



relative humidity can be monitored and a highly reproducible signal occurs upon cycling between dry and water containing nitrogen flows. The water sorption capacity of the films was found to be 25–30 wt %. However, it is necessary to take into account that water vapor is also a common interfering gas and must be addressed in the design of MOF-based sensing systems.

Experiment has shown that response and recovery times of the above-mentioned sensors depend on the nature, thickness, and structure of used material. For example, while the charcoal coating exhibited good sensitivity and reproducibility, recovery times upon purging with clean air were on the order of 8–10 min.

A variety of organophosphine transition metal complexes have been used for the detection of  $\text{SO}_2$  (Cook et al. 1989). Cook et al. (1989) used triphenyl- and tribenzylphosphine compounds as ligands bound to Cu and Mn. Varying the ligand affects the Lewis acid strength of the metal complex and, hence, its ability to bind  $\text{SO}_2$ . One complex (bis(tribenzylphosphine)copper(II) thiophenolate-[Cu(PBza)<sub>2</sub>]SPh) exhibited a reversible response to  $\text{SO}_2$  that was linear in the range 10–1,000 mg/L. The coating exhibited good stability in laboratory air and retained sensitivity to  $\text{SO}_2$  even after 2–3 months. Selectivity was also favorable, with little or no interference from  $\text{O}_2$ ,  $\text{CO}_2$ ,  $\text{NH}_3$ ,  $\text{CO}$ , or  $\text{NO}_2$ . Other transition metal compounds which engage in irreversible redox reactions with  $\text{SO}_2$  have demonstrated good sensitivity (Pribil and Bilkova 1992). A typical sensor signal and sensor calibration curve for vic-dioxime-based QCM device is shown in Fig. 13.7. Şen et al. (2010) and Harbeck et al. (2011) have shown that using 10-MHz quartz crystal microbalance sensors and a vic-dioxime-based sensing layer, an extraordinary high sensitivity (up to 260 Hz/ppm) to the test various vapors and detection limits in the low parts-per-billion range can be obtained. At the same time, it was established that the humidity influence and cross-interferences to common volatile organic compounds are low.

**Table 13.10** Responses of different SAW sensors towards different gases

Sensitive layer	Structure	Analyte gas	Operating frequency (MHz)	Frequency shift (Hz)
<i>Conventional SAW-based gas sensors</i>				
WO <sub>3</sub> /Ru	248 rotated Y-cut quartz	3 ppm of NO	261	50,000
Doped WO <sub>3</sub>	YZ LiNbO <sub>3</sub>	30 ppm of H <sub>2</sub> S	60	10,000
WO <sub>3</sub> /Au	YZ LiNbO <sub>3</sub>	100 ppm H <sub>2</sub> S	38.15	5,000
Pb-Pc	YZ LiNbO <sub>3</sub>	10 ppm of NO <sub>2</sub>	110	154
Catalyzed Pb-Pc	YZ LiNbO <sub>3</sub>	10 ppm of NO <sub>2</sub>	110	330
Tetra-4- <i>tert</i> -butyl Si-Pc dichloride	ST quartz	100 ppm of NO <sub>2</sub>	98.6	420
Au	288 rotated Y-cut quartz	500 ppb of Hg	261	4,000
WO <sub>3</sub>	278 quartz	10 ppm of H <sub>2</sub> S	260	4,000
WO <sub>3</sub>	YZ LiNbO <sub>3</sub>	27 ppm of H <sub>2</sub> S	60	9,900
Pt/WO <sub>3</sub>	Langasite	1,000 ppm of H <sub>2</sub> S	167.14	6,000
<i>Multilayered SAW-based gas sensors</i>				
TiO <sub>2</sub>	SiO <sub>2</sub> /ST quartz	10,000 ppm	63.04	45,000
ZnO	ZnO/908 rotated ST quartz	50 ppm of O <sub>2</sub>	90	11,000
ZnO	ZnO/908 rotated ST quartz	100 ppm of C <sub>2</sub> H <sub>8</sub>	90	11,000
Pd/Pc	YZ LiNbO <sub>3</sub>	2 % H <sub>2</sub>	–	5,000
Cu-Pc	SiO <sub>2</sub> /908 rotated ST quartz	1 ppm of NO <sub>2</sub>	100	1,400
WO <sub>3</sub>	ZnO/368 YX LiTaO <sub>3</sub>	500 ppm of ethanol	167.75	119,000
WO <sub>3</sub>	ZnO/368 YX LiTaO <sub>3</sub>	1 % H <sub>2</sub>	164.07	24,700
Au-WO <sub>3</sub>	ZnO/368 YX LiTaO <sub>3</sub>	1 % H <sub>2</sub>	165.7	755,000
SWCNTs	SiO <sub>2</sub> /ST cut X-propagating quartz	50 ppm of isopropanol	433	8,000

Source: Reprinted with permission from Ippolito et al. (2009). Copyright 2009 Springer, New York



**Table 13.11** Cluster classification of coatings for use in a QCM sensor array

Group	Compound	Comments
A	Poly(butadieneacrylonitrile); poly(butadiene) (–OH terminated); octadecylvinyl ether/maleic; anhydride copolymer blend; poly(vinyl stearate); poly(butadiene methacrylate); poly(1-butadiene)	Generally exhibited highest sensitivity to test vapors, especially phosphonates (DMMP, DIMP) and octane
B	Poly( <i>p</i> -vinyl phenol); methyl vinyl ether; polystyrene; poly(vinyl butyral); poly(vinyl carbazole)	Exhibit some selectivity to dimethyl phosphite and esters
C	Poly(ethylene glycol methyl ether); phenoxy resin; poly(methyl methacrylate); poly(vinyl chloride)	Semi-selective response to water vapor
D	Poly(caprolactone)triol; abietic acid; polyethylene; collodion; carnauba wax	Exhibit sensitivity/selectivity for DIMP; collodion exhibits greatest response to phosphonates of all tested coatings
E	Ethyl cellulose; poly(caprolactone); DC 11; poly(caprolactone)triol 2X	Some selectivity for dichloropentane vs most test vapors (except DIMP)
F	Polyvinyl isobutyl ether; poly-1-butene	Generally poor sensitivity/selectivity for test vapors

Source: Data from Carey et al. (1986)

Organic semiconductors such as phthalocyanine (Pc) films have been studied extensively as coatings for (partially) reversible detection of NO<sub>2</sub> (Ricco et al. 1985; Nieuwenhuizen and Nederlof 1988) and other chemicals (Kurosawa et al. 1990). Other coordination and/or charge-transfer reagents have been used successfully for the detection of NH<sub>3</sub> (Lai et al. 1986), toluene diisocyanate (Fielden et al. 1984), phosgene (Suleiman and Guilbault 1984b), and organophosphorus compounds (Guilbault et al. 1981).

Recently, nanomaterials have gained much attention as sensitive layers towards a variety of gases and vapors. Their potential to increase response by one order of magnitude over those of conventional sensing layers is being widely investigated. For example, polyvinyl alcohol (PVA) and polyacrylic acid (PAA) nanofibrous membranes spun on QCMs have exhibited responses of 730 Hz towards NH<sub>3</sub> concentrations of 200 ppm (Ding et al. 2004). Of all nanomaterials, carbon nanotubes have received the most attention for sensing applications. Multi-walled carbon nanotube (MWCNT) coated QCMs have been reported for relative humidity (RH) sensing applications, in which frequency shifts between 2.5 kHz and 10 kHz have been recorded for RH values between 5 and 97 % (Zhang et al. 2005). Table 13.10 provides a summary of the performance of several other SAW-based gas and vapor sensors towards various analytes.

However, it is necessary to recognize that organic polymers form the most common type of coating used with AW sensors due to their capability to reversibly sorb vapors (Ballantine et al. 1997). Moreover, thin films of many polymeric materials exhibit good adhesive properties and are easily applied to most substrates. In addition, relatively rapid diffusion and a high capacity for organic solutes make amorphous polymers attractive as sensor coatings. One demonstrated advantage of using polymer coatings to detect organic solvents is that two independent acoustic wave propagation parameters (i.e., frequency and attenuation) can be measured for a single device/coating combination, enhancing the information content of the sensor response. This is due to the fact that two different acoustic wave perturbations are generally involved when solvent is sorbed by a polymer layer: changes in mass loading and changes in polymer viscoelastic properties; the latter results from plasticization (i.e., softening) of the polymer by the absorbing solvent. The attenuation (i.e., insertion loss) response is due solely to changes in viscoelasticity, while the frequency response results from a combination of viscoelastic and mass-loading effects. Because each of the two perturbations depends on a different combination of the physicochemical properties of the absorbed species, they are, in general, independent of one another.

The variety of functionalities that can be incorporated into polymers makes it possible to optimize selected sorptive interactions and maximize sensitivity for given analytes. This feature of polymers is especially important for designing sensor arrays for electronic noses. Specificity of polymer interaction with different vapors, which was determined by Carey et al. (1986), is shown in Table 13.11.

As is indicated in many chapters of our handbook, in the development of a gas sensor for a given application, numerous factors affecting performance must be considered. Among these are sensitivity, selectivity, reversibility, response time, dynamic range, stability, reliability, and environmental (e.g., temperature) effects. Some of these concerns dictate the preferred substrate and/or acoustic mode; others are important in the selection of the coating or in establishing optimal operating conditions. These criteria play an important role in the design of a complete sensor system. For example, the high degree of selectivity afforded by carefully choosing an analyte/coating chemical interaction makes this class of sensors particularly attractive. Unfortunately, the price of selectivity is often an irreversible response and limited lifetime (Ballantine et al. 1997).

Although nonporous surfaces do not provide the sensitivity and limit of detection associated with porous layers, smooth surfaces have nonetheless been investigated. Nonspecific adsorption of a range of volatile organic compounds on smooth quartz and metal surfaces was given a degree of specificity by directly heating the device surface using a metal meander line. The form of the resulting thermal desorption signature depended upon the adsorbed species (Martin et al. 1987) and can be used in some applications for identification of adsorbed vapors.

For a better understanding of AW-based gas sensors, the reader is referred to several published reviews. Comprehensive surveys detailing the developments of AW sensors have been compiled by D'Amico and Verona (1989), Ballantine and Wohltjen (1989), Grate et al. (1993a, b), Martin et al. (1996), Vellekoop (1998), Cheeke and Wang (1999), Drafts (2001), Ippolito et al. (2009), Vashist and Korotcenkov (2011), Voinova and Jonson (2011), and Afzal and Dickert (2011).

## References

- Afzal A, Dickert FL (2011) Surface acoustic wave sensors for chemical applications. In: Korotcenkov G (ed) *Chemical sensors: comprehensive sensor technologies*, vol 4, Solid state devices. Momentum, New York, pp 447–484
- Ameloot R, Stappers L, Fransaeer J, Alaerts L, Sels BF, De Vos DE (2009) Patterned growth of metal-organic framework coatings by electrochemical synthesis. *Chem Mater* 21:2580–2582
- Ballantine DS, Wohltjen H (1989) Surface acoustic wave devices for chemical analysis. *Anal Chem* 61:704–715
- Ballantine DS Jr, White RM, Martin SJ, Ricco AJ, Zellers ET, Frye GC, Wohltjen H (1996) Acoustic wave sensors: theory, design, and physico-chemical applications. In: Levy M, Stern R (eds) *Applications of modern acoustics*. Academic, San Diego
- Ballantine DS Jr, White RM, Martin SJ, Ricco AJ, Frye GC, Zellers ET, Wohltjen H (1997) Acoustic wave sensors: theory, design, and physico-chemical applications. Academic, San Diego
- Bein T, Brown K, Frye GC, Brinker CJ (1989) Molecular sieve sensors for selective detection at the nanogram level. *J Am Chem Soc* 111:7640–7641
- Bryant A, Poirier M, Riley DL, Vetelino JF (1983) Gas detection using surface acoustic wave delay lines. *Sens Actuators* 4:105–111
- Carey WP, Beebe KR, Kowalski BR, Ilman DL, Hirschfeld T (1986) Selection of adsorbates for chemical sensor arrays by pattern recognition. *Anal Chem* 58:149–153
- Cheeke JDN, Wang Z (1999) Acoustic wave gas sensors. *Sens Actuators B* 59:146–153
- Cheremisinof PN, Ellerbusch F (eds) (1980) *Carbon adsorption handbook*. Science, Ann Arbor, pp 241–279
- Comyn J (ed) (1985) *Permeation of gases and vapors in polymers*. Elsevier, London
- Cook RL, MacDuff RC, Sammels AF (1989) Organophosphine transition metal complexes as selective surfaces for the reversible detection of sulfur dioxide with piezoelectric crystal sensors. *Anal Chim Acta* 217:101–109
- D'Amico A, Verona E (1989) SAW sensors. *Sens Actuators* 17:55–66

- D'Amico A, Paima A, Verona E (1982) Palladium-surface acoustic wave interaction for hydrogen detection. *Appl Phys Lett* 41:300–301
- D'Amico A, Petri A, Verardi P, Verona E (1987)  $\text{NH}_3$  surface acoustic wave gas detector. *Proc IEEE Ultrason Symp* 1987:633–636
- Ding B, Kim JH, Miyazaki Y, Shiratori SM (2004) Electrospun nanofibrous membranes coated quartz crystal microbalance as gas sensor for  $\text{NH}_3$  detection. *Sens Actuators B* 101:373–380
- Drafts B (2001) Acoustic wave technology sensors. *IEEE Trans Microw Theory* 49:795–802
- Edmonds TE, Hephher MJ, West TS (1988) Studies on the adsorption of nitrogen dioxide onto manganese dioxide-coated quartz piezoelectric crystals. *Anal Chim Acta* 207:67–75
- Fachberger R, Bruckner G, Knoll G, Hauser R, Binasch J, Reindl L (2004) Applicability of  $\text{LiNbO}_3$ , langasite and  $\text{GaPO}_4$  in high temperature SAW sensors operating at radio frequencies. *IEEE Trans Ultrason Ferroelectr Freq Control* 51:1427–1431
- Fanget S, Hentz S, Puget P, Arcamone J, Matheron M, Colinet E, Andreucci P, Duraffourg L, Myers E, Roukes ML (2011) Gas sensors based on gravimetric detection—a review. *Sens Actuators B* 160:804–821
- Fechele AC, Wlodarski W, Kalantar-Zadeh K, Holland AS, Antoszewski J, Kaciulis S, Pandolfi L (2006) SAW-based gas sensors with rf sputtered  $\text{InO}_x$  and PECVD  $\text{SiN}_x$  films: response to  $\text{H}_2$  and  $\text{O}_3$  gases. *Sens Actuators B* 118:362–367
- Ferrari V (2004) Acoustic-wave piezoelectric and pyroelectric sensors based on PZT thick films. In: Yurish SY, Gomes MTSR (eds) *Smart sensors and MEMS*, vol 181, NATO science series II: mathematics, physics and chemistry. Springer, New York, pp 125–154
- Ferrari V, Marioli D, Taroni A, Ranucci E (2000) Multisensor array of mass microbalances for chemical detection based on resonant piezo-layers of screen-printed PZT. *Sens Actuators B* 68:81–87
- Fielden PR, McCallum JJ, Stanios T, Alder JF (1984) Detection of toluene diisocyanate with a coated quartz piezoelectric crystal: part 4. A portable automatic detector with humidity correction. *Anal Chim Acta* 162:85–96
- Fritze H (2011) High-temperature bulk acoustic wave sensors. *Meas Sci Technol* 22:012002
- Fritze H, Tuller HL (2001) Langasite for high temperature bulk acoustic wave applications. *J Appl Phys Lett* 78:976–977
- Fritze H, Schulz M, She H, Tuller HL (2006) Sensor application-related defect chemistry and electromechanical properties of langasite. *Solid State Ionics* 177:2313–2316
- Grate JW, Martin SJ, White RM (1993a) Acoustic-wave microsensors. *Anal Chem* 65:A940–A948
- Grate JW, Martin SJ, White RM (1993b) Acoustic-wave microsensors. *Anal Chem* 65:A987–A996
- Guilbault GG, Affolter J, Tomita Y, Kolesar ES Jr (1981) Piezoelectric crystal coating for detection of organophosphorus compounds. *Anal Chem* 53:2057–2060
- Harbeck M, Sen Z, Gürol I, Gümüş G, Musluoglu E, Ahsen V, Öztürk ZZ (2011) Vic-dioximes: a new class of sensitive materials for chemical gas sensing. *Sens Actuators B* 156:673–679
- Ippolito SJ, Trinchi A, Powell DA, Wlodarski W (2009) Acoustic wave gas and vapor sensors. In: Comini E, Faglia G, Sberveglieri G (eds) *Solid state gas sensing*. Springer, New York, pp 261–304
- Jakubik WP, Urbaczyk MW, Kochowski S, Bodzenta J (2002) Bilayer structure for hydrogen detection in a surface acoustic wave sensor system. *Sens Actuators B* 82:265–271
- Kholkin AL, Kiselev DA, Kholkina LA, Safari A (2009) Smart ferroelectric ceramics for transducer applications, Chapter 9.1. In: Schwartz M (ed) *Smart materials*. CRC, Boca Raton
- King WH (1964) Piezoelectric sorption detector. *Anal Chem* 36:1735–1739
- Korotcenkov G (ed) (2011) *Chemical sensors: comprehensive sensor technologies*, vol 4, Solid state devices. Momentum, New York
- Kreno LE, Leong K, Farha OK, Allendorf M, Van Duyne RP, Hupp JT (2012) Metal-organic framework materials as chemical sensors. *Chem Rev* 112:1105–1125
- Kurosawa S, Kamo N, Matsui D, Kobatake Y (1990) Gas sorption to plasma-polymerized copper phthalocyanine film formed on a piezoelectric crystal. *Anal Chem* 62:353–359
- Lai CSI, Moody GJ, Thomas JDR (1986) Piezoelectric quartz crystal detection of ammonia using pyridoxine hydrochloride supported on a polyethoxylate matrix. *Analyst* 111:511–515
- Lakin KM (2005) Thin film resonator technology. *IEEE Trans Ultrason Ferroelectr* 52:707–716
- Lang SB (2005) Pyroelectricity: from ancient curiosity to modern imaging tool. *Phys Today* 58:31–36
- Lee L-H (1991) *Fundamentals of adhesion*. Plenum, New York
- Lee JH, Yoon KH, Hwang KS, Park J, Ahn S, Kim TS (2004) Label free novel electrical detection using micromachined PZT monolithic thin film cantilever for the detection of C-reactive protein. *Biosens Bioelectron* 20:269–275
- Lee Y, Lim G, Moon W (2006) A self-excited micro cantilever biosensor actuated by PZT using the mass micro balancing technique. *Sens Actuators A* 130–131:105–110
- Lozano J, Fernandez MJ, Fontecha JL, Aleixandre M, Santos JP, Sayago I, Arroyo T, Cabellos JM, Gutierrez FJ, Horrillo MC (2006) Wine classification with a zinc oxide SAW sensor array. *Sens Actuators B* 120:166–171
- Martin SJ, Schweizer KS, Schwartz SS, Gunshor RL (1984) Vapor sensing by means of a ZnO-on-Si surface acoustic wave resonator. *Proc IEEE Ultrason Symp* 1984:207–213

- Martin SJ, Ricco AJ, Ginley DS, Zipperian TE (1987) Isothermal measurements and thermal desorption of organic vapors using SAW devices. *IEEE Trans Ultrason Ferroelectr Freq Control* 34:142–147
- Martin SJ, Frye GC, Spates JJ, Butler MA (1996) Gas sensing with acoustic devices. *Proc IEEE Ultrason Symp* 1996:423–434
- Monreal FJ, Marl CM (1987) The use of polymer materials as sensitive elements in physical and chemical sensors. *Sens Actuators* 12:129–144
- Mortet V, Williams OA, Haenen K (2008) Diamond: a material for acoustic devices. *Phys Stat Sol* 205(5):1009–1020
- Nieuwenhuizen MS, Nederlof AJ (1988) Surface acoustic wave gas sensor for nitrogen dioxide using phthalocyanines as chemical interfaces. Effects of nitric oxide, halogen gases, and prolonged heat treatment. *Anal Chem* 60:236–240
- Özgür Ü, Alivov Ya I, Liu C, Teke A, Reshchikov MA, Doğan S, Avrutin V, Cho S-J, Morkoç H (2005) A comprehensive review of ZnO materials and devices. *J Appl Phys* 98:041301
- Pribil R, Bilkova E (1992) The use of a piezoelectric crystal to determine sulphur dioxide in gases. *Talanta* 39:361–366
- Ricco AJ, Martin SJ (1992) Thin metal film characterization and chemical sensors: monitoring electronic conductivity, mass loading and mechanical properties with surface acoustic wave devices. *Thin Solid Films* 206:94–101
- Ricco AJ, Martin SJ, Zipperian TE (1985) Surface acoustic wave gas sensor based on film conductivity changes. *Sens Actuators* 8:319–333
- Richter D, Fritze H, Schneider T, Hauptmann P, Bauersfeld N, Kramer KD, Wiesner K, Fleischer M, Karle G, Schubert A (2006) Integrated high temperature gas sensor system based on bulk acoustic wave resonators. *Sens Actuators B* 118:466–471
- Rosen CZ, Hiremath BV, Newnham R (eds) (1992) *Piezoelectricity*. Springer-Verlag, New York
- Roy S, Basu S (2002) Improved zinc oxide film for gas sensor applications. *Bull Mater Sci* 25:513–515
- Sanchez-Pedreno JAO, Drew PKP, Alder JF (1986) The investigation of coating materials for the detection of nitrobenzene with coated quartz piezoelectric crystals. *Anal Chim Acta* 182:285–291
- Scheide EP, Taylor JK (1974) Piezoelectric sensor for mercury in air. *Environ Sci Technol* 8:1087–1091
- Schulz M, Sauerwald J, Richter D, Fritze H (2009) Electromechanical properties and defect chemistry of high-temperature piezoelectric materials. *Ionics* 15:157–161
- Schwartz RW, Ballato J, Haertling GH (2004) Piezoelectric and electro-optic ceramics. In: Buchanan RC (ed) *Ceramic materials for electronics*. Dekker, New York, pp 207–315
- Şen Z, Gürol I, Gümüş G, Musluoğlu E, Harbeck M, Ahsen V, Öztürk ZZ (2010) Organophosphate sensing with vic-dioximes using QCM sensors. *IEEE SENSORS 2010 Conference*, pp 2127–2130
- Setter N (ed) (2002) *Piezoelectric materials in devices*. EPFL Swiss Federal Institute of Technology, Lausanne
- Smith RT, Welsh FS (1971) Temperature dependence of the elastic, piezoelectric, and dielectric constants of lithium tantalate and lithium niobate. *J Appl Phys* 42:2219–2230
- Smythe R, Helmbold RC, Hague GE, Snow KA (2000) Langasite, langanite, and langatate bulk-wave Y-cut resonators. *IEEE Trans Ultrason Ferroelectr Freq Control* 47:355–360
- Suleiman AA, Guilbault GG (1984a) Mercury displacement in the determination of sulfur dioxide with a piezoelectric crystal detector. *Anal Chem* 56:2964–2966
- Suleiman A, Guilbault GG (1984b) A coated piezoelectric crystal detector for phosgene. *Anal Chim Acta* 162:97–102
- Tadigadapa S, Mateti K (2009) Piezoelectric MEMS sensors: state-of-the-art and perspectives. *Meas Sci Technol* 20:092001–092030
- Tuller HL (2003) Defect engineering: design tools for solid state electrochemical devices. *Electrochim Acta* 48:2879–2887
- Uchino K, Ito Y (2009) Smart ceramics: transducers, sensors, and actuators, Chapter 9.2. In: Schwartz M (ed) *Smart materials*. CRC, Boca Raton
- Vashist SK, Korotcenkov G (2011) Microcantilever-based chemical sensors. In: Korotcenkov G (ed) *Chemical sensors: comprehensive sensor technologies*, vol 4, Solid state devices. Momentum, New York, USA, pp 321–376
- Vellekoop MJ (1998) Acoustic wave sensors and their technology. *Ultrasonics* 36:7–14
- Voinova M, Jonson M (2011) The quartz crystal microbalance. In: Korotcenkov G (ed) *Chemical sensors: comprehensive sensor technologies*, vol 4, Solid state devices. Momentum, New York, pp 377–445
- Wang QM, Shen DM, Bulow M, Lau ML, Deng SG, Fitch FR, Lemcoff NO, Semanscin J (2002) Metallo-organic molecular sieve for gas separation and purification. *Microporous Mesoporous Mater* 55:217–230
- Wang W, He S, Li S, Pan Y (2006) Enhanced sensitivity of SAW gas sensor based on high frequency stability oscillator. *Smart Mater Struct* 15:1525–1530
- Weber J, Albers WM, Tuppurainen J, Link M, Gabl R, Wersing W, Schreiter M (2006) Shear mode FBARs as highly sensitive liquid biosensors. *Sens Actuators A* 128:84–88
- Wohltjen H (1984) Chemical microsensors and microinstrumentation. *Anal Chem* 56:87A–103A

- Wood GO, Moyer ES (1991) A review and comparison of adsorption isotherm equations used to correlate and predict organic vapor cartridge capacities. *Am Ind Hyg Assoc J* 52:235–242
- Yanagitani T, Kiuchi M, Matsukawa M, Watanabe Y (2007) Characteristics of pure-shear mode BAW resonators consisting of (1120) textured ZnO films. *IEEE Trans Ultrason Ferroelectr Freq Control* 54:1680–1686
- Ye ZG (ed) (2008) *Handbook of advanced dielectric piezoelectric and ferroelectric mater: synthesis characterization and applications*. Woodhead, Cambridge
- Zhang J, Hu J, Zhu ZQ, Gong H, O’Shea SJ (2004) Quartz crystal microbalance coated with solgel-derived indium-tin oxide thin films as gas sensor for NO detection. *Colloid Surf A* 236:23–30
- Zhang YS, Yu K, Xu RL, Jiang DS, Luo LQ, Zhu ZQ (2005) Quartz crystal microbalance coated with carbon nanotube films used as humidity sensor. *Sens Actuators A* 120:142–146
- Zhang S, Yu F, Xia R, Fei Y, Frantz E, Zhao X, Yuan D, Chai BHT, Snyder D, Shrout TR (2011) High-temperature ReCOB piezocrystals: recent developments. *J Crystal Growth* 318:884–889
- Zhou X, Zhang J, Jiang T, Wang X, Zhu Z (2007) Humidity detection by nanostructured ZnO: a wireless quartz crystal microbalance investigation. *Sens Actuators A* 135:209–214

## Chapter 14

# Materials for Optical, Fiber Optic, and Integrated Optical Sensors

Optical sensors can be used for detection and determination of chemical or physical parameters by measuring changes in optical properties. In general, optical, fiber optic, and optical-integrated gas sensor systems include an optical source (laser, LED, laser diode, etc.); optical fiber or planar waveguide (PW); a sensing or modulator element (which transduces the measurand to an optical signal); monochromator (or optical filters to select specific absorption wavelengths); a sample holder or a sample presentation interface; an optical detector, allowing for transmittance or reflectance measurements at the wavelength of interest; and processing electronics (oscilloscope, optical spectrum analyzer, etc.) (Modlin and Milanovitch 1991; Burgess 1995; Vurek 1996; Allen 1998; Bansal 2004; McDonagh et al. 2008; Korotcenkov et al. 2011). It is evident that, in order to be able to perform detection using integrated and fiber optics, the working wavelengths must be included within the transmission windows of fibers and planar waveguides (Brenici and Baldini 1991).

### 14.1 General View on Optical Gas Sensing

As a rule the optical signal in gas sensor arises from the interaction of gas molecules with an incident electromagnetic radiation, which can take place at all frequency and wavelength ranges (see Table 14.1). Every gas has specific properties and therefore has specific interaction with electromagnetic radiation. This means that the results of these interactions can be used for gas molecule identification. However, for optical gas sensing, usually narrower spectral region is used, from infrared (IR) region to ultraviolet (UV) region. These regions have specific spectral characterization presented in Table 14.2. The appropriate conversion functions are presented in Table 14.3.

We need to say that various methods can be used for gas analysis (Korotcenkov et al. 2011). However, absorption spectroscopy is still one of the most commonly used methods in optical gas sensing (Kraft 2006). It has been established that, for many applications, absorption spectroscopic detection is a reliable method of detecting various gases. For example, many gases can be monitored directly via absorption infrared (IR) and near-infrared (NIR) spectroscopy. IR and NIR measures the vibrational transitions of molecular bonds. In the mid-IR region of the spectrum, the incident radiation excites the fundamental transitions between the ground state of a vibrational mode and its first excited state. The most prominent absorption bands occurring in the NIR region are related to overtones and combinations of fundamental vibrations of  $-\text{CH}$ ,  $-\text{NH}$ , and  $-\text{OH}$  (and  $-\text{SH}$ ) functional groups that are characteristic of organic matter (Reich 2005). Therefore, IR and NIR spectroscopy have been widely used for detection of gases such as  $\text{H}_2\text{O}$ ,  $\text{CO}$ , and  $\text{CO}_2$  (Zhang et al. 2000; Zhang and Wu 2004),  $\text{NO}_2$  (Ashizawa et al. 2003),  $\text{CH}_4$  (Chévrier et al. 1995),  $\text{O}_2$ ,  $\text{NO}$ ,  $\text{NH}_3$ ,  $\text{HF}$ , and  $\text{H}_2\text{S}$  (Allen 1998).

**Table 14.1** Interaction of atoms and molecules with electromagnetic radiation

Wavelength range	Effect
Radio frequency range 100 m–1 cm	Electron spin causes a very small magnetic dipole; inverting the spin causes a change of the dipole's spatial direction that interacts with the magnetic part of the radiation and leads to absorption or emission
Microwave range 1 cm–10 $\mu\text{m}$	Molecules with permanent polar dipole moment align according to the electric component of the radiation (rotation); this leads to a wavelength-dependent absorption or emission
Infrared (IR) range 100–0.78 $\mu\text{m}$	Oscillations of the atoms in the molecules that cause a change of the dipole moment interact with the electric component of the radiation (IR-active). If the dipole moment in the molecule remains constant for specific oscillation modes, it is IR-inactive
Visible (VIS)/ultraviolet (UV) range 0.78 $\mu\text{m}$ –100 nm	Alternating electric field of the radiation induces a periodic deflection of the electrons in the molecules and thus a change in the dipole moment; it causes the absorption of the radiation at resonance frequency of the deflection

Source: Reprinted with permission from Zosel et al. (2011). Copyright 2011 IOP

**Table 14.2** Spectral regions important for optical sensors

Range	$h\nu$ (eV)	$\lambda$ (nm)	$\nu$ ( $\text{cm}^{-1}$ )
Infrared	0.025–0.4	3,000–50,000	200–3,300
Near-infrared	0.4–1.6	780–3,000	3,100–13,000
Visual	1.6–3.3	380–780	13,000–26,000
Red	1.6–1.9	625–780	13,000–16,000
Orange	1.9–2.1	590–625	16,000–17,000
Yellow	2.1–2.2	565–590	17,000–18,000
Green	2.2–2.4	520–565	18,000–19,000
Cyan	2.4–2.5	500–520	19,000–20,000
Blue	2.5–2.8	435–500	20,000–23,000
Violet	2.8–3.2	380–435	23,000–26,000
Ultraviolet	3.2–6.2	200–380	26,000–50,000

$\lambda$ , wavelength;  $\nu = \lambda^{-1}$ , wave number;  $h\nu$ , energy of photons

**Table 14.3** Parameters and units usually used in spectroscopy

Quantity	Relationship	Usual units
Wavelength	$\lambda$	$\mu\text{m}$ , nm
Wave number	$\nu = 1/\lambda$ (cm)	$\text{cm}^{-1}$
Frequency	$\nu = c/\lambda$ (m)	Hz
Energy	$h\nu = 1.24/\lambda$ ( $\mu\text{m}$ )	eV

$c = 3 \times 10^8$  m/s

Wavelengths preferable for gas detection are listed in Table 14.4. NIR absorption bands are typically broad, overlapping, and 10–100 times weaker than their corresponding fundamental mid-IR absorption bands. These characteristics severely restrict sensitivity in the classical spectroscopic sense and require chemometric data processing to relate spectral information to sample properties. The low absorption coefficient, however, permits high penetration depth and, thus, an adjustment of sample thickness.

**Table 14.4** Absorption lines of several gases and vapors used for gas analysis

Analyte	$\lambda_{\text{abs}}$	Analyte	$\lambda_{\text{abs}}$
UV range			
CO <sub>2</sub>	133, 145 nm	Phenols	266, 270–400 nm
Ethene	171 nm	Bilirubin	452 nm
Nitrates	210 nm	Nitrogen dioxide	496 nm
O <sub>3</sub>	254 nm		
Near-IR range			
O <sub>2</sub>	0.763 $\mu\text{m}$	CO	1.55 $\mu\text{m}$
HF	1.27, 1.33 $\mu\text{m}$	H <sub>2</sub> S	1.57 $\mu\text{m}$
H <sub>2</sub> O	1.3–1.4, 1.8, 1.94 $\mu\text{m}$	CO <sub>2</sub>	1.57, 2.01 $\mu\text{m}$
CH <sub>4</sub>	1.3, 1.65 $\mu\text{m}$	C <sub>3</sub> H <sub>8</sub>	1.68 $\mu\text{m}$
HBr	1.34 $\mu\text{m}$	HCl	1.75 $\mu\text{m}$
N <sub>2</sub> O	1.52 $\mu\text{m}$	NO	1.8 $\mu\text{m}$
Mid-IR range			
NH <sub>3</sub>	2.25, 3.03, 5.7 $\mu\text{m}$	H <sub>2</sub> S	3.72, 3.83 $\mu\text{m}$
CH <sub>4</sub>	2.3, 3.2–3.5, ~7.7 $\mu\text{m}$	HBr	3.77 $\mu\text{m}$
CO	2.33, 4.6, 4.8, 5.9 $\mu\text{m}$	N <sub>2</sub> O	4.3, 4.4, ~8 $\mu\text{m}$
CO <sub>2</sub>	2.7, 4.26, ~13 $\mu\text{m}$	HI	4.39 $\mu\text{m}$
H <sub>2</sub> O	2.75–2.85 $\mu\text{m}$	Carbonyl sulfide	4.87 $\mu\text{m}$
C <sub>2</sub> H <sub>2</sub>	3.07 $\mu\text{m}$	HNO <sub>3</sub>	5.81 $\mu\text{m}$
CH <sub>3</sub> Cl	3.29 $\mu\text{m}$	NO <sub>2</sub>	6.17–6.43, 15.4–16.3 $\mu\text{m}$
C <sub>3</sub> H <sub>8</sub>	3.3 $\mu\text{m}$	SO <sub>2</sub>	7.35, 19.25 $\mu\text{m}$
HCl	3.4 $\mu\text{m}$	H <sub>2</sub> O <sub>2</sub>	7.79 $\mu\text{m}$
Acetone	3.4 $\mu\text{m}$	HCOOH	8.98 $\mu\text{m}$
H <sub>2</sub> CO	3.6 $\mu\text{m}$		

Source: Data from Allen (1998), Mihalcea et al. (1998), Werle (1998), Kalinina et al. (2010), etc.

The growing interest in IR and NIR spectroscopy is probably a direct result of its major advantages over other analytical techniques, namely, easy sample preparation without any pretreatments, the possibility of separating the sample measurement position and spectrometer by use of fiber optic probes, and the prediction of chemical and physical sample parameters from a single spectrum (Reich 2005; Anderson et al. 2005; Kraft 2006). This means that a single spectrum allows several analytes to be determined simultaneously. Moreover, gas absorption spectroscopy enables identification and quantification of components in gas mixtures with little interference from other gases.

In its simplest form, the IR and NIR spectroscopy techniques involve confining a sample of target material (gas) in an optical absorption cell and measuring its absorptions at specific IR or NIR wavelengths, which are characteristic of the vibrational modes of the molecule. The system components usually include an IR source, a monochromator (or optical filters to select specific absorption wavelengths), a sample holder or a sample presentation interface, and a detector, allowing for transmittance or reflectance measurements at the wavelength of interest. At present, gas analyzers working in IR and NIR spectral regions usually are designed using nondispersive infrared (NDIR) gas sensors and Fourier transform infrared (FTIR) spectroscopy. NDIR sensors use band-pass filtering to select the specific analyte absorption wavelength, as opposed to dispersion by a prism or a grating as employed in a spectrometer. An FTIR spectrometer consists of an interferometer, usually a Michelson type, which generates an interferogram from the IR emission of the sample and then performs a Fourier transform to obtain the spectrum. Current FTIR spectrometers offer precise quantification of a wide range of analytes for concentrations down to single-digit parts-per-billion levels and are now available as integrated and relatively compact units compared to the complex and bulky units offered in the past (McDonagh et al. 2008).



However, it is necessary to know that IR sensors can only monitor specific gases that have nonlinear molecules. In addition, it is necessary to know that the signals of IR sensors can be affected by water vapor and other gases present in the atmosphere. For example, oxygen and ozone have strong absorption in the ultraviolet region but essentially zero in the visible and infrared regions, except for isolated peaks. Methane ( $\text{CH}_4$ ) has a couple of very small wavelength regions in which it absorbs strongly, and these occur at about 3.5 and 8  $\mu\text{m}$ . Carbon dioxide has a more complex absorption spectrum, with isolated peaks at about 2.6 and 4  $\mu\text{m}$ , and a shoulder, or complete blackout, of infrared radiation beyond about 13  $\mu\text{m}$ . The plot for water vapor shows an absorption spectrum more complex even than that of carbon dioxide, with numerous broad peaks in the infrared region between 0.8 and 10  $\mu\text{m}$ . The total spectrum of all atmospheric gases is given in Fig. 14.1. Absorption spectra of water are presented in Fig. 14.2.

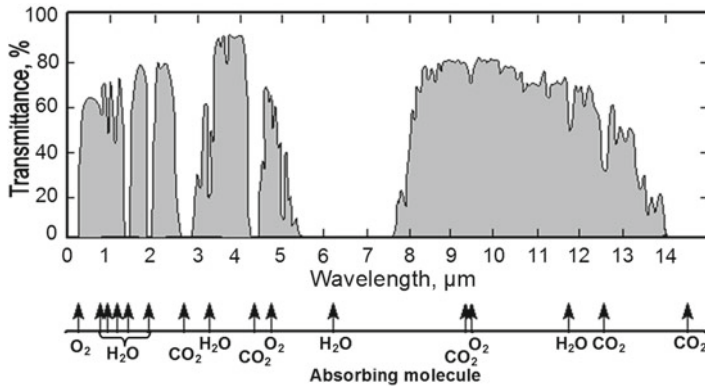


**Fig. 14.1** Transmission spectra of atmosphere (Data from <http://nldr.library.ucar.edu/collections/technotes/asset-000-000-000-650.pdf>; <http://www.astro.virginia.edu/~mfs4n/ir/atmtrans.html>; [http://en.wikipedia.org/wiki/File:Atmospheric\\_Transmission.png](http://en.wikipedia.org/wiki/File:Atmospheric_Transmission.png))

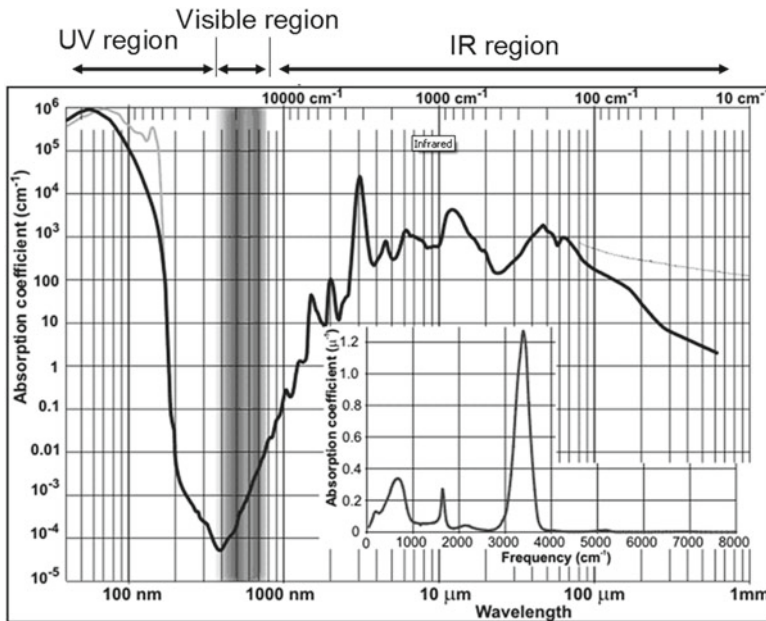


**Fig. 14.2** Absorption spectra of liquid water (Data from <http://www.lsbu.ac.uk/water/vibrat.html>; <http://omlc.ogi.edu/spectra/water/index.html>; [http://en.wikipedia.org/wiki/Electromagnetic\\_absorption\\_by\\_water](http://en.wikipedia.org/wiki/Electromagnetic_absorption_by_water))

Given the transmission spectra of the atmosphere, one can conclude that NIR gas detection technology, in general, is best suited to the detection of gases which have characteristic absorption lines in the ranges of 3–5 or 8–13  $\mu\text{m}$ , i.e., outside those spectral regions where broad and strong water-related absorption features prevail (see Fig. 14.1). Potentially interesting molecules that satisfy this condition are  $\text{CO}_2$ ,  $\text{CO}$ ,  $\text{N}_2\text{O}$ , and a wide range of hydrocarbon species. Also included in this group are hydrogenated fluorocarbon gases such as tetrafluoroethane ( $\text{CF}_3\text{CH}_2\text{F}$ ). Examples that do not satisfy this condition are  $\text{NO}_2$  species and  $\text{NH}_3$  (Spannhake et al. 2009).

Many molecules also absorb ultraviolet or visible light of different wavelengths. Some examples of molecules are presented in Table 14.4. Therefore, these molecules can be detected using UV spectroscopy as well (Kraft 2006). When a molecule absorbs a photon from the UV/vis region, the corresponding energy is captured by one (or several) of its outermost electrons. Ultraviolet–visible spectroscopy (UV = 200–400 nm, visible = 400–800 nm) corresponds to electronic excitations between the energy levels that correspond to the molecular orbitals of the system. In particular, transitions involving  $\pi$  orbital and ion pairs ( $n$  = nonbonding) are important, and so UV/vis spectroscopy is used mostly for identifying conjugated systems which tend to have stronger absorptions (Baldini et al. 2006). Absorbance is directly proportional to the path length and the concentration of the absorbing species. This means that an absorption spectrum can show a number of absorption bands corresponding to structural groups in the molecule (Rouessac and Rouessac 2007).

To date, direct UV absorption sensing has been used mainly in environmental applications to monitor pollutants in the atmosphere such as ozone and  $\text{NO}_2$  (Wu et al. 2006), hydrocarbons, and volatile organic compounds (VOCs) (Lin et al. 2004). Fiber optic UV systems for gas and vapor analysis have been reviewed by Eckhardt et al. (2007). The strong absorbance of vapors and gases in the UV region is advantageous and has resulted in a compact detection system of good accuracy.

## 14.2 Fibers for Optical Gas Sensors

Fiber optic gas sensors are the most popular type of optical gas sensors. An optical fiber consists of at least three components: a core, a cladding, and a light-impermeable jacket (see Fig. 14.3). The core is the thin center of the fiber where the light travels. Therefore, generally the core is a cylindrical, flexible, and transparent long strand made either from a glass, plastic, silica, or other ceramic materials. The cladding is the outer optical material which surrounds the core and functions to reflect the light back into the core by the total internal reflection principle (Lacey 1982; Cheo 1985). This occurs when the refractive index of the core ( $n_1$ ) is higher than that of the surrounding cladding ( $n_2$ ). As a result, light beams are reflected toward the inside of the guide by internal total reflection.

Depending on the wavelength of the light input, waveguide geometry, and distribution of its refractive indices, several modes can propagate through the fiber, resulting in the so-called single- and multimode optical fibers. Table 14.5 provides a summary of the typical properties of various optical silica-based fiber types (e.g., single- and multimode). Both fiber types are used in the construction of

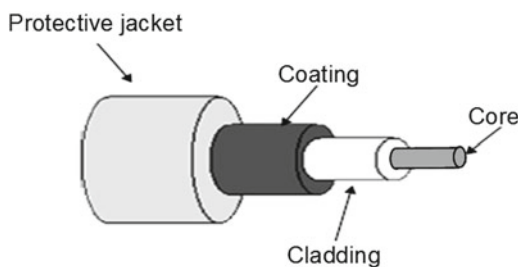


**Fig. 14.3** Schematic diagram of fiber

**Table 14.5** Typical characteristics of single-mode and multimode silica-based fibers

Element	Single-mode fiber ( $\mu\text{m}$ )	Multimode fiber ( $\mu\text{m}$ )	Material
Core	2–10	50–150	Silica based
Cladding	80–120	100–250	Doped silica
Coating	250	250	Polymer
Buffer	900	900	Plastic

Source: Data from Krohn (1988)

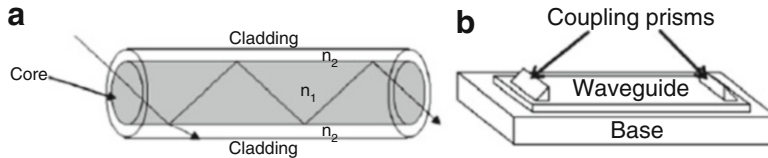


**Fig. 14.4** Basic setup of (a) cylindrical light guides, e.g., fiber optic guides. (b) Planar waveguide configuration

fiber optic gas sensors. In deciding between single-mode and multimode fibers used, we need to take into account that a large-core diameter and a higher numerical aperture give to multimode fibers several advantages in comparison with single-mode fibers, since they make it easier for fiber connection to be made and light is launched into a multimode fiber with ease. In addition, multimode fibers permit the use of LEDs rather than lasers as the radiation source, which saves costs. LEDs are cheaper and have longer lifetimes. On the other hand, as the number of modes increase, the effect of modal dispersion in multimode fibers increases as well. Differences among the group velocities of the modes result in a spread of travel times and are accompanied by the broadening of a light pulse as it travels through the fiber. This effect limits how often adjacent pulses can be launched without resulting in pulse overlap at the far end of the fiber. Modal dispersion therefore limits the speed at which multimode optical fiber communications systems can operate. However, it is necessary to note that in recent decades graded-index multimode fibers have been developed, which use variations in the composition of the glass in the core to compensate for different path lengths of the modes and have much better parameters. They offer hundreds of times more bandwidth than conventional step-index fibers. We need also to take into account that single-mode fibers are more sensitive to strain variation. A planar waveguide sensor can consist of thin planar layers instead of optical fibers. The principle of measurement is shown in Fig. 14.4.

At present, usually two common types of materials normally used for manufacturing optical fibers are glass and plastic. In polymer optical fibers, traditionally PMMA (acrylic) is the core material, and fluorinated polymers are the cladding material. Since the late 1990s however, much higher performance polymer optical fibers based on perfluorinated polymers (mainly polyperfluorobutylvinylether) have begun to appear in the marketplace. Glass optical fiber is most often (though not always) fabricated from very pure silica or  $\text{SiO}_2$  (Syms and Cozens 1993). This has a refractive index of  $n = 1.458$  at  $\lambda_0 = 850$  nm. Dopants useful for fabrication of silica-based fibers include germania ( $\text{GeO}_2$ ) and phosphorus pentoxide ( $\text{P}_2\text{O}_5$ ), both of which increase the refractive index of silica, and boric oxide ( $\text{B}_2\text{O}_3$ ) and fluorine ( $\text{F}_2$ ), which reduce it. Thus, a typical fiber might consist of a  $\text{GeO}_2$ : $\text{SiO}_2$  core with a  $\text{SiO}_2$  cladding. Alternatively, a pure  $\text{SiO}_2$  core could be used, with a  $\text{B}_2\text{O}_3$ : $\text{SiO}_2$  cladding. The boundary between the core and cladding may either be abrupt (step-index fiber) or gradual (graded-index fiber). Glass fibers exhibit higher light transmission characteristics in comparison with plastic fibers, which range from the visible end of the electromagnetic spectrum to the near-IR region (see Fig. 14.5). Both UV and mid-IR absorption bands result in a fundamental limit to the attenuation which one can achieve in the silica system. This occurs despite the fact that the Rayleigh scattering contribution decreases as  $\lambda^{-4}$ , and the ultraviolet Urbach absorption edge decreases even faster with increasing  $\lambda$ .

**Fig. 14.5** Absorption bands of some common gases within the transmission window for silica fiber (Reprinted with permission from Dakin et al. (1995). Copyright 1995 Elsevier)

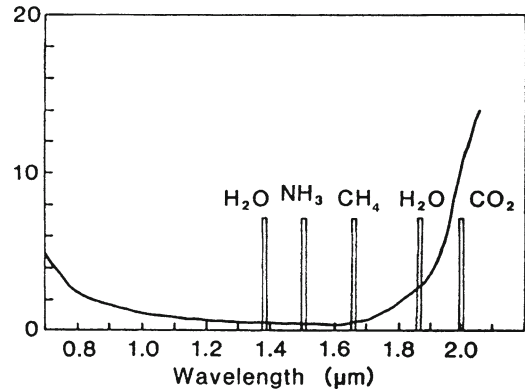


**Table 14.6** Categories of IR fibers with a common example to illustrate each subcategory

Main	Subcategory	Examples
Glass	Heavy-metal fluoride (HMFG)	ZrF <sub>4</sub> -BaF <sub>2</sub> -LaF <sub>3</sub> -AlF <sub>3</sub> -NaF (ZBLAN)
	Germanate	GeO <sub>2</sub> -PbO
	Chalcogenide	As <sub>2</sub> S <sub>3</sub> and AsGeTeSe
Crystal	Polycrystalline (PC)	AgBrCl
	Single crystal (SC)	Sapphire
Hollow waveguide	Metal/dielectric film	Hollow glass waveguide
	Refractive index < 1	Hollow sapphire at 10.6 μm

Source: Data from Harrington (2002)

The infrared absorption increases with long wavelengths and becomes dominant beyond wavelengths of about 1.6 μm, resulting in a fundamental loss minimum near 1.55 μm (Bass and Van Stryland 2002). Therefore, silica fibers with a low OH content guarantee low attenuations for wavelength values included between 500 and 1,750 nm. Therefore, low-loss silica-core fibers are preferred where fiber lengths are long, at which fiber losses become considerable. Silica-based fibers also have better thermal stability than plastic fibers. On the other hand, plastic fibers are less brittle and less expensive to use. Therefore, the low-cost, low-temperature processes by which polymers can be fabricated have led to continued research into the applications of plastic fiber to technologies which require low cost and easy connectivity and that are not loss-limited. The additional flexibility of these materials makes them attractive for large-core, short-length applications in which one wishes to maximize the light insertion.

However, there are several strong absorption regions in the near IR which tend to limit the application of plastic fibers in this region. Therefore, in the mid-IR region, materials which exhibit better infrared transparency usually are used for fiber fabrication. Infrared optical fibers may be defined as fiber optics that transmit radiation with wavelengths greater than approximately 2 μm (Harrington 2002). IR fiber optics may logically be divided into three broad categories: glass, crystalline, and hollow waveguides. Materials used for their fabrication are listed in Table 14.6. Two of the most important representative materials suitable for application in IR fibers are the heavy-metal fluoride glasses and the chalcogenide glasses. A key feature of these IR fibers is their ability to transmit longer wavelengths than most oxide glass fibers can. In some cases, the transmittance of the fiber can extend well beyond 20 μm. However, while both classes exhibit better IR transparency, neither has yet improved to the point of serious competition with silica materials. Harrington (2002) indicates that, compared to silica, IR fibers usually have higher losses, larger refractive indices, and larger  $dn/dT$  values. Other low-loss fiber materials that have been investigated include low-melting-point silicate glasses (soda-lime silicates, germanosilicates, and borosilicates) and halide crystals (TlBrI, TlBr, KCl, CsI, and AgBr). Plastic-based fibers have been designed as well.

**Table 14.7** Selected properties of optical fibers used as sensors

Fiber/parameter	Wavelength ( $\mu\text{m}$ )	Attenuation	Refractive index, core	Max. use temperature ( $^{\circ}\text{C}$ )
Silica	0.2–4	0.5 $\text{dBm}^{-1}$ (1.5 $\mu\text{m}$ )	1.458	800
Chalcogenide	3–10	0.5 $\text{dBm}^{-1}$ (6 $\mu\text{m}$ )	2.9	300
Fluoride	0.2–4.3	0.02 $\text{dBm}^{-1}$ (2.6 $\mu\text{m}$ )	1.51	250
Sapphire	0.2–4	20 $\text{dBm}^{-1}$ (3 $\mu\text{m}$ )	1.7	>1,500
Single-mode photonic crystal	0.4–3	<1 $\text{dBm}^{-1}$ (16 $\mu\text{m}$ )	1.0 (core) 1.46 (cladding)	800
AgBr/Cl	3.3–15	0.7 $\text{dBm}^{-1}$ (10.6 $\mu\text{m}$ )	2.0	400
PMMA	0.4–0.8	0.1 $\text{dBm}^{-1}$ (600 nm) 30 $\text{dBm}^{-1}$ (800 nm)	1.492	80

PMMA poly(methyl methacrylate)

Source: Data from suppliers and Fernando and Degamber (2006)

**Table 14.8** Acceptance angles ( $\theta_c$ ) and numerical apertures (NA) of different types of optical fibers

Fiber material and transmission range (nm)	$\Theta_{\text{max}}$ (deg)	NA ( $\lambda < 587 \text{ nm}$ , $n_0 = 1$ )
Glass (400–1,600)	26.5	0.45
	32.5	0.54
	35.0	0.57
	40.0	0.64
	60.0	0.86
Quartz (250–1,000)	12.5	0.22
	15.0	0.26
PMMA (400–800)	27.5	0.46
	30.0	0.50

PMMA poly(methyl methacrylate) (acrylic glass)

Source: Data from Haus (2010)

As it was shown before, the spectral transmission of an optical fiber is determined by the material used in its core and cladding. Selected parameters of several commercially available optical fibers used in chemical sensors are presented in Tables 14.7 and 14.8. In particular, these tables show a list of typical acceptance angles, transmission ranges, and numerical apertures. The numerical aperture (NA) is an important parameter for the familiar light-beam approach. It provides a connection between the maximum angle of incidence  $\theta_{\text{max}}$ , at which the core of the fiber will take in light that will be contained within the core, and the refractive indices of corresponding materials:

$$\text{NA} = n_0 \cdot \sin(\theta_{\text{max}}) = \frac{\sqrt{n_1^2 - n_2^2}}{n_0} \quad (14.1)$$

The refractive index  $n_0$  belongs to the medium surrounding the fiber. For air,  $n_0 = 1$ .

### 14.3 Planar Waveguide and Integrated Optical Sensors

Planar and integrated optical gas sensors have more complicated configuration. Typical configuration of planar waveguide (PW) is shown in Fig. 14.4. Detailed descriptions of planar waveguide-based chemical sensor (PWCSs) can be found in review papers by McDonagh et al. (2008), Lambeck (2006), Sparrow et al. (2009), and Campbell (2010). Comparing integrated optic sensors with microelectronic

**Table 14.9** Materials acceptable for integrated optical gas sensors

Substrate	Guiding layer
Glass or fused quartz	Various glasses; Ta <sub>2</sub> O <sub>5</sub> , Nb <sub>2</sub> O <sub>5</sub> ; polymers
Glass	Mixed metal oxide layers
LiNbO <sub>3</sub> or LiTaO <sub>3</sub>	Metal oxide layers
GaAs or InP	Ga <sub>1-x</sub> Al <sub>x</sub> As; Ga <sub>1-x</sub> In <sub>x</sub> As <sub>1-y</sub> Py
Quartz crystal	Metal oxides

Source: Data from Selvarajan and Asoundi (1995)

devices, we would like to say that whereas microelectronics focuses chiefly on silicon technology, integrated optics still makes use of a variety of materials such as glass, silicon, metal oxides, polymers, liquid crystals, and Group III–V compound semiconductors, each with different waveguide fabrication technologies. At its core, PW gas sensors comprise a planar substrate (e.g., glass, plastic, or silicon) that forms the basis of the sensor chip. In some cases, this substrate acts as the waveguide, while in others an additional waveguide layer is deposited onto the substrate. The basic requirements of a thin-film optical guide material are that it be transparent to the wavelength of interest and that it has a refractive index higher than that of the medium in which it is embedded (Selvarajan and Asoundi 1995). Usually, a layer of film on top of a substrate (of lower index) serves as the guide. In channel optical waveguides, light is confined in the film not only across its thickness but also across its lateral direction. To realize this, the waveguide in its cross section should be surrounded in all directions by media having lower indices of refraction. Thus, in terms of total internal reflection, guidance can be considered to be the result of rays which propagate within the high-refractive-index region, suffering total internal reflection at the boundary interfaces with the media of lower refractive indices. Thus, materials that enable light-mode propagation are characterized by a high refractive index and low attenuation <3 dB/cm. Especially, metal oxides or nitrides meet these optical requirements, and hence, SiO<sub>2</sub>, SiOXNY, Si<sub>3</sub>N<sub>4</sub>, TiO<sub>2</sub>, Ta<sub>2</sub>O<sub>5</sub>, ZnO, LiNbO<sub>3</sub>, and Nb<sub>2</sub>O<sub>5</sub> are the typical waveguide materials. With regard to the waveguide layer, several configurations have been employed that impart various optical functionalities to the sensor platform. In many cases, the light that propagates within the waveguide facilitates the operation of the platform as a sensor through the interaction of its evanescent field with the sensing environment above the waveguide.

Materials used in integrated optic sensor fabrication are listed in Table 14.9. Integrated optics in glass has advantages because of using the same material basis as fibers, so that efficient light coupling is possible. However, integrated optics in solid-state materials such as silicon or on semiconducting substrates such as GaAs or InP allows simple integration of optical and electronic functions. Absorption in such waveguides is relatively high but acceptable for short path lengths in integrated optical sensors. Semiconductor waveguides are often made as ridges, because of the ease with which a mesa structure may be made by etching. Ridge guides can also be made in amorphous material on semiconducting substrates (Syms and Cozens 1993). One common system involves silicon oxynitride guides, constructed on a silicon dioxide buffer layer, which in turn lies on a silicon substrate. Silicon oxynitride has a relatively high refractive index but one which is lower than that of the silicon, for which  $n \approx 3.5$ . The two are therefore separated by a thick layer of SiO<sub>2</sub>, which acts as a low-index ( $n \approx 1.47$ ) spacer. Other systems use doped silica (e.g., a SiO<sub>2</sub>/TiO<sub>2</sub> mixture) on top of the silica buffer layer. These are important, since they allow the fabrication of waveguides in a form compatible with VLSI electronics. ZnO can also be used as the waveguiding material. Its high refractive index (>2.0) enables high surface sensitivity. Furthermore, ZnO shows the electrooptic effect: by applying an electric field across a layer of this material, the optical refractive index is changed, which can be used for linearizing the sensor signal (Heideman et al. 1996).

There are several ways by which planar waveguides and sensors in IO form can be realized (Selvarajan and Asoundi 1995; Buck 1995). The type of material chosen more or less determines the process technology to be employed. In the case of glass, wet and dry ion-exchange techniques are commonly used

for fabricating mostly passive IO components such as splitter/combiners. Polymer waveguides on glass and other substrates, on the other hand, are formed by spin or dip coating. While this process is simple, precise thickness and uniformity control are difficult. Plasma polymerization and the Langmuir–Blodgett method of formation are other techniques used in the case of polymers. In case of metal oxide, there are two accepted approaches for planar waveguide fabrication (Schmitt and Hoffmann 2010). In the first approach, the substrate material is modified, e.g., by ion exchange in  $\text{SiO}_2$  or  $\text{LiNbO}_3$  (Syms and Cozens 1993; Korishko et al. 2000; Hu et al. 2001). For example, titanium metal can be diffused into lithium niobate or lithium tantalate substrates. The additional impurities cause a required change in refractive index. In the second approach, a waveguide layer is deposited on top of a substrate material (coating), as is done with metal oxides or nitrides (Worhoff et al. 1999). Here, high-refractive-index waveguides can be achieved more easily, but often they are porous and lack sufficient chemical resistance (Schmitt and Hoffmann 2010). For semiconductor crystalline layers and quantum-well structures, growth epitaxial methods (LPE, MBE, MOCVD) are appropriate in the best way.

## 14.4 Light Sources for Optical Gas Sensors

As it was shown before, optical IR, NDIR, and UV gas sensors need light sources for the excitation of the gas molecules in the wavelength range for the particular gas (see Table 14.4). Of course, for optimal gas sensor operation these light sources should correspond to the following requirements (Zosel et al. 2011):

- Rugged construction
- High emissivity
- Long lifetime
- Low cost
- Small size
- Low power consumption
- High pulse rates and, hence, a low thermal time constant for light modulation to offset thermal background signals

At present, there are many types of light sources which operate using different principles. IR radiation sources used in gas sensors are listed in Table 14.10. Therefore, the selection of optimal sources is an important part of gas sensor design. Of course, the choice of emitter to be used in the gas sensor is driven by the requirements of the particular application. For example, polyaniline transducer-based sensors for ammonia show maximum absorbance change at 632.8 nm, so when polyaniline is used as a transducer in optical fiber sensors for ammonia sensing, a He–Ne laser (632.8 nm) source is best for maximum sensor response. However, analysis shows that in optical, fiber optic gas sensors and various portable gas analyzers, semiconductor-based light sources (LEDs and laser diodes) offer the best advantages in terms of size, cost, power consumption, and reliability (Selvarajan and Asoundi 1995). Spectral regions of infrared lasers possible on the laser market are shown in Fig. 14.6.

The selection of the light source for optical gas sensors depends also on the wavelength region in which the transducer shows the maximum response. The emitter must also match the detector to give an optimal “optopair” configuration (Table 14.11). It can be seen that pyroelectric detectors and thermopiles during  $\text{CO}_2$  detection work better in combination with incandescent IR lamps, while photodiodes and photoresistors better operate with LED. Therefore, we have to recognize that thermal sources, such as incandescent lamps, are still used in NDIR systems in industry (see Table 14.12). The same we can say about UV lamps used for UV spectroscopy. The characteristics of some lamp type UV sources are shown in Table 14.13.

However, we need to note that the use of LEDs and laser diodes instead of bulky, high-power-consuming light sources such as thermal IR sources, tungsten-halogen, or deuterium lamps (Johnston 1992; Reich 2005) is the common tendency in manufacturing gas sensors, especially

**Table 14.10** IR radiation sources used in gas sensors

Emission	Type	Properties
Thermal	Wound filament	High-power output with high reliability
	Ribbon filament	Higher pulse rates of up to 200 Hz, modulation depth of 50 %, often used with reflectors to direct entire radiation out of package
	Thin-film filament	High-volume production, low output power due to small filament size
	MEMS system (hot plate)	Thin-film filaments on thin membranes (of silicon), 1,200 °C with 10.7 mW radiation power from 1 m <sup>2</sup> emission area
Photon	IR-LED	Optically pumped LEDs based on III-V semiconductors
	Laser diode	Narrower bandwidth than LEDs

Source: Reprinted with permission from Zosel et al. (2011). Copyright 2011 IOP

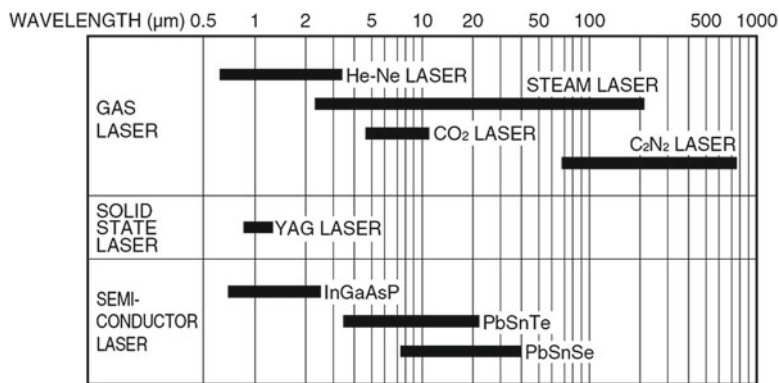


**Fig. 14.6** Wavelength regions of major infrared lasers (From Hamamatsu Photonics; <http://sales.hamamatsu.com/assets/applications/SSD/>)

**Table 14.11** Optimal optopairs of radiation source and detector for CO<sub>2</sub> detection (4.2 μm)

Optopair	Time constant (s)	Relative limit of detection (ppm-cm)/(mW·√s)
Thermal + thermopile	0.1	160
Thermal + pyrodetector	0.1	50–160
Thermal + photoresistor	0.1	0.3
Thermal + photodiode	0.1	0.7
LED + thermopile	0.01	100
LED + pyrodetector	0.1	100
LED + photoresistor	10 <sup>-6</sup>	2 × 10 <sup>-3</sup>
LED + photodiode	10 <sup>-8</sup>	0.5 × 10 <sup>-3</sup>

Source: Data extracted from Sotnikova et al. (2010)

designed for portable devices. In general, thermal sources have two main shortcomings: the first is their broadband radiation, which results in wasted energy because only a narrow band is absorbed by the target gas; the second is their slow response time which precludes fast modulation. For fast modulation with a thermal source, one must use an optical chopper in the system configuration.

Features of LEDs include very low coherence length, broad spectral width, low sensitivity to back reflected light, and high reliability. LED sources can be easily integrated with photodiode array detectors



**Table 14.12** Some commonly used mid-IR sources

	Sources	Lifetime (h)	Modulation	Range ( $\mu\text{m}$ )
Thermal source	IR lamp	40,000	<2 Hz	0.2–5
	Nanoamorphous carbon films	25,000	<100 Hz	1–20
	Surface textured thin metal filament	25,000	<10 Hz	2–20
Quantum laser	Lead–salt diode lasers	10,000	10 kHz	3–30
	Antimonide lasers	2,000	10 KHz	2–4
	Quantum cascade lasers	7,000	10 KHz	4–12

Source: Data extracted from Hecht (1992), Bewley et al. (2008), Nelson (2009)

**Table 14.13** Characteristics of lamp type UV sources

Lamp type	Wavelength range (nm)
Mercury vapor	
Low pressure	253.7 nm (peak) and weaker lines in the near-UV and visible range
Medium pressure	~100–700
Deuterium	~115–400
Xenon arc	~300–1,300 nm with dominated lines between 750 and 1,000 nm
Excimer	172 (Xe <sub>2</sub> *), 193 (ArF*), 222 (KrCl*), 248 (KrF*), 283 (XeBr*), 308 (XeCl*), 351 (XeF*)
Metal halide	~320–700
Zinc or Cadmium	213.9 nm (peak), plus other weaker lines in the UV range

through fiber optics, waveguides, and microscope objectives. Simplicity of use and low power consumption make LEDs a much more attractive option than tungsten lamps in microfluidic devices (O'Toole and Diamond 2008). Laser diodes (LDs) also have great advantages. They exhibit high coherence, narrow line width, and high optical output power, all of which are essential in interferometric sensors. Single-mode fibers may require coherent LD sources as well. High-performance Mach–Zehnder and Fabry–Perot sensors also need single-mode lasers. The lasers used for gas analysis span the UV, visible, and near- and mid-IR spectral regions, with wavelengths ranging from 0.3 to >2  $\mu\text{m}$  for conventional diode lasers (see Table 14.14) and from 2 to >4  $\mu\text{m}$  for recently developed quantum cascade lasers (QCLs) (Hvozdar et al. 2002; Kosterev and Tittel 2002; Duxbury et al. 2005). QCLs are semiconductor lasers based on transitions in a multiple-quantum-well heterostructure (Faist et al. 1994). The emission wavelength depends mainly on the quantum-well thickness rather than on the size of the band gap, as is the case with conventional diode lasers. This has allowed, using the same base semiconductors (InGaAs and AlInAs grown on InP), the manufacture of lasers with an emission wavelength ranging from 3.5 to 17  $\mu\text{m}$  (Werle et al. 2002). Thus, QCLs can operate at wavelengths in the MIR range, which match well with the fundamental vibrational absorption bands of many gases and other chemical species—in comparison to conventional diode sources, where the laser emission generally matches the weaker overtone bands (Duxbury et al. 2005; Grouiez et al. 2008) (see Table 14.14). In addition, due to specific mechanism of recombination, QCLs can operate at near room temperature and produce more optical power (tens of milliwatts) of radiation within a broad range of frequencies. Thus, QCLs can be made to operate over a much larger range than lead–salt lasers, covering significant parts of both the infrared and submillimeter regions, and with higher output power. In mid-IR range, lead–salt diode lasers (LSDL), made from IV–VI semiconductor materials, also can be used. These lasers can operate in the 3–30- $\mu\text{m}$  spectral region. However, lead–salt conventional diode lasers can operate only at liquid nitrogen temperature; it limits the range of uses (Nelson 2009).

It is necessary to note that the presence of a diode laser in the required spectral region is the main factor determining ability to design portable gas analyzers suitable for field applications. Even though the power of a diode laser can be low, being highly monochromatic and tuned to the key absorption wavelength, it allows all of the energy to be absorbed by the gas molecules which

**Table 14.14** Typical parameters of monochromatic LDs which can be used in gas sensing

Laser type	Wavelength	Power	Comments
Gallium nitride (GaN) lasers	Blue/violet to near UV (400–480 nm)	From 5 mW up to 500 mW (CW)	Room temperature
Aluminum gallium arsenide (AlGaAs) lasers	NIR or visible (750–1,000 nm)	From 10 mW up to 0.4 W (CW)	Room temperature, low cost
Vertical cavity lasers (GaAs; InP)	NIR or visible (650–2,000 nm)	1–100 mW (CW)	Room temperature, widely tunable
Indium gallium arsenide phosphide (InGaAsP) lasers	NIR (1,200–2,000 nm)	From 10 mW up to 1 W (CW)	Room temperature, low cost
Antimonide (GaSb; AlGaAsSb; InGaAsSb; InGaSb) lasers	NIR to mid-IR (2,000–4,000 nm)	≥1 mW CW	Room temperature or cooled
QCLs	Mid-IR (3,000–15,000 nm)	Tens of mW CW, tens of W pulsed	Falling prices, no need now for cryogenic cooling
Lead–salt (PbS; PbTe; PbSe; PbSnTe; PbSnSe; PbCdSe; PbSSe) lasers	Mid-IR (3,000–30,000 nm)	<1 mW CW	Require cryogenic cooling

Source: Data from Nichia Corporation (2007), Philips Lumileds (2007), Optoelektronik (2007), etc.

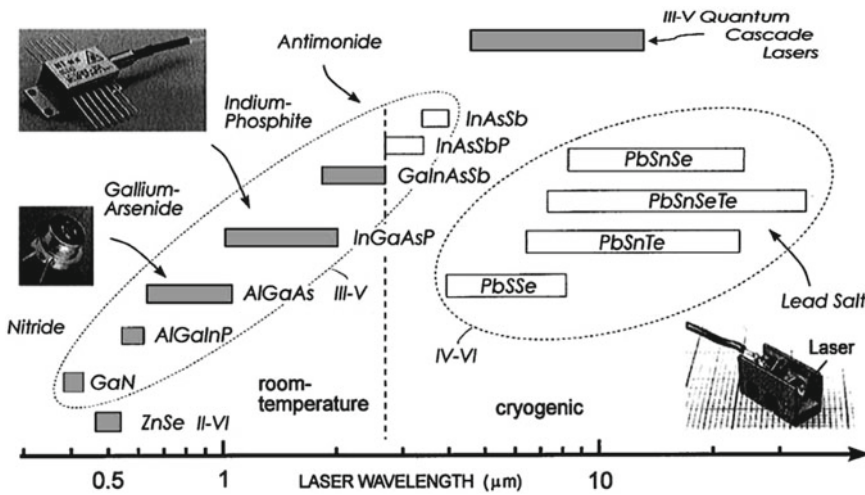


**Fig. 14.7** Spectral coverage of the visible to infrared region by different semiconductor laser materials: while for *p-n*-junction lasers room-temperature operation is only possible up to 2–3 μm for Group III–V materials, quantum cascade lasers become a promising alternative to the cryogenic cooled Group IV–VI lead–salt diode lasers (Reprinted with permission from Werle et al. (2002). Copyright 2002 Elsevier)

is not usually the case in non-laser-based devices. As a result, diode laser sensing systems can have higher sensitivity and selectivity. Therefore, while FTIR is well suited to multicomponent analysis of gases and other chemical species for a range of processes, laser spectroscopy is the method of choice for trace gas analysis, because a spectrally narrow laser source probes a narrow absorption feature of the analyte. Thus, lasers and laser diodes are potentially key components within future generations of optical gas sensors. Comprehensive reviews of diode laser-based gas sensor systems have been provided by Werle et al. (1998, 2002) and Allen (1998).

However, it is necessary to know that LDs in general are susceptible to reflected (feedback) light and temperature changes. They are also less reliable and more expensive. In addition, it is necessary to know that at present it is still difficult to make LDs, especially tunable diode lasers that operate at wavelengths greater than 2.2 μm at room temperature. Spectral regions for commercially available LDs and materials used for their fabrication are shown in Fig. 14.7.

We would like to note that the designing of tunable diode lasers is one of the most promising approaches used for the development of gas analyzers aimed for detection of a specific gas (Somesfalean et al. 2005). Gas analyzers based on tunable diode lasers are considerably simpler in comparison with conventional systems. A *tunable laser* is a laser whose wavelength of operation can be altered in a controlled manner. There are many types and categories of tunable lasers. They exist in the gas, liquid, and solid states. Among the types of tunable lasers are excimer lasers, CO<sub>2</sub> lasers, dye lasers (liquid and solid state), transition-metal solid-state lasers, semiconductor crystal and diode lasers, and free-electron lasers (Duarte 1995).

For the design of tunable laser, various approaches can be used. For example, one can organize the tuning of the laser output across the *linewidth* of the laser transition (0.4–0.5-nm wavelength range). This range can be achieved by placing wavelength-selective optical elements into the laser's *optical cavity*, to provide selection of a particular *longitudinal mode* of the cavity. Most laser gain media have a number of transition wavelengths on which laser operation can be achieved. For example, Nd:YAG laser in addition to the principal 1,064-nm output line has weaker transitions at wavelengths of 1,052 nm, 1,074 nm, 1,112 nm, 1,319 nm, and a number of other lines. If a *dispersive* element, such as a *prism*, is introduced into the optical cavity, tilting of the cavity's mirrors can cause tuning of the laser as it "hops" between different laser lines. Such schemes are common in *argon-ion lasers*, allowing tuning of the laser to a number of lines from the *ultraviolet* and *blue* through to *green* wavelengths. However, the most promising tunable lasers for spectroscopy are multiple distributed feedback (DFB) and distributed Bragg reflector (DBR) cavity lasers, including *vertical cavity surface-emitting lasers* (VCSELs). These lasers are common diode lasers which have ridged structures along the entire cavity for DFB and at each section for DBR that act as distributed or discrete reflectors at the wavelength of interest. The tuning range of such lasers is typically a few nanometers, up to a maximum of approximately 4 nm. It was found that when mounted with external optics, typical diode lasers can be tuned in wider range mainly in the red and near infrared. Using this approach one can design tunable sensors with the tuning range from a few nanometers to tens of nanometers. Of course, the diode laser can be tuned by directly changing the active region temperature (of the cold stage where the diode is mounted) or by changing the ohmic heating of the active region by adjusting the laser drive current (Nadezhdinskii 1996).

One can find, for example, in Hanna et al. (2002) and Magnuson et al. (2008), examples of *tunable lasers* used in gas analyzers. In analyzers based on tunable lasers, the narrow-band laser radiation is scanned over an isolated absorption line, specific for the species to be studied, and the concentration is retrieved from the measured absorbance according to the Beer–Lambert law (Ingle and Crouch 1988). Such lasers have been used for detecting species with absorption bands in the near-infrared region, such as CO<sub>2</sub> at 1,604 nm (Cooper et al. 1993), water vapor at 1,303 nm and CO at 1,604 nm (Riris et al. 1994), NO at 1,800 nm (Sonnenfroh and Allen 1997), CO and CO<sub>2</sub> at 1,577 nm (Lytkine et al. 2006), O<sub>2</sub> at 760 nm (Weldon et al. 1997), and CH<sub>4</sub> at 1,650 nm (Chou et al. 1997). In UV range, tunable lasers also can be used. In particular, in diode laser-based sensor system for UV absorption measurements of the NO molecule in the 226-nm region, which was developed by Hanna et al. (2002), the single-mode 395-nm external-cavity diode laser (ECDL) is sum-frequency-mixed with the output of frequency-doubled, diode-pumped Nd:YAG laser in a beta-barium-borate (BBO) crystal to produce 40 nW of tunable radiation at 226.8 nm. The wavelength of the 395-nm external-cavity diode laser (ECDL) is then scanned over NO absorption lines to produce fully resolved absorption spectra. The estimated NO gas detection limit of the system for demonstrated absorption sensitivity of  $2 \times 10^{-3}$  is 0.2 ppm per meter of path length at 300 K.

## 14.5 Detectors for Optical Gas Sensors

There are two types of detectors: quantum detectors, also known as photodetectors, and thermal detectors, which can be used in optical gas sensors (see Table 14.15). A quantum detector responds to individual photons, which are the quanta of radiation. A thermal detector responds to temperature changes caused by

**Table 14.15** Various infrared detectors used in optical nondispersive infrared gas sensors

		Spectral response ( $\mu\text{m}$ )	Operating temperature (K)	Detectivity ( $\text{Cm Hz}^{1/2}/\text{W}$ )
Thermal detectors	Thermopiles <sup>a</sup>	2–15	300	$1.8 \times 10^8$
	Pyroelectric <sup>b</sup>	2–20	300	$2 \times 10^8$
	Bolometer <sup>c</sup>	8–14	300	$1 \times 10^9$
Quantum detectors <sup>d</sup>	InSb	2–6	213	$2 \times 10^9$
	PbSe	1.5–5.8	300	$1 \times 10^8$
	HgCdTe	2–16	77	$2 \times 10^{10}$

Company: <sup>a</sup>PerkinElmer; <sup>b</sup>IGM&I Co. Ltd; <sup>c</sup>Raytheon; <sup>d</sup>Hamamatsu

Source: Data from Nelson (2009)

the radiation power incident upon it. There are several types of thermal detectors available, including thermopiles, pyroelectric, and bolometer (Nelson 2009; Budzier and Gerlach 2011). The most desirable features of thermal detectors are the high linearity of their signal as a function of the infrared radiation power and their uniform response independent of wavelength. Possibility to operate without cooling is other advantage of thermal detectors.

Due to the large progress of micromechanical manufacturing procedures, thermopiles became inexpensive thermal sensors that are available in large numbers (Graf et al. 2007). A thermopile is an array of thermocouples connected in series. A thermocouple is a pair of junctions of dissimilar materials that produce voltage when one side of the junctions has a different temperature from the other (Seebeck effect). The so-called reference junction is kept at a known temperature by bonding it to a mass with a stable temperature. The other, so-called active, junction is exposed to incident radiation. Connecting many thermocouples in series increases the voltage and therefore allows greater sensitivity. Some thermopile detectors have a built-in thermistor that measures the reference temperature and thus allows the temperature of the target to be calculated. An important advantage of thermopiles is the fact that they can be easily integrated using standard technologies of semiconductor manufacturing—which leads to low-cost mass production. The unique properties of the thermopile are its inherently stable response to DC radiation and its relative insensitivity to ambient temperature variations. If thermopiles are read out with a high impedance amplifier, they exhibit no  $1/f$  noise. Of the various types of thermal detectors, thermopiles have the fewest requirements, making them often the simplest to incorporate into infrared systems. Thermopiles typically operate over a broad range of temperatures without cooling or temperature stabilization (Foote and Jones 1998). No electrical bias is required; the devices passively generate a voltage signal in response to incident radiation. Thus, for some applications thermopile detectors can be supported by simpler, lower power, more reliable systems than either bolometers or pyroelectric or ferroelectric detectors. However, their DC response eliminates the need for a chopper.

The ideal material for thermopile should have high thermoelectric coefficient, low thermal conductivity, and low volume resistivity. Therefore, various metals, semiconductors, and many other thermoelectric materials may be used for thermopile design (Graf et al. 2007). However, good electrical conductors, such as gold, copper, and silver, have relatively poor thermoelectric power (see Table 14.16). Only metals with higher resistivity, especially bismuth and antimony, possess high thermoelectric power in combination with low thermal conductivity, which is why they are the best known thermoelectric materials. Doping of these materials with selenium (Se) or tellurium (Te) can further improve the thermoelectric coefficient. Use of semiconductor materials—such as silicon (crystalline or polycrystalline)—as thermoelectric materials provides other advantages. The resistivity and thermoelectric power can be altered by changing the dopant concentration; resistivity increases faster than the square root of thermoelectric power, as does the internal resistance. Thus, the dopant concentration must be optimized for high-sensitivity/noise ratios. The basic advantage of silicon, therefore, is compatibility with CMOS-standard processes. Typical parameters of micromachined thermopiles are presented in Table 14.17.

**Table 14.16** Seebeck coefficients in metal and semiconductors ( $T=320\text{--}320\text{ }^\circ\text{C}$ , Pt is reference electrode)

Sample	$\alpha_a$ ( $\mu\text{V/K}$ )	Sample	$\alpha_a$ ( $\mu\text{V/K}$ )
<i>p</i> -Si	450	Pb	-1.05
<i>p</i> -Ge	420	Al	-1.66
Sb	48.9	Pt	-5.28
Cr	21.8	Pd	-10.7
Fe	15	K	-13.7
Ca	10.3	Co	-13.3
Mo	5.6	Ni	-19.5
Au	1.94	Constantan	-37.25
Cu	1.83	Bi	-73.4
In	1.68	<i>n</i> -Si	-450
Ag	1.51	<i>n</i> -Ge	-548
W	0.9		

Source: Data from Graf et al. (2007)

**Table 14.17** Typical characteristics of different micromachined thermopiles

Sort	Area ( $\text{mm}^2$ )	$D^*$ ( $10^7\text{ cm Hz}^{1/2}/\text{W}$ )	$R$ ( $\mu\text{V/W}$ )	Material	$\tau$ (ms)
CB	15.2	5		<i>p</i> -Si/Al	
	0.77	1.5	25	Al/poly	300
MB	0.12	1.7	12	Al/poly	10
	0.15	2.4	150	<i>n,p</i> -poly	22
	0.12	1.78	28	Al/poly AMS	20
	0.42	71	184	InGaAs/InP	
M	0.25	9.3	48	<i>n</i> -poly/Al	20
	0.2	55	180	Bi/Sb	19
	0.2	77	500	$\text{Bi}_{0.5}\text{Sb}_{1.5}\text{Te}_3/\text{Bi}_{0.87}\text{Sb}_{0.13}$	44
C	0.785	29	23.5	Bi/Sb	32
	0.06	25	194	Si	12
	0.37	5.6	36	CMOS	<6
	0.6	24	80	CMOS	<40
	0.49	21	110	BiSb/NiCr	40

CB cantilever beam thermopile, MB micro bridge thermopile, M membrane thermopile, C commercial thermopiles, R responsivity,  $\tau$  time constant of response,  $D^*$  specific detectivity

Source: Data from Graf et al. (2007)

Pyroelectric materials are an active material in pyroelectric detectors (Norkus et al. 2006; Budzier and Gerlach 2011). Parameters of these materials are listed in Table 14.18. The three most commonly used pyroelectric materials in such detectors are triglycine sulfate (TGS), lithium tantalate, and ceramic material based on lead zirconate (PZ), including lead zirconate titanate (PZT) (Porte 1987; Izyumskaya et al. 2007).

Triglycine sulfate (TGS) is a colorless water-soluble crystal which is grown from solution; its chemical formula is  $(\text{NH}_2\text{CH}_2\text{COOH})\cdot 3\text{H}_2\text{SO}_4$ . It is hygroscopic and rather fragile, so that special precautions are necessary when it is being processed; and its low Curie temperature ( $49\text{ }^\circ\text{C}$ ) is a major disadvantage, particularly for detectors which are required to meet military specifications. A number of variants on pure TGS have been introduced which lessen these disadvantages, and it remains the favored material for applications where sensitivity is of prime importance. Lithium tantalate,  $\text{LiTaO}_3$ , gives inferior performance to TGS, due to its lower pyroelectric coefficient and slightly higher relative permittivity. It has the advantages, however, of a very high Curie temperature ( $620\text{ }^\circ\text{C}$ ) and insolubility in water.

**Table 14.18** Characteristics of pyroelectric materials (thermal conductivity is included for reference)

Material	$T_c$ (°C)	$\epsilon_r$	$P$ ( $10^{-8}$ C/cm <sup>2</sup> K)	$C$ (J/cm <sup>3</sup> K)	$K$ ( $10^{-3}$ W/cm K)
TGS	49.5	38	3.5	2.4	6.4
DTGS	61	18	2.7	3.5	6.5
LiTaO <sub>3</sub>	618	54	2.3	3.1	40
Sr <sub>0.48</sub> Ba <sub>0.52</sub> Nb <sub>2</sub> O <sub>6</sub>	115	380	6.5	2.3	
PbTiO <sub>3</sub>	460	100–200	3–11	3.2	32
PZT ceramics	200	250–800	5–8	2.4	11
PVF	120	8–11	0.24	2.4	1.3

$T_c$  Curie temperature;  $\epsilon_r$  dielectric constant;  $P$  pyroelectric coefficient;  $C$  volumetric specific heat;  $K$  thermal conductivity

Source: Hamamatsu Photonics (<http://sales.hamamatsu.com/assets/applications/SSD/>)

Detectors made of this material have responsivities which are independent of temperature over a wide range. The performance of PZ and PZT is generally comparable with, or better than, lithium tantalate, except in the case of large area detectors. One of the major advantages of ceramic over a single crystal is that it is relatively easy to produce large blocks of uniform material. This is generally achieved by the hot-pressing technique. There is no need to consider orientation during this processing since the ceramic can be poled in any desired direction by the application of a 3 kV/mm field at about 150 °C. Other materials such as polyvinylidene fluoride (PVDF) and strontium barium niobate (SBN) can also be applied (Guggilla et al. 2006). When exposed to incident radiation, the resulting temperature change causes a large electrical polarization of the active material. The electrical polarization induces a charge proportional to the incident power on nearby electrodes. The pyroelectric effect requires a change in temperature to produce a change in polarization. This means that only changes in incident radiation can be measured. When response from a stationary object is required, a radiation chopper is used. Such choppers can be rotating. The advantage of the pyroelectric detector is its high responsivity: a pyroelectric detector can output signals that are orders of magnitude higher than thermopiles, which makes the pyroelectric detector easier to interface to external circuitry (Nelson 2009). Additionally, the pyroelectric detector can be made with a fast response time close to 1 ms, an order of magnitude faster than the thermopile. Another important design consideration derives from the fact that pyroelectric materials are a subgroup of piezoelectric materials. Any external stress, mechanical vibration, or electric field can cause an electric signal that will interfere with the measured response. Furthermore, any small changes in environment temperature will further compromise the measurements. To compensate for these effects, a second pyroelectric element, identical to the measurement unit, is set up with a light-blocking layer. Any environmental changes create the same voltage on both elements, and therefore, any voltage difference between them is due to the incident light. Normally, it has high noise. Recent data show that the detectivity (the equivalent of the signal-to-noise ratio) of the pyroelectric detector and thermopiles is similar (see Table 14.15).

A bolometer is a simple resistance thermometer. The responsive element changes temperature when it absorbs incident radiation. The electrical resistance of the responsive element changes due to the temperature change. In general, for thermal detectors, all the quantities should be minimized to obtain the smallest noise-equivalent power (NEP). To optimize the detector sensitivity, materials with the lowest thermal conductivity  $G$  and a small  $1/f$  noise constant should be chosen. At the same time, it must be possible to integrate the temperature sensing material together with signal read-out electronics (e.g., a CMOS wafer) in a cost-efficient way. Today, the most common bolometer temperature sensing materials are vanadium oxide (VO<sub>x</sub>), amorphous silicon ( $\alpha$ -Si), and silicon diodes. Simple alternatives for temperature sensing material are thin film metals. They are easy to integrate with CMOS process and the  $1/f$  noise is low. Temperature coefficient of resistance (TCR) is unfortunately also very low (e.g., titanium up to 0.35 %/K), which results in low-performance detectors.

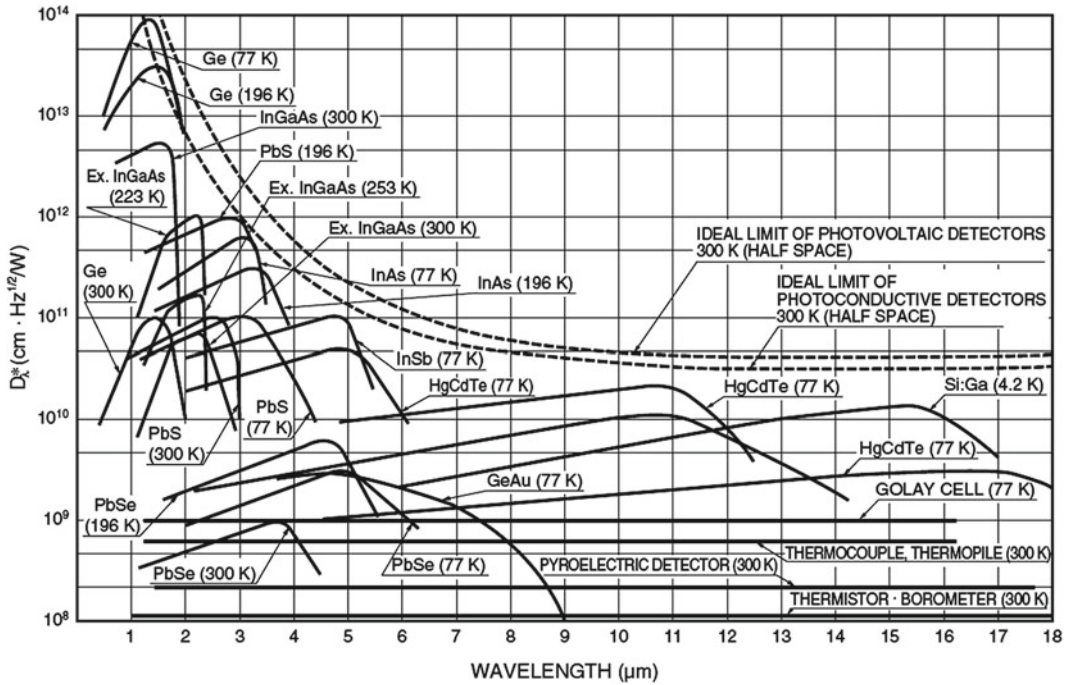


**Fig. 14.8** Operating ranges for some infrared detectors with recommended operating temperatures (From Hamamatsu Photonics; <http://sales.hamamatsu.com/assets/applications/SSD/>)

Titanium is preferred due to its low thermal conductance. Another alternative is polycrystalline silicon–germanium (SiGe) with approximately 30 % Ge, amorphous germanium–silicon–oxygen compounds ( $\text{Ge}_x\text{Si}_{1-x}\text{O}_y$ ), or semiconducting  $\text{YBa}_2\text{Cu}_3\text{O}_7$  (Niklaus et al. 2007). The noise-equivalent temperature difference (NETD) of state-of-the-art uncooled infrared bolometer is typically limited by the  $1/f$  noise from the bolometer temperature sensing material (Richards 1994). The  $1/f$  noise constant is a material parameter that can vary several orders of magnitude for different materials, and even small variations of the material composition can dramatically change the  $1/f$  noise constant. For most materials,  $1/f$  noise constant is not very well documented in literature; however, monocrystalline materials can have a significantly lower  $1/f$  noise constant as compared to amorphous or polycrystalline materials. Thus, one way to reduce the NETD of a bolometer may be the use of monocrystalline temperature sensing bolometer materials (Niklaus et al. 2007).

Regarding photodetectors, we can say that semiconductor photodiodes (PDs), avalanche photodiodes (APDs), and photodiode arrays (PDA) are the most suitable detectors in optical gas sensors (Selvarajan and Asundi 1995). PDs are extremely versatile and have been employed in various configurations. PDs are popular because of their rapid response and wide linear range, which is typically three to four orders of magnitude better than that of phototransistors (PTs). Regarding materials that are preferable for PD fabrication, we can say that Si PDs are good for visible and near-IR wavelengths; Ge, InGaAs/InP, InGaAsP/InP, InGaAsSb, AlGaAsSb/InGaAsSb, and HgCdTe PDs are good for the 0.9- to 2.2- $\mu\text{m}$  range (Refaat et al. 2003) (see Fig. 14.8), while wide-bandgap semiconductors such as GaN and AlGaP are acceptable for the UV spectral range (see Table 14.19) (Monroy et al. 2003). Generally, there is no bandwidth limitation due to the detector as such, although the associated electronic circuits can impose some limitations.

In addition, photomultiplier tubes, light-dependent resistors (LDRs), and phototransistors (PTs) can be used in optical sensors (O’Toole and Diamond 2008). However, PTs have slow response times

**Table 14.19** Performance of some commercial UV photodetectors

Material	Si	GaP	Diamond	SiC	GaN	GaN	AlGaN	AlGaN
Spectral range (nm)	1,100–200	200–520	130–225	219–380	360–250	365–200	320–200	280–200
$\lambda_{\text{max}}$ (nm)	850	440	200	275	360			
Responsivity (A/W)	0.14 at 254 nm	0.15 at $\lambda_{\text{max}}$	0.15 at $\lambda_{\text{max}}$	~0.16 at $\lambda_{\text{max}}$	0.1 at $\lambda_{\text{max}}$	0.1 at 325 nm	~0.8 at 310 nm	0.03 at 275 nm

Source: Data from Monroy et al. (2003)



**Table 14.20** Specifications of LIDAR systems

Parameter/type	DIAL (2 $\mu\text{m}$ )	DIAL (2 $\mu\text{m}$ )	CAL (532-Ch)	CAL (1064-Ch)
<i>Transmitter</i>				
Laser wavelength	2,053 nm	2,053 nm	532 nm	1,064 nm
Laser	Ho:Tm:LuLiF laser		Frequency-doubled Nd:YAG laser	
Laser energy	42 mJ	90 mJ	56 mJ	42 mJ
Laser pulse width	180 ns	130 ns	15 ns	15 ns
Repetition rate	5 Hz	5 Hz	20 Hz	20 Hz
<i>Receiver</i>				
Telescope diameter	0.4 m	0.4 m	0.28 m	0.28 m
Optical efficiency	47 %	58 %	61.4 %	44 %
Detector type	APD	HPT	PMT	APD
Detector	InGaAs (p-i-n)	Sb-based HPT	MP-943	Si APD C30955E
Sampling rate	5 MS/s	5 MS/s	5 MS/s	5 MS/s

*DIAL* differential absorption LIDAR, *CAL* compact aerosol LIDAR, *HPT* heterojunction phototransistors, *PMT* photomultiplier tubes, *APD* avalanche photodiodes

*Source:* Data from Refaat et al. (2003, 2011)

in comparison with PDs and APDs. Most PTs have response times measured in tens of microseconds, which is approximately 100 times slower than photodiodes. They also have the disadvantage of having small active areas and high noise levels. LDRs, while inexpensive and small in size, are not commonly employed in optical sensors because they, similarly to PTs, have slow response times in comparison to photodiodes. In addition they are nonlinear devices. LDRs are more ideally employed for light presence/absence detection than for accurate measurements of light intensity.

We would like to say that in this chapter, we cannot give recommendation regarding optimal use of all types of light sources and detectors, because the configuration of optical gas sensors depends on the approach used for both gas sensor design and target gas. Moreover, even for similar application sensor systems can have different configuration. This situation is illustrated in Table 14.20, where the specifications of the LIDAR systems designed for CO<sub>2</sub> measurements are summarized.

## 14.6 Other Elements of Optical Gas Sensors

Regarding other materials used in optical gas sensor fabrication, we can say that a number of different materials are available as lens or window materials (Allen 1998). These materials should be chosen to provide good transmission properties at the wavelength of interest. For high-sensitivity applications, adding an antireflection coating to the window at the laser wavelength reduces etalon background fringes in the transmission data. Transparency characteristics for various optical materials are shown in Fig. 14.9. Fused silica windows are satisfactory for most visible and near-IR applications at moderate temperatures. Special IR-grade quartz should be used for applications near 1.4  $\mu\text{m}$ , due to a material absorption band in normal quartz that can affect the properties of antireflection coatings and lead to severe etalons. In the near-IR, CaF<sub>2</sub> or sapphire optics can occasionally be useful as well. In the mid-IR, common materials are chalcogenide glasses, ZnSe, CaF<sub>2</sub>, and KBr (Kraft 2006). Indicated materials have been used to create thin-film coating and filter material. Table 14.21 lists some of the common IR materials and their characteristics, and Fig. 14.7 shows transparency curves of some optical materials.

Common to refractive elements in both wavelength ranges is the problem of chromatic aberration. Therefore, *mirror optics* is usually applied in particular in the mid-IR. Reflecting coatings applied to a surface for operation in the visible and near-infrared ranges can be silver, aluminum, chromium,

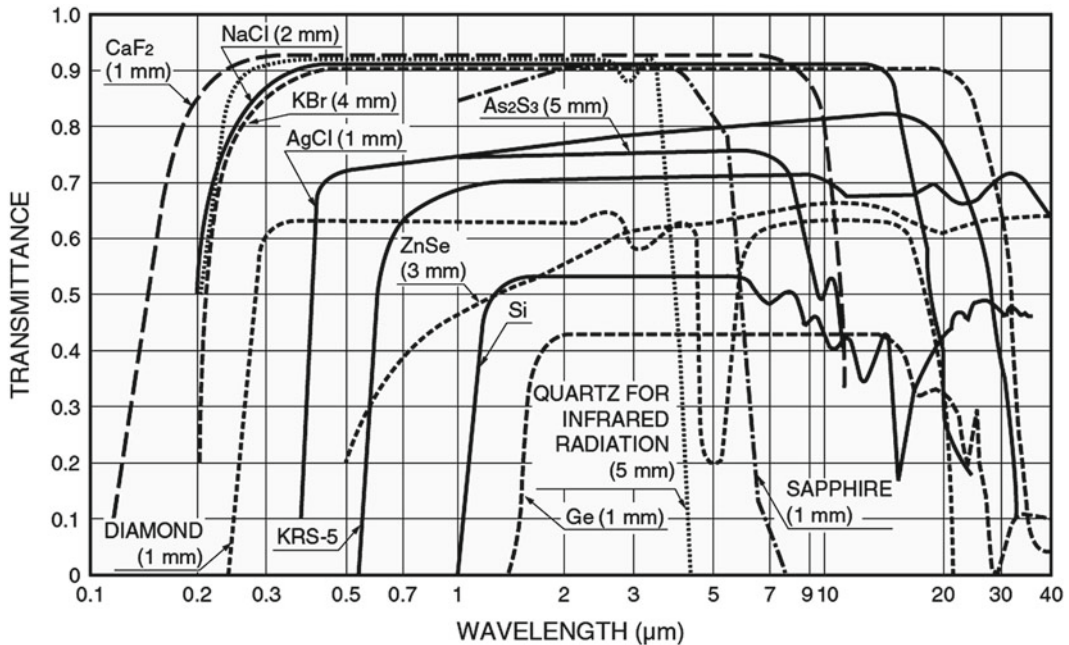


**Fig. 14.9** Transparency characteristics for various optical materials (From Hamamatsu Photonics; <http://sales.hamamatsu.com/assets/applications/SSD/>)

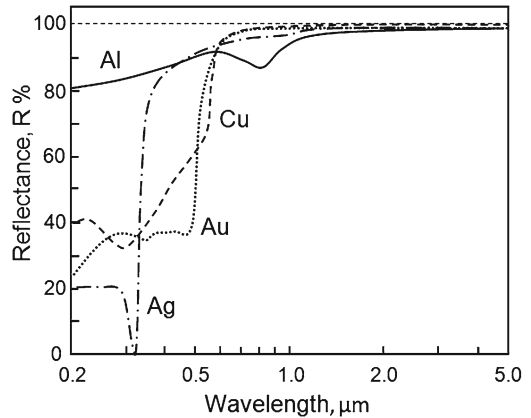
**Table 14.21** Common infrared coating materials

Material	Wavelength range ( $\mu\text{m}$ )	Refractive index @ ( $\mu\text{m}$ )
Sapphire	0.1–5.0	1.76
BaF <sub>2</sub>	0.2–11	1.47
CaF <sub>2</sub>	0.2–8	1.41
Silicon	1.1–10	3.42
ZnSe	0.6–20	2.49
KBr	0.5–25	1.54

and rhodium. However, the mirrors used are usually aluminum-coated ones. Gold is preferable for the far-infrared spectral range devices (see Fig. 14.10). By selecting an appropriate coating, the reflectance may be achieved of any desired value from 0 to 1. The best mirrors for broadband use have pure metallic layers, vacuum-deposited or electrolytically deposited on glass, fused silica, or metal substrates. Before the reflective layer deposition, to achieve a leveling effect a mirror may be given an undercoat of copper, zirconium–copper, or molybdenum. While near-IR mirrors are usually protected by thin SiO<sub>2</sub> layers, unprotected mirrors have to be used in the mid-IR. Disadvantages of mirror optics are the elevated space consumption and the higher prices in comparison to refractive optics, especially comparing nonstandard mirrors against nonstandard lenses. In total, mirror optics are so preferable to fibers and refractive optics, at least in the mid-IR, that in some technical applications they are used to replace waveguides to transport IR radiation between source, sensor head, and spectrometer. More detailed descriptions and parameters of components used during IR and UV–vis measurements can be found in the literature (Kraft 2006; Haus 2010).

Planar couplers, polarizers, and phase modulators required for integrated optical gas sensors can easily be realized as a single chip on lithium niobate. A planar LiNbO<sub>3</sub> phase modulator consists of a

**Fig. 14.10** Spectral reflectance of some mirror coatings at normal incidence (Data from Baumeister (2004), Ridgway (2004), <http://www.tydexoptics.com/materials1/coatings/mccoatings/>)



titanium-diffused monomode channel waveguide and a pair of oriented electrodes. Through application of an electrical voltage to the electrodes, the refractive index of the waveguide and hence the phase of the optical signal passing through it can be altered. Amorphous layers on silicon are also useful in developing certain passive components, such as grating and channel waveguides in sensing and communication applications

## References

- Allen MG (1998) Diode laser absorption sensors for gas-dynamic and combustion flows. *Meas Sci Technol* 9:545–562
- Anderson MS, Andringa JM, Carlson RW, Conrad P, Hartford W, Shafer M, Soto A, Tsapin AI, Dybwad JP, Wadsworth W, Hand K (2005) Fourier transform infrared spectroscopy for Mars science. *Rev Sci Instrum* 76:034101
- Ashizawa H, Yamaguchi S, Endo M, Ohara S, Takahashi M, Nanri K, Fujioka T (2003) Development of a nitrogen dioxide gas sensor based on mid-infrared absorption spectroscopy. *Rev Laser Eng* 31:151–155
- Baldini F, Chester AN, Homola J, Martellucci S (eds) (2006) *Optical chemical sensors*. Springer, Dordrecht
- Bansal L (2004) Development of a fiber optic chemical sensor for detection of toxic vapors. Ph.D. thesis, Drexel University, Philadelphia, PA
- Bass M, Van Stryland EW (eds) (2002) *Fiber optic handbook: fiber, devices, and systems for optical communications*. McGraw-Hill, New York
- Baumeister PW (2004) *Optical coating technology*. SPIE Press, Bellingham, Washington, DC
- Bewley WW, Canedy CL, Kim M, Kim CS, Nolde JA, Larrabee DC, Lindle JR, Vurgaftman I, Meyer JR (2008) Interband cascade laser progress. *Proc SPIE* 6909:69090X-1–69090X-10
- Brenci M, Baldini F (1991) Fiber optic optrodes for chemical sensing. In: *Proceedings of the 8th IEEE optical fiber sensors conference*, New York, pp 313–319
- Buck JA (1995) *Fundamentals of optical fibers*. Wiley, Chichester
- Budzier H, Gerlach G (2011) *Thermal infrared sensors: theory, optimization and practice*. Wiley, New York
- Burgess LW (1995) Absorption-based sensors. *Sens Actuators B* 29:10–15
- Campbell DP (2010) Planar-waveguide interferometers for chemical sensing. In: Zourob M, Lakhtakia A (eds) *Chemical sensors and biosensors: methods and applications*. Springer, Berlin, pp 55–113
- Cheo PK (1985) *Fibre optics: devices and systems*. Prentice-Hall, Englewood Cliffs, NJ
- Chévrier J-B, Baert K, Slater T, Verbist A (1995) Micromachined infrared pneumatic detector for gas sensor. *Microsyst Technol* 1:71–74
- Chou S-I, Baer DS, Hanson RK (1997) Diode laser absorption measurements of  $\text{CH}_3\text{Cl}$  and  $\text{CH}_4$  near 1.65  $\mu\text{m}$ . *Appl Opt* 36:3288–3293
- Cooper DE, Martinelli RU, Carlisle CB, Riris H, Bour DB, Menna RJ (1993) Measurement of  $^{12}\text{CO}_2$ : $^{13}\text{CO}_2$  ratios for medical diagnostics with 1.6- $\mu\text{m}$  distributed-feedback semiconductor diode lasers. *Appl Opt* 32:6727–6731
- Dakin JP, Edwards HO, Weigl BH (1995) Progress with optical gas sensors using correlation spectroscopy. *Sens Actuators B* 29:87–93
- Duarte FJ (ed) (1995) *Tunable lasers handbook*. Academic, New York

- Duxbury G, Langford N, McCulloch MT, Wright S (2005) Quantum cascade semiconductor infrared and far-infrared lasers: from trace gas sensing to non-linear optics. *Chem Soc Rev* 34:921–934
- Eckhardt HS, Klein K-F, Spangenberg B, Sun T, Grattan KTV (2007) Fibre-optic UV systems for gas and vapour analysis. *J Phys Conf Ser* 85:012018
- Faist J, Capasso F, Sivco DL, Sirtori C, Hutchinson AL, Cho AY (1994) Quantum cascade laser. *Science* 264:553–555
- Fernando GF, Degamber B (2006) Process monitoring of fibre reinforced composites using optical fibre sensors. *Int Mater Rev* 51(2):65–106
- Footo MC, Jones EW (1998) High-performance micromachined thermopile linear arrays. *Proc SPIE* 3379:192–197
- Graf A, Arndt M, Sauer M, Gerlach G (2007) Review of micromachined thermopiles for infrared detection. *Meas Sci Technol* 18:R59–R75
- Grouiez B, Parvitte B, Joly I, Courtois D, Zeninari V (2008) Comparison of a quantum cascade laser used in both CW and pulsed modes: application to the study of SO<sub>2</sub> lines around 9 μm. *Appl Phys B* 90:177–186
- Guggilla P, Batra AK, Currie JR, Aggarwal MD, Alim MA, Lal RB (2006) Pyroelectric ceramics for infrared detection applications. *Mater Lett* 60:1937–1942
- Hanna SF, Barron-jimenez R, Anderson TN, Lucht RP, Caton JA, Walther T (2002) Diode-laser-based ultraviolet absorption sensor for nitric oxide. *Appl Phys B* 75:113–117
- Harrington A (2002) Infrared fibers. In: Bass M, Van Stryland EW (eds) *Fiber optic handbook: fiber, devices, and systems for optical communications*, Chap 14. McGraw-Hill, New York
- Haus J (2010) *Optical sensors: basics and applications*. Wiley-VCH, Weinheim
- Hecht J (1992) *The laser guidebook*, 2nd edn. McGraw-Hill, New York
- Heideman RG, Veldhuis GJ, Jager EWH, Lambeck PV (1996) Fabrication and packaging of integrated chemo-optical sensors. *Sens Actuators B* 35–36:234–240
- Hu H, Lu F, Chen F, Shi B-R, Wang K-M, Shen D-Y (2001) Monomode optical waveguide in lithium niobate formed by MeV Si<sup>+</sup> ion implantation. *J Appl Phys* 89:5224–5226
- Hvozdar L, Pennington N, Kraft M, Karlowatz M, Miziakoff B (2002) Quantum cascade lasers for mid-infrared spectroscopy. *Vib Spectrosc* 30:53–58
- Ingle JDJ, Crouch SR (1988) *Spectrochemical analysis*. Prentice-Hall, Englewood Cliffs, NJ
- Izyumskaya N, Alivov Y-I, Cho S-J, Morko c H, Lee H (2007) Processing, structure, properties, and applications of PZT thin films. *Crit Rev Sol State Mater Sci* 32:111–202
- Johnston SF (1992) Gas monitors employing infrared LEDs. *Meas Sci Technol* 3:191–195
- Kalinina K, Stoyanov N, Molchanov S, Kizhaev S, Zhurtanov B, Yakovlev Y (2010) Mid-Infrared LEDs based on GaSb-InAs heterostructures for portable sensing systems. *Annu Bull Austral Inst High Energy Mater* 1:117–123
- Korishko YN, Fedorov VA, Feoktistova OY (2000) LiNbO<sub>3</sub> optical waveguide fabrication by high-temperature proton exchange. *J Lightwave Technol* 18:562–568
- Korotcenkov G, Cho BK, Sevilla F III, Narayanaswamy R (2011) Optical and fiber optic chemical sensors. In: Korotcenkov G (ed) *Chemical sensors: comprehensive sensor technologies*, vol 5, Electrochemical and optical sensors. Momentum Press, New York, pp 311–476
- Kosterev AA, Tittel FK (2002) Chemical sensors based on quantum cascade lasers. *IEEE J Quantum Electron* 38:582–590
- Kraft M (2006) Vibration spectroscopic sensors. In: Baldini F, Chester AN, Homola J, Martellucci S (eds) *Optical chemical sensors*. Springer, Dordrecht, pp 117–155
- Krohn DA (1988) *Fiber optic sensors: fundamentals and applications*, vol 138. Instrument Society of America, Research Triangle Park, NC
- Lacey EA (1982) *Fibre optics*. Prentice-Hall, Englewood Cliffs, NJ
- Lambeck PV (2006) Integrated optical sensors for the chemical domain. *Meas Sci Technol* 17:R93–R116
- Lin T, Sree R, Tseng S, Chiu K, Wu C, Lo J (2004) Volatile organic compound concentrations in ambient air of Kaohsiung petroleum refinery in Taiwan. *Atmos Environ* 38:4111–4122
- Lytikine A, Jager W, Tulip J (2006) Gas phase chemical analysis using long wavelength vertical-cavity surface-emitting lasers. *Opt Eng* 45:1–7
- Magnuson JK, Anderson TN, Lucht RP, Vijayarathy UA, Oh H, Annamalai K, Caton JA (2008) Application of a diode-laser-based ultraviolet absorption sensor for *in situ* measurements of atomic mercury in coal-combustion exhaust. *Energy Fuel* 22:3029–3036
- McDonagh C, Burke CS, MacCraith BD (2008) Optical chemical sensors. *Chem Rev* 108:400–422
- Mihalcea RM, Baer DS, Hanson RK (1998) Diode-laser absorption measurements of CO<sub>2</sub> near 2.0 mm at elevated temperatures. *Appl Opt* 37(36):8341–8347
- Modlin DN, Milanovitch FP (1991) Instrumentation for fiber optic chemical sensors. In: Wolfbeis OS (ed) *Fiber optic chemical sensors and biosensors*, vol 1. Chemical Rubber Company, Boca Raton, FL, pp 237–302
- Monroy E, Omnes F, Calle F (2003) Wide-bandgap semiconductor ultraviolet photodetectors. *Semicond Sci Technol* 18:R33–R51
- Nadezhdinskii A (1996) Diode laser frequency tuning. *Spectrochim Acta A* 52:959–965

- Nelson A (2009) Applications of functional thin films and nanostructures in gas sensing. In: Zribi A, Fortin J (eds) *Functional thin films and nanostructures for sensors*. Springer, New York, pp 85–102
- Nichia Corporation (2007) Specifications for chip type UV LED, Model NCSU034A(T). Nichia Corporation, Tokushima
- Niklaus F, Vieider C, Jakobsen H (2007) MEMS-based uncooled infrared bolometer arrays – a review. *Proc SPIE* 6836:68360D-1–68360D-15
- Norkus V, Chvedov D, Gerlach G, Kohler R (2006) Performance improvements for pyroelectric infrared detectors. *Proc SPIE* 6206:62062X
- Optoelektronik (2007) Jumbo LED ELJ - 850 - 629, Product Datasheet 10 EPIGAP
- O'Toole M, Diamond D (2008) Absorbance based light emitting diode optical sensors and sensing devices. *Sensors* 8:2453–2479
- Philips Lumileds (2007) Technical datasheet DS51: Power Light Source LUXEON® K2, Product Datasheet 9, Philips Lumileds, San Jose, CA
- Porte SG (1987) Materials for pyroelectric detectors. *Mater Design* 8(2):120–124
- Refaat TF, Abedin MN, Koch GJ, Ismail S, Singh UN (2003) Infrared detectors characterization for CO<sub>2</sub> DIAL measurement. *Proc SPIE* 5154:65–73
- Refaat TF, Ismail S, Koch GJ, Rubio M, Mack TL, Notari A, Collins JE, Lewis J, De Young R, Choi Y, Abedin MN, Singh UN (2011) Backscatter 2- $\mu$ m Lidar validation for atmospheric CO<sub>2</sub> differential absorption Lidar applications. *IEEE Trans Geosci Remote Sens* 49(1):572–580
- Reich G (2005) Near-infrared spectroscopy and imaging: basic principles and pharmaceutical applications. *Adv Drug Deliv Rev* 57:1109–1143
- Richards PL (1994) Bolometers for infrared and millimeter waves. *J Appl Phys* 76(1):1–24
- Ridgway ST (2004) Optical coatings for CHARA reflective optics. CHARA Technical Report No. 911, October 2004
- Riris H, Carlisle CB, Carr LW, Cooper DE, Martinelli RU, Menna RJ (1994) Design of an open path near-infrared diode laser sensor: application to oxygen, water, and carbon dioxide vapor detection. *Appl Opt* 33:7059–7066
- Rouessac F, Rouessac A (2007) *Chemical analysis: modern instrumentation methods and techniques*. Wiley, Chichester
- Schmitt K, Hoffmann C (2010) High-refractive-index waveguide platforms for chemical and biosensing. In: Zourob M, Lakhtakia A (eds) *Chemical sensors and biosensors: methods and applications*. Springer, Berlin, pp 21–54
- Selvarajan A, Asoundi A (1995) Photonics, fiber optic sensors and their applications in smart structures. *J Non-Destruct Eval* 15(2):41–56
- Somesfalean G, Sjöholm M, Persson L, Gao H, Svensson T, Svanberg S (2005) Temporal correlation scheme for spectroscopic gas analysis using multimode diode lasers. *Appl Phys Lett* 86:184102
- Sonnenfroh DM, Allen MG (1997) Absorption measurements of the second overtone band of NO in ambient and combustion gases with a 1.8  $\mu$ m room temperature diode laser. *Appl Opt* 36:7970–7977
- Sotnikova GY, Gavrilov GA, Aleksandrov SE, Kapralov AA, Karandashev SA, Matveev BA, Remennyy MA (2010) Low voltage CO<sub>2</sub>-gas sensor based on III–V mid-IR immersion lens diode optopairs: where we are and how far we can go? *IEEE Sens J* 10:225–234
- Spannhake J, Helwig A, Schulz O, Muller G (2009) Micro-fabrication of gas sensors. In: Comini E, Faglia G, Sberveglieri G (eds) *Solid state gas sensing*. Springer, New York, pp 1–46
- Sparrow IJG, Smith PGR, Emmerson GD, Watts SP, Riziotis C (2009) Planar Bragg grating sensors—fabrication and applications: a review. *J Sens* 2009:607647
- Syms RRA, Cozens JR (1993) *Optical guided waves and devices*. Academic, London
- Vurek GG (1996) Optical sensors for biomedical applications. In: Schultz JS, Taylor RF (eds) *Handbook of chemical and biological sensors*, Chap 15. IOP, Bristol
- Weldon V, O'Gorman J, Perez-Camacho JJ, McDonald D, Hegarty J, Connolly JC, Morris NA, Martinelli RU, Abeles JH (1997) Laser diode based oxygen sensing: a comparison of VCSEL and DFB laser diodes emitting in the 762 nm region. *Infrared Phys Technol* 38:325–329
- Werle P (1998) A review of recent advances in semiconductor laser based gas monitors. *Spectrosc Acta A* 54:197–236
- Werle P, Slemr F, Maurer K, Kormann R, Mucke R, Janker B (2002) Near- and mid-infrared laser-optical sensors for gas analysis. *Opt Lasers Eng* 37:101–114
- Worhoff K, Lambeck PV, Driessen A (1999) Design, tolerance analysis, and fabrication of silicon oxynitride based planar optical waveguides for communication devices. *J Lightwave Technol* 17:1401–1407
- Wu B, Chang C, Sree U, Chiu K (2006) Measurement of non-methane hydrocarbons in Taipei City and their impact on ozone formation in relation to air quality. *J Anal Chim Acta* 576:91–99
- Zhang G, Wu X (2004) A novel CO<sub>2</sub> gas analyzer based on IR absorption. *Opt Lasers Eng* 42:219–231
- Zhang G, Lui J, Yuan M (2000) Novel carbon dioxide gas sensor based on infrared absorption. *Opt Eng* 39:2235–2240
- Zosel J, Oelßner W, Decker M, Gerlach G, Guth U (2011) The measurement of dissolved and gaseous carbon dioxide concentration. *Meas Sci Technol* 22:072001

## Chapter 15

# Materials for Electrochemical Gas Sensors with Liquid and Polymer Electrolytes

In previous chapters we mainly discussed solid electrolyte gas sensors designed for application at increased temperature. In the present chapter our attention will be focused on the ambient-temperature liquid and polymer electrolyte gas sensors which are used mostly for medical and industrial hygiene applications. As shown in Chap. 1 (Vol. 1), electrochemical gas sensors usually include filter, membrane (or capillary), electrolyte solution – in which the two or three electrodes (working or sensing electrode, WE, reference electrode, RE, and counter electrode, CE) are immersed, and membrane. The electrochemical gas sensor produces a current or voltage when exposed to a gas/vapor containing an electroactive analyte because the analyte diffuses into the electrochemical cell, to the working electrode surface, and thereon participates in an electrochemical reaction that either produces or consumes electrons (i.e., a redox reaction) (Stetter et al. 2011).

It is clear that each part of the sensor influences the overall performance and analytical characteristics of the sensor. The application of electrochemical sensors to gas-phase analytes involves a unique gas/liquid/solid boundary (analyte–electrolyte–electrode) and an interfacial transport process that frequently controls the response characteristics and analytical performance of the electrochemical gas sensor. It is often the major goal of research to find the link between the analytical performance of the electrochemical sensor and the construction/design and materials from which the sensor is made, as well as the many factors included in the testing of the sensor, such as mass transfer of the analyte to the electrode (Stetter et al. 2011). This means that the choice of appropriate materials for sensor construction and an efficient sensor geometry, and the selection of porosity/composition of materials to enable the gaseous analyte to transport effectively and efficiently to the interface of the electrode/electrolyte where a fast, reversible, redox reaction can occur, are critical to obtaining optimal sensor operation and performance. This interfacial redox reaction provides the charge-transfer reaction of the analyte and the analyte's characteristic sensor signal (Stetter and Li 2008). The materials that participate in specific chemical interactions and their fundamental electronic and electrochemical properties, and their stability, will control sensory reaction thermodynamics and kinetics. Therefore, the selectivity of an electrochemical gas sensor can be realized by optimizing the electrode material to facilitate or catalyze only selected reactions or by control of the sensing electrode potential to select an applied bias that thermodynamically favors either the oxidation reaction or the reduction reaction for a particular analyte. The dimensions of the sensor device also have a profound effect on a gas sensor's analytical performance, including the observed sensitivity, selectivity, response time, and signal stability. The “minor” details of sensor design can have a profound influence on the accuracy, precision, background current, noise, stability, lifetime, and selectivity of the resulting sensor. Note that often the choice of optimum sensor materials and geometry for a given application are not obvious.

## 15.1 Membranes

The gas permeable membrane can be used to regulate the gas flow into the sensor, and it can aid selectivity, allowing only the analyte gas to pass, as well as provide a barrier to prevent the leakage of the electrolyte from the interior of the sensor. Both porous and nonporous membranes can be used for hydrogen and some other gases. Hydrophobic porous membranes are used with aqueous electrolytes since the pores are not wetted by the aqueous solution but allow the transport of dissolved gases to the electrode–electrolyte interface. The choice of membrane, its pore size, and its thickness can determine sensitivity and response time of the sensor in some cases. For example, a low concentration gas sensor with very high sensitivity uses a coarse-high-porosity hydrophobic membrane and less restricted capillary to allow more gas molecules to pass through per unit time to produce higher sensitivity. However, this design also allows more of the electrolyte's water molecules to escape out to the environment and the sensor can dry out faster. Depending on the electrolyte, drying out can change the electrolyte concentration, the solubility of the analyte, and the conductivity of the electrolyte, and these changes will often negatively affect the sensor signal/noise ratio and lower sensitivity and response time.

Several types of porous and gas-permeable membranes exist and can be made of polymeric or inorganic materials. Most common are the commercially available very thin solid polytetrafluoroethylene (PTFE or Teflon) films, microporous Teflon films, or silicone membranes. Issues concerning the choice of membrane include permeability to the analyte of interest, ability to prevent electrolyte leakage, manufacturability, and the thickness and durability of the membrane (Stetter and Li 2008). In a number of cases the rate of mass transport through the membrane controls the limiting current and, hence, the sensitivity of the sensor. In particular, an increase in membrane thickness decreases the sensor sensitivity. Ideally, the gas membrane must have a constant permeability to the target gaseous analyte during sensor operation over a wide temperature range and should possess mechanical, chemical, and environmental stability. Electrochemical hydrogen sensors typically use membranes of Teflon (see Table 15.1). Expanded polytetrafluoroethylene (ePTFE) membrane is a chemically stable

**Table 15.1** Examples of electrochemical H<sub>2</sub> sensors based on liquid and polymer electrolytes

Gas	Electrolyte	Membrane	Electrode material	Sens. type	LOD (H <sub>2</sub> )	Upper range
H <sub>2</sub> -air	6 N KOH or 5 N H <sub>2</sub> SO <sub>4</sub>	Teflon	Pt			
H <sub>2</sub>	5 M H <sub>2</sub> SO <sub>4</sub>	Teflon	Pt/C			4,000 ppm
H <sub>2</sub>	9 M H <sub>2</sub> SO <sub>4</sub>	PTFE	Au			
H <sub>2</sub>	1 M H <sub>2</sub> SO <sub>4</sub>	Nafion	Pt–Ag/AgCl	A	<1 %	16 % ppm
H <sub>2</sub> -N <sub>2</sub>	1.0 M NaOH	PTFE	Pt/C	A	<0.1 %	2 %
H <sub>2</sub> -air	H <sub>2</sub> SO <sub>4</sub>	Teflon	Pt–Ag/AgCl	A	<0.2 %	0.2–4 %
H <sub>2</sub> -N <sub>2</sub>	H <sub>2</sub> SO <sub>4</sub>	Teflon	Pt–Ag/AgCl	A	<0.4 %	1–100 %
H <sub>2</sub> -air	Nafion	PTFE	Pt/C	A	<50 ppm	12,000 ppm
H <sub>2</sub> -N <sub>2</sub> (CO <sub>2</sub> )	Nafion	Ionic polymer	Pt			10 %
H <sub>2</sub> -N <sub>2</sub>	Nafion		Pt	A	10 ppm	10 %
H <sub>2</sub> -N <sub>2</sub>	0.5 M H <sub>2</sub> SO <sub>4</sub>	PTFE	Pt/C	A	<0.1 %	2 %
H <sub>2</sub> -argon	Nafion	Teflon	Pt/C	A	<10 ppm	4 %
H <sub>2</sub> -argon	PVA/H <sub>3</sub> PO <sub>4</sub>	Teflon	Pd and Pt	A	<10 ppm	
H <sub>2</sub>	Nafion/0.1 M H <sub>2</sub> SO <sub>4</sub>		Pt			5,000 ppm
H <sub>2</sub> -air	Nafion		Pt	A,P	20 ppm	4,000 ppm
H <sub>2</sub> -air	Nafion		Pt	P	30 ppm	1,000 ppm
H <sub>2</sub>	Nafion	Teflon	Pt	A	<10 ppm	1,000 ppm
H <sub>2</sub> -air	PBI/H <sub>3</sub> PO <sub>4</sub>		Pt/C–Ag/AgCl	P	<10 <sup>-4</sup> Pa	1 Pa

PTFE polytetrafluoroethylene or Teflon, PVA polyvinyl alcohol, PBI Polybenzimidazole, A amperometric, P potentiometric, LOD limit of detection

Source: Reprinted with permission from Korotcenkov et al. (2009). Copyright 2009 American Chemical Society

substance and has high gas permeability without permeation of aqueous electrolytes. However, other materials can also be used. For example, a semipermeable membrane composed of an acrylonitrile butadiene copolymer can be used to detect selectively the partial pressure of oxygen in blood samples by allowing oxygen transport and effectively preventing the transport of the other species present in the sample (Stetter and Li 2008).

## 15.2 Electrolytes

As follows from the principles of electrochemical sensors, the electrolyte is part of the electric circuit of an electrochemical sensor system. The role of the electrolyte is to transport charge within the sensor, contact all electrodes effectively, solubilize the reactants and products for efficient transport, and be stable chemically and physically under all conditions of sensor operation (Stetter and Li 2008). So, for electrochemical gas sensor applications, the electrolyte solution needs to support both counter electrode and sensing electrode reactions, form a stable reference potential with the reference electrode, be compatible with the materials of construction, and be stable over long periods of time under various operating conditions. An electrolyte can be either/both ion-conducting or/and electron-conducting. Examples of commonly used electrolytes include aqueous electrolytes, nonaqueous electrolytes, polymers, ionic liquids, and solid electrolytes (Dawson et al. 2000; Stetter and Li 2008). Detailed discussion of the indicated electrolytes can be found in other sections of this book. On the other hand, the modifying coating is not a part of the electric circuit, although ion transport and electron transport sometimes take place within the coating or at the coating/electrode interface. The difference between the electrolyte and the electrode modifying coating is not always obvious, and sometimes the classification in a structure is a bit arbitrary.

Prior to 1970, electrolyte solutions for amperometric sensors were mainly aqueous in nature. Even nowadays, aqueous solutions are still used as the electrolytes for gas sensing, e.g., acid or halide electrolytic solutions are used for acidic gas (Imaya et al. 2005) and for other gas-detection applications (Ho and Hung 2001). As illustrated in the preceding examples, aqueous electrolytes are effective in many electrochemical gas sensors. Examples of commonly used electrolytes in  $H_2$  sensors are presented in Table 15.1. Liquid electrolytes used for designing other electrochemical sensors are listed in Table 15.2. One can observe that most electrochemical gas sensors utilize  $H_2SO_4$  and NaOH liquid electrolytes and Nafion as polymer electrolyte.

In some cases hydrogels or an electrolyte inside a porous matrix are used to replace free liquid electrolytes to raise viscosity, lower evaporation rates, and resist leakage of the electrolyte from sensor devices. The polymers or hydrogels can prevent the evaporation of electrolyte during sensor fabrication, especially for microsensor devices where very small amounts of electrolyte are used (Stetter and Li 2008).

In addition to inorganic materials, in electrochemical gas sensors one can also use biological materials such as hydrogenases (Bonanos 2001), a class of enzymes that catalyze the interconversion among  $H_2$ , protons ( $H^+$ ), and electrons. The enzymes can be found in many phylogenetically different microorganisms, including *Thiocapsa roseopersicina*, *Allochromatium vinosum*, *Clostridium pasteurianum*, and *Ralstonia eutropha*. The bio- $H_2$ -sensor's detection signal was generated in a flow cell in which gaseous  $H_2$  was transported to an aqueous phase and oxidized by hydrogenase using benzyl viologen as an artificial electron acceptor. Reduced  $BV^+$  was subsequently detected by chronoamperometry. The net current obtained was proportional to the  $H_2$  concentration in the gas phase. This branch of amperometry using biomaterials has addressed many sensing problems in medical applications, but this particular design has limited sensitivity and stability and will require additional research to achieve practicality in many of the known field applications.



**Table 15.2** Amperometric sensors for electroactive gases

Analyte	Type	Arrangement	Detection limit (ppm)	Upper limit of dynamic range (ppm)
H <sub>2</sub>	SPE <sup>a</sup>	Pt/Nafion/0.1 M H <sub>2</sub> SO <sub>4</sub>	n/a	5,000
	GDE <sup>a</sup>	Teflon-bonded WC/5 M H <sub>2</sub> SO <sub>4</sub>	n/a	40,000
CH <sub>4</sub>	SPE	Pt/Nafion/10 M H <sub>2</sub> SO <sub>4</sub>	1,300	80 %
	GDE	Teflon-bonded Pt/2 M NaClO <sub>4</sub>	60,000	100 %
C <sub>2</sub> H <sub>4</sub>	SPE	Au/Nafion/0.5 M H <sub>2</sub> SO <sub>4</sub>	0.001	500
CH <sub>2</sub> CH <sub>2</sub>	SPE	Pt/Nafion/10 M H <sub>2</sub> SO <sub>4</sub>	0.015	100
O	SPE	Au/Nafion/0.5 M H <sub>2</sub> SO <sub>4</sub>	0.013	1
CH <sub>2</sub> O	SPE	Au/Nafion/1 M NaOH	0.002	0.5
C <sub>2</sub> H <sub>5</sub> OH	SPE	Au/Nafion/1 M NaOH	1	476
CO	SPE	Pt/Nafion/1 M H <sub>2</sub> SO <sub>4</sub>	1.7	33,000
CO <sub>2</sub>	GDE	GoreTex/Pt/0.5 M H <sub>2</sub> SO <sub>4</sub>	<5 % <sup>b</sup>	50 %
	GDE	Teflon/Pt/DMSO	40,000	100 %
	Clark	Nonporous Teflon/Au/DMSO	n/a	15
O <sub>2</sub>	SPE	Pt/Nafion/1 M H <sub>2</sub> SO <sub>4</sub>	n/a	5 %
	GDE	Silicon-sieve/Pt/Nafion/H <sup>+</sup>	n/a	80 %
	Clark	Nonporous Teflon/Au/DMSO	n/a	90 %
O <sub>3</sub>	SPE <sup>c</sup>	Au/Nafion/H <sub>2</sub> SO <sub>4</sub>	0.2	350
	SPE	Au/Nafion/1 M HClO <sub>4</sub>	0.22	44,800
N <sub>2</sub> O	Clark	Nonporous Teflon/Au/DMSO	n/a	90 %
NO	SPE	Au, Pt/Nafion/10 M H <sub>2</sub> SO <sub>4</sub>	0.0010	1
	SPE <sup>c</sup>	Au/ <i>a</i> -ZrPO <sub>4</sub> /TiH <sub>x</sub>	0.2	20
	GDE	Silicon-sieve/Au/Nafion/H <sup>+</sup>	5	100
	SPE <sup>d</sup>	Au/NASICON-NaNO <sub>2</sub>	n/a	1
NO <sub>2</sub>	SPE	Au, Pt/Nafion/10 M H <sub>2</sub> SO <sub>4</sub>	0.004	1
	SPE <sup>d</sup>	Au/NASICON-NaNO <sub>2</sub>	0.01	1
	SPE	C, Au/ <i>a</i> -ZrPO <sub>4</sub> /TiH <sub>x</sub>	0.01; 0.1	20
	SPE	Au/PVC/TBAHFPe	0.075	5
	SPE	C/PVC/TBAHFPe	0.08	2.2
	SPE	Au/Nafion/0.5 M H <sub>2</sub> SO <sub>4</sub>	n/a	100
	SPE	Au/Nafion/1 M HClO <sub>4</sub>	0.2	7
SO <sub>2</sub>	SPE	Au/Nafion, ADP/1 M NaOH	0.0005	0.1
	SPE	Au/Nafion/0.5 M H <sub>2</sub> SO <sub>4</sub>	0.0025	0.1
	SPE	Pt/Nafion/1 M HClO <sub>4</sub>	0.18	4,500
	GDE	Teflon/Au/5 M H <sub>2</sub> SO <sub>4</sub> in DMSO	0.5	200
	SPE	Teflon/Au, Au/Nafion/4 M H <sub>2</sub> SO <sub>4</sub>	n/a	50
	GDE	Teflon-bonded Au/0.33 M H <sub>3</sub> PO <sub>4</sub>	n/a	500
H <sub>2</sub> S	SPE	Ag/Nafion/0.01 M HClO <sub>4</sub> + 0.99 M NaClO <sub>4</sub>	0.045	450

Source: Reprinted with permission from Knake et al. (2005). Copyright 2005 Elsevier

SPE solid polymer electrolyte, GDE gas diffusion electrodes (description see later), Clark Clark-type gas sensor, SPE solid polymer-electrolyte-electrode

<sup>a</sup>Galvanic mode

<sup>b</sup>(Absorptive) preconcentration step followed by anodic oxidation or cathodic reduction

<sup>c</sup>With porous Teflon membrane as additional diffusion barrier

<sup>d</sup>Operating temperature >150 °C

### 15.3 Electrodes

The material of choice for the sensor's electrodes can be different for each function. The RE needs to establish a stable potential. The counter electrode, CE, or auxiliary electrode should be able to catalyze its half-cell reaction over an extended period. In addition, of course, the SE should be the ideal catalyst for its sensing reaction and be selective for it (Chang et al. 1993; Stetter and Li 2008). All of the electrodes need to be stable, manufacturable, and good interfaces for the electrochemistry.

**Table 15.3** Reference and sensing electrode materials used in H<sub>2</sub> electrochemical sensors

Electrode material	Electrode type	Examples	Working temperature
Ag/Ag <sup>+</sup>	RE	(Ag/AgSO <sub>4</sub> ; Ag/AgCl)	RT
Hydrated oxides	RE	(NiO; PbO <sub>2</sub> ; etc.)	RT
Ag	SE	Ag-loaded epoxy resin	<100 °C
Au	SE; RE		<500 °C
Pd	SE(WE)		>600 °C
Pt	SE; RE		>600 °C
Pt/C	SE(WE)	Pt-carbon	
Pt-alloy	SE(WE)	Pt–Au; Ag; Cu; Ni	>500 °C
Transition metal hydrides	RE; CE	(ZrHx; TiHx; ThHx; NbHx)	
Metal oxides	SE(WE)	ITO; ZnO; SnO <sub>2</sub> ; CdO	up to 700 °C
Nanocomposites	SE	(Au/CuO; Au/Nb <sub>2</sub> O <sub>5</sub> ; Au/Ga <sub>2</sub> O <sub>3</sub> )	up to 700 °C

RE reference electrode, SE sensing or working (WE) electrode, CE counter electrode

Source: Reprinted with permission from Korotcenkov et al. (2009). Copyright 2009 American Chemical Society

Materials used as reference or sensing electrodes in H<sub>2</sub> electrochemical sensors are presented in Table 15.3.

In an electrochemical sensor, the working electrode is made from a noble metal, such as platinum or gold, that is capable of making a defined interface with the electrolyte in the cell and is in a porous structure to allow efficient diffusion of the gas phase to a large and reactive electrode/electrolyte interface (Chang et al. 1993; Jordan et al. 1997; Stetter and Li 2008). Palladium, silver, iridium, and rhodium have also been used as electrochemical sensing electrodes, but not so often. The noble metals generally exhibit excellent stability in electrolyte solutions under polarized potentials that may be corrosive to other metals. The noble metals also have high electrocatalytic activity toward analytes like CO, H<sub>2</sub>S, O<sub>2</sub>, Cl<sub>2</sub>, and NO.

Carbons, including graphite and glassy carbon, are also popular materials for working electrodes. Using Pt/C composite (Lu et al. 2005) nanoscale materials in gas-diffusion electrodes maximizes the effective electrode surface area and, because carbon is conductive, the electrode achieves a better combination of such properties as conductivity-porosity. Carbon provides good electrical contact between the grains of noble metal in the porous matrix. Using thick film technology, a few milligrams of the carbon slurry paste can be added along with Pt grains. Research has shown that carbon nanotubes, which have high conductivity, excellent strength, and chemical stability, can also be used for fabrication of working electrodes in electrochemical gas sensors. It was established that CNT modified electrodes have excellent electrochemical properties, such as a wide potential window, small background current, and high electrocatalytic activities, which are superior to those of traditional carbon electrodes. In addition, CNTs provide large surface areas and can be functionalized for specific reactivity.

The counterelectrode (CE) must also be stable in the electrolyte and efficiently perform the complementary half-cell reaction that is the opposite of the analyte reaction (Chang et al. 1993). Therefore, a Pt electrode is also very often used as the CE in an electrochemical gas sensor.

The reference electrode, or RE, also presents challenges for electrochemical sensors and especially miniaturized sensors where a small, stable, and long-lived RE is needed (Cao et al. 1992; Chou 1999). The reference electrode in an electrochemical cell should have a high degree of reversibility as well. It is known that, for a sensor requiring an external driving voltage, it is important to have a stable and constant potential at the sensing electrode. In reality, the sensing electrode potential does not remain constant due to the continuous electrochemical reaction taking place on the surface of the electrode. It causes deterioration of the performance of the sensor over extended periods of time. To improve the performance of the sensor, a reference electrode is introduced. This reference electrode is placed

within the electrolyte in close proximity to the sensing electrode. The main function of reference electrode is to maintain a fixed stable constant potential at the sensing electrode. No current flows to or from the reference electrode. The gas molecules react at the sensing electrode and the current flow between the sensing and the counter electrode is measured and is typically related directly to the gas concentration. The value of the voltage applied to the sensing electrode makes the sensor specific to the target gas. Experiment has shown that for optimal operation of an electrochemical gas sensor the reference electrode must form a stable potential with the electrolyte, be compatible with the sensor manufacture, and, generally, not be sensitive to temperature ( $T$ ), pressure ( $P$ ), relative humidity (RH), or other contaminants or reactants in the sensor system. The RE must be able to maintain the WE at a constant electrochemical potential during the sensing application.

For traditional sensors, calomel,  $\text{Hg}/\text{HgCl}_2$ , and silver–silver chloride,  $\text{Ag}/\text{AgCl}$ , are the most commonly used. This is based on the high degree of reversibility of the oxidation–reduction reaction involving  $\text{Hg}-\text{HgCl}_2$  and  $\text{Ag}-\text{AgCl}$ . However, for practical fabrication processing,  $\text{Ag}/\text{AgCl}$  is simpler compared to a calomel reference electrode. Because mercury has a relatively high vapor pressure it does not lend itself well in any fabrication process using a vacuum or low-pressure environment. Therefore, a silver/silver chloride ( $\text{Ag}/\text{AgCl}$ ) reference electrode is commonly used for this purpose in many electrochemical applications (Ives and Janz 1961). Usually a silver film is first deposited by either thick- or thin-film metallization, serving as the base of the reference electrode. The silver film can then be chlorided electrochemically, forming the  $\text{Ag}/\text{AgCl}$  electrode. However it was found that  $\text{Ag}/\text{AgCl}$  electrodes maintain a fixed potential only when the chloride concentration is fixed, and its lifetime is limited because silver chloride can gradually dissolve in aqueous solutions. This means that the basic design of the  $\text{Ag}/\text{AgCl}$  RE can be unstable in many electrolytes. For example, the  $\text{AgCl}$  layer may dissolve in an electrolyte such as sulfuric acid, causing the  $\text{Ag}/\text{AgCl}$  RE potential to change as the chloride layer is dissolved. In addition, free chloride ions in the electrolyte may form complexes with the platinum particles on the WE and CE. This can have deleterious effects on the chemical stability of the electrodes and adversely affect the sensor performance. For resolving this problem Chao et al. (2005) proposed to protect  $\text{Ag}/\text{AgCl}$  electrode by Nafion. Nafion is a cation-exchange membrane that allows only small cations such as protons in the electrolyte to move freely from the bulk solution to the  $\text{Ag}/\text{AgCl}$  wire surface. Anions such as  $\text{Cl}^-$  will not readily diffuse into the electrolyte because of the electric repulsion (Donnan exclusion) within the positively charged Nafion ion-exchange layer. Thus, the protective Nafion coating both minimizes the dissolution of chloride ions into the bulk solution and, at the same time, maintains ionic contact between the RE and the bulk solution. However, it was found that, simultaneously with stability improvement, the solid Teflon membrane on the RE electrode slowed the response time of the sensor from 5 % to 90 % signal from a few seconds to a few minutes (Chao et al. 2005).

The other popular reference electrode is a Pt/air electrode (Bay et al. 1972), which is not a classical reference electrode but is sometimes called a pseudo-reference electrode because, while it forms a stable potential, the potential is not that of a well-defined thermodynamic reaction and the electrode must be calibrated with an electrode of known potential. In a two-electrode system, a single electrode, called the auxiliary electrode, can function as both the RE and the CE for the purposes of a given analytical experiment (Stetter and Li 2008).

We need to note that the metallization processes used for the fabrication of various electrodes in electrochemical sensors, especially of microminiaturized construction, are of considerable importance (Liu 1996). Metallization of the electrode element can be accomplished by thick- or thin-film techniques. Each technique has its merits and limitations, and the choice between the two techniques depends on the requirements. The thin-film electrode is geometrically well defined. Compared to thick-film electrodes, they are more uniform, reproducible, and can have a smaller structure. For thin-film sensing elements, a structure in the order of nanometers is feasible, whereas the thick-film sensing element has to be much larger. However, thin-film electrodes are not as porous as thick-film ones, unless the thin-film element is extremely thin. In addition, thin-film electrodes are

relatively dense and do not have the electrocatalytic properties that porous electrodes have. Therefore, in many instances, the surface of the thin film is chemically or electrochemically modified to enhance its electrocatalytic activity. For instance, thin platinum film electrodes can be platinized electrochemically, forming a porous platinum black layer. This platinum black layer is electrocatalytically more active than the thin platinum film. Thin-film processes are more capital and labor intensive and the process is more complicated than thick-film processes. Thin-film deposition is also a batch process which may produce sensors of limited numbers of silicon substrates. This is very desirable in prototype development, for it allows modification on prototypes with minimum cost. However, both thick-film and thin-film metallization for electrochemical sensor development are generally used.

## 15.4 Gas Diffusion Electrodes

As demonstrated by Clark et al. (1953), a membrane diffusion barrier for the working electrode offers several advantages over a bare electrode (Hitchman 1978). For instance, the membrane eliminates interferences from ions and other substances to which it is impermeable, thus improving the selectivity for the analyte of interest. Also, the membrane serves as a diffusion layer for gaseous analytes. By appropriate selection of the membrane material and size, one can control the analytical characteristics of a sensor, permitting the analysis of several analytes over a wide range of concentrations.

The earliest Teflon-bonded diffusion electrodes were prepared by Niedrach and Alford (1965) for use in fuel cells. Experiment has shown that a fuel cell with indicated diffusion electrodes can also be used as a gas sensor if the configuration is appropriate. The gas diffusion electrode (GDE) was first deployed for reducing gases by Bay et al. (1972) with free electrolyte and also for  $H_2$  sensors using a Nafion polymer electrolyte by La Conti and Maget (1971). It should be noted that the development of the gas-diffusion electrode (GDE)—porous electrodes which allow the diffusion of the analyte gas to reaction points where the electrode is in contact with an internal electrolyte solution—was a major achievement in the evolution of modern electrochemical gas sensors. The Niedrach electrode provided a model for the contemporary gas-diffusion electrode, being “semihydrophobic” and allowing an open porous electrode of the finely dispersed metal catalyst yet not allowing complete penetration by the electrolyte.

The original Niedrach electrode consisted of a sintered Teflon–Pt catalyst covered with a porous Teflon film. These electrodes are prepared by mixing Teflon emulsion with a high-surface-area noble metal catalyst powder and then depositing the slurry on a metal wire screen or on the surface of a totally hydrophobic porous Teflon film. The metal grid in the GDE serves as current collector (Niedrach and Alford 1965). Mechanical stability is obtained by heating to sinter the materials together. The resulting gas-diffusing electrode consists of highly interlocked matrices of gas pores, electrolyte channels, electronically conducting paths, and electrocatalytic surfaces. This type of electrode architecture possesses gas-filled pores that are partially wetted, thus forming triple points. GDE is porous enough to effect efficient gas permeation, has sufficient metal catalyst to be a good electronic conductor, and is hydrophilic enough to make intimate contact with the electrolyte for ionic conduction and facilitation of electrochemical reactions involving gases. The electrochemical cell that is based on a gas diffusion electrode composed of a porous PTFE membrane and a porous electrode is shown in Fig. 15.1a.

Its performance was evaluated in hydrogen–oxygen and hydrogen–air fuel cells at ambient temperature in 6 N KOH and 5 N  $H_2SO_4$ . In both cases it was shown that water was efficiently retained in the electrolytic solutions and did not leak into the gas fuel feed stream. It was established that gas-diffusion electrodes based on back-side metallized porous membranes (Cao and Stetter 1991; Cao et al. 1992; Chang et al. 1993) are not affected by evaporation of water because the porous electrode is directly in contact with the bulk of the electrolyte solution. The mass transfer of analyte from the

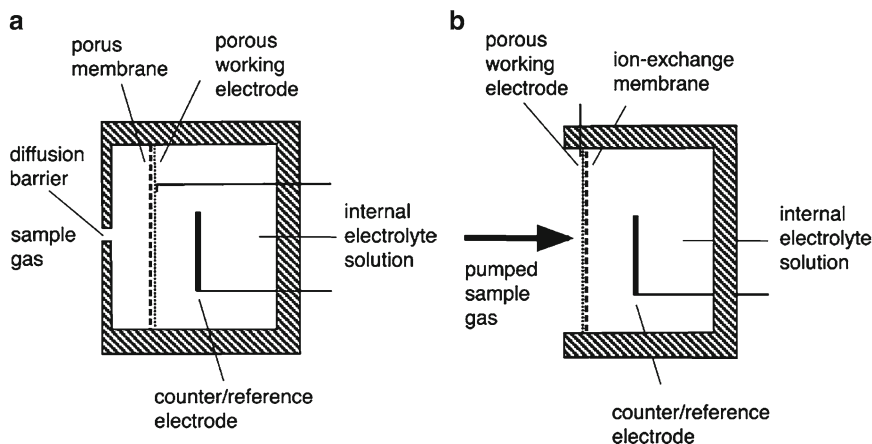


**Fig. 15.1** Schematic of a cell based on (a) a gas-diffusion electrode (GDE) composed of a porous PTFE-membrane and a porous electrode and (b) a metallized solid polymer electrolyte (SPE) membrane (Reprinted with permission from Knake et al. (2005). Copyright 2005 Elsevier Science)

sample to the working electrode can be faster in comparison with the classical configuration, resulting in shorter response times and higher currents that lead to higher sensitivity. Also, the real surface area of the electrode can be several orders of magnitude higher, allowing species with relatively poor electroactivity to produce measurable currents. Therefore GDEs are especially valuable in those cases when the kinetics of the electrochemical reaction is very slow, such as the oxidation of hydrocarbons and CO. Examples of the earliest of these sensors reveal excellent practical sensor characteristics (Bay et al. 1974; Blurton and Stetter 1978). The design of GDE electrochemical sensors has been shown to provide fast responses, high sensitivities, and low detection limits (Stetter et al. 1977; Blurton and Stetter 1978; Mosley et al. 1991; Sundmacher et al. 2005). Experiment has shown that Pt/Nafion electrodes can be successfully applied for amperometric NO and NO<sub>2</sub> sensing as well (Ho and Hung 2001; Ho et al. 2005).

According to Sundmacher et al. (2005), the GDE combines the following functions: (1) a catalytic function within the electrode structure for electrochemical reactions; (2) electrons released in the anodic reaction or consumed in the cathodic reaction at the reaction sites have to be collected, i.e., the electrode composite must be electrically conductive; (3) ions in the membrane must be transported towards the reaction sites, i.e., the electrode needs to house some electrolyte to have ionic conductivity; and (4) non-charged reactants have to be transported towards the reaction sites, primarily via pore diffusion inside the electrode structure. Thus, gas-diffusion electrodes (GDE) have highly efficient three-phase boundaries, where the reacting gas, metallic electrode, and electrolyte meet together and react. The mechanism of transport is often modeled as a process consisting of diffusion through the air filled pores of the porous current collector, diffusion to the triple phase boundary, and electron transfer occurring just as the analyte reaches the three phases where electrodes, ion-exchange membrane or electrolyte, and gas phase meet. All indicated functions are important for operation of electrochemical sensors and therefore optimal electrode design requires a perfectly executed balance of the different functions. For example, the ratio between hydrophilic metal and hydrophobic PTFE is very crucial and subject to optimization in order to find a compromise between formation of efficient triple points and prevention of the gas-filled pores from being flooded by the electrolyte solution (Otagawa et al. 1985).

At present there are several variants of GDEs designed for sensors applications [see, for example, the review of Knake et al. (2005)]. The electrolyte solution can be contained in a porous matrix such as PVC, and the porous electrode might then be deposited directly onto this substrate. A mechanically

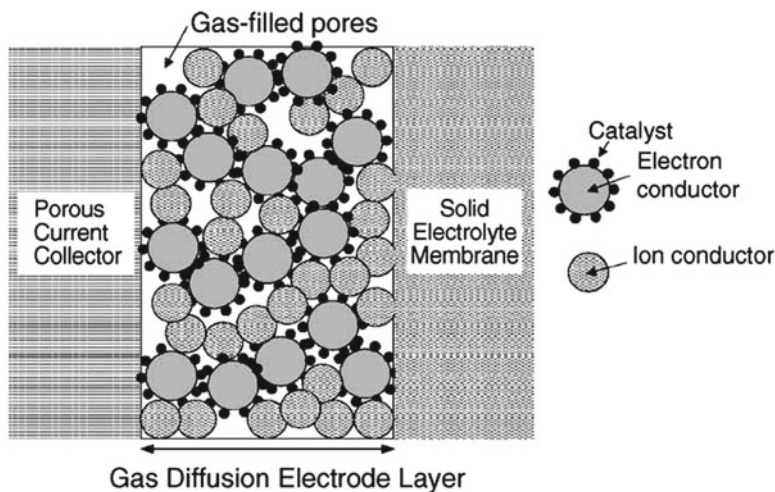


**Fig. 15.2** Schematic illustration of gas diffusion electrode (GDE) (Reprinted with permission from Sundmacher et al. (2005). Copyrights 2005 Elsevier)

stable electrode can also be constructed by coating a carbon fleece with a mixture of platinum black (or platinum impregnated carbon particles) and PTFE particles, followed again by heat treatment. Two such electrodes can then be pressed onto opposite sides of an ion-exchange membrane such as Nafion to obtain an electrochemical cell for gases. Bergman (1968) suggested a design that consisted of a porous working electrode which was vapor-deposited onto the backside of a thin nonporous oxygen-permeable PTFE membrane. Later, porous PTFE was employed to create the metallized membrane electrode (MME) as this allows for the higher mechanical strength of a thicker material. This configuration was subsequently widely adopted for gas sensors. The MME has been reviewed by Opekar (1989). More efficient membrane bonded electrodes can be obtained by mixing a powder of a finely dispersed electrode metal with a binder and applying this mixture to the back of a porous PTFE-membrane. Different procedures such as painting, spraying, and pressing may be used, and this might also involve the use of heat for sintering the binder (which often consists of PTFE-powder).

Figure 15.2 shows a schematic of a typical GDE manufactured by using fuel cell technologies. As can be seen, GDEs are generally composed of a sintered composite (e.g., powdered Teflon and noble metal black) with two or three similar gas diffusion electrodes separated by an aqueous electrolyte or an ion conducting membrane (Bay et al. 1972; Kordesch and Simader 1996; Paganin et al. 1996). By using well-defined particle size distributions, one can adjust the electrode pore structure. This in turn offers the possibility to optimize the transport properties of the GDE with respect to the non-charged reactants. As a result, the catalytically active surface area of the electrode can be several orders of magnitude higher in comparison with standard electrodes, allowing species with relatively poor electroactivity to produce measurable currents.

Parameters of the presently most used Pt-based gas-diffusion electrodes are given in Table 15.4. The gas diffusion electrodes (GDEs) used in amperometric electrochemical gas sensors are semihydrophobic (Bay et al. 1972; Kordesch and Simader 1996; Paganin et al. 1996). Usually they are composed of two layers deposited on an appropriate support. A diffusion layer is prepared with a suspension of PTFE (for example, DuPont TM 30) with high surface area carbon (Cabot XC-72, 250 m<sup>2</sup>/g). Nafion® (DuPont) is a proton exchange material, and, as such, an ionic conductor. Onto this layer the catalytic layer is deposited using several procedures (Paganin et al. 1996; Ren et al. 1996). The catalytic layer contains metal nanoparticles (usually Pt) anchored on a carbon support. Platinum-based metal nanoparticles of around 2–5 nm are often used for fabrication of gas-diffusion electrodes

**Table 15.4** Description of the standard gas diffusion electrodes

Electrode	ETEK	SORAPECH2	SORAPECO2
Platinum loading (mg/cm <sup>2</sup> )	0.5	0.2	0.35
NAFION (mg/cm <sup>2</sup> )	Unknown	1	0.8
Roughness factor	5	80	150
Active layer (10 <sup>-6</sup> m)	10	5	5
Diffusion layer (10 <sup>-6</sup> m)	250	250	250

Source: Reprinted with permission from Rosini and Siebert (2005). Copyrights 2005 Elsevier

(Kordesch and Simader 1996; Paganin et al. 1996; Vielstich et al. 2003) as is fuel-cell grade Pt black. The result is a matrix that has pores, electrolyte channels, electronic pathways, and electrocatalytic surfaces intermixed. The material is a good electronic conductor, porous to gases, and can conduct ions in and around the catalyst which presents a very high electroactive area. It is important to note that for the last 20 years the content of Pt in GDEs, expressed in mass of Pt per unit of geometric area, has decreased more than ten times from 5 mg/cm<sup>2</sup> Pt to 0.2–0.4 mg/cm<sup>2</sup> Pt. The mixture is filtered on a support (a carbon cloth or a carbon paper, totally hydrophobic).

As can be seen in Fig. 15.1a, the first gas-diffusion electrodes were designed based on back-side metallized porous membranes and the presence of liquid electrolyte. However, there is other approach to diffusion electrode design (Knake et al. 2005). It was found that the liquid electrolyte in a GDE could be replaced by a solid, ionically conductive polymer. Thus, whole electrode–electrolyte assemblies consisting of porous electrodes and ion-exchange polymers were manufactured. This arrangement is depicted in Fig. 15.1b. When using SPE-membrane-based sensors, the electrodes face the sample gas and, therefore, essentially no diffusion barrier is present. Furthermore, they have usually been used in systems with a forced gas flow.

The gas electrode, in which a porous metal layer is bound to an ion-conducting membrane such as Nafion design, was first reported in the mid-1980s (Katayama-Aramata et al. 1983; Kita et al. 1984; Kita and Nakajima 1986; Enea 1987). This arrangement is often referred to as an SPE-electrode, because the ion-exchange membrane material is usually termed solid polymer–electrolyte (SPE). This acronym refers to the use of an ionically conducting membrane as an integral element in a device. The electrodes are mounted in the cell housing such that the electrode faces the gas phase directly while the backside of the SPE-membrane is in contact with the liquid electrolyte phase and can be seen as its continuation. It should be noted that, under the highly acidic or basic conditions normally used, Nafion is highly hydrated and, although it is a cation exchanger, anions might pass through the membrane. Thus, the electrode reaction at the front side of a Nafion-membrane which is contacted in the back by a solution of 1 M NaOH takes place under basic conditions. The direct exposure of the porous working electrode to the gas phase leads to an efficient transport of the analyte to the electrode. The arrangement was originally proposed for use in fuel cells but was soon adapted for sensing applications as well (Schiavon et al. 1989). Table 15.2 shows that at present SPE-electrodes are the most used configuration in liquid and polymer-based in electrochemical gas sensors. The topic has been reviewed by Bontempelli et al. (1997), Opekar (1989), and by Opekar and Stulik (1999). Opekar and Stulik (1999) have shown that the procedure of metal-membrane contacts' forming is one of the most important steps in fabrication of SPE gas diffusion electrodes. In particular they emphasize four of the methods used most often:

- *Mechanical procedures.* An electrode of a suitable shape and material, e.g., a fine mesh, can be pressed, under ambient or elevated temperature, onto the surface of a membrane, or a wire can be tightly wound around a solid or polymer electrolyte tube. Screen printing is also a mechanical procedure for depositing material from an ink onto a surface.
- *Physical vapor deposition (PVD) and chemical vapor deposition (CVD) plating.* These procedures permit formation of electrodes of various shapes on the surface of membranes and solid electrolytes,

but the electrodes often have poor mechanical stability and are destroyed by changes in the membrane dimensions due to test-medium humidity variations. However, vacuum evaporation (or sputtering) is one of the principal methods for preparation of planar sensors, with electrodes produced photolithographically on an inert support (glass, ceramic).

- *Chemical deposition.* A metal can be deposited from a solution, especially in cases where the electrode is produced on the surface of membranes and solid electrolytes, by chemical reduction of a suitable metal compound. This approach was patented for platinum and gold electrodes, but it can also be used for other metals (e.g., Ni, Cu, Ag).
- *Impregnation.* The polymer or solid electrolyte membrane is immersed in a solution of a suitable compound of the metal to be deposited and is saturated with the solution; the saturation can be accelerated for Nafion by adding methanol to the solution. The membrane is then immersed, one or both sides, in a solution of a strong reductant so the metal deposits where the reductant is placed. The procedure can be repeated to obtain a thicker metal film.

Of course, every method has both advantages and disadvantages, and some detailed information is available in reviews (Opekar 1989; Opekar and Stulik 1999).

As indicated earlier, electrochemical gas sensors based on metallized porous PTFE-membranes form the basis of a very successful range of products available from several manufacturers. However, it should be noted that cells based on gas diffusion electrodes (GDE) (e.g., for oxygen and ethanol) are sometimes not interrogated amperometrically (Stetter and Li 2008), i.e., by applying a fixed potential to the working electrode and measuring the resulting current, but applied as galvanic fuel cells. In this case, the cells are constructed with a counter electrode system which has an appropriate potential conducive to spontaneous current flow in the presence of the analyte. This can then be evaluated indirectly by measuring the voltage created on a load resistor.

In addition it is necessary to take into account that each electrochemical gas sensor can have a unique design and a different set of materials and geometries for membranes, electrolytes, and electrodes in order to take advantage of the chemical properties of a specific target analyte and to survive under various operating conditions. Many gases can be measured with an appropriately designed electrochemical gas sensor, such as H<sub>2</sub>, O<sub>2</sub>, CO, NO<sub>2</sub>, NO, O<sub>3</sub>, SO<sub>2</sub>, H<sub>2</sub>S, and organic vapors with electroactive functional groups such as alcohols or aldehydes. Therefore, the discovery of unique combinations of materials, geometries, and methods can give both improvement of electrochemical gas sensors' parameters and wider use of electrochemical gas sensors in various applications.

## References

- Bay HW, Blurton KF, Lieb HC, Oswin HG (1972) Electrochemical measurement of carbon monoxide. *Intern Lab* 1(5):37–41
- Bay HW, Blurton KF, Sedlak JM, Valentine AM (1974) Electrochemical technique for the measurement of carbon monoxide. *Anal Chem* 46(12):1837–1839
- Bergman I (1968) Metallized membrane electrode: atmospheric oxygen monitoring and other applications. *Nature* 218:266
- Blurton KF, Stetter JR (1978) A sensitive electrochemical detector for gas chromatography. *J Chromatogr* 155:35–45
- Bonanos N (2001) Oxide-based protonic conductors: point defects and transport properties. *Solid State Ion* 145:265–274
- Bontempelli G, Comisso N, Toniolo R, Schiavon G (1997) Electroanalytical sensors for nonconducting media based on electrodes supported on perfluorinated ion-exchange membranes. *Electroanalysis* 9:433–443
- Cao Z, Stetter JR (1991) Amperometric gas sensors. In: Madou M, Joseph JP (eds) *Opportunities for innovation: chemical and biological sensors*. NIST Publication GCR 91-593-1, U.S. Department of Commerce, Gaithersburg, MD
- Cao Z, Buttner WJ, Stetter JR (1992) The properties and applications of amperometric gas sensors. *Electroanalysis* 4:253–266
- Chang SC, Stetter JR, Cha CS (1993) Amperometric gas sensors. *Talanta* 40:461–477



- Chao Y, Buttner WJ, Yao S, Stetter JR (2005) Amperometric sensor for selective and stable hydrogen measurement. *Sens Actuators B* 106:784–790
- Chou J (1999) Hazardous gas monitors: a practical guide to selection, operation, and applications. McGraw-Hill Professional, New York, NY
- Clark LC, Wolf R, Granger D, Taylor Z (1953) Continuous recording of blood oxygen tensions by polarography. *J Appl Physiol* 6:189–193
- Dawson GA, Hauser PC, Kilmartin PA, Wright GA (2000) CO<sub>2</sub> gas sensing at microelectrodes in nonaqueous solvents. *Electroanalysis* 12:105–110
- Enea O (1987) On the electrocatalytic oxidation of methanol vapors at Au-Nafion electrodes. *J Electroanal Chem* 235:393–401
- Hitchman ML (1978) Measurements of dissolved oxygen. Wiley, New York, NY
- Ho KC, Hung WT (2001) An amperometric NO<sub>2</sub> gas sensor based on Pt/Nafion® electrode. *Sens Actuators B* 79:11–18
- Ho KC, Liao JY, Yang CC (2005) A kinetic study for electrooxidation of NO gas at a Pt/membrane electrode-application to amperometric NO sensor. *Sens Actuators B* 108:820–827
- Imaya H, Ishiji T, Takahashi K (2005) Detection properties of electrochemical acidic gas sensors using halide-halate electrolytic solutions. *Sens Actuators B* 108:803–807
- Ives DJG, Janz GJ (eds) (1961) Reference electrodes: theory and practice. Academic, New York, NY
- Jordan LR, Hauser PC, Dawson GA (1997) Humidity and temperature effects on the response to ethylene of an amperometric sensor utilizing a gold-Nafion electrode. *Electroanalysis* 9:1159–1162
- Katayama-Aramata A, Nakajima H, Fujikawa K, Kita H (1983) Metal electrodes bonded on solid polymer electrolyte membranes (SPE)—the behaviour of platinum bonded on SPE for hydrogen and oxygen electrode processes. *Electrochim Acta* 28:777–780
- Kita A, Fujikawa K, Nakajima H (1984) Metal electrodes bonded on solid polymer electrolyte membranes (SPE)-II. The polarization resistance of Pt-Nafion electrode. *Electrochim Acta* 29:1721–1724
- Kita H, Nakajima H (1986) Metal electrodes bonded on solid polymer electrolyte membranes (SPE)-III. CO oxidation at Au-SPE electrodes. *Electrochim Acta* 31:193–200
- Knake R, Jacquinet P, Hodgson AWE, Hauser PC (2005) Amperometric sensing in the gas-phase. *Anal Chim Acta* 549:1–9
- Kordesch K, Simader G (1996) Fuel cells and their applications. VCH, New York, NY
- Korotcenkov G, Han S-D, Stetter JR (2009) Review of electrochemical hydrogen sensors. *Chem Rev* 109(3):1402–1433
- Liu C-C (1996) Electrochemical sensors: microfabrication techniques. In: Taylor RF, Schultz JS (eds) Handbook of chemical and biological sensors. IOP, Bristol, Ch. 16
- La Conti S, Maget HJR (1971) Electrochemical detection of H<sub>2</sub>, CO, and hydrocarbons in inert or oxygen atmospheres. *J Electrochem Soc* 118:506–510
- Lu X, Wu S, Wang L, Su Z (2005) Solid-state amperometric hydrogen sensor based on polymer electrolyte membrane fuel cell. *Sens Actuators B* 107:812–817
- Mosley PT, Norris J, Williams DE (eds) (1991) Techniques and mechanisms in gas sensing. Adam Hilger, New York, NY
- Niedrach LW, Alford HR (1965) A new high-performance fuel cell employing conducting-porous-teflon electrodes and liquid electrolytes. *J Electrochem Soc* 112:117–124
- Opekar F (1989) Analytical applications of metallized membrane electrodes. *Electroanalysis* 1:287–295
- Opekar F, Stulik K (1999) Electrochemical sensors with solid polymer electrolytes. *Anal Chim Acta* 385:151–162
- Otagawa T, Zaromb S, Stetter JR (1985) Electrochemical oxidation of methane in nonaqueous electrolytes at room temperature. *J Electrochem Soc* 132:2951–2957
- Paganin VA, Ticianelli EA, Gonzalez ER (1996) Development and electrochemical studies of gas diffusion electrodes for polymer electrolyte fuel cells. *J Appl Electrochem* 26:297–304
- Ren X, Wilson MS, Gottesfeld S (1996) High performance direct methanol polymer electrolyte fuel cells. *J Electrochem Soc* 143:L12–L15
- Rosini S, Siebert E (2005) Electrochemical sensors for detection of hydrogen in air: model of the non-Nernstian potentiometric response of platinum gas diffusion electrodes. *Electrochim Acta* 50:2943–2953
- Schiavon G, Zotti G, Bontempelli G (1989) Electrodes supported on ion-exchange membranes as sensors in gases and low-conductivity solvents. *Anal Chim Acta* 221:27–41
- Stetter JR, Sedlak JM, Blurton KF (1977) Electrochemical gas chromatographic detection of hydrogen sulfide at ppm and ppb levels. *J Chromatogr Sci* 15:125–128
- Stetter JR, Li J (2008) Amperometric gas sensors: a review. *Chem Rev* 108:352–366
- Stetter JR, Korotcenkov G, Zeng X, Liu Y, Tang Y (2011) Electrochemical gas sensors: fundamentals, fabrication and parameters. In: Korotcenkov G (ed) Chemical sensors: comprehensive sensor technologies, vol 5, Electrochemical and optical sensors. Momentum Press, New York, NY, pp 1–89
- Sundmacher K, Rihko-Struckmann LK, Galvita V (2005) Solid electrolyte membrane reactors: status and trends. *Catal Today* 104:185–199
- Vielstich W, Lamm A, Gasteiger HA (eds) (2003) Handbook of fuel cell -fundamentals, technology and applications, vol 2. Wiley, Chichester, Part 3

## Chapter 16

# Materials for Capacitance-Based Gas Sensors

### 16.1 General Discussions

Capacitance-type sensors are a huge part of existing sensor types in both research and industry, as they offer significant advantages in terms of simplicity of fabrication, sensitivity, and low-power operation (Ishihara and Matsubara 1998; Kummer et al. 2004; Chatzandroulis et al. 2011). In such a structure, the capacitance between the two electrodes is given by

$$C = \epsilon_r \epsilon_0 \frac{A}{d}, \quad (16.1)$$

where  $\epsilon_r$  and  $\epsilon_0$  are the relative and vacuum permittivity constants, respectively,  $A$  is the plate surface area, and  $d$  is the plate distance. From this equation it is evident that only three ways exist to effect a change in the capacitance of that device: (1) alter the distance  $d$  between the two plates, (2) alter the overlapping area  $A$  between the two plates, and (3) change the dielectric permittivity between the plates. In capacitance-type gas sensing, two different approaches have been followed to date (Hagleitner et al. 2001; Chatzandroulis et al. 2011). In one approach, the variations in device capacitance result from a change in the dielectric permittivity of a gas-sensitive material (permittivity-type gas sensors). In a permittivity-based capacitance-type chemical sensor, a chemically sensitive material is placed either between a top and bottom electrode or on top of an interdigitated electrode (IDE) structure (Lin et al. 1991). The change in capacitance depends on the adsorption of the analyte on top of the sensitive layer and also on the absorption of the analyte within the sensitive layer. Both processes change the thickness (swelling) and permittivity of the sensitive layer.

Chatzandroulis et al. (2011) believe that interdigital electrode capacitance-type gas sensors are the most likely candidates for integrating a gas sensor on a thin-film flexible substrate. Use of a flexible substrate reduces fabrication costs even further and allows for integration with other sensors and electronic circuits. Moreover, it is compatible with a new generation of electronic devices made out of polymer materials (known as organic electronic devices), which represent the future in bringing fabrication costs down and thus opening the field to a variety of applications such as monitoring humidity and temperature monitoring of goods vulnerable to environmental conditions, for example, foods, medical supplies, aircraft, and automotive replacement parts. In addition, flexible substrates are ideal for deployment on curved surfaces or for integration on cloths for application in wearable sensors. It should be noted that for IDE capacitance-type gas sensors, the thickness of the sensing layers is very important (Hagleitner et al. 2001; Kummer et al. 2004) (see Fig. 16.1). For example, for a layer thickness of less than half the periodicity, swelling of the polymer on analyte absorption always results in a capacitance increase, regardless of the dielectric constant of the absorbed analyte. This is due to the increased poly-

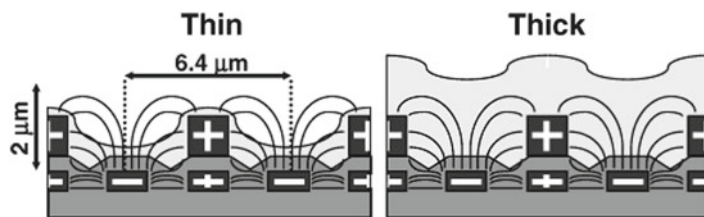


**Fig. 16.1** Configuration of electric field lines in capacitance sensors with different thickness of sensitive (polymer) films (Reprinted with permission from Kummer et al. (2004). Copyright 2004 American Chemical Society)

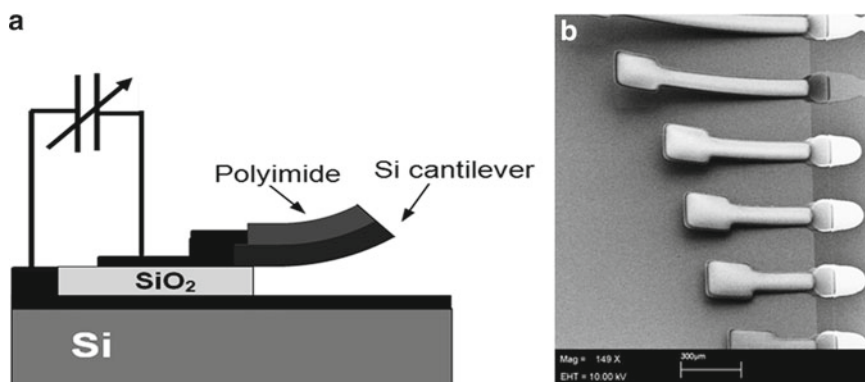


**Fig. 16.2** (a) Schematic diagram and (b) top-surface view of cantilevers covered with polyimide and with a square-shaped end for increased capacitance (Reprinted with permission from Chatzandroulis et al. (2002). Copyright 2002 Elsevier)

mer/analyte volume within the field line region exhibiting a larger dielectric constant than that of the air it displaces. On the other hand, the capacitance change for a polymer layer thickness larger than half the periodicity of the electrodes is determined by the ratio of the dielectric constants of analyte and polymer. If the dielectric constant of the polymer is lower than that of the analyte, the capacitance will be increased, and if the polymer dielectric constant is larger, the capacitance will be decreased.

In the other approach, researchers have developed capacitance-type gas sensors and sensor arrays of silicon/polymer bimorphs operating in either resonance or static bending (Britton et al. 2000; Chatzandroulis et al. 2002; Lavrik et al. 2004; Lang et al. 2005; Goeders et al. 2008; Nordström et al. 2008). The operation principle of bimorph gas sensors relies on the detection of changes in the mechanical properties of a structure which typically consists of a cantilever or a membrane covered by a chemically selective layer. The analyte absorption/adsorption on the selective layer material (usually a polymer) induces mass and surface stress changes due to overlying polymer swelling that result in a change in the device resonance frequency and/or bending, which are then detected as a change in capacitance. In capacitive readout, the capacitance is measured between a flexible and a fixed electrode which are separated by a small gap. The flexible electrode is a conductor on the cantilever or membrane, and the fixed electrode is a conductor on the substrate (Chatzandroulis et al. 2011). One of the examples of cantilever-based sensors is shown in Fig. 16.2. A capacitive-type humidity sensor consisting of a hydrophilic (polyimide) layer that covers the top surface of a silicon cantilever was developed by Chatzandroulis et al. (2002). The Si cantilevers had square-shaped ends for increased capacitance and various lengths (500–2,500  $\mu\text{m}$ ). We note that, in general, a bimorph cantilever is more sensitive than a similar bimorph membrane because the latter is clamped peripherally instead of having one clamped edge as in the case of a cantilever.

MIS, Schottky diode, and p–n-junction-based gas sensors can also be of capacitance type. The construction and principles of operation of such sensors can be found in the Introduction and review papers (Lundstrom 1981).

## 16.2 Polymer-Based Capacitance Gas Sensors

It should be noted that the most widely used materials in capacitance-type gas sensors are polymers (Chatzandroulis et al. 2011). They are particularly suitable for sensing organic vapors and other types of analytes (see Table 16.1) because they exhibit rapid reversible vapor sorption and are easy to apply

**Table 16.1** Capacitance-type gas and humidity polymer-based sensors

Sensor type	Sensitive material	Target species	Reference	
<i>Permittivity-based sensors</i>				
IDE	Polyimide; BCB	Humidity	Laville and Pellet (2002)	
	Polyimide	Humidity	Chandran et al. (1991), Boltshauser and Baltes (1991), Boltshauser et al. (1991), Shibata et al. (1996), Park et al. (2001), Dai (2007), Lee et al. (2008)	
	Poly CA, poly CAB, MMA, PVP, and mixtures thereof	Humidity	Oprea et al. (2008)	
	BBCB	Humidity	Pecora et al. (2008)	
	Polar PEUT; PDMS	<i>n</i> -Octane, <i>n</i> -hexane, humidity, and mixtures thereof	Kummer et al. (2006)	
	PHEMA; PMMA; PHEMA; EPR	Ethanol, methanol, toluene, humidity	Kitsara et al. (2006)	
	PDMS	<i>n</i> -Hexane, toluene, <i>n</i> -octane, 1-propanol, and ethyl acetate	Igreja and Dias (2006)	
	Parallel plate	APTMOS, PTMOS	CO <sub>2</sub>	Menil et al. (1995)
		Polyimide	Humidity	Kang and Wise (2000)
		SXFA	Acetone, ethyl alcohol, ethyl acetate	
OV225		Toluene	Patel et al. (2003)	
PECH; PEVA; SXFA; OV275		CEE		
SXFA		DIMP, DMMP		
SXFA		Ethanol	McCorkle et al. (2005)	
PAPPS; SXFA; OV225; PEO; AuHFA; PECH; ADIOL; HC; PEI		Warfare agents, toxic industrial chemicals	Mlsna et al. (2006)	
Heteropolysiloxane	CO <sub>2</sub>	Endres et al. (1999)		
<i>Bimorph-based sensors</i>				
Cantilevers	Polyimide	Humidity	Chatzandroulis et al. (2002)	
	PDMS	Toluene	Amírola et al. (2005), Rodríguez et al. (2004)	
	PECH	Octane	Amírola et al. (2005)	
	Gold	Mercury	Britton et al. (2000)	
	Palladium	Hydrogen		
Membranes	PVAc; PHEMA; PDMS; PMMA; EPN	Humidity	Chatzandroulis et al. (2004)	
	Alkanethiol coatings with hydroxyl, carboxyl, and methyl end groups	IPA, toluene	Satyanarayana et al. (2006)	
	Alkanethiol coatings with COOH and NH <sub>3</sub> end groups	IPA, humidity	Lim et al. (2007)	

(continued)

**Table 16.1** (continued)

Sensor type	Sensitive material	Target species	Reference
	PAAM	Humidity, IPA	Park et al. (2007)
	PEG	Acetone	
	PVA	Methanol	
	PIB	DMMP, humidity, ethanol	Park et al. (2008)
	Single-walled carbon nanotubes	CO <sub>2</sub>	Sivaramakrishnan et al. (2008)

*APTOS* 3-amino-propyl-trimethoxysilane, *AuHFA* fluoroalcohol-coated gold nanospheres, *BBCB* bisbenzocyclobutene, *BCB* benzocyclobutene, *CA* cellulose acetate, *CAB* cellulose acetate-butyrate, *CEE* chloroethyl ether, *DIMP* diisopropyl methylphosphonate, *DMMP* dimethyl methylphosphonate, *EPR* epoxidized novolac, *IPA* isopropanol, *OV-225* cyanopropyl methyl phenylmethyl silicone, *OV-275* dicyanoallyl silicone, *PAAM* polyallylamine hydrochloride, *PAPPS* propylaminopropyl polysiloxane, *PDMS* poly(dimethylsiloxane), *PECH* polyepichlorohydrin, *PEG* polyethylene glycol, *PEI* polyethyleneimine, *PEO* polyethylene oxide, *PEVA* polyethylene-co-vinyl acetate, *PEUT* poly(ether urethane), *PHEMA* poly(2-hydroxyethyl methacrylate), *PIB* polyisobutylene, *PMMA* poly(methyl methacrylate), *PTMOS* propyltrimethoxysilane, *PVA* polyvinyl alcohol, *PVP* polyvinylpyrrolidone, *SXFA* siloxane fluoroalcohol

Source: Data extracted from Chatzandroulis et al. (2011)

as thin or thick films by a variety of techniques. Moreover, the polymer layer can be chosen according to its affinity to the particular set of molecules one wishes to detect. However, Chatzandroulis et al. (2011) reported that the selection of the most suitable polymer for a capacitance-type sensor application is rather difficult because, in many cases, the analyte molecules should be detected at trace-level concentrations. This is a very challenging task, especially for gas detection, taking into account that in real environments the analyte of interest is not the only substance dissolved in an inert gas (e.g., nitrogen or synthetic air). Several other substances and at much higher concentrations, e.g., humidity, that may interfere with the targeted analyte are usually present (James et al. 2005). Therefore it is necessary to develop techniques that enable the detection of low analyte concentrations, even in the presence of humidity, that is, to find ways to recover expectedly small analyte signals on the background of large water signals (Kummer et al. 2004).

The first capacitance-type polymer sensing devices based on polyimide films were designed in the early 1980s as humidity sensors (Sheppard et al. 1982; Delapierre et al. 1983). It is necessary to note that the humidity sensor is the best known capacitive-type sensor. Since water has an abnormally large dielectric constant ( $\epsilon_r \sim 80$ ), changes in relative permittivity by the adsorption of water provide a simple detection mechanism. For comparison, the relative permittivity of polymers such as polyimides is known to range from 3 to 6. In relation to other types of humidity sensors, the capacitive type has the advantage of high sensitivity over a wide humidity range (Ishihara and Matsubara 1998). As a rule, humidity sensors operate in the range from 10 to 90–95 % RH. Furthermore, the response and recovery times are less than 10–30 s. Capacitive humidity sensors are commercially available from, for example, Sensirion (<http://www.sensirion.com/>), Vaisala (<http://www.vaisala.com/>), and Humirel (<http://www.humirel.com/>). A detailed description of the material acceptable for humidity sensor design can be found in Chap. 18 (Vol. 1). Later on, capacitance-type gas sensors using various polymer layers as sensitive material were developed for the detection of volatile organic compounds (Endres and Drost 1991; Cornila et al. 1995; Meanna Perez and Freyre 1997; Josse et al. 1996; Casalini et al. 1999; Domansky et al. 2001). Figure 16.3 illustrates operating characteristics of capacitance-type sensors realized as monolithic CMOS microsystems (Li et al. 2007). The capacitive sensor was based on two sets of interdigitated electrode structures, which correspond to the two plates of a standard capacitor. The dimensions of the capacitor are 814  $\mu\text{m} \times 824 \mu\text{m}$ , and it includes 128 finger pairs. The electrode width and spacing are 1.6  $\mu\text{m}$ . The nominal capacitance of the interdigitated capacitor was a few picofarads, whereas capacitance changes upon analyte absorption were in the range of a few attofarads. It is seen that the frequency changes of the thick-layer capacitive sensor upon exposure to ethanol and toluene have different directions, which correspond to the dielectric

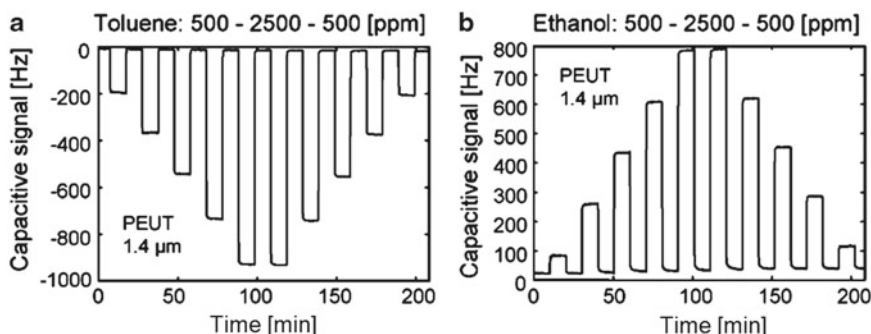


**Fig. 16.3** Sensor responses of the capacitive sensors upon exposure to various concentrations of (a) toluene and (b) ethanol. The analyte concentrations included 500–2,500 ppm, up and down. The capacitive sensor has been coated with 1.4- $\mu\text{m}$ -thick polar poly(ether urethane) (PEUT) layer (Reprinted with permission from Li et al. (2007). Copyright 2007 Elsevier)

constants of the analytes. Ethanol with a dielectric constant of 24.3, which is larger than that of the polymer PEUT (4.8), leads to a capacitance increase and, hence, a positive frequency shift, whereas toluene with a dielectric constant of 2.36 leads to a capacitance decrease and a negative frequency shift. The detection of CO and CO<sub>2</sub> gases was also demonstrated (Endres et al. 1999; Sivaramakrishnan et al. 2008). Polymeric materials used for capacitance sensor design are listed in Table 16.1. The thickness of the polymeric films can be varied from 100 nm to hundreds of micrometers.

Experiments have shown that capacitance-based gas sensors can detect vapors and gases with concentration in the ppm range. For example, Kitsara et al. (2006) reported on detection limits for PDMS-covered cantilevers below 50 ppm for toluene and 10 ppm for octane. Rodríguez et al. (2004), using frequency multiplication and PDMS as the active layer, established that the sensors had sensitivity to concentrations of toluene as low as 25 ppm. For gases the sensitivity is lower. Sivaramakrishnan et al. (2008) found that capacitance-based sensors with membranes coated by a single-walled nanotube (SWNT) film can detect CO<sub>2</sub> with concentrations from 3.2 to 10.4 %.

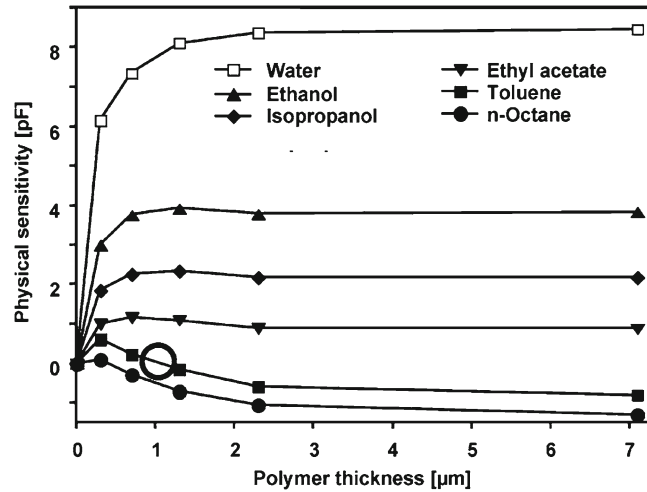
Regarding the role of polymer type in sensor response, one can say that results depend on many factors and vary over a wide range. For example, according to Chatzandroulis et al. (2004), among poly(hydroxyethyl methacrylate) (PHEMA), poly(methyl methacrylate) (PMMA), poly(vinyl acetate) (PVAc), epoxidized novolac (EPN), and polydimethylsiloxane (PDMS) layers, PHEMA-, PVAc-, and PMMA-coated membranes exhibited a strong response upon exposure to methanol and ethanol vapors. In all cases the response to methanol was higher than for ethanol. This was attributed to the longer chain length of the ethanol molecules. The smaller size of the methanol molecule greatly facilitates its diffusion into the polymer layer compared to ethanol or other larger molecules.

High sensitivity to water, due to its abnormally large dielectric constant, is the main problem for capacitance-type devices. This effect is shown in Fig. 16.4 for PEUT-based CMOS sensors (Kummer et al. 2004). Therefore, the compensation of humidity influence or humidity control is required for correct operation of capacitance-type sensors in a real environment.

## 16.3 Other Materials

In addition to polymers that are used extensively for capacitive gas sensors, several other materials have been suggested and applied so far, for either polar or nonpolar analytes. In certain cases these sensors have proved to be very good candidates for the sensing of substances, such as NO<sub>2</sub>, for which polymers are not suitable. The most interesting results were obtained using porous materials such as

**Fig. 16.4** Measured dependence of the physical sensitivity,  $\Delta C/\varphi_A$ , on the layer thickness,  $h$ , for analytes with various dielectric constants. Low  $\epsilon_A$ : *n*-octane (1.93) and toluene (2.36). High to very high  $\epsilon_A$ : ethyl acetate (5.88), 2-propanol (18.5), ethanol (24.3), and water (76.6) (Reprinted with permission from Kummer et al. (2004). Copyright 2004 American Chemical Society)



silicon carbide, porous alumina, porous silicon, and a porous sensing matrix on the base of Ni/Si nanowire composites and carbon nanotubes (Chatzandroulis et al. 2011).

In particular, Connolly et al. (2005) designed  $\text{NH}_3$  capacitive sensor with 500-nm-thick porous SiC film. The response in humidity was very low for  $\text{RH} < 50\%$ , which was attributed to the porous dimensions. The exact sensing mechanism is still not clear, but  $\text{NH}_3$  levels as low as  $\sim 0.5$  ppm were detected. Porous alumina ( $\text{Al}_2\text{O}_3$ ) has also been examined as a sensing material for capacitive gas sensors and in particular for humidity measurements (Nahar and Khanna 1982; Timar-Horvath et al. 2008). The  $\text{Al}_2\text{O}_3$ -based humidity sensor was a volume-effect device based on physical adsorption. At low humidity, the walls of the pores are lined with one-molecular-thickness liquid layer. As the humidity increases, after saturating the walls, due to a capillary condensation effect, the water starts condensing in the pores (Boucher 1976; Neimark and Ravikovitch 2001). It was established that the water molecules, even at a partial pressure higher than the saturated vapor pressure  $P_0$ , tend to condense in capillary pores with a radius below the Kelvin radius  $r$ , which is defined as function (1) (Boucher 1976):

$$r = \frac{-2\gamma V_L \cos\theta}{RT \ln(p/p_0)}, \quad (16.2)$$

where  $\theta$  is the contact angle of liquor and wall of capillary pore,  $V_L$  is the molecular volume of liquor,  $\gamma$  is the surface tension of liquor,  $R$  is the gas constant ( $R = 8.314 \text{ J} \times (\text{mol} \times \text{K})^{-1}$ ),  $T$  is the absolute temperature (K), and  $r$  is the Kelvin radius of the capillary pores.

Porous silicon is another sensitive material of interest (Rittersma et al. 2000; Fürjes et al. 2003; Erdamar et al. 2007; Korotcenkov and Cho 2010). For example, Kim et al. (2000) fabricated capacitive alcohol gas sensors using a porous silicon (PSi) layer for the measurement of breath alcohol concentration. Kim et al. (2000) have shown that, since the PSi layer shows high adsorption against ethanol along with a large internal surface area, detecting low alcohol gas concentrations (0–0.5 %) without any heating may be realized in comparison with conventional metal oxide sensors. Erdamar et al. (2007) examined two porous Si nanostructure types as capacitive sensors for water and acetone vapors. In the case of humidity, it was found that, for an increase from 25 to 75 % RH, the capacitance doubles and that it depends on the measuring frequency. However, it is necessary to take into account that the control of the microstructure of the porous film is of great importance in ensuring good sensing characteristics and acceptable reproducibility. Furthermore, it was found necessary to leave the upper electrode thin and porous for rapid response (Ishihara and Matsubara 1998). Other advantages and disadvantages of porous materials for gas sensor design can be found in Chap. 5 (Vol. 1).

Molecular sieves can also be applied for design capacitance gas sensors. It was demonstrated that bipolar interactions between adsorbates and molecular sieves are of potential use in capacitive-type gas sensors.

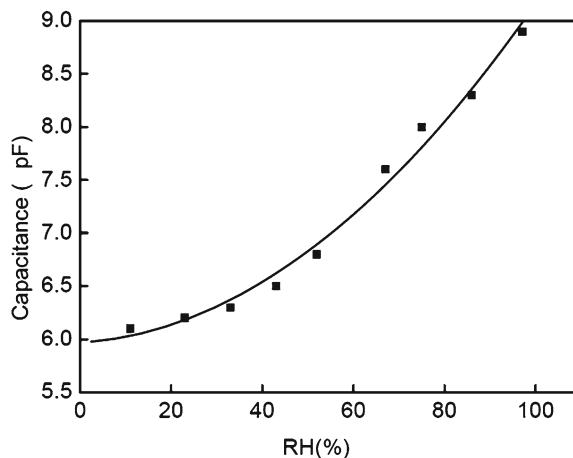


**Fig. 16.5** Capacitance response of MWCNTs-based sensors to RH. The area and the thickness of the MWCNTs-SiO<sub>2</sub> film were 1×0.8 cm and about 175 μm, respectively. The role of SiO<sub>2</sub> powder was to increase the adhesive properties of the film. The CNTs were first purified by heating at 400 °C. They were then functionalized by a H<sub>2</sub>SO<sub>4</sub> and HNH<sub>3</sub> mixture (v/v=3:1) at 100 °C for 2 h to functionalize the CNTs with -OH and -COOH groups, which can make the CNTs hydrophilic and thus increase the sensor sensitivity (Reprinted from Chen et al. (2009a). Published by MDPI)

In particular, Alberti et al. (1991) proposed zeolite-based sensors for detection of hydrocarbons such as butane and Balkus et al. (1997) used thin film aluminophosphate (AIPO)-5 molecular sieve as the dielectric phase in a capacitance-type chemical sensor for CO and CO<sub>2</sub>. AIPO-n is a family of phosphorus molecular sieves which, similar to zeolites, have ordered molecular-sized pores. The AIPO-5 structure used for the dielectric layer consists of four- and six-membered rings of alternating phosphate and aluminum ions bridged by oxygen. These rings are arranged to produce one-dimensional channels 0.73 nm in diameter. The properties of AIPO-n are reviewed in detail by Ishihara and Takita (1996), and one of the attractive properties of these materials is their heat stability. The properties of zeolites as they relate to zeolite-based gas sensors are discussed in a special section in Vol. 2.

Carbon nanotubes (CNTs) have been explored as potential candidates for capacitance-type gas sensors by Snow et al. (2005), Brahim et al. (2008), and others. In particular, Snow et al. (2005) have shown that the capacitance of SWCNTs was proved to be highly sensitive to a broad group of polar and nonpolar vapors (e.g., chlorobenzene, water, acetone). In the presence of a dilute chemical vapor, molecular adsorbates are polarized by the fringing electric fields radiating from the surface of an SWCNT electrode, which causes an increase in its capacitance. Such SWCNT chemicapacitors were proved fast, highly sensitive, and completely reversible. Brahim et al. (2008) explored the CNTs modified by transition metals (e.g., Ti, Fe, Ni, Co) for NO<sub>2</sub> monitoring, for which polymers are not suitable. By varying the nature of the transition metal infiltrated into the CNT, significantly different responses among the hybrid sensors upon exposure to parts per million levels of NO<sub>2</sub> were recorded. Some hybrid materials demonstrated superior sensitivity and an approximately twofold increase in the detection of NO<sub>2</sub> at room temperature compared to the pristine single-walled carbon nanotube (SWCNT) sensor. Chen et al. (2009b) have shown that the sandwich-structured capacitive sensor with vertically aligned CNT arrays had an acceptable response to ammonia and formic acid as well. The sensor response was reproducible and stable. Chen et al. (2009b) have found that, compared to CNT film sensors, the as-fabricated CNT arrays capacitive sensor had a faster rate of gas diffusion and desorption. The 90 % response time was about 100 s for 15 ppm NH<sub>3</sub> and 20 s for 175 ppm HCOOH. The 90 % recovery time was about 150 s for 15 ppm NH<sub>3</sub> and only 70 s for 175 ppm HCOOH. Since MWCNTs have porous structures and capillary condensation occurs in the MWCNT films, humidity sensors can be designed as well (Chen et al. 2009a) (see Fig. 16.5). It was found that the 90 % response and recovery times of sensors operated at room temperatures were 45 s and 15 s, respectively.



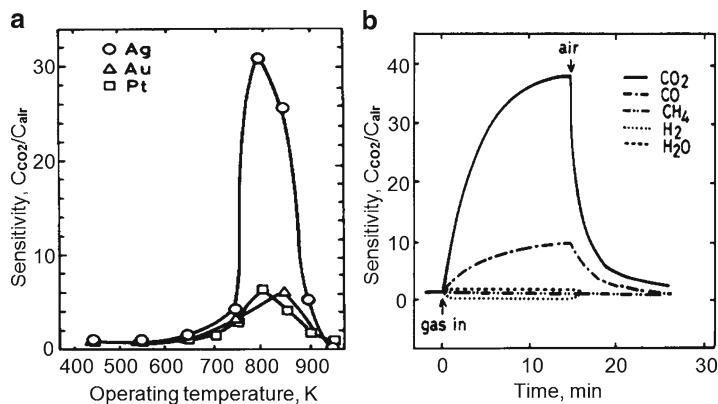


**Fig. 16.6** (a) Effects of electrode on the sensitivity to 2 % CO<sub>2</sub> of Ag added CuO–BaTiO<sub>3</sub>. (b) Typical sensor responses of Ag-added CuO–BaTiO<sub>3</sub> to 2 % CO<sub>2</sub>, CO, CH<sub>4</sub>, H<sub>2</sub>, and 2.8 % H<sub>2</sub>O. (Amount of Ag was 1 mol %, and operating and precalcination temperatures were 692 and 973 K, respectively) (Reprinted with permission from Ishihara et al. (1995b). Copyright 1995 Elsevier)

The application of conventional semiconductors in capacitance sensors is limited as a rule by MIS and Schottky diode-based devices, which are applied mainly for hydrogen detection up to the ppb range (Lundstrom 1981). Most of these sensors use Pd or Pt as metal electrode, SiO<sub>2</sub> as dielectric layer, and Si, GaN, or SiC as semiconductor (Lloyd Spetz and Savage 2003). As indicated in the Introduction, the mechanism of sensitivity of such devices is based on hydrogen dissociative adsorption on catalytically active metal, diffusion through thin metal film, and adsorption of hydrogen atoms at the metal–insulator interface with the forming dipole layer. Research has shown that these structures can also be used for detection of ammonia and hydrogen sulfide with threshold sensitivity in the ppm range (Lundstrom 1981). However, in this case the mechanism of response is different. Triple phase boundaries have proved to be significant for generation of specific gas response, e.g., for NH<sub>3</sub> or H<sub>2</sub>S (Lofdahl et al. 2001). The use of particles as the electrode material increases the occurrence of triple phase boundaries where the catalytic metal, the insulator, and the test gas molecules are in contact. In particular, Salomonsson et al. (2005) proposed such an approach to design MISiC sensors with Ru and RuO<sub>2</sub> electrode materials.

Research has shown that metal oxides can be used for the design of capacitance-based gas sensors as well. In particular, capacitive-type sensors for hydrogen (Schoeneberg et al. 1990), ammonia (Winqvist et al. 1985), O<sub>2</sub>, CO (Kang and Kim 1993), and humidity (Silverthorne et al. 1989) were designed using semiconductor metal oxides such as ZnO and SnO<sub>2</sub>. These MOX capacitive-type sensors are based on changes in the depletion layer caused by changes in work function of the metal on exposure to the gas.

Metal oxide solid electrolytes can also be incorporated in capacitance-type gas sensors (Ishihara and Matsubara 1998; Zamani et al. 2005). Usually such sensors are used for CO<sub>2</sub> detection and are based on depletion layer control at p–n junctions formed in oxide semiconductor powders. For these purposes a mechanical mixture of n-type BaTiO<sub>3</sub> and p-type metal oxides such as PbO, NiO, CuO, and Co<sub>3</sub>O<sub>4</sub> can be used (Ishihara et al. 1990, 1991a, b, 1992a, b). These mixed metal oxides exhibit high sensitivity with optimum operating temperatures below 800 K. The decrease in the height of the potential barrier at intergrain interface due to interaction with CO<sub>2</sub> leads to a narrowing depletion layer, leading to an increase in capacitance. Since the reactivity of carbon dioxide is weak, output signals from CO<sub>2</sub> sensors are generally small, making selectivity an important target in the development of CO<sub>2</sub> sensors. In this context the addition of noble metals to semiconductor type gas sensors is sometimes effective in enhancing the sensing characteristics. For example, the addition of Ag in CuO–BaTiO<sub>3</sub> decreases the lower limit of CO<sub>2</sub> detection up to 50 ppm (Ishihara et al. 1992b). Furthermore, the effects of Ag additions were observed only on CO<sub>2</sub> sensitivity, making CuO–BaTiO<sub>3</sub>:Ag more selective for CO<sub>2</sub>. Operating characteristics of CuO–BaTiO<sub>3</sub>:Ag-based capacitance CO<sub>2</sub> sensors are shown in Fig. 16.6.

**Table 16.2** NO<sub>x</sub>-sensing characteristics of capacitance sensors based on binary mixed oxides

	$T_{oper}^a$ (°C)	Air level (nF)	Sensitivity <sup>b</sup> $C_{air}/C_{NO}$	90 % Response (s)	90 % Recovery (min)
WO <sub>3</sub> -ZnO	470	0.289	2.26	8	45
WO <sub>3</sub> -CuO	381	1.738	2.08	15	35
WO <sub>3</sub> -NiO	365	0.145	1.74	10	15
WO <sub>3</sub> -SnO <sub>2</sub>	176	0.144	7.74	210	55
WO <sub>3</sub> -MgO	319	0.030	1.22	210	35
WO <sub>3</sub> -Fe <sub>2</sub> O <sub>3</sub>	384	1.204	2.25	15	<sup>c</sup>
NiO-V <sub>2</sub> O <sub>3</sub>	170	158	1.74	180	<sup>c</sup>
NiO-BaTiO <sub>3</sub>	509	0.077	0.68	360	25
NiO-SrTiO <sub>3</sub>	—	—	1.00	—	—
NiO-ZnO	262	0.679	20.4	30	<sup>c</sup>
NiO-SnO <sub>2</sub>	218	0.471	7.68	61	<sup>c</sup>
NiO-In <sub>2</sub> O <sub>3</sub>	261	250	0.32	85	11
NiO-BaSnO <sub>3</sub>	—	—	1.00	—	—
ZnO-SnO <sub>2</sub>	265	0.091	4.15	22	<sup>c</sup>
ZnO-In <sub>2</sub> O <sub>3</sub>	373	844	0.33	24	15
CoO-In <sub>2</sub> O <sub>3</sub>	129	0.040	0.06	193	<sup>c</sup>

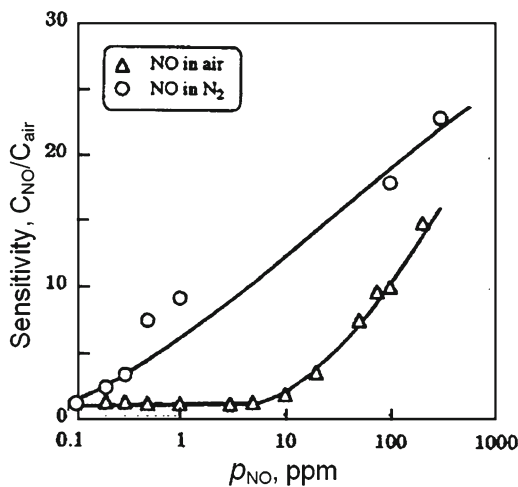
<sup>a</sup>Temperature at the maximum sensitivity

<sup>b</sup>Sensitivity to 100 ppm NO

<sup>c</sup>Capacity did not restore to the air level within 60 min

Source: Data extracted from Ishihara and Matsubara (1998)

**Fig. 16.7** Sensitivity to NO on CoO-In<sub>2</sub>O<sub>3</sub> against NO concentration in N<sub>2</sub> and in air (Reprinted with permission from Ishihara and Matsubara (1998). Copyright 1998 Springer)



Capacitive-type NO<sub>x</sub> sensors based on the same principle (p-n junction) were also investigated (Ishihara et al. 1995a, b, 1996). Table 16.2 summarizes the sensitivity to 100 ppm NO over various mixed oxides. The capacitance of the mixed oxide generally decreased upon exposure to NO. Among the mixed oxides examined, it was found that a large capacitance increase was observed on CoO-In<sub>2</sub>O<sub>3</sub> upon exposure to 100 ppm NO as shown in Table 16.2. It was reported that this CoO-In<sub>2</sub>O<sub>3</sub> mixed oxide has high sensitivity to NO, rather low sensitivity to CO, CO<sub>2</sub>, SO<sub>2</sub>, and H<sub>2</sub>O, and clearly no sensitivity to NO<sub>2</sub> (Ishihara et al. 1996). The sensitivity to NO in N<sub>2</sub> and air is shown in Fig. 16.7. The capacitance of CoO-In<sub>2</sub>O<sub>3</sub> becomes more sensitive to NO at low-oxygen partial pressure.

## References

- Alberti K, Haas J, Plog C, Fetting F (1991) Zeolite coated interdigital capacitors as a new type of gas sensor. *Catal Today* 8:509–513
- Amírola J, Rodríguez A, Castañer L, Santos JP, Gutiérrez J, Horrillo MC (2005) Micromachined silicon microcantilevers for gas sensing applications with capacitive read-out. *Sens Actuators B* 111–112:247–253
- Balkus KJ, Ball LJ, Gnade BE, Anthony JM (1997) A capacitance type chemical sensor based on  $\text{AlPO}_4$ -5 molecular sieves. *Chem Mater* 9:380–386
- Boltshauser T, Baltes H (1991) Capacitive humidity sensors in SACMOS technology with moisture absorbing photo-sensitive polyimide. *Sens Actuators A* 26:509–512
- Boltshauser T, Chandran L, Baltes H, Bose F, Steiner D (1991) Humidity sensing properties and electrical permittivity of new photosensitive polyimides. *Sens Actuators B* 5:161–164
- Boucher EA (1976) Review porous materials: structure, properties and capillary phenomena. *J Mater Sci* 11:1734–1750
- Brahim S, Colbern S, Gump R, Grigorian L (2008) Tailoring gas sensing properties of carbon nanotubes. *J Appl Phys* 104:024502
- Britton CL Jr, Jones RL, Oden PI, Hu Z, Warmack RJ, Smith SF, Bryan WL, Rochelle JM (2000) Multiple-input microcantilever sensors. *Ultramicroscopy* 82:17–21
- Casalini R, Kilitziraki M, Wood D, Petty MC (1999) Sensitivity of the electrical admittance of a polysiloxane film to organic vapors. *Sens Actuators B* 56:37–44
- Chandran L, Baltes H, Korvink J (1991) Three-dimensional modeling of capacitive humidity sensors. *Sens Actuators A* 25:243–247
- Chatzandroulis S, Tserepi A, Goustouridis D, Normand P, Tsoukalas D (2002) Fabrication of single crystal Si cantilevers using a dry release process and application in a capacitive-type humidity sensor. *Microelectron Eng* 61–62:955–961
- Chatzandroulis S, Tegou E, Goustouridis D, Polymenakos S, Tsoukalas D (2004) Capacitive-type chemical sensors using thin silicon-polymer bimorph membranes. *Sens Actuators B* 103:392–396
- Chatzandroulis S, Tsouti V, Raptis I, Goustouridis D (2011) Capacitance-type chemical sensors. In: Korotcenkov G (ed) *Chemical sensors: comprehensive sensor technologies*, vol 4, Solid state sensors. Momentum Press, New York, pp 229–260
- Chen W-P, Zhao Z-G, Liu X-W, Zhang Z-X, Suo C-G (2009a) A capacitive humidity sensor based on multi-wall carbon nanotubes (MWCNTs). *Sensors* 9:7431–7444
- Chen Y, Meng F, Li M, Liu J (2009b) Novel capacitive sensor: fabrication from carbon nanotube arrays and sensing property characterization. *Sens Actuators B* 140:396–401
- Connolly EJ, Timmer B, Pham HTM, Groeneweg J, Sarro PM, Olthuis W, French PJ (2005) A porous SiC ammonia sensor. *Sens Actuators B* 109:44–46
- Cornila C, Hierlemann A, Lenggenhager R, Malcovati P, Baltes, Hierlemann H, Noetzel G, Weimar U, Göpel W (1995) Capacitive sensors in CMOS technology with polymer coating. *Sens Actuators B* 25–27:357–361
- Dai C-L (2007) A capacitive humidity sensor integrated with micro heater and ring oscillator circuit fabricated by CMOS-MEMS technique. *Sens Actuators B* 122:375–380
- Delapierre G, Grange H, Chambaz B, Destannes L (1983) Polymer based capacitive humidity sensor—characteristics and experimental results. *Sens Actuators A* 4:97–104
- Domansky K, Liu J, Wang LQ, Engelhard MH, Baskaran S (2001) Chemical sensors based on dielectric response of functionalized mesoporous silica films. *J Mater Res* 16:2810–2816
- Endres HE, Drost S (1991) Optimization of the geometry of gas sensitive interdigital capacitors. *Sens Actuators B* 4:95–98
- Endres HE, Hartinger R, Schwaiger M, Gmelch G, Roth M (1999) A capacitive CO sensor system with suppression of the humidity interference. *Sens Actuators B* 57(1–3):83–87
- Erdamar O, Bilen B, Skarlatos Y, Aktas G, Inci MN (2007) Effects of humidity and acetone on the optical and electrical properties of porous silicon nanostructures. *Physica Status Solidi C* 4:601–603
- Fürjes P, Kovács A, Dücsó Cs, Ádám M, Müller B, Mescheder U (2003) Porous silicon-based humidity sensor with interdigital electrodes and internal heaters. *Sens Actuators B* 95:140–144
- Goeders KM, Colton JS, Bottomley LA (2008) Microcantilevers: sensing chemical interactions via mechanical motion. *Chem Rev* 108:522–542
- Hagleitner C, Hierlemann A, Lange D, Kummer A, Kerness N, Brand O, Baltes H (2001) Smart single-chip gas sensor microsystem. *Nature* 414:293–296
- Igreja R, Dias CJ (2006) Dielectric response of interdigital chemocapacitors: the role of the sensitive layer thickness. *Sens Actuators B* 115:69–78
- Ishihara T, Matsubara S (1998) Capacitive type gas sensors. *J Electroceram* 2(4):215–228
- Ishihara T, Takita Y (1996) Property and catalysis of aluminophosphate-based molecular sieves. In: Spivey JJ (ed) *Catalysis*, vol 12. Royal Society of Chemistry, Great Britain, pp 21–51

- Ishihara T, Kometani K, Hashida M, Takita Y (1990) Mixed oxide capacitor of BaTiO<sub>3</sub>-PbO as a new type CO<sub>2</sub> gas sensor. *Chem Lett* 1990:2033–2036
- Ishihara T, Kometani K, Hashida M, Takita Y (1991a) Application of mixed oxide capacitor to the selective carbon dioxide sensor. *J Electrochem Soc* 138:173–176
- Ishihara T, Kometani K, Mizuhara Y, Takita Y (1991b) Mixed oxide capacitor of CuO–BaSnO<sub>3</sub> as a sensor for CO<sub>2</sub> detection over a wide range of concentration. *Chem Lett* 1991:1711
- Ishihara T, Kometani K, Mizuhara Y, Takita Y (1992a) Application of a mixed oxide capacitor to the selective carbon dioxide sensor. *J Electrochem Soc* 139:2881–2885
- Ishihara T, Kometani K, Mizuhara Y, Takita Y (1992b) Mixed oxide capacitor of CuO–BaTiO<sub>3</sub> as a new type CO<sub>2</sub> gas sensor. *J Am Ceram Soc* 75:613–618
- Ishihara T, Sato S, Takita Y (1995a) Capacitive-type sensors for the selective detection of nitrogen oxides. *Sens Actuators B* 24–25:392–395
- Ishihara T, Kometani K, Nishi Y, Takita Y (1995b) Improved sensitivity of CuO–BaTiO<sub>3</sub> capacitive-type CO<sub>2</sub> sensor by additives. *Sens Actuators B* 28:49–54
- Ishihara T, Sato S, Fukushima T, Takita Y (1996) Capacitive gas sensor of mixed oxide CoO–In<sub>2</sub>O<sub>3</sub> to selectively detect nitrogen monoxide. *J Electrochem Soc* 143:1908–1914
- James D, Scott SM, Ali Z, O'Hare WT (2005) Chemical sensors for electronic nose systems. *Microchim Acta* 149:1–17
- Josse F, Lukas R, Zhou RN, Schneider S, Everhart D (1996) AC impedance-based chemical sensors for organic solvent vapors. *Sens Actuators B* 36:363–369
- Kang WP, Kim CK (1993) Gas sensitivities of silicon MIS capacitors incorporated with catalyst and adsorptive oxide layers. *J Electrochem Soc* 140:L125–L127
- Kang U, Wise K (2000) A high speed capacitive humidity sensor with on-chip thermal reset. *IEEE Trans Electron Devices* 47(4):702–710
- Kim S-J, Jeon BH, Choi K-S, Min N-K (2000) Capacitive porous silicon sensors for measurement of low alcohol gas concentration at room temperature. *Solid State Electrochem* 4:363–366
- Kitsara M, Goustouridis D, Chatzandroulis S, Beltsios K, Raptis I (2006) A lithographic polymer process sequence for chemical sensing arrays. *Microelectron Eng* 83:1192–1196
- Korotcenkov G, Cho BK (2010) Porous semiconductors: advanced material for gas sensor applications. *Crit Rev Solid State Mater Sci* 35(1):1–37
- Kummer AM, Hierlemann A, Baltes H (2004) Tuning sensitivity and selectivity of complementary metal oxide semiconductor-based capacitive chemical microsensors. *Anal Chem* 76:2470–2477
- Kummer AM, Burg TP, Hierlemann A (2006) Transient signal analysis using complementary metal oxide semiconductor capacitive chemical microsensors. *Anal Chem* 78:279–290
- Lang HP, Hegner M, Gerber C (2005) Cantilever array sensors. *Mater Today* 8:30–36
- Laville C, Pellet C (2002) Comparison of three humidity sensors for a pulmonary function diagnosis microsystem. *IEEE Sensors J* 2(2):96–101
- Lavrik NV, Sepaniak MJ, Datskos PG (2004) Cantilever transducers as a platform for chemical and biological sensors. *Rev Sci Instrum* 75:2229–2253
- Lee C-Y, Wu G-W, Hsieh W-J (2008) Fabrication of micro sensors on a flexible substrate. *Sens Actuators A* 147:173–176
- Li Y, Vancura C, Barrettino D, Graf M, Hagleitner C, Kummer A, Zimmermann M, Kirstein K-U, Hierlemann A (2007) Monolithic CMOS multi-transducer gas sensor microsystem for organic and inorganic analytes. *Sens Actuators B* 126:431–440
- Lim SH, Jaworski J, Satyanarayana S, Wang F, Raorane D, Lee S-W, Majumdar A (2007) Nanomechanical chemical sensor platform. In: *Proceedings of the 2nd IEEE international conference on nano/micro engineered and molecular systems, Bangkok, Thailand, 16–19 Jan 2007*, pp 886–889
- Lin J, Müller S, Obermeier E (1991) Two-dimensional and three-dimensional as basic elements for chemical sensors interdigital capacitors. *Sens Actuators B* 5:223–226
- Lloyd Spetz A, Savage S (2003) Advances in FET chemical gas sensors. In: Choyke WJ, Matsunami H, Pensl G (eds) *Recent major advances in SiC*. Springer, Berlin, pp 879–906
- Lofdahl M, Utaiasin C, Carlsson A, Lundstrom I, Eriksson M (2001) Gas response dependence on gate metal morphology of field-effect devices. *Sens Actuators B* 80:183–192
- Lundstrom I (1981) Hydrogen sensitive MOS structures. Part 1. Principles and applications. *Sens Actuators* 1:403–426
- McCorkle DL, Warmack RJ, Patel SV, Mlsna T, Hunter SR, Ferrell TL (2005) Ethanol vapor detection in aqueous environments using micro-capacitors and dielectric polymers. *Sens Actuators B* 107:892–903
- Meanna Perez JM, Freyre C (1997) A poly(ethylene terephthalate)-based humidity sensor. *Sens Actuators B* 42:27–30
- Menil F, Lucat C, Debeda H (1995) The thick-film route to selective gas sensors. *Sens Actuators B* 24–25:415–420
- Mlsna TE, Cemalovic S, Warburton M, Hobson ST, Mlsna DA, Patel SV (2006) Chemicapacitive microsensors for chemical warfare agent and toxic industrial chemical detection. *Sens Actuators B* 116:192–201
- Nahar RK, Khanna VK (1982) A study of capacitance and resistance characteristics of an Al<sub>2</sub>O<sub>3</sub> humidity sensor. *Int J Electron* 52:557–567

- Neimark AV, Ravikovitch PI (2001) Capillary condensation in MMS and pore structure characterization. *Microporous Mesoporous Mater* 44–45:697–707
- Nordström M, Keller S, Lillemose M, Johansson A, Dohn S, Haefliger D, Blagoi G, Havsteen-Jakobsen M, Boisen A (2008) SU-8 cantilevers for bio/chemical sensing: fabrication, characterisation and development of novel read-out methods. *Sensors* 8:1595–1612
- Oprea A, Bârsan N, Weimar U, Bauersfeld ML, Ebling D, Wöllenstein J (2008) Capacitive humidity sensors on flexible RFID labels. *Sens Actuators B* 132:404–410
- Park S, Kang J, Park J, Mun S (2001) One-bodied humidity and temperature sensor having advanced linearity at low and high relative humidity range. *Sens Actuators B* 76:322–326
- Park KK, Lee HJ, Yaralioglu GG, Ergun AS, Oralkan Ö, Kupnic M, Quate CF, Khuri-Yakub BT, Braun T, Ramseyer J-P, Lang HP, Hegner M, Gerber C, Gimzewski JK (2007) Capacitive micromachined ultrasonic transducers for chemical detection in nitrogen. *Appl Phys Lett* 91:094102
- Park KK, Lee HJ, Kupnic M, Oralkan Ö, Khuri-Yakub BT (2008) Capacitive micromachined ultrasonic transducer as a chemical sensor. In: *Proceedings of the 7th IEEE conference on sensors, IEEE sensors, Lecce, Italy, 26–29 Oct 2008*, pp 5–8
- Patel SV, Mlsna TE, Fruhberger B, Klaassen E, Cemalovic S, Baselt DR (2003) Chemicapacitive microsensors for volatile organic compound detection. *Sens Actuators B* 96:541–553
- Pecora A, Maiolo L, Cuscunà M, Simeone D, Minotti A, Mariucci L, Fortunato G (2008) Low-temperature polysilicon thin film transistors on polyimide substrates for electronics on plastic. *Solid State Electron* 52:348–352
- Rittersma ZM, Splinter A, Bödecker A, Benecke W (2000) A novel surface-micromachined capacitive porous silicon humidity sensor. *Sens Actuators B* 68:210–217
- Rodríguez A, Amírola J, Millán M, Horrillo MC, Sayago I, García M, Gutiérrez FJ (2004) Electromechanically coupled feedback loops for microsystems. Application to volatile organic compounds (VOC) sensors. In: *Proceedings of the 3rd IEEE conference on sensors, IEEE sensors, vol 1. Vienna, Austria, 24–27 Oct 2004*, pp 154–157
- Salomonsson A, Roy S, Aulin C, Ojamae L, Kall PO, Strand M, Sanati M, Lloyd Spetz A (2005) RuO<sub>2</sub> and Ru nanoparticles for MISiC-FET gas sensors. In: *Proceedings of MSTI-Nanotech-2005 conference, vol 2*, pp 269–272. <http://www.nsti.org>
- Satyanarayana S, McCormick DT, Majumdar A (2006) Parylene micro membrane capacitive sensor array for chemical and biological sensing. *Sens Actuators B* 115:494–502
- Schoeneberg U, Hosticka BJ, Zimmer G, Maclay GJ (1990) A novel readout technique for capacitive gas sensors. *Sens Actuators B* 1:58–61
- Sheppard NF, Day DR, Lee HL, Senturia SD (1982) Microdielectrometry. *Sens Actuators A* 2:263–274
- Shibata H, Ito M, Asakura M, Watanabe K (1996) A digital hygrometer using a polyimide film relative humidity sensor. *IEEE Trans Instrum Meas* 45(3):564–569
- Silverthorne SV, Watson CW, Baxtor RD (1989) Characterization of a humidity sensor that incorporates a CMOS capacitance measuring circuit. *Sens Actuators* 19:371–383
- Sivaramakrishnan S, Rajamani R, Pappenfus TM (2008) Electrically stretched capacitive membranes for stiffness sensing and analyte concentration measurement. *Sens Actuators B* 135:262–267
- Snow ES, Perkins FK, Houser EJ, Badescu SC, Reinecke TL (2005) Chemical detection with a single-walled carbon nanotube capacitor. *Science* 307:1942–1944
- Timar-Horvath V, Juhasz L, Vass-Varnai A, Perlaky G (2008) Usage of porous Al<sub>2</sub>O<sub>3</sub> layers for RH sensing. *Microsyst Technol* 14:1081–1086
- Winqvist F, Spetz A, Armgarth M, Lundstrom I (1985) Biosensors based on ammonia sensitive metal-oxide-semiconductor structures. *Sens Actuators* 8:91–100
- Zamani C, Shimanoe K, Yamazoe N (2005) A new capacitive-type NO<sub>2</sub> gas sensor combining an MIS with a solid electrolyte. *Sens Actuators B* 109:216–220

## Chapter 17

# Sensing Layers in Work-Function-Type Gas Sensors

### 17.1 Work-Function-Type Gas Sensors

Classical work-function-type gas sensors are specific devices based on the Kelvin method. The Kelvin method (“vibrating capacitor/condenser method,” “capacitive probe method”), using a so-called Kelvin probe (KP) or Kelvin oscillator, is an established tool for measuring the work function of a sample or, more precisely, the contact potential between the sample and a reference.

Using this method, the change in the work function due to the reaction of the material with surrounding gas can be measured. When the surface of the metal and the electroactive material are held parallel to each other and separated by a dielectric material, there is a potential difference across the surface due to transfer of charges. This potential difference is produced by the difference between the work functions of the two materials and formed from a bulk term and a surface dipole term. Gases interact with the surface dipole of one or both materials that constitute the Kelvin probe. The extent to which the gases can interact with the surface dipole determines the amount of work-function shift (Bergstrom et al. 1997). Gases, of course, can change bulk properties of materials as well.

A schematic diagram illustrating the operating principle of work-function-type gas sensors is shown in Fig. 17.1. The traditional KP, as described by Lord Kelvin (1898), consists of a flat circular electrode (termed the reference electrode) suspended above and parallel to a stationary electrode (the sample under study), thus creating a simple capacitor. The charge on the capacitor due to the contact potential can be measured – with some difficulty – using an electrometer or via the discharging current after moving one plate away. In 1932, Zisman introduced an improved measurement procedure. He mounted a vibrating reference surface just above the sample, the discharging current then varying periodically as the tip vibrates, the amplitude depending on the difference between the contact potential and an external voltage. This technique led to the development of systems that automatically track shifts in the contact potential and, thus, the work function of the sample, if the reference electrode is unaffected. Reviews related to KP measurements have been carried out by Engelhardt et al. (1970), Surplice and D’Arcy (1970), Belier et al. (1995), Zanolari et al. (1997), and Doll et al. (1998).

A major advantage of this method is that it is a noncontact and nondestructive way of measuring. Additionally, it is not expected to influence the electrical or chemical structure of the material. The technique is very simple, but fast, accurate, and versatile: it can, in principle, be used in many environments. However, experience has shown that for practical sensor applications Kelvin probes are not suitable due to the necessary instrumentation and the limits to miniaturization. Most probes are rather macroscopic with a reference electrode the size of a few millimeters or centimeters. In addition, this method of measurement is complicated in comparison with other methods used in gas sensing and requires specific conditions and equipment. As a result, these devices are not available on the sensor

**Fig. 17.1** Schematic diagram illustrating experimental setup: Kelvin probe (Reprinted with permission from Bögner et al. (1998). Elsevier)

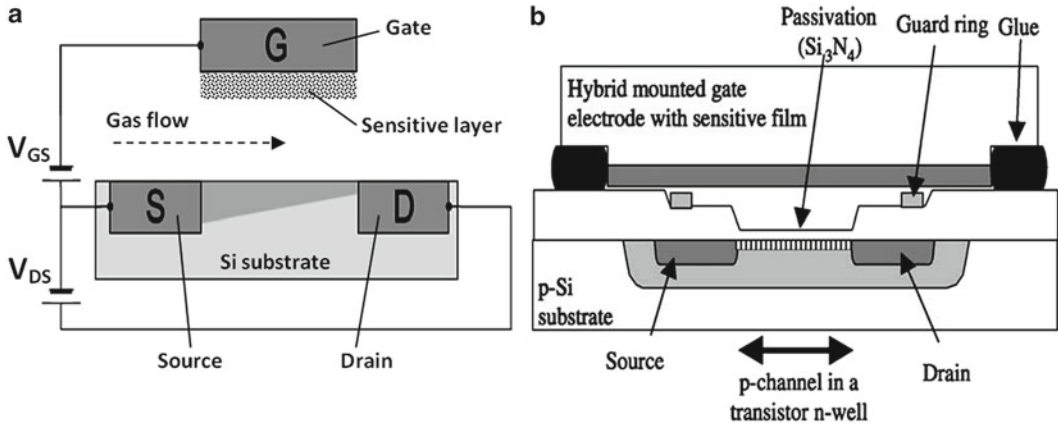
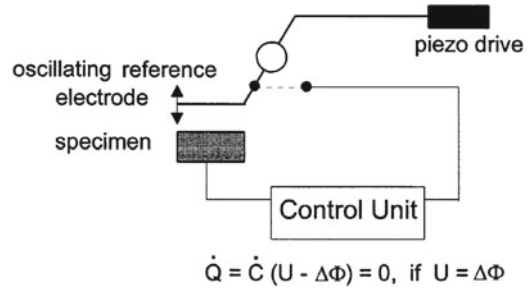


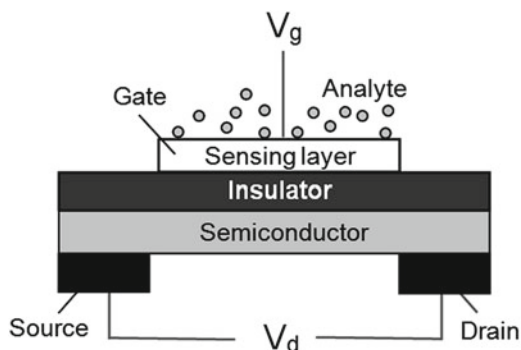
**Fig. 17.2** (a) Schematics of GasFET-type sensor and (b) one of variants of GasFET realization (Reprinted with permission from Burgmair et al. (2003b). Copyright 2003 Elsevier)

market. The Kelvin probe is more widely used for research on gas adsorption and interaction with solids during gas-sensing effect study (Barsan and Weimar 2003; Pokhrel et al. 2008). However, in spite of this situation, many organic and inorganic materials have been tested with the KP during the past few decades. It was found that the KP is an effective test tool to screen and characterize possible sensing layers for field-effect devices such as GasFETs, where materials demonstrating large work function changes during interaction with gas are required (Fleischer 2008). Schematically, GasFETs are shown in Fig. 17.2. The insulation of the transistor channel has to be made of a chemically inert material to avoid additional gas reactions at this surface; otherwise, an additional potential change occurs there. The usage of LPCVD-deposited  $\text{Si}_3\text{N}_4$  has been shown to be a good choice. The idea of a GasFET was introduced by Janata and coworkers (Josowicz and Janata 1986; Cassidy et al. 1986) and until recently has been under investigation (Bergstrom et al. 1997; Domansky et al. 1998; Fleischer et al. 2001; Burgmair et al. 2003a, b; Lampe et al. 2005; Stegmeier et al. 2010).

It should be noted that materials acceptable for GasFET sensors can be used in MOSFET gas sensors (see Fig. 17.3), which also operate due to change of work function of sensing layers. This configuration of sensor is also widely used to detect various gases and vapors (Liess et al. 1996; Covington et al. 2001; Bufon and Heinzl 2006). It is known that when two chemically different plates are electronically connected, an electric field is created at their interface. This field is proportional to the difference of work functions of the two plate materials (Janata and Josowicz 1998), and both source–drain current and turn-on voltage are governed by it. Interaction between analyte molecules and the sensing layer is able to change the work function of the sensing material and thus can affect the source–drain current or gate voltage (Janata 1990, 2003).

The advantage of GasFETs in comparison with conventional MOSFET- and FET-based gas sensors is the free choice of the sensing material. Moreover, in contrast to classical semiconducting metal-oxide

**Fig. 17.3** Schematic configuration of MOSFET gas sensors



gas sensors, the gas-sensing properties do not depend on the morphology of the sensing materials. Such a possibility gives significant additional freedom in design. In a GasFET, the gases come into direct contact with the insulator face of the gate electrode. Therefore the current in this device in general relies on potential changes upon gas exposure of a sensitive material deposited on the gate electrode. The disadvantage of the GasFET in comparison with conventional MOSFET- or FET-based sensors is that the modulation  $\delta I_{SD}/\delta V_G$  is weakened significantly by the air gap (by a factor of about 100), necessitating transistors with very steep characteristics. Following work by Gergintschew et al. (1996), Fleischer et al. (2001), and Pohle et al. (2003), several options have been introduced to make more efficient use of the generated voltage. One significant improvement consists of the formation of a larger area capacitor built from the suspended gate and a floating gate. The floating gate then transmits the potential coming from the gas-sensitive layer to a small FET device with a short channel (Pohle et al. 2003). This basically minimizes the loss of sensing signal due to weak coupling via the air gap.

Experiment has shown that this potential change can be measured in the same way with the Kelvin probe. The transferability of the KP result to the GasFET has been shown in the meantime by Burgmair et al. (2002) and Oprea et al. (2005). This means that materials with large changes in work function measured by KPs are materials which can be successfully used as sensing layer in GasFETs. Therefore, in this chapter we will briefly consider materials studied by KP. It was established that, for various sensitive layers, work-function shifts upon gas adsorption in the order of several hundred millivolts are possible; however, in many cases the signal is only in the range of 10–50 mV.

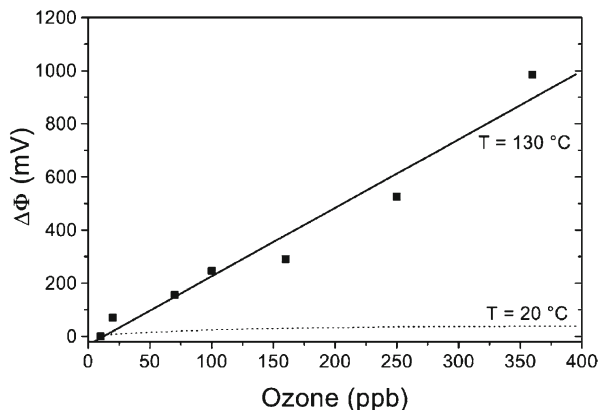
## 17.2 Materials Tested by KP

### 17.2.1 Metallic Layers

Metal layers were the first materials studied by KPs and used as a gate in GasFETs. Next to Pd (Cassidy et al. 1986; Fleischer et al. 2001), which is a classical gate of MOSFET- and FET-type hydrogen gas sensors (Lundström et al. 1975), other noble metals such as Au and Pt were tested. Burgmair et al. (2003b) established that Pt layers also can work as a sensing layer in  $H_2$  sensors. With the adsorption of  $H_2$  on Pt, amazingly high surface potential changes of 500 mV and more are observed. The reason for this can be seen in the high reactivity of Pt to  $H_2$  even at room temperatures. It was demonstrated that the signal is fully reversible and the baseline is stable. Very fast response times (<10 s) have been observed at room temperature. Moreover, a wide detection range is available. It is an important result because Pd as a sensing layer for  $H_2$  sensors has strong disadvantages during operation at RT (see Chap. 4 (Vol. 1)). However, Pt-based highly sensitive layers also have shortcomings. The problem with high sensitivities is that the strong reaction with  $H_2$  implies a strong influence on the “natural” adsorbates on these sensing layers (Moos et al. 2009). In this case, it is removal of the



**Fig. 17.4** Concentration dependence of the signal amplitudes at 130 and 20 °C for a gold layer (Reprinted with permission from Zimmer et al. (2001). Copyright 2001 Elsevier)



adsorbed oxygen on the Pt surface, which is reconstituted only after long periods, thus causing some hysteresis effects after repeated strong  $H_2$  exposure. This leads to a new operation strategy for reactive Pt, which is further coated with a gas diffusion filter (Senft et al. 2007). Now, the differences in the diffusion of  $O_2$  and  $H_2$  cause the major sensing effect, significantly improving the reproducibility of the sensor readings for  $H_2$ .

Stegmeier et al. (2010) have shown that Pt is acceptable for RT VOCs detection as well. However, for this purpose, a thermal activation process in an oxygen-containing atmosphere is a necessary prerequisite. The VOC detection at room temperature seems to be dependent on the existence of reactive oxygen species on the surface, which can be generated during thermal activation. It was found that the activity of generated oxygen species depends on the material system, for example, platinum powder grain size and platinum dispersion on the support.

Zimmer et al. (2001) found that Au and Pt can be used as ozone sensing layers. Hybrid suspended gate FET devices with a sensitive layer of platinum or gold were proven to be well suited as reproducible ozone detection from the low ppb region up to 500 ppb and higher. However, the same research has shown that gold and platinum at room temperature are also very sensitive to other gases. For some gases, the work-function shift for the same concentrations is even higher than for ozone. The heated samples are much more sensitive (see Fig. 17.4) and selective toward ozone. Regarding platinum in particular, all oxidizing gases are below 30 % of the ozone amplitude. This means that room temperature is not suitable for ozone detection by KP using Au and Pt as sensing layers, and operation at increased temperature is more efficient for application. Operating at 130 °C, gold shows a nearly linear dependence on ozone concentration with high signals (Fig. 17.4) and little humidity influence. Platinum at 130 °C performs well with a fast response time and low cross-sensitivities to other gases. Filippini et al. (2002) reported that Au has shown good sensitivity to  $NO_2$  as well. Sulima et al. (2005) reported that gold is also a suitable sensitive layer for the detection of chlorine gas. Chlorine converts gold into gold chloride, and at temperatures of 190 °C gold chloride decomposes again. Therefore, reversible measurement cycles are possible. Kiss et al. (2000) have shown that a mixed phase of Pt/Cu can be used for the design of CO sensors. Semi-noble metals like Ag are reported to be sensitive to  $H_2S$  and  $Cl_2$ .

### 17.2.2 Inorganic Layers

During the past few decades, many inorganic materials have been tested. Experiment has shown that ionic films like hydrated potassium halogenides provide excellent work-function sensor signals for ozone detection at room temperature (Doll et al. 1996). Figure 17.5a shows the work-function changes at RT of various materials exposed to  $O_3$  (~300 ppb in air). It is seen that KI has maximum response.

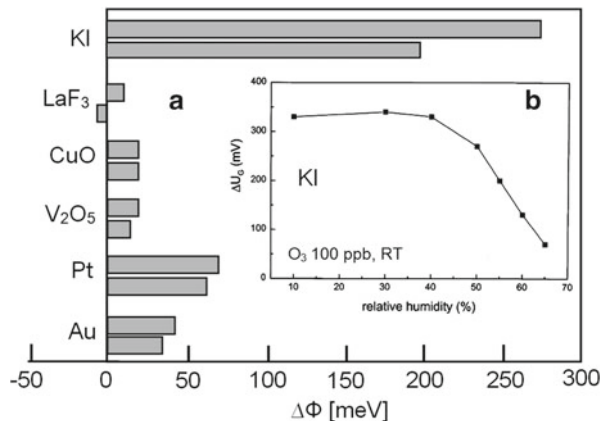


**Fig. 17.5** (a) Work-function changes at RT of various materials exposed to O<sub>3</sub> at a concentration of approx. 300 ppb in air. Minimum and maximum amplitudes are shown. (b) Humidity dependence of KI work-function changes during interaction with O<sub>3</sub> (100 ppb) measured at 25 °C ((a) Reprinted with permission from Doll et al. 1996 and (b) Fuchs et al. (1998). Copyright 1996 and 1998 Elsevier)

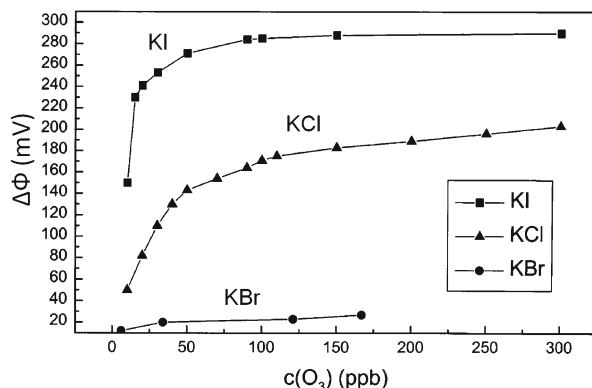


**Fig. 17.6** Work-function shifts vs ozone concentration for KI, KCl, and KBr measured at 25 °C and 30 % RH (Reprinted with permission from Fuchs et al. (1998). Copyright 1998 Elsevier)

Hybrid suspended gate FET with a thin potassium iodide (KI) sensitive layer were proven to be well suited as a reproducible ozone sensor operating at room temperature with an excellent resolution in the low ppb region (Fuchs et al. 1998). However, it was established that, for low concentrations of ozone, the adsorption is too slow to reach saturation within the exposure time of 60 min, whereas at concentrations bigger than 100 ppb, the signal shows saturation (Fig. 17.6). Moreover, KI response to O<sub>3</sub> is strongly dependent on the air humidity (see Fig. 17.5b). Work-function change is independent of humidity only in the range 20–45 % RH. Below 20 % RH, the high noise amplitude prevents a reliable ozone measurement, while above 45 % RH the  $\Delta\Phi$  strongly decreases. It should be stressed that the impact of humidity strongly limits the applicability of the sensor to moderate ambient conditions. So, KI-based GasFET may preferably be applied as a threshold indicator for a concentration of 80–100 ppb ozone in air with low RH (Fuchs et al. 1998). It was also found that, in the long term, KI-based sensors do not retain their properties: signal amplitudes decrease, independent of humidity. It was assumed that such behavior is due to an agglomeration of the KI layer occurring after several weeks of ozone exposure.

Regarding other alkali halides that are expected to be suitable sensitive layers, one can say that KCl does not exhibit such a high slope for small ozone concentrations as does KI. In Fig. 17.5, a comparison between KI, KCl, and KBr is depicted. Although the signals are not as high as for KI and response times are about 30 min, KCl is a suitable layer because of its higher resolution in the interesting region between 50 and 120 ppb (Fuchs et al. 1998). The application of KBr is questionable because this material shows rather low sensitivity with respect to ozone.

Semiconducting inorganic layers tested by KP include thin and thick layers of SnO<sub>2</sub> (Flietner et al. 1994; Barsan et al. 1999; Wöllenstein et al. 2000; Karthigeyan et al. 2001) and many other oxides like iron oxide (Gurlo et al. 2004), Ga<sub>2</sub>O<sub>3</sub> (Stegmeier et al. 2010), ZrO<sub>2</sub> (Miyahara et al. 1988), mixed aluminum and nickel oxides (Bögner et al. 1998), IrO<sub>2</sub> (Karthigeyan et al. 2002, 2004), TiO<sub>2</sub> (Ostrick et al. 2000b), and Cr<sub>1.8</sub>Ti<sub>0.2</sub>O<sub>3</sub> (CTO) (Burgmair et al. 2002). Normally, studies are concentrated on simple gases like O<sub>2</sub>, H<sub>2</sub>, CO, NO<sub>2</sub>, NH<sub>3</sub>, and humidity. Experiments carried out with these metal oxides have shown that the response of metal oxide-based sensors is more stable in comparison with alkali halide-based sensors (Karthigeyan et al. 2001). However, elevated temperatures are usually necessary for proper operation of metal oxide-based sensing layers. For example, the sensitivity of a Ga<sub>2</sub>O<sub>3</sub> thin film to CO, H<sub>2</sub>, and CH<sub>4</sub> measured with a Kelvin probe at RT is low; only at high operation temperature can significant gas signals be detected. Similar results were obtained using SnO<sub>2</sub> thin films (Karthigeyan et al. 2001; Lampe et al. 2005). The response time of the samples was also very slow. Therefore, it was concluded that metal oxide thin films are not suitable for the measurement of reducing gases by work-function change at room temperature. As a rule, acceptable response appears at operation temperatures exceeded 100 °C. For example, an interesting stable and reversible reaction of NO<sub>2</sub> on iridium oxide with low cross-sensitivity to other gases (CO, H<sub>2</sub>, Cl<sub>2</sub>) except for NH<sub>3</sub> was found at 130 °C (Karthigeyan et al. 2002). The base line is completely recovered after the removal of multiple NO<sub>2</sub> exposure under different humidity conditions. Karthigeyan et al. (2001) reported that SnO<sub>2</sub>-based sensors also had good sensitivity to NO<sub>2</sub> at  $T_{\text{oper}} = 130$  °C. They obtained ~100 mV work-function change to 5 ppm concentration at 130 °C. Also a little influence of humidity on the work function was observed. It was found that, from the tested metal oxides, only Cr<sub>1.8</sub>Ti<sub>0.2</sub>O<sub>3</sub> (CTO) can operate at low temperatures (Burgmair et al. 2002). Burgmair et al. (2002) studied Cr<sub>1.8</sub>Ti<sub>0.2</sub>O<sub>3</sub> films and established that, as expected for a reducing gas,  $\Delta\Phi$  is negative and reversible. For GasFETs the sensitivity amounts to about -30 mV per decade of ammonia concentration at room temperature. The response time ( $t_{90}$ ) is ~2 min for  $C_{\text{NH}_3} > 20$  ppm. Moreover, at room temperature, CTO has a low cross-sensitivity to water vapor, both in terms of the dependence of the ammonia response and in terms of the humidity influencing the sensor baseline signal (~ -15 mV). The sensitivity decreases with increasing temperature.

Much better results for metal oxides such as SnO<sub>2</sub> or Ga<sub>2</sub>O<sub>3</sub> are produced using Pd- and Pt-activated thick films of these materials (Lampe et al. 2005; Stegmeier et al. 2010). Lampe et al. (2005) reported that, for SnO<sub>2</sub>:Pd sensors, an acceptable response is observed even at low temperatures (40 °C) (see Fig. 17.7). The gas response even at low CO concentrations is high ( $\Delta\Phi$ : 30 mV/3 ppm CO), and the response time ( $t_{90} < 1$  min) is low. Similar results were found by using ethanol %F : 25 mV/10 vpm EtOH) as the target gas. However, Kelvin probe measurements showed that a preliminary activation step – heating the film at 175–200 °C for 5–30 min in wet synthetic air – is necessary to get a high CO and EtOH sensitivity at low operation temperatures (Lampe et al. 2005). This effect was discussed above with reference to Pt layers. Obviously, some reactive oxygen species are formed during the thermal activation which are then stored in the sensing material. Using only Pt as the sensing layer, the gas sensitivity declines after a few hours after thermal activation (Stegmeier et al. 2008). Using Pt/Ga<sub>2</sub>O<sub>3</sub> systems, the gas sensitivity is preserved at least one order of magnitude longer. This means that the oxide enhances the lifetime of the activated species.

Other inorganic materials were also studied by KP. Studies on gas sensitivity are reported for carbonates, especially BaCO<sub>3</sub>, being sensitive to CO<sub>2</sub> and NO<sub>2</sub> even at ambient temperature (Ostrick et al. 1999, 2000a, 2003), TiN (Ostrick et al. 2000b) as ammonia sensitive layers, and LaF<sub>3</sub> as oxygen (Cho et al. 1991; Choi et al. 1993) and ozone (Doll et al. 1996) sensing layers. The sensitivity of barium carbonate to CO<sub>2</sub> in work-function-type gas sensors is due to the formation of bicarbonate

**Fig. 17.7** Kelvin probe measurements of a Pd-activated SnO<sub>2</sub> thick film. Response to different CO concentrations at about 40 °C (Reprinted with permission from Lampe et al. (2005). Copyright 2005 Elsevier)

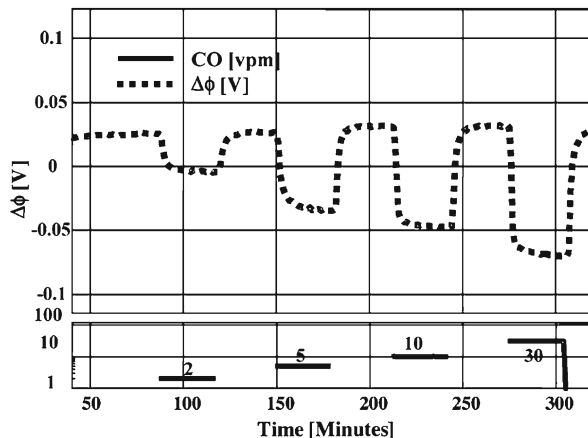
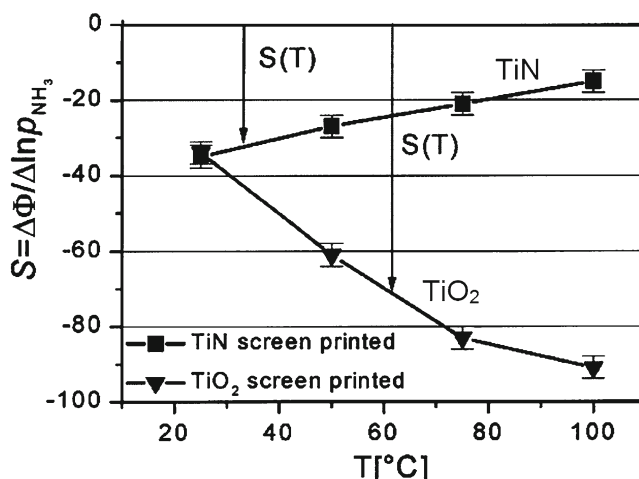


**Fig. 17.8** Temperature dependence of the sensitivity of TiN and TiO<sub>2</sub> to ammonia (Reprinted with permission from Ostrick et al. (2000b). Copyright 2000 Elsevier)



species at the surface (Ostrick et al. 2003). However, it was established that BaCO<sub>3</sub> films completely lose their CO<sub>2</sub> sensitivity in absolutely dry atmospheres. IR spectroscopic investigations have shown that the CO<sub>2</sub> detection process is a reversible formation of dimeric HCO<sub>3</sub><sup>-</sup> in the water film on the surface (Ostrick et al. 2000a). Mixed oxide systems based on BaTiO<sub>3</sub>/CuO (Simon et al. 2003) are also suitable for room temperature detection of CO<sub>2</sub>. The sensitivity is perhaps correlated with the formation of a surface phase of BaCO<sub>3</sub>.

Ostrick et al. (2000b) reported that the exposure of TiN to ammonia (400–100 ppm) in wet synthetic air at room temperature leads to a reversible decrease of  $\Delta\Phi$ . A change of the work function was equal to ~30 meV/decade of increasing ammonia concentration at room temperature. The response time ( $t_{90}$ ) to 1 ppm was ~1 min. The sensitivity was a typical room temperature effect as it decreased at higher temperatures up to 100 °C (Fig. 17.8). As can be seen, TiO<sub>2</sub>-based sensors have a higher response. However, the response of TiN-based sensors has a low cross-sensitivity to humidity. It was found that the sensitivity to ammonia does not depend on the relative humidity: the work-function change due to humidity changes is as low as ~2 meV for an increase of 10 % in relative humidity. Such behavior is a great advantage of TiN-based sensors.

### 17.2.3 Organic Layers

The organic materials most exhaustively studied by KP are the conducting polymers such as polypyrrole (Josowicz and Janata 1986; Blackwood and Josowicz 1991; Topart and Josowicz 1992a, b; Cabala et al. 1997; Hatfield et al. 2000), *p*-polyphenylene (Blackwood and Josowicz 1991), and polyaniline (Domansky et al. 1998). Thiol-functionalized porphyrins were also studied (Di Natale et al. 1998). As a rule, this research related to interaction with volatile organic compounds (VOCs) like methanol, ethanol, hydrocarbons, and chlorinated hydrocarbons. It confirmed that these polymers, especially after appropriate doping, are promising for RT VOCs sensors. Results reported by Blackwood and Josowicz (1991) are presented in Table 17.1. It is seen that the measured work-function changes for polypyrrole and *p*-polyphenylene depend on the conditions of the preparation of the film. In particular, the Kelvin probe results show that the polymer films' response to organic vapor is influenced both by the nature of the solvent from which the film was originally grown and by the type of anion with which it is doped.

However, we note that other gases and vapors were tested as well – for example, Cabala et al. (1997) in research used dimethyl methylphosphonate (DMMP), tetrachloroethene (PER), and NO<sub>2</sub> (see Fig. 17.9). Cabala et al. (1997) have shown that PP layers have high sensitivity to DMMP and NO<sub>2</sub> up to 87 mV (ppm decade)<sup>-1</sup> to NO<sub>x</sub> and low sensitivity to PER. The detection range during this study was 0.4–40 ppm for NO<sub>x</sub> and 2–40 ppm for DMMP. The most sensitive layer for DMMP detection was found to be NiPcTS-doped PP, whereas CuPcTS-doped PP shows the highest sensitivity to NO<sub>x</sub>. In addition, they established that the use of MPcTS (M=Cu, Ni) as a dopant for PP preparation enhances the stability of PP in comparison to PP doped with small anions, and makes PP practically insensitive to ambient air. Cabala et al. (1997) also established that increasing the content of small anions in mixtures with MPcTS decreases the response time of PP samples from the order of hours to minutes. The competitive doping of PP with a mixture of small anions and MPcTS slightly decreases the sensitivity but enhances the selectivity of the measurements.

Langmuir–Blodgett (LB) or self-assembled monolayer (SAM) thin films of porphyrins were also studied (Di Natale et al. 1998; D'Amico et al. 2000a, b; Andersson et al. 2001). It was found that these layers are sensitive to ethanol and triethylamine. Testing with KPs has shown that phthalocyanines can work as ozone (Bouvet et al. 2001) and NO<sub>2</sub> (Gu et al. 1998) sensitive layers. Simon et al. (2000) reported that nonconducting polymers like polyvinylpyrrolidone can be used as humidity-sensitive layers. After a detailed study, Harbeck (2005) concluded that polyacrylic acid (PAA) seems to be most suitable among the different polymers—poly(4-vinylphenol) (PVPh), polystyrene (PS), poly(acrylonitrile-*co*-butadiene) (PAB), and poly(cyanopropylphenyl-siloxane) (PCPhS)—for ammonia detection with the KP and, presumably, the GasFET. PAA shows a large signal and high sensitivity in addition to low humidity sensitivity. In addition, the long time stability is excellent.

Blackwood and Josowicz (1991) analyzing results of vapors' influence on work function of various polymer structures (see Table 17.1) concluded that the magnitude and direction of any vapor-induced shift in the work function of a conducting polymer,  $\Phi$ , is directly related to the relative value of  $\Phi$  and the electronegativity of the vapor  $\chi_M$ . It has also been shown that  $\Phi$  varies with the growth conditions, and thus, once a method of accurately controlling the initial work functions of the polymer films is obtained, it may be possible to predict the response of any film to any particular organic vapor. Therefore it should become possible to produce relatively high-sensitivity gas sensors by choosing a film for which the magnitude of  $\Phi - \chi_M$  is large. However, a lower limit on the value of the work function of the polymer,  $\Phi$ , will be set by the fact that a practical sensor must be stable in its normal environment, which is usually air.

**Table 17.1** Changes induced in the work function (WF) measured vs Au in various polymer films by exposure to vapors

Vapor (concentration)	Polymer film deposited from	WF in N <sub>2</sub> (meV)	WF in vapor (meV)	ΔWF (meV)	Donor or acceptor
MeOH (4.6 × 10 <sup>-3</sup> mol/dm <sup>3</sup> )	PPP-TOS/AcCN	60	100	40	Acceptor
	PP-Fe(CN) <sub>6</sub> /H <sub>2</sub> O	210	145	-65	Acceptor
	PP-TOS/AcCN	265	165	-100	Donor
	PP-TOS/CH <sub>2</sub> Cl <sub>2</sub>	415	275	-140	Donor
	PPP;TCNQ-TOS/AcCN	490	200	-290	Donor
	PPP-CIO <sub>4</sub> /AcCN	590	260	-330	Donor
	PP;TCNQ-TOS/AcCN	615	265	-350	Donor
	PPP-TOS/AcCN	60	215	155	Acceptor
	PP-Fe(CN) <sub>6</sub> /H <sub>2</sub> O	210	260	50	Acceptor
	PP-TOS/AcCN	265	255	-10	Weak donor
CHCl <sub>3</sub> (1.2 × 10 <sup>-3</sup> mol/dm <sup>3</sup> )	PP-TOS/CH <sub>2</sub> Cl <sub>2</sub>	415	365	50	Donor
	PPP;TCNQ-TOS/AcCN	490	435	-55	Donor
	PPP-CIO <sub>4</sub> /AcCN	590	485	-105	Donor
	PP;TCNQ-TOS/AcCN	615	485	-130	Donor
	PPP-TOS/AcCN	60	210	150	Acceptor
	PP-Fe(CN) <sub>6</sub> /H <sub>2</sub> O	210	235	25	Acceptor
	PP-TOS/AcCN	265	280	15	Weak acceptor
	PP-TOS/CH <sub>2</sub> Cl <sub>2</sub>	415	335	-80	Donor
	PPP;TCNQ-TOS/AcCN	490	530 <sup>a</sup>	-40 <sup>a</sup>	Donor
	PPP-CIO <sub>4</sub> /AcCN	590	430 <sup>a</sup>	-160	Donor
i-PrOH (0.4 × 10 <sup>-3</sup> mol/dm <sup>3</sup> )	PP;TCNQ-TOS/AcCN	615	660 <sup>a</sup>	-45 <sup>a</sup>	Donor
	PPP-TOS/AcCN	60	170	110	Acceptor
	PP-Fe(CN) <sub>6</sub> /H <sub>2</sub> O	210	220	10	Weak acceptor
	PP-TOS/AcCN	265	230	-35	Donor
	PP-TOS/CH <sub>2</sub> Cl <sub>2</sub>	415	350	-65	Donor
	PPP;TCNQ-TOS/AcCN	490	370	-120	Donor
	PPP-CIO <sub>4</sub> /AcCN	590	410	-180	Donor
	PP;TCNQ-TOS/AcCN	615	470	-145	Donor
	PPP-TOS/AcCN	60	80	20	Weak acceptor
	PP-Fe(CN) <sub>6</sub> /H <sub>2</sub> O	210	225	15	Weak acceptor
C <sub>6</sub> H <sub>14</sub> (1.6 × 10 <sup>-3</sup> mol/dm <sup>3</sup> )	PP-TOS/AcCN	265	260	-5	Weak donor
	PP-TOS/CH <sub>2</sub> Cl <sub>2</sub>	415	405	-10	Weak donor
	PPP-CIO <sub>4</sub> /AcCN	590	580	-10	Weak donor
	PPP-TOS/AcCN	60	50	-10	Weak donor

PP polypyrrole, PPP *p*-polyphenylene, AcCN acetonitrile, CIO<sub>4</sub> LiClO<sub>4</sub>, TCNQ 7,7,8,8-tetracyanoquinodimethane, TOS tetraethylammonium *p*-toluenesulfonate

Source: Reprinted with permission from Blackwood and Josowicz (1991). Copyright 1991 American Chemical Society

<sup>a</sup>Unstable

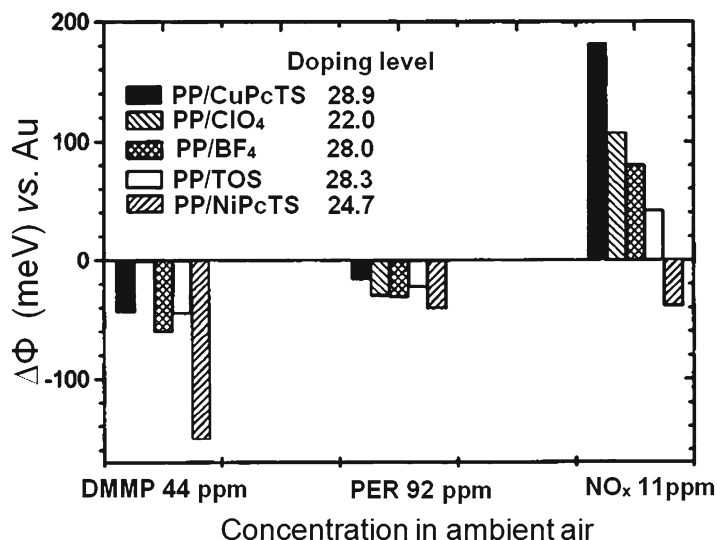


**Fig. 17.9** Comparison of the work-function change,  $\Delta\Phi$ , of PP layers doped with various anions in the presence of  $\text{NO}_x$ , PER, and DMMP in ambient air. The doping level is given for each of the PP layers. Compounds used for doping: *CuPcTS* copper phthalocyanine tetrasulfonate tetrasodium salt, *NiPcTS* nickel phthalocyanine tetrasulfonate tetrasodium salt, *TOS* sodium toluene-*p*-sulfonate, *BF<sub>4</sub>*-sodium tetrafluoroborate, *CIO<sub>4</sub>* - perchlorate (Reprinted with permission from Cabala et al. (1997). Copyright 1997 Royal Society of Chemistry)

## References

- Andersson M, Holmberg M, Lundström I, Lloyd-Spetz A, Martenson P, Paolesse R, Falconi C, Proiett E, Di Natale C, D'Amico A (2001) Development of a ChemFET sensor with molecular films of porphyrins as sensitive layer. *Sens Actuators B* 77:567–571
- Barsan N, Weimar U (2003) Understanding the fundamental principles of metal oxide based gas sensors; the example of CO sensing with  $\text{SnO}_2$  sensors in the presence of humidity. *J Phys Condens Matter* 15:R813–R839
- Barsan N, Heilig A, Kappler J, Weimar U, Göpel W (1999) CO–water interaction with Pd-doped  $\text{SnO}_2$  gas sensors: simultaneous monitoring of resistances and work functions. In: Proceedings of European conference on solid state transducers, Eurosensors XIII, September 6–9, Hague, The Netherlands, pp 183–184
- Belier JP, Lecoer J, Koehler C (1995) Improved Kelvin method for measuring contact potential differences between stepped gold surfaces in ultrahigh vacuum. *Rev Sci Instrum* 66(12):5544–5547
- Bergstrom PL, Patel NY, Schwank JW, Wise KD (1997) A micromachined surface work-function gas sensor for low-pressure oxygen detection. *Sens Actuators B* 42:195–204
- Blackwood D, Josowicz M (1991) Work function and spectroscopic studies of interactions between conducting polymers and organic vapors. *J Phys Chem* 95:493–502
- Bögner M, Fuchs A, Scharnagel K, Winter R, Doll T, Eisele I (1998) Thin  $(\text{NiO})_{1-x}(\text{Al}_2\text{O}_3)_x$ , Al doped and Al coated NiO layers for gas detection with HGSFET. *Sens Actuators B* 47:145–152
- Bouvet M, Guillaud G, Leroy A, Maillard A, Spirkovitch A, Tourmilhac F-G (2001) Phthalocyanine-based field-effect transistor as ozone sensor. *Sens Actuators B* 73:63–70
- Bufon CCB, Heinzel T (2006) Polypyrrole thin-film field-effect transistor. *Appl Phys Lett* 89:012104
- Burgmair M, Wöllenstein J, Böttner H, Karthigeyan A, Anothainart K, Eisele I (2002) Ti-substituted chromium oxide in work function type sensors: ammonia detection at room temperature with low humidity cross sensitivity. In: Proceedings of international workshop on materials and technologies for chemical sensors, Sept. 2001, Brescia (Italy). (Paper was not published in a journal; it can be found at <http://forschung.unibw.de/berichte/2002/7ut0fvd1htxsoquwk7yl5hkzsvu8aa.pdf>)
- Burgmair M, Zimmer M, Eisele I (2003a) Humidity and temperature compensation in work function gas sensor FETs. *Sens Actuators B* 93:271–275
- Burgmair M, Frerichs H-P, Zimmer M, Lehmann M, Eisele I (2003b) Field effect transducers for work function gas measurements: device improvements and comparison of performance. *Sens Actuators B* 95:183–188

- Cabala R, Meister V, Potje-Kamloth K (1997) Effect of competitive doping on sensing properties of polypyrrole. *J Chem Soc Faraday Trans* 93:131–137
- Cassidy J, Pons S, Janata J (1986) Hydrogen response of palladium coated gate field effect transistor. *Anal Chem* 58:1757–1761
- Cho WI, Yi CW, Ju JB, Cho BW, Yun KS (1991) Characteristics of a thin-film LaF<sub>3</sub> solid electrolyte for oxygen sensing. *Sens Actuators B* 5:149–153
- Choi SK, Yi CW, Cho WI, Cho JJB, Yun KS, Yamazoe N (1993) A MOSFET type sensor for oxygen sensing LaF<sub>3</sub> as a gate material. *Sens Actuators B* 13:45–48
- Covington JA, Gardner JW, Briand D, de Rooij NF (2001) A polymer gate FET sensor array for detecting organic vapours. *Sens Actuators B* 77:155–162
- D'Amico A, Di Natale C, Paolesse R, Macagnano A, Mantini A (2000a) Metalloporphyrins as basic material for volatile sensitive sensors. *Sens Actuators B* 65:209–215
- D'Amico A, Di Natale C, Paolesse R, Mantini A, Goletti C, Davide F, Filosofi G (2000b) Chemical sensing materials characterization by Kelvin probe technique. *Sens Actuators B* 70:254–262
- Di Natale C, Paolesse R, Mantini A, Macagnano A, Boschi T, D'Amico A (1998) Kelvin probe investigation of self-assembled-monolayers of thiol derivatized porphyrins interacting with volatile compounds. *Sens Actuators B* 48:368–372
- Doll T, Lechner J, Eisele I, Schierbaum K-D, Göpel W (1996) Ozone detection in the ppb range with work function sensors operating at room temperature. *Sens Actuators B* 34:506–510
- Doll T, Scharnagl K, Winter R, Bogner I, Eisele I, Ostrik B, Schoning M (1998) Work function gas sensors – reference layers and signal analysis. In: *Proceedings of European conference on solid state transducers, Eurosenors XII*, Southampton, UK, 13–16 Sept, pp 143–146
- Domansky K, Baldwin DL, Grate JW, Hall TB, Li J, Josowicz M, Janata J (1998) Development and calibration of field-effect transistorbased sensor array for measurement of hydrogen and ammonia gas mixtures in humid air. *Anal Chem* 70:473–481
- Engelhardt HA, Feulner P, Pfnür H, Menzel D (1970) An accurate and versatile vibrating capacitor for surface and adsorption studies. *J Phys E Sci Instrum* 10:1133–1136
- Filippini D, Fraigi L, Aragon R, Weimar U (2002) Thick film Au gate field-effect devices sensitive to NO<sub>2</sub>. *Sens Actuators B* 81:296–300
- Fleischer M (2008) Advances in application potential of adsorptive-type solid state gas sensors: high-temperature semi-conducting oxides and ambient temperature GasFET devices. *Meas Sci Technol* 19:042001
- Fleischer M, Ostrick B, Pohle R, Simon E, Meixner H, Bilger C, Daeche F (2001) Low-power gas sensors based on work-function measurement in low-cost hybrid flip-chip technology. *Sens Actuators B* 80:169–173
- Flietner B, Doll T, Lechner J, Leu M, Eisele I (1994) Fabrication of a hybrid field-effect structure for gas detection with diverse sensitive materials. *Sens Actuators B* 18–19:632–636
- Fuchs A, Bogner M, Doll T, Eisele I (1998) Room temperature ozone sensing with KI layers integrated in HSGFET gas sensors. *Sens Actuators B* 48:296–299
- Gergintschew Z, Kornetzky P, Schipanski D (1996) The capacitively controlled field effect transistor (CCFET) as a new low power gas sensor. *Sens Actuators B* 35–36:285–289
- Gu C, Sun L, Zhang T, Li T, Zhang X (1998) High-sensitivity phthalocyanine LB film gas sensor based on field effect transistor. *Thin Solid Films* 327–329:383–386
- Gurlo A, Sahn M, Oprea A, Barsan N, Weimar U (2004) A *p*- to *n*-transition on  $\alpha$ -Fe<sub>2</sub>O<sub>3</sub>-based thick film sensors studied by conductance and work function change measurements. *Sens Actuators B* 102:291–298
- Harbeck M (2005) New applications of organic polymers in chemical gas sensors. PhD Thesis, University of Tübingen, Germany
- Hatfield JV, Covington JA, Gardner JW (2000) GasFETs incorporating conducting polymers as gate materials. *Sens Actuators B* 65:253–256
- Janata J (1990) Potentiometric microsensors. *Chem Rev* 90:691–703
- Janata J (2003) Electrochemical microsensors. *Proc IEEE* 91:864–869
- Janata J, Josowicz M (1998) Chemical modulation of work function as a transduction mechanism for chemical sensors. *Acc Chem Res* 31:241–248
- Josowicz M, Janata J (1986) Suspended gate field effect transistor modified with polypyrrole as alcohol sensor. *Anal Chem* 58:514–517
- Karthigeyan A, Gupta RP, Scharnagl K, Burgmair M, Zimmer M, Sharma SK, Eisele I (2001) Low temperature NO<sub>2</sub> sensitivity of nano-particulate SnO<sub>2</sub> film for work function sensors. *Sens Actuators B* 78:69–72
- Karthigeyan A, Gupta RP, Scharnagl K, Burgmair M, Sharma SK, Eisele I (2002) A room temperature HSGFET ammonia sensor base on iridium oxide thin film. *Sens Actuators B* 85:145–153
- Karthigeyan A, Gupta RP, Scharnagl K, Burgmair M, Sulima T, Venkataraj S, Sharma SK, Eisele I (2004) Iridium oxide as low temperature NO<sub>2</sub>-sensitive material for work function-based gas sensors. *IEEE Sens J* 4(2):189–194
- Kelvin LF (1898) Contact electricity of metals. *Philos Mag J Sci* 46(278):82–120



- Kiss G, Varhegyi EB, Mizsei J, Krafcsik OH, Kovacs K, Negyesi G, Ostrick B, Meixner H, Reti F (2000) Examination of the CO/Pt/Cu layer structure with Kelvin probe and XPS analysis. *Sens Actuators B* 68:240–243
- Lampe U, Simon E, Pohle R, Fleischer M, Meixner H, Frerichs H-P, Lehmann M, Kiss G (2005) GasFETs for the detection of reducing gases. *Sens Actuators B* 111–112:106–110
- Liess M, Chinn D, Petelenz D, Janata J (1996) Properties of insulated gate field-effect transistors with a polyaniline gate electrode. *Thin Solid Films* 286:252–255
- Lundström I, Shivaraman AS, Lundkvist L (1975) Hydrogen sensitive MOS field effect transistor. *Appl Phys Lett* 26:55–57
- Miyahara Y, Tsukada K, Miyagi H (1988) Field-effect transistor using a solid electrolyte as a new oxygen sensor. *J Appl Phys* 63(7):2431–2434
- Moos R, Sahner K, Fleischer M, Guth U, Barsan N, Weimar U (2009) Solid state gas sensor research in Germany – a status report. *Sensors* 9:4323–4365
- Oprea A, Simon E, Fleischer M, Frerichs H-P, Wilbertz C, Lehmann M, Weimar U (2005) Flip-chip suspended gate field effect transistors for ammonia detection. *Sens Actuators B* 111:582–586
- Ostrick B, Mühlsteff J, Fleischer M, Meixner H, Doll T, Kohl C-D (1999) Adsorbed water as key to room temperature gas sensitive reactions in work function type sensors: the carbonate-carbon dioxide system. *Sens Actuators B* 57:115–119
- Ostrick B, Fleischer M, Meixner H, Kohl C-D (2000a) Investigation of the reaction mechanisms, in work function type gas sensors at room temperature by studies of the cross sensitivity to oxygen and water: the carbonate-carbon dioxide system. *Sens Actuators B* 68:197–202
- Ostrick B, Pohle R, Fleischer M, Meixner H (2000b) TiN in work function type sensors: a stable ammonia sensitive material for room temperature operation with low humidity cross sensitivity. *Sens Actuators B* 68:234–239
- Ostrick B, Fleischer M, Meixner H (2003) The influences of interfaces and interlayers on the gas sensitivity in work function type sensors. *Sens Actuators B* 95:271–274
- Pohle R, Simon E, Fleischer M, Meixner H, Frerichs H-P, Lehmann M, Verhoeven H (2003) Realisation of a new sensor concept: improved CCFET and SGFET type gas sensors in hybrid flip-chip technology. In: *Proceedings of the 12th international conference on solid-state sensors, actuators and microsystems, TRANSDUCERS 2003*, June, pp 135–138
- Pokhrel S, Simion CE, Quemener V, Barsan N, Weimar U (2008) Investigations of conduction mechanism in Cr<sub>2</sub>O<sub>3</sub> gas sensing thick films by ac impedance spectroscopy and work function changes measurements. *Sens Actuators B* 133:78–83
- Senft C, Galonska T, Widanarto W, Frerichs H-P, Wilbertz C, Eisele I (2007) Stability of FET-based hydrogen sensors at high temperatures. In: *Proceedings of IEEE sensors 2007 conference*, Atlanta, GA, October, pp 189–192
- Simon E, Fleischer M, Meixner H (2000) Polyvinylpyrrolidone: a new material for humidity sensing using work function read out. In: *Proceedings of 8th international meeting on chemical sensors, IMCS-2000*, July 3–5, Basel, Switzerland, p 194
- Simon E, Lampe U, Pohle R, Fleischer M, Meixner H, Frerichs H-P, Lehmann M, Verhoeven H (2003) Novel carbon dioxide gas sensors based on field effect transistors. In: *Proceedings of the 12th Transducers 2003*, Boston, MA, USA, June, p 204
- Stegmeier S, Fleischer M, Hauptmann P (2008) Detections of VOCs with activated Pt and supported Pt sensing layers by the change of work function at room temperature. In: *Proceedings of Eurosensors XXII*, Dresden, Germany, September, pp 1424–1427
- Stegmeier S, Fleischer M, Hauptmann P (2010) Thermally activated platinum as VOC sensing material for work function type gas sensors. *Sens Actuators B* 144:418–424
- Sulima T, Knittel T, Freitag G, Widanarto W, Eisele I (2005) A gas FET for chlorine detection. In: *Proceedings of IEEE sensors 2005 conference*, Irvine, CA, October–November, pp 113–115.
- Surplice NA, D'Arcy RJ (1970) A critique of the Kelvin method of measuring work functions. *J Phys E Sci Instrum* 3:477–482
- Topart P, Josowicz M (1992a) Transient effects in the interaction between polypyrrole and methanol vapor. *J Phys Chem* 96:8662–8666
- Topart P, Josowicz M (1992b) Characterization of the interaction between poly(pyrrrole) films and methanol vapor. *J Phys Chem* 96:7824–7830
- Wöllenstein J, Ihlenfeld F, Jaegle M, Köhner G, Böttner H, Becker WJ (2000) Gas-sensitive p-GaAs field effect device with catalytic gate. *Sens Actuators B* 68:22–26
- Zanoria ES, Hammall K, Danyluk S, Zharin AL (1997) The nonvibrating Kelvin probe and its application for monitoring surface wear. *J Test Eval* 25(2):233–238
- Zimmer M, Burgmair M, Scharnagl K, Karthigeyan A, Doll T, Eisele I (2001) Gold and platinum as ozone sensitive layer in work-function gas sensors. *Sens Actuators B* 80:174–178
- Zisman WA (1932) A new method of measuring contact potential differences in metals. *Rev Sci Instrum* 3:367–370

# Chapter 18

## Humidity-Sensitive Materials

### 18.1 Humidity Sensors

Moisture is present in various concentrations in most surroundings. Because of water's unique properties, humidity greatly influences both living organisms and materials (Fitzpatrick et al. 2002; Amin et al. 2004; Prowse et al. 2011). Therefore humidity measurement and control is vital to many manufacturing processes in such as the textiles, food processing, paper, semiconductor, and petrochemical industries. In the automobile industry, humidity sensors are used in rear-window defoggers and motor assembly lines. Humidity sensors find applications in diverse areas such as medical science, packaging, cryogenic processes, environmental monitoring, meteorology, flood-warning systems, and for actuating early warning systems or adjusting the amount of water in agricultural irrigation systems. In the medical field, humidity sensors are used in respiratory equipment, sterilizers, incubators, pharmaceutical processing, and biological products. There are many domestic applications, such as intelligent control of the living environment in buildings, cooking control for microwave ovens, and intelligent control of laundries (Patisier 1999; Chen and Lu 2005; Fraden 2010; Liu et al. 2011; Khanna 2012).

Humidity is a measure of the amount of water vapor in a gas that can be a mixture, such as air, or a pure gas, such as nitrogen or argon. Based on measurement techniques, the most commonly used units for humidity measurement are relative humidity (RH), dew/frost point (D/F PT), and parts per million (ppm) (Chen and Lu 2005). Relative humidity (RH) is the ratio of the partial pressure of water vapor present in a gas to the saturation vapor pressure of the gas at a given temperature. RH is a function of temperature, and, thus, it is a relative measurement. The RH measurement is expressed as a percentage. Dew point is the temperature (above 0 °C) at which the water vapor in a gas condenses to liquid water. Frost point is the temperature (below 0 °C) at which the vapor condenses to ice. D/F PT is a function of the pressure of the gas but is independent of temperature and is therefore an absolute humidity measurement. Parts per million (ppm) represents water vapor content by volume fraction (ppmv) or, if multiplied by the ratio of the molecular weight of water to that of air, as ppmw. PPM is also an absolute measurement. Although this measurement unit is more difficult to conceive, it has extensive applications in industry, especially for trace moisture measurement. Figure 18.1 shows the correlation between relative humidity (RH), parts per million by volume (ppmv), and dew/frost point (D/F PT).

There are many types of devices such as mirror-chilled hygrometers, psychrometers, optical sensors, and solid-state sensors which can be used for humidity control (Nitta 1981; Rittersma 2002). Mirror-based dew point sensors have better accuracy, but these devices are more costly to make and use (Chen and Lu 2005). Solid-state humidity sensors can be fabricated at low cost and used for moisture control more conveniently. Solid-state humidity sensors are broadly classified into three types: gravimetric (QCM and SAW), resistive, and capacitive, according to the output form of the sensor

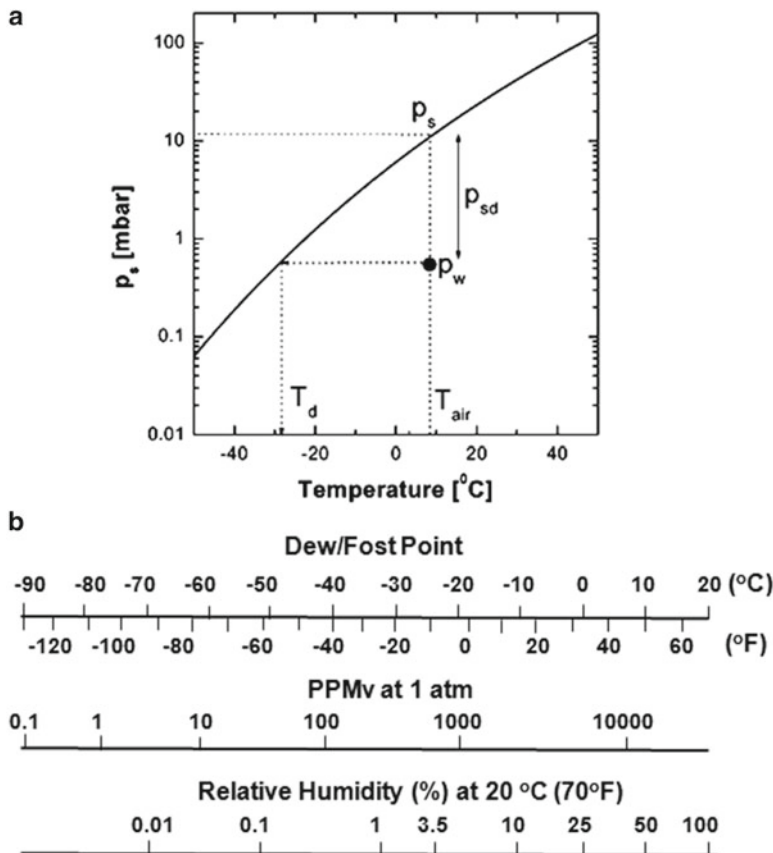


**Fig. 18.1** (a) Water saturation pressure vs temperature and (b) correlation among humidity units: relative humidity (RH), dew/frost point (D/F PT), and parts per million by volume fraction (ppmv) (Reprinted with permission from (a) Rittersma (2002) and (b) Chen and Lu (2005). Copyright 2002 and 2005 Elsevier)

(Hijikigawa et al. 1983; Rittersma 2002; Wang et al. 2005; Khanna 2012). These sensors have different humidity-sensing behaviors. In a quartz crystal microbalance (QCM) (Gerlach and Sager 1994) and SAW sensors (Hoyt et al. 1998) coated with a hygroscopic layer, the change of frequency caused by the mass change due to water adsorption acts as a measure of humidity. A number of publications on the relationship between polymers and their hygroscopic properties have been presented (Mercer and Goodman 1991; Sakai 1993; Lin et al. 1993). The resistance or impedance of the resistive-type sensor usually decreases as the relative humidity increases. As we discussed before (Chap. 2 (Vol. 1)), this effect has a strong influence on the operating characteristics of conductometric metal oxide and polymer gas sensors. In contrast, the capacitance of capacitive-type humidity sensor based on solid-state porous matrix increases with humidity. For polymer-based sensors, the direction of capacitance change depends on the principles of operation. One can find in Rittersma (2002) the principles of operation and constructions of capacitance sensors. Most humidity capacitance-type sensors based on porous materials operate because the relative electrical permittivity of sensitive layers undergoes a change upon exposure to a humid atmosphere. This effect takes place due to the adsorption of water molecules in its micropores (Kim et al. 2000). Due to the polar structure of the  $\text{H}_2\text{O}$  molecule, water exhibits a very high permittivity  $\epsilon_w = 80$  at room temperature. Dielectric materials have considerably smaller permittivity and, therefore, the permittivity of dielectric films shows a huge increase upon adsorption of water.

**Table 18.1** Kelvin radius at different RH

RH (%)	$r$ (nm)
11	0.4906 $x$
23	0.7369 $x$
33	1.095 $x$
43	1.283 $x$
52	1.656 $x$
67	2.704 $x$
75	3.764 $x$
86	7.180 $x$
97	35.55 $x$

*Source:* Reprinted from Chen et al. (2009). Published by MDPI

In addition to adsorption–chemisorption processes, capillary condensation phenomena are also involved when considering the fine structure of the porous matrix. According to the basic theory of adsorption on a porous matrix (Adamson and Gast 1997), when the vapor molecules are first physisorbed onto the porous material, capillary condensation will occur if the micropores are narrow enough. The critical size of pores for a capillary condensation effect is characterized by the Kelvin radius. In the case of water the condensation of vapor into the pores can be expressed by a simplified Kelvin equation (Ponec et al. 1974):

$$r_k = \frac{2\gamma V_M \cos\theta}{\rho RT \ln(\%RH/100)} \quad (18.1)$$

where  $\gamma$  is the surface tension of vapor in the liquid phase,  $V_M$  is molecular volume,  $\theta$  is contact angle, and  $\rho$  is the density of vapor in the liquid phase. In this equation, the thickness of the adsorbed layer has been ignored. While  $V_M$  and surface tension  $\gamma$  are constants at room temperature, the possibility of controlling the condensation by simply changing the contact angle  $\theta$  becomes attractive.

The values of Kelvin radius, calculated for water vapors in accordance with Eq. (18.1), are presented in Table 18.1. For these calculations, the following data and assumptions were used: the contact angle between the liquor and the wall of concave ( $\theta$ ) is constant; the  $V_L$  and  $\gamma$  are  $1.8 \times 10^{-2}$  L/mol and 72.8 mN/m (20 °C), respectively; the temperature ( $T$ ) is about 293 K; and  $x = \cos \theta$ . It is seen that the Kelvin radius increases with the relative humidity, and the rate of change (the slope) also increases with relative humidity. This means that the pores with smaller diameter are filled first, while bigger pores are filled later.

It should be noted that optical humidity sensors as a rule use similar effects, which were discussed above (Russell and Flecher 1985; Ballantine and Wohltjen 1986; Boltinghouse and Abel 1989; Wang et al. 1991; Kharaz and Jones 1995; Ando et al. 1996; Zhou et al. 1998; Skrdla et al. 1999; Alvarez-Herrero et al. 2004). The water adsorption in a porous matrix produces a variation in the optical response of the device, because the refractive index of the layer changes when the hydration of sensing material takes place and the pores are filled or emptied. The water adsorption isotherms and, therefore, the sensor response depend on the size and shape of the pores. One can find in Posch and Wolfbeis (1988), Otsuki and Adachi (1993), Papkovsky et al. (1994), Costa-Fernandez et al. (1997), Costa-Fernandez and Sanz-Medel (2000), Choi and Tse (1999), Choi and Shuang (2000), and Bedoya et al. (2001, 2006) a description of optical humidity sensors used and other principles.

Thus, the performance of a humidity sensor based on a porous sensing layer is determined by its nano- and microscopic dimensions, including pore size, thickness of the porous layer, size distribution of the surface structural unit, regularity of the surface morphology, and electrode distance (Kim et al. 2000; Di Francia et al. 2002). This fact indicates that the regularity and controllability of porous structures are of great importance in sensor applications. For example, due to water condensation in

nanosize pores, it is difficult to prepare rapid humidity sensors on the basis of nanoporous material (Bjorkqvist et al. 2004). Water transport in nanoporous material is described by Knudsen diffusion. Experiment has shown that the characteristics of humidity sensors are strongly affected by the hydrophilic/hydrophobic properties of the walls (Yarkin 2003). Based on the Kelvin equation, the Kelvin radius becomes smaller when the surface becomes more hydrophobic.

It should be noted that capacitive humidity sensors are often preferred for application because of their high sensitivity, linear output response, smaller temperature dependence, and lower power dissipation than other humidity sensors (Kang and Wise 2000). The capacitive sensors are characterized by higher stability as well. Most air pollutants, except some solvents (e.g., acetone, alcohol, benzene, and ethyl alcohol), have imperceptible effects on their performance (Dey and Munshi 2008). However, we have to note that, despite considerable research in the field of humidity sensor design, humidity sensors continue to suffer from slow response, low accuracy (% RH), and considerable long-term drift. A clear understanding of underlying physicochemical phenomena together with accurate modeling and simulation of humidity sensor characteristics is therefore still extremely important. One can find in review by Khanna (2012) a detailed description of humidity sensor operation and approaches to humidity sensor simulation.

## 18.2 Materials Acceptable for Application in Humidity Sensors

Experiment has shown that, while many materials are sensitive to humidity (Viviani et al. 2001; Chen and Lu 2005; Cao et al. 2011), reliable and repeatable application of these materials for monitoring humidity has been found to be extremely complicated. The humidity-sensing materials are roughly grouped under three headings: organic polymers, conductive metal oxides, and porous dielectric ceramics (Sakai et al. 1996; Chakraborty et al. 1999; Rittersma 2002; Chen and Lu 2005). Other materials such as porous silicon, porous SiC (Korotcenkov and Cho 2010a, b), and carbon nanotubes (Cao et al. 2011) can also be used. The most popular materials used for designing humidity sensors are listed in Table 18.2.

**Table 18.2** Materials tested as sensing layers in humidity sensors

Type of material (sensor type)	Examples
Polymers (resistance type)	Polyelectrolytes (quaternary ammonium salts, sulfonate salts, and phosphonium salts); KOH-H <sub>2</sub> O-doped PVA; poly( <i>p</i> -diethynylbenzene) or PDEB; poly(propargyl benzoate) (PPBT); <i>p</i> -diethynylbenzene- <i>co</i> -propargyl alcohol; ethynylbenzene- <i>co</i> -propargyl alcohol (copolymer); polymethyl methacrylate, etc.
Polymers (capacitance type)	Polyimides; polyethersulfone (PES); polysulfone (PSF); divinyl siloxane benzocyclobutene (BCB); cellulose acetate butyrate (CAB); hexamethyldisilazane (HMDSN); poly(methyl methacrylate) (PMMA); poly(vinyl cinnamate)
Conductive metal oxides (resistance type)	(Ionic): ZrO <sub>2</sub> ; ZnO-Y <sub>2</sub> O <sub>3</sub> ; TiO <sub>2</sub> -Bi <sub>2</sub> O <sub>3</sub> ; Mg-based ferrite; MgCr <sub>2</sub> O <sub>4</sub> ; BaSrTiO <sub>3</sub> ; BaMO <sub>3</sub> (with M = Ti, Zr, Hf, or Sn); MnWO <sub>4</sub> ; ZnCr <sub>2</sub> O <sub>4</sub> -LiZnVO <sub>4</sub> ; LiCl-doped MnWO <sub>4</sub> ; etc. (Electronic): SnO <sub>2</sub> ; ZnO; In <sub>2</sub> O <sub>3</sub> ; Fe <sub>2</sub> O <sub>3</sub> ; Sr <sub>1-x</sub> La <sub>x</sub> SnO <sub>3</sub> ; etc.
Porous dielectric ceramics (capacitance type)	Anodic Al <sub>2</sub> O <sub>3</sub> ; SiO <sub>2</sub>
Porous semiconductors (capacitance type)	Porous silicon; porous SiC; MnWO <sub>4</sub> ; WO <sub>3</sub>
Other materials	Multiwalled carbon nanotube (MWCNT); carbon nitride CN <sub>x</sub> ; phthalocyanines

PVA poly(vinyl alcohol)

### 18.2.1 Polymers

As indicated earlier, humidity sensors are usually developed using two approaches based on resistance and capacitance measurements. The ability of a porous polymer membrane to sense humidity is based on water adsorption. The presence of an adsorbed layer of water at the surface reduces the total sensor impedance due to the increase in the ionic conductivity and increases the capacitance due to the high dielectric constant of water. From general considerations, microporous hydrophilic polymers are the best material for application in resistance type humidity sensors (Yamazoe and Shimizu 1986; Casalbore-Micelia et al. 2005). Polyvinyl alcohol (PVA) is one such polymer which has an OH group at every other carbon in the backbone chain. A group of organic polymers, which have constituent ionic monomers such as sodium styrenesulfonate and exhibit ionic conductivity, are called polymer electrolytes. The ionic conductivity of such polymers increases with an increase in water adsorption due to increases in the ionic mobility and/or charge carrier concentrations. However, one of the serious shortcomings of hydrophilic polymers is that they are soluble in water, so they cannot be used at high humidities or in a place where dew may form (Sakai et al. 1996). For resolving this problem, the hydrophilic sites or hydrophilic polymers were introduced by graft polymerization or impregnation into hydrophobic polymers such as polyethylene. Random or block copolymerization can also be used. As a result, humidity sensors based on polyethylene film or a sintered alumina plate both impregnated with a hydrophilic polymer having a quaternary ammonium group or a sulfonate group such as poly(*N,N*-dimethyl-3,5-dimethylene) piperidium chloride or polystyrene sulfonate were designed (Sakai et al. 1996). Humidity sensors based on hydrophilic polymers such as poly-(2-acrylamido-2-methylpropane sulfonate) or poly-(2-hydroxy-3-methacryloxypropyl trimethylammonium chloride) grafted onto the surface of the pores of porous polyethylene and polytetrafluoroethylene (PTFE) films were also tested and shown to meet the parameters acceptable for real application (Sakai et al. 1986, 1996). These sensors, composed of modified porous polymer films, are resistive to water. They are even washable in water. Sakai et al. (1986) have shown that the grafted copolymer films are stable for long periods of time. Their characteristics as humidity sensors do not change even after the sensors have been immersed in water. One disadvantage of this type of sensor is the rather complicated chemical procedures for preparing the material. Wang et al. (1998) prepared films of differently modified polyvinyl alcohol (PVA) and phthalocyanine-silicon (bis-(dimethacryloxyethyl-amine-ethoxy)-(phthalocyanine)-silicon) and examined their impedance changes with changes in relative humidity. They established that the content of the hydrophilic group as well as its hydrophilicity really plays a crucial role in determining the response of the polymer film to relative humidity. A significant difference in sensing behavior was observed between molecular and ionic forms of TA film, namely, the molecular TA film showed almost no response while the ionic form TA film showed a large conductometric response to relative humidity.

The introduction of cross-linkers in polymers is another approach to stabilize polymers during their interaction with water (Sakai et al. 1996, 2000; Lee et al. 2004; Suna et al. 2010). In particular, using this approach, sensors based on either polyelectrolyte or doped acetylene-type polymers have been improved. The polymers mentioned above are not sufficiently resistive to water. The formation of cross-linked polymer networks on the surface of this type of substrate made the polymer coating insoluble in water but sensitive to humidity. The indicated approach was applied to poly(2-hydroxy-3-methacryloxypropyl-trimethyl ammonium chloride), organoalkoxysilanes [ $\text{RSi}(\text{OC}_2\text{H}_5)_3$ ] poly(vinylpyridine), and poly(chloromethyl styrene). In the case of poly(vinylpyridine) and poly(chloromethyl styrene), the degree of reaction should be as high as possible in order to reduce hysteresis. It was found that the cross-linking of poly(methyl methacrylate) (PMMA) also promoted the improvement of PMMA-based humidity sensors. Matsuguchi et al. (1991) observed the decrease of the hysteresis and the temperature coefficient. Durability in the presence of organic vapors was also much improved. The cross-linking of PMMA was carried out using divinylbenzene or ethylene glycol dimethacrylate.

**Fig. 18.2** The DC resistance measurements at 25 °C for various relative humidity values for devices fabricated on (1) polycarbonate, (2) cellulose acetate, and (3) nylon membranes, respectively (Reprinted with permission from Yang et al. (2006). Copyright 2006 Elsevier)

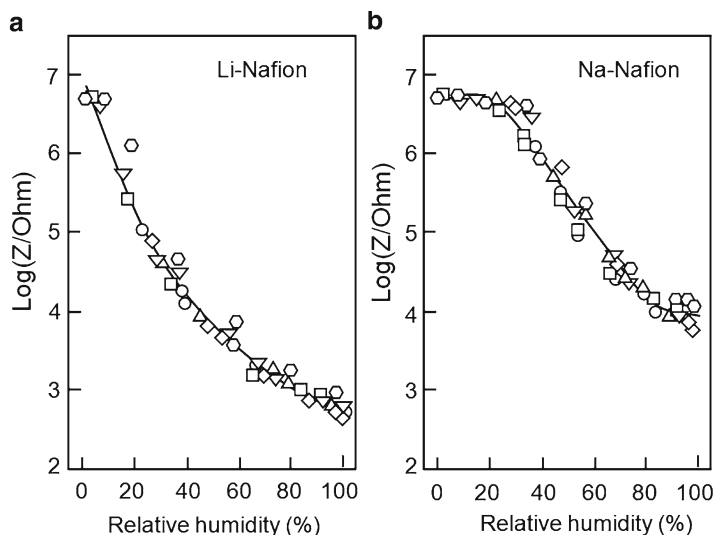
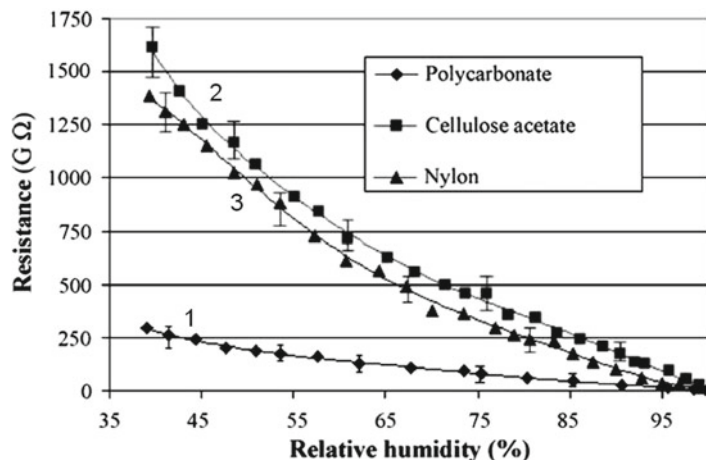
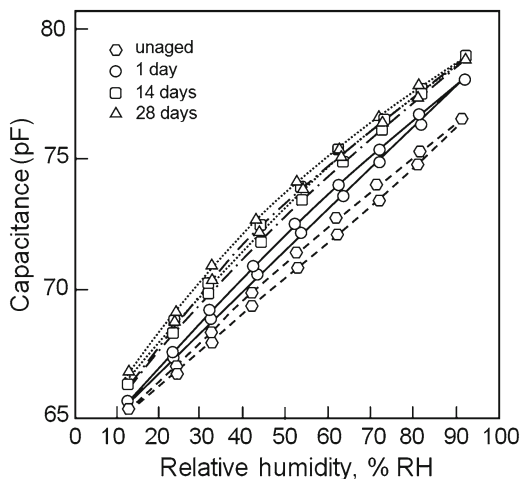


**Fig. 18.3** The relative humidity responses of (a) Li-Nafion and (b) Na-Nafion at different steps of the stability tests: *circles*—original untreated sample, immediately after preparation; *squares*—after treatment at 100 % RH for 3 days at room temperature; *triangles*—after immersion in water for 5 h at room temperature; *inverted triangles*—after heating at 120 °C for 2 h; *diamonds*—after heating at 100 °C and 100 % RH for 3 h; and *hexagons*—after treatment with C<sub>2</sub>H<sub>5</sub>OH/CH<sub>3</sub>OH water solution for 2 weeks (Reprinted with permission from Wang et al. (1998). Copyright 1998 Elsevier)

Yang et al. (2006) have shown that nanoporous polymer membranes of polycarbonate (PC), cellulose acetate (CA), and polyester (nylon) can also be used for humidity sensor design (see Fig. 18.2). There are also reports regarding humidity sensors based on poly(ethyleneterephthalate) (Meanna Perez and Freyre 1997), polyphosphazene (Anchisini et al. 1996), Nafion (Wang et al. 1998), and many other polymers. In particular, Wang et al. (1998) studied sulfonated tetrafluoroethylene-based fluoropolymer-copolymer (Nafion) in different ionic forms (H<sup>+</sup>, Li<sup>+</sup>, and Na<sup>+</sup>) and examined the impedance changes under influence on relative humidity. The comparison of operating properties of H-, Li-, and Na-Nafion film-based humidity sensors has shown that the Li-Nafion film exhibited the greatest sensitivity and stability (see Fig. 18.3). Moreover, it was established that Nafion-based films have good stability against various environments such as high temperature, high relative humidity, and alcohol vapor.

**Fig. 18.4** Capacitance vs RH of Kapton® HN-based humidity sensor in the unaged state and after aging for 1, 14, and 28 days at 85 °C/85 % RH (Reprinted with permission from Ralston et al. (1996). Copyright 1996 Elsevier)



Regarding the role of polymer type in sensor response, one can say that results depend on many factors and vary over a wide range. For example, according to Chatzandroulis et al. (2004), among poly(hydroxyethyl-methacrylate) (PHEMA), poly(methyl methacrylate) (PMMA), poly(vinyl acetate) (PVAc), epoxidized novolac (EPN), and polydimethylsiloxane (PDMS) layers, PHEMA presented the highest response to water vapor. This can be explained by the formation of hydrogen bonds between the OH group of PHEMA and water molecules. On the other hand, both PMMA and PVAc, lacking a high hydrogen-bonding capability, showed considerably lower sensitivity, whereas EPN and PDMS, being more hydrophobic, presented the lowest response to humidity.

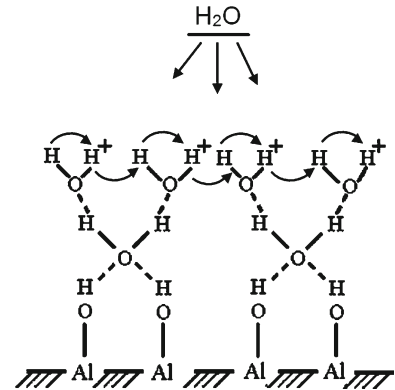
Various polyimides in the form of films and resins have been used extensively in relative humidity sensors of the capacitance type because of their toughness and thermal stability (Yamazoe and Shimizu 1986; Mercer and Goodman 1991; Kuroiwa et al. 1993). It is known that these polymers are insoluble in water. For example, Ralston et al. (1996) characterized the performance of 13 polyimide films in relative humidity-sensing applications. In Fig. 18.4 the hysteresis loop for the Kapton® HN-based sensor is shown as a typical example. The humidity-sensing characteristics of polyimide-based devices are excellent except for instability at high humidities and at high temperatures. Sakai et al. (1996) believed that these disadvantages arise for two reasons: (1) unreacted sites are likely to be present and (2) microvoids may arise from volatile by-products such as water. New designs based on polyimide oligomers improved parameters of sensors (Matsuguchi et al. 1993). It was established that these oligomers polymerize, forming cross-linking bonds, without evolving by-products. The cross-linking leads to a rigid hydrophobic film which does not contain microvoids and is chemically and thermally stable. As a result, improved polyimides have been successfully applied to Si chips as humidity-sensitive dielectrics with high mechanical strength, high temperature capability, and high resistance to chemical attack. The best sensors give an almost linear signal with relative humidity, and have hysteresis less than 1–3 %, and response times less than 10–30 s. Long-term stability and a good durability against high relative humidity (90–95 % RH) and dew condensation have also been claimed.

Experiment has shown that cellulose acetate (CA) or cellulose acetate butyrate (CAB) can also be used for these purposes (Sakai et al. 1996; Yang et al. 2006). However, many problems such as hysteresis, stability at high humidities and at high temperature, and durability on exposure to some kinds of organic vapors still remain to be solved. Sadaoka et al. (1988) also established that the hysteresis for the various cellulose derivatives-based sensors was caused by the formation of clusters of sorbed water molecules.

In general, polymers usually cannot withstand higher humidity levels and elevated temperatures for long periods (Yamazoe and Shimizu 1986; Arai and Seiyama 1991). Polymer humidity sensors



**Fig. 18.5** Schematic illustration of buildup of adsorbed water layers upon an alumina surface (idea from Fleming 1981)



can also show hysteresis or degradation upon exposure to some solvents or to electrical shocks. However, the response characteristics are more linear than those of porous ceramics. From a technological point of view, polymers have the great advantage that they can be added at the end of the fabrication sequence of a CMOS process.

Regarding response and recovery times of polymer-based humidity sensors, one can say that the porosity of the humidity-sensitive polymer is important to obtain quick responses, because the response and recovery times are determined by the time it takes for water vapor to diffuse into or out from a polymer film to reach an equilibrium (Yamazoe and Shimizu 1986). The polymer film should therefore be as thin as possible for quick response. Tsuchitani et al. (1985) believe that, besides the film thickness, an increase in hydrophobicity of the constituent ionic monomer appears to shorten the response time, while the mole fraction of the constituent ionic monomer to non-ionic monomer strongly affects the sensing characteristics.

### 18.2.2 Metal Oxide Ceramics

Porous metal oxides form another large group of materials acceptable for application in humidity sensors. It is well known that water molecules undergo chemisorption and physisorption on the surface of oxides (Thiel and Madey 1987; Henderson 2002; Traversa 1995). Chemisorption, which is the stronger process, causes dissociation of water molecules to form surface hydroxyls. After hydroxyl formation, the next water molecule will be physisorbed through hydrogen double bonds on the two neighboring hydroxyl groups, and a proton may be transferred from a hydroxyl group to the water molecule to form an H<sub>3</sub>O<sup>+</sup> ion. The water molecules in the first physisorbed layer cannot move or rotate freely. At higher humidity levels, each water molecule will be singly bonded to a hydroxyl group, as illustrated in Fig. 18.5, and proton hopping between adjacent water molecules in the continuous water layer takes place. Thus, the water molecules in the second and succeeding layers can rotate more freely, which is important for Grotthuss-type transport of protons. Grotthuss-type or “free-proton” mechanism is related to the transport of protons (H<sup>+</sup>) and any assembly that carries protons (OH<sup>-</sup>, H<sub>2</sub>O, H<sub>3</sub>O<sup>+</sup>, NH<sub>4</sub><sup>+</sup>, HS<sup>-</sup>, etc.) between relatively stationary host anions (Grotthuss 1806). The Grotthuss mechanism requires close proximity of water molecules, which are firmly held but able to rotate. In other words, from the second physisorbed layer, water molecules become mobile and finally almost identical to the bulk liquid water, and the Grotthuss mechanism becomes dominant. The conduction process in this case occurs by attachment of a proton to a water molecule, thereby forming a hydronium ion; the hydronium ion releases another proton to a second water molecule that accepts this proton while releasing a third proton, and so on through the liquid. Hence, the dominant

charge carrier in a high-moisture atmosphere is the  $H^+$  (proton). The concentration of  $H^+$  increases with increasing humidity, and it moves freely through the water-like layer. However, this mechanism indicates that sensors based purely on water-phase protonic conduction would not be quite as sensitive to low humidity, where the water vapor could rarely form continuous mobile layers on the sensor surface. We need to note that sensors based on the above-mentioned mechanism of conductivity can operate at low temperature ( $<100\text{ }^\circ\text{C}$ ) and are widely accepted for many ionic ceramics, also of the non-oxide type (Traversa 1995).

Transport by any other species is termed “vehicle mechanism.” Vehicle mechanism is most frequently encountered in aqueous solution and other liquid/melts. In solids, vehicle mechanism is usually restricted to materials with open structures (channels, layers) to allow passage of large ions and molecules. Compounds with less water would be expected to conduct by vehicle mechanism in which a nucleophilic group such as  $H_2O$  or  $NH_3$  acts as a proton carrier. The electron tunneling between donor water sites is also possible in humidity-sensitive materials (Yeh et al. 1989). The tunneling effect, along with the energy induced by the surface anions, enables electrons to hop along the surface that is covered by the immobile layers and therefore contributes to the conductivity. This mechanism can be used for explaining sensitivity to low humidity levels, at which there is no effective protonic conduction (Traversa 1995). The classification of proton conductors according to the preparation method, chemical composition, structural dimensionality, mechanism of conduction, etc., has been summarized in a comprehensive book on proton conductors (Colomban 1992).

In semiconducting metal oxides, the mechanism of sensitivity to humidity is different. It is known that water molecules act as an electron-donating gas on semiconductive oxides, causing the decrease of resistance of  $n$ -type oxides and increase of resistance of  $p$ -type oxides. In fact, semiconductor gas sensors, which are widely used to detect reducing gases, are known to suffer from interfering effects of water vapor under certain conditions (Barsan and Ionescu 1983). Because the conductivity is caused by the surface concentration of electrons, this sensing style is usually called “electronic type.” However, the water layer formed by the physical adsorption may be somewhat proton-conductive. Therefore, at room temperatures the conductivity of ceramic semiconducting materials is actually due to addition of both electrons and protons (ionic), unless at high temperatures ( $>100\text{ }^\circ\text{C}$ ) when moisture cannot effectively condense on the surface. At higher temperatures ( $T > 100\text{ }^\circ\text{C}$ ), chemisorption of water molecules is only responsible for changes in the electrical conductivity of ceramics.

To date a number of metal oxides have been tested (Gusmano et al. 1992; Ichinose 1993; Traversa and Bearzotti 1995; Vijayamohan et al. 1996; Dellwo et al. 1997; Xu et al. 1998; Neri et al. 1999; Thosko and Zvevditz 1999; Qu et al. 2000a; Chen and Lu 2005; Pandey and Tiwari 2010) (see Table 18.2). For example, Rezlescu et al. (2005) studied the microstructure and humidity sensitivity of four compositions of an Mg-based ferrite:  $MgFe_2O_4 + CaO$ ,  $Mg_{0.5}Cu_{0.5}Fe_{1.8}Ga_{0.2}O_4$ ,  $Mg_{0.5}Zn_{0.5}Fe_2O_4 + KCl$ , and  $MgMn_{0.2}Fe_{1.8}O_4$ . Ruther et al. (2000) analyzed humidity microsensors based on silica aerogel. Wang et al. (2005) fabricated humidity sensors from nanometer barium titanate powder,  $BaTiO_3$ . Qu and Meyer (1997) proposed a thick-film humidity sensor based on porous  $MnWO_4$  material. Jain et al. (1999) reported about  $ZrO_2$ - $TiO_2$ -based sensors with superior sensing properties compared to other materials.  $ZrO_2$ - $TiO_2$  is characterized by high mechanical strength, resistance to chemical attack, and thermal stability. Because of the immense surface-to-volume ratio and the abundant void fraction, very high sensitivities of the order of several thousand percent can be obtained with porous metal oxide ceramics. Generally, ceramic humidity sensors are more chemically and thermally stable than the polymeric types. Reviews of ceramics for humidity sensors have been presented by Seiyama et al. (1983), Traversa (1995), and Chen and Lu (2005).

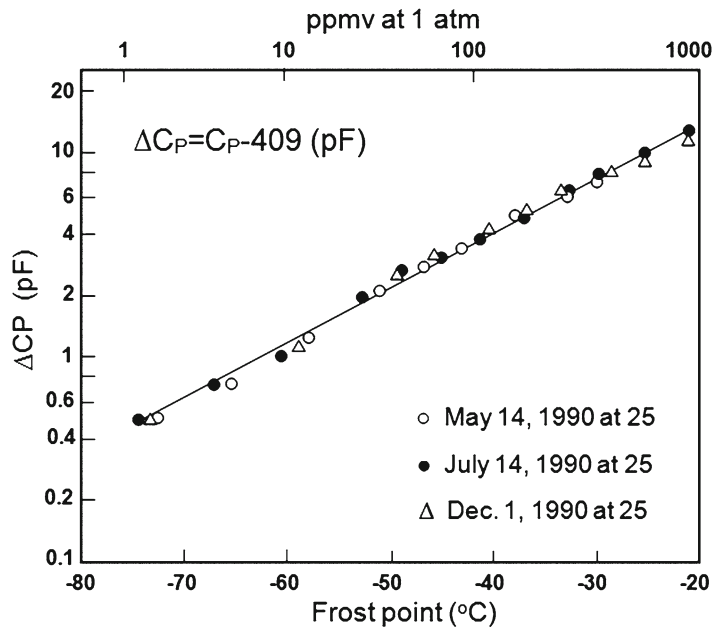
One of the first ceramics to be used in humidity capacitance-type sensors was porous  $Al_2O_3$ , obtained by electrochemical etching of aluminum under anodic bias. The first humidity-sensitive  $Al_2O_3$  layer formed through anodization on Al metal surface was reported in 1953.  $Al_2O_3$  exhibits a pore size distribution that depends on the etching parameters such as current density (Masuda et al. 1993). The material is today used in many commercial humidity sensors—on the one hand because

the etching technology is well established, and on the other because  $\text{Al}_2\text{O}_3$  has proved to be stable at elevated temperature and at high humidity level (Khanna and Nahar 1984; Sberveglieri et al. 1994, 1995; Nahar and Khanna 1998; Mai et al. 2000; Nahar 2000; Varghese and Grimes 2003; Cheng et al. 2011). Humidity sensors based on porous anodic aluminum oxide ( $\text{Al}_2\text{O}_3$ ) thin film exhibit high sensitivity and rapid response, and they are useful in a wide range of humidity detection scenarios (Nahar 2000). Sensor parameters of  $\text{Al}_2\text{O}_3$ -based devices (sensitivity, humidity range, response time, stability, etc.) strongly depend on the thickness and the density of the porous layer and size of the pores (Banerjee and Sengupta 2002; Varghese et al. 2002). For example, the response time of ceramic humidity sensors is generally limited by diffusion (Cunningham and Williams 1980; Seiyama et al. 1983). This means that the response and recovery times are controlled by pore size (Sun et al. 1989). It is also clear from the empirical point of view that, for design devices with highly humidity-sensitive properties over a wide range of humidity, it is necessary to use ceramics with a large pore volume and a wide dispersion of pore sizes from nano- to macropores (Traversa 1995). The diameters and depths of the pores can be controlled by the technological parameters such as concentration and temperature of the electrolyte and the current density in the anodizing cell. Therefore, the detection limit could be set very low by shrinking the pore size (the minimum detectable humidity decreases as the pore radius decreases). In particular, Chen et al. (1990) achieved sensitivity as low as 1 ppmv by optimizing pore size. Thus, control of microstructure of the film is again important for sensing characteristics, and the film preparation conditions should be carefully chosen. To obtain quick responses, the upper electrode should be as thin and porous as possible.

The primary problem of anodized amorphous  $\text{Al}_2\text{O}_3$ , discussed before, is that, when exposed for a long duration in high humidity, significant degradation in the sensitivity and drift in the capacitance characteristics would be expected (Chen and Lu 2005). There is a major drawback for aluminum oxide sensors – long-term calibration drift (Emmer et al. 1985). Nahar (2000) believed that this effect was caused by the widening of the pores due to diffusion of the adsorbed water. However, in other research it was found that the basic reason for long-term drift of sensors using porous anodic aluminum oxide films is related to the structure transformation of  $\text{Al}_2\text{O}_3$  during use. It was established that anodic aluminum oxide contains  $\alpha$ - $\text{Al}_2\text{O}_3$ ,  $\gamma$ - $\text{Al}_2\text{O}_3$ , and amorphous phases. The  $\alpha$ -phase of  $\text{Al}_2\text{O}_3$  is stable, while the  $\gamma$ -phase and amorphous  $\text{Al}_2\text{O}_3$  suffer from degradation. When the structure is exposed to a humid atmosphere, the  $\gamma$ -phase or amorphous  $\text{Al}_2\text{O}_3$  changes to  $\gamma$ - $\text{Al}_2\text{O}_3 \cdot \text{H}_2\text{O}$  (boehmite) (Young 1961). This irreversible phase change causes volume expansion of aluminum oxide, resulting in the gradual decrease of surface area and porosity (Emmer et al. 1985). Many researchers tried to improve the anodic aluminum oxide sensors by optimization of anodization process (Varghese et al. 2002; Varghese and Grimes 2003), aging the aluminum oxide in boiling water or macerating the films in some ion solutions (Emmer et al. 1985). Mai et al. (2000) proposed to use thermal annealing at about 400 °C. However, the drift cannot be completely eliminated. Even commercial aluminum oxide moisture sensors have to be calibrated twice a year to ensure their accuracy (Chen and Lu 2005). This problem seriously hinders the widespread use of aluminum oxide moisture sensors. Chen and Jin (1992) proposed other approaches to stability improvement. In order to overcome this difficulty, the  $\alpha$ - $\text{Al}_2\text{O}_3$  film was re-anodized in diluted sulfuric acid or borax solution for a short time to form a thin barrier layer. The fabricated sensors showed high sensitivity for moisture level from 1,000 to 1 ppmv or  $-20$  to  $-76$  °C dew/frost point (D/F PT) (see Fig. 18.6). The sensors also demonstrated excellent long-term stability. For more than 6 months there was no drift of data. The response was also very fast. From the low to the high moisture level, the response time is about 5 s and from the high to the low moisture level about 20 s. Therefore, the long-term calibration drift occurring in  $\gamma$ - $\text{Al}_2\text{O}_3$  film sensors was eliminated in the  $\alpha$ - $\text{Al}_2\text{O}_3$  film sensors.

It should be noted that other metal oxides used in humidity sensors did not show parameters comparable with parameters of  $\text{Al}_2\text{O}_3$ -based devices (Chen and Lu 2005). It was also found that metal oxide ceramics are highly sensitive to contaminants such as dust and smoke (Clayton et al. 1985; Nakajima et al. 1999). This means that they require maintenance, e.g., by heating them from time to

**Fig. 18.6** Operating characteristics of  $\alpha$ - $\text{Al}_2\text{O}_3$ -based capacitance humidity sensors during long-term stability test (Data from Chen and Jin 1992)



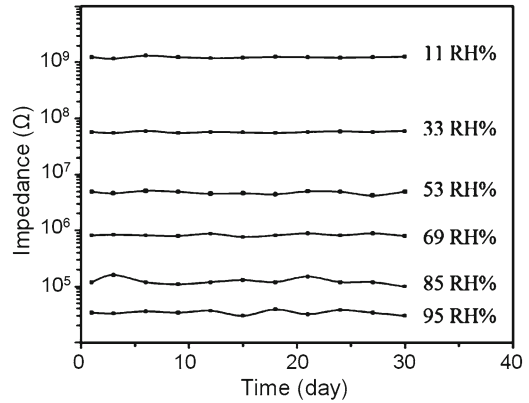
time and evaporating condensed vapor. Temporary heating could also be a solution for drift due to the formation of chemisorbed OH-groups. Visscher and Kornet (1994) found that capacitive sensors drifted to a higher output over a longer period. Ceramic humidity sensors with integrated refresh heaters have been presented by Kang and Wise (1999) and Qu and Meyer (1998). Here, the heater was placed on the backside of the sensor to optimize the chip size.

For application in resistive humidity sensors, things are not so clear regarding metal oxides (Traversa 1995). In the literature, one can find numerous pieces of research focused on finding appropriate conducting materials, which can be either ionic or electron conductors (She et al. 1994; Lee et al. 1994; Chakraborty 1995; Golonka et al. 1997; Chakraborty et al. 1998; Serin et al. 2000). Ying et al. (2000) investigated  $\text{TiO}_2$ - $\text{K}_2\text{O}$ - $\text{LiZnVO}_4$  in the range 10–99 % RH. Qu et al. (2000b) studied  $\text{Ba}_{1-x}\text{Sr}_x\text{TiO}_3$ . Feng et al. (1998) tested Nafion and Nafion/ $\text{SiO}_2$  composite films. Yagi and Ichikawa (1993) described humidity sensors with a  $\text{Y}_2\text{O}_3$ -doped  $\text{ZrO}_2$  electrolyte. Shimizu et al. (1985) reported on humidity sensors based on  $\text{MgAl}_2\text{O}_4$  and  $\text{MgFe}_2\text{O}_4$ . However, results presented in the literature do not make it easy to select the most acceptable metal oxide, because the unified basis for comparison is absent. Moreover, every developer believes that his material is better.

Research has shown that the conduction mechanism in ionic conductors at low relative humidity is usually related to the migration of the protons dissociated from the surface hydroxyl groups, while at higher relative humidity, Grotthuss-type proton conduction takes place through capillary-condensed water (Yamazoe and Shimizu 1986). Seiyama et al. (1983) established that the introduction of small amounts of alkali ions has a favorable effect on ceramic humidity sensors. The alkali ions added act as dominant charge carriers instead of protons and thus often endow the sensors with higher humidity sensitivity as well as base resistance stability. Recently, this approach was used by Songa et al. (2009) for  $\text{SnO}_2$ , by Qi et al. (2009) for  $\text{TiO}_2$ , and by Anbia and Fard (2011) for  $\text{Ti}_{0.9}\text{Sn}_{0.1}\text{O}_2$ -based humidity sensors and has shown that sensing characteristics can really be improved (see Fig. 18.7).

As has also been found in this type of ceramic sensor, the base resistance of the element gradually increases during operation (Yamazoe and Shimizu 1986). This drift seems to be related to the formation of stable chemisorbed OH-groups on the surface of metal oxides, which impede Grotthuss-type proton conduction. The presence of temporal drift is one of the main disadvantages of resistive humidity

**Fig. 18.7** Stability test of  $\text{Ti}_{0.9}\text{Sn}_{0.1}\text{O}_2$ -based humidity sensors doped by KCl (Reprinted with permission from Anbia and Fard (2011). Copyright 2011 Elsevier)



sensors, because the presence of the temporal drift requires periodical recalibration of the device. To overcome this unfavorable phenomenon, it was proposed to use heat cleaning at temperatures above 400 °C before each operation. Yagi and Nakata (1992) have shown that in many cases a once-a-day cycle of heat cleaning is enough for recovering the sensor's performance in a normal atmosphere. This allows long continuous measurement and provides a nearly maintenance-free ceramic humidity sensor with improved reliability and precision. The surface hydroxyl ions are removed by heating to temperatures higher than 400 °C (Morimoto et al. 1969; Egashira et al. 1978, 1981).

Moreover, humidity sensors are usually exposed to atmospheres that contain a number of impurities, such as dust, dirt, oil, smoke, alcohol, and solvents. The adhesion or adsorption of these compounds on the ceramic surface causes irreversible changes in the sensor's response. Contaminants act in the same way as chemisorbed water and may also be removed by heating. Commercial sensors based on ceramic-sensing elements were equipped with a heater for regeneration (Nitta 1981). The surface-related phenomena of humidity sensing by ceramics make these materials less resistant than polymers to surface contamination because of their porous structure. Nonlinear behavior of humidity-resistance characteristics is also a disadvantage of this type of humidity sensor (Traversa 1995). Another drawback of some resistive sensors is their significant temperature dependencies when installed in an environment with large (>10 °F) temperature fluctuations. This means that simultaneous temperature compensation is required for accuracy. Conductance-type sensors with integrated temperature compensation were presented by Wang et al. (1993) and Qu and Meyer (1997).

### 18.2.3 Porous Semiconductors (Silicon and Other)

The attractive properties of porous semiconductors, especially porous silicon, notably very large surface-to-volume ratio (typically > 500 m<sup>2</sup>/cm<sup>3</sup>), controllable structure through formation parameters, and CMOS compatibility, enable development of microminiaturized humidity sensors with improved sensitivity and reduced size. Porous silicon (PSi) is usually obtained by anodic or galvanic etching of silicon in hydrofluoric acid (Korotcenkov and Cho 2010b). Porous silicon-based humidity sensors operating on the capacitive principle have been demonstrated by a few authors (Connolly et al. 2002, 2004a; Fürjes et al. 2003; Xu et al. 2005; Islam et al. 2005; Islam and Saha 2006). One advantage of PSi as a sensor material is the possibility to integrate it with already existing silicon technology. In some applications, even a coarse control of operation environments, a simple and cheap humidity sensor is desirable (e.g., inside a mobile phone). Besides PSi-based devices, capacitance-type humidity sensors were also designed based on porous SiC (Connolly et al. 2002, 2004a).

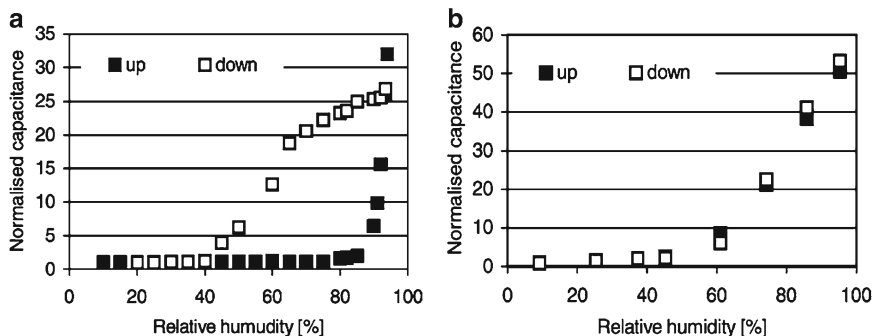


**Fig. 18.8** Hysteresis effect in as-prepared PSi-based humidity sensors (a) without any heating and (b) with refreshing before each measurement (20 s, 120 mW). Up and down indicate the direction of humidity change (Reprinted with permission from Fürjes et al. (2003). Copyright 2003 Elsevier)

However, research has shown that in most cases porous semiconductor-based humidity sensors in capacitance configuration operate efficiently only in the range of relative humidity higher than 10–20 % (Connolly et al. 2002, 2004a; Fürjes et al. 2003; Xu et al. 2005). Slow response, due to the limited mass transportation and capillary condensation, is another disadvantage of capacitance-type sensors (Connolly et al. 2004b). According to Connolly et al. (Connolly et al. 2002), even the fastest SiC-based humidity sensors have response times of about 120 s when the RH changed from 10 % to 90 %. As shown by Fürjes et al. (2003), excessive thickness of the PSi layer would make the absorption and desorption processes much more difficult and lead to a long response time. Therefore, the optimization of porous layer thickness is needed for achievement of optimal parameters of humidity sensors.

Poor linearity of operating characteristics can be added to the disadvantages of porous semiconductor-based RH sensors (see Fig. 18.8). Research carried out by O'Halloran et al. (1999) showed that this parameter of humidity sensors can be improved by changing the current density used to form the porous layer. It has been shown that it is possible to form a device that is linear over the humidity range 10–90 % RH. However, porous silicon layers formed at such low current density values show a long response time and poor sensitivity in comparison to layers formed using higher values of current density.

Large hysteresis is also a common problem in humidity sensing based on adsorption (see Fig. 18.8a). Bjorkqvist et al. (2004) established that the hysteresis is related to the size and geometry of the pores and how the presence of moisture changes this geometry. Widening of the pore size in PSi structures might solve the hysteresis problem. For example, a TC-PSi humidity sensor with larger pores designed by Bjorkqvist et al. (2006) showed only slight hysteresis above 75 % RH. In addition, larger pores should reduce the response time. Unfortunately, the increase of pore size also reduces the sensitivity. Because of that, the pore size in the range 2–10 nm is optimal for effective humidity sensing in the low RH range, whereas material with larger (20–100 nm) pores is more preferable for the design of humidity sensors for high RH values (Seiyama et al. 1983; Connolly et al. 2002).

It follows from the above that humidity sensors based on PSi have disadvantages that can restrain their commercialization (Connolly et al. 2004b). However, research carried out during recent years has shown that the operating parameters of PS-based humidity sensors can be considerably improved. For example, Xu et al. (2005) showed that for PS-based humidity sensors prepared by hydrothermal etching, when the RH changed from 11 % to 95 %, the capacitance showed an increase over 1,500 % at a frequency of 100 Hz. Only about 15 and 5 s were needed for the capacitance to reach 90 % of its final/initial values during an RH-increasing process and an RH-decreasing process, respectively. For hydrothermal etching, samples are usually placed in a closed stainless steel tank, which makes it possible to carry out treatments for a long time at high temperature without loss of etchant.

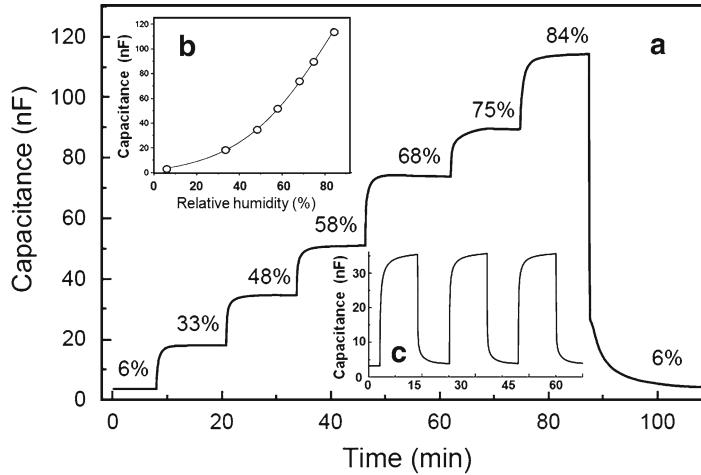


**Fig. 18.9** (a) Dynamic response of the capacitance of a TC-PSi humidity sensor. Electrical parameters were measured using 85 Hz frequency. (b) Dependence of the capacitance on relative humidity measured using 85 Hz frequency. (c) Repeatability of a TC-PSi humidity sensor. Relative humidity is changed between 6 and 58 %. Capacitance was measured using 120 Hz frequency (Reprinted with permission from Bjorkqvist et al. (2004). Copyright 2004 Elsevier)

Xu et al. (2005) believed that the fast response to humidity of Si-NPPA sensors might be due to the regular morphology and suitable thickness of the sensing layer.

Carbonization of the PSi surface is another promising approach to optimization of humidity sensors. The long-term stability studies of differently stabilized PSi samples have shown that the thermal carbonization (TC) of PSi is an even more efficient stabilizing method than thermal oxidation (Bjorkqvist et al. 2006). Thermal carbonization is a stabilizing method that exploits the dissociation of acetylene at high temperatures (Salonen et al. 2002). A thermally carbonized PSi surface has been found to be stable in humid air and even in harsh environments. This treatment also changes the originally hydrophobic PSi surface to hydrophilic, thus improving its humidity-sensing properties. Moreover, the sensitivity of TC-PSi is presumably better due to its larger specific surface area. A recent report on a TC-PSi humidity sensor showed good sensitivity (see Fig. 18.9a) and repeatability of the sensor (Fig. 18.9c) but also inappropriate hysteresis (Bjorkqvist et al. 2004).

Another method contributing to the improvement of PSi-based humidity sensors' parameters was proposed by Allongue et al. (1997) and Bjorkqvist et al. (2006). It was found that both sensitivity and recovery time extremes may be improved through annealing of PSi structures at 200 °C. It was established that the continuous heating reduced the hysteresis drastically but also decreased the sensitivity. With periodical refreshing, the sensitivity was nearly the same as without heating, but the hysteresis was negligible. This means that the application of chemical sensor refreshing before every measuring step is highly recommended. Investigations have shown that the application of internal heating filaments allowed a more rapid reaching of the desired temperature values around the active part of the chip than for heaters placed outside of the porous silicon structure (Fürjes et al. 2003) (see Fig. 18.8b). The humidity sensors realized in the frame of the proposed approach usually consist of three parts (Rittersma et al. 2000): (1) a humidity-sensitive capacitor with a PSi dielectric, (2) two integrated thermoresistors, and (3) a refresh resistor. The capacitor is formed between a meshed top electrode and a low-ohmic backside of the sensor.

It should be noted that in each case mentioned, reduced hysteresis is mostly based on a smaller amount of condensed water (Bjorkqvist et al. 2006). In a capacitive-type sensor, this also means lower

sensitivity. However, the sensitivity of the PSi humidity sensor even after the proposed modifications is still adequate for accurate humidity measurements.

In closing it is necessary to say that, in spite of the progress achieved in the development of PSi humidity sensors, commercial devices utilize either porous metal oxides ( $\text{Al}_2\text{O}_3$ ,  $\text{TiO}_2$ , etc.) or polymer films to detect humidity. A good humidity sensor has to fulfill several requirements, such as high sensitivity over a wide range of humidity, short response time, small hysteresis, and especially good long-term stability. As indicated before, these are difficult to meet concurrently for PSi-based devices (Bjorkqvist et al. 2004). When ease of manufacture and low cost are added to the list, the situation becomes even more complicated.

### 18.2.4 Other Materials and Approaches

LiCl was the first electrolyte used for fabrication of humidity sensors. This device, the Dunmore- or LiCl dew point sensor, was invented in 1938, named after its inventor (Dunmore 1938), and was used for over 40 years, being the only electrical moisture-sensing device available at the time. This device operates on the principle that lithium chloride solution immersed in a porous binder changes its ionic conductivity depending on the relative humidity of the surrounding atmospheric air. The device is integrated with a heater and a temperature sensor, which are connected to a control circuit to keep the vapor pressure of the saturated LiCl solution equal to the vapor pressure of the atmosphere. The humidity measurement is achieved by measurement of the dew point temperature. Several efforts have been made to improve this device, e.g., by measuring the conductance with a pair of interdigital electrodes of noble metals (Dunmore 1939; Mathews 1963). A wide relative humidity range of 10–100 % can be measured using this device. These sensors show rather slow responses to humidity but a fairly good stability and have been widely used in radiosonde circuits as well as in instruments for medical services. However, their use in very humid environments should be avoided so as not to lower the accuracy and lifetime. The major advantage of this sensor is that it is suitable for batch fabrication. However, it requires regular maintenance of the LiCl solution to guarantee the stable operation of the device, which is an important disadvantage (Yamazoe and Shimizu 1986).

Regarding other materials acceptable for application in humidity sensors, during the last few decades a number of materials were tested as sensing layer for humidity sensors. For example, Cao et al. (2011) showed that in the 11–98 % relative humidity (RH) range, the resistances of chemically treated and untreated multi-wall carbon nanotube (MWCNT)-based humidity sensors increased by 120 % and 28 %, respectively. Tao et al. (2009) proposed capacitive humidity sensors based on another type of nanomaterial, Ni/Si nanowire composites. The evaluation showed that the lack of Ni causes much smaller responses compared to the Ni-coated SiNWs. In the particular case of 500 °C annealing of the Ni/SiNWs, the response recording was close to one order of magnitude higher than the response of the uncoated SiNWs. It was concluded that the humidity sensor based on as-synthesized nanocomposites exhibited high sensitivity and fast response time due to its unique large surface-to-volume ratio and electrical properties.

Řeboun and Hamáček (2008) established that organic semiconductors such as phthalocyanines can also be used for humidity sensor design. Phthalocyanines are stable up to temperatures around 400 °C and have high sensitivity to humidity and gases (Snow and Barger 1989). However, it was found that the phthalocyanine films after a lengthy humidity exposure (RH ~90 %) are close to quasi-liquid phase and they are spread on the electrode system and can be washed out from the substrate. To achieve the appropriate stability of the organic film, Řeboun and Hamáček (2008) proposed to mix water-soluble phthalocyanines with an acrylate resin. They found that with the concentration of acrylate resin in phthalocyanine 1:3 or higher, the long-term stability of electrical parameters is sufficient for humidity changes detection in the range from 20 % to 90 %.



Research has shown that zeolites (Neumeier et al. 2008) and mesoporous silica (Wagner et al. 2011) are also promising materials for incorporation in humidity sensors. Sensors based on the indicated materials are capable of detecting traces of humidity in processes where high temperatures are required.

## References

- Adamson AW, Gast AP (1997) Physical chemistry of surface. Wiley, New York
- Allongue P, de Villeneuve CH, Bernard MC, Peo JE, Boutry-Forveille A, Levy-Clement C (1997) Relationship between porous silicon formation and hydrogen incorporation. *Thin Solid Films* 297:1–4
- Alvarez-Herrero A, Guerrero H, Levy D (2004) High-sensitivity sensor of low relative humidity based on overlay on side-polished fibers. *IEEE Sens J* 4(1):52–56
- Amin MN, Hossain MA, Roy KC (2004) Effects of moisture content on some physical properties of lentil seeds. *J Food Eng* 65(1):83–87
- Anbia M, Fard SEM (2011) Improving humidity sensing properties of nanoporous TiO<sub>2</sub>-10 mol % SnO<sub>2</sub> thin film by co-doping with La<sup>+</sup> and K<sup>+</sup>. *Sens Actuators B* 160:215–221
- Anchisini R, Faglia G, Gallazzi MC, Sberveglieri G, Zerbi G (1996) Polyphosphazene membrane as a very sensitive resistive and capacitive humidity sensor. *Sens Actuators B* 35(36):99–102
- Ando M, Kobayashi T, Haruta M (1996) Humidity-sensitive optical absorption of Co<sub>3</sub>O<sub>4</sub> film. *Sens Actuators B* 32:157–160
- Arai H, Seiyama T (1991) Humidity control. In: Gopel W, Hesse J, Zemel JN (eds) *Sensors, a comprehensive survey*, vol 3, part II. VCH, Weinheim, pp 981–1012
- Ballantine DS, Wohltjen H (1986) Optical waveguide humidity detector. *Anal Chem* 58:2883–2885
- Banerjee G, Sengupta K (2002) Pore size optimisation of humidity sensor – a probabilistic approach. *Sens Actuators B* 86:34–41
- Barsan N, Ionescu R (1983) The mechanism of the interaction between CO and an SnO<sub>2</sub> surface: the role of water vapour. *Sens Actuators B* 12:71–75
- Bedoya M, Orellana G, Moreno-Bondi MC (2001) Fluorescence optosensor for humidity measurement in air. *Helv Chim Acta* 84:2628–2639
- Bedoya M, Diez MT, Moreno-Bondi M, Orellana G (2006) Humidity sensing with a luminescent Ru(II) complex and phase-sensitive detection. *Sens Actuators B* 113:573–581
- Bjorkqvist M, Salonen J, Paski J, Laine E (2004) Characterization of thermally carbonized porous silicon humidity sensor. *Sens Actuators A* 112:244–247
- Bjorkqvist M, Paski J, Salonen J, Lehto V-P (2006) Studies on hysteresis reduction in thermally carbonized porous silicon humidity sensor. *IEEE Sens J* 6(3):542–547
- Boltinghouse F, Abel K (1989) Development of an optical relative humidity sensor: cobalt chloride optical absorbency sensor study. *Anal Chem* 61:1863–1866
- Cao CL, Hu CG, Fang L, Wang SX, Tian YS, Pan CY (2011) Humidity sensor based on multi-walled carbon nanotube thin films. *J Nanomater* 2011:707303
- Casalbore-Micelia G, Camaioni N, Li Y, Martelli A, Yang M-J, Zanelli A (2005) Water sorption in polymer electrolytes: kinetics of the conductance variation. *Sens Actuators B* 105:351–359
- Chakraborty S (1995) The humidity dependent conductance of Al<sub>2</sub>(SO<sub>4</sub>)·16H<sub>2</sub>O. *Smart Mater Struct* 4:368–369
- Chakraborty S, Nemoto K, Hara K, Lai PT (1998) Humidity sensors using a mixture of ammonium paratungstate pentahydrate and aluminium sulphate. *Smart Mater Struct* 7:569–571
- Chakraborty S, Nemoto K, Hara K, Lai PT (1999) Moisture sensitive field effect transistors using SiO<sub>2</sub>/Si<sub>3</sub>N<sub>4</sub>/Al<sub>2</sub>O<sub>3</sub> gate structure. *Smart Mater Struct* 8:274–277
- Chatzandroulis S, Tegou E, Goustouridis D, Polymenakos S, Tsoukalas D (2004) Capacitive-type chemical sensors using thin silicon-polymer bimorph membranes. *Sens Actuators B* 103:392–396
- Chen Z, Jin M-C (1992) An alpha-alumina moisture sensor for relative and absolute humidity measurement. In: *Proceedings of the 27th annual conference of IEEE Industry Application Society, Houston, TX*, vol 2, pp 1668–1675
- Chen Z, Lu C (2005) Humidity sensors: a review of materials and mechanisms. *Sens Lett* 3(4):274–295
- Chen Z, Jin M-C, Zhen C (1990) Humidity sensors with reactively evaporated Al<sub>2</sub>O<sub>3</sub> films as porous dielectrics. *Sens Actuators B* 2:167–171
- Chen W-P, Zhao Z-G, Liu X-W, Zhang Z-X, Suo C-G (2009) A capacitive humidity sensor based on multi-wall carbon nanotubes (MWCNTs). *Sensors* 9:7431–7444
- Cheng B, Tian B, Xie C, Xiao Y, Lei S (2011) Highly sensitive humidity sensor based on amorphous Al<sub>2</sub>O<sub>3</sub> nanotubes. *J Mater Chem* 21:1907–1912

- Choi MMF, Shuang S (2000) Fluorescent optode membrane based on organogel for humidity sensing. *Analyst* 125:301–305
- Choi MMF, Tse OL (1999) Humidity-sensitive optode membrane based on a fluorescent dye immobilized in gelatin film. *Anal Chim Acta* 378:127–134
- Clayton WA, Preud PJ, Baxter RD (1985) Contamination resistant capacitive humidity sensor. In: Proceedings of the conference on humidity and moisture, Washington, DC, pp 535–544
- Colomban P (ed) (1992) Proton conductors. Cambridge University Press, New York
- Connolly EJ, O'Halloran GM, Pham HTM, Sarro PM, French PJ (2002) Comparison of porous silicon, porous polysilicon and porous silicon carbide as materials for humidity sensing applications. *Sens Actuators B* 99:25–30
- Connolly EJ, Pham HTM, Groeneweg J, Sarro PM, French PJ (2004a) Relative humidity sensors using porous SiC membranes and Al electrodes. *Sens Actuators B* 100:216–220
- Connolly EJ, Timmer B, Pham HTM, Groeneweg J, Sarro PM, Olthuis W, French PJ (2004b) Porous SiC as an ammonia sensor. In: Proceedings of IEEE sensors conference, vol 1, article M2P-P.21, pp 178–181
- Costa-Fernandez JM, Sanz-Medel A (2000) Air moisture sensing materials based on the room temperature phosphorescence quenching of immobilized mercurochrome. *Anal Chim Acta* 407:61–69
- Costa-Fernandez JM, Diaz-Garcia ME, Sanz-Medel A (1997) A critical comparison of different solid supports to develop room-temperature phosphorescence sensing phases of air moisture. *Sens Actuators B* 38–39:103–109
- Cunningham RE, Williams RJJ (1980) Diffusion in gases and porous media. Plenum, New York
- Dellwo U, Keller P, Meyer J-U (1997) Fabrication and analysis of a thick-film humidity sensor based on  $\text{MnWO}_4$ . *Sens Actuators A* 61:298–302
- Dey D, Munshi S (2008) An artificial neural network based system for measurement of humidity and temperature using capacitive humidity sensor and thermistor. *Sens Transducers J* 97(10):1–10
- Di Francia G, Noce MD, Ferrara VL, Lancellotti L, Morvillo P, Quercia L (2002) Nanostructured porous silicon for gas sensor application. *Mater Sci Technol* 18:767–771
- Dunmore FW (1938) An electrometer and its application to radio meteorography. *J Res Nat Bur Stand* 20:723–744
- Dunmore FW (1939) An improved electric hygrometer. *J Res Nat Bur Stand* 23:701–714
- Egashira M, Kawasumi S, Kagawa S, Seiyama T (1978) Temperature programmed desorption study of water adsorbed on metal oxides. I. *Bull Chem Soc Jpn* 51:3144–3149
- Egashira M, Nakashima M, Kawasumi S, Seiyama T (1981) Temperature programmed desorption study of water adsorbed on metal oxides. 2. Tin oxide surfaces. *Z Phys Chem* 85:4125–4130
- Emmer I, Hajek Z, Repa P (1985) Surface adsorption of water vapour on hydrated layers of  $\text{Al}_2\text{O}_3$ . *Surf Sci* 162:303–309
- Feng CD, Sun SL, Wang H, Segre CU, Stetter JR (1998) Humidity sensitive properties of Nafion® and sol-gel derived  $\text{SiO}_2$ /Nafion composite thin films. *Sens Actuators B* 40:217–222
- Fitzpatrick S, McCabe JF, Petts CR, Booth SW (2002) Effect of moisture on polyvinylpyrrolidone in accelerated stability testing. *Int J Pharm* 246(1–2):143–151
- Fleming WJ (1981) A physical understanding of solid state humidity sensors. *Soc Automot Eng Trans Section 2*, 90:1656–1667
- Fraden J (2010) Handbook of modern sensors: physics, designs, and applications. Springer, New York
- Fürjes P, Kovács A, Cs D, Ádám M, Müller B, Mescheder U (2003) Porous silicon-based humidity sensor with interdigital electrodes and internal heaters. *Sens Actuators B* 95:140–144
- Gerlach G, Sager K (1994) A piezoresistive humidity sensor. *Sens Actuators A* 43:181–184
- Golonka LJ, Licznarski BW, Nitsch K, Terycz H (1997) Thick-film humidity sensors. *Meas Sci Technol* 8:92–98
- Grothuss CJD (1806) Sur la décomposition de l'eau et des corps qu'elle tient en dissolution à l'aide de l'électricité galvanique. *Ann Chim (Paris)* 58:54–73
- Gusmano G, Montesperelli G, Traversa E, Bearzotti A, Petrocco G, D'Amico A, Di Natale C (1992) Magnesium aluminium spinel thin film as a humidity sensor. *Sens Actuators B* 7:460–463
- Henderson MA (2002) The interaction of water with solid surfaces: fundamental aspects revisited. *Surf Sci Rep* 46:1–308
- Hijikigawa M, Miyoshi S, Sugihara T, Jinda A (1983) A thin-film resistance humidity sensor. *Sens Actuators* 4:307–315
- Hoyt AE, Ricco AJ, Bartholomew JW, Osbourn GC (1998) SAW sensors for the room-temperature measurement of  $\text{CO}_2$  and relative humidity. *Anal Chem* 70:2137–2145
- Ichinose N (1993) Humidity sensitive characteristics of the  $\text{MO-WO}_3$  (M = Mg, Zn, Ni, Mn) system. *Sens Actuators B* 13(14):100–103
- Islam T, Saha H (2006) Modeling of an aged porous silicon humidity sensor using ANN technique. *Sens Transducers J* 72(10):731–739
- Islam T, Pramanik C, Saha H (2005) Modeling, simulation and temperature compensation of porous polysilicon capacitive humidity sensor using ANN technique. *Microelectron Reliab* 45:697–703

- Jain MK, Bhatnagar MC, Sharma GL (1999) Effect of Li<sup>+</sup> doping on ZrO<sub>2</sub>-TiO<sub>2</sub> humidity sensor. *Sens Actuators B* 55:180–185
- Kang U, Wise KD (1999) A robust high-speed capacitive humidity sensor integrated on a polysilicon heater. In: *Proceedings of Transducers'99*, Sendai, Japan, pp 1674–1677
- Kang U, Wise KD (2000) A high-speed capacitive humidity sensor with on-chip thermal reset. *IEEE Trans Electron Dev* 47(4):702–710
- Khanna VK (2012) Detection mechanisms and physico-chemical models of solid-state humidity sensors. In: Korotcenkov G (ed) *Chemical sensors: simulation and modelling*, Vol. 3: Solid state devices. Momentum, New York
- Khanna VK, Nahar RK (1984) Effect of moisture on the dielectric properties of porous alumina films. *Sens Actuators* 5:187–198
- Kharaz A, Jones BE (1995) A distributed optical fibre sensing system for multipoint humidity measurements. *Sens Actuators A* 46–47:491–493
- Kim SJ, Park JY, Lee SH, Yi SH (2000) Humidity sensors using porous silicon layer with mesa structure. *J Phys Appl Phys* 33:1781–1784
- Korotcenkov G, Cho BK (2010a) Porous semiconductors: advanced material for gas sensor applications. *Crit Rev Solid State Mater Sci* 35(1):1–37
- Korotcenkov G, Cho BK (2010b) Silicon porosification: state of the art. *Crit Rev Solid State Mater Sci* 35(3):153–260
- Kuroiwa T, Hayashi T, Ito A, Matsuguchi M, Sadaoka Y, Sakai Y (1993) A thin film polyimide based capacitive type relative humidity sensor. *Sens Actuators B* 13(14):89–91
- Lee D, Yuk J, Lee N, Uchino K (1994) Humidity-sensitive properties of Nb<sub>2</sub>O<sub>5</sub>-doped Pb(Zr, Ti)O<sub>3</sub>. *Sens Mater* 5(4):231–240
- Lee C-W, Choib B-K, Gong M-S (2004) Humidity sensitive properties of alkoxy silane-crosslinked polyelectrolyte using sol-gel process. *Analyst* 129(7):651–656
- Lin J, Heurich M, Obermeier E (1993) Manufacture and examination of various spin-on glass films with respect to their humidity-sensitive properties. *Sens Actuators B* 13(14):104–106
- Liu YJ, Shi J, Zhang F, Liang H, Xu J, Lakhtakia A, Fonash SJ, Huang TJ (2011) High-speed optical humidity sensors based on chiral sculptured thin films. *Sens Actuators B* 156:593–598
- Mai LH, Hoa PTM, Binh NT, Ha NTT, An DK (2000) Some investigation results of the instability of humidity sensors based on alumina and porous silicon materials. *Sens Actuators B* 66:63–65
- Masuda H, Nishio K, Baba N (1993) Fabrication of a one-dimensional microhole array by anodic oxidation of aluminium. *Appl Phys Lett* 63:3155–3157
- Mathews DA (1963) Review of the lithium chloride radiosonde hygrometer. In: *Proceedings of the conference on humidity and moisture*, vol VI, Washington, DC, pp 219–227
- Matsuguchi M, Sadaoka Y, Sakai Y, Kuroiwa T, Ito A (1991) A capacitive-type humidity sensor using cross-linked poly(methylmethacrylate) thin films. *J Electrochem Soc* 138:1862–1865
- Matsuguchi M, Sadaoka Y, Nosaka K, Ishibashi M, Sakai Y, Kuroiwa T, Ito A (1993) Effect of sorbed water on the dielectric properties of acetylene-terminated polyimide resins and their application to a humidity sensor. *J Electrochem Soc* 140:825–829
- Meanna Perez JM, Freyre C (1997) A poly(ethyleneterephthalate)-based humidity sensor. *Sens Actuators B* 42:27–30
- Mercer FW, Goodman TD (1991) Effect of structural features and humidity on the dielectric constant of polyimides. *High Perform Polym* 3(4):297–310
- Morimoto T, Nagao M, Fukuda F (1969) The relation between the amounts of chemisorbed and physisorbed water on metal oxides. *J Phys Chem* 73:243–248
- Nahar RK (2000) Study of the performance degradation of thin film aluminum oxide sensor at high humidity. *Sens Actuators B* 63:49–54
- Nahar RK, Khanna VK (1998) Ionic doping and inversion of the characteristic thin film porous Al<sub>2</sub>O<sub>3</sub> humidity sensor. *Sens Actuators B* 46:35–41
- Nakajima A, Miazusawa Y, Yokoyama T, Chakraborty S, Hara K (1999) Highly durable humidity sensor fabricated on a sapphire substrate. In: *Proceedings of Transducers'99*, Sendai, Japan, pp 1672–1673
- Neri G, Bonavita A, Pace C, Patane S, Arena A, Allegrini M, Galvagno S (1999) Iron oxide-based thin films for humidity sensors. In: *Proceedings of Eurosensors XIII*, Hague, The Netherlands, 12–15 September, pp 149–152
- Neumeier S, Echterhof T, Bolling R, Pfeifer H, Simon U (2008) Zeolite based trace humidity sensor for high temperature applications in hydrogen atmosphere. *Sens Actuators B* 134:171–174
- Nitta T (1981) Ceramic humidity sensor. *Ind Eng Chem Prod Res Dev* 20:669–674
- O'Halloran GM, van der Vlist W, Sarro PM, French PJ (1999) Influence of the formation parameters on the humidity sensing characteristics of a capacitive humidity sensor based on porous silicon. In: *CD proceedings of the 13th European conference on solid-state transducers, EUROSENSORS XIII*, The Hague, September 12–15, pp 117–120
- Otsuki S, Adachi K (1993) Effect of humidity on the fluorescence properties of a medium-sensitive fluorophore in a hydrophilic polymer film. *J Photochem Photobiol A Chem* 71:169–173

- Pandey NK, Tiwari K (2010) Morphological and relative humidity sensing properties of pure ZnO nanomaterial. *Sens Transducers* 122(11):9–19
- Papkovsky DB, Ponomarev GV, Chernov SF, Ovchinnikov AN, Kurochkin IN (1994) Luminescence lifetime-based sensor for relative air humidity. *Sens Actuators B* 22:57–61
- Patissier B (1999) Humidity sensors for automotive, appliances and consumer applications. *Sens Actuators B* 59: 231–234
- Ponec V, Knor Z, Cerný S (1974) Adsorption on solids. Butterworth, London, p 405
- Posch H, Wolfbeis OS (1988) Optical sensors. Part 13: fiber-optic humidity sensor based on fluorescence quenching. *Sens Actuators* 15:77–83
- Prowse MS, Wilkinson M, Puthoff JB, Mayer G, Autumn K (2011) Effects of humidity on the mechanical properties of gecko setae. *Acta Biomater* 7(2):733–738
- Qi Q, Fenga Y, Zhanga T, Zheng X, Lu G (2009) Influence of crystallographic structure on the humidity sensing properties of KCl-doped TiO<sub>2</sub> nanofibers. *Sens Actuators B* 139:611–617
- Qu W, Meyer J-U (1997) Thick-film humidity sensor based on porous MnWO<sub>4</sub> material. *Meas Sci Technol* 8:593–600
- Qu W, Meyer JU (1998) A novel thick-film ceramic humidity sensor. *Sens Actuators B* 40:175–182
- Qu W, Wlodarski W, Meyer JU (2000a) Comparative study on micromorphology and humidity sensitive properties of thin-film and thick-film humidity sensors based on semiconducting MnWO<sub>4</sub>. *Sens Actuators B* 64:76–82
- Qu W, Green R, Austin M (2000b) Development of multi-functional sensors in thick-film and thin-film technology. *Meas Sci Technol* 11:1111–1118
- Ralston ARK, Klein CF, Thoma PE, Denton DD (1996) A model for the relative environmental stability of a series of polyimide capacitance humidity sensors. *Sens Actuators B* 34:343–348
- eboun J, Hamáček A (2008) Organic materials for humidity sensors. In: Proceedings of IEEE sensor conference, 26–29 October, Lecce, Italy, G003, pp 473–477
- Rezlescu N, Rezlescu E, Popa PD, Tudorache F (2005) A model of humidity sensor with a Mg-based ferrite. *J Optoelectron Adv Mater* 7(2):907–910
- Rittersma ZM (2002) Recent achievements in miniaturised humidity sensors – a review of transduction techniques. *Sens Actuators A* 96:196–210
- Rittersma ZM, Splinter A, Bodecker A, Benecke W (2000) A novel surface-micromachined capacitive porous silicon humidity sensor. *Sens Actuators B* 68:210–217
- Russell AP, Flecher KS (1985) Optical sensor for the determination of moisture. *Anal Chim Acta* 170:209–216
- Ruther P, Burg M, Steinert C, Paul O (2000) Humidity microsensors using silica aerogel thin films. In: Proceedings of Eurosensors XIV, Copenhagen, Denmark, 27–30 August, pp 51–52
- Sadaoka Y, Matsuguchi M, Sakai Y, Takahashi K (1988) Effect of sorbed water on the dielectric constant of some cellulose thin films. *J Mater Sci Lett* 7:121–124
- Sakai Y (1993) Humidity sensors using chemically modified polymeric materials. *Sens Actuators B* 13(14):82–85
- Sakai Y, Sadaoka Y, Ikeuchi K (1986) Humidity sensors composed of grafted copolymers. *Sens Actuators* 9:125–131
- Sakai Y, Sadaoka Y, Matsuguchi M (1996) Humidity sensors based on polymer thin films. *Sens Actuators B* 35–36:85–90
- Sakai Y, Matsuguchi M, Hurukawa T (2000) Humidity sensor using cross-linked poly(chloromethyl styrene). *Sens Actuators B* 66:135–138
- Salonen J, Laine E, Niinisto L (2002) Thermal carbonization of porous silicon surface by acetylene. *J Appl Phys* 91(1):456–461
- Sberveglieri G, Rinchetti G, Groppelli S, Faglia G (1994) Capacitive humidity sensor with controlled performances, based on porous Al<sub>2</sub>O<sub>3</sub> thin film grown on SiO<sub>2</sub>-Si substrate. *Sens Actuators B* 18(19):551–553
- Sberveglieri G, Murri R, Pinto N (1995) Characterisation of porous Al<sub>2</sub>O<sub>3</sub>-SiO<sub>2</sub>/Si sensor for low and medium humidity ranges. *Sens Actuators B* 23:177–180
- Seiyama T, Yamazoe N, Arai H (1983) Ceramic humidity sensors. *Sens Actuators* 4:85–96
- Serin N, Serin T, Unal B (2000) The effect of humidity on electronic conductivity of an Au/CuO/Cu<sub>2</sub>O/Cu sandwich structure. *Semicond Sci Technol* 15:112–116
- She Y-E, Jiang B-Y, Liu J-Z (1994) Si-Mg-Al-O system ceramic humidity sensor. *Sens Actuators A* 40:151–153
- Shimizu Y, Arai H, Seiyama T (1985) Theoretical studies on the impedance-humidity characteristics of ceramic humidity sensors. *Sens Actuators* 7:11–22
- Skrdl PJ, Saavedra SS, Armstrong NR, Mendes SB, Peyghambarian N (1999) Sol-gel-based planar waveguide sensor for water vapor. *Anal Chem* 71:1332–1337
- Snow AW, Barger WR (1989) Phthalocyanine films in chemical sensors. In: Kadish KM, Smith KM, Guillard R (eds) Phthalocyanines – properties and applications. VCH, New York, pp 343–392
- Songa X, Qi Q, Zhang T, Wang C (2009) A humidity sensor based on KCl-doped SnO<sub>2</sub> nanofibers. *Sens Actuators B* 138:368–373
- Sun HT, Ming-Tang W, Ping L, Xi Y (1989) Porosity control of humidity-sensitive ceramics and theoretical model of humidity-sensitive characteristics. *Sens Actuators* 19:61–70

- Suna A, Wanga Y, Li Y (2010) Stability and water-resistance of humidity sensors using crosslinked and quaternized polyelectrolytes films. *Sens Actuators B* 145:680–684
- Tao B, Zhang J, Miao F, Li H, Wan L, Wang Y (2009) Capacitive humidity sensors based on Ni/SiNWs nanocomposites. *Sens Actuators B* 136:144–150
- Thiel PA, Madey TE (1987) The interaction of water with solid surfaces: fundamental aspects. *Surf Sci Rep* 7:211–385
- Thosko N, Zvevditza N (1999) Humidity sensor using  $\text{TiO}_2$ - $\text{Bi}_2\text{O}_3$  ceramics. In: *Proceedings of Sensor 99, Nurnberg*, 18–20 May, pp 641–646
- Traversa E (1995) Ceramic sensors for humidity detection: the state-of-the-art and future developments. *Sens Actuators B* 23:1335–1356
- Traversa E, Bearzotti A (1995) A novel humidity-detection mechanism for ZnO dense pellets. *Sens Actuators B* 23:181–186
- Tsuchitani S, Sugawara T, Kinjo H, Ohara S (1985) Humidity sensor using ionic copolymer. In: *Digest of technical papers, 3rd International conference on solid-state sensors and actuators (Transducers' 85)*, Philadelphia, PA, USA, June 11–14, pp 210–212
- Varghese OK, Grimes CA (2003) Metal oxide nanoarchitectures for environmental sensing. *J Nanosci Nanotechnol* 3(4):277–293
- Varghese OK, Gong D, Paulose M, Ong KG, Grimes CA, Dickey EC (2002) Highly ordered nanoporous alumina films: effect of pore size and uniformity on sensing performance. *J Mater Res* 17(5):1162–1171
- Vijayamohan K, Mulla IS, Pradhan SD (1996) Humidity-sensing behaviour of surface-modified zirconia. *Sens Actuators A* 57:217–221
- Visscher GJW, Kornet JG (1994) Long-term tests of capacitive humidity sensors. *Meas Sci Technol* 5:1294–1302
- Viviani M, Buscaglia MT, Buscaglia V, Leoni M, Nanni P (2001) Barium perovskites as humidity sensing materials. *J Eur Ceram Soc* 21(10–11):1981–1984
- Wagner T, Krotzky S, Weiß A, Sauerwald T, Kohl C-D, Roggenbuck J, Tiemann M (2011) A high temperature capacitive humidity sensor based on mesoporous silica. *Sensors* 11:3135–3144
- Wang K, Seiler K, Haug JP, Lehmann B, West S, Hartman K, Simon W (1991) Hydration of trifluoroacetophenones as the basis for an optical humidity sensor. *Anal Chem* 63:970–974
- Wang H, Xu T, Zhang S, Lu T (1993) A multi-channel temperature and humidity monitor. *Meas Sci Technol* 4:164–169
- Wang H, Feng CD, Suin SL, Segre CU, Stetter JR (1998) Comparison of conductometric humidity-sensitive polymers. *Sens Actuators B* 40:211–216
- Wang J, Wang X-H, Wang X-D (2005) Study on dielectric properties of humidity sensing nanometer materials. *Sens Actuators B* 108:445–449
- Xu CN, Miyazaka K, Watanabe T (1998) Humidity sensors using manganese oxides. *Sens Actuators B* 46:87–96
- Xu YY, Li XJ, He JT, Hai XH, Wang Y (2005) Capacitive humidity sensing properties of hydrothermally-etched silicon nano-porous pillar array. *Sens Actuators B* 105:219–222
- Yagi H, Ichikawa K (1993) Humidity sensing characteristics of a limiting current type planar oxygen sensor for high temperatures. *Sens Actuators B* 13(14):92–95
- Yagi H, Nakata M (1992) Humidity sensor using  $\text{Al}_2\text{O}_3$ ,  $\text{TiO}_2$  and  $\text{SnO}_2$  prepared by sol-gel method. *J Ceram Soc Jpn* 100:152–156
- Yamazoe N, Shimizu Y (1986) Humidity sensors: principles and applications. *Sens Actuators* 10:379–398
- Yang B, Aksak B, Lin Q, Sitti M (2006) Compliant and low-cost humidity nanosensors using nanoporous polymer membranes. *Sens Actuators B* 114:254–262
- Yarkin DG (2003) Impedance of humidity sensitive metal/porous silicon/n-Si structures. *Sens Actuators A* 107:1–6
- Yeh Y, Tseng T, Chang D (1989) Electrical properties of porous titania ceramic humidity sensors. *J Am Ceram Soc* 72:1472–1475
- Ying J, Wan C, He P (2000) Sol-gel processed  $\text{TiO}_2$ - $\text{K}_2\text{O}$ - $\text{LiZnVO}_4$  ceramic thin films as innovative humidity sensors. *Sens Actuators B* 63:165–170
- Young L (1961) *Anodic oxide films*. Academic, New York
- Zhou Q, Shahriari MR, Kritz D, Sigel GH (1998) Porous fiber-optic sensor for high-sensitivity humidity measurements. *Anal Chem* 60:2317–2320

## Chapter 19

# Materials for Field Ionization Gas Sensors

As stated in Chap. 1, there are two types of gas sensors: the chemical type and the physical type. All sensors discussed previously in this volume are chemical-type devices. However, application of the chemical-type gas sensor is limited by several disadvantages, such as the potential difficulties in detecting gases with low adsorption energies, poor diffusion kinetics or poor charge transfer with nanotubes, high working temperature (except for the CNT-based sensors), and higher power consumption for conventional conductometric gas sensors. It is also challenging to use this technique to distinguish between gases or gas mixtures; gases in different combinations could produce the same net change in conductance as produced by a single pure gas. Chemical-type sensors are also very sensitive to changes in environmental conditions (moisture and temperature), and chemisorption could cause irreversible changes in the properties of gas-sensing materials (Modi et al. 2003).

Field ionization gas sensors do not have the disadvantages indicated because these devices work by fingerprinting the ionization characteristics of distinct gases. Field ionization (FI) is a quantum tunneling phenomenon whereby an atom or a molecule is ionized in the presence of a very high electric field, typically of order  $10^{10}$  V/m (Gomer 1961). This type of sensor can detect gases regardless of their adsorption energies. However, conventional gas ionization sensors are limited by their huge, bulky architecture, high power consumption, and risky high-voltage operation. Research carried out during the last decade has shown that the indicated disadvantages of gas ionization sensors can be overcome by the use of 1D structures (Modi et al. 2003; Hui et al. 2006; Wang et al. 2011). A schematic diagram illustrating the construction of modern gas ionization sensors is shown in Fig. 19.1. SEM images of 1D structures used in field ionization gas sensors are shown in Fig. 19.2.

It was established that the sharp tips of nanotubes generate very high electric fields at relatively low voltages, lowering breakdown voltages severalfold in comparison to traditional electrodes, and thereby enabling compact, battery powered and safe operation of such sensors (Modi et al. 2003; Riley et al. 2003). For example, physical gas sensors based on carbon nanotubes demonstrated low breakdown voltage and showed good sensitivity and selectivity. In many research projects carbon MWNTs were grown by chemical vapor deposition (CVD) on an  $\text{SiO}_2$  substrate, were 25–30 nm in diameter, and from 30 mm (Modi et al. 2003) to 2  $\mu\text{m}$  (Hui et al. 2006) in length. Several curves illustrating the operating characteristics of field ionization gas sensors are shown in Figs. 19.3 and 19.4.

It was found that these sensors can detect many gases, such as air, He, Ar, and gas mixtures, without gas separation (Modi et al. 2003). We need to note that ionization gas sensors such as photo-ionization detectors (PID), flame-ionization detectors (FID), or electron-capture detectors (ECD) are not suitable for direct application to gas mixtures. These detectors work in conjunction with a gas chromatography setup that separates the mixture into distinct bands that can then be qualitatively and quantitatively analyzed (Modi et al. 2003). In addition, FID has poor selectivity and requires bulky and hazardous

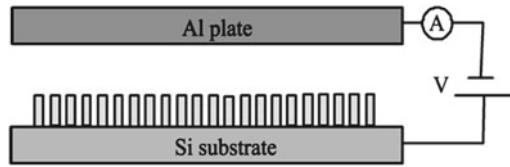


**Fig. 19.1** Schematic diagram of gas-ionized sensor with 1D electrodes. Controlled DC voltage is applied between the anode (vertically aligned nanotube film) and the cathode (Al sheet), which are separated by an insulator. The distance between the two electrodes could be adjusted in a range of 20–200  $\mu\text{m}$  by the thickness of the plastic film or glass

**Fig. 19.2** (a) Cross-sectional SEM image of MWNT (Reprinted with permission from Hui et al. (2006). Copyright 2006 IOP). (b) SEM image of ZnO nanorods. TEM images of the nanorods. (c) Individual bare ZnO nanorod. (d) Pd/ZnO nanorod with palladium capping by 120 s sputtering, respectively (Reprinted from Wang et al. (2011). Published by Springer)

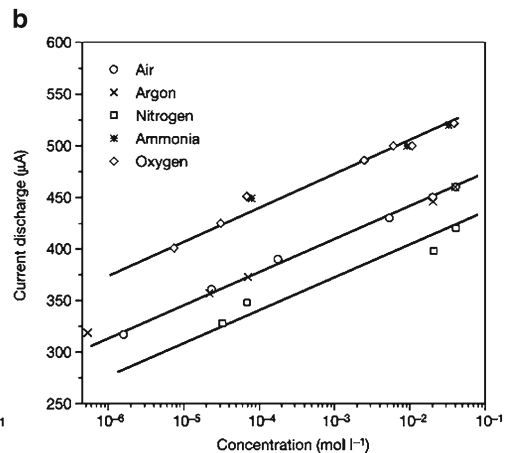
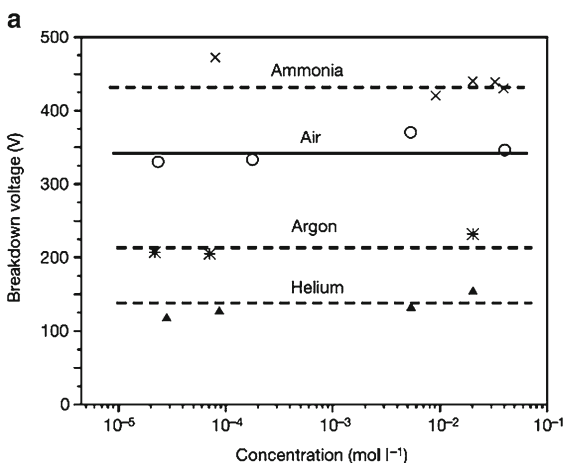
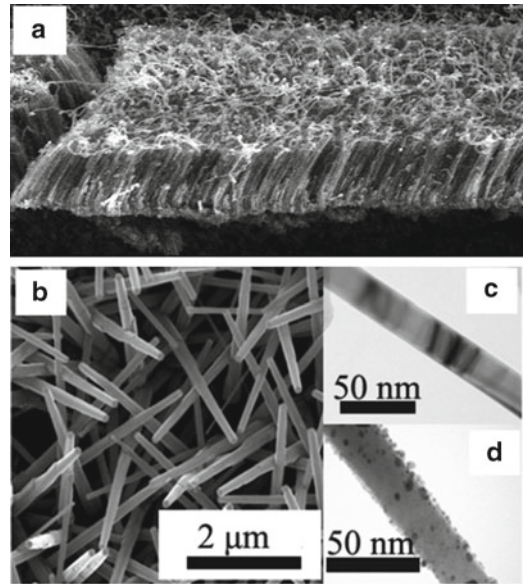


**Fig. 19.3** Effect of gas concentration on (a) electrical breakdown and (b) current discharge. It is seen that breakdown voltages vary only slightly with gas concentration and the discharge current varies logarithmically with concentration (Reprinted with permission from Modi et al. (2003). Copyright 2003 Nature Publishing Group)

**Fig. 19.4** Current–voltage ( $I$ – $V$ ) curves for  $\text{NH}_3$ ,  $\text{CO}_2$ ,  $\text{N}_2$ ,  $\text{O}_2$ , He, Ar, and air, showing distinct breakdown voltages; ammonia displays the highest breakdown voltage, and helium the lowest (Reprinted with permission from Modi et al. (2003). Copyright 2003 Nature Publishing Group)

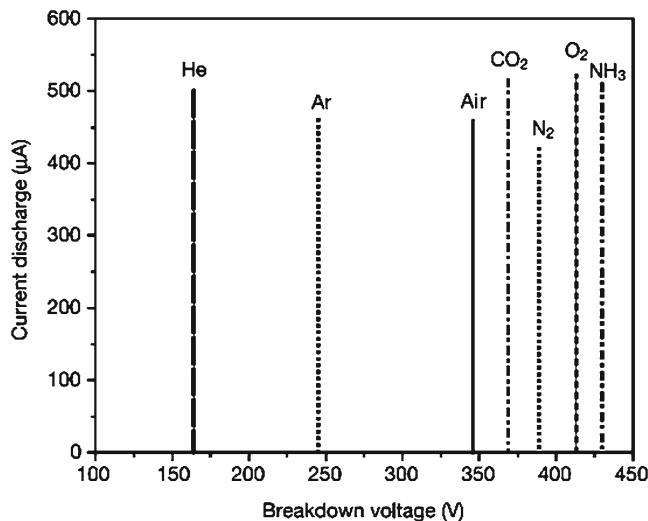
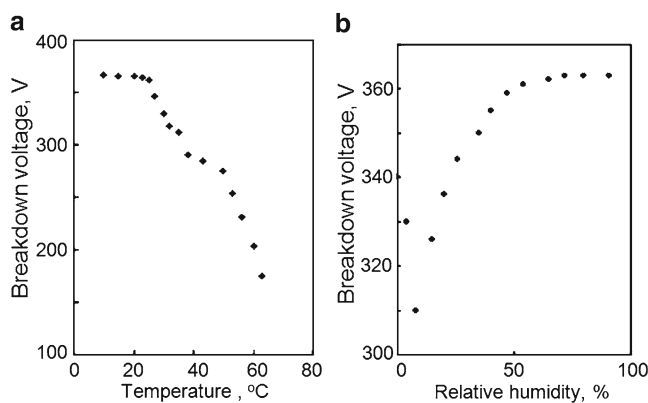


**Fig. 19.5** Effects of environmental factors on the operating characteristics of carbon MWNT-based field ionization gas sensors: (a) temperature and (b) relative humidity (Reprinted with permission from Hui et al. (2006). Copyright 2006 IOP)

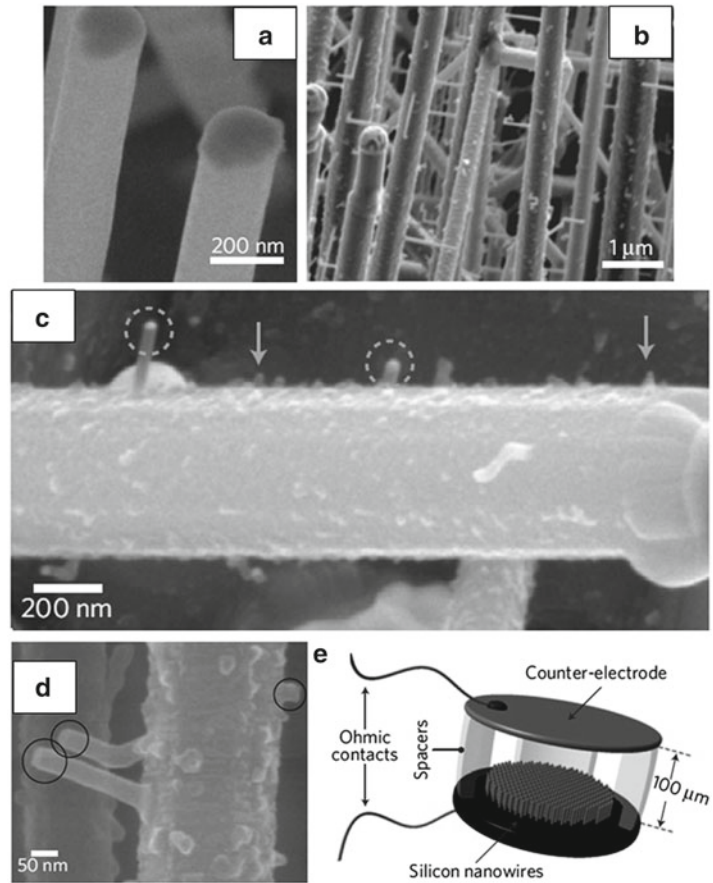


hydrogen storage tanks during operation, PID with better selectivity is limited to a small range of analytes, and ECD detectors are hazardous because they contain radioactive electron emitters. In contrast, the nanotube sensor is compact, safe to use, and requires low power to operate. Moreover, it was found (see Fig. 19.5) that field ionization gas sensors were not so sensitive to extraneous factors such as temperature, humidity, and gas flow (Hui et al. 2006). This means that such devices offer several practical advantages over previously reported nanotube gas sensor systems (Collins et al. 2000; Kong et al. 2000). It was found that the simple, low-cost sensors described here could be deployed for a variety of applications, such as environmental monitoring, sensing in chemical processing plants, and gas detection for counterterrorism. Unfortunately, the sensitivity of field ionization gas sensors is low in comparison with conductometric gas sensors. For example, below 1 % concentration the breakdown of Ar ceases and the breakdown voltage rises sharply to the value for pure air. Higher sensitivity up to 25 ppm was achieved only by using a gas chromatograph. However, the test indicated that the nanotube ionization microsensors (with proper calibration) shows promise for room temperature detection of gases at the percentage level in mixtures with air with fast response (application of the breakdown electric field results in a stable discharge within 20 ms) (Abdel-Salam et al. 2000).

However, the same research established that CNT-based ionization gas sensors show poor stability because carbon nanotubes can easily be oxidized and degraded in the oxygen-containing atmosphere (Wang et al. 2005; Liao et al. 2008). In addition, we have to say that, even when greatly decreasing the gaseous breakdown voltages to a range of 100–450 V (Modi et al. 2003; Hui et al. 2006; Wang et al. 2011),



**Fig. 19.6** Nanowires used to measure anomalous semiconductor-assisted gas ionization: (a) a close-up SEM image of smooth silicon nanowires after annealing in HCl; (b, c) SEM micrographs of a forest of, and a single, whiskered silicon nanowire that showed low-voltage FI; (d) SEM images of whiskered nanowires after removal of gold catalyst for the tips; (e) a three-dimensional schematic illustration of the device used to measure gas ionization on both types of nanowire. Note that the nanowires were planted at the anode.  $d_{\text{gap}} = 100 \mu\text{m}$  is the spacing between anode and cathode (Reprinted with permission from Sadeghian and Islam (2011). Copyright 2011 Nature Publishing Group)



such voltages are still hazardous to use. Moreover, CNT-based field ionization sensors operate in corona discharge mode. Corona discharges are difficult to control and they generate excessive heat that may destroy sharp and slender CNTs. For resolving this problem, Sadeghian and Kahrizi (2007, 2008) proposed to use a sparse array of vertically aligned gold nanorods as substitutes for CNTs. Recently, using the indicated approach, Sadeghian and coworkers (2008, 2011) have obtained threshold field ionization voltages of 0.2–9 V (depending on the measured gas) by incorporating whisker-covered gold nanowires on the cathode. With such an approach, sensors with high sensitivity, high selectivity, long durability, and (ultra)low-power operation ( $P < 10 \mu\text{W}$  with ionization currents  $\leq 1 \mu\text{A}$ ) are made possible. Sadeghian and Islam (2011) have shown that silicon nanowires can also be used for semiconductor-assisted gas ionization (see Fig. 19.6).

Liao et al. (2008) and Wang et al. (2011) have shown that metal oxide nanowires and nanorods, which are stable at room temperatures, can also be used for stable field ionization gas sensors instead of CNTs. In particular, Liao et al. (2008) used ZnO nanowires and Wang et al. (2011) used ZnO nanorods. However, it was found that 1D ZnO nanostructures with relatively larger tip radii, compared with CNTs, need higher breakdown voltage (see Fig. 19.7). For resolving this problem, Wang et al. (2011) proposed modifying ZnO nanorods by Pd nanoparticles. The results obtained have shown that the breakdown voltage decreases appreciably for the Pd/ZnO nanorod-based sensor compared with the bare ZnO nanorod. This means that the modification of the surface of 1D ZnO nanostructures to obtain lower breakdown voltage can be one of the key issues for gas sensor applications.

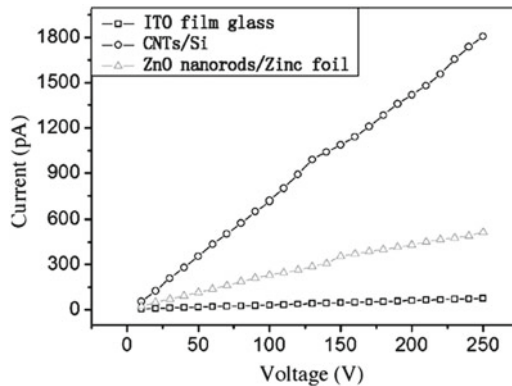


**Fig. 19.7** Effect of work voltages on prebreakdown current in air ( $T=25\text{ }^{\circ}\text{C}$ ; 48.7 % RH) for sensors with (1) CNTs and (2) ZnO nanorod electrodes. ITO films used as other electrode (inter-electrode gap is 50  $\mu\text{m}$ ). Here, CNTs are 30–40 nm in diameter, and the diameter of ZnO nanorods is 80–120 nm (Reprinted with permission from Huang et al. (2009). Copyright 2009 Elsevier)

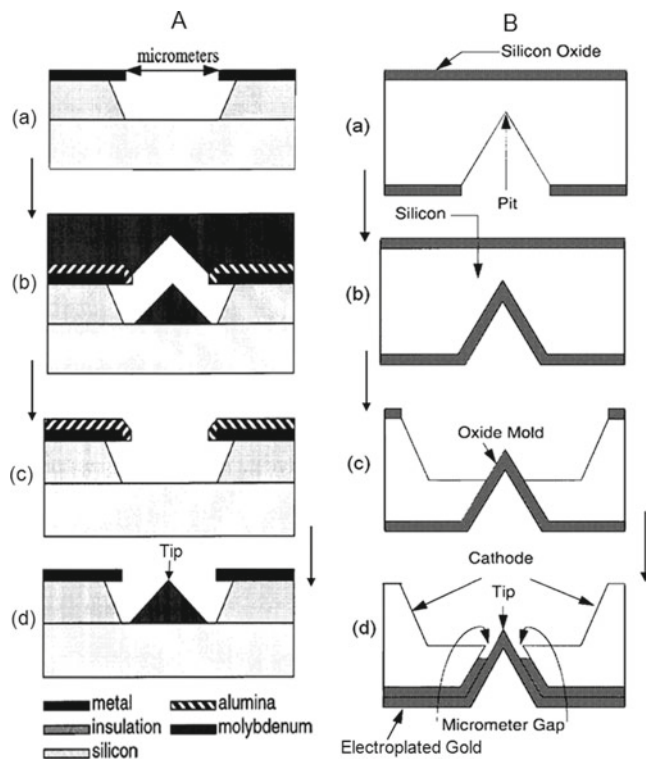


**Fig. 19.8** Fabrication sequence for one single tip proposed by (A) Spindt (1968, 1992) and (B) Ghodsian et al. (1998). (Idea from Spindt (1968) and Ghodsian et al. (1998))

Ghodsian et al. (1998) have shown that micromachining technology also makes it possible to design low-cost field ionization gas sensors with low working voltage. A technological process designed by Ghodsian et al. (1998) (see Fig. 19.8) allowed one to achieve a high resolution gap between the tip and a second electrode with a mask that has millimeter resolution and this gap can easily be controlled accurately with the oxide thickness. Due to the small distance between electrodes, the gas sensor could operate

with only 5 V applied voltage and could detect sample gas down to 14 ppm. Since the technology is based on bulk micromachining, the sensors can easily be integrated with a micromachined gas chromatography system. Ghodsian et al. (1998) believe that this will eventually improve the yield and manufacturing cost of micromachined gas chromatography system for remote environmental monitoring.

## References

- Abdel-Salam M et al (2000) High voltage engineering – theory and practice. Dekker, New York
- Collins P, Bradley K, Ishigami M, Zettl A (2000) Extreme oxygen sensitivity of electronic properties of carbon nanotubes. *Science* 287:1801–1804
- Ghodsian B, Parameswaran M, Syrzycki M (1998) Gas detector with low-cost micromachined field ionization tips. *IEEE Electron Device Lett* 19(7):241–243
- Gomer R (1961) Field emission and field ionization. Harvard University Press, Cambridge, MA
- Huang J, Wang J, Gu C, Yu K, Meng F, Liu J (2009) A novel highly sensitive gas ionization sensor for ammonia detection. *Sens Actuators A* 150:218–223
- Hui G, Wu L, Pan M, Chen Y, Li T, Zhang X (2006) A novel gas-ionization sensor based on aligned multi-walled carbon nanotubes. *Meas Sci Technol* 17:2799–2805
- Kong J, Franklin NR, Zhou C, Chapline MG, Peng S, Cho K, Dai H (2000) Nanotube molecular wires as chemical sensors. *Science* 287:622–625
- Liao L, Lu HB, Shuai M, Li JC, Liu YL, Liu C, Shen ZX, Yu T (2008) A novel gas sensor based on field ionization from ZnO nanowires: moderate working voltage and high stability. *Nanotechnology* 19:175501
- Modi A, Koratkar N, Lass E, Wei B, Ajayan PM (2003) Miniaturized gas ionization sensors using carbon nanotubes. *Nature* 424:171–174
- Riley DJ, Mann M, MacLaren DA, Dastoor PC, Allison W, Teo KBK, Amaratunga GAJ, Milne W (2003) Helium detection via field ionization from carbon nanotubes. *Nano Lett* 3:1455–1458
- Sadeghian RB, Islam MS (2011) Ultralow-voltage field-ionization discharge on whiskered silicon nanowires for gas-sensing applications. *Nat Mater* 10:135–140
- Sadeghian RB, Kahrizi M (2007) A novel miniature gas ionization sensor based on freestanding gold nanowires. *Sens Actuators A* 137:248–255
- Sadeghian RB, Kahrizi M (2008) A novel miniature gas ionization sensor based on freestanding gold nanowires. *IEEE Sens J* 8(2):161–169
- Spindt CA (1968) A thin-film field-emission cathode. *J Appl Phys* 39(7):3504–3505
- Spindt CA (1992) Microfabricated field-emission. *Surf Sci* 266:145–154
- Wang MS, Peng LM, Wang JY, Chen Q (2005) Electron field emission characteristics and field evaporation of a single carbon nanotube. *J Phys Chem B* 109:110
- Wang H, Zou C, Tian C, Zhou L, Wang Z, Fu D (2011) A novel gas ionization sensor using Pd nanoparticle-capped ZnO. *Nanoscale Res Lett* 6:534

## Chapter 20

# Gas Sensors Based on Thin-Film Transistors

### 20.1 Thin-Film Transistors

Experiment has shown that sensors based on the field-effect transistor (FET) offer a simple, efficient, and low-cost sensing platform for various applications, in particular for flexible electronics. Thin-film FET-based (TFTs) gas sensors utilize very simple construction. Two electrodes (“source” and “drain”) in contact with the semiconductor are used to apply a source–drain voltage and measure the source–drain current that flows through the semiconductor layer, while a third electrode (“gate”) is used to modulate the magnitude of the source–drain current. Figure 20.1 shows a conventional TFT in which the active semiconductor layer is exposed to the analyte of interest on one side, and the gate electrode is separated from the active layer by an insulator on the other. The gate can be used to switch the transistor “on” (high source–drain current) and “off” (negligible source–drain current). It should be noted that the structure with a highly conductive bottom substrate as a gate is not practical for real-life applications; however, it is very useful for lab prototyping printed transistors, especially for investigating semiconducting materials. Usually such substrates consist of thermally oxidized, highly doped silicon.

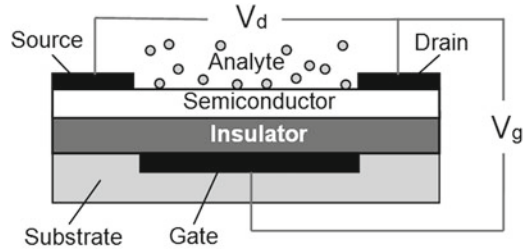
In real TFTs, for example printed TFTs designed for flexible electronics, a gate is usually fabricated from metals such as gold (Au) or silver (Ag), but other options are possible. Some of the often used insulator materials are organic polymer dielectrics, such as polyvinyl alcohol (PVA) and polyvinyl phenol (PVP); however, a multitude of other materials are currently being researched for this purpose. The source and drain contacts can be printed using something metallic in nature or a conducting polymer, such as poly(3,4-ethylenedioxythiophene):poly(styrenesulfonate) (PEDOT:PSS). Of course, other variants are possible.

With zero gate bias, the TFT is a chemiresistor that measures the variation of the film conductivity upon exposure to a chemical species. Depending on the semiconducting material used as the active layer, the mobile charge carriers can either be electrons (n-type material) or holes (p-type material). The source–drain current is controlled by both the gate electrode via an electric field applied across an insulating layer (gate dielectric) and the analyte–semiconductor interaction. It is known that analyte–semiconductor interaction, following electron transfer between analyte molecules and sensing layer, is able to change the concentration and mobility of free charge carriers and the work function of the semiconductor [see Chaps. 2 and 5 (Vol. 1)], which causes responses in the source–drain current (Janata and Josowicz 1998).

The variation of the source-to-drain current,  $I_D$ , as a function of the source-to-drain voltage,  $V_D$ , and of the grid voltage,  $V_G$ , is a well-established equation (Guillaud et al. 1990):

$$I_D = \frac{Z\mu C_i}{L} V_D \left( V_G - V_T - \frac{V_D}{2} \right), \quad (20.1)$$

**Fig. 20.1** Schematic cross section of a field-effect gas-sensing transistor. The analyte of interest is represented by gray circles. The applied source–drain voltage  $V_d$  and gate voltage  $V_g$  are also shown



where  $Z$  is the channel length,  $L$  the inter-electrode distance,  $C_i$  the capacitance of the insulator per unit surface, and  $V_T$  the threshold voltage – see Eq. (20.2). In molecular TFT,  $V_T$  has been associated with the presence of traps of structural origin or ions or other impurities at the semiconductor–dielectric material interface (Horowitz et al. 1990; Guillaud et al. 1998):

$$V_T = -\frac{ehn_0}{C_i} \quad (20.2)$$

where  $h$  is the thickness of the sensing layer and  $n_0$  the density of charge carriers without grid voltage.

Thus, an individual  $I$ – $V$  curve has a linear region at  $V_D \ll (V_G - V_T)$  and a saturation region at  $V_D > (V_G - V_T)$ . At  $V_D = V_G - V_T$ , the  $I_D = f(V_D)$  curve reaches a maximum and a pinch off of the channel occurs. For  $V_D > V_G - V_T$  the channel is no longer continuous and the corresponding current is called saturation current – see Eq. (20.3):

$$I_{DS} = \frac{Z\mu C_i}{2L} (V_G - V_T)^2 \quad (20.3)$$

The curve  $\sqrt{I_{DS}} = f(V_G)$  enables deduction of the mobility  $\mu$ , which is called the field-effect mobility. The channel length  $L$  (distance between the source and drain electrodes) and the thickness of dielectric layer determine the range of the voltage sweeps. The magnitude of  $L$  is also important in minimizing the effect of the contact resistance, which must be kept to a small fraction of the total channel resistance (Torsi and Dodabalapur 2005).

It is clear that the sensing effect in TFT can be improved by reducing the free charge carrier density and the thickness of the active part of the TFT and by increasing the mobility of charge carriers and capacitance of the insulating material, i.e., decreasing the thickness of the insulator (Bouvet 2006).

In comparison with chemiresistors, transistors provide more parameters for measurements and thus may give more detailed information about the analyte, which can be used for its reliable detection. For example, Torsi et al. (2000) demonstrated that, in addition to measuring the bulk conductivity of the semiconductor upon exposure to chemical species, threshold voltage and field-effect mobility can also be measured and used for analysis. This means that transistors in principle are more selective devices than conventional chemiresistors. Moreover, the detection limit and sensitivity of the sensors based on transistor are better than those of chemiresistors because of the signal amplification of transistor devices (Torsi et al. 2001). Of course, in the present case we are comparing TFTs with conventional polymer-based chemiresistors. Composite-based chemiresistors have considerably higher sensitivity [see Chap. 2 (Vol. 1)]. Torsi et al. (2001) also demonstrated that transistors, in addition to higher sensitivity, also showed a larger dynamic range and superior reversibility in comparison with simple resistors. Bouvet et al. (2001a, b) provided evidence that their TFT gas sensor performed better than a similar resistor-type sensor in terms of drift, sensitivity, signal-to-noise ratio, response time, lifetime, and operating temperature. The disadvantages of these devices are, as with other semiconductor devices, their preparation is slightly complicated and the characterization of a transistor is more difficult than a chemiresistor.

As indicated before, the semiconductor, which interacts with analyte, is the main element in thin-film transistor-based gas sensors. Research has shown that for fabrication of these devices both organic and inorganic semiconductors can be used.

## 20.2 Gas-Sensing Characteristics of Organic Thin-Film Transistors

An organic semiconductor (OSC) is an organic material with semiconductor properties. Research has shown that there are two major overlapping classes of organic semiconductors. Semiconducting properties can be discovered in single molecules, short-chain oligomers, so-called organic charge-transfer complexes, and various linear-backbone conductive polymers [see Chap. 3 (Vol. 1)]. Semiconducting small molecules (aromatic hydrocarbons) include the polycyclic aromatic compounds pentacene, anthracene, tetracene, diindenoperylene, perylenediimides, tetracyanoquinodimethane, and rubrene. Polymeric organic semiconductors, conjugated polymers, include poly(3-hexylthiophene) (P3HT), polyfluorene, poly 2,5-thienylene vinylene, poly(*p*-phenylene vinylene) (PPV), and polyacetylene (PA) and its derivatives.

Organic semiconductors, organic macromolecules with  $\pi$ -conjugated backbones, are attractive because of their unique electric and electronic properties (Covington et al. 2001, Chen et al. 2004; Bobacka and Ivaska 2010; Potje-Kamloth 2010). Almost all organic solids are insulators. However, when their constituent molecules have  $\pi$ -conjugate systems, there is the possibility of converting these materials into a conducting state. Charge injection (holes or electrons) into the conjugated backbone of the polymer is called doping. It leads to the formation of a self-localized electronic state within the previously forbidden semiconductor bandgap and causes a chain deformation around the charge. The prime source of localization of charge carriers in conducting polymers is structural disorder, which decreases the conductivity by lowering the charge carrier mobility. Thus, the added charge on the polymer is not a free electron or hole but is a localized particle connected with a chain deformation, which is known as a polaron or bipolaron state depending on the degree of doping. The creation of polaron or bipolaron electronic defects allows charge transport within a single chain (Bassler and Kohler 2012). Typical current carriers in organic semiconductors are holes and electrons in  $\pi$ -bonds. To match conventions between the physicist and chemist, a polymeric cation-rich material is called p-doped, and a polymeric anion-rich material is called n-doped. Besides this charge injection, doping in polymers also implies the insertion or the repulsion of counterions, that is, dopant anions, in order to maintain charge neutrality (Potje-Kamloth 2010).

Doping in polymers can be accomplished in a number of ways: chemically, electrochemically, and photochemically, as well as by charge injection at the metal–insulator–semiconductor interface. In the case of electrochemical and/or chemical doping, the neutral polymer chain is oxidized (p-doping) or reduced (n-doping). Because every monomer is a potential redox site, conjugated polymers can be doped to a high density of charge carriers; the doping level is up to five orders of magnitude greater than that in common inorganic semiconductors. The induced electrical conductivity is permanent until the charge carriers are purposely removed by undoping, that is, by reversing the (electro)chemical reaction at the redox sites of the polymer chain. However, though high density of carriers and their possible spatial delocalization, in organic semiconductors charge carriers cannot participate in electronic transport similar to the transport in inorganic semiconductors. Electrons in organic semiconductors can move via  $\pi$ -electron cloud overlaps, especially by hopping, tunneling, and related mechanisms (Bassler and Kohler 2012). Polycyclic aromatic hydrocarbons and phthalocyanine salt crystals are examples of this type of organic semiconductor. It was established that the dopant compounds play a very important role in hopping transport. For thermally activated hopping, the charge transport follows the relation  $\mu \approx \left( -\frac{E_a}{kT} \right)$ . The mobility in most OTFTs increases with increasing gate bias, which is attributed to filling of the tail states of the density of states (DOS).

**Table 20.1** Bandgap of several organic semiconductors used in TFTs design

Organic semiconductor	Abbreviation	Bandgap (eV)
Trans-polyacetylene	PA	1.4
Polythiophene	PT	2.0–2.1
Polyaniline	PAni	2.2
Rubrene(5,6,11,12-tetraphenyl-naphthalene)		2.2
Poly( <i>p</i> -phenylene vinylene)	PPV	2.5
Poly( <i>p</i> -phenylene)	PPP	2.8–3.0
Polypyrrole	PPy	3.2

Table 20.1 summarizes bandgaps for several of the most commonly used organic semiconductors. It is important that conductivities of organic semiconductors and Fermi levels can be controllably changed at will by chemical and electrochemical doping methods. This means that the characteristics of electronic devices utilizing them can be modified by request.

The first organic thin-film FET-based (OTFTs) transistors were reported in the mid-1980s (Ebisawa et al. 1983; Kudo et al. 1984), and by the end of 1980s it had been shown that these devices can be used for gas detection. Several groups observed that the source–drain current could be sensitive to the presence of specific gases. In particular, Laurs and Heiland (1987) fabricated transistors based on various phthalocyanines and observed that the source–drain currents increased by orders of magnitude in the presence of oxygen, iodine, and bromine. Assadi et al. (1990) reported that the source–drain currents of poly(3-hexylthiophene) transistors decreased upon exposure to ammonia. Ohmori et al. (1991) demonstrated that water vapor and chloroform gas also enhanced the source–drain currents of poly(3-butylthiophene) transistors. In each of these early reports, the changes in source–drain currents were observed to be reversible. Since the year 2000, interest in this area has greatly intensified, and now we have a lot of review papers related to this subject of research (Torsi 2000; Torsi and Dodabalapur 2005; Mabeck and Malliaras 2006; Wang et al. 2006; Guo et al. 2010). Table 20.2 summarizes organic semiconductors, which were tested as sensing layer in OTFTs, and analytes, which can be detected using these materials. One can find detailed discussions of organic semiconductors acceptable for application in TFTs in reviews prepared by Hasegawa and Takeya (2009) and Yamashita (2009). All the above-mentioned devices are based on p-type conductivity. N type OTFTs are as yet poorly developed (Yamashita 2009). It is seen that mainly OTFTs can be used for detection of water vapors and vapors of organic solvents (Covington et al. 2001). However, as experiment has shown, gases such as O<sub>2</sub>, NO<sub>2</sub>, N<sub>2</sub>, O<sub>3</sub>, H<sub>2</sub>, and SO<sub>2</sub> can also be detected. The optimal thickness of organic semiconductor in TFT-based sensors usually vary in the range from tens to several hundreds of nanometers depending on the material used. For too thin and too thick films, the gate modulation is very weak. Moreover, it is impossible to reach saturation point with great thickness.

Typical operating characteristics of OTFTs are shown in Fig. 20.2. These results were obtained by Zhu et al. (2002), who studied pentacene-based TFT as a humidity sensor.

Experiment has shown that organic thin-film transistors (OTFTs) offer a great deal of promise for applications in gas sensing (Torsi 2000; Mabeck and Malliaras 2006; Bouvet 2006). These sensors have advantages typical of all polymer-based devices and organic electronics (Yamashita 2009) [Chap. 3 (Vol. 1)]. Organic semiconductors can be deposited using low-temperature processes on a variety of substrates, including mechanically flexible plastics, and can operate at room temperatures [see Chaps. 3 and 7 (Vol. 1)]. This means that a low-cost approach—no vacuum processing, no lithography, low-cost substrates—can be used for gas sensor fabrication (Chang et al. 2006). For example, for sensor fabrication one can use novel low-cost technologies such as soft lithography and ink-jet printing. Thin films of organic semiconductors deposited using the methods indicated are mechanically robust and flexible. All the above-mentioned factors testify that OTFTs are promising elements for flexible electronics (Chang et al. 2006; Yamashita 2009). Moreover, easy modification in conducting polymer structures provides a simple route to sensing materials with different work functions and

**Table 20.2** Summary of OTFT-based gas sensors

Active layer	Analytes
Phthalocyanines(metallophthalocyanines)	Oxygen, iodine, bromine (Laurs and Heiland 1987); nitrogen dioxide (Hu et al. 2000; Bouvet 2006); ozone (Bouvet et al. 2001a, b; Bouvet 2006); alcohols, ketones, thiols, nitriles, esters, ring compounds (Crone et al. 2001)
9,10-ter-anthryleneethynylene	NO and NO <sub>2</sub> (Marinelli et al. 2009)
Naphthalene tetracarboxylic derivatives	Nitrogen, oxygen (Torsi et al. 2000); water vapor (Torsi et al. 2000, 2001); alcohols, ketones, thiols, nitriles, esters, ring compounds (Crone et al. 2001)
Pentacene	Water vapor (Zhu et al. 2002; Li et al. 2005); 1-pentanol (Wang et al. 2004)
Oligothiophenes	Alcohols (Someya et al. 2002); ketones, thiols, nitriles, esters, ring compounds (Crone et al. 2001)
Polythiophenes	Ammonia (Assadi et al. 1990); Water vapor (Kang et al. 2005), chloroform (Ohmori et al. 1991); alcohols, ketones, thiols, nitriles, esters, ring compounds, alkanes (Crone et al. 2001; Torsi et al. 2003a, b, 2004); 2,4,6-trinitrotoluene (TNT) vapors (Bentes et al. 2004)
Poly(phenylene ethynylene)	Volatile chiral molecules (Tanese et al. 2004)
Poly(3-methylthiophene)	Oxygen, hydrogen (Thackeray and Wrighton 1986)
Polyaniline	Water vapor (Chao and Wrighton 1987); sulfur dioxide (Gaponik et al. 1997)
Polypyrrole	Oxygen (Bufon and Heinzl 2006)
Bilayer—OH6OPT/6PTTP6	Dimethyl methylphosphonate (DMMP) (Huang et al. 2007)
PEDOT/PSS	Water vapor (Nilsson et al. 2002)

*OH6OPT* 5,5-bis(4-hydroxyhexyloxyphenyl)-2,2" bithiophene, *6PTTP6* 5,5-bis(4-*n*-hexyl-phenyl)-2,2" bithiophene, *PEDOT* poly(3,4-ethylenedioxythiophene), *PSS* poly(styrenesulfonate)

selectivities to analytes, which ensure high performance transistor configured sensors. Furthermore, it is possible to integrate covalently recognition elements directly with the organic semiconductor to provide highly specific interactions with chosen analytes. Miniaturization of these devices is straightforward, so portability, small sample volumes, and arrays with many elements are achievable. In addition, they provide a response (current change) that is easy to measure with simple instrumentation. With these advantages, it is feasible that single-use, disposable sensors could be realized using OTFTs.

However, it should be noted that at the same time OTFT-based sensors have all the disadvantages peculiar to polymer-based devices: bad temporal and thermal stability (Yamashita 2009), low selectivity to vapors of organic solvents, and high sensitivity to water vapors. For example, the major problem with pentacene, which shows the highest hole mobility of 3.0 cm<sup>2</sup> V/s in thin-film OTFTs, as well as many other organic conductors, is its rapid oxidation in air to form pentacenequinone (Hasegawa and Takeya 2009). In addition, pentacene has low solubility in solvents. Good solubility is crucial for device fabrication using solution methods such as ink-jet printing. Li et al. (2005) studied OTFT with different p-channel organic semiconductors and various device structures and established that all the p-channel organic semiconductors investigated showed degraded transistor performance with increased humidity. Torsi et al. (2002) found that above 70 °C the grains in alkyl-substituted  $\alpha$ -thiophene oligomers



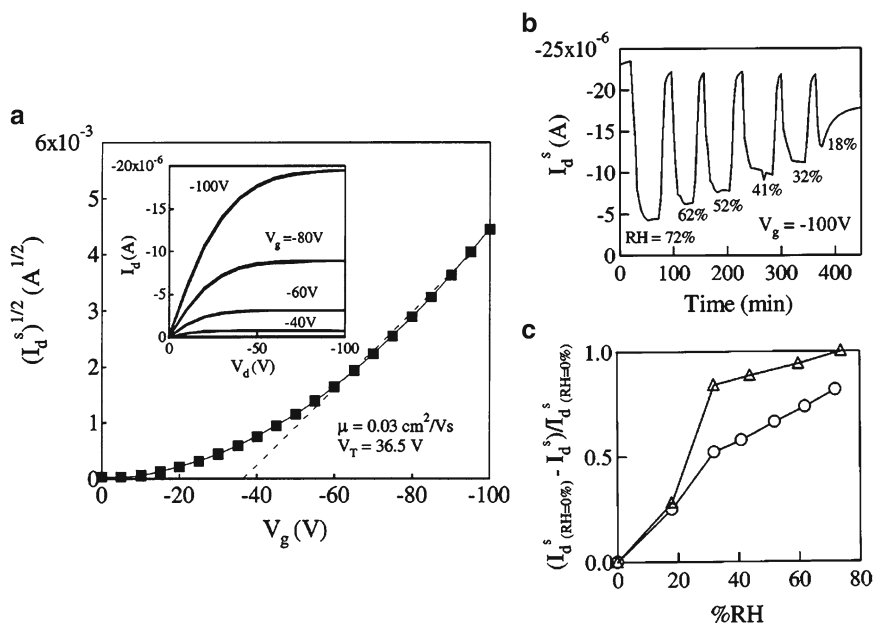


**Fig. 20.2** Operating characteristics of pentacene-based TFT. The channel length  $L$  is  $100\ \mu\text{m}$  and the channel width  $W$  is  $3\ \text{mm}$ . (a) Square root of the saturation current as a function of the gate voltage in a vacuum. The *dashed line* is a fit to obtain the hole mobility. *Inset* shows the drain current vs drain voltage characteristics measured in a vacuum. (b) Time dependence of the saturation current measured at a gate voltage of  $-100\ \text{V}$  and a drain voltage of  $-100\ \text{V}$ . The OTFT was exposed to wet  $\text{N}_2$  gas with different RH and vacuum, alternatively. (c) The saturation current measured at  $V_g = -100\ \text{V}$  and  $V_d = -100\ \text{V}$  as a function of relative humidity for two OTFTs. The *circles* are for the OTFT with a  $50\text{-nm}$ -thick pentacene layer; the *triangles* are for the OTFT with a  $100\text{-nm}$ -thick pentacene layer (Reprinted with permission from Zhu et al. (2002). Copyright 2002 American Institute of Physics)

films begin to coalesce, and a more regular, terraced morphology with a low surface roughness is observed. This type of morphology reduced the ability of gases to adsorb, decreasing the sensor response. In addition, we have to say that in many cases OTFTs' parameters such as composition, doping, thickness of insulator and sensing layers, grain size, and inter-electrode distance are not optimized, and therefore the operating characteristics of these devices are far from ideal.

Analysis of the results presented in Table 20.2 testifies that OTFTs and polymer-based chemiresistors, discussed in Chap. 3 (Vol. 1), use the same sensing materials and detect the same gases and vapors. This means that the mechanisms of analyte interaction with polymers discussed in Chap. 3 (Vol. 1) can be used to explain the gas-sensing effects observed in OFETs. However, we have to note that due to the complicated nature of this phenomenon and the possibility of using it in OTFTs organic semiconductors with different structures, we do not have a unified explanation for all the effects observed and every case requires an individual approach. In addition it is necessary to take into account that a resistor is sensitive to bulk mobility changes, whereas a transistor is sensitive not only to changes in the channel mobility but also to the number of trapped or otherwise immobile charges at the insulator–semiconductor interface, which give rise to a threshold shift (Torsi et al. 2002). This means that the mechanisms of sensitivity for different TFTs can have distinctive features.

For example, it is known that the response in TFTs may depend on both the conductivity and the work function of the polymer. However, experiment has shown that sometimes it is difficult to separate the influences of the various forms of modulation. For example, Polk et al. (2002) found that localized energy states in polyaniline can affect the value of the work function but do not affect the conductivity of the polymer.

Torsi et al. (2003a, b) have shown that the modification of the molecular structure of the active material also has a strong influence on the mechanism of sensitivity in TFTs' gas sensors. Torsi et al. (2003a, b) fabricated polymer transistors using two different types of active layers based on the same polythiophene backbone: one with alkyl side chains and the other with alkoxy side chains. These two chemically different transistors were exposed to a range of organic vapors, including alcohols, alkanes, and ketones. Polythiophene transistors with alkyl side chains showed responses that were correlated with the alkyl chain length of the analyte, whereas the transistors with alkoxy side chains showed responses that were correlated with the dipole moment of the analyte. These results demonstrate the enhancement in selectivity that can be achieved with OTFT sensors by tuning the active organic semiconductor via chemical synthesis. As an example of pushing this idea further, Tanese et al. (2004) proposed OTFT sensors based on active polymeric layers bearing enantioselective pendant groups for the detection of volatile chiral molecules.

Torsi et al. (2002) and Someya et al. (2002) fabricated oligothiophene-based transistors with a range of different oligothiophene film morphologies and studied their responses to alcohol vapors. Devices with larger numbers of grain boundaries showed larger responses when exposed to 1-pentanol, whereas devices without grain boundaries showed almost no response. They also observed that there was no swelling of the oligothiophene films upon exposure to the alcohol vapors, which suggests that the sensor response is due to surface interactions rather than bulk interactions. In addition to depositing organic films with a range of different grain sizes, they also varied the source–drain channel length in order to control the number of grain boundaries per device systematically. Their results indicate that the sensing of alcohol vapors with oligothiophene transistors is primarily due to semiconductor–analyte interactions at grain boundaries. They have proposed that vapor molecules adsorb more readily at grain boundaries, where they are closer to the conducting channel at the interface with the dielectric and can more strongly affect the electrical response. Li et al. (2005) established that in pentacene-type and other p-type TFTs, the sensitivity to humidity can be explained in terms of a decrease in the pentacene hole mobility in the presence of water vapor. The presence of polar water molecules can reduce the hole mobility by trapping charges at grain boundaries, thereby reducing the source–drain current. Assadi et al. (1990) also believed that the changes observed in poly(3-hexylthiophene)-based TFTs during interaction with ammonia are due to mobility variations rather than to variations in doping.

One can find a more detailed analysis of the sensing mechanisms of OTFT-based gas sensors in reviews by Someya et al. (2010) and Duarte and Dodabalapur (2012). They have shown that environmental molecules (“analytes”) can have very special effects on OFETs. Noncovalent bonds such as hydrogen bonds and  $\pi$  interactions cause attractions between analytes and organic semiconductors (OSCs) that exceed simple van der Waals interactions. The interactions can occur on the surfaces of OSC films, between crystallites that make up a polycrystalline OSC solid, in the free volume of OSCs that are either amorphous or intentionally supplied with flexible side chains, or at interfaces between organic semiconductors and dielectrics or electrodes (Someya et al. 2010). Many analytes are dipolar and thus induce local fields that are superimposed on the gate voltage, altering effective charge carrier mobilities. Duarte and Dodabalapur (2012) concluded that OTFTs are typically injection-limited devices, and the increase in the current during interaction with polar analytes most likely occurs due to the dipole interaction at the contact interface with the image charge, which decreases the barrier for hole injection. According to Duarte and Dodabalapur (2012), there are two phenomena that occur in the large channel devices ( $L > 1 \mu\text{m}$ ) when exposed to a polar analyte. The first is the percolation of the polar species through the grain boundaries where they interact with charges to produce trapping effects and increased potential barriers. These effects produce a decrease in drain current based on the polarizability of the organic semiconductor. The second effect is the alignment of the analyte dipoles in such a way that they act as added charge and an increase in drain current occurs. Depending on the carrier density (high gate bias or low gate bias operation), either trapping or the added charge phenomena will dominate. An increase in drain current may also occur due to the dielectric interface affecting the dipole interaction at the organic semiconductor/analyte interface. Regarding nonpolar

analytes, one can say that they also could conceivably alter mobilities through induced dipoles and disruption of molecular packing in the organic semiconductors (Someya et al. 2010). Furthermore, depending on the relative positions of OSC and analyte carrier energy levels, analytes can cause the trapping of mobile carriers by localizing them on the analyte molecules or doping by donating or extracting electrons from the organic semiconductor matrix. The effects of doping and trapping on OSC conductivity and interfacial potential barriers can be profound.

We also need to take into account that in nanoscale devices (short-channel devices), the analyte molecules modulate the charge carrier injection at the source and drain electrodes. For small channel length, the number of grain boundaries within a channel decreases so that the amount of effect of grain boundaries on electrical transport and chemical sensing reduces and other factors become more important. As a result, when the channel length is comparable with or smaller than the grain size of polycrystalline organic molecules or conjugated polymers, we might possibly observe the electrical transport and chemical sensing behavior within the body of grains; the mechanism of this might be different from that in large-scale devices in which grain boundaries dominate. Wang et al. (2006) believe that electrical transport in very short-channel-length organic transistors ( $L < 50$  nm) is contact limited. Due to analyte molecules diffusion near the source/drain contacts through the porous semiconductor layer, the analyte molecules can affect the behavior of the contact. Wang et al. (2006) have shown on the example of P3HT-based OTFT that the behavior of nanoscale OTFT sensors is remarkably different from that of their microscale counterparts. For OTFTs of such small dimensions the drain current typically increases by a factor of  $>5$  in response to the analyte ( $>10$  for some devices). The smaller the channel length, the stronger this effect. This means that nanoscale-dimension sensors are more sensitive. This provides a strong argument for employing nanoscale channel-length devices for sensing.

In closing, it is necessary to recognize that the published data do not enable one to conclude whether organic semiconductor might be optimal for TFT-based gas sensor design. There are only particular statements. For example, Bouvet (2006) concluded that phthalocyanines cannot be used in transistors for humidity and VOC sensing, even though they could be used favorably in such devices. Phthalocyanines work better with oxidizing species such as ozone and nitride dioxide, which act as true dopants, whereas water and volatile organic compounds act as traps and lead to a decrease in the current. Crone et al. (2001) and Torsi et al. (2002) found that the sensing response increased as the length of the organic semiconductor's hydrocarbon end group increased. They believe that this is because of the elongated lamellar morphology and looser molecular packing, which enable greater access of analyte vapor and increased surface area and change the electronic or spatial barriers between grains. The alkyl chains therefore facilitate adsorption of the analyte molecules by the sensing film. This adsorption mechanism could be a combination of hydrophobic interactions, intercalation to fill defect vacancies, and simple surface binding. All these processes are favored at grain boundaries. Huang et al. (2007) found that fabrication of a bilayer structure—[5,5'-bis(4-hydroxyhexyloxyphenyl)-2,2''bithiophene (OH6OPT)] on the surface of 5,5'-bis(4-*n*-hexyl-phenyl)-2,2''bithiophene (6PTTP6)—led to faster response times and higher sensitivity (up to 150 ppm) for dimethyl methylphosphonate (DMMP) compared to a single 6PTTP6 layer. Marinelli et al. (2009) have shown that using a 9,10-bis[(10-decylantracene-9-yl)ethynyl]anthracene ( $D_{3A}$ ) oligomer amorphous organic semiconductor with good stability in air makes it possible to design effective  $NO_x$  OTFT sensor. The  $D_{3A}$  OTFT used at room temperature exhibited differential sensitivity to NO and  $NO_2$ .  $NO_2$  detection down to 250 ppb could be achieved with very low cross-sensitivity to interfering species such as hydrogen sulfide and carbon monoxide (see Fig. 20.3). However, the temporal drift is present in operating characteristics of these sensors all the same.

The absence of general rules, which can be used for selection of optimal organic semiconductors, means that for every analyte we have to search specific OSC and specific functionalization to achieve the required sensitivity and selectivity.

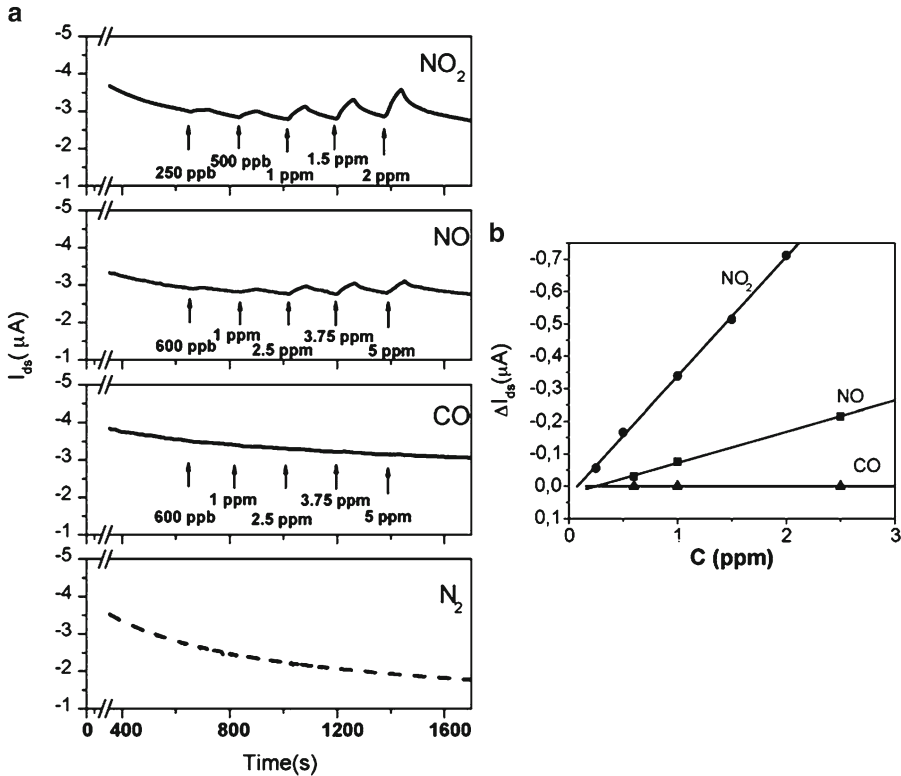


**Fig. 20.3** (a) Typical  $I_{DS}$  transient response curves of  $D_{3A}$  OTFT upon exposure to different concentrations of  $NO$ ,  $NO_2$ , and  $CO$ . Baseline current in  $N_2$  is reported as well. (b) Plot of  $\Delta I_{DS}$  response vs analyte concentration at  $V_g = -40$  V. The resulting film 10 nm thick of  $D_{3A}$  was deposited directly onto a  $SiO_2$  (100 nm)/n-doped Si substrate where Au/Ti source (S) and drain (D) pads were photolithographically patterned with channel width and length of  $W = 11,230$  and  $L = 30 \mu m$ , respectively (Reprinted with permission from Marinelli et al. (2009). Copyright 2009 Elsevier)

## 20.3 Metal Oxide-Based Thin-Film Transistors

It is usually assumed that TFT-based gas sensors should operate at room temperature. From this point of view, conventional metal oxides such as  $SnO_2$ ,  $In_2O_3$ ,  $WO_3$ , and  $ZnO$  are not promising for application in this type of gas sensor in spite of the presence of metal-oxide-based TFTs designed for other applications (Nomura et al. 2004, 2006; Fortunato et al. 2012; Park et al. 2012). Metal oxide gas sensors must typically be operated between 200 and 400 °C to insure rapid kinetics. Moreover, for stable operation high-temperature annealing is usually required. However, attempts to incorporate metal oxides in RT TFT-based sensors, due to their high stability, are being made. It should be said that these approaches gave positive results. It was found that Zn-based amorphous oxide semiconductors (AOSs), for example amorphous In-Ga-ZnO (a-IGZO), satisfy all the requirements of materials aimed at application in TFT-based gas sensors (Takagi et al. 2005; Kamiya et al. 2010). As an n-type semiconductor, amorphous  $InGaZnO_4$  is transparent with an optical bandgap of 3.1–3.3 eV (Nomura 2008).

The main advantages of Zn-based AOS for TFT design are high electron mobility even in amorphous form, scalability, uniformity, and the availability of low-temperature processes (Nomura et al. 2004; Kamiya and Hosono 2010). Thin films of amorphous  $InGaZnO_4$  are usually obtained from a polycrystalline ceramic target by using physical deposition techniques such as pulsed laser deposition and radio frequency sputtering at room temperature (Hosono and Nomura 2008). Formation of amorphous  $InGaZnO_4$

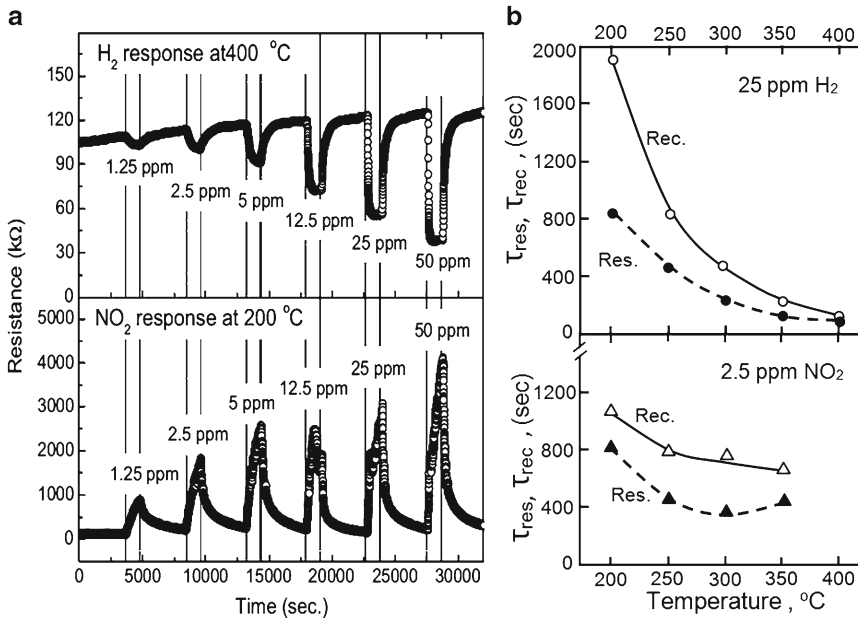


**Fig. 20.4** (a) Dynamic sensing transient of an a-IGZO thin film as a function of H<sub>2</sub> and NO<sub>2</sub> concentrations at 400 °C and 200 °C, respectively. (b) Temperature dependencies of response/recovery time constants evaluated from the gas response transient characteristics of an a-IGZO films during H<sub>2</sub> and NO<sub>2</sub> detection. The a-IGZO thin films were deposited by RF-magnetron sputtering, using a polycrystalline InGaZnO<sub>4</sub> target, at room temperature, onto alumina substrates, fitted with gold interdigitated electrodes (Au-IDEs). The film thickness was ~100 nm (Reprinted with permission from Yang et al. (2012). Copyright 2012 Elsevier)

requires an extremely high cooling rate, i.e., amorphous a-IGZO can be fabricated only in the form of a thin film, not in bulk form. The amorphous nature of a-IGZO films has been reported to remain stable up to relatively high temperatures (~500–600 °C) (Yang et al. 2012). Electron mobilities in the system In-Ga-Zn-O range from 5 to 39 cm<sup>2</sup>/Vs. While the highest value of mobility, 39 cm<sup>2</sup>/Vs, is obtained around the samples containing the maximum In<sub>2</sub>O<sub>3</sub> fraction, the lowest value of mobility is obtained in Ga-rich samples. However, though Ga<sup>3+</sup> is a carrier killer, the presence of Ga is necessary to stabilize the a-IGZO film (Kumomi et al. 2008). The explanation is that high electron mobility, unusual for the amorphous state, is achieved by employing heavy metal oxides, owing to spatial overlap between vacant s-orbitals of neighboring cations at the conduction band minimum (Kamiya and Hosono 2010). They also have a large process window in the choice of gate insulators. It was also found that the properties of AOS-based channel layers are easily influenced by various environment conditions. In particular, it was established that the conductivity of Zn-based oxide materials are sensitive to oxygen partial pressure and humidity (Kang et al. 2007; Park et al. 2008). This property is the main requirement for application in TFT-based gas sensors. In particular, Kang et al. (2007) produced IGZO TFT-based gas sensors and showed that IGZO-based TFT have stable characteristics and even at low temperatures have strong responses to oxygen partial pressure variations. They reported a turn-on voltage shift for IGZO TFTs from -7 to -54 V as the pressure in the chamber decreased from 760 to 8.5 × 10<sup>-6</sup> Torr and a return to the initial voltage upon re-exposure to air. The oxygen adsorption and desorption processes are assumed to be the main source of this considerable shift in turn-on voltage. However, during the following research, it was established that even for IGZO the kinetics of response and especially recovery processes after interaction with oxygen, NO<sub>2</sub>, or water is very slow. For example, Park et al. (2008) established that for recovery of the initial state after interaction with oxygen and water, annealing in vacuum at T = 100 °C for ~300 min is required. Yang et al. (2012) have shown that IGZO-based TFT gas sensors operate with acceptable recovery times only at increased temperatures (see Fig. 20.4). Such parameters create difficulties for real application of IGZO-based TFT gas sensors.

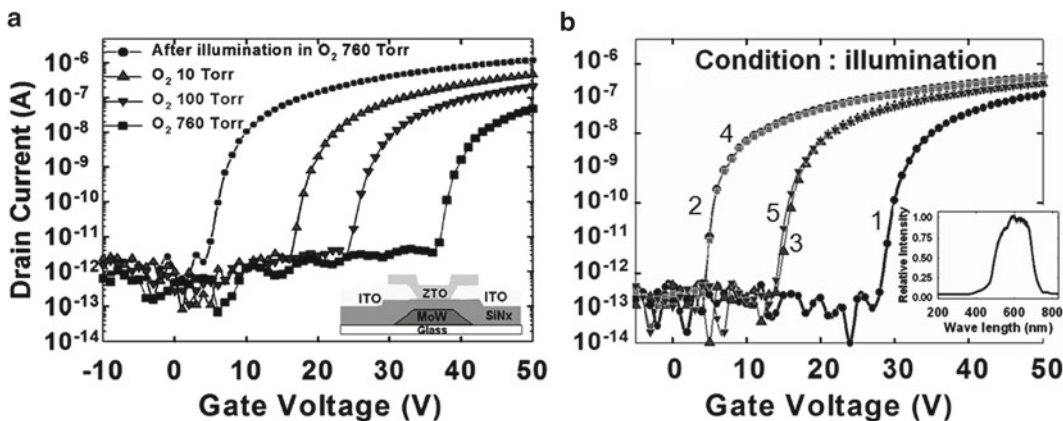


**Fig. 20.5** (a) Transfer  $I_D$ - $V_G$  characteristics of a-ZTO TFTs in different oxygen partial pressures at room temperature (10 Torr, 100 Torr, and 760 Torr) and after illumination of visible light with an intensity of 5,000 lux in oxygen ambient of 760 Torr, respectively. The inset shows the schematic cross-sectional view of a fabricated bottom-gate a-ZTO TFT. (b)  $I_D$ - $V_G$  characteristics of a-ZTO TFTs after 120 s illumination time and subsequent relaxation for 120 s in oxygen ambient: (1) oxygen ambient, 760 Torr; (2) reset; (3) adsorption; (4) reset; (5) adsorption (Reprinted with permission from Chen et al. (2012). Copyright 2012 American Institute of Physics)

Chen et al. (2012) have shown that the illumination of ZTO films considerably reduces recovery time after interaction with oxygen even without additional heating. Chen et al. (2012) established that after illumination with visible light ( $\lambda_{\max} = 600$  nm) for 120 s in oxygen-rich ambient, a significant increase in drain current of nearly  $10^4$  times occurs with fixed gate and drain voltages (see Fig. 20.5a). The transfer curve exhibits an obvious negative shift due to the oxygen desorption by photogenerated holes. It is expected that an optimized method of illumination can help to reset the electrical characteristics or distinguish the on/off state of this reliable oxygen sensor. Figure 20.5b shows a shift phenomenon that still occurs after experimental repetition. This suggests that the reset and adsorbed operation of an oxygen sensor can be reproduced by visible light illumination. However, even in this case the duration of measurement cycles is too long for in situ measurements. In addition, the incorporation of a light source in the device complicates the fabrication and exploitation of gas sensors.

It was established that IGZO layers can also be used in hybrid TFT-based gas sensors (see Fig. 20.6a), which can operate at low temperatures without illumination (Zan et al. 2011). In particular, a sensitive and reversible response to 100 ppb ammonia and 100 ppb acetone was obtained at room temperature by IGZO-based hybrid TFT sensor. However, in this case IGZO does not act as a sensing layer. The organic layer, serving as a second gate, forms a  $p$ - $n$  junction with the  $a$ -IGZO film. Zan et al. (2011) used P3HT and CuPc films for these purposes. Oxidizing or reducing vapor molecules act like electron acceptors or electron donors to change the potential of the organic layer and the current of  $a$ -IGZO TFT.

## 20.4 Other Materials in Thin-Film Transistor-Based Gas Sensors

Experiment has shown that we do not have a large choice of inorganic materials which could be used for designing TFT-based gas sensors aimed at operation at room temperatures. Besides polymers and metal oxides, discussed above, graphene and chalcogenides only have a real chance to be incorporated in TFT-based gas sensors. However, despite the fact that chalcogenide-based TFTs have been developed (Mitzi et al. 2004; Seon et al. 2009; Salas-Villasenor et al. 2010), gas sensing properties of these devices are still not studied. Gas-sensing characteristics of chalcogenide-based chemiresistors were discussed earlier in Chap. 5 (Vol. 1). At present in the literature one can only find information about  $\text{MoS}_2$ -based TFT gas sensors.  $\text{MoS}_2$  is a dichalcogenide with a layer structure.

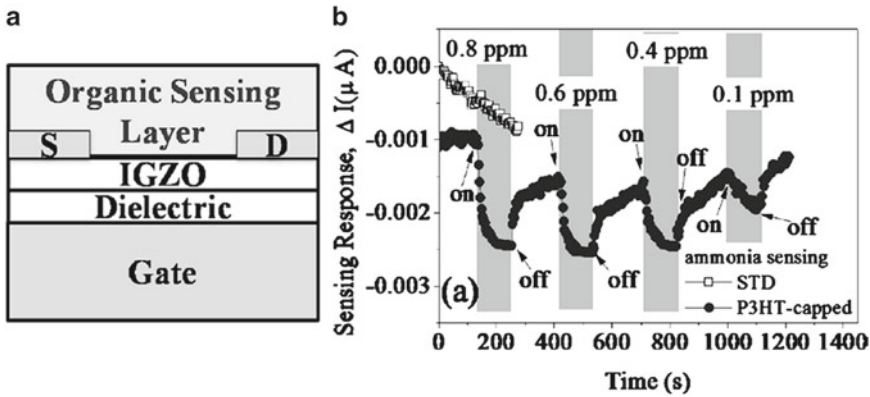


**Fig. 20.6** (a) Schematic diagram of hybrid organic-capped *a*-IGZO TFT. (b) Drain current variation ( $\Delta I$ ) in STD and P3HTcapped device as a function of time exposed to different concentration of ammonia at  $V_G - V_T = 0.3$  V,  $V_D = 1$  V. The thickness of the *a*-IGZO layer was 50 nm and the thickness of the P3HT film was 20 nm. STD means that *a*-IGZO TFT does not have organic layer (Reprinted with permission from Zan et al. (2011). Copyright 2011 American Institute of Physics)

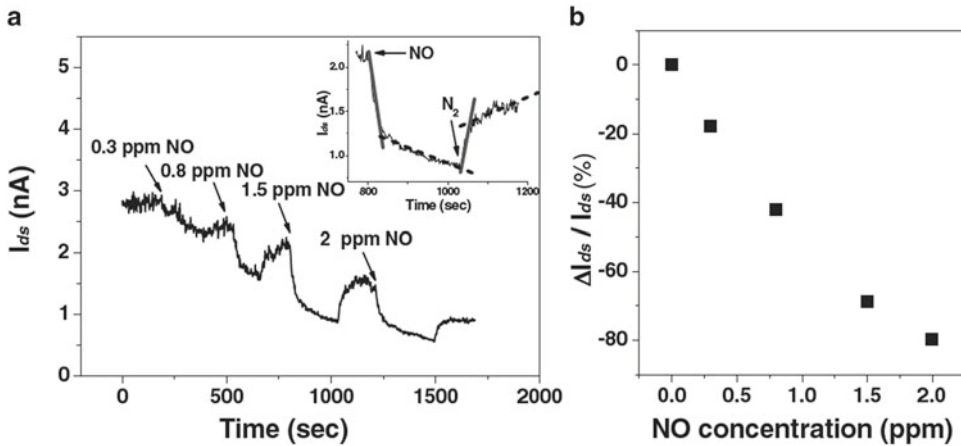


**Fig. 20.7** NO sensor based on 2L  $\text{MoS}_2$  TFT device. (a) Real-time current response after exposure of the 2L  $\text{MoS}_2$  FET to NO with increased concentration. *Inset*: a typical adsorption and desorption process of NO on the 2L  $\text{MoS}_2$  TFT. (b) Plot of the percent change in current as a function of NO concentration (Reprinted with permission from Li et al. (2012). Copyright 2012 Wiley-VCH Verlag)

Li et al. (2012) fabricated a TFT based on single- and multilayer  $\text{MoS}_2$  films using the mechanical exfoliation method and tested the sensitivity of these devices to NO. The average height of a single layer of  $\text{MoS}_2$  was  $\sim 0.8$  nm. The fabricated  $\text{MoS}_2$  FET devices show n-type doping behavior. It was found that the FET sensors based on bilayer (2L), trilayer (3L), and quadrilayer (4L)  $\text{MoS}_2$  films exhibited a high sensitivity to NO with a detection limit of 0.8 ppm (see Fig. 20.7), while the single-layer (1L)  $\text{MoS}_2$  device showed a rapid but unstable response. Functionalization of the  $\text{MoS}_2$  thin film with Pt nanoparticles (PtNPs) further increased the sensitivity of the TFT sensor by  $\sim 3$  times (see Fig. 20.8) (He et al. 2012a).

However, the same experiment has shown that even sensors with multilayer structure show a drift of characteristics, and the complete desorption of adsorbed NO molecules upon  $\text{N}_2$  flow is very slow (see insert in Fig. 20.8a), which is possibly due to the strong chemisorption of NO on the  $\text{MoS}_2$  surface.

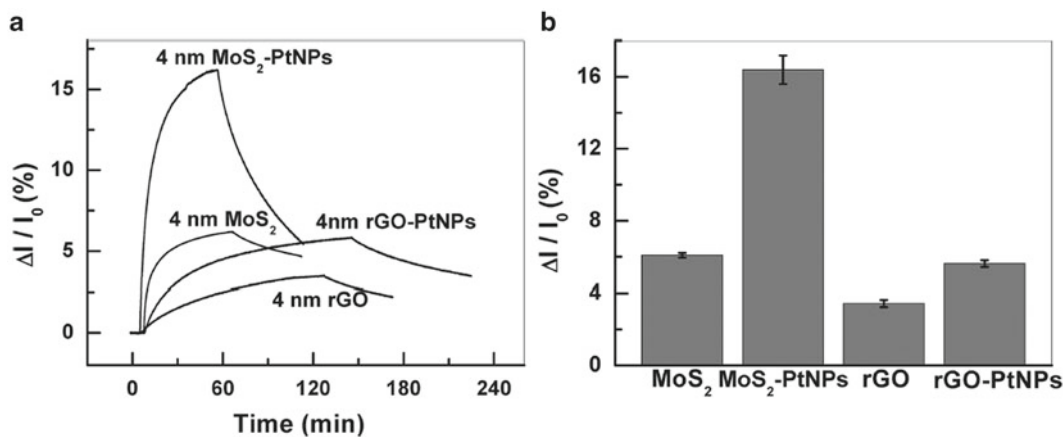


**Fig. 20.8** (a) Typical current response of TFT sensor on PET upon exposure of 1.2 ppm  $\text{NO}_2$  with channel of rGO, rGO-PtNPs,  $\text{MoS}_2$ , and  $\text{MoS}_2$ -PtNPs, respectively. (b) The current change of TFT sensor on PET with channel of rGO, rGO-PtNPs,  $\text{MoS}_2$ , and  $\text{MoS}_2$ -PtNPs, respectively (Reprinted with permission from He et al. (2012a, b). Copyright 2012 Wiley-VCH Verlag)

$\text{MoS}_2$ -based sensors with surfaces functionalized by Pt nanoparticles also have too slow a response and recovery (see Fig. 20.8a). In addition, we have to note that the proposed technology of sensor fabrication is too complicated for mass production. We are not sure that this technology can guarantee the fabrication of active channels with reliable and reproducible sensing performance.

The same situation arises with graphene TFT gas sensors based on mechanically cleaved single-layer graphene (Schedin et al. 2007). These sensors showed high sensitivity. However, the prospects of these devices in the sensor market will depend on the possibility of depositing graphene thin films by conventional methods such as CVD or chemical synthesis of reduced graphene oxide (rGO). Therefore, the design of these technologies has attracted much interest. Importantly, the emergence of rGO, one kind of solution-processable graphene derivative, has boosted the studies on the graphene-based thin-film transistor (TFT) (He et al. 2011, 2012b; Lee et al. 2012), since it is compatible with conventional thin-film technologies such as spin coating (Fowler et al. 2009) and ink-jet printing (Dual et al. 2010). However, graphene without proper surface functionalization (Berashevich and Chakraborty 2010) is a semimetal (Geim and Novoselov 2007; Meric et al. 2008) with a zero band-gap, resulting in weak switching properties. Graphene-based gas sensors will be discussed in more detail in Chaps. 1 and 25 (Vol. 2).

Gas-sensing properties of rGO-based TFTs designed by He et al. (2012a, b) are shown in Fig. 20.8a. It is seen that these sensors also have slow responses at room temperature. The same results were obtained by Zhang et al. (2012). The arrays of rGO sensors were fabricated from a patterned film by a simple shadow mask method. Gas sensors showed acceptable sensitivity and recyclable usage in sensing  $\text{NH}_3$ . The rGO sensor exhibited at room temperature a decrease of about 10 % in conductance with the exposure to 1,000 ppm  $\text{NH}_3$ . Of course such sensitivity is low in comparison with the sensitivity of conventional gas sensors. In addition, response and recovery times during interaction with  $\text{NH}_3$  exceeded 50 min. It is too long for real applications. The drift of characteristics in the indicated sensors is also present.

With some reservations, CNTs-based FET sensors with bottom-gate configuration can also be attributed to TFT sensors. Carbon nanotubes (CNTs) are one-dimensional molecular structures, which demonstrate very high carrier mobility in field-effect transistors (Avouris et al. 2007). Carbon-based gas sensors will be discussed in detail in Chap. 1 (Vol. 2). In this chapter we will briefly analyze the prospects for CNTs in TFT-based gas sensor design.



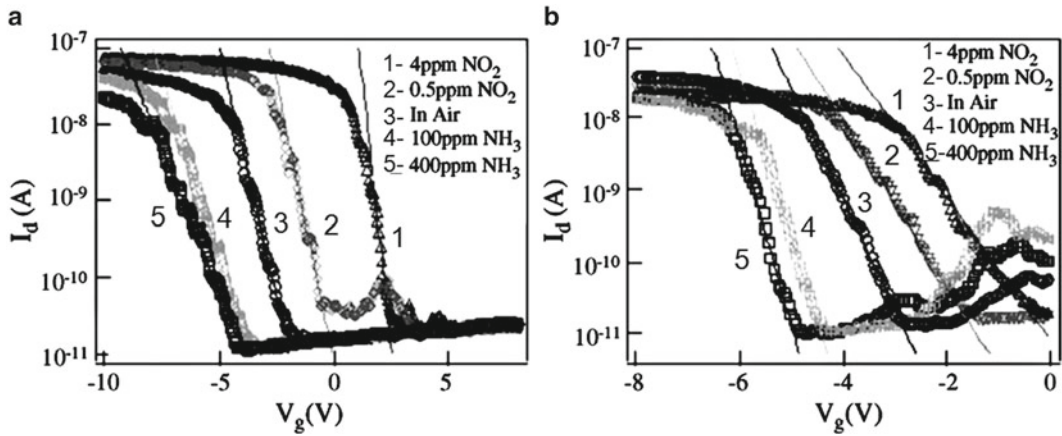


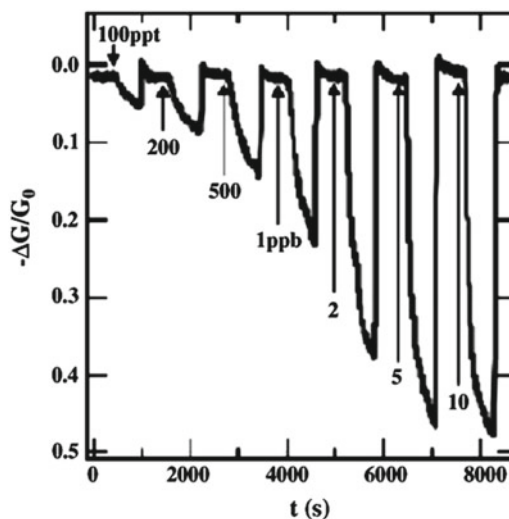
**Fig. 20.9** Operating characteristics of FET gas sensors based on individual SWCNT after exposure to different concentrations of  $\text{NO}_2$  and  $\text{NH}_3$  for two configurations. (a) The center covered by poly(methyl methacrylate) (PMMA) configuration. (b) Contact-covered configuration. The SWCNT was  $4 \mu\text{m}$  long. The measurements show a change of the transfer characteristics for both configurations (Reprinted with permission from Liu et al. (2005). Copyright 2005 American Institute of Physics)

It is considered that CNTFET-based sensors in comparison with existing technologies have advantages such as compactness, the ability to work at room temperature with a low power consumption, and very fast response times (Bondavalli et al. 2009). It is known that CNTs can be of two types: single-wall carbon nanotubes (SWCNTs) and multi-wall carbon nanotubes (MWCNTs) (Saito et al. 1998). It must be pointed out that the research related to TFT-based gas sensor design has essentially focused on SWCNTs, which can be semiconducting or metallic, depending on their chirality (Saito et al. 1998); MWCNTs are only metallic and therefore unsuitable for fabricating transistors. Experiment has shown that CNTs-based FET sensors fabricated using individual carbon nanotubes are sensitive to various analytes such as  $\text{NO}_2$ ,  $\text{NH}_3$ , and vapors and can operate at ppm and ppb levels (Kong et al. 2000; Liu et al. 2005; Snow et al. 2006; Bondavalli et al. 2009). Operating characteristics of sensors designed by Liu et al. (2005) are shown in Fig. 20.9.

However, the utilization of a single SWCNT presents some important issues (Bondavalli et al. 2009). First, considering that up to now no method exists to fabricate only semiconducting SWCNTs, one cannot predict whether an SWCNT is metallic or semiconducting. Second, it is quite laborious to identify the position of a single SWCNT using fine observation methods such as atomic force microscopy (AFM). From an industrial point of view, AFM is not a suitable solution for the mass manufacture of sensors. Third, considering that the CNTFET electrical characteristics are dependent on the single SWCNT physical characteristics (bandgap in particular, which depends on diameter for semiconductor specimens), it is very difficult to obtain reproducible devices.

The use of SWCNT mats as channels in FET sensors resolves some of the above-mentioned problems. In particular, it has been established that SWCNT mats, through a percolation effect, can show semiconductor behavior even without separation on semiconducting and metallic CNTs. According to Bondavalli et al. (2009), only two conditions must be fulfilled: the distance between the two electrodes must be larger than the SWCNT length (otherwise metallic nanotubes could cause a short circuit) and the areal density of the SWCNT mat has to exceed slightly the percolation threshold for semiconducting specimens (remember that SWCNTs always come in mixtures of metallic (m) and semiconductor (s) specimens, with the approximate ratio  $s/m=2$ ; therefore, conditions can be found where the s-SWCNTs will percolate, whereas the m-SWCNTs will not, yielding an overall semiconductor behavior). In many pieces of work, including Novak et al. (2003) and Snow et al. (2003), this approach was realized with high efficiency.

**Fig. 20.10** Resistance change of CNT-based FET with PEI functionalization as a function of time during interaction with  $\text{NO}_2$ . CNTFETs were functionalized using polyethyleneimine (PEI) simply by immersion. Desorption is achieved using UV light (Reprinted with permission from Qi et al. (2003). Copyright 2003 American Chemical Society)



In addition, during the same research, it was established that CNT-based sensors, similar to the sensors discussed in previous sections, have too long a recovery process after interaction with analyte. Depending on measurement conditions, the recovery time was varied from 30 min to 12 h (Kong et al. 2000; Liu et al. 2005). Experiment has shown that recovery time could be dramatically reduced simply by applying a reverse bias for around 200 s (Hopkins and Lewis 2001). Researchers thought that the Coulomb interaction between the analyte and the negative charges induced in the channel by the gate voltage reduces the desorption barrier. The same method has been employed by Chang et al. (2007). UV illumination, due to photodesorption of adsorbed species, also promotes a decrease in recovery times of CNTs-based gas sensors after interaction with analyte. Figure 20.10 illustrates that using UV illumination stable operation of CNT-based sensors with acceptable recovery times can be achieved. It is seen that the kinetics in this cases will be limited by response processes.

The following optimization of CNT-based gas sensors can be achieved through functionalization of carbon nanotubes (Qi et al. 2003; Bondavalli et al. 2009). For example, Shim et al. (2001) have shown that CNTFET functionalization by polyethyleneimine (PEI) considerably increases sensitivity to  $\text{NO}_2$ . The PEI coated CNTFETs showed a much higher sensitivity to  $\text{NO}_2$  compared to bare CNTFETs: the CNTFET sensors could detect a concentration of 100 ppt and saturated at 3 ppb. This value of 100 ppt constitutes up to now the lowest gas concentration ever detected by a CNTFET gas sensor. This behavior is linked to the doping effect of high-density amines from the PEI molecules on carbon nanotubes. Information related to CNTs functionalization may also be found in Chap. 25 (Vol. 2) of this book.

## References

- Assadi A, Gustafsson G, Willander M, Svensson C, Inganas O (1990) Determination of field-effect mobility of poly (3-hexylthiophene) upon exposure to  $\text{NH}_3$  gas. *Synth Met* 37:123–130
- Avouris P, Chen Z, Perebeinos V (2007) Carbon-based electronics. *Nat Nanotechnol* 2:605–615
- Bassler H, Kohler A (2012) Charge transport in organic semiconductors. *Top Curr Chem* 312:1–66
- Bentes E, Gomes HL, Stallinga P, Moura L (2004) Detection of explosive vapors using organic thin-film transistors, vol. 2. Proceedings of IEEE sensors conference, Vienna, 24–27 Oct, pp 766–769
- Berashevich J, Chakraborty T (2010) Doping graphene by adsorption of polar molecules at the oxidized zigzag edges. *Phys Rev B* 81:205431

- Bobacka J, Ivaska A (2010) Chemical sensors based on conducting polymers. In: Cosnier S, Karyakin A (eds) *Electropolymerization: concepts, materials and applications*. Wiley-VCH, Weinheim, pp 173–187
- Bondavalli P, Legagneux P, Pribat D (2009) Carbon nanotubes based transistors as gas sensors: state of the art and critical review. *Sens Actuators B* 140:304–318
- Bouvet M (2006) Phthalocyanine-based field-effect transistors as gas sensors. *Anal Bioanal Chem* 384:366–373
- Bouvet M, Leroy A, Simon J, Tournilhac F, Guillaud G, Lessnick P, Maillard A, Spirkovitch S, Debliquy M, de Haan A, Decroly A (2001a) Detection and titration of ozone using metallophthalocyanine based field effect transistors. *Sens Actuators B* 72:86–93
- Bouvet M, Guillaud G, Leroy A, Maillard A, Spirkovitch S, Tournilhac FG (2001b) Phthalocyanine-based field-effect transistor as ozone sensor. *Sens Actuators B* 73:63–70
- Bufon CCB, Heinzel T (2006) Polypyrrole thin-film field-effect transistor. *Appl Phys Lett* 89:012104
- Chang JB, Liu V, Subramanian V, Sivula K, Luscombe C, Murphy A, Liu JS, Frechet JMJ (2006) Printable polythiophene gas sensor array for low-cost electronic noses. *J Appl Phys* 100:014506
- Chang YW, Oh JS, Yoo SH, Choi HH, Yoo K-H (2007) Electrically refreshable carbon nanotube-based gas sensors. *Nanotechnology* 18:435504
- Chao S, Wrighton MS (1987) Characterization of a solid-state polyaniline-based transistor: water vapor dependent characteristics of a device employing a poly(vinyl alcohol)/phosphoric acid solid-state electrolyte. *J Am Chem Soc* 109:6627–6631
- Chen H, Josowicz M, Janata J, Potje-Kamloth K (2004) Chemical effects in organic electronics. *Chem Mater* 16:4728–4735
- Chen Y-C, Chang T-C, Li H-W, Chung W-F, Wu C-P, Chen S-C, Lu J, Chen Y-H, Tai Y-H (2012) High-stability oxygen sensor based on amorphous zinc tin oxide thin film transistor. *Appl Phys Lett* 100:262908
- Covington JA, Gardner JW, Briand D, de Rooij NF (2001) A polymer gate FET sensor array for detecting organic vapours. *Sens Actuators B* 77:155–162
- Crone B, Dodabalapur A, Gelperin A, Torsi L, Katz HE, Lovinger AJ, Bao Z (2001) Electronic sensing of vapors with organic transistors. *Appl Phys Lett* 78:2229–2231
- Dual V, Surwade SP, Ammu S, Agnihotra SR, Jain S, Roberts KE, Park S, Ruoff RS, Manohar SK (2010) All-organic vapor sensor using inkjet-printed reduced graphene oxide. *Angew Chem Int Ed* 49:2154–2157
- Duarte D, Dodabalapur A (2012) Investigation of the physics of sensing in organic field effect transistor based sensors. *J Appl Phys* 111:044509
- Ebisawa F, Kurokawa T, Nara S (1983) Electrical properties of polyacetylene/polysiloxane interface. *J Appl Phys* 54:3255–3259
- Fortunato E, Barquinha P, Martins R (2012) Oxide semiconductor thin-film transistors: a review of recent advances. *Adv Mater* 24:2945–2986
- Fowler JD, Allen MJ, Tung VC, Yang Y, Kaner RB, Weiller BH (2009) Practical chemical sensors from chemically derived graphene. *ACS Nano* 3:301–306
- Gaponik NP, Shchukin DG, Kulak AI, Sviridov DV (1997) Polyaniline-based microelectrochemical transistor with the electrocatalytic gate. *Mendeleev Commun* 7(2):70–71
- Geim AK, Novoselov KS (2007) The rise of graphene. *Nat Mater* 6:183–191
- Guillaud G, Al SM, Maitrot M, Simon J, Bouvet M (1990) Field-effect transistors based on intrinsic molecular semiconductors. *Chem Phys Lett* 167:503–506
- Guillaud G, Simon J, Germain J-P (1998) Metallophthalocyanines: gas sensors, resistors and field effect transistors. *Coord Chem Rev* 178:1433–1484
- Guo Y, Yu G, Liu Y (2010) Functional organic field-effect transistors. *Adv Mater* 22:4427–4447
- Hasegawa T, Takeya J (2009) Organic field-effect transistors using single crystals. *Sci Technol Adv Mater* 10(2):024314
- He Q, Wu S, Gao S, Cao X, Yin Z, Li H, Chen P, Zhang H (2011) Transparent, flexible, all-reduced graphene oxide thin film transistors. *ACS Nano* 5:5038–5044
- He Q, Zeng Z, Yin Z, Li H, Wu S, Huang X, Zhang H (2012a) Fabrication of flexible MoS<sub>2</sub> thin-film transistor arrays for practical gas-sensing applications. *Small* 8(19):2994–2999. doi:10.1002/sml.201201224
- He Q, Wu SX, Yin ZY, Zhang H (2012b) Graphene-based electronic sensors. *Chem Sci* 3:1764–1772
- Hopkins AR, Lewis NS (2001) Detection and classification characteristics of arrays of carbon black/organic polymer composite chemiresistive vapor detectors for the nerve agent stimulants dimethyl methylphosphonate and diisopropyl methylphosphonate. *Anal Chem* 73:884–892
- Horowitz G, Peng X, Fichou D, Garnier F (1990) The oligothiophene-based field-effect transistor: how it works and how to improve it? *J Appl Phys* 67:528–532
- Hosono H, Nomura K (2008) Factors controlling electron transport properties in transient amorphous oxide semiconductors. *J Non-Cryst Solids* 354:2796–2800
- Hu W, Liu Y, Xu Y, Liu S, Zhou S, Zhu D, Xu B, Bai C, Wang C (2000) The gas sensitivity of a metal-insulator-semiconductor field-effect-transistor based on Langmuir–Blodgett films of a new asymmetrically substituted phthalocyanine. *Thin Solid Films* 360:256–260

- Huang J, Miragliotta J, Becknell A, Katz HE (2007) Hydroxy-terminated organic semiconductor-based field-effect transistors for phosphonate vapor detection. *J Am Chem Soc* 129:9366–9376
- Janata J, Josowicz M (1998) Chemical modulation of work function as a transduction mechanism for chemical sensors. *Acc Chem Res* 31:241–248
- Kamiya T, Hosono H (2010) Material characteristics and applications of transparent amorphous oxide semiconductors. *NPG Asia Mater* 2:15–22
- Kamiya T, Nomura K, Hosono H (2010) Present status of amorphous In–Ga–Zn–O thin-film transistors. *Sci Technol Adv Mater* 11:044305
- Kang HS, Lee JK, Lee JW, Joo J, Ko JM, Kim MS, Lee JY (2005) Humidity dependent characteristics of thin film poly(3,4-ethylenedioxythiophene) field-effect transistor. *Synth Met* 155:176–179
- Kang D, Lim H, Kim C, Song I (2007) Amorphous gallium indium zinc oxide thin film transistors: sensitive to oxygen molecules. *Appl Phys Lett* 90:192101
- Kong J, Franklin N, Chou C, Pan S, Cho KJ, Dai H (2000) Nanotube molecular wires as chemical sensors. *Science* 287:622–625
- Kudo K, Yamashina M, Moriizumi T (1984) Field effect measurement of organic dye films. *Jpn J Appl Phys* 23:130–130
- Kumomi H, Nomura K, Kamiya T, Hosono H (2008) Amorphous oxide channel TFTs. *Thin Solid Films* 516:1516–1522
- Lauris H, Heiland G (1987) Electrical and optical properties of phthalocyanine films. *Thin Solid Films* 149:129–142
- Lee S-K, Jang HY, Jang S, Choi E, Hong BH, Lee J, Park S, Ahn J-H (2012) All graphene-based thin film transistors on flexible plastic substrates. *Nano Lett* 12(7):3472–3476
- Li D, Borkent E-J, Nortrup R, Moon H, Katz H, Bao Z (2005) Humidity effect on electrical performance of organic thin-film transistors. *Appl Phys Lett* 86:042105
- Li H, Yin ZY, He QY, Li H, Huang X, Lu G, Fam DWH, Tok ALY, Zhang Q, Zhang H (2012) Fabrication of single- and multilayer MoS<sub>2</sub> film-based field-effect transistors for sensing NO at room temperature. *Small* 8(1):63–67
- Liu X, Luo Z, Han S, Tang T, Zhang D, Zhou C (2005) Band engineering of carbon nanotube field-effect transistors via selected area chemical gating. *Appl Phys Lett* 86:243501
- Mabeck JT, Malliaras GG (2006) Chemical and biological sensors based on organic thin-film transistors. *Anal Bioanal Chem* 384:343–353
- Marinelli F, Dell'Aquila A, Torsi L, Tey J, Suranna GP, Mastrorilli P, Romanazzi G, Nobile CF, Mhaisalkar SG, Cioffi N, Palmisano F (2009) An organic field effect transistor as a selective NO<sub>x</sub> sensor operated at room temperature. *Sens Actuators B* 140:445–450
- Meric I, Han MY, Young AF, Ozyilmaz B, Kim P, Shepard KL (2008) Current saturation in zero-bandgap, top-gated graphene field-effect transistors. *Nat Nanotechnol* 3:654–659
- Mitzi DB, Kosbar LL, Murray CE, Copel M, Afzali A (2004) High-mobility ultrathin semiconducting films prepared by spin coating. *Nature* 428:299–303
- Nilsson D, Kugler T, Svensson PO, Berggren M (2002) An all-organic sensor–transistor based on a novel electrochemical transducer concept printed electrochemical sensors on paper. *Sens Actuators B* 86:193–197
- Nomura K (2008) Bandgap states in transparent amorphous oxide semiconductor, In–Ga–Zn–O, observed by bulk sensitive X-ray photoelectron spectroscopy. *Appl Phys Lett* 92:202117
- Nomura K, Ohta H, Takagi A, Kamiya T, Hirano M, Hosono H (2004) Room temperature fabrication of transparent flexible thin-film transistors using amorphous oxide semiconductors. *Nature* 432:488–492
- Nomura K, Takagi A, Kamiya T, Ohta H, Hirano M, Hosono H (2006) Amorphous oxide semiconductors for high-performance flexible thin-film transistors. *Jpn J Appl Phys* 45:4303–4308
- Novak JP, Snow ES, Houser EJ, Park D, Stepnowski JL, McGill RA (2003) Nerve agent detection using networks of single-walled carbon nanotubes. *Appl Phys Lett* 83(19):4026–4029
- Ohmori Y, Takahashi H, Muro K, Uchida M, Kawai T, Yoshino K (1991) Gas-sensitive Schottky gated field effect transistors utilizing poly(3-alkylthiophene) films. *Jpn J Appl Phys* 30:L1247–L1249
- Park JS, Jeong JK, Chung HJ, Mo YG, Kim HD (2008) Electronic transport properties of amorphous indium–gallium–zinc oxide semiconductor upon exposure to water. *Appl Phys Lett* 92:072104
- Park JS, Maeng W-J, Kim H-S, Park J-S (2012) Review of recent developments in amorphous oxide semiconductor thin-film transistor devices. *Thin Solid Films* 520:1679–1693
- Polk BJ, Potje-Kamloth K, Josowicz M, Janata J (2002) Role of protonic and charge transfer doping in solid-state polyaniline. *J Phys Chem* 106:11457–11462
- Potje-Kamloth K (2010) Gas sensing with conducting polymers. In: Cosnier S, Karyakin A (eds) *Electropolymerization: concepts, materials and applications*. Wiley-VCH, Weinheim, pp 153–171
- Qi P, Vermesh O, Grecu M, Javey A, Wang Q, Dai H, Peng S, Cho KJ (2003) Towards large arrays of multiplex functionalized carbon nanotube sensors for highly sensitive and selective molecular detection. *Nano Lett* 3:347–351
- Saito R, Dresselhaus G, Dresselhaus MS (eds) (1998) *Physical properties of carbon nanotubes*. Imperial College Press, London

- Salas-Villasenor AL, Mejia I, Hovarth J, Alshareef HN, Cha DK, Ramirez-Bon R, Gnade BE, Quevedo-Lopez MA (2010) Impact of gate dielectric in carrier mobility in low temperature chalcogenide thin film transistors for flexible electronics. *Electrochem Solid State Lett* 13(9):H313–H316
- Schedin F, Geim AK, Morozov SV, Hill EW, Blake P, Katsnelson MI, Novoselov KS (2007) Detection of individual gas molecules adsorbed on graphene. *Nat Mater* 6:652–655
- Seon J-B, Lee S, Kim JM, Jeong H-D (2009) Spin-coated CdS thin films for *n*-channel thin film transistors. *Chem Mater* 21:604–611
- Shim M, Javey A, Kam NWS, Dai H (2001) Polymer functionalization for air-stable *n*-type carbon nanotube field-effect transistors. *J Am Chem Soc* 123:11512–11513
- Snow ES, Novak JP, Campbell PM, Park D (2003) Random networks of carbon nanotubes as an electronic material. *Appl Phys Lett* 82(13):2145
- Snow ES, Perkins FK, Robinson JA (2006) Chemical vapour detection using single walled carbon nanotubes. *Chem Soc Rev* 35:790–798
- Someya T, Katz HE, Gelperin A, Lovinger AJ, Dodabalapur A (2002) Vapor sensing with  $\alpha$ ,  $\omega$ -dihexylquarterthiophene field-effect transistors: the role of grain boundaries. *Appl Phys Lett* 81:3079–3081
- Someya T, Dodabalapur A, Huang J, See KC, Katz HE (2010) Chemical and physical sensing by organic field-effect transistors and related devices. *Adv Mater* 22:3799–3811
- Takagi A, Nomura K, Ohta H, Yanagi H, Kamiya T, Hirano M, Hosono H (2005) Carrier transport and electronic structure in amorphous oxide semiconductor, a-InGaZnO<sub>4</sub>. *Thin Solid Films* 486:38–41
- Tanese MC, Torsi L, Cioffi N, Zotti LA, Colangiuli D, Farinola GM, Babudri F, Naso F, Giangregorio MM, Sabbatini L, Zambonin PG (2004) Poly(phenylene ethynylene) polymers bearing glucose substituents as promising active layers in enantioselective chemiresistors. *Sens Actuators B* 100:17–21
- Thackeray JW, Wrighton MS (1986) Chemically responsive microelectrochemical devices based on platinumized poly(3-methylthiophene): variation in conductivity with variation in hydrogen, oxygen, or pH in aqueous solution. *J Phys Chem* 90:6674–6679
- Torsi L (2000) Novel applications of organic based thin film transistors. *Microelectron Reliab* 40:779–782
- Torsi L, Dodabalapur A (2005) Organic thin-film transistors as plastic analytical sensors. *Anal Chem* 77:381–387
- Torsi L, Dodabalapur A, Sabbatini L, Zambonin PG (2000) Multi-parameter gas sensors based on organic thin-film-transistors. *Sens Actuators B* 67:312–316
- Torsi L, Dodabalapur A, Cioffi N, Sabbatini L, Zambonin PG (2001) NTCDA organic thin-film-transistor as humidity sensor: weaknesses and strengths. *Sens Actuators B* 77:7–11
- Torsi L, Lovinger AJ, Crone B, Someya T, Dodabalapur A, Katz HE, Gelperin A (2002) Correlation between oligothiophene thin film transistor morphology and vapor responses. *J Phys Chem B* 106:12563–12568
- Torsi L, Tanese M, Cioffi N, Gallazzi M, Sabbatini L, Zambonin P, Raos G, Meille S, Giangregorio MM (2003a) Side-chain role in chemically sensing conducting polymer field-effect transistors. *J Phys Chem B* 107:7589–7594
- Torsi L, Tafuri A, Cioffi N, Gallazzi MC, Sassella A, Sabbatini L, Zambonin PG (2003b) Regioregular polythiophene field-effect transistors employed as chemical sensors. *Sens Actuators B* 93:257–262
- Torsi L, Tanese MC, Cioffi N, Gallazzi MC, Sabbatini L, Zambonin PG (2004) Alkoxy-substituted polyterthiophene thin-film-transistors as alcohol sensors. *Sens Actuators B* 98:204–207
- Wang L, Fine D, Dodabalapur A (2004) Nanoscale chemical sensor based on organic thin-film transistors. *Appl Phys Lett* 85:6386–6388
- Wang L, Fine D, Sharma D, Torsi L, Dodabalapur A (2006) Nanoscale organic and polymeric field-effect transistors as chemical sensors. *Anal Bioanal Chem* 384:310–321
- Yamashita Y (2009) Organic semiconductors for organic field-effect transistors. *Sci Technol Adv Mater* 10(2):024313
- Yang DJ, Whitfield GC, Cho NG, Cho P-S, Kim I-D, Saltsburg HM, Tuller HL (2012) Amorphous InGaZnO<sub>4</sub> films: gas sensor response and stability. *Sens Actuators B* 171–172:1166–1171
- Zan H-W, Li C-H, Yeh C-C, Dai M-Z, Meng H-F, Tsai C-C (2011) Room-temperature-operated sensitive hybrid gas sensor based on amorphous indium gallium zinc oxide thin-film transistors. *Appl Phys Lett* 98:253503
- Zhang J, Hu PA, Zhang R, Wang X, Yang B, Cao W, Li Y, He X, Wang Z, O'Neill W (2012) Soft-lithographic processed soluble micropatterns of reduced graphene oxide for wafer-scale thin film transistors and gas sensors. *J Mater Chem* 22:714–718
- Zhu ZT, Mason JT, Dieckmann R, Malliaras GG (2002) Humidity sensors based on pentacene thin-film transistors. *Appl Phys Lett* 81:4643–4645

## Author Biography



**Ghenadii Korotcenkov** has more than 40 years experience as a teacher and scientific researcher. He received his Ph.D. in Physics and Technology of Semiconductor Materials and Devices in 1976, and his Habilitate Degree (Dr. Sci.) in Physics and Mathematics of Semiconductors and Dielectrics in 1990. For many years he led the scientific Gas Sensor Group and managed various national and international scientific and engineering projects carried out in the Laboratory of Micro- and Optoelectronics, Technical University of Moldova. Since 2008, Korotcenkov has been a research Professor in Gwangju Institute of Science and Technology, Republic of Korea.

Korotcenkov's research results are well known in the study of Schottky barriers, MOS structures, native oxides, and photoreceivers on the base of III–V compounds. His current research interests include material sciences and surface science, focused on metal oxides and solid-state gas sensor design.

Korotcenkov is the author or editor of 16 books and special issues, 12 invited review papers, 19 book chapters, and more than 190 peer-reviewed articles. He is a holder of 18 patents. His research activities have been honored by Award of the Supreme Council of Science and Advanced Technology of the Republic of Moldova (2004), The Prize of the Presidents of Ukrainian, Belarus and Moldovan Academies of Sciences (2003), Senior Research Excellence Award of Technical University of Moldova (2001, 2003, 2005), Fellowship from International Research Exchange Board (1998), and National Youth Prize of the Republic of Moldova (1980), among others.

# Index

## A

- Alarm systems, 1, 28, 37, 83, 289
- Ammonia (NH<sub>3</sub>) sensor, 11, 35, 36, 68, 80, 130, 186, 233, 275, 338, 370
- Analyte, 11, 75, 119, 168, 197, 235, 255, 287, 300, 309, 331, 353, 365, 378, 411, 415
- Auxiliary materials, 200, 214, 217, 356, 358

## B

- Bimetallic catalysts
  - Pd/Rh, 279
  - Pt/Pd, 279
  - Ru/Pd, 279, 280

## C

- Calorimetric (combustion-type) gas sensors
  - catalytic bead, 287–289
  - catalytic sensors, 287,
  - pellistors, 287, 288, 290
- Cantilever-based sensor platforms
  - cantilever bending, 235, 237
  - cantilevers, 234–239
    - microcantilever, 234–239
    - nanoelectromechanical systems, 234
    - piezoresistive cantilever, 238
    - polymer-based microcantilevers, 238–239
    - silicon-based microcantilevers, 235–238
- Cantilever-based sensors, 125, 139, 160, 186, 366
  - vibrational frequency, 20
- Capacitance gas sensor fabrication
  - aluminophosphate (AlPO<sub>5</sub>)-5, 371
  - carbon nanotubes (CNTs), 371
  - metal oxides, 13, 50, 94, 370, 372
  - polymer based capacitance gas sensors, 119, 367–369
  - porous alumina (Al<sub>2</sub>O<sub>3</sub>), 370
  - porous silicon (PSi), 370
  - SiC, 370, 372
  - zeolite, 371

- Capacitance gas sensors
  - advantages/disadvantages, 370
  - detection limits, 369
  - operation, 366, 369
- Carbon dioxide (CO<sub>2</sub>), 1, 50, 119, 184, 197, 233, 256, 275, 294, 322, 329, 356, 367, 382, 411
  - sensors, 11, 29, 35, 69, 83, 206–210, 213, 214, 372
- Carbon monoxide (CO), 3–6, 11, 13, 16, 20, 22, 24, 34, 36, 38, 50, 66–70, 74, 78, 79, 82, 86, 87, 93, 97, 99, 101, 119, 129, 133, 134, 141, 143, 154, 156, 160, 161, 169, 178, 182, 184–186, 189, 214, 231, 233, 253, 256, 257, 259, 261–265, 273, 275, 278–283, 288, 289, 294, 298, 300, 322, 329, 333, 342, 356, 357, 360, 363, 369, 371–373, 380–383, 422, 423
  - sensors, 84, 256, 296–298, 380
- Catalysts in conductometric gas sensors
  - bimetallic catalysts, 279–280
  - noble metal, 273–276, 279, 281–283
  - noble metal-metal oxide composites, 283
  - transition metals, 92, 273, 280
- Catalytically active filters
  - insulating layer, 299
  - metal oxides (MOXs)
    - CuO, 93, 298
    - MnO<sub>2</sub>, 299
  - noble metal films
    - Pd, 250, 299, 300
    - Pt, 250, 261, 299, 300
- Ceramic sensors, 279, 399
- Chemiresistors, 27, 30, 50–52, 71–77, 83, 89, 100, 101, 119, 122, 124, 139, 183, 184, 186, 189, 231, 415, 416, 420, 425
- Chemochromic materials
  - polyoxo compounds, 102, 103
  - V<sub>2</sub>O<sub>5</sub>, 102, 103
  - WO<sub>3</sub>, 101–103
- Cold sensors, 26

- Composite, 82, 83, 87, 93, 95, 96, 121, 123, 129, 131, 138, 141, 142, 145, 163, 183, 200, 205, 238, 249, 261, 262, 264, 265, 283, 296, 357, 360, 361, 370, 399, 403, 416
  - Conductometric gas sensor operation
    - chemical mechanism, 277, 278
    - conductivity, 15, 51, 71, 278
    - Debye length, 71
    - electronic mechanism, 277, 278
    - grain boundary, 75
    - grain size effect, 17, 71–73, 96
    - Schottky barrier, 255, 278
    - sensing mechanism, 277
    - spillover, 255, 276–277, 279, 281, 282
    - UV light activation, 85
  - Conductometric gas sensors, 17, 24, 28, 29, 34, 51, 77, 78, 81, 84, 92, 94, 117, 122, 138, 145, 252, 253, 255–260, 266, 273–283, 409, 411
- D**
- Detectors for optical sensors
    - advantages/disadvantages, 344
    - bolometer, 343, 345, 346
    - photodetector, 342, 346, 347
    - photodiode, 338, 339, 346, 348
    - photoreceivers, 171
    - photoresistor, 338, 339
    - pyrodetector, 339
    - requirements, 343
    - thermopile, 338, 339, 343–345
    - UV photodetectors, 347
- E**
- Electrical sensors, 13
  - Electrochemical cell, 62, 136, 197, 353, 357, 359, 361
  - Electrochemical sensors
    - auxiliary layer, 200
    - cross sensitivity, 212–215
    - diffusion barrier, 13, 29
    - electrode, 13, 29, 30, 132, 197–201, 262, 353, 355, 357, 358, 360
    - electrolytes, 13, 124, 131, 136, 140, 198, 201, 211, 262, 353, 355
    - membranes, 124, 197, 354–355, 360
    - Nernst equation, 135, 197
    - triple phase boundary (TPB), 360
  - Electrochemical sensor types
    - amperometric, 13, 15, 30–32, 131, 241, 355, 360, 361
    - conductometric, 13, 30, 131
    - mixed potential gas sensor, 30, 261
    - potentiometric
      - sensors of Type I, 197
      - sensors of Type II, 212
      - sensors of Type III, 212
  - Electrode materials
    - adhesion metal, 258
    - Ag, 257, 357
    - aluminum-doped zinc oxide (AZO), 259
    - Au, 255, 257, 354, 357
    - graphite interdigitated electrodes, 242
    - interdigitated electrodes requirements, 259
    - ITO electrode, 64
    - NiFe, 258
    - polycrystalline silicon, 259, 266
    - Pt, 255, 257, 259–261, 354, 357
    - sensing electrodes, 207, 261, 262, 357
    - TiSi<sub>2</sub>, 259
  - Electrodes for solid electrolyte-based sensors
    - requirements, 260
    - sensing electrodes, 260–266
  - Electrodes in electrochemical sensors
    - auxiliary electrode, 356, 358
    - counter electrode (CE), 13, 353, 355, 356, 358, 363
    - gas diffusion electrodes (GDE), 13, 357–363
    - permselective electrode, 125
    - reference electrode (RE), 13, 353, 355, 357, 358
    - sensing electrode (SE), 353, 355, 357, 358
    - working electrodes (WE), 353, 357, 358
  - Electrolytes for electrochemical sensors
    - liquid electrolytes
      - H<sub>3</sub>PO<sub>4</sub>, 356
      - H<sub>2</sub>SO<sub>4</sub>, 355
      - NaOH, 355
    - polymer electrolytes, 353–363
      - Nafion, 354–356, 358–363
    - requirements, 358
    - solid state electrolytes, 353
  - Electronic nose, 5, 10, 27, 28, 34, 37, 50, 52, 85, 168, 242, 311, 325
    - sensor array, 5, 27, 52, 168, 242, 325
  - Environmental monitoring, 2, 26, 27, 177, 240, 389, 411, 414
    - sensor, 27, 28, 211
- F**
- FET-based sensors, 13, 25, 37, 186, 378, 379, 415, 426–428
  - Fiber optic sensors, 21, 25, 35, 37, 51, 102, 119, 153, 157, 186, 329–350
  - Fibers for gas sensors
    - cladding, 333, 334, 336
    - core, 333–336
    - glass optical fibers, 334
    - IR fibers, 335
    - light-impermeable jacket, 333
    - multimode fibers, 334
    - polymer optical fibers, 334
    - single mode fibers, 334, 336
  - Field ionization gas sensors
    - advantages/disadvantages, 409, 411
    - conventional gas ionization sensors, 409
    - 1D-based gas ionization sensors, 409, 410
      - carbon MWNTs, 409, 411
      - silicon nanowires, 412
      - ZnO nanowires, 412
    - electron-capture detectors (ECD), 409, 411
    - flame-ionization detectors (FID), 409



- micromachining field ionization gas sensors, 413, 414
  - operation, 409, 411, 412
  - photo-ionization detectors (PID), 409, 411
  - Figaro sensors, 13, 14, 16, 266, 297
  - Filters in gas sensors
    - catalytically active filters, 298–300
    - passive filters, 293–298
  - Flexible sensor platforms
    - microheating elements, 230
    - plastic-flexible foil, 233, 234
    - polyethylenes (PEN), 230–233
    - polyethylenimine (PEI), 231–233
    - polyimide (PI), 230–234
    - polyphenylene sulfide (PPS), 231, 232
    - Polytetrafluoroethylene (PTFE), 230
  - Fluoride ion conductors
    - advantages/disadvantages, 214–217
    - LaF<sub>3</sub>, 214–217
    - PbF<sub>2</sub>, 214, 215
    - Sn/SnF<sub>2</sub>, 215
  - Fluorine sensors, 13, 214, 216
    - SiC/epi-SiC/SiO<sub>2</sub>/LaF<sub>3</sub>/Pt, 216
- G**
- Gas detectors, 1, 25
  - Gas diffusion electrodes (GDE)
    - composition, 360, 361
    - fabrication, 357, 361, 362
    - function, 360
    - parameters, 361, 363
  - Gases
    - asphyxiant gases, 2
    - combustible gases, 1, 3, 34, 50, 275, 287–289
    - flammable gas, 1, 3, 4, 23, 34
    - hydrocarbons (HCs), 3, 16, 24, 38, 66, 68, 101, 103, 155, 175, 214, 287, 296, 333
    - oxidizing gases, 49, 50, 84, 143, 233, 380
    - reducing gases, 16, 34, 49, 50, 58, 73, 76, 79, 84, 85, 101, 103, 143, 233, 274, 278, 359, 382, 397
    - toxic gases, 1, 3, 5, 9, 34
    - vapors of organic solvents, 16, 320, 418, 419
    - volatile organic compounds (VOCs), 3, 4, 7, 9, 13, 31, 34, 98, 119, 122, 125, 126, 130, 168, 231, 233, 266, 273, 294, 301, 322, 333, 368, 380, 384, 422
    - water vapors, 202, 206, 208, 211, 215, 217
  - Gas-permeable membranes
    - Nafion, 119, 125, 354
    - polytetrafluoroethylene (PTFE or Teflon), 119, 354
    - silicone membranes, 354
  - Gas preconcentrators
    - adsorbent, 295
    - microfabricated preconcentrator, 300
    - microtrap, 300
  - Gas sensing effect, 39, 71, 175, 245, 347, 420
  - Gas sensor operation
    - AC measurements, 16
    - adsorption, 15, 19, 39
    - calibration, 29, 32, 35
    - catalytic reaction, 23
    - chemisorption, 16
    - classification, 13–26
    - DC measurements, 16, 17
    - desorption, 76, 77, 98, 132, 140, 161, 162, 185, 255, 279, 280, 282, 290, 295, 301, 325, 371, 401, 424–426, 429
    - detection limit, 32
    - diffusion, 13, 15, 29
    - heterogeneous catalysis, 51
    - interference, 23, 27, 28, 32–34
    - life time, 32, 139, 298, 353, 358, 382, 416
    - long-term drift, 39
    - operating temperature, 17, 24, 26, 32
    - oxygen chemisorption, 16
    - parameters, 22, 23, 29, 35
    - physisorption, 396
    - power consumption, 17, 24–33
    - receptors, 21, 27, 97, 278
    - recognition element, 21, 22, 419
    - recovery time, 31, 95, 96, 123, 139, 161, 169, 186, 189
    - reliability, 26, 27, 39, 125, 182, 266, 290, 339
    - requirements, 26–30, 39, 40, 53, 68, 93, 141, 243–244, 257, 260, 266, 274, 318, 338, 343, 358, 424
    - response, 26, 39, 94, 125, 129, 159, 170, 180, 187, 202, 255–257, 318, 353, 369, 380, 382, 411
    - response time, 35, 39, 52, 89, 93, 140
    - selectivity, 26, 28, 30, 34, 40, 52, 139, 143, 262, 353, 409, 411, 412
    - sensitivity, 18, 26, 31, 34, 93, 143, 170, 256, 261, 353, 354, 365, 380, 382, 409, 411, 412
    - stability, 100, 143, 172, 180, 261, 319, 353, 354
    - surface species, 22, 102, 168, 174, 212, 214
    - transducer, 21, 99, 128, 278, 312, 317, 338
  - Gas sensor types, 94, 99, 122, 127, 140, 167, 233, 243, 287–291, 365–368, 370–372, 377–386, 409
  - Glass optical fibers
    - chalcogenide glasses, 335, 348
    - halide crystals, 335
    - heavy-metal fluoride glasses, 335
    - silica, 334
    - silicate glasses, 335
- H**
- High temperature sensors, 52, 64, 66, 67, 314–317
  - Hotplates, 167, 168, 225, 233
    - micromachined hotplates, 17, 221–228
  - Hot sensors, 26
  - Humidity, 1, 51, 136, 161, 169, 202, 231, 257, 283, 293, 310, 363, 365, 380, 389, 411, 418
  - Humidity sensors, 35, 89, 93, 94, 139, 141, 142, 217, 232, 233, 235, 310, 366, 368, 370, 371, 389–392, 418

## Humidity sensors materials

- LiCl dew point sensor, 403
- metal oxides, 390, 392, 396–400, 403
- polymers, 390, 392–397, 400, 403
- porous semiconductors, 392, 400–403

## Humidity sensors operation

- adsorption-chemisorption, 391
- capillary condensation, 370, 371, 391, 401
- Knudsen diffusion, 392
- methods of measurements, 389, 403
- protonic conduction, 397
- relative humidity (RH), 389–391, 393–395, 399, 401–403
- surface hydroxyl groups, 399
- vehicle mechanism, 397

Hydrogen (H<sub>2</sub>), 1, 62, 117, 154, 170, 197, 233, 262, 275, 289, 294, 316, 354, 367, 379, 395, 411, 419

Hydrogen (H<sub>2</sub>) sensors

- high temperature hydrogen sensors, 63, 64, 66, 67
- low temperature hydrogen sensors, 62, 66

Hydrogen sulfide (H<sub>2</sub>S), 3, 5, 6, 8, 13, 22, 32–36, 50, 70, 77–79, 82, 84–88, 95, 97, 119, 122–124, 128–130, 133, 134, 143, 154, 161, 189, 208, 212, 213, 233, 275, 289, 291, 297, 313, 321, 323, 329, 331, 356, 357, 363, 372, 380, 422  
sensors, 233, 355

**I**

## Infrared coating materials

- BaF<sub>2</sub>, 349
- CaF<sub>2</sub>, 349
- KBr, 349
- sapphire, 349
- silicon, 349
- ZnSe, 349

## Inorganic layers in work function gas sensors

- BaCO<sub>3</sub>, 382, 383
- potassium chloride (KCl), 381, 382
- potassium iodide (KI), 380–382
- TiN, 382, 383

Integrated optical sensors (IOS), 170, 171, 329–350

## Ion conductors

- Ag<sub>2</sub>SO<sub>4</sub>, 198, 199, 211, 212
- β-alumina, 198, 206, 208, 211
- Ba(NO<sub>3</sub>)<sub>2</sub>, 210
- CaCO<sub>3</sub>–Na<sub>2</sub>CO<sub>3</sub>, 208
- CeO–BaCO<sub>3</sub>/CuO, 5210
- K<sub>2</sub>SO<sub>4</sub>, 211
- LiCO<sub>3</sub>, 210
- Li<sub>2</sub>CO<sub>3</sub>–CaCO<sub>3</sub>, 210
- Li<sub>2.88</sub>PO<sub>3.73</sub>N<sub>0.14</sub>, 207, 208
- Li<sub>2</sub>SO<sub>4</sub>, 211, 212
- Na<sub>2</sub>CO<sub>3</sub>, 38, 206
- Na<sub>2</sub>CO<sub>3</sub> + BaCO<sub>3</sub>, 206, 208
- NaNO<sub>2</sub>, 210
- NaNO<sub>2</sub> + Li<sub>2</sub>CO<sub>3</sub>, 210
- NASICON, 53, 133, 206, 208, 210, 211
- Na<sub>2</sub>SO<sub>4</sub>, 38, 211, 212
- Na<sub>2</sub>SO<sub>4</sub>–Li<sub>2</sub>SO<sub>4</sub>–Y<sub>2</sub>(SO<sub>4</sub>)<sub>3</sub>–SiO<sub>2</sub>, 211

## IR fibers

- crystal, 335
- glass, 335
- hollow waveguide, 335

**L**

## Light sources in optical sensors

- advantages/disadvantages, 338, 340
- IR source, 338, 340
- laser diodes (LD), 338, 340, 341
- light emitted diodes (LED), 338, 339
- quantum cascade lasers (QCLs), 340, 341
- requirements, 338
- thermal source, 338–340
- tunable laser, 342
- UV sources, 338, 340

**M**

Magnetic gas sensors, 20–21

Mass-sensitive gas sensors, 18–20

## Materials for heater fabrication

- Cr–Ni alloy, 266
- polysilicon, 266, 267
- Pt, 266
- requirements, 266
- RuO<sub>2</sub>, 266
- TiSi<sub>2</sub>, 267

## Membranes for electrochemical sensors

- gas-permeable membranes, 124–125, 354
- permselective membranes, 125

## Metal-based gas sensors

- advantages/disadvantages, 52, 84
- cantilever-based H<sub>2</sub> sensor, 160
- conductometric sensors, 71
- fiber optic sensors, 333–336
- interferometric sensors, 159
- limitations, 68–70
- optical sensors, 329–333
- optimization, 39, 58
- plasmon resonance sensors, 93
- thermoelectric hydrogen sensors, 101, 159

Metal cluster, 277, 278, 281–283

## Metal films

- Ag, 156, 162
- Au, 156, 157, 162
- Pd, 154, 161, 321
- Pd-based alloys, 160
- sub-layer, 161

## Metal layers in work function gas sensors

- Au, 379, 380
- Pt, 379, 380

## Metal oxide composites

- Au–MeO<sub>x</sub>, 265
- CuO–ZnO, 265

## Metal oxide gas sensors

- advantages, 52
- disadvantages, 52
- grain size, 71–73, 75, 82, 94–96

- porosity, 62, 71–73, 82
- sensing mechanism, 276–279, 421
- specific surface area, 73, 82
- Metal oxide heterostructures
  - CuO/ZnO, 87, 89
  - SnO<sub>2</sub>/CuO, 87, 88
- Metal oxide p–n homojunction, 85–89
- Metal oxides (semiconducting), 71–92
- Metal oxides as sensing electrodes
  - CdO, 260
  - La<sub>0.6</sub>Ca<sub>0.4</sub>CoO<sub>3</sub>, 216
  - La<sub>0.8</sub>Ca<sub>0.2</sub>MnO<sub>3</sub>, 216
  - LaCoO<sub>3</sub>, 216
  - LaCrO<sub>3</sub>, 216
  - LaFeO<sub>3</sub>, 216
  - LaMnO<sub>3</sub>, 216
  - NiO, 85, 92, 93, 101
  - In<sub>2</sub>O<sub>3</sub>, 52, 71, 73, 74, 77–81, 84, 85, 94, 95, 97
  - SnO<sub>2</sub>, 260
  - ZnO, 260
- Metal oxides binary
  - Co<sub>3</sub>O<sub>4</sub>, 93
  - CuO, 78
  - Fe<sub>2</sub>O<sub>3</sub>, 78, 79
  - Ga<sub>2</sub>O<sub>3</sub>, 78, 79
  - indium oxide (In<sub>2</sub>O<sub>3</sub>), 77–79, 81
  - NiO, 85, 92, 93, 100
  - tin dioxide (SnO<sub>2</sub>), 77–81
  - titanium dioxide (TiO<sub>2</sub>), 77–79
  - tungsten oxide (WO<sub>3</sub>), 77–81
  - zinc oxide (ZnO), 77–81
- Metal oxides complex, 78–83
  - Cr<sub>2-x</sub>Ti<sub>x</sub>O<sub>3+2x</sub> (CTO), 79, 84
- Metal oxides for capacitance sensors
  - CoO–In<sub>2</sub>O<sub>3</sub>, 373
  - CuO–BaTiO<sub>3</sub>, 80, 372
- Metal oxides in humidity sensors
  - porous Al<sub>2</sub>O<sub>3</sub>, 94, 397
  - TiO<sub>2</sub>–K<sub>2</sub>O–LiZnVO<sub>4</sub>, 399
  - Ti<sub>0.9</sub>Sn<sub>0.1</sub>O<sub>2</sub>, 399–400
- Metal oxides in work function gas sensors
  - Cr<sub>1.8</sub>Ti<sub>0.2</sub>O<sub>3</sub> (CTO), 382
  - Ga<sub>2</sub>O<sub>3</sub>, 382
  - SnO<sub>2</sub>, 382
- Metal oxides mixed
  - SnO<sub>2</sub>–In<sub>2</sub>O<sub>3</sub> (ITO), 80
  - SnO<sub>2</sub>–ZnO, 80, 81
- Metal oxide solid electrolytes
  - apatite family, 54
  - Bi<sub>2</sub>O<sub>3</sub>, 55, 56, 68, 69
  - CeO<sub>2</sub>, 54–56, 67, 70
  - fluorite-type oxides, 67
  - LAMOX family, 56–57
  - Y<sub>2</sub>O<sub>3</sub>, 55, 56, 60, 66
  - yttria-stabilized zirconia (YSZ), 55, 58, 60, 63, 64, 66, 70
  - ZrO<sub>2</sub>, 58–62, 70
- Methane (CH<sub>4</sub>), 7, 11, 13, 20–24, 34–36, 38, 50, 64, 66, 67, 78, 79, 85, 86, 98, 99, 103, 126, 133, 161, 186, 208, 231, 263, 264, 273, 275, 283, 288–291, 293, 294, 297–299, 329, 331, 332, 342, 356, 372, 382
- sensors, 296
- Micromachining hotplates
  - bulk micromachining, 227
  - CMOS technology, 228
  - mechanical layer, 226, 227
  - porous silicon, 225–227
  - sacrificial etchant, 227
  - sacrificial layer, 225–228
  - surface micromachining, 225–228
- MOS-diode sensors, 18, 168
- MOSFET-based sensors, 378, 379
- N**
- Nanocomposite, 88, 92, 262, 265
- Nanoparticles, 37, 71, 81, 182, 233, 238, 241, 255, 264, 265, 281, 282, 287, 289, 361, 412, 426, 427
- Nitrogen oxides (NO<sub>x</sub>), 2–5, 7, 11, 13, 34–36, 38, 50, 69, 78, 79, 81, 119, 141, 156, 178, 187, 199, 200, 210, 215, 296, 302, 384, 386, 422
  - sensors, 80, 210–211, 214, 373
- Noble metal-based composites
  - Au–TiO<sub>2</sub>, 289
  - Pt/alumina, 290
- Noble metal catalysts
  - Au, 250, 261, 273, 274
  - Pd, 250, 265, 273, 274
  - Pt, 250, 261, 265, 273, 274
  - Rh, 262, 265, 273, 274
- O**
- Optical gas sensor components
  - detectors, 342–348
  - infrared coating materials, 349
  - lens, 348, 349
  - light sources, 338–342
  - mirror optics, 348, 349
  - monochromator, 329, 331
  - optical filters, 329, 331
  - requirements, 337, 338, 343
  - window materials, 348
- Optical gas sensors
  - absorption infrared (IR) spectroscopy, 22, 329, 331, 339
  - absorption lines, 331, 333, 342
  - absorption spectroscopy, 22, 329, 331
  - advantages, 331
  - Fourier-transform infrared (FTIR) spectroscopy, 331
  - indicator dyes, 22
  - LIDAR systems, 348
  - near-infrared (NIR) spectroscopy, 329, 331
  - quenching of fluorescent, 128
  - UV–vis spectroscopy, 128, 333

- Organic layers in work function gas sensors  
 dimethyl-methylphosphonate (DMMP), 384, 386  
 polypyrrole (PP), 384  
*p*-polyphenylene (PPP), 384, 385  
 tetrachloroethene (PER), 384  
 thiol functionalized porphyrins, 384
- Oxygen (O<sub>2</sub>), 2, 53, 119, 178, 198, 260, 281, 298, 313, 329, 356, 372, 380, 399, 411, 418
- Oxygen sensors  
 high temperature oxygen sensors, 54–62, 89  
 lambda sensors, 54  
 low temperature oxygen sensors, 52, 66, 76
- Ozone (O<sub>3</sub>), 2–4, 6, 7, 13, 22, 34–38, 72–74, 85, 97, 119, 138, 240–242, 300, 332, 333, 380–382, 384, 419, 422  
 sensors, 97, 240
- P**
- Palladium (Pd)-based alloys in gas sensors  
 Pd–Ag, 162  
 Pd–Au, 162  
 Pd–Ni, 162
- Palladium (Pd)-based hydrogen sensors  
 dipole layer, 18, 155  
 hydrogen diffusion, 154  
 lattice expansion, 153, 160, 163  
 mechanism of sensing, 155  
 Pd-gate, 18  
 resistance change, 153, 154
- Paper-based gas sensors  
 cellulose microfibril network, 241  
 cellulose sheet, 240  
 filter paper, 240–242  
 glossy paper, 242  
 trapping reagent, 240
- Passive filters  
 Al<sub>2</sub>O<sub>3</sub>, 294, 296, 299  
 charcoal filter, 297  
 polymer gas separation membranes, 296  
 SiO<sub>2</sub>, 294, 296, 298, 299
- Perovskites  
 advantages, 58  
 BaTiO<sub>3</sub>, 91  
 BaZrO<sub>3</sub>, 64, 70  
 CaZrO<sub>3</sub>, 63, 70  
 KCa<sub>2</sub>Nb<sub>3</sub>O<sub>10</sub>, 63  
 La<sub>2</sub>CuO<sub>4+δ</sub> (lanthanum cuprate), 92  
 LaGaO<sub>3</sub> (LSGM), 57  
 SrTi<sub>(1-x)</sub>Fe<sub>x</sub>O<sub>3</sub>, 52, 92  
 SrTiO<sub>3</sub>, 52, 91
- Physical gas sensors, 409
- Piezoelectric-based gas sensors  
 advantages, 310, 311, 314, 317, 321, 324  
 bulk acoustic wave (BAW), 307, 309, 312, 316  
 crystal microbalance (QCM), 18–20, 33, 51, 123, 125, 139, 140, 142, 160, 307, 310, 319, 321, 322, 324, 389, 390  
 high temperature devices, 314–317  
 interdigital transducers (IDTs), 307, 312–314  
 limitations, 316, 317  
 operation temperature, 315, 316  
 oscillator, 18–20  
 piezoelectricity, 307  
 piezoelectric MEMS devices, 317–318  
 QCM-based sensors, 139, 145  
 resonant frequency, 20, 307, 309  
 SAW-based sensors, 18, 311–314  
 sensing layer, 318–325  
 surface acoustic wave (SAW), 19, 20, 307–312, 314, 320, 321, 323, 324
- Piezoelectric crystal resonators  
 film bulk acoustic resonator, 19, 308, 311  
 thin-film bulk acoustic resonator, 307, 312  
 thin-film resonators, 307, 310
- Piezoelectric materials  
 aluminum nitrate (AlN), 310, 311, 317  
 comparison, 310, 311  
 gallium orthophosphate (GaPO<sub>4</sub>), 316  
 langasite (La<sub>3</sub>Ga<sub>5</sub>SiO<sub>14</sub>, LGS), 316  
 lead zirconate titanate (PZT), 310, 317  
 lithium niobate (LiNbO<sub>3</sub>), 309, 310, 312  
 lithium tantalate (LiTaO<sub>3</sub>), 310, 312  
 oxyborates ReCa<sub>4</sub>O(BO<sub>3</sub>)<sub>3</sub>, 316  
 quartz, 309–312  
 ZnO, 310, 311, 317
- Planar waveguides  
 configuration, 337  
 glass, 337, 338  
 metal oxides (ZnO, TiO<sub>2</sub>, LiNbO<sub>3</sub>, LiTaO<sub>3</sub>, etc.), 337  
 quartz crystal, 337  
 semiconductors (GaAs, InP, etc.), 337, 338
- Plasmon resonance gas sensors, 93, 156
- Polymer choosing  
 hydrophilic polymers, 393  
 hydrophobic polymers, 139, 144, 393
- Polymer electrolytes  
 hydrogels, 124, 136, 355  
 Nafion, 131–135, 354  
 polyelectrolyte, 124, 393  
 poly(hydroxyethyl methacrylate) (PHEMA), 131, 369, 395  
 poly(vinyl pyridine) (PVPy), 131, 393  
 PVA/H<sub>3</sub>PO<sub>4</sub> electrolyte, 134, 144, 354  
 sulfonated polybenzimidazole (PBI), 134, 144  
 sulfonated polyether ether ketone (S-PEEK), 134
- Polymer field-effect transistors (PolyFET), 126, 127
- Polymer for capacitance gas sensors  
 polydimethylsiloxane (PDMS), 367, 369  
 polyimides, 367, 368
- Polymer gas sensor operation  
 de-doping, 138, 143  
 dipole-dipole interaction, 131, 141  
 doping, 122, 127, 129, 130, 143  
 hydrogen bonding, 131, 141  
 π-bonding, 117  
 protonation, 124, 130, 143  
 redox reaction, 129  
 swelling, 122, 130, 131, 137, 138
- Polymer gas sensors advantages, 144

- Polymer gas sensors disadvantages  
 sensitivity to air humidity, 28  
 sensitivity to oxidizers (ozone), 74  
 sensitivity to UV radiation, 97, 138
- Polymer optical fibers  
 perfluorinated polymers, 334  
 PMMA (acrylic), 334
- Polymer(s)  
 advantages, 144  
 backbone, 128–130, 134, 143  
 chain, 117, 118, 129, 130, 417  
 conjugated polymers, 117, 118, 127, 128, 143  
 deposition, 122, 134, 137, 145, 359  
 films, 122, 127, 129, 131, 137, 138, 140, 145, 146,  
 319, 366, 384, 385, 393, 396, 403  
 gas-permeable membranes, 124, 125, 324  
 limitations, 136–139  
 mechanism of conductivity, 128–129  
 polymerization, 118, 120–122, 131, 141, 145  
 synthesis, 121
- Polymers conducting (CPs)  
 polyaniline (PANI), 118, 122, 127, 128, 130, 131,  
 138, 139, 141, 143, 199  
 poly(etherurethane) (PEUT), 125, 369  
 polypyrrole (PPy), 118, 122, 126, 128, 141, 145  
 polythiophene (PT), 118, 127, 128, 130, 131, 141, 143  
 poly(vinyl alcohol) (PVA), 124, 143  
 poly(vinylidene fluoride) (PVDF), 128  
 poly(vinylidene fluoride-trifluoroethylene)  
 (P(VDF-TrFE)), 128
- Polymers in humidity sensors  
 polyimides, 230, 233, 235, 366–368, 392, 395  
 polymer stabilization, 127, 142, 143  
 polyvinyl alcohol (PVA), 142, 393
- Porous semiconductor-based gas sensors, 175–180  
 advantages/disadvantages, 176–180  
 Si, 175–180
- Porous semiconductors in humidity sensors  
 porous SiC, 370, 392, 400  
 porous silicon (PSi), 392, 400–402  
 PSi stabilization, 402
- Portable sensors, 25, 26, 28–30  
 battery life, 28
- Proton ion conductors  
 $H_3Mo_{12}PO_{40} \cdot 29H_2O$ , 202  
 $H_3PW_{12}O_{40} \cdot 29H_2O$ , 202, 203  
 $HSbP_2O_8 \cdot 10H_2O$ , 202  
 $H_4SiW_{12}O_{40} \cdot 28H_2O$ , 202, 203  
 $HUO_2PO_4 \cdot 4H_2O$ , 202, 203  
 $P_2O_5-SiO_2$ , 187, 202, 203  
 $Sb_2O_5 \cdot H_2O-H_3PO_4$ , 202, 205  
 $Sn_{0.9}In_{0.1}P_2O_7$ , 206
- Pyroelectric materials  
 lead zirconate (PZ), 311, 344  
 lead zirconate titanate (PZT), 99, 344, 345  
 $LiTaO_3$ , 99, 344, 345  
 $NiO$ , 100  
 polyvinylidene fluoride (PVDF), 99  
 $SiGe$ , 99, 346  
 strontium barium niobate (SBN), 345  
 triglycine sulphate (TGS), 99, 344
- R**
- Reference electrode (RE) in electrochemical sensors  
 calomel,  $Hg/HgCl_2$ , 328  
 Pt/air, 328  
 silver-silver chloride,  $Ag/AgCl$ , 328
- Resistive sensors, 15, 18, 32, 89, 129, 139, 154, 169,  
 233, 293, 389, 390, 399, 400
- Room temperature sensors, 17, 94, 96, 159
- S**
- Schottky diode, 14, 18, 32, 50, 127, 156, 169, 171,  
 173–175, 366
- Schottky diode-based sensors, 18, 372
- Semiconductor-based gas sensors, 16, 18, 25, 93, 255,  
 281, 283, 296, 372, 397
- Semiconductor compound III–V-based gas sensors,  
 170–172  
 advantages/disadvantages, 171–172
- Semiconductor compound II–VI-based gas sensors  
 advantages/disadvantages, 183, 185  
 $CdS$ , 182–185  
 $CdSe$ , 182–184  
 $ZnS$ , 182–185  
 $ZnSe$ , 182, 183
- Semiconductor glasses-based gas sensors  
 advantages/disadvantages, 186, 187  
 chalcogenide glasses, 186–187  
 other glasses, 187–188
- Semiconductor sensors, 25, 296
- Sensing effect, 39, 71, 156, 173, 273, 377, 380, 416, 420
- Sensing electrodes in solid electrolyte-based sensors  
 hydrides ( $MeHx$ ), 265  
 metal oxide composites, 262  
 metal oxides, 262, 263  
 Pt, 261–265  
 Pt-based alloy, 262
- Sensing layer for piezoelectric-based gas sensors  
 classification of coatings, 324  
 requirements, 318–319  
 sensing mechanism, 320–325  
 solid adsorbents, 320  
 sorptive interaction, 319–320
- Sensing materials, 21, 24, 30, 38, 39, 49, 68, 72, 73, 77,  
 80, 93, 94, 100, 101, 129, 131, 137, 153, 159,  
 167, 174, 177, 183, 187, 229, 231, 242
- Sensing materials for work function gas sensors  
 inorganic layers, 380–383  
 metal layers, 379–380  
 metal oxides, 378, 382  
 organic layers, 384–386
- Sensor applications  
 agriculture, 3, 10  
 environment control, 2–10  
 industry, 1–3  
 medicine, human diseases, 10–13  
 in situ monitoring, 52
- Sensor fabrication  
 calcination, 66, 249, 290, 291  
 chemical deposition, 363  
 chemical vapor deposition (CVD), 225, 300, 362–363

- Sensor fabrication (*cont.*)
- electrophoretic deposition, 299
  - immobilization, 241
  - impregnation, 240, 363
  - ink-jet printing, 230, 418, 419, 427
  - physical vapor deposition (PVD), 362–363
  - planar sensors, 136, 224
  - sensor packaging
    - material requirements, 243–244
    - packaging layer, 243
  - successive ionic layer deposition (SILD), 299
  - surface functionalization, 427
  - thick film technology, 25
  - thin film technology, 25
- Sensor platforms
- cantilever-based sensor platforms, 234–235
  - conventional sensor platforms
    - alumina ( $\text{Al}_2\text{O}_3$ ), 223, 224
  - dissipation power, 392
  - flexible sensor platforms, 228–234
  - melting point, 224, 231, 232
  - micromachining hotplates, 225–228
  - multi-parameter sensing platform, 233
  - paper-based gas sensors, 240–242
- Silicon-based gas sensors
- advantages/disadvantages, 167
  - MOS-based sensors, 168
  - Si:H, 169, 170
- Solid electrolyte
- fluoride ion conductors, 214–217
  - ideal solid electrolyte, 200–201
  - ion conductors, 197, 200, 208, 210, 212
  - metal oxide solid electrolytes, 53–70
  - oxygen diffusion, 50
  - oxygen ion conductors, 198
  - perovskites, 203, 216, 217
  - proton ion conductors, 201–204, 206
- Solid electrolyte gas sensors
- advantages, 52
  - limitation, 68–70
- Sorbents
- activated carbon, 294, 296, 297, 301
  - aluminas, 294
  - graphitized carbon blacks, 301
  - molecular sieves, 294, 296, 301
  - porous polymers, 295, 300
  - silicas, 294
  - zeolites, 294
- Space-charge region, 74, 75
- Stoichiometry, 52, 56, 91, 188, 273, 316, 317
- Sulfur dioxide ( $\text{SO}_2$ ), 8, 9, 13, 419
- Sulfur dioxide ( $\text{SO}_2$ ) sensors, 35, 212, 363
- Surface functionalization, 27, 183, 427
- Surface modifiers
- additives, 273–279, 283
  - catalysts, 273–283
  - catalytic activity, 279, 281
  - sensitization mechanisms, 276–279
- Surface reaction, 16, 77, 80, 255, 273, 275, 277
- T**
- Tellurium-based gas sensors
- advantages/disadvantages, 188
  - operation, 189–190
- Thermoelectric materials
- BiTe, 181
  - PbTe, 181
  - SiGe, 24, 99, 181, 182
- Thermometric sensor
- advantages/disadvantages, 287
  - Curie temperature, 99
  - pyroelectric detectors, 25
  - pyroelectric sensors, 23–25
  - Seebeck effect, 24
  - thermoconductivity-based sensors, thermal
    - conductivity, 23
  - thermoelectric gas sensors,  $\text{SrTi}_{1-x}\text{Fe}_x\text{O}_{3-\delta}$ , 100
- Thick film sensors, 25, 74, 92, 103
- Thick film technology
- conductor pastes, 251
  - dielectric inks, 251
  - drop-coating, 249
  - organic carrier, 250, 252, 253
  - organic vehicle, 249, 252, 253
  - powders, 251
  - screen meshes, 250
  - screen-printing, 249
  - sol-gel, 73, 81
  - tape casting, 249
  - thick-film adhesion, 252
  - thick-film ink, 250
- Thin film sensors, 137, 259
- Thin film technology
- chemical vapor deposition, 182
  - magnetron sputtering, 182, 424
  - spray pyrolysis, 73, 256, 276
- Transition metal catalysts, 51, 83, 84, 91–93, 101, 153, 263, 274, 275, 280, 322
- Cu, 51, 273
- W**
- Wide-band-gap semiconductor-based
- gas sensors
    - advantages/disadvantages, 172–173
    - GaN, 172–175
    - SiC, 172–174
- Wireless sensing, 27, 37
- Work function, 13, 14, 18, 19, 32, 37, 50, 93, 119, 126, 127, 129, 131, 138, 151, 174, 177, 255, 273, 278, 372, 415, 418, 420
- Work function gas sensors
- advantages/disadvantages, 377–378
  - GasFET, 378, 379, 381, 382, 384
  - Kelvin probe (KP), 377–379, 382–384
  - sensing materials, 378, 382
- Working electrodes (WE) in electrochemical sensors
- carbons, 357
  - Pt/C, 135, 206, 357